

67-5-2-V

THE JOURNAL OF PHYSICAL CHEMISTRY

Volume 72

JANUARY—APRIL 1968

PAGES 1—1404

FREDERICK T. WALL, *Editor*

MARILYN H. PERRIN AND ROBERT G. LINCK, *Assistant Editors*

EDITORIAL BOARD

R. BERSOHN
S. BRUNAUER
L. F. DAHL
J. R. FRESCO
G. J. HILLS
M. KASHA
C. KEMBALL

W. KLEMPERER
A. KUPPERMANN
F. A. LONG
R. A. MARCUS
W. J. MOORE
W. A. NOYES, JR.
B. S. RABINOVITCH

R. E. RICHARDS
F. S. ROWLAND
W. G. SCHNEIDER
R. L. SCOTT
R. SEIFERT
S. I. WEISSMAN
B. H. ZIMM

CHARLES R. BERTSCH, *Senior Production Editor*

JOSEPH H. KUNEY
Director of Business Operations
Director of Publications Research

RICHARD L. KENYON
Director of Publications

DAVID E. GUSHEE
Publication Manager, Journals

EASTON, PA.
MACK PRINTING COMPANY
1968

THE JOURNAL OF PHYSICAL CHEMISTRY

Volume 72, Number 1 January 1968

Reactions of Tritium Atoms Produced by Electron Impact on T_2 with Solid Propene and Propane	R. D. Shores and H. C. Moser	1
The Fragmentation of Skeletal Bonds of Cyclic Alkanes in Mass Spectra	Kozo Hirota and Yoshio Niwa	5
Equations for the Description of Isothermal Diffusion in Multicomponent Systems Containing Pairs of Chemically Equivalent Components	John Grover Albright	11
d^2 and d^8 Configurations in an Axial Model Field	Donald R. Scott and F. A. Matsen	16
Spin-Free Quantum Chemistry. V. Spin Density	F. A. Matsen and A. A. Cantu	21
The Effect of Temperature on Dielectric Properties of Water-in-Oil Emulsions	I. D. Chapman	33
A Comparative Study of Pheophytin <i>a</i> and Pheophytin <i>b</i> Monolayers	W. E. Ditmars, Jr., and Q. Van Winkle	39
Adsorption of 1,1-Diphenyl-2-picrylhydrazyl on Solid Acid Catalysts	Haruo Imai, Yoshio Ono, and Tominaga Keii	46
Dielectric Properties of Ice and Water Clathrates	Wallace S. Brey, Jr., and Howard P. Williams	49
The Reaction of O with Alcohols in Gas-Phase Radiolysis	John M. Warman	52
Excess Thermodynamic Functions of Some Binary Nonelectrolyte Mixtures. I. Measurements of Excess Gibbs Free Energy, Enthalpies, and Volumes of Mixing	S. N. Bhattacharyya and A. Mukherjee	56
Excess Thermodynamic Functions of Some Binary Nonelectrolyte Mixtures. II. Analyses of g^E , h^E , and v^E Data in Terms of a Generalized Quasi-Lattice Theory	S. N. Bhattacharyya, R. C. Mitra, and A. Mukherjee	63
Electron Spin Resonance Study of Some Trifluoromethylnitrobenzene Anion Radicals	J. W. Rogers and W. H. Watson	68
Surface Potentials of Aqueous Electrolyte Solutions	N. L. Jarvis and M. A. Scheiman	74
The Kinetics of Dissociation of Hydrogen Fluoride behind Incident Shock Waves	Jay A. Blauer	79
Rates of Reactions of Oxygen Atoms with Solid and Liquid Sulfur (and Selenium)	F. Cramarossa, E. Molinari, and B. Roio	84
Stochastic Approach to Nonequilibrium Thermodynamics of First-Order Chemical Reactions. II. Open Systems	Kenji Ishida	92
Electrolytes in High Surface Area Systems. I. The Reaction between Lithium Chloride-Acetone Solutions and Silica Gel, an Unusual Addition Reaction	Russell Maatman, Abel Geertsema, Harold Verhage, Glenn Baas, and Michael Du Mez	97
Electrolytes in High Surface Area Systems. II. The Reaction between Aqueous Dichromate and Silica Gel	Russell W. Maatman and Allan Kramer	104
Kinetics of the Reaction of Fluorine with Difluoramino Radicals and the Dissociation of Fluorine	R. W. Diesen	108
Mechanism for Controlling the Reactivity of Lead Azide	V. R. Pai Verneker and A. C. Forsyth	111
Stability Order in Metal Chelate Compounds. V. Bivalent Metal Complexes of 2-Pyridylmethyl Phosphate	Yukito Murakami and Makoto Takagi	116
Nuclear Magnetic Resonance of Oxygen-17 and Chlorine-35 in Aqueous Hydrochloric Acid Solutions of Cobalt(II). I. Line Shifts and Relative Abundances of Solution Species	A. H. Zeltmann, N. A. Matwyoff, and L. O. Morgan	121
On the Tait and Related Empirical Equations of State	George A. Neece and David R. Squire	128
Application of the Electron-Donation Model for Hydrogen Absorption to Palladium-Rich Alloys. Hydrogen-Gold-Palladium	K. Allard, A. Maeland, J. W. Simons, and Ted B. Flanagan	136
Investigation of the Validity of Several Approximations in Measurements of Cation-Ligand Association Constants by a Conductance Method	J. B. Ezell and W. R. Gilkerson	144
Differential Diffusion Coefficients of Hexamethylenetetramine Aqueous Solutions	L. Costantino, V. Crescenzi, and V. Vitagliano	149

Perkin-Elmer announces its new analytical GC/DF mass spectrometer

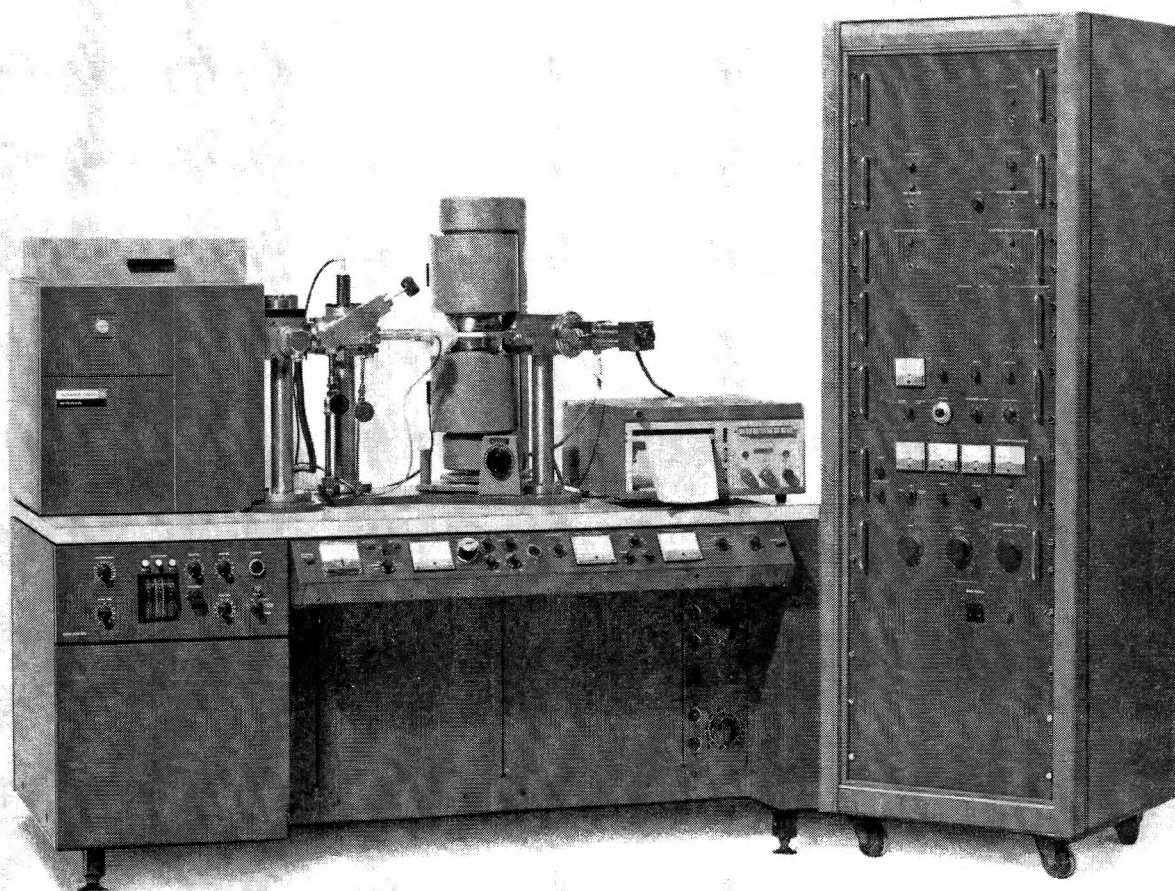
Designed for every instrumentation laboratory, the Model 270 provides complete capability and simplicity – at moderate cost.

- ☐ Double-focusing Nier-Johnson mass analyzer
- ☐ Resolves mass peaks to M/e 1000; scans to M/e 3300
- ☐ Built-in Perkin-Elmer Model 900 GC inlet system and sample enricher
- ☐ Heated direct solids sampling system
- ☐ Differential pumping
- ☐ High-sensitivity electron multiplier detector

- ☐ Fast and repetitive scanning system
- ☐ High-speed multi-channel oscillographic recorder
- ☐ Readily accessible controls
- ☐ Compact laboratory size
- ☐ Much lower cost than any other mass spectrometer in this performance range

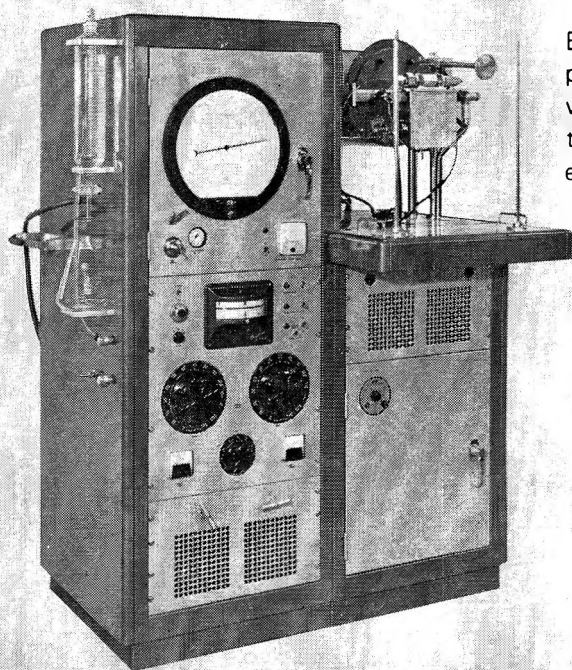
For more data, write Instrument Division, Perkin-Elmer Corporation, 715 Main Avenue, Norwalk, Connecticut 06852, or your nearest Perkin-Elmer office.

PERKIN-ELMER



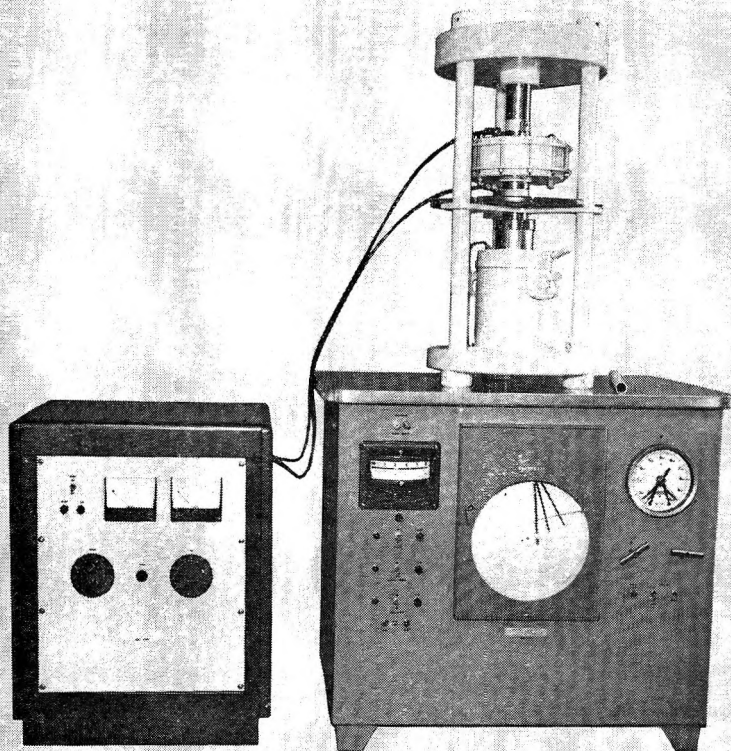
This instrument is instantly available to you under Perkin-Elmer's low cost lease plan.

Conformational Isomerism of 1,1'-Disubstituted Azo Compounds	Gavriella Gabor and Kedma H. Bar-Eli	153
Convective Diffusion in Capillaries	Allen R. Overman and Raymond J. Miller	155
Ionic Reactions of Unsaturated Compounds. I. Polymerization of Acetylene	Jean H. Futrell and Thomas O. Tiernan	158
Studies of Free-Radical Species from the Reactions of Titanium(III) Ions with Hydrogen Peroxide	Koichi Takakura and Bengt Rånby	164
Metal-Ammonia Solutions. II. Internal Reflection Spectroscopy of Alkali Metal-Ammonia Solutions	D. F. Burow and J. J. Lagowski	169
The Proton Magnetic Resonance Spectra of Diethyl Vinylphosphonate and Substituted Vinylphosphonates	M. P. Williamson, S. Castellano, and C. E. Griffin	175
Density and Heat of Fusion of Folded-Chain Polyethylene Crystals	Fumiyuki Hamada, Bernhard Wunderlich, Takuji Sumida, Seiichi Hayashi, and Akio Nakajima	178
The Cobalt-60 γ Radiolysis of Cysteine in Deaerated Aqueous Solutions at pH Values between 5 and 6	Verna Gaye Wilkening, Manohar Lal, Meta Arends, and D. A. Armstrong	185
Triplet Methylene Radical Reaction with <i>cis</i> -Butene-2	D. F. Ring and B. S. Rabinovitch	191
Solvent-Dependent H-H Couplings in Hexachlorobicyclo[2.2.1]heptenes	Stanford L. Smith and Richard H. Cox	198
Sublimation of Ammonium Perchlorate	P. W. M. Jacobs and A. Russell-Jones	202
Complexes in Calcium Phosphate Solutions	A. Chughtai, R. Marshall, and G. H. Nancollas	208
Osmotic Coefficients of Aqueous Solutions of Tri- <i>n</i> -alkylsulfonium Halides at 25°	Siegfried Lindenbaum	212
Polymer Studies by Gel Permeation Chromatography. II. The Kinetic Parameters for Styrene Polymerizations	James A. May, Jr., and William B. Smith	216
Fluorine Bomb Calorimetry. XXIII. The Enthalpy of Formation of Carbon Tetrafluoride	Elliott Greenberg and Ward N. Hubbard	222
Dose and Concentration Dependence of Hydrogen Transfer in the Radiolysis of Dilute Solutions of Cyclopropane in <i>n</i> -Hexane and Cyclohexane.	Stefan J. Rząd and Robert H. Schuler	228
Computed Activation Energies and Rate Constants for Forward and Reverse Transfers of Hydrogen Atoms	S. W. Mayer and L. Schieler	236
Infrared Spectra of Kaolin Mineral-Dimethyl Sulfoxide Complexes	S. Olejnik, L. A. G. Aylmore, A. M. Posner, and J. P. Quirk	241
Infrared Spectra of the Beryllium Halides	Alan Snelson	250
Energy Transfer in Radiolysis of Rare Gas-C ₂ F ₆ Liquid Mixtures	Alicja Sokolowska and Larry Kevan	253
Electromotive Force Studies in Aqueous Solutions at Elevated Temperatures. IX. The Thermodynamic Properties of Hydrochloric Acid-Gadolinium Chloride Mixtures	M. H. Lietzke and R. W. Stoughton	257
Sound Velocities, Adiabatic Compressibilities, and Free Volumes in Aniline Solutions	D. D. Deshpande and L. G. Bhatgadde	261
The Crystal Structure of Dipotassium Tetranitroethide	Maurice Dyke and Ronald L. Sass	266
Estimation of the Isomerization Rate of Nitrous Acid	I. C. Hisatsune	269
Diffusion Potential Decay Accompanying Transient-State Diffusion of Electrolytes in Ideal Solutions	Gary E. Spalding	272
Light Scattering and Refractometry of a Monodisperse Polymer in Binary Mixed Solvents	K. Okita, A. Teramoto, K. Kawahara, and H. Fujita	278
Electron Spin Resonance Spectrum of Tetrakis(<i>p</i> -methoxyphenyl)ethylene Cation Radical	Jorge A. Valenzuela and Allen J. Bard	286
Carbon-13 Nuclear Magnetic Resonance Studies of 3-Substituted Pyridines	H. L. Retcofsky and R. A. Friedel	293
The Ultraviolet Spectrum of the Nitrate Ion in Molten Mixtures of Alkali Metal Nitrates	Charles R. Boston, David W. James, and G. Pedro Smith	293
Isosbestic Points and Internally Linear Spectra Generated by Changes in Solvent Composition Temperature	Jorulf Brynestad and G. Pedro Smith	293
Kinetics of Aluminum Ion Hydrolysis in Dilute Solutions	Lloyd P. Holmes, David L. Cole, and Edward M. Eyring	301
The Photochemistry of NCS ⁻ in Solution	M. Luria and A. Treinin	305
The Enthalpy of Fusion of Linear Polyethylene	L. Mandelkern, A. L. Allou, Jr., and M. Gopalan	309



BARNES VOLUMETRIC HYDROTHERMAL SYSTEMS give pressures to 15,000 psi and temperatures to 600°C. With vacuum system, aliquot sampler, and liquid volume indicator, this apparatus provides a complete high pressure system for exploring new frontiers in volumetric chemistry.

OPPOSED ANVIL PRESSURE SYSTEMS. Based on principles developed by Bridgman, samples are loaded between opposed anvils or pistons. Pressures to over 2,000,000 psi can be produced, and at lower pressures samples can be heated to 1500°C. with the internal heating accessory.



Think what you could accomplish at *REALLY* high pressures...

A virtually unlimited field of study is now yours with these ultra-high pressure systems. You can explore the effects of pressure on thousands of known chemical reactions. More important, you can now investigate reactions possible **only** under high pressures.

For instance, enthalpy determinations directly from the Clapeyron equation take on new significance with ultra-high pressures. Likewise, syntheses of dense phases, hot pressing, isostatic pressing, and direct P-V-T mea-

surements are extended to new importance.

TEM-PRES RESEARCH can give you this capability plus options that custom-engineer any system to your own requirements: thermal and corrosive environments; fluid pressures; electrical measurements of pressurized specimens; ignition; continuous mixing; and a variety of other needs.

Write today for technical data on TEM-PRES RESEARCH High Pressure Systems.

TEM-PRES RESEARCH

1401 S. Atherton, State College, Pa. 16801 (814) 237-7631

CARBORUNDUM



One year old and flourishing —

INTERNATIONAL JOURNAL OF QUANTUM CHEMISTRY

HONORARY EDITORIAL BOARD

W. Heitler

Robert S. Mulliken

John C. Slater

EDITORIAL BOARD

Editor-in-Chief: Per-Olov Löwdin

Assistant Editors: Jean-Louis Calais

Charles A. Coulson

Raymond Daudel

Joseph O. Hirschfelder

Laurens Jansen

Masao Kotani

Roy McWeeny

Yngve Öhrn

Ruben Pauncz

Clemens Roothaan

Harrison Shull

With the end of 1967, the *International Journal of Quantum Chemistry* will complete its first year of publication. Founded to offer worldwide circulation to original papers in quantum mechanics and its applications to the theory of atoms, molecules, and crystals, the *Journal* has, in its one year of existence, devoted its pages to the most brilliant and thorough contributions to these subjects. In it have appeared the results of research on the fundamental concepts and mathematical structure of quantum chemistry, on applications to atoms, to molecules, and to crystals, on applications to molecular biology, and on the computational methods of quantum chemistry.

The *International Journal of Quantum Chemistry* is published bimonthly. Volume II (1968) will also include the proceedings of the 1968 symposium to be held at Sanibel Island.

Subscription: \$60.00

Foreign postage: \$3.00

INTERSCIENCE PUBLISHERS, a division of
JOHN WILEY & SONS, Inc., 605 Third Avenue, New York, N. Y. 10016



RESEARCH IN PHYSICAL PHARMACY

An opportunity to conduct research work in physical pharmacy in an established laboratory awaits the recent recipient of a Bachelor's or Master's Degree in Physical Pharmacy or Physical Chemistry. Working under the general direction of a PhD, the research assistant is encouraged to exercise initiative and good judgment.

Interested applicants send resumes showing full details of education and experience to:

J. J. Kuhn, Jr., *Employment Manager*

McNEIL LABORATORIES, INC.

Camp Hill Road

Fort Washington, Pa. 19034

An Equal Opportunity Employer

CIRCUIT DESIGNERS

**for advanced
microelectronic
circuit synthesis.**

**Managerial,
Engineering and
Research candidates
wanted
for novel thin-film
circuit development.**

**New business
opportunity offers
growth potential
for Electronic
Circuit Engineers.**

Send resume to General Electric Co., Rm.
105-A, P.O. Box 112, Main Post Office,
Schenectady, N.Y. 12301.

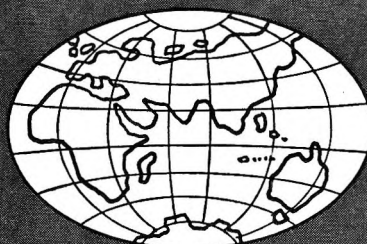
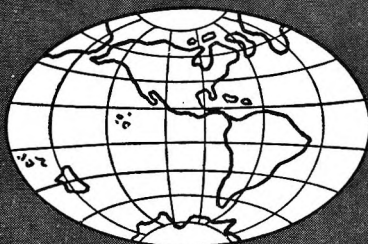
GENERAL  ELECTRIC

An equal opportunity employer, M/F.

AUTHOR INDEX

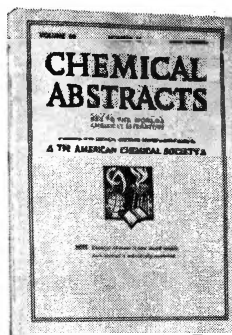
- Albright, J. G., 11
Allard, K., 136
Allou, A. L., Jr., 309
Anacker, E. W., 379
Arends, M., 185
Armstrong, D. A., 185
Attwood, D., 339
Aylmore, L. A. G., 241
- Baas, G., 97
Bär, F., 369
Bard, A. J., 286
Bar-Eli, K. H., 153
Bertozzi, G., 353
Bhatgadde, L. G., 261
Bhattacharyya, S. N., 56, 63
Blauer, J. A., 79
Boston, C. R., 293
Brey, W. S., Jr., 49
Brinton, R. K., 321
Brynestad, J., 296
Burow, D. F., 169
- Cantu, A. A., 21
Castellano, S., 175
Chandross, E. A., 378
Chapman, I. D., 33
Chughtai, A., 208
Clarke, J. K. A., 327
Cole, D. L., 301
Coleman, C. F., 365
Costantino, L., 149
Cox, R. H., 198
Cramarossa, F., 84
Crescenzi, V., 149
- Dahms, H., 362
Dandy, A. J., 334
Deshpande, D. D., 261
Diesen, R. W., 108
- Ditmars, W. E., Jr., 39
Du Mez, M., 97
Dyke, M., 266
- Eckstrom, H. C., 369
Eyring, E. M., 301
Ezell, J. B., 144
- Farren, G. M., 327
Flanagan, T. B., 136
Forsyth, A. C., 111
Friedel, R. A., 290
Fujita, H., 278
Fukuzawa, K., 371
Futrell, J. H., 158
- Gabor, G., 153
Geertsema, A., 97
Gilkerson, W. R., 144
Gopalan, M., 309
Greenberg, E., 222
Griffin, C. E., 175
- Hamada, F., 178
Hartland, S., 318
Hayashi, S., 178
Hermann, A., 364
Hirota, K., 5
Hisatsune, I. C., 269
Holmes, L. P., 301
Hou, K. C., 348
Horne, R. A., 376
Hubbard, W. N., 222
- Imai, H., 46
Ishida, H., 367
Ishida, K., 92
- Jacobs, P. W. M., 202
James, D. W., 293
Jarvis, N. L., 74
Johnson, J. S., Jr., 360
- Kawahara, K., 278
Keii, T., 46
Kevan, L., 253
Kramer, A., 104
Kubokawa, Y., 356
- Lagowski, J. J., 169
Lahaye, J., 348
Lal, M., 185
Levison, S. A., 358
Lietzke, M. H., 257
Lindenbaum, S., 212
Luria, M., 305
- Maatman, R., 97, 104
Maeland, A., 136
Mandelkern, L., 309
Marcus, R. A., 358
Maricle, D. L., 377
Marshall, R., 208
Matsen, F. A., 16, 21
Matwiyoff, N. A., 121
May, J. A., Jr., 216
Mayer, S. W., 236
Miller, R. J., 155
Mitra, R. C., 63
Miyama, H., 371
Miyata, H., 356
Molinari, E., 84
Morgan, L. O., 121
Moser, H. C., 1
Mukherjee, A., 56, 63
Murakami, Y., 116
- Nakajima, A., 178
Nancollas, G. H., 208
Neece, G. A., 128
Niwa, Y., 5
- Okita, K., 278
- Olejniak, S., 241
Ono, Y., 46
Overman, A. R., 155
- Palmer, H. B., 348
Paul, R., 375
Posner, A. M., 241
Prausnitz, J. M., 330
- Quirk, J. P., 241
- Rabinovitch, B. S., 191
Rånby, B., 164
Retcofsky, H. L., 290
Rigby, M., 330
Ring, D. F., 191
Rogers, J. W., 68
Roio, B., 84
Rubalcava, H. E., 327
Rush, R. M., 360
Russell-Jones, A., 202
Rzad, S. J., 228
- Sass, R. L., 266
Sato, H., 367
Scheiman, M. A., 74
Schieler, L., 236
Schott, H., 380
Schuler, R. H., 228
Scott, D. R., 16
Shores, R. D., 1
Simons, J. W., 136
Smith, G. P., 293, 296
Smith, S. L., 198
Smith, W. B., 216
Smith, W. H., 369
Snelson, A., 250
Sokolowska, A., 253
Soldani, G., 353
Spalding, G. E., 272
Sperling, L. H., 345
- Squire, D. R., 128
Stern, J. H., 364
Stoughton, R. W., 257
Sugishima, K., 367
Sumida, T., 178
- Takagi, M., 116
Takakura, K., 164
Teramoto, A., 278
Tiernan, T. O., 158
Tobolsky, A. V., 345
Treinin, A., 305
Tschuikow-Roux, E., 375
Tsubomura, H., 367
- Valenzuela, J. A., 286
Van Winkle, Q., 39
Verhage, H., 97
Verneker, V. R. P., 111
Visco, R. E., 378
Vitagliano, V., 149
- Walton, J. C., 375
Warman, J. M., 52
Watson, W. H., 68
Whittington, S. G., 372
Wilkening, V. G., 185
Williams, H. P., 49
Williams, P. J., 372
Williamson, M. P., 175
Wunderlich, B., 178
- Yamamoto, N., 367
Yao, S. J., 373
Yoshinaga, K., 367
Young, R. P., 376
- Zeltmann, A. H., 121
Zweig, A., 377
Zwolinski, B. J., 373

Only CHEMICAL ABSTRACTS funnels the flow of world wide chemical and chemical engineering data your way



CHEMICAL ABSTRACTS is the only complete and comprehensive chemical abstracting service in the world which can provide you with data and ideas to keep your research, development, production or educational activities moving forward. It is compiled through the systematic collecting, analyzing, and processing of articles and papers from nearly 12,000 journals published in 100 countries and in more than 50 languages. Also processed are patents issued by 25 countries and irregular publications such as books, conference proceedings and government bulletins.

Issues are published each week and are indexed by subject, author, and patent number for fast, easy reference to specific areas of



interest. Seven volume indexes are issued every six months providing you with the keys to the entire literature of chemistry.

Through CHEMICAL ABSTRACTS you can keep on top of all information published anywhere on anything in the world of chemistry. Users consistently report significant savings in time, money and effort by avoiding duplication in research . . . capitalizing on the findings of others . . . learning about new methods and processes.

Act now to have CHEMICAL ABSTRACTS on your desk or in your library. Write for complete information and subscription prices to: E. G. Johnson, Subscriber Information Dept. CA.



CHEMICAL ABSTRACTS SERVICE

American Chemical Society
Columbus, Ohio 43216

THE JOURNAL OF PHYSICAL CHEMISTRY

Volume 72, Number 2 February 1968

Symposium on Inorganic Photochemistry

Photochemistry of Some Square-Planar and Octahedral Platinum Complexes Vincenzo Balzani and Vittorio Carassiti	383
Photochemistry of the Aqueous Nitrate System. I. Excitation in the 300-m μ Band Malcolm Daniels, R. V. Meyers, and E. V. Belardo	389
Electron Spin Resonance Studies of the Photooxidation and Reduction of Cobalt Complexes D. R. Eaton and Susan R. Suart	400
Hydroxyl Radical Kinetics by Kinetic Spectroscopy. III. Reactions with H ₂ O ₂ in the Range 300–458°K N. R. Greiner	406
Ligand Substitution Reactions of Hexacyanoferrate(III) and Azide Induced by Flash Photolysis Donald J. Kenney, Guido G. Clinckemaillie, and Brother Cyril Leo Michiels	410
Photochemistry of Complex Ions. V. The Photochemistry of Some Square-Planar Platinum(II) Complexes Jayarama R. Perumareddi and Arthur W. Adamson	414
<hr/>	
Reexamination of Homogeneous Nucleation and Condensation of Water Welby G. Courtney	421
Condensation of Water in a Cloud Chamber Welby G. Courtney	433
Radiometric Determination of the Volume Change on Mixing in the Liquid Cadmium–Cadmium Chloride System J. Mościński and L. Suski	441
Concentration Fluctuations in Dilute Polymer Solutions. I. A Theoretical Treatment of Flow-Time Fluctuations in a Capillary Viscometer Michael J. Eitel	448
Infrared Studies of Intermediates of the Ammonia Synthesis on Iron Toshiko Nakata and Sanjuro Matsushita	453
Thermodynamics of the Solution of Mercury Metal. I. Tracer Determination of the Solubility in Various Liquids James N. Spencer and Adolf F. Voigt	464
Thermodynamics of the Solution of Mercury Metal. II. The Free-Volume Theory James N. Spencer and Adolf F. Voigt	471
The Vapor Pressure, Vapor Dimerization, and Heat of Sublimation of Aluminum Fluoride, Using the Entrainment Method Ralph F. Krause, Jr., and Thomas B. Douglas	475
Electron Paramagnetic Resonance and Optical Studies of the Oxidation of Aniline by Copper(II) Acetate Alan Van Heuvelen and Larry Goldstein	481
Coulometric Titration of Wustite Frank E. Rizzo and Jack V. Smith	485
Interactions Responsible for the Selective Adsorption of Nonionic Organic Compounds on Alumina. Comparisons with Adsorption on Silica L. R. Snyder	489
Studies of Gas-Phase Reactions of CF ₃ Radical with Methylchlorosilanes W. J. Cheng and M. Szwarc	494
Mathematical Formulation of Rotor Deceleration Experiments in Ultracentrifugation Wilhelm Godschalk	498
The Reaction of Magnesium Metal with Magnesium Chloride Michael Krumpelt, Jack Fischer, and Irving Johnson	506
The Radiolysis of Some Heavy Water Solutions at pD 1.3–13 Z. D. Draganić, O. I. Mićić, and M. T. Nenadović	511
Reactions of Hydrocarbons with Mixtures of Active Nitrogen and Hydrogen Atoms. I. "Normal" Reactions; Reactions of Alkenes and Alkanes David R. Safrany and Walter Jaster	518
Reactions of Active Nitrogen with Organic Substrates. VII. Molecular Origins of Products of Reaction with Propene. II Yoiti Titani and Norman N. Lichtin	526
The Crystal Structures of Bismuth Halide Complex Salts. II. Bispiperidinium Pentabromobismuthate(III) W. Gant McPherson and Edward A. Meyers	532
Electronic Structure and Photochemistry of Flavins. IV. σ -Electronic Structure and the Lowest Triplet Configuration of a Flavin Pill-Soon Song	536

conductivity meter, anyone?

Whatever your requirements, why not turn to the people who know most about conductivity measurement? Whether you need a general purpose, wide range meter with moderate accuracy, a precision laboratory bridge with 0.1% accuracy, a direct reading meter with output for a remote recorder, an electrodeless system for highly corrosive fluids, or almost anything else, we can probably supply what you require. Contact your local Beckman Sales Office or write direct.



Beckman*

INSTRUMENTS, INC.

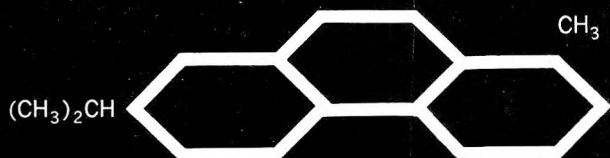
CEDAR GROVE OPERATIONS
89 Commerce Road
Cedar Grove, New Jersey 07009

INTERNATIONAL SUBSIDIARIES: Geneva; Munich; Glenrothes, Scotland; Tokyo; Paris; Capetown; London; Mexico City.

Formerly Industrial Instruments, Inc.

The Photolysis of Perfluoroazomethane	E-Chung Wu and O. K. Rice	542
Aluminum-27 Nuclear Magnetic Resonance of Trialkylaluminum Complexes	L. Petrakis and H. E. Swift	546
Proton Magnetic Resonance Studies of Proton Exchange in Ethylenediamine-Water and Ammonia-Water Systems	Mohammed Alei, Jr., and Alan E. Florin	550
The Powder Patterns and Lattice Constants of Ammonia-boron Trifluoride and Ammonium Tetrafluoroborate	A. P. Caron, J. L. Ragle, M. E. Yorke, and H. Yeh	556
Thermodynamics of the Lead Storage Cell. The Heat Capacity and Entropy of Lead Dioxide from 15 to 318°K	J. A. Duisman and W. F. Giauque	562
Heats of Immersion in the Thorium Oxide-Water System. III. Variation with Specific Surface Area and Outgassing Temperature	E. L. Fuller, Jr., H. F. Holmes, C. H. Secoy, and J. E. Stuckey	573
Reaction of the Deuterated Electron, e_d^- , with e_d^- , D, OD, and D_2O	Edwin J. Hart and E. M. Fielden	577
Investigation of Micelle Structure by Fluorine Magnetic Resonance. II. Effects of Temperature Changes, Added Electrolyte, and Counterion Size	Norbert Muller and Ronald H. Birkhahn	583
Bubbles: A Boundary-Layer "Microtome" for Micron-Thick Samples of a Liquid Surface	Ferren MacIntyre	589
Photochemical Generation of Nitrogen Dioxide in Aqueous Solutions	Michael Ottolenghi and Joseph Rabani	593
Porous Glass as an Ionic Membrane	Inci Altug and Michael L. Hair	599
Thermodynamics of High-Temperature High-Pressure Solutions. Argon in Molten Sodium Nitrate	James L. Copeland and Lawrence Seibles	603
Theory of the Radial Distribution Function	Jack Cohn	608
Mechanism of $O(^3P)$ Addition to Condensed Films. II. Propene, 1-Butene, and Their Mixtures	Ralph Klein and Milton D. Scheer	616
Magnesium Ion Catalysis of Hydrolysis of Isopropyl Methylphosphonofluoridate. The Charge Effect in Metal Ion Catalysis	J. Epstein and W. A. Mosher	622
Rate Constants of OH with HO_2 , O_2^- , and $H_2O_2^+$ from Hydrogen Peroxide Formation in Pulse-Irradiated Oxygenated Water	Knud Sehested, Ole Lang Rasmussen, and Hugo Fricke	626
Analytical Potential Models and the Properties of Noble Gases	J. P. O'Connell and J. M. Prausnitz	632
Thermodynamic Properties of Gases in Propellants. II. Solubilities of Helium, Nitrogen, and Argon Gas in Hydrazine, Methylhydrazine, and Unsymmetrical Dimethylhydrazine	E. T. Chang, N. A. Gokcen, and T. M. Poston	638
Energetics of the Adsorption of Water Vapor on "Pure" Silver Iodide	M. L. Corrin and John A. Nelson	643
Temperature Dependence of Contact Angle and of Interfacial Free Energies in the Naphthalene-Water-Air System	J. B. Jones and Arthur W. Adamson	646
Nuclear Magnetic Resonance Studies of Hydrogen Bonding. II. The Pyrrole-Dimethyl Sulfoxide System	David M. Porter and Wallace S. Brey, Jr.	650
The Reversible Hydration of 2- and 4-Pyridinecarboxaldehydes. II. General Acid-Base and Metal Ion Catalysis	Y. Pocker and J. E. Meany	655
Nuclear Magnetic Resonance Studies of Inorganic Fluorides. V. Fluorosilanes	R. B. Johannesen, F. E. Brinckman, and T. D. Coyle	660
Crystal and Molecular Structures of Three Dihalobenzocyclobutenes	George L. Hardgrove, Lieselotte, K. Templeton, and David H. Templeton	668
Interaction Virial Coefficients in Hydrocarbon Mixtures	E. M. Dantzler, C. M. Knobler, and M. L. Windsor	676
Electrical Conductances of Aqueous Sodium Chloride Solutions from 0 to 800° and at Pressures to 4000 Bars	Arvin S. Quist and William L. Marshall	684
The Thermal Decomposition of Solid <i>cis</i> -Diazidotetraamminecobalt(III) Azide	Taylor B. Joyner	703
Some Upper Limits for the Single-Step Double-Displacement Reaction in Recoil Tritium Systems	Y.-N. Tang and F. S. Rowland	707
Isotopic Exchange between <i>p</i> -Nitrobenzyl Chloride and Chloride Ions as Studied by Electrodeposition	P. Beronius and H. Johansson	713
Valence Shell Calculations on Polyatomic Molecules. II. CNDO SCF Calculations on Monosubstituted Benzenes	John E. Bloor and Donna L. Breen	716
Electron Spin Resonance and Optical Studies of <i>t</i> -Butyl Peroxide Ions Produced by γ Irradiation	Tadamasa Shida	723
Analysis of the Ionic Composition of the Diffuse Double Layer in Mixed Electrolytes by Charge-Step Chronocoulometry	Fred C. Anson	727

Would you believe



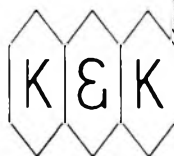
retene

**is just 1 of 30,000
rare chemicals
available for
immediate delivery?**

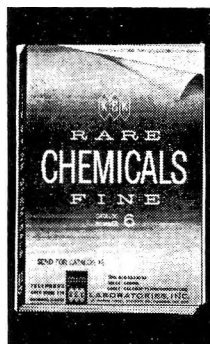
Almost any rare chemical, in any quantity, on hand and available for immediate delivery. K & K probably has the largest in stock supply of chemicals available anywhere . . . and those hard to find chemicals are our specialty.

Orders received are usually shipped in 24 hours or less and that means 5 mg or 500 lbs. Check K & K, a dependable source for any chemical you need.

Our 224 page catalogue available, free — just write for it.



LABORATORIES, INC.
DEPT. P-268
121 Express Street, Engineers Hill
Plainview, New York 11083



K & K LABORATORIES, INC.
DEPT. P-268
121 Express Street, Engineers Hill
Plainview, New York 11803

Gentlemen:
Please send me a copy of your latest catalogue.

NAME _____

STREET ADDRESS _____

CITY & STATE _____ ZIP CODE _____

Ordered Fluids and Liquid Crystals



ADVANCES IN CHEMISTRY SERIES **63**

Ordered Fluids and Liquid Crystals

ADVANCES IN CHEMISTRY SERIES No. 63

Twenty-two studies on characterization, properties, and occurrence of these phenomena in many substances, including:

- the polymorphism of tristearin
- characterization of mesomorphic phases by nmr spectroscopy
- interfaces in nematic liquids
- liquid crystals as ordered components of living substances
- liquid crystalline nature of phospholipids
- the structure of synthetic polypeptides in solution by polarization of fluorescence
- order and structure in concentrated polymer solutions and gels
- field dependence of the magnetic susceptibility of the liquid crystal phase of *p*-azoxyanisole

332 pages with index cloth bound (1967) 9.50 postpaid in U.S. and Canada; plus 20 cents foreign and PUAS.

Set of L. C. cards free with library orders.

Order from

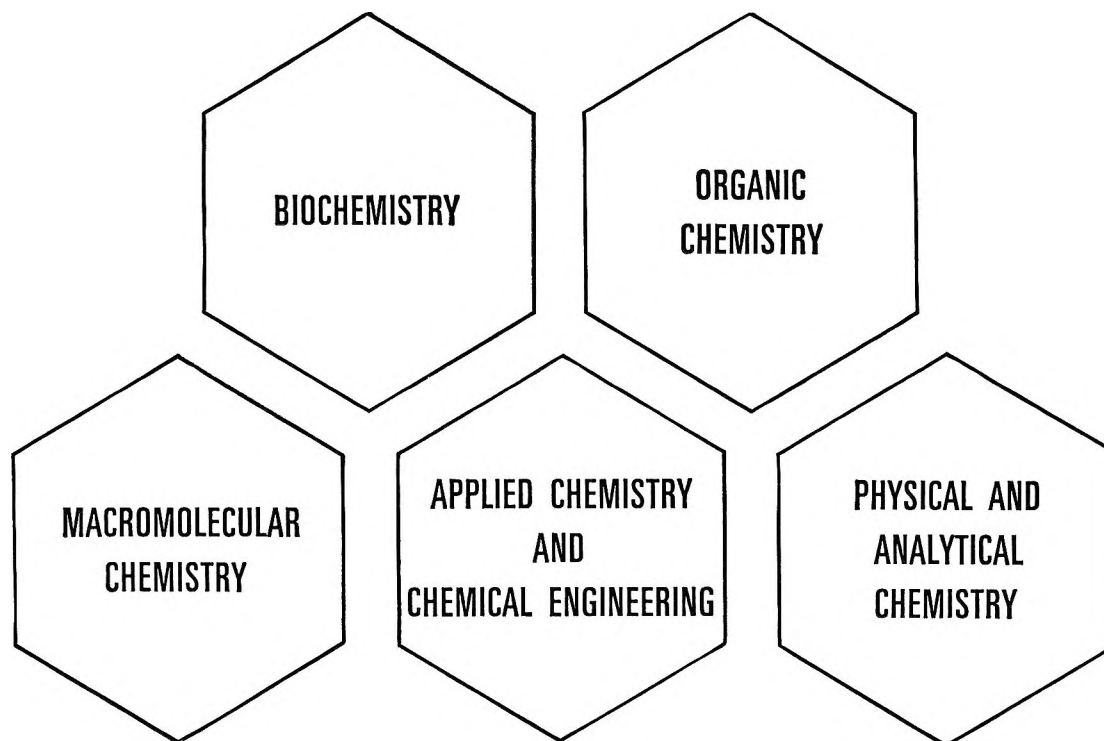
Dept. M
Special Issues Sales
American Chemical Society
1155 Sixteenth St., N.W.
Washington, D.C. 20036

NOTES

The Effect of Salts of Organic Acids and Bases on the Thermal Transition of Ribonuclease	Eugene E. Schrier and Lois D. Mackey	733
A Nuclear Magnetic Resonance Investigation of Paramagnetic Relaxation in Viscous Solutions	Lawrence S. Frankel	736
Pyrolysis and Energetics of Halocarbons in Cryochemical Studies of Divalent Carbon	W. J. Martin and H. A. McGee, Jr.	738
The Anion and Cation Radicals of N,N-Dimethyl- <i>p</i> -nitroaniline	R. F. Nelson and R. N. Adams	740
Ion-Solvent-Molecule Interactions in the Gas Phase. Enthalpies and Entropies for the Reactions $\text{NH}_4^+(\text{NH}_3)_{n-1} + \text{NH}_3 = \text{NH}_4^+(\text{NH}_3)_n$	S. K. Searles and P. Kebarle	742
Reaction of Oxygen Atoms with ICN.	Q. J. F. Grady, C. G. Freeman, and L. F. Phillips	743
Crystal-Field Splitting of Fundamentals in the Raman Spectrum of Rhombic Sulfur	A. T. Ward	744
The Determination of Activation Energies in Solid-State Kinetic Processes	H. N. Murty, D. L. Biederman, and E. A. Heintz	746
Some New Modes of Aerosol Particle Motion: Photodiffusiophoresis	J. R. Brock	747
Intramolecular Comparison of the Insertion into the C-H Bonds of Alkanes by Singlet Methylene Radicals	J. W. Simons, C. J. Mazac, and G. W. Taylor	749
Solubility of Benzene in Concentrated Aqueous Solutions of Tetraalkylammonium Bromides	Henry E. Wirth and Antonio LoSurdo	751
On the Temperature Dependence of the Viscosity of Organic Glasses.	G. A. von Salis and H. Labhart	752
The Effect of Temperature on Magnetically Nonequivalent Protons in an Asymmetric Azo Compound	Stanley Seltzer and Stamatios G. Mylonakis	754

COMMUNICATIONS TO THE EDITOR

Chemiluminescent Reactions of Fluorescein Dyes in Aqueous Solution.	L. I. Grossweiner and A. F. Rodde, Jr.	756
Excited-Molecule Reactions in the Radiolysis of Peptides in Concentrated Aqueous Solution	Michael A. J. Rodgers and Warren M. Garrison	758
The Reaction of Nitrous Oxide with Excited Molecules in the Radiolysis and Photolysis of Liquid Alkanes	R. A. Holroyd	759
Chlorine Nuclear Quadrupole Resonance in $(\text{C}_2\text{H}_5)_4\text{NAsCl}_6$	J. V. DiLorenzo and R. F. Schneider	761
Electrical Conductivity of Liquid and Saturated Vapor of BiCl_3 and HgCl_2 to Their Critical Temperatures	L. F. Grantham and S. J. Yosim	762
High Internal Excitation Energies of Products Following Energetic Substitution of Tritium for Hydrogen in Methyl Isocyanide	Cheng T. Ting and F. S. Rowland	763
Electron Capture Processes in Irradiated Gaseous HCl	G. R. A. Johnson and J. L. Redpath	765
Activation Energies for Reactions of the Hydrated Electron	B. Cercek and M. Ebert	766



Look into **CHEMICAL ABSTRACTS** Section Groupings for efficient and economical coverage of specific interest areas.

Abstracts of the world's chemical literature published regularly in **CHEMICAL ABSTRACTS** are also published in separate issues or "Section Groupings" covering five general areas in the field of chemistry. These Section Groupings are published every other week and contain both the abstracts and a keyword index made up of significant terms selected from the abstracts. Taken together, the five Section Groupings include all abstracts published in CA.

The Section Groupings are extremely valuable as personal desk copies for immediate reference and for browsing in specific subject areas. If your individual interest or that of

your organization is limited to a particular phase of chemistry, a CA Section Grouping can provide you with a comprehensive and economical abstracting service.

Section Groupings can also be used as alerting tools in conjunction with the issue keyword indexes and as retrospective search tools in conjunction with the volume and collective indexes to **CHEMICAL ABSTRACTS** in your company or institution library.

Complete information on **CHEMICAL ABSTRACTS** Section Grouping subscriptions can be obtained by writing to: E. G. Johnson, Subscriber Information Dept. CASG.



CHEMICAL ABSTRACTS SERVICE

American Chemical Society
Columbus, Ohio 43216

AUTHOR INDEX

- Adams, R. N., 740
Adamson, A. W., 414, 646
Alei, M., Jr., 550
Altug, I., 599
Anson, F. C., 727

Balzani, V., 383
Belardo, E. V., 389
Beronius, P., 713
Biederman, D. L., 746
Birkhahn, R. H., 583
Bloor, J. E., 716
Breen, D. L., 716
Brey, W. S., Jr., 650
Brinckman, F. E., 660
Brock, J. R., 747

Carassiti, V., 383
Caron, A. P., 556
Cercek, B., 766
Chang, E. T., 638
Cheng, W. J., 494
Clinckemallie, G. G., 410
Cohn, J., 608
Copeland, J. L., 603
Corrin, M. L., 643
Courtney, W. G., 421, 433
Coyle, T. D., 660

Daniels, M., 389
Dantzler, E. M., 676
DiLorenzo, J. V., 761

Douglas, T. B., 475
Draganić, Z. D., 511
Duisman, J. A., 562

Eaton, D. R., 400
Ebert, M., 766
Eitel, M. J., 448
Epstein, J., 622

Fielden, E. M., 577
Fischer, J., 506
Florin, A. E., 550
Frankel, L. S., 736
Freeman, C. G., 743
Fricke, H., 626
Fuller, E. L., Jr., 573

Garrison, W. M., 758
Giauque, W. F., 562
Godschalk, W., 498
Gokcen, N. A., 638
Goldstein, L., 481
Grady, Q. J. F., 743
Grantham, L. F., 762
Greiner, N. R., 406
Grossweiner, L. I., 756

Hair, M. L., 599
Hardgrove, G. L., 668
Hart, E. J., 577
Heintz, E. A., 746
Holroyd, R. A., 759
Holmes, H. F., 573

Jaster, W., 518
Johannesen, R. B., 660

Johansson, H., 713
Johnson, G. R. A., 765
Johnson, I., 506
Jones, J. B., 646
Joyner, T. B., 703

Kebarle, P., 742
Kenney, D. J., 410
Klein, R., 616
Knobler, C. M., 676
Krause, R. F., Jr., 475
Krumpelt, M., 506

Labhart, H., 752
Lichtin, N. N., 526
LoSurdo, A., 751

MacIntyre, F., 589
Mackey, L. D., 733
Marshall, W. L., 684
Martin, W. J., 738
Matsushita, S., 458
Mazac, C. J., 749
McGee, H. A., Jr., 738
McPherson, W. G., 532
Meany, J. E., 655
Meyers, E. A., 532
Meyers, R. V., 389
Michiels, C. L., 410
Micić, O. I., 511
Mościński, J., 441
Mosher, W. A., 622
Muller, N., 583
Murty, H. N., 746
Mylonakis, S. G., 754

Nakata, T., 458
Nelson, J. A., 643
Nelson, R. F., 740
Nenadović, M. T., 511

O'Connell, J. P., 632
Ottolenghi, M., 593

Perumareddi, J. R., 414
Petrakis, L., 546
Phillips, L. F., 743
Pocker, Y., 655
Porter, D. M., 650
Poston, T. M., 638
Prausnitz, J. M., 632

Quist, A. S., 684

Rabani, J., 593
Ragle, J. L., 556
Rasmussen, O. L., 626
Redpath, J. L., 765
Rice, O. K., 542
Rizzo, F. E., 485
Rodde, A. F., Jr., 756
Rodgers, M. A. J., 758
Rowland, F. S., 707, 763

Safrany, D. R., 518
Scheer, M. D., 616
Schneider, R. F., 761
Schrier, E. E., 733
Searles, S. K., 742
Secoy, C. H., 573

Sehested, K., 626
Seibles, L., 603
Seltzer, S., 754
Shida, T., 723
Simons, J. W., 749
Smith, J. V., 485
Snyder, L. R., 489
Song, P.-S., 536
Spencer, J. N., 464, 471
Stuckey, J. E., 573
Suart, S. R., 400
Suski, L., 441
Swift, H. E., 546
Szwarc, M., 494

Tang, Y.-N., 707
Taylor, G. W., 749
Templeton, D. H., 668
Templeton, L. K., 668
Ting, C. T., 763
Titani, Y., 526

Van Heuvelen, A., 481
Voigt, A. F., 464, 471
von Salis, G. A., 752

Ward, A. T., 744
Windsor, M. L., 676
Wirth, H. E., 751
Wu, E.-C., 542

Yeh, H., 556
Yorke, M. E., 556
Yosim, S. J., 762



NEW
WILEY
AND
INTERSCIENCE
BOOKS
IN
YOUR
FIELD

FOR MORE INFORMATION ABOUT
ANY OF THESE BOOKS ON
PHYSICAL CHEMISTRY,
WRITE TO:

JOHN WILEY & SONS, INC.
605 Third Avenue
New York, N. Y. 10016

INTERMOLECULAR FORCES

Edited by JOSEPH O. HIRSCHFELDER. Volume 12 in the Advances in Chemical Physics Series (*Interscience*). 1967 446 pages \$22.50

CHEMISTRY OF DISSOCIATED WATER VAPOR AND RELATED SYSTEMS

By M. VENUGOPALAN and R. A. JONES. Monographs on Chemistry, Physical Chemistry Section (*Interscience*). 1968 463 pages \$19.50

PERSPECTIVES IN STRUCTURAL CHEMISTRY

Volume 1

Edited by J. D. DUNITZ and J. A. IBERS. An *Interscience* book. 1967 199 pages \$9.95

MACROMOLECULAR REVIEWS,

Volume 2

Edited by A. PETERLIN, M. GOODMAN, S. OKAMURA, B. H. ZIMM, and H. F. MARK. An *Interscience* Book. 1967 295 pages \$13.50

SPECTROSCOPIC CALCULATIONS FOR A MULTIELECTRON ION

By H. H. THEISSING and P. J. CAPLAN. An *Interscience* book. 1966 209 pages \$10.00

MÖSSBAUER EFFECT DATA INDEX, 1958-1965

Compiled by A. H. MUIR Jr., K. J. ANDO, and H. M. COOGAN. An *Interscience* book. 1966 351 pages \$9.00

THE FORMATION AND PROPERTIES OF PRECIPITATES

By ALAN G. WALTON. Volume 23 in the Chemical Analysis Series (*Interscience*). 1967 232 pages \$11.00

INTERNAL REFLECTION SPECTROSCOPY

By N. J. HARRICK. An *Interscience* book. 1967 327 pages \$16.50

PROGRESS IN PHYSICAL ORGANIC CHEMISTRY

Edited by ANDREW STREITWIESER Jr. and R. W. TAFT. *Interscience* books. Volume 4: 1967 303 pages \$15.50. Volume 5: 1967 358 pages \$16.00

ADVANCES IN ELECTROCHEMISTRY AND ELECTROCHEMICAL ENGINEERING

Edited by PAUL DELAHAY and CHARLES W. TOBIAS. *Interscience* books. Volume 5: 1967 325 pages \$14.50. Volume 6: 1967 481 pages \$19.00

RADICAL IONS

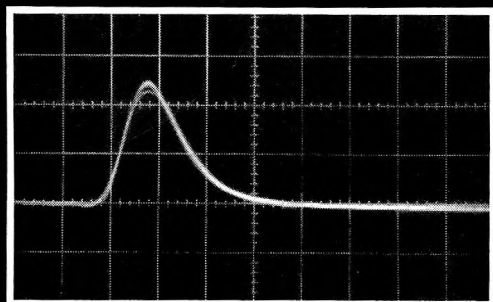
Edited by E. T. KAISER and LARRY J. KEVAN. Reactive Intermediate Series (*Interscience*). 1968 *In press* \$30.00

THE JOURNAL OF PHYSICAL CHEMISTRY

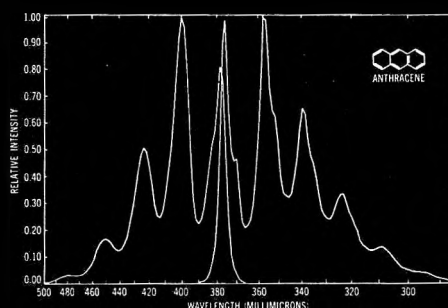
Volume 72, Number 3 March 1968

Isopiestic Measurements of the Osmotic and Activity Coefficients for the Systems $\text{HClO}_4\text{--LiClO}_4\text{--H}_2\text{O}$, $\text{HClO}_4\text{--NaClO}_4\text{--H}_2\text{O}$, and $\text{LiClO}_4\text{--NaClO}_4\text{--H}_2\text{O}$	R. M. Rush and J. S. Johnson	767
Photodecomposition of Aqueous Solutions of Barium Azide	V. R. Pai Verneker and M. Blais	774
Study of the Explosive Behavior of Barium Azide	V. R. Pai Verneker and L. Avrami	778
Reductions by Monovalent Zinc, Cadmium, and Nickel Cations	D. Meyerstein and W. A. Mulac	784
Calorimetric Determination of the Heat of the Sodium-Lithium Ion-Exchange Reaction in Anhydrous Methanol	A. Schwarz	789
A Comparison of Quinine Bisulfate and 9,10-Diphenylanthracene as Fluorescence Standards	R. Rusakowicz and A. C. Testa	793
Ion-Solvent Interaction. VI. A Thermodynamic Approach to Preferential Solvation in Mixed Solvents	J. Padova	796
Calculation of Fractionation Factors for Carbon and Oxygen Isotopic Exchange in the System Calcite-Carbon Dioxide-Water	Y. Bottinga	800
Reactions of the Primary Reducing Species in the Radiolysis of Liquid 2-Propanol	J. C. Russell and G. R. Freeman	808
The Yields of the Primary Reducing Species in the Radiolysis of Liquid Ethanol	J. C. Russell and G. R. Freeman	816
Proton Magnetic Resonance Studies of Mixed Aluminum Alkyls. I. Aluminum Trialkyls	Osamu Yamamoto and Kikuko Hayamizu	822
Dilute Solution Properties of Styrene-Methyl Methacrylate Random Copolymers	Tadao Kotaka, Yoji Murakami, and Hiroshi Inagaki	829
Diffuse Double Layer of Weak Electrolytes with Field Dissociation	Gilles G. Susbielles and Paul Delahay	841
The Effect of Hydrogen Bonding on the Kinetics of the Urethane Reaction	Adolf E. Oberth and Rolf S. Bruenner	845
Thermodynamic Data from Fluorescence Spectra. II. Hydrophobic Bond Formation in Binary Complexes	Donald K. Kunimitsu, A. Young Woody, Evelyn R. Stimson, and Harold A. Scheraga	856
The Electrical Conductivity of 0.10 <i>M</i> Potassium Chloride Water-Alcohol Solutions under Hydrostatic Pressure	R. A. Horne, D. S. Johnson, and R. P. Young	866
The Rate of Oxidation of Nitrite Ions in Dilute Solutions of Sodium Nitrite in Molten Lithium Perchlorate	David W. James	876
Reactions of the Hydrated Electron in Alkaline Solution	Nathan Klein, Conrad N. Trumbore, James E. Fanning, Jr., and John W. Warner	880
Implications and Use of Spectral Shifts in Polymerization Studies of Metal Ions	Jack I. Morrow and Joel Levy	885
Theoretical Relations among Rate Constants, Barriers, and Brønsted Slopes of Chemical Reactions	R. A. Marcus	891
The Effect of Solutes and Temperature on the Structure of Water	O. D. Bonner and G. B. Woolsey	899
Relationship between the DTA Peak and the Maximum Reaction Rate.	K. Akita and M. Kase	906
SCFMO Calculations of Heteroatomic Systems with the Variable- β Approximation. III. Electronic Spectra of Anions of Hydroxyaromatics	Kichisuke Nishimoto and Leslie S. Forster	914

Investigating molecular structure?



+



= Theory
of
quenching
dynamics

Dr. George Hammond of the chemistry department at California Institute of Technology obtained complete fluorometric data for a fluorescence quenching theory by adding the τ of anthracene in the presence of quenchers to the invariance of the emission spectrum.

Now you can get complete fluorometric data by adding decay time to spectral information.

The TRW Decay Time Fluorometer gives you accurate decay time from 10 milliseconds down to 1.7 nanosecond. Use it if your work is determining the structure of proteins, amino acids and

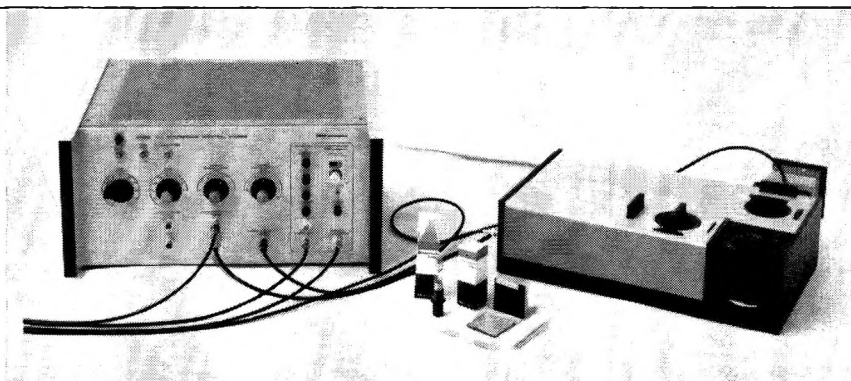
other fluorescing compounds. Use it if you are studying fluorescing crystals, or the basic structure of molecules, or fluorescence quenching; or if you are measuring molecular volume.

Absorption and interference filters used with a high aperture optical system permit greater sensitivity in the TRW Decay Time Fluorometer than has previously been achieved by other methods.

Decay time range: From 10 milliseconds to 1.7 nanosecond

Sensitivity: 5.0 P/B quinine sulfate

Multiple decay: Resolve single components of multiple exponential decays



Write or call us for more details on this new fluorometry technique and equipment. Dept. JPC-68

TRWINSTRUMENTS

Main Office: 139 Illinois Street, El Segundo, California 90245 • (213) 535-0854

East Coast: 580 Mineola Avenue, Carle Place, New York 11514 • (516) 248-6377

TRW®

A Potentiometric Study of Acid-Base Equilibria in 1,1,3,3-Tetramethylguanidine	Joseph A. Caruso and Alexander I. Popov	918
The Solid-State Radiation Chemistry of Selected Transition Metal Chelates of Glycine and Alanine	W. Carl Gottschall, Jr., and Bert M. Tolbert	922
Properties of Organic-Water Mixtures. VI. Activity Coefficients of Sodium Chloride in Saturated Water-Pyridine Mixtures at 5 and 25°	Richard J. Raridon, Willis H. Baldwin, and Kurt A. Kraus	925
Detailed Studies of a One-Electron, Two-Photon Ionization in a Rigid Organic Solution at 77°K	K. D. Cadogan and A. C. Albrecht	929
Nuclear Magnetic Resonance and Ultraviolet Spectroscopy of Phenylmagnesium Bromide, Phenyllithium, and Pyridine	Gideon Fraenkel, David G. Adams, and Ronald R. Dean	944
Nuclear Magnetic Resonance and Ultraviolet Spectroscopy of Substituted Aromatic Organometallic Compounds of Lithium, Magnesium, and Calcium	Gideon Fraenkel, Shlomo Dayagi, and Sadao Kobayashi	953
Vibrational Intensities. XVIII. Infrared Band Shapes for Some Liquid Methyl Iodide Bands	C. E. Favelukes, A. A. Clifford, and Bryce Crawford, Jr.	962
Vapor-Phase Charge-Transfer Complexes. II. The $2I_2 \rightleftharpoons I_4$ System	Milton Tamres, Walter K. Duerksen, and John M. Goodenow	966
Correlation of Molecular Structure with Fluorescence Spectra in Rare Earth Chelates. I. Internal Stark Splitting in Tetraethylammonium Tetrakis(dibenzoylmethido)europate(III)	Sven Bjorklund, Nicolae Filipescu, N. McAvoy, and J. Degnan	970
Electrical Phenomena Associated with the Transport of Ions and Ion Pairs in Liquid Ion-Exchange Membranes. III. Experimental Observations in a Model System	J. L. Walker, Jr., G. Eisenman, and J. P. Sandblom	973
Nuclear Magnetic Resonance Analyses and Parameters for Some Monohalosubstituted Fluorobenzenes	J. E. Loemker, J. M. Read, and J. H. Goldstein	991
Photochromism: Spectroscopy and Photochemistry of Pyran and Thiopyran Derivatives	Ralph S. Becker and Jaroslav Kolc	997
Nuclear Magnetic Resonance Studies of Proton-Exchange Kinetics of N-Methylacetamide and N-Acetylglycine N-Methylamide	James E. Bundschuh and Norman C. Li	1001
Dipole Moments of 1-Alkylpyrazoles in Nonpolar and Polar Solvents	Joseph D. Broadus and John D. Vaughan	1005
Critical Bond Length in Radical Combination and Unimolecular Dissociation Reactions	E. Tschuikow-Roux	1009
Radical Yield in γ -Irradiated Aqueous Alkaline Solutions of Fremy's Salt	N. Th. Rakintzis and Gabriel Stein	1011
Study of Dielectric Relaxation in Benzene Solutions of Some Hydroxy- and Methoxybenzaldehydes	J. P. Shukla, S. I. Ahmad, D. D. Shukla, and M. C. Saxena	1013
The Activity of Lithium in Lithium Amalgams	David R. Cogley and James N. Butler	1017
Dissociation of Lithium and Sodium Salts in Ethereal Solvents	D. Nicholls, C. Sutphen, and M. Szwarc	1021
Gas-Phase Radiolysis of Benzene	Robert R. Hentz and Stefan J. Rząd	1027
Tellurium Vapor Pressure and Optical Density at 370-615°	R. F. Brebrick	1032
The Conductance of the Trialkylsulfonium Iodides in Water, Methanol, and Acetonitrile at 10 and 25°	D. Fennell Evans and T. L. Broadwater	1037
High-Temperature Infrared Spectroscopy of Pyridine Adsorbed on Faujasites	P. E. Eberly, Jr.	1042
Measurement of Activities in Gallium-Indium Liquid Alloys	G. J. Macur, R. K. Edwards, and P. G. Wahlbeck	1047
Isotopic Exchange of Oxygen on Platinum Powder	Y. L. Sandler and D. D. Durigon	1051
Pressure Dependence of Dielectric Constant and Density of Liquids	James F. Skinner, E. L. Cussler, and Raymond M. Fuoss	1057
Thermodynamics of Aqueous Mixtures of Electrolytes and Nonelectrolytes. IV. Transfer of Hydrochloric Acid from Water to Aqueous Acetic Acid at 25°	J. H. Stern and J. Nobileone	1064
Physicochemical Properties of Sulfolane	Mario Della Monica, Liliana Jannelli, and Ugo Lamanna	1068

NOTES

On the Reaction of D_2^+ with Cyclohexane	Jean H. Futrell, Fred P. Abramson, and Thomas O. Tiernan	1071
An Infrared Study of Hydroxyl Groups on Sepiolite	F. R. Cannings	1072

Mass spectrometry on a mass scale proves RMU-6 performance

The Morgan-Schaffer Corporation, Montreal, a Canadian service laboratory doing mass spectrometry on a pay-as-you-go basis, is yielding some unusual insights into the capabilities of the Hitachi Perkin-Elmer RMU-6.

In a recent letter to Perkin-Elmer, Dr. James E. Morgan wrote, "The reliability of our RMU-6D enables us to give each customer's problem the individual attention it deserves. Our instrument is probably being used harder and more efficiently than in the usual laboratory. During 18 months operation, our customers have not experienced any disruption in service, which is probably the best testimonial that could be given to an instrument as temperamental as a mass spectrometer.

"Our active accounts are fairly evenly split between universities and industry. Approximately 70% of these accounts are distributed uniformly across the U.S., with

most of the remainder in Canada. (We do have some customers in Ireland, Israel, Italy and Venezuela.)

"Most of our spectra (~80%) are produced for organic structural elucidation. The remaining 20% are largely isotopic analysis, quality control and quantitative gas analysis.

"It is difficult to classify all the types of compounds we have examined. The majority, however, fall into the following classifications:

- ☐ long chain fatty acid esters and alcohols;
- ☐ long chain aliphatic hydrocarbons (e.g. C_{30} - C_{40} paraffins from insect cuticle waxes);
- ☐ organo-metallics (porphyrins, ferrocenes, selenium, silicon and boron compounds);
- ☐ amino acids, peptides, etc. (the highest M.W. compound for which we have obtained a complete spectrum was a cyclic

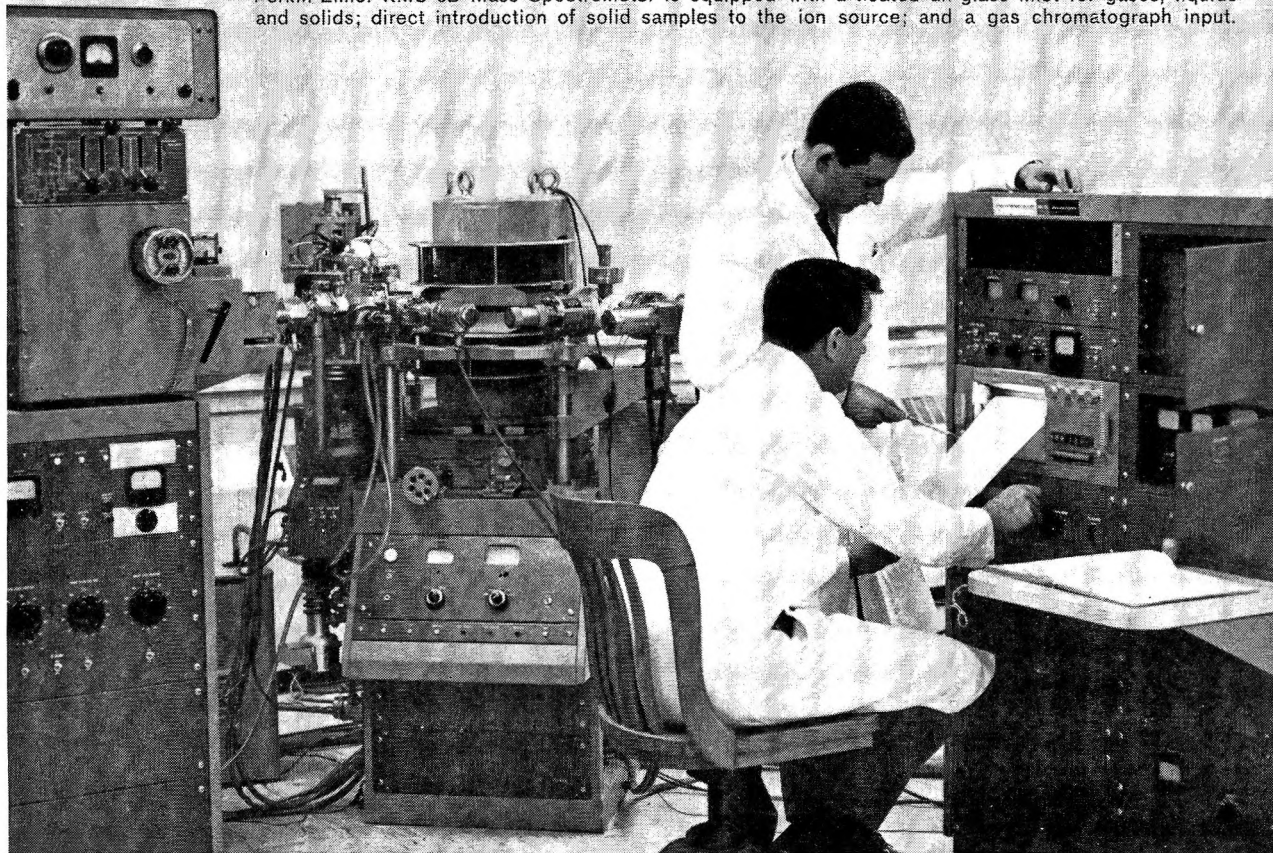
depsipeptide of M.W. 1,110 amu);

- ☐ sugar derivatives—nucleosides, glucosides, ribosides, etc.;
- ☐ synthetic and natural alkaloids, steroids and hormones;
- ☐ highly condensed, high M.P. (>300°C) aromatic hydrocarbons;
- ☐ chlorinated insecticides, terpenes and isotopically labelled compounds."

If you are dependent upon reliable mass spectrometry and want more information on the RMU-6 series instruments, the High Resolution Double-Focusing System, the Digital Data Acquisition System, the GC/Helium Separator System, High Sensitivity Detector and accessories, write to Instrument Division, Perkin-Elmer Corporation, 808 Main Avenue, Norwalk, Conn. 06852.

PERKIN-ELMER

Drs. James E. Morgan and Robert Schaffer are shown in their Montreal laboratory. Their Hitachi Perkin-Elmer RMU-6D Mass Spectrometer is equipped with a heated all-glass inlet for gases, liquids and solids; direct introduction of solid samples to the ion source; and a gas chromatograph input.

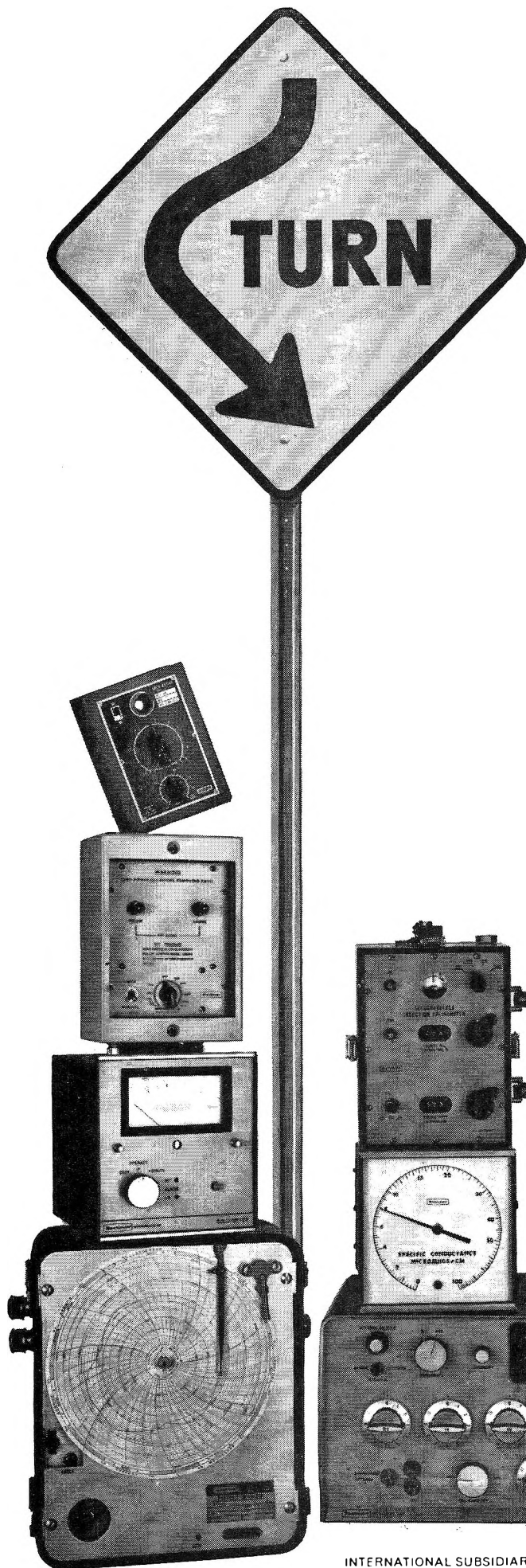


This instrument is instantly available to you under Perkin-Elmer's low cost lease plan.

Aliphatic Semidiones. VIII. Hyperfine Splitting by Oxygen and Carbon Atoms in Semidiones	Glen A. Russell and Graham R. Underwood	1074
The Argon-Sensitized Radiolysis of Methane and Ethane in the Liquid Phase	Norman V. Klassen	1076
The Action of Lead Monoxide as an Inorganic Photosensitizer	W. C. Tennant	1078

COMMUNICATIONS TO THE EDITOR

The Reaction of Nitrogen Atoms with N_2O_5	G. Liuti, S. Dondes, and P. Harteck	1081
Homogeneous Chemical Kinetics with the Rotating Disk Electrode. The ECE Mechanism	Stewart Karp	1082
Evidence for the Formation of a Surface Complex as the Rate-Determining Step in the Polarographic Reduction of Certain Nickel(II)-Organic Amine Complexes. Effect of the Structure of the Electrical Double Layer	Harry B. Mark, Jr., Lowell R. McCoy, Emilia Kirowa-Eisner, and Hubert C. MacDonald, Jr.	1083



to the people who know most about conductivity

Your conductivity measurements take a turn for the better when you use instruments designed and manufactured by specialists with more than three decades of experience.

Whatever your needs — an electrodeless system for highly corrosive fluids — a direct reading meter with output for remote recording — a wide range meter with moderate accuracy — or a general purpose instrument — chances are we can supply the unit that is exactly right for the job. For prompt attention to your conductivity measurement needs, contact your local Beckman Sales Office — or write direct.

Beckman®

INSTRUMENTS, INC.

CEDAR GROVE OPERATIONS

89 COMMERCE ROAD
CEDAR GROVE, NEW JERSEY • 07009

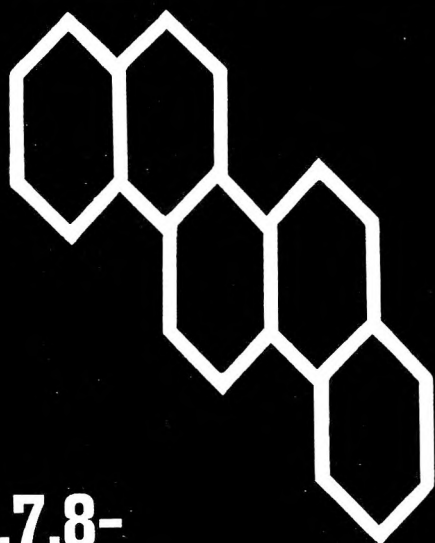
INTERNATIONAL SUBSIDIARIES: Geneva; Munich; Glenrothes, Scotland; Tokyo; Paris; Capetown; London; Mexico City.

THE JOURNAL OF PHYSICAL CHEMISTRY

Volume 72, Number 4 April 1968

Pyrex Membrane Potential in Binary Nitrate Melts	A. G. Keenan, K. Notz, and F. L. Wilcox	1085
An X-Ray Study of Formamide and Solutions of Potassium Iodide in Formamide	R. J. DeSando and G. H. Brown	1088
A Sessile Drop Study of Liquid-Solid Adhesion for the System Indium(l)-Aluminum Using Ultrahigh Vacuum Techniques	R. G. Aldrich and D. V. Keller, Jr.	1092
Mass Spectrometric Studies at High Temperatures. XXII. The Stabilities of Tantalum Pentafluoride and Tantalum Oxytrifluoride	K. F. Zmbov and J. L. Margrave	1099
Vaporization Studies on Arsenic	C. C. Herrick and Roy C. Feber	1102
Spectroscopy of Alkali Metals in Fused Alkali Metal Salts	J. F. Rounsaville and J. J. Lagowski	1111
Dielectric Properties of Polycrystalline Barium Trititanate and Barium Tetratitanate	G. W. Marks and C. E. Antoniak	1117
Properties of Ethylene-Methacrylic Acid Copolymers and Their Sodium Salts: Infrared Studies	W. J. MacKnight, L. W. McKenna, B. E. Read, and R. S. Stein	1122
A Spectroscopic Study of Binuclear Copper Complexes in Aqueous Poly(methacrylic acid) Solutions	J. C. Leyte, L. H. Zuiderweg, and M. van Reisen	1127
Acid-Base Reactions in Concentrated Aqueous Quaternary Ammonium Salt Solutions. III. Dicarboxylic Acids	Joseph Steigman, Richard De Iasi, Harvey Lilienfeld, and Donald Sussman	1132
Volume Changes on Mixing Solutions of Alkali Halides and Symmetrical Tetraalkylammonium Halides. II. Effects of Deuterium Oxide and Temperature	Wen-Yang Wen and Kenichi Nara	1137
The Effect of Impurities on the Spin-Lattice Relaxation of Ammonium Chloride	D. E. Woessner and B. S. Snowden, Jr.	1139
Internal Reflectance Spectroscopy at Optically Transparent Electrodes	V. S. Srinivasan and T. Kuwana	1144
Electrolytic Hydrogen Evolution Reaction on Aluminum in Acidic Solutions	A. K. Vijh	1148
Structure and Properties of Poly- γ -benzyl-L-glutamate Cast from Dimethylformamide	A. J. McKinnon and A. V. Tobolsky	1157
The Vapor Pressure and Melting Points of Xenon Difluoride and Xenon Tetrafluoride	Felix Schreiner, Geraldine N. McDonald, and Cedric L. Chernick	1162
Radiolytic Formation and Decomposition of Ozone	John T. Sears and James W. Sutherland	1166
The Surface of a Carbon with Sorbed Oxygen on Pyrolysis.	Marcellus T. Coltharp and Norman Hackerman	1171
Spectroscopic Studies of Isotopically Substituted 2-Pyridones.	Robert A. Coburn and Gerald O. Dudek	1177
Very Low Pressure Pyrolysis. III. <i>t</i> -Butyl Hydroperoxide in Fused Silica and Stainless Steel Reactors	S. W. Benson and G. N. Spokes	1182
Mathematical Analysis of Dropping Mercury Electrode. I. Solution of Diffusion Equation for Variable Mercury Flow Rate	J. L. Duda and J. S. Vrentas	1187
Mathematical Analysis of Dropping Mercury Electrode. II. Prediction of Time Dependence of Mercury Flow Rate	J. L. Duda and J. S. Vrentas	1193
Properties of Organic-Water Mixtures. VII. Self-Diffusion Coefficients of Na ⁺ in Ethylene Glycol-Water and Glycerol-Water Mixtures at 25°	Arthur E. Marcinkowsky, Harold O. Phillips, and Kurt A. Kraus	1201

Would you believe



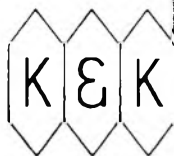
**1,2,7,8-
dibenzphenanthrene**

**is just 1 of 30,000
rare chemicals
available for
immediate delivery?**

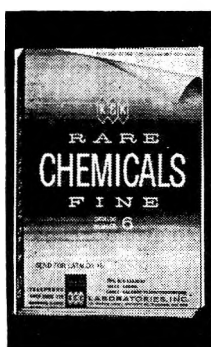
Almost any rare chemical, in any quantity, on hand and available for immediate delivery. K & K probably has the largest in stock supply of chemicals available anywhere . . . and those hard to find chemicals are our specialty.

Orders received are usually shipped in 24 hours or less and that means 5 mg or 500 lbs. Check K & K, a dependable source for any chemical you need.

Our 224 page catalogue available, free — just write for it.



LABORATORIES, INC.
DEPT. P-468
121 Express Street, Engineers Hill
Plainview, New York 11083



LABORATORIES, INC.
DEPT. P-468
121 Express Street, Engineers Hill
Plainview, New York 11803
Gentlemen:
Please send me a copy of your latest
catalogue.

NAME _____

STREET ADDRESS _____

CITY & STATE _____

ZIP CODE _____

**THEY'RE NEW—
THEY'RE IMPORTANT—
THEY'RE FROM MCGRAW-HILL**

BONDING THEORY

By DONALD J. ROYER, Georgia Institute of Technology. *McGraw-Hill Series in Undergraduate Chemistry*. 259 pages; \$10.75

Providing a general introduction to bonding theory and quantum chemistry at the intermediate level, this book covers those essentials of the subject which the average practicing chemist should know about bonding theory. It is designed for the non-specialist in theoretical chemistry and employs an approach that is basically informal and nonrigorous.

QUANTUM CHEMISTRY

By F. L. PILAR, University of New Hampshire. 736 pages; \$15.50

This book offers a useful introduction to those theoretical aspects of quantum theory needed to understand and appreciate the formalism of the relatively recent literature and research work in the area of the electronic structure of atoms and molecules.

EXPERIMENTS IN PHYSICAL CHEMISTRY, 2nd Edition

By DAVID P. SHOEMAKER and CARL W. GARLAND, both of Massachusetts Institute of Technology. 490 pages; \$9.95

A junior-senior level lab text for the standard physical chemistry laboratory course, providing 47 experiments, each accompanied by a careful theoretical description. The approach is concerned with testing and illustrating theoretical principles and developing a research orientation.

QUANTUM THEORY OF MAGNETIC RESONANCE PARAMETERS

By JASPER D. MEMORY, North Carolina State University. *McGraw-Hill Series in Advanced Chemistry*. Available Spring, 1968.

With unique coverage, this book provides an introduction to the application of quantum chemistry methods in the calculation of nuclear magnetic resonance shielding parameters, spin-spin coupling constants, and electron spin resonance hyperfine coupling constants.

THE PRINCIPLES OF CURRENT METHODS FOR THE STUDY OF ELECTROCHEMICAL REACTIONS

By BORIS B. DAMASKIN, Moscow State University; translated by GLEB MAMANTOV, University of Tennessee. 128 pages; \$4.95

This book deals with the principles of relaxation methods employed to study the kinetics of fast electrode processes.

Write today for your examination copies



McGraw-Hill Book Company
330 West 42nd Street
New York, New York 10036

The Binding of Cholate and Glycocholate Anions by Anion-Exchange Resins	James Blanchard and J. Graham Nairn	1204
Computer Evaluation of Entropy Titration Data. Calorimetric Determination of Log β_1 , ΔH° , and ΔS° Values for the Silver(I)- and Copper(II)-Pyridine Systems	Reed M. Izatt, Delbert Eatough, Richard L. Snow, and James J. Christensen	1208
Solubilization Behavior of Sodium Dodecylpolyoxyethylene Sulfates in Relation to Their Polyoxyethylene Chain Lengths	Fumikatsu Tokiwa	1214
The A_2B_2 Aromatic Proton Nuclear Magnetic Resonance Spectra of <i>para</i> -Substituted Anilines, Diphenylamines, and Triphenylamines	Robert D. Allendoerfer, Griffith Smith, and Robert I. Walter	1217
Varietal Differences in Gelatin, Egg Albumin, and Casein in Relation to Sorption-Desorption Hysteresis with Water	K. Subba Rao and Bhagwan Das	1223
The Reduced Equation of State of Argon and Xenon	Eugene M. Holleran	1230
Vapor Pressures of the Isotopic Waters and Ices	W. Alexander Van Hook	1234
An Electron Paramagnetic Resonance Study of the Bonding in Copper Complexes	Virginia Chapin Swett and Emily Pitcher Dudek	1244
Mechanism of Gaseous Siloxane Reaction with Silica. I	William Hertl	1248
Current Dependence of Water Transport in Cation-Exchange Membranes	N. Lakshminarayanaiah and V. Subrahmanyam	1253
Metachromasy of a Thiocarbocyanine Dye in Aqueous Solution: The Formation of Dimers and Trimers	J. F. Padday	1259
Studies of Concentrated Polymer Solutions by the Fluorescence Polarization Method. II. Polyacrylamide in Water	T. Yanagida, A. Teramoto, and H. Fujita	1265
Enthalpy and Entropy Increments above 298°K and a Σ -Plot Treatment of Vaporization Data for Niobium Pentachloride	F. J. Keneshea, D. Cubicciotti, G. Withers, and H. Eding	1272
Diffuse Transition and Melting in Fluorite and Anti-Fluorite Type of Compounds: Heat Content of Potassium Sulfide from 298 to 1260°K	A. S. Dworkin and M. A. Bredig	1277
Electronic and Electron Spin Resonance Spectra of the Perfluoro-2,1,3-benzoselenadiazole Anion Radical	J. Fajer, B. H. J. Bielski, and R. H. Felton	1281
A Floating Spherical Gaussian Orbital Model of Molecular Structure. III. First-Row Atom Hydrides	Arthur A. Frost	1289
Thermodynamics of the λ Transition in Sodium Nitrate	William Klement, Jr.	1294
Studies of Chloroform as Hydrogen Donor to Some Organophosphorus Compounds and Long-Chain Tertiary Alkylamines	Sanji Nishimura, Charles H. Ke, and Norman C. Li	1297
The Kinetics of the Rearrangement of 2',4'-Dinitro-2-aminodiphenyl Ether in Methyl Alcohol-Carbon Tetrachloride Solutions	Frances Wright Balfour and Thomas F. Fagley	1300
Adsorption and Oxidation of Carbon Monoxide on Platinized Platinum Electrodes	M. W. Breiter	1305
The Brønsted α and Isotope Effects for Vinyl Ether Hydrolysis	Maurice M. Kreevoy and Robert Eliason	1313
Electron Spin Resonance Line Width of the Hexaaquochromic Ion as a Criterion of Outer-Sphere Coordination Interactions.	K. M. Sancier	1317
The Study of the Hindered Rotation of Methyl Groups Using Nuclear Magnetic Resonance	Joseph H. Noggle	1324
Phase Diagrams of the Bismuth Trihalides at High Pressure	A. J. Darnell and W. A. McCollum	1327
Molecular Addition Compounds of Tin(IV) Chloride with Ethyl Esters of Dicarboxylic Acids in Benzene and Methylene Chloride	Andrzej Kemula and Reynold T. Iwamoto	1334
Chlorine Nuclear Quadrupole Resonance Study of Some Molecular Adducts of Phosphorus Oxychloride	Max T. Rogers and James A. Ryan	1340
Excess Properties of Some Aromatic-Alicyclic Systems. III. Analysis of H^E and V^E Data in Terms of the Theory of Flory	G. C. Benson and Jaswant Singh	1345
Solution Kinetics <i>via</i> Fluorescence Quenching—Transient and Solvent Effects	J. Q. Umberger	1350
Reduction Potentials of Complex Ions. The Tris(pyridine-2-aldoxime)iron(III)-Tris- (pyridine-2-aldoxime)iron(II) System	George I. H. Hanania, Dennis H. Irvine, and Fahd R. Shurayh	1355
Mean Activity Coefficient of Polyelectrolytes. VIII. Osmotic and Activity Coefficients of Polystyrenesulfonates of Various Gegenions	Norio Ise and Tsuneo Okubo	1361
Mean Activity Coefficient of Polyelectrolytes. IX. Activity Coefficients of Polyethylenesulfonates of Various Gegenions	Norio Ise and Kiyotsugu Asai	1366

1967-68 LABORATORY GUIDE

to Instruments, Equipment and Chemicals

1 Laboratory Supply Houses 11 LG

2 Product Classifications 25 LG


3 Instruments & Equipment 51 LG

4 Chemicals & Services 243 LG

5 Trade Names 313 LG

6 Books 355 LG

7 Company Directory 383 LG

 an American Chemical Society Publication

The beginning of a requisition

This is where laboratory chemists, life scientists, physicists and engineers turn first to find who sells what, to inquire about products, to locate sales offices, to consult vendors, to create lists of bidders, to place orders.

The definitive ACS LABORATORY GUIDE is issued annually in July to subscribers to the ACS Research Journals.

Mean Activity Coefficient of Polyelectrolytes. X. Activity Coefficients of Polyphosphates of Various Gegenions	Norio Ise and Tsuneo Okubo	1370
Metal-Ammonia Solutions. III. Spectroscopy of Quaternary Ammonium Radicals	R. K. Quinn and J. J. Lagowski	1374
A Temperature-Jump Study of the Kinetics of the Formation of the Monosulfato Complex of Iron(III)	Francesco Paolo Cavasino	1378

NOTES

Chemistry of Crystalline Aluminosilicates. IV. Factors Affecting the Formation of Zeolites X and B	George T. Kerr	1385
Aliphatic Semidiones. IX. Hyperfine Splittings by Nitrogen Atoms Attached to a Paramagnetic Center	Glen A. Russell, John McDonnell, and Charles Myers	1386
On the Kinetics of Color Development in the Landolt ("Iodine Clock") Reaction	John A. Church and Sanford A. Dreskin	1387
Complete Proton and Naturally Occurring ^{33}S Hyperfine Splittings in the Thianthrene Cation Radical	H. J. Shine and Paul D. Sullivan	1390
Small Tunneling Effect in the Electron Paramagnetic Resonance Spectrum of Cu^{2+} -CaO at 1.2°K	R. E. Coffman, D. L. Lyle, and D. R. Mattison	1392
The Radiolysis of Liquid Nitrous Oxide	M. G. Robinson and G. R. Freeman	1394
Influence of the Solvent Structure on Ion-Pair Association	Filippo Conti, Pietro Delogu, and Gianfranco Pistoia	1396

COMMUNICATIONS TO THE EDITOR

Estimation of Bond Dissociation Energies of N-H Bonds by Correlation with HT Yields from Recoil Tritium Abstraction	T. Tominaga and F. S. Rowland	1399
X-Ray Evidence for Residual Water in Calcined Divalent Cation Faujasite-Type Zeolites	D. H. Olson	1400
Production of $\text{N}_2(\text{A}^3\Sigma)$ and $\text{CO}(\text{a}^3\pi)$ by $\text{Hg}(\text{I}^1\text{P}_1)$ Photosensitization; Pressure Dependence of 2537-Å Emission	A. Granzow, M. Z. Hoffman, N. N. Lichtin, and S. K. Wason	1402
Reactions of Tetranitromethane with Hydroxide Ion and Nitrite Ion	Donald J. Glover	1402
Homogeneous Periodic Reactions	D. H. Shaw and H. O. Pritchard	1403

AUTHOR INDEX

- Aldrich, R. G., 1092
 Allendoerfer, R. D., 1217
 Antoniak, C. E., 1117
 Asai, K., 1366
 Balfour, F. W., 1300
 Benson, G. C., 1345
 Benson, S. W., 1182
 Bielski, B. H. J., 1281
 Blanchard, J., 1204
 Bredig, M. A., 1277
 Breiter, M. W., 1305
 Brown, G. H., 1088
 Cavasino, F. P., 1378
 Chernick, C. L., 1162
 Christensen, J. J., 1208
 Church, J. A., 1387
 Coburn, R. A., 1177
 Coffman, R. E., 1392
 Coltharp, M. T., 1171
 Conti, F., 1396
 Cubicciotti, D., 1272
 Darnell, A. J., 1327
 Das, B., 1223
 De Iasi, R., 1132
 Delogu, P., 1396
 DeSando, R. J., 1088
 Dreskin, S. A., 1387
 Duda, J. L., 1187, 1193
 Dudek, E. P., 1244
 Dudek, G. O., 1177
 Dworkin, A. S., 1277
 Eatough, D., 1208
 Eding, H., 1272
 Eliason, R., 1313
 Fagley, T. F., 1300
 Fajer, J., 1281
 Feber, R. C., 1102
 Felton, R. H., 1281
 Freeman, G. R., 1394
 Frost, A. A., 1289
 Fujita, H., 1265
 Glover, D. J., 1402
 Granzow, A., 1402
 Hackerman, N., 1171
 Hanania, G. I. H., 1355
 Herrick, C. C., 1102
 Hertl, W., 1248
 Hoffman, M. Z., 1402
 Holleran, E. M., 1230
 Irvine, D. H., 1355
 Ise, N., 1361, 1366, 1370
 Iwamoto, R. T., 1334
 Izatt, R. M., 1208
 Ke, C. H., 1297
 Keenan, A. G., 1085
 Keller, D. V., Jr., 1092
 Kemula, A., 1334
 Keneshea, F. J., 1272
 Kerr, G. T., 1385
 Klement, W., Jr., 1294
 Kraus, K. A., 1201
 Kreevoy, M. M., 1313
 Kuwana, T., 1144
 Lagowski, J. J., 1111, 1374
 Lakshminarayanaiah, N., 1253
 Leyte, J. C., 1127
 Li, N. C., 1297
 Lichtin, N. N., 1402
 Lilenfeld, H., 1132
 Lyle, D. L., 1392
 MacKnight, W. J., 1122
 Marcinkowsky, A. E., 1201
 Margrave, J. L., 1099
 Marks, G. W., 1117
 Mattison, D. R., 1392
 McCollum, W. A., 1327
 McDonald, G. N., 1162
 McDonnell, J., 1386
 McKenna, L. W., 1122
 McKinnon, A. J., 1157
 Myers, C., 1386
 Nairn, J. G., 1204
 Nara, K., 1137
 Nishimura, S., 1297
 Noggle, J. H., 1324
 Notz, K., 1085
 Okubo, T., 1361, 1370
 Olson, D. H., 1400
 Padday, J. F., 1259
 Phillips, H. O., 1201
 Pistoia, G., 1396
 Pritchard, H. O., 1403
 Quinn, R. K., 1374
 Rao, K. S., 1223
 Read, B. E., 1122
 Robinson, M. G., 1394
 Rogers, M. T., 1340
 Rounsaville, J. F., 1111
 Rowland, F. S., 1399
 Russell, G. A., 1386
 Ryan, J. A., 1340
 Sancier, K. M., 1317
 Schreiner, F., 1162
 Sears, J. T., 1166
 Shaw, D. H., 1403
 Shine, H. J., 1390
 Shurayh, F. R., 1355
 Singh, J., 1345
 Smith, G., 1217
 Snow, R. L., 1208
 Snowden, B. S., Jr., 1139
 Spokes, G. N., 1182
 Srinivasan, V. S., 1144
 Steigman, J., 1132
 Stein, R. S., 1122
 Subrahmanyam, V., 1253
 Sullivan, P. D., 1390
 Sussman, D., 1132
 Sutherland, J. W., 1166
 Swett, V. C., 1244
 Teramoto, A., 1265
 Tobolsky, A. V., 1157
 Tokiwa, F., 1214
 Tominaga, T., 1399
 Umberger, J. Q., 1350
 Van Hook, W. A., 1234
 van Reisen, M., 1127
 Vijh, A. K., 1148
 Vrentas, J. S., 1187, 1193
 Walter, R. I., 1217
 Wason, S. K., 1402
 Wen, W.-Y., 1137
 Wilcox, F. L., 1085
 Withers, G., 1272
 Woessner, D. E., 1139
 Yanagida, T., 1265
 Zmbov, K. F., 1099
 Zuiderweg, L. H., 1127

THE JOURNAL OF PHYSICAL CHEMISTRY

Registered in U. S. Patent Office © Copyright, 1968, by the American Chemical Society

VOLUME 72, NUMBER 1 JANUARY 15, 1968

Reactions of Tritium Atoms Produced by Electron

Impact on T₂ with Solid Propene and Propane¹

by R. D. Shores and H. C. Moser

Department of Chemistry, Kansas State University, Manhattan, Kansas 66502 (Received August 15, 1967)

A beam of electrons of 30–50 eV energy was used to dissociate T₂ gas in a region adjacent to a surface of solid propene or propane at 77°K. The principal tritium-containing products from propene reactions were HT, propene, propane, 2,3-dimethylbutane, 2-methylpentane, *n*-hexane, and 4-methyl-1-pentene. The principal tritium-containing hydrocarbon products from propane reactions were methane, ethane, ethene, propane, and propene. The products are interpreted as having resulted from various reactions of hot and thermal T atoms. The T atoms are proposed to result from the decomposition of the ³Σ_u state of molecular T₂ yielding T atoms with energies of 2.2–5.2 eV.

Introduction

Theoretical considerations indicate that molecular hydrogen should be excited to the ³Σ_u state when bombarded with 8.8-eV electrons and should dissociate into two normal H atoms each with 2.2 eV kinetic energy.² Hydrogen atoms produced by bombardment with electrons of higher energy should also result primarily from dissociation of the ³Σ_u state.³ These atoms should have an energy spread from 2.2 to 5.2, with the most probable energy around 3.7 eV.²

Experimental work in 1927 by Glockler, Baxter, and Dalton⁴ and by Hughes and Skellett⁵ verified that bombardment of hydrogen with low-energy electrons produces H atoms by a direct dissociative process. Both groups of workers studied reactions of the hydrogen atoms that were produced by this technique and followed the progress of reaction by measuring the decrease in hydrogen pressure. The dissociative process began at 11.4–11.5 eV and increased rapidly with increasing electron energy. Dorsch and Kallmann⁶ verified the earlier reports. They reacted H atoms produced by electron bombardment with PbCl₂. The H atoms reduced the PbCl₂, and the metallic lead darkened the walls of the container.

In the present study, we have sought to obtain information for making a comparison between the chemical reactions of H atoms resulting from electron impact and reactions of both thermal and "hot" atoms produced by other processes.

Experimental Section

The reactant gases were CP grade propene (Matheson Co.), propene-*d*₆ (Volk Radiochemical Co.), and research grade propane (Phillips Petroleum Co.). All were used without further purification. Carrier-free tritium, obtained from Oak Ridge National Laboratory, was purified on introduction into the vacuum system by diffusion through a heated palladium thimble. The

(1) Taken in part from the Ph.D. Thesis of R. D. Shores, Kansas State University, Manhattan, Kan., 1966. Work performed under Contract AT(11-1)-584 with the U. S. Atomic Energy Commission.

(2) H. S. W. Massey and E. H. S. Burhop, "Electronic and Ionic Impact Phenomena," Oxford University Press, London, 1952, p 232.

(3) O. A. Schaeffer and J. M. Hastings, *J. Chem. Phys.*, **18**, 1048 (1950).

(4) G. Glockler, W. P. Baxter, and R. H. Dalton, *J. Am. Chem. Soc.*, **49**, 58 (1927).

(5) A. H. Hughes and A. M. Skellett, *Phys. Rev.*, **30**, 11 (1927).

(6) K. E. Dorsch and H. Kallmann, *Z. Physik*, **53**, 80 (1929).

HT content of the tritium was determined to be less than 6 mole %.

An electron gun-reaction vessel design similar to the one used by Hughes and Skellett⁵ was employed. The reaction vessel was a cylindrical glass tube 2.8 cm o.d. \times 15 cm. The electrons were emitted from a directly heated platinum ribbon coated with the oxides of barium and strontium which was suspended inside a glass tube (12 mm o.d.). The grid was attached to the end of the glass tube and consisted of a small copper plate (diam, 1 cm) with four 0.36-mm holes drilled in it and was placed 1 mm from the cathode. Thus the thermionic cathode was practically isolated from the remainder of the reaction vessel by the copper grid and the glass tube. The plate was a circular copper disk (diam, 1.6 cm) and was placed 9.2 cm below the grid. Both the grid and the plate were maintained at ground potential, and a negative potential was applied to the cathode. The electrons were collimated by means of an axial magnetic field of 200 gauss which was produced by a solenoid.

Since the energy of the bombarding electrons was usually above the ionization potential of molecular tritium, arrangement was made for collection of positive ions in the reaction system. The inside wall of the reaction vessel was silvered, and a coil of tungsten wire was positioned 1 mm from the silvered surface. During a reaction, the coil of wire was maintained at ground potential (the same potential as the plate) and the silvered surface upon which the hydrocarbon reactant was deposited was maintained at a potential of +20 v.

Hydrocarbon reactant (7–30 μ moles) was introduced at low pressure (0.01 torr) and frozen on the inside of the reaction chamber at 77°K. After adjusting the electron current, carrier-free tritium was released into the reaction vessel. The total reaction time varied from 1 to 15 min.

Following reaction, the products which were gases at 77°K (HT, DT, T₂, and methane) were trapped in a sampler containing molecular sieve at 77°K. The hydrogen species were separated on a 6-ft "moderately activated" alumina column⁷ immersed in liquid nitrogen. After removal of the liquid nitrogen, methane was eluted from the alumina. The remaining products were trapped at 77°K and transferred to a gas chromatograph. A two-stage column with a section of ethylene glycol-silver nitrate and a section of dimethyl-sulfolane or isoquinoline was used to separate the products. The tritium in the products was counted by passing the gas chromatograph effluent stream through an ionization chamber which was connected to a vibrating reed electrometer.

Results

Table I gives results of reactions of T atoms with solid propene and solid propane. The electron energy

was varied from 20 ev in some reactions to 30, 40, or 50 ev in others. An increase in accelerating voltage increased the electron current and the amount of tritium incorporated but did not change the product distribution appreciably.

Table I: Hydrocarbon Products from Tritium Atom Reactions with Solid Propene and Propane

Products	Tritium distribution, %	
	Propene ^a	Propane ^b
C	1.2 \pm 0.4	28.2 \pm 3.4
C=C	1.5 \pm 0.3	6.2 \pm 1.2
C-C	0.6 \pm 0.2	10.0 \pm 1.1
C-C=C	30.8 \pm 0.9	3.8 \pm 1.3
C-C-C	39.1 \pm 1.1	49.0 \pm 1.6
C ₄	0.3 \pm 0.1	2.8 \pm 0.5
C-C-C-C	8.0 \pm 1.4	
$\begin{array}{c} \text{C} \quad \text{C} \\ \quad \\ \text{C}-\text{C}-\text{C}-\text{C}=\text{C} \end{array}$	5.2 \pm 0.6	
$\begin{array}{c} \text{C} \\ \\ \text{C}-\text{C}-\text{C}-\text{C}-\text{C} \end{array}$	7.8 \pm 1.7	
$\begin{array}{c} \text{C} \\ \\ \text{C}-\text{C}-\text{C}-\text{C}-\text{C}=\text{C} \end{array}$	1.2 \pm 0.1	
C-C-C-C-C-C	4.3 \pm 2.0	

^a 13–30 μ moles of propene; T₂ pressure, 5×10^{-4} torr. Average of 13 reactions. ^b 7 μ moles of propane; T₂ pressure, 1×10^{-3} torr; electron energy, 30 ev. Average of 20 reactions.

The yields from reactions of tritium atoms with solid propene and propane are given in Table II. The yield from propene was about 50 times as large as that from propane.

Table II: Yields of Products from Tritium Atom Reactions with Solid Propene and Propane

	Compound reacted		
	Propene-d ₆	Propene	Propane
Length of reaction, min	1	1	1
Plate current, μ a	20–30	8	7
T ₂ pressure, torr	5×10^{-4}	1×10^{-3}	1×10^{-3}
Products	Yield of products, μ curies		
HT	8.3	<i>a</i>	<i>a</i>
DT	1.0		
Unreacted T ₂	85.0	152	180
CH ₄	<i>b</i>	0.53	0.18
Condensed products at 77°K	12.9	14.5	0.22

^a Not reported because part of the HT was not formed at the solid film. (See below.) ^b Not measured.

(7) E. H. Carter, Jr., and H. A. Smith, *J. Phys. Chem.*, **67**, 1512 (1963).

The cross section for electron-induced dissociation of tritium gas was estimated from the yield of hydrocarbon products in the propene system by assuming that each tritium that was produced subsequently reacted to form a tritiated hydrocarbon product. Thus, the cross section for dissociation induced by 40-ev electrons was estimated to be $0.34 \times 10^{-16} \text{ cm}^2$. Corrigan and Von Engel⁸ and Ramien⁹ have reported cross sections of $0.2\text{--}0.3 \times 10^{-16} \text{ cm}^2$ for atomization of hydrogen by electrons.

Blank reactions were run with the thermionic cathode maintained at its regular operating temperature but no electron current between the cathode and grid or plate. The yield of tritiated products for these blank reactions was insignificant except for the yield of HT, which was similar to that from other reactions in which an electron current was maintained. The yield of HT was large for all reactions (5–25 μcuries) but did not amount to a sizable fraction of the total amount of T₂ in the system (150–200 μcuries), and thus the isotopic composition of the T₂ was nearly constant during reaction. Reactions (see Table II) were run with propene-*d*₆ to determine if the HT came from the hydrocarbon film or from other parts of the system. The yield of DT was only about one-eighth of the yield of HT, indicating that most of the HT did not come from the hydrocarbon film. This is not surprising because the T atoms produced by thermal atomization at the cathode, though essentially isolated from the propene surface, were free to bombard other surfaces (mostly glass) where hydrogen isotope exchange could occur.

Discussion

Both systems (propane or propene) yielded a set of tritiated products which were the same as those that one would predict from characteristic hot reactions of recoil tritium atoms. Also produced were products more characteristic of thermal tritium atoms than hot tritium atoms. Specific cases of both types of reactions will be discussed.

The over-all mechanism preferred by the authors involves first the production of hot tritium atoms by dissociation of ³Σ_uT₂ followed by either hot or thermal reactions of the tritium atoms which occur predominantly on the surface of the solid hydrocarbon.

Tritium Atom Reactions with Propene. The product distribution from reactions with propene indicates that a significant fraction of the tritium atoms reacted before reaching thermal equilibrium with the solid film. Tritium atoms thermalized to 77°K react with solid propene to produce isopropyl free radicals,¹⁰ which then react by disproportionation or combination to yield tritium-labeled propene, propane, and 2,3-dimethylbutane. Two other C₃ radicals, *n*-propyl and allyl, are formed by reactions of hot tritium atoms as evidenced by the presence of the combination products: 2-methylpentane, *n*-hexane, 3-methyl-1-pentene, and 1-

hexene. Allyl radicals formed by the abstraction of hydrogen from propene were not labeled, and therefore the resulting dimer, 1,5-hexadiene, was not detected.

A comparison of the relative amounts of C₃ radicals that reacted by combination to form C₆ products is given in Table III. The distributions were calculated from the various yields of C₆ products, and they show that the tritium atoms from electron-induced dissociation of T₂ are chemically "hotter" than those from the thermal dissociation of T₂ at 2420°K. The numbers in Table III are not percentages of the three radicals in the reacting films, except for the case where only *sec*-propyl radicals were present, because the radicals also reacted by disproportionation. *sec*-Propyl undergoes disproportionation more readily than *n*-propyl¹¹ so that the ratio of *sec*-propyl to *n*-propyl was probably higher than 52/28. Thus the T atoms which bombarded solid propene at 77°K in the present study reacted with solid propene much more discriminately at the site of the double bond than do recoil T atoms with propene in the gas phase.¹²

Table III: Distribution of C₃ Radicals That Reacted by Combination to Form C₆ Compounds

Method of producing T atoms	Radical content (%) of combination products		
	<i>sec</i> - Propyl	<i>n</i> - Propyl	Allyl
Electron bombardment	52	28	20
Thermal dissociation at 2420°K ¹⁰	69	17	14
Thermal dissociation at 1450°K ¹⁰	80	11	9
Thermal dissociation and moderation at 77°K ¹⁰	100	0	0

The reactions previously discussed which produce either C₃ or C₆ compounds account for over 95% of the hydrocarbon products. Methane and ethylene are the principal remaining products and are proposed to arise from reactions of hot tritium atoms.¹³ Thus hot addition of a tritium to a propene molecule may produce methyl radicals and labeled ethylene, and a hot tritium atom may replace a vinyl radical to produce labeled methane.

Lee, Musgrave, and Rowland¹⁴ observed that hydrogen abstraction was one of the most important reactions

(8) S. J. B. Corrigan and A. Von Engel, *Proc. Roy. Soc. (London)*, **A69**, 615 (1956).

(9) H. Ramien, *Z. Physik*, **70**, 353 (1931).

(10) H. B. Yun and H. C. Moser, *J. Phys. Chem.*, **67**, 2806 (1963).

(11) J. A. Kerr and A. F. Trotman-Dickenson, "Progress in Reaction Kinetics," Vol. I, Pergamon Press, New York, N. Y., 1961, p 107.

(12) D. Urech and R. Wolfgang, "Chemical Effects of Nuclear Transformations," Vol. II, International Atomic Energy Agency, Vienna, 1961, p 99.

(13) R. Wolfgang, *Ann. Rev. Phys. Chem.*, **16**, 15 (1965).

(14) J. K. Lee, B. Musgrave, and F. S. Rowland, *J. Am. Chem. Soc.*, **82**, 3545 (1960).

of recoil tritium atoms with propene. In the present study, appreciable quantities of HT were formed, but most of the HT was not formed from reactions with propene. Experiments with C_3D_6 (see Table II) yielded only one-eighth as much DT as HT, which indicates that only a small part of the HT was the result of abstraction reactions with the propene film. In the present study, abstraction reactions were not as important as addition of tritium in the propene system.

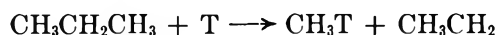
The occurrence of direct displacement of T for H in propene, a process important with recoil atoms, could not be proved in our system since propene-T was a product of three other possible reactions: (a) radical-radical, (b) atom-radical disproportionation of tritium-labeled propyl radicals, and (c) decomposition by CH rupture¹⁵ of excited tritium-labeled propyl radicals following the addition of a T atom to propene.

However, the occurrence of (c) above and/or direct displacement seems most reasonable for the formation of propene-T in several experiments in which the occurrence of (a) and (b) were not likely. In these experiments, propene and nitric oxide were frozen together, and the result was the elimination of all C_6 compounds, indicating that the nitric oxide had blocked radical-radical reactions ((a) above). In contrast, the yield of propene-T was still significant. Reaction b above, can also be discounted for the most part because had (b) occurred to any significant extent, atom-radical combination would have occurred also.¹⁶ The result would have been that the amount of tritium in propene-T and propane-T would have been similar. In the experiments where nitric oxide was present, the ratio of the amount of tritium in propene to that in propane was in the range of 6-20, indicating that not much T atom-propyl radical combination occurred.

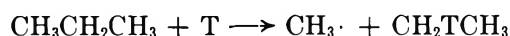
T-Atom Reactions with Propane. The principal tritium-labeled products from propane reactions were propane and methane. Only tentative mechanisms can be proposed for this system at the present time. The tritium-labeled propane could reasonably come from either or both of two different processes: (1) a two-step process in which a propyl radical is formed followed by tritium atom addition to this free radical, or (2) a di-

rect displacement of T for H. We obtained evidence for the occurrence of both processes. For example, neither the presence of 2-methylpropene (a good hydrogen atom scavenger) nor nitric oxide in the propane matrix reduced the labeled propane yield to less than 60% of the amount from a pure propane matrix, which gives indication that a process not requiring a second tritium atom or a propyl radical was occurring at least part of the time. On the other hand, the presence of propene as a product seems most reasonably explained on the basis of reactions of labeled propyl radicals as intermediates.

The methane could come from the displacement of an ethyl radical by T



The alternate displacement of methyl by T would produce labeled ethane



These reactions have been proposed for recoil tritium atoms and are processes which are proposed to occur in in about 10^{-14} sec.¹³ An alternate mechanism for the formation of methane could involve labeled methyl radicals as intermediates, but this process does not seem as likely as the former. The labeled methyl radicals could result from the decomposition of excited propane formed by tritium atom addition to propyl radicals, but this process would be quite improbable due to the ease of deactivation of excited propane in this system. Apparently, tritium atoms add to isopropyl radicals without significant decomposition of the excited propane.¹⁶

Part of the methane may have arisen from reactions other than at the hydrocarbon film. The yield of methane increased with electron beam current but was not directly proportional to it. In contrast, the yield of tritiated propane was found to be directly proportional to the electron beam current in the range of 2-36 μ a.

(15) R. Wolfgang, *Progr. Reaction Kinetics*, **3**, 142 (1965).

(16) K. W. Watkins and H. C. Moser, *J. Phys. Chem.* **70**, 1137 (1966).

The Fragmentation of Skeletal Bonds of Cyclic Alkanes in Mass Spectra¹

by Kozo Hirota and Yoshio Niwa

Department of Chemistry, Faculty of Science, Osaka University, Toyonaka, Osaka, Japan
(Received October 19, 1966)

In order to extend the application of molecular orbital theory to fragmentation in mass spectra, scission probabilities of skeletal C-C bonds in cyclic alkanes have been calculated. By introducing a new assumption necessary to handle the fragmentation of ring compounds, a satisfactory agreement between theory and experiment has been obtained for four cyclic alkanes (C_5H_{10} , C_6H_{12} , C_7H_{14} , and C_8H_{16}). The above results have been obtained using only one arbitrary constant for all the cyclic alkanes. It has been concluded that the theory can explain the mass spectra of cyclododecane ($C_{12}H_{24}$) and others of this kind of compound, if the scheme of the statistical theory is taken into account in the secondary decomposing processes of the initial fragments.

Introduction

The "molecular orbital (MO) theory" of mass spectra was found to be very useful in predicting, quantitatively, the initial fragmentation of skeletal bonds of several alkanes,² alkyl ketones,³ and alkyl amines,⁴ the number of such compounds reaching more than 20. This theory, therefore, may play a complimentary role to the statistical theory of Rosenstock, *et al.*,⁵ which was proposed in order to explain all mass spectral peaks, postulating a total reaction scheme peculiar to the molecule, as well as rate constants and lifetimes of each intermediate included in the scheme.

It is a characteristic of the MO theory that no reaction scheme is required, and only a few arbitrary parameters are necessary in calculation. These parameters, in some cases, can be estimated from the ionization potentials of the molecules studied. Notwithstanding such advantages, the MO theory includes a fundamental postulate too bold to be acknowledged by some researchers who favor the kinetic viewpoint. Therefore, additional examples of application may be desirable so as to show that the success is not fortuitous.

As a result, studies on several cyclic alkanes (C_5H_{10} , C_6H_{12} , C_7H_{14} , C_8H_{16} , and $C_{12}H_{24}$) were begun in order to extend the theory to compounds other than normal alkanes and also to discuss the range of applicability of this theory and to suggest a generalized theory.

Theory

Conceptually, the basis of the MO theory is quite different from that of the statistical theory. First, such a particular scheme is implicitly included in the theory that scission of skeletal bonds of molecules occurs just after electron bombardment without at any time localizing excess energy at any particular bond or, to put it quantitatively, within the time of one molecular vibration. This fundamental postulate may be ac-

cepted as a kind of autoionization⁶ of the superexcited ionic species. Therefore, the theory makes it unnecessary to introduce the idea of the activated complex, which is indispensable in statistical theory. Of course, the processes which proceed *via* the activated complex may be shown in most of the actual mass spectra, as indicated by the appearance of metastable peaks. However, as far as initial fragmentation processes of the skeletal bonds are concerned, the above scheme will be applied initially to be followed by slow decomposition of the initial fragments. Occurrence of such secondary processes has been confirmed by isotopic tracer techniques.

Lower cycloalkanes are suited to the investigation of the applicability of the above scheme because their mass spectra measured by different researchers are nearly identical. Also, the amounts of the ions, if grouped together according to number of carbon atoms, coincide with each other very well, as shown in Table I, where the observed probabilities of bond scission are proportional to the grouped amount of ions, as will be explained in Figure 3. The data have been recalculated from the API catalog of mass spectral data⁷ as well as from our unpublished data.

In spite of differences in the apparatus used and in the operating conditions, agreement is unexpectedly good, and it is especially noteworthy that the scission prob-

(1) Report VII on molecular-orbital theory for mass spectra; preliminary report, *Tetrahedron Letters*, 5757 (1966).

(2) (a) K. Fueki and K. Hirota, *Nippon Kagaku Zasshi*, **80**, 1202 (1959); **81**, 212 (1960); (b) J. C. Lorquet, *Mol. Phys.*, **9**, 101 (1965).

(3) M. Hatada and K. Hirota, *Bull. Chem. Soc. Japan*, **38**, 599 (1965); *Z. Physik. Chem. (Frankfurt)*, **44**, 328 (1965).

(4) K. Hirota and M. Itoh, *Bull. Chem. Soc. Japan*, **39**, 1406 (1966).

(5) H. M. Rosenstock, *et al.*, *Proc. Natl. Acad. Sci. U. S.*, **38**, 667 (1952).

(6) R. L. Platzman, *Radiation Res.*, **17**, 419 (1962).

(7) American Petroleum Institute Research Project No. 44.

Table I: Observed Probabilities of C-C Bond Scissions (%) Determined from API Mass Spectral Data^a

Serial no.	Electron current, μ A	Ionizing voltage, v	Probability			
			No. of C-C bonds			
			1	2	3	4
Cyclopentane						
116	8.0	50	16.7	83.3		
182	9.0	50	16.6	83.4		
182	8.0	70	17.1	82.9		
Cyclohexane						
118	8.0	50	8.5	54.1	37.4	
216	9.0	50	8.9	54.6	36.5	
216	9.0	70	9.1	54.5	36.4	
1585	100	70	9.4	55.2	35.4	
1589	20	50	9.3	54.7	36.0	
1589	20	70	9.4	54.9	35.7	
1605	34.5	70	9.1	55.0	35.9	
H.-N.	50	25	10.2	53.3	36.5	
H.-N.	50	80	9.6	53.5	36.9	
Cycloheptane						
478	9.0	50	6.9	31.8	61.3	
478	9.0	70	7.0	31.9	61.1	
930	10.5	70	7.4	33.3	59.3	
1277	10.5	70	7.2	32.5	60.3	
Cyclooctane						
842	52.0	70	2.3	24.1	50.1	23.5

^a The temperature of the ionization source is 245 or 250°, except the unknown one (no. 1589). The apparatus used was CEC No. 21-102 or 21-103, except no. 1585, 1589, 1605 (Metropolitan-Vickers Type Ms-2), and H.-N. (Hetachi RMU-2).

ability of cyclohexane remains practically invariant, even if the ionizing voltage is lowered to 25 v. This finding seems to suggest that successive slow scission of the C-C bonds of initial fragments occurs very rarely in above four cycloalkanes.

Now, in the case of normal alkanes,² the scission probability of each C-C bond was calculated under the original assumption that the probability of scission at the *i*th bond is proportional to the charge density of the highest occupied (HO) level at that bond.⁸ However, the above assumption is insufficient for evaluating the fragmentation of superexcited species of cyclic alkanes because it gives us only the probability of opening the ring, thus forming only the parent ion. Therefore, it becomes necessary to introduce a new assumption to evaluate the probability of another bond scission occurring successively to or actually simultaneously with the first one.

Like the superexcited species produced by electron bombardment, the molecular cationic species is assumed whose electron distribution is the same as that of its neutral molecule, except that an electron from the HO level has been stripped off. Though this assumption may now be a tentative one, the theory will be extended for the two following reasons.

First, taking the fundamental postulate into consideration, the superexcited state in question may just correspond to the activated complex in the statistical theory. Secondly, the possibility of fragmentation from other superexcited states will be investigated in another paper.

The actual procedure of calculation will be explained, citing cyclopentane as an example.

Due to the loss of an electron by electron bombardment, a skeletal scission occurs at a bond which is then numbered zero (*cf.* Figure 1.). The parent ion thus produced may be regarded as taking two configurations, A and B, neglecting highly excited configurations. The number of energy levels in each configuration is increased by one over that of neutral cyclopentane. This arises from the splitting of the bond 0 into two sp^3 hybrid orbitals, and the energy of the two highest levels, I and II, are approximately equal, as shown in the figure, where the two levels correspond to the non-bonding MO's. The electron deficiency, or positive charge, is almost completely localized at the bonds S in configuration A. This configuration may contribute to the formation of the parent ion. In addition to configuration A, one must consider a configuration in which the positive charge is distributed over all the bonds, *i.e.*, configuration B. As assumed in the cases of *n*-alkanes, configuration B may contribute to the skeletal bond scission, and the probability is assumed to be proportional to the positive charge density in the highest σ -bonding orbital III; *i.e.*, $C_i^2(\text{III})^{9,10}$ would give the probability of *i*th bond scission, which scission would cause the fragmentation of cyclic alkanes.

Now it should be unnecessary to explain the procedure on other alkanes of different carbon numbers.

Calculation

In order to determine the charge density of each C-C bond, the LCBO-MO treatment¹¹ will be adopted as in the previous reports. According to this treat-

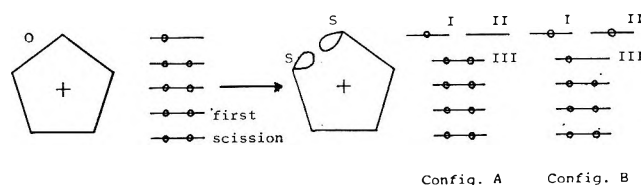


Figure 1. The configurations of the parent ion. In configuration B, the electron population may be drawn as shown in the figure because of the same symmetry of the MO's II and III.

(8) R. Thompson, "Applied Mass Spectrometry," Institute of Petroleum, London, 1953, p 154.

(9) See Calculation.

(10) G. G. Hall, *Proc. Roy. Soc. (London)*, **A205**, 541 (1951).

(11) R. D. Brown, *J. Chem. Soc.*, 2615 (1953); due to the approximation to be adopted, the result is the same even if the equivalent orbital treatment is used.

ment, we can give the ionization potential from the HO orbital ψ (I) of the molecule concerned, using the molecular orbital made by the linear combination of all the bond orbitals ϕ_i 's (LCBO) of the bonds constituting the molecule; *i.e.*

$$\psi(\text{I}) = \sum_i C_i(\text{I})\phi_i; \quad \sum_i C_i^2(\text{I}) = 1 \quad (1)$$

where i is the number of the bond and $C_i(\text{I})$ is the expansion coefficient of ψ (I) with respect to the i th bond orbital.

In order to evaluate the scission probability of each C-C bond, the charge densities $C_i^2(\text{I})$ thus calculated were used in the cases of normal alkanes. However, since all the bonds of the above four alkanes are of the same nature, it can be seen that the probability of the first bond scission is equal for all bonds. Therefore, the problem to be investigated is now the calculation of the probability of the second bond scission in the "polymethylene" ion, which is produced by the first scission. For example, in the case of cyclopentane, it becomes necessary to calculate the charge density $C_i^2(\text{III})$ (*cf.* Figure 1).

For the sake of simplicity in calculation, each CH_2 group is regarded as a single united atom. Secular equations of each polymethylene ion are constructed, neglecting the nondiagonal matrix elements which correspond to the interaction between nonadjacent bonds as well as all overlap integrals.

The electron density on each C-C bond, as calculated using this approximation, is essentially equal to that found using a rigorous treatment.¹ Details will be shown in the Appendix,¹¹ where the result for *n*-octane is cited as an example.

Therefore, all the matrix elements can be classified into coulombic integrals or exchange integrals, and these integrals will be denoted by α and β , respectively, except for three special cases which will be explained. They are introduced because of the presence of the outermost sp^3 hybrid orbitals: the diagonal matrix element (α_0) for the outermost sp^3 hybrid orbital; the diagonal element (α_1) for the terminal C-C bond orbitals; and the nondiagonal element (β_0) involving these two bond orbitals (*cf.* Figure 2). However, it is possible to assume that $\beta_0 = 0$,¹² and therefore the two levels whose eigenvalues are equal to α_0 correspond to the two highest energy levels. By omitting these two levels, the secular determinant (Δ_0) can be simplified into a secular equation of lower degree (Δ), in which α_0 is not included. Then, for the sake of simplicity, α_1 was replaced by $\alpha + m_1\beta$ where m_1 is a free parameter. An example of such a secular equation is shown for cyclopentane by eq 2, which gives a fourth-order de-

$$\Delta = \begin{vmatrix} \lambda + m_1 & 1 & 0 & 0 \\ 1 & \lambda & 1 & 0 \\ 0 & 1 & \lambda & 1 \\ 0 & 0 & 1 & \lambda + m_1 \end{vmatrix} = 0 \quad (2)$$

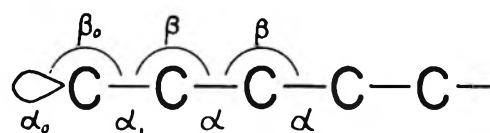


Figure 2. Matrix elements of the polymethylene ion.

terminant, where $(\alpha - E)/\beta$ has been substituted by λ .

Thus, $C_i^2(\text{III})$'s were calculated from those belonging to the MO of highest energy in the secular equation of the Δ type. It will be pointed out in the Discussion that the use of λ has meaning beyond that of a mere calculating procedure.

Results

As mentioned above, estimation of only one parameter, m_1 , in eq 2 was necessary to solve the secular equations numerically. Its value was estimated to be 0.8, because it was found to give the best coincidence between the observed and calculated probabilities of bond scissions of cyclopentane. The calculated $C_i^2(\text{III})$'s for the other three cyclic alkanes are denoted in Figure 3, where the adopted numbering of the bonds is not essential to the result.

According to the procedure described in the theoretical part, the scission probability of each kind of bond was then calculated, and the probabilities thus obtained on the four alkanes were plotted in per cent against each bond number in Figure 4, where the curves denote the calculated values and the bond numbers correspond to the ones shown in Figure 3. Agreement between the observed and calculated values is better than expected, considering that there may be some experimental errors

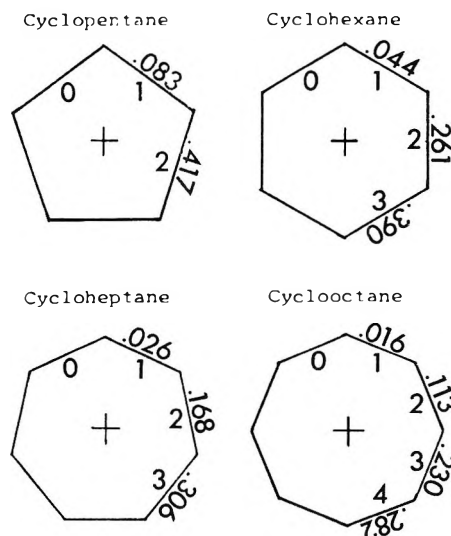


Figure 3. Bond numbering of the polyethylene ion produced from each cyclic alkane and $C_i^2(\text{III})$ for these ions.

(12) Actually, the result was practically insensitive to variations in the adopted β_0 value, indicating this approximation to be reasonable.

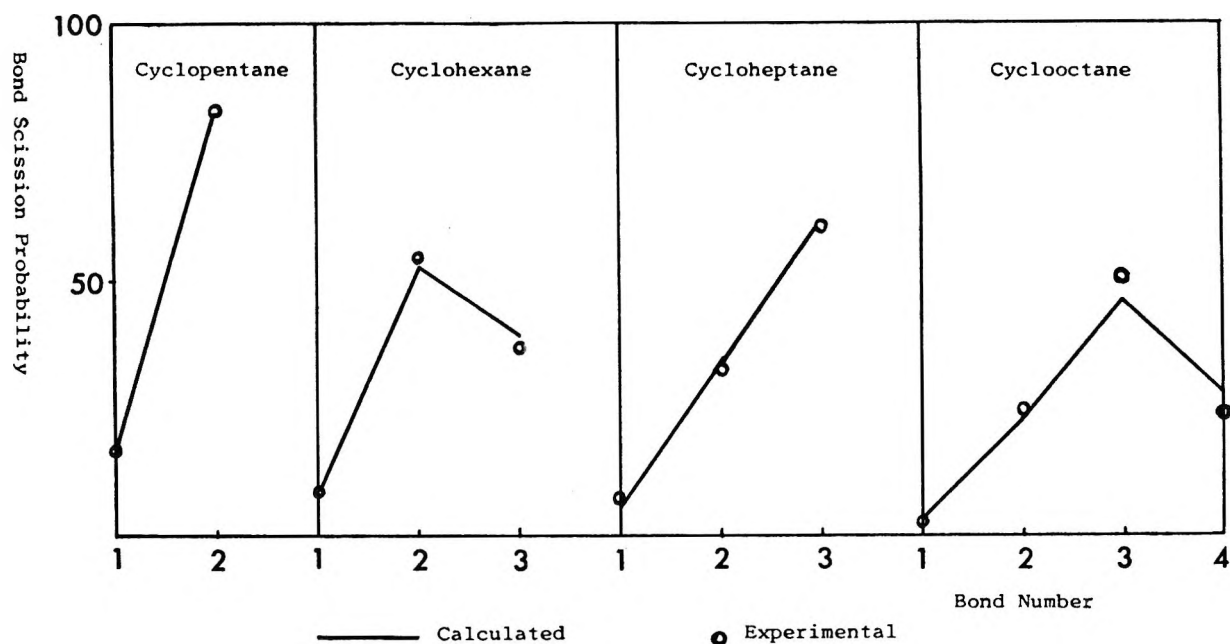


Figure 4. Bond-scission probabilities of cyclic alkanes in mass spectra.

Table II: Effect of the Parameter m_1 on the Theoretical Results

	Bond no.	0.3	0.5	0.8 ^a	1.0	1.3
Cyclopentane	1	22.75	20.00	16.55	14.64	12.27
	2	77.25	80.00	83.45	85.36	87.73
Cyclohexane	1	12.95	11.04	8.80	7.64	6.26
	2	51.15	51.65	52.15	52.36	52.55
	3	35.90	37.31	39.05	40.00	41.19
Cycloheptane	1	8.01	6.69	5.21	4.47	3.61
	2	34.47	34.13	33.64	33.33	32.91
	3	57.52	59.18	61.15	62.20	63.48
Cyclooctane	1	5.29	4.35	3.32	2.83	2.26
	2	23.97	23.38	22.64	22.22	21.68
	3	44.28	45.05	45.94	46.38	46.92
	4	26.47	27.22	28.10	28.57	29.14

^a The final result was obtained using this value.

in the spectra.¹³ The agreement is even better than those obtained in the cases of *n*-alkanes.^{2a} This may be partly due to the fact that the inductive effect¹⁴ at the terminal CH₂ group of the parent ion was, if it exists, introduced automatically by the parameter m_1 . However, it is noteworthy that a slight change of the adjustable parameter m_1 does not alter the conclusion qualitatively, as is shown in Table II.

Discussion

Now that such a quantitative explanation has been found to be satisfactory for cycloalkanes, the MO theory of mass spectra becomes more convincing than before as far as the scission of the skeletal C-C bonds is concerned. The above result may, in turn, teach us the plausibility of the second assumption added to the original theory.

Then, it may be interesting that even such a static approach is effective in explaining a kinetic phenomenon, and it is noteworthy that an important conclusion can be derived from the result if the basis of the theory is considered; *i.e.*, all the fragment ions accompanying C-C bond scission are produced within the time of one molecular vibration. However, since the detailed processes during that time cannot be explained now, it must be admitted that the present method must remain a semiempirical tool until these processes are clarified completely.

Concerning C-H bond scission, which is less frequent

(13) Contribution of the metastable peaks to the result could be neglected because of their small amount compared with the total peaks.

(14) G. G. Hall, *Bull. Soc. Chim. Belges*, **73**, 305 (1960).

than C-C bond scission, nothing was mentioned in the above discussion because of the approximate nature of the united-atoms method adopted in the present study. In order to discuss the scission of all the bonds generally, it might be necessary to introduce the successive process of the initially produced ions into the total scheme of fragmentation. These successive decomposition processes may be inevitably introduced in other cases, and especially easy transfer of a proton may occur, making the mass spectra more complex. This is the reason why it was mentioned in the Introduction that the MO theory is complimentary to the statistical theory for explaining mass spectra.

In connection to the above discussion, it might be mentioned that Beckey^{15a} and Lorquet and Hall^{15b} already have proposed a relation favorable to the MO theory to explain the bond scission of lower alkane molecules in field-ionization mass spectra.

It is interesting to note that secular equations including the α and β values can also be used for the case of the normal alkanes, and the scission probabilities of their C-C bonds are determinable without any knowledge of them. This result suggests that the fragmentation of both alkanes does not depend on the arbitrary selection of some particular α and β values, and is also suggestive of an understanding of the general mechanism of fragmentation and indicates that the good agreement in this paper is not fortuitous.

Prediction on Higher Cyclic Alkanes¹⁶

In the case of n -alkanes higher than octane, it was pointed out experimentally that lower fragments increased more rapidly than expected from theory; *i.e.*, peaks corresponding to C_3 or C_4 fragments are always the most abundant in the spectra of higher alkanes. This result may be explained by the occurrence of secondary fragmentation brought about by localization of excess energy at a particular bond, as shown experimentally in cases of higher alkanes. Therefore, the above result, though concluded to be fatal to the theory,¹⁷ is not incompatible with the generalized theory.

On the other hand, if the above reasoning is true, higher cycloalkanes may give lower fragments more abundantly than expected from theory. According to our preliminary experiment on cyclododecane, $C_{12}H_{24}$, at ordinary ionizing voltage (80 v), the maximum of the fragment distribution seems to lie at the peaks of $C_3 + C_9$ fragments but not at twice the peaks of C_6 fragments, as required by simple theory. See the data in Table IIIA, which form a contrast to the cases of lower cycloalkanes. If this finding can be explained by the successive decomposition of the initial fragments, it is expected that in the case of mass spectra of cyclododecane measured at lower ionizing voltage the maximum of the fragment distribution would shift to the region of central bond scission and the distribution would come closer to the calculated value, because the

Table III: Fragment Distribution of Cyclododecane, $C_{12}H_{24}$ ^{a,b}

A. Ionizing Voltage, 80 v; Electron Current, 58 μ a; Temperature of Ion Source, 190°						
C_1	0.0	C_{11}	0.0	$C_1 + C_{11}$	0.0	0.9
C_2	8.4	C_{10}	0.3	$C_2 + C_{10}$	8.7	6.5
C_3	29.9	C_9	0.5	$C_3 + C_9$	30.4	15.7
C_4	27.9	C_8	1.7	$C_4 + C_8$	29.6	25.7
C_5	17.1	C_7	4.4	$C_5 + C_7$	21.5	33.2
C_6	9.8			C_6	9.8	18.0
Total (C_1 - C_{11}) = 100%						
$C_{12}/\sum_{i=1}^{11} C_i = 0.011$						
B. Ionizing Voltage, 30 v; Electron Current, 58 μ a; Temperature of Ion Source, 220°						
C_1	0.0	C_{11}	0.0	$C_1 + C_{11}$	0.0	0.9
C_2	0.9	C_{10}	1.3	$C_2 + C_{10}$	2.2	6.5
C_3	12.7	C_9	1.9	$C_3 + C_9$	14.6	15.7
C_4	27.5	C_8	4.6	$C_4 + C_8$	32.1	25.7
C_5	24.0	C_7	9.3	$C_5 + C_7$	33.3	33.2
C_6	17.8			C_6	17.8	18.0
Total (C_1 - C_{11}) = 100%						
$C_{12}/\sum_{i=1}^{11} C_i = 0.025$						

^a Using a Hitachi RMU for 7 hr. ^b Intensity of the parent ion at B is 1.56 times that at A.

excess energy given to the molecule decreases as the energy of the bombarding electron is decreased. This expectation was found to be true as shown by the data in Table IIIB, where the order of abundance of fragments is

$$2C_6 > C_5 + C_7 > C_4 + C_8 >$$

$$C_3 + C_9 > C_2 + C_{10} > C_1 + C_{11}$$

The observed bond-scission probability coincides well with the calculated one.

It can be said, therefore, that the above finding gives us further evidence of the reliability of the MO theory.

Conclusion

The LCBO-MO theory can be used quantitatively to correlate calculated electron densities in various bonds with the yields of fragment ions and is thus a potentially useful tool for predicting fragmentation patterns of hydrocarbons.

Acknowledgment. The authors express their sincere thanks to Dr. Keiji Kuwata and others in our Department, and also to Dr. Mitio Inokuti, Argonne

(15) (a) H. D. Beckey, *Z. Naturforsch.*, **19**, 71 (1964); (b) J. C. Lorquet and G. G. Hall, *Mol. Phys.*, **9**, 29 (1965).

(16) This section was added by the kind suggestion of the referees.

(17) N. D. Coggeshall, *J. Chem. Phys.*, **30**, 505 (1959).

National Laboratory, Argonne, Illinois, for his valuable discussion.

Appendix

Expansion Coefficients of the MO at Each Bond Orbital of Normal Octane. In order to examine the reliability of the method adopted in the present paper, expansion coefficients of the HO-MO at the i th bond, $C_i^2(I)$, will be compared with the results of two other methods of a higher degree of precision, selecting n -octane as an example.

The results obtained by the three methods are compared in Table IV, where $C_i^2(I)$'s are shown against the number of the C-C bond:¹⁸ A, the present method (united-atom approximation); B, Hall's method (All CH bonds are taken into account, but the two outermost CH bonds are disregarded.);^{2a} and C, Lorquet's method (all CH bonds and the inductive effect).^{2b}

From Table IV it can be concluded that the united-atom approximation is sufficient for us to derive the

Table IV: $C_i^2(I)$ of n -Octane (%)^a

No. of C-C bond	1, 7 ^b	2, 6 ^b	3, 5 ^b	4 ^b	Ref
A	0.0366	0.1250	0.2134	0.2500	13
B	0.0362	0.1235	0.2108	0.2470	2a
C	0.03	0.12	0.21	0.24	2b

^a Due to the contribution of C-H bonds, the total of $C_i^2(I)$ does not reach 100% in the cases of B and C. ^b $\begin{array}{cccc} \text{C} & \text{---} & \text{C} & \text{---} & \text{C} & \text{---} & \text{C} \\ & & 1 & & 2 & & 3 & & 4 \end{array}$
 $\begin{array}{cccc} \text{C} & \text{---} & \text{C} & \text{---} & \text{C} & \text{---} & \text{C} \\ & & 5 & & 6 & & 7 \end{array}$

charge density at the HO-MO. This conclusion may also be applied to the polymethylene ions, considering that the difference of charge density between neutral and cationic species is negligibly small, as far as alkanes are concerned.²

(18) G. R. Lester, *Advan. Mass Spectry., Proc. Conf.*, 1, 287 (1959).

Equations for the Description of Isothermal Diffusion in Multicomponent Systems Containing Pairs of Chemically Equivalent Components

by John Grover Albright^{1,2}

Institute for Enzyme Research, University of Wisconsin, Madison, Wisconsin 53706
(Received December 16, 1966)

Since an understanding and examination of experimental data for diffusion in systems with chemically equivalent components would aid in the interpretation of data from systems in which the components are chemically different, equations are presented for the description of isothermal diffusion in multicomponent systems where each chemically different component becomes recognized as a *pair* of chemically equivalent components. These equations use the n^2 mutual diffusion coefficients and the $n + 1$ intradiffusion (tracer-diffusion) coefficients for a system with $n + 1$ chemically different components to obtain the $(2n + 1)^2$ diffusion coefficients for the $n + 1$ *pairs* of chemically equivalent components. A volume-fixed frame of reference has been used in the derivation of these equations. Equations are also presented for the thermodynamic description of the same type of system. These latter equations use the coefficients $R_{i,k}$, due to Onsager, that relate the gradient of chemical potential of each component to the flows of all of the components of the system. The equations presented in this article may easily be expanded to describe systems where each chemically different component becomes recognized as a set of any number of chemically equivalent components.

Background

Tracer-diffusion coefficients represent an important measurable property in the study of transport processes in liquid systems. Usually a tracer component is detectable by radioactive properties and is added to an experimental system in such minute amounts that its concentration is several orders of magnitude less than the concentrations of other components already present in the system which are essentially unaltered by the addition. Tracer-diffusion coefficients are measured under the condition that the system is in thermal equilibrium and that all other components are essentially homogeneously distributed throughout the system. In this case the rate of diffusion of the tracer component is proportional to its own concentration gradient according to Fick's first law and the diffusion process may be described by one diffusion coefficient, the tracer-diffusion coefficient.

Of particular importance are the measurements of tracer-diffusion coefficients in experimental systems where the added tracer components are chemically equivalent with regard to the diffusion process to components already present in these systems. In this case the tracer-diffusion coefficient is equal to the intradiffusion coefficient for intradiffusion between the two chemically equivalent components. The term intradiffusion was introduced and carefully defined in a previous article.³ In the process of intradiffusion only

the two chemically equivalent components are diffusing and there is no flow or concentration gradient of any of the other components in the system. Concentration gradients and consequent flows of the two diffusing components are opposite in direction and equal in magnitude, and the sum of the concentrations of these components is constant with time and position. Intradiffusion coefficients depend on the total concentration of the chemically equivalent components, along with the concentrations of all of the other components in the system, but are independent of the concentration ratio of the chemically equivalent components. Tracer-diffusion coefficients represent a property measured at one limit of this ratio. An intradiffusion coefficient may conveniently be regarded as a property ascribed to a single chemical component of a system even though its measurement does necessitate the presence of two separately identifiable forms of the component or in reality two components. If a system is composed of only two chemically equivalent components, then the intradiffusion coefficient will be a self-diffusion coefficient; however, the latter term is a misnomer when

(1) Department of Chemistry, Texas Christian University, Fort Worth, Texas 76129.

(2) This research was supported in part by Public Health Service Research Grant AM-05177 from the National Institute of Arthritis and Metabolic Diseases.

(3) J. G. Albright and R. Mills, *J. Phys. Chem.*, **69**, 3120 (1965).

applied to systems that also contain chemically different components.

When all of the diffusion coefficients are known for a system with chemically different components, the measurement of intradiffusion coefficients for one or more of these components allows an expansion of the description of the system. In a previous article,³ equations were presented which treated a binary system as a ternary system upon recognition of the solute component as two chemically equivalent components. The more general case of a multicomponent system will now be considered where the intradiffusion coefficients have been measured for all of the components and each component is identified as a *pair* of chemically equivalent components. Expressions will be derived for the diffusion coefficients in flow equations which are written to include all of these identifiable components. Also, in a parallel derivation, the thermodynamic coefficients due to Onsager⁴ will be obtained for this expanded description. Specifically, the case of a system that contains $n + 1$ chemically different components will be considered where n may be any finite positive integer. The diffusion coefficients and the thermodynamic coefficients, $R_{i,k}$, for this system and the intradiffusion coefficients of each of the $n + 1$ components in this system will be assumed to be available.⁵⁻¹² Also, the molecular weight of each component and the density of the system as a function of composition will be assumed to be known. These quantities will be used to obtain expressions for diffusion coefficients and Onsager's coefficients which describe the same system as containing $n + 1$ pairs of chemically equivalent components for a total of $2(n + 1)$ components.

Expressions for Diffusion Coefficients

General Equations. Independent flow equations for describing isothermal diffusion at constant pressure in a system containing n chemically different solute components may be written¹³

$$-(\mathbf{J}_i)_v = \sum_{k=1}^n (D_{i,k})_v \nabla c_k \quad (i = 1, 2, \dots, n) \quad (1)$$

Here cgs units may be adopted where \mathbf{J}_i is the flow of component i with the units moles/cm² sec, $(D_{i,k})_v$ are diffusion coefficients with the units cm²/sec, and c_i is the concentration of component i in moles/cm³ where ∇c_i is the concentration gradient. Subscript v denotes the volume-fixed frame of reference which is identical with an apparatus-fixed frame of reference in a closed cell if there is no volume change on mixing. This frame of reference is defined by the equation

$$\sum_{i=0}^n \bar{V}_i (\mathbf{J}_i)_v = 0 \quad (2)$$

Here the solvent is designated as component zero and \bar{V}_i is the partial molal volume of component i in cm³/mole.

When each of the $n + 1$ components is identified as two chemically equivalent components, the component designated as i in eq 1 will in the following be designated as components $2i$ and $2i + 1$.¹⁴ In this expanded description the independent flow equations for isothermal diffusion may be written

$$-(\mathbf{J}_{2i})_v = (D_{2i,1})_v \nabla c_1 + \sum_{k=1}^n (D_{2i,2k})_v \nabla c_{2k} + (D_{2i,2k+1})_v \nabla c_{2k+1} \quad (i = 1, 2, \dots, n) \quad (3a)$$

$$-(\mathbf{J}_{2i+1})_v = (D_{2i+1,1})_v \nabla c_1 + \sum_{k=1}^n (D_{2i+1,2k})_v \nabla c_{2k} + (D_{2i+1,2k+1})_v \nabla c_{2k+1} \quad (i = 0, 1, \dots, n) \quad (3b)$$

The equation for the volume-fixed frame of reference becomes

$$\sum_{i=0}^{2n+1} \bar{V}_i (\mathbf{J}_i)_v = 0 \quad (4)$$

Since eq 1, 3a, and 3b represent the same system where the only difference is the ability to identify the members of each *pair* of chemically equivalent components, the following relations apply

$$c_i = c_{2i} + c_{2i+1} \quad (i = 0, 1, \dots, n) \quad (5)$$

$$(\mathbf{J}_i)_v = (\mathbf{J}_{2i})_v + (\mathbf{J}_{2i+1})_v \quad (i = 0, 1, \dots, n) \quad (6)$$

$$\bar{V}_i = \bar{V}_{2i} = \bar{V}_{2i+1} \quad (i = 0, 1, \dots, n) \quad (7)$$

In obtaining expressions relating the coefficients in eq 3a and 3b to the coefficients in eq 1 and to intradiffusion coefficients, two types of experimental situations will be considered: the case of intradiffusion and the case where the concentration ratios of the chemically equivalent components are constants independent of time

(4) L. Onsager, *Ann. N. Y. Acad. Sci.*, **46**, 241 (1945).

(5) At present, experimental data are available for ternary systems; see, for example, ref 6. Theory for the experimental measurement of systems containing four different components has been presented by Kim.⁹ General solutions to the continuity equations for arbitrary boundary conditions for an n -component system have been given by Toor^{10,11} and by Stewart and Prober.¹²

(6) H. Fujita and L. J. Gosting, *J. Am. Chem. Soc.*, **78**, 1099 (1956).

(7) P. J. Dunlop and L. J. Gosting, *J. Phys. Chem.*, **63**, 86 (1959).

(8) D. G. Miller, *ibid.*, **63**, 570 (1959).

(9) H. Kim, *ibid.*, **70**, 562 (1966).

(10) H. L. Toor, *A.I.Ch.E. J.*, **10**, 448 (1964).

(11) H. L. Toor, *ibid.*, **10**, 460 (1964).

(12) W. E. Stewart and R. Prober, *Ind. Eng. Chem. Fundamentals*, **3**, 224 (1964).

(13) See, for example, J. G. Kirkwood, *et al.*, *J. Chem. Phys.*, **33**, 1505 (1960).

(14) This may be illustrated by considering a system containing four chemically different components ($n = 3$). If only chemically different components can be recognized, the components of this system are assigned the numbers $i = 0, 1, 2, 3$. When, however, it is recognized that each of these components is actually a *pair* of chemically equivalent but separately identifiable components, the eight components are assigned the numbers $2i = 0, 2, 4, 6$ and $2i + 1 = 1, 3, 5, 7$, respectively, for $i = 0, 1, 2, 3$.

and position. These same cases will be considered in finding expressions for Onsager's coefficients.

Case of Intradiffusion. For the intradiffusion between any pair of components $\bar{2i}$ and $\bar{2i} + 1$ the following equations apply where $D_{\bar{i}}^{\dagger}$ is the intradiffusion coefficient of component \bar{i} ¹⁵

$$-(\mathbf{J}_{\bar{2i}})_{\mathbf{v}} = D_{\bar{i}}^{\dagger} \nabla c_{\bar{2i}} \quad (i = 0, 1, \dots, n) \quad (8)$$

$$\nabla c_{\bar{2i}} = -\nabla c_{\bar{2i}+1} \quad (i = 0, 1, \dots, n) \quad (9)$$

$$(\mathbf{J}_{\bar{2i}})_{\mathbf{v}} = -(\mathbf{J}_{\bar{2i}+1})_{\mathbf{v}} \quad (i = 0, 1, \dots, n) \quad (10)$$

where for every other pair of components, i.e., $\bar{2j} \neq \bar{2i}$ and $\bar{2j} + 1 \neq \bar{2i} + 1$

$$(\mathbf{J}_{\bar{2j}})_{\mathbf{v}} = (\mathbf{J}_{\bar{2j}+1})_{\mathbf{v}} = \nabla c_{\bar{2j}} = c_{\bar{2j}+1} = 0 \quad (j = 0, 1, \dots, n) \quad (11)$$

When eq 8 and the equations obtained by inserting eq 10 into eq 8 are substituted in the left sides of eq 3a and 3b and eq 9 and 11 are applied, the following equations may be readily obtained

$$\begin{aligned} D_{\bar{i}}^{\dagger} &= (D_{\bar{2i}, \bar{2i}})_{\mathbf{v}} - (D_{\bar{2i}, \bar{2i}+1})_{\mathbf{v}} \\ &= -(D_{\bar{2i}+1, \bar{2i}})_{\mathbf{v}} + (D_{\bar{2i}+1, \bar{2i}+1})_{\mathbf{v}} \end{aligned} \quad (i = 1, 2, \dots, n) \quad (12)$$

Application of eq 9 and 11 to eq 3a and 3b rewritten for flows of components $\bar{2j}$ and $\bar{2j} + 1$ gives the equations

$$\begin{aligned} (D_{\bar{2j}, \bar{2i}})_{\mathbf{v}} &= (D_{\bar{2j}, \bar{2i}+1})_{\mathbf{v}} \\ (j = 1, 2, \dots, n; j \neq i; i = 1, 2, \dots, n) \end{aligned} \quad (13a)$$

$$\begin{aligned} (D_{\bar{2j}+1, \bar{2i}})_{\mathbf{v}} &= (D_{\bar{2j}+1, \bar{2i}+1})_{\mathbf{v}} \\ (j = 0, 1, \dots, n; j \neq i; i = 1, 2, \dots, n) \end{aligned} \quad (13b)$$

For the intradiffusion of the chemically equivalent components $\bar{0}$ and $\bar{1}$ where component $\bar{0}$ is the solvent

$$\begin{aligned} -(\mathbf{J}_{\bar{2j}})_{\mathbf{v}} &= -(\mathbf{J}_{\bar{2j}+1})_{\mathbf{v}} = (D_{\bar{2j}, \bar{1}})_{\mathbf{v}} \nabla c_{\bar{1}} = \\ (D_{\bar{2j}+1, \bar{1}})_{\mathbf{v}} \nabla c_{\bar{1}} &= 0 \quad (j = 1, 2, \dots, n) \end{aligned} \quad (14)$$

$$-(\mathbf{J}_{\bar{1}})_{\mathbf{v}} = (D_{\bar{1}, \bar{1}})_{\mathbf{v}} \nabla c_{\bar{1}} = D_{\bar{0}}^{\dagger} \nabla c_{\bar{1}} \quad (15)$$

Thus

$$\begin{aligned} (D_{\bar{k}, \bar{1}})_{\mathbf{v}} &= \delta_{k,1} D_{\bar{0}}^{\dagger} \quad (k = 1, 2, \dots, 2n + 1; \\ \delta_{k,1} &= 0, k \neq 1; \delta_{k,1} = 1, k = 1) \end{aligned} \quad (16)$$

Case of Constant Concentration Ratios. If homogeneous mixtures of each pair of chemically equivalent components are used to prepare the solutions for a diffusion experiment, the ratio of the two concentrations of each pair will be a constant independent of time and position for the experiment; otherwise, the diffusion process would partially separate a homogeneous mixture of the two components in contradiction to the assumption that they are chemically equivalent.

With constant concentration ratios the flows and concentration gradients may be written

$$(\mathbf{J}_{\bar{i}})_{\mathbf{v}} = (c_{\bar{i}}/c_{\bar{2i}})(\mathbf{J}_{\bar{2i}})_{\mathbf{v}} = (c_{\bar{i}}/c_{\bar{2i}+1})(\mathbf{J}_{\bar{2i}+1})_{\mathbf{v}} \quad (i = 0, 1, \dots, n) \quad (17)$$

$$\nabla c_{\bar{i}} = (c_{\bar{i}}/c_{\bar{2i}})\nabla c_{\bar{2i}} = (c_{\bar{i}}/c_{\bar{2i}+1})\nabla c_{\bar{2i}+1} \quad (i = 0, 1, \dots, n) \quad (18)$$

By applying eq 16 (with $k \neq 1$), 17, and 18 to eq 3a and 3b and equating terms with eq 1, the following expressions are easily found

$$\begin{aligned} (D_{\bar{2i}, \bar{2k}})_{\mathbf{v}} \left(\frac{c_{\bar{i}}}{c_{\bar{2i}}} \right) \left(\frac{c_{\bar{2k}}}{c_{\bar{k}}} \right) + (D_{\bar{2i}, \bar{2k}+1})_{\mathbf{v}} \left(\frac{c_{\bar{i}}}{c_{\bar{2i}}} \right) \left(\frac{c_{\bar{2k}+1}}{c_{\bar{k}}} \right) &= (D_{\bar{i}, \bar{k}})_{\mathbf{v}} \\ (i = 1, 2, \dots, n; k = 1, 2, \dots, n) \end{aligned} \quad (19a)$$

$$\begin{aligned} (D_{\bar{2i}+1, \bar{2k}})_{\mathbf{v}} \left(\frac{c_{\bar{i}}}{c_{\bar{2i}+1}} \right) \left(\frac{c_{\bar{2k}}}{c_{\bar{k}}} \right) + \\ (D_{\bar{2i}+1, \bar{2k}+1})_{\mathbf{v}} \left(\frac{c_{\bar{i}}}{c_{\bar{2i}+1}} \right) \left(\frac{c_{\bar{2k}+1}}{c_{\bar{k}}} \right) &= (D_{\bar{i}, \bar{k}})_{\mathbf{v}} \\ (i = 1, 2, \dots, n; k = 1, 2, \dots, n) \end{aligned} \quad (19b)$$

The following results may be obtained from eq 12, 13a, and 13b by substituting eq 19a and 19b and applying eq 5

$$\begin{aligned} (D_{\bar{2i}, \bar{2k}})_{\mathbf{v}} &= (D_{\bar{2i}, \bar{2k}+1})_{\mathbf{v}} + \delta_{i,k} D_{\bar{i}}^{\dagger} = \\ \frac{c_{\bar{2i}}}{c_{\bar{i}}} [(D_{\bar{i}, \bar{k}})_{\mathbf{v}} - \delta_{i,k} D_{\bar{i}}^{\dagger}] + \delta_{i,k} D_{\bar{i}}^{\dagger} \end{aligned} \quad (i = 1, 2, \dots, n; k = 1, 2, \dots, n) \quad (20a)$$

$$\begin{aligned} (D_{\bar{2i}+1, \bar{2k}+1})_{\mathbf{v}} &= (D_{\bar{2i}+1, \bar{2k}})_{\mathbf{v}} + \delta_{i,k} D_{\bar{i}}^{\dagger} = \\ \frac{c_{\bar{2i}+1}}{c_{\bar{i}}} [(D_{\bar{i}, \bar{k}})_{\mathbf{v}} - \delta_{i,k} D_{\bar{i}}^{\dagger}] + \delta_{i,k} D_{\bar{i}}^{\dagger} \end{aligned} \quad (i = 1, 2, \dots, n; k = 1, 2, \dots, n) \quad (20b)$$

where $\delta_{i,k}$ is again the Kronecker δ .

In finding expressions for diffusion coefficients in the flow equation for component $\bar{1}$, the case where the concentration ratio, $c_{\bar{0}}/c_{\bar{1}}$, is a constant independent of time and position is considered. By applying eq 13b and 16 and then eq 5 to eq 3b for component $\bar{1}$, the following equation may be obtained

$$-(\mathbf{J}_{\bar{1}})_{\mathbf{v}} = D_{\bar{0}}^{\dagger} \nabla c_{\bar{1}} + \sum_{k=1}^n (D_{\bar{1}, \bar{2k}})_{\mathbf{v}} \nabla c_{\bar{k}} \quad (21)$$

Equation 2 on substitution of eq 1 gives

$$\bar{V}_0(\mathbf{J}_0)_{\mathbf{v}} = - \sum_{i=1}^n \bar{V}_i(\mathbf{J}_i)_{\mathbf{v}} = \sum_{i=1}^n \sum_{k=1}^n \bar{V}_i(D_{\bar{i}, \bar{k}})_{\mathbf{v}} \nabla c_{\bar{k}} \quad (22)$$

(15) By definition the frame of reference for the intradiffusion coefficients coincides with the volume-fixed frame of reference and the subscript \mathbf{v} may be omitted. Also the intradiffusion coefficients are referred to here as properties of the chemically different components of eq 1 and 2 and are identified by the component numbers, i , used in those equations.

At constant pressure, the following equation will apply⁴

$$\sum_{i=0}^n \bar{V}_i \nabla c_i = 0 \quad (23)$$

Application of eq 18 and 23 to the term involving ∇c_i in eq 21 leads to the equation

$$(\mathbf{J}_i)_v = \sum_{k=1}^n \left(D_0^\dagger \frac{c_i \bar{V}_k}{c_0 \bar{V}_0} - (D_{i,2k})_v \right) \nabla c_k \quad (24)$$

By relating \mathbf{J}_0 to \mathbf{J}_i with eq 17, eq 22 may be written

$$(\mathbf{J}_i)_v = \sum_{k=1}^n \nabla c_k \sum_{i=1}^n \frac{c_i \bar{V}_i}{c_0 \bar{V}_0} (D_{i,k})_v \quad (25)$$

By equating coefficients of ∇c_k in eq 24 and 25, the following result may be obtained

$$\begin{aligned} (D_{i,2k})_v &= (D_{i,2k+1})_v = \\ &- \sum_{i=1}^n \frac{c_i \bar{V}_i}{c_0 \bar{V}_0} [(D_{i,k})_v - \delta_{i,k} D_0^\dagger] \\ &\quad (k = 1, 2, \dots, n) \end{aligned} \quad (26)$$

For actual experimental applications the ratio of the partial molal volumes would be related to density in grams per cubic centimeter and molecular weights by¹⁶

$$\frac{\bar{V}_i}{\bar{V}_0} = \frac{M_i - (\partial \rho / \partial c_i)_{T,P,c_k \neq 0,i}}{M_0} \quad (i = 1, 2, \dots, n) \quad (27)$$

Equations 16, 20a, 20b, 26, and 27 permit the diffusion coefficients $(D_{i,k})_v$ for the expanded system to be calculated from the intradiffusion coefficients, D_0^\dagger , and the diffusion coefficients, $(D_{i,k})_v$, for the unexpanded system of chemically different components; the molecular weights and concentration derivatives of density are also needed in eq 27. These equations give a better understanding of diffusion coefficients in multicomponent systems. For example, eq 16 suggests that if component 1 in a multicomponent system is similar to but not identical with the solvent with regard to properties of diffusion, then the cross-term diffusion coefficients, $(D_{k,1})_v$, may be expected to be small although not zero. Of course, the numbering of components becomes arbitrary and the cross-term diffusion coefficients, $(D_{k,j})_v$, would be expected to be small if it were component j that was similar to the solvent. Although all of the intradiffusion coefficients are assumed to be known for these equations, some of the $(D_{i,k})_v$ may be calculated when fewer of the intradiffusion coefficients are known.

Expressions for Onsager's Coefficients

General Equations. From the theory of the thermodynamics of irreversible processes as presented by Onsager,⁴ the isothermal diffusion process considered in the last section may be described by the linear laws for chemically different components as

$$\mathbf{X}_i = \sum_{k=0}^n R_{i,k} \mathbf{J}_k \quad (i = 0, 1, \dots, n) \quad (28)$$

Here, \mathbf{X}_i is a generalized force that is applied to component i and the terms $R_{i,k}$ are thermodynamic transport coefficients.^{17,18} In the case of isothermal diffusion

$$\mathbf{X}_i = -\nabla \mu_i \quad (i = 0, 1, \dots, n) \quad (29)$$

where $\nabla \mu_i$ is the gradient of chemical potential of component i . Onsager includes the following additional relations in his description

$$\sum_{k=0}^n R_{i,k} c_k = 0 \quad (i = 0, 1, \dots, n) \quad (30)$$

$$R_{i,k} = R_{k,i}$$

$$(i = 0, 1, \dots, n; k = 0, 1, \dots, n) \quad (31)$$

Because of eq 30 the coefficients $R_{i,k}$ will be independent of the frame of reference for the flows¹⁹ and with this description all of the coefficients $R_{i,k}$ will be unique. Equations 31 are the Onsager reciprocal relations (ORR).

As in the preceding development for diffusion coefficients, each component will be recognized as two chemically equivalent components which may be separately identified from differences that do not alter the rate of diffusion of the molecules. The component numbered i then becomes components numbered $2i$ and $2i + 1$. In this case diffusion may be described by

$$\begin{aligned} \mathbf{X}_{2i} &= \sum_{k=0}^n R_{2i,2k} \mathbf{J}_{2k} + R_{2i,2k+1} \mathbf{J}_{2k+1} \\ &\quad (i = 0, 1, \dots, n) \end{aligned} \quad (32a)$$

$$\begin{aligned} \mathbf{X}_{2i+1} &= \sum_{k=0}^n R_{2i+1,2k} \mathbf{J}_{2k} + R_{2i+1,2k+1} \mathbf{J}_{2k+1} \\ &\quad (i = 0, 1, \dots, n) \end{aligned} \quad (32b)$$

where

$$\mathbf{X}_i = -\nabla \mu_i \quad (i = 0, 1, \dots, 2n + 1) \quad (33)$$

$$\sum_{k=0}^{2n+1} R_{i,k} c_k = 0 \quad (i = 0, 1, \dots, 2n + 1) \quad (34)$$

(16) This expression may be derived by applying the equations $\sum_{i=0}^n \bar{V}_i c_i = 1$ and $\sum_{i=0}^n M_i c_i = \rho$ to eq A-7 of ref 7 when the units of that equation are converted to moles per cubic centimeter. It should be emphasized that $\rho = f(c_1, \dots, c_n)$ when determining $\partial \rho / \partial c_i$.

(17) The term friction coefficient was applied to the quantities $R_{i,k}$ by Laity.¹⁸ Actually, as shown by Laity's development, it is the terms $-R_{i,k}$ with $i \neq k$ that are closely related to the concept of friction between components i and k .

(18) R. W. Laity, *J. Phys. Chem.*, **63**, 80 (1959).

(19) The flows relative to two arbitrary frames of reference, A and B, will be related to each other by the equation $(\mathbf{J}_i)_A = (\mathbf{J}_i)_B + c_i \mathbf{v}_{BA}$ where \mathbf{v}_{BA} is the velocity of frame B relative to frame A. If this relation is substituted into eq 28, the sum of terms associated with \mathbf{v}_{BA} is zero according to eq 30.

$$R_{i,\bar{k}} = R_{k,\bar{i}} \quad (i = 0, 1, \dots, 2n+1; k = 0, 1, \dots, 2n+1) \quad (35)$$

The chemical potentials are related to the concentrations by the equations

$$\mu_i = (\mu_i)^0 + RT \ln \gamma_i c_i \quad (i = 0, 1, \dots, n) \quad (36)$$

$$\mu_{\bar{i}} = (\mu_{\bar{i}})^0 + RT \ln \gamma_{\bar{i}} c_{\bar{i}} \quad (i = 0, 1, \dots, 2n+1) \quad (37)$$

where γ_i is the activity coefficient of component i (or $\gamma_{\bar{i}}$ of \bar{i}). Here, R is the gas constant and T is the absolute temperature. Because components $2i$ and $2i+1$ are chemically equivalent to each other and to i , it is evident that

$$\gamma_i = \gamma_{2i} = \gamma_{2i+1} \quad (i = 0, 1, \dots, n) \quad (38)$$

Case of Intradiffusion. In obtaining expressions which relate the coefficients $R_{i,\bar{k}}$ to the coefficients $R_{i,k}$ and D_i^\dagger , the case of intradiffusion will first be considered. For the process of intradiffusion, eq 8-11 apply. The activity coefficients become constants and for each pair of intradiffusing components the gradients of chemical potential may be written

$$\nabla \mu_{2i} = \frac{RT}{c_{2i}} \nabla c_{2i} \quad (i = 0, 1, \dots, n) \quad (39a)$$

$$\nabla \mu_{2i+1} = \frac{RT}{c_{2i+1}} \nabla c_{2i+1} \quad (i = 0, 1, \dots, n) \quad (39b)$$

The left sides of eq 32a and 32b may be expressed in terms of concentration gradients by means of eq 33, 39a, and 39b, and the J_{2k+1} on the right sides may be replaced by J_{2k} with eq 10. Consideration separately of the intradiffusion of each pair of components $2k$ and $2k+1$ and application of eq 8 for that pair and eq 11 for the other components leads to the relations

$$R_{2i,2k} - R_{2i,2k+1} = \frac{\delta_{i,k} RT}{c_{2i} D_i^\dagger} \quad (i = 0, 1, \dots, n; k = 0, 1, \dots, n) \quad (40a)$$

$$R_{2i+1,2k+1} - R_{2i+1,2k} = \frac{\delta_{i,k} RT}{c_{2i+1} D_i^\dagger} \quad (i = 0, 1, \dots, n; k = 0, 1, \dots, n) \quad (40b)$$

Case of Constant Concentration Ratios. Equations 40a and 40b provide half the information necessary to relate the coefficients $R_{i,\bar{k}}$ to the coefficients $R_{i,k}$ and D_i^\dagger . The rest of the information is obtained by considering the experimental case where the ratios of the concentrations of the chemically equivalent components are constants independent of time or position. For this case eq 17 and 18 apply and eq 18 and 36-38 may be used to show that

$$\nabla \mu_i = \nabla \mu_{2i} = \nabla \mu_{2i+1} \quad (i = 0, 1, \dots, n) \quad (41)$$

By applying eq 17, 33, and 41 to eq 32a and 32b and equating the resulting terms with terms in eq 28 and 29, the following equations are obtained.²⁰

$$R_{2i,2k} c_{2k} + R_{2i,2k+1} c_{2k+1} = R_{i,k} c_k \quad (i = 0, 1, \dots, n; k = 0, 1, \dots, n) \quad (42a)$$

$$R_{2i+1,2k} c_{2k} + R_{2i+1,2k+1} c_{2k+1} = R_{i,k} c_k \quad (i = 0, 1, \dots, n; k = 0, 1, \dots, n) \quad (42b)$$

Finally eq 40a, 40b, 42a, and 42b may be solved to yield the results

$$\begin{aligned} R_{2i,2k+1} &= R_{2i,2k} - (\delta_{i,k} RT / c_{2i} D_i^\dagger) \\ &= R_{i,k} - (\delta_{i,k} RT / c_i D_i^\dagger) \end{aligned} \quad (i = 0, 1, \dots, n; k = 0, 1, \dots, n) \quad (43a)$$

$$\begin{aligned} R_{2i+1,2k} &= R_{2i+1,2k+1} - (\delta_{i,k} RT / c_{2i+1} D_i^\dagger) \\ &= R_{i,k} - (\delta_{i,k} RT / c_i D_i^\dagger) \end{aligned} \quad (i = 0, 1, \dots, n; k = 0, 1, \dots, n) \quad (43b)$$

These equations show that the cross-term coefficients $R_{i,k}$ with $i \neq k$ in eq 28 are equal to the four coefficients $R_{2i,2k}$, $R_{2i+1,2k}$, $R_{2i,2k+1}$, and $R_{2i+1,2k+1}$ in eq 32a and 32b. This is consistent with the concept that the coefficients $-R_{i,k}$ with $i \neq k$ represent a measure of friction between molecules of type i and k ; such friction should be dependent on the chemical environment of the system and not on the manner in which the chemically equivalent forms of the components are identified. The coefficients $R_{2i,2i+1}$ and $R_{2i+1,2i}$ of eq 32a and 32b have no counterpart in eq 28 and are related to "friction" between chemically equivalent molecules. The terms $R_{i,i}$ in eq 28 are shown by eq 30 to be an average "friction" of component i with all of the other components in the system.

Thermodynamic equations in which flows are equated to the sum of the products of transport coefficients and generalized driving forces have been commonly used in the description of diffusion processes.^{7,8} The procedures used in this article could be applied to finding expanded descriptions in terms of the intradiffusion coefficients for these cases. This was done for the special case considered in ref 3 and it is apparent that the general expressions for this description would not have the simplicity of eq 43a and 43b.

Acknowledgments. The author wishes to thank Dr. L. J. Gosting for his many helpful suggestions in the preparation of this article. Special thanks go to Mrs. Sharon R. Albright for her help in the preparation of the manuscript.

(20) Since these equations are independent of frame of reference, the flows, J_i , are all independent.

d² and d⁸ Configurations in an Axial Model Field

by Donald R. Scott¹

Department of Chemistry, Texas Technological College, Lubbock, Texas

and F. A. Matsen

Molecular Physics Group, The University of Texas, Austin, Texas (Received January 10, 1967)

The splitting of the electronic energy levels of the d² and d⁸ free ions by an axial (C_n, n > 4) model field is investigated. The model-field matrix elements are tabulated, and the resulting eigenvalues are listed. The electronic ground states and spectra of d² and d⁸ axial compounds are discussed in general, and those of Ti(C₅H₅)₂, V(C₅H₅)₂⁺, and Ni(C₅H₅)₂ are discussed in detail.

Introduction

The effect of ligands on the electronic properties of transition metal ions has been studied by two methods: molecular-orbital theory and model-field theory.² The former approach invokes both ligand and metal orbitals, while the latter invokes only metal orbitals. A model field is one which reflects accurately the symmetry of the field in that portion of Hilbert space which is under study.³ Model fields are expressed in terms of parameters which are determined from experimental data and which permit some accommodation for the neglect of configuration interaction⁴ and for metal-ligand electron interchange. In the early development of the theory, the parameters were evaluated by representing the ligands as point charges or point dipoles. This so-called crystal-field theory was generally unsuccessful when used nonempirically and has been replaced by the more realistic model-field theory.

In this paper the splitting of the d² and d⁸ free-ion levels by an axial model field is investigated.⁵ The results are used to discuss the ground states and optical spectra of axial d² and d⁸ compounds. Metallocenes of the types M(C_nH_n)X, where X = NO or C_nH_n, have axial symmetry C_n; and if X is C_nH_n, some additional symmetry. Within a dⁿ configuration, the model fields have the same form for all these C_n compounds, n > 4. The effects of other symmetries, e.g., inversion, can be ignored.

Axial Model Field. The general expansion of a model field is

$$V_{MF} = \sum_K \sum_Q \lambda_Q^K V_Q^K$$

where V_Q^K are the components (spherical harmonics) of a tensor operator of rank K and λ_Q^K are expansion coefficients. We require that the model field Hamiltonian, V_{MF} , commute with all symmetry operations, G_i , of point group C_n

$$[V_{MF}, G_i] = 0$$

for $G_i \in C_n$. Generally

$$G_i V_Q^K G_i^{-1} = \sum_{Q'}^{K} [G_i]^{K}_{Q'Q} V_{Q'}^K$$

where G_i^{-1} is the inverse of G_i , and $[G_i]^{K}_{Q'Q}$ are the matrix elements of the representation of G_i . But for C_n groups

$$[G_i]^{K}_{Q'Q} = \delta_{Q'Q} \exp \frac{2\pi i Q}{n}$$

Therefore, V_{MF} and G_i commute if, and only if

$$\exp \frac{2\pi i Q}{n} = 1$$

and

$$Q = 0, \pm n, \pm 2n, \dots$$

The representation of V_Q^K in the $|dM\rangle$ (free-ion kets) basis is by the Wigner-Eckart theorem

$$\langle dM | V_Q^K | dM' \rangle = (-1)^{2-M} \begin{pmatrix} 2 & K & 2 \\ \bar{M} & Q & M' \end{pmatrix} \langle d || V^K || d \rangle$$

where $\bar{M} = -M$, $\begin{pmatrix} 2 & K & 2 \\ \bar{M} & Q & M' \end{pmatrix}$ is a 3-j symbol, and $\langle d || V^K || d \rangle$ is the reduced matrix element.⁶ From the

(1) Materials Sciences Laboratory, Lockheed-Georgia Co., Marietta, Ga.

(2) Model-field theory is commonly referred to as crystal- or ligand-field theory in its applications to metal ions.

(3) J. S. Griffith, *J. Chem. Phys.*, **41**, 576 (1964); O. R. Plummer and F. A. Matsen, to be published.

(4) K. Rajnak and B. G. Wybourne, *J. Chem. Phys.*, **41**, 565 (1964).

(5) Previous studies on this subject are: (a) T. S. Piper and R. L. Carlin, *ibid.*, **33**, 1208 (1960); (b) J. T. Hougen, G. E. Leroi, and J. C. James, *ibid.*, **34**, 1670 (1961); (c) R. A. Berg and O. Sinanoglu, *ibid.*, **32**, 1082 (1960); (d) C. K. Jorgensen, *Mol. Phys.*, **7**, 417 (1963); (e) C. W. DeKock and D. M. Gruen, *J. Chem. Phys.*, **44**, 4387 (1966); **46**, 1096 (1967).

(6) B. R. Judd, "Operator Techniques in Atomic Spectroscopy," McGraw-Hill Book Co., Inc., New York, N. Y., 1963, p 42.

Table I: Axial Model Field Matrix Elements for d² and d⁸^a

<i>LM</i>	<i>L'M'</i>	<i>D_s</i>	<i>D_t</i>	<i>LM</i>	<i>L'M'</i>	<i>D_s</i>	<i>D_t</i>
44	44	-4	-2	31	31	3/5	1
43	43	-1	3	31	11	$-\frac{4}{5}(\sqrt{6})$	$\sqrt{6}$
42	42	8/7	11/7	30	30	4/5	6
42	22	$-\frac{4}{7}\sqrt{3}$	$-\frac{30}{7}\sqrt{3}$	30	10	-12/5	-4
41	41	17/7	-9/7	22	22	6/7	-4/7
41	21	$-\frac{4}{7}(\sqrt{6})$	$\frac{5}{7}(\sqrt{6})$	21	21	-3/7	16/7
40	40	20/7	-18/7	20	20	-6/7	-24/7
40	20	$-\frac{24}{35}(\sqrt{5})$	$\frac{20}{7}(\sqrt{5})$	20	00	$-\frac{2}{5}(\sqrt{70})$	0
40	00	0	$-2\sqrt{14}$	11	11	7/5	0
33	33	-1	3	10	10	-14/5	0
32	32	0	-7				

^a Numbers listed under *D_s* and *D_t* are the coefficients which correspond to *a* and *b* in $\langle LM|V_{MF}(1) + V_{MF}(2)|L'M'\rangle = aD_s + bD_t$ for d². $\langle LM|V_{MF}(1) + V_{MF}(2)|L'M'\rangle = \langle L\bar{M}|V_{MF}(1) + V_{MF}(2)|L'\bar{M}'\rangle$. Matrix elements for d⁸ are obtained by changing the signs of the coefficients of *D_s* and *D_t* for the d² matrix element. Zero matrix elements not listed.

properties of the 3-j symbols, $\begin{pmatrix} 2 & K & 2 \\ \bar{M} & Q & M' \end{pmatrix}$ is nonzero only if $K < 5$. Since $\langle d||V^K||d\rangle$ is zero for K odd, $K = 0, 2, 4$. Furthermore, $|Q| \leq K \leq 4$, and, from above, $Q = 0, \pm n, \pm 2n, \dots$ for C_n . Therefore, $|Q| \leq 4$; and for C_n ($n > 4$), $Q = 0$. The effective and exact model field for C_n fields ($n > 4$) is therefore (neglecting V_0^0 , which contributes nothing to the splitting of the levels)

$$V_{MF} = \lambda_0^2 V_0^2 + \lambda_0^4 V_0^4 \quad C_n (n > 4)$$

For $Q = 0$, the 3-j symbol $\begin{pmatrix} 2 & K & 2 \\ \bar{M} & Q & M' \end{pmatrix}$ is zero for $M \neq M'$. Consequently, the axial model-field potential is diagonal in the $|dM\rangle$ representation with eigenvalues

$$E(\sigma) = 2D_s - 6D_t \quad M = 0$$

$$E(\pi) = D_s + 4D_t \quad M = \pm 1$$

$$E(\delta) = -2D_s - D_t \quad M = \pm 2$$

where $D_s = (-1/\sqrt{70})\langle d||V^2||d\rangle$ and $D_t = (-1/3\sqrt{70})\langle d||V^4||d\rangle$. Since the model field is the same for any $n > 4$, we have used the C_∞ designation for states.

The d⁹ eigenvalues may be obtained from the d¹ values by treating d⁹ as a d¹ positive hole configuration. Changing the signs of *D_s* and *D_t* yields

$$E(\sigma^1\pi^4\delta^4) = -2D_s + 6D_t$$

$$E(\sigma^2\pi^3\delta^4) = D_s - 4D_t$$

$$E(\sigma^2\pi^4\delta^3) = 2D_s + D_t$$

Two- and Eight-Electron Systems. The spin-free model field Hamiltonian for the two-electron system is

$$V_{MF} = V_{MF}(1) + V_{MF}(2) + \frac{e^2}{r_{12}}$$

We take the free ion kets, $|d^2, LM\rangle$, as basis kets. The kets with $L = 0, 2, 4$ (S, D, G) are symmetric to electron interchange (singlets), and those with $L = 1, 3$ (P, F) are antisymmetric (triplets). The coulombic interaction is diagonal in this basis, and the eigenvalues are expressed in terms of Racah parameters. To evaluate the model field matrix elements, we note that

$$\begin{aligned} \langle d^2, LM|V_0^K(i)|d^2, L'M'\rangle = \\ (-1)^{L-M} \begin{pmatrix} LK & L' \\ \bar{M} & OM' \end{pmatrix} \langle d^2, L||V^K(i)||d^2, L'\rangle \end{aligned}$$

where

$$\begin{aligned} \langle d^2, L||V^K(1)||d^2, L'\rangle = (-1)^{L'+K} [(2L+1) \times \\ (2L'+1)]^{1/2} \begin{Bmatrix} L & K & L' \\ 2 & 2 & 2 \end{Bmatrix} \langle d||V^K||d \rangle \end{aligned}$$

and

$$\langle d^2, L||V^K(2)||d^2, L'\rangle = (-1)^{L+L'} \langle d^2, L||V^K(1)||d^2, L'\rangle.$$

It follows that the matrix elements $\langle d^2, LM||V_0^K(1) + V_0^K(2)||d^2, L'M'\rangle$ are zero unless $M = M'$ (imposed by the axial field) and $L + L'$ is even. Since the spin-free Hamiltonian commutes with the group of permutations on the electron coordinates, the symmetric states (singlets) do not interact with the antisymmetric states (triplets). The model field matrix elements are listed in Table I.

The dimension of the d² representation is 25×25 . However, the axial symmetry of the model field and the zero matrix elements between even and odd L kets results in a reduction to one 3×3 matrix: $^1S(\sigma) \cdot ^1D(\sigma) \cdot ^1G(\sigma)$; four 2×2 matrices: $^3F(\sigma) \cdot ^3P(\sigma)$; $^3F(\pi) \cdot ^3P(\pi)$, $^1G(\pi) \cdot ^1D(\pi)$, $^1G(\delta) \cdot ^1D(\delta)$; and four 1×1 matrices: $^1G(\gamma)$, $^1G(\phi)$, $^3F(\delta)$, $^3F(\phi)$. The eigenvalues are listed on the next page.

$${}^3F(\phi) = -Ds + 3Dt + A - 8B$$

$${}^3F(\delta) = -7Dt + A - 8B$$

$${}^3F(\pi) \cdot {}^3P(\pi) = \frac{2Ds + Dt + 2A - B}{2} \pm \frac{[16Ds^2 - 40DsDt + 24BDs - 30BDt + 225B^2 + 25Dt^2]^{1/2}}{2}$$

$${}^3F(\sigma) \cdot {}^3P(\sigma) = \frac{-2Ds + 6Dt + 2A - B}{2} \pm \frac{[36Ds^2 + 120DsDt - 108BDs - 180BDt + 100Dt^2 + 225B^2]^{1/2}}{2}$$

$${}^1G(\gamma) = -4Ds - 2Dt + A + 4B + 2C$$

$${}^1G(\phi) = -Ds + 3Dt + A + 4B + 2C$$

$${}^1G(\delta) \cdot {}^1D(\delta) = \frac{2Ds + Dt + 2A + B + 4C}{2} \pm \frac{[4Ds^2 + 225Dt^2 + 60DsDt + 4BDs + 30BDt + 49B^2]^{1/2}}{2}$$

$${}^1G(\pi) \cdot {}^1D(\pi) = \frac{2Ds + Dt + 2A + B + 4C}{2} \pm \frac{[16Ds^2 + 25Dt^2 - 40DsDt + 40BDs - 50BDt + 49B^2]^{1/2}}{2}$$

$${}^1G(\sigma) \cdot {}^1D(\sigma) \cdot {}^1S(\sigma) =$$

$$\begin{vmatrix} \frac{20}{7}Ds - \frac{18}{7}Dt + A + 4B + 2C - \epsilon & -\frac{24}{35}\sqrt{5}Ds + \frac{20}{7}\sqrt{5}Dt & -2\sqrt{14}Dt \\ -\frac{24}{35}\sqrt{5}Ds + \frac{20}{7}\sqrt{5}Dt & -\frac{6}{7}Ds - \frac{24}{7}Dt + A - 3B + 2C - \epsilon & -\frac{2\sqrt{70}}{5}Ds \\ -2\sqrt{14}Dt & -\frac{2\sqrt{70}}{5}Ds & A + 14B + 7C - \epsilon \end{vmatrix} = 0$$

The d^3 eigenvalues or matrices may be obtained from these by changing the signs of all model field matrix elements. The e^2/r_{12} terms are left unchanged.

Results and Discussion

d^2 . The splitting of the d^2 free-ion levels under an axial model field is illustrated in Figure 1 as a function of Ds/B and B/Ds , a measure of field strength. It should be noted that the mode of presentation is different from and clearer than the conventional Orgel plot. The plotted curves were calculated for $C = 4B$, a value approximately correct for Ti^{2+} and V^{3+} free ions, and for $Dt/Ds = 0.65$. The correlations between the free-ion levels and the strong-field configurations are not unique, since the relative positions of the strong field configurations depend upon the values of Ds and Dt .

The detailed positions of the various levels depend

upon the particular values of Ds , Dt , B , and C . However, examination of plots of the d^2 levels computed with $C = 4B$ and $Dt/Ds = 0 - 1.0$ leads to some generalizations. (See Figure 1.) For these parameter values, a 3F level will be the ground state except for very strong fields; *e.g.*, for $Ds = Dt$ and $C = 4B$, the ${}^1D(\sigma)$ state becomes the ground state at $B/Ds \cong 0.04$. The ${}^1D(\sigma)$ state drops below the triplet states because the σ^2 configuration producing the ${}^1D(\sigma)$ state is below the $\sigma\delta$ and δ^2 configurations for these parameter values.

Usually, the ${}^3F(\delta)$ state is the lowest triplet state for weak and intermediate fields ($B/Ds > 0.1$, $C = 4B$). However, for $Dt = 0$, ${}^3F(\phi)$ is lowest for weak and intermediate fields ($B/Ds > 0.3$, $C = 4B$); and ${}^3F(\sigma)$ is lowest for stronger fields since the δ^2 configuration is the lowest one for this set of parameters. The ${}^3F(\sigma)$ level is also the ground state for $Dt/Ds \cong 0.6$ and $C = 4B$ for strong fields ($B/Ds < 0.1$). Since the values of Ds , Dt , B , and C cited are reasonable ones (the very strong field compounds may be the exceptions), most d^2 axial field compounds should have triplet ground states.

An example of an axial field d^2 compound is $V(C_5H_5)_2^+$. Reference to Figure 1 shows that for a Dt/Ds ratio of 0.65, similar to that found for ferrocene^{7a,b} and a B/Ds ratio of 0.08, either the ${}^3\Sigma^-$ or the ${}^3\Delta$ state could be the ground state. The experimental magnetic moment of $V(C_5H_5)_2^+$ is 2.86 ± 0.06 B.M.,⁸ in good agreement with a "spin only" calculation of 2.83 B.M.

for two unpaired electrons. On the basis of these limited data, the ground state for this complex appears to be the ${}^3\Sigma^-[{}^3F(\sigma)]$ level, since the other triplet states would be expected to contribute orbital angular momentum to the magnetic moment. A ${}^3\Sigma^-$ ground state indicates a very strong field compound, but the fact that the $C_5H_5^-$ ligands do present a very strong field is shown in the experimentally determined B/Ds ratio of 0.08, found for ferrocene by analysis of the electronic spectrum.^{7a,b}

Other strong-field d^2 complexes are titanocene, $Ti(C_5H_5)_2$, and the recently synthesized⁹ zirconocene, $Zr(C_5H_5)_2$. Titanocene was originally stated to be

(7) (a) D. R. Scott and R. S. Becker, *J. Organometal. Chem.*, **4**, 409 (1965); (b) D. R. Scott, Ph.D. Dissertation, University of Houston, Houston, Texas, 1965; (c) D. R. Scott, *J. Organometal. Chem.*, **6**, 429 (1966).

(8) E. O. Fischer and U. Piesbergen, *Z. Naturforsch.*, **11b**, 758 (1956).

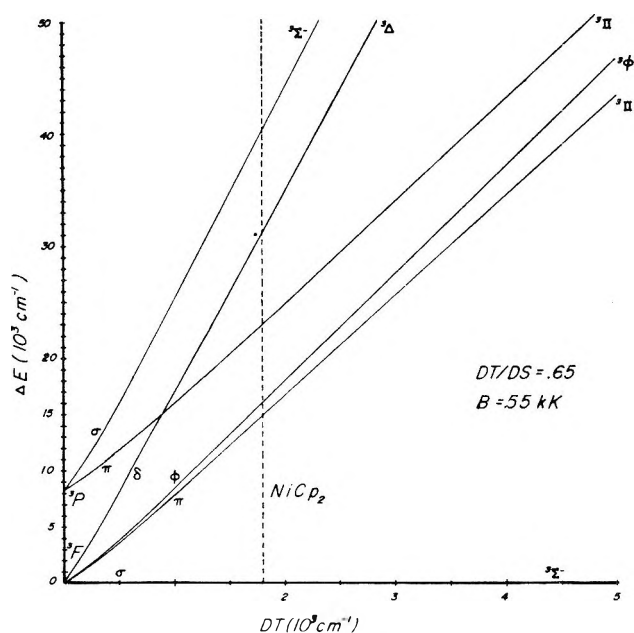


Figure 3. Triplet levels of d^8 in an axial model field.

Acknowledgments. We wish to thank Dr. Lawrence Ellzey, of the Molecular Physics Group, for many helpful discussions, and Dr. Ed Rodriguez for programming aid at various times. The eigenvalues for the graphs

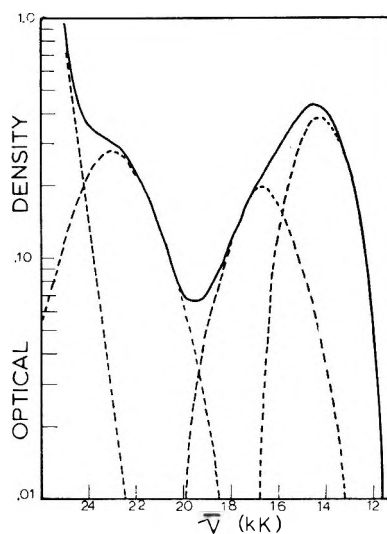


Figure 4. Ligand field bands of nickelocene.

were calculated on the CDC 1604 computer at the University of Texas. This research was supported in part by a grant from the Petroleum Research Fund, administered by the American Chemical Society, to D. R. Scott, and by the Robert A. Welch Foundation of Houston, Texas.

Spin-Free Quantum Chemistry.¹ V. Spin Density

by F. A. Matsen and A. A. Cantu

Molecular Physics Group, The University of Texas, Austin, Texas 78712 (Received April 24, 1967)

In the spin-free formulation of quantum chemistry, the eigenstates of a system are spinless and are characterized by partitions $[2^p, 1^{N-2p}]$ which identify certain irreducible representations of the permutation group and which also identify the spin states by $S = N/2 - p$. We define a spin-free unpaired electron density operator from which the unpaired electron density in a particular permutation (spin) state can be computed. The integral of the unpaired electron density is equal to the valence of the system. Rules are determined for evaluating matrix elements of this operator. We consider the helium ($1s2s$) 3S atom, the lithium ($1s^22s$) 2S atom, and the methyl and allyl radicals. The unpaired electron density at a nucleus can be determined from the isotropic magnetic hyperfine interaction. When used in this way, the unpaired electron density is called "spin density." The fact that the hyperfine interaction constant is proportional to the spin-free unpaired electron density implies that spin is not a dynamical variable in the computation of hyperfine interaction constants.

I. Introduction

In this paper, we introduce the *unpaired electron density*, a spin-free concept related to chemical valence. In section IV and Appendix B we prove that the unpaired electron density is identical with the spin density employed in the discussion of hyperfine interactions. Thus we show that spin densities can be obtained in a spin-free formulation. This proves that spin does not have a dynamical role in determining hyperfine interaction constants just as it has no dynamical role in singlet-triplet splittings. In sections V through VIII, we present a spin-free discussion of the hyperfine-interactions for several chemical systems which have been previously treated in the conventional spin formulation. This is done to illustrate the method and to see how certain effects which have previously been attributed to spin dynamics arise merely from the permutational symmetry of the system wavefunction. We begin with a brief review of spin-free quantum chemistry.²

A spin-free electronic Hamiltonian for an N -electron system is

$$H = \sum_{i=1}^N H_i + \sum_{i<j=1}^N \frac{e^2}{r_{ij}} \quad (1.1)$$

where H_i is a one-electron operator and e^2/r_{ij} is the coulombic energy between electrons i and j . Now

$$[H, P] = 0 \text{ for } P \in S_N \quad (1.2)$$

where S_N is the group of permutations on the spin-free coordinates of the electrons. As a consequence of (1.2), the eigenstates of the system lie in spaces called *permutation states* each characterized by the partition $[\lambda]$ of N . The Pauli exclusion principle excludes all permutation states except those with

$$[\lambda] = [2^p, 1^{N-2p}] \quad 0 \leq p \leq \frac{N}{2} \quad (1.3)$$

The allowed states can also be characterized by the following indices: the *pair number*, p ; the *multiplicity*

$$m = N - 2p + 1 \quad (1.4)$$

the *spin*

$$S = \frac{N}{2} - p \quad (1.5)$$

the *valence*

$$v = m - 1 = 2S = N - 2p \quad (1.6)$$

The last of these gives the number of unpaired electrons.

An N -electron primitive ket $|\gamma\rangle$ can be projected into the $[\lambda]$ th permutation state by the matrix basis

$$\{e_{rs}^{[\lambda]} : r, s = 1, \dots, f^{[\lambda]}\} \quad (1.7)$$

of the invariant subalgebra $A^{[\lambda]}$ of the $(N!)$ dimensional permutation algebra A_N . A linearly independent portion of the projected set

$$\{e_{rs}^{[\lambda]}|\gamma\rangle \equiv |\gamma; [\lambda]rs\rangle : r, s = 1, \dots, f^{[\lambda]}\} \quad (1.8)$$

is used for finding a matrix of H .³ For a unitary matrix basis we find that (paper I²)

(1) Supported by the Robert A. Welch Foundation, Houston, Texas.

(2) For more details, see paper I: F. A. Matsen, "Advances in Quantum Chemistry," Vol. I, P. O. Lowdin, Ed., Academic Press Inc., New York, N. Y., 1964; paper II: F. A. Matsen, *J. Phys. Chem.*, **68**, 3282 (1964); paper III: F. A. Matsen, A. A. Cantu, and R. D. Poshusta, *ibid.*, **70**, 1558 (1966); paper IV: F. A. Matsen, *ibid.*, **70**, 1568 (1966).

(3) Here the permutations in the expanded form of the matrix basis permute the electron coordinates of $|\gamma\rangle$.

$$\langle \gamma; [\lambda]rs | H | \gamma; [\lambda']tu \rangle = \delta^{[\lambda][\lambda']} \delta_{r,t} \langle \gamma; [\lambda]rs | H | \gamma; [\lambda]ru \rangle \quad (1.9)$$

$$= \delta^{[\lambda][\lambda']} \delta_{r,t} \langle \gamma | H | \gamma; [\lambda]su \rangle \quad (1.10)$$

Thus since the r index in $|\gamma; [\lambda]rs\rangle$ is just a degeneracy index, one needs only work with the set

$$\{|\gamma; [\lambda]rs\rangle: r = \text{fixed}, s = 1, \dots, f^{[\lambda]}\} \quad (1.11)$$

This spans a subspace, $V(\gamma, [\lambda], r)$ —space, of the $[\lambda]$ th permutation state. Since the matrix of H in $V(\gamma, [\lambda], r)$ is independent of r , we choose $r = 1$. Thus one needs only project $|\gamma\rangle$ with the unitary matrix basis

$$\{e_{1s}^{[\lambda]}: s = 1, \dots, f^{[\lambda]}\} \quad (1.12)$$

which spans a subalgebra⁴ $A_1^{[\lambda]}$ of $A^{[\lambda]}$. For the allowed $[\lambda]$'s, a second basis for $A_1^{[\lambda]}$ is the *structure basis*

$$\{\kappa^{[\lambda]} \equiv \kappa: \kappa = \text{I, II, } \dots, f^{[\lambda]}\} \quad (1.13)$$

This basis is easier to construct and it relates directly to chemical structure. For an allowed $[\lambda]$

$$f^{[\lambda]} = \frac{N!(N - 2p + 1)}{p!(N - p + 1)!} \quad (1.14)$$

II. The Structure Kets

The structure basis (1.13) is used to project a primitive ket into a subspace, $V(\gamma; [\lambda], 1)$, of the allowed $[\lambda]$ th permutation state. A normalized projected ket, called a (pure) *structure ket*, is

$$|\gamma; \kappa^{[\lambda]}\rangle \equiv |\gamma; \kappa\rangle \equiv \frac{\kappa}{\sqrt{C}} |\gamma\rangle \quad (2.1)$$

where

$$C = \langle \gamma | \kappa^\dagger \kappa | \gamma \rangle \quad (2.2)$$

For $|\gamma\rangle$ an orbital product of distinct orthonormal orbitals

$$C = 2^p (N - p)! p! \quad (2.3)$$

The structure basis element $\kappa^{[\lambda]} \equiv \kappa$, called a structure operator is obtained² from a Young tableau $T_\kappa^{[\lambda]}$ which is constructed from a particular (canonical) pair diagram $D_\kappa^{[\lambda]}$ (see Table I)

$$D_\kappa^{[\lambda]} \longrightarrow T_\kappa^{[\lambda]} \longrightarrow \kappa^{[\lambda]} \quad (2.4)$$

Only $f^{[\lambda]}$ (1.14) of the structure operators are linearly independent. A particular set of such structure projectors which we call the structure basis is that associated with the set of *canonical* diagrams $D_\kappa^{[\lambda]}$. Paper I has an aufbau procedure for obtaining these. For a $|\gamma\rangle$ not invariant under any permutation of electron coordinates, e.g., an orbital product of distinct orbitals, there result $f^{[\lambda]}$ linearly independent (pure) structure kets on projection with the structure basis. For κ' a noncanonical structure operator

$$\kappa' = \sum_{\kappa \in \text{canonical}}^{f^{[\gamma]}} a_{\kappa\kappa'} \kappa \quad (2.5)$$

and for $|\gamma\rangle$ not invariant under any permutation of electron coordinates

$$|\gamma; \kappa'\rangle = \sum_{\kappa \in \text{canonical}}^{f^{[\lambda]}} a_{\kappa\kappa'} |\gamma; \kappa\rangle \quad (2.6)$$

This is known as Rumer's rule.

While the techniques outlined here are applicable to any type of primitive ket, we will for simplicity restrict our discussion mainly to orbital products (atomic or molecular)

$$|\gamma\rangle = |ab \cdots n\rangle \quad (2.7)$$

Here the position of the orbital in the ket gives the electron assignment. With such kets one can associate structure diagrams $D_\kappa^{[\lambda]}(\gamma)$ in which the electron indices are replaced by the orbital to which they are assigned in $|\gamma\rangle$. A structure ket $|\gamma; \kappa\rangle$ is said to *pair* orbitals a and b if and only if it is invariant under the interchange of orbitals a and b . See Table I.

We remark now briefly on $|\gamma\rangle$'s whose orbitals are *not* distinct. Suppose $|\gamma\rangle$ contains q orbitals, each of which has two electrons assigned. Two cases result. First, if the pair number p of $[\lambda] = [2^p, 1^{N-2p}]$ is less than q , then $\kappa^{[\lambda]}|\gamma\rangle = 0$ for all κ ; i.e., $|\gamma\rangle$ has no component in the $[\lambda]$ th permutation state. Second, for $p \geq q$, not all structure kets are zero. The number of (nonzero) linearly independent structure kets, which we denote by $f^{[\lambda]}(\gamma)$, is less than or equal to $f^{[\lambda]}$. For simplicity, we assign the $2q$ orbitals to the first $2q$ electrons. Then $f^{[\lambda]}(\gamma)$ is found by counting only those canonical $D_\kappa^{[\lambda]}(\gamma)$ such that the doubly occupied orbitals are always paired with each other. Note that the normalization constant C of (2.3) is different for these cases. For orthonormal orbitals

$$C = 2^{p+q} (N - p)! p! \quad (2.8)$$

See Table I.

The structure kets of the $[\lambda]$ th permutation state are used in finding a matrix of the system Hamiltonian. An eigenvalue problem results. The K th eigenket in the $[\lambda]$ th permutation state is (assumed normalized)

$$|\gamma; K^{[\lambda]}\rangle \equiv |\gamma; K\rangle \equiv |K\rangle = \sum_{\kappa=1}^{f^{[\lambda]}(\gamma)} b_{\kappa K} |\gamma; \kappa\rangle \quad (2.9)$$

Note that the $b_{\kappa K}$'s are functions of $|\gamma\rangle$. If $b_{\kappa K} = 1$ and $b_{\kappa' K} = 0$ for all $\kappa' \neq \kappa$, then

$$|\gamma; K\rangle = |\gamma; \kappa\rangle \quad (2.10)$$

(4) This subalgebra is called a *minimal right ideal* of $A^{[\lambda]}$. See F. A. Matsen and R. D. Poshusta, "Algebras, Ideals and Quantum Mechanics With Applications From the Symmetric Group," Molecular Physics Group Technical Report, The University of Texas, Austin, Texas, to be published in "Theorie des Groupes en Physique Classique et Quantique," by T. Kahan, Ed., Dunod Cie., Paris.

Table I: Structure Kets Formed from Orbital Product Kets^a

Case of Distinct Orbitals													
N	$[\lambda]$	p	m	$ \gamma\rangle$	$f^{[\lambda]}(\gamma)$	$D_{\kappa}^{[\lambda]}(\gamma)$	$T_{\kappa}^{[\lambda]}$	$\kappa[\lambda]$	$ \gamma; \kappa\rangle$				
1	[1]	0	Doublet	$ a\rangle$	1	\underline{a}	<table><tr><td>1</td></tr></table>	1	$\mathbf{I}^{[1]} = g$	$ a\rangle$			
1													
2	[1 ²]	0	Triplet	$ ab\rangle$	1	$\underline{a} \quad \underline{b}$	<table><tr><td>1</td></tr><tr><td>2</td></tr></table>	1	2	$\mathbf{I}^{[1^2]} = g - (12)$	$\frac{1}{\sqrt{2}}\{ ab\rangle = ba\rangle\}$		
1													
2													
	[2]	1	Singlet		1	$\underline{a} \rightarrow \underline{b}$	<table><tr><td>1</td><td>2</td></tr></table>	1	2	$\mathbf{I}^{[2]} = g + (12)$	$\frac{1}{\sqrt{2}}\{ ab\rangle + ba\rangle\}$		
1	2												
3	[1 ³]	0	Quartet	$ abc\rangle$	1	$\underline{a} \quad \underline{b}$ $\quad \underline{c}$	<table><tr><td>1</td></tr><tr><td>2</td></tr><tr><td>3</td></tr></table>	1	2	3	$\mathbf{I}^{[1^3]} = g - (12) - (13)$ $\quad - (23) + (123)$ $\quad + (132)$	$\frac{1}{\sqrt{6}}\{ abc\rangle - bac\rangle - cba\rangle$ $\quad - acb\rangle + cab\rangle + bca\rangle\}$	
1													
2													
3													
	[2,1]	1	Doublet		2	$\underline{a} \rightarrow \underline{b}$ $\quad \underline{c}$	<table><tr><td>1</td><td>2</td></tr><tr><td>3</td><td></td></tr></table>	1	2	3		$\mathbf{I}^{[2,1]} = [g - (13)][g + (12)]$ $\quad = g + (12) - (13)$ $\quad - (123)$	$\frac{1}{2}\{ abc\rangle + bac\rangle$ $\quad - cba\rangle - cab\rangle\}$
1	2												
3													
					$\underline{a} \quad \underline{b}$ $\quad \nearrow \underline{c}$	<table><tr><td>3</td><td>2</td></tr><tr><td>1</td><td></td></tr></table>	3	2	1		$\mathbf{II}^{[2,1]} = -\mathbf{I}^{[2,1]}(13)$ $\quad = g - (13) + (23)$ $\quad - (132)$	$\frac{1}{2}\{ abc\rangle - cba\rangle$ $\quad + acb\rangle - bca\rangle\}$	
3	2												
1													
					$\underline{a} \quad \underline{b}$ $\quad \searrow \underline{c}$	<table><tr><td>1</td><td>3</td></tr><tr><td>2</td><td></td></tr></table>	1	3	2		$\mathbf{III}^{[2,1]} = -\mathbf{I}^{[2,1]}(23)$ $\quad = (12) - (23)$ $\quad - (123) + (132)$	$\frac{1}{2}\{ bac\rangle - acb\rangle$ $\quad - cab\rangle + bca\rangle\}$	
1	3												
2													
Case of Repeated Orbitals													
N	$[\lambda]$	p	m	$ \gamma\rangle$	$f^{[\lambda]}(\gamma)$	$D_{\kappa}^{[\lambda]}(\gamma)$			$ \gamma; \kappa\rangle$				
2	[2]	1	Singlet	$ aa\rangle$	1	$\underline{a} \quad \underline{a}$			$ aa\rangle$				
3	[2,1]	1	Doublet	$ aac\rangle$	1	$\underline{a} \rightarrow \underline{a}$ $\quad \underline{c}$			$\frac{1}{\sqrt{2}}\{ aac\rangle - caa\rangle\}$				

^a Note, for *N* = 3 and *p* = 1, by Rumer's rule

$$|\gamma; \text{III}\rangle = |\gamma; \text{I}\rangle - |\gamma; \text{II}\rangle$$

(noncanonical) (canonical)

or symbolically

<i>a</i>	<i>b</i>	<i>a</i> → <i>b</i>	<i>a</i> <i>b</i>
↘	↗	↗	↘
<i>c</i>	<i>c</i>	<i>c</i>	<i>c</i>

III I II

and we say that there exists *perfect pairing* according to κ (or *D*_κ^[λ](γ)).

The expectation value of a spin-free operator Θ is

$$\Theta_K \equiv \langle \gamma; K | \Theta | \gamma; K \rangle = \sum_{\kappa, \kappa' = I}^{f^{[\lambda]}(\gamma)} b_{\kappa K} b_{\kappa' K} \Theta_{\kappa \kappa'} \quad (2.11)$$

where

$$\Theta_{\kappa \kappa'} \equiv \langle \gamma; \kappa | \Theta | \gamma; \kappa' \rangle \quad (2.12)$$

By Rumer's rule, eq 2.5, it is possible to express (2.12) as expression 2.13.

$$\langle \gamma \kappa | \Theta | \gamma \kappa' \rangle = \sum_{\substack{\kappa'' \text{ canonical} \\ \text{and noncanonical}}} C_{\kappa \kappa''} \langle \gamma; \kappa'' | \Theta | \gamma; \kappa'' \rangle \quad (2.13)$$

Consequently

$$\langle \gamma; K | \Theta | \gamma; K \rangle = \sum_{\substack{\kappa'' \text{ canonical} \\ \text{and noncanonical}}} d_{\kappa'' K} \langle \gamma; \kappa'' | \Theta | \kappa'' \rangle \quad (2.14)$$

where

$$d_{\kappa'' K} = \sum_{\kappa, \kappa' \text{ canonical}} b_{\kappa K} b_{\kappa' K} C_{\kappa \kappa''} \quad (2.15)$$

See Table II.

Volume 72, Number 1 January 1968

Table II: Matrix Elements

Here we abbreviate $|\gamma; \kappa\rangle = |\kappa\rangle$ and $|\gamma; K\rangle = |K\rangle$
 For $N = 3$, $[\lambda] = [2, 1]$, $f^{[2, 1]}(\gamma) = 2$, by Rumer's rule (2.6),
 $|\text{III}\rangle = |\text{I}\rangle - |\text{II}\rangle$

Thus

$$\langle \text{III} | \mathbf{o} | \text{III} \rangle = \langle \text{I} | \mathbf{o} | \text{I} \rangle + \langle \text{II} | \mathbf{o} | \text{II} \rangle - 2 \langle \text{I} | \mathbf{o} | \text{II} \rangle$$

and

$$\langle \text{I} | \mathbf{o} | \text{II} \rangle = \frac{1}{2} \{ \langle \text{I} | \mathbf{o} | \text{I} \rangle + \langle \text{II} | \mathbf{o} | \text{II} \rangle - \langle \text{III} | \mathbf{o} | \text{III} \rangle \}$$

For

$$|K\rangle = b_{IK}|I\rangle + b_{IIK}|II\rangle$$

We have

$$\begin{aligned} \langle K | \mathbf{o} | K \rangle &= b_{IK}^2 \langle \text{I} | \mathbf{o} | \text{I} \rangle + b_{IIK}^2 \langle \text{II} | \mathbf{o} | \text{II} \rangle + \\ &2b_{IK}b_{IIK} \langle \text{I} | \mathbf{o} | \text{II} \rangle = d_{IK} \langle \text{I} | \mathbf{o} | \text{I} \rangle + \\ &d_{IIK} \langle \text{II} | \mathbf{o} | \text{II} \rangle + d_{IIIK} \langle \text{III} | \mathbf{o} | \text{III} \rangle \end{aligned}$$

where

$$\begin{aligned} d_{IK} &= b_{IK}^2 + b_{IIK}b_{IIIK} \\ d_{IIK} &= b_{IIK}^2 + b_{IK}b_{IIIK} \\ d_{IIIK} &= -b_{IK}b_{IIK} \end{aligned}$$

Finally, if \mathbf{o} commutes with all permutations of S_N , then (paper III)

$$\langle \gamma; \kappa | \mathbf{o} | \gamma; \kappa' \rangle = \sum_{P \in S_N} (P)_{\kappa\kappa'} \langle \gamma | \mathbf{o} | \gamma; P \rangle \quad (2.16)$$

where the numbers $(P)_{\kappa\kappa'}$ are the Pauling numbers and $|\gamma; P\rangle \equiv P|\gamma\rangle$.

III. The Unpaired Electron Density

The total electron density operator at the point \vec{r} for an N -electron system is

$$\mathbf{e}(\vec{r}) \equiv \sum_{i=1}^N \mathbf{e}^i(\vec{r}) \quad (3.1)$$

where

$$\mathbf{e}^i(\vec{r}) \equiv \delta(\vec{r} - \vec{r}_i) \quad (3.2)$$

The electron density at \vec{r} for the eigenket $|K\rangle$ is then

$$\rho_K(\vec{r}) \equiv \langle K | \mathbf{e}(\vec{r}) | K \rangle \quad (3.3)$$

By (2.11)

$$\rho_K(\vec{r}) = \sum_{\kappa, \kappa'=I}^{f^{[\lambda]}(\gamma)} b_{\kappa K} b_{\kappa' K} \langle \gamma; \kappa | \mathbf{e}(\vec{r}) | \gamma; \kappa' \rangle \quad (3.4)$$

Since

$$[\mathbf{e}(\vec{r}), P] = 0 \text{ for } P \in S_N$$

then by (2.16)

$$\rho_K(\vec{r}) = \sum_{\kappa, \kappa'=I}^{f^{[\lambda]}(\gamma)} \sum_{P \in S_N} b_{\kappa K} b_{\kappa' K} (P)_{\kappa\kappa'} \langle \gamma | \mathbf{e}(\vec{r}) | \gamma; P \rangle \quad (3.5)$$

For $|\gamma\rangle$ a product of distinct orthonormal orbitals the only nonzero terms in (3.5) are those for which $P = \mathcal{I}$. Thus

$$\rho_K(\vec{r}) = \left\{ \sum_{\kappa} |b_{\kappa K}|^2 + 2 \sum_{\kappa < \kappa'} (g)_{\kappa\kappa'} b_{\kappa K} b_{\kappa' K} \right\} \times \{ |a(\vec{r})|^2 + |b(\vec{r})|^2 + \dots + |n(\vec{r})|^2 \} \quad (3.6)$$

Since the first term in braces is just $\langle K | K \rangle = 1$, then

$$\rho_K(\vec{r}) = \{ |a(\vec{r})|^2 + |b(\vec{r})|^2 + \dots + |n(\vec{r})|^2 \} \quad (3.7)$$

We now define the unpaired electron density operator at \vec{r} for the allowed $[\lambda]$ th permutation state as⁵

$$\begin{aligned} \hat{\mathbf{e}}_I^{[\lambda]}(\vec{r}) &\equiv \hat{\mathbf{e}}(\vec{r}) \equiv \sum_{i=1}^N \mathbf{e}^i(\vec{r}) - 2 \sum_{i=1}^p \mathbf{e}^{2i}(\vec{r}) \\ &\equiv \sum_{i=1}^N \mathbf{e}^i(\vec{r}) X_i \end{aligned} \quad (3.8) \quad (3.9)$$

where X_i takes values of ± 1 according to (3.8) and p is as in (1.3). The unpaired electron density at \vec{r} for the eigenket $|K\rangle$ in the $[\lambda]$ th permutation state is then

$$\hat{\rho}_K(\vec{r}) \equiv \langle K | \hat{\mathbf{e}}(\vec{r}) | K \rangle \quad (3.10)$$

and by (2.14)

$$\hat{\rho}_K(\vec{r}) = \sum_{\kappa \text{ canonical and noncanonical}} d_{\kappa''K} \langle \kappa'' | \hat{\mathbf{e}}(\vec{r}) | \kappa'' \rangle \quad (3.11)$$

We note that the valence of any ket in the $[\lambda]$ th permutation state is given by

$$v = \int \hat{\rho}_K(\vec{r}) d\vec{r} = N - 2p \quad (3.12)$$

For a primitive ket which is a product of orthonormal orbitals, the diagonal elements $\langle \kappa | \hat{\rho}(\vec{r}) | \kappa \rangle$ have a simple graphical interpretation: nonzero unpaired electron densities occur only for unpaired orbitals. See Table III.

Off-diagonal elements can be obtained from diagonal elements by means of (2.13). For a graphical generalization of this, see Appendix A.

IV. The Isotropic Magnetic Hyperfine Hamiltonian

For a system in the K th electronic state of the $[\lambda]$ th permutation state, the isotropic (contact) contribution to the magnetic interaction of the total spin angular momentum S with each nuclear spin angular momenta \vec{I}_a is given by the effective isotropic hyperfine Hamiltonian⁶

$$H_K^{\text{eff}}(\text{cont}) = \sum_a A_K(a) \vec{S} \cdot \vec{I}_a \quad (4.1)$$

Here the sum extends over all the nuclei in the system. $[\lambda] = [2^p, 1^{N-2p}]$ and S are related by

(5) The subscript I in (3.8) is to indicate that the operator is defined with respect to reference tableau I in order to have consistency with the structure basis which is also built with respect to table I. A consequence of this is that when the structure basis is used, a simple graphical definition results.

(6) A. Abragam and M. H. L. Pryce, *Proc. Roy. Soc. (London)*, **A205**, 135 (1951).

Table III: Unpaired Electron Density of Structure Kets Built from Orthonormal Orbitals^a

N	$[\lambda]$	$\hat{\rho}(\vec{r})$	$ \gamma\rangle$	$D_K^{[\lambda]}(\gamma)$	κ	$\langle\gamma \kappa \hat{\rho}(\vec{r}) \gamma;\kappa\rangle$
1	[1]	$\rho^1(\vec{r})$	$ a\rangle$	$\underset{\cdot}{a}$	I	$ a(\vec{r}) ^2$
2	[1 ²]	$\rho^1(\vec{r}) + \rho^2(\vec{r})$	$ ab\rangle$	$\underset{\cdot}{a} \quad \underset{\cdot}{b}$	I	$ a(\vec{r}) ^2 + b(\vec{r}) ^2$
	[2]	$\rho^1(\vec{r}) - \rho^2(\vec{r})$		$\underset{\cdot}{a} \rightarrow \underset{\cdot}{b}$	I	0
3	[1 ³]	$\rho^1(\vec{r}) + \rho^2(\vec{r}) + \rho^3(\vec{r})$	$ abc\rangle$	$\underset{\cdot}{a} \quad \underset{\cdot}{b} \quad \underset{\cdot}{c}$	I	$ a(\vec{r}) ^2 + b(\vec{r}) ^2 + c(\vec{r}) ^2$
	[2,1]	$\rho^1(\vec{r}) - \rho^2(\vec{r}) + \rho^3(\vec{r})$		$\underset{\cdot}{a} \rightarrow \underset{\cdot}{b} \quad \underset{\cdot}{c}$	I	$ c(\vec{r}) ^2$
				$\underset{\cdot}{a} \quad \underset{\cdot}{b} \quad \underset{\cdot}{c}$	II	$ a(\vec{r}) ^2$
				$\underset{\cdot}{a} \quad \underset{\cdot}{b} \quad \underset{\cdot}{c}$	III	$ b(\vec{r}) ^2$
			$ aac\rangle$	$\underset{\cdot}{a} \rightarrow \underset{\cdot}{a} \quad \underset{\cdot}{c}$	I	$ c(\vec{r}) ^2$

^a For $N = 3$, $[\lambda] = [2,1]$, and $|K\rangle = b_{IK}|\gamma;I\rangle + b_{IIK}|\gamma;II\rangle$; by Table II, $\hat{\rho}_K(\vec{r}) = (b_{IK}^2 + b_{IIK}b_{IIIK})|c(\vec{r})|^2 + (b_{IIK}^2 + b_{IIIK}b_{IIK})|a(\vec{r})|^2 - b_{IK}b_{IIIK}|b(\vec{r})|^2$. For $b_{IK} = b_{IIIK} = 1/\sqrt{3}$, $\hat{\rho}_K(\vec{r}) = (2/3)|a(\vec{r})|^2 - (1/3)|b(\vec{r})|^2 + (2/3)|c(\vec{r})|^2$. For $1 \approx |b_{IK}| \gg |b_{IIIK}|$, $\hat{\rho}_K(\vec{r}) \approx |c(\vec{r})|^2 + b_{IIIK}\{|a(\vec{r})|^2 - |b(\vec{r})|^2\}$.

$$S = \frac{N}{2} - p \quad (4.2)$$

The hyperfine interaction constant is given by (Appendix B)

$$A_K(a) = \frac{B(a)}{2S} \hat{\rho}_K(\vec{r}_a) \quad (4.3)$$

where $\hat{\rho}_K(\vec{r}_a)$ is the unpaired electron density at the a th nucleus for the K th state of the $[\lambda]$ th permutation state, and

$$B(a) = \frac{16\pi\beta_e\gamma_a\hbar}{3} \quad (4.4)$$

where β_e is the Bohr magneton (9.273×10^{-21} erg/gauss) and γ_a is the nuclear gyromagnetic ratio for nucleus a .

It follows that a determination of $A_K(a)$ is also a determination of the unpaired electron density at nucleus a . When used in this connection, $\hat{\rho}_K(r_a)$ is called the *spin density*. The phrase, "vector density of electron spin angular momentum,"⁷ has been applied to the quantity $\hat{\rho}_K(\vec{r}_a)\vec{S}$.

V. The Helium Atom^{8a} (1s2s) ³S

For He³ ($I = 1/2$) in the lowest ³S state^{8b}

$$\left|\frac{A_K}{h}\right| = 4493.14 \text{ Mc/sec (exptl)} \quad (5.1)$$

and by (4.3)

$$|\hat{\rho}_K(0)| = 2.649(a_0^{-3}) \text{ (exptl)} \quad (5.2)$$

For

$$|\gamma\rangle = |1s2s\rangle \quad (5.3)$$

one has for the triplet ($[\lambda] = [1^2]$) eigenket

$$|\gamma;K\rangle = 1/\sqrt{2}\{|1s2s\rangle - |2s1s\rangle\} \quad (5.4)$$

and by (3.10)

$$\hat{\rho}_K(0) = |1s(0)|^2 + |2s(0)|^2 - 1s(0)2s(0)\langle 1s|2s\rangle \quad (5.5)$$

$$\approx |1s(0)|^2 + |2s(0)|^2 \quad (5.6)$$

Using hydrogenic functions with $Z = 2$ for 1s and $Z = 1$ for 2s, the calculated unpaired electron density at the nucleus is

$$\hat{\rho}_K(0) = 2.586(a_0^{-3}) \text{ (calcd)} \quad (5.7)$$

VI. The Lithium Atom (1s²2s) ²S_{1/2}

For the ground-state doublet of lithium⁹

$$\left|\frac{A_K}{h}\right| = 401.186 \text{ Mc/sec (exptl)} \quad (6.1)$$

and by (4.3)

$$|\hat{\rho}_K(0)| = 0.2313(a_0^{-3}) \text{ (exptl)} \quad (6.2)$$

(7) H. M. McConnell and J. Strathdee, *Mol. Phys.*, **2**, 129 (1959).

(8) (a) This section follows a development by S. M. Blinder, "Advances in Quantum Chemistry," Vol. 2, P. O. Lowdin, Ed., Academic Press Inc., New York, N. Y., 1965; (b) G. Weinreich and V. W. Hughes, *Phys. Rev.*, **95**, 1451 (1954).

(9) P. Kush and H. Taub, *ibid.*, **75**, 1477 (1949).

Table IV: Analysis of Lithium Eigenkets, Computed Energy, and Unpaired Electron Density

Primitive ket $ \gamma\rangle^a$	Symmetry of core	Eigenket $ \gamma;K\rangle$	Existence of ^b core polarization	Computed energy (Hartree)	$\rho_K(0)$ in (a_0^{-3}) ^c
$ 1s1s2s\rangle^d$	Symmetric	$ \gamma;I\rangle$	No	-14.83584 ^d	0.1666
$ 1s1s'2s\rangle^d$	Asymmetric	$ \gamma;I\rangle$	No	-14.8872 ^d	0.3002
$ 1s1s'2s\rangle^e$	Asymmetric	$b_{IK} \gamma;I\rangle + b_{IIK} \gamma;II\rangle$	Yes	-14.8873 ^e	0.2418
$ \theta(1,2)\rangle 2s\rangle + \theta_1'(1,2,3)\rangle$ 41-term C.I. by Weiss ^f	Symmetric	$ \gamma;I\rangle$	No	-14.95244 ^f	0.2053
$ \theta(1,2)\rangle 2s\rangle + \theta_1'(1,2,3)\rangle + \theta_2'(1,2,3)\rangle$ 45-term C.I. by Weiss ^f	Asymmetric (in θ_2')	$ \gamma;I\rangle + \gamma;II\rangle - \theta_2';I\rangle$	Yes	-14.95420 ^f	0.2065
$ \Phi(1,2)\rangle Q\rangle + C(1,2,3)\rangle$ core and core-valence correlated by Berg- gren and Wood ^g	Symmetric	$ \gamma;I\rangle$	No	-14.95260 ^g	0.2285
$ \Phi(1,2)\rangle Q\rangle + C'(1,2,3)\rangle$ core and core-valence correlated by Berg- gren and Wood ^g	Asymmetric (in C')	$\frac{1}{\sqrt{2}}\{s - (13)\} \gamma\rangle^c$	Does not fit our defi- nition because of quartet component	-14.95262 ^g	0.2294
Experimental				-14.9561 ^h	0.2313 ⁱ

^a The first four primitive kets are built from Slater orbitals; note that $2s(0) = 0$. θ_1' has a Slater $1s$ assigned to the third electron and thus, $\theta_1'|_{r_3=0} \neq 0$. ^b Note that core polarization makes a significant difference in $\hat{\rho}_K(0)$, but not on E , when $|\gamma\rangle|_{r_3=0} = 0$. When $|\gamma\rangle|_{r_3=0} \neq 0$ structure ket $|\gamma;I\rangle$ contributes to most of $\hat{\rho}_K(0)$. ^c This ket corresponds to an "unrestricted Hartree-Fock-like" ket in the conventional language. It is not a pure permutation (spin) state since it can be decomposed into two doublet components and one quartet component. For example, if $|\gamma\rangle = |abc\rangle$ is made of orthonormal orbitals, then $1/\sqrt{2}\{s - (13)\}|\gamma\rangle = 1/3\{\sqrt{2}|\gamma;I^{(2,1)}\rangle + \sqrt{2}|\gamma;II^{(2,1)}\rangle + \sqrt{3}|\gamma;I^{(1,1)}\rangle\}$. Because of this mixture, the first-order perturbation treatment discussed in Appendix B for obtaining the hyperfine constant would give obscure results for the hyperfine constant since the treatment calls explicitly for eigenfunctions of S^2 , i.e., pure spin states. ^d R. P. Hurst, J. D. Gray, C. H. Brigman, and F. A. Matsen, *Mol. Phys.*, **1**, 189 (1958). ^e C. H. Brigman and F. A. Matsen, *J. Chem. Phys.*, **27**, 829 (1957); see also E. A. Burke and J. F. Mulligan, *ibid.*, **28**, 995 (1958). ^f A. W. Weiss *Phys. Rev.*, **122**, 1826 (1961); see also J. B. Martin and A. W. Weiss, *J. Chem. Phys.*, **39**, 1618 (1963). Here θ is a 35-term C. I. singlet (symmetric) function for Li^+ . θ_1' is a six-term C. I. function for Li and θ_2' , a four-term C. I. function of Li . Further, $\theta_1'|_{r_3=0} \neq 0$, and $\theta_2'|_{r_3=0} \neq 0$. ^g K. F. Berggren and R. F. Wood, *Phys. Rev.*, **130**, 198 (1963). Here Φ is symmetric and contains core correlation, Q is "flexible" $2s$, $Q(0) \neq 0$, C and C' both contain core-valence correlation, C is symmetric and C' is not. Further, $C|_{r_3=0} \neq 0$, $C'|_{r_3=0} \neq 0$. ^h C. W. Scherr, J. N. Silverman, and F. A. Matsen, *Phys. Rev.*, **127**, 830 (1962). ⁱ These were obtained by Burke¹⁰ and some by Martin and Weiss. ^j Measured by Kush and Taub.⁹

We exhibit a number of primitive kets and the unpaired electron densities which are calculated from them. (See Table IV.) If

$$(12)|\gamma\rangle = |\gamma\rangle \quad (6.3)$$

the primitive ket is said to have a *symmetric core*. Only structure ket $|\gamma;I\rangle$ can thus be projected out of a primitive ket with a symmetric core. If the core is not symmetric, the two linearly independent kets $|\gamma;I\rangle$ and $|\gamma;II\rangle$ can be projected. If structure ket $|\gamma;II\rangle$ is included, the treatment is said to permit *core polarization*.¹⁰ Thus, deviations from perfect pairing in $D_1^{(2,1)}$ introduce core polarizations. (See Figure 1.)

Because core polarization can have a large effect on the computed hyperfine constant, it has sometimes been referred to as "spin-polarization." The phrase, spin polarization, has also been employed in discussion of the unrestricted Hartree-Fock functions.

VII. The Methyl Radical

The hyperfine interaction constants for methyl (C^{12}) and methyl (C^{13}) have been determined.¹¹ Analysis

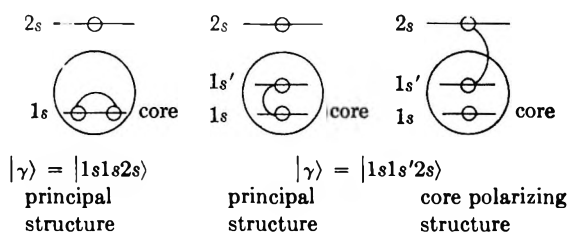


Figure 1. Schematic representation of core polarization for $|\gamma\rangle = |1s1s2s\rangle$ and $|\gamma\rangle = |1s1s'2s\rangle$.

of the data shows that the hyperfine interaction constants for the three protons are identical, so the three hydrogen atoms are equivalent and the molecule has symmetry C_{3v} . The constants are

$$|A_K(H)| = 25 \pm 2 \text{ gauss} \quad (\text{for the three protons}) \quad (\text{exptl}) \quad (7.1)$$

(10) For a more extensive discussion of core polarization, see E. A. Burke, *Phys. Rev.*, **135**, A621 (1964).

(11) T. Cole, H. O. Pritchard, N. R. Davidson, and H. M. McConnell *Mol. Phys.*, **1**, 406 (1958).

$$|A_K(C)| = 41 \pm 3 \text{ gauss (exptl)} \quad (7.2)$$

which by (4.3) are related to $\hat{\rho}_K(H)$ and $\hat{\rho}_K(C)$.

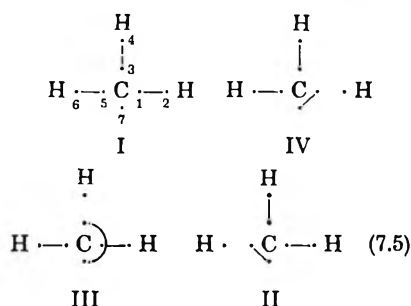
We follow the treatment given by Karplus and Fraenkel¹² to interpret these results theoretically. We take as the spin-free primitive ket

$$|\gamma\rangle = |c_1 h_1 c_2 h_2 c_3 h_3 c_4\rangle \quad (7.3)$$

where

$$c_i = C_{is}2s + C_{ix}2p_x + C_{iy}2p_y + C_{iz}2p_z \quad (7.4)$$

is centered on the carbon and h_i is a $1s$ orbital on proton i . Orbitals c_1, c_2 , and c_3 are taken as equivalent. Some of the more important structures for the $[\lambda] = [2^3, 1]$ ($S = 1/2$) state are the principal structure and those with the unpaired electron on a proton



Structures II, III, and IV are of the "no bond" forms which are sometimes employed in discussion of hyperconjugation.¹³ The eigenket for the ground-state doublet, 2A_1 , is then

$$|\gamma; K\rangle = C_I |\gamma; I\rangle + C_{II} \{ |\gamma; II\rangle + |\gamma; III\rangle + |\gamma; IV\rangle \} \quad (7.6)$$

Thus

$$\begin{aligned} \hat{\rho}_K(\vec{r}) = & C_I^2 \hat{\rho}_{II}(\vec{r}) + 2C_I C_{II} \{ \hat{\rho}_{I\ II}(\vec{r}) + \hat{\rho}_{I\ III}(\vec{r}) + \hat{\rho}_{I\ IV}(\vec{r}) \} + \\ & \frac{2}{3} \{ \hat{\rho}_{II\ II}(\vec{r}) + \hat{\rho}_{II\ III}(\vec{r}) + \hat{\rho}_{II\ IV}(\vec{r}) + \\ & C_{II}^2 \{ \hat{\rho}_{III\ II}(\vec{r}) + \hat{\rho}_{III\ III}(\vec{r}) + \hat{\rho}_{III\ IV}(\vec{r}) + \\ & \hat{\rho}_{IV\ II}(\vec{r}) + 2\hat{\rho}_{IV\ III}(\vec{r}) + 2\hat{\rho}_{IV\ IV}(\vec{r}) + \\ & 2\hat{\rho}_{III\ IV}(\vec{r}) \} - \frac{4}{3} \{ \hat{\rho}_{I\ II}(\vec{r}) + \hat{\rho}_{I\ III}(\vec{r}) + \\ & \hat{\rho}_{I\ IV}(\vec{r}) \} \} \quad (7.7) \end{aligned}$$

Here, as (2.12)

$$\hat{\rho}_{\kappa\kappa'}(\vec{r}) = \langle \gamma; \kappa | \hat{\rho}(\vec{r}) | \gamma; \kappa' \rangle \quad (7.8)$$

Orthogonality is assumed among the seven orbitals in (7.3). Then on using (A.30), (7.7) becomes

$$\begin{aligned} \hat{\rho}_K(\vec{r}) = & \{ \Gamma(c_1) + \Gamma(c_2) + \Gamma(c_3) \} |c_1(\vec{r})|^2 + \\ & \Gamma(c_4) |c_4(\vec{r})|^2 + \{ \Gamma(h_1) + \Gamma(h_2) + \\ & \Gamma(h_3) \} |h_1(\vec{r})|^2 \quad (7.9) \end{aligned}$$

where, as (A.29)

$$\Gamma(j) = \sum_{\kappa, \kappa'=I}^{IV} b_{\kappa K} b_{\kappa' K} \gamma_{\kappa\kappa'}(j) \Delta_{\kappa\kappa'} \quad (7.10)$$

which for the present case one has $b_{IK} = C_I + C_{II}$ and $b_{IIK} = b_{IIIK} = b_{IVK} = -2/3 C_{II}$.

In Table VI of Appendix A, we tabulate the coefficients $\gamma_{\kappa\kappa'}(j)$ and $\Delta_{\kappa\kappa'}$.

If the system is planar, then c_1, c_2 , and c_3 are sp^2 hybrids, which we denote by t , and c_4 , a $2p$ orbital. Thus since $2p(C) = 2p(H) = 0$, $h(C) \cong 0$, and $t(H) \cong 0$, then by using (7.9) and Table VI one has

$$\hat{\rho}_K(C) = 2/3 \{ 3C_I C_{II} + C_{II}^2 \} |t(C)|^2 \quad (7.11)$$

$$\hat{\rho}_K(H) = -2/3 \{ 3C_I C_{II} - C_{II}^2 \} |h(H)|^2 \quad (7.12)$$

Using semiempirical techniques, Karplus and Fraenkel obtain¹² C_I and C_{II} in the form

$$\Gamma(t) = 2/9 (3C_I C_{II} + C_I^2) = 0.04747 \quad (7.13)$$

$$\Gamma(h) = -2/9 (3C_I C_{II} - C_I^2) = -0.04531 \quad (7.14)$$

Using values given by Jucys¹⁴ for the orbital densities, they obtain¹⁵

$$A_K(C) = 56.54 \text{ gauss (calcd)} \quad (7.15)$$

$$A_K(H) = -23.00 \text{ gauss (calcd)} \quad (7.16)$$

Improved unpaired electron density calculations have been done (Karplus and Fraenkel) by including $1s$ contributions. This makes a considerable improvement. Further improvement was made by considering incomplete orbital following.¹⁶ This corrects for the sensitivity of $A_K(C)$ to deviations from linearity.

VIII. The Allyl Radical

For the allyl radical, we assume that the protons on the end carbon atoms are equivalent. The esr spectrum¹⁷ gives

$$(\text{averaged}) |A_e(H)| = 14.38 \text{ gauss} \quad (\text{end protons}) \quad (8.1)$$

$$|A_m(H)| = 4.06 \text{ gauss} \quad (\text{middle proton}) \quad (8.2)$$

The first theoretical explanation of these results, and of similar results for a large class of conjugated radicals,

(12) M. Karplus and G. K. Fraenkel, *J. Chem. Phys.*, **35**, 1312 (1961).

(13) M. J. S. Dewar, "Hyperconjugation," The Ronald Press Co., New York, N. Y., 1962.

(14) A. Jucys, *Proc. Roy. Soc. (London)*, **A173**, 59 (1939); *Fiz. Zh.*, **11**, 49 (1947).

(15) A_K (in gauss) = $(1/g_e \beta_e) A_K$ (in ergs).

(16) D. M. Schrader and M. Karplus, *J. Chem. Phys.*, **40**, 1593 (1964).

(17) R. M. Fessenden and R. H. Schuler, *ibid.*, **39**, 2147 (1963). Note that A (gauss) = $(1/g_e \beta_e) A$ (ergs). Further, the actual data asserted a slight nonequivalence of the end protons; we give the averaged result.

was successfully given by McConnell.¹⁸ He first observed a linear relation between the $A(H)$'s and the unpaired π -orbital density $\Gamma(C)$'s of the respectively attached carbons.

$$A(H) = Q\Gamma(C) \quad (8.3)$$

This implies that such conjugated systems cannot be treated as purely π -electron systems and that it is necessary for determining $A(H)$ to include structure kets which leave a hydrogen atom with an unpaired electron. McConnell's theoretical results for Q is

$$Q = -22.5 \text{ gauss} \quad (8.4)$$

From the above data, if (8.3) is a valid expression, an "experimental" Q_{exptl} can be constructed. Using the fact that (A.33)

$$2\Gamma_e(C) + \Gamma_m(C) = 1 \quad (8.5)$$

and the assumption that $\Gamma_e(C)$ and $\Gamma_m(C)$ have opposite signs (justified later), one has

$$|Q|_{\text{exptl}} = 2[\text{averaged } A_e(H)] - A_m(H) \quad (8.6)$$

$$= 24.7 \text{ gauss} \quad (8.7)$$

Thus the "experimental" $\Gamma(C)$'s can be obtained. See Table V.

Table V: Unpaired π -Orbital Density of Allyl Radical

Calculations	$\Gamma_e(C)$	$\Gamma_m(C)$
Simple molecular orbital ^a	0.5	0
Simple valence bond ^b	0.666	-0.333
Valence bond with complete ^c configuration interaction	0.62	-0.23
Molecular orbital with ^a com- plete configuration inter- action	0.6	-0.2
Experimental, $ Q_{\text{exptl}} = 24.7$ gauss ^d	0.58	-0.16

^a See, e.g., H. M. McConnell, *J. Chem. Phys.*, **28**, 1188 (1959).

^b See Table III. ^c H. C. Lefkovits, J. Fain, and F. A. Matsen, *J. Chem. Phys.*, **23**, 1690 (1955); also, D. J. E. Ingram, "Free Radicals," Butterworth and Co. Ltd., London, 1953, p 133.

^d O. Chalvet and R. Daudel, *J. Chim. Phys.*, **49**, 629 (1952); also, H. M. McConnell, *J. Chem. Phys.*, **28**, 1188 (1959). ^e See ref 17.

In Table V are the calculated π -orbital densities for several different π -electron treatments of the allyl radical. In the simple valence bond treatment, one takes

$$|\gamma\rangle = |\pi_a \pi_b \pi_c\rangle \quad (8.8)$$

where π_a , π_b , and π_c are taken to be orthonormal π orbitals on each of the carbon atoms. The unpaired π -orbital density associated with each of the carbon atoms is determined in Table III and reported in

Table V. Note that the assumption made of $\Gamma_m(C)$ and $\Gamma_e(C)$ having opposite signs is justified.

IX. Summary

We have defined the spin-free concept of the unpaired electron density and discussed its computation for several systems. We have related it to the hyperfine interaction constant and have shown it to be identical with the widely used spin density.

In Appendix B, it is stated that the derivation of the isotropic magnetic hyperfine interaction constant rests on a *first-order perturbation treatment*. Within this approximation we obtained this constant in the spin-free framework. Thus our formulation emphasizes the important point that spin is not a dynamical variable in the computation of the hyperfine interaction constant and that only spin-free dynamics prevail.

Appendix A

Evaluation of $\langle \gamma; \kappa | \hat{\rho}(\vec{r}) | \gamma; \kappa' \rangle$ for Doublet State. We consider the case of $N(\text{odd})$ and $p = (N - 1)/2$ ($m = \text{doublet}$). Further, we take the special case of

$$|\gamma\rangle = |\phi_1 \phi_2 \dots \phi_N\rangle \quad (A.1)$$

where the orbitals are real, distinct, and orthonormal. The set of $\{C_{\kappa''\kappa'}\}$ of (2.13) result from Rumer's rule, eq 2.5. They also arise from the algebraic expression

$$Z_{\kappa\kappa'} + Z_{\kappa'\kappa} = 2 \sum_{\substack{\kappa'' \text{ canonical} \\ \text{and noncanonical}}} C_{\kappa\kappa''\kappa'} Z_{\kappa''\kappa'} \quad (A.2)$$

where

$$Z_{\kappa\kappa'} \equiv \frac{\kappa^\dagger \kappa'}{C} \equiv \frac{\kappa^\dagger \kappa'}{2^p (N - p)! p!} \quad (A.3)$$

The matrix element of (A.2) over the ket (A.1) is the same as (2.13) with $\Theta = I$, the identity operator, and (A.1) for the primitive ket.

Since (paper III²)

$$Z_{\kappa\kappa'} = \sum_{P \in S_N} (P)_{\kappa\kappa'} P \quad (A.4)$$

where the coefficients are the Pauling numbers, then (A.2) becomes (with the usual sum of κ'')

$$\sum_{P \in S_N} [(P)_{\kappa\kappa'} + (P)_{\kappa'\kappa}] P = 2 \sum_{P \in S_N} \left[\sum_{\kappa''} C_{\kappa\kappa''\kappa'} (P)_{\kappa''\kappa'} \right] P \quad (A.5)$$

Thus equating coefficients

$$(P)_{\kappa\kappa'} + (P)_{\kappa'\kappa} = 2 \sum_{\kappa''} C_{\kappa\kappa''\kappa'} (P)_{\kappa''\kappa'} \quad (A.6)$$

For the case of N (odd) and $p = (N - 1)/2$, the Pauling numbers are obtained as follows.

(a) Consider the case of $N' = N + 1$ (even) and $p' = N'/2$ (singlet). Define $|\gamma g\rangle \equiv |\phi_1 \phi_2 \phi_3 \dots \phi_N\rangle |g\rangle$.

(18) H. M. McConnell, *J. Chem. Phys.*, **24**, 632, 764 (1956). See also H. M. McConnell and D. B. Chestnut, *ibid.*, **28**, 107 (1958).

Here, N' and g are called the ghost integer and ghost orbital, respectively.

(b) Construct the diagrams $D_{\kappa}^{p'}(\gamma g)$ and $D_{\kappa}^{p'}(\gamma g)$ such that g has the head of an arrow and on the removal of g , one obtains $D_{\kappa}^p(\gamma)$ and $D_{\kappa}^{p'}(\gamma)$, respectively.

(c) Construct the diagram $PD_{\kappa}^{p'}(\gamma g)$ by first permuting the integers (orbitals) of $D_{\kappa}^{p'}(\gamma g)$ according to P and then returning the integers (orbitals) to their original order carrying along the new head and tail assignment.

(d) Construct the superposition diagram $[D_{\kappa}PD_{\kappa'}] \equiv [D_{\kappa}^{p'}(\gamma g)PD_{\kappa'}^{p'}(\gamma g)]$ and denote by i , the number of islands formed and by r , the number of arrow reversals needed to obtain a head to head and tail to tail diagram.

(e) Then

$$(P)_{\kappa\kappa'} = \epsilon(P)(-1)^r 2^{i-N'/2} \quad (\text{A.7})$$

We shall only consider two permutations; the identity g and a transposition, say (ij) . For these (A.7) becomes

$$(g)_{\kappa\kappa'} = (-1)^r 2^{i-N'/2} \quad (\text{A.8})$$

$$= \langle \gamma; \kappa | \gamma; \kappa' \rangle \quad (\text{A.9})$$

$$\equiv \Delta_{\kappa\kappa'} \quad (\text{A.10})$$

and

$$\begin{aligned} ((ij))_{\kappa\kappa'} &= ((ij))_{\kappa'\kappa} \\ &= \Delta_{\kappa\kappa'} \begin{cases} 1 \text{ for } i \text{ and } j \text{ in the same island of } [D_{\kappa}D_{\kappa'}] \text{ and separated by an odd number of lines} \\ -2 \text{ for } i \text{ and } j \text{ in the same island of } [D_{\kappa}D_{\kappa'}] \text{ and separated by an even number of lines} \\ -1/2 \text{ for } i \text{ and } j \text{ in different islands of } [D_{\kappa}D_{\kappa'}] \end{cases} \end{aligned} \quad (\text{A.11})$$

Here r and i in (A.8) refer to the superposition diagram $[D_{\kappa}D_{\kappa'}]$. Further

$$((ij))_{\kappa''\kappa'''} = \begin{cases} 1 \text{ for } i \text{ and } j \text{ paired in } [D_{\kappa''}D_{\kappa'''}] \\ -1/2 \text{ for } i \text{ and } j \text{ unpaired in } [D_{\kappa''}D_{\kappa'''}] \end{cases} \quad (\text{A.12})$$

This follows since $[D_{\kappa''}D_{\kappa'''}]$ is merely $D_{\kappa''}$ with each line occurring twice (superimposed), i.e., there are $N'/2$ degenerate islands. We divide the collection of superposition diagrams $\{[D_{\kappa''}D_{\kappa'''}]\}$ into two sets: one has points i and j doubly paired and the other set has the remaining diagrams. We denote the sum of the $C_{\kappa\kappa'}$'s that correspond to the first set by

$$\sum_{\kappa''} C_{\kappa\kappa'} \quad (\text{A.13})$$

and the remaining sum of $C_{\kappa\kappa'}$'s by

$$\sum_{\kappa'''} C_{\kappa\kappa'} \quad (\text{A.14})$$

For $P = (ij)$, eq A.6 becomes

$$((ij))_{\kappa\kappa'} = \sum_{\kappa''} C_{\kappa\kappa'} - 1/2 \sum_{\kappa'''} C_{\kappa\kappa'} \quad (\text{A.15})$$

For $P = g$, eq A.6 becomes

$$\Delta_{\kappa\kappa'} = \sum_{\kappa''} C_{\kappa\kappa'} = \sum_{\kappa''} C_{\kappa\kappa'} + \sum_{\kappa'''} C_{\kappa\kappa'} \quad (\text{A.16})$$

From (A.15) and (A.16), one can solve for (A.13)

$$\sum_{\kappa''} C_{\kappa\kappa'} = 1/3 [2((ij))_{\kappa\kappa'} + \Delta_{\kappa\kappa'}] \quad (\text{A.17})$$

For the case we are considering, the diagonal unpaired electron density matrix elements can be obtained graphically.

$$\hat{\rho}_{\kappa''\kappa'''}(\vec{r}) = \langle \gamma; \kappa'' | \hat{\rho}(\vec{r}) | \gamma; \kappa''' \rangle = |\phi_i(\vec{r})|^2 \quad (\text{A.18})$$

where ϕ_i is the orbital bonded to g in $D_{\kappa''}^{p'}(\gamma g)$. This follows from the fact that ϕ_i is the unpaired orbital in $D_{\kappa''}^{p'}(\gamma)$.¹⁹ Consider now an off-diagonal matrix element which by (2.13) is

$$\hat{\rho}_{\kappa\kappa'}(\vec{r}) = \langle \gamma; \kappa | \hat{\rho}(\vec{r}) | \gamma; \kappa' \rangle = \sum_{\kappa''} C_{\kappa\kappa'} \langle \gamma; \kappa'' | \hat{\rho}(\vec{r}) | \gamma; \kappa'' \rangle \quad (\text{A.19})$$

We divide the set of superposition diagrams $\{[D_{\kappa''}D_{\kappa'''}]\}$ into N sets each characterized by g bonded to one of the N integers (orbitals). Then

$$\hat{\rho}_{\kappa\kappa'}(\vec{r}) = \sum_{j=1}^N \sum_{\kappa''} C_{\kappa\kappa'} \langle \gamma; \kappa'' | \hat{\rho}(\vec{r}) | \gamma; \kappa'' \rangle \quad (\text{A.20})$$

By (A.18)

$$\hat{\rho}_{\kappa\kappa'}(\vec{r}) = \sum_{j=1}^N \left[\sum_{\kappa''} C_{\kappa\kappa'} \right] |\phi_j(\vec{r})|^2 \quad (\text{A.21})$$

and by (A.17)

$$\hat{\rho}_{\kappa\kappa'}(\vec{r}) = \sum_{j=1}^N 1/3 [2(gj)_{\kappa\kappa'} + \Delta_{\kappa\kappa'}] |\phi_j(\vec{r})|^2 \quad (\text{A.22})$$

We define

$$\gamma_{\kappa\kappa'}(j) \equiv \frac{1}{3\Delta_{\kappa\kappa'}} [2((gj))_{\kappa\kappa'} + \Delta_{\kappa\kappa'}] \quad (\text{A.23})$$

$$= \begin{cases} 1 \text{ for } j \text{ and } g \text{ in the same island of } [D_{\kappa}D_{\kappa'}] \text{ and separated by an odd number of lines} \\ -1 \text{ for } j \text{ and } g \text{ in the same island of } [D_{\kappa}D_{\kappa'}] \text{ and separated by an even number of lines} \\ 0 \text{ for } j \text{ and } g \text{ in different islands} \end{cases} \quad (\text{A.24})$$

Then, as shown in (A.25)

(19) This can be shown by expanding κ'' into its sum of permutations and using the orthogonality of orbitals.

$$\hat{\rho}_{\kappa\kappa'}(\vec{r}) = \sum_{j=1}^N \Delta_{\kappa\kappa'} \gamma_{\kappa\kappa'}(j) |\phi_j(\vec{r})|^2 \quad (\text{A.25})$$

This is a form of the Schug formula.²⁰

For

$$|\gamma; K\rangle = \sum_{\kappa=I}^{f[\lambda]} b_{\kappa K} |\gamma; \kappa\rangle \quad (\text{A.26})$$

where $[\lambda] = [2^{(N-1)/2}, 1]$, a double state

$$\hat{\rho}_K(\vec{r}) = \sum_{\kappa, \kappa'=I}^{f[\lambda]} b_{\kappa K} b_{\kappa' K} \langle \gamma; \kappa | \hat{\rho}(\vec{r}) | \gamma; \kappa' \rangle \quad (\text{A.27})$$

By (A.25)

$$\hat{\rho}_K(\vec{r}) = \sum_{j=1}^N \left[\sum_{\kappa, \kappa'=I}^{f[\lambda]} b_{\kappa K} b_{\kappa' K} \Delta_{\kappa\kappa'} \gamma_{\kappa\kappa'}(j) \right] |\phi_j(\vec{r})|^2 \quad (\text{A.28})$$

We define the *unpaired orbital density* to be

$$\Gamma(j) \equiv \sum_{\kappa, \kappa'=I}^{f[\lambda]} b_{\kappa K} b_{\kappa' K} \Delta_{\kappa\kappa'} \gamma_{\kappa\kappa'}(j) \quad (\text{A.29})$$

Thus (A.28) becomes

$$\hat{\rho}_K(\vec{r}) = \sum_{j=1}^N \Gamma(j) |\phi_j(\vec{r})|^2 \quad (\text{A.30})$$

The form (A.30) was used by Karplus and Fraenkel in their treatment of methyl radical (see ref 12). Some of these results were obtained earlier by McConnell²¹ and McLachlan.²²

An important property of $\Gamma(j)$ is obtained by

$$\int \hat{\rho}_K(\vec{r}) d\vec{r} = \sum_{j=1}^N \Gamma(j) \int |\phi_j(\vec{r})|^2 d\vec{r} \quad (\text{A.31})$$

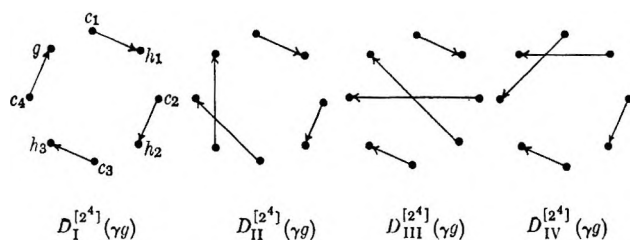
$$= \sum_{j=1}^N \Gamma(j) \quad (\text{A.32})$$

and by (3.12), we have

$$\sum_{j=1}^N \Gamma(j) = 1 \quad (\text{A.33})$$

For $|\gamma\rangle$ having doubly occupied orbitals we use the $|\gamma; \kappa\rangle$'s that always pair the doubly occupied orbitals. For this case the result (A.30) still holds; however, in (A.29) we use $f^{[\lambda]}(\gamma)$ instead of $f^{[\lambda]}$.

In conclusion, we tabulate $\gamma_{\kappa\kappa'}(j)$ and $\Delta_{\kappa\kappa'}$ for the methyl radical discussed in section VII. The pair diagrams associated with the chemical structures in (7.5) are taken to be

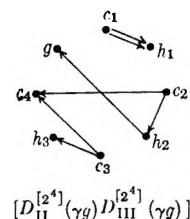


Here we use the notions of the ghost orbital g . Using these structures one obtains Table VI.

Table VI: $\gamma_{\kappa\kappa'}(j)$ and $\Delta_{\kappa\kappa'}$ for Methyl Radical

$\kappa\kappa'$	c_1	c_2	c_3	c_4	h_1	h_2	h_3	$\Delta_{\kappa\kappa'}$
I I	0	0	0	1	0	0	0	1
I II	0	0	-1	1	0	0	1	$1/2$
I III	0	-1	0	1	0	1	0	$1/2$
I IV	-1	0	0	1	1	0	0	$1/2$
II II	0	0	0	0	0	0	1	1
II III	0	-1	-1	1	0	1	1	$1/4$
II IV	-1	0	-1	1	1	0	1	$1/4$
III III	0	0	0	0	0	1	0	1
III IV	-1	-1	0	1	1	1	0	$1/4$
IV IV	0	0	0	0	1	0	0	1

As an example of how Table VI was constructed, we consider $\kappa = \text{II}$ and $\kappa' = \text{III}$.



Thus

$$\Delta_{\text{II III}} = (-1)^{2'-4} = 1/4$$

c_1 and h_1 are not in the island containing g and thus, according to (A.24), $\gamma_{\text{II III}}(c_1) = \gamma_{\text{II III}}(h_1) = 0$. Further, since h_2 , h_3 , and c_4 are an odd number of lines away from g and c_2 and c_3 are an even number of lines away from g , then, by (A.24), $\gamma_{\text{II III}}(h_2) = \gamma_{\text{II III}}(h_3) = \gamma_{\text{II III}}(c_4) = 1$ and $\gamma_{\text{II III}}(c_2) = \gamma_{\text{II III}}(c_3) = -1$.

Appendix B: Derivation of Eq 4.3

The isotropic contribution to the magnetic hyperfine interaction for a system of N electrons and M nuclei is given by the Fermi contact term²³

$$H(\text{cont}) = \sum_{a=1}^M \sum_{i=1}^N B(a) \mathbf{g}^i(a) \vec{S}_i \cdot \vec{I}_a \quad (\text{B.1})$$

where

$$\mathbf{g}^i(a) = \delta(\vec{r}_i - \vec{r}_a) \quad (\text{B.2})$$

\vec{r}_a being the center of nuclei a , and $B(a)$ is as in (4.4). This operator is considered as a perturbation to an N -electron spin-free Hamiltonian. Abragam and

(20) J. C. Schug, T. K. Brown, and M. Karplus, *J. Chem. Phys.*, **35**, 1873 (1961).

(21) H. M. McConnell, *ibid.*, **30**, 126 (1959).

(22) A. D. McLachlan, *Mol. Phys.*, **2**, 223 (1959).

(23) E. Fermi, *Z. Physik*, **60**, 320 (1930).

Pryce²⁴ have obtained $H_K^{\text{eff}}(\text{cont})$ of (4.1) from $H(\text{cont})$ by a first-order perturbation treatment. McConnell¹⁸ and McWeeny²⁵ and others have expounded on the evaluation of $A_K(a)$ in $H_K^{\text{eff}}(\text{cont})$. They obtain $A_K(a)$ as (compare with 4.3)

$$A_K(a) = \frac{B(a)}{2S} Q_K(a) \quad (\text{B.3})$$

where

$$Q_K(a) \equiv \langle K; SS | q(\vec{r}_a) | K; SS \rangle \quad (\text{B.4})$$

$$|K; SS\rangle = \alpha |K\rangle |SS\rangle \text{ (normalized)} \quad (\text{B.5})$$

$$q(\vec{r}_a) = \sum_{i=1}^N \delta(\vec{r}_i - \vec{r}_a) S_{iz} \quad (\text{B.6})$$

Here $|K; SS\rangle$ is the antisymmetric space-spin ket for the K th electronic state. It is an eigenfunction of S^2 and S_z . One refers to $q(\vec{r})$ as the "spin density" operator at \vec{r} and to $Q_K(\vec{r})$ as the "spin density" at \vec{r} of the K th electronic state. We prove the following theorem.

$$Q_K(\vec{r}) = \hat{\rho}_K(\vec{r}) \quad (\text{B.7})$$

where $\hat{\rho}_K(\vec{r})$ is the spin-free unpaired electronic density (3.10).

Proof: we begin by considering the eigenstate $|K; SS\rangle$. As used here, it is an exact zero-order eigenstate to the unperturbed spin-free Hamiltonian of the system. However, exact eigenstates are seldom found and only approximations are encountered. $|K; SS\rangle$ can be approximated by a suitable choice of a primitive ket $|\gamma\rangle$. The approximate eigenket to $|K; SS\rangle$ takes the form

$$|\gamma; KSS\rangle = N^{(S)} \alpha |\gamma\rangle |KSS\rangle \text{ (normalized)} \quad (\text{B.8})$$

where $N^{(S)}$ is a normalization constant

$$\alpha = \frac{1}{\sqrt{N!}} \sum_{P \in SN} \epsilon(P) P^e \otimes P^s \quad (\text{B.9})$$

is the antisymmetrizer in which P^e and P^s permute electron and electron spin coordinates, respectively, and

$$|KSS\rangle = \sum_{t=1}^{f^{[S]}} a_{Kt} |tSS\rangle \quad (\text{B.10})$$

In (B.10), $|tSS\rangle$ is the t th linearly independent spin eigenket of S^2 and S_z and $f^{[S]}$ is $f^{[\lambda]}$ of (1.14) where $[\lambda]$ and S are related by (1.5). The spin eigenket $|tSS\rangle$ can be obtained by projecting on an eigenket $|M_S = S\rangle$ of S_z with an operator φ_i^S

$$|tSS\rangle = \varphi_i^S |M_S = S\rangle \quad (\text{B.11})$$

A direct relation exists between the set $\{\varphi_i^S\}$ and the set $\{\kappa^{[\lambda]}\}$ of structure projectors. In fact, if we take

$$|M_S = S\rangle \equiv |k^s(N)\rangle \equiv |\alpha \beta \dots \alpha \beta \alpha \dots \alpha\rangle \quad (\text{B.12})$$

φ_i^S may be taken as²⁶

$$\varphi_i^S = N_i^{[\lambda]} P_i^{[\lambda]} \sigma_{i1}^{[\lambda]} = \sigma_{i1}^{[\lambda]} N_i^{[\lambda]} P_i^{[\lambda]} \quad (\text{B.13})$$

where $N_i^{[\lambda]}$ is the antisymmetric sum of permutations on columns of $T_I^{[\lambda]}$ and $P_i^{[\lambda]}$ is the symmetric sum of permutations on rows of $T_I^{[\lambda]}$

$$T_I^{[\lambda]} = \begin{array}{|c|c|c|c|c|c|} \hline 1 & 3 & \dots & 2p-1 & 2p+1 & \dots & N \\ \hline 2 & 4 & \dots & 2p & & & \\ \hline \end{array} \quad (\text{B.14})$$

$$[\bar{\lambda}] = \overbrace{[2^p, 1^{N-2p}]} = [N-p, p] \text{ and } p = N/2 - S$$

Since

$$\alpha \{g^e \otimes P^s\} = \epsilon(P) \alpha \{P^{-1e} \otimes g^s\} \quad (\text{B.15})$$

one can show that

$$\alpha \{g^e \otimes \varphi_i^S\} = \alpha \{\kappa^{[\lambda]} \otimes g^s\} \quad (\text{B.16})$$

where $\kappa^{[\lambda]}$ is the κ th structure operator and $[\lambda] = \overbrace{[N-p, p]} = [2^p, 1^{N-2p}]$. Thus for (B.8)

$$|\gamma; KSS\rangle = N^{(S)} \alpha |\gamma\rangle |KSS\rangle \quad (\text{B.17})$$

by (B.10)

$$= N^{(S)} \sum_{\kappa} a_{\kappa K} \alpha |\gamma\rangle |KSS\rangle \quad (\text{B.18})$$

by (B.11), (B.12), and (B.13)

$$= N^{(S)} \sum_{\kappa} a_{\kappa K} \alpha |\gamma\rangle \varphi_i^S |k(N)\rangle \quad (\text{B.19})$$

by (B.16)

$$= N^{(S)} \sum_{\kappa} a_{\kappa K} \alpha \kappa^{[\lambda]} |\gamma\rangle |k(N)\rangle \quad (\text{B.20})$$

and by (2.1)

$$= N^{(S)} \sum_{\kappa} \sqrt{C} a_{\kappa K} \alpha |\gamma; \kappa^{[\lambda]}\rangle |k(N)\rangle \quad (\text{B.21})$$

By (2.9)

$$|\gamma; KSS\rangle = N^{(S)} \alpha |\gamma; K^{[\lambda]}\rangle |k(N)\rangle \quad (\text{B.22})$$

where $|\gamma; K^{[\lambda]}\rangle$ is normalized. We now obtain $N^{(S)}$

$$1 = (N^{(S)})^2 \langle k(N) | \langle \gamma; K^{[\lambda]} | \alpha^\dagger \alpha | \gamma; K^{[\lambda]} \rangle | k(N) \rangle \quad (\text{B.23})$$

Using

$$\alpha^\dagger = \alpha; \quad \alpha^2 = \sqrt{N}! \alpha \quad (\text{B.24})$$

one has

(24) A. Abragam and M. H. L. Pryce, *Proc. Roy. Soc. (London)* **A205**, 135 (1951).

(25) R. McWeeny, *J. Chem. Phys.*, **42**, 1717 (1965); see also R. McWeeny and Y. Mizuno, *Proc. Roy. Soc. (London)*, **A259**, 554 (1961).

(26) This corresponds to Pauling's method of obtaining eigenkets of S^2 and S_z : L. Pauling, *J. Chem. Phys.*, **1**, 280 (1933). Note that $P_I^{[\bar{\lambda}]}$ is not necessary since $P_I^{[\bar{\lambda}]} |k^s(N)\rangle = (N-p)! |k^s(N)\rangle$. The reason for its inclusion is apparent later.

$$1 = (N^{(S)})^2 \sum_{P \in S_N} \epsilon(P) \langle k(N) | \langle \gamma; K^{[\lambda]} | P \times \\ | \gamma; K^{[\lambda]} \rangle P | k(N) \rangle \quad (\text{B.25})$$

$$= (N^{(S)})^2 \sum_{P \in S_N} \langle \gamma; K^{[\lambda]} | \epsilon(P) P | \gamma; K^{[\lambda]} \rangle \times \\ \langle k(N) | P | k(N) \rangle \quad (\text{B.26})$$

However, by definition of $|k(N)\rangle$, (B.12)

$$\langle k(N) | P | k(N) \rangle = \begin{cases} 0 & \text{if } P \notin \mathcal{O}_I^{[\bar{\lambda}]} \\ 1 & \text{if } P \in \mathcal{O}_I^{[\bar{\lambda}]} \end{cases} \quad (\text{B.27})$$

where $\mathcal{O}_I^{[\bar{\lambda}]}$ is the group of permutations on rows of $T_I^{[\bar{\lambda}]}$, (B.14). Thus, using $\mathcal{O}_I^{[\bar{\lambda}]} = \mathfrak{N}_I^{[\lambda]}$, (B.26) becomes

$$1 = (N^{(S)})^2 \langle \gamma; K^{[\lambda]} | \sum_{P \in \mathfrak{N}_I^{[\lambda]}} \epsilon(P) P | \gamma; K^{[\lambda]} \rangle \quad (\text{B.28})$$

Using

$$N_I^{[\lambda]} = \sum_{P \in \mathfrak{N}_I^{[\lambda]}} \epsilon(P) P \quad (\text{B.29})$$

and

$$N_I^{[\lambda]} \mathbf{k}^{[\lambda]} = (N - p)! p! \mathbf{k}^{[\lambda]} \quad (\text{B.30})$$

or

$$N_I^{[\lambda]} | \gamma; K^{[\lambda]} \rangle = (N - p)! p! | \gamma; K^{[\lambda]} \rangle \quad (\text{B.31})$$

we have

$$1 = (N^{(S)})^2 (N - p)! p! \langle \gamma; K^{[\lambda]} | \gamma; K^{[\lambda]} \rangle \quad (\text{B.32})$$

$$1 = (N^{(S)})^2 (N - p)! p! \quad (\text{B.33})$$

or

$$N^{(S)} = \sqrt{(N - p)! p!} \quad (\text{B.34})$$

Thus

$$| \gamma; KSS \rangle = \frac{1}{\sqrt{(N - p)! p!}} \mathcal{Q} | \gamma; K^{[\lambda]} \rangle | k(N) \rangle \quad (\text{B.35})$$

We now use (B.35) in (B.4) and obtain

$$Q_{\mathbf{K}}(\vec{r}) = \langle \gamma; KSS | q(\vec{r}) | \gamma; KSS \rangle \quad (\text{B.36})$$

$$= \frac{1}{(N - p)! p!} \langle k(N) | \langle \gamma; K^{[\lambda]} | \times \\ \mathcal{Q} q(\vec{r}) \mathcal{Q} | \gamma; K^{[\lambda]} \rangle | k(N) \rangle \quad (\text{B.37})$$

However

$$[q(\vec{r}), P^* \otimes P^*] = 0 \text{ for } P^* \otimes P^* \in S_N^* \otimes S_N^* \quad (\text{B.38})$$

Hence

$$\mathcal{Q} q(\vec{r}) = q(\vec{r}) \mathcal{Q} \quad (\text{B.39})$$

and by (B.24), (B.36) becomes

$$Q_{\mathbf{K}}(\vec{r}) = \frac{1}{(N - p)! p!} \sum_{P \in S_N} \epsilon(P) \langle k(N) | \times \\ \langle \gamma; K^{[\lambda]} | q(\vec{r}) P | \gamma; K^{[\lambda]} \rangle P | k(N) \rangle \quad (\text{B.40})$$

Substituting for $q(\vec{r})$, (B.6), and separating out the spin and the spin-free matrix elements, we have

$$Q_{\mathbf{K}}(\vec{r}) = \frac{1}{(N - p)! p!} \sum_{i=1}^N \sum_{P \in S_N} \langle \gamma; K^{[\lambda]} | \mathfrak{g}^i \epsilon(P) P \times \\ | \gamma; K^{[\lambda]} \rangle \langle k(N) | S_{iz} P | k(N) \rangle \quad (\text{B.41})$$

For the spin matrix element, we have

$$\langle k(N) | S_{iz} P | k(N) \rangle = \begin{cases} 0 & \text{if } P \notin \mathcal{O}_I^{[\bar{\lambda}]} \\ 1/2 X_i & \text{if } P \in \mathcal{O}_I^{[\bar{\lambda}]} \end{cases} \quad (\text{B.42})$$

and

$$X_i = \begin{cases} 1 & \text{if } i \in \text{first row of } T_I^{[\bar{\lambda}]} \\ -1 & \text{if } i \in \text{second row of } T_I^{[\bar{\lambda}]} \end{cases} \quad (\text{B.43})$$

Thus, using (B.42), (B.43), and $\mathcal{O}_I^{[\bar{\lambda}]} = \mathfrak{N}_I^{[\lambda]}$, (B.41) becomes

$$Q_{\mathbf{K}}(\vec{r}) = \frac{1}{(N - p)! p!} \sum_{P \in \mathfrak{N}_I^{[\lambda]}} \langle \gamma; K^{[\lambda]} | \sum_{i=1}^N \mathfrak{g}^i X_i \epsilon(P) P | \gamma; K^{[\lambda]} \rangle \quad (\text{B.44})$$

By (B.29), (B.31), and (3.9) we have

$$Q_{\mathbf{K}}(\vec{r}) = \langle \gamma; K^{[\lambda]} | \hat{\rho}(\vec{r}) | \gamma; K^{[\lambda]} \rangle \quad (\text{B.45})$$

and by (3.10)

$$Q_{\mathbf{K}}(\vec{r}) = \hat{\rho}_{\mathbf{K}}(\vec{r}) \quad (\text{B.46})$$

The Effect of Temperature on Dielectric Properties of Water-in-Oil Emulsions

by I. D. Chapman

Department of Chemistry, Trent University, Peterborough, Ontario, Canada (Received February 27, 1967)

The real and imaginary parts of the dielectric constants of a number of water-in-oil emulsions have been measured at frequencies between 30 cps and 100 kc/sec over a range of temperatures from -45 to 25° . An abrupt change in dielectric properties occurred at about -37° and was thought to be caused by the freezing of supercooled water droplets in the emulsions. The dielectric behavior of the ice-oil system was consistent with theories of interfacial polarization.

I. Introduction

The study of the dielectric properties of emulsions has been confined mainly to being a part of a general study of the dielectric properties of heterogeneous systems. This type of work has had as its object the testing of theories concerning heterogeneous systems. However, the chief value of dielectric techniques to the chemist has been to provide information about the nature of the molecules, atoms, and ions in liquids and solids. For example, the effect of structure on inter- and intramolecular forces in liquids and the elucidation of the configurational structures of molecules have been studied using the dielectric techniques.

Very little work has been done to attempt to apply dielectric techniques to this end in emulsion studies. This type of work requires information on the dielectric properties of materials, not only as a function of the applied frequency but also as a function of the measuring temperature. It is apparent that there is a lack of data on the effect of temperature on the dielectric properties of emulsions. While the real part of the dielectric constant alone can sometimes provide useful information on the processes occurring in the dielectric medium, the effect of frequency and temperature changes on the losses in the dielectric can often allow a decision to be made between two possible mechanisms¹ which observation on the real part of the dielectric constant alone would not allow. Because water-in-oil emulsions have been observed to exhibit dielectric dispersion,² it therefore seemed appropriate to make a preliminary study on the effect of temperature on the dielectric properties of water-in-oil emulsions in order to see if dielectric techniques could indeed be applied to a study of the nature of the dispersed phase.

II. Experimental Section

The emulsions were made in a blender from distilled water and paraffin oil. The oil contained magnesium stearate in concentrations up to $0.02 M$ in order to stabilize the emulsions. Both microscopic observation and measurement of dielectric properties con-

firmed that the emulsions were stable over a sufficiently long period (*i.e.*, 5–6 hr) in order for the required number of frequency and temperature spectra to be recorded.

The measuring cell was made of two concentric steel cylinders; the outer cylinder was at ground potential and was insulated from the high potential inner cylinder by Teflon spacers. The cell was calibrated with pure liquids of known dielectric constant and had an empty cell capacitance of 36.5 pf. The cell snugly fitted into a cooling jacket from which it was electrically insulated. Methanol, which had been cooled with Dry Ice, was circulated through the jacket and allowed cell temperatures as low as -45° to be achieved and controlled to $\pm 0.1^{\circ}$. During the cooling of the cell, an atmosphere of dry nitrogen was maintained over the cell to prevent the condensation of atmospheric water on the cell and leads. It was necessary to add small amounts of the emulsion to the cell during the cooling process due to the contraction of the liquid in the cell. This was done with a hypodermic syringe, whose needle fitted into a small hole in the top Teflon spacer. A second hole allowed the worker to see when there was a sufficient quantity of emulsion in the cell and allowed the emulsion to expand on heating. After the above procedure, the cell capacitance always returned to the value first recorded at room temperature before cooling. Great care was taken during the filling process to see that no air bubbles were trapped in the liquid. For this reason, it was found necessary to pump briefly on the emulsion after it had been made to remove any air. It was not thought that this short time of pumping was sufficient to remove any appreciable quantity of water.

The capacitance and resistance of the cell were measured with a General Radio capacitance measurement bridge, Type 1610B, which had a frequency range from 30 cps to 100 kc/sec.

(1) H. Fröhlich, "Theory of Dielectrics," Oxford University Press, London, 1958.

(2) T. Hanai, *Kolloid-Z.*, **177**, 57 (1961).

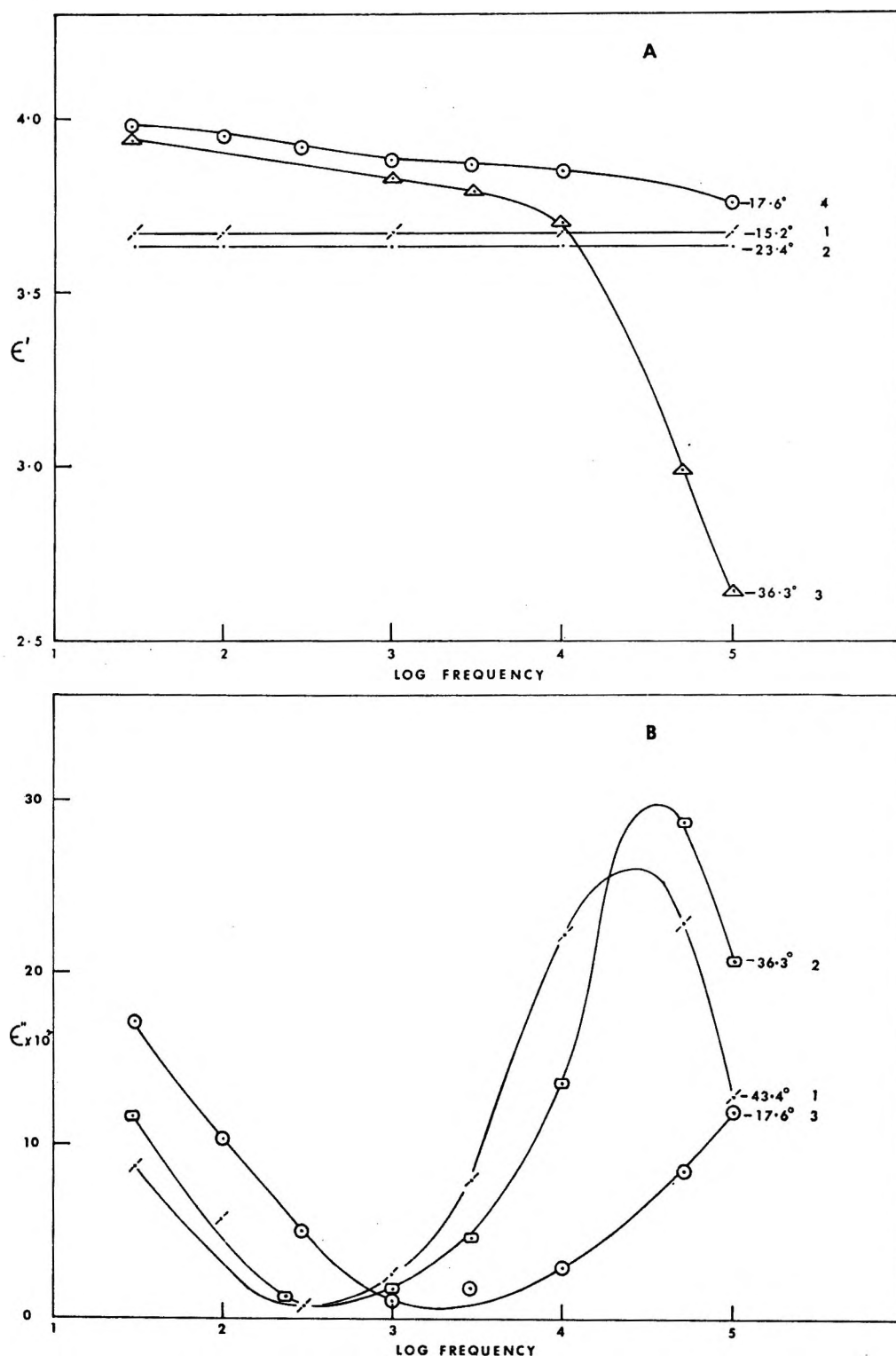


Figure 1. The frequency dependence of the real and imaginary parts of the dielectric constant of an 18% water-in-oil emulsion at various temperatures. The numbers by each curve indicate the sequence in which the data were obtained.

For all emulsions, the electrical measurements were made during one temperature cycle of the cell and contents from 25 to -45° and back. The frequency spectra of the dielectric constants were measured at each successive temperature during which the temperature of the cell remained constant.

III. Results

The real and imaginary parts of the dielectric constant of an 18% water-in-oil emulsion are plotted in Figures 1A and B for a number of temperatures and frequencies. At temperatures above -37° , no losses were observed and the dielectric constant of the emulsion at any given

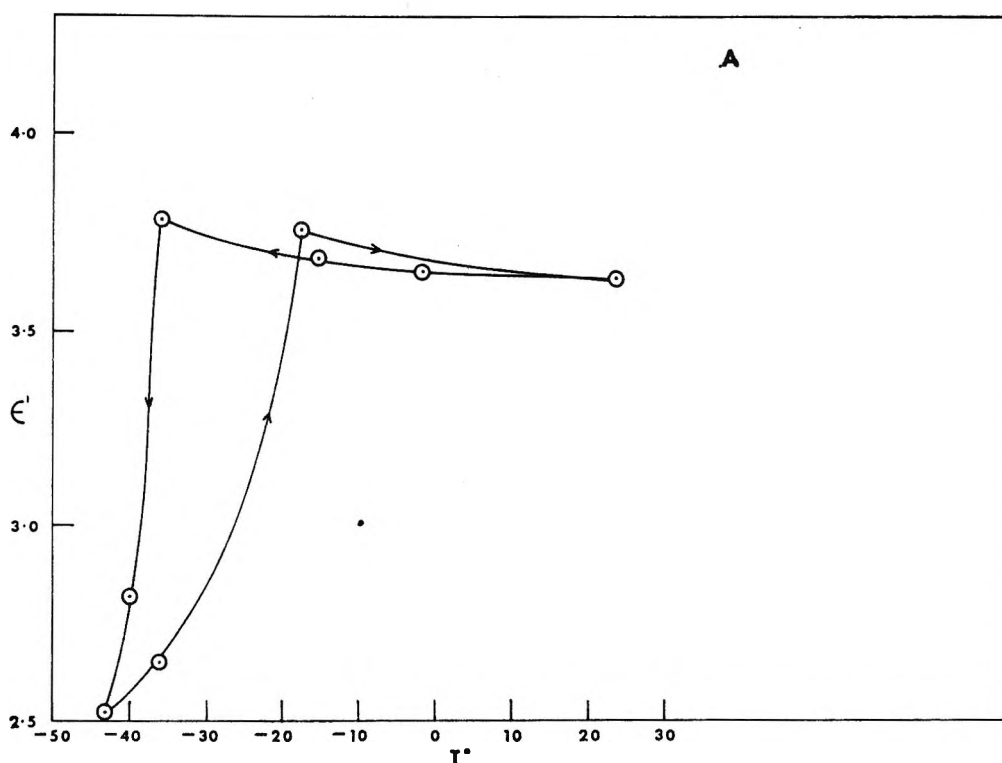


Figure 2A. The temperature dependence of the real and imaginary parts of the dielectric constant of an 18% water-in-oil emulsion at 100 kc/sec.

temperature was constant at all frequencies, although it increased slightly as the temperature was reduced. Below -37° , there was a decrease in the dielectric constant of the emulsion as the frequency increased, and dielectric losses were observed. At frequencies higher than 3 kc/sec, the losses rose to a maximum and then decreased as the frequency increased to 100 kc/sec. Fairly large losses were also observed at frequencies below 3 kc/sec; these losses rose rapidly as the frequency decreased. These effects are shown with the curves drawn from data recorded at -43.4° . As the temperature was raised, the loss maxima occurred at slightly different frequencies, the frequency at which the maximum occurred increasing as the temperature increased, as shown in Figure 1B curve 2. By about -17° there was no longer a maximum in the loss curve and the low-frequency losses had become quite large. The real part of the dielectric constant was almost constant except at the very highest measuring frequencies, where it slightly decreased in value. The losses at all frequencies were negligible at 0° and the dielectric constant returned to the value observed on first cooling.

The variation in the real and imaginary parts of the dielectric constant with temperature are shown in Figure 2 for a constant measuring frequency of 100 kc/sec. As already noted, the value of the real part of the dielectric constant of the emulsion increased slightly as the temperature was reduced until about -37° , when it abruptly decreased in value, continuing to

fall as the temperature was reduced further to -45° . As the temperature was raised, the dielectric constant rose gradually until it returned to a value close to that observed during the cooling at about -18° . The value at room temperature was exactly that recorded before cooling commenced. The losses at 100 kc/sec only became appreciable at about -37° , then rose as the temperature fell to -45° , and still continued to rise on warming the emulsion, rising to a maximum at -35° then falling to 0 by 0° .

The effect of the concentration of water in the emulsions on the losses is shown in Figure 3. At the given temperature, the losses appear to vary directly with the concentration of water and the loss maxima occur at about the same frequency.

IV. Discussion

From the results, it is apparent that an abrupt change in the properties of the emulsion occurred at about -37° . Since the oil by itself did not exhibit any losses at any frequency or temperature down to -45° , it is probable the change involved the water. Liquid water does not exhibit dielectric dispersion at these frequencies, while dielectric dispersion has been observed at these frequencies for ice. The relationship between the dielectric constant and the temperature of the emulsion, as shown in Figure 2A, is typical of a freezing liquid. The abrupt change in the dielectric constant of the emulsion as the temperature is lowered is usually due to an order-disorder transition, which,

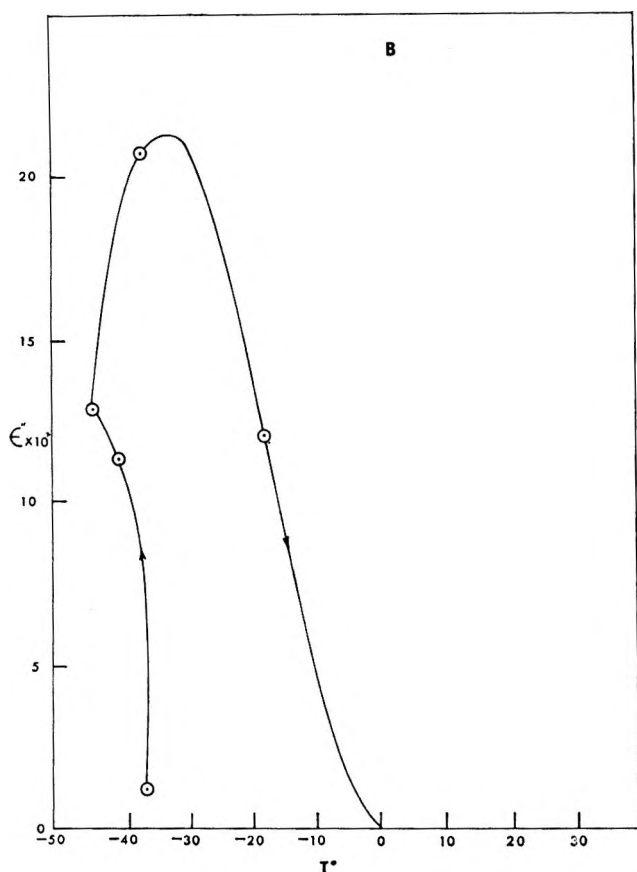


Figure 2B. See caption to Figure 2A.

as Fröhlich¹ is careful to point out, may or may not occur at the melting temperature of the solid. In this case, however, it would appear that it must be at or close to the freezing point of the supercooled liquid. As the temperature is increased, there is a gradual increase in the dielectric constant of the emulsion until it returns to a value close to that observed on cooling. The temperature at which this happens certainly does not occur at the melting point of the ice, although the data on the real part of the dielectric constant are insufficient to settle this point since the contribution of the dielectric constants of ice and supercooled water to that of the emulsion would be very similar. However, since the losses persist up to 0°, it would appear that the ice does not melt until that temperature.

The supercooling of water in the form of small droplets, while not well documented for emulsions, is a well known phenomenon in other systems. Cwilog³ showed that water droplets in a cloud chamber spontaneously froze at about -41° in dust-free atmospheres. Similarly, Lafargue⁴ observed that water droplets in air froze at -41°, independent of the concentration of dissolved ions. Supercooling of water to this extent occurs in systems where the size of the water droplet is very small, below 60 μ. Mohler's work⁵ on the expansion of water below 0° in fine capillaries, and Hodgson and McIntosh's work⁶ on the expansion of water-

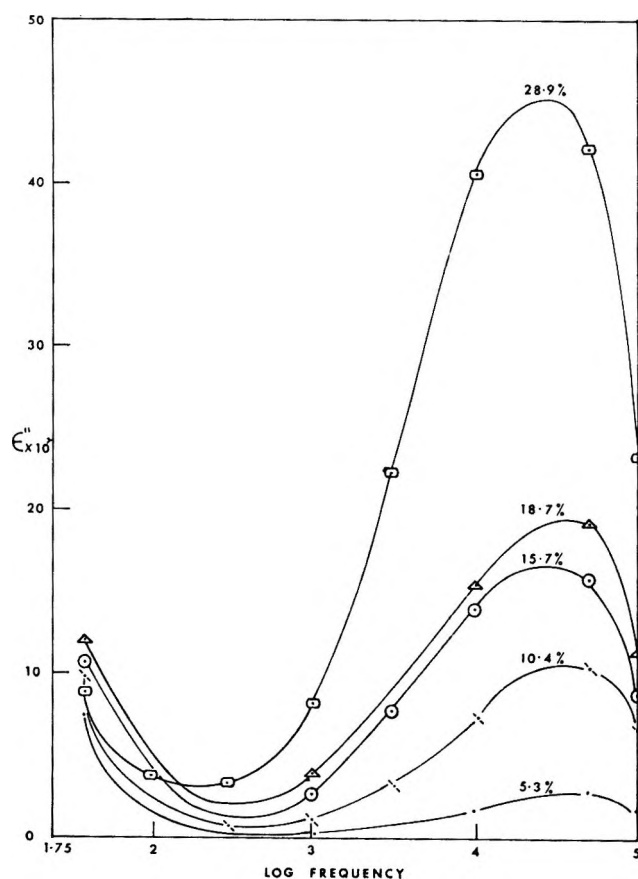


Figure 3. The frequency dependence of the imaginary part of the dielectric constant of water in oil emulsions of various concentrations at -40°.

saturated porous glass rods show that, provided the dimensions of the container which holds the water are small enough, supercooling can also occur in systems where the water particles are not spherical.

The explanation for the phenomenon of supercooling of liquids in very small droplets is not fully understood. Cwilog showed that the temperature at which the supercooled water froze depended on the presence or absence of suitable sublimation nuclei upon which the ice crystals might form. Thus, depending on the atmosphere around the water droplets, he reported freezing occurred between -27° in heavily contaminated atmospheres and -41° in dust-free atmospheres. Lafargue argued that spontaneous nucleation occurred at -41° because the structure of the water was such at that temperature that it was able to nucleate upon itself. Weyl⁷ has suggested that the water in the interior of a droplet has a normal atomic structure, whereas the surface film of the same droplet has a different atomic structure. It then follows that a water

(3) B. W. Cwilog, *Proc. Roy. Soc. (London)*, **A190**, 137 (1947).

(4) C. Lafargue, *Compt. Rend.*, **230**, 2022 (1950).

(5) J. F. Mohler, *Phys. Rev.*, **35**, 236 (1912).

(6) C. Hodgson and R. McIntosh, *Can. J. Chem.*, **38**, 958 (1960).

(7) W. A. Weyl, *J. Colloid. Sci.*, **6**, 389 (1951).

droplet has to have a certain minimum size in order to be stable. The transition from one type of structure to another type requires a finite distance, which will be a function of the temperature since the structure of water changes with temperature. Therefore, at a given temperature below the normal freezing point, a particular size must exist where a droplet of water is stable in the liquid state but not as ice. Weyl reported that the spontaneous freezing temperature of water does indeed decrease with a decrease in size of droplet. Weyl also suggested that the presence of highly polarizable ions alters the distribution of atoms in the surface layer and so allows the structure of the water droplets to change to that of the normal arrangement and hence allows freezing to occur.

The diameter of the water droplets in the emulsion was in the range 10–50 μ . The proportion of small droplets increased as the concentration of water increased, although all emulsions contained some larger particles. At any frequency and below -37° , the losses which were observed in emulsions of differing water content varied directly with the water content at a given temperature as shown in Figure 3. For those emulsions which contained concentrations of water in excess of 15%, the losses at any given frequency increased as the temperature was lowered below the inception of freezing at -37° . Therefore, more water must have frozen, thus increasing the losses. This effect can be seen in Figure 2B. As can be seen from Figure 1B, the losses at 100 kc would normally be expected to decrease as the temperature decreased, since a decrease in temperature causes the loss maximum to shift to lower frequencies, making the losses on the high frequency side of the peak fall. The increase in the losses as the temperature was raised, also shown in Figure 2B, is of course the reverse of that process; that is, the loss maximum shifts to be a higher frequency as the temperature is raised. Thus, previous observations in other systems are confirmed; the spontaneous freezing temperature of the water decreases as the particle size decreases.

It is unlikely that the nucleation could be suddenly induced in emulsions by dust or other entrapped particles. Furthermore, the presence of magnesium and stearate ions from the emulsifier in the surface layer of the water did not prevent supercooling. Therefore, the surface state of the stabilized water droplets in emulsions does not seem to be an important factor in the mechanism which controls nucleation and subsequent freezing. Lafargue's theory of spontaneous nucleation, while stating that the lowest temperature at which liquid water can exist is -41° , does not explain the range of temperature over which the water froze.

The curves shown in Figure 1 are typical of heterogeneous systems where the dielectric dispersion arises from interfacial polarization. The mechanism of

interfacial polarization arises from the migration of charge carriers, under the influence of an applied field, through one or both of the phases of the heterogeneous system. A charge accumulates at the interface and induces a mirror image which gives rise to a dipole moment.

The classic example of interfacial polarization is the Maxwell-Wagner two-layer condenser. The analysis of such a system gives rise to a frequency-dependent dielectric behavior characterized by a complex dielectric constant

$$\epsilon^* = \epsilon' - j\epsilon'' \quad (1)$$

The real and imaginary parts of this dielectric constant can be expressed by

$$\epsilon' = \epsilon_\infty + \frac{\epsilon_0 - \epsilon_\infty}{1 + w^2\tau^2} \quad (2)$$

$$\epsilon'' = \frac{\epsilon_\infty\tau}{w\tau_1\tau_2} + \frac{(\epsilon_0 - \epsilon_\infty)w\tau}{1 + w^2\tau^2} \quad (3)$$

ϵ_0 and ϵ_∞ are the equilibrium and limiting high-frequency dielectric constants, τ is the relaxation time for the composite dielectric, τ_1 , τ_2 refer to the relaxation times of the individual phases, and $w = 2\pi \times$ frequency. From eq 2, it can be seen that ϵ' will fall from a value of ϵ_0 at $w = 0$ to ϵ_∞ at $w \rightarrow \infty$. The right-hand side of eq 3 is made up of two parts—the first an ohmic conductivity term, the second a relaxation term. Thus, the second term suggests that ϵ'' will rise from zero to a maximum and then fall to zero over the appropriate range of frequencies. The first term indicates that ϵ'' will tend to infinitely as $w \rightarrow 0$. The sum of these two terms indicates that ϵ'' will be large at low frequencies, will fall then rise to a maximum at intermediate frequencies, and then fall to zero as $w \rightarrow \infty$.

The tendency to large losses at low frequencies is the feature that differentiates interfacial polarization from the Debye-type relaxation observed with orientational polarization. These large losses at low frequencies are clearly seen in Figure 1B. Although the formulas were originally derived for a two-layer condenser, Wagner⁸ has shown that one phase may be dispersed as spheres in the other phase without changing the complex permittivity of the composite dielectric. Wagner solved his equations for the special case of a low concentration of suspended spheres in a nonconducting medium. His expressions related ϵ_0 and ϵ_∞ to the dielectric constants of the two phases and their volume fractions. At the concentrations of water in these emulsions, Wagner's expressions do not hold since they do not take into account the interaction between the conducting regions. The results instead are considered in relation to a recent successful extension of Wagner's theory by Hanai.²

(8) K. W. Wagner, *Arch. Electrotech.*, 2, 371 (1914).

Hanai assumed that Wagner's relationships hold for the infinitesimal process where infinitesimally small quantities of the dispersed phase are added to the system. By a succession of these infinitesimal additions, the system reaches the final volume fraction ϕ . From this basic equation, so deduced, he obtained expressions pertinent to water-in-oil emulsions, where the conductivity of the water is very much greater than that of the oil. The following expressions were shown to give good agreement with data obtained from his measurements on water-in-oil emulsions

$$\epsilon_0 = \frac{\epsilon_1}{(1 - \phi)^3} \quad (4)$$

$$\frac{\epsilon_2 - \epsilon_\infty}{\epsilon_2 - \epsilon_1} \left(\frac{\epsilon_1}{\epsilon_\infty} \right)^{1/3} = 1 - \phi \quad (5)$$

ϵ_1 and ϵ_2 refer to the dielectric constants of the oil and water, respectively.

In this work, ϵ_1 was calculated from measurements using oil alone. The value 2.18 was constant over the temperature range -38 to -48° . If the arguments of the earlier part of the discussion are correct, ϵ_2 refers not to liquid water but to ice in the above range of temperatures. Auty and Cole⁹ measured the dielectric constant of ice and showed that at frequencies above 1 kc/sec, the dielectric constant of ice was 3.10 in the same temperature range.

Table I compares the observed and the calculated values of ϵ_0 and ϵ_∞ for various volume fractions of water.

Table I

Volume fraction	ϵ_0		ϵ_∞	
	a	b	a	b
0.099	3.11	2.98	2.36	2.30
0.151	3.65	3.57	2.38	2.33
0.179	3.92	3.94	2.38	2.35
0.226	4.78	4.76	2.44	2.38
0.280	5.78	5.84	2.45	2.45

* Measured. ^b Calculated from eq 4 and 5.

At the highest measuring frequency of 100 kc, $\epsilon'' \neq 0$, and therefore $\epsilon' \neq \epsilon_\infty$. The values of ϵ_∞ in Table I were obtained from a Cole-Cole plot of ϵ'' vs. ϵ' . The curve was extrapolated at the high frequency end to $\epsilon'' = 0$, the intercept of the ϵ' axis giving the value of ϵ_∞ .

The agreement between the measured and calculated data is excellent. The assumption that the dispersed phase is ice would appear correct and the dielectric behavior of the system appears consistent with theories

of interfacial polarization. Furthermore, the relaxation frequencies are an order of magnitude higher than those observed by Auty and Cole for ice in the same temperature range where the effect was assumed to be due to orientational polarization.

In order to establish the nature of the charge carrier in the mechanism of interfacial polarization, it would be helpful to know the activation energy of the migration of the carrier from one site to the next. This can be found by plotting $\log \tau$ against $1/T$. τ is related to T by the expression

$$\tau = A \exp B/RT$$

τ is the reciprocal of w_{\max} where w_{\max} is the frequency at which ϵ'' is a maximum. A and B are constants, although B is also identified with the activation energy for the relaxation process. A straight line was plotted from the data which are listed in Table II.

Table II

$\tau \times 10^4$	$1/T \times 10^4$
6.3	4.38
4.2	4.29
3.9	4.24
2.7	4.17

The slope of the line gave a value of 7.8 kcal/mole for B . This is very close to the value of 8-9 kcal/mole calculated by Riehl¹⁰ for the activation energy for the migration of a proton in ice from one water molecule to the next and suggests that the charge carriers are protons.

In summary, it would appear that the interfacial region does not have any discernible effect upon the dielectric properties of the water-in-oil emulsions below the freezing point of the water. The phenomena appear to be explicable on the basis of interfacial polarization in a system of conducting spheres in a nonconducting medium. In such a system, however, it would be difficult to see any effect due to surface conductivity. As O'Konski¹¹ points out, the effect of the bulk conductivity will mask any surface conductivity, even in the case where the bulk conductivity is that of ice and not water.

Acknowledgments. The author wishes to thank the National Research Council of Canada and Trent University for their generous financial support of this work, and Mr. M. Beswick for his help in taking many of the data.

(9) R. P. Auty and R. H. Cole, *J. Chem. Phys.*, **20**, 1309 (1952).

(10) N. Riehl, *Zh. Fiz. Khim.*, **29**, 1372 (1955).

(11) C. T. O'Konski, *J. Phys. Chem.*, **64**, 605 (1960).

A Comparative Study of Pheophytin *a* and Pheophytin *b* Monolayers

by W. E. Ditmars, Jr., and Q. Van Winkle

Department of Chemistry, The Ohio State University, Columbus, Ohio 43210 (Received February 17, 1967)

Monomolecular films of pheophytin *a* and pheophytin *b* at air-water interfaces have been prepared and studied. If the pH of the aqueous subphase is less than about 5.0 and if low-intensity diffuse green lighting is used, the films are chemically stable. At higher pH's, the pheophytins undergo a chemical change that appears to be essentially allomerization. Surface pressure and surface potential of the pheophytins as a function of molecular area at 21° have been studied at pH 4.0 and 3.0. Decrease of pH results in an increase of molecular area and of apparent surface moment at given values of surface pressure. The phenomena, and the chemical stabilization, are evidence of salt formation by entry of one or two protons at the center of the chlorin ring. The results are discussed in terms of a simple model. A method is described for analyzing the composition of dilute benzene or ether solutions containing mixtures of chlorophyll *a*, allomerized chlorophyll *a*, pheophytin *a*, and allomerized pheophytin *a*.

Introduction

There is considerable evidence that the chlorophylls, *in vivo*, exist in the form of oriented noncrystalline monolayers,¹ lying at what is essentially an oil-water interface. Monolayer studies of the chlorophylls and their closely related derivatives *in vitro* provide useful information about their intermolecular interaction properties. In particular, insight can be gained into conditions necessary for chemical stability and the variations of interfacial dipolar characteristics with change of molecular composition and superficial environment.

As a surface chemistry problem, study of the chlorophyll and derivative monolayers presents unusual difficulties not only because of their chemical and photochemical instability, but also because of problems of obtaining homogeneously spread films. These problems may, in part, account for the lack of agreement in recent work.^{2,3} Qualitative comparison shows differences in surface pressure (π) by as much as a factor of 2 for given values of area per molecule (σ).

Exploratory work in this laboratory on the chemical stability of chlorophyll and pheophytin monolayers is in general agreement with observations made by Colmano,⁴ Rosoff and Aron,² and Bellamy, *et al.*³ Our findings differ from those of the latter authors in several respects, however. We find that at air-buffer (pH 8.0-9.0) interfaces, in dim, diffuse green light, homogeneously spread monolayers of chlorophyll *a*, pheophytin *a*, and pheophytin *b* undergo a chemical change that appears to be essentially allomerization (*i.e.*, oxidation of the cyclopentanone ring). Allomerization of the pheophytins occurs to the extent of about 75% in 4.5 hr. In the same period, chloro-

phyll *a* undergoes about 11% allomerization. We found that the pheophytins were stable ($\leq 5\%$ decomposition) for periods of at least 6 hr if the pH of the aqueous phase was equal to or less than 4.5. A comparative study was made of their surface pressures (π) and surface potentials (ΔV) as a function of molecular area (σ). Film pressure (π) and surface potential (ΔV) measurements were made simultaneously at $21 \pm 0.5^\circ$. The only published work found, for the pheophytins under similar experimental conditions, is that of Rosoff and Aron.² These authors apparently studied only pheophytin *a* and indicate that the properties are the same at pH 8.0 as at pH 4.0. This is in variance with our observations on chemical stability as a function of pH and with our findings that, at pH 4.0, areas per molecule at given values of π are at least 20% greater than those reported at pH 8.0.

Experimental Section

A. Materials. All solvents and reagents were CP analytical grade. The solvents used in the spectroscopic analyses with determinants were saturated with water and contained dissolved oxygen and carbon dioxide in amounts probably $\geq 10^{-5}$ M. The distilled water used had a specific resistance of 8×10^6 ohms/cm. Benzene and ether were evaluated as spreading solvent.

(1) For example, see: Brookhaven Symposia in Biology, No. 11, "The Photochemical Apparatus—Its Structure and Function," Brookhaven National Laboratory, Upton, N. Y. (Available from the Office of Technical Services, Department of Commerce, Washington 25, D. C.), 1958, J. J. Wolken, p 87; J. A. Bergeron, p 118; R. Sager, p 101.

(2) M. Rosoff and C. Aron, *J. Phys. Chem.*, **69**, 21 (1965).

(3) W. D. Bellamy, G. L. Gaines, Jr., and A. G. Tweet, *J. Chem. Phys.*, **39**, 2528 (1963).

(4) G. Colmano, *Biochim. Biophys. Acta*, **47**, 454 (1961).

Table I: Visible Absorption Parameters of the Pheophytins

Ref	Red molar absorption coeff, $\epsilon_R \times 10^{-4}$	$\lambda R(\max)$, $m\mu$	$\lambda B(\max)$, $m\mu$	B/R	R(min)	R/505 ^a	R _{1/2} , $m\mu$	B _{1/2} , $m\mu$
Pheophytin a (mol wt 871), Ethyl Ether								
This research	5.30	667.0	408.5	2.03	18.1	4.52	16.6	51.8
Zscheile and Comar	5.14	665.0	401	2.14	18	4.38	17.0	
Smith and Benitez	5.55	667	408.5	2.07		4.37		
Holt and Jacobs	5.10	666	408.5	2.10	~23	4.44	16.5	
Pheophytin a, Benzene								
This research	5.42	670.2	414.3	2.03	19.2	4.97	18.4	47.9
Bellamy, Gaines, and Tweet	4.88	669	414	2.06	16.3	4.65	19.0	50
Pheophytin b (mol wt 885.2), Ethyl Ether								
This research	3.18	654.3	433.2	4.89	7.33	2.97	16.0	16.2
Zscheile and Comar	3.27	653	433	5.32	8.0	2.92	16.0	22.0
Smith and Benitez	3.73	655	434	5.15		2.96		
Holt and Jacobs	3.30	654.8	432	5.26	~10	3.0	17.0	18.0

^a The ratio is that of the optical densities of the peaks of the main red band and the second green band. The latter for pheophytin b occurs at 522.1 $m\mu$.

The latter was adopted since it was found to give more homogeneously spread films. Surface-active impurities derived from the materials used could have given the following probable positive errors in π : 0.05 dyne/cm for $210 \text{ \AA}^2 \geq \sigma \geq 155 \text{ \AA}^2$, 0.1 dyne/cm for $150 \text{ \AA}^2 \geq \sigma \geq 130 \text{ \AA}^2$, and 0.2 dyne/cm for $125 \text{ \AA}^2 \geq \sigma \geq 100 \text{ \AA}^2$.

Double recrystallization of the Baker reagent grade phthalate salt, used to prepare the 0.025 *M* buffer solutions, had no detectable influence on experimental accuracy (see below). Within experimental error, increase or decrease of buffer concentration by a factor of 2, use of a citrate buffer, and use of unbuffered HCl substrate gave the same results.

Crystalline samples of chlorophyll *a* and chlorophyll *b* were prepared by a method similar to that of Jacobs, Vatter, and Holt.⁵ The pheophytins were prepared by treating acetone solutions of the chlorophylls with degassed 10% (by volume) HCl solution for 1 min with agitation and then were transferred by washing to ethyl ether or benzene. All operations were carried out in dim, diffuse green light or in total darkness.

The purity of the pheophytins was estimated to be 90% or better, the main impurity being 5–7% allomerized pheophytin. A comparison of spectral parameters of this work and those reported in the literature⁶ is given in Table I. The values of the molar extinction coefficients of this work were calculated from the measured optical densities of the pheophytin solutions of known concentration. The accuracies of the concentrations depended on those of the parent chlorophyll solutions. The crystalline chlorophylls were thoroughly desiccated to remove water before solution preparation. Samples were taken from different prep-

arations of crystals whose spectroscopic parameters agreed to within better than 1%. A detailed comparison (unpublished) of molar extinction coefficients of this work and those available in the literature indicated an absolute purity of 97% or better for the chlorophylls used in this research.

B. Monolayer Stability Test Procedure. The monolayer was spread at an area per molecule ($\geq 240 \text{ \AA}^2$) corresponding to pressures less than 0.1 dyne/cm. At the end of a test period, about 57% of the monolayer was compressed onto a large glass plate, collected in a known volume of reagent grade solvent, and analyzed spectroscopically. All of the apparatus (glassware and nickel tongs) used in transferring the monolayer were thoroughly cleaned and wetted with the aqueous substrate used for testing. It was essential that the plate remain completely wetted during the whole time of transfer (5 min); partial drying resulted in the occurrence of allomerization on the plate.

C. Correlation of Spectroscopic Data. Spectroscopic measurements, at 25°, were made with a Cary 14 recording spectrophotometer run on automatic slit control.

Pheophytinization and allomerization of the chlorophylls are the simplest decomposition processes that can occur under many usual laboratory conditions when water, carbon dioxide, and oxygen are present to

(5) E. E. Jacobs, A. E. Vatter, and A. S. Holt, *Arch. Biochem. Biophys.*, **53**, 228 (1954).

(6) F. P. Zscheile and C. L. Comar, *Botan. Gaz.*, **102**, 463 (1941); J. H. C. Smith and A. Benitez in "Modern Methods of Plant Analysis," K. Paech and M. V. Tracey, Ed., Vol. 4, Springer-Verlag, Berlin, 1955, p 142; A. S. Holt and E. E. Jacobs, *Am. J. Botany*, **41**, 710 (1954).

interact.⁷ Study of the spectral changes of dilute solutions in instances where decomposition had occurred suggested that mixtures of pheophytinized and allomerized products can be formed. Using the optical densities of pure solutions with known concentrations of chlorophyll *a*, pheophytin *a*, allomerized chlorophyll *a*, and allomerized pheophytin *a*, the spectra of solutions in which decomposition had occurred were analyzed by the standard method of determinants.

The allomerized chlorophyll *a* was prepared by the method which Holt⁸ used to prepare fraction 2 (the lactone with the expanded isocyclic ring structure). This compound is predominantly formed when water is present. The visible absorption spectrum is the same whether a hydroxyl group or a methoxy group is present on the C-10 atom. Allomerized pheophytin *a* was obtained by the procedure used to prepare the pheophytins, but using a solution of allomerized chlorophyll *a* as the starting material.

The optical densities and wavelengths used for the four components and values of the denominator determinants are given in Table II. The optical densities are arrayed in the order which gives the value of the determinant. Wavelengths in the regions of the maxima of the primary red and blue bands were chosen to minimize the effect of small errors. By calculating

Table II: Optical Density (*d*) Values and Wavelengths for $0.99 \times 10^{-6} M$ Solutions at 25° and Values of the Denominator Determinants Used for Component Correlation

Wave-length, mμ	Optical density			Pheo <i>a</i>
	Chl <i>a</i>	Allom chl <i>a</i>	Allom pheo <i>a</i>	
A. For Benzene (H ₂ O, O ₂ , CO ₂) Solutions				
667.5	0.723	0.226	0.282	0.501
405.0	0.569	0.652	0.989	0.902
427.5	0.840	0.646	0.283	0.465
415.0	0.633	0.907	0.720	1.088
Determinant <i>A</i> = -96.8686×10^{-3}				
405.0	0.569	0.652	0.989	0.902
662.5	0.696	0.343	0.182	0.329
427.5	0.840	0.646	0.283	0.465
415.0	0.633	0.907	0.720	1.088
Determinant <i>B</i> = $+40.1329 \times 10^{-3}$				
B. For Ethyl Ether (H ₂ O, O ₂ , CO ₂) Solutions				
420	0.796	0.955	0.347	0.609
665	0.659	0.221	0.300	0.505
415	0.690	0.983	0.521	0.882
405	0.688	0.725	0.902	1.022
Determinant <i>C</i> = $+46.11707 \times 10^{-3}$				
405	0.688	0.725	0.902	1.022
415	0.690	0.983	0.521	0.882
667.5	0.477	0.121	0.344	0.525
420	0.796	0.955	0.347	0.609
Determinant <i>D</i> = $+39.917798 \times 10^{-3}$				

the unknown concentrations from two different sets of simultaneous equations, the possibility of spurious correlations is reduced.

Use of the method to analyze the changes in pigment samples from numerous tests on decomposition during pigment preparation, storage in solutions, and in monolayers showed that, in the absence of extensive photo-bleaching, pheophytinization and/or allomerization were the predominant decomposition reactions. An uncertainty of $\pm 5\%$ or less was found in the concentrations of the four components, if extensive allomerization had not occurred. Where extensive allomerization was indicated, concentration uncertainties as large as $\pm 10\%$ were found, indicating that more than one type of allomerized product had been formed.

The percentage decomposition of pheophytin *b* in the monolayer stability tests was estimated by determining the change in the ratio of the peak optical densities of the main blue band and the blue satellite band. The percentage recovery was estimated from knowledge of the amount spread and comparison of the peak optical densities of the red, blue, and blue satellite bands with those from a solution of known concentration of pure pigment. On the basis of the similarities in the type spectroscopic changes to those caused by transformation of pheophytin *a* into allomerized pheophytin *a*, it seems likely that the primary intact-ring product was the allomerized form of pheophytin *b*.

D. Surface Measurement Apparatus and Procedures. The Wilhelmy plate method⁹ was used to measure surface pressure (precision ± 0.02 dyne/cm). Microscope cover glasses, slightly etched in hot Haemosol (Meinecke and Co., Inc.) and trisodium phosphate preserved a zero contact angle, whereas tantalum and platinum did not. Etching caused adsorption of the pheophytins on the wet glass at $\pi < 0.1$ dyne/cm. To obtain zero contact angle and reproducible adsorption the slide was inserted after the monolayer was spread. The correction for surface concentration, due to adsorption, was determined for each run.

Surface potentials (precision ± 8 mv or better) were measured with both the vibrating disk and the ionizing electrode methods.¹⁰ The latter method provided for scanning over the entire surface. To prevent irreversible changes in the film with use of the polonium electrode,^{11,12} it was held at a distance of 1 cm from the surface during the brief period of automatic recording of

(7) For example, E. I. Rabinowitch, "Photosynthesis," Interscience Publishers, Inc., New York, N. Y., 1945-1956, pp 400, 452, 462, 1773-1774.

(8) A. S. Holt, *Can. J. Biochem. Physiol.*, **36**, 439 (1958).

(9) For example, W. D. Harkins, "Physical Chemistry of Surface Films," Reinhold Publishing Corp., New York, N. Y., 1952, pp 121-124.

(10) For example, A. W. Adamson, "Physical Chemistry of Surfaces," Interscience Publishers, Inc., New York, N. Y., 1960, p 119.

(11) Similar observations have been made for protein monolayers.¹²

(12) J. F. Chambers, *Australian J. Chem.*, **16**, 180 (1963).

measurements and removed from the surface at other times.

The following procedure gave satisfactory results in obtaining homogeneously spread films. A 10^{-4} *M* solution of the pigment was added dropwise in increments of ~ 0.005 cc/10 sec. The drops were distributed evenly over the surface such that the initial total surface area of the film was from 40 to 80 cm² greater than that corresponding to the start of measurable changes of surface pressure. The initial area per molecule was from 230 to 245 Å². A well-spread monolayer showed variations in ΔV (surface potential) of ± 20 mv or less at $\pi < 1.0$ dyne/cm and ± 2 mv at higher compression. These variations were reproducible on decompression and recompression provided that the collapse pressure had not been greatly exceeded. More rapid spreading led to large variations in ΔV (± 50 to ± 150 mv) over the surface that persisted on high compression. With improper spreading, smaller values of π at given σ 's were observed, which indicated three-dimensional aggregation that was not reversible in the time of measurement (5 hr). Use of a spreading peg (wire, slide, etc.)¹³ did not, in itself, lessen heterogeneity.

Compression and decompression of the films were completely reversible if the area per molecule was not reduced to less than about 85 Å² and if the rate of area change was 9 Å²/molecule min or less. Equilibration times of 5–10 min were allowed between area changes corresponding to about 4% of the total area per molecule.

Results

The surface pressure and surface potential data are summarized in Figures 1 and 2 and Table III. The experimental accuracy in area per molecule, for a given value of π , is estimated to be $\pm 3\%$. The average deviation in surface potential was found to be ± 8 mv over the whole range of π . Film collapse, as evidenced by decrease of surface pressure and surface potential with time, was observed at compressions several dynes per centimeter above the highest values recorded in the table.

The surface potentials are positive in sign. This suggests that the ester groups are anchored in the water phase, with the phytol group and the chlorin head oriented in the air phase. The smaller over-all surface moments of the pheophytin *b* systems are probably due primarily to the presence of the carbonyl group at the 3 position on the chlorin ring. The average difference at both pH's is about 0.5 Debye unit.

The compressibilities, at compressions greater than about 1.0 dyne/cm, are characteristic of liquid expanded films, ranging from 0.08 cm/dyne for pheophytin *b* at low compressions and pH 3.0 to 0.022 cm/dyne for pheophytin *a* at high compressions and pH 4.0. Decrease of pH results in an increase of compressibility. The pheophytin *b* monolayers show greater compress-

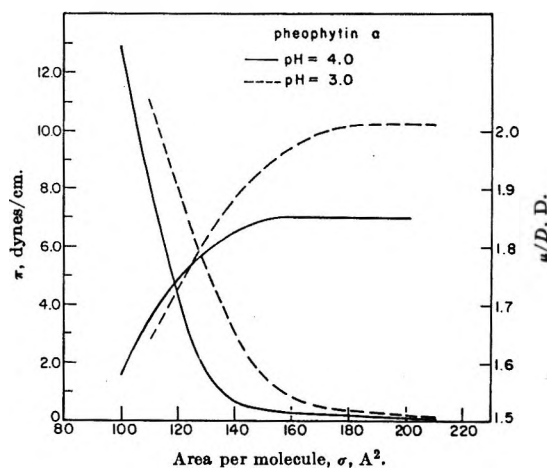


Figure 1. Film pressure (π , dynes/cm) and surface moment (μ/D , D.) vs. area per molecule (σ , Å² per molecule) for pheophytin *a* monolayers at air–water (0.025 *M* phthalate buffer) interfaces; pH 4.0 and 3.0; temperature 21°.

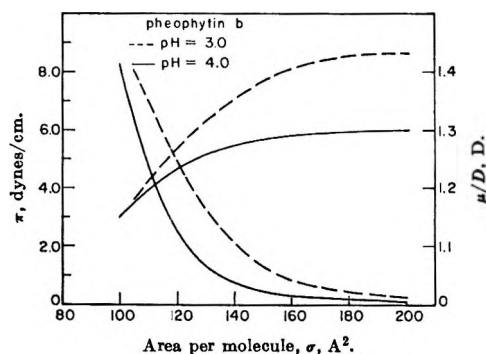


Figure 2. Film pressure (π , dynes/cm) and surface moment (μ/D , D.) vs. area per molecule (σ , Å² per molecule) for pheophytin *b* monolayers at air–water (0.025 *M* phthalate buffer) interfaces; pH 4.0 and 3.0; temperature 21°.

sibility than the pheophytin *a* films at a given pH, at compressions above about 1.0 dyne/cm. In the same range, the areas per molecule of the *b* systems are smaller than those of the *a* by an average of about 7% at pH 4.0 and 9% at pH 3.0 for the same value of π .

Alexander¹³ and later Trurnit and Colmano¹⁴ made comparative studies of chlorophyll *a* and chlorophyll *b* monolayers. While their results cannot be compared directly with those of this research, there are certain features which are in common. Their work showed that the chlorophyll *b* films had greater compressibilities than the *a* films, and, at given values of π , showed smaller values of molecular area. Alexander's work showed that the surface moment of chlorophyll *b* films was about 0.27 D. less than that of the *a* films.

As shown in Figures 1 and 2 the pheophytins are characterized by a decrease of over-all surface moment

(13) A. E. Alexander, *J. Chem. Soc.*, 1813 (1937).

(14) For example, H. J. Trurnit, and G. Colmano, *Biochim. Biophys. Acta*, **31**, 434 (1959).

Table III: Film Pressure (π) and Surface Potential (ΔV) Values for Pheophytin *a* and *b* at pH 4.0 and 3.0

Area/ molecule, Å ²	Pheophytin <i>a</i>				Pheophytin <i>b</i>			
	pH 3.0		pH 4.0		pH 3.0		pH 4.0	
	π , dynes/cm ²	ΔV , mv	π , dynes/cm	ΔV , mv	π , dynes/cm	ΔV , mv	π , dynes/cm	ΔV , mv
100			12.85	597			8.25	434
105			10.46	586	8.03	423	6.35	422
110	11.04	561	8.25	573	6.92	415	4.90	410
115	9.50	553	6.24	561	5.83	407	3.65	399
120	8.00	544	4.35	548	4.90	398	2.62	387
125	6.56	536	2.80	535	4.02	390	1.84	377
130	5.30	527	1.60	521	3.30	381	1.27	364
135	4.10	517	1.04	508	2.63	372	0.98	354
140	3.05	508	0.68	492	2.10	364	0.75	342
145	2.25	497	0.50	480	1.64	355	0.62	333
150	1.50	486	0.41	463	1.29	347	0.50	322
155	1.05	476	0.36	450	1.01	339	0.40	313
160	0.80	464	0.31	436	0.83	330	0.35	303
165	0.63	454	0.27	424	0.70	322	0.30	295
170	0.50	442	0.24	412	0.60	314	0.29	286
175	0.42	431	0.21	401	0.50	306	0.25	279
180	0.37	420	0.18	387	0.45	298	0.23	271
185	0.30	409	0.16	377	0.35	290	0.18	263
190	0.27	398	0.14	367	0.30	283	0.15	257
195	0.23	388	0.12	358	0.25	275	0.12	249
200	0.20	379	0.10	349	0.20	269	0.10	244
205	0.17	369						
210	0.15	361						

(μ/D) with decrease of σ at compressions above about 1.0 dyne/cm, at which point the compressibility has greatly decreased. Above about 1.0 dyne/cm, μ/D decreases linearly with increase of π up to the collapse pressure.

The pheophytins show an expansion in area per molecule, at a given value of π , with decrease of pH. Decrease of pH from 4.0 to 3.0 results in an average increase of 8% in σ for $\pi > 1.0$ dyne/cm. The expansion below 1.0 dyne/cm averages about 13%. Comparison of the data of Bellamy, *et al.*,³ on pheophytin *a* at pH 8.0 with the present data at pH 4.0 shows an average expansion of 20% in σ at the lower pH for $\pi > 1.0$ dyne/cm. The average compressibility, in the range of 1.0–11.0 dynes/cm, increases from 0.018 cm/dyne at pH 8.0 to 0.024 cm/dyne at pH 4.0. Table IV shows the effect of pH on surface moment.

While a detailed investigation of the factors affecting monolayer stability has not been made, certain features can be outlined. At pH's less than 5.0, the allomerization of the pheophytins is retarded to about 0.7%/hr in periods up to 20 hr. There is indication that other, slower reactions also occur. At pH 8.0, the rate of allomerization of the pheophytins is about 11%/hr. The corresponding allomerization rate for chlorophyll *a* is about 2.5%/hr. No pheophytin or allomerized pheophytin appears to be formed. When the monolayer is under an inert atmosphere (~ 100 ppm of O₂), and at high pH, the rate of allomerization of chlorophyll decreases to about 0.8%/hr. The effect on the pheo-

Table IV: Effect of pH on μ/D for Pheophytin *a*

Ref	pH	π , dynes/cm	μ/D , Debye units
Bellamy, <i>et al.</i>	8.0	1.0	1.52
Bellamy, <i>et al.</i>	8.0	10.0	1.41
This research	4.0	1.0	1.82
This research	4.0	10.0	1.64
This research	3.0	1.0	1.96
This research	3.0	10.0	1.67

phytins has not yet been evaluated. Additives such as β -carotene, lecithin, or phytol in chlorophyll *a* monolayers appear to have little effect on the rate of decomposition.

Discussion

A plausible interpretation of the stabilization of pheophytin monolayers by low pH and the concurrent expansion of the films and increase of μ/D with decrease of pH from 8.0 to 4.0 is that salt formation occurs with entry of a least one proton into the center of the ring. On this basis, the further expansion when the pH is decreased from 4.0 to 3.0 can be viewed as an increase in the degree of protonation.¹⁵

The strong perturbing effect of acid on the visible

(15) A. Neuberger and J. Scott [*Proc. Roy. Soc. (London)*, **A213**, 307 (1952)] present evidence that the closely related porphyrin derivatives can exist in mono- and diprotonated forms.

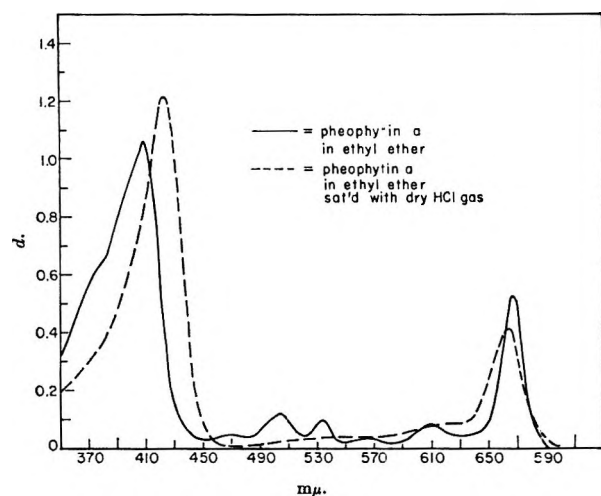


Figure 3. Visible absorption spectra of pheophytin *a* (10^{-6} *M*) in ethyl ether and in ethyl ether saturated with dry HCl gas.

absorption spectrum of pheophytin *a*, shown in Figure 3,¹⁶ can also be interpreted as arising from entry of protons into the center of the ring. The effect is reversed upon removal of acid. Addition of protons to the center of the chlorin ring of pheophytin *a* would tend to produce the same symmetry as that of chlorophyll *a*. The changes effected by the acid make the pheophytin *a* spectrum resemble that of chlorophyll *a*. Strong perturbing effects of acid on the spectrum of allomerized pheophytin *a* are also observed.

Certain features of the pheophytin monolayers can be interpreted on the basis of a simple model. From a scale molecular model based on known atomic radii and bond angles, it was determined that the chlorin head with the ester groups can be approximated by a rigid rectangular parallelepiped, $13.1 \times 13.1 \times 4.5$ Å, and the phytol tail by a flexible cylinder with a length of 20 Å and a diameter of 5.8 Å. With the head and tail folded together and the plane of the head perpendicular to the air-water interface, the smallest excluded area is about 90 Å² (this includes the unoccupiable interstitial area between close-packed molecules). With the ester groups oriented in the water, this would be the smallest observable area per molecule for a monomolecular film of the pure pigment. If the angle of the folded unit, with respect to a normal to the interface, is increased to 42°, the smallest excluded area is about 110 Å². The collapse areas in the range 100–110 Å², observed in this work, are consistent with the tilted, folded configuration. If the chlorin head were inverted into the water and both head and tail made perpendicular to the interface, molecular areas of 75 Å² or less would be observed. The sign of the surface potential would probably be reversed.

Figure 4 shows an idealized cross-sectional view, in the plane of the interface, of a probable local arrangement of monolayer molecules and their counterions at an average area per molecule of 130 Å². The rectangles

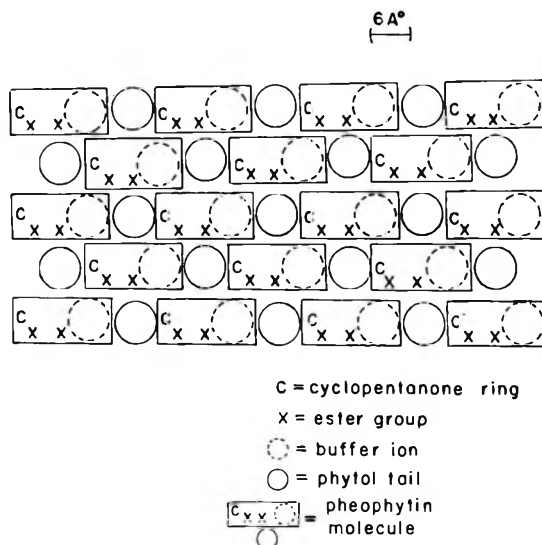


Figure 4. Arrangement of pheophytin molecules at an air-water interface at an average area of 130 Å² per molecule. A plan view of the plane of the interface. Rectangles represent the cross section of the chlorin head oriented at 42° to the normal to the interface.

represent cross-sectional projections of the heads, with the angle of tilt taken to be 42° from the normal. The closed circles are projections of the tails, and the dashed circles inside the head areas are projections of the phthalate counterions, considered to lie beneath the heads in the aqueous phase. The units are drawn to scale of the approximate molecular dimensions. The letter C's designate the position of the cyclopentanone ring, and the X's show the position of the ester groups. In addition to the horizontal displacement of alternate rows of molecules as shown in Figure 4, it is visualized that a relative vertical displacement between alternate rows occurs. This would further reduce the net lateral coulombic repulsion interactions. Vertical displacement of a molecule into the surface of the water, due to nearest neighbor repulsions, will be opposed by the work required for hydrophobic immersion of the hydrocarbon parts of the molecule. Dispersion interactions, which make the main contribution to the effective cohesive pressure, will be large for head-tail and head-head interactions and small for tail-tail interactions. In this closely packed array, kinetic motions of the molecular units about their equilibrium positions and axial rotational motions of the phytol tails will contribute to the thermal pressure. Random wagging motions of the tails will be largely frozen out.

The observed small increase of surface moment with increase of area per molecule can be simply interpreted as resulting from a decrease in the degree of relative vertical displacement between neighboring molecules,

(16) Similar observations were made for $\alpha,\beta,\gamma,\delta$ -tetraphenylchlorin: G. D. Dorough and F. M. Neunneken, *J. Am. Chem. Soc.*, **74**, 3974 (1952).

accompanied by a slight increase in separation of some of the heads and their counterions.

At film pressures less than about 1.0 dyne/cm, pheophytin monolayers are characterized by compressibilities larger than those for cohering liquid films and by small fluctuations in the surface potential over the surface. The consistency and reproducibility of the phenomena make it unlikely that surface contaminants are the cause. A reasonable interpretation is that the films are characterized by coexisting regions of different states of molecular ordering. One type of region would consist of molecules in the ordered local array suggested in Figure 4, while the other would consist of a more or less random interdispersion of heads and tails, characterized by a significantly increased kinetic motion of the tails. In the more disordered region, intermolecular coulombic repulsions would be less and could thereby result in a further decrease in the degree of relative vertical displacement and an increase in the separation of some of the heads and their counterions. This would account for the variations in surface moment (about ± 0.06 D. from the average value shown in Figures 1 and 2) over the surface.

The areas per molecule where collapse begins to occur are similar for the pheophytin *a* and *b* systems. Collapse pressures for the *b* systems, however, are considerably smaller. From the viewpoint of the proposed model, these phenomena can be related rather simply to the presence of the 3-position carbonyl groups on the pheophytin *b* head units. As the film is compressed, the molecules approach a close-packed ordered array with increasing degree of relative vertical displacement between alternate rows of molecules. In the vertical staggering arrangement, intermolecular configurations

are possible where there are ion-dipole attractions between neighboring positively charged head centers and 3-position carbonyl groups. Increase of degree of relative vertical staggering by compression can increase ion-dipole attractions. These interactions, not present in the pheophytin *a* monolayers, will contribute to the cohesive pressure and tend to promote relative vertical displacement. Consequently, less compressional work is required to reduce film area and reach the collapse configuration.

Increase of angle of tilt of the chlorin heads (with respect to a normal to the interface) with decrease of pH may account in part for both the increase of area where film collapse begins and the relatively small increase of apparent surface moment. At the area of start of film collapse the monolayer molecules are probably in the closest packed state. By the present model, angles of tilt of 31° at pH 4.0 for pheophytin *a* and *b*, 37° at pH 3.0 for pheophytin *b*, and 42° at pH 3.0 for pheophytin *a* are calculated.

If stabilization of the pheophytin monolayers against allomerization results as a consequence of protonation at low pH, as seems likely, the following can be visualized. Protons, in the center of the chlorin ring, can act as strong electron acceptors. Such attraction transmitted to the cyclopentanone ring would decrease its electron density. This would increase the potential barrier in the first step of the allomerization process.

Acknowledgments. We take pleasure in acknowledging the assistance of H. F. Blanck, Jr., in development of the determinantal method of analysis. The research work has been generously supported by grants from the National Science Foundation (GB2254) and the National Institute of Health (5R01 GM10856-06).

Adsorption of 1,1-Diphenyl-2-picrylhydrazyl on

Solid Acid Catalysts

by Haruo Imai, Yoshio Ono, and Tominaga Keii

Department of Chemical Engineering, Tokyo Institute of Technology, Meguro, Tokyo, Japan
(Received March 14, 1967)

Adsorption of 1,1-diphenyl-2-picrylhydrazyl (DPPH) on some silica-alumina catalysts has been studied mainly by the electron spin resonance (esr) method. The peak height of the esr spectrum of DPPH decreases upon addition of silica-alumina catalyst to benzene solution of DPPH. This decrease of the peak height is attributed to the chemisorption, not physical adsorption, of DPPH on the catalyst. From the investigation of some reactions of DPPH with a few acids, it is concluded that DPPH is adsorbed on Lewis acid sites, losing its unpaired electron, and on Brønsted acid sites, obtaining a proton from silica-alumina catalyst. With the use of silica-alumina poisoned with ethyl acetate, it was found that the number of Lewis acid sites was $5 \times 10^{12}/\text{cm}^2$ and that of Brønsted acid sites was $1 \times 10^{12}/\text{cm}^2$.

Introduction

Many adsorption methods of measuring the acidity of solid acid catalysts have been proposed.¹⁻⁵ Among them, the method utilizing *n*-butylamine¹ is well known as the most useful one. However, this method also has some disadvantages in that the experimental procedure requires the use of optical spectrometry.

In the present work, adsorption of 1,1-diphenyl-2-picryl-2-hydrazyl (DPPH) on silica-alumina catalysts has been studied in connection with the surface acidity of the catalysts.

Experimental Section

Silica-alumina (17% alumina) was prepared by coprecipitation with hydrolysis of ethyl orthosilicate and aluminum isopropoxide. Alumina and silica gel were obtained with hydrolysis of the corresponding compounds mentioned above. These were dried at 120° for 2 hr and then activated in air at 550° for 2 hr. Their specific surface areas, measured by the nitrogen adsorption method, were 280, 244, and 183 m²/g, respectively. Sodium-exchanged silica-alumina and aluminum were prepared by immersing the activated catalysts overnight in a 1 *N* sodium hydroxide aqueous solution and washing with water. The catalysts evacuated after overnight contact with ethyl acetate or *n*-butylamine were found to be poisoned. Silica gel treated with hydrogen fluoride was obtained by immersing silica gel in a 10% hydrogen fluoride solution and washing with water. DPPH was recrystallized from ethyl ether at room temperature. The analytical grade benzene and carbon tetrachloride were dried with silica gel and used as solvents.

The esr measurements were carried out at room

temperature with spectrometer JES 3110-X with 100 kc/sec field modulation. The cell used for the measurements is a quartz tube (8 mm in diameter) as illustrated in Figure 1. DPPH was used as a benzene solution (1.7×10^{-3} *M*) which was saturated completely with nitrogen. A part of about 0.4 cc of the DPPH solution was put into the cell, and the cell was set in the cavity of the esr spectrometer as illustrated in Figure 1A. A small amount of the catalyst, previously heated *in vacuo* for 2 hr at 500°, was sealed into a glass ampoule. The catalyst was added to the cell by breaking the ampoule under a nitrogen stream from a branch of the cell. After mixing the catalyst with the solution for a few minutes, the esr measurements were carried out. Changes in the amount of DPPH were monitored by measuring the peak height of a first-derivative representation of the esr signal.

In the optical spectrometric studies, the catalyst used was pressed into a plate about 0.1 mm in thickness.

Results and Discussion

When a small amount of silica-alumina catalyst was added to the DPPH solution, the peak height decreased very rapidly and levelled off at a new value. The peak height decreased with successive addition of the cata-

(1) H. A. Benesi, *J. Am. Chem. Soc.*, **78**, 5490 (1956).

(2) H. P. Leftin and W. K. Hall, *Actes Congr. Intern. Catalyse*, **2°**, Paris, **1**, 1353 (1961).

(3) R. L. Richardson and S. W. Benson, *J. Phys. Chem.*, **61**, 405 (1957).

(4) (a) D. M. Brouwer, *J. Catalysis*, **1**, 372 (1962); (b) W. K. Hall, *ibid.*, **1**, 53 (1962).

(5) Y. Trambouze, *Advan. Catalysis*, **9**, 544 (1957).

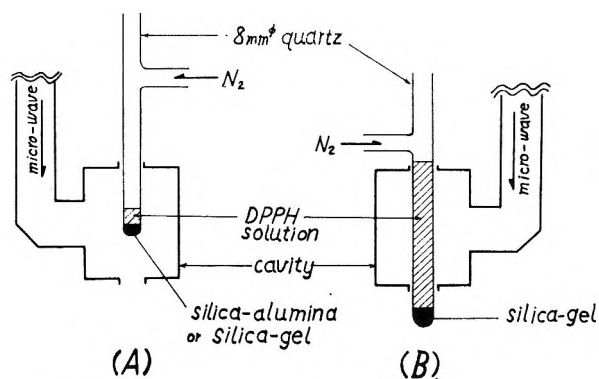


Figure 1. Apparatus.

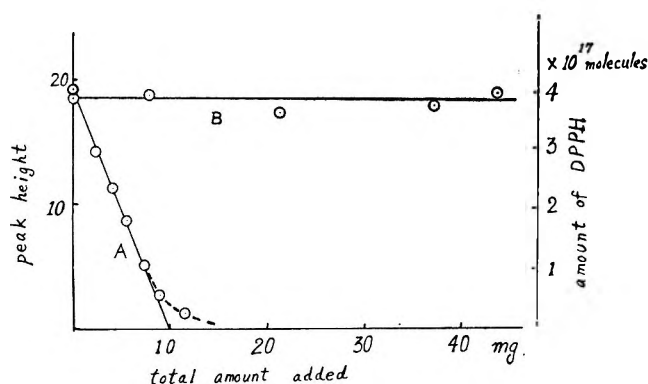


Figure 2. Change in the peak height of DPPH with the successive addition of silica-alumina (A) and silica gel (B).

lyst, as shown in Figure 2A, where the abscissa represents the total amount of the catalyst added to the solution. The peak height in the absence of the catalyst corresponds to 4.1×10^{17} molecules/0.4 cc. The extrapolation of the straight line of Figure 2A to the abscissa indicates 10 mg of the catalyst, which shows that the slope of the line is 4.1×10^{17} molecules/10 mg, i.e., 1.5×10^{13} molecules/cm². When carbon tetrachloride was used as solvent instead of benzene, the same results were obtained. Accordingly, the value 1.5×10^{13} molecules/cm² may be considered as the saturation amount of chemisorbed DPPH on the surface of the silica-alumina at the experimental temperature, 25°. The adsorption isotherm at 25° was measured by changing the initial concentration of the solution from 1×10^{-4} to 2×10^{-3} mole/l. The observed isotherm (Figure 3) is a Langmuir type with a saturation value of 1.6×10^{13} molecules/cm².

A similar experiment for silica gel showed no decrease in the peak height, as illustrated in Figure 2B. However, using a large amount of the solution (4 cc) and the cell set as in Figure 1B, the adsorption isotherm as shown by B in Figure 3 was obtained.

From these adsorption experiments, the adsorption of DPPH on the surface of the silica-alumina sample can be considered as "chemical" and that on the silica gel as "physical." Furthermore, it should be noted that

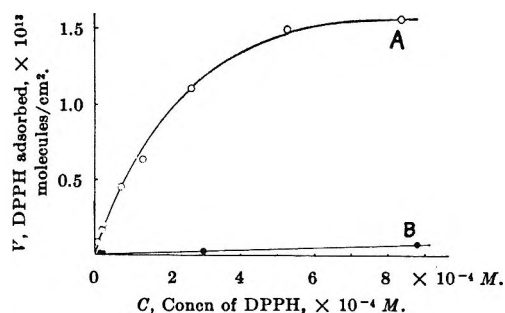


Figure 3. Adsorption isotherms of DPPH by silica-alumina (A) and silica gel (B) at 25°.

the saturation amount of chemisorption, 1×10^{13} molecules/cm², corresponds to the total number of surface acid sites of the silica-alumina sample.

It is very interesting to clarify the nature of this "chemisorption." As is well known, the acid sites of the surface of a silica-alumina catalyst are divided into Lewis acid and Brønsted acid. In order to know the interactions of DPPH with these acid sites, reactions of DPPH with the following acids have been carried out. Antimony pentachloride and aqueous acetic acid were used as examples of a Lewis acid and a Brønsted acid, respectively. When DPPH was added to antimony pentachloride in carbon tetrachloride, the color of the solution changed from violet to green. No esr signal was obtained from this solution. However, the green solution changed its color again to violet and gave the esr signal of DPPH upon the addition of water, which decomposes antimony pentachloride. In order to discover the stoichiometry of the reaction of DPPH with antimony pentachloride, esr measurements have been made for the solution using a variety of mole ratios, $0 < [\text{SbCl}_5]/[\text{DPPH}] < 1$. These various solutions were made from DPPH in carbon tetrachloride in a concentration of 10^{-3} mole/l., and antimony pentachloride in carbon tetrachloride in a concentration of 10^{-3} mole/l. The observed relations between the esr peak heights of the solution mixtures and the mole ratios is shown in Figure 4; one mole of DPPH reacts with one mole of antimony pentachloride, i.e., one DPPH loses its unpaired electron through the attack of one Lewis acid.

It must be noted that the behavior of DPPH is very similar to that of perylene. (1) It is well known that perylene forms its cation radical with charge transfer to a Lewis acid such as AlCl_3 . (2) The radical is also formed when perylene adsorbs on Lewis acid sites of silica-alumina or alumina,^{4,6} and (3) perylene develops a violet color peculiar to the radical in concentrated sulfuric acid, while DPPH turns green in concentrated sulfuric acid as well as in a antimony pentachloride-carbon tetrachloride solution. These similarities strongly suggest that DPPH forms a charge-transfer

 (6) B. D. Flockhart and R. C. Pink, *J. Catalysis*, **4**, 90 (1965).

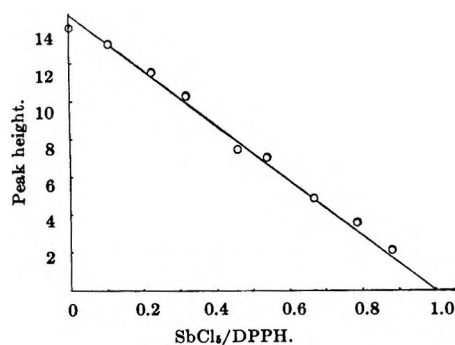


Figure 4. Stoichiometry of the reaction of DPPH with antimony pentachloride.

complex with the Lewis acid or Lewis sites of silica-alumina.

The solution of DPPH in glacial acetic acid showed a violet color and the same spectrum as did DPPH in benzene. Upon adding a small amount of water, this violet color changed to red and the esr signal disappeared. The infrared spectrum of this red solution was completely identical with that of 1,1-diphenyl-2-picrylhydrazine.

The optical spectra of DPPH obtained in benzene, concentrated sulfuric acid, diluted aqueous acetic acid, and on the silica-alumina catalyst are shown in Figure 5. When the spectrum from the adsorbed DPPH (b) is compared with those from DPPH in diluted acetic acid (c) and concentrated sulfuric acid (d), the band at 700 m μ can be assigned to DPPH adsorbed on Lewis acid sites, and the band from 350 to 450 m μ to the superimposed one from DPPH adsorbed on Lewis acid sites and on Brønsted acid sites.

From these experimental results, it can be concluded that DPPH is adsorbed on both Lewis sites and Brønsted sites of the surface of the catalyst.

In order to confirm this conclusion concerning the nature of the surface acidity, the chemisorption on some poisoned catalysts was examined, using the same procedure as was used to get Figure 2. The saturation amounts of chemisorption obtained with various samples are summarized in Table I. From the fact that no chemisorption occurred on silica-alumina or alumina poisoned with *n*-butylamine which is chemisorbed on both kinds of acid sites,¹ it is clear that DPPH is chemisorbed on acid sites. The fact that no chemisorption occurred on alumina poisoned with ethyl acetate, which is a Lewis base, shows that Lewis sites on the surface of alumina are responsible for chemisorption

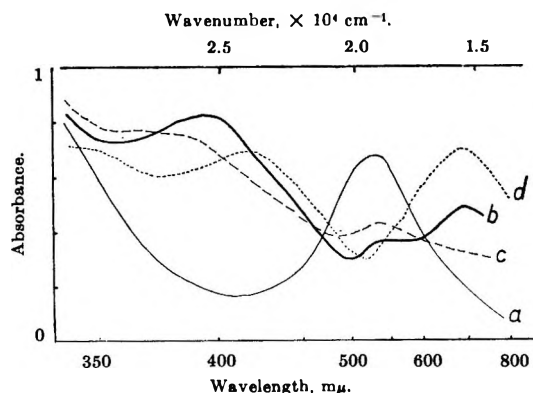


Figure 5. Visible absorption spectra of DPPH in benzene (a), on silica-alumina (b), in dil CH₃COOH (c), and in concd H₂SO₄ (d).

Table I: Chemisorption Amounts of DPPH (molecules/cm²)

	Silica-alumina	Alumina	Silica gel
Nontreatment	1.5×10^{13}	2.8×10^{13}	0
Poisoned with <i>n</i> -butylamine	0	0	...
Poisoned with ethyl acetate	1.0×10^{13}	0	...
Base exchange with aq NaOH	2.7×10^{13}	2.3×10^{13}	...
Treated with aq HF	5.5×10^{13}

of DPPH. On the other hand, the fact that a considerable amount of chemisorption occurred on silica-alumina even after the same poisoning shows that the latter catalyst has Brønsted sites also. The decrease of the adsorption amount by a sodium-exchange treatment indicates that some Lewis sites as well as Brønsted sites were poisoned by the treatment, in accordance with the result obtained by Pink.⁶ Chemisorption occurs on silica gel pretreated with hydrogen fluoride, which is a Brønsted acid. From these results, it is clear that DPPH is adsorbed chemically on both Lewis acid sites and Brønsted acid sites. Supposing that Lewis sites on the surface of the silica-alumina were completely poisoned with ethyl acetate, the total number of Brønsted sites should be $1.0 \times 10^{13}/\text{cm}^2$; the number of Lewis sites should be $5 \times 10^{12}/\text{cm}^2$. These values agree with those obtained by the use of other adsorbates: Lewis sites are $5 \times 10^{12}/\text{cm}^2$ (triphenylmethane)² and $2 \times 10^{12}/\text{cm}^2$ (perylene)⁴; total acid sites are $3 \times 10^{13}/\text{cm}^2$ (*n*-butylamine).⁷

(7) T. Shiba, M. Sato, H. Hattori, and K. Yoshida, *Shokubai* (Sapporo), 6, 80 (1964).

Dielectric Properties of Ice and Water Clathrates

by Wallace S. Brey, Jr., and Howard P. Williams

Department of Chemistry, University of Florida, Gainesville, Florida 32601 (Received March 17, 1967)

Dielectric properties of clathrate compounds of dichlorofluoromethane and trichlorofluoromethane as well as of ice formed in various ways have been measured in the audio-frequency region over ranges of temperatures between -30 and $+2^\circ$. All the materials except pure ice show distributions of relaxation times, the distributions for the clathrates being more extensive than those for the impure ice samples. Ice samples formed in the presence of impurities as well as the clathrates all exhibit greater low-frequency conductivity than does pure ice. However, while impurities have little effect on the magnitude of the frequency at which maximum loss occurs in ice, the loss maximum is at substantially higher frequencies in the clathrates. The activation energies for reorientation are slightly larger for the clathrates than for ice.

Both ice and the water clathrate compounds of non-polar molecules, which contain a host lattice somewhat resembling that of ice, have a region of dielectric absorption in the audiofrequency range. Study of the characteristics of this absorption has been very valuable as a tool for understanding something of the structure of the clathrate and of the rotational behavior of the enclathrated molecules.

In a previous paper,¹ capacitance and loss measurements were reported for the hydrate of trichlorofluoromethane (Refrigerant-11 or R-11), and the variation of the frequency of maximum loss with temperature was interpreted in terms of an apparent activation energy. Davidson and co-workers have carried out dielectric measurements in the audiofrequency range on a number of water clathrates.²⁻⁵ For mixtures of acetone or ethanol with water, they have used dielectric absorption as a criterion for the existence of hydrate at low temperatures.

In the present paper, we report results of measurements of dielectric properties of the hydrate of dichlorofluoromethane (R-21), together with additional results for the hydrate of trichlorofluoromethane. The hydrate of the latter is known to have a structure of type II.^{6,7} Almost certainly, the hydrate of dichlorofluoromethane has the same structure, which is characteristic of somewhat larger molecules, although this has not been directly established. To determine whether the effects of other foreign molecules, too large to form clathrates, on the dielectric properties of ice are similar to the effects of the enclathrated molecules, we have also investigated the dielectric properties of samples of ice frozen in the presence of either urea or dioxane. Parameters in which the clathrates differ from pure ice include the magnitude of low-frequency conductivity, the magnitude of the frequency at which the loss maximum occurs at a given temperature, and the distribution of relaxation times,

and ice samples frozen in the presence of impurities are compared in each of these respects.

Experimental Section

Except for the electrode size and the procedure of handling the sample, the measurements were made as previously described.¹ The 350M Balsbaugh cell, used in the earlier work and referred to here as cell I, was modified from some of the measurements by replacement of the $7/8$ -in. diameter inner electrode with a $1/2$ -in. diameter stainless steel electrode. The modified cell is referred to as cell II. It was also found convenient to alter the outer electrode, essentially the sample container, by constructing the bottom as a screw cover, using a Teflon gasket as a seal. The inverted cell could then be filled to the desired extent with solid sample with the inner electrode already in place, and then closed by screwing on the bottom cap, without disturbing the solid sample.

The other difference in technique involved covering the sample with the corresponding liquid fluoromethane. As described previously,¹ the hydrate of trichlorofluoromethane may change in crystal form and dielectric properties with time. In the present work, we have established that this change does not occur in the presence of excess liquid trichlorofluoromethane, and this is consistent with the proposal that aging effects result from the loss of the enclathrated molecule. Blank

- (1) W. S. Brey, Jr., and J. W. Legg, *J. Phys. Chem.*, **67**, 1737 (1963).
- (2) G. J. Wilson and D. W. Davidson, *Can. J. Chem.*, **41**, 264 (1963).
- (3) D. W. Davidson and G. J. Wilson, *ibid.*, **41**, 1424 (1963).
- (4) D. W. Davidson, M. M. Davies, and K. Williams, *J. Chem. Phys.*, **40**, 3449 (1964).
- (5) A. D. Potts and D. W. Davidson, *J. Phys. Chem.*, **69**, 996 (1965).
- (6) M. von Stackelberg and H. R. Müller, *Z. Elektrochem.*, **58**, 25 (1954).
- (7) T. A. Wittstruck, W. S. Brey, A. M. Buswell, and W. H. Rodebush, *J. Chem. Eng. Data*, **6**, 343 (1961).

runs showed no dielectric loss in the pure liquid fluoromethane.

Dichlorofluoromethane was obtained from the Matheson Co. as Genetron-21 and was distilled from the original container into a chilled Pyrex test tube, fitted with a standard-taper joint. After addition of an equal volume of water and after several minutes of shaking the tube and cooling it in an ice bath, the hydrate precipitated from solution. The hydrate of trichlorofluoromethane, the latter obtained as Freon-11, was prepared in the same way. The solid hydrate was broken up with a stainless steel spatula before being placed in the cell; at this point it had an appearance similar to that of granulated sugar. In the cell, the hydrate crystals were lightly tamped and then covered with liquid fluoromethane.

Ice from pure water and from aqueous solutions was prepared directly in the dielectric cells by slowly immersing the bottom of the cell in a bath of Dry Ice and acetone, so that freezing would occur in a regular way from the bottom of the cell upward. The ice was then annealed at least 24 hr at -5° . The water used to prepare the ice had a specific conductivity of less than 1×10^{-6} mho and was degassed by several cycles of freezing, pumping, and thawing before the final freezing step. Ice was also prepared by freezing from degassed aqueous solutions $6.77 \times 10^{-3} M$ in urea, $2.34 \times 10^{-3} M$ in dioxane, and $1.00 \times 10^{-5} M$ in dioxane, respectively. The urea was Fisher Certified reagent grade and the dioxane was Baker Analyzed reagent grade.

Results and Discussion

In Figure 1 are shown Cole-Cole plots for ice frozen in each of the two cells, based on data obtained at -10° . Given for purposes of comparison, these plots form very nice circular arcs with centers falling on the axis of abscissas, indicating only a single relaxation time. This behavior is that found previously for ice.⁸

Figure 2 includes plots of loss against frequency as measured at -10° for ice formed from solutions $2.34 \times 10^{-3} M$ in dioxane and $6.77 \times 10^{-3} M$ in urea. Both here and in Figure 3, where the same data are plotted in Cole-Cole form, there is seen to be an upward turn on the low-frequency side of the absorption maximum. This indicates that there is a considerable amount of low-frequency conductivity. This is quite reasonable for ice formed in the presence of urea, which may be contaminated by the slow formation of ammonium cyanate ions. However, no such explanation can be advanced for this behavior in the presence of dioxane, where we may attribute the results to the effect of surface polarization.

Results for the two clathrate compounds at -10° are presented in the form of Cole-Cole plots in Figure 4. The location of the center of a Cole-Cole circular arc is an indication of the distribution of relaxation times.⁹

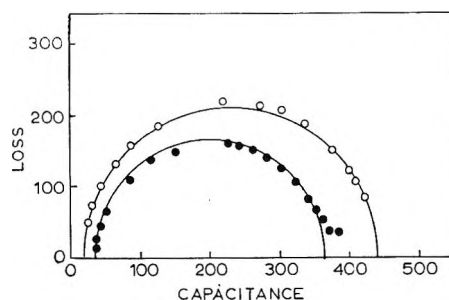


Figure 1. Cole-Cole plots for pure ice at -10° . Numerical values are those of capacitance and loss as measured directly on the cell containing the sample; these are proportional, respectively, to the real and imaginary parts of the dielectric constant; shaded circles are results for cell I, and open circles are results for cell II.

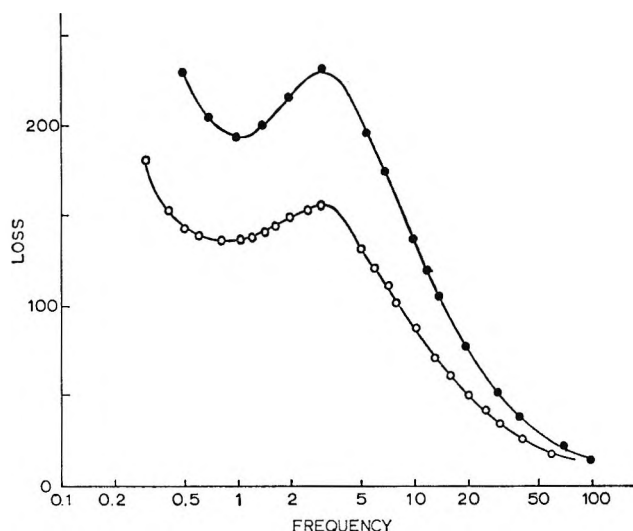


Figure 2. Relative dielectric loss at -10° plotted against frequency in kc/sec for ice frozen from $2.34 \times 10^{-3} M$ dioxane solution (closed circles, cell II) and from $6.77 \times 10^{-3} M$ urea solution (open circles, cell I).

Values for the angle $\alpha\pi/2$, related to this location, are given for the various solids in Table I. The larger this angle, the greater the breadth of distribution of relaxation times. At -10° , the value of the angle increases from 3° for the ice from dioxane, through 7° for ice from a solution of urea, to 12° and 14° for the two clathrates. Thus the ice formed in the presence of impurities lies intermediate between pure ice and the clathrate structure. The behavior of the two hydrates is quite similar, despite the fact that dichlorofluoromethane contains a hydrogen atom and might be expected to have somewhat different interactions with the water lattice from those of trichlorofluoromethane.

For the two clathrates, the value of α is quite strongly temperature dependent. The increase of α with decreasing temperature indicates that the various relaxa-

(8) R. P. Auty and R. H. Cole, *J. Chem. Phys.*, **20**, 1309 (1952).

(9) K. S. Cole and R. H. Cole, *ibid.*, **9**, 341 (1941).

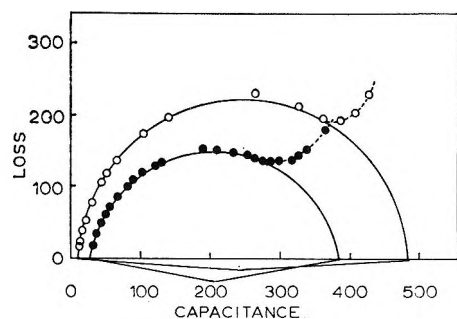


Figure 3. Cole-Cole plots of the data shown in Figure 2. Numerical values are as described for Figure 1; closed circles are for ice formed in the presence of urea, and open circles for ice formed in the presence of dioxane.

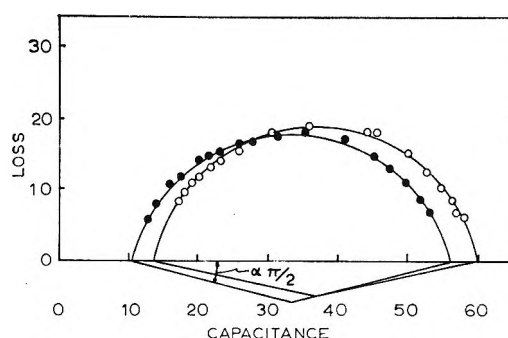


Figure 4. Cole-Cole plots for the hydrates of trichlorofluoromethane (closed circles) and of dichlorofluoromethane (open circles) at -10° in cell II. Numerical values are as described for Figure 1.

Table I: Frequency of Loss Maximum and Parameter for Distribution of Relaxation Times

Material	Temp, °C	Frequency of max loss, kc	$\alpha\pi/2$, deg
Pure ice in cell I	-10	3.50	0
Pure ice in cell II	-2	7.16	0
	-5	5.60	0
	-10	3.47	0
	-15	2.38	0
Ice from $2.34 \times 10^{-3} M$ dioxane solution, in cell II	-2	6.8	4
	-5	5.4	4
	-10	3.3	3
	-15	2.2	3
Ice from $6.76 \times 10^{-3} M$ urea solution, in cell I	-5	5.0	6
	-10	3.2	7
	-15	2.8	9
Trichlorofluoromethane clathrate in cell II	+2	35	10
	-5	20	13
	-10	11.2	14
	-19	4.5	15
Dichlorofluoromethane clathrate in cell II	-5	58	11
	-10	30	12
	-16	18	15
	-22	8.8	18
	-30	4.3	22

tion times, which are averaged together at room temperature, are becoming more resolved at the lower temperatures. The structure of the clathrate contains water molecules in several different environments. By analogy with the behavior of ice, it seems reasonable that the motion of defects is responsible for relaxation. The distribution of relaxation times between several distinct regions must then be attributed to a difference in activation energy for motion, which results from the difference in lattice location of the particular oxygen atoms past which the defects migrate.

In Table I are also given the frequencies at which maximum loss occurs. For ice, with $\alpha = 0$, these were obtained from plots of $\log \tan \phi$ against \log frequency, where ϕ is the loss angle. The logarithms of the frequency of maximum loss are plotted against reciprocal

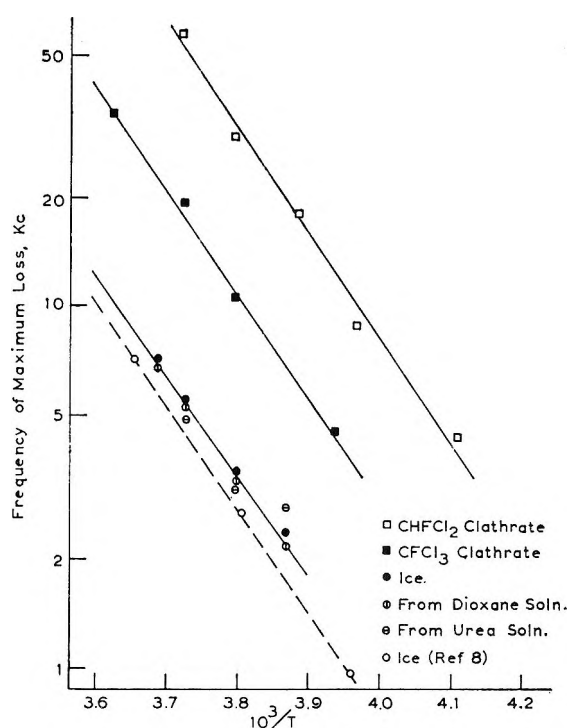


Figure 5. Arrhenius plots of the logarithm of the frequency of maximum dielectric loss against the reciprocal of absolute temperature.

temperature in Figure 5, where data of Auty and Cole⁸ for ice are also included. There is no substantial difference between the values for ice formed in the presence of impurities and our values for pure ice. However, the magnitude of the frequency of maximum loss at a given temperature is larger for the clathrate of trichlorofluoromethane than for ice, and larger still for the clathrate of dichlorofluoromethane. For ice formed from the solution $1.00 \times 10^{-5} M$ in dioxane, the results, not given in detail here, are also indistinguishable in all respects, within the experimental error, from those for pure ice.

The data plotted in Figure 5 for the two clathrates are based on observations extending over the widest

range of temperature for which measurements were made on single samples. Measurements were performed at one, two, or three temperatures on several other samples of each of the hydrates, and the frequencies of maximum loss were found to vary somewhat from sample to sample, depending in all likelihood upon the fraction of the interelectrode space filled by solid. However, there was no indication in any of the measurements that the slopes of the log frequency *vs.* reciprocal temperature plots would be different from those shown, or that the order of frequency of maximum loss could vary from that indicated in Figure 5.

Apparent activation energies may be calculated from the slopes of the plots in Figure 5. For ice, the value found is 12.8 ± 0.5 kcal/mole, compared to Auty and Cole's value of 13.25 kcal/mole. Within somewhat larger experimental uncertainties, the values for ice frozen in the presence of dioxane or urea are identical. For the clathrate of trichlorofluoromethane, the activation energy is 13.3 ± 0.6 kcal/mole, and for the clathrate of dichlorofluoromethane, it is 13.9 ± 0.8 kcal/mole. Thus the activation energy would appear to increase in the order ice < trichlorofluoromethane hydrate < dichlorofluoromethane hydrate, although the

variation is not much greater than the experimental error.

The activation energy found for the hydrate of trichlorofluoromethane is larger than that reported previously.¹ This is undoubtedly a result of the difference in technique in the present study, involving maintenance of constant clathrate composition by using an excess of liquid fluoromethane. It is interesting that the activation energies found here are almost twice as great as those reported for hydrates of such molecules as ethanol⁵ and acetone.² Any experimental errors, such as those attributable to the presence of a liquid phase contributing to the relaxation itself, or the presence of air gaps in the solid, would be expected to decrease the activation energy rather than increase it, so that the present values may be viewed as lower limits if not strictly correct. Thus we conclude that the halomethane molecules produce less drastic changes in the hydrogen-bonded solid structure than do the more asymmetric molecules such as ethanol and acetone and, further, that the hydrogen in dichlorofluoromethane probably has no appreciable interaction with the lattice.

Acknowledgment. This research was supported by a grant (GM-10861) from the National Institutes of Health.

The Reaction of O^- with Alcohols in Gas-Phase Radiolysis¹

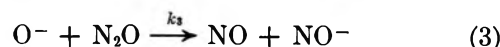
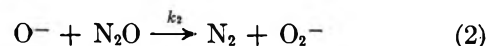
by John M. Warman

Radiation Research Laboratories, Mellon Institute, Pittsburgh, Pennsylvania 15213 (Received March 27, 1967)

The addition of MeOH, EtOH, or *i*-PrOH to an alkane- N_2O (4%) mixture markedly increases the yield of nitrogen, $G(N_2)$, to a limiting value of $\sim 3G_e$ (where G_e is the yield of electrons). The addition of *t*-BuOH decreases $G(N_2)$ toward a value of $\sim G_e$. The results can be explained in terms of the reaction of the O^- ion (formed on electron capture by N_2O) with the alcohol. Two mechanisms for reaction appear to occur: one leading to products which can react with N_2O to give two molecules of N_2 (rate constant k_{O^-+ROH}), the other leading to products which do not react with N_2O (rate constant $k^*_{O^-+ROH}$). Using CO_2 as a competitive O^- ion scavenger, the rate constants k_{O^-+ROH} and $k^*_{O^-+ROH}$ have been determined relative to $k_{O^-+CO_2}$. Possible reaction mechanisms are discussed.

Introduction

When an alkane-4% N_2O mixture is irradiated, the yield of nitrogen, $G(N_2)$, is $1.55G_e$. This has been explained^{2,3} by the occurrence of reactions 1-3 with $k_2/k_3 = 1.22$.

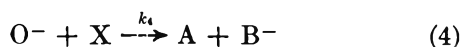


(1) Supported in part by the U. S. Atomic Energy Commission.

(2) G. R. A. Johnson and J. M. Warman, *Nature*, **203**, 73 (1964); *Trans. Faraday Soc.*, **61**, 512 (1965).

(3) J. M. Warman, *Nature*, **213**, 381 (1967).

If a substance X, which can react with O^- , is added to this system then, $G(N_2)$ will change



The degree and direction of change will depend upon the rate constant ratio $k_4/(k_2 + k_3)$ and the nature of the products of reaction 4. If the products of (4) do not subsequently react with N_2O , then $G(N_2)$ will decrease, in the limit to G_e , as is found for $X = CO_2$.³ If the products of (4) further react with N_2O to form N_2 then $G(N_2)$ will increase, as is found for $X = \text{acetone}$.³ The work presented here illustrates the use of this system for studying the reaction of O^- with alcohols.

Experimental Section

Propane, butane (Philips Research Grade), nitrous oxide, carbon dioxide, and sulfur hexafluoride (Matheson) were distilled several times (through a cold spiral) on a vacuum line. Methanol (Baker Analyzed Reagent), ethanol (Commercial Solvents Corp.), 2-propanol (Eastman Spectro Grade) and 2-methyl-2-propanol (Eastman) were used without further purification. All reagents were deaerated by a freeze-pump-thaw cycle.

The pressure of each constituent of the mixture to be irradiated was measured in a known volume prior to transfer to a common bulb at -196° . The resulting mixture was then warmed to room temperature and expanded into a volume containing the radiation vessels. The resultant total pressure was ~ 630 mm. The vessels were Pyrex cylinders of 160 cm³ volume and 20 cm length.

A 2000-curie Co^{60} source was used to irradiate the samples. Dosimetry was based on $G(C_2H_4 \rightarrow H_2) = 1.31$.⁴ G values were based on the total energy absorbed by all constituents of the gas mixture, using the relevant stopping powers.⁴ The dose rate in the present experiments was $\sim 3 \times 10^{13}$ ev/cm³ sec. The highest total dose used was 2×10^{17} ev/cm³.

The products which were noncondensable at -196° were transferred to a gas buret by means of a single-stage diffusion pump and a Toepler pump. After pressure-volume measurement, the gas composition was determined mass spectrometrically.

Results

All G values (yield of product per 100 ev absorbed) were obtained from the slopes of linear yield dose plots, e.g. see Figure 1. G values are given in terms of G_e (the yield of electrons per 100 ev absorbed), which for these experiments $= 100/W_{n-C_4H_{10}} = 4.35$.⁴ "The system" is synonymous with a mixture of 600 mm of alkane and 25 mm of N_2O . The alkane used in these experiments was n -butane. Several points were repeated using propane and no difference in $G(N_2)$ was detectable.

The addition of small amounts ($<0.5\%$) of ethanol

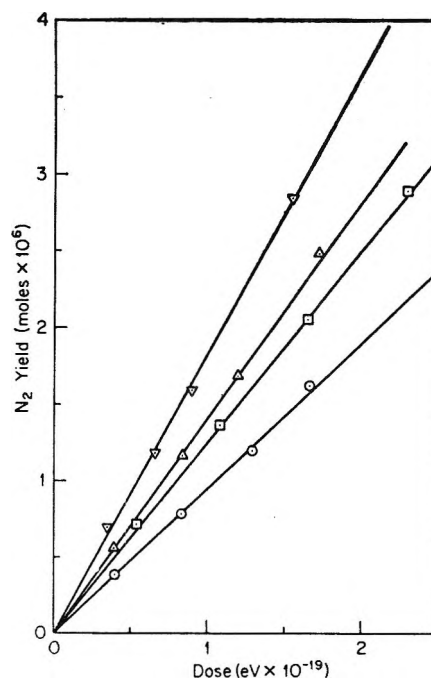


Figure 1. Yield vs. dose plots for the formation of nitrogen from the mixtures: $n-C_4H_{10}$ (600 mm)- N_2O (25 mm)- i -PrOH (15 mm)- CO_2 , with $[CO_2]/[i-PrOH] =$ 0 (∇), 0.19 (Δ), 0.54 (\square), 1.33 (\circ).

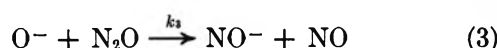
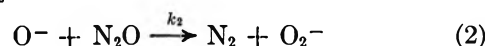
to the system markedly increased $G(N_2)$ from the value of $1.55 G_e$ found in the absence of additive (Figure 2). On increasing $[EtOH]$, $G(N_2)$ reached a limiting value of $2.8 G_e$. For $[EtOH]/[N_2O] = 0.6$ (for which $G(N_2) = 2.8 G_e$), the addition of 0.2% SF_6 reduced $G(N_2)$ to $<0.15 G_e$. For $[MeOH]/[N_2O]$ and $[i-PrOH]/[N_2O] \sim 0.6$, $G(N_2) = 2.95 G_e$ and $2.6 G_e$, respectively. The yield of N_2 from a mixture with $[ROH]/[N_2O] \sim 0.6$ decreased with increasing concentration of added CO_2 (Figure 3). The addition of t -BuOH to the system decreased $G(N_2)$ to a value of $1.1 G_e$ at the highest concentration used (Figure 2).

Discussion

The formation of nitrogen, on irradiation of alkane- N_2O (4%) mixtures, has been shown to be due to electron capture²



At this concentration of N_2O , electron scavenging is virtually complete (98% for n -butane) and $G(N_2) = 1.55 G_e$ ($G_e = 4.35$ for n -butane). The additional yield of nitrogen, $0.55 G_e$, over that expected from reaction 1 has been shown³ to be due to the subsequent reaction of O^- with N_2O



with $k_2/k_3 = 1.22$.

(4) G. G. Meisels, *J. Chem. Phys.*, **41**, 1510 (1964).

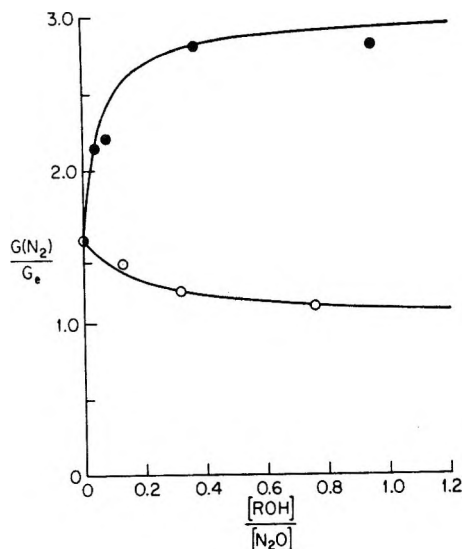


Figure 2. The effect of ethanol (●) and *t*-butanol (○) on $G(N_2)$ from a mixture of *n*-butane (600 mm)– N_2O (25 mm). The upper curve is calculated (see Discussion).

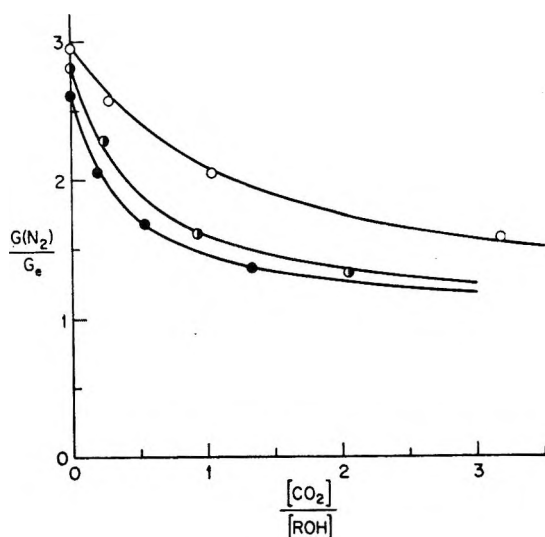
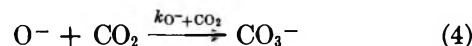


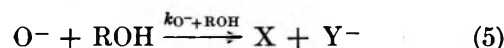
Figure 3. The effect of CO_2 on $G(N_2)$ from a mixture of *n*-butane (600 mm)– N_2O (25 mm)–ROH (~ 15 mm), where ROH is methanol (○), ethanol (◐), and 2-propanol (●). (For $[CO_2]/[MeOH] \sim 3$, $P_{MeOH} = 8.5$ mm.)

The addition of small amounts of methanol, ethanol, or 2-propanol to the system *n*-butane–4% N_2O markedly increase $G(N_2)$. As the alcohol concentration is increased a limiting $G(N_2) \sim 3G_e$ is reached (Figure 2). The decrease of $G(N_2)$ from this value to $<0.15G_e$ on the addition of only 0.2% SF_6 (an efficient electron scavenger) indicates the electron to be the primary precursor of at least 95% of the N_2 . Since N_2O is the only constituent which can capture thermal electrons, then the primary process in N_2 formation must be reaction 1. The only reactive product of (1) is O^- . The effect of added alcohol must therefore be due to its reaction with O^- , directly, or with the products of reac-

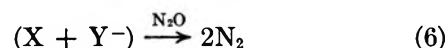
tion 2 and/or 3. Carbon dioxide has been found to undergo a fast reaction with O^- ^{5,6}



but is relatively inert to the radical and ionic products of hydrocarbon radiolysis. The addition of $\sim 2\%$ CO_2 to an alkane–4% N_2O mixture³ completely scavenges O^- and prevents the occurrence of reactions 2 and 3. If then the effect, due to the addition of the alcohols, requires reactions 2 and/or 3 to occur, then the addition of $\sim 2\%$ CO_2 to the alcoholic systems should decrease $G(N_2)$ from $\sim 3G_e$ to G_e . It is found, however, that at this concentration ($2\% CO_2 = [CO_2]/[ROH] \sim 0.7$ (Figure 3)), $G(N_2)$ is still considerably greater than G_e . The effect on $G(N_2)$ of the addition of alcohol must therefore be due to the reaction of O^- with the alcohol



The limiting yield of $3G_e$ can be explained if the products of (5) react with N_2O to form 2 molecules of N_2 .



At sufficiently low $[ROH]/[N_2O]$, competition between reaction 5 and reactions 2 and 3 should occur and be apparent as a fall off in $G(N_2)$ from the limiting value of $\sim 3G_e$. The rate constant ratio, $k_{O^-+ROH}/(k_2 + k_3)$, should then be calculable from the expression

$$G(N_2) = G_e \left[1 + \frac{0.55 + 2 \frac{k_{O^-+ROH}}{k_2 + k_3} \frac{[ROH]}{[N_2O]}}{1 + \frac{k_{O^-+ROH}}{k_2 + k_3} \frac{[ROH]}{[N_2O]}} \right] \quad (A)$$

obtained from a steady-state treatment of reactions 1–3, 5, and 6. The fall off from the limiting yield with decreasing $[ROH]/[N_2O]$, Figure 2, occurs, however, in a region where the error in measuring $[ROH]$ is large. The ratio $k_{O^-+ROH}/(k_2 + k_3)$ cannot, therefore, be determined accurately from these results.

The addition of CO_2 to the alcoholic systems, in the region of limiting $G(N_2)$, should result in simple competition between reactions 4 and 5. Thus $G(N_2)$ should decrease from $\sim 3G_e$ and tend toward G_e with increasing $[CO_2]/[ROH]$. A steady-state treatment of this competition gives as the expected dependence of $G(N_2)$ on $[CO_2]/[ROH]$

$$G(N_2) = G_e \left[1 + \frac{2}{1 + \frac{k_{O^-+CO_2}}{k_{O^-+ROH}} \frac{[CO_2]}{[ROH]}} \right] \quad (B)$$

Accordingly a plot of $2G_e/(G(N_2) - G_e)$ vs. $[CO_2]/[ROH]$ should be a straight line of slope equal to $k_{O^-+CO_2}/k_{O^-+ROH}$.

(5) J. L. Moruzzi and A. V. Phelps, *J. Chem. Phys.*, **45**, 4617 (1966).

(6) W. L. Fite and J. A. Rutherford, *Discussions Faraday Soc.*, **37**, 1964.

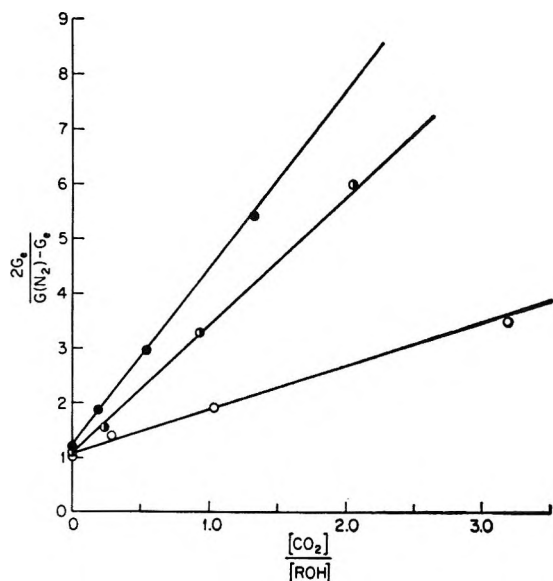
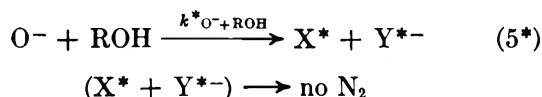


Figure 4. Illustration of the linear dependence of $2G_e/(G(N_2) - G_e)$ on $[CO_2]/[ROH]$ according to eq B (see Discussion), where ROH is methanol (○), ethanol (◐), and 2-propanol (●).

k_{O^-+ROH} . Good linearity was found for the three alcohols investigated (Figure 4). From the slopes, $k_{O^-+ROH}/k_{O^-+CO_2} = 1.19, 0.44$, and 0.35 for MeOH, EtOH, and *i*-PrOH, respectively.

The ratio $k_{O^-+CO_2}/(k_2 + k_3) = 44$ has been determined in other experiments,⁷ from which $k_{O^-+EtOH}/(k_2 + k_3) = 19.4$. The upper curve in Figure 2 was calculated using this value in expression A. The agreement with experiment is good with the experimental points lying somewhat below the predicted curve, however.

The effect of *t*-BuOH on $G(N_2)$ was studied in an attempt to elucidate the mechanism of reaction 5. Thus, if the increase in $G(N_2)$, found with MeOH, EtOH, and *i*-PrOH, is due to O^- attack on the α -H atom (the hydrogen atom on the carbon atom adjacent to the hydroxyl group), then the absence of an α -H atom in *t*-BuOH should prohibit reaction. $G(N_2)$ would then be expected to be unaltered by the addition of *t*-BuOH. If reaction 5 involves the hydroxyl group, then $G(N_2)$ should increase as for the other alcohols. In fact, *t*-BuOH decreased $G(N_2)$ to a limiting yield of $\sim G_e$ (Figure 2). It would therefore appear that *t*-BuOH reacts with O^- to form species which do not further contribute to N_2 formation.



Accordingly, $G(N_2)$ should obey the expression

$$G(N_2) = G_e \left[1 + \frac{0.55}{1 + \frac{k_{O^-+ROH} [ROH]}{k_2 + k_3 [N_2O]}} \right] \quad (C)$$

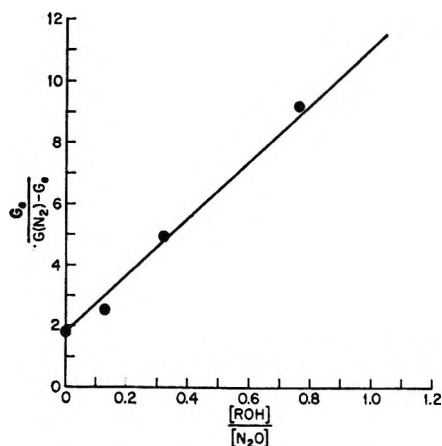


Figure 5. Illustration of the linear dependence of $G_e/(G(N_2) - G_e)$ on $[ROH]/[N_2O]$ according to eq C (see Discussion), where ROH is *t*-butanol.

A plot of $G_e/(G(N_2) - G_e)$ vs. $[t\text{-BuOH}]/[N_2O]$ should then be a straight line of slope $1/k_{O^-+ROH}/(k_2 + k_3)$. Such a plot is shown in Figure 5, from which $k_{O^-+t\text{-BuOH}}/(k_2 + k_3) = 5.1$, resulting in $k_{O^-+t\text{-BuOH}}/k_{O^-+CO_2} = 0.12$.

As mentioned previously, the N_2 yields, determined on the addition of EtOH (Figure 2), were slightly lower than predicted using eq A and the rate-constant ratio, $k_{O^-+EtOH}/(k_2 + k_3)$, determined by the CO_2 competition method. In the case of MeOH, no discrepancy was detectable, but for *i*-PrOH the discrepancy was even greater than for EtOH. This can be explained in view of the *t*-BuOH results, if both reaction 5 and 5* occur with EtOH and *i*-PrOH. Equation B, describing the effect of CO_2 , should then be replaced by (D). (For simplicity k_{O^-+ROH} , $k_{O^-+ROH}^*$, and $k_{O^-+CO_2}$ have been reduced to k , k^* and k_{CO_2} , respectively, in this paragraph.)

$$G(N_2) = G_e \left[1 + \frac{2 \frac{k}{(k + k^*)}}{1 + \frac{k_{CO_2} [CO_2]}{(k + k^*) [ROH]}} \right] \quad (D)$$

According to (D), a plot of $2G_e/(G(N_2) - G_e)$ vs. $[CO_2]/[ROH]$ should be a straight line of slope k_{CO_2}/k and

Table I

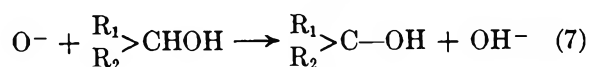
ROH	$\frac{k_{O^-+ROH}}{k_{O^-+CO_2}}$	$\frac{k_{O^-+ROH}^*}{k_{O^-+CO_2}}$
CH ₃ OH	1.19	^a
C ₂ H ₅ OH	0.44	0.03
(CH ₃) ₂ CHOH	0.35	0.06
(CH ₃) ₃ COH	0	0.12

^a Immeasurable.

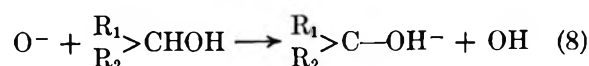
(7) J. M. Warman, *J. Phys. Chem.*, **71**, 4066 (1967).

intercept $(k + k^*)/k$. From the slopes and intercepts of the plots in Figure 4, values of k/k_{CO_2} and k^*/k_{CO_2} can be obtained. These values are listed in Table I.

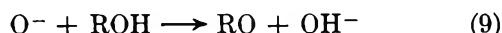
The present results are insufficient to define specifically the nature of reactions 5, 5*, and 6. However, the observation that *t*-BuOH does not undergo reaction 5, whereas MeOH, EtOH, and *i*-PrOH do, would suggest the necessity of an α -hydrogen atom for this reaction to occur. Reaction 5 therefore, most probably involves either hydrogen atom abstraction



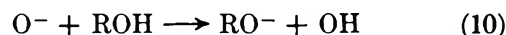
or proton abstraction



from the α -carbon atom. Reaction 5*, which occurs with EtOH, *i*-PrOH, and *t*-BuOH, could then be hydrogen atom abstraction



or proton abstraction



from the hydroxyl group. Apart from the hydroxyl radical, which would be expected to react exclusively with the hydrocarbon under the present conditions, the fate of the products of reactions 7-10 cannot be predicted.

Preliminary mass-spectrometric studies⁸ indicate reaction between O^- and alcohols to occur. With MeOH, using SO_2 as the source of O^- , secondary ions of mass 17 (OH^-) and 31 (H_3CO^-) are observed. However, the probable excess kinetic energy of the O^- ions in these experiments makes extrapolation of these data to radiolysis conditions somewhat doubtful.

Acknowledgment. The author wishes to thank Mr. G. K. Buzzard for carrying out the mass spectrometric analyses.

(8) G. K. Buzzard and J. M. Warman, work in progress.

Excess Thermodynamic Functions of Some Binary Nonelectrolyte

Mixtures. I. Measurements of Excess Gibbs Free

Energy, Enthalpies, and Volumes of Mixing

by S. N. Bhattacharyya and A. Mukherjee¹

Indian Association for the Cultivation of Science, Jadavpur, Calcutta, India (Received March 22, 1967)

Excess Gibbs free energies, enthalpies, and volumes of the systems toluene-fluorobenzene and methylcyclohexane-fluorobenzene have been measured at different temperatures over the entire mole fraction range. The excess Gibbs free energies have been studied at 50, 60, and 70°, the excess enthalpies at 10, 25, and 40°, and the excess volumes at 40° for all the systems.

I. Introduction

A very recent trend in the field of molecular theories of solutions is to extend these theories to more general cases such as mixtures of polyatomic molecules having wide differences in size and weak orientational forces. Two major approaches to a molecular theory of solutions, rigid lattice theories and deformable lattice theories, are already fairly well developed. The rigid lattice models have been extensively used before, but

lately a generalized quasi-lattice model, originally due to Barker,¹ has been applied with considerable success to mixtures of polyatomic molecules and polymer solutions, particularly where strong orientational forces like hydrogen bonds are involved.¹⁻³ The attractive

(1) J. Barker, *J. Chem. Phys.*, **20**, 1526 (1952).

(2) J. R. Goates, R. L. Snow, and M. R. James, *J. Phys. Chem.*, **67**, 335 (1961).

(3) J. B. Ott, J. R. Goates, and R. L. Snow, *ibid.*, **66**, 1301 (1962).

feature of this theory is that it can take into account the effects due to the difference in the number of sites occupied by the component molecules of the mixture and also of those molecular interactions which are directional in character. This theory could also be applied, with much profit, to general cases as mentioned above. Very little systematic work has been done until now along these lines, particularly in interpreting both excess free energies and enthalpies of such nonelectrolyte mixtures.

With this object in view, we have measured the excess Gibbs free energy g^E , excess enthalpy h^E , and excess volume v^E of the systems toluene-fluorobenzene and methylcyclohexane-fluorobenzene. Bhattacharyya, Anantaraman, and Palit have already measured the excess functions for the systems benzene-fluorobenzene and cyclohexane-fluorobenzene.⁴ A good volume of data already exists in the literature on allied systems such as benzene-cyclohexane or toluene-cyclohexane so our investigations, along with data that are available, would enable us to test very systematically the scope and applicability of the Barker quasi-lattice theory.

The deformable lattice theory of solution due to Prigogine may, as well, be utilized for the analysis of the experimental excess functions. Bhattacharyya, Anantaraman, and Palit⁴ demonstrated that average potential theory could effectively be extended to a mixture composed of spherical nonpolar molecules and spherical weakly polar molecules. In reality, a polyatomic molecule would be nonspherical in shape and would be the source of other types of weak orientational forces. It has lately been shown⁵ that with the help of a single potential all types of weak forces, central, dipolar, globular, or those due to polarizabilities, that are encountered in a real solution could be approximated. This could very well be tested in our proposed investigations. Moreover, an attempt would be made to eliminate the limitations inherent in the average potential model; i.e., the theory could be applied to systems where the force constants of the molecules are very close to each other by utilizing some of the features of the deformable lattice theories of polymer mixtures which are in a rapid state of development.

The results of the measurements of h^E and v^E of the system toluene-fluorobenzene at 25° have been reported earlier.⁶ Samples of fluorobenzene from a different source have been used for present work. To ensure that the results obtained with the two samples are not different, a few more measurements of h^E at 25° have been made. As the two sets of data have been found to be in agreement with each other within experimental error, the combined data of this system for h^E at 25° have been subjected to analysis. The experimental methods used and the results obtained for this work are described in this paper. The applications of the generalized rigid-lattice theory and deformable-

lattice theory to the data are reported in two subsequent papers.

II. Experimental Section

Measurement of g^E . A dynamic-type equilibrium still has been designed and built to measure g^E . The still is similar to the one developed by Brown and Ewald,⁷ with certain modifications, as it appears to fulfill the requirements suggested by Fowler.⁸ The sample tubes with magnetically operated ball valves used by Brown and Ewald have been replaced in the still by overflow traps, as the former were found to be troublesome. The stopcock over the disengagement chamber for introduction of liquid mixture to the still has also been eliminated, the mixture being introduced through the overflow tubes. The same tubes, of which the overflow tubes are an integral part, are designed with a view to minimize any error caused by a change in composition of the equilibrium samples due to evaporation during their removal. At the sampling end is a specially designed ground joint with a capillary opening which has been used for this purpose, the sample being taken out with a long needle immediately after the still is stopped. The capacity of the boiler has been made deliberately as large as 180 ml to obtain very accurate results. The traps each hold about 8 ml. The disengagement chamber has been altered to take a ten-junction copper-constantan thermocouple, and a drip counter has been built into the condensate return. The drip counter also prevents liquid from flowing back to the vapor condensate trap as a result of surging during the initial stages of boiling.

The equilibrium still is connected to a manostat and manometer system, which is the same as that of Scatchard, Raymond, and Gilmann⁹ and which has been used before in this laboratory. An Invar scale cathetometer with a precision of ± 0.02 mm was used to read the heights of the mercury. The 90-l. manostat and the manometer were kept in oil and air thermostats, respectively, where the temperatures were maintained at $35 \pm 0.01^\circ$. The mercury heights were corrected for the mean temperature and the gravitational constant. The correction for the weight of the column of the confining gas over the mercury in the lower arm of the manometer to the line of condensation and the weight of the column of vapor from the line of condensation to the lower end of the thermometer well is

(4) S. N. Bhattacharyya, A. V. Anantaraman, and S. R. Palit, *Trans. Faraday Soc.*, **59**, 1101, (1963); *Indian J. Chem.*, **1**, 459 (1963).

(5) S. N. Bhattacharyya, *Indian J. Phys.*, **41**, 579 (1967).

(6) S. N. Bhattacharyya and A. Mukherjee, *Indian J. Phys.*, **38**, 93 (1964).

(7) I. Brown and A. H. Ewald, *Australian J. Sci. Res.*, **A5**, 306 (1953); I. Brown, *ibid.*, **A3**, 530 (1952).

(8) R. T. Fowler, *Ind. Chemist*, **24**, 717 (1948).

(9) G. Scatchard, C. L. Raymond, and H. H. Gilmann, *J. Am. Chem. Soc.*, **60**, 1275 (1938).

less than 0.008 mm, so this correction was not applied. No correction has been made for the pressure gradient required to accelerate the vapor from the disengagement chamber to the condenser as this is believed to be negligible. The pressure of the vacuum side of the manometer was checked by a McLeod gauge and was always kept below 0.005 mm. The ten-junction thermocouple was calibrated by measuring the vapor pressure of pure benzene at various temperatures and subsequently fixing the temperatures by the data of Scatchard, Wood, and Mochel.¹⁰ For this, benzene was purified with special care, and its density was repeatedly checked until it agreed quite well with the standard values in the literature. A LN K2 potentiometer was used for temperature measurements with a precision of $\pm 0.005^\circ$.

The composition of the sample was determined by the technique of density measurements.¹¹ Single-stem pycnometers of about 4-ml capacity were used for density measurements. A semimicro Mettler balance was used for weighings. The weights and optical scale of the balance were recalibrated against its own 1-g weight. The bath for the pycnometers was kept constant to $\pm 0.002^\circ$. The heights of liquid and its meniscus were read by a travelling microscope. The weights were corrected to vacuum from the temperature, pressure, and humidity of the balance room. Mixtures of known composition were prepared in a large pycnometer of 15-ml capacity. Corrections were applied for the weights of the first component expelled from the pycnometer as vapor when the second component was added. The error in the density measurements has been calculated to be not more than three parts in 10^5 .

The molar excess Gibbs free energy, g^E , has been calculated taking into account the deviation of the vapor mixture from the perfect gas assumptions.¹¹⁻¹³ If we allow an error of ± 0.002 mm in p , the pressure, ± 0.0005 in x and y , the liquid phase and vapor phase composition each, and $\pm 0.005^\circ$ in the temperature determination, the over-all error in the g^E measurement would be less than ± 2 joules mole⁻¹ near the equimolar composition for any of the measurements reported here. The error would be greater than this at both ends of the composition scale.

Measurement of v^E . The volume change of mixing has been determined from the data of the densities of the pure components and those of mixtures of known composition prepared to determine the unknown compositions of the samples from the equilibrium still.

Measurement of h^E . The heat of mixing has been measured by an adiabatic-isothermal twin microcalorimeter, designed and constructed by Bhattacharyya and Das.¹⁴ This calorimeter was used extensively by Bhattacharyya, Anantaraman, and Palit⁴ for their work on chlorobenzene and fluorobenzene systems. With this calorimeter, the uncertainty in measurements

of magnitude 0.1 joule of heat in the system is about 5%. It can be expressed as a roughly constant percentage above 1 joule and is estimated to be less than 0.5%. Below 1 joule, uncertainty, expressed as a percentage, gradually increases but the absolute accuracy, expressed in joule mole⁻¹, remains roughly constant at about 1 joule mole⁻¹.

The density of benzene at 40° was found to be 0.85763, which compares favorably with Timmermans' value¹⁵ of 0.85769, and with the API value¹⁶ of 0.8577. The densities of toluene, methylcyclohexane, and fluorobenzene at 40° were 0.84793, 0.75300, and 0.99981, respectively, which compare well with the existing data.¹⁵⁻¹⁷ (See Tables I and II.)

Table I: Vapor Pressure of Pure Compounds (mm)

Compounds	Vapor pressure, this work	Vapor pressure, other work
Temp 50°		
Benzene	271.34	271.34 ¹⁰
Fluorobenzene	230.21	229.42 ^a
Toluene	91.86	92.11 ¹⁵
Methylcyclohexane	138.63	138.32 ¹⁵
Temp 60°		
Benzene	391.66	391.66 ¹⁰
Fluorobenzene	333.71	333.84 ^a
Toluene	137.86	138.96 ¹⁵
Methylcyclohexane	202.00	202.80 ¹⁵
Temp 70°		
Benzene	551.03	551.03 ¹⁰
Fluorobenzene	474.29	473.47 ^a
Toluene	202.70	203.75 ¹⁵
Methylcyclohexane	288.97	289.89 ¹⁵

^a D. W. Scott, *et al.*, *J. Am. Chem. Soc.*, **78**, 5457 (1956).

III. Results and Discussion

Excess Enthalpy h^E . Plots of excess heat *vs.* mole fraction gave, approximately, a parabola at all the

(10) G. Scatchard, S. E. Wood, and J. M. Mochel, *J. Am. Chem. Soc.*, **61**, 3206 (1938).

(11) M. L. McGlashan, J. E. Prue, and I. E. J. Sainsbury, *Trans. Faraday Soc.*, **50**, 1284 (1954).

(12) J. S. Rowlinson, "Liquid and Liquid Mixtures," Butterworth and Co., London, 1959, Section 4.3.

(13) A. V. Anantaraman, Ph.D. Thesis, Calcutta University, Calcutta, India, 1962.

(14) S. N. Bhattacharyya and S. K. Das, *Indian J. Phys.*, **31**, 33 (1959).

(15) J. Timmermans, "Physico-Chemical Constants of Pure Organic Compounds," Elsevier Publishing Co., Amsterdam, The Netherlands, 1950.

(16) "Selected Values of Physical and Thermodynamic Properties of Hydrocarbons and Related Compounds," American Petroleum Institute Research Project 44, Carnegie Press, Pittsburgh, Pa., 1953.

(17) A. I. Vogel, *J. Chem. Soc.*, 644 (1948).

Table II: Second Virial Coefficients (B_{11}) and Molar Volumes (V_1) of Pure Compounds (ml per mole)

Compounds	$-B_{11}/V_1$		
	50°	60°	70°
Fluorobenzene ^a	-1403/100.0	-1295/102.0	-1199/104.0
Toluene ^{b,17}	-2018/109.8	-1858/111.1	-1716/112.3
Methylcyclohexane ^{c,16}	-1714/132.1	-1607/133.7	-1509/135.3

^a See footnote a, Table I. ^b R. J. L. Audon, J. D. Cox, E. F. G. Herington, and J. F. Martin, *Trans. Faraday Soc.*, **53**, 1074 (1957). ^c Calculated using Berthelot's empirical equation (cf., J. D. Lambert, G. A. H. Roberts, J. S. Rowlinson, and V. J. Wilkinson, *Proc. Roy. Soc. (London)*, **A106**, 113 (1949)).

temperatures. For each system, the data were fitted to an expression of the type

$$h^E = x_1 x_2 \sum_{p=0}^n A_p (x_1 - x_2)^p \quad (1)$$

where x_1 indicates the mole fraction of the nonpolar component in the mixture. The sum in (1) consists of $n + 1$ terms, corresponding to integral values of p from 0 to n in all cases. Forms of (1) with more than four coefficients were never used. Values of the coefficient A_p , determined by trial and error, are collected in Table V. The experimental data for h^E have been plotted in Figures 1 and 2. The smooth curves in these figures represent the values calculated from eq 1 and the coefficients in Table III.

The curves for both the systems are slightly asymmetrical, each showing either a minimum or a maximum occurring very near $x_1 = 0.5$.

The system toluene-fluorobenzene has a small minimum near $x = 0.5$ at all the temperatures studied. The interesting feature of this system is the increase of excess enthalpy with temperature, the equimolar values being -62, -55, and -49 joules/mole at 10, 25, and 40°, respectively.

The system methylcyclohexane-fluorobenzene, on the other hand, shows a large maximum very near $x_1 = 0.5$ at all the temperatures. The excess enthalpies have been found to decrease, in this case, with increase in temperature, the equimolar values being 790, 738, and 692 joules/mole at 10, 25, and 40°, respectively.

Excess Gibbs Free Energy g^E . To reduce the time required to reach equilibrium, which is often as much as 6 hr, the pressure of the still was not disturbed after the system approached fairly close to a steady state. Hence the equilibrium temperature was close, but not exactly equal, to the required temperature, and the difference between these sometimes exceeded $\pm 0.5^\circ$. A correction was therefore applied so that the correct value of the vapor pressure in a given series of experiments refers to the same round value of temperature. For this, g^E was calculated at first at the exact observed

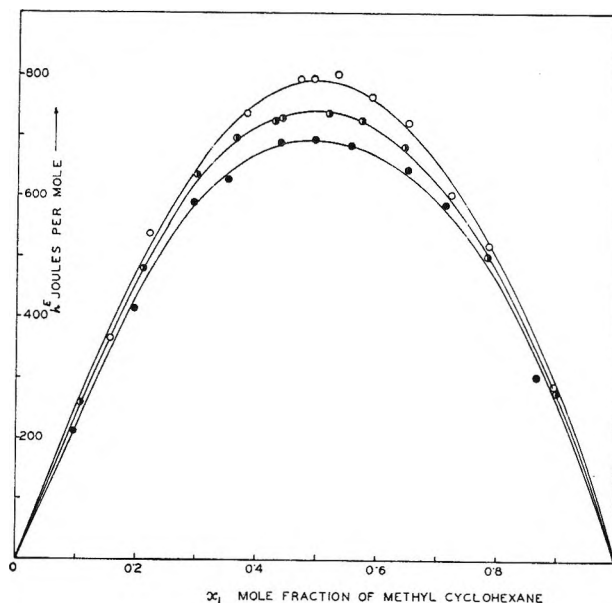


Figure 1. Excess enthalpies h^E ; methylcyclohexane-fluorobenzene system; experimental points: \circ , 10°; \bullet , 25°; and \bullet , 40°. The smoothed curves are from eq 1, with the coefficients from Table V.

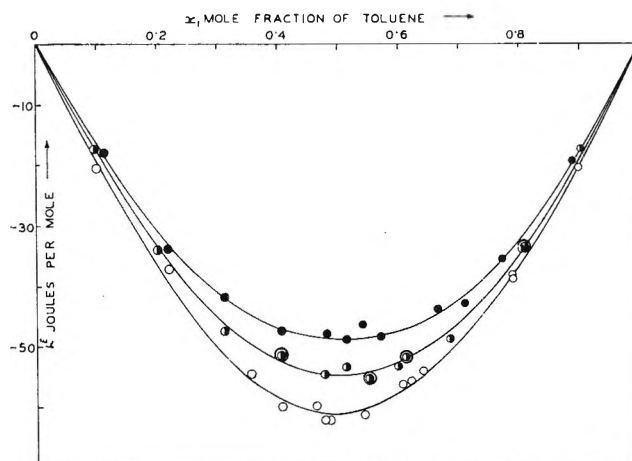


Figure 2. Excess enthalpies h^E , toluene-fluorobenzene system; experimental points: \circ , 10° (this work); \bullet , 25° (this work); \bullet , 25° (from ref 7); and \bullet , 40° (this work). The smoothed curves are from eq 1 with the coefficient from Table V.

temperature, and then the well known method of successive approximations was applied over magnified graphs to obtain dg^E/dT at the specified temperature range and at different compositions. This gave us directly the magnitude of the correction necessary for each of the observations.

We have tested our experimental data of p , x , and y for consistency in simultaneous measurements, based on the test suggested by Rowlinson.¹⁸ The results of the graphical integration of the left-hand side and right-hand side of eq 4.96 of ref 18 are summarized in Table

(18) J. S. Rowlinson, "Liquid and Liquid Mixtures," Butterworth and Co., 1959, Chapters 4, 5.

Table III: Coefficients of Eq 1, 3, and 9 in Joules or Milliliters per Mole

System	Excess function	Temp, °C	A_0 B_0 or C_0	A_1 B_1 or C_1	A_2 B_2 or C_2	A_3 B_3 or C_3	A_4 B_4 or C_4
$C_6H_5CH_3 + C_6H_5F$	h^E	10	-246.0	10.26	53.49	-26.89	-25.54
		25	-220.0	-3.57	4.93	-7.43	24.85
		40	-196.0	-4.46	-35.59	-9.31	66.19
	h^E	10	3160	41.3	-454.1	-444.4	386.6
		25	2952	-109.1	164.2	496.0	-546.3
		40	2760	-69.4	461.3	434.0	-948.6

	
	
$C_6H_{11}CH_3 + C_6H_5F$	g^E	50	1484	-57.1	137.4	189.8	-682.8
		60	1452	-34.8	-181.9	195.8	-365.1
		70	1400	-25.3	-331.4	186.0	-302.9
	v^E
		40	2.34	0.2706	0.1729	-0.4343	0.9768
	

Table IV

System	Temp, °C	Area, left-hand side of eq 4.96, ref 18	Area, right-hand side of eq 4.96, ref 18
$C_6H_5CH_3 + C_6H_5F$	50	-0.0150	-0.0126
	60	-0.0145	-0.0158
	70	-0.0225	-0.0211
$C_6H_{11}CH_3 + C_6H_5F$	50	-0.0075	-0.0080
	60	-0.0097	-0.0104
	70	-0.0100	-0.0135

IV. It is seen that the difference between them nowhere exceeds 0.0035 and may be taken as quite adequate for both the systems at all the temperatures.

As for the excess heat, h^E , a plot of excess Gibbs free energy against mole fraction gave almost symmetrical parabolas at all the temperatures; these data are summarized in Tables V and VI. (See Figures 3-5.)

The excess Gibbs free energy g^E of the system toluene-fluorobenzene has been found to be positive, but very small. The value of g^E at all temperatures is so small that its absolute values over the entire composition range are of the same order as our experimental error, which is ± 2 joules mole⁻¹, as estimated earlier. All of the data, except one or two points, are within

$$g^E = Bx_1x_2 \pm 2 \text{ joules mole}^{-1} \quad (2)$$

where B is 24, 28, and 32 joules per mole at 50, 60, and 70°, respectively. Such a low value of g^E obviously produced a large scattering in absolute values and no attempt was made to fit any curve. For the same reason, it is very difficult to come to any conclusion regarding the shape of the curve or the temperature derivative of the equimolar values. The equimolar g^E may be taken to be 6 ± 2 and 8 ± 2 joules mole⁻¹ at 50, 60, and 70°, respectively.

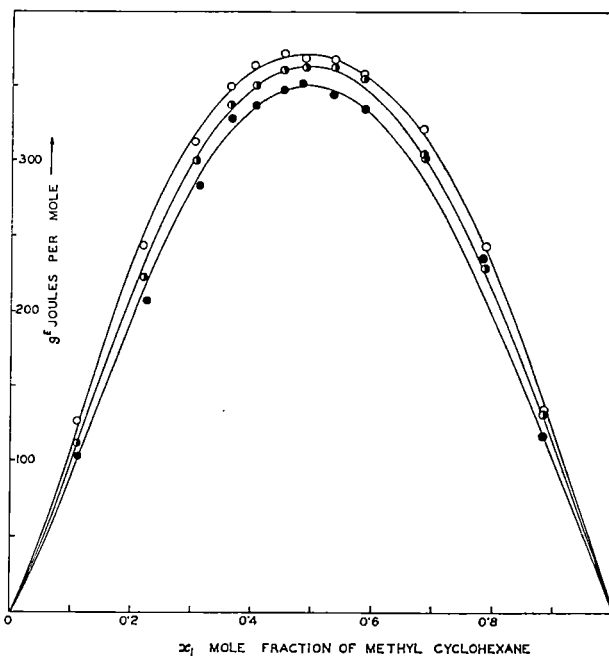


Figure 3. Excess Gibbs free energies; methylcyclohexane-fluorobenzene system; experimental points: \circ , 50°; \bullet , 60°; and \bullet , 70°. Smoothed curves are from eq 3 with the coefficients from Table V.

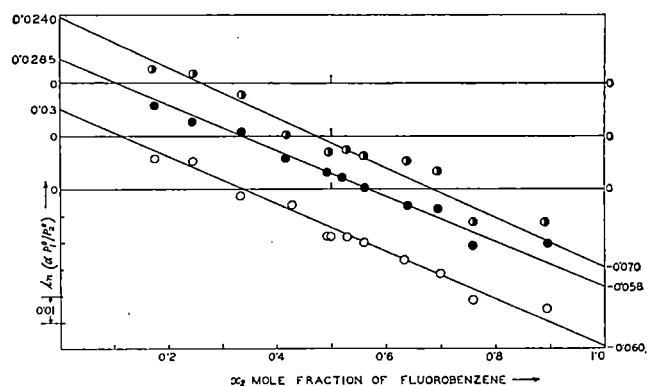


Figure 4. Test for consistency; toluene-fluorobenzene system; experimental points: \circ , 50°; \bullet , 60°; and \bullet , 70°.

Table V: Excess Gibbs Free Energy of Mixing
System: Toluene-Fluorobenzene

Temp, °C	x_1 , mole fraction of toluene in liquid phase	y_1 , mole fraction of toluene in vapor phase	p , mm	g^E , joules mole ⁻¹
50.00	1.0000	1.0000	91.86	...
49.96	0.8249	0.6500	116.30	+1.9
50.115	0.7546	0.5486	126.86	+2.1
49.93	0.6532	0.4405	138.28	+2.9
49.855	0.5808	0.3568	149.30	+5.3
49.58	0.5035	0.2914	157.96	+8.2
50.275	0.5010	0.2902	162.65	+8.1
49.69	0.4711	0.2655	162.92	+5.4
49.585	0.4384	0.2411	166.55	+4.5
50.115	0.3610	0.1881	180.55	+2.3
49.745	0.3034	0.1520	185.85	+3.3
49.96	0.2396	0.1160	195.95	+1.6
49.93	0.1067	0.0475	214.50	+1.6
50.00	0.0000	0.0000	230.21	...
60.00	1.0000	1.0000	137.86	...
59.93	0.8258	0.6594	172.10	+2.3
60.01	0.7559	0.5600	186.30	+2.5
60.035	0.6649	0.4499	205.50	+5.0
60.095	0.5831	0.3684	220.80	+7.9
60.23	0.5073	0.3016	236.68	+7.3
60.13	0.5053	0.3025	235.64	+8.7
60.12	0.4724	0.2731	243.90	+3.9
59.93	0.4401	0.2489	242.52	+4.4
60.35	0.3620	0.1942	265.42	+0.9
60.01	0.3048	0.1571	273.48	+2.3
60.12	0.2415	0.1207	286.72	+2.5
60.23	0.1088	0.0500	314.62	+2.1
60.00	0.0000	0.0000	333.71	...
70.00	1.0000	1.0000	202.70	...
70.02	0.8269	0.6702	250.65	+3.6
70.04	0.7552	0.5674	270.60	+4.3
70.35	0.6641	0.4595	298.00	+3.3
70.41	0.5824	0.3785	320.25	+4.7
70.135	0.5067	0.3111	337.95	+8.7
70.355	0.5052	0.3099	340.80	+7.7
70.02	0.4730	0.2810	346.50	+9.7
70.34	0.4397	0.2566	359.00	+10.4
70.305	0.3622	0.2003	379.00	+4.2
70.255	0.3049	0.1626	393.90	+3.8
70.04	0.2518	0.1318	404.80	+3.9
70.135	0.1109	0.0532	445.55	+3.2
70.00	0.0000	0.0000	474.29	...

Table VI: Excess Gibbs Free Energy of Mixing
System: Methyl Cyclohexane-Fluorobenzene

Temp, °C	x_1 , mole fraction of methyl cyclo- hexane in liquid phase	y_1 , mole fraction of methyl cyclo- hexane in vapor phase	p , mm	g^E , joules mole ⁻¹	g^E , cor to 50°, joules mole ⁻¹
50.00	1.0000	1.00000	138.63
49.99	0.8852	0.7527	163.45	+134.3	+134.3
49.98	0.7915	0.6295	179.66	+243.6	+243.6
49.99	0.6868	0.5191	194.50	+321.2	+321.2
50.05	0.5875	0.4384	205.33	+356.9	+357.0
49.745	0.5409	0.4036	207.10	+367.8	+367.5
49.99	0.4998	0.3662	213.05	+367.8	+367.8
50.00	0.4544	0.3455	215.86	+371.5	+371.5
49.98	0.4046	0.3147	218.97	+364.0	+364.0
49.875	0.3663	0.2883	220.34	+249.5	+349.5
49.98	0.3053	0.2487	223.50	+311.2	+311.2
50.05	0.2218	0.1902	226.75	+243.7	+243.7
50.00	0.1100	0.0127	228.46	+126.4	+126.4
50.00	0.0000	0.0000	230.21
60.00	1.0000	1.0000	202.00
59.95	0.8851	0.7595	236.00	+130.8	+130.8
60.215	0.7916	0.6341	260.97	+229.3	+229.5
59.95	0.6888	0.5234	279.95	+303.6	+303.7
59.825	0.5885	0.4417	293.96	+354.6	+354.4
60.04	0.5384	0.4056	302.37	+362.8	+362.7
60.22	0.4881	0.3672	310.40	+362.8	+363.0
59.89	0.4553	0.3472	309.74	+359.7	+359.6
59.835	0.4073	0.3157	313.59	+350.3	+350.1
60.30	0.3664	0.2890	322.37	+337.5	+337.8
60.04	0.3077	0.2492	322.75	+300.2	+300.2
59.97	0.2209	0.1887	325.00	+222.7	+222.7
60.02	0.1099	0.1008	329.45	+111.5	+111.5
60.00	0.0000	0.0000	333.71
70.00	1.0000	1.0000	288.97
70.02	0.8855	0.7665	334.84	+117.8	+117.8
70.13	0.7932	0.6417	370.15	+236.1	+236.2
70.02	0.6883	0.5294	396.94	+302.0	+302.0
70.135	0.5904	0.4482	418.12	+333.9	+334.1
70.005	0.5374	0.4068	427.27	+343.7	+343.7
70.01	0.4885	0.3725	434.92	+350.9	+350.9
70.035	0.4557	0.3493	440.06	+347.1	+347.2
70.05	0.4072	0.3169	446.55	+336.5	+336.6
70.31	0.3667	0.2896	456.21	+328.5	+328.8
70.01	0.3147	0.2537	454.80	+282.4	+282.4
70.05	0.2254	0.1887	459.90	+207.6	+207.6
70.005	0.1123	0.0976	466.08	+102.1	+102.1
70.00	0.0000	0.0000	474.29

For the methylcyclohexane-fluorobenzene system, the data were fitted to an equation exactly the same as the type used for h^E

$$g^E = x_1 x_2 \sum_0^n B_p (x_1 - x_2)^p \quad (3)$$

As for the "excess heat" case, here also a value of n greater than 3 was never used. The experimental data of g^E have been plotted in Figure 3.

The curves for this system have been found to be slightly asymmetrical, having a large maximum near $x_1 = 0.5$ for each temperature. In this case, g^E has

been found to decrease with increases of temperature; their equimolar values are 370, 360 and 350 joules mole⁻¹ at 50, 60, and 70°, respectively. The values of the coefficients B_p are summarized in Table III.

The density-composition equation used for the analysis of the composition of the liquid and vapor phases are as follows.

System: toluene-fluorobenzene

$$x_{\text{tol}} \text{ or } y_{\text{tol}} = \xi - 0.12873\xi(1 - \xi) \quad (4)$$

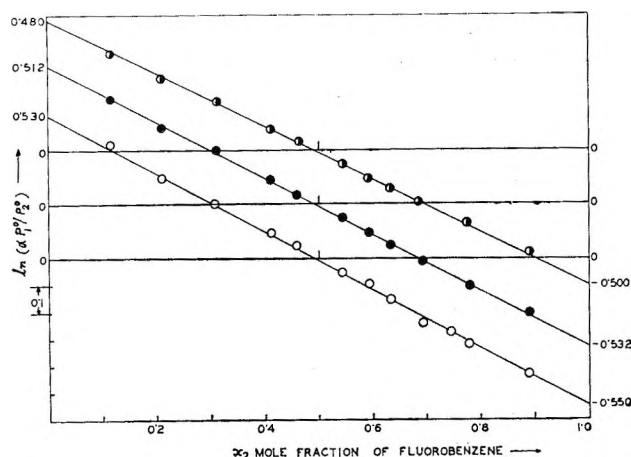


Figure 5. Test for consistency; methylcyclohexane-fluorobenzene system; experimental points: O, 50°; ●, 60°; and ◐, 70°.

System: methylcyclohexane-fluorobenzene

$$x_{mc} \text{ or } y_{mc} = 0.99774\xi -$$

$$0.36795\xi(1 - \xi) + 0.07306\xi(1 - \xi)(1 - 2\xi) \quad (5)$$

where ξ is defined by

$$\xi = \frac{d_1 - d_{mixt}}{d_1 - d_2} \quad (6)$$

$d_1 > d_2$ and d_1 is the density of the liquids.

The difference between the experimental value of x_1 and that calculated from eq 4 and 5 did not exceed ± 0.0006 , except at one point in the entire composition range, which is fairly close to our experimental error.

The experimental value of g^E at 25° can be found by extrapolation from the results obtained at 50, 60, and 70°. For the methylcyclohexane-fluorobenzene system, the average equimolar dg^E/dT over the experimental temperature range is -1.0 joule mole $^{-1}$ deg $^{-1}$, and the equimolar g^E at 25° turns out to be 395 joules mole $^{-1}$. It is interesting to note that the equimolar h^E at 25° calculated from g^E data by the classical relation

$$h^E = g^E - T \frac{\partial g^E}{\partial T} \quad (7)$$

is 693 joules mole $^{-1}$ and compares well with the direct calorimetric determination, which is 738 joules mole $^{-1}$.

For the toluene-fluorobenzene system, there is considerable uncertainty about the value of the temperature derivative of g^E , due to the fact that the absolute equimolar g^E values are small enough to be comparable to experimental accuracy, and the procedure as outlined above would not give good results. It is meaningless to calculate h^E from g^E data for the same reason. In order to extrapolate g^E to 25°, the best method in this case would be to accept the average equimolar value of this system as 7 ± 2 joules mole $^{-1}$ at the

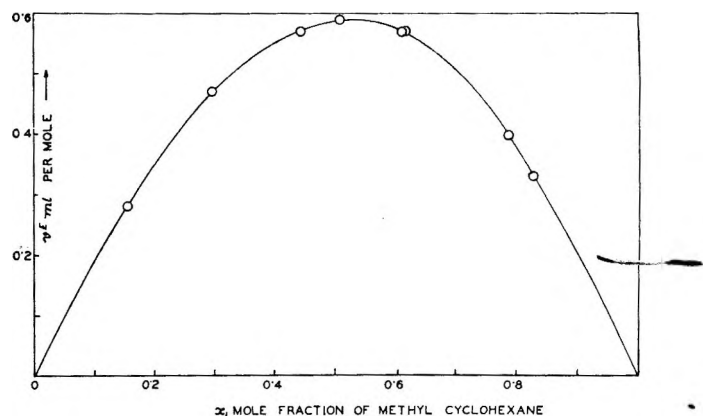


Figure 6. Excess volumes; methylcyclohexane-fluorobenzene system; O, experimental points at 40°. The smoothed curve is from eq 9, with the coefficients from Table V.

average temperature 60° and then extrapolate it to 25° with a dg^E/dT which is consistent with the experimental equimolar h^E of -55 joules/mole with the help of relation 7. The equimolar value of g^E at 25° obtained in this way is -0.2 ± 2 joule mole $^{-1}$.

Excess Volume v^E . The excess volume has been calculated from the density measurements as described before. As in the case of g^E , the volume change is very small and positive for the system toluene-fluorobenzene. Because of such small magnitudes, a plot of v^E against x would show considerable scattering, and neither a plot nor a curve fitting was attempted. For the same reason, it is not possible to say anything about the shape of the v^E vs. x curve. All the data for the excess volume at 40° are within the range

$$v^E = Cx_1x_2 \pm 0.005 \text{ ml mole}^{-1} \quad (8)$$

with $C = 0.10 \pm 0.005$ ml mole $^{-1}$, with an experimental error as previously discussed. Equation 8 has also been found to be valid for the excess volume at 25° reported earlier.⁶ Hence, the equimolar value of v^E at both the temperatures may be taken to be 0.025 ± 0.005 ml mole $^{-1}$. The temperature coefficient of v^E of this system is thus found to be either absent or within experimental error in this temperature range.

The excess volume of the system methylcyclohexane-fluorobenzene was studied only at 40°. Unfortunately, the stock sample of fluorobenzene was exhausted and the v^E at 25° could not be determined. It is well known that, except for a very few systems, the temperature coefficient of v^E is usually very small and hence the equimolar value of v^E at 40° has been taken to be the same as that at 25° in later theoretical analysis. The error introduced in this way has been taken to be small and within the limits of theoretical approximations. The v^E vs. mole fraction data at 40° are presented in Figure 6. The data were smoothed out with the help of an equation similar to (1), viz.

$$v^E = x_1 x_2 \sum_0^3 C_p (x_1 - x_2)^p \quad (9)$$

The coefficients C_p were calculated as in the treatment of calorimetric data and were collected in Table III. The excess volumes of this system are positive and large; the v^E vs. x curve is quite asymmetric with the maximum occurring at $x_1 = 0.53$ toward the nonpolar

end of the scale. The equimolar value of v^E is 0.59 ml mole⁻¹ at 40°.

Acknowledgment. This work was supported by the C.S.I.R. India and forms part of a program of the C.S.I.R. Research Unit. Thanks are due to Professor S. R. Palit, Head of the Physical Chemistry Department, I.A.C.S., Calcutta, India.

Excess Thermodynamic Functions of Some Binary

Nonelectrolyte Mixtures. II. Analyses of g^E , h^E , and v^E

Data in Terms of a Generalized Quasi-Lattice Theory

by S. N. Bhattacharyya, R. C. Mitra, and A. Mukherjee

Indian Association for the Cultivation of Science, Jadavpur, Calcutta, India (Received March 22, 1967)

The experimental data on molar excess enthalpies, Gibbs free energies, and volumes of the systems toluene-fluorobenzene and methylcyclohexane-fluorobenzene presented in part I of this series have been examined from the point of view of a generalized quasi-lattice treatment. Although this approach cannot provide an independent estimate of excess enthalpy and free energy, it is nonetheless possible to predict the excess functions in terms of various molecular interaction pairs once these are obtained uniquely from the analysis of data of other carefully chosen allied binary mixtures.

I. Introduction

The results of measurements of the molar excess enthalpy, h^E , Gibbs free energy, g^E , and volume, v^E , at different temperatures for the systems toluene-fluorobenzene and methylcyclohexane-fluorobenzene were reported in part I¹ of this series. The present paper describes an attempt to interpret the data based on the generalized quasi-lattice theory as developed by Barker² in a very systematic way. This theory was originally formulated to take into account the molecular interactions which are strongly directional, as in hydrogen-bonded systems, and also the effects arising out of the large difference in molecular size of the parent molecules constituting the mixture. The theory could be extended to the general case of mixtures of nonelectrolytes where the strong angle-dependent forces would be replaced by comparatively much weaker ones or even may be completely absent, while the molecules constituting the mixture may continue to be very different in size. The systems to be analyzed here obviously come under this category. Systematic works

already attempted in this direction are very few,^{3,4} and practically no work has been done to interpret both excess free energies and enthalpies of such nonelectrolyte mixtures.

II. Quasi-Lattice Theory

In his generalized rigid-lattice model, Barker assumes that in the solution a molecule of type i occupying r_i sites in a z co-ordinated lattice has $(q_i z)$ contact points. These contact points are divided into various classes, μ, ν, \dots , the number in the μ th class being Q_μ^i . The thermodynamics can then be expressed in terms of interaction energies for all possible combinations of these contact points. The final expressions for

(1) S. N. Bhattacharyya and A. Mukherjee, *J. Phys. Chem.*, **72**, 56 (1968).

(2) J. Barker, *J. Chem. Phys.*, **20**, 1526 (1952).

(3) J. B. Ott, J. R. Goates, and R. L. Snow, *J. Phys. Chem.*, **67**, 515 (1963).

(4) I. A. McLure, J. E. Bennet, A. E. P. Watson, and G. C. Benson, *ibid.*, **69**, 2759 (1965).

the molar excess enthalpy and free energy, according to him, are

$$h^E = -2RT \left[\sum_i \sum_{\mu, \nu} (X_\mu^i X_\nu^i - x_i X_\mu^i X_\nu^i) \eta_{\mu\nu}^{ii} \ln \eta_{\mu\nu}^{ii} + \sum_{i \neq j} \sum_{\mu, \nu} X_\mu^i X_\nu^j \eta_{\mu\nu}^{ij} \ln \eta_{\mu\nu}^{ij} \right] \quad (1)$$

$$g^E = \sum_i x_i \mu_i^E \quad (2)$$

$$\mu_i^E = RT \left[\sum_\mu Q_\mu^i \ln (X_\mu^i / x_i X_\mu^{i1}) + r_i (1/z - 1) \ln \left(\sum_i r_i x_i / r_i \right) \right] \quad (3)$$

Here the molar interchange energy for a contact between the types of molecules i and j and areas of classes μ and ν is denoted by $U_{\mu\nu}^{ij}$. The terms $U_{\mu\nu}^{ij}$ and $\eta_{\mu\nu}^{ij}$ are defined by

$$2U_{\mu\nu}^{ij} = 2^*U_{\mu\nu}^{ij} - {}^*U_{\mu\mu}^{ii} - {}^*U_{\nu\nu}^{jj} \quad (4)$$

$$\eta_{\mu\nu}^{ij} = \exp(-U_{\mu\nu}^{ij}/RT) \quad (5)$$

the starred parameters indicating the net interaction energies of various pairs. The parameters X_μ^i are the solutions of the equations

$$X_\mu^i \sum_j X_\nu^j \eta_{\mu\nu}^{ij} = (Q_\mu^i/2)x_i \quad (6)$$

and X_μ^{i1} are the values of X_μ^i for $x_1 = 1$.

The theory was applied with considerable success by Barker himself² and later by Goates, Snow, and James⁵ and Ott, Goates, and Snow⁶ for alcohol in nonpolar solvent systems. The application of the theory may also be extended to cases of nonpolar or weakly dipolar mixtures where strong specific interactions are absent, but where the component molecules are very different in size and shape. The only notable works in this direction are those of Ott, Goates, and Snow³ and McLure, Bennett, Watson, and Benson.⁴ The former applied Barker's theory to describe only the heats of mixing of several aromatic-aliphatic, aromatic-alicyclic, and hydrocarbon-halogen substituted hydrocarbon systems and neglected, as before, the volume change of mixing. The latter group extensively and in a very systematic way studied heats of mixing and volume change of mixing of some aromatic-alicyclic systems and recalculated the heats of mixing at constant pressure as energies of mixing at constant volume. Goates, *et al.*, reported many discrepancies in the same interaction constants calculated from different systems and attributed it to the limiting number of data and to the crudeness of the theory. Benson, *et al.*, also found that the data for all of their systems could not be fitted by a single value of U_{12} ; the values vary by as much as $\pm 14\%$. All of these works support, in a more or less satisfactory way, the general validity of Barker's theory applied to nonpolar systems, as far as heats of mixing are concerned.

Three major drawbacks are very apparent in these applications of Barker's theory to nonpolar systems.

(a) One of the drawbacks of the quasi-lattice theory

lies in the arbitrary way the number of sites could be assigned to different molecules. The assumption that a carbon atom occupies one site of a fourfold coordinated lattice (*i.e.*, $z = 4$) would no doubt allow assignment of the contact surfaces of a molecule in terms of its molecular structure, but it would not necessarily ensure equal volume per segment in different molecules. The latter is important from the point of view of the theory of *r-mer* solutions and is one of the factors governing the shapes of the plots of the excess functions against mole fraction, particularly when the interaction is weak ($U_{ij} \ll RT$). Similarly, the assumption that a chlorine, bromine, or oxygen atom occupies a single site is also quite arbitrary. This is well illustrated in the case of the C_6H_{14} - C_6F_{14} system.³ Each fluorine atom was assigned one site, which resulted in a high distortion of the calculated h^E curve. Neglect of this particular aspect may also be partly responsible for the discrepancies observed by both Goates, *et al.*, and Benson, *et al.*, in the value of the same interaction constant calculated from different systems.

This arbitrariness may partly be removed by selecting a suitable reference molecule (say benzene or an *n*-alkane) and assigning it a number of sites r_{ref} , with a fixed coordination number, so that the number of contact surfaces so obtained are related to its molecular structure. Now the number of sites for a particular molecule could be fixed unambiguously from the consideration that its volume per segment should be equal to that of the reference molecule as far as is practicable.

(b) Another limitation of the application of quasi-lattice theory lies in the fact that the assignment of interaction energies is often somewhat arbitrary, and different sets may be found which fit the experimental excess energy equally well. Such a situation was encountered mainly in those systems where attempts were made to calculate more than one interaction energy from a single set of experimental data of one system only. Naturally, we can, if possible, select systems in such a way that only one interaction energy is to be chosen to fit a single set of experimental data, all other interaction energies being already known or having been previously determined. Using the treatment outlined in (a), one can get a unique value for each interaction pair in this way.

(c) It may be noticed that very little work has been done to calculate excess free energy for the nonpolar systems or systems having weak noncentral interactions. Goates, *et al.*, never tried to calculate the excess free energy of any of their systems. Benson, *et al.*,⁴ did mention about the discrepancy of their calculated excess free energies and entropies of some of their aromatic-alicyclic systems, but did not furnish any details. It

(5) J. R. Goates, R. L. Snow, and M. R. James, *J. Phys. Chem.*, **65**, 335 (1961).

(6) J. B. Ott, J. R. Goates, and R. L. Snow, *ibid.*, **66**, 1301 (1962).

is obvious that they used for their calculation of f^E the same interchange energies that were obtained from their calculation of u^E .

We ourselves did some preliminary calculations of the f^E for the benzene-cyclohexane system, for which very reliable experimental data exist. We used the same interchange energy, number of contact points, and coordination number used by Benson, *et al.*, and obtained similar results. We found that $f^E \simeq u^E$ and that s^E is small and negative, whereas experimental f^E is much less, about half that of u^E .

These findings are not at all surprising because the benzene-cyclohexane system has only one type of contact pair and the molecular volumes of the components here are not too different. Hence, it is expected that the generalized quasi-lattice theory would essentially reduce it to the case of a strictly regular solution with the quasi-chemical approximation. It is very well known that this theory can predict only the combinatorial part of excess entropy. For molecules of near-equal size, this turns out to be very small and negative when $U_{ij} \ll RT$. A rigid lattice theory, as such, is unable to take into account any contribution from the noncombinatorial entropy. The latter may be, and usually is, quite large in magnitude in nonpolar systems or systems involving weak interactions, and almost the entire excess entropy that is encountered there would be noncombinatorial in origin. This, precisely, is the reason for the discrepancy between theoretical predictions and experimental results observed by Benson and co-workers and cannot be rectified by simply reassigning the contact energies or number of sites.

In contrast, in the systems containing very strong interaction like a hydrogen bond (*i.e.*, $U_{ij} \ll RT$), the combinatorial part of the entropy can far outweigh the noncombinatorial part. The Q - C approximation, being a fairly good approximation for the calculation of combinatorial entropy, may take into account the entire excess entropy in such systems. The latter may explain the success of Barker and Goates, *et al.*,^{5,6} in their calculation of free energies for the solutions of alcohol in nonpolar solvents.

Contribution due to noncombinatorial excess entropy can be incorporated in a rigid-lattice model by following the intuitive method, suggested by Guggenheim.⁷ It requires the use of a temperature-dependent but concentration-independent "cooperative free energy" term ω_{ij} , instead of U_{ij} , in the Q - C approximation. Naturally X_μ^i and f^E are to be calculated using this temperature-dependent ω_{ij} . For the calculation of u^E , X_μ^i is to be taken as in f^E , but now the interchange energy U_{ij} is independent of temperature and connected with ω_{ij} by a Gibbs-Helmholtz equation

$$U_{ij} = \omega_{ij} - T \frac{\partial \omega_{ij}}{\partial T} \quad (7)$$

With these modifications, expressions 2 and 3 remain unaltered but (1) and (6) may be rewritten as

$$\mu_\nu^E = -2RT \left[\sum_i \sum_{\mu, \nu} (X_\mu^i X_\nu^i - x_i X_\mu^i X_\nu^i) \times \right. \\ \left. \xi_{\mu\nu}^{ii} \ln \eta_{\mu\nu}^{ii} + \sum_{i \neq j} \sum_{\mu, \nu} X_\mu^i X_\nu^j \xi_{\mu\nu}^{ij} \ln \eta_{\mu\nu}^{ij} \right] \quad (8)$$

$$X_\mu^i \sum_\nu X_\nu^j \xi_{\mu\nu}^{ij} = (Q_\mu^i/2) x_i \quad (9)$$

where

$$\xi_{\mu\nu} = \exp(-\omega_{ij}/RT) \quad (10)$$

III. Discussion

Along with a correction due to the volume change of mixing, we have adopted procedure (a)-(c) for our calculations. Among the various mixing processes developed to convert excess functions measured at constant pressure to experimental values at constant volume,^{8,9} those constant volume values obtained by "mixing at constant volume per segment" or the so-called "process 3" have been held by many workers to represent truly the rigid-lattice models. But as very meagre thermodynamic data of the pure components are available to pursue such a correction in our case, we are compelled to adopt the so called "process 2" or simply the "constant-volume process" of ref 9. It may also be mentioned here that there are also opinions that all these processes are really developed to rationalize a model far removed from reality.¹⁰ For "process 2" the following thermodynamic relations may be written, neglecting the higher order terms

$$f_v^E - g_v^E = \frac{v}{2\beta} (v^E/v)^2 \quad (11)$$

$$\mu_v^E - h_v^E = v^E T (\alpha/\beta) \quad (12)$$

Here α , the coefficient of thermal expansion, and β , the isothermal compressibility, are those of the mixtures and have been estimated by assuming additivity on a volume-fraction basis from the pure components. See Table I.¹¹⁻¹⁴

The right-hand side of eq 11 is so small in the systems

(7) E. A. Guggenheim, *Trans. Faraday Soc.*, **44**, 1007 (1948); *Nuovo Cimento*, Suppl 2, **6**, 181 (1949); E. A. Guggenheim, "Mixtures," Oxford University Press, 1952.

(8) G. Scatchard, *Trans. Faraday Soc.*, **33**, 160 (1937); J. H. Hildebrand and R. L. Scott, "Solubility of Non Electrolytes," Reinhold Publishing Corp., New York, N. Y., 1949; R. L. Scott, *Discussions Faraday Soc.*, **44**, 15 (1953).

(9) M. L. McGlashan, J. W. Morcom, and A. G. Williamson, *Trans. Faraday Soc.*, **57**, 601 (1961).

(10) S. N. Bhattacharyya, D. Patterson, and T. Somecynsky, *Physica*, **30**, 1276 (1964).

(11) G. A. Holder and E. Whalley, *Trans. Faraday Soc.*, **58**, 2095 (1962).

(12) Y. Wada, *J. Phys. Soc. Japan*, **4**, 280 (1949).

(13) "Selected Values of Properties of Hydrocarbons and Related Compounds," American Petroleum Institute Research Project 44, Carnegie Press, Pittsburgh, Pa., 1953.

(14) "Physical Properties of Chemical Compounds," American Chemical Society, Washington, D. C., 1955.

Table I: Isothermal Compressibility (β) and Coefficient of Thermal Expansion (α) of Pure Compounds at 25°

Compounds	$10^3\beta$, cm ² /atom	$10^3\alpha$, cm ³ /deg	Ref
Benzene	98.12	1.217	11, 12
Toluene	94.73	1.071	12, 13
Cyclohexane	115.20	1.261	11, 13
Methylcyclohexane	122.52	1.440	12, 13
Fluorobenzene	95.86 ^a	1.100	13, 14

^a Estimated.

investigated by us that it may safely be neglected, or in our cases $f_v^E \simeq g_p^E$.

We have assumed a fourfold coordinated lattice and assigned five sites to the benzene molecule, which we have taken as reference. Component molecules of the mixtures are then assigned such a number of sites as to make the volumes per site for all the molecules practically equal to each other. Fractional numbers have also been accepted so long as they give an integral number of contact points for a molecule. In this way, we obtain $r_B = 5$, $r_F = 5.5$, $r_C = 6$, $r_T = 6$, and $r_M = 7$, where the subscripts, B, F, C, T, and M refer to benzene, fluorobenzene, cyclohexane, toluene, and methylcyclohexane, respectively. To these molecules various contact surfaces have then been assigned. These are: benzene: $r_B = 5$, $q_{Bz} = 12$, $Q_H^B = 12$; fluorobenzene: $r_F = 5.5$, $q_{Fz} = 13$, $Q_F^F = 2$, $Q_H^F = 11$; cyclohexane: $r_C = 6$, $q_{Cz} = 14$, $Q_{h_1}^C = 14$; toluene: $r_T = 6$, $q_{Tz} = 14$, $Q_{h_2}^T = 3$, $Q_H^T = 11$; methylcyclohexane: $r_M = 7$, $q_{Mz} = 16$, $Q_{h_2}^M = 3$, $Q_{h_1}^M = 13$. Thus, the fluorobenzene molecule has two types of contact points, aromatic hydrogen (H) and fluorine (F). The toluene molecule also has two types, aromatic hydrogen (H) and aliphatic hydrogen (h_2), and the methyl cyclohexane molecule has two types of contact points, alicyclic hydrogen (h_1) and aliphatic hydrogen (h_2). Of the various interaction pairs possible from these combinations, the system fluorobenzene-methylcyclohexane possesses all of them. These are (1) the fluorine-aromatic hydrogen pair, $\omega_{FH} = \omega_1$; (2) the aromatic hydrogen-alicyclic hydrogen pair, $\omega_{Hh_1} = \omega_2$; (3) the fluorine-alicyclic hydrogen pair, $\omega_{Fh_1} = \omega_3$; (4) the aromatic hydrogen-aliphatic hydrogen pair, $\omega_{Hh_2} = \omega_4$; (5) the fluorine-aliphatic hydrogen pair, $\omega_{Fh_2} = \omega_5$; and lastly (6) the alicyclic hydrogen-aliphatic hydrogen pair, $\omega_{h_1h_2} = \omega_6$. Out of the six possible interaction pairs, we have put $\omega_6 = 0$, which is reasonable.

We have tried to find out, as argued in (b), these five interaction pairs, more or less uniquely, from five other systems, excluding fluorobenzene-methylcyclohexane, for which reliable experimental data exist. We have selected for these systems (1) benzene-fluorobenzene, (2) cyclohexane-fluorobenzene, (3) benzene-cyclohexane,

(4) toluene-cyclohexane, and (5) toluene-fluorobenzene. Of these, the experimental h^E , g^E , and v^E of the first two systems are taken from Bhattacharyya, Anantaraman, and Palit.^{15,16} The h^E and v^E of (3) and (4) has been obtained from the work of Benson and co-workers.⁴ The g^E of these two systems are taken from Scatchard, Wood and Mochel,¹⁷ and Myers,¹⁸ respectively. We ourselves have measured h^E , g^E , and v^E of (5).¹

We have, by trial and error, first tried to find out the correct value of the only unknown, ω_{ij} , involved in any system so that eq 9 is exactly satisfied, and at the same time, the experimental f_v^E is correctly predicted at, or very near, equimolar concentration. These give us the correct ω_{ij} and x_μ^i and are in turn used for u^E calculations. With ω_{ij} and x_μ^i thus obtained, U_{ij} is adjusted to predict the correct experimental u_v^E at or near equimolar concentration from eq 8. Computations were performed with the help of desk calculators (we followed the method outlined by Barker²) in absence of electronic computer facilities, and the calculations over the entire mole fraction range were not pursued. The results of the calculations of all the systems at equimolar composition and 25° have been summarized in Tables II and III.

(1) Cooperative free energy, ω_1 , and interchange energy, U_1 , of the interaction pair between fluorine (F) and aromatic hydrogen contacts (H) were obtained from the benzene-fluorobenzene system. Only one kind of interaction pair is involved in this system.

(2) $\omega_2(U_2)$, representing aromatic (H), and alicyclic (h_1) contacts were obtained from the system benzene-cyclohexane. This system also possesses only one kind of interaction pair.

(3) The system cyclohexane-fluorobenzene has three interaction parameters of which $\omega_1(U_1)$ and $\omega_2(U_2)$ may now be put equal to values that have been found from (1) and (2). The third, $\omega_3(U_3)$, representing the interaction between the fluorine (F) and alicyclic hydrogen (h_1) contact, has been found out from the f^E and u^E data of this system.

(4) The interaction parameter, $\omega_4(U_4)$, for aromatic (H) and aliphatic (h_2) contacts has been determined from the toluene-cyclohexane system. The other parameter involved here is $\omega_3(U_3)$, which has been taken to be the same as that obtained from the benzene-cyclohexane system.

(5) From the fluorobenzene-toluene system, the interaction parameters $\omega_5(U_5)$ for the fluorine (F) and aliphatic (h_2) contacts were calculated. The other pa-

(15) S. N. Bhattacharyya, A. V. Anantaraman, and S. R. Palit, *Trans. Faraday Soc.*, **59**, 1101 (1963).

(16) S. N. Bhattacharyya, A. V. Anantaraman, and S. R. Palit, *Indian J. Chem.*, **1**, 459 (1963).

(17) G. Scatchard, S. E. Wood, and J. M. Mochel, *J. Am. Chem. Soc.*, **61**, 3206 (1938).

(18) H. S. Myers, *Ind. Eng. Chem.*, **47**, 2215 (1955).

Table II: The Interaction Parameters Involved in the Systems and Their Values Calculated in Joules Mole⁻¹

System	Parameters involved	Parameters already known	Unknown parameters determined	Exptl excess function used for calcn	Calcd values of the parameters
(1) Benzene + fluorobenzene	ω_1 U_1		ω_1 U_1	f^E u^E	26.3 -251.8
(2) Benzene + cyclohexane	ω_2 U_2		ω_2 U_2	f^E u^E	103.9 184.0
(3) Cyclohexane + fluorobenzene	$\omega_1, \omega_2, \omega_3$ U_1, U_2, U_3	ω_1, ω_2 U_1, U_2	ω_3 U_3	f^E u^E	585.1 125.0
(4) Toluene + cyclohexane	ω_2, ω_4 U_2, U_4	ω_2 U_2	ω_4 U_4	f^E u^E	190.7 95.7
(5) Toluene + fluorobenzene	$\omega_1, \omega_4, \omega_5$ U_1, U_4, U_5	ω_1, ω_4 U_1, U_4	ω_5 U_5	f^E u^E	101.6 -736.7

Table III: Thermodynamic Molar Quantities of Mixtures at Equimolar Concentration and 25°

System	$\alpha \times 10^3$, deg ⁻¹	$\beta \times 10^3$, ml ² joule ⁻¹	v^E , ml mole ⁻¹	h_p^E exptl, joules mole ⁻¹	u_p^E exptl, joules mole ⁻¹	u_p^E calcd, joules mole ⁻¹	g_p^E exptl, joules mole ⁻¹	g_p^E calcd, joules mole ⁻¹
C ₆ H ₆ + C ₆ H ₅ F	1.16	95.74	0.08	10	-19	-19 ^a	0	1 ^a
C ₆ H ₆ + <i>c</i> -C ₆ H ₁₂	1.24	107.5	0.58	805	582	582 ^a	325	325 ^a
<i>c</i> -C ₆ H ₁₂ + C ₆ H ₅ F	1.24	107.3	0.79	912	670	670 ^a	566	566 ^a
<i>c</i> -C ₆ H ₁₂ + C ₆ H ₅ CH ₃	1.17	105.9	0.52	625	438	438 ^a	397	397 ^a
C ₆ H ₅ CH ₃ + C ₆ H ₅ F	1.19	106.2	0.03	-55	-66	-66 ^a	0	0 ^a
<i>c</i> -C ₆ H ₁₁ CH ₃ + C ₆ H ₅ F	1.30	111.2	0.59	738	537	568 ^b	395	360 ^b

^a Adjusted. ^b Predicted.

rameters involved in this system are $\omega_1(U_1)$ and $\omega_4(U_4)$, which were assigned the values obtained from (1) and (4).

(6) We tried next to predict f^E and u^E of the system methylcyclohexane-fluorobenzene with the help of these five sets of parameters evaluated from the five systems as described above (*cf.* Table II). The calculated values of f^E and u^E of this system (*cf.* Table III) came out to be 360 and 568 joules mole⁻¹ at equimolar concentration and 25° while the experimental results were 396 and 537 joules mole⁻¹, respectively. Although the theoretical values are not in strict quantitative agreement with the experimental results, these are within 10% of it and demonstrates the more or less consistent character of the values of the "cooperative free energy" and energy of interchange of various interaction pairs obtained in this way.

It may be pointed out that calculations of this type demand extreme accuracy of experimental results.

There is a tendency that small experimental errors of the individual systems add up in the course of calculation, causing an appreciable error in the final prediction. Uncertainty as to the validity of "process 2" might be responsible also for some error in the calculation of u^E . Unlike alcohol solutions, even small interaction energies are important in the systems involving only weak interactions. From the chemical point of view, in general, no two contact points of the same class but belonging to different molecules (such as the aliphatic hydrogens substituted to an aromatic ring and aliphatic hydrogen substituted to an alicyclic ring) would strictly be exactly identical. The last drawback may cause an appreciable discrepancy in the predicted results.

Acknowledgment. This work was supported by the C.S.I.R. Research Unit. Thanks are due to Professor S. R. Palit, Head of the Physical Chemistry Department, I.A.C.S., Calcutta, India.

Electron Spin Resonance Study of Some Trifluoromethylnitrobenzene Anion Radicals

by J. W. Rogers and W. H. Watson

Department of Chemistry, Texas Christian University, Fort Worth, Texas 76129 (Received April 11, 1967)

The electron spin resonance (esr) spectra of the anion radicals of 3-trifluoromethyl-4-nitrophenol and 2-trifluoromethylnitrobenzene show pronounced line-width alternation. This is interpreted as arising from the hindered rotation of the trifluoromethyl group and the extreme variations in the instantaneous hyperfine constants of the equivalent fluorine atoms. Solvent studies in N,N-dimethylformamide, dimethyl sulfoxide, and acetonitrile indicate that radical-solvent interactions are important. A specific model is proposed to explain the observed line-width alternations. The two-electron reduction of 2-trifluoromethylnitrobenzene yields a paramagnetic species whose esr spectrum is consistent with the loss of coupling to the nitrogen nucleus. Only the monoanion radical spectra are observed for the high-voltage reduction of 3-trifluoromethyl-4-nitrophenol and 3-trifluoromethylnitrobenzene. These radicals probably are formed by electron transfer from the multi-negative anions to the neutral species. The ultraviolet-visible spectrum of 2-trifluoromethylnitrobenzene was recorded as a function of time and electrolysis voltage. Some speculations are made concerning the reduction processes in these systems.

Introduction

In recent years, many investigators have studied the esr spectra of radical anions formed by the reduction of various aromatic molecules.¹⁻⁵ Through these studies, a considerable quantity of data has been accumulated on π -electron densities, bonding, and structure. More recently, the phenomenon of line-width alternation was recognized and has received considerable attention.⁶⁻¹¹ A theory of line widths has been developed by Fraenkel which allows a quantitative description of linewidths to be given.¹²⁻¹⁴ In general, these effects are minor and result in only slight line broadening; however, for 2-trifluoromethylnitrobenzene and its derivatives, the effects are so pronounced that the broadened lines frequently are difficult to detect. A study of these highly perturbed systems is of interest, and a study which complements the work described in this paper has recently been reported.¹⁵

The experimental technique developed by Geske and Maki, in which an electrode is used as a selective reducing agent to generate radicals *in situ*, has proven to be useful in the esr study of radical reduction products.¹⁶ The major attention has been focused on study of organic anion radicals prepared by the one-electron reduction of the parent molecule.¹⁻⁵ In general, the two-electron reduction step results in a diamagnetic product or products; however, some anion radicals generated electrochemically at applied potentials considerably above the first polarographic wave have been mentioned in the literature.¹⁷⁻²⁰

In the 2-trifluoromethylnitrobenzene system, we have observed the esr spectrum of a paramagnetic species generated at a potential corresponding to the second polarographic wave. Hyperfine interaction

- (1) A. H. Maki and D. H. Geske, *J. Am. Chem. Soc.*, **83**, 1852 (1960).
- (2) P. H. Rieger and G. K. Fraenkel, *J. Chem. Phys.*, **37**, 2795 (1962).
- (3) P. H. Rieger and G. K. Fraenkel, *ibid.*, **39**, 609 (1963).
- (4) S. H. Glarum and J. H. Marshall, *ibid.*, **41**, 2182 (1964).
- (5) P. L. Kolker and W. A. Waters, *J. Chem. Soc.*, 1136 (1964).
- (6) J. H. Freed and G. K. Fraenkel, *J. Chem. Phys.*, **37**, 1156 (1962).
- (7) J. H. Freed, P. H. Rieger, and G. K. Fraenkel, *ibid.*, **37**, 1881 (1962).
- (8) J. H. Freed and G. K. Fraenkel, *ibid.*, **41**, 699 (1964).
- (9) J. H. Freed and G. K. Fraenkel, *ibid.*, **40**, 1815 (1964).
- (10) A. Hudson, C. Lagercrantz, and G. R. Luckhurst, *Mol. Phys.*, **11**, 321 (1966).
- (11) A. Carrington, *ibid.*, **5**, 425 (1962).
- (12) J. H. Freed and G. K. Fraenkel, *J. Chem. Phys.*, **39**, 326 (1963).
- (13) J. H. Freed and G. K. Fraenkel, *J. Am. Chem. Soc.*, **86**, 3477 (1964).
- (14) G. K. Fraenkel, *J. Phys. Chem.*, **71**, 139 (1967).
- (15) E. G. Janzen and J. L. Gerlock, presented at the 152nd National Meeting of the American Chemical Society, New York, N. Y., Sept 1966; private communication.
- (16) D. H. Geske and A. H. Maki, *J. Am. Chem. Soc.*, **82**, 2671 (1960).
- (17) P. H. Rieger, I. Bernal, W. H. Reinmuth, and G. K. Fraenkel, *ibid.*, **85**, 683 (1963).
- (18) I. Bernal and G. K. Fraenkel, *ibid.*, **86**, 1671 (1964).
- (19) R. D. Allendoerfer and P. H. Rieger, *ibid.*, **88**, 3711 (1966).
- (20) J. Q. Chambers and R. N. Adams, *J. Electroanal. Chem.*, **9**, 400 (1965).

with the nitrogen nucleus is not observed, and the nitro group either has been eliminated or reduced.

Experimental Section

The anion radicals were prepared by electrolytic reduction of a 10^{-3} M solution of the reductant in N,N-dimethylformamide (DMF), dimethyl sulfoxide (DMSO), and acetonitrile (CH_3CN), using tetra-*n*-propylammonium perchlorate as the supporting electrolyte. All potentials were measured between the mercury cathode in the electrolysis vessel and an aqueous saturated calomel reference electrode. The diffusion of small quantities of water through the salt bridge must be considered, since traces of water can greatly alter the appearance of the spectrum. Spectra were always obtained with and without the calomel reference electrode. The general experimental techniques were similar to those described by Geske and Maki.¹⁶

Spectroquality solvents were used. DMF was dried over calcium hydride, and DMSO was vacuum distilled after standing over calcium hydride. Acetonitrile was used without further purification. Tetra-*n*-propylammonium perchlorate was prepared by the addition of an aqueous solution of the hydroxide to an equivalent amount of perchloric acid. The hydroxide was obtained as a 10% aqueous solution from Eastman Kodak Co. The salt was recrystallized from aqueous acetonitrile, 20%, washed with a large quantity of water, and dried over phosphorus pentoxide.

The parent compounds were obtained from K & K Laboratories, Inc. The 2-trifluoromethylnitrobenzene was recrystallized from a 20% solution of ethanol in petroleum ether, mp 32°. The 3-trifluoromethylnitrobenzene, bp 202°, and 3-trifluoromethyl-4-nitrophenol, mp 78°, were used without further purification. The two trifluoromethylnitrobenzene isomers were checked by gas chromatography and were found to be chromatographically pure, *i.e.*, much less than 1% total impurities. The trace contaminants were identified as isomers of the main constituent. Reference compounds 2-aminobenzotrifluoride and trifluorotoluene were obtained from Aldrich Chemical Co., Inc., and 2-trifluoromethylphenol was obtained from K & K Laboratories.

Polarographic data at a single concentration and 25° were obtained using a Sargent Model XV recording polarograph. All polarographic measurements were made in the same electrolysis vessel used in the esr experiments, and an aqueous saturated calomel reference electrode was used throughout. No *iR* correction was made for the electrolysis vessel.

A conventional X-band spectrometer, employing a Strand Labs cylindrical reflection cavity operating in the TE₀₁₁ mode, was used. A 9-in. Varian magnet with Field Dial control was used in conjunction with 6-kc field modulation. The sample cell was cooled by a

JEOLCO-JES-VT-2 temperature controller adapted to the Strand Labs cavity. Temperature was monitored with a thermocouple placed approximately 2 cm from the sample. The hyperfine lines from potassium peroxyaminedisulfonate in water were used to calibrate the magnetic-field sweep.

The ultraviolet-visible spectra of electrochemically generated species were recorded on a Cary Model 15 spectrophotometer. A pool of mercury was placed in the bottom of a regular quartz ultraviolet cell and a platinum wire, sealed in a glass tube, was placed beneath the surface. A platinum electrode was inserted into the upper portion of the cell and the two electrodes connected to a voltage bridge. The upper electrode was masked from the optical path of the instrument. Identical solutions were placed in the reference and sample cells and the spectrum recorded to check for a linear base line. An appropriate voltage could be applied, and transient or new species with absorption bands in the ultraviolet or visible regions of the spectrum could be recorded. Quantitative measurements were not possible because of concentration gradients, diffusion, and reaction. The pure solvents were checked to ensure that they were not responsible for any new absorption bands.

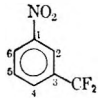
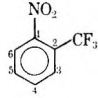
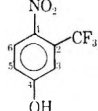
Results and Discussion

The reduction voltages in all solvents were determined from polarographic studies and are indicated in Table I. The first polarographic wave for 2-trifluoromethylnitrobenzene and 3-trifluoromethylnitrobenzene corresponds to a one-electron addition to form the anion radical. The first polarographic wave for 3-trifluoromethyl-4-nitrophenol involves the reduction of the phenolic proton, while the second wave corresponds to the addition of an electron to form the phenoxy anion radical. Only 2-trifluoromethylnitrobenzene yielded an additional paramagnetic species at higher polarographic potentials.

3-Trifluoromethylnitrobenzene. The esr spectrum of the monoanion radical of 3-trifluoromethylnitrobenzene was recorded in the solvents DMSO and DMF. The coupling constants are listed in Table I and are in good agreement with those obtained in acetonitrile.¹⁶ The solvent effects are consistent with numerous other studies. The coupling-constant assignment is in agreement with molecular-orbital calculations and other investigators.¹⁶ The minimum line widths are about 130 mgauss in DMF and 240 mgauss in DMSO.

Reduction at the second polarographic wave yields the monoanion radical as the only paramagnetic species. This is assumed to occur *via* electron transfer between a diamagnetic dianion and the neutral species, $\text{A}^{2-} + \text{A} \rightarrow 2\text{A}^{\cdot -}$. Prolonged reduction at higher voltages, with the calomel reference electrode in the system, yields a spectrum which differs superficially with the low-voltage spectrum. This spectrum is

Table I: Coupling Constants^a for Trifluoromethylnitrobenzene Anion Radicals^b

Compound	Solvent	Electrolysis voltage	A_N	A_2	A_3	A_4	A_5	A_6
	DMSO	-1.0	8.64	3.22	1.18 ^c	4.32	1.18	3.22
	DMF	-1.0	8.73	3.27	1.28	4.03	1.01	3.27
	DMF(4H ₂ O)	-1.0	8.85	3.27	1.16	4.43	1.16	3.27
	CH ₃ CN	-1.0	8.32	8.51 ^c	0.87 ^d	3.90	1.23 ^d	3.20
	DMSO	-1.0	7.96	9.34	0.85	4.31	1.26	3.07
	DMF	-1.0	7.67	9.64	0.87	4.36	1.26	3.06
	DMF ^e	-2.0	...	6.7 ^c	1.2 ^f	5.2 ^f	2.3 ^f	2.3 ^f
	CH ₃ CN	-2.0	12.62	8.63 ^c	0.38 ^d	...	1.09 ^d	2.68
	DMSO	-2.0	12.10	9.24	0.38 ^g	...	1.09	2.71
	DMF	-2.0	12.00	9.67	0.38	...	1.09	2.71

^a The following coupling constants were obtained by Prof. E. G. Janzen (private communication): 3-trifluoromethylnitrobenzene in CH₃CN, $A_N = 8.84$, $A_F = 1.2$, $A_2^H = 3.01$ and 3.21 , $A_m^H = 1.00$, $A_p^H = 4.05$; and 3-trifluoromethyl-4-nitrophenol in CH₃CN (numbered as indicated in the table), $A_N = 12.1$, $A_F = 8.38$, A_3^H and $A_5^H = 1.06$ and 0.32 , and $A_6^H = 2.68$. ^c In gauss and at room temperature unless otherwise specified. ^e Quartet splitting assigned to trifluoromethyl groups. ^d Assignments are consistent but ambiguous. ^e Temperature, -20°. ^f Assignment ambiguous. ^g Resolved with low modulation, narrow sweep widths, and long sweep times.

identical with that obtained upon reduction with a solvent composed of 0.4% water in DMF, Table I. Prolonged electrolysis at the higher voltages permits water to diffuse into the system from the reference electrode system.

3-Trifluoromethyl-4-nitrophenol. The esr spectra of 3-trifluoromethyl-4-nitrophenol in DMSO, DMF, and CH₃CN are shown in Figure 1. The paramagnetic species was short-lived and the esr signal disappeared with a few minutes after electrolysis had ceased. The spectrum in DMF contained six groups of four lines with no overlapping components. The four lines were composed of two doublets. Without additional information, these spectra could not be readily interpreted as arising from hyperfine interactions with the ring substituents; however, the spectrum of 3-trifluoromethyl-4-nitrophenol in CH₃CN contains additional features. The six groups of four sharp lines are still present, but prominent broad lines are now observed between the six groups of lines. This might suggest the simultaneous existence of two or more paramagnetic species, or a line-broadening phenomenon, which affects a particular class of transitions. Esr spectra recorded as a function of modulation amplitude are consistent with the latter interpretation.

The theory of line widths developed by Fraenkel¹³ can be used to interpret the esr data. This theory assumes that the total spin Hamiltonian can be divided into two parts

$$\hbar\mathcal{H} = \hbar\mathcal{H}_0 + \hbar\mathcal{H}_1(t) \quad (1)$$

The time-independent zero-order Hamiltonian, \mathcal{H}_0 , yields a sharp lined spectrum, but $\mathcal{H}_1(t)$ is a fluctuating time-dependent perturbation which causes relaxation and line broadening. The perturbing Hamiltonian¹²

for the modulation of the isotropic interaction can be written as

$$\hbar\mathcal{H}_1(t) = \{\hbar|\gamma_e|\sum_i [a_i(t) - \bar{a}_i]I_{i1}\} \cdot S \quad (2)$$

where $a_i(t)$ is the instantaneous value of the isotropic hyperfine splitting and $\bar{a}_i = \langle a_i(t) \rangle$. The correlation functions $g_{ij}(\tau)$, which are needed to calculate the line widths, are

$$g_{ij}(\tau) = \gamma_e^2 \langle [a_i(t) - \bar{a}_i] [a_j(t + \tau) - \bar{a}_j] \rangle \quad (3)$$

where i and j refer to the various nuclei. The spectral densities are calculated from the Fourier transform of the correlation functions

$$J_{ij}(\omega) = (1/2) \int_{-\infty}^{\infty} g_{ij}(\tau) \exp(-i\omega\tau) d\tau \quad (4)$$

where $\omega/2\pi$ is the frequency of the transition induced by the perturbation.

The three-jump model for nuclei with spin one-half has been developed by Fraenkel.¹³ There are a number of possible conformations that are consistent with such a mechanism. It has been suggested that p- π overlap is an important factor in these systems.¹⁵ This would involve overlap of a p orbital on the fluorine atom with a π orbital of the nitro group. The magnitude or significance of such an interaction is difficult to evaluate, and we feel that the data in this paper are consistent with other interpretations.

The line broadening depends upon large differences in the instantaneous hyperfine constants of the equivalent nuclei of the trifluoromethyl group and a jump frequency of the same order of magnitude as the frequency difference between the two instantaneous hyperfine values. A possible conformation might involve two

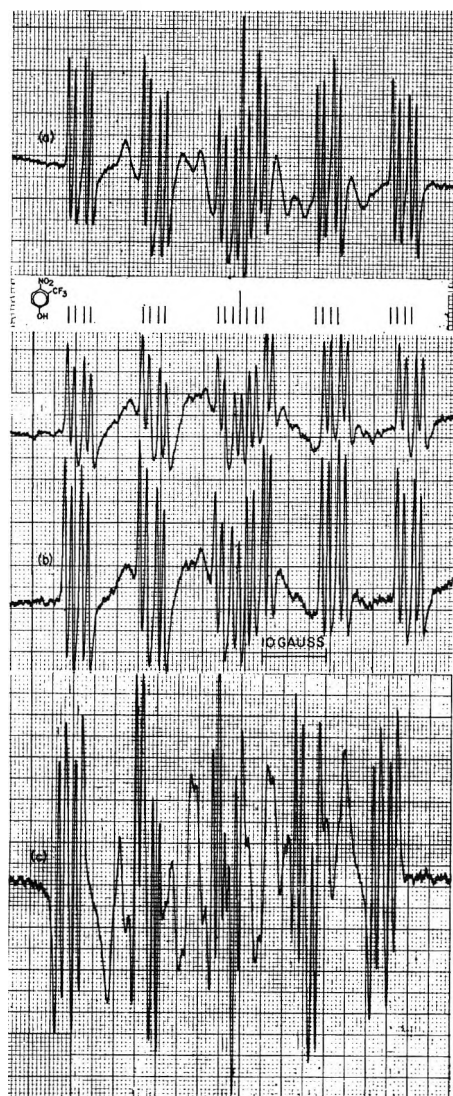
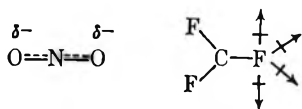


Figure 1. The esr spectra of the anion radical of 3-trifluoromethyl-4-nitrophenol in (a) DMSO, (b) DMF, and (c) CH_3CN .

fluorine atoms adjacent to the negative nitro group and the other surrounded by the positive ends of the solvent



dipoles. The solvent-radical complexes would fluctuate rapidly and only the time-averaged value would be observed. A solvent dependence should be observed in the spectra, since the solvent polarity should affect the average value of the instantaneous hyperfine constant and possibly the jump frequency.

A continuous rotation of the trifluoromethyl group would lead to the same qualitative conclusions as the three-jump mechanism. The three-jump mechanism is more convenient for computations and has been used in this article.

The three-jump model can be simplified if we assume

all nonsecular contributions are negligible, $(\omega_0\tau_0)^2 \gg 1$, and the only spectral densities of importance are those for which $\omega = 0$. In this model, $\tau_0 = 1/3k_1$, where k_1 is the rate constant for the jump, and $\omega_0/2\pi$ is the Larmor frequency. We have neglected anisotropic intramolecular dipolar interactions between the unpaired electron and the nuclear magnetic moments which may contribute to the line broadening.

The spectral densities can be written as

$$J_{11}(0) = J_{22}(0) = J_{33}(0) =$$

$$\gamma^2[1/3(a_1^2 + 2a_2^2) - \bar{a}^2]/3k_1 \quad (5)$$

$$J_{12}(0) = J_{13}(0) = J_{23}(0) = -(1/2)J_{11}(0) \quad (6)$$

The secular contribution of the modulation of the hyperfine splitting to the line width of the k th line is given by

$$[T_2^{(k)}]^{-1} = \sum_{ij} J_{ij}(0)m_i m_j \quad (7)$$

where m_i is the z component of the spin angular momentum of nucleus i . Substitution of the spectral densities, eq 5 and eq 6, into eq 7 shows that, under the above assumptions, there is no line-broadening contribution to the $M = \pm(3/2)$ lines while there is a contribution of $J_{11}(0)$ to the lines corresponding to $M = \pm(1/2)$.

The assumption of line-width alternation permits a reasonable set of coupling constants to be assigned to the spectra of 3-trifluoromethyl-4-nitrophenol obtained in the three solvents, Table I. If the spectra are recorded at the same low modulation, the $M = \pm 1/2$ lines are absent in DMF, noticeable in DMSO, and prominent in CH_3CN . The trend can be seen in Figure 1. The line-broadening effects are approximately in the same order as the polarity of the solvent, and this is interpreted as indication of a solvent interaction with the CF_3 group. The spectrum of 3-trifluoromethyl-4-nitrophenol in CH_3CN can be reconstructed, and excellent agreement is obtained, except for small frequency shifts due to secular terms which have not been included in the analysis. Under normal recording conditions, the sharpest lines are approximately 450 mgauss wide; however, low modulation and slow sweeps reduce the line widths to about 130 mgauss and a 0.38-gauss coupling constant can be extracted from the spectrum.

The spectrum of the 3-trifluoromethyl-4-nitrophenol anion radical in DMF and CH_3CN was recorded at several temperatures. In DMF, the intensity of the sharp lines decreased as the temperature was lowered, and the spectrum was unobservable at approximately -45° . No significant broadening of the sharp lines occurred. If electrolysis was discontinued at -45° and the solution immediately warmed, the spectrum reappeared. This is postulated to involve a temperature-dependent equilibrium of transient paramagnetic and diamagnetic species. The diamagnetic species

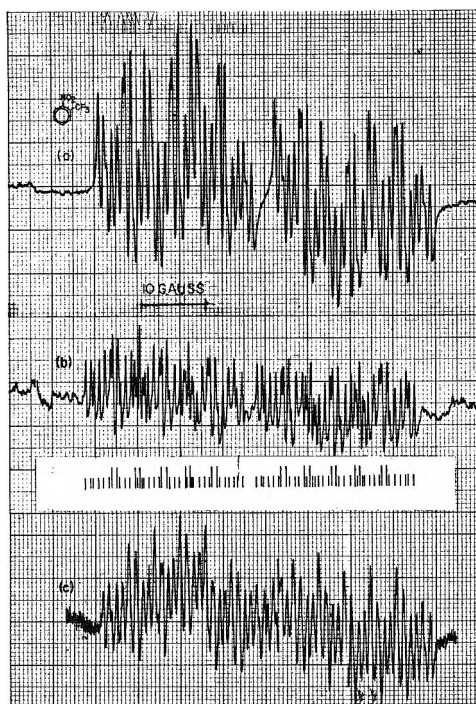


Figure 2. The esr spectra of the anion radical of 2-trifluoromethylnitrobenzene generated at -1.0 v in (a) DMF, (b) DMSO, and (c) CH₃CN.

might be a short-lived dimer dianion. When 3-trifluoromethyl-4-nitrophenol in CH₃CN was cooled, the prominent broad lines further broadened until they disappeared. The sharp lines decreased in intensity without broadening until, at -45° , the spectrum was not observed.

A small sample of DPPH was placed in the cavity along with the usual electrolysis vessel. The anion radical of 3-trifluoromethyl-4-nitrophenol was generated and the esr spectrum recorded as the temperature lowered. The intensity of the DPPH spectrum increased, as expected. Polarograms were run at room temperature and at -8° . There was a noticeable decrease in diffusion current, but not of sufficient magnitude to account for the disappearance of the spectrum. It was concluded that the disappearance of the spectrum upon lowering the temperature was consistent with the postulate of a shift in equilibrium between the anion radical and some diamagnetic species.

2-Trifluoromethylnitrobenzene. The esr spectra of the 2-trifluoromethylnitrobenzene anion radical generated at -1.0 v in the solvents DMSO, DMF, and acetonitrile are shown in Figure 2. If line-width alternation is assumed, the spectra can be fitted by a reasonable set of coupling constants, Table I. The line widths are approximately 280 mgauss. There are no indications of the broadened lines in any of these spectra.

The spectrum of the anion radical of 2-trifluoromethylnitrobenzene in DMF and CH₃CN was recorded at several temperatures. The intensity of the lines decreased as the temperature was lowered, and at -4°

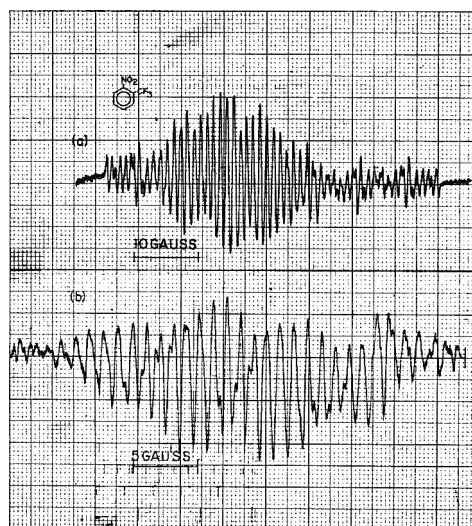


Figure 3. The esr spectrum of an anion radical of 2-trifluoromethylnitrobenzene generated at -1.0 v: (a) superimposed spectra at room temperature in DMF, and (b) spectrum of new species resolved at -20° .

the spectrum was not observed. The line widths did not increase significantly as the temperature was lowered, and the spectrum did not reappear upon warming the solution.

When the reduction potential was raised to -2.0 v, a second spectrum appeared superimposed upon the first, Figure 3. The two spectra could be resolved by lowering the temperature to -4° , where only the high-voltage spectrum was observed, although the end lines frequently were lost in the background. The spectrum is simple in appearance, but it is not interpretable in terms of the original ring substituents. The most reasonable set of hyperfine constants is obtained when coupling to the nitrogen nucleus is assumed to be negligible. This phenomenon has been observed in the high-voltage reduction of aromatic polynitro compounds.¹⁷⁻²⁰

It has been shown that the reduction of polynitro-mesitylenes and -durenes¹⁹ can yield amines and a variety of intermediates. These reductions involve proton transfer from an activated methyl group to a nitro group. The reductions were observed to occur between the first two polarographic waves, and the addition of a proton donor increased the formation of amine product.

2-Trifluoromethylnitrobenzene does not contain an activated methyl group, and protons must be abstracted from either the solvent or the ring itself. The solvent protons would be most susceptible to abstraction, but there is no precedent for such a mechanism in nitro-group reduction. The unknown paramagnetic species is not formed in the presence of a proton donor, and the spectrum is not that of 2-aminobenzotrifluoride. The amine is not the paramagnetic contributor; however,

the unknown species might be a paramagnetic intermediate in the reduction process.

The reduction of *o*- and *p*-dinitrobenzene in wet DMF yielded the corresponding nitrophenols.²⁰ The nitro group was assumed to be displaced by the attack of a hydroxyl ion, which was generated during the reduction of a nitro group in the presence of water. This mechanism does not appear applicable unless small quantities of water remain in the solvent after drying. The unknown paramagnetic species can be generated in wet solvent, but the spectrum does not correspond to that of an authentic sample of 2-trifluoromethylphenol. No paramagnetic species was obtained upon reduction of trifluorotoluene.

The behavior of the 2-trifluoromethylnitrobenzene system during reduction differs from that observed in systems where amine formation occurs. The paramagnetic species is formed only above the second polarographic wave. The spectrum of the anion radical is also observed above the second polarographic wave. This can be interpreted in terms of a dianion, which either transfers an electron to the neutral species or decomposes with possible loss of a nitro group. Dimer formation with subsequent decomposition to the anion radical and the unknown paramagnetic species is an additional possibility. Reactions involving the trifluoromethyl group also have been considered, but we have no evidence that such reactions occur.

A study of the ultraviolet-visible spectrum as a function of reduction potential and time should yield information concerning the reduction process. The electrolysis of 3-trifluoromethyl-4-nitrophenol cannot be monitored in the visible portion of the spectrum due to the intense band obtained upon formation of the phenoxyl ion. The compound 2-trifluoromethylnitrobenzene does not present this problem, and the various spectra are shown in Figure 4.

When the electrolysis voltage is set at a value below -1.0 v with respect to saturated calomel, a small band appears at approximately $420\text{ m}\mu$ and does not increase in intensity after the first few minutes of electrolysis. This band remains indefinitely after electrolysis has terminated. It is assumed that this corresponds to the reduction of an impurity which is completed after a short period of electrolysis, or some phenomena associated with the increased surface area of the mercury electrode. This material was never observed in the electrolysis cell used in the esr studies.

When the electrolysis voltage is raised above -1.0 v, a band immediately appears at approximately $474\text{ m}\mu$. When electrolysis is continued at this voltage, an additional band at $445\text{ m}\mu$ begins to grow and soon becomes more prominent than the one at $475\text{ m}\mu$. Two intense bands appear in the ultraviolet, and the one at $325\text{ m}\mu$ remains after electrolysis has terminated. The $325\text{-m}\mu$ band is assumed to represent product formation. If the electrolysis voltage is suddenly raised, the band

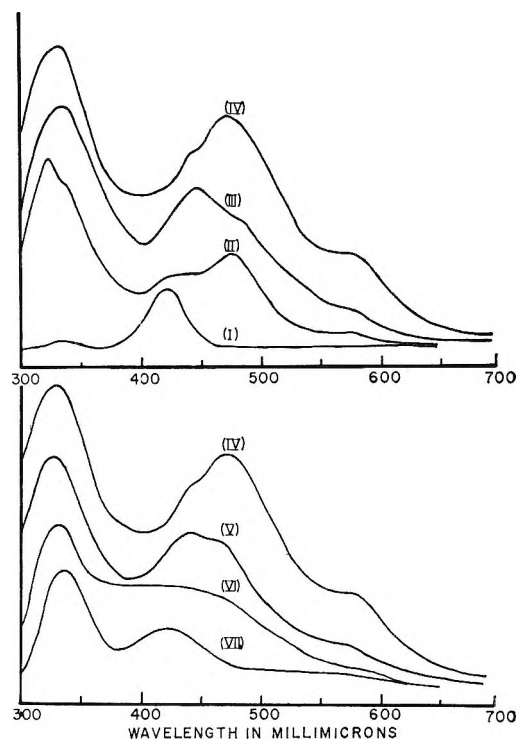


Figure 4. The ultraviolet-visible spectrum of 2-trifluoromethylnitrobenzene as a function of reduction potential and time: (I) potential below first polarographic wave, (II) voltage increased to first polarographic wave, -1.0 v, (III) generation at the first polarographic wave until steady-state concentration obtained, (IV) potential raised to -2.0 v, (V) 20 min after electrolysis terminated, (VI) 40 min after electrolysis terminated, and (VII) final stable species.

at $475\text{ m}\mu$ is increased in intensity relative to the $445\text{-m}\mu$ band; however, after a few minutes the band at $445\text{ m}\mu$ again becomes more prominent. If electrolysis is terminated, the band at $475\text{ m}\mu$ decreases more rapidly than that at $445\text{ m}\mu$, and after a short period they both disappear. The band at $325\text{ m}\mu$ appears to decrease in intensity; however, the decrease is due to diffusion of this species throughout the cell and the disappearance of a transient species whose absorption band overlaps the one at $325\text{ m}\mu$. The band at $475\text{ m}\mu$ is assumed to be the anion radical, and the band at $445\text{ m}\mu$ the diamagnetic intermediate. If electrolysis is maintained at constant voltage for a period of time, a steady-state concentration of each is obtained. Both of these species then disappear and a permanent product is formed.

A number of reaction schemes are possible. The formation of an unstable dianion dimer which then reacts or decomposes to form a neutral product represents a likely path; however, no definite evidence has been presented for this speculation.

At the highest voltage, a band also appears at $575\text{ m}\mu$, and this is assumed to be the second paramagnetic species generated above -2.0 v. This band also disappears after electrolysis has ceased. It is impossible to

obtain rates from these data because of concentration gradients, diffusion, and other variables.

The 2-trifluoromethylnitrobenzene and 3-trifluoromethyl-4-nitrophenol systems have proven to be interesting. The pronounced line-width alternation can be adequately explained by the theory of Fraenkel, and there is evidence for a significant contribution to the perturbation from a fluctuating radical-solvent interaction. Some general features of the high-voltage electrochemical reduction have been discussed, but the diamagnetic intermediates and products have

not been identified. Additional studies utilizing preparative electrochemical techniques are being made now. The fate of the nitro group during high-voltage reduction is of interest, and we hope that a detailed reaction scheme for the reduction can be developed.

Acknowledgment. We wish to express our appreciation to the Robert A. Welch Foundation and the Texas Christian University Research Foundation for their financial support. We wish to acknowledge NASA for a NASA Traineeship (J. W. R.) and Mr. A. E. Nobles for obtaining the ultraviolet and visible spectra.

Surface Potentials of Aqueous Electrolyte Solutions

by N. L. Jarvis and M. A. Scheiman

Surface Chemistry Branch, Chemistry Division, U. S. Naval Research Laboratory, Washington, D. C. 20390
(Received April 17, 1967)

The effect of added electrolytes on the surface potential of water was determined using the radioactive-electrode technique. Changes in surface potential, ΔV , were found to vary from 64 mv for Na_2SO_4 at 1.8 *m* to -180 mv for NaSCN at 7.5 *m*. The group Ia chlorides in water gave surface-potential differences that decreased in the order $\text{K}^+ = \text{NH}_4^+ > \text{Na}^+ > \text{Li}^+$, while the surface potentials of the group IIa cations decreased in the order $\text{Ba}^{2+} > \text{Sr}^{2+} > \text{Mg}^{2+}$. At a constant anion concentration of 2 *m*, the surface-potential differences due to the sodium salts were in the order $\text{SO}_4^{2-} > \text{CO}_3^{2-} > \text{CH}_3\text{COO}^- > \text{Cl}^- > \text{NO}_3^- > \text{Br}^- > \text{I}^- > \text{SCN}^-$. In general, the anion with the smaller hydration energy gave the greatest decrease in surface potential. The magnitude of each surface-potential change, however, does not appear to be a simple function of the hydration energy. The surface-potential changes must also involve the orientation and structure of the water molecules at the water-air interface, which may be only partially dependent upon the ionic properties as determined in bulk solution.

Introduction

Inorganic electrolytes are known to have a marked effect on the surface tension of water;^{1,2} less well known is their influence on the surface potential of water.³⁻⁵ The surface tensions of aqueous electrolyte solutions increase linearly with concentration, except perhaps at very low concentrations where Jones and Ray¹ reported an apparent surface tension minimum. On the basis of the Gibbs adsorption equation, Langmuir⁶ concluded that the increase in surface tension indicates a deficiency of solute in the surface layer, in the case of a KCl solution the layer of pure solvent being about 4 Å thick. Calculations by Harkins and co-workers^{7,8} substantiated this value and indicated that for chlorides of the group Ia cations the thickness of this pure solvent layer will decrease from 5 Å for 0.1 *M* solutions to

almost 3 Å for 2 *M* solutions. Several theoretical explanations of the negative surface excess have been proposed,^{9,10} but none will satisfactorily explain or pre-

- (1) G. Jones and W. A. Ray, *J. Am. Chem. Soc.*, **59**, 187 (1937); **63**, 288 (1941).
- (2) W. Drost-Hansen, *Ind. Eng. Chem.*, **57**, 18 (1965).
- (3) A. Frumkin, *Z. Physik. Chem.*, **109**, 34 (1924).
- (4) J. W. Williams and V. A. Vigfusson, *J. Phys. Chem.*, **35**, 345 (1931).
- (5) J. E. B. Randles, *Discussions Faraday Soc.*, **24**, 194 (1957).
- (6) I. Langmuir, *J. Am. Chem. Soc.*, **39**, 1848 (1917).
- (7) W. D. Harkins and H. M. McLaughlin, *ibid.*, **47**, 2083 (1925).
- (8) W. D. Harkins and E. C. Gilbert, *ibid.*, **48**, 604 (1926).
- (9) C. Wagner, *Physik. Z.*, **25**, 474 (1924).
- (10) L. Onsager and N. N. T. Samaras, *J. Chem. Phys.*, **2**, 528 (1934).

dict the surface tensions of all aqueous electrolyte solutions.

Surface-potential values for aqueous electrolyte solutions have been reported by Frumkin³ and Randles.⁵ Although their values differed in some instances, they did agree that the surface potentials of a series of anions become more negative in the order $F^- > Cl^- > Br^- > NO_3^- > I^- > ClO_4^- > SCN^- > PF_6^-$. Haydon¹¹ suggested that an acceptable general explanation for these results must consider the water structure, as influenced by the ions and the proximity of the interface, including contributions due to the oriented solvent dipoles and any electrokinetic potential established at the interface. Randles⁵ noted a correlation between the magnitudes of the surface-potential differences and the "real" hydration energies of certain cations and anions, but an attempted quantitative explanation was found in poor agreement with the experimental results. Several questions have also been raised^{4,12} regarding the surface-potential method used by Frumkin and Randles. The method they employed was essentially that of Kenrick,¹³ which measures the potential difference between two flowing liquid surfaces. Randles had the aqueous electrolyte solution flow down the inner surface of a glass tube while the reference liquid, 1 M NaCl, flowed from a fine glass tip, in the form of a jet, down the axis of the tube. In the present study, the surface potentials of a variety of inorganic electrolytes were measured by the ionizing-electrode method, similar to that proposed by Guyot.¹⁴

Experimental Section

The ionizing electrode used in this study consisted of a series of thin polonium 210 strips attached to the face of a 2 × 2 in. brass plate. The electrode was mounted approximately 1 cm above the substrate liquid. A calomel electrode with a saturated KCl salt bridge was used in the solution. The potential difference between the polonium electrode and the water surface was measured with a high impedance Keithley Model 610A electrometer. The sensitivity of the experimental apparatus was ± 1 mv. With the exception of NaI and NaSCN, the salts used in this investigation were all reagent grade chemicals. NaCl, NaNO₃, NaSO₄, KCl, KI, NH₄Cl, and MgCl₂ were from the Baker Chemical Co., while NaBr, Na(C₂H₃O₂), LiCl, MgSO₄, (NH₄)₂SO₄, BaCl₂, SrCl₂, Mg(NO₃)₂, and Ca(NO₃)₂ were from Fisher Scientific Co. The NaI was USP grade from Fisher, and NaSCN was CP grade from Baker Chemical. All solutions of these salts were prepared in triply distilled water, the final two distillations being from an all-quartz apparatus. The pH values of several of the ionic solutions were also determined as a function of concentration.

Significant amounts of surface-active organic contamination were observed in several of the salts. A number of procedures were used in an attempt to re-

move this contamination. Aqueous solutions of certain of the electrolytes were percolated through activated adsorbents such as Florisol or charcoal. NaI, NaBr, and LiCl were recrystallized several times prior to use, while other salts such as NaCl were heated to near their melting points to remove the trace organic matter. Each of these procedures was only partially successful. It was found that the remaining traces of surface-active contamination could be controlled by surface-chemical techniques. Concentrated solutions of the salts were prepared and then poured into glass dishes 1.8 cm deep and 16.0 cm in diameter, until the liquid level was well above the rim of the dish. The rim of the dish was lightly coated with wax to make it hydrophobic. A Teflon-covered magnetic stirring bar was used to assure uniform solution concentration. When contamination was present, the surface potential of the solution would change rapidly with time as the contaminating organic material adsorbed at the interface. Waxed glass barriers were used to sweep the adsorbed material to one side of the dish where it could be removed with an aspirator. The sweeping procedure was repeated until the initial surface-potential values were reproducible; it was then assumed that the interface immediately after sweeping was free of contamination. The change in surface potential with concentration was determined by successive dilutions of the saturated solution, finally extrapolating the surface potential to zero concentration. The potential between the electrode and water at zero concentration does not indicate the actual potential of a water surface, as the potential of the reference ionizing electrode was unknown. The reported surface potentials are the differences between the potential extrapolated to zero concentration and those measured at each given solution concentration. All surface-potential measurements were carried out in an enclosed Lucite glove box, at a temperature of $20 \pm 0.2^\circ$. All glassware was cleaned, prior to use, in hot nitric and sulfuric acid and then rinsed profusely with distilled water.

The surface tension of each salt solution was determined as a function of concentration. The measurements were made using a Cenco duNouy ring tensiometer, with a precision of approximately ± 0.1 dyne/cm. In these experiments, the surfaces of the salt solutions were again swept with the movable barrier to remove the adsorbed surface-active contaminants. The surface tension measurements were made at $25 \pm 1^\circ$.

Results

The surface potentials due to the electrolytes are

- (11) D. A. Haydon in "Recent Progress in Surface Science," Vol. 1, J. F. Danielli, K. G. A. Pankhurst, and A. C. Riddiford, Ed., Academic Press, New York, N. Y., 1964.
- (12) J. Koefoed, *Discussions Faraday Soc.*, **24**, 233 (1957).
- (13) F. B. Kenrick, *Z. Physik. Chem.*, **19**, 625 (1896).
- (14) J. Guyot, *Ann. Phys.*, **2**, 506 (1924).

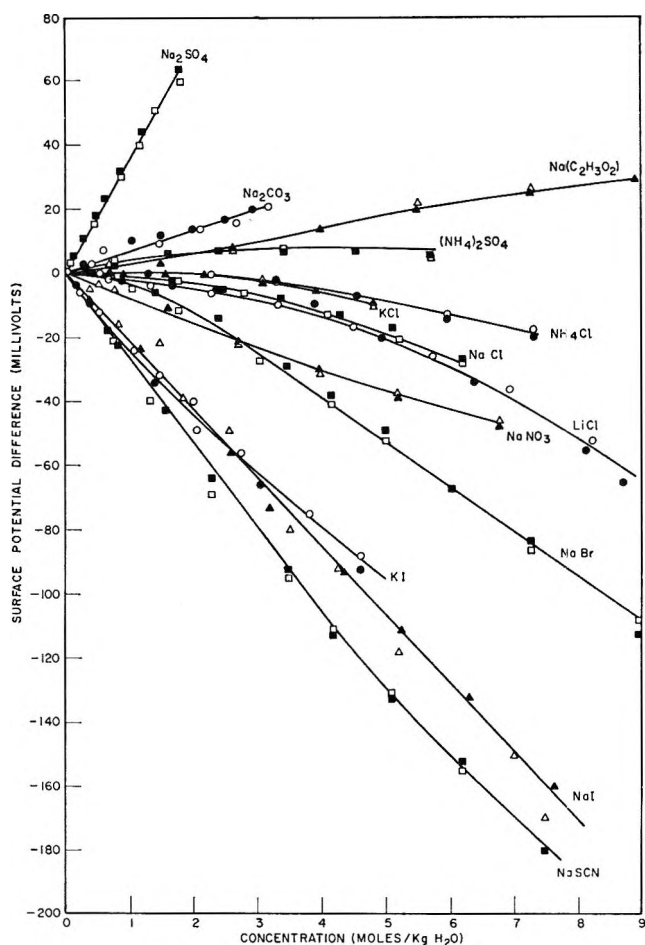
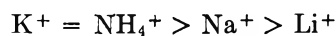
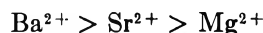


Figure 1a. Surface potential difference vs. solution concentration for aqueous solutions of inorganic electrolytes. Electrolytes with monovalent cations.

plotted in Figures 1a and 1b as a function of concentration (moles of salt/kg of water). In most cases, the concentration range extends approximately to saturation. Data for at least two, and in some cases three, independent runs are plotted. The results are in moderately good agreement with those of Frumkin,³ for concentrations of one and two mole equivalents of anion per kg of water. His surface-potential values at a concentration of 2 *m* were from 2 to 15 mv more negative than those given in Figure 1a. The present results for $(\text{NH}_4)_2\text{SO}_4$ and Na_2CO_3 are about 7 mv more positive than Frumkin's at equivalent concentrations. The largest difference was for Na_2SO_4 , for which Frumkin reported $\Delta V = +2.5$ mv at a concentration of one mole of anion, compared to +35 mv in Figure 1a. The surface potentials given in Figure 1a for KI agreed within 5 mv with similar measurements reported by Randles,⁶ up to a concentration of 3 *m*. The general agreement between the results of the present study and those of Frumkin and Randles indicates that the two experimental methods are indeed measuring the same surface phenomenon. The surface potentials of solutions of the group Ia chlorides were found to decrease in the order



The values for these chlorides are in good agreement with values reported by Randles,⁵ and show the same decrease with increasing energy of cation hydration.¹⁵ The same trend was observed for the chlorides of the group IIa cations in Figure 1b, where the cations having the greatest energy of hydration again gave the lowest potential. The surface potentials decreased in the order



The data indicate that the cations studied to date have a less pronounced effect on surface potential than the anions. Figure 2 shows the surface potentials of the chloride salts plotted as a function of the chloride concentration. At 3 *m*, the ΔV 's of all the chlorides fell within a range of 14 mv, while at 1 *m*, they were grouped within a span of only 4 mv, hardly more than the precision of the experimental technique. Only at concentrations above 4 or 5 *m* did the cations appear to have a marked effect upon surface potential.

The relative importance of the anions on surface potential is further reinforced by observing the differences in surface potential of a series of sodium salts. At a constant anion concentration of 2 *m*, their sur-

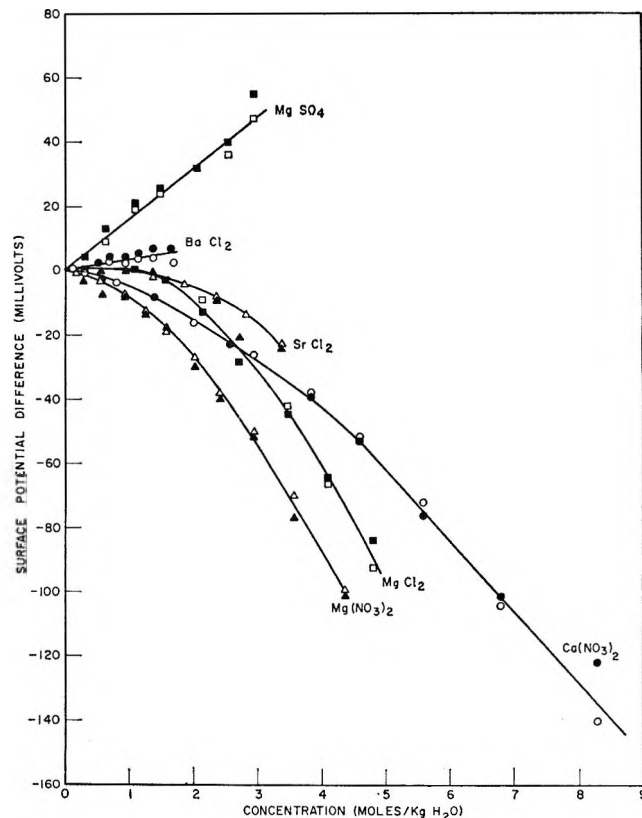


Figure 1b. Plots as described in Figure 1a for electrolytes with divalent cations.

(15) W. M. Latimer, K. S. Pitzer, and C. M. Slansky, *J. Chem. Phys.*, **7**, 108 (1939).

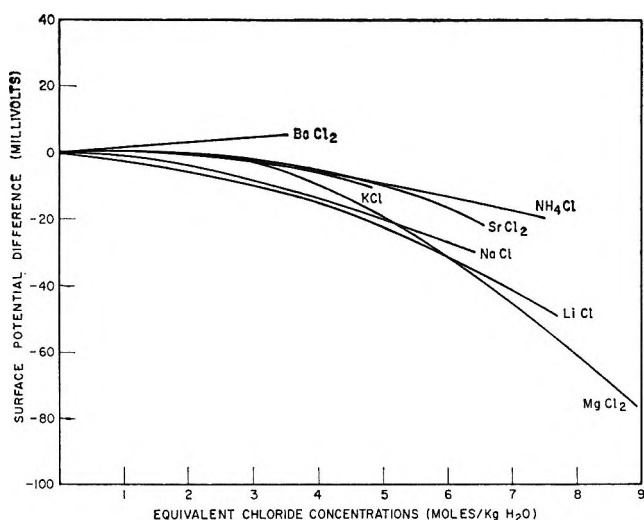
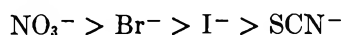
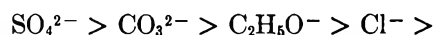
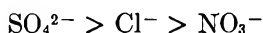


Figure 2. Surface potentials of various chloride salt solutions as a function of chloride concentration (mole-equivalents of Cl^- per kg of water).

face potentials cover a range of over 100 mv, decreasing in the order



In contrast with the cations, the anions with the smaller hydration energies apparently give the lowest surface potentials. The same general trend was observed for salts of Mg^{2+} , whose surface potentials also decreased in the order



From the results, it appears the effect of an ion upon surface potential is related in some manner to the structure of the water molecules in the ionic co-sphere, as influenced by ionic charge and ionic radius. Randles showed this to be true, for certain electrolytes at least, by plotting ΔV against the differences in "real" hydration energies of the ions. However, ionic properties such as hydration energy, ionic entropy, and the so-called structure-making or structure-breaking properties of ions are determined in bulk solution where the anions and cations are uniformly distributed and subjected to a more or less symmetrical force field. At the interface, the anions and cations may not be uniformly distributed, and it is obvious that the forces operating on a molecule will be unsymmetrical. Weyl,¹⁶ Good,¹⁷ and Fletcher¹⁸ have argued that the water molecules at the water-air interface have a preferential orientation, with the oxygen atoms outermost. A result of this orientation is the establishment of an electrical double layer at the surface, with the outermost portion of the double layer being negative and the innermost part being positive. With the positive portion of the double layer directed into the solution, one might expect a preferential accumulation of the anions near the interface.

Another difficulty in interpreting ΔV measurements is determining what part of the surface potential arises from the electrostatic forces associated with the ionic charge and what part may be due simply to a change in the orientation of the water dipoles in the vicinity of the ion. On the basis of the Helmholtz equation, even a small change in the average orientation of the surface water molecules could be sufficient to cause the observed changes in surface potential and could lead to an increase, as well as a decrease in ΔV . Surface tension *vs.* concentration curves are given in Figure 3 for each of the electrolytes. A comparison of surface tension data with the surface potentials shows little if any correlation between the two measurements. The poor correlation is not surprising, for even though both techniques are measuring properties of an interfacial phase, the properties are somewhat unrelated, one arising from the intermolecular forces of attraction and the other from the electrical properties of the surface molecules.

Conclusions

The presence of electrolytes in solution can greatly alter the surface potential of water. In many cases, it appears as though the anions primarily determine the sign of the potential and, to a great extent, its magnitude. This suggests that the anions may be preferentially associated with the water molecules near the surface, being attracted by the positive side of the double layer, which is directed toward solution. From this picture of a water surface, a negative change in surface potential seems to follow logically from the

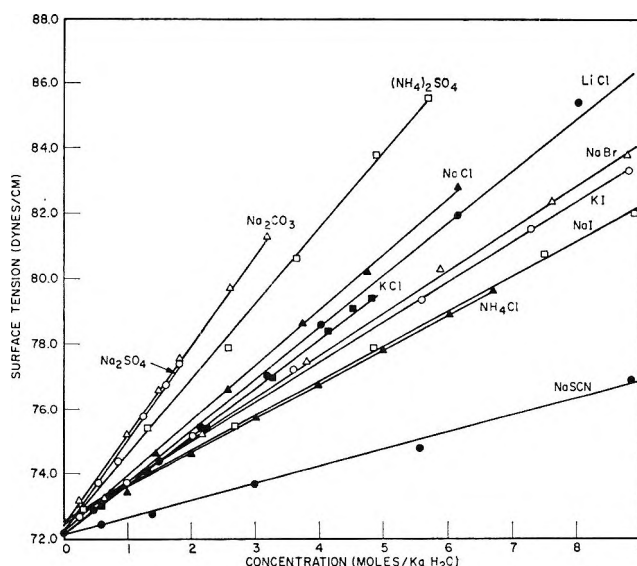


Figure 3a. Surface tension *vs.* concentration for aqueous electrolyte solutions. Electrolytes with monovalent cations.

(16) W. A. Weyl, *J. Colloid Sci.*, **6**, 389 (1951).

(17) R. J. Good, *J. Phys. Chem.*, **61**, 810 (1957).

(18) N. H. Fletcher, *Phil. Mag.*, **7**, 255 (1962).

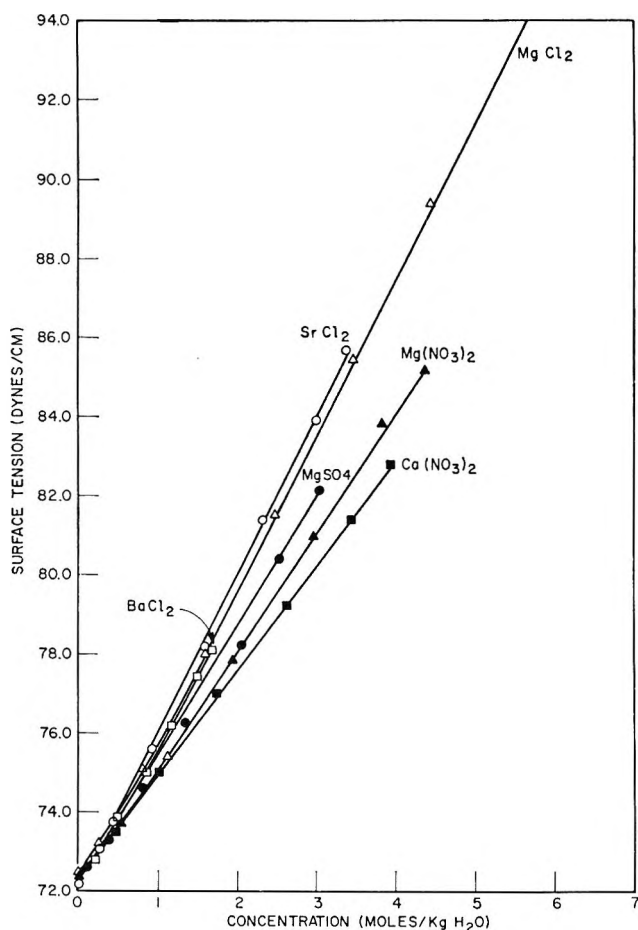


Figure 3b. Plots as described in Figure 3a for electrolytes with divalent cations.

addition of an electrolyte to the solution. It is difficult to explain the occurrence of a positive ΔV if one assumes that the potential changes arise solely from the electrostatic potential at the interface, for this would

mean that the cations are approaching closer to the interface, and thus closer to the positive side of the double layer, than are the anions. In addition to the electrostatic effect, it is possible the ions may influence ΔV by changing the orientation of the polar water molecules in the surface. A relatively small change in the average orientation of the surface water molecules should be sufficient to give ΔV changes of the magnitude shown in Figure 1. If it is true that in each case the anions are less strongly repelled from the surface than the cations, then it must be assumed that the anions SO_4^{2-} , CO_3^{2-} , and $\text{C}_2\text{H}_3\text{O}_2^-$ are reorienting the water in such a way as to overcome the negative electrostatic contribution to surface potential and give a resulting positive ΔV . It is interesting that those anions giving a positive potential change are all so-called "structure-making" anions, as opposed to Cl^- , NO_3^- , I^- , Br^- , and SCN^- which are classed as "structure-breaking." Thus the groups of anions giving rise to surface potentials of different signs are known to interact differently with the water structure. Several orientations for water molecules in the vicinity of an anion have been postulated;¹⁹⁻²¹ however, the problem of constructing a model that is in good agreement with experimental data seems extremely difficult. The theory proposed by Randles took into account only the electrostatic potentials of the ions and their adsorption, or repulsion, by the surface double layer. As he pointed out, the poor agreement between his theory and his experimental results showed that the molecular structure of the water in association with the ions cannot be ignored.

(19) E. J. W. Verwey, *Rec. Trav. Chim.*, **61**, 127 (1942).

(20) J. B. Hasled, D. M. Ritson, and C. H. Collie, *J. Chem. Phys.*, **16**, 1 (1948).

(21) F. Vaslow, *J. Phys. Chem.*, **67**, 2773 (1963).

The Kinetics of Dissociation of Hydrogen Fluoride

behind Incident Shock Waves

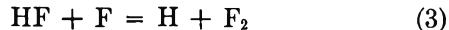
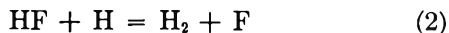
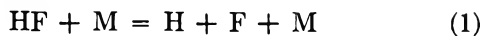
by Jay A. Blauer

Air Force Rocket Propulsion Laboratory, Research and Technology Division, Air Force Systems Command, Edwards, California 93523 (Received April 20, 1967)

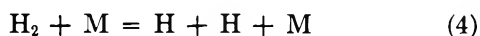
The rate of dissociation of HF behind incident shock waves has been studied in the temperature range of 3700–6100°K. The course of dissociation was followed by monitoring the emission intensity of the 1–0 band of HF centered at 2.5 μ . The experimental results gave values of $k_1 = (0.47 \times 10^{19})T^{-1} \exp(-134,100/RT)$ and $k_2 = 2 \times 10^{12} \exp(-35,000/RT)$ for the bimolecular rate constants of the reactions $\text{HF} + \text{M} = \text{H} + \text{F} + \text{M}$ and $\text{H} + \text{HF} = \text{H}_2 + \text{F}$, respectively. The rate of the fluorine exchange reaction $\text{HF} + \text{F} = \text{H} + \text{F}_2$ was found to be of no consequence to the present study, even though large amounts of F_2 were added to the gaseous mixtures used.

Introduction

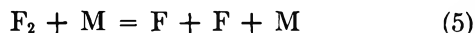
The dissociation of HF can proceed by at least three separate paths



The exchange reactions 2 and 3 will of course be followed by the reactions



and



Data concerning the rates of reactions 4 and 5 have appeared in published form in numerous papers^{1–5} and were not subjected to further investigation in the present study.

When this investigation was initiated, no published data were available concerning the dissociation rate of HF, although two other studies were under way in other laboratories.^{3,6} The results of Jacobs, *et al.*,³ have since appeared in published form. Jacobs proceeded by adding various amounts of H_2 to the gaseous mixtures under investigation, with the intent of obtaining definitive values for the rates of reactions 1, 2, and 4. In the study being reported herein, various amounts of F_2 were added to the gaseous mixtures in an attempt to study not only reactions 1 and 2, but also reaction 3. Jacobs has suggested⁷ that, based upon his results, the addition of large amounts of F_2 to the gaseous mixture should permit a study of reaction 3.

Although Levy and Copeland^{8,9} have reported investigations of the kinetics of the hydrogen-fluorine

system, their data have not yet been reduced to actual rate constants for any of the reactions listed above.

The choice of an infrared-emission technique for following the course of the dissociation was made possible by the results of Malkmus¹⁰ concerning the infrared emissivity of HF at temperatures between 1800 and 7000°K, and optical densities between 10^{-2} and 10 atm cm. Calculations based upon these results show that if the experimental conditions are held within the boundaries for temperature and optical density of 3500–7000°K and 0.01–0.5 atm cm, respectively, the emission intensity of the gas will be directly proportional to the partial pressure of HF in the reacting mixture. Furthermore, this proportionality is found to be independent of temperature in the range cited. The maximum error incurred in the assumption of this proportionality within the prescribed range of experimental conditions is 15%.

Experimental Section

The shock tube designed by Avco is of stainless steel and has an inside diameter of 1.5 in. The over-all length of the test section is 25 ft, and the entire inside

- (1) J. P. Rink, *J. Chem. Phys.*, **36**, 262 (1962).
- (2) G. Careri, *ibid.*, **21**, 749 (1953).
- (3) T. A. Jacobs, R. R. Geidt, and N. Cohen, *ibid.*, **43**, 3688 (1965).
- (4) D. Britton and C. D. Johnson, *J. Phys. Chem.*, **64**, 742 (1960).
- (5) R. L. Oglukian, Technical Report No. AFRPL-TR-65-152, Oct 1965.
- (6) J. F. Spinnler, "Quarterly Progress Report in Interior Ballistics," No. P-64-22, Defense Documentation Center No. AD355643, Rohm and Haas Co., Huntsville, Ala., Nov 1964.
- (7) Personal communication.
- (8) J. B. Levy and B. K. Copeland, *J. Phys. Chem.*, **67**, 2156 (1963).
- (9) J. B. Levy and B. K. Copeland, *ibid.*, **69**, 408 (1965).
- (10) W. Malkmus, General Dynamics-Convair Report, No. ZPh-119, 1961.

surface is finished to a grade-8 smoothness. The observation port is equipped with sapphire windows held in compression by close-tolerance brass collets. Window-shock tube sealing is effected with indium wire gaskets. The driver, having an over-all length of 66 in., was separated from the downwind section by means of scribed diaphragms of cold-rolled steel. The downwind section was in turn separated from a 55-gallon dump tank by means of a thin sheet of Mylar.¹¹

Shock detection was by means of ionization probes having a spatial resolution of 1 mm and placed at intervals of 30 in. along the entire length of the downwind section. Shock detectors were also placed 5.25 in. from the center, on each side of the observation port. The outputs of all the probes were fed to a Tektronix-535 oscilloscope, equipped with a raster sweep and Radionics Model TWM crystal-driven timing generator.

Infrared radiation was detected and its intensity measured by means of an indium antimonide detector¹² used in a photoconductive mode. Signal amplification consisted of two stages of capacitance-coupled cascade amplification with cathode followers for interstage coupling and as output stages.¹³ Spectral resolution was by means of a Perkin-Elmer prism monochromator.

Wire screens of known blocking efficiency for radiant energy were placed between the monochromator and a blackbody source of radiant energy to test the linearity of the response of the analytical system to radiant intensity. The linearity of response was found to be good within 5% over the entire range of radiant intensity considered in this study.

After amplification the detector output was fed to a Tektronix Model 535 dual-trace oscilloscope. The data were recorded on 3000-speed Polaroid film by means of a Fairchild Type F29.6 camera. Time markers and calibrated voltage markers were placed on the film by means of a Radionics Model TWM crystal-driven timing generator and an SRC (Systems Research Corp.) Model 3512B dc power supply, respectively.

Argon, hydrogen, and hydrogen fluoride, having stated purities of 99.998%, 99.998%, and 99.9%, respectively, were purchased from Matheson and used without further purification. Mass spectrometric analysis, using argon as an internal standard, indicated the presence of less than 0.01% O₂, 0.03% N₂, and trace amounts of SiF₄ as the only impurities in the HF used, and only trace amounts (*ca.* less than 0.01%) of H₂O and N₂ in the Ar and H₂ used. Gaseous F₂ with a minimum purity of 98.2% was purchased from Allied Chemical Corp. A mass analysis revealed the presence of 0.7% O₂ and 0.2% HF as the only significant impurities. After passage through a column of NaF pellets, the gas was used without further purification.

Mixtures of Ar, HF, H₂, and F₂ which contained 0–4% HF, 0–0.32% H₂, and 0–6% F₂ were prepared and stored in stainless steel tanks, which had been passivated

with gaseous F₂ at 20 psi for 1 week. Heise gauges, whose scales could be read to 0.1% of full scale, were used in all mixing operations. Immediately before using a gaseous mixture in a test, its HF and F₂ contents were determined by reading its optical densities at 2.5 and 0.285 μ , respectively, on a Beckman DK-2 spectrophotometer, equipped with a stainless steel absorption cell having sapphire windows. Calibration of the spectrophotometer was accomplished by determining the optical densities of freshly mixed samples of F₂, HF, and Ar. Beer's law described the results, provided the partial pressure of HF was kept below 100 torr in all operations.

Prior to each test it was found necessary to condition the walls of the shock tube and the absorption cell of the Beckman DK-2 to the presence of HF. This was accomplished by passing the test gas through the entire apparatus until the optical density at 2.5 μ was reproducible over a period of 10 min. Only by following this procedure could reproducible results be obtained. The apparatus was then reevacuated, and a fresh sample was admitted to the desired test pressure (*ca.* 10–40 torr). The gaseous pressure within the tube was measured by means of a Wallace and Tiernan, 0–100 torr, gauge. The test was then conducted using a helium driver.

Results and Discussion

On the assumption of transparent gas radiation, the concentration of HF in the reacting mix is related to signal output of the analytical system by means of the equation

$$(\text{HF}) = \frac{(\text{HF})_0}{V_0} (V) \quad (6)$$

where the subscript refers to the conditions immediately behind the shock wave. The value of (HF)₀ was found *via* a solution of the Rankine-Hugoniot equations. Due to the extreme instability of F₂ under the experimental conditions,^{4,5} it was assumed totally dissociated within the shock front itself. The value of V₀ was found by simple logarithmic extrapolation of the oscilloscope trace to the initial conditions; see Figure 1 and Figure 2. These initial trace heights are shown in comparison to the initial concentrations of HF in the reacting mix in Table I. The constancy of the ratio of V₀/(HF)₀ as tabulated in the last column of the table demonstrates the validity of our calculations based upon the results of Malkmus.¹⁰

Resort was made to the method of initial slopes for the evaluation of the rate constant of reaction 1. The results are illustrated in Figure 3 as a function of tem-

(11) Trade name.

(12) Purchased from Santa Barbara Research Center, Goleta, Calif.

(13) The analytical system was designed by William Netusil of Rocketdyne, Inc., Canoga Park, Calif., Contract AF 04(611)-8502.

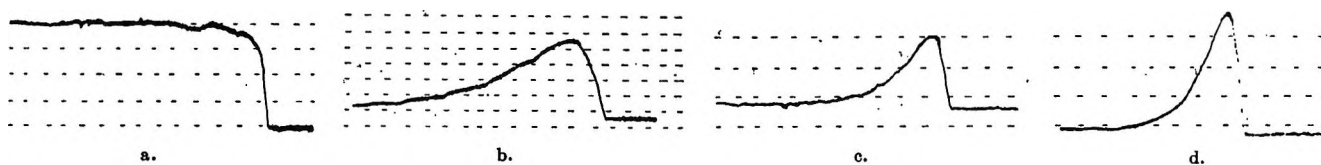


Figure 1. Reaction profile for: (a) shot no. 71; 2.06% HF, 0.375% H₂, 3231°K, 10-μsec time markers, and 0.2-v ordinate divisions; (b) shot no. 99: 2.23% HF, 1.48% F₂, 5367°K, 5-μsec time marks, and 0.1-v ordinate divisions; (c) shot no. 58: 2.35% HF, 1.80% F₂, 4871°K, 10-μsec time marks, 0.2-v ordinate divisions; (d) shot no. 60; 2.47% HF, 1.80% F₂, 5862°K, 10-μsec time marks, 0.1-v ordinate division.

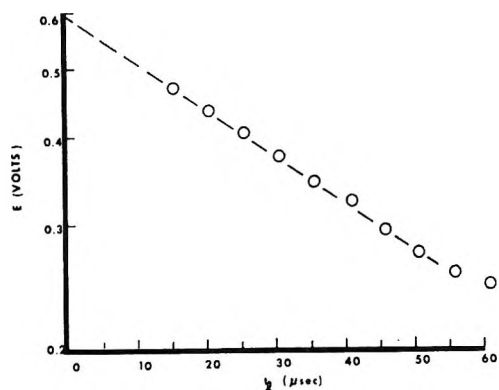


Figure 2. Logarithmic extrapolation illustrated for shot no. 52: 5.84% F₂, 3.02% HF, 5283°K.

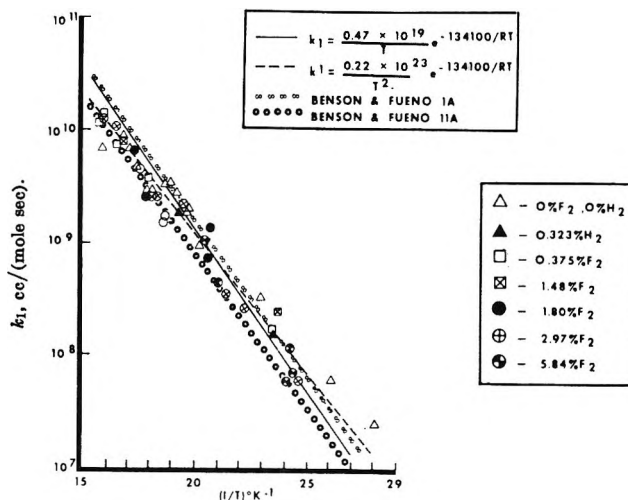


Figure 3. Temperature dependence of initial rates.

Table I: Internal Consistency of Initial Emission Intensities

Run no.	T, °K	(HF) ₀ × 10 ⁴ , mole/cc	V ₀ , v	V ₀ /(HF) ₀ × 10 ⁻⁶
First Set ^a				
49	4175	0.238	1.04	4.4
53	4264	0.285	1.54	5.4
50	4312	0.185	0.95	5.1
54	4426	0.426	2.23	5.2
51	4784	0.176	0.89	5.1
52	5283	0.112	0.59	5.3
47	5613	0.200	0.87	4.4
Second Set				
71	3231	0.086	0.82	9.5
69	3932	0.081	0.71	8.8
70	3961	0.102	0.92	9.0
72	4260	0.185	1.37	7.4
66	6105	0.098	0.68	7.0
67	6276	0.077	0.82	10.6
68	6365	0.077	0.76	9.9

^a Refers to individual settings for bias current and amplifier-plate voltage.

perature and are tabulated in Table II. The relationship

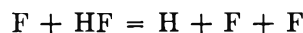
$$k_1 = \frac{0.47 \times 10^{19}}{T} e^{-134,100/RT} \quad (7)$$

gives the best simple fit to all of the experimental data, although the cascade model of Benson and Fueno¹⁴ does reproduce the data very well from a standpoint of

temperature dependence and absolute magnitude.¹⁵ The activation energy is assumed identical with the endothermicity of the reaction. The result given in eq 7 agrees favorably with the result obtained by Jacobs, *et al.*,³ *i.e.*

$$k_1 = \frac{1.1 \times 10^{19}}{T} e^{-134,100/RT} \quad (8)$$

The absence of any pronounced effect of large amounts of atomic fluorine upon the initial slope (see Figure 3) suggests that reaction 3 is either insignificant in comparison to reaction 1 over the entire ranges of temperature and concentration utilized or identical with the reaction



with the efficiency of F atoms as a third body being roughly equivalent to that of argon.

The over-all reduction of the rate data proceeded by matching observed and calculated reaction profiles. The computed profiles were obtained by means of a nonequilibrium computer program¹⁶ that involved an

(14) S. W. Benson and T. Fueno, *J. Chem. Phys.*, **36**, 1957 (1962).

(15) Our calculations utilize a collision diameter for the collision complex of HF which is just half that given by the procedures of ref 14. This is to account for the difference in relative efficiency of energy transfer for collisions occurring with the heavy F end and the light H end of the complex.

(16) Furnished by Dr. T. A. Jacobs of Aerospace Corporation, El Segundo, Calif.

Table II: Compositions and Shock Parameters for Individual Shots

Shot no.	%HF	%H ₂	%F ₂	P _i , ^a mm	U _s , ^b mm/μsec	T _i , °K ^c	T _e , °K ^d	(HF) ₀ × 10 ⁷ , moles/cc	k ₁ × 10 ⁻¹¹ , cc/mole sec
40	2.17	0.00	0.00	31.5	2.455	5563	5053	1.44	0.0282
41	2.12	0.00	0.00	31.5	2.410	5370	4872	1.43	0.000539
42	2.12	0.00	0.00	31.5	2.410	5379	4881	1.43	0.0337
43	2.12	0.00	0.00	31.5	2.363	5174	4676	1.43	0.0201
44	3.03	0.00	0.00	40.0	2.324	4970	4386	2.55	0.00953
45	2.95	0.00	0.00	40.0	2.019	3822	3613	2.43	0.000574
46	2.95	0.00	0.00	40.0	1.983	3696	3525	2.43	0.000233
47	2.95	0.00	0.00	32.0	2.477	5613	4917	2.00	0.0278
48	Velocity trace failed		
49	2.52	0.00	5.84	40.0	2.270	4138	4053	2.38	0.000539
50	2.45	0.00	5.84	32.0	2.272	4145	4046	1.85	0.00109
51	3.12	0.00	5.84	24.0	2.437	4784	4410	1.76	0.00430
52	3.02	0.00	5.84	15.8	2.469	4914	4414	1.17	0.0105
53	3.02	0.00	5.84	40.0	2.262	4110	4011	2.85	0.000666
54	3.75	0.00	0.00	54.1	2.191	4426	4039	4.26	0.00333
55	3.75	0.00	0.00	12.0	2.555	5905	4996	0.963	0.0679
56	2.02	5.00	0.00	40.0	2.278	4499	3794	1.74	0.0000
57	2.36	0.00	1.80	31.5	2.346	4824	4469	1.59	0.00694
58	2.35	0.00	1.80	18.9	2.358	4871	4473	0.949	0.0161
59	2.52	0.00	1.80	31.5	2.551	5672	5161	1.71	0.0244
60	2.47	0.00	1.80	18.9	2.595	5862	5350	1.01	0.0635
61	3.57	0.00	0.00	18.9	2.641	6314	5479	1.37	0.0693
62	1.34	0.00	0.922	18.9	2.589	6022	5739	0.570	0.0822
63	1.39	0.00	0.922	18.9	2.656	6320	6054	0.559	0.127
64	1.39	0.00	0.922	18.9	2.150	4218	4041	0.546	0.00305
65	1.92	0.00	0.375	18.9	2.474	5613	5146	0.766	0.0371
66	1.92	0.00	0.375	24.0	2.583	6102	5623	0.977	0.0741
67	1.92	0.00	0.375	18.9	2.624	6276	5808	0.770	0.140
68	1.92	0.00	0.375	18.9	2.646	6365	5909	0.771	0.116
69	2.07	0.00	0.375	18.9	2.050	3932	3711	0.807	0.0000
70	2.06	0.00	0.375	24.0	2.058	3961	3747	1.02	0.0000
71	2.06	0.00	0.375	18.9	1.849	3231	3203	0.790	0.0000
72	2.06	0.00	0.375	40.0	2.140	4260	3992	1.71	0.0000
73	0.984	0.00	0.00	40.0	2.161	4425	4166	0.808	0.00320
74	0.984	0.00	0.00	40.0	1.871	3379	3323	0.792	0.0000
75	0.984	0.00	0.00	40.0	1.775	3068	3043	0.784	0.000
76	1.03	0.00	0.00	32.0	2.250	4768	4528	0.681	0.00784
77	1.02	0.00	0.00	24.0	2.339	5150	4851	0.508	0.0213
78	1.02	0.00	0.00	18.9	2.359	5216	4966	0.400	0.0278
79	2.05	0.00	2.97	40.0	2.171	4089	3989	1.75	0.000614
80	2.05	0.00	2.97	24.0	2.330	4700	4385	1.06	0.00355
81	2.05	0.00	2.97	24.0	2.285	4522	4426	1.06	0.00256
82	2.05	0.00	2.97	16.0	Velocity trace failure	
83	2.05	0.00	2.97	24.0	2.042	3621	3603	1.04	0.0000
84	Defective oscillogram		
85	1.93	0.00	2.97	24.0	2.554	5635	5209	1.00	0.0266
86	1.95	0.00	2.97	24.0	2.526	5513	5089	1.01	0.0256
87	1.95	0.00	2.97	24.0	2.442	5155	4768	1.01	0.0229
88	1.95	0.00	2.97	12.0	2.663	6109	5669	0.510	0.104
89	0.852	0.00	0.00	24.0	2.382	5320	5096	0.452	0.0341
90	0.911	0.00	0.00	24.0	2.489	5784	5558	0.455	0.0469
91	1.96	0.323	0.00	24.0	2.553	5977	5432	0.992	0.0930
92	1.97	0.323	0.00	24.0	2.418	5390	4859	0.991	0.0333
93	1.97	0.323	0.00	24.0	1.716	2849	2816	0.940	0.0000
94	1.97	0.323	0.00	24.0	2.374	5206	4687	0.989	0.0185
95	1.97	0.323	0.00	24.0	2.592	6153	5602	0.998	0.0775
96	0.00	0.00	0.00	24.0	2.366	5300	5300	0.000	...
97	0.00	0.232	0.00	24.0	2.354	5124	4614	0.983	0.0183
98	1.97	0.323	0.00	24.0	2.138	4274	3931	0.976	0.00149
99	2.23	0.00	1.48	31.9	2.452	5367	4893	1.47	0.0166
100	2.16	0.00	1.48	31.9	2.463	5413	4938	1.46	0.0146
101	2.16	0.00	1.48	16.0	2.543	5756	5253	0.736	0.0466

^a Initial total pressure. ^b Shock velocity. ^c Temp of gas immediately behind shock wave. ^d Temp of gas at equilibrium.

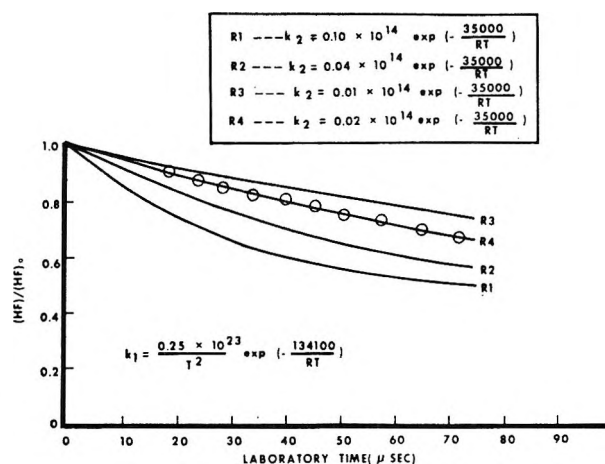


Figure 4. Illustration of the dependence of the reaction profile on the value of k_2 : 1.97% HF, 0.32% H_2 , 4274°K (initially), shot no. 98.

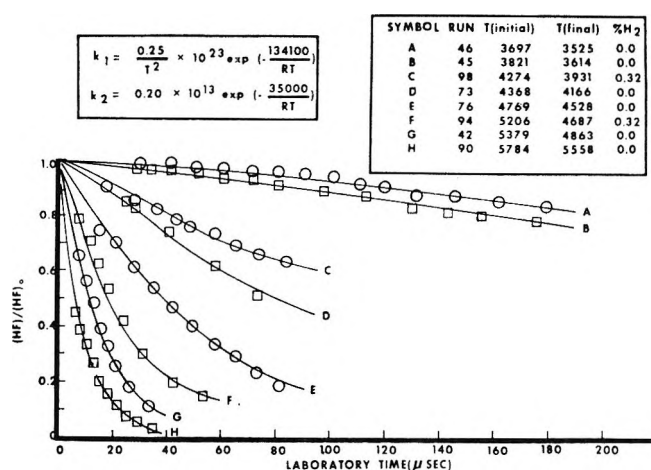


Figure 7. Comparison of computed and observed reaction profiles for mixes containing no added fluorine; k_2 has the best value.

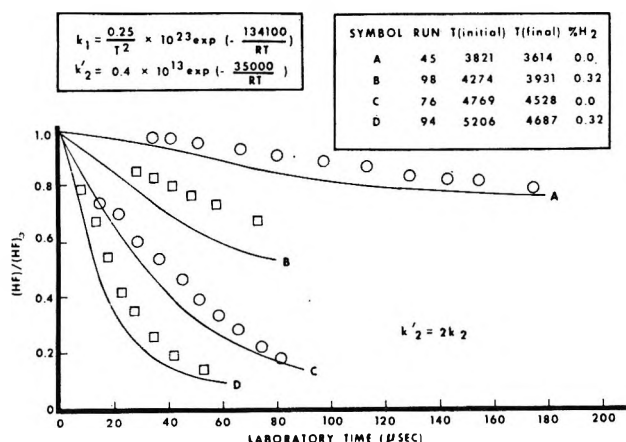


Figure 5. Comparison of computed and observed reaction profiles for mixes containing no added fluorine; k_2 is too large.

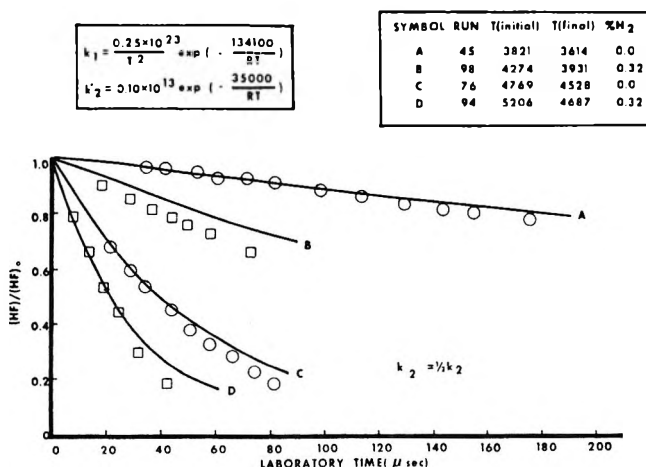


Figure 6. Comparison of computed and observed reaction profiles for mixes containing no added fluorine; k_2 is too small.

integration technique, which utilized both temperature and time as independent variables. The initial estimate of reaction 2 was taken from ref 3 as

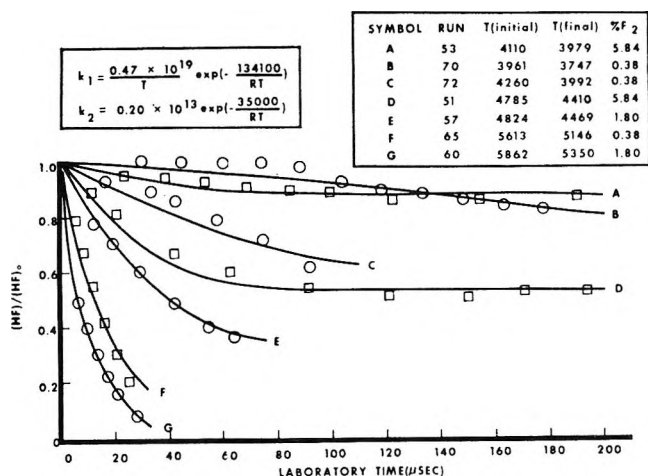


Figure 8. Comparison of computed and observed reaction profiles for mixes containing added fluorine.

$$k_2 = 1 \times 10^{13} e^{-35,000/RT} \quad (9)$$

Here, as before, the activation energy is approximated by the endothermicity of the reaction. The procedure was an iterative one involving variations in only one of the rate constants at a time.

Figure 4 illustrates the effect upon one reaction profile of shifting the value of k_2 while the value of k_1 is held fixed. The value of k_1 is shown in this figure as

$$k_1 = \frac{0.25 \times 10^{23}}{T^2} e^{-134,100/RT} \quad (10)$$

due to the fact that a T^{-2} temperature dependence seems to fit the data for mixtures not containing F_2 slightly better than a T^{-1} dependence, whereas the reverse is true for mixes containing F_2 . The difference between expressions 7 and 10 is not statistically significant. The best fit to the experimental data is given for

$$k_2 = 0.2 \times 10^{13} e^{-35,000/RT} \quad (11)$$

A comparison of the observed and computed reaction profiles for 15 separate tests are shown in Figures 5–8. The results confirm eq 11. The values given by eq 11 are one-fifth as large as the results of Jacobs, *et al.*,³ see eq 9. Although this difference is statistically significant (see Figure 4), there is no satisfactory means of making an *a priori* judgment between the two results.

Conclusions

In conclusion, the rate constants for reactions 1 and 2 have been evaluated in the temperature range of 3700 to 6100°K in F₂–HF–H₂–Ar mixes. The results are in reasonable agreement with the results of Jacobs, *et al.*³

The presence of large amounts of atomic F in the reacting mix has no pronounced effect upon the rate of

dissociation, other than for the simple mass action suppression of reactions 1 and 2. The third body efficiency of atomic F for recombination of H and F is not grossly different from that of Ar.

The cascade model of Benson and Fueno for calculating atomic recombination rates reproduces the absolute magnitude of these rates very well, although little can be said regarding the temperature dependence due to the degree of scatter in the data.

Acknowledgments. We wish to thank Dr. T. A. Jacobs and Dr. N. Cohen of Aerospace Corp of El Segundo, Calif. for assistance in the planning stage of this research and for providing the nonequilibrium computer program used in the computation of reaction profiles.

Rates of Reactions of Oxygen Atoms with Solid and Liquid

Sulfur (and Selenium)

by F. Cramarossa, E. Molinari, and B. Roio

Istituto di Chimica Generale e Inorganica dell'Università, Bari, Italy

Accepted and Transmitted by The Faraday Society (May 2, 1967)

The kinetics of the heterogeneous oxidation of solid and liquid sulfur by gaseous oxygen atoms has been studied in the temperature region 50–160°. Rates of selenium oxidation have been determined between 200 and 330°. Primary reaction products are SO and SeO which undergo further oxidation in the gas phase. The dependence of the rates on the concentration of oxygen atoms is different below and above the melting point, and the dependence on the temperature is complex. The chemical and the evaporation regimes of the reaction have both been observed. The kinetics is affected by the interplay of homogeneous and heterogeneous reactions.

The interaction of gaseous atoms with surfaces has been the subject of a number of investigations in recent times, mostly in connection with the catalytic behavior of surfaces toward atom recombination.

A variety of chemical reactions of atoms with solids is reported in the literature. Kinetic studies of these reactions are, however, limited to a few systems only: C + H,¹ C + O,^{2,3} Ge + H,⁴ and Mo, W + O.⁵ The common feature of these systems is that the reaction products are volatile at the temperatures of the experiments. Rate-limiting conditions imposed by diffusion of the reactants across the surface layer formed by the products are therefore absent.

In the present work the kinetics of the reaction of oxygen atoms with solid and liquid sulfur has been studied between 50 and 160°. Rate measurements of the oxidation of selenium, performed between 200 and 330°, will also be reported. However, the kinetics of

(1) A. B. King and H. Wise, *J. Phys. Chem.*, **67**, 1163 (1963).

(2) D. E. Rosner and H. D. Allendorf, *AIAA J.*, **3**, 1523 (1965).

(3) J. D. Blackwood and F. K. McTaggart, *Australian J. Chem.*, **12**, 114, 553 (1959).

(4) K. M. Sancier, S. R. Morrison, and H. U. D. Wiesendanger, *J. Catalysis*, **5**, 361 (1966).

(5) D. E. Rosner and H. D. Allendorf, *J. Chem. Phys.*, **40**, 3441 (1964); *J. Electrochem. Soc.*, **114**, 305 (1967).

the latter reaction was not studied in detail for reasons which will become apparent in the course of the discussion.

These reactions are exothermic and the reaction products are volatile. Three different reaction regimes are therefore to be expected: (1) the chemical or kinetic regime, (2) the external diffusion regime, and (3) the evaporation regime in which the oxidation reactions are "forced off" the surface.^{2,6}

Experimental Section

A scheme of the flask reactor which was used in most of the experiments is given in Figure 1. A tubular reactor of similar design ($R = 1.4$ cm; $L = 7$ cm) was used in some of the runs. The gas stream containing the oxygen atoms entered the reactor at point 1 and condensable products were trapped beyond point 2 in a liquid nitrogen trap. Rates of weight loss were determined by following the changes of the length of the thermostated quartz spring balance by means of a precision cathetometer. Two balances of sensitivities 25 and 66 mg/mm, respectively, for sulfur and for selenium, have been used after calibration. Oxygen atoms were produced by means of a microwave discharge in an argon-oxygen stream at a total pressure of 2 torr and an argon flow rate of $0.60 \text{ cm}^3/\text{sec}$.⁷ The concentration of the atoms could be varied by changing the $\text{O}_2:\text{Ar}$ ratio (0.05–0.3).

The absolute concentration of the atoms was mea-

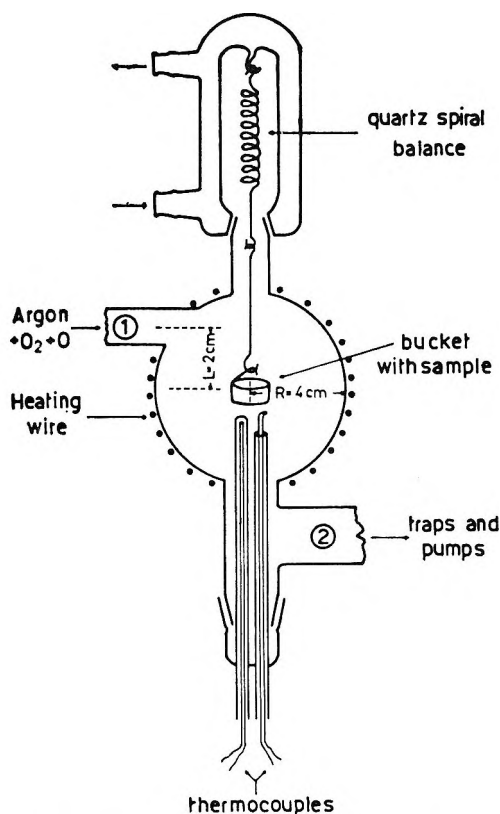


Figure 1. Schematic diagram of the flask reactor.

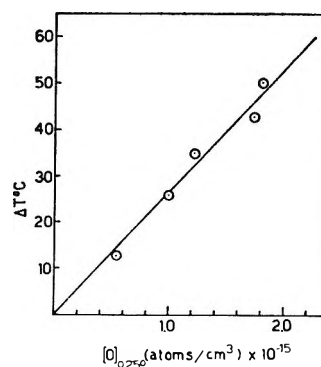


Figure 2. Temperature increase of the catalytic probe as a function of atom concentration.

sured at the position of the sample by chemical titration with NO_2 .⁸ The concentration of NO at the extinction point, where $[\text{NO}] = [\text{O}]$, was determined by mass spectrometric analysis.⁷ The temperature increase of a copper-constantan thermocouple with a catalytic silver tip placed at the position of the sample and of a similar reference thermocouple placed in a side arm at point 1 was linear with the concentration of oxygen atoms as measured by chemical titration (Figure 2).

Rates of reaction were determined by means of isothermal experiments and of experiments in which the temperature was increased linearly with the time. In both cases the temperature of the sample must be determined in the presence of oxygen atoms. In fact, when atoms are present, the temperature of the sample increases to a steady value which depends on the concentration of the atoms. Calibration runs were therefore performed at different concentrations of oxygen atoms; the temperature of a thin copper-constantan thermocouple immersed in the sample and protected by thin glass capillaries was determined as a function of the temperature of a reference thermocouple placed inside the reactor and protected by glass (Figure 1).

Rates of oxidation were successively measured under identical conditions, with the sample suspended to the spring balance. In the case of nonisothermal experiments, reproducible rates can be determined at any temperature from the curves which give the length of the balance, the sample temperature, and the reference temperature as a function of the time.

Pure sulfur and selenium have been used after outgassing *in situ* of the melts.

Results

The Reaction with Sulfur. Rates of weight loss of the sulfur sample, expressed as atoms/sec cm^2 of geometric surface, determined in the flask reactor

(6) D. E. Rosner, *AIChE J.*, **2**, 593 (1964).

(7) E. Molinari, F. Cramarossa, A. Pullo, and L. Triolo, *J. Catalysis*, **4**, 341 (1965).

(8) F. Kaufman, *Progr. Reaction Kinetics*, **1**, 1 (1961).

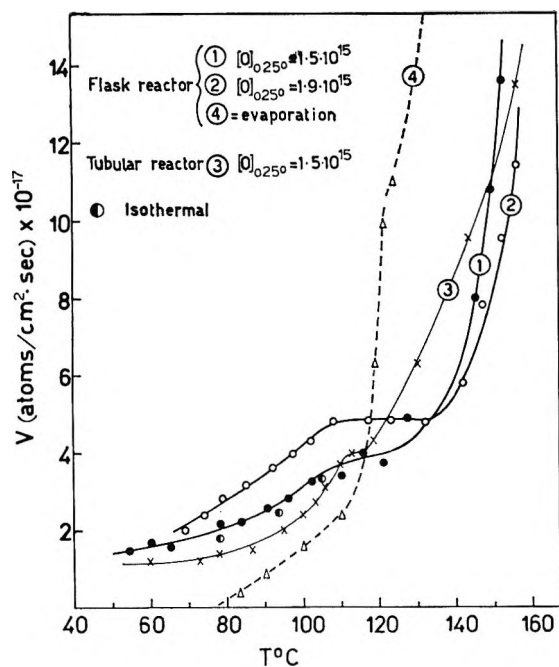


Figure 3. Rates of weight loss of sulfur as a function of the temperature.

have been plotted as a function of temperature in Figure 3 for two different samples at different concentrations of the oxygen atoms. Rate values obtained in the tubular reactor have also been plotted for comparison. It can be noticed that between 110 and 120° the rates remain constant. This behavior can reasonably be attributed to a decrease of the effective surface of solid sulfur when melting is approached. By assuming that the geometric and the effective surfaces of the liquid coincide, one can estimate the roughness factor of the solid by extrapolation of the low-temperature rates up to the melting point. Values of the roughness factor have been found to be between 1.10 and 1.25 for different samples. Rates of evaporation measured in an argon-oxygen stream are represented by the dotted line of Figure 3. Differences of the evaporation rates observed with pure argon are within the experimental errors. The results of Figure 3 have been obtained by the rising-temperature technique. Figure 4 shows the results of isothermal rate measurements. Rate values derived from the slopes of the straight lines have also been plotted in Figure 3. The agreement between isothermal and nonisothermal rates is within the experimental errors. The dependence of the rates on the concentration of oxygen atoms was determined on the same sample by the rising-temperature technique at different concentrations. Log V -log $[O]$ plots obtained at different temperatures are given in Figure 5. The slopes of these curves give a reaction order of 0.36 ± 0.03 , independent of temperature. Qualitative analysis of the products collected in the cold trap downstream from the sulfur sample showed the presence of SO_2

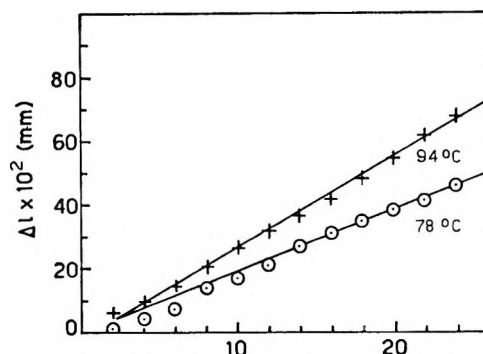


Figure 4. Decrease of the balance length as a function of time at constant temperature.

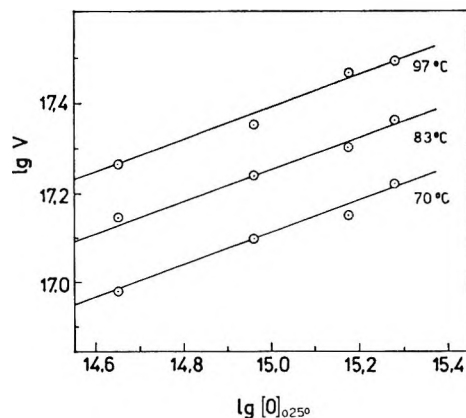


Figure 5. Rates of weight loss as a function of atom concentration for three different temperatures.

and SO_3 . The evolution of H_2S observed upon addition of water was attributed to SO (probably present as $(S_nO)_x$ in the condensed products) which reacts with formation of H_2S , H_2SO_3 , and S .⁹

Mass spectrometric analysis of the gas collected between the sample and the trap confirms the presence of SO . The relative abundance of these products changes with experimental conditions but no systematic quantitative analysis has been made.

The reaction is accompanied by a blue luminescence which, in the case of the reactor flask, extends upstream from the sample to the admission point of the gases. The extension of the luminescence downstream depends on the experimental conditions and ranges from a few centimeters to about 1 m, decreasing with increasing temperature of the sample. The intensity of the luminescence within the flask increases with increasing temperature. However, when temperatures in the neighborhood of 155–160° are reached, the luminescence is suddenly extinguished in the flask and is concentrated over a very short distance within the lateral tube near the admission point of the gas. The behavior observed in the tubular reactor is similar.

(9) "Gmelins Handbuch der anorganischen Chemie," 8th ed, Verlag Chemie, Weinheim, 1953, Part B1, p 177.

The following differences should, however, be mentioned. The extension of the luminescence downstream is again dependent on the experimental conditions but is completely extinguished when the sample temperature reaches about 105° . A rather sharply defined region of luminescence has been observed, extending upstream from the sample for a distance which increases with increasing temperature. At temperatures above about 130° this luminosity detaches itself from the sulfur surface leaving a dark zone behind, whose thickness increases with the temperature. The distances of the two luminous fronts from the sample surface are both functions of the linear velocity of the gas stream and of the concentration of the atoms.

The Reaction with Selenium. Rates of oxidation and of evaporation of selenium, determined by the rising-temperature technique, have been plotted in Figure 6. Rates of evaporation at 301° compare favorably with a previous determination by Brewer as given in ref 10. The oxidation reaction of selenium is accompanied by the emission of a blue-lilac luminescence. This luminescence behaves very much like the one observed for sulfur and extinction occurs in the flask reactor at temperatures in the neighborhood of 290° .

Discussion

The Reaction with Sulfur. From the data of Figure 3 it is possible to calculate the reaction probability ϵ expressed as the ratio between the observed rate and the number of oxygen atoms striking the unit surface in unit time, calculated according to the kinetic theory of gases. By equating ϵ to $\exp(-E/RT)$ the activation energy can be determined at each temperature. If this calculation is performed, one finds that at constant temperature ϵ decreases with increasing concentration of oxygen atoms, as expected from the observed reaction order (0.36). The activation energy decreases with increasing temperature, for a constant concentration of the atoms (from 3.3 to 2.3 kcal/mole between 50 and 150° and $[O]_{25^\circ} = 1.5 \times 10^{15}$ atoms/cm³). This result is a clear indication that the rate of reaction cannot be expressed as the number of oxygen atoms striking the unit surface in unit time with the necessary activation energy. In the following paragraphs an attempt will therefore be made to evaluate the factors which are likely to influence the observed kinetics.

Diffusional Effects. The observed values of ϵ range from about 5×10^{-3} to about 2×10^{-1} , pointing to a comparatively fast heterogeneous reaction. It is therefore necessary to ascertain whether diffusion of oxygen atoms to the surface might perturb the kinetics of the process. In order to evaluate the influence of diffusion, use has been made of the dimensionless analysis of the problem as developed by Wise, *et al.*¹¹

It will at first be assumed that the main sink for

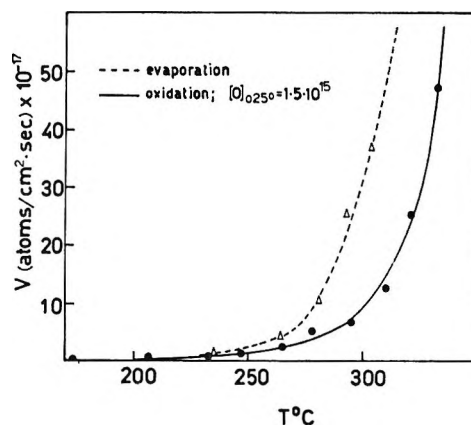


Figure 6. Rates of weight loss of selenium as a function of the temperature.

oxygen atoms is the heterogeneous reaction with sulfur. The following quantities must be evaluated under the experimental conditions prevailing in the flask and in the tubular reactor: $L_1/F' = L/\delta'R$ and $F'V = Rv/D$, where L is the distance between the inlet point of the gas and the sample surface, R the reactor radius, v the linear velocity of the gas, D the interdiffusion coefficient of oxygen atoms in the gaseous mixture (≈ 135 cm²/sec at 2 torr and 25°); $\delta' = 4D/\epsilon'\bar{c}R$, with \bar{c} the mean atom velocity, and $\epsilon' = \epsilon a/a_0$, where a ($= 1$ cm²) and a_0 are the cross-sectional areas of the sample and of the reactor, respectively.¹² From the calculated values of L_1/F' and $F'V$ the ratio $u = [O]_s/[O]_0$ of the concentration of the atoms at the sample surface $[O]_s$ to the concentration at the gas inlet $[O]_0$ can be evaluated by means of the graphs of ref 11. In Table I, values of u at three different temperatures have been reported for the two types of reactor and for $[O]_{0,25^\circ} = 1.5 \times 10^{15}$ atoms/cm³. One appreciates that in the case of the flask reactor the values of u below the melting point (119°) are close to 1. This means that the corrections for diffusion are well within the experimental errors. It is therefore justified to conclude that the reaction with the solid takes place in the chemical regime and that the measured order of reaction and the activation energies should be those of the chemical process. The situation is different at temperatures above the melting point, but, as will be discussed later, other perturbing factors will come into play in this temperature region. In the tubular reactor the situation is intermediate between the chemical and the diffusional regime. The rates should therefore be lower in the tubular reactor as actually observed below 110° (Figure 3). If one

(10) C. F. Powell in "Vapor Deposition," C. F. Powell, J. H. Oxley, and J. M. Blocher, Ed., John Wiley and Sons, Inc., New York, N. Y., 1966, p 224.

(11) H. Wise and C. M. Ablow, *J. Chem. Phys.*, **35**, 10 (1961); H. Wise, C. M. Ablow, and D. J. Schott, *ibid.*, **39**, 2063 (1963).

(12) C. M. Ablow, A. Motz, and H. Wise, *ibid.*, **43**, 10 (1965).

remembers that the order of the reaction is 0.36, the ratio of the velocities observed in the two reactors is in fair agreement with the ratio which can be calculated from the data of Table I.

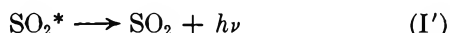
Table I: Values of $[O]_s/[O]_0$ at Different Temperatures

	Temp., °C		
	50	100	150
Flask reactor	0.96	0.94	0.71
Tubular reactor	0.83	0.68	0.33

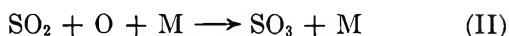
The Removal of Oxygen Atoms in the Gas Phase. While diffusion effects appear to be unimportant in the flask reactor below the melting point, another factor should be considered which might affect both the reaction order and the activation energy of the heterogeneous process. As previously mentioned, the heterogeneous oxidation is accompanied by a luminescence which extends both upstream and downstream from the sample for a length which depends on the experimental conditions. This luminescence has recently been investigated by Rolfes, Reeves, and Harteck,¹³ by Clyne, Halstead, and Thrush,¹⁴ and by Halstead and Thrush.¹⁵ It corresponds to the so-called SO_2 afterglow which has its origin in the reaction



followed by



The rate of reaction I at 25° has been measured by Halstead and Thrush¹⁵ under conditions very similar to those prevailing in the present experiments. Reactions I and I' are followed by the reaction



the rate of which has also been measured by Halstead and Thrush.¹⁵ Reactions I and II represent additional sinks for oxygen atoms which might affect their concentration at the sample surface.

The diffusion coefficient of SO in the gas mixture can be evaluated from the kinetic theory of gases (≈ 53 cm²/sec at 25°). The length of back-diffusion against the gas stream, corresponding to a reduction of the concentration to 0.01 of its value at the sample surface, can be calculated according to the expression

$$c_z/c_0 = \exp(-vx/D) = 10^{-2} \quad (1)$$

where v is the linear velocity of the gas. This calculation shows that back-diffusion of SO can easily extend up to the point of gas inlet, in the absence of reaction with oxygen atoms. It is therefore necessary to evaluate the decrease of the concentration of the atoms which takes place between the point of gas inlet and

the sample surface as a result of the combined action of reactions I and II.

A simplified treatment of this problem is reported in the Appendix. According to this treatment the observed rate V_{obsd} is given by

$$V_{\text{obsd}} = k[O]_s^m = k[O]_0^m \times [1 - k_1[Ar]ABV_{\text{obsd}}\tau]^m \quad (2)$$

where m is the *true* reaction order of the heterogeneous process, k_1 the rate constant of reaction I, τ the residence time. (For other symbols see the Appendix.) Equation 2 shows that, depending on the value of m and on the magnitude of the other quantities which are temperature dependent, both the *observed* reaction order and the activation energy might differ from those corresponding to the heterogeneous reaction. Under the present experimental conditions one finds that the true reaction order m coincides, within the errors, with the observed order (0.36 ± 0.03). The ratio $[O]_s/[O]_0$ is 0.85 at 50°, and its variation with the temperature is such as to maintain the value of $[O]_s$ approximately constant in the temperature range of interest. This value will be used in subsequent calculations.

When evaporation of molecular sulfur becomes appreciable, an additional series of homogeneous reactions should be considered which can initiate immediately above the surface: $S_{\text{vap}} + O \rightarrow SO$, followed by reactions I and II. (S_{vap} will mainly be S_8 in the temperature region investigated. The schematic reaction $S_{\text{vap}} + O \rightarrow SO$ includes any reaction step of the kind: $S_n + O \rightarrow SO + S_{n-1}$, with $n = 1-8$). These reactions will determine a further decrease of the concentration of the oxygen atoms at the surface.

The presence of this additional series of homogeneous reactions allows one to interpret the extinction of the luminescence observed in the flask reactor and the progressive detachment of the luminous front from the sulfur surface in the tubular reactor. In fact, if the reaction $S_{\text{vap}} + O \rightarrow SO$ is faster than the successive reactions, extinction of the luminescence occurs whenever the concentration of S_{vap} is such as to remove the oxygen atoms completely from the gas phase. The situation would in fact be similar to that encountered in the chemical titration of oxygen atoms with NO_2 .⁸ A dark region is therefore to be expected extending from the surface up to the point where oxygen atoms are completely removed by S_{vap} . A qualitative explanation of the different behavior observed in the two reactors can be found if one remembers that linear gas velocities are higher in the tubular reactor by a factor of about 8.

(13) T. R. Rolfes, R. R. Reeves, and P. Harteck, *J. Phys. Chem.*, **69**, 849 (1965).

(14) M. A. A. Clyne, C. J. Halstead, and B. A. Thrush, *Proc. Roy. Soc. (London)*, **A295**, 355 (1966).

(15) C. J. Halstead and B. A. Thrush, *ibid.*, **A295**, 363 (1966).

The Heterogeneous Oxidation. One important observation, which can be considered as the clue to the oxidation mechanism, is that above about 120° the rates of weight loss in the presence of atoms are significantly lower than the rates of free evaporation (Figure 3). This observation is strongly suggestive of a surface highly covered by chemisorbed oxygen atoms which block the evaporation of sulfur molecules. Evaporation thus becomes possible only from that fraction of the surface which is free from adsorbed oxygen. In the stationary state of the oxidation reaction the rate of oxygen atom chemisorption on the fraction of free surface ($1 - \sigma$) can be equated to the rate of oxygen desorption (in the form of SO) from the covered fraction σ of the surface

$$k_a Z [O]_s (1 - \sigma) = k_d \sigma \quad (3)$$

where $k_a = k_{0a} \exp(-E_a/RT)$, $k_d = k_{0d} \exp(-E_d/RT)$, and $Z = \bar{c}/4$, with \bar{c} the mean atom velocity. This is essentially the mechanism originally proposed by Langmuir for the high-temperature oxidation of tungsten and successively applied to other cases of chemical evaporation in the presence of volatile reaction products.¹⁶

From eq 3 one derives

$$1 - \sigma = \frac{k_d}{k_d + Z k_a [O]_s} \quad (4)$$

and the expression for the rate of oxidation

$$V_{ox} = Z [O]_s k_a \frac{k_d}{k_d + Z k_a [O]_s} \quad (5)$$

The over-all rate of weight loss V_{obsd} is given by

$$V_{obsd} = V_{ox} + V_{ev} \quad (6)$$

where $V_{ox} = k_a Z [O]_s (1 - \sigma)$ and $V_{ev} = K_{ev}(1 - \sigma)$, with K_{ev} the rate of evaporation of sulfur in the absence of oxygen atoms. The kinetic treatment will first be developed on the assumption that the sticking probability of oxygen atoms on the fraction of free surface is unity; i.e., $k_a = 1$.

Below 100° the rate of evaporation can be neglected, the observed rates coincide with V_{ox} , and the experimental data can be inserted in eq 5 together with the calculated values of Z and $[O]_s$. Values of k_d can thus be calculated at different temperatures and different concentrations of oxygen atoms. It is found that in the temperature region under consideration $k_d \ll Z(O)_s$. From this it follows (eq 5) that k_d will show a dependence on $[O]_s$ of the form

$$k_d = k_d' [O]_s^{0.36} \quad (7)$$

A plot of $\log k_d'$ vs. $1/T$ gives a straight line from which an apparent activation energy E_d of 5.0 kcal/mole can be calculated. If one admits that eq 7, written in the form $k_d = k_{0d}' \exp(-E_d/RT) [O]_s^{0.36}$, is valid up to

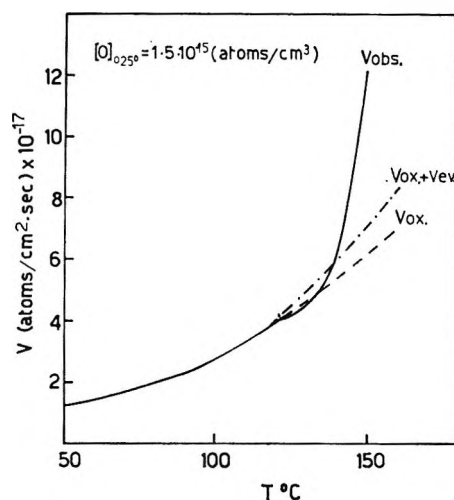


Figure 7. Observed and calculated rates for sulfur.

160°, values of $(1 - \sigma)$ can be determined as a function of temperature by means of eq 4. Values of $(1 - \sigma)$ derived according to the above treatment range between 0.8×10^{-2} and 3×10^{-2} .

The over-all rate of weight loss can thus be calculated up to 160° by means of eq 6. In Figure 7, observed and calculated rates have been compared for $[O]_{0.25^\circ} = 1.5 \times 10^{15}$ atoms/cm³. The low-temperature data have been corrected for the roughness factor. The agreement cannot be considered satisfactory in that calculated rates are higher than the observed one between 120 and 130° and definitely lower above 130°.

The above calculation has, however, neglected the consumption of oxygen atoms caused by the reaction $S_{vap} + O = SO$ which has been discussed in a preceding paragraph. In fact, when evaporation becomes appreciable, one observes the so-called "evaporation regime" superposed to the "kinetic regime" of the heterogeneous process.

In order to evaluate the influence of a decrease of the concentration of oxygen atoms on the over-all rates, the curves of Figure 8 have been calculated. This can be done by means of eq 6 and of the values of $(1 - \sigma)$ which can be determined as a function of $[O]_s$, as previously discussed. The dotted lines of this figure, which connect the rates observed with $[O]_{0.25^\circ} = 1.5 \times 10^{15}$ and $[O]_{0.25^\circ} = 1.9 \times 10^{15}$ atoms/cm³, show that the values of $[O]_s$ regularly decrease with increasing temperature as expected. It should be pointed out that diffusional effects, which become important above 119°, also contribute to the decrease of $[O]_s$. The rather puzzling observation of the negative dependence of the rates on $[O]_0$ above the melting point (Figure 3, curves 1 and 2) finds its interpretation in the two dotted curves of Figure 8. The ignorance of the rate con-

(16) J. F. Dettonre, T. G. Knorr, and E. H. Hall in "Vapor Deposition," C. F. Powell, J. H. Oxley, and J. M. Blocher, Ed., John Wiley and Sons, Inc., New York, N. Y., 1966, p 88.

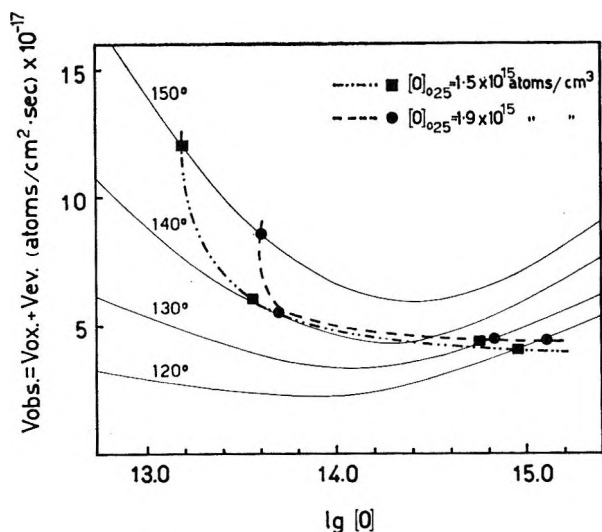
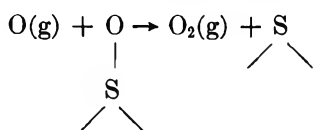


Figure 8. Over-all rates as a function of atom concentration for different temperatures.

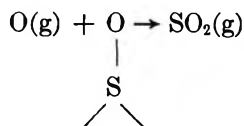
stants for the reaction $S_{\text{vap}} + O \rightarrow SO$ and the complexity of the system do not allow an *a priori* calculation of $[O]_s$.

A qualitative understanding of the complex behavior observed above the melting point is thus possible on the basis of the model discussed and with the additional condition that the sticking probability of the oxygen atoms is unity ($k_a = 1$). The condition $k_a \ll 1$ should be ruled out in that it leads to calculated rates above the melting point much higher than the observed ones.

The Heterogeneous Recombination of Oxygen Atoms. The surface of sulfur can act as a catalyst for the recombination of oxygen atoms. Rates of recombination much higher than the rates of oxidation would perturb the observed kinetics in that rapid removal of the atoms at the surface would shift the reaction into a diffusion-controlled regime. Recombination coefficients on sulfur would, however, be difficult to measure in that the oxidation reaction is fast. An indirect indication that the rates of recombination on the sulfur surface should be lower than the rates of oxidation might come, however, from the observation that the recombination reaction is likely to proceed according to⁸



and the rate of this reaction should be comparable with or lower than the rate of the reaction



The latter reaction represents a mechanism of desorp-

tion alternative to the unimolecular process discussed in the preceding paragraph ($v_d = k_d \sigma$). It can, however, be shown that this mechanism would lead to a first-order dependence of the rates on $[O]_s$ and should therefore play a negligible role between 50 and 100°.

The Reaction with Selenium. The data of Figure 6 show that significant values for the rates can be determined only above about 250°, and one again finds that the rates of evaporation are definitely higher than the rates of oxidation. The reaction with selenium can thus be studied only in a temperature range where the regime of the reaction is composite and where a detailed kinetic study would be of little significance. It should be noted that the rates of reaction with selenium are comparable with the rates observed with sulfur around the respective melting points (119 and 219°). The behavior of the luminescence observed during the oxidation of selenium suggests that the primary product of the heterogeneous process is a lower oxide of selenium, very likely SeO , previously identified in discharge tubes.

Conclusion

As a conclusion to the kinetic analysis carried on in the preceding pages, a comment on the observed dependence of k_d on $[O]_s$ (eq 7) is appropriate. This dependence is suggestive of a decrease of the heat of adsorption with increasing surface coverage. In fact, σ is an increasing function of $[O]_s$. The rate constant k_d could therefore be written in the form $k_d = k_{od} \exp[-(E_d - E([O]_s))/RT]$ with $\exp(E([O]_s)/RT) = k_{od}'/k_{od}[O]_s^{0.36}$. A different approach to the problem would be to consider that desorption of SO takes place by a mechanism of *induced desorption*.¹⁷ This mechanism is based on the observation that the energy liberated during adsorption might not be accommodated by the solid at a sufficient rate. Incomplete accommodation by the solid of the energy released at the surface by heterogeneous processes has been experimentally demonstrated in the case where the interacting species are atoms^{18,19} and has recently been invoked to interpret the observed influence of atomic species on the kinetics of catalytic reactions.⁷ Theoretical aspects of these effects have recently been examined by Majuga and Sokolov.²⁰

One consequence of this mechanism is that the rate of desorption cannot be treated as independent of the rate of adsorption in that the former becomes a function of the rate of energy release during adsorption.^{17b} Effects of this type should become particularly impor-

(17)(a) E. Molinari, *Z. Physik. Chem. (Frankfurt)* **6**, 1 (1956); (b) E. Molinari, *Gazz. Chim. Ital.*, **86**, 551 (1956).

(18) P. Hartek, R. R. Reeves, and G. Mannella, *Can. J. Chem.*, **38**, 1648 (1960).

(19) B. J. Wood, J. S. Mills, and H. Wise, *J. Phys. Chem.*, **67**, 1462 (1963).

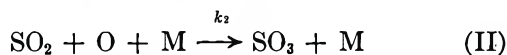
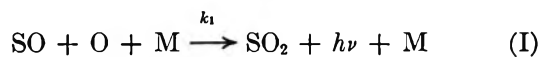
(20) V. V. Majuga and N. D. Sokolov, *Dokl. Akad. Nauk SSSR*, **165**, 625 (1966).

tant when atomic species interact with surfaces. The observed dependence of k_d on $[O]_s^{0.36}$ might thus be attributed to the increase of the rate constant for desorption k_d caused by the increase of the rate of adsorption with increasing concentration of oxygen atoms. In this case one writes k_d in the form $k_d = k_{0d}e^{Ed/R\theta}$, $e^{-Ed/RT}$,¹⁷ where θ is the so-called compensation temperature, a function of $[O]_s$.

Acknowledgment. Partial support of this work by the National Research Council of Italy is gratefully acknowledged.

Appendix

The rate of formation of SO(g) can be written as: $V_{\text{obsd}} = d[SO]/dt = k[O]_s^m$, where k is the rate constant for the heterogeneous process, $[O]_s$ the concentration of oxygen atoms at the sample surface, and m the true reaction order. Oxygen atoms disappear from the gas phase according to the two reactions



where M is argon. The rate constants at 25° have been measured¹⁴ and their values are: $k_1 = (3.2 \pm 0.4) \times 10^{17}$ and $k_2 = (4.7 \pm 0.8) \times 10^{15} \text{ cm}^6 \text{ mole}^{-2} \text{ sec}^{-1}$.

The contribution of the second reaction to the consumption of the atoms can be neglected without serious error. The rate of the homogeneous disappearance of the atoms can then be written as

$$\frac{d[O]}{dt} = k_1[O][SO][Ar]$$

$[O]_s$ will be given by

$$[O]_s = [O]_0 - \int_0^\tau \frac{d[O]}{dt} dt$$

where $[O]_0$ is the concentration of the atoms at the inlet point of the gas and τ the residence time between the point of inlet and the sample surface. By putting $[SO] = [SO] = [SO]_s a = AaV_{\text{obsd}}$ and $[O] = [\bar{O}] = [O]_0 b$, one obtains

$$[O]_s = [O]_0(1 - k_1[Ar]BAV_{\text{obsd}}\tau) \quad (A1)$$

with $B = ab$ and $V_{\text{obsd}} = k[O]_s^m = k[O]_0^m [1 - k_1[Ar]ABV_{\text{obsd}}\tau]^m$, which is eq 2. The ratio of the rates observed at two different values of $[O]_0$ will be

$$\log \frac{V_{\text{obsd}_1}}{V_{\text{obsd}_2}} = m \log \frac{[O]_{0,1}}{[O]_{0,2}} + m \log \frac{1 - k_1[Ar]_1 A_1 B V_{\text{obsd}_1} \tau_1}{1 - k_1[Ar]_2 A_2 B V_{\text{obsd}_2} \tau_2} \quad (A2)$$

From this equation m and B can be derived by graphical solution as follows. k_1 , A , τ , and $[Ar]$ can be calculated for any value of $[O]_0$ and of the temperature (the activation energy of termolecular reaction I can be assumed to be zero without serious errors). By means of eq A2, one plots m as a function of B for any couple of experimental values of V_{obsd} . The point of intersect of two such m - B curves will determine the values of m and B . The ratio $[O]_s/[O]_0$ can then be derived from eq A1.

Stochastic Approach to Nonequilibrium Thermodynamics of

First-Order Chemical Reactions. II. Open Systems

by Kenji Ishida

Radiochemistry Laboratory, Japan Atomic Energy Research Institute, Tokai-mura, Naka-gun, Ibaraki-ken, Japan (Received May 8, 1967)

The nonequilibrium thermodynamics for an open system, in which first-order chemical reactions and particle exchanges with a heat bath are taking place, is stochastically formulated through the probability distribution governing the open system. A stochastic entropy is also defined for such a nonequilibrium system, and it has completely the same form as for a closed system. The entropy production and the relation between entropy and fluctuation are discussed in comparison with the results obtained for the corresponding closed system.

Introduction

In a previous paper¹ (hereafter referred to as I), we studied the stochastic nonequilibrium thermodynamics of first-order chemical reactions in the closed system, in which the probability distribution for reaction states was determined by the stochastic theory of the reaction process. We then started with the correlation of entropy to probability

$$S = -k \sum_i \langle N_i \rangle \ln \{p_i(t)/q_i\} + S_e \quad (1)$$

where S_e denotes the entropy for the equilibrium state, k is Boltzmann's constant, $\langle N_i \rangle$ the mean number of molecules of species i , $p_i(t)$ the probability for a molecule i to be found in the reaction system at time t , and q_i the corresponding probability in thermal equilibrium. In particular, we investigated both entropy production and relation of fluctuation to entropy in comparison with conventional irreversible thermodynamics.

It is known from statistical mechanics² that the statistical entropies for canonical, grand canonical, and other ensembles can be in general defined by

$$S = -k \sum_{\epsilon} p(\epsilon) \ln p(\epsilon)$$

since the probability, $p(\epsilon)$, of the realization of the quantum state, ϵ , is found for all types of ensembles. Similar considerations can be also made for formula 1, since we can stochastically find the probability distribution for the reaction states in an open system. We may, therefore, regard formula 1 as of general applicability to closed systems as well as to open systems. Here, "open" is used in the sense that the transport of matter into and out of the system is allowed.

In order to pass to stochastic nonequilibrium thermodynamics for an open system, in which first-order

reactions and particle exchanges with the surroundings take place, we must begin with the derivation of the probability distribution appropriate to the open system.

Stochastic Model for Open System

We consider the stochastic model^{3,4} for an open system immersed in an infinite heat bath of constant temperature, T . This system consists of r species A_1, A_2, \dots, A_r , between which all possible first-order reactions of the type $A_i \rightleftharpoons A_j$ occur, and which is open with respect to all the species. The state of such an open system at any time, t , is specified by $\{N_i\}$, denoting a set of numbers of molecules, (N_1, N_2, \dots, N_r) . The process through which a particle leaves the system is assumed to be first order. The probability, p_{i0} , per molecule for a transition from system to heat bath in unit time is given by

$$p_{i0} = \alpha_{i0} N_i$$

where the subscript zero denotes the heat bath and the rate constant, α_{i0} , is independent of N_i and t . On the other hand, according to Gans' model, the entry of a particle into the system from an infinite heat bath is a zero-order process. Such a process is called a Poisson process in the theory of stochastic processes.⁵ That is, the transition probability, p_{0i} , per unit time is constant

$$p_{0i} = \beta_i$$

(1) K. Ishida, *J. Phys. Chem.*, **70**, 3806 (1966).

(2) R. Kubo, "Statistical Mechanics," North-Holland Publishing Co., Amsterdam, 1965, p 31. Refer also to N. Nagasako, *Bull. Chem. Soc. Japan*, **35**, 179 (1962), and E. T. Jaynes, *Phys. Rev.*, **106**, 620 (1957).

(3) P. J. Gans, *J. Chem. Phys.*, **33**, 691 (1960).

(4) T. L. Hill and I. W. Plesner, *ibid.*, **43**, 267 (1965).

(5) S. Karlin, "A First Course in Stochastic Processes," Academic Press, New York, N. Y., 1966, p 13.

where β_i depends only on i . Of course, the rate constants, α 's and β 's, are positive and independent of time, but are functions of temperature. With these remarks in mind, we can now set up the differential difference equation for the probability distribution, $P(\{N_i\};t)$, governing the open system. Following the method of Gans,³ we have

$$\begin{aligned} dP(\{N_i\};t)/dt = & -\sum_{i=1}^r \sum_{j=1}^r \alpha'_{ij} N_i P(\{N_i\};t) - \\ & \sum_{i=1}^r \alpha_{i0} N_i P(\{N_i\};t) - \sum_{i=1}^r \beta_i P(\{N_i\};t) + \sum_{i=1}^r \sum_{j=1}^r \alpha'_{ij} \times \\ & (N_i + 1) P(\{N_i\}_{i \neq i, j} + N_i + 1, N_j - 1; t) + \\ & \sum_{i=1}^r \alpha_{i0} (N_i + 1) P(\{N_i\}_{i \neq i}, N_i + 1; t) + \\ & \sum_{i=1}^r \beta_i P(\{N_i\}_{i \neq i}, N_i - 1; t) \quad (2) \end{aligned}$$

where α_{ij} is the rate constant of $A_i \rightarrow A_j$ and primed summations indicate omission of the term $j = i$.

We introduce the initial condition as follows. If each of the species A_1, A_2, \dots, A_r behaves as an ideal gas, it is physically plausible that the expected initial probability distribution is of the form

$$P(\{N_i\};0) = \prod_{i=1}^r \frac{\exp(-\langle N_i^0 \rangle) \langle N_i^0 \rangle^{N_i^0}}{N_i^0!} \quad (3)$$

in which $\langle N_i^0 \rangle$'s are the mean numbers of molecules in the initial population, since in the case of the classical treatment of an ideal gas as a grand canonical ensemble,⁶ the distribution law (3) is an equilibrium probability distribution.

We have now to derive the probability distribution for the open system of interest. Defining the generating function by

$$G(\{z_i\};t) = \sum_{N_1=0}^{\infty} \cdots \sum_{N_r=0}^{\infty} \prod_{i=1}^r z_i^{N_i} P(\{N_i\};t) \quad (4)$$

and solving (2), under the initial condition (3), by means of the method of generating functions, we obtain, in exactly the same way as Gans did³

$$G(\{z_i\};t) = \exp \left\{ \sum_{i=1}^r M_i(t) (z_i - 1) \right\} \quad (5)$$

which is of the type of the generating function of a Poisson distribution. From this we have, according to (4)

$$P(\{N_i\};t) = \prod_{i=1}^r \frac{\exp\{-M_i(t)\} \{M_i(t)\}^{N_i}}{N_i!} \quad (6)$$

In (5) or (6), $M_i(t)$ denotes the mean number of molecules and takes the form⁸

$$\begin{aligned} M_i(t) = & B^{-1} \sum_{j=1}^r \sum_{k=1}^r B^{kj} \{ -\beta_j \lambda_k^{-1} + \\ & (\langle N_j^0 \rangle + \beta_j \lambda_k^{-1}) \exp(\lambda_k t) \} b_{ki} \\ = & M_i(\infty) + B^{-1} \sum_{j=1}^r \sum_{k=1}^r B^{kj} \{ \langle N_j^0 \rangle + \\ & \beta_j \lambda_k^{-1} \} b_{ki} \exp(\lambda_k t) \quad (7) \end{aligned}$$

where the mean number of molecules in the equilibrium state, $M_i(\infty)$, is given by

$$M_i(\infty) = -B^{-1} \sum_{j=1}^r \beta_j \sum_{k=1}^r \lambda_k^{-1} B^{kj} b_{ki} \quad (8)$$

When the probability distribution governing an open system is given by (6), the probability distribution for the sum $\sum_{i=1}^r N_i = N$ can be shown to be, by convolution⁹

$$P(N;t) = \frac{\exp\{-M(t)\} \{M(t)\}^N}{N!} \quad (9)$$

where N is the total number of molecules and its mean

$$M(t) = \sum_{i=1}^r M_i(t) \quad (10)$$

Our central interest, however, is in obtaining the probability distribution for an open system with an arbitrary but fixed N . Let $X_i(t)$ ($i = 1, 2, \dots, r$) and $X(t) = \sum_{i=1}^r X_i(t)$ be random variables which assume positive integers. The conditional probability, such that the random variable $X_i(t)$ takes N_i as its realized value, given the random variable $X(t)$ and assuming an arbitrarily fixed value N , is expressed in the form

$$\begin{aligned} Pr\{X_1(t) = N_1, X_2(t) = \\ N_2, \dots, X_r(t) = N_r | X(t) = N\} \\ Pr\{X_1(t) = N_1, X_2(t) = \\ N_2, \dots, X_r(t) = N_r\} \\ = \frac{N_2, \dots, X_r(t) = N_r\}}{Pr\{X(t) = N\}} \\ = \left\{ \prod_{i=1}^r \exp\{-M_i(t)\} \{M_i(t)\}^{N_i} / N_i! \right\} / \\ \{ \exp\{-M(t)\} \{M(t)\}^N / N! \} \\ = \frac{N!}{\prod_{i=1}^r N_i!} \prod_{i=1}^r \{p_i(t)\}^{N_i} \quad (11) \end{aligned}$$

(6) N. Nagasako, *Bull. Chem. Soc. Japan*, **35**, 179 (1962). See also C. Kittel, "Elementary Statistical Physics," John Wiley and Sons, Inc., New York, N. Y., 1958, p 66.

(7) See ref 3. Refer also to I. M. Krieger and P. J. Gans, *J. Chem. Phys.*, **32**, 247 (1960).

(8) B , B^{kj} , b_{ki} , and λ_k are used in the same meaning as in the paper of Gans.

(9) W. Feller, "An Introduction to Probability Theory and its Applications," 2nd ed, John Wiley and Sons, Inc., New York, N. Y., 1957; p 250.

where (6) and (9) have been used and $p_i(t) = M_i(t)/M(t)$. It should be noted that in the multinomial distribution (11) for open system, the total number of molecules, N , can be assumed to be variable, but for a closed system it is inevitably constant as in (26) of paper I.

Entropy Production

We are now in a position to obtain the stochastic entropy production. Since the probability of a state in the open system with an arbitrarily fixed N is $\prod_{i=1}^r \{p_i(t)\}^{N_i}$, the entropy, according to (1), is given by

$$S = -k \sum_{i=1}^r M_i(t) \ln \{p_i(t)/p_i(\infty)\} + S_e \quad (12)$$

where $p_i(\infty) = M_i(\infty)/M(\infty)$ corresponds to q_i in formula (1). From this, we can readily obtain as the entropy production

$$dS/dt = -\sum_{i=1}^r \{dM_i(t)/dt\} \ln \{p_i(t)/p_i(\infty)\} \quad (13)$$

It has been shown in conventional irreversible thermodynamics,¹⁰ however, that whether the system under consideration is closed or open, the entropy production is invariably nonnegative. Therefore, (13) must also satisfy the inequality $dS/dt \geq 0$, where the equality holds for the equilibrium state.

The next problem is to express (13) in terms of rates and affinities. To do this, we break up the equation into

$$dS/dt = -k \sum_{i=1}^{r-1} \{dM_i(t)/dt\} \ln \{p_i(t)/p_i(\infty)\} - k \{dM_r(t)/dt\} \ln \{p_r(t)/p_r(\infty)\} \quad (14)$$

On the other hand, from (2), we can easily derive the rate equation with respect to the mean

$$dM_i(t)/dt = -v_i + w_i \quad (15)$$

where the reaction rate, v_i , is given by

$$v_i = \sum_{j=1}^r \alpha_{ij} M_i(t) - \sum_{j=1}^r \alpha_{ji} M_j(t)$$

just as in the case of closed system (see paper I), and the rate of the transport process between system and external environment, w_i , is given by

$$w_i = \beta_i - \alpha_{i0} M_i(t)$$

Rearranging the equation $\sum_{i=1}^r dM_i(t)/dt = dM(t)/dt$, we have

$$dM_r(t)/dt = \sum_{i=1}^{r-1} v_i + w_r \quad (16)$$

where $\sum_{i=0}^r v_i = 0$ and $dM(t)/dt = \sum_{i=1}^r w_i$ have been used.

The substitution of (15) and (16) into (14) leads directly to

$$dS/dt = k \sum_{i=1}^{r-1} v_i \{ \ln [p_i(t)/p_i(\infty)] - \ln [p_r(t)/p_r(\infty)] \} - k \sum_{i=1}^r w_i \ln [p_i(t)/p_i(\infty)] \quad (17)$$

which is the same as

$$dS/dt = k \sum_{i=1}^{r-1} v_i \{ \ln [M_i(t)/M_i(\infty)] - \ln [M_r(t)/M_r(\infty)] \} - k \sum_{i=1}^r w_i \{ \ln [M_i(t)/M_i(\infty)] - \ln [M(t)/M(\infty)] \} \quad (18)$$

The first sum is the entropy production due to chemical reactions and agrees completely with

$$(dS/dt)_{\text{closed}} = \frac{1}{T} \sum_{i=1}^{r-1} v_i A_i^{\text{ch}} \quad (19)$$

where A_i^{ch} denotes the chemical affinity of the reaction between components i and r

$$A_i^{\text{ch}} = kT \{ \ln [M_i(t)/M_i(\infty)] - \ln [M_r(t)/M_r(\infty)] \} \quad (20)$$

The second sum on the right-hand side of (18) is the entropy production due to particle exchange with the external environment. If we define the affinity corresponding to the transport of component i by

$$A_i^{\text{tr}} = kT \{ \ln [M_i(t)/M_i(\infty)] - \ln [M(t)/M(\infty)] \} \quad (21)$$

and take into account (20), we get as a thermodynamic expression of (18)

$$dS/dt = \frac{1}{T} \sum_{i=1}^{r-1} v_i A_i^{\text{ch}} - \frac{1}{T} \sum_{i=1}^r w_i A_i^{\text{tr}} \quad (22)$$

We finally must make a simple remark about the entropy production (18) or (22). As is clear from above, the entropy production for an open system includes that for the closed system as a special case, where $w_i = 0$ for all i . From a mathematical standpoint, however, this originates in the probability distributions governing these systems themselves. The total number of molecules assumed in the probability distribution for the closed system is only constant valued. On the other hand, in the open system, where the distribution law has in form been the same multinomial distribution as in the closed system, but a conditional one, the total number of molecules is able to assume any value, that is to say, it can be regarded as a random variable.

(10) I. Prigogine, "Introduction to Thermodynamics of Irreversible Processes," 2nd ed, Interscience Publishers, Inc., New York, N. Y., 1961, pp 28, 78.

Entropy and Fluctuation

Before discussing the relation of fluctuation to entropy for open system in the state close to equilibrium, we shall briefly describe that for the case of a closed system. We first write the stochastic entropy in the form

$$(\Delta S/k)_{\text{closed}} = -\sum_{i=1}^r M_i(t) \ln \{M_i(t)/M_i(\infty)\} \quad (23)$$

where $\Delta S = S - S_e$ denotes the deviation of entropy from its equilibrium value. Let us now introduce the stoichiometric coefficient of A_i in the reaction $A_i \rightarrow A_j$, ν_{ij} , and the degree of advancement, ξ_{ij} , by means of $M_i(t) - M_i(\infty) = \sum_{j=1}^r \nu_{ij}(\xi_{ij} - \xi_{ij}^{(e)})$. Developing the right-hand side of (23) in the Taylor series with respect to $\sum_{j=1}^r \nu_{ij}(\xi_{ij} - \xi_{ij}^{(e)})$, we obtain

$$(\Delta S/k)_{\text{closed}} = -\frac{1}{2} \sum_{i=1}^r \frac{1}{M_i(\infty)} \left\{ \sum_{j=1}^r \nu_{ij}(\xi_{ij} - \xi_{ij}^{(e)}) \right\}^2 \quad (24)$$

where $\xi_{ij}^{(e)}$ is the equilibrium value of ξ_{ij} and $\sum_{i=1}^r \sum_{j=1}^r \nu_{ij}(\xi_{ij} - \xi_{ij}^{(e)}) = 0$ has been used. This may be also written in a bilinear form

$$(\Delta S/k)_{\text{closed}} = -\frac{1}{2} \left\{ \sum_{i \neq j}^{1/2r(r-1)} \left(\frac{1}{M_i(\infty)} + \frac{1}{M_j(\infty)} \right) (\xi_{ij} - \xi_{ij}^{(e)})^2 + 2 \sum_{i=1}^r \frac{1}{M_i(\infty)} \sum_{j \neq i'}^r \nu_{ij} \nu_{ij'} (\xi_{ij} - \xi_{ij}^{(e)}) (\xi_{ij'} - \xi_{ij'}^{(e)}) \right\} \quad (25)$$

where $\nu_{ij}^2 = 1$, $\nu_{ij} + \nu_{ji} = 0$ and $\xi_{ij} - \xi_{ij}^{(e)} = \xi_{ji} - \xi_{ji}^{(e)}$ have been used and $1/2r(r-1)$ denotes the number of all possible reactions.

We now return to the open system. Similarly, we start with

$$\Delta S/k = -\sum_{i=1}^r M_i(t) \{ \ln [M_i(t)/M_i(\infty)] - \ln [M(t)/M(\infty)] \} \quad (26)$$

By following the same procedure as in the derivation of (24), we have for the open system

$$\Delta S/k = -\frac{1}{2} \left\{ \sum_{i=1}^r x_i^2/M_i(\infty) - \left(\sum_{i=1}^r x_i \right)^2/M(\infty) \right\} \quad (27)$$

where we emphasize that the new parameter $x_i = M_i(t) - M_i(\infty)$ is not the degree of advancement.

Since for closed system x_i becomes $\sum_{j=1}^r \nu_{ij}(\xi_{ij} - \xi_{ij}^{(e)})$, (27) includes (24) as a special case. Equation 27 can be also be written as

$$\Delta S/k = -\frac{1}{2} \sum_{i \neq j}^{1/2r(r-1)} \frac{M(\infty)}{M_i(\infty)M_j(\infty)} \times \{p_j(\infty)x_i - p_i(\infty)x_j\}^2 \quad (28)$$

We see here that in the state close to equilibrium $\Delta S/k \leq 0$ holds also for the open system. The Poisson distribution has the property that variance is equal to the mean. Thus, using the variances $\sigma_{i,e}^2$ and $\sigma_e^2 = \sum_{i=1}^r \sigma_{i,e}^2$ in place of $M_i(\infty)$ and $M(\infty)$, respectively, we have

$$\Delta S/k = -\frac{1}{2} \sum_{i \neq j}^{1/2r(r-1)} (\sigma_e^2/\sigma_{i,e}^2 \sigma_{j,e}^2) \times \{p_j(\infty)x_i - p_i(\infty)x_j\}^2 \quad (29)$$

which explicitly represents the relationship between entropy and fluctuation. This problem will be taken up again in the following section.

Example and Discussion

Further progress in the understanding of the results obtained in the previous sections will be greatly helped by an illustration of simple systems. Let us first consider an open system, O, in which one single reaction $A \rightleftharpoons B$ occurs.¹¹ Of course, we suppose that this system has the same well-defined temperature, T , as an infinite heat bath. Then, according to (11), the probability distribution for such a system is given by

$$P(N_A, N_B; t) = \frac{(N_A + N_B)!}{N_A! N_B!} \times \left\{ \frac{M_A(t)}{M_A(t) + M_B(t)} \right\}^{N_A} \left\{ \frac{M_B(t)}{M_A(t) + M_B(t)} \right\}^{N_B} \quad (30)$$

In consequence, we have as the entropy production

$$dS/dt = \frac{v}{T} \{ kT \ln [M_A(t)/M_A(\infty)] - kT \ln [M_B(t)/M_B(\infty)] \} - \frac{1}{T} \sum_{\gamma=A,B} w_\gamma \times \{ kT \ln [M_\gamma(t)/M_\gamma(\infty)] - kT \ln [M(t)/M(\infty)] \} \quad (31)$$

where $v = \alpha_{AB}M_A(t) - \alpha_{BA}M_B(t)$, $w_\gamma = \beta_\gamma - \alpha_{\gamma_0}M_\gamma(t)$ ($\gamma = A, B$) and $M(t) = M_A(t) + M_B(t)$.

It is interesting to compare (31) with the entropy production in the open system, O', discussed by Prigogine.¹² This system consists of two open subsystems I and II, but is closed as a whole and maintained at uniform temperature, T . We suppose, moreover, that the reaction $A \rightleftharpoons B$ occurs only in subsystem I.¹³ Since the whole system I + II is closed, we obtain a multinomial distribution, in the same way as in paper I

(11) If reaction $A \rightleftharpoons B$ occurs only in the system just considered, it may be regarded as a catalytic reaction.

(12) Reference 10, p 28.

(13) See footnote 11.

$$P(N_A^I, N_B^I, N_A^{II}, N_B^{II}; t) = \frac{N!}{\prod_{\gamma} \prod_{\rho} N_{\gamma}^{\rho}!} \prod_{\gamma} \prod_{\rho} \{p_{\gamma}^{\rho}(t)\}^{N_{\gamma}^{\rho}} \quad (32)$$

where the total number of molecules, $N = \sum_{\gamma} \sum_{\rho} N_{\gamma}^{\rho}$, is fixed and $\sum_{\gamma} \sum_{\rho} p_{\gamma}^{\rho}(t) = 1$ ($\rho = A, B$; $\gamma = I, II$).

Thus we have as the entropy production for an open system O'

$$dS/dt = \frac{v}{T} \{ kT \ln [M_A^I(t)/M_A^I(\infty)] - kT \ln [M_B^I(t)/M_B^I(\infty)] \} - \frac{1}{T} \sum_{\gamma} w'_{\gamma} \{ kT \ln [M_{\gamma}^I(t)/M_{\gamma}^I(\infty)] - kT \ln [M_{\gamma}^{II}(t)/M_{\gamma}^{II}(\infty)] \} \quad (33)$$

where $w'_{\gamma} = \beta_{\gamma} M_{\gamma}^{II}(t) - \alpha_{\gamma} M_{\gamma}^I(t)$ is the rate of transport process between two subsystems.¹⁴ It is important, here, to note that the difference between (31) and (33) is due to that between two probability distributions (30) and (32). Since affinity and chemical potential can be expressed, respectively, by

$$A^I = kT \ln [M_A^I(t)/M_A^I(\infty)] - kT \ln [M_B^I(t)/M_B^I(\infty)]$$

and

$$\mu_{\gamma}^{\rho} = \mu_{\gamma,e}^{\rho} + kT \ln [M_{\gamma}^{\rho}(t)/M_{\gamma}^{\rho}(\infty)]$$

(33) reduces to

$$dS/dt = A^I v/T - \frac{1}{T} \sum_{\gamma} w'_{\gamma} (\mu_{\gamma}^I - \mu_{\gamma}^{II}) \quad (34)$$

which is in agreement with the equation deduced by Prigogine.¹⁵ In the probability problem, however, it is necessary to turn to a more detailed discussion of the distribution law in the open system O'. It follows from (32) that the marginal distribution¹⁶ of subsystem II is

$$P_{II}(N_A^{II}, N_B^{II}; t) = \frac{N!}{\prod_{\gamma} N_{\gamma}^{II}! (N - \sum_{\gamma} N_{\gamma}^{II})!} \times \prod_{\gamma} \{p_{\gamma}^{II}(t)\}^{N_{\gamma}^{II}} \cdot \left\{ \sum_{\gamma} p_{\gamma}^I(t) \right\}^{N - \sum_{\gamma} N_{\gamma}^{II}} \quad (35)$$

Since the conditional probability $Pr\{I|II\}$ of subsystem I, given subsystem II, is defined by

$$Pr\{I|II\} = \frac{P(N_A^I, N_B^I, N_A^{II}, N_B^{II}; t)}{P_{II}(N_A^{II}, N_B^{II}; t)}$$

we have, using eq 32 and 35

$$Pr\{I|II\} = \frac{(N_A^I + N_B^I)!}{N_A^I! N_B^I!} \left\{ \frac{p_A^I(t)}{p_A^I(t) + p_B^I(t)} \right\}^{N_A^I} \times \left\{ \frac{p_B^I(t)}{p_A^I(t) + p_B^I(t)} \right\}^{N_B^I} \quad (36)$$

where the total number of molecules in subsystem I, $N_A^I + N_B^I = N^I$, can take on any value. This distribution law is in form consistent with the distribution law (30) for the open system O. We can therefore say that the entropy production for subsystem I in open system O' has the same physical meaning as that for open system O. We emphasize that such discussions are possible only by the stochastic study of nonequilibrium thermodynamics of chemical reactions.

For the open system O near equilibrium, we have, according to formula 28

$$\Delta S/k = -\frac{1}{2} \frac{M(\infty)}{M_A(\infty)M_B(\infty)} \times \{p_B(\infty)x_A - p_A(\infty)x_B\}^2 \quad (37)$$

Since $M_A(\infty) = \sigma_{A,e}^2$ and $M_B(\infty) = \sigma_{B,e}^2$, it follows that

$$\frac{M(\infty)}{M_A(\infty)M_B(\infty)} = \frac{1}{\sigma_{A,e}^2} + \frac{1}{\sigma_{B,e}^2} \quad (38)$$

On the other hand, the binomial distribution of open system O in equilibrium state has the variance, i.e., the fluctuation

$$\sigma_e^2 = M(\infty)p_A(\infty)p_B(\infty) = M_A(\infty)M_B(\infty)/M(\infty) \quad (39)$$

Using (38) and (39), we can write (37) in the form

$$\Delta S/k = -1/2(1/\sigma_e^2)\{p_B(\infty)x_A - p_A(\infty)x_B\}^2 \quad (40)$$

where $1/\sigma_e^2 = 1/\sigma_{A,e}^2 + 1/\sigma_{B,e}^2$. This is the expression of the relation of fluctuation to entropy for the open system O. If this system is closed, the parameters x_A and x_B are replaced by $-(\xi - \xi^{(e)})$ and $\xi - \xi^{(e)}$, respectively. We then have

$$(\Delta S/k)_{\text{closed}} = -1/2(1/\sigma_e^2)_{\text{closed}}(\xi - \xi^{(e)})^2 \quad (41)$$

where $p_A(\infty) + p_B(\infty) = 1$ has been used. This is identical with eq 42 in paper I. We can see also from this example that the nonequilibrium thermodynamics of an open system contains that of the closed system as a special case. From the stochastic point of view, such a proposition is ascribed to the difference between the probability distribution for the open system and that for the closed system.

(14) It is supposed, for the open system O', that the transport of particles between subsystems I and II is a first-order process. α_{γ} and β_{γ} denote the rate constants for the transport of species γ from I to II and from II to I, respectively.

(15) Reference 10, p 29. If we set $T^I = T^{II} = T$ and $v^{II} = 0$ in eq 3.53, we have eq 34.

(16) Reference 9, p 201.

Electrolytes in High Surface Area Systems. I. The Reaction between Lithium Chloride-Acetone Solutions and Silica Gel, an Unusual Addition Reaction^{1a}

by Russell Maatman,^{1b} Abel Geertsema, Harold Verhage,
Glenn Baas, and Michael Du Mez

Department of Chemistry, Dordt College, Sioux Center, Iowa (Received May 12, 1967)

A reaction between LiCl dissolved in acetone and silica gel is described. General methods for distinguishing between adsorption and exchange are given. Both cation and anion react reversibly without ion exchange. This is an unusual example of salt addition (as contrasted with exchange) to a noncrystalline surface. The amount of reaction is enhanced by the addition of small amounts of water, but with further addition there is less reaction. From Langmuir plots, the equilibrium constant for surface complex formation, K , was found to be $2-6 \times 10^2$ l. mole⁻¹. LiNO₃ and NaI react less extensively, with $K \sim 10$ l. mole⁻¹. The site concentration varied from 0.2–0.6 mmole g⁻¹, depending upon the amount of water present. LiCl does not add to the gel surface when *n*-propyl, *n*-butyl, or isoamyl alcohol is the solvent. These observations are interpreted to mean that Li⁺, Cl⁻, or both add to polar surface sites, which involve water added to the surface, that excess water (or alcohol) destroys surface sites by further adsorption, and that excess water stabilizes the ions in solution. Salt addition to the gel surface is similar to molecule addition. It was shown that LiCl and LiNO₃ can be removed from acetone by silica gel powder in a chromatographic column.

Introduction

We showed earlier that alkali metal nitrates dissolved in H₂O, CH₃OH, or C₂H₅OH react at the most only slightly with the surface of silica gel.^{2,3} An incidental observation in these studies was that LiNO₃ in acetone reacts extensively with the gel surface. Polar molecules, such as fatty acids, are known to react with surfaces which are more polar than the solvent.⁴ Adamson states that if both the positive and negative ions of an electrolyte are adsorbed, "...the situation is essentially the same as for molecular adsorption."⁵ Addition of ions to crystalline solids is well known; we decided to determine whether the reaction observed with silica gel, at most much less crystalline than the materials usually used for ion adsorption (*e.g.*, BaSO₄), is analogous to molecular adsorption.

The reaction of both cation and anion with porous oxide surfaces is not unexpected. The reaction may occur because there are present easily exchanged cationic and anionic groups on the surface (*e.g.*, aqueous alkaline earth salt ions exchange with H⁺ and OH⁻ of the alumina surface⁶); because the salt is slightly soluble (*e.g.*, aqueous silver salts are adsorbed by silica-alumina, Fe₂O₃, and Fe₂O₃-SiO₂⁷); or because a new phase forms (*e.g.*, CuCl₂ forms Cu₂(OH)₃Cl on the surface of hydrated Al₂O₃⁸).

There is not much information on silica gel ion reaction in nonaqueous systems, and the pattern is not

evident. For example, French and Howard observed, at the most, only slight absorption by silica gel of transition metal salts dissolved in dioxane or quinoline.⁹ Strazhesko and Yankovskaya noted, using tracer methods, some cation uptake from CH₃OH, acetone, and dioxane by silica gel.¹⁰

(1) (a) Acknowledgment is made to the donors of The Petroleum Research Fund, administered by the American Chemical Society, for partial support of this research. This work was also supported by Atomic Energy Commission Contract AT(11-1)-1354, and by the National Science Foundation Program for High School Teachers. (b) Correspondence should be sent to this author.

(2) D. L. Dugger, J. H. Stanton, B. N. Irby, B. L. McConnell, W. W. Cummings, and R. W. Maatman, *J. Phys. Chem.*, **68**, 757 (1964).

(3) J. L. Daniel and R. W. Maatman, *J. Miss. Acad. Sci.*, **9**, 70 (1963).

(4) (a) H. N. Holmes and J. B. McKelvey, *J. Phys. Chem.*, **32**, 1522 (1928); (b) Y. Morinaga and I. Nakamori, *Kyushu Kogei Seni Daigaku Kogiegakubu Kenkyu Hokoku*, **12**, 59 (1962).

(5) A. W. Adamson, "Physical Chemistry of Surfaces," Interscience Publishers, New York, N. Y., 1960, p. 590.

(6) K. C. Williams, J. L. Daniel, W. J. Thomson, R. I. Kaplan, and R. W. Maatman, *J. Phys. Chem.*, **69**, 250 (1965).

(7) (a) O. I. Dmitrenko and A. A. Ryabinina, *Kolloid. Zh.*, **15**, 29 (1953); (b) O. I. Dmitrenko, *Chemisation Socialistic Agr.* (U. S. S. R.), **9**, No. 5, 46 (1940); (c) V. A. Kargin, P. S. Vasil'ev, and O. I. Dmitrenko, *Russ. J. Phys. Chem.*, **14**, 1628 (1940).

(8) H. Schafer and W. Neugebauer, *Naturwissenschaften*, **38**, 561 (1951).

(9) C. M. French and J. P. Howard, *Trans. Faraday Soc.*, **52**, 712 (1956).

(10) D. N. Strazhesko and G. F. Yankovskaya, *Ukr. Khim. Zh.*, **25**, 471 (1959).

To investigate the reaction of nonaqueous salt solutions with silica gel, we treated the gel under various conditions with LiNO_3 , LiCl , and NaI , dissolved in acetone. Most of the experiments were with LiCl . Acetone was the solvent of choice because of the initial observation and because there is no complicating reaction of acetone with the silica gel surface.¹¹ In a few additional experiments, various alcohols were used as solvent for comparison purposes, since alcohols do react with the gel surface.

Methods

Determination of the Reaction Isotherm. When a solution is mixed with a porous solid, the total amount of solute in the pores of one gram of the solid at equilibrium, y_{tot} , is given by

$$y_{\text{tot}} = \frac{c_i V - c_f(V - WP)}{W} \quad (1)$$

where V ml of solution of concentration c_i is mixed with W g of solid of pore volume P (ml g^{-1}), and where c_f is the final concentration of the liquid external to the pores. To determine y_r , the amount of reacted solute per gram, y_{tot} is diminished by $c_f P$. In the present investigation (except for one case where the assumption is not needed) $y_r \gg c_f P$, and there is little error involved in neglecting the correction which takes into account the inability of the solute to "see" the whole pore volume.¹² The reaction isotherm is a plot of y_r vs. c_f . If there is a time-invariant shoulder in the reaction isotherm, the reaction is reversible.⁶

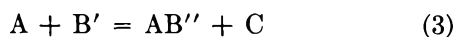
Determination of the Nature of the Surface Reaction. A distinction between exchange and adsorption reactions can be made by examination of the shape of the reaction isotherm, since the two kinds of reaction do not lead to curves of the same shape. This is a difficult comparison to make, given the usual experimental error. There are other means of distinguishing between these two kinds of surface reaction.

First, exchange can sometimes be detected by observing exchange products in solution. Inability to find such products is, however, no proof of absence of exchange, since it is not always certain which materials should be tested for; also, the amounts sought in systems with only slight reaction can be too small to detect. Even when a supposed exchange product is detected, one may actually find a secondary product.

Second, a distinction between exchange and adsorption may be made by analyzing the reaction isotherm in detail. We can show this by examining the equations for the two types of reaction. For adsorption



where A is the solute, B the adsorption site, and AB the surface complex. For exchange



where B' is the exchange site and C is the substance released from the surface. (B' decomposes into $B'' + C$.) The adsorption equilibrium constant is (neglecting the deviation of activity coefficients from unity)

$$K_a = [AB]/[A/V][B] = [AB]/[A/V]\{D - [AB]\} \quad (4)$$

where $[AB]$ and $[B]$ are the amounts per unit weight of solid, in moles, of surface sites covered and uncovered, respectively, D is the number of moles of adsorption sites per unit weight of solid, and $[A/V]$ is the equilibrium concentration of solute. The exchange equilibrium constant is

$$K_e = [AB''] [C/V] / [A/V] [B'] = [AB''] [C/V] / [A/V] \{D' - [AB'']\} \quad (5)$$

The adsorption or exchange isotherm is a plot of $[AB]$ or $[AB'']$ vs. $[A/V]$. Equation 4 shows that such a plot for adsorption is independent of V . (For these equations, it is assumed for simplicity that $W = 1$ g.) On the other hand, eq 5 shows that because of the $[C/V]$ factor, even though species C is not detected, such a plot for exchange does depend upon V . Thus the reaction isotherm is unique for adsorption, but not for exchange, where there is a curve for every value of V . Observing a family of reaction isotherms, therefore, indicates exchange occurs, even if there are also non-exchange reactions occurring.

Another way of using the reaction isotherm to distinguish between exchange and adsorption is to attempt the so-called Langmuir plot. Equation 4, for adsorption, can be rearranged to

$$[AB]/[A/V] = -K_a[AB] + K_a D \quad (6)$$

A linear plot of $[AB]/[A/V]$ vs. $[AB]$ thus indicates adsorption, providing a similar plot of the same data assuming exchange is not linear. In what follows it is shown that a similar plot in an exchange reaction is not linear.

We first obtain an expression for $[AB'']$ from eq 5

$$[AB''] = K_e D' [A/V] / \{ [C/V] + K_e [A/V] \} \quad (7)$$

If no more than a negligible amount of species C is introduced from other sources

$$[AB''] = [C] \quad (8)$$

From eq 5 and 8

$$[C/V] = -K_e [A/V] / 2 + \{ K_e^2 [A/V]^2 + 4 K_e [A/V] [D'/V] \}^{1/2} / 2 \quad (9)$$

From eq 7 and 9, the quantity $[C/V]$ is eliminated and

(11) G. Blyholder and W. V. Wyatt, *J. Phys. Chem.*, **70**, 1745 (1966).

(12) B. L. McConnell, K. C. Williams, J. L. Daniel, J. H. Stanton, B. N. Irby, D. L. Dugger, and R. W. Maatman, *J. Phys. Chem.*, **68**, 2941 (1964).

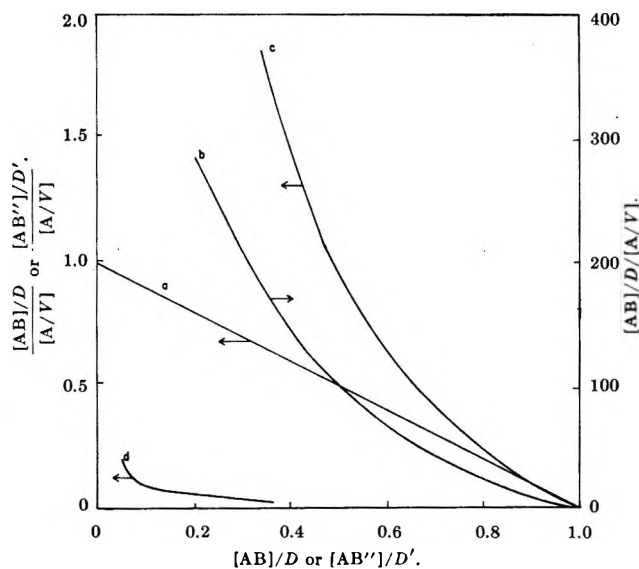
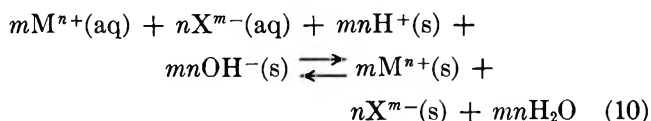


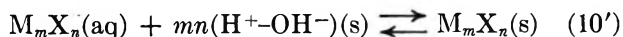
Figure 1. Attempted Langmuir plots for adsorption and exchange, with amount adsorbed expressed as fraction of saturation value. (a) adsorption, with $K_a = 1$; (b) exchange, with $K_e = 1$ and $D'/V = 0.01$; (c) exchange, with either $K_e = 1$ and $D'/V = 1$ or $K_e = 10$ and $D'/V = 10$; (d) exchange, with $K_e = 1$ and $D'/V = 100$. See text.

plots of $[AB'']/[A/V]$ vs. $[AB'']$ for various values of the system parameters, K_e and D'/V , can be constructed. In Figure 1, it is shown that such plots are linear for adsorption and definitely nonlinear—easily seen even with normal experimental error—for widely varying values of the parameters in the exchange system. Equation 5 can be rearranged to show that a plot of $\{[A]/[AB'']\}$ vs. $[A]/[AB'']^2$, at constant volume, is linear in exchange systems. The analytical treatment of cases in which the exchanging ions are not of the same valence is obviously much more complicated.

Even with the use of these tests, there is at least one case in which exchange might be thought to be adsorption. Suppose both the cation and anion of the solute exchange for solvent cation and anion of the surface. The over-all effect is that of a "molecule" ("kome") of salt adsorbing. For the salt M_nX_n



where (s) refers to species of the surface phase. Since in aqueous solutions the production of water will not be observed, reaction 10 will appear to be, if there is equivalent anion and cation exchange



where there is "coupled" exchange and $(H^+-OH^-(s))$ denotes a double site which can accommodate both anion and cation. Since reaction 10' is in the form of reaction 2, adsorption will appear to occur where there is actually exchange. The alumina-salt reaction is

apparently in this category.⁶ If, however, the exchange is not coupled, it can be detected. For example, in the case cited nonequivalent exchange would lead to a pH change.

Experimental Section

Materials. Except where noted, the silica gel was Davison Code 40 silica gel, 6–12 mesh, washed with nitric acid as described elsewhere.¹³ After washing, the gel was dried in an oven and calcined for 2 hr in air at 450°, except where other temperatures are specified. The temperature of calcining, surface area (BET, measured in the sorptometer described elsewhere¹⁴) in m²/g, and pore volume (amount of liquid acetone taken up by pores) in ml/g for the various gels are 250°, 480, 0.43; 450°, 445, 0.37; 650°, 401, 0.33. The gel in the chromatographic columns was Baker Reagent silica gel powder, used as received.

Reagent acetone was used either as received, with ~0.2 vol % H₂O (where vol % H₂O is obtained by comparing the volume of water with the total solution volume), or after drying over Linde 3A molecular sieve. Except where noted, the dry acetone was used. Isoamyl, *n*-butyl, and *n*-propyl alcohols (Eastman White Label) were used as received. Other materials were of reagent grade.

Procedure. In the batch experiments, V/W varied from 1.25 to 5.83 ml/g; in most experiments 20 ml of solution was mixed with 12 g of gel. After an equilibration period of at least 2 days, aliquots were removed for analysis. All experiments were at room temperature, $22 \pm 3^\circ$. Except where noted, the acetone used was dried.

In preparing acetone–water–LiCl solutions, it was noted that LiCl solubility passes through a minimum as the water content is varied. With 0.05 M LiCl the salt precipitated, as water was added, at 1.0 vol % H₂O and it redissolved at 4.7 vol % H₂O; the effect was reversible. Precipitation was not observed with 0.01 M LiCl.

In the column experiments, 10 g of silica gel powder was placed on a glass-wool plug in a 100-ml buret of 0.58 cm² cross section. After the column was just covered with acetone, 50 ml of salt solution was passed through with a flow rate of 0.9 ml/min; liquid flow was continued by elution with acetone.

Analytical. For the alkali metal salt solutions, 10-ml aliquots, from the initial and the equilibrated solution, were evaporated until free of liquid, either in the air or in a rotating vacuum evaporator. The residue, after being dissolved in 10 ml of water, was analyzed with the appropriate electrode and a calomel reference electrode

(13) (a) S. Åhrland, I. Grenthe, and B. Noren, *Acta Chem. Scand.*, **14**, 1059 (1960); (b) J. Stanton and R. W. Maatman, *J. Colloid Sci.*, **18**, 132 (1963).

(14) H. L. Lutrick, K. C. Williams, and R. W. Maatman, *J. Chem. Educ.*, **41**, 93 (1964).

in the Beckman GS pH meter. With all LiCl solutions, chloride was determined using an Ag-AgCl electrode; in LiNO₃ experiments, lithium was determined using a general cation electrode; in NaI experiments, sodium was determined using a sodium ion electrode. Greater precision was obtained with the chloride electrode than with the cation electrodes, and therefore a careful comparison of Li⁺ and Cl⁻ of the same solution was not practical.

Water in acetone and in the LiCl-acetone solutions was determined using a 10% ethofat-chromosorb T column in an Aerograph 90-P gas chromatograph. The presence of LiCl did not affect the analysis.

Results

Aqueous aluminum nitrate reacts with silica gel by ion exchange.² To show that varying V/W in exchange systems does indeed lead to a family of reaction isotherms, the results for aqueous Al(NO₃)₃-silica gel are given in Table I. Isotherm dependence upon V/W is seen even though ion exclusion is not separated out. The validity of this test is therefore assumed.

Table I: Dependence of Aqueous Aluminum Nitrate-Silica Gel Reaction upon V/W ^a

c_i , M, Al(NO ₃) ₃	Moles of Al/g of gel, $\times 10^4$ ^b		
	V/W , 1.25 ml/g	V/W , 2.50 ml/g	V/W , 5.00 ml/g
0.02	1.37	1.93	3.15
0.04	1.85	2.85	4.18
0.08	3.00	4.74	...

^a Davison Silica gel of 491 m²/g, BET, used as received; 25-ml solution was used with contact for a minimum of 2 days.

^b Total of both reacted and unreacted aluminum in pores per gram of gel; values reported are those rounded off from isotherm.

To investigate reversibility in the acetone-salt-gel systems, the effect on the isotherm of solution-silica gel contact time was studied. The low-concentration results are shown in Figure 2, where there are virtually identical isotherms for contact times of 9, 15, and 80 days. The existence of a shoulder proves reversibility.⁶

The effect of the water of both the calcined gel and the initial solution is of interest. For anhydrous solutions, there are, in Figure 3, isotherms for LiCl reacting with gels calcined at various temperatures, thus varying both water content and surface area. In Figure 4, the points and dashed curves are for similar experiments, except that the solvent used contained ~ 0.2 vol % H₂O; for reference, the curves of Figure 3 are included. In Figure 5, the effect of water in the initial solution is given for LiCl solutions of three different initial salt concentrations. The change in the water content of the salt solutions (and also of solutions containing no salt) was measured, and the results are given in Table II.

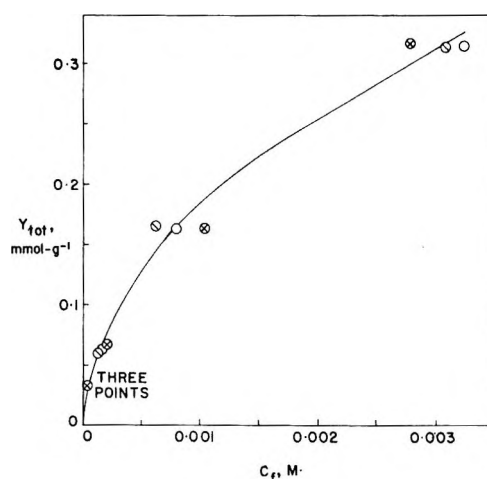


Figure 2. LiCl adsorption for various equilibration times: O, 9 days; ⊖, 15 days; ⊗, 80 days. All three times at the one place so indicated. The initial solution contained 0.2% H₂O.

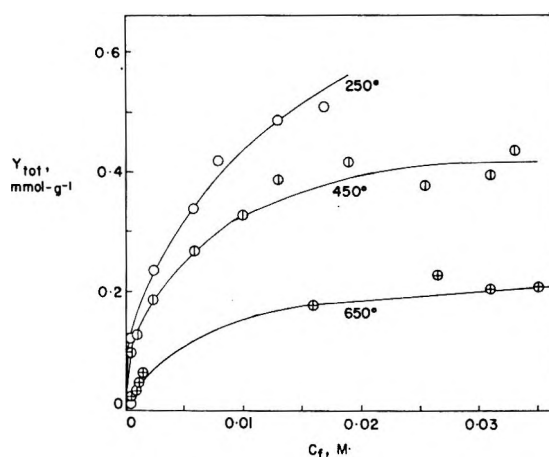


Figure 3. LiCl adsorption by gels calcined at various temperatures: O, 250°; ⊖, 450°; ⊕, 650°.

In Figure 6, there is an isotherm comparison of LiCl, LiNO₃, and NaI, all in acetone containing ~ 0.2 vol % H₂O.

Two experimental approaches to determine whether the reaction in acetone is exchange or addition were used. In Figure 7, the absence of an effect of varying V/W on the LiCl isotherm indicates the reaction involves the two ions in equivalent amounts. (See Methods.) Where equivalent reaction is the same as addition, the Langmuir plot should be linear. Linear plots are seen in Figure 8. A summary of the Langmuir constants (including those for curves not shown) is given in Table III. There are also given, in Table III, the y_{tot} values (read from the isotherms) at $c_i = 2 \times 10^{-4}M$, thus permitting a direct comparison between systems by the "initial slope" method.¹⁵

Proof that LiCl and LiNO₃ can be removed from acetone by the use of a silica gel adsorption column is

(15) Reference 5, p 579.

Table II: Silica Gel Adsorption of Water from LiCl-H₂O-Acetone Solutions^a

Initial vol % H ₂ O	c_i , LiCl							
	0.00 M		0.01 M		0.02 M		0.04 M	
	Eq H ₂ O ^b	ν^c H ₂ O	Eq H ₂ O ^b	ν^c H ₂ O	Eq H ₂ O ^b	ν^c H ₂ O	Eq H ₂ O ^b	ν^c H ₂ O
0.5	0.20	3.3	0.20	3.3	0.10	4.4
1.0	0.6	3.7	0.50	5.5	0.40	6.7	0.40	6.7
2.0	1.3	6.5	1.0	11	1.0	11	0.90	12
5.0	3.6	13	3.4	18	3.3	19	3.1	21

^a 20-ml solution mixed with 10 or 12 g of gel calcined at 450°. (Not shown: with no water in initial solution, none appears in equilibrium solution.) For the amount of salt reaction in these experiments, see Figure 5. ^b Volume % H₂O in equilibrium solution.

^c In mmole of H₂O adsorbed per gram of gel, calculated on basis of difference between initial and final water concentrations.

Table III: Salt-Gel Adsorption Constants

Salt	Treat- ment, ^a °C	Water, vol % ^b	Site density mmole g ⁻¹ ^c	K , M ⁻¹ ^d	ν , mmole g ⁻¹ ^e
LiNO ₃	450	0.2	0.28	12	<i>f</i>
NaI	450	0.2	0.19	11	<i>f</i>
LiCl	450	0.2	0.50	610	6.0×10^{-2}
LiCl	650	0.2	0.36	290	2.7×10^{-2}
LiCl	250	0	0.62	290	8.0×10^{-2}
LiCl	450	0	0.48	260	4.6×10^{-2}
LiCl	650	0	0.23	370	1.4×10^{-2}

^a Temperature at which gel was calcined. ^b Water in solvent initially. ^c Determined from Langmuir plot; $\pm 10\%$ estimated error. ^d Equilibrium constant for salt adsorption, determined from Langmuir plot; $\pm 10\%$ estimated error. ^e Amount of salt adsorbed at $c_i = 2 \times 10^{-4}$ M. ^f Too small to measure; see Figure 6.

given by the elution curves of Figure 9. The Figure also shows there is no salt adsorption when isoamyl, *n*-butyl, or *n*-propyl alcohol is the solvent.

Discussion

The Water Effect. The solution and the surface compete for water, even when the surface is the source of the water. Increasing the calcination temperature decreases the amount of water in the gel¹⁶ and, therefore, it also decreases the amount of water in the equilibrium system. In Figures 3 and 4, it is shown that the amount of reaction also decreases with increased calcining temperature or addition of a small amount of water to the system. (The decrease in surface area as the calcining temperature is increased (see Experimental) is much smaller than the decrease in the amount of reaction.) With water added to the initial solution, there is a maximum in the amount of reaction at ~ 2 vol % H₂O (Figure 4). (Adsorption by gels calcined above the standard temperature, 450°, would have to be shown in Figure 5 as a function of *negative* added water values.)

The site densities, in Table III, suggest that a factor contributing to the greater amount of reaction at the

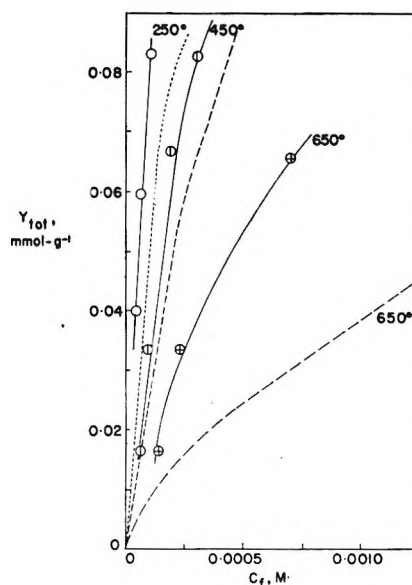


Figure 4. LiCl adsorption by gels calcined at various temperatures. Experimental points and solid curves for solvent with 0.2% H₂O initially: O, 250°; ⊕, 450°; ⊗, 650°. Dashed curves for anhydrous solution, taken from Figure 3.

higher water levels (still in the low-water concentration range) is the increased number of sites. In related experiments, it has been shown that the amount of CH₃OH vapor^{17a,b} or methyl red in benzene solution^{17c} which adsorbs on silica gel increases with increasing water content of the gel.

Adsorption, Not Exchange. In the Results, it was shown that cation and anion react in equivalent amounts. Equivalent exchange of cation and anion cannot, however, be distinguished from adsorption (*i.e.*, addition) when the exchange products are initially present in excess. (See Methods.) This occurs when H⁺ and OH⁻ are the exchange products and water is the solvent. In the salt-acetone-silica gel experiments,

(16) R. K. Iler, "The Colloid Chemistry of Silica and Silicates," Cornell University Press, Ithaca, N. Y., 1955, pp 236, 237.

(17) (a) L. G. Ganichenko, V. F. Kiselev, and K. G. Krasil'nikov, *Dokl. Akad. Nauk SSSR*, **125**, 1277 (1959); (b) M. M. Egorov, T. S. Egorova, V. F. Kiselev, and K. G. Krasil'nikov, *Vestn. Mosk. Univ. Ser. Mat. Mekh., Astron., Fiz., Khim.*, **13**, 203 (1958); (c) ref 16, p 238.

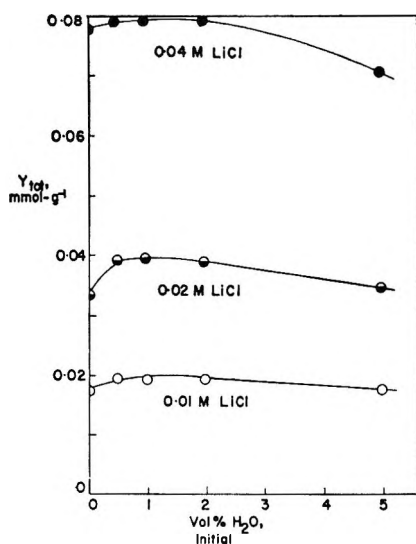


Figure 5. LiCl adsorption as a function of initial water composition of the solution. $V/W = 2.0 \text{ ml g}^{-1}$; salt molarities of initial solutions indicated on curves. For water uptake in same experiments, see Table II.

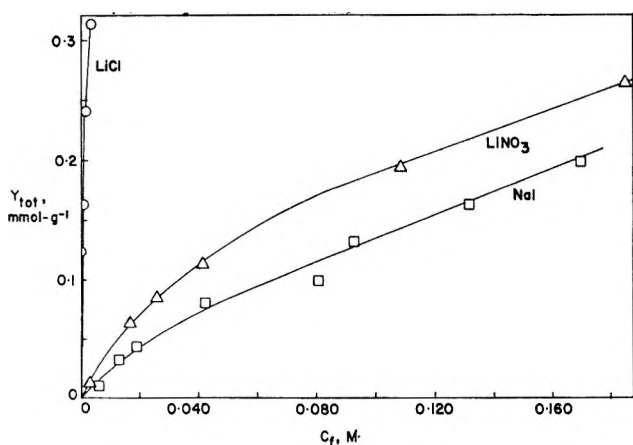
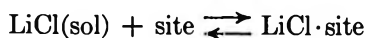


Figure 6. LiCl, LiNO_3 , and NaI adsorption; initial solution contained 0.2 vol % H_2O .

the solvent cannot be produced by any combination of exchange products, and we deduce that the salt-surface reaction is a true addition reaction. This is an unusual example of salt addition (as contrasted with exchange) to a surface as noncrystalline as silica gel. There is some question, for example, as to whether the reported addition of silver salts to various oxide surfaces is actually an example of equivalent exchange.⁷

Further Remarks. The distribution of LiCl between the gel and liquid phases depends upon the stabilities and concentrations of the species in the reaction (where (sol) refers to the solution)



a reaction formally similar to molecule-gel-liquid systems. Thus, Puri, *et al.*, showed that fatty acid adsorption by silica gel from toluene solution increases as the moisture content of the gel increases, and that the

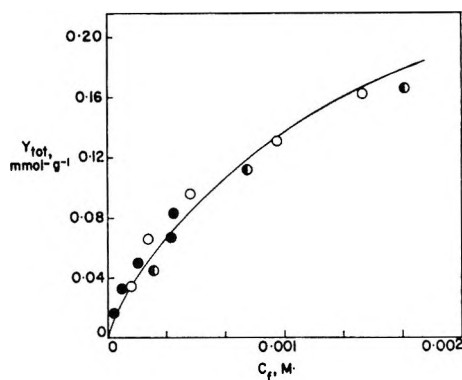


Figure 7. LiCl adsorption at various values of V/W . ●, $V/W = 1.67 \text{ ml g}^{-1}$; ○, $V/W = 3.33 \text{ ml g}^{-1}$; ◐, $V/W = 5.83 \text{ ml g}^{-1}$.

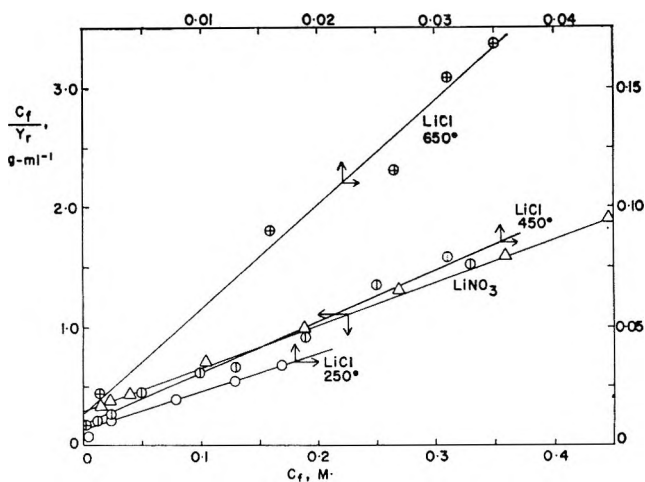


Figure 8. Langmuir plots: ○, LiCl, 250° gel; ◐, LiCl, 450° gel; ●, LiCl, 650° gel; Δ, LiNO_3 , 0.2 vol % H_2O , 450° gel.

adsorption is greater if the acid is more soluble in water.¹⁸ The chief complicating factor in the salt experiments is that changing the water content of the system alters the surface in a different way at low water concentration than at high concentration. The LiCl solubility experiment (with a minimum in solubility between 1.0 and 4.7 vol % H_2O) probably indicates that varying the water content of the solution also changes the affinity of LiCl for the solution phase in a different way at low water concentration than at high. Several additional observations are made. (1) The adsorption sites are polar and probably distinct. Discussion: If the Langmuir conditions are met, as they seem to be (Figure 8), the sites are distinct. Since ions adsorb, the sites are polar. For the largest maximum in an adsorption isotherm (LiCl, 250° gel) there are 8×10^{13} sites cm^{-2} , which are $\sim 35 \text{ \AA}$ apart, if they are distributed uniformly over the surface. For comparison, Iler¹⁶ shows that the silica gel surface contains *ca.* 80×10^{13} bound hydroxyls per cm^2 when saturated

(18) B. R. Puri, R. K. Sud, and M. L. Lakhanpal, *J. Indian Chem. Soc.*, **31**, 612 (1954).

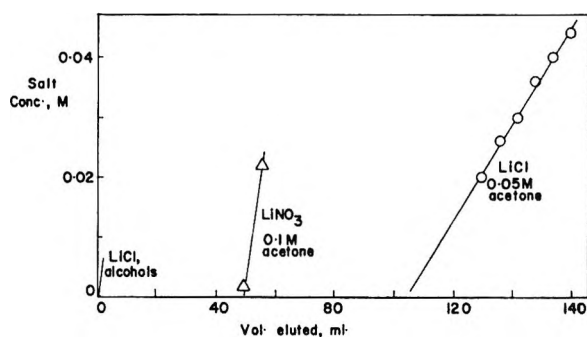


Figure 9. Elution curves. Salt (with initial concentration) and solvent: curve at left is 0.05 *M* LiCl in *n*-butyl, *n*-propyl, and isoamyl alcohols; Δ , 0.1 *M* LiNO₃ in 0.2 vol % H₂O in acetone; \circ , 0.05 *M* LiCl in 0.2 vol % H₂O in acetone.

and $40\text{--}60 \times 10^{13}$ bound hydroxyls per cm² when calcined at 300–600°. Therefore, the reactive site of interest in the present work could be a certain fraction of the bound hydroxyls. Recently, Snyder and Ward discovered a new kind of reactive site on the gel surface;¹⁹ while these need not be the same sites as those upon which ions adsorb, the fact of their recent discovery suggests there may be other sets of heretofore unknown sites. (2) The adsorption order is, with the strongest adsorption first, alcohol > salt ion(s) > acetone. Discussion: When the solvent is alcohol, salt adsorption was not detected in the silica gel columns nor was reaction detected in the earlier work when C₂H₅OH and CH₃OH were the solvents.³ If one salt ion is the primary adsorbate, the ion of opposite charge also adsorbs to preserve electrical neutrality.

Simultaneous adsorption of cation and anion is much more likely, however. The dielectric constant of acetone is 20.7 (at 25°) and salts of the type used are less than 30% dissociated in 0.1 *M* solution in acetone.²⁰ Thus in the lowest concentrations used ($\sim 1 \times 10^{-4}$ *M*) the salts were largely dissociated; in the highest (~ 0.4 *M*), associated. Addition of ions, one at a time, is improbable in the associated high-concentration solutions. Since the low concentration and high concentration solutions behaved similarly, we suggest that simultaneous adsorption is probable over the whole concentration range studied. There is also appreciable association in some of the alcohol solutions; such association would not be a factor, since there is no doubt that the polar alcohol molecules adsorb on the gel surface. (3) At equilibrium LiCl(sol) and the surface compete

for water. Discussion: The data of Table I indicate that some of the water reacts either with the surface or with the LiCl-site complex. The amount of water (on a molar basis) which adsorbs is from 5 to 35 times the maximum number of sites recorded in Table II. Also, salt adsorption apparently enhances water adsorption. (4) Above ~ 2 vol % H₂O, adsorption of salt diminishes because water affects both LiCl(sol) and the sites of reaction 1. Discussion: Li⁺ is a structure former in water, and the LiCl solutions are therefore stabilized by the addition of enough water. Even though LiCl adsorption brings water to the surface (Table I), appreciable energy to dehydrate Li⁺ partially is probably needed for adsorption to occur. Furthermore, addition of water to the surface hydrolyzes the Si–O–Si bond; in this concentration range, water may destroy sites by hydrolysis or addition onto previously existing sites. In 100% water, salts of the type studied here do not detectably adsorb (*i.e.*, add), although there is slight ion exchange.² (5) Even though in dilute solution the least soluble molecules tend to adsorb most,²¹ the situation is more complex in the salt–acetone–silica gel system. Discussion: At 22° the solubilities of LiCl and NaI in acetone are, respectively, 0.62 and 0.16 *m*,²² the same as the order of reactivities. To expect more adsorption with lower solubility is an oversimplification, since the individual stabilities of the salt crystals must be considered. This is more of a problem than it is with molecule deposition, since the energies of molecular crystals are much smaller than the energies of salt crystals.

While we have not described the nature of the surface complex formed, we have described a reversible addition reaction of salt ions to the gel surface; we have also given evidence which suggests the same surface complex involves the anion, the cation, and some of the surface hydroxyls.

Acknowledgments. We acknowledge with appreciation the preliminary work of Mr. John Daniel and the surface area measurements of Mr. Arlyn Schaap.

(19) L. R. Snyder and J. W. Ward, *J. Phys. Chem.*, **70**, 3941 (1966).

(20) R. A. Robinson and R. H. Stokes, "Electrolyte Solutions," Butterworth and Co., Ltd., London, 1959, p 550.

(21) R. S. Hansen and R. P. Craig, *J. Phys. Chem.*, **58**, 211 (1954).

(22) See J. W. Mellor "A Comprehensive Treatise on Inorganic and Theoretical Chemistry," Vol. II, John Wiley and Sons, Inc., New York, N.Y., pp 543, 606.

Electrolytes in High Surface Area Systems. II. The Reaction between Aqueous Dichromate and Silica Gel^{1a}

by Russell W. Maatman^{1b} and Allan Kramer

Department of Chemistry, Dordt College, Sioux Center, Iowa 51250 (Received May 12, 1967)

Aqueous solutions of the heavier alkali metal dichromates react reversibly with the surface of silica gel. The amount of reaction is increased when the solution is 2–6 *M* with respect to H_2SO_4 . With the acid solutions, the amount of reaction is the same for all five alkali metal dichromates. With both the acidic and nonacidic systems, the reaction has been shown to be either adsorption or equivalent exchange of cation and anion. While there is more reaction with acid present than without acid added, the order of increasing amounts of reaction at low concentration of dichromate salt is $6\text{ M} < 4\text{ M} < 2\text{ M H}_2\text{SO}_4$. At high concentrations of dichromate salt, the order is reversed. These facts are shown to be consistent with a reaction scheme in which $\text{Cr}_2\text{O}_7^{2-}$ adds to a surface site produced by reaction of H^+ with the surface. In this scheme, increasing acid concentration produces more sites but it also removes reactive $\text{Cr}_2\text{O}_7^{2-}$ to form HCr_2O_7^- and $\text{H}_2\text{Cr}_2\text{O}_7$. The dependence of the nonacidic solution reaction upon the nature of the cation may arise from the greater tendency of the higher atomic number alkali metal ions to form ion pairs in certain systems and from a smaller solution stability of the dichromate salts of the same alkali metals.

Introduction

While studying the behavior of solute ions in the pores of high surface area oxides, we noted that under certain conditions aqueous dichromate reacts slightly with the surface of silica gel.

Others have reported reactions between oxy molecules or ions of Cr(VI) and silica or silica gel. For example, chromic acid–silanol and siloxanol esters have been made.² Dibbs showed that H_2SO_4 – $\text{Na}_2\text{Cr}_2\text{O}_7$ mixtures deposit on quartz a Cr-containing material not removed with water.³ In a dried CrO_3 –silica gel mixture, prepared by heating gel previously impregnated with chromic acid, CrO_3 bonds weakly to the surface.⁴ Iler found the chromate ion to be unique among inorganic anions in its ability to retard the gelling rate of silica gel, probably because of the formation of a silicochromic acid.⁵ Oxidation of a silica surface by permanganate⁶ suggests acidic dichromate solutions might also oxidize the surface. The reaction of the aqueous ion with the preformed gel which we observed, eventually shown to be reversible, differs from all these in one or more respects, and the reactions observed by others differ from each other as well. Yet there seems to be a basic tendency for oxy ions and/or molecules of Si and Cr to react, and the cited reactions probably all depend upon this basic tendency.

While cations exchange with the weakly acidic hydrogen of the surface silanol groups of the gel,⁷ the possibility of anion reaction with the surface by addition

to the protonated hydroxyl of the surface silanol group has been questioned.⁸ Anion reaction has been ascribed to known impurities.⁹ No anion reaction with the surface was found with aqueous HI, H_2SO_4 , and H_3PO_4 ,¹⁰ or with chloride and nitrate salts.¹¹ At very low concentrations, however, in electrokinetic experiments, several of the common anions are preferentially adsorbed by the silica surface.¹² At very high pH's silica gel adsorbs OH^- .¹³

(1) (a) This work was partially supported by Atomic Energy Commission Contract AT (11-1)-1354. Acknowledgment is made to the donors of The Petroleum Research Fund, administered by the American Chemical Society, for partial support of this research. (b) Correspondence should be sent to this author.

(2) C. R. Hare, University Microfilms, Library of Congress Card No., Microfilm, 61-2695.

(3) H. P. Dibbs, *Can. J. Chem.*, **40**, 565 (1962).

(4) J. Deren and J. Haber, *Bull. Acad. Polon. Sci., Ser. Sci. Chim.*, **12**, 663 (1964).

(5) R. K. Iler, *J. Phys. Chem.*, **56**, 678 (1952).

(6) E. D. Richardson and C. D. Poncher, *Research*, **11**, 247 (1959).

(7) D. L. Dugger, J. H. Stanton, B. N. Irby, B. L. McConnell, W. W. Cummings, and R. W. Maatman, *J. Phys. Chem.*, **68**, 757 (1964).

(8) S. Ahrland, I. Grenthe, and B. Noren, *Acta Chem. Scand.*, **14**, 1059 (1960).

(9) F. Umland and K. Kirchner, *Z. Anorg. Allgem. Chem.*, **280**, 211 (1955).

(10) D. N. Strazhesko and G. F. Yankovskaya, *Ukr. Khim. Zh.*, **25**, 471 (1959).

(11) (a) J. Stanton and R. W. Maatman, *J. Colloid Sci.*, **18**, 878 (1963); (b) B. L. McConnell and R. W. Maatman, *J. Miss. Acad. Sci.*, **9**, 81 (1963).

Experimental Section

Materials. The silica gel is the acid-washed and calcined (2 hr in air at 450°) gel, surface area of 445 m² g⁻¹ (BET), used in the earlier work.¹⁴ Rb₂Cr₂O₇ and Cs₂Cr₂O₇, supplied by K & K Laboratories, were used as received. The other materials were of reagent grade.

Procedure. Salt solution (*V* ml) of concentration *c_i* was mixed with *W* g of gel (usually *V/W* was 2.08 ml/g) and after 3–5 days at room temperature (22 ± 3°), an aliquot of the solution contacting the gel was analyzed iodometrically to determine *c_t*, the dichromate concentration. In some experiments the initial solution was 2–6 *M* with respect to H₂SO₄. This concentration is high enough so that the initial and equilibrated solutions are of almost the same acidity. The acid solutions were of the same yellow color as the non-acid solutions. The amount of salt taken into the pores per gram of gel, *y_{tot}*, is given by

$$y_{\text{tot}} = \frac{c_i V - c_t (V - WP)}{W}$$

where *c_i* is the concentration of the solution used with the gel of *P* ml g⁻¹ pore volume.

pH's were measured on a Beckman GS pH meter. In a typical case, a solution of 0.0475 *M* Cs₂Cr₂O₇ of pH 4.26 became 0.0366 *M* upon equilibration, with a pH of 3.72. Since this pH change is small and about what one would expect with the small amount of cation exchange there is in these systems, and therefore not of interest here, no other pH's are reported.

Several gel samples, which had been equilibrated with either acidified or unacidified dichromate, were washed extensively with the same solution, lacking only the dichromate salt. By washing, the yellow tint disappeared, indicating that the dichromate was removed.

Results and Discussion

Reversibility and the Nature of the Reaction. The data of Table I show that dichromate uptake at various acidities is not a function of time, even though the maximum on the reaction isotherm (see below) is not achieved at the concentrations used. Thus the gel reaction with dichromate is reversible, using the criterion discussed earlier.¹⁵ The data of Table II show that the amount of reaction (for the determination of *y_r*, the amount of reaction, see below) does not depend upon *V/W* at virtually constant *c_t*. Thus the reaction is either equivalent exchange or adsorption, but not nonequivalent exchange, according to the criterion of part I.¹⁴ The absence of a significant pH change in the nonacidic systems (see Experimental Section) is consistent with the conclusion that the reaction is either equivalent exchange or adsorption.

The Isotherms. To determine the amount of dichromate in the pores which reacts with the surface,

Table I: Effect of Time on Dichromate Uptake^a

H ₂ SO ₄ concn	Equil time, days	<i>y_{tot}</i> , mmole g ⁻¹
0 <i>M</i> ^b	2	0.0197
	3	0.0175
	4	0.0178
	5	0.0187
	7	0.0187
4 <i>M</i> ^c	3	0.106
	6	0.113
	10	0.106
6 <i>M</i> ^d	3	0.117
	6	0.117
	10	0.112

^a 25 ml of K₂Cr₂O₇ mixed with 12 g of gel. ^b *c_t* = 0.0254–0.0267 *M*. ^c *c_t* = 0.178–0.183 *M*. ^d *c_t* = 0.177–0.179 *M*.

Table II: Effect of *V/W* on Dichromate Uptake

	<i>V/W</i> , ml g ⁻¹	<i>c_t</i> , <i>M</i>	<i>y_r</i> , mmole g ⁻¹
Nonacid ^a	2.08	0.0234	0.0143
	2.50	0.0248	0.0136
	3.13	0.0251	0.0161
	4.17	0.0270	0.0137
	6.25	0.0280	0.0139
4 <i>M</i> H ₂ SO ₄ ^b	2.08	0.180	0.0382
	2.92	0.186	0.0367
	3.75	0.189	0.0381
	4.58	0.189	0.0443
	5.42	0.191	0.0432
	6.25	0.193	0.0362

^a 25 ml of 0.0303 *M* Cs₂Cr₂O₇ mixed with varying amounts of gel; the points lie on the Cs₂Cr₂O₇ curve of Figure 1. ^b 12 g of gel mixed with varying amounts of 0.199 *M* K₂Cr₂O₇.

y_r, as contrasted with the dichromate dissolved in the pore volume liquid, *y_{tot}* is diminished by *c_tP* to produce the isotherms of Figures 1 and 2; this procedure assumes¹⁶ that the high-concentration increment in *y_{tot}* (with increasing *c_i*) is due entirely to unreacted salt in the pores. Since there is a plateau in two of the resulting isotherms (for the nonacid systems), the assumption is justified. (In alkaline solution, CrO₄²⁻ is partially excluded from the surface region of animal

(12) (a) D. J. O'Connor and A. S. Buchanan, *Trans. Faraday Soc.*, **52**, 397 (1956); (b) D. P. Benton and G. A. H. Elton, *ibid.*, **49**, 1213 (1953).

(13) W. M. Heston, R. K. Iler, and G. W. Sears, *J. Phys. Chem.*, **64**, 147 (1960).

(14) R. W. Maatman, A. Geertsema, H. Verhage, G. Baas, and M. Du Mez, *ibid.*, **72**, 97 (1968).

(15) K. C. Williams, J. L. Daniel, W. J. Thomson, R. I. Kaplan, and R. W. Maatman, *ibid.*, **69**, 250 (1965).

(16) D. Ledebor, E. Post, W. Bruxvoort, R. De Jong, and R. Maatman, *J. Catalysis*, **4**, 480 (1965).

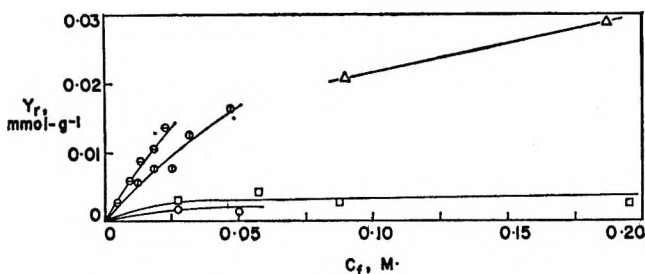


Figure 1. Isotherms for reacted dichromate, no added acid: \ominus , Cs^+ ; \oplus , Rb^+ ; Δ , K^+ ; \square , Na^+ ; \circ , Li^+ .

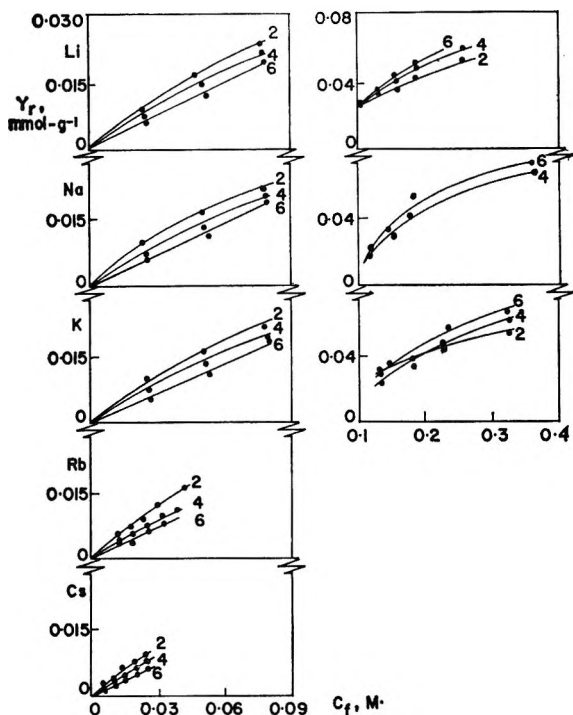


Figure 2. Isotherms for reacted dichromate for indicated salts; numbers on curves indicate initial H_2SO_4 molarity. Note that ordinates are contracted for curves at right.

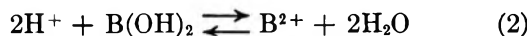
charcoal,¹⁷ there are several other pairs of ions where the smaller unhydrated ion, with its higher charge density, tends to hydrate more and therefore is excluded more from the surface region.^{7,18} At high concentrations the scatter is large in both Figures 1 and 2 because y_r is determined by finding the difference between two relatively large quantities.

Chromium Species Present. Since there are several aqueous Cr(VI) species, it is necessary to specify which species are present. With aqueous $\text{K}_2\text{Cr}_2\text{O}_7$ there is virtually no hydrolysis¹⁹ and in its spectrum only $\text{Cr}_2\text{O}_7^{2-}$ is seen.²⁰ In dichromate solution, evidence of the trichromate and tetrachromate ($\text{Cr}_3\text{O}_{10}^{2-}$ and $\text{Cr}_4\text{O}_{13}^{2-}$) could not be found.¹⁹ We therefore assume for our nonacid solutions that chromium is present only as $\text{Cr}_2\text{O}_7^{2-}$.

At very high acidities it is possible to condense the dichromate to form the trichromate and tetrachro-

mate.²¹ The high concentrations of Cr(VI) ²² and acid²¹ needed for condensation were not achieved in our systems; this conclusion was confirmed by the lack of the characteristic dark red or brown colors associated with the higher chromates. Dichromate can add one²³ or two²⁴ protons, and we therefore conclude that in our acid solutions $\text{Cr}_2\text{O}_7^{2-}$, HCr_2O_7^- , and $\text{H}_2\text{Cr}_2\text{O}_7$ may be present.

Proposed Reaction Schemes. The following reaction scheme is suggested for the acid systems.



(The effect of $\text{H}_2\text{Cr}_2\text{O}_7$ formation is considered separately below.) B(OH)_2 represents a certain group of surface sites. For our purpose, an equivalent alternative is the modification of reactions 2 and 3 so that there is no water produced in reaction 2, in which case B'H_2^{2+} is the site produced in reaction 2 and used in reaction 3. In any event, the number of reaction sites is small (from Figure 2, the largest amount of reaction was at $c_f = 0.7 \text{ M}$, 6 M acid, where y_r was $0.14 \text{ mmole g}^{-1}$, or $1.9 \times 10^{13} \text{ sites cm}^{-2}$) and they are seen only under unusual circumstances; consequently, they may have been overlooked earlier.

The suggested scheme is consistent with several observations. First, at constant acidity the amount of dichromate reaction does not depend upon which metal cation is present: the isotherms (Figure 2) for the various salts at the same acidity are superimposable, except that there is an inevitable scatter at high c_f , as mentioned above. Second, dichromate reaction with the surface is either addition or there is an equivalent amount of cation and anion exchange. In the proposed reaction scheme, the large excess of acid (compared to the dichromate concentration) which we used provides the sites so that reaction 3 is the dichromate addition reaction which was observed. Third, the scheme suggests that if reaction 2 is important, there ought to be more reaction with acid than without acid, as is actually seen.

The quantitative effect of the acid is more complicated, since increasing acidity has opposite effects on the concentrations of the two reactants of reaction 3.

(17) J. W. Mellor, "A Comprehensive Treatise on Inorganic and Theoretical Chemistry," Vol. XI, John Wiley and Sons, Inc., New York, N. Y., 1962, p 338.

(18) R. W. Dalton, J. L. McClanahan, and R. W. Maatman, *J. Colloid Sci.*, **17**, 207 (1962).

(19) Reference 17, p 222.

(20) E. Viterbi and G. Krausz, *Gazz. Chim. Ital.*, **57**, 690 (1927).

(21) Reference 17, pp 349-352.

(22) Reference 17, p 219.

(23) (a) E. Spitalsky, *Z. Anorg. Chem.*, **54**, 265 (1907); (b) K. Beck and P. Stegmüller, *Arch. kaiser. Gesundh.*, **34**, 446 (1910).

(24) Reference 17, p 214.

Figure 2 illustrates this complexity; at low c_t , reactivity diminishes with increased acidity, while the order is reversed at high c_t . To explain the acid effect, reaction 1 is considered in more detail. For the equilibrium solution we can write

$$K = \frac{[\text{HCr}_2\text{O}_7^-]}{[\text{H}^+][\text{Cr}_2\text{O}_7^{2-}]} = \frac{[\text{HCr}_2\text{O}_7^-]}{[\text{H}^+]\{c_t - [\text{HCr}_2\text{O}_7^-]\}} \quad (4)$$

where K is the equilibrium quotient. Rearranging

$$\frac{[\text{Cr}_2\text{O}_7^{2-}]}{c_t} = \frac{1}{K[\text{H}^+] + 1} \quad (5)$$

K , the equilibrium quotient, would be expected to be large at all acidities, since the equilibrium constant for reaction 1 is 1×10^3 .²³ Therefore, in spite of the nonideality of these solutions at 2–6 M H_2SO_4 , $K[\text{H}^+] \gg 1$ in that acid range. We use eq 5 only to show that the fraction of chromium in solution which is in the form of free $\text{Cr}_2\text{O}_7^{2-}$ is (with the qualification noted below) *approximately* inversely proportional to the acidity and, at any one acidity, independent of c_t . The nonideality of these solutions prevents making more than this approximation, but for our purposes we need no more.

To make a meaningful comparison between the acid isotherms of Figure 2, y_r at equal concentrations of free dichromate should be compared. Figure 3 is thus constructed using the approximation derived from eq 5. In this figure, y_r is shown as a function of free $\text{Cr}_2\text{O}_7^{2-}$. The absolute amount of free $\text{Cr}_2\text{O}_7^{2-}$ is not known, and therefore the abscissa scale is arbitrary; comparisons at constant acidity are made by assuming (eq 5) that the concentration of free $\text{Cr}_2\text{O}_7^{2-}$ is proportional to c_t . The 2 M isotherm is assigned the same shape it has in Figure 2 (where the isotherms of a given acidity are identical); to compare isotherms of different acidities the 4 M and 6 M isotherm abscissas are changed. For the 4 M isotherm of Figure 3, the abscissa of each point is one-half its value in Figure 2, and for the 6 M isotherm the abscissa of each point is contracted to one-third its Figure 2 value. Thus, by assuming that the concentration of free $\text{Cr}_2\text{O}_7^{2-}$ at constant c_t is inversely proportional to $[\text{H}^+]$, the three acid isotherms are put on a comparable basis. (Using the factors 2 and 3 for contraction stems from the assumption that $[\text{H}^+]$ in the 2, 4, and 6 M solutions varies in the ratio 1:2:3. The assumption is in error to the extent that equilibria involving HSO_4^- , HCr_2O_7^- , etc., are not constant in the 2–6 M acid range. The conclusion, however, does not depend upon the exact value of the ratio.)

We are thus able to see that at any value of free $\text{Cr}_2\text{O}_7^{2-}$, y_r increases with acidity; the complicated matter of isotherm-crossing in Figure 2 is thus accounted for. By considering reactions 2 and 3 alone, one would indeed expect that increasing acidity would

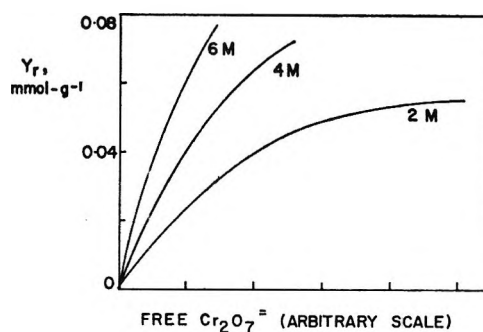
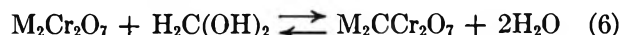


Figure 3. Reacted dichromate as a function of free dichromate. H_2SO_4 concentrations on curves. See text.

increase the amount of reaction. (To the extent that HCr_2O_7^- reacts to form $\text{H}_2\text{Cr}_2\text{O}_7$, $[\text{H}^+]$ in eq 5 approaches $[\text{H}^+]^2$, bringing about an even larger spread in the curves of Figure 3.) This analysis indicates increasing acidity, for a fixed concentration of free $\text{Cr}_2\text{O}_7^{2-}$ increases the amount of reaction if $\text{B}(\text{OH})_2$ (or B') were a fixed group of sites. Yet the isotherm shapes in Figure 2 or 3 suggest that at the higher acidities the site density may increase. The hydrated surface is known to be heterogeneous, with hydroxyl groups attached to Si, and it is possible that the number of releasable hydroxyl groups (or the number of sites which can receive protons) increases as the acidity increases.

If there is a small amount of reaction at even high acid concentration, much less reaction of dichromate with the surface would be expected in the nonacidic systems. This is verified by comparing Figures 1 and 2. For nonacidic systems the reaction suggested is equivalent anion-cation exchange



where C is a site containing ionizable OH^- and H^+ ; presumably H^+ is part of surface hydroxyls. An equally likely reaction, and one apparently not distinguishable from reaction 6, is salt adsorption on site C' , without the elimination of water. If reaction 6 is correct, these sites could well be within the group designated by $\text{B}(\text{OH})_2$ in reaction 2: the presence of large amounts of acid in the system would then render reaction 6 of negligible importance. The dependence of the isotherm upon the nature of the metal ion is expected if reaction 6 (or its adsorption equivalent, using C') is correct.

With respect to the increasing tendency for reaction with the dichromates of the higher atomic number alkali metals, it should be mentioned that there is some evidence for greater tendency for ion pairing with these alkali metals,^{11b} and it is possible that the surface complex is stabilized by ion pairing with the metal ion. Another factor may be a decrease in solution stability as the atomic number of the alkali metal increases. Alkali metal dichromate solubilities, which depend in

part upon the stabilities of the saturated solutions, do indeed decrease markedly as the atomic number of the alkali metal increases. The reported dichromate solubilities at 20° (in some cases interpolated or extrapolated from other temperatures) are, in molalities: Li⁺, 5.37;²⁵ Na⁺, 6.78; K⁺, 0.41; Rb⁺, 0.18;²³ Cs⁺, 0.060.²⁷

Work in progress includes a study of the behavior of electrolytes in systems containing high surface area carbonaceous materials.

Acknowledgments. The preliminary experimental work carried out by J. Daniel, A. Leenstra, D. Leenstra, and R. Blankespoor is acknowledged with thanks.

(25) W. H. Hartford and K. A. Lane, *J. Am. Chem. Soc.*, **70**, 647 (1948).

(26) Reference 17, p 339.

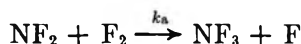
(27) S. M. Arkhipov, P. D. Komissarova, and N. A. Druz, *Zh. Neorg. Khim.*, **9**, 498 (1964).

Kinetics of the Reaction of Fluorine with Difluoramino Radicals and the Dissociation of Fluorine¹

by R. W. Diesen

Chemical Physics Research Laboratory, The Dow Chemical Company, Midland, Michigan 48640
(Received May 15, 1967)

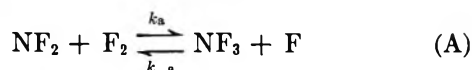
The rate of the exothermic free-radical reaction



has been directly determined by measuring the disappearance of molecular fluorine and the initial rate of NF₃ formation in the temperature range 1100–1600°K by means of a shock tube coupled to a TOF mass spectrometer. The Arrhenius expression $k_a = 4.8 \times 10^9 \exp(-14,400/RT) \text{ M}^{-1} \text{ sec}^{-1}$ is obtained for the rate constant which when extrapolated ($\sim 10^7$) to near room temperature is in reasonable agreement with the data (corrected) of Levy and Copeland² although the activation energy is ~ 5 kcal/mole higher. The dissociation of fluorine in neon was also studied in the temperature range 1400–2000°K where $k_F = 2.0 \times 10^{10} \exp(-35,000/RT) \text{ M}^{-1} \text{ sec}^{-1}$ is an Arrhenius fit to the data.

Introduction

The exothermic free radical abstraction reaction



represents an elementary reaction involving species important in the decomposition of the simple nitrogen-fluorine compounds. Levy and Copeland² have investigated the reaction of molecular fluorine with tetrafluorohydrazine near room temperature and deduced a value of k_a from the kinetic data in the temperature range 300–350°K (35–85°C) yielding a substantial activation energy of 9.6 kcal/mole. At higher temperatures, near 1800°K, Diesen³ presents data which suggest that k_a may be orders of magnitude higher than the extrapolated value of the room temperature data.

Reaction A can be essentially isolated in the temperature range 1100–1500°K and was studied in some detail as a continuing program of evaluating elementary reactions involving simple nitrogen-fluorine species.

The present results when coupled with the room temperature data represent a range of 10^8 in k_a . In addition, the rate constant for the dissociation of fluorine in neon is evaluated in the temperature interval 1400–2000°K, a range below that of ref 4.

Experimental Section

The shock tube-mass spectrometer apparatus and

(1) This work was sponsored by the U. S. Office of Naval Research under Contract No. Nonr 3814(00).

(2) J. B. Levy and B. K. W. Copeland, *J. Phys. Chem.*, **69**, 3700 (1965).

(3) R. W. Diesen, *J. Chem. Phys.*, **45**, 759 (1966).

operation have been previously reported.^{4,5} The shock wave serves to compressively heat the gas, and the reacting gas behind the reflected shock wave is continuously sampled by a 1-3-mil orifice and analyzed every 25 μ sec by a TOF mass spectrometer (0.5 μ sec electron-beam pulse). The individual spectra (75 v) are displayed on an oscilloscope and are recorded and resolved by a high-speed drum camera. The conditions of proper sampling and other important experimental considerations are treated in detail elsewhere.^{4,6}

Reaction mixtures were made from Matheson research grade neon and argon, DuPont tetrafluorohydrazine of 99+ % purity, and General Chemical fluorine of 99% purity. All mixtures reported are in mole % and all concentrations are in molar units (*M*), moles/liter. Argon was added at 0.25% to serve as an internal pressure standard.⁵

The reflected shock conditions were calculated from the Rankine-Hugoniot relations and the experimental shock velocities as previously described.⁵

Results and Discussion

Reaction A can be studied by following the time dependence of one or all of the species involved. Two procedures were used here to simplify the interpretation of the data.

Procedure I. Initial Rate of NF_3 Formation. The initial rate of NF_3 is conveniently measured experimentally, since the parent peak (*m/e* 71) can be directly measured with no interference in the mass spectrum and is a direct measure of reaction A as long as other processes involving NF_3 are unimportant. The rate expression

$$d(\text{NF}_3)/dt = k_a(\text{NF}_2)(\text{F}_2) + k_d(\text{NF}_2)(\text{Ne}) - k_6(\text{NF}_3)(\text{Ne}) - k_{-a}(\text{NF}_3)(\text{F})$$

for NF_3 formation is obtained where the first term is the reaction of interest, reaction A, the second term considers the known³ NF_3 formation from the thermal decomposition of NF_2 , with an effective rate constant k_d , the third term the thermal loss of NF_3 with a rate constant k_6 , and the last term the back reaction with fluorine atoms. For a sample containing 1 mole % of NF_2 and F_2 in neon, it is calculated from the data of ref 3 and the equilibrium constant⁷ for reaction A that for 10% reaction the correction terms to reaction A is less than 10% below 1500°K, as confirmed by "blank" runs with NF_2 or NF_3 in the absence of F_2 .

The data points for the time dependence of NF_3 formation for two runs are given in Figure 1. All of the calculated rate constants for reaction A are summarized in Figure 2 in terms of an Arrhenius plot, including the rate constants determined from the fluorine analysis.

Procedure II. First Order Disappearance of F_2 . The rate expression at the top of the next page

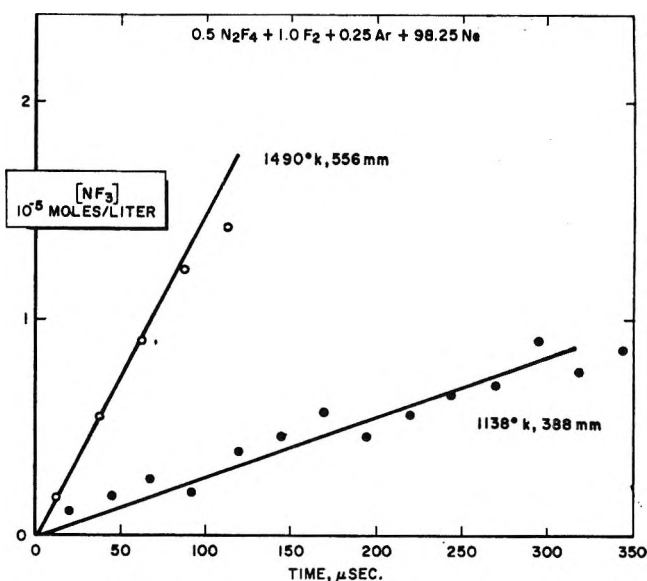


Figure 1. Time dependence of NF_3 formation for a reactant composition $1.0\text{F}_2 + 0.50\text{N}_2\text{F}_4 + 0.25\text{Ar} + 98.25\text{Ne}$. The temperatures and pressures indicated are for reflected shock conditions. For all practical purposes, the dissociation of N_2F_4 into NF_2 is instantaneous behind the reflected shock wave, i.e., $(\text{NF}_2)_0 = 2(\text{N}_2\text{F}_4)_0$.

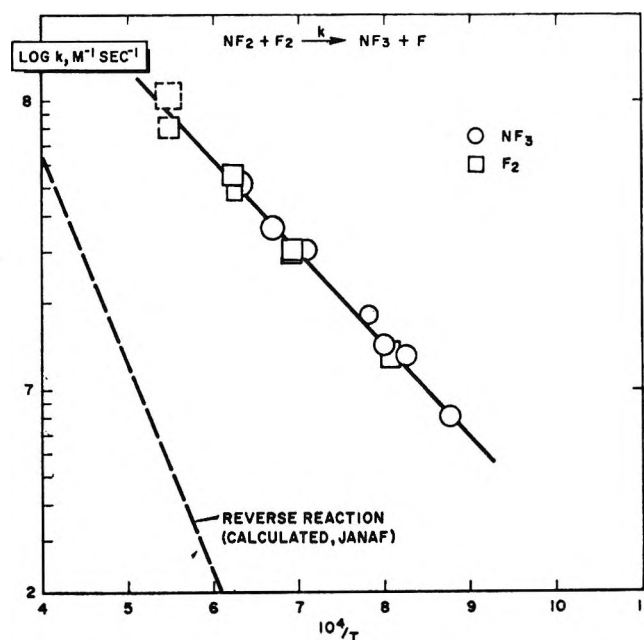


Figure 2. Arrhenius plot of k_a : O, results from NF_3 analysis; □, results from F_2 analysis. (Two highest values required large corrections and are considered less reliable.) Dashed line represents the value of k_{-a} calculated from the equilibrium constant, ref 7, and k_a is represented by the solid line.

(4) R. W. Diesen, *J. Chem. Phys.*, **44**, 3662 (1966).

(5) R. W. Diesen and W. J. Felmlee, *ibid.*, **39**, 2115 (1963).

(6) W. J. Felmlee, R. V. Petrella, and R. W. Diesen, "Mass Spectral Studies of Kinetics Behind Shock Waves: Direct Sampling and Flash Photolysis of NO_2 ," ONR Technical Report SL 175311a, The Dow Chemical Co., Midland, Mich., May 1966.

(7) "JANAF Thermochemical Tables," The Dow Chemical Co., Midland, Mich., Sept 1965.

$$-d \ln (F_2)/dt = k_a(NF_2) + k_{F_2}(Ne)$$

is derived for the first-order disappearance of F_2 , where the first term is the contribution of reaction A and the second term is the competing thermal dissociation process with a rate constant k_{F_2} . For an excess of NF_2 to F_2 , it is seen that a log plot of F_2 vs. time should be a straight line with a slope given by a sum of two constant (almost⁸) terms. The second term, the dissociation, becomes a significant term at higher temperatures and thus it was necessary to determine k_{F_2} in neon over the temperature range of interest. The logarithmic decay of F_2 , alone and in an excess of NF_2 , is shown in Figure 3. The calculated values^{9,10} of k_{F_2} in neon and k_a are shown in Figure 4 and Figure 2.

The Arrhenius expression

$$k_{F_2} = 2.0 \times 10^{10} \exp(-35,000/RT) M^{-1} \text{ sec}^{-1}$$

is calculated for the dissociation of F_2 in neon from the solid line in Figure 3. These results are in essential agreement with those of ref 4 in absolute value, but with a higher activation energy. It appears that the last two data points of ref 4 are systematically¹⁰ "high" by a factor of 2. It is also seen that the dissociation rate constant in argon reported by ref 11 is systematically higher by about a factor of 2. Considering the scatter of the results, the factor of 2 between neon and argon is in fair agreement with the value of 50% reported in ref 4 at higher temperatures near 2000°K.

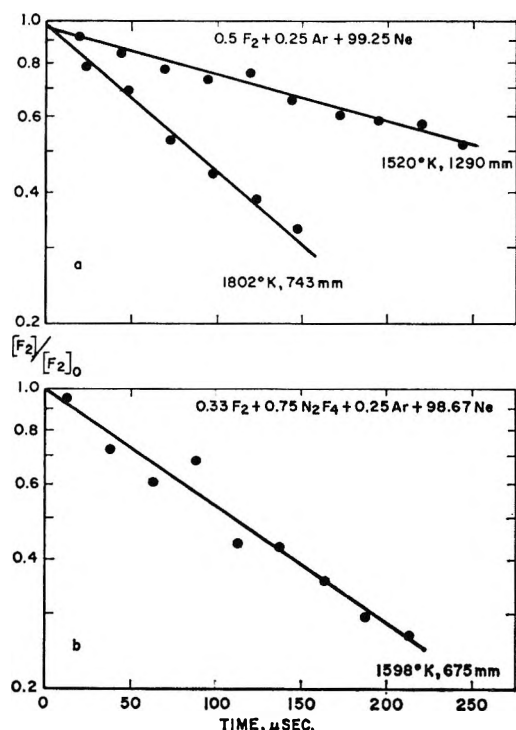


Figure 3. First-order decay of molecular fluorine ($[F_2]/[F_2]_0$, fraction of F_2 remaining): (a) $0.50F_2 + 0.25Ar + 99.25Ne$; (b) $0.33F_2 + 0.75N_2F_4 + 0.25Ar + 98.67Ne$ mole %.

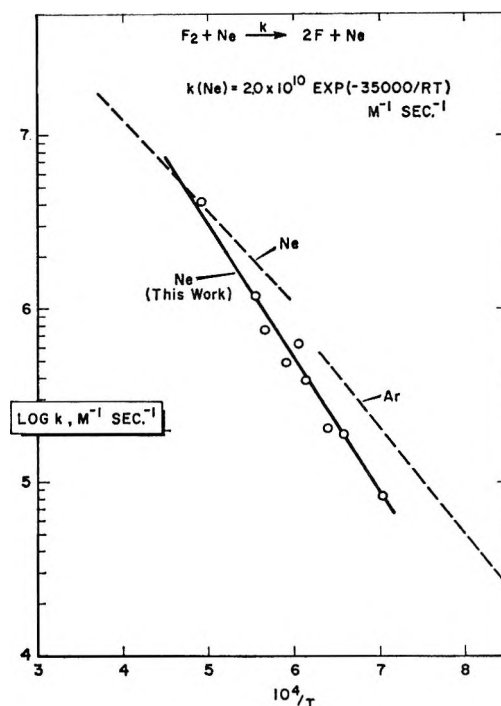


Figure 4. Arrhenius plot of the observed dissociation rate constant for fluorine. Solid line represents data of this work for 0.5% fluorine in neon and the dashed lines represent the data for ref 4 in neon and ref 11 in argon.

The solid line in Figure 2 yields

$$k_a = 4.8 \times 10^9 \exp(-14,400/RT) M^{-1} \text{ sec}^{-1}$$

The activation energy of 14.4 kcal/mole is significantly higher than the value of 9.7 reported by Levy and Copeland. As can be seen in Figure 5, an extrapolation of the present results to near room temperature is in reasonable agreement with the data of Levy and Copeland, when their results are corrected¹² downward by a factor of ~ 2.7 .

Considering the long extrapolation, the agreement (or disagreement) may be quite fortuitous. However, in spite of the relatively large uncertainty of $\sim 25\%$ in the absolute value of k_a of this work and the relative

(8) For complete reaction, (NF_2) varies between 1.5 and 1.23 mole %. To calculate k_a , (NF_2) is taken as constant at the average concentration of the amount of reaction for a given run. This leads to a limit of uncertainty of about 10% in k_a , which is partially compensated by the exothermicity of the reaction and is well within the estimated over-all uncertainty of $\sim 25\%$ (as contrasted to the average deviation of 6% of the data points from the Arrhenius fit).

(9) One data point at 1288°K was excluded and considered unreliable (see ref 10). At face value $k = 4.0 \times 10^4 M^{-1} \text{ sec}^{-1}$.

(10) These data points were deduced from relatively low-pressure experiments yielding small changes in slope and can be partially explained by a minor resolution change with time within the 15% uncertainty determined by direct experiment in ref 4.

(11) D. J. Seery and D. Britton, *J. Phys. Chem.*, **70**, 4074 (1966); the equation used is the revised "best" choice of four different equations for fluorine in argon. For previous equations see C. D. Johnson and D. Britton, *ibid.*, **68**, 3032 (1964).

(12) To be consistent with the data of L-C and of ref 7, the preexponential factor reported by L-C needs to be lowered by a factor of 2.7.

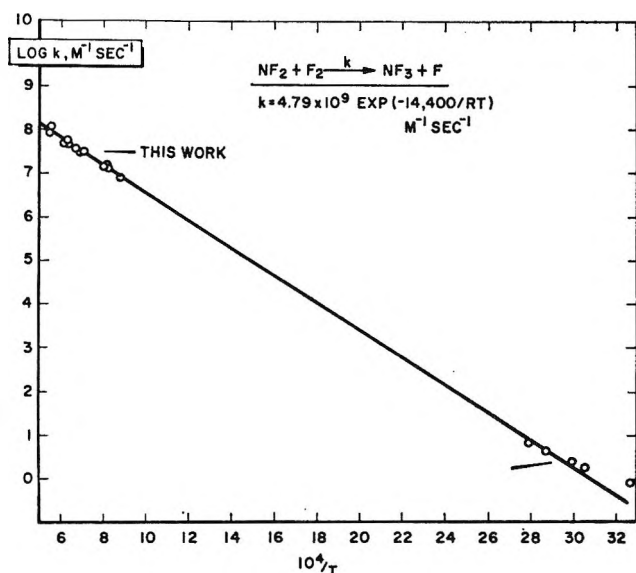
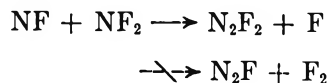


Figure 5. Arrhenius plot of k_a , comparing this work with the low temperature data of ref 2 (see arrow at lower right).

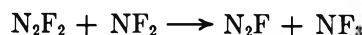
disagreement¹³ with the temperature dependence of L-C, the large range of 10^8 in k_a covered by the two sets of data closely defines an Arrhenius activation energy; to change the activation energy by 1 kcal necessitates an error of >3 in the absolute value of k_a between the two sets of data.

The present results definitively exclude reaction A

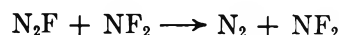
as an important reaction for NF_3 formation in the decomposition of NF_2 reported in ref 3. It is here suggested that the reaction of NF with NF_2 gives



followed by



along with



as a "follow on" sequence kinetically indistinguishable from that suggested in ref 3. The decomposition of N_2F_2 and its reactions with NF_2 are currently being investigated.

Acknowledgment. The author is indebted to R. K. Tarzwell for obtaining the experimental data.

(13) The disagreement cannot be completely explained. In part, a heterogeneous reaction may be contributing to the observed rate of L-C at the lower temperatures, a possibility not excluded by a surface to volume change of 2 at 348.16°K. Also, a small temperature dependence of the Arrhenius activation energy is a real possibility. Until these uncertainties are resolved, preferably by direct measurements at intermediate temperatures, it is difficult to define the uncertainty limits of the Arrhenius parameters describing the two sets of data. An uncertainty of ± 0.5 kcal/mole for the activation energy and $\pm 50\%$ for the preexponential factor are suggested.

Mechanism for Controlling the Reactivity of Lead Azide

by V. R. Pai Verneker¹ and A. C. Forsyth

Explosives Laboratory, Picatinny Arsenal, Dover, New Jersey (Received May 16, 1967)

It has been shown that (1) the reactivity of $\alpha\text{-PbN}_6$ increases as the particle size decreases; (2) when iron is incorporated as Fe^{3+} up to 1×10^{-2} mole % (acidic medium), it makes $\alpha\text{-PbN}_6$ less reactive; (3) when iron is carried by $\alpha\text{-PbN}_6$ as $(\text{FeN}_3)^{2+}$, a very marked enhancement in reactivity results; (4) a change in the optical absorption of $\alpha\text{-PbN}_6$ is also caused by iron doping; and (5) $\alpha\text{-PbN}_6$ prepared from lead nitrite and hydrazoic acid is the least reactive and the absorption edge of this preparation is at 300 $\text{m}\mu$, in contrast to 420 $\text{m}\mu$, which is the absorption edge of $\alpha\text{-PbN}_6$ prepared by other conventional methods.

Introduction

A great deal of work has been done on the thermal decomposition of $\alpha\text{-PbN}_6$.²⁻⁶ However, the role of crystal defects (vacancies, dislocations, interstitials, and foreign ions) has not been studied in any great detail. Jach⁷ investigated the effects of defects created

by reactor irradiation and showed that the rate of thermal decomposition of $\alpha\text{-PbN}_6$ can be enhanced.

(1) Research Institute for Advanced Studies, Baltimore, Md. 21227.

(2) W. E. Garner and A. S. Gomm, *J. Chem. Soc.*, 2123 (1931).

(3) W. E. Garner, A. S. Gomm, and H. R. Hales, *ibid.*, 1393 (1933).

The defects caused by reactor irradiation could be of different kinds and so it is hard to attribute the sensitization of α -PbN₆ to any one or two principal defects. Jach explains his results in terms of nuclei or potential nuclei created by reactor irradiation. In attempting to explain the initial stages of the thermal decomposition of unirradiated α -PbN₆, Jach states that the activation energy for the surface reaction is lower than that for the bulk reaction, and so at lower temperatures the surface reaction predominates over the bulk reaction.

The object of the present investigation is to determine how the reactivity of α -PbN₆ is influenced by particle size, the incorporation of an impurity (iron) and the method of preparation of α -PbN₆.

Experimental Section

Material Preparation. α -PbN₆ was prepared in two ways, by the reaction of an aqueous solution of lead nitrite with an acetone solution of hydrazoic acid and by the reaction of aqueous solutions of lead acetate and sodium azide or barium azide. The acidity was controlled in the first process by adjusting the concentration of hydrazoic acid and in the second process by the addition of nitric acid.

An aqueous solution of ferric azide was prepared by reacting metallic iron of spectral grade with hydrazoic acid. An excess of acid had to be maintained to avoid hydrolysis. Fe⁶⁹ was obtained from Oak Ridge National Laboratory, Tenn., in the form of ferric chloride. This was diluted with hydrazoic acid.

Lead azide doped with iron was prepared in the following manner. To a known amount of an acetone solution of hydrazoic acid was added a calculated amount of ferric azide solution and 1 μ curie of Fe⁶⁹. To this solution, a known amount of an aqueous solution of lead nitrite was added with constant stirring. The final volume in all cases was kept constant as was the ratio of acetone to water. Before filtering to separate the lead azide formed, a known amount of the supernatant liquid was pipetted into a measuring vial to determine the radioactivity due to Fe⁵⁹ remaining in solution. Lead azide doped with iron was then separated, dried, and desiccated. The dried product was then sieved so as to collect samples of a desired particle size. When lead azide was prepared by the second method, the dopant (iron) was added to the aqueous solution of either sodium or barium azide and the rest of the procedure was the same as described above.

Uptake of Iron by Lead Azide. In order to determine the mechanism of uptake of iron by lead azide, the azide was partially precipitated from the solution and a study was made of the distribution of iron in both the solid and the solution. Details of this type of study are discussed by Wahl and Bonner.⁸

Determination of the Reactivity of the Solid. The thermal sensitivity of lead azide was determined by

measuring the time for a 40-mg sample (constant particle size) to explode at a fixed temperature. The apparatus used for this study has been described previously.⁹ To study the thermal decomposition of α -PbN₆, a conventional vacuum system was used and an alphanatron gauge served to monitor the pressure of the nitrogen gas evolved in the decomposition. The sample was contained in a glass cell and this was heated by immersion in an oil bath, which was maintained at a temperature fixed within $\pm 0.1^\circ$. Reactivity was determined by measuring the time taken for the gas pressure to build from one arbitrary value to another. This procedure was adopted because to obtain a full pressure-time curve at the temperatures under investigation, required 6–8 hr. Furthermore, α -PbN₆ undergoes what is termed an aging effect; *i.e.*, its reactivity changes with time.

Except when a study was made of the effect of particle size, in all experiments where a comparison of the reactivities of different samples was made, care was taken to use the same amount of sample (by weight) and the same particle size. Finally, measurements of the optical absorption were done using a diffuse reflectance technique.

Results and Discussion

Figure 1 shows the effect of the particle size on the reactivity of α -PbN₆. The surface area was not measured, but can be calculated from the average particle size, considering the particles as spheres. Although this assumption is not strictly true, the results definitely show that the reactivity increases as the surface area increases. This may mean that the thermal reaction starts at defect centers and that these are more abundant on the surface.

In Figure 2 are depicted results on the uptake of iron by α -PbN₆. Of the two coefficients, D is seen to be constant, *i.e.*, iron is distributed homogeneously within the azide crystal.⁸ The data do not fit any adsorption isotherm. The D value is independent of the pH from 4 to 6 and does not show any change when the iron:lead ratio is changed from 10^{-3} mole % to 10^{-5} mole %. As iron azide and lead azide are not isomorphous, this mechanism of uptake is called anomalous mixed crystal formation,⁸ where iron goes into the crystal either substitutionally or interstitially.

Figure 3 shows how the reactivity of α -PbN₆ is affected by doping α -PbN₆ with different concentrations

(4) W. E. Garner, *Proc. Roy. Soc. (London)*, **A246**, 203 (1958).

(5) B. Reitzner, *J. Phys. Chem.*, **65**, 948 (1961).

(6) B. Reitzner, *ibid.*, **66**, 421 (1962).

(7) J. Jach, *Trans. Faraday Soc.*, **59**, 947 (1963).

(8) A. C. Wahl and N. A. Bonner, "Radioactivity Applied to Chemistry," John Wiley and Sons, Inc., New York, N. Y., 1951, p 102.

(9) A. J. Clear, "Standard Laboratory Procedures for Sensitivity, Bruisance, and Stability of Explosives," Picatinny Arsenal Technical Report FRL-TR-25, Jan 1961.

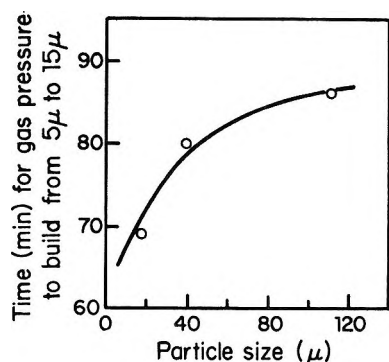


Figure 1. Reactivity of α -PbN₆ as a function of particle size at 240°.

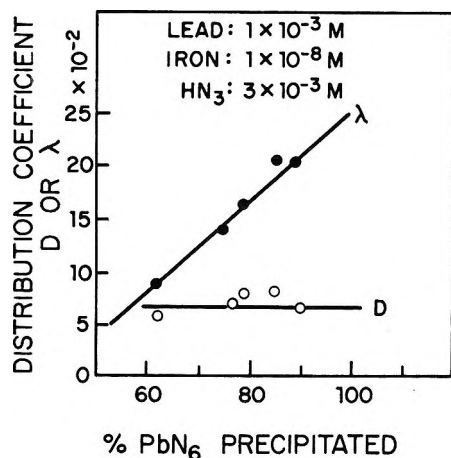
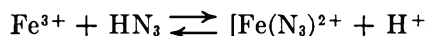


Figure 2. Study of the uptake of iron (using Fe^{59} tracer) by α -PbN₆ using the distribution laws (iron in the solid/iron in the solution) = D (azide in the solid/azide in the solution) and \log (total iron/iron in solution) = $\lambda \log$ (total azide/azide in solution).

of iron. The α -PbN₆ used in this experiment was prepared by reaction of spectral grade lead nitrite with HN₃. Besides the iron, no other significant impurities were present. One sees a marked initial decrease in reactivity, which peaks when the doping is of the order of 1×10^{-2} mole %. Thereafter the drop in reactivity decreases, and when the doping is of the order of 1×10^{-1} mole %, the reactivity attains the value of the reactivity of the undoped sample. The only variable, apart from the concentration of iron, which was changed, was the ratio $[\text{Fe}]:[\text{HN}_3]$. It is reported in the work of Ricca¹⁰ and Wallace¹¹ that iron can exist either as Fe^{3+} or $[\text{Fe}(\text{N}_3)]^{2+}$ and that, as the proton concentration drops, $[\text{Fe}(\text{N}_3)]^{2+}$ is favored



In these experiments, as the doping increased, so did the ratio $\text{Fe}:\text{HN}_3$. It is, therefore, possible that with high dopant concentrations, some $[\text{Fe}(\text{N}_3)]^{2+}$ could have been incorporated in the α -PbN₆. Although it is extremely dangerous to work with high concentrations of HN₃, one experiment was done to dope α -PbN₆ with

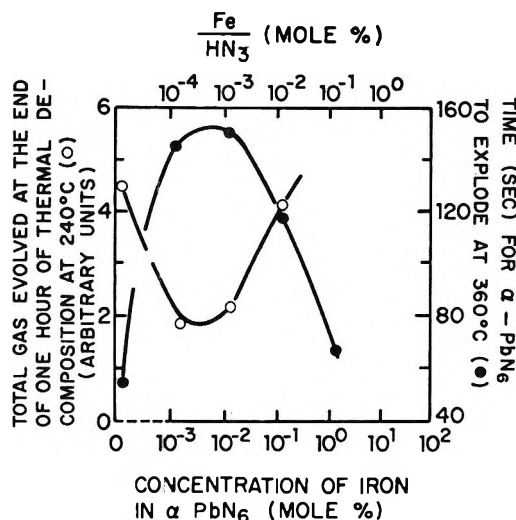
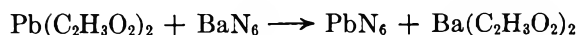


Figure 3. Reactivity of α -PbN₆ as a function of the concentrations of Fe^{3+} dopant in α -PbN₆.

iron and to bring the ratio of $\text{Fe}:\text{HN}_3$ down from 1×10^{-2} to 1×10^{-5} . As a result, the reactivity (as measured by the gas evolved) dropped from 4.1 to 2.5. Under the conditions of the experiment, therefore, one may say that iron is incorporated into α -PbN₆ in the form of Fe^{3+} . This then would give rise to cation vacancies in the crystal of α -PbN₆. It is very tempting, therefore, to say that cation vacancies decrease the reactivity of α -PbN₆. However, as there is a limit to the number of cation vacancies which can exist in the crystal, one would expect a saturation effect for the decrease in reactivity. If the result of the single experiment ($\text{Fe}:\text{HN}_3 = 1 \times 10^{-5}$ mole %) is valid, then this is explained. Experiments were then conducted to determine the effect of high doping with Fe^{3+} using a different method to prepare α -PbN₆.

Lead acetate was treated with sodium azide in a nitric acid solution keeping the pH between 2 and 2.5. The results of these experiments are presented in Figure 4. One sees that, after the initial decrease in reactivity, there is, in fact, an increased reactivity. Since there is a high concentration of sodium ions present in the solution along with Fe^{3+} , Na^+ can also get into the crystal. Sodium doping would then produce anion vacancies. To overcome this, α -PbN₆ was prepared from the following reaction



The results of these experiments are shown in Figure 5. One can see an initial decrease in reactivity, but, on further doping, the reactivity attains the value of the reactivity of undoped α -PbN₆. In the same figure, one can also see that the reactivity of α -PbN₆ prepared

(10) B. Ricca, *Gazz. Chim. Ital.*, **75**, 71 (1945).

(11) R. M. Wallace and E. K. Dukes, *J. Phys. Chem.*, **65**, 2094 (1961).

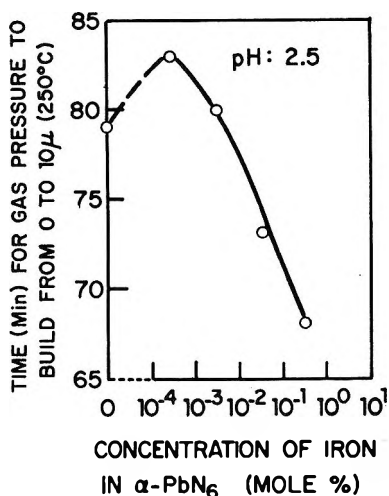


Figure 4. Reactivity of α -PbN₆ as a function of the concentration of Fe³⁺ dopant in α -PbN₆.

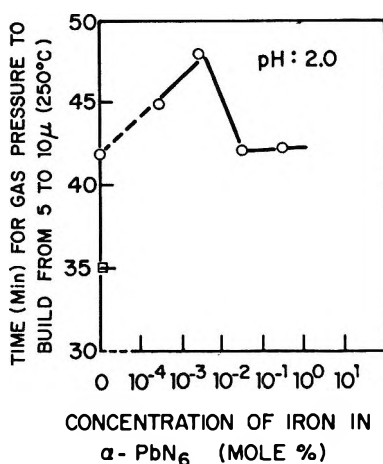


Figure 5. Reactivity of α -PbN₆ vs. concentration of Fe³⁺ dopant in α -PbN₆: prepared from Pb(C₂H₃O₂)₂ + BaN₃, ○; and in α -PbN₆ prepared from Pb(C₂H₃O₂)₂ + NaN₃, □.

from NaN₃ is much greater than that prepared from BaN₃.

In Figure 6 are presented results showing how the reactivity of α -PbN₆ is influenced by doping α -PbN₆ with iron in the form of the complex [FeN₃]²⁺. As stated earlier, whether iron exists as Fe³⁺ or [FeN₃]²⁺ is primarily determined by the pH. From the experiments conducted to this point, it was not clear whether [FeN₃]²⁺ is adsorbed either on the surface or internally at dislocations, or whether this complex gets into the crystal either substitutionally or interstitially. It is possible that [FeN₃]²⁺ itself is unstable at the temperature of the experiment and thus starts the reaction. It is equally conceivable that the incorporation of a colored ion like [FeN₃]²⁺ may well change the bulk properties of α -PbN₆. Until this is resolved, it is not possible to define the exact mechanism of the enhancement in the reactivities.

In Table I are presented data on the optical absorp-

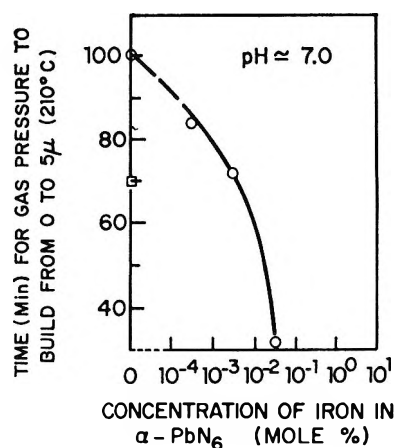
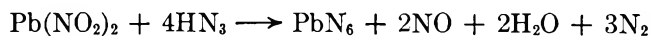


Figure 6. Reactivity of α -PbN₆ vs. concentration of [FeN₃]²⁺ in α -PbN₆ prepared from Pb(C₂H₃O₂)₂ + BaN₃, ○, and in α -PbN₆ prepared from Pb(C₂H₃O₂)₂ + NaN₃, □.

tion of α -PbN₆ prepared by different methods and α -PbN₆ doped with Fe³⁺ or [FeN₃]²⁺. As single crystals of α -PbN₆ are difficult to grow, the measurements were made using the reflectance technique on powders. From the data, it is clear that α -PbN₆ prepared from NaN₃ or BaN₃ starts to absorb at 420 mμ. This is not dependent on the pH, and doping with Fe³⁺ does not change the absorption edge. However, doping with [FeN₃]²⁺ shifts the edge to 680 mμ. It is not clear from the spectrum whether the absorption due to the colored [FeN₃]²⁺ is superimposed on the intrinsic absorption of α -PbN₆ or whether the intrinsic absorption itself has changed. Further, it is also noted that when α -PbN₆ is prepared by reacting lead nitrite with HN₃, the absorption edge shifts to 300 mμ. From the table, one can see that this α -PbN₆ is the least reactive. All of the other undoped preparations absorb at 420 mμ, but still show differences in reactivities. The samples prepared from an acidic medium are less reactive than those prepared from a neutral medium. It is difficult to draw inferences from this set of experiments, because samples prepared from acidic medium could well have contained nitrate ions and nitrate ions could decrease the reactivity of α -PbN₆. However, it can be inferred with reasonable certainty that sodium ions increase the reactivity of α -PbN₆ and that the least reactive preparation of α -PbN₆ is from the reaction



In solids which are purely ionic, one can speak in terms of either Schottky or Frenkel defects. However, α -PbN₆ is not 100% ionic and this makes it hard to argue in terms of these defects. In spite of this, one can speculate on models to explain these results, *i.e.*, initial decrease in reactivity followed by the regaining of the original reactivity. When Fe³⁺ is incorporated in a crystal of α -PbN₆, cation vacancies are created, and, to maintain an equilibrium following the law of

Table I: Effect of Doping on the Optical and Thermal Properties of Lead Azide

Iron, mole %	Method of preparation	pH	Absorption edge, mμ	Time for gas pressure to build from 0 to 5 μ (220°), min
0	BaN ₆ + Pb(AC) ₂	2.5	420	95
0	BaN ₆ + Pb(AC) ₂	7.0	420	48
0	NaN ₃ + Pb(AC) ₂	2.5	420	65
0	NaN ₃ + Pb(AC) ₂	7.0	420	33
0	HN ₃ + Pb(NO ₂) ₂	3.5	300	120
10 ⁻⁴ -10 ⁻¹ {	BaN ₆ + Pb(AC) ₂	2.0	420	...
10 ⁻⁴ -10 ⁻¹ { (Fe ³⁺)	NaN ₃ + Pb(AC) ₂	2.0	420	...
10 ⁻⁴ -10 ⁻¹ {	BaN ₆ + Pb(AC) ₂	7.0	680	...
10 ⁻⁴ -10 ⁻¹ { [(FeN ₃) ₂ ⁺]	NaN ₃ + Pb(AC) ₂	7.0	680	...

mass action, this results in a decrease in anion vacancies. Since anion vacancies are good electron traps, a decrease in their concentration will result in drop in reactivity. As the doping increases there results, along with the production of cation vacancies, an increasing concentration of Fe³⁺. This Fe³⁺ can form an associated complex with a cation vacancy and also act as a good electron trap. This will result, therefore, in an apparent enhancement in reactivity. If one now considers Frenkel defects, then it follows that as the iron doping increases, the vacancy concentration likewise increases and the added vacancies depress the equilibrium concentration of interstitial lead ions. The ionic conduc-

tivity would therefore decrease and so would the reactivity. However, as the doping increases further, the vacancy diffusion mechanism becomes more important than the interstitial diffusion of lead ions and so the conductivity, and usually the reactivity, could increase. Experiments on the conductivity of AgBr doped with Ca²⁺ show similar results.¹² Further investigations will have to be done to determine the conductivity, color center behavior, and similar properties of α-lead azide before the actual mechanism of the change in reactivity can be defined.

(12) C. Kittel, "Introduction to Solid State Physics," John Wiley and Sons, Inc., New York, N. Y., 1960, p 483.

Stability Order in Metal Chelate Compounds. V.¹ Bivalent Metal

Complexes of 2-Pyridylmethyl Phosphate

by Yukito Murakami and Makoto Takagi

*Department of Organic Synthesis, Faculty of Engineering, Kyushu University, Hakozaki, Fukuoka, Japan
(Received May 18, 1967)*

The complex formation between 2-pyridylmethyl phosphate and the bivalent metal ions, Mg(II), Mn(II), Co(II), Ni(II), Cu(II), and Zn(II), was investigated by means of a potentiometric method. Where the chelate system became complicated by the formation of a protonated complex, a nonlinear least-squares method was successfully applied to the analysis of data with the aid of an electronic computer. The resulting stability order of the 1:1 complex with respect to the bivalent metals has been found to follow the sequence: $\text{Mg} < \text{Co} \sim \text{Mn} < \text{Zn} \sim \text{Ni} \ll \text{Cu}$. The donor group of a significant coordination ability in this metal complex formation seems to be the phosphate group, and the pyridyl nitrogen plays merely a minor role in such a process. Meanwhile, the copper ion has been shown to form a chelate ring with the present ligand by involving both the pyridyl nitrogen and the phosphate group. A plausible structure of the copper chelate based on the stability data has been proposed. The formation of metal chelates of a 2:1 molar ratio of ligand to metal ion has not been detected under present experimental conditions.

Introduction

In the course of our investigation on the hydrolysis of organic orthophosphates and the metal catalysis in such reactions, 2-pyridylmethyl phosphate² was found to undergo a catalytic hydrolysis in the presence of copper(II) ion, while other bivalent (alkaline earth or transition) metal ions exhibited no catalytic activity under comparable experimental conditions.³ Thus, it was aimed in the present work to explore the interaction of several bivalent metal ions with 2-PMP in terms of stability constants and to obtain a clue to understanding the catalytic mechanism of metal ions in the hydrolysis reaction of phosphates. The method of nonlinear least squares coupled with the use of an electronic computer was adopted in this work to estimate stability constants in cases where the metal complex system became involved by the coexistence of protonated complexes.

Experimental Section

Materials. 2-PMP was prepared and purified according to the method reported previously.⁴ A stock solution of this phosphate was usually prepared just before use, or otherwise kept frozen in a refrigerator for protection from hydrolysis. The bivalent metal nitrates, $\text{Mg}(\text{NO}_3)_2 \cdot 6\text{H}_2\text{O}$, $\text{Co}(\text{NO}_3)_2 \cdot 6\text{H}_2\text{O}$, $\text{Ni}(\text{NO}_3)_2 \cdot 6\text{H}_2\text{O}$, $\text{Cu}(\text{NO}_3)_2 \cdot 3\text{H}_2\text{O}$, $\text{Zn}(\text{NO}_3)_2 \cdot 6\text{H}_2\text{O}$, and the sulfate, $\text{MnSO}_4 \cdot n\text{H}_2\text{O}$, of analytical grade were the products of the Wako Pure Chemical Industries, Ltd. These salts were dissolved in carbonate-free water for

preparation of the stock solutions, which were standardized by a conventional chelatometric titration.

Potentiometric Measurements of Hydrogen Ion Concentration. The apparatus and procedures for potentiometric measurements have been described in a previous paper.⁵ All of the measurements were made on the solutions maintained at $25.0 \pm 0.1^\circ$ and the ionic strength of 0.10 (KNO_3). The total concentration of the ligand was kept constant ($1.00 \times 10^{-3} M$), while those of the metal ions were varied (1.00×10^{-3} and $5.00 \times 10^{-4} M$). Each potentiometric titration was checked by duplicate runs. After the completion of each measurement, the titrating solution was analyzed for inorganic phosphate, and decomposition of the ligand during the titration was found to proceed to a negligible extent.

Mathematical Treatment of Data

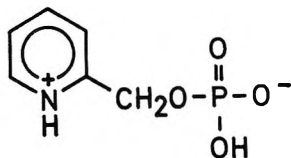
Acid Dissociation of the Ligand. Since 2-PMP has a tribasic nature, three acid dissociation constants are defined as follows

- (1) (a) Contribution No. 126 from the Department of Organic Synthesis, Faculty of Engineering, Kyushu University; (b) Part IV: Y. Murakami and M. Takagi, *Bull. Chem. Soc. Japan*, **38**, 828 (1965).
- (2) 2-Pyridylmethyl phosphate is abbreviated hereafter as 2-PMP.
- (3) Y. Murakami and M. Takagi, to be published.
- (4) Y. Murakami, M. Takagi, and H. Nishi, *Bull. Chem. Soc. Japan*, **39**, 1197 (1966).
- (5) Y. Murakami, *J. Inorg. Nucl. Chem.*, **24**, 679 (1962).

$$K_{H_3L} = \frac{[H_2L][H^+]}{[H_3L^+]}; \quad K_{H_2L} = \frac{[HL^-][H^+]}{[H_2L]}$$

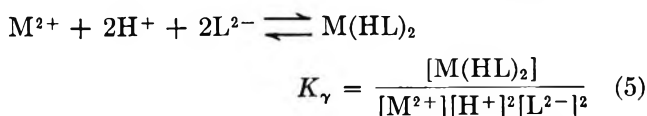
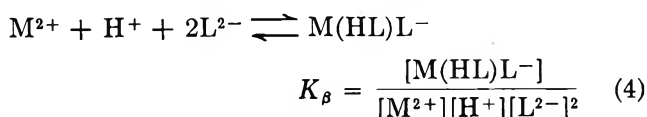
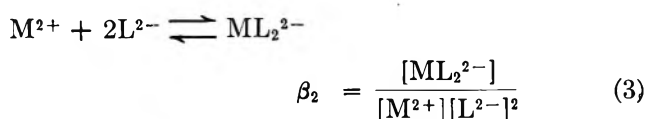
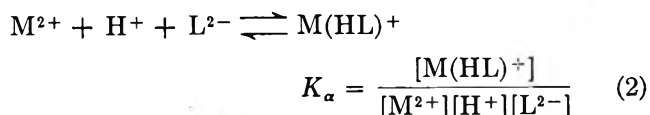
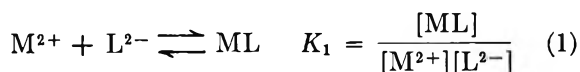
$$K_{HL} = \frac{[L^{2-}][H^+]}{[HL^-]}$$

where H_2L stands for the neutral species represented by I, and the brackets indicate the concentration. A usual algebraic method described previously⁶ was employed for the evaluation of these constants.



I

Complex-Forming Equilibria. The 2-PMP molecule has two coordination sites, *i.e.*, an aromatic nitrogen and a phosphate group. Whether they behave in conjunction with each other to form chelate compounds or separately to yield simple metal complexes, there is no *a priori* settlement. Apart from these considerations, the subsequent analysis showed that the following reaction scheme may suffice to cover all the probable solution equilibria responsible for the present experimental conditions



If the complex formations are restricted to those due to eq 1 and 3, a functional relationship, which is linear in unknown parameters, can easily be derived for each titration point, and the evaluation of formation constants is quite straightforward by the aid of usual algebraic methods.⁶

Meanwhile, if all the solution equilibria indicated above are taking place to a significant extent, the following two equations are derived under the considera-

tion of ionic neutrality, as well as mass balance for ligand and metal

$$p[L]^3 + q[L]^2 + r[L] = -P \quad (6)$$

$$p'[L]^3 + q'[L]^2 + r'[L] = T_L \quad (7)$$

where

$$p = Q(\beta_2 + K_\beta[H] + K_\gamma[H]^2)$$

$$q = (P - 2T_M)(\beta_2 + K_\beta[H] + K_\gamma[H]^2) + Q(K_1 + K_\alpha[H]) - T_M(2\beta_2 + K_\beta[H])$$

$$r = (P - T_M)(K_1 + K_\alpha[H]) + Q - T_M K_1$$

$$p' = R(\beta_2 + K_\beta[H] + K_\gamma[H]^2)$$

$$q' = (2T_M - T_L)(\beta_2 + K_\beta[H] + K_\gamma[H]^2) + R(K_1 + K_\alpha[H])$$

$$r' = (T_M - T_L)(K_1 + K_\alpha[H]) + R$$

and

$$P = T_{OH} + [H] - [OH]$$

$$Q = \frac{[H]}{K_{HL}} \left(\frac{[H]^2}{K_{H_3L}K_{H_2L}} - 1 \right) - 2$$

$$R = \frac{[H]^3}{K_{H_3L}K_{H_2L}K_{HL}} + \frac{[H]^2}{K_{H_2L}K_{HL}} + \frac{[H]}{K_{HL}} + 1$$

In the above equations T_L , T_M , and T_{OH} are, respectively, the total concentration of the ligand, the metal ion, and the base added to the system. Through division of eq 6 by eq 7, the following equation, which is then quadratic in $[L]$ is derived

$$\alpha[L]^2 + \beta[L] + \gamma = 0 \quad (8)$$

where

$$\alpha = (Q + PR/T_L)(\beta_2 + K_\beta[H] + K_\gamma[H]^2)$$

$$\beta = (Q + PR/T_L)(K_1 + K_\alpha[H]) + T_M\{2(P/T_L - 1)(\beta_2 + K_\beta[H] + K_\gamma[H]^2) - 2\beta_2 - K_\beta[H]\}$$

$$\gamma = (Q + PR/T_L) + T_M\{(P/T_L - 1)(K_1 + K_\alpha[H]) - K_1\}$$

Equations 6 and 7 are apparently nonlinear with respect to equilibrium constants and are the implicit expression of functional relationships for a number of unknown parameters (equilibrium constants), which are combined with known variables and constants. Thus, the method proposed by Rubin,⁷ which has been proved to be useful for this purpose irrespective of an explicit or an implicit nature of functional relationship, was applied to the present problem.

(6) Y. Murakami, K. Nakamura, and M. Tokunaga, *Bull. Chem. Soc. Japan*, **36**, 669 (1963).

(7) D. I. Rubin, *Chem. Eng. Progr. Symposium Ser.*, **59**, 90 (1963).

For clarity in this computational procedure, it is desirable to derive an explicit expression which does not carry the unknown variable $[L]$. This is successfully performed by the combination of eq 7 and 8. In the course of this mathematical manipulation, it should be noticed that the values of β_2 , K_β , and K_γ are conveniently assumed to be zero under the experimental conditions where only the 1:1 complexes are significantly formed, and eq 8 reduces to the first-order expression in $[L]$. In the nonlinear least-squares method, an iterative calculation is performed to minimize the residual sum of squares

$$U = \sum_{i=1}^N \{T_L(\text{obs})_i - T_L(\text{calc})_i\}^2$$

until

$$\max_j \left| \frac{\Lambda_j^1 - \Lambda_j^0}{\Lambda_j^0} \right| < \epsilon$$

holds.^{7,8}

All the calculation processes were programmed by means of Kyushu Daigaku Algol (ALGOL-H) and carried out on Okitac 5090-H electronic computer of the Computation Center of Kyushu University.

Results

Acid Dissociation Constants. The acid dissociation constants of 2-PMP have already been reported.⁴ They were measured again for assurance and substantially the same values were obtained: pK_{H_2L} , 1.8; pK_{HL} , 4.42; and pK_{HL} , 6.30.

Titration Curves. Titration curves for a 1:1 molar ratio of ligand to metal ion are shown partly in Figure 1. It is seen that the interactions between 2-PMP and the bivalent metals are not pronounced except for the copper(II). Nevertheless, the order of complex-forming ability may be placed with respect to metal ions in the increasing manner: $Mg < Co \sim Mn < Zn \sim Ni \ll Cu$. For the first transition metal ions, pH readings of the system became unstable and drifted continuously, on standing near and above $a = 2.0$ (a being the degree of neutralization of the ligand), probably because of their hydrolytic tendencies, so that the equilibrated data were not obtained for these cases. This phenomenon was found less significant for the copper(II) system.

Equilibrium Constants for Magnesium, Manganese, Cobalt, Nickel, and Zinc Systems. In the region where $a < 1$, we have not observed any significant differences between titration curves for these metal complex systems and that for the ligand only. This means that the complex formation is mainly with the diionic species of the ligand and that the formation of any protonated complex needs not be considered in the first approximation. Analyses showed this is the case. A usual algebraic method⁶ gave the stability constants listed in Table I. Only a 1:1 (metal:ligand) complex was de-

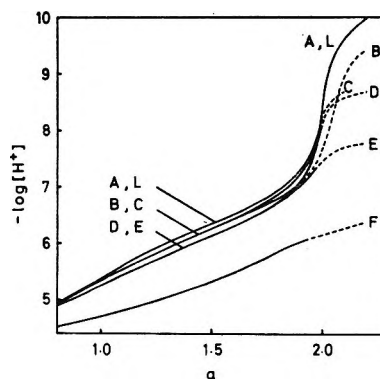


Figure 1. Titration curves for 2-pyridylmethyl phosphate-bivalent metal systems with 1:1 molar ratio of ligand to metal ion at $25.0 \pm 0.1^\circ$ and $\mu = 0.10$ (KNO_3): A, Mg; B, Mn; C, Co; D, Ni; E, Zn; F, Cu; L, ligand alone; initial concentration of ligand, $1.001 \times 10^{-3} M$; a = moles of base added per mole of ligand. Dotted lines indicate nonequilibrated regions.

Table I: Stability Constants of Metal Complexes of Some Organic Phosphates^a

Ligand	Metal ion	Log K_1^b	Log K_{MHL}^c
2-Pyridylmethyl phosphate ^d $pK_{H_2L} = 1.8$ $pK_{HL} = 4.42$ $pK_{HL} = 6.30$	Mg(II) ^f	~ 1.7	
	Mn(II) ^f	2.44 ± 0.05	
	Co(II) ^f	2.27 ± 0.04	
	Ni(II) ^f	2.85 ± 0.02	
	Cu(II)	4.44 ± 0.01	2.23 ± 0.03
	Zn(II) ^f	2.83 ± 0.04	
Adenosine-3-phosphate ¹¹ $pK_{H_2L} = 3.63$ $pK_{HL} = 5.80$	Mg(II)	1.89	
	Mn(II)	2.28	
	Co(II)	2.24	
	Ni(II)	2.79	
	Cu(II)	2.96	
	Zn(II)	2.60	
Adenosine-5-phosphate ¹¹ $pH_{H_2L} = 3.81$ $pK_{HL} = 6.21$	Mg(II)	1.97	
	Mn(II)	2.40	
	Co(II)	2.64	
	Ni(II)	2.84	
	Cu(II)	3.18	
	Zn(II)	2.72	
α -D-Glucose-1-phosphate ¹²	Zn(II)	2.34	
	Co(II)	2.12	
2-Aminoethyl phosphate ^{11,13,d} $pK_{H_2L} = 5.57$ $pK_{HL} = 10.12$	Mg(II) ^f	1.70	1.25
	Mn(II) ^f	2.56	1.72
	Cu(II)	6.39	1.94

^a Temperature = 25.0° , $\mu = 0.10$. ^b $K_1 = [ML]/[M^{2+}][L^{2-}]$.

^c $K_{MHL} = [MHL^+]/[M^{2+}][HL^-]$. ^d Temperature was maintained within $\pm 0.1^\circ$ of precision and the ionic strength was kept constant with KNO_3 . ^e $\mu = 0.15$. ^f Stability constant was calculated from the titration data of 1:1 molar ratio of ligand-metal. The stability constant varies slightly with the molar ratio.

tected for each metal ion, consistent with the fact that the \bar{n} value (average number of ligands bound per metal ion) does not exceed 0.25 at $a = 1.68$, even for the nickel system.

(8) N is the number of observations. Λ_j^0 indicates the approximation at one stage and Λ_j^1 stands for the next approximation to Λ_j , the j th parameter to be determined. ϵ is a preassigned tolerance for convergence, and a value of 0.001 was assigned for it in the present investigation.

A minor inconsistency was observed, however, for nickel around $a = 1$ in the analysis mentioned above. This seems to be caused by some contribution of the formation of a 1:1 protonated complex represented by eq 2. Making use of the nonlinear least-squares method under the consideration of eq 1 and 2, the U values were found to become considerably smaller than those obtained without considering eq 2. Thus, it seems probable that the protonated complex was actually formed in this system. However, the analysis of the system for concentrations of each ionic species showed that the concentration of the specified proton complex never exceeded 2% of T_L at maximum. Moreover, the estimated equilibrium constant itself is very small and suffers variation among independent titrations. For example, 1:1 and 1:2 (metal:ligand) titration data for the nickel system gave the following equilibrium constants: T_M/L_L , 1.0, 0.5; $\log K_1$, 2.86, 2.82; $\log K_\alpha$, 7.36, 7.73. Presently, there exists some uncertainty for the formation of a protonated complex and the corresponding equilibrium constant for the nickel chelate system.

Equilibrium Constants for Copper System. In accordance with a preliminary survey of the potentiometric data, the a range between 0.60 and 1.50 in the titration curve for a 1:1 molar ratio of ligand to metal ion was selected for calculation. The treatment of data along the procedure for the linear case proved to be quite unsatisfactory, only giving an approximate value of the stability constant, $K_1 \sim 10^4$. On the other hand, referring to the stability constants of the copper chelate of 2-pyridylmethanol,⁹ K_α was estimated to be around the order of 10^9 . This set of constants (K_1 and K_α) was used as a starting set in order to get the best set of values by means of the iterative least-squares method. In practice, several starting sets were employed, varying the K_α value over 10^2 -fold range, in order to ensure that the best set of constants was independent of a starting set. One of the results obtained by this computation is shown in Table II. In the course of inspection of the titration curve for a 2:1 molar ratio of ligand to metal ion, the value of U was found to be relatively large in comparison with that obtained for the 1:1 ratio case. Thus, the data were analyzed for three cases by considering the following sets of equilibrium constants: (a) K_1 , K_α , β_2 , K_β , and K_γ ; (b) K_1 , K_α , β_2 , and K_β ; (c) K_1 , K_α , and β_2 . Nevertheless, these treatments failed to give reasonable improvement.

Stability constants evaluated in the present investigation are summarized in Table I.

Discussion

Computational Method. It has been shown in the preceding section that the nonlinear least-squares method proposed by Rubin⁷ could successfully be applied to the evaluation of stability constants for relatively simple systems such as treated in this work. A

Table II: Result of Calculation for the 2-PMP-Cu(II) System: ($T_M/T_L = 1$)^a

a	$T_L(\text{obsd}) \times 10^3$	$T_L(\text{calcd}) \times 10^3$	$D \times 10^3$	$D/T_L(\text{obsd}) \times 10^2, \%$	$[L] \times 10^6$
0.602	0.9952	1.0300	-0.0348	-3.49	0.4326
0.662	0.9946	0.9543	0.0403	4.05	0.4807
0.722	0.9940	0.9860	0.0080	0.80	0.5850
0.781	0.9934	1.0501	-0.0566	-5.70	0.7265
0.842	0.9929	0.9526	0.0402	4.05	0.7768
0.902	0.9923	0.9872	0.0051	0.51	0.9310
0.962	0.9917	0.9333	0.0584	5.89	1.0250
1.022	0.9911	0.9933	-0.0023	-0.22	1.2500
1.082	0.9905	0.9973	-0.0068	-0.68	1.4420
1.141	0.9899	0.9809	0.0090	0.90	1.6313
1.201	0.9893	0.9978	-0.0085	-0.85	1.9001
1.262	0.9887	0.9913	-0.0026	-0.26	2.1728
1.321	0.9881	1.0378	-0.0497	-5.02	2.5981
1.381	0.9876	1.0167	-0.0291	-2.95	2.9353
1.441	0.9870	0.9906	-0.0036	-0.36	3.3085
1.501	0.9864	0.9608	0.0256	2.59	3.7376

$$|D/T_L(\text{obsd}) \times 10^2|_{\text{av}} = 2.40$$

^a $K_1 = 0.2763 \times 10^6$, $K_\alpha = 0.3363 \times 10^9$, $U = 0.1536 \times 10^{-7}$. ^b $D = T_L(\text{obsd}) - T_L(\text{calcd})$.

starting set of only a crude approximation was sufficient to obtain the best refined set of stability constants concerned. In principle, this method may find wide applicability in the more complicated systems where the other equilibria such as hydrolyses of the metal ions or complex species are introduced. However, in general, U is not a simple function of unknown parameters, and several minima would be present in close proximity to the best set of parameters. If this were the case, the set of the approximate parameters to be given at the start would be critical. Thus, the use of either several sets of starting approximation or a good set of starting parameters, which may be obtainable from the other computational technique, *e.g.*, graphical method, would eliminate these uncertainties.

It is advisable by all means to check the consistency between the observed and the calculated data. This was performed along the two lines: regeneration of the titration curves by the use of the evaluated stability constants, and analyses of the system for the concentrations of all the ionic species concerned. The agreement between the observed and the calculated pH values is quite satisfactory as seen in Table III, and this provides convincing support to the constants obtained here. Concentrations of all the components, ligand and complex species, which take part in equilibrium were calculated for the varying degree of neutralization, a , as illustrated in Figure 2, and each species is seen to vary its concentration in a plausible manner.

(9) Y. Murakami and M. Takagi, *Bull. Chem. Soc. Japan*, **38**, 828 (1965).

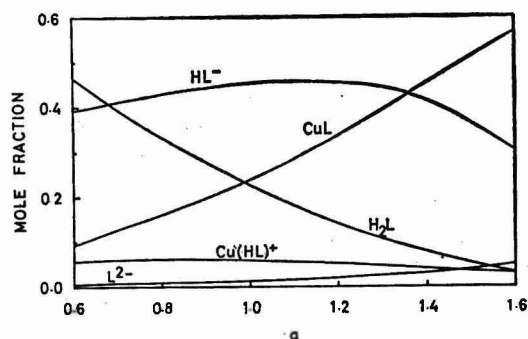


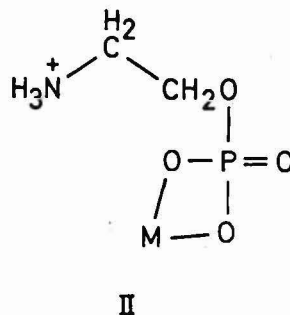
Figure 2. Distribution of 2-pyridylmethyl phosphate and the corresponding copper(II) complex species in the course of titration of 2-pyridylmethyl phosphate-copper(II) system with 1:1 molar ratio of ligand to metal ion: $t = 25.0 \pm 0.1^\circ$; $\mu = 0.10$ (KNO_3); initial concentration of ligand, $1.001 \times 10^{-3} \text{ M}$; a = moles of base added per mole of ligand.

Table III: Comparison between Observed and Calculated Values of pH for the 2-PMP-Cu(II) System ($T_M/T_L = 1$)

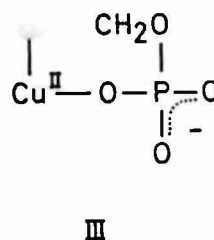
a	$-\text{Log} [\text{H}^+](\text{obsd})$	$-\text{Log} [\text{H}^+](\text{calcd})$	Difference
0.361	4.101	4.107	-0.006
0.481	4.225	4.228	-0.003
0.602	4.344	4.343	0.001
0.722	4.455	4.455	0.000
0.842	4.565	4.567	-0.002
0.962	4.677	4.680	-0.003
1.082	4.798	4.798	0.000
1.201	4.925	4.925	0.000
1.321	5.071	5.067	0.004
1.441	5.228	5.228	0.000
1.561	5.413	5.422	-0.009
			$ \text{Difference} _{\text{av}} = 0.0025$

Stability Constants and Plausible Structures of Complexes. Adenosine-3-phosphate and adenosine-5-phosphate were found to yield metal complexes with various bivalent metals with participation of only the phosphate group.¹⁰ Later, this viewpoint was supported by the fact that α -D-glucose-1-phosphate yielded some bivalent metal complexes¹² with the stability constants of approximately the same order of magnitude as those of the above two phosphates; the stability data are taken from the literature¹¹⁻¹⁴ as listed in Table I. Meanwhile, the formation of a protonated complex was confirmed only for the copper system. This means that the heterocyclic nitrogen alone demonstrates an extremely low tendency to form the coordinate bond with those bivalent metal ions employed in this work. Thus, from the comparison of these stability constants which appeared in the literature with the present data, it may be seen for the present ligand that the donor group playing the major role in the metal complex formation, with exception of the copper system, is the phosphate group, and the pyridyl nitrogen has merely a minor or nearly a negligible coordination ability.

On the other hand, 2-aminoethyl phosphate, which is structurally related to the present ligand, forms the protonated complexes with some bivalent metal ions. Since in these complexes the proton is attached to the amino nitrogen, on the contrary to what is assumed for 2-PMP, the structure shown by II was postulated.¹⁴



Upon deprotonation in the copper complex, the resulting metal complex gained a much increased stability. This suggests that the metal chelate ring involving both the amino nitrogen and the phosphate group of the ligand is definitely formed. The similar chelate ring formation seems to be true for the copper complex of 2-PMP; this is in agreement with the comparatively higher value of the stability constant than those for the complexes of adenosine phosphates. In conclusion, structure III is presented here for the copper complex



of 2-PMP. It is not unreasonable for 2-PMP to yield a seven-membered chelate ring when examined by means of a molecular structural model, and chelate rings involving more than six members have been proposed for other phosphate-containing ligands, *e.g.*, O-phosphorylated peptides¹⁴ and salicyl phosphate.¹⁵

The 1:2 complex CuL_2^{2-} , which did not form to a significant extent under present experimental conditions, seems to have much lower stability than the

(10) A. E. Martell and G. Schwarzenbach, *Helv. Chim. Acta*, **39**, 653 (1956).

(11) M. M. T. Khan and A. E. Martell, *J. Am. Chem. Soc.*, **84**, 3037 (1962).

(12) Br. E. Doody, E. R. Tucci, R. Scruggs, and N. C. Li, *J. Inorg. Nucl. Chem.*, **28**, 833 (1966).

(13) R. Österberg, *Acta Chem. Scand.*, **14**, 471 (1960).

(14) R. Österberg, *ibid.*, **16**, 2434 (1962).

(15) G. E. Mont and A. E. Martell, *J. Am. Chem. Soc.*, **88**, 1387 (1966).

1:1 complex as mentioned previously, in contrast to the 2-aminoethyl phosphate chelate system (the difference between successive stability constants, 0.39 in log *K* unit). Such a low stability of the 1:2 complex may be

ascribed to the two dominating factors: the low basicity of pyridyl nitrogen and the steric effect of the pyridine ring, which may generate a strong repulsive force against the second ligand.

Nuclear Magnetic Resonance of Oxygen-17 and Chlorine-35 in

Aqueous Hydrochloric Acid Solutions of Cobalt(II). I. Line Shifts

and Relative Abundances of Solution Species^{1a}

by A. H. Zeltmann, N. A. Matwiyoff,^{1b} and L. O. Morgan^{1c}

University of California, Los Alamos Scientific Laboratory, Los Alamos, New Mexico 87544
(Received May 24, 1967)

The nmr spectra of oxygen-17 and chlorine-35 were observed for cobalt(II) chloride solutions at hydrochloric acid concentrations from 0.4 to 16 *m*. Downfield line shifts for both nuclear species were interpreted in terms of complexes present. Relative abundances of complex species were correlated by semi-thermodynamic equilibrium constants, and values of ΔH and ΔS were obtained for each equilibrium from temperature dependences of line shifts. Complex species found to be important were $\text{Co}(\text{H}_2\text{O})_6^{2+}$, $\text{CoCl}(\text{H}_2\text{O})_5^+$, $\text{CoCl}_2(\text{H}_2\text{O})_4$, $\text{CoCl}_3(\text{H}_2\text{O})_3^-$, and CoCl_4^{2-} . The last one predominates at the highest hydrochloric acid concentrations. Relative abundances of the three four-coordinate complexes were found to be compatible with spectrophotometric observations at 619, 658, and 684 m μ . Isotropic spin-exchange coupling constants in the complexes and the corresponding fractional *s* characters of the unpaired electrons in the ligand atoms were found to be: octahedral chlorine-35, 2.53×10^6 cps, 0.0019; tetrahedral chlorine-35, 6.89×10^6 cps, 0.0052; octahedral oxygen-17, 1.34×10^7 cps, 0.0101; and tetrahedral oxygen-17, 3.26×10^7 cps, 0.0242. Data reported elsewhere by Horrocks and Hutchinson on proton shifts in aqueous cobalt(II) thiocyanate solutions were reinterpreted, taking into account the trend to increasing tetrahedral coordination with increasing thiocyanate substitution in the complex species, to demonstrate that the assumption of constant Fermi contact interaction for ligand nuclei in a given symmetry is valid. For protons a small pseudo-contact term improves the data fit somewhat. The pseudo-contact term is unimportant for oxygen-17 and chlorine-35 interactions, where Fermi contact terms are large.

Introduction

The nmr spectrum of oxygen-17 in aqueous cobalt(II) perchlorate solutions has been investigated by several groups,²⁻⁴ and that of chlorine-35 in aqueous cobalt(II) chloride solutions at hydrochloric acid concentrations as high as 9.3 *M*⁵ also has been investigated. In both cases, there is appreciable line broadening attributable to the paramagnetic species, and large downfield line shifts are observed. In hydrochloric acid solutions, a very large increase in shift occurs in the intermediate concentration range, which appears to be associated

with the color change from pink to blue. Chesnut⁵ attributed the shifts in low concentration of hydrochloric

(1) (a) Work performed under the auspices of the U. S. Atomic Energy Commission. (b) Department of Chemistry, Pennsylvania State University, University Park, Pa. 16802. Visiting Staff Member. (c) Department of Chemistry, The University of Texas, Austin, Texas 78712. Consultant.

(2) J. A. Jackson, J. F. Lemons, and H. Taube, *J. Chem. Phys.*, **32**, 553 (1960).

(3) T. J. Swift and R. E. Connick, *ibid.*, **37**, 307 (1962).

(4) F. Klanberg, J. P. Hunt, and H. V. Dodgen, *Inorg. Chem.*, **2**, 139 (1963).

(5) D. B. Chesnut, *J. Chem. Phys.*, **33**, 1234 (1960).

acid to the presence of a single octahedral chloro cobalt(II) species, undergoing rapid exchange with chloride ions, and the enhanced shifts in concentrated solutions to a single tetrahedral species present in low abundance. Spectroscopists, working with concentrated hydrochloric acid solutions of cobalt(II) salts, have assumed the predominant species to be CoCl_4^{2-} .⁶ Cotton, Goodgame, and Goodgame⁷ compared the spectra of cobalt(II) in concentrated hydrochloric acid solutions with those of known CoCl_4^{2-} salts in organic solvents and concluded that the tetrahedral species present is principally $\text{CoCl}_3(\text{H}_2\text{O})^-$.

The present work was undertaken to determine the distribution of species over the entire range of acid concentrations and to establish the presence or absence of water molecules in the coordination sphere of the highest chloro complex. Although the value of the first formation constant has been reported by a number of investigators,⁸⁻¹⁵ the results vary over a wide range. Best values for K_1 lie in the region 0.2-0.7, but each is subject to some qualification, which creates doubt as to its validity. Nevertheless, it seems probable that the monochlorocobalt(II) ion, most likely $\text{CoCl}(\text{H}_2\text{O})_5^+$, is formed with a stability constant from 0.1 to 1. Results of most investigations suggest the formation of higher complexes, but no stability constants are reported. In most instances, experimental results suggest that only a single species is observed in addition to monochlorocobalt(II) and that it is anionic and tetrahedral.

From previous results of magnetic resonance measurements of oxygen-17 and chlorine-35 line shifts in cobalt(II) solutions, it appeared that determination of both, in the same solutions, might permit an accounting of the several species to be made. With some judicious assumptions, that has proved to be the case, and the results of those measurements are reported in the following sections.

Experimental Section

Reagent grade cobaltous chloride hexahydrate was used without further purification. The salt was analyzed by means of displacement of hydrogen ions from a cation-exchange resin. The resultant acid solution was titrated with standard sodium hydroxide solution and the cobalt(II) equivalence determined. The salt was found to have the composition $\text{CoCl}_2 \cdot 5.98\text{H}_2\text{O}$. Spectrographic analysis gave the following maximum abundances of transition metal impurities: Ni, 0.01%; Fe, 0.003%; Cu, 0.0005%; Cr, 0.001%; and Mn, 0.005%.

In most cases, hydrochloric acid was added by passing gaseous hydrogen chloride (Matheson) into the solution, but in a few instances Baker's Analyzed hydrochloric acid solution was added. In each solution the O^{17} was 1.7% or more. Descriptions of the preparation

of H_2O^{17} from NO^{17} and of the techniques of the magnetic measurements have been given previously.¹⁶

Results

Downfield shifts of both O^{17} and Cl^{35} were observed in all hydrochloric acid solutions of cobalt(II) chloride, relative to line-center positions in solutions of equivalent hydrochloric acid solutions in the absence of added paramagnetic salts. In the majority of cases, exchange between coordinated species, Cl^- or H_2O , and the corresponding entity in bulk solution was found to be rapid, so that³

$$\Delta\omega_N = p_N \Delta\omega_{\text{Co(N)}} \quad (1)$$

in which p_N is the number of ligands N complexed relative to total N present and $\Delta\omega_{\text{Co(N)}}$ is given by¹⁷

$$\frac{\Delta\omega_{\text{Co(N)}}}{\omega_N} = (1/2)S(S+1)(A_N/kT)(g_{\text{eff}}\beta/\hbar\gamma_N) \quad (2)$$

A_N is the spin exchange coupling constant (in ergs), g_{eff} is the effective g factor observed for the paramagnetic species, γ_N is the magnetogyric ratio for the nuclei, and ω is the resonant frequency of the unshifted nuclei. $T\Delta\omega_N$ is constant with change in temperature, if there is no change in species and exchange is rapid enough to give complete averaging. The latter was found to be true in all except oxygen-17 shifts at the lowest hydrochloric acid concentrations at 27°. Corrections were made using comprehensive line-broadening data to be reported in a latter communication.

Observed shift values are listed in Table I, columns 10 and 12, for a series of solutions in which hydrochloric acid concentration was varied from 0.424 to 15.69 *m*. Data are given in terms of $\Delta\omega'_{\text{Co(N)}}/\omega_N$ ($N = \text{O}^{17}$ or Cl^{35}), where

$$\Delta\omega'_{\text{Co(N)}} = \Delta\omega_N/p_N' \quad (3)$$

and

$$p_N' = \text{moles of Co(II)}/\text{moles of N} \quad (4)$$

(6) T. Dreisch and W. Trommer, *Z. Physik. Chem.*, **B37**, 37 (1937), and references cited therein.

(7) F. A. Cotton, D. M. L. Goodgame, and M. Goodgame, *J. Am. Chem. Soc.*, **83**, 4690 (1961).

(8) P. Job, *Compt. Rend.*, **196**, 181 (1933); **198**, 827 (1934).

(9) D. F. C. Morris and E. L. Short, *Electrochim. Acta*, **7**, 385 (1962).

(10) J. M. Smithson and R. J. P. Williams, *J. Chem. Soc.*, 457 (1958).

(11) M. W. Lister and P. Rosenblum, *Can. J. Chem.*, **38**, 1827 (1960).

(12) B. Tremillon, *Bull. Soc. Chim. France*, 1483 (1958).

(13) S. Tribalat and J. M. Caldero, *Compt. Rend.*, **255**, 925 (1962).

(14) R. A. Robinson and J. B. Brown, *Trans. Roy. Soc. New Zealand*, **77**, 1 (1948).

(15) R. H. Herber and J. W. Irvine, *J. Am. Chem. Soc.*, **80**, 5622 (1958).

(16) A. H. Zeltmann and L. O. Morgan, *J. Phys. Chem.*, **70**, 2807 (1966).

(17) N. Bloembergen, *J. Chem. Phys.*, **27**, 595 (1957).

Table I: Oxygen-17 and Chlorine-35 Line Shifts in Aqueous HCl Solutions at 27 ± 1°

Molality		α_{\pm}	α_1	α_0	α_1	α_2	α_3	α_4	$(\Delta'\omega_{\text{Co}(\text{O}^{17})}/\omega_{\text{O}^{17}}) \times 10^4$		$(\Delta'\omega_{\text{Co}(\text{Cl}^{35})}/\omega_{\text{Cl}^{35}}) \times 10^4$	
HCl	CoCl ₂								Exptl ^a	Calcd	Exptl ^b	Calcd
0.424	0.109	0.491	0.973	0.922	0.078	(1003) ^c	999	3.7	3.1
0.932	0.117	0.975	0.951	0.852	0.148	(993) ^c	987	6.1	6.6
1.99	0.123	2.39	0.898	0.689	0.310	0.002	(968) ^c	959	11.2	14.1
3.41	0.122	5.64	0.814	0.457	0.534	0.010	(930) ^c	919	21.2	25.9
3.89	0.115	7.22	0.798	0.390	0.595	0.015	(896) ^c	908	25.7	29.8
5.79	0.139	18.8	0.672	0.159	0.752	0.080	0.007	0.002	849	861	52.9	54.9
6.66	0.123	27.7	0.615	0.096	0.727	0.148	0.021	0.008	812	835	75.1	77.3
7.88	0.133	44.8	0.541	0.040	0.565	0.273	0.070	0.051	726	728	146	136
8.21	0.139	51.3	0.520	0.029	0.490	0.306	0.094	0.082	694	678	168	162
8.97	0.157	71.7	0.467	0.011	0.279	0.335	0.159	0.215	538	505	245	245
9.70	0.138	93.9	0.425	0.004	0.136	0.285	0.195	0.380	398	420	328	315
10.20	0.168	114	0.397	0.001	0.072	0.223	0.199	0.504	300	317	348	357
11.00	0.136	151	0.355	...	0.023	0.134	0.177	0.666	199	195	392	401
12.00	0.152	213	0.308	...	0.005	0.061	0.132	0.802	99.6	104.4	428	431
12.30	0.134	234	0.295	...	0.003	0.048	0.119	0.830	90.0	87.7	435	436
12.68	0.139	264	0.279	...	0.002	0.035	0.103	0.860	75.0	70.0	438	441
13.55	0.157	344	0.246	0.017	0.074	0.909	44.9	43.0	447	450
14.26	0.150	422	0.222	0.010	0.056	0.935	33.6	29.6	447	454
14.66	0.151	470	0.209	0.007	0.048	0.945	31.8	24.4	453	455
15.69	0.160	618	0.180	0.003	0.032	0.965	27.0	15.0	456	458

^a Resonant frequency = 8.000 Mc/sec. ^b Resonant frequency = 5.000 Mc/sec. ^c Corrected for incomplete averaging.

The relation between p_N' and p_N is

$$p_N = p_N' n \alpha_m \quad (5)$$

and α_m is the fraction of total cobalt(II) in species m , which contains n coordinated groups containing nucleus N. That breakdown is done to facilitate reduction of data in terms of species and coordination number. For example, in cobalt(II) perchlorate solution the principal species is $\text{Co}(\text{H}_2\text{O})_6^{2+}$, $\Delta\omega_{\text{Co}(\text{O}^{17})}/\omega_{\text{O}^{17}} = 0.101$, $\alpha_0 = 1.00$, and $n = 6$. Then, $\Delta\omega_{\text{Co}(\text{O}^{17})}/\omega_{\text{O}^{17}} = 0.0169$.

Behavior of $T\Delta\omega'_{\text{Co}(\text{N})}/\omega_N$ as functions of temperature for several hydrochloric acid concentrations is shown in Figures 1 and 2. At the lowest concentrations, the shifts for O¹⁷ at room temperature and below were not at their saturation (rapid averaging) values. The 27° values, listed in Table I, were corrected for incomplete exchange.³ Shifts for Cl³⁵ were in the limiting region for all solutions at 27°.

Measured extinction coefficients were obtained at 684, 658, and 619 mμ for a large number of cobalt(II) chloride solutions in the hydrochloric acid concentration range covered by the magnetic resonance measurements. Spectra were observed using a Cary Model 14 visible-ultraviolet spectrometer, the cell compartment of which was kept at 26 ± 0.2°. Cobalt(II) concentrations for those measurements were in the range 0.001–0.02 m ; 1-cm cells were used for the measurement at the lower concentrations of cobalt(II) and 1-mm cells for those at the higher concentrations. The spectra of standard aqueous solutions of methylene blue (pH 2.0) were used to obtain the relative path lengths. The data are shown as individual points in Figure 3. The system conformed

to Beer's law throughout the range represented. Above 15 m HCl, the spectrum does not change and ϵ at a given wavelength is constant to the limit of solubility of hydrochloric acid and lithium chloride. Each experimental point represents a separate sample, for which cobalt(II) and hydrochloric acid analyses were carried out.

Analysis of Shift Data. A qualitative indication of the nature of changes in the cobalt(II) hydrochloric acid solutions may be obtained by casual examination of the tabulated and plotted results. In Figure 1, the rapid rise with temperature at low HCl of normalized oxygen-17 shifts in the low temperature region is the result of increasing exchange rate for H₂O. In cobalt(II) perchlorate aqueous solution, values become constant at about 35°. Cobalt(II) chloride in hydrochloric acid solutions produces oxygen-17 shifts, which decrease at higher temperatures because of increasing chloro complex formation; the mean H₂O coordination number \bar{n} decreases. The opposite effect is seen in Figure 2 for chlorine-35 shifts as \bar{n} for Cl[−] increases.

Tabulated shifts at 27° show the effects of increasing hydrochloric acid concentration, as a decrease in oxygen-17 shift values is offset by increase in those for chlorine-35. At the highest concentration, the observed oxygen-17 shift is less than 3% of the values observed at very low concentrations of hydrochloric acid. It is apparent that very little exchanging H₂O remains in cobalt(II) complexes at that point. In the 5–9 m hydrochloric acid range, the relative decrease in oxygen-17 shifts is considerably larger than the corresponding increase in chlorine-35, suggesting a decrease in total co-

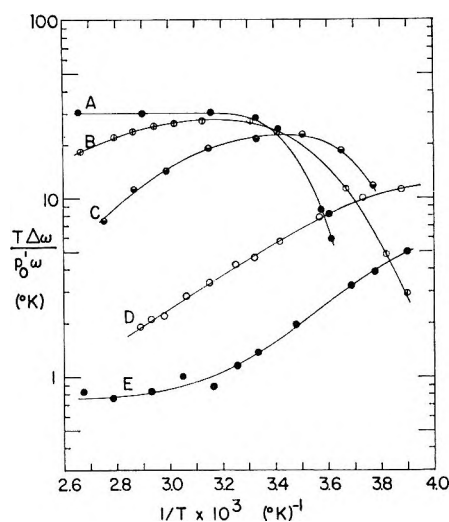


Figure 1. Temperature dependence of 8-Mc/sec O^{17} shifts in cobalt (II) solutions: (A) $\text{Co}(\text{ClO}_4)_2$ in 0.017 m HClO_4 , $p_{O'} = 0.00203$; (B) CoCl_2 in 5.73 m HCl , $p_{O'} = 0.002032$; (C) CoCl_2 in 7.8 m HCl , $p_{O'} = 0.002401$; (D) CoCl_2 in 11.3 m HCl , $p_{O'} = 0.003854$; and (E) CoCl_2 in 13.8 m HCl , $p_{O'} = 0.004493$.

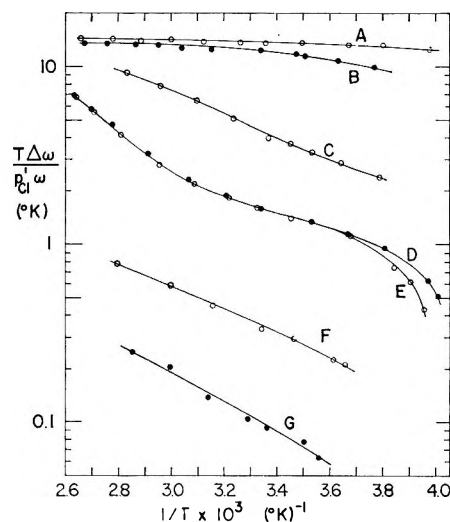


Figure 2. Temperature dependence of 5-Mc/sec Cl^{36} shifts in cobalt(II) chloride solutions: (A) 13.8 m HCl , $p_{\text{Cl}'} = 0.01748$; (B) 11.3 m HCl , $p_{\text{Cl}'} = 0.01826$; (C) 7.8 m HCl , $p_{\text{Cl}'} = 0.01651$; (D) 5.73 m HCl , $p_{\text{Cl}'} = 0.01894$, measured at 3 Mc/sec; (E) same solution as D measured at 5 Mc/sec; (F) 2.0 m HCl , $p_{\text{Cl}'} = 0.0445$; and (G) 0.424 m HCl , $p_{\text{Cl}'} = 0.1683$.

ordination number. That decrease parallels the change in solution color from pink to blue and the increase in ϵ_{av} at 684, 658, and 619 $m\mu$. ϵ_{av} is the absorbance in a 1-cm cell divided by cobalt(II) molarity.

Quantitative treatment of the data was based on equilibria among the several proposed complex species. A number of combinations were tried, including dehydration of the various chloro species without gain of Cl^- , change in total coordination number at later stages, and

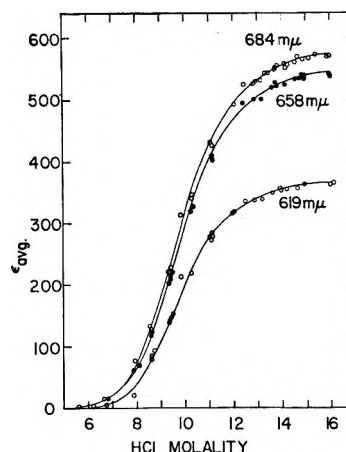
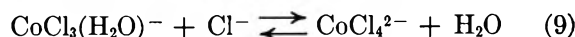
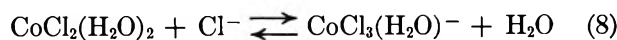
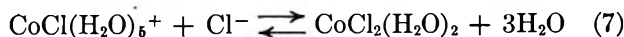


Figure 3. ϵ_{avg} as a function of HCl molality; the circles represent experimental data. The solid lines were calculated using the following equations: $\epsilon_{619} = 13.8\alpha_2 + 167.8\alpha_3 + 372.9\alpha_4$; $\epsilon_{658} = 72.1\alpha_2 + 180.1\alpha_3 + 555.7\alpha_4$; and $\epsilon_{684} = 76.2\alpha_2 + 203.7\alpha_3 + 585.7\alpha_4$.

restriction to fewer species. The minimum number of steps among the appropriate species is represented by the equations



Designating the cobalt(II) species by the fractional abundances, α_m , with m specifying the number of coordinated Cl^- , the successive equilibrium constants are with $a_1 = \text{water activity}$ and $a_{\pm\text{Cl}} = \text{mean Cl}^- \text{ activity}$

$$K_1 = (\alpha_1/\alpha_0)(a_1/a_{\pm}) \quad (10)$$

$$K_2 = (\alpha_2/\alpha_1)(a_1^3/a_{\pm}) \quad (11)$$

$$K_3 = (\alpha_3/\alpha_2)(a_1/a_{\pm}) \quad (12)$$

$$K_4 = (\alpha_4/\alpha_3)(a_1/a_{\pm}) \quad (13)$$

wherein it is assumed that the ratio of activity coefficients for the cobalt(II) complexes is constant. Thus, the equilibrium constants are semi-thermodynamic. That procedure is open to question where the charge type of the species changes and the nature of the medium varies significantly over the range of validity of the equation. Nevertheless, some such assumption is necessary and that one has proved to be reasonable in a number of instances.¹⁸⁻²⁰

It was assumed that ligand-shift values depend upon coordination number and configuration only. Thus,

(18) J. Bjerrum, *Kgl. Danske Videnskab. Selskab., Mat.-Fys. Medd.*, 22, No. 18 (1946).

(19) R. Nasänen, *Acta Chem. Scand.*, 4, 140, 816 (1950).

(20) G. A. Gamlen and D. O. Jordan, *J. Chem. Soc.*, 1435 (1953).

with octahedral complexes in the low hydrochloric acid concentration region and tetrahedral species at high concentrations, there are four shift parameters to be considered: $\Delta\omega^{\text{oct}}_{\text{Co}(\text{O}^{17})}$, $\Delta\omega^{\text{oct}}_{\text{Co}(\text{Cl}^{35})}$, $\Delta\omega^{\text{tet}}_{\text{Co}(\text{O}^{17})}$, and $\Delta\omega^{\text{tet}}_{\text{Co}(\text{Cl}^{35})}$. Those parameters and the several K 's were varied to obtain best fit to experimental data. A CDC 6600 subroutine was written for a least-squares program²¹ to obtain the best set of shifts and constants and to calculate net shift values on the basis of those parameters. Stoichiometric and ionic-strength corrections were built into the program as described below. Calculated net shift values are listed in Table I, columns 11 and 13, for the constants given in Table II. Relative abundances of the species which correspond to the listed constants are presented in Table I and plotted in Figure 4.

Table II: Equilibrium Parameters for Cobalt(II) Species in Aqueous Hydrochloric Acid Solutions^a

Equilibrium constant (300°K)	ΔH_f^b kcal/mole	ΔS_f^b entropy units
K_1 0.17 ± 0.06	2.9 ± 1.0	$+6.1 \pm 3.1$
K_2 $(1.7 \pm 0.4) \times 10^{-3}$	2.1 ± 1.0	-5.6 ± 3.4
K_3 $(3.1 \pm 0.9) \times 10^{-3}$	11.3 ± 1.3	$+26.2 \pm 4.4$
K_4 $(8.8 \pm 1.7) \times 10^{-3}$	0.80 ± 0.4	-6.7 ± 1.4

^a Based on $(\Delta\omega^{\text{oct}}_{\text{Co}(\text{O}^{17})}/\omega_{\text{O}^{17}}) = (1.68.6 \pm 2.2) \times 10^{-4}$; $(\Delta\omega^{\text{tet}}_{\text{Co}(\text{O}^{17})}/\omega_{\text{O}^{17}}) = (394.5 \pm 23.0) \times 10^{-4}$; $(\Delta\omega^{\text{oct}}_{\text{Co}(\text{Cl}^{35})}/\omega_{\text{Cl}^{35}}) = (44.2 \pm 14.0) \times 10^{-4}$; $(\Delta\omega^{\text{tet}}_{\text{Co}(\text{Cl}^{35})}/\omega_{\text{Cl}^{35}}) = (115.6 \pm 1.2) \times 10^{-4}$; all at 300°K. ^b In calculations of this quantity, no account was taken of the variation of activity coefficients with temperature. This quantity therefore includes a contribution due to that effect.

Approximate values of the K 's were used to calculate fractions of each complex species. The approximate ionic strength was then obtained by the relation

$$\mu = m_{\text{HCl}} + m_{\text{CoCl}_2}(3\alpha_0 + \alpha_1 + \alpha_4) \quad (14)$$

With

$$c/\mu = 0.9972 + 0.01817m_{\text{HCl}} - 0.015m_{\text{CoCl}_2} \quad (15)$$

values of $\gamma_{\pm}(\text{HCl})$ were calculated²² for solutions up to 4 m HCl. For higher concentrations, those values were obtained from the data of Akerlöf and Teare.²³ In each instance, the activity of water, a_1 , was gotten by integration of the Gibbs–Duhem equation over the appropriate range of γ_{\pm} . The activity values were then used to determine best values of the K 's by least-squares fit of shift data for both oxygen-17 and chlorine-35. Calculations were then repeated to refine the activity coefficients. Free chloride-ion concentrations were obtained from

$$[\text{Cl}^-] = m_{\text{HCl}} + m_{\text{CoCl}_2}(2\alpha_0 + \alpha_1 - \alpha_3 - 2\alpha_4) \quad (16)$$

Chloride activities are given by $a_{\pm} = \gamma_{\pm}[\text{Cl}^-]$.

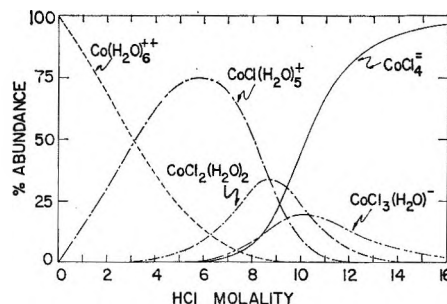


Figure 4. Abundances of the indicated cobalt complexes as a function of HCl molality; CoCl_2 molality, 0.11–0.16.

The mean ion activities of HCl have been used throughout this work in place of single chloride-ion activities which are unobtainable. Because we are primarily concerned with presenting equations which will readily permit the recovery of species concentrations over a wide range of hydrochloric acid concentrations, we are satisfied that the procedure is reasonable. Earlier attempts to obtain thermodynamic constants were made by approximating mean ionic activity coefficients from data on stand-in substances. However, truly suitable stand-in salts for which adequate data are available are not to be found. Standard deviations of the various parameters resulting from the data-fitting process are much larger than those for the parameters obtained by the procedure outlined previously. The added computational difficulty in recovering data from the listed constants when stand-in activities are used makes that method much less attractive than the one used here.

Horrocks and Hutchinson²⁴ have correctly suggested that the validity of the isotropic shift method of determining \bar{n} for a ligand may be questioned for pmr shifts since pseudo-contact interactions become important when a large g -tensor anisotropy is accompanied by a relatively small contact interaction coupling constant. However, ¹⁷O and ³⁵Cl hyperfine coupling constants are large, 1.34×10^7 cps and 2.53×10^6 cps, respectively, and this effect does not invalidate the isotropic shift method as is shown in the calculation below.

The electron–proton coupling constants for the equatorial and axial methanol OH protons of the complexes $(\text{H}_2\text{O})\text{Co}(\text{CH}_3\text{OH})_5^{2+}$ and $\text{ClCo}(\text{CH}_3\text{OH})_5^+$ have been determined directly: $A_M^{\text{eq}} = 2.9 \times 10^5$ cps, $A_M^{\text{axial}} = 6.0 \times 10^5$ cps, and $A_M^{\text{eq}} = 4.9 \times 10^5$ cps, and $A_M^{\text{axial}} = 3.3 \times 10^6$ cps, respectively.^{25,26} For these complexes,

(21) This program is based on R. H. Moore and R. K. Zeigler, Los Alamos Scientific Laboratory Report LA-2367, Los Alamos, N. M., Oct 1959, available from the Office of Technical Services, U. S. Department of Commerce, Washington, D. C.

(22) H. S. Harned and B. B. Owen, "The Physical Chemistry of Electrolyte Solutions," 3rd ed, Reinhold Publishing Corp., New York, N. Y., 1958, p 469.

(23) G. Akerlöf and J. W. Teare, *J. Am. Chem. Soc.*, **59**, 1855 (1937).

(24) W. DeW. Horrocks, Jr., and J. R. Hutchinson, *J. Chem. Phys.*, **46**, 1703 (1967).

(25) Z. Luz and S. Meiboom, *ibid.*, **40**, 1058 (1964).

(26) Z. Luz, *ibid.*, **41**, 1748 (1964).

the average A_M values, from which the chemical shifts in the rapid-exchange limit can be calculated, are 3.5×10^5 cps and 4.6×10^5 cps, respectively. These values are nearly the same as the A_M values measured for the unsubstituted complex $\text{Co}(\text{CH}_3\text{OH})_6^{2+}$: 3.9×10^5 cps, and 4.5×10^5 cps, respectively (the difference in the A_M values for this complex was attributed by Luz²⁶ to experimental error and "salt effects"). These data, which are a result of direct measurement, demonstrate that the A_M values for the mixed complexes are not significantly different from those of the unsubstituted complexes even for pmr measurements. The complex, $(\text{CH}_3\text{OH})_5\text{CoCl}^+$, should be reasonably similar to the chloro-aquo complex of $\text{Co}(\text{II})$, which we studied.

Equations 3 and 4 of ref 24 may be considered to define a coupling constant A_p . Rewriting eq 3

$$A_e = \frac{-\Delta\nu_e}{\nu} \frac{\gamma_{H^1}}{\gamma_e} \frac{3kT}{g\beta S(S+1)}$$

If ratios of A_e and A_p are to be meaningful, the coupling constants must be in the same units

$$A_p = \frac{-\Delta\nu_p}{\nu} \frac{\gamma_{H^1}}{\gamma_e} \frac{3kT}{g\beta S(S+1)}$$

Since

$$\frac{\Delta\nu_p}{\nu} = -\beta^2 S(S+1) \times \frac{(3g_{||}^2 + g_{||}g_{\perp} - 4g_{\perp}^2)}{45kT} \frac{(3\cos^2\chi - 1)}{r^3}$$

We may substitute for $\Delta\nu_p/\nu$ in the previous equation to find the following definition of $A_p(\text{H}^1)$

$$A_p(\text{H}^1) = \beta \frac{\gamma_{H^1}}{\gamma_e} \times \frac{(3g_{||}^2 + g_{||}g_{\perp} - 4g_{\perp}^2)}{15} \frac{(3\cos^2\chi - 1)}{r^3(\text{Co-H})}$$

Cobalt-hydrogen and cobalt-oxygen distances were estimated from data of Bullen²⁷ for cobalt(II) bis-acetylacetonate dihydrate. Therefore

$$A_p(\text{O}^{17}) = \beta \frac{\gamma_{\text{O}^{17}}}{\gamma_e} \frac{(3g_{||}^2 + g_{||}g_{\perp} - 4g_{\perp}^2)}{15} \frac{(3\cos^2\chi - 1)}{r^3(\text{Co-O})}$$

$$A_p(\text{O}^{17}) = \frac{\gamma_{\text{O}^{17}}}{\gamma_{H^1}} \frac{r^3(\text{Co-H})}{r^3(\text{Co-O})} A_p(\text{H}^1)$$

Anticipating that $A_p(\text{O}^{17})$ is negligible relative to $A_e(\text{O}^{17})$

$$A_M = A_p + A_e \simeq A_e = 1.34 \times 10^7 \text{ cps}$$

$$\frac{A_e(\text{O}^{17})}{A_p(\text{O}^{17})} = \frac{1.34 \times 10^7}{\frac{1.72 \times 10^5}{2} \frac{5.772}{42.577} \left(\frac{2.75 \times 10^{-8}}{2.05 \times 10^{-8}} \right)^3}$$

$$\frac{A_e(\text{O}^{17})}{A_p(\text{O}^{17})} = 494$$

A similar calculation may be made for ^{35}Cl , indicating that the pseudo-contact interaction may be neglected in that case also.

An alternate interpretation of the results for the cobalt(II) thiocyanate system²⁴ follows, assuming that temperature-dependence data would show the system to be in the fast-exchange region. Using four thiocyanate equilibria, analogous to eq 6-9 of this work, the proton data may be fitted quite well with the following two-parameter equation

$$\Delta\nu = (6p^{(6)} + 5p^{(5)})\Delta\nu_M^{\text{oct}} + (2p^{(2)} + p^{(1)})\Delta\nu_M^{\text{tet}}$$

where the individual terms refer to the complexes $\text{Co}(\text{H}_2\text{O})_6^+$, $\text{Co}(\text{NCS})(\text{H}_2\text{O})_5^+$, $\text{Co}(\text{NCS})_2(\text{H}_2\text{O})_2$, and $\text{Co}(\text{NCS})_3(\text{H}_2\text{O})^-$, respectively, with $\Delta\nu_M^{\text{oct}} = 4670$ cps and $\Delta\nu_M^{\text{tet}} = 22,390$ cps. The fit may be improved by assuming a pseudo-contact interaction contribution to the proton shift equal to about 20% of $\Delta\nu_M^{\text{oct}}$ for $\text{Co}(\text{NCS})(\text{H}_2\text{O})_5^+$. The two parameters then are $\Delta\nu_M^{\text{oct}} = 4530$ cps and $\Delta\nu_M^{\text{tet}} = 21,160$ cps.

Discussion

It is apparent from the relative mole fractions of species shown in Figure 4 that attempts to recover specific species distributions of the four coordinate complexes by most available methods, such as spectrophotometry, would be quite difficult, if not impossible. Solid curves in Figures 3 are those calculated from the concentrations given in Table I and least-squares deviation estimation of the molar extinction parameter. The curves were calculated using the following equations

$$\epsilon_{619} = 13.8\alpha_2 + 167.8\alpha_3 + 372.9\alpha_4$$

$$\epsilon_{658} = 72.1\alpha_2 + 180.1\alpha_3 + 555.7\alpha_4$$

and

$$\epsilon_{684} = 76.2\alpha_2 + 203.7\alpha_3 + 585.7\alpha_4$$

The fit to experimental data is better than the experimental error over the entire range of hydrochloric acid concentration. If the procedure is reversed and the observed data are interpreted in terms of expected cobalt(II) species, a single four-coordinate species suffices to rationalize the experimental results. The spectrophotometric method is not sensitive enough to the presence of the intermediate species to serve the analysis of the system.

In the treatment of successive equilibria, Bjerrum,¹⁸ Nasänen,¹⁹ and Gamlen and Jordan²⁰ eliminated water activity from their formulations. While this resulted in somewhat different equilibrium constants, when our data were treated in the same manner it did not lead to different interpretation. It was noted that the weighted variance of computed and experimental shifts was larger than in the treatment using water activity and

(27) G. J. Bullen, *Acta Cryst.*, **11**, 703 (1959).

the average deviation was greater than the experimental error of an individual shift determination.

Although the relative abundances of dichloro and trichloro complexes are low, their presence indicates the pathway by which successive coordination of chloride occurs and confirms CoCl₄²⁻ as the dominant species in concentrated hydrochloric acid solution. While there are apparently significant differences between the spectra of CoCl₄²⁻ in concentrated hydrochloric acid solutions and those in organic solvents⁷ the oscillator strengths of the former are not more than 8–10% less than those of the latter. The oscillator strength of (Φ₄As)₂CoCl₄ in CH₂Cl₂ is 5.38×10^{-3} as compared to 5.30×10^{-3} for the cobalt(II) species in 16 *m* HCl. That difference is presumably attributable to relatively strong ion-solvent coupling in aqueous solution.

Ligand shifts may be interpreted in terms of isotropic hyperfine coupling constants in the complex ions using eq 2. Static magnetic susceptibilities of octahedral and tetrahedral cobalt(II) species were taken to be 5.00 and 4.80 Bohr magnetons, respectively. Nuclear magnetogyric ratios are 3.628×10^3 radians sec⁻¹ gauss⁻¹ for oxygen-17 and 2.624×10^3 for chlorine-35. The several coupling constants are listed in Table III, together with the estimated fractional *s* character in the ligand atoms. The latter are based on $(A_{2s}/h)_{O^{17}} = 4.61 \times 10^9$ sec⁻¹ and $(A_{3s}/h)_{Cl^{35}} = 4.46 \times 10^9$ sec⁻¹, calculated from Hartree functions,^{28,29} and ³⁰

$$f_s = 2SA_N/A_{ns} \quad (17)$$

The ratio of coupling constants in tetrahedral and octahedral configurations is 2.49 for oxygen-17 and 2.80 for chlorine-35, as compared with 2.25 estimated from unpaired electron occupancy of σ antibonding orbitals in tetrahedral and octahedral cobalt(II). Our value of (A/h) for oxygen-17 in octahedral configuration is slightly lower than that reported by Swift and Connick,³ 1.48×10^7 sec⁻¹. That value was obtained from the shift listed by Jackson, Lemons, and Taube.² Our value for the coupling constant is based on much larger observed shifts from a variety of samples, and the oxygen-17 concentration was considerably greater.

The constant reported here is believed to be the better of the two.

The ratio of *f_s* values for oxygen-17 and chlorine-35 in octahedral species is 5.3, while that in tetrahedral is 4.7. It is generally true that fractional *s* character increases from fluorine to nitrogen in the second row of the periodic table. In CuF₂(H₂O)₂, the *f_s* for fluorine is 0.0055 and that for oxygen is 0.011.³¹ It is also to be expected that increased separation of *s* and *p* levels in chlorine, as compared to fluorine, decreases the *s* character of the bonding hybrid. Those two factors may be responsible for the rather large observed ratios.

Table III: Isotropic Spin-Exchange Coupling Constants for Oxygen-17 and Chlorine-35 in Cobalt(II) Complexes

Nucleus	Symmetry	Principal species used	$(A/h) \times 10^{-7}$, radian sec ⁻¹	$(A/h) \times 10^{-6}$, cps	$f_s \times 10^4$
Cl ³⁵	Octahedral	CoCl(H ₂ O) ₅ ⁺	1.59	2.53	1.9
Cl ³⁵	Tetrahedral	CoCl ₄ ²⁻	4.33	6.89	5.2
O ¹⁷	Octahedral	Co(H ₂ O) ₆ ²⁺	8.40	13.4	10.1
		CoCl(H ₂ O) ₅ ⁺			
O ¹⁷	Tetrahedral	CoCl ₃ (H ₂ O) ⁻	20.5	32.6	24.2

Acknowledgments. We are indebted to Dr. W. Burton Lewis and others for helpful comments during discussions of the work reported here. We also wish to thank Patricia Stein who made many of the measurements, Dr. B. B. McInteer and Mr. R. M. Potter of the Los Alamos Scientific Laboratory for supplying the enriched NO¹⁷, and Mr. S. V. Hooker of Pennsylvania State University for recording some of the electronic absorption spectra.

(28) D. R. Hartree, W. Hartree, and B. Swirles, *Phil. Trans. Roy. Soc. London*, **A238**, 229 (1940).

(29) D. R. Hartree and W. Hartree, *Proc. Roy. Soc. (London)*, **A156**, 45 (1936).

(30) F. Keffer, T. Oguchi, W. O. Sullivan, and J. Yamashita, *Phys. Rev.*, **115**, 1553 (1959).

(31) R. G. Shulman and B. J. Wyluda, *J. Chem. Phys.*, **35**, 1498 (1961).

On the Tait and Related Empirical Equations of State

by George A. Neece¹ and David R. Squire

U. S. Army Research Office, Duke Station, Durham, North Carolina (Received May 26, 1967)

The nature of the empirical parameters in the Tait equation and related empirical equations of state are examined and the dependence of these parameters upon the intermolecular-pair potential is investigated. The empirical parameters of the various equations of state considered are shown to be rather simply related. Explicit theoretical relationships for the parameters of a slightly modified form of the Tait equation, $(-1/v)(\partial v/\partial p)_T = C/[p + B(T)]$, are derived. The semiquantitative dependence of the Tait parameters on repulsive and attractive forces is obtained from the investigation of a hard-sphere model and a hard-sphere model with attractive forces. Quantitative dependence of the parameters in the various equations considered is found from the consideration of a classical equation of state valid at high number densities, which is derived from the cell model of Lennard-Jones and Devonshire. This equation of state gives the explicit dependence of the pressure upon all the parameters of the Mie potential. Values for the compressibility factors at high densities calculated using this equation of state are found to be in excellent agreement with those values calculated by the numerical integration of the free volume integral and associated integrals. The C and B parameters calculated from this theoretical equation of state are shown to depend upon both the attractive and repulsive forces. It is found in agreement with experimental observations that the C parameter is only slightly temperature dependent, and that the B parameter is a decreasing function of the temperature. The theoretically calculated C and B parameters for solid argon are found to be in good agreement with the experimentally determined values.

I. Introduction

Toward the end of the nineteenth century, Tait,² a noted Scottish mathematician and physicist, studied the compressibilities of glass, mercury, and water, and in the course of these studies he introduced an empirical equation which historically is usually written in the following form

$$-\frac{1}{v_0} \left(\frac{\partial v}{\partial p} \right)_T = \frac{C^*}{p + B^*(T)} \quad (1)$$

where p is the pressure, v_0 is a reference volume, and C^* and B^* are constants characteristic of the material being studied. During the intervening years, this empirical equation has proved to be very successful for both liquids and solids. Experimental data have been obtained and the two Tait parameters, C^* and B^* , have been experimentally determined and qualitatively discussed for a variety of liquid systems.³⁻⁷ The C^* parameter has been found to be nearly independent of temperature and density for a given liquid; the values for C^* have been found to range from 0.089 for liquid hydrocarbons to 0.149 for liquid water. The B^* parameter has been found to be a decreasing function of the temperature and is usually several hundred atmospheres in magnitude.

Often the Tait equation is modified so that the left-

hand side of the equation may be identified with the isothermal compressibility, K

$$-\frac{1}{v} \left(\frac{\partial v}{\partial p} \right)_T = \frac{C}{p + B(T)} \quad (2)$$

Frequently, this modified form is identified as the Tait equation.⁸ For dense systems the values of the parameters for the above equations will differ only slightly as may be seen from the following relationships between the parameters of eq 1 and 2

$$C^* = \frac{v}{v_0} \frac{C}{1 + C} \quad (3)$$

$$B^* + p = \frac{B + p}{1 + C}$$

- (1) Department of Chemistry, Cornell University, Ithaca, N. Y.
- (2) P. G. Tait, "Physics and Chemistry of the Voyage of H.M.S. Challenger," Vol. II, Part IV, 1888 S.P. LXI.
- (3) A. Carl, *Z. Physik. Chem.*, **101**, 238 (1922).
- (4) R. E. Gibson, *J. Am. Chem. Soc.*, **56**, 4 (1934).
- (5) R. E. Gibson and O. H. Loeffler, *J. Phys. Chem.*, **43**, 207 (1939).
- (6) R. E. Gibson and O. H. Loeffler, *Ann. N. Y. Acad. Sci.*, **51**, 727 (1949); contains a rather complete bibliography.
- (7) W. G. Cutler, R. H. McMickle, W. Webb, and R. W. Scieszler, *J. Chem. Phys.*, **29**, 727 (1958).
- (8) "Handbook of Chemistry and Physics," 47th ed, Chemical Rubber Publishing Co., Cleveland, Ohio, 1966, p F9.

Thus, it can be seen that it matters little which empirical form one chooses to describe the isothermal behavior of dense systems.

The Murnaghan equation⁹ for solids at high pressures is given by the expression

$$p = b^{-1}K_0 \left[\left(\frac{v_0}{v} \right)^b - 1 \right] \quad (4)$$

where K_0 is the bulk modulus corresponding to the reference volume v_0 and b is a constant. The integrated form of eq 2 is equivalent to eq 4 with the following relationships holding between the parameters of the two equations

$$b = \frac{1}{C} \quad (5)$$

$$K_0 = \frac{B}{C}$$

Experimental work has shown that eq 1 and 2 closely fit observed compressibilities over several thousand atmospheres for numerous liquids and solutions. MacDonald¹⁰ has pointed out the applicability of eq 1 and 2 in considerable detail.

In addition, eq 2 seems to describe the compressibilities of highly compressed gases quite well as is indicated in Figure 1 where $-v(\partial p/\partial v)_T$ vs. p is plotted for highly compressed argon gas¹¹ at 328°K and solid argon¹² at 77°K; according to eq 2, the slopes of these lines should be C^{-1} and the intercepts BC^{-1} . The insensitivity of the C parameter for argon to temperature can also be noted from Figure 1. Unfortunately, the data available on liquid argon are over such a short pressure range (pressures not exceeding 200 atm) that they were not plotted on the figure.

Although the Tait equation has been used for many years and is thought to be one of the most successful empirical equations for describing the isothermal equilibrium properties of liquids and solids,^{8,13} little theoretical work has been done on the equation. Kirkwood and Bethe¹⁴ have derived a modified form of the equation for extremely high pressures. Ginnell¹⁵ has interpreted the Tait equation in terms of his theory of molecular association. Recently Nanda and Simha,¹⁶ utilizing the principle of corresponding states, have examined the relationship between the Tait parameters and a theoretical equation of state, derived from a cell theory for oligomer and polymer liquids. However, in none of these investigations are the Tait parameters related to the parameters of the potential of intermolecular interaction. It has been suggested⁵ from qualitative arguments that C^* is a constant independent of the temperature, because it depends only on the repulsive forces between molecules, and that B^* represents the net internal pressure of the liquid; i.e., an increase in the attractive potential

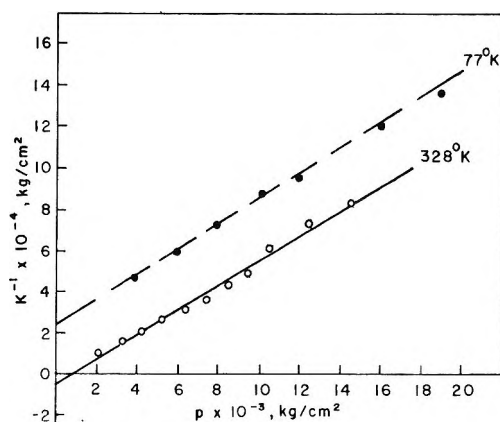


Figure 1. The inverse of the isothermal compressibility plotted vs. the pressure for solid argon at 77°K from Stewart,¹² ---, and for gaseous argon at 328°K from Bridgman,¹¹ —.

between molecules, a decrease in temperature, and an increase in free volume all cause B^* to increase. It has been found experimentally that C^* is nearly independent of temperature and volume, and that B^* is a decreasing function of the temperature. The C and B parameters of the modified equation behave similarly. The empirical b parameter of the Murnaghan equation, which was derived from the theory of finite strain, is not theoretically well understood. It has been generally observed that the b parameter is nearly independent of volume and temperature.¹⁷

In this paper we have attempted to relate the parameters of eq 1 and 2 to the parameters of an intermolecular-pair potential and to analyze the temperature dependence and other properties of these empirical parameters. In the following section, expressions are derived for the parameters of the Tait equation for a model in which there are only repulsive forces and compared with those derived from a model to which attractive forces have been added. In the third section, we derive from cell theory an equation of state which is accurate at high densities and which contains, explicitly, the dependence of the pressure upon the parameters of a general Mie potential. From this equation of state, the C and B of eq 2 are derived and their behaviors described.

(9) F. D. Murnaghan, "Finite Deformation of an Elastic Solid," John Wiley and Sons, Inc., New York, N. Y., 1951, Chapter 4.

(10) J. R. MacDonald, *Rev. Mod. Phys.*, **38**, 669 (1966).

(11) P. W. Bridgman, *Proc. Am. Acad. Arts Sci.*, **70**, 1 (1935).

(12) J. W. Stewart, *J. Phys. Chem. Solids*, **1**, 146 (1956).

(13) J. O. Hirschfelder, C. F. Curtiss, and R. B. Bird, "Molecular Theory of Gases and Liquids," John Wiley and Sons, Inc., New York, N. Y., 1954, p 261.

(14) J. G. Kirkwood and H. Bethe, "The Pressure Wave Produced by an Underwater Explosion," OSRD Report No. 588, Part 1, Department of Commerce Bibliography No. PB 32182.

(15) R. Ginnell, *J. Chem. Phys.*, **34**, 1249 (1961).

(16) V. S. Nanda and R. Simha, *J. Phys. Chem.*, **68**, 3158 (1964).

(17) J. J. Gilvarry, *J. Appl. Phys.*, **28**, 1253 (1957).

II. Tait Parameters from a Rigid-Sphere Model

In order to show in a semiquantitative way the dependence of the Tait parameters on repulsive and attractive forces, we consider first a system of rigid spheres and then a rigid-sphere system with attractive forces. An equation of state for a system of rigid spheres has been theoretically derived both from the scaled-particle theory¹⁸ and from solutions of the Percus-Yevick integral equation.^{19,20} This equation of state is given by

$$p_0 = \frac{kT}{v} \frac{(1 + y + y^2)}{(1 - y)^3} \quad (6)$$

where

$$y = \frac{\pi\sigma^3}{6v}$$

and v is the volume per molecule and σ is the diameter of a rigid sphere in the system. This equation of state should best be applicable at very high temperatures where attractive forces can be neglected. At lower temperatures, it is necessary to include the effects of attractive forces on the equation of state. Widom²¹ has shown that if the attractive forces in a system of rigid spheres provide a uniform negative potential, then thermodynamic consistency demands that the equation of state be given by

$$p = p_0 - \frac{a'}{v^2} \quad (7)$$

Guggenheim²² has shown that eq 7 works quite well for liquid argon at densities and temperatures between those at the triple and critical points.

From eq 1 the following general relationships can be obtained for calculating the C^* and B^* parameters

$$C^* = \frac{-\left(\frac{\partial p}{\partial v}\right)_T}{v_0 \left(\frac{\partial^2 p}{\partial v^2}\right)_T} \quad (8)$$

$$B^* = -\left[C^*v_0 \left(\frac{\partial p}{\partial v}\right)_T + p\right] \quad (9)$$

By taking the appropriate derivatives of eq 6 and 7, one can find the Tait C^* parameters to be

$$C^* = \frac{(1 + 2y)(1 - y)}{2(1 + 5y)} \quad (10)$$

for rigid spheres and

$$C^* = \frac{(1 + 2y)^2(1 - y) - \frac{2a'(1 - y)^6}{kTv}}{2(1 + 5y)(1 + 2y) - \frac{6a'}{kTv}(1 - y)^5} \quad (11)$$

for eq 7 where we have used the approximation

$$v \left(\frac{\partial^2 p}{\partial v^2}\right)_T \cong v_0 \left(\frac{\partial^2 p}{\partial v^2}\right)_T$$

At high temperatures, the temperature-dependent terms in the numerator and denominator in eq 11 become small and eq 11 reduces to eq 10. The C^* parameter of eq 10 is temperature independent, but it is density dependent through the y parameter, which in turn is directly proportional to the density.

The value of the y parameter is less than or equal to 0.740, and for $0.5 \leq v^*/v \leq 1.0$, C^* is of the order of 10^{-1} . For small variations of the density, which at high densities correspond to very large pressure changes, C^* does not change rapidly. The effect of adding an attractive term to the hard-sphere equation of state is to reduce the value of C^* by several per cent and to introduce into the C^* expression temperature-dependent terms. The variation with temperature of the C^* parameter in eq 11 is not very great, principally because the temperature-dependent terms occur as corrective terms in a ratio of two temperature-dependent expressions so that C^* varies only as the numerator changes relative to changes in the denominator of eq 11. At the triple point of argon, the empirically fitted values²² of y and a'/kTv are 0.427 and 8.56, respectively, so that $C^* = 0.108$. If the temperature-dependent terms are omitted, then $C^* = 0.169$. (From least-squares fits of plots of K^{-1} vs. p ,²³ the average value of C^* is 0.112 ± 0.02 for liquid argon.)

From this example, it seems that by considering only repulsive forces in the system, one can find the correct order of magnitude of C^* , but the attractive terms are very important at liquid temperatures and densities.

The B^* parameter can be found from eq 6-8 to be

$$B^* = -\frac{kT}{v} \frac{(1 + 6y + 2y^3)}{2(1 - y)^3(1 + 5y)} \quad (12)$$

for rigid spheres and

$$B^* = -\frac{kT}{v} \frac{1 - y^3 - C^*(1 + 2y)^2}{(1 - y)^4} + \frac{a'}{v^2} (1 - 2C^*) \quad (13)$$

for eq 7. The B^* parameter for rigid spheres is always negative; the B^* parameter for hard spheres with attractive forces contains a negative term, which is linearly dependent upon the temperature, and a positive temperature-independent term. (Here we are considering the temperature dependence of C^* param-

(18) H. Reiss, H. L. Frisch, and J. L. Lebowitz, *J. Chem. Phys.*, **31**, 369 (1959).

(19) M. S. Wertheim, *Phys. Rev. Letters*, **8**, 321 (1963).

(20) E. Thiele, *J. Chem. Phys.*, **38**, 1959 (1963).

(21) B. Widom, *ibid.*, **39**, 2808 (1963).

(22) E. A. Guggenheim, *Mol. Phys.*, **9**, 43 (1965).

(23) A. Van Itterbeck and O. Verbeke, *Physica*, **26**, 931 (1960).

eter to be negligible.) The positive term arises from the presence of attractive forces in the system. We thus conclude that the B^* parameter is a decreasing function of the temperature which depends strongly on both attractive and repulsive forces in the system.

III. Relationship of the Tait Parameters to the Mie Potential

In the preceding section it was demonstrated that the dependence of the Tait parameters on the intermolecular pair potential can be ascertained from the consideration of theoretical equations of state. By the nature of the equations considered, the nature of the dependence of the Tait parameters upon the intermolecular potential is necessarily limited to being only semiquantitative in character. However, the explicit dependence of the parameters of the Tait and related empirical equations of state upon the parameters of an intermolecular-pair potential such as a Mie potential can be successfully obtained from the consideration of a suitable model applicable to condensed systems.

In this section a classical equation of state valid at high number densities is derived from the cell model of Lennard-Jones and Devonshire. The equation is in excellent agreement with the numerically calculated results, under the conditions mentioned, and gives the explicit dependence of the pressure upon all the parameters of the pair potential used. The parameters of eq 2 are then calculated from this equation of state and their dependence upon the parameters of the intermolecular-pair potential and the temperature are analyzed.

In recent years several authors^{24,25} have pointed out that the cell model is indeed an excellent model for solids and high-density systems. Equation of state calculations based upon this model have been carried out for solid argon²⁶ and the results are in excellent agreement with experiment.

We proceed following the well-established approach beginning with the free-volume theory of liquids and solids for which the Helmholtz free energy is given by the relation

$$A = NkT \ln \frac{v_f \alpha}{\Lambda^3} + \frac{N\phi^*(0)}{2} \quad (14)$$

and

$$\Lambda = \frac{h}{(2\pi mkT)^{1/2}}$$

where v_f is the free volume per molecule, $N\phi^*(0)/2$ is the energy of the system when all the molecules are located at the centers of their cells, and α is the communal entropy term which is usually considered to be a constant and for crystalline solids is set equal to unity. In the one-shell LJD theory,²⁷ it is assumed that the nearest neighbors are smeared over a sphere of radius

equal to the nearest neighbor distance a , and v_f is given by

$$v_f = \int 4\pi r^2 \exp \left[-\frac{\Psi(r)}{kT} \right] dr \quad (15)$$

where

$$\Psi(r) = \phi(r) - \phi(0) \quad (16)$$

and

$$\phi(r) = \frac{c}{2} \int_0^\pi U(R) \sin \theta d\theta \quad (17)$$

where

$$R^2 = r^2 + a^2 - 2ar \cos \theta$$

$$a^3 = \gamma v$$

Here, v is the volume per molecule, and $U(R)$ is the potential of interaction.

Lennard-Jones and Ingham,²⁸ who included the effects of all shells, obtained the following general result for $\phi_\gamma^*(0)$

$$\phi_\gamma^*(0) = \frac{\epsilon}{n - m} \left[mc_\gamma f_{n,\gamma} \left(\frac{r^*}{a} \right)^n - nc_\gamma f_{m,\gamma} \left(\frac{r^*}{a} \right)^m \right] \quad (18)$$

where c_γ is the number of nearest neighboring molecules for the geometry indicated by γ , and $f_{n,\gamma}$ is a coefficient derived by adding the contributions to $\phi_\gamma^*(0)$ by all shells in which the molecules interact with a central molecule with a potential inversely proportional to r^n . The values of these coefficients are given in Table I for the Lennard-Jones 6:12 potential for the cubic lattices.

Table I: Values of $c_\gamma f_{12,\gamma}$ and $c_\gamma f_{6,\gamma}$

Lattice geometry	c_γ	γ	$c_{12,\gamma}$	$c_{6,\gamma}$
Simple cubic	6	1	6.2021	8.40192
Body-centered cubic	8	$3\sqrt{3}/4$	9.1142	12.2533
Face-centered cubic	12	$\sqrt{2}$	12.1318	14.4539

It is to be noted that $\phi_\gamma^*(0)$ is different from the lattice energy found by considering eq 17, since the lattice energy, $\phi(0)$, derived from eq 17 is based upon a one-shell calculation. Equation 17 can be applied to each shell surrounding a central molecule with appropriate changes of c and a . When three shells are considered

(24) W. L. Hoover and B. J. Alder, *J. Chem. Phys.*, **45**, 2361 (1966).

(25) J. A. Barker, "Lattice Theories of the Liquid State," Macmillan and Co., Ltd., New York, N. Y., 1963, Chapter 3.

(26) H. G. David and S. D. Harmann, *J. Chem. Phys.*, **38**, 3037 (1963).

(27) J. E. Lennard-Jones and A. F. Devonshire, *Proc. Roy. Soc. (London)*, **A163**, 53 (1937).

(28) J. E. Lennard-Jones and A. E. Ingham, *ibid.*, **A107**, 636 (1925).

Table II: A Comparison of One-Shell and Three-Shell Integrals for $c\epsilon/kT = 18.701^a$

v/v^*	g	g_I	g_m	G	g_L	g_M
1.00	2.172 (−4)	2.732 (−5)	5.886 (−6)	2.273 (−4)	2.952 (−5)	6.671 (−6)
0.95	1.491 (−4)	1.471 (−5)	3.202 (−6)	1.551 (−4)	1.573 (−5)	3.595 (−6)
0.90	1.009 (−4)	7.716 (−6)	1.695 (−6)	1.043 (−4)	8.179 (−6)	1.887 (−6)
0.85	6.722 (−5)	3.938 (−6)	8.716 (−7)	6.910 (−5)	4.138 (−6)	9.620 (−7)
0.80	4.399 (−5)	1.949 (−6)	4.341 (−7)	4.499 (−5)	2.032 (−6)	4.754 (−7)
0.75	2.821 (−5)	9.321 (−7)	2.086 (−7)	2.873 (−5)	9.650 (−7)	2.269 (−7)
0.70	1.768 (−5)	4.287 (−7)	9.634 (−8)	1.794 (−5)	4.410 (−7)	1.041 (−7)
0.65	1.079 (−5)	1.884 (−7)	4.248 (−8)	1.090 (−5)	1.927 (−7)	4.565 (−8)
0.60	6.371 (−6)	7.853 (−8)	1.774 (−8)	6.420 (−6)	7.991 (−8)	1.897 (−8)

^a The symbols g , g_I , g_m , G , g_L , and g_M are the same as those used in ref 29. The number in parentheses is the power of 10 by which the entry is to be multiplied.

and $\phi(0)$ is found in this manner, the coefficient of the repulsive terms in $\phi(0)$ and $\phi^*_\gamma(0)$ are almost the same, but those for the attractive terms are quite different. Often it has been the custom to use for one-shell calculations $\phi_\gamma(0)$ derived from eq 17. On the other hand, for three-shell calculations, a $\phi^*_\gamma(0)$, derived from eq 18 and Table I, is used. We choose as the lattice energy for solids $\phi^*_\gamma(0)$ of eq 18. (In an ideal cell model for a perfectly ordered solid, one would choose to calculate both the lattice energy and the free volume by a consideration of the interaction of a molecule with all of its surrounding shells. Fortunately, the equation of state in the temperature and density regions where the model is most applicable is quite insensitive to the number of shells used in a calculation of the free volume term, as we shall show shortly.)

Calculations of the three-shell integrals at high densities with $T = 77^\circ\text{K}$ and $\epsilon/k = 120^\circ\text{K}$ (corresponding to argon) were made and are compared to the single-shell integrals in Table II. All of our calculations of the various LJD integrals were done on an IBM 7072 computer using Simpson's rule. Accuracy to four significant figures was obtained by successively doubling the number of intervals until there was four place agreement. A direct comparison was made of our computed values for the three-shell integrals with the corresponding calculations of Wentorf, *et al.*,²⁹ and nearly exact agreement was found except at very low temperatures and high densities. Even under these conditions, the differences were found to be only a few per cent in most cases. It is evident from a consideration of these data that as the density increases, the differences in the one- and three-shell integrals correspondingly diminish. In Table III, it is noted that the free-volume contributions to the compressibility factors for the one-shell integrals become nearly equal at high densities, and from Table IV it can be seen that the compressibility factors for one-shell and three-shell calculations are virtually indistinguishable at high densities. The reasons for this can be seen by considering the relative contributions of the lattice energy and the free volume to the compressibility factors; the

Table III: A Comparison of Contributions to the Compressibility Factor for $c\epsilon/kT = 18.701$

v/v^*	Free-volume contribution to $p v/kT$			$\phi^*(0)$ contribution to $p v/kT$
	1 shell	3 shells	Approx	
1.00	8.38	8.52	9.50	−7.24
0.95	8.28	8.39	9.09	−3.49
0.90	8.17	8.27	8.75	+2.02
0.85	8.06	8.14	8.47	10.09
0.80	7.94	8.01	8.23	21.93
0.75	7.83	7.89	8.03	39.43
0.70	7.72	7.77	7.87	65.55
0.65	7.62	7.67	7.71	105.21
0.60	7.54	7.57	7.59	166.64

Table IV: A Comparison of Compressibility Factors for $c\epsilon/kT = 18.701$

v/v^*	$p v/kT$		
	1 shell	3 shells	Approx
1.00	1.14	1.28	2.26
0.95	4.79	4.90	5.60
0.90	10.19	10.29	10.77
0.85	18.15	18.23	18.56
0.80	29.87	29.94	30.16
0.75	47.26	47.32	47.46
0.70	73.27	73.32	73.42
0.65	112.83	112.88	112.92
0.60	174.18	174.21	174.23

relative change of these contributions with increasing densities can be found in Table III where it may be observed that the lattice energy term changes rapidly and at high densities is by far the dominant term. Thus, at high ρ it hardly matters whether the free-volume contribution is calculated using one shell or three shells.

In the derivation of the high-density equation of state which follows, we limit ourselves to one-shell consider-

(29) R. H. Wentorf, Jr., R. J. Buehler, J. O. Hirschfelder, and C. F. Curtiss, *J. Chem. Phys.*, **18**, 1484 (1950).

ations in determining the free volume and use for the pair-potential function the Mie potential

$$U(R) = \frac{\epsilon}{n-m} \left[m \left(\frac{r^*}{R} \right)^n - n \left(\frac{r^*}{R} \right)^m \right] \quad n > m \quad (19)$$

Using eq 16-18 we find that the potential field is given by the relation

$$\Psi[r(x)] = \phi_{n,m}(x) - \phi_{m,n}(x) \quad (20)$$

where

$$\phi_{n,m} = \frac{c\epsilon m}{2|m-n|} \left(\frac{r^*}{a} \right)^n \times \left[\frac{(1+x)^{n-2} - (1-x)^{n-2}}{(n-2)(1-x^2)^{n-2}} - 2 \right] \quad (21)$$

and

$$x = \frac{r}{a}$$

The usual procedure at this point has been to evaluate the free-volume integral numerically using eq 15, 20, and 21, and then to tabulate v_f and the associated integrals for different values of potential function parameters. Instead, we proceed by first expanding $\Psi(x)$ as given by eq 20 and retaining only the quadratic term, so that

$$\frac{\Psi(x)}{kT} \approx \lambda x^2 \quad (22)$$

where

$$\lambda = \frac{c\epsilon mn}{6kT(n-m)} \left[(n-1) \left(\frac{r^*}{a} \right)^n - (m-1) \left(\frac{r^*}{a} \right)^m \right] \quad (23)$$

Thus, in this approximation the free volume is

$$v_f = 4\pi a^3 \int_0^{0.55267} \exp(-\lambda x^2) x^2 dx \quad (24)$$

where the upper limit on the integral is that for a face-centered cubic lattice. At high number density, ρ , the value of the integral is insensitive to this limit and the results derived below are also valid for other cubic lattices. The free-volume contribution to the equation of state in this approximation is given by

$$kT \left(\frac{\partial \ln v_f}{\partial v} \right)_T = \frac{kT}{v} - \frac{kT \frac{\partial \lambda}{\partial v} \int_0^{0.55267} \exp(-\lambda x^2) x^4 dx}{\int_0^{0.55267} \exp(-\lambda x^2) x^2 dx} \quad (25)$$

At high ρ and low T , λ is very large, and the ratio of the two integrals in eq 25 is $3/(2\lambda)$. Consequently

$$\left(\frac{\partial \ln v_f}{\partial v} \right)_T = \frac{1}{v} - \frac{3}{2} \frac{\partial \ln \lambda}{\partial v} \quad (26)$$

and the compressibility factor is given by

$$\frac{pv}{kT} = 1 + \frac{1}{2} \frac{n(n-1) \left(\frac{v^*}{v} \right)^{(n-m)/3} - m(m-1)}{(n-1) \left(\frac{v^*}{v} \right)^{(n-m)/3} - (m-1)} + \frac{c_\gamma mn\epsilon}{6kT(n-m)} \left[f_{n,\gamma} \left(\frac{v^*}{v} \right)^{n/3} - f_{m,\gamma} \left(\frac{v^*}{v} \right)^{m/3} \right] \quad (27)$$

where

$$v^* = \gamma^{-1} r^{*3}$$

For $n = 12$, $m = 6$, and $c_\gamma = 12$, the lattice energy contribution to the compressibility factor is given by

$$\left(\frac{pv}{kT} \right)_{\phi^*(0)} = \frac{24\epsilon}{kT} \left[1.0110 \left(\frac{v^*}{v} \right)^4 - 1.2045 \left(\frac{v^*}{v} \right)^2 \right] \quad (28)$$

and the free-volume contribution is

$$\left(\frac{pv}{kT} \right)_{v_f} = 1 + \frac{66 \left(\frac{v^*}{v} \right)^2 - 15}{11 \left(\frac{v^*}{v} \right)^2 - 5} \quad (29)$$

In Table III, the free-volume contribution computed using eq 29 is compared with the numerically calculated one-shell and three-shell contributions; it is evident that the agreement is good and that it improves with increasing density. The compressibility factors computed using eq 28 and 29 are compared with the one shell and three shell numerically evaluated compressibility factors in Table IV. It is noted that the compressibility factors computed in this approximation at high densities are virtually indistinguishable from the numerically calculated values.

In the derivation of eq 27, we have used an expansion of $\Psi(x)/(kT)$ in which only the quadratic term was retained. To discuss this approximation briefly, we consider the expansion of eq 20, retaining the x^4 term

$$\frac{\Psi(x)}{kT} = \lambda(x^2 + \lambda^* x^4) \quad (30)$$

It can be shown that λ^* , which is temperature independent, decreases slowly with increasing density and is equal to approximately 10 over the range $1.25 \leq v^*/v \leq 2$. On the other hand, λ is a rapidly increasing function of the density; for $c\epsilon/kT = 18.7$ corresponding to argon at 77°K and $m = 6$, $n = 12$, the coefficient λ increases from 712 to 5834 as v^*/v increases from 1.25 to 2.

We conclude from the fact that $\lambda^* x^4 \approx 10x^4$ that this term is less than 5% of x^2 for $x < 0.07$, but for a large value of λ , say 2000, if $x = 0.07$, then $\lambda x^2 = 10$, and the integrand in the free-volume expression

given by eq 15 is very small, relative to its maximum value of approximately $(\lambda e)^{-1}$. Thus, for large values of λ corresponding to high ρ and low T , the x^4 term does not become important relative to the x^2 term until after the integrand in eq 15 is virtually zero. Similarly, one can show that higher order terms in the expansion of eq 16 can be neglected for high ρ and low T .

From eq 27, one can derive expressions for the C and B parameters of eq 2 and for the parameters of the Murnaghan equation and Tait equation for dense systems at low temperatures, which depend explicitly upon the parameters of a Mie potential and upon the density and temperature. The complete expressions for the B and C parameters as determined from eqs 2 and 27 are given by the equations

$$\frac{1}{C} + 1 = \frac{v^2 \left(\frac{\partial^2 p}{\partial v^2} \right)_T}{-v \left(\frac{\partial p}{\partial v} \right)_T} \quad (31)$$

$$B = -C^* v \left(\frac{\partial p}{\partial v} \right)_T - p$$

where

$$p = Tj_1 + j_2$$

$$-v \left(\frac{\partial p}{\partial v} \right)_T = -Tj_3 + j_4 + p \quad (32)$$

$$v^2 \left(\frac{\partial^2 p}{\partial v^2} \right)_T = p -$$

$$v \left(\frac{\partial p}{\partial T} \right)_v - \frac{(n-m+6)}{3} Tj_1 + Tj_5 + 2j_4 + j_6$$

with the j_i 's defined by the relations

$$j_1 = \frac{k}{v} \left[1 + \frac{1}{2} \frac{n(n-1)t^{n-m} - m(m-1)}{(n-1)t^{n-m} - (m-1)} \right]$$

$$j_2 = \frac{c\gamma mn\epsilon}{6(n-m)v} [f_{n,\gamma} t^n - f_{m,\gamma} t^m] \quad (33)$$

$$j_3 = \frac{k}{6v} \frac{(n-m)^2(n-1)(m-1)t^{n-m}}{[(n-1)t^{n-m} - (m-1)]^2}$$

$$j_4 = \frac{c\gamma \epsilon mn}{18(n-m)v} [nf_{n,\gamma} t^n - mf_{m,\gamma} t^m]$$

$$j_5 = \frac{k}{9v} \frac{(n-m)^3(m-1)(n-1)t^{2(n-m)}}{[(n-1)t^{n-m} - (m-1)]^3}$$

$$j_6 = \frac{c\gamma \epsilon mn}{54(n-m)v} [n^2 f_{n,\gamma} t^n - m^2 f_{m,\gamma} t^m]$$

with

$$t = \left(\frac{v^*}{v} \right)^{1/3}$$

A relatively simple expression for the C parameter can be derived from the preceding equations if some of the unimportant terms are dropped. Equation 31 shows the C parameter depends upon changes in the pressure with specific volume. A consideration of Table III shows that at high densities the change with density of the $\phi^*_{\gamma}(0)$ contribution to the pressure is over two orders of magnitude larger than the change in the free-volume contribution. Neglecting the contributions to the C parameter from free-volume contributions to pressure, one can show that

$$C = \frac{\left(\frac{v^*}{v} \right)^{(n-m)/3} f_{n,\gamma}(9+3n) - f_{m,\gamma}(9+3m)}{\left(\frac{v^*}{v} \right)^{(n-m)/3} f_{n,\gamma}(3+n)^2 - f_{m,\gamma}(3+m)^2} \quad (34)$$

One will note immediately that the expression above is independent of temperature. The temperature-dependent terms in C were lost when the free-volume contributions were dropped. In the complete expression, the temperature-dependent terms occur as small subtractive terms in the numerator and denominator of eq 31, and at high densities, these terms have a small effect on the value of C . The dependence of the C parameter upon the density is not small over all ranges of the density as Figure 2 shows. There C is plotted vs. v^*/v for $n = 12$, $m = 6$, $f_{n,\gamma} = 1.011$, and $f_{m,\gamma} = 1.2045$. However, for compressibility experiments carried out at high pressures and high densities, C can be considered to be nearly a constant, as the following illustration will show. In compressibility experiments on solid argon at 77°K, v^*/v ranges from about 1.15 to 1.34 as the pressure is changed from 4000 to 16,000 kg/cm². Over this range of pressure the theoretical value of C is 0.146 ± 0.015 including all the temperature-dependent terms (excluding the temperature-dependent terms C has a value of 0.129 ± 0.010 over this pressure range). Hence, within experimental accuracy, C is indeed nearly a constant over this pressure range.

From eq 31 and 32, one can express the B parameter by the relation

$$B = [C(j_2 + j_4) - j_2] - [j_1 + C(j_3 - j_1)]T \quad (35)$$

The algebraic expressions in square brackets in eq 35 are positive at high densities. The most important facts to notice about this expression are that B is a linearly decreasing function of the temperature, if the dependence of the C parameter upon the temperature is neglected, and that B depends not only upon n , m , and v^* , but also upon ϵ . (The C parameter given by eq 34 does not depend upon the well depth parameter ϵ .) The temperature-dependent and the temperature-independent terms in B at low temperatures are the same order in magnitude. Since B depends upon the difference between these two large positive terms in brackets, it is quite sensitive to small changes in the

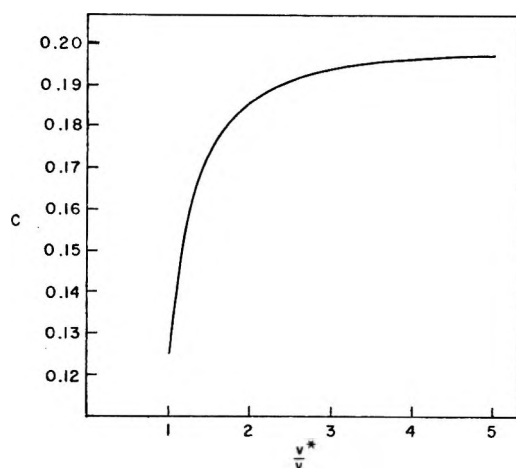


Figure 2. The C parameter plotted vs. the inverse of the reduced specific volume for a Mie potential with $n = 12$, $m = 6$, $f_{n,\gamma} = 1.011$, and $f_{m,\gamma} = 1.2045$.

parameters in each term, and it is particularly sensitive to the $v^* = \gamma^{-1}r^*$ parameter. The C parameter is not as sensitive as B to the v^* parameter, and hence B would be expected to change more than C as one considers molecules of different sizes. For solid argon at 77°K the experimentally determined values from a least-squares analysis of Stewart's data¹¹ for C and B are 0.168 ± 0.002 and 3940 ± 140 kg/cm², respectively, while over the same range of densities eq 32 predicts C to be 0.146 ± 0.015 and B to be 3680 ± 660 kg/cm². Both theoretical values are in good agreement with experiment.

IV. Discussion

Many empirical isotherms for liquids have been proposed over the years, and, as remarked by Moelwyn-Hughes,³⁰ they bear the marks of considerable similarity. In his book referenced above the following isotherm is introduced for liquids

$$v = v^0 [1 + \omega K^0 (p - p^0)]^{-1/\omega} \quad (36)$$

where v^0 is the volume and K^0 is the isothermal compressibility of the system at some reference pressure, p^0 ; ω is a constant which is experimentally determined by

$$\left(\frac{\partial \frac{1}{K}}{\partial p} \right)_T = \omega \quad (37)$$

Equation 36 can be shown to be identical with the Murnaghan equation and to the isotherm obtained from eq 2 where the B and C parameters are related in the following way to the parameters in the Moelwyn-Hughes equation

$$C = \frac{1}{\omega}$$

$$B = \frac{1}{K^0} - \omega p^0 \quad (38)$$

As discussed by Moelwyn-Hughes, eq 36 has some theoretical basis, since it has been shown that for molecules which obey Mie's potential, ω can be approximately derived from a harmonic oscillator model.³¹ A simple expression for ω for this model is found to be equal to $(n + m + 6)/3$ at a single value of the density, which he discusses. It is to be noted that eq 34 leads to this same result when v^*/v and the summation coefficients are set equal to unity.

In summary, the theoretical expressions derived for the Tait parameters, from eq 1 and 27, yield results which are in agreement with experimental observations in that C^* is found to be nearly temperature independent and 0.1 in order of magnitude, and B^* is found to be a decreasing function of the absolute temperature and more dependent on the particular substance than the C^* parameter. Good agreement was found between the theoretically calculated values of the C and B parameters and the experimentally determined values for solid argon. Finally, eq 5 and 34 indicate that the b parameter is nearly independent of temperature and depends only slightly on the specific volume if the range of pressures is not too wide, as observed experimentally.

Glossary of Symbols

a	Nearest neighbor distance
a'	van der Waals cohesive energy
A	Helmholtz free energy
b	Dimensionless parameter in the Murnaghan equation
B	Temperature-dependent parameter in the modified Tait equation
B^*	Temperature-dependent parameter in the Tait equation
c	Number of nearest neighbors
C	Dimensionless parameter in the modified Tait equation
C^*	Dimensionless parameter in the Tait equation
h	Planck's constant
k	The Boltzmann constant
K_0	Bulk modulus corresponding to reference volume, v_0
K	Isothermal compressibility
m	Integer exponent in the attractive energy term in the Mie potential
n	Integer exponent in the repulsive energy term in the Mie potential
N	Avogadro's number
p	Pressure

(30) E. A. Moelwyn-Hughes, "States of Matter," Interscience Publishers, Inc., New York, N. Y., 1961, Chapter V.

(31) E. A. Moelwyn-Hughes, *J. Phys. Chem.*, **55**, 1246 (1951).

r^*	Length parameter in the Mie potential	ϵ	Energy parameter in the Mie potential
T	Absolute temperature	ρ	Number density
U	Mie potential function	σ	Rigid-sphere diameter
v	Volume per molecule	$\phi(r)$	Interaction energy of a molecule with its neighbors
v_f	Free volume per molecule	$\phi(0)N/2$	Lattice energy (one shell)
w	Molecular mass	$\phi^*(0)N/2$	Lattice energy (all shells)
α	Communal entropy	ω	Experimentally determined constant equal to $1/C$
γ	Numerical constant that depends on the geometry of the lattice		

Application of the Electron-Donation Model for Hydrogen Absorption

to Palladium-Rich Alloys. Hydrogen-Gold-Palladium

by K. Allard, A. Maeland, J. W. Simons, and Ted B. Flanagan

Chemistry Department, University of Vermont, Burlington, Vermont 05401 (Received May 31, 1967)

Detailed data for absorption of hydrogen by a series of gold-palladium alloys have been obtained in the low-content α phase. Heats of absorption at infinite dilution determined from the extrapolation of the isosteric heats are: 5980 (cal/mole of H_2) (5.7), 7000 (15.3), 7540 (18.8), 9040 (26.5), and 9340 (44.7), where the number in parentheses refers to the atom per cent of gold in the alloy. Entropies of absorption have been obtained and are compared to values calculated from a model of localized protons treated as three-dimensional oscillators. Results are interpreted in terms of a model where both gold and hydrogen are assumed to donate electrons to the empty combined s and d bands of the palladium.

Introduction

The absorption of hydrogen by palladium-rich alloys is of interest from several points of view. Such investigations serve as useful tests of the electron-donation model for proton absorption proposed by Mott¹ for pure palladium-hydrogen and extended to a statistical mechanical model by Lacher.² It may also prove to be feasible to probe the band shape of palladium and its alloys by utilizing the data on hydrogen absorption. Finally, it may be pointed out that palladium alloys have frequently been utilized to show the influence of the electronic band of metals upon heterogeneous reactions.³ It appears to the present authors that the role of the electronic band structure of metals in influencing reactions of chemical interest should be probed with absorption systems such as those described here *before* the more complex problem of the correlation of electronic structure with surface catalysis is attempted. The main reasons for this suggested sequence

is that absorption data can be treated using bulk metallic properties, whereas heterogeneous catalytic data must be interpreted using more poorly characterized surface properties. In addition, these absorption systems are not as subject to the experimental problems associated with surfaces, *e.g.*, irreproducibility arising from contamination.

Although there have been data available on hydrogen absorption by palladium alloys, aside from the early work of Sieverts at elevated temperatures,⁴ the majority of the data at temperatures below approximately 120°

(1) N. F. Mott and H. Jones, "Theory of Metals and Alloys," Clarendon Press, Oxford, 1936; N. F. Mott, *Advan. Phys.*, **13**, 325 (1964).

(2) J. R. Lacher, *Proc. Roy. Soc. (London)*, **A161**, 525 (1937).

(3) *E.g.*, G. Bond, "Catalysis by Metals," Academic Press, London, 1962.

(4) Sieverts' extensive contributions are reviewed by F. A. Lewis, "The Palladium Hydrogen System," Academic Press, London, 1967.

have been determined using electrochemical techniques.^{4,5} This research has established the general features of the absorption behavior, such as the free energy and enthalpy changes corresponding to the $\alpha \rightarrow \beta$ phase transformation and the final hydrogen content at equilibrium (25°, 1 atm). The present investigation represents the first attempt to determine electrochemically equilibrium data of a series of palladium-rich alloys using the H₂-He dilution technique developed by Simons and Flanagan⁶ for the α phase of hydrogen-palladium.

An important exception to the above is the hydrogen-transfer catalyst method utilized by Wicke, Brodowsky, and their co-workers⁷ to determine hydrogen absorption behavior near room temperature. Aside from constituting an important experimental advance in this area of research, their analysis of their data also represents an important contribution. Specifically, these workers have investigated rather thoroughly hydrogen absorption by silver-palladium^{7b} and have done some research of a more preliminary nature on nickel-palladium,⁸ rhodium-palladium,⁸ tin-palladium,⁸ and lead-palladium alloys.⁸

The gold-palladium alloy system behaves similarly to the silver-palladium system with respect to hydrogen absorption, in that the absorption of hydrogen into the two-phase region becomes more exothermic as gold is added⁹ despite the fact that neither gold nor silver absorb hydrogen in their pure states. This present work reports detailed isothermal data of absorption of hydrogen by the gold-palladium alloy system in the low hydrogen content α phase, where problems associated with hysteresis are usually absent, and its interpretation in terms of the extended statistical mechanical model following a treatment of the absorption problem for pure palladium.^{6,10}

Electron-Donation Models of Proton Absorption

It is useful to discuss and develop the theories of hydrogen absorption in order to have the necessary equations for the interpretation of the data of the present study. The authors favor the model in which the hydrogen is absorbed as protons and its electrons are donated to the empty combined s-d bands of the metal.¹ (In the metal, the protons must be screened by electrons from the metallic bands; Mott has suggested that d-band electrons pile up to screen the protons.) It appears to us that the evidence in favor of this model for palladium and its alloys is rather convincing. Mackleit and Schindler¹¹ recently have shown directly from low-temperature electronic heat-capacity measurements that the density of states in the d band of palladium decreases with absorption of hydrogen. The present authors¹⁰ have shown that if the effect due to the filling of the empty s-d bands of palladium is included in the Lacher model, it is predicted that the heat of absorption decreases at high hydrogen contents, as

has been observed experimentally.¹² With reference to hydrogen absorption, it has been shown that the addition of tin or lead to palladium is about four times as effective as hydrogen or silver in the filling of d bands.⁸ There are still difficulties present in the model,¹³ but the above observations constitute strong evidence in its favor. A successful interpretation of the data obtained for palladium alloys in terms of this model will offer further evidence in its favor.

Wicke and Nernst^{12c} have employed an approach based on an earlier treatment by Wagner based on eq 1

$$RT \ln p_{H_2}^{1/2} = \mu_H =$$

$$\mu_{0H} + RT \ln \frac{n}{1-n} + \Delta\mu_H(n) \quad (1)$$

where n is H/Pd (or H/metal for alloys), and Brodowsky¹⁴ has further divided $\Delta\mu_H(n)$ into $\Delta\mu_{H+}(n) + \Delta\mu_e(n)$, where $\Delta\mu_{H+}(n)$ corresponds to the H-H interaction term and $\Delta\mu_e(n)$ corresponds to electronic terms due to band filling. From plots of $RT \ln p^{1/2}(1-n)/n$ vs. n (at small n), $\Delta\mu_{0H}$ and $\Delta\mu_H(n)$ are obtained. Brodowsky argues that the initial dependence of $\Delta\mu_e(n)$ upon n is small and will be neglected. This allows $\Delta\mu_{H+}(n)$ to be evaluated from the quasi-chemical approximation; i.e., the initial slope of $\Delta\mu_{H+}(n)$ is $12RT[1 - e(-W/RT)]$ where W is the apparent pair interaction energy in the lattice, which arises from strain and consequent aggregation of interstitial protons.^{14,15} Since $\Delta\mu_{H+}(n)$ is now known, $\Delta\mu_e(n)$ can be evaluated experimentally. Essentially the same treatment is employed by these workers for hydrogen absorption by palladium-rich alloys, e.g., ref 7b. An important new finding arises from their study of the silver-palladium alloys, namely, that the heat of absorption at infinite dilution ($n \rightarrow 0$) becomes more exothermic as the silver content increases. This trend may be inferred from

(5) E.g., F. A. Lewis, *Platinum Metals Rev.*, **4**, 132 (1960); **5**, 21 (1961).

(6) J. W. Simons and T. B. Flanagan, *J. Phys. Chem.*, **69**, 3773 (1965).

(7) See, for example: (a) *Techn. Bull. Englehard Ind. Inc.*, **7**, 41 (1966); (b) H. Brodowsky and E. Poeschel, *Z. Physik. Chem.*, **44**, 143 (1965); (c) H. Brodowsky, *Z. Naturforsch.*, **22a**, 130 (1967).

(8) H. Brodowsky and H. Husemann, *Ber. Bunsenges. Physik. Chem.*, **70**, 626 (1966).

(9) A. Maeland and T. B. Flanagan, *J. Phys. Chem.*, **69**, 3575 (1965).

(10) J. W. Simons and T. B. Flanagan, *Can. J. Chem.*, **43**, 1665 (1965).

(11) C. A. Mackleit and A. I. Schindler, *Phys. Rev.*, **146**, A463 (1966).

(12) (a) P. S. Perminov, A. A. Orlov, and A. N. Frumkin, *Dokl. Akad. Nauk SSSR*, **84**, 749 (1952); (b) P. L. Levine and K. E. Weale, *Trans. Faraday Soc.*, **56**, 357 (1960); (c) E. Wicke and G. H. Nernst, *Z. Elektrochem.*, **68**, 224 (1964).

(13) T. R. P. Gibb, J. MacMillan, and R. J. Roy, *J. Phys. Chem.*, **70**, 3024 (1966).

(14) H. Brodowsky, *Z. Physik. Chem.*, **44**, 129 (1965).

(15) M. von Stackelberg and P. Ludwig, *Z. Naturforsch.*, **19a**, 93 (1964).

studies of the two-phase free-energy changes,^{16,17} but such an inference is ambiguous. This surprising finding has introduced the necessity for a further interaction to be introduced into the statistical model, an interaction between the absorbed protons and the silver atoms. It is our opinion that the general features of the treatment of Brodowsky and co-workers are valid; it represents the first detailed interpretation of absorption by palladium-rich alloys. Two details deserve comment, however: firstly, the assumption of $n_s = 1$ is implicit in their treatment, and this choice may not be correct; secondly, the assumption that $\Delta\mu_o(n)$ is not significant as $n \rightarrow 0$ may be examined further.^{7b,c} The treatment given below discusses these points, and, in addition, the method outlined here has certain virtues, because the entropy and enthalpy terms are evaluated and discussed separately. It should also be pointed out that it makes little difference whether the Bragg-Williams² or quasi-chemical approximations⁷ are employed in this research, because for the small values of n employed here the two treatments have an identical functional dependence upon n .

The extended Lacher model for pure palladium-hydrogen was given recently as¹⁰

$$\ln p^{1/2} = \ln \frac{f^{1/2}}{Q(T)} + \frac{\ln \frac{n}{n_s}}{1 - \frac{n}{n_s}} + \frac{W_H}{RT} + \frac{X_d}{2RT} + \frac{2W_{HH}}{RT} \frac{n}{n_s} + \frac{We(n)}{RT} \quad (2)$$

where the terms are defined as before.¹⁰ This equation accounts for the alteration in the energy of electron donation with band filling by use of the $We(n)$ term. The combined s-d density-of-states relationship for palladium established by Hoare and co-workers¹⁸ from electronic heat capacities of silver-palladium, empirically, can be approximated by

$$N(E)_{s+d} = 4e^{-6.85E} \quad (3)$$

where E (ev) is the energy of the band relative to the Fermi level of pure palladium; this approximation is quite good to $E > 0.3$ ev (Figure 1). This is a better and more convenient approximation to the band shape than that employed previously.¹⁰ The rigid-band model upon which the band shape is based,¹⁸ has been shown to be erroneous.¹⁹ However, since both addition of hydrogen and silver or gold result in an apparent value of 0.6 hole in the d band, the use of the band established using silver and the rigid-band approximation may not be inappropriate for the case of hydrogen absorption.

For any gold-palladium alloy we have from eq 3

$$n = 0.584e^{-6.85E_{Au}} [1 - e^{-6.85\Delta E_H}] \quad (4)$$

where E_{Au} is the energy of the band corresponding to a

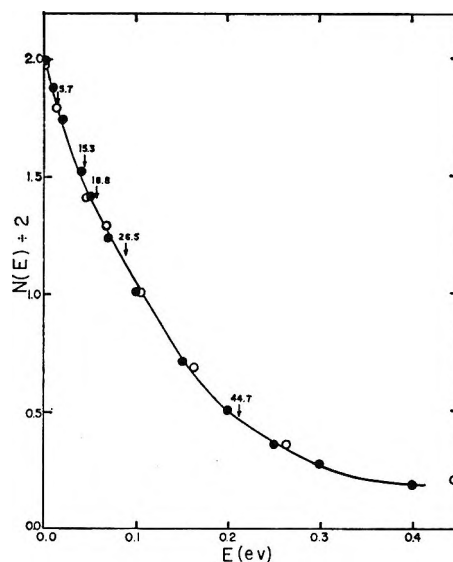


Figure 1. Density-of-states for the combined s and d bands of pure palladium for one spin direction based on specific-heat measurements of silver-palladium: O, data of ref 18; ●, approximate fit to data of ref 18 given by $2e^{-6.85E}$. The arrows represent the energy corresponding to the gold alloys used here, if gold donates its electron to the combined s-d bands of palladium.

given fraction of gold and ΔE_H is the energy increment corresponding to a given value of n ; i.e., $\Delta E_H = E - E_{Au}$ where E is the actual energy of the band at any value of n . For small values of n , ΔE_H is also small and eq 4 can be approximated by

$$\Delta E_H \simeq e^{6.85E_{Au}} n / 4.0 \quad (5)$$

This shows that for increasing gold contents, the energy of electron donation will be altered by the $e^{6.85E_{Au}}$ term, and, in addition, this should be directly proportional to n for small n . In this research, the poorest case of the approximation is for the 44.8% Au-Pd alloy and eq 4 is a good approximation to eq 3 for this alloy, to $n \leq 0.04$. This allows eq 2 to be rewritten in a more general form

$$\ln p^{1/2}(1 - \theta)/\theta = C_1 + (C_2/RT) + (C_3/RT)\theta = B(T, \theta) \quad (6)$$

where θ is n/n_s , C_1 , C_2 , and C_3 are determined from the experimental data, and C_3 includes the H-H interaction and the effect given by eq 5; these two effects operate in different directions. Equation 6 has been employed before for pure palladium-hydrogen,⁶ and as in the treatments given earlier,^{12c} $B(T, \theta)$ is plotted against θ , and $C_1 + (C_2/RT)$ is obtained as the intercept and C_3/RT

(16) F. A. Lewis and W. H. Schurter, *Naturwissenschaften*, **47**, 177 (1960).

(17) A. C. Makrides, *J. Phys. Chem.*, **68**, 2160 (1964).

(18) F. E. Hoare and B. Yates, *Proc. Roy. Soc. (London)*, **A240**, 42 (1957); F. E. Hoare, J. C. Mathews, and J. C. Walling, *ibid.*, **A216**, 502 (1953).

(19) J. J. Vuillemin and M. G. Priestley, *Phys. Rev. Letters*, **14**, 307 (1965).

Table I: Hydrogen Absorption Data for Several Gold-Palladium Alloys

n	273.2°K	298.0°K	323.2°K	348.0°K	n	273.2°K	298.0°K	323.2°K	348.0°K
	$P(\text{atm}) \times 10^4$	$P(\text{atm}) \times 10^4$	$P(\text{atm}) \times 10^4$	$P(\text{atm}) \times 10^4$		$P(\text{atm}) \times 10^4$	$P(\text{atm}) \times 10^4$	$P(\text{atm}) \times 10^4$	$P(\text{atm}) \times 10^4$
5.7% Au					18.8% Au				
0.0040	3.06	8.71	21.97	42.21	0.0031	0.406	1.18	2.06	3.30
0.0062	6.59	18.11	44.42	93.94	0.0040	0.568	1.75	2.87	4.57
0.0082	10.97	29.35	71.37	149.83	0.0057	0.761	2.42	3.99	6.38
0.0102	16.36	42.98	105.21	211.95	0.0066	1.04	2.96	5.11	7.88
0.0123	22.59	57.78	141.22	282.29	0.0075	1.29	3.79	6.45	9.51
0.0144	29.15	73.55	182.89	361.31	0.0083	1.53	4.44	7.60	11.41
0.0165	24.55	90.05	225.28	450.22	0.0090	1.89	5.23	8.96	13.36
0.0185		106.05	261.98	535.47	0.0099	2.18	6.01	10.33	15.70
0.0206		122.95	302.46	641.05	0.0107	2.48	6.65	11.65	18.02
0.0227		140.35	344.17	732.56	0.0116	2.79	7.77	13.13	20.68
0.0248		157.74	388.91	837.09	0.0123	3.12	8.67	14.81	23.23
0.0300			489.38	1085.66	0.0133	3.45	9.52	16.44	26.09
0.0350				1308.38	0.0140	3.79	10.54	18.12	29.51
0.0400				1505.29	0.0147	4.20	11.57	20.13	32.66
44.7% Au					0.0156	4.57	12.60	22.36	36.16
					0.0164	4.98	13.31	23.92	39.45
0.005	0.556	0.986		8.48	0.0180	5.80	14.62	28.19	46.62
0.010	1.21	3.79		37.13	0.0197	6.70	17.76	32.51	54.28
0.015	1.98	9.53	26.27	90.59	0.0214	7.55	20.11	36.92	62.76
0.020	8.64	19.19	52.26	178.46	0.0230	8.43	22.78	41.94	71.00
0.025	15.65	33.66	86.69	305.62	0.0247	9.42	25.21	45.88	79.74
0.030	29.27	56.73	129.32	496.89	0.0288	11.55	31.85	57.42	102.79
0.035	41.04	89.68	208.16	751.69	0.0329	13.76	40.24	69.78	125.03
0.040	61.95	135.67	314.92	1105.8	0.0370	15.54	48.13	82.89	145.61
0.045	88.98	192.54	455.95	1553.6	0.0412	17.21	56.24	99.85	165.92
0.050	125.75	263.57	650.91	2169.7	0.0494	20.40	72.18	121.45	201.81
0.055	176.33	362.26	912.64	2893.8	0.0576	23.38	87.02	147.54	240.17
0.060	245.27	501.85	1282.2	3851.9	0.0658	25.45	98.74	170.12	277.70
0.065	341.14	684.24	1762.2	5096.5	0.0743	27.01	108.22	188.92	316.44
0.070	473.58	942.31	2422.0	6275.0					

as the slope. The value of $2RC_1$ will be called ΔS° (the entropy change upon absorption when $\theta = 0.5$ and $dC_3/dT = 0$) and $2C_2$ will be called $\Delta \bar{H}^\circ$ ($\theta \rightarrow 0$). For palladium-hydrogen, $C_3 = -11,038$ cal/mole; therefore, the predominant effect is the H-H attractive interaction, and effects due to band filling may be present, but are not detectable because they have been obscured by the attractive interaction.

Results and Discussion

Heat of Absorption. When palladium is alloyed with gold, extensive single-phase (α) absorption of hydrogen can occur in certain of these alloys.⁹ One goal of this research was to utilize this fact in order to show directly from the isosteric heats of absorption, determined from the Clausius-Clapeyron equation, that the heat increases with n . This was not possible for pure palladium in the temperature range studied because the α -phase content is so small that any increase in the heat was within experimental error.⁶ Previously, the increase in the heat was shown to exist with the aid of eq 1 or its equivalent, eq 6.^{6,7b,12c} Admittedly, these equations are very general, but they do assume localized absorption and an interaction which depends linearly

upon θ , and it is reassuring that the isosteric heats generally agree with those predicted by the equations (see below).

A series of slow runs with H₂-He mixtures were made and are illustrated in Figure 2. The data are a composite of runs from different specimens, and a variety of surface activation procedures. It is believed that these data, which can be converted to P vs. n , utilizing relationships between R/R_0 and n determined elsewhere for these alloys (Table I), correspond closely to equilibrium. The most important fact showing that these data closely approach equilibrium is that any further reduction in the H₂ partial pressure, and its accompanying slowing of the absorption run, did not significantly alter the relationships obtained. Plots of $p^{1/2}$ vs. n show straight-line behavior at small values of n , and these generally pass through the origin; i.e., the data follow Sieverts' law as expected for equilibrium data. It was not possible to use this experimental technique for alloys with gold contents of 44.7%. This is, in all probability, due to the fact that diffusion is too slow for the attainment of equilibrium using this technique (0-60°).

The isosteric heats of absorption are shown as a

Table II: Thermodynamic Parameters for Hydrogen Absorption in the α Phase by Au-Pd Alloys at 25°

% Au	$-\Delta\bar{S}^\circ$ eu/mole of H ₂	$-\Delta\bar{H}^\circ$ cal/mole of H ₂	$-2C_2$ cal/mole of H ₂	$\frac{d\Delta\bar{H}}{dn}$	$2C_3^b$	$2C_3^c$	$\frac{dC_3^c}{dT}$
0	25.9 ^a	(4623) ^a	4623 ^a	...	-22,075	-22,075	...
5.7	29.3	5980	6440	-43,400	-21,258	-19,886	37.4
15.3	11.2	7000	8300	-37,600	-18,750	-12,366	32.0
18.8	32.2	7540	7140	-20,600	-12,540	-10,542	10.5
26.5	31.6	9040	8480	-14,400	-6,600
44.7	32.2	9340	9440	+21,160	+14,388	+7,874	-8.0

^a Reference 6. \bar{H}° was not determined directly in ref 6, but was obtained from $2C_2$. ^b Calculated using $n_s = 1$. ^c Calculated using $n_s = \text{Pd}/(\text{Au} + \text{Pd})$.

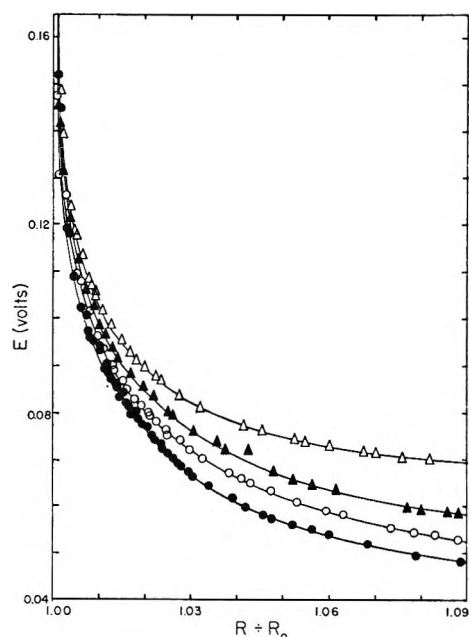


Figure 2. Electrode potentials of 18.8% Au-Pd alloy vs. standard hydrogen electrode, plotted against relative resistance of the specimen: Δ , 273°K; \blacktriangle , 298°K; \circ , 310°K; and \bullet , 320°K.

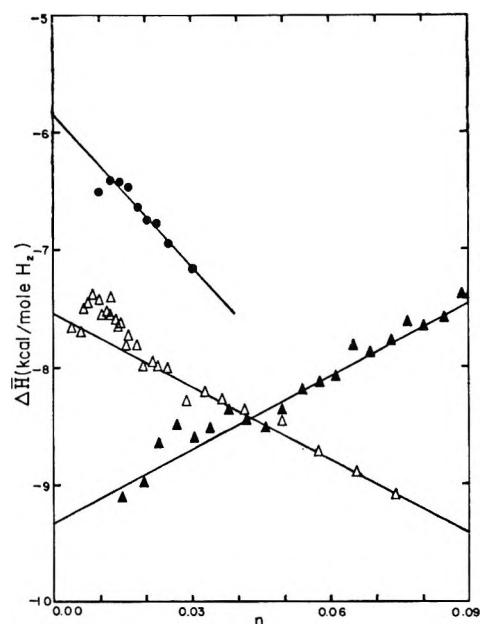


Figure 3. Typical plots of isosteric heats of absorption against n , H/M: \bullet , 5.7%; Δ , 18.8%; and \blacktriangle , 44.7% Au-Pd.

function of n for various alloys (Figure 3). It may be seen that $\Delta\bar{H}$ is approximately a linear function of n for the small values of n studied here. Scatter of the data is considerable at very small values of n and these have not been weighted as much as larger values. The slope $\partial\Delta\bar{H}/\partial n$ becomes less negative with gold content and, in fact, the 44.7% alloy shows an increase in $\Delta\bar{H}$ with n (Table II). This latter observation is in keeping with the electron-donation model, *i.e.*, the density-of-states has declined to a value low enough so that the filling in of the band predominates over the H-H interaction. The important quantities, $\Delta\bar{H}^\circ$, can also be obtained by extrapolation to $n = 0$ (Figure 3). These values are plotted in Figure 4, where they are compared to the data of silver-palladium.^{7b} It is of interest that the differences between the added gold or added silver content are less marked when the fundamental quantity $\Delta\bar{H}^\circ$ is plotted against per cent of added metal rather than $\Delta H_{\alpha \rightarrow \beta}$. The reason for this is that in the

case of, for example, the 10% Ag and Au alloys β_{\min} is $\sim 0.44^{7b}$ and 0.37, respectively (the latter value is obtained by interpolation between the 8.7 and 11.90% Au alloys⁹). Accompanying the transformation in the silver alloy, there is a larger contribution from H-H interaction because β_{\min} corresponds to a larger H content than in the comparable gold alloy. This illustrates the caution which must be used in employing only the thermodynamic parameters characteristic of the $\alpha \rightarrow \beta$ phase change when generalizing about the properties of the alloy systems toward hydrogen absorption. Figure 4 shows that $\Delta\bar{H}^\circ$ increases with percentage of added metal; the gold data are linear to approximately 26.5% and extrapolate back to the value for pure palladium.⁶ The value for the 44.7% alloy shows a marked deviation from this linearity; this is in accordance with the electron-donation model. The fact that the heat of absorption increases with added metal means that gold in palladium, analogously to silver in palladium,^{7b,16,17} exhibits an apparent interaction between the added metal and the hydrogen, and

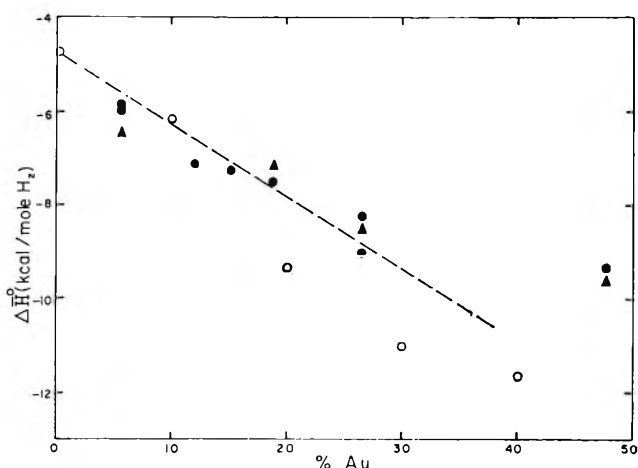


Figure 4. Heats of absorption at infinite dilution ($n \rightarrow 0$) compared to comparable values for silver-palladium alloys (ref 7b): ●, from extrapolated values of $\Delta\bar{H}$ (where two values are given, these represent values determined by two different workers at different times); ▲, calculated values of $2C_2$; ○, values for silver-palladium.^{7b}

allowance must be made for this in the models for hydrogen absorption by alloys. The origin of this interaction is subject to controversy,^{7b,17} but recent results by Wicke, Brodowsky, and their co-workers^{7,9} offer strong evidence in favor of an interaction arising from the relief of strain by the congregation of interstitial protons, the energy of which is perturbed by the nature of the added metal; *i.e.*, the presence of large compressible added atoms increases the apparent interaction. Gold fits into the picture in a qualitative way, *i.e.*, its compressibility and size are greater than that of palladium. There are, therefore, at least two effects governing the relationship between $\Delta\bar{H}^\circ$ and percentage of added gold, the H-Au interaction and the effect of filling the combined s-d bands of palladium (these, of course, operate in different directions). It can be shown from the approximate band shape (eq 3) that the initial energy of electron donation increases in a linear way with fraction of gold in the alloy to include at least the 18.8% gold alloy; therefore, a nearly linear relationship observed between $\Delta\bar{H}^\circ$ and percentage gold (0 to 18.8%, Table I) is not inconsistent with the electron-donation model. Both the H-Au interaction and the electron-donation energy change in direct proportion to the gold content (Figure 4), and the H-Au interaction is the most important factor.

It is useful, in order to test the model of absorption, to calculate the heats of absorption from eq 6 and to compare them with the isosteric heats. Some typical plots of B (eq 6) *vs.* θ are shown in Figure 5. It may be seen that the plots are reasonably linear; C_3 is obtained from the slope, and C_1 and C_2 are obtained from the temperature dependence of the intercepts of the B plots (Table II). Equation 6 may be plotted using various values for n_s ; Figure 5 shows $n_s = 1$ and

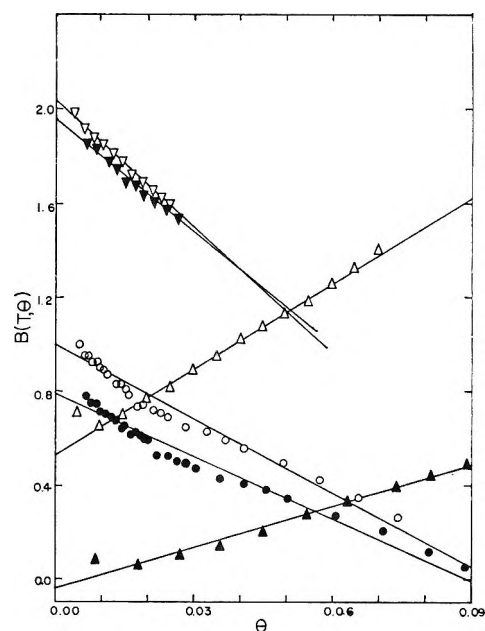


Figure 5. Representative $B(T, \theta)$ *vs.* θ plots for several gold contents: open symbols represent n_s chosen as 1; filled symbols represent n_s chosen as fraction of palladium; ▼, 5.7%; ○, ●, 18.8%; and ▲, △, 44.7% Au-Pd.

0.552 (fraction of palladium) for the 44.7% alloy. There is no basis for choice between $n_s = 1$ or $n_s =$ fraction of palladium, on the basis of the B plots; both exhibit approximately the same degree of linearity. The values of C_1 , C_2 , and C_3 are determined from these plots and the heats can be calculated from

$$\Delta\bar{H}(\theta) = -2RT^2 \left(\frac{\partial \ln p^{1/2}}{\partial T} \right)_\theta = 2C_2 + 2C_3\theta - 2T\theta \left(\frac{dC_3}{dT} \right) \quad (7)$$

The last term on the right-hand side of this equation must be included in order to get reasonable agreement with the more directly determined values. It is also theoretically expected that C_3 should have a significant temperature dependence.⁷ In earlier work with pure palladium,⁶ Simons and Flanagan found good agreement between an average isosteric heat and that evaluated *via* eq 7 without including the dC_3/dT term. The reasons for this is that while dC_3/dT may be large for pure palladium (its value may be estimated by extrapolation of the data for the alloys given in Table II), the limiting concentration of hydrogen in the α phase of pure palladium is so small that on an average $-2T\theta \cdot (dC_3/dT)$ contributes less than 200 cal; whereas, in the alloys, which have larger values of θ , this term becomes more important. The remarkable agreement between the average isosteric heat of 4780 ± 100 cal/mole with the average value of 4777 determined from eq 4 in ref 6 (which has an incorrect sign—it should read, $2C_2 + 2C_3n = -4623 - 22,075n$) must be regarded as fortuitous, although, coincidentally, ref 12c gives 4777

for this value too, again taking $n = 0.007$ for the average value of n . The temperature dependence of C_1 has been omitted because it cannot be evaluated directly from the data; estimates based on the Einstein model give the value of $RT^2(dC_1/dT)$ of the order of 300 cal/mole.

Values of dC_3/dT can be determined directly from the slopes of the B plots for the alloys, or, alternatively, dC_3/dT can be obtained by differentiation of eq 7 with respect to θ , *i.e.*

$$\frac{\partial \Delta \bar{H}(\theta)}{\partial \theta} = 2C_3 - 2T \left(\frac{dC_3}{dT} \right) \quad (8)$$

upon substitution of this value for dC_3/dT into eq 7, we obtain

$$\Delta H(\theta) = 2C_2 + \theta(\partial \Delta \bar{H}(\theta)/\partial \theta) \quad (9)$$

This procedure now becomes essentially an expansion of $\Delta \bar{H}(\theta)$ about $\theta = 0$ since $2C_2 = \Delta \bar{H}^\circ$ and the dependence of $\Delta \bar{H}$ on θ essentially duplicates the results of the directly determined isosteric heats, except that this procedure does give two methods to obtain $\Delta \bar{H}^\circ$, and it allows us to determine dC_3/dT (Table II) for use in the entropy calculations (see below). It can be seen from the form of eq 9 that in the relationships between $\Delta \bar{H}(n)$ *vs.* n , it makes no difference which value of n_s is chosen. To show the validity of eq 7 then, we must use an independent value of dC_3/dT ; for the 44.76% Au alloy, these data appear good and the $\Delta \bar{H}(n)$ values agree reasonably well with those determined from the Clausius–Clapeyron equation. It should also be mentioned that the value of $2C_2$ agrees quite well with that of $\Delta \bar{H}^\circ$ (Table II). There is no basis for judgment in the choice between $n_s = 1$ and $n_s = \text{fraction of palladium}$ from these heats of absorption.

Entropy of Absorption. The entropy of absorption is determined experimentally from $2F[(\partial E)/(\partial T)_n]$ and is shown as a function of n for several alloys in Figure 6. The entropy of absorption also can be determined from eq 6, *i.e.*

$$\Delta \bar{S} = 2RC_1 + 2\theta(dC_3/dT) + 2R \ln [\theta/(1 - \theta)] \quad (10)$$

and in addition $\Delta \bar{S}$ can be calculated from the Einstein model, *i.e.*

$$\Delta \bar{S} = 2R \ln [\theta/(1 - \theta)] - S^\circ_{H_2} + 2S_a - 2\theta(dC_3/dT) \quad (11)$$

where $S^\circ_{H_2} = 31.21$ (298°K) and S_a is the entropy of a proton treated as a localized three-dimensional isotropic oscillator. In earlier work by the authors on α -phase palladium–H₂,⁶ a value of ν_H was employed corresponding to the β phase, since the α -phase value of ν_H was then unavailable. Recently, a determination of ν_H for the α phase has been made using neutron scattering.²⁰ The value of ν_H for the alloys may be somewhat different from this, but in the absence of

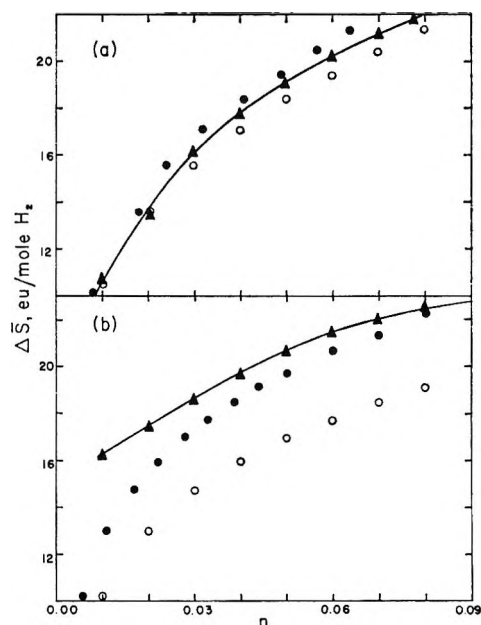


Figure 6. Representative plots of isosteric entropy of absorption *vs.* n : (a) 18.8% Au–Pd and (b) 44.7% Au–Pd; and ▲, experimental values; ●, calculated values using $n_1 = \text{fraction of palladium}$; and ○, calculated values using $n_s = 1$.

specific data the value for α Pd–H₂ will be employed. One of the authors²¹ has found that the hydrogen is located in the octahedral holes in the α phase of the 15.3% gold–palladium alloy. It was also found that ν_H changed with n , but this effect is believed not to alter seriously the value of S_a for the small values of n employed in this research. Again in the earlier work,⁶ the last term in eq 6 was omitted, but its contribution is small in the α -Pd–H₂ system because θ is small.

The value of dC_1/dT is a relatively small term (eq 9) and has been omitted. If n_s is chosen as fraction of palladium, the agreement of $\Delta \bar{S}(n)$ with the experimental values is somewhat better than for $n_s = 1$ for the 44.7% Au alloy, where the differences between the two values of n_s are the greatest. This is the only evidence in favor of this choice for n_s , and further work must be done to allow a choice to be made, *e.g.*, determination of ν_H in the alloys by neutron scattering.

Values of $\Delta \bar{S}^\circ$ ($\theta = 0.5$, $dC_3/dT = 0$) are equal to $2RC_1$ and are shown in Table II. The variation in the entropy of absorption is small enough in the change from the 5.7 to 44.7% Au to be accounted for by a change in ν_H with gold content. The changes in $\Delta \bar{S}^\circ$ are comparable to those observed for the silver–palladium system.^{7b}

The equilibrium value of n is, of course, attained when $\Delta \bar{H} = T\Delta \bar{S}$ and, for example, the 44.7% Au–Pd alloy

(20) W. Kley, J. Peretty, R. Rubin, and G. Verson, Symposium on Inelastic Scattering of Neutrons by Condensed Systems, Brookhaven National Laboratory, Upton, N. Y., 1965.

(21) A. Maeland, presented at the 153rd National Meeting of the American Chemical Society, Miami Beach, Fla., April 1967.

reaches $n = 0.107$ at 25° , 1 atm of H_2 . No unexpected effects operate and the main reason that absorption ceases in this alloy at a rather low value of n is that the heat of absorption declines with n , so that $T\Delta\bar{S} = \Delta\bar{H}$ at $n = 0.107$. The internal consistency of the data for this alloy can be shown from the fact that experimentally determined plots of $T\Delta\bar{S}$ vs. $\Delta\bar{H}$ intersect at values of n close to those determined by direct analysis of the hydrogen content of samples at equilibrium. Plots of $\Delta\bar{G}$ vs. n for the 44.7% alloy are quite linear from $n = 0.06$ – 0.10 ; this is expected if the logarithmic relationship holds, *i.e.*, $\ln p^{1/2} (\text{atm}) = A(T) + B(T)n$. Wicke, Brodowsky, and co-workers have shown that this relationship holds for silver-palladium alloys.⁷ Flanagan and Simons²² have shown recently that this previously empirical relationship follows from the effect of filling in of the combined s-d bands of palladium by hydrogen. Thus, the fact that the data of the 44.7% Au-Pd alloy follow the logarithmic relationship at relatively low values of added hydrogen supports the electron-donation model, *i.e.*, both gold and hydrogen act as electron donors to the empty s-d bands of palladium.

Role of the Added Gold in the Filling in of the Combined s-d Bands of Palladium. Equation 2 can be rewritten in a form suitable for alloys as

$$\ln p = 2C_1^0 + 2 \ln \frac{\theta}{1-\theta} + \frac{2C_2^0}{RT} + \frac{2W_M}{RT} + \frac{2W_e^M}{RT} + \frac{2}{RT}(2W_{HH}^M + 5770n_s e^{6.85W_e^M})\theta \quad (12)$$

where C_1^0 , C_2^0 are the values corresponding to pure palladium-hydrogen, W_M and W_e^M are the changes in the energy relative to pure palladium introduced by the added metal for the H-lattice interaction and the shift of the Fermi energy by the added metal at $n \rightarrow 0$ and W_{HH}^M is the H-H interaction as perturbed by the added metal and the last term accounts for the filling in of the s-d bands of the alloy by hydrogen using eq 4. Expressing C_2 and C_3 in terms of the parameters of eq 12, we have $C_2 = C_2^0 + W_M + W_e^M$ and $C_3 = 2W_{HH}^M + 5770n_s e^{6.85W_e^M}$. Now if the approximate band shape is employed, we may obtain W_M and W_{HH}^M . This is, admittedly, a questionable procedure, but at the present stage of development there is no other possibility for separation of these effects and this procedure yields results which serve as a semiquantitative test for the electron-donation model. For example, by employing the experimental values of C_2^0 , C_2 and the calculated values of W_e^M for the various gold alloys

Table III: Some Parameters for Absorption of Hydrogen by Au-Pd Alloys Derived from the Density-of-States Curve for Palladium

Alloy, % Au	W_{Au} , cal	$2W_{HH}^{Au}$, cal	E_L , cal
0	0	-16,807	8403
5.7	-1232	-15,398	7699
15.3	-1662	-12,809	6404
18.8	-2573	-12,187	6093
26.6	-3959	-10,970	5485
44.7	-7319	-10,378	5189

(Table III), where W_{Au} represents W_M for the specific case of gold-palladium alloys, *etc.*, n_s has been taken as the fraction of palladium in the alloy in the calculations shown in Table III, since this value appears to give more reasonable results. It can be seen that the energy of the inclusion of the proton into the lattice (W_{Au}) decreases almost linearly (more favorable entry into the lattice) with gold content; this holds true even for the high gold-content alloy (44.7% Au). This effect could not have been seen from the values of C_3 (Table II). Similarly values of $2W_{HH}^{Au}$ decrease with gold content. These approximate calculations show that the electron-donation model allows the values of C_2 and C_3 to be broken down into terms which show quite reasonable trends with gold content.

It is concluded that the data of the present research are compatible with the electron-donation model in which both gold and hydrogen donate electrons to the combined s-d band of palladium. In addition, the results are in qualitative agreement with the strain model introduced to account for the H-H^{14,15} and H-M⁷ interaction. For example, Brodowsky¹⁴ gives $E_L \simeq C_2$, which may be modified for the density-of-states effect so that in our terminology $E_L \simeq -W_{HH}$, where E_L is the energy needed to insert an isolated proton into the lattice. Now W_{Au} and E_L should be related, *i.e.*, if the strain effect lowers the energy necessary to incorporate a proton into the lattice, then the decrease in W_{Au} should be equal to the decrease in E_L . This is roughly seen to be the case.

Acknowledgment. Financial support of this research by the U. S. Atomic Energy Commission is gratefully acknowledged. The authors are indebted to Englehard Industries, Inc., for the loan of the gold-palladium alloys used in this research.

(22) T. B. Flanagan and J. W. Simons, *J. Phys. Chem.*, **70**, 375C (1966).

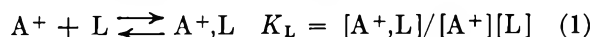
Investigation of the Validity of Several Approximations in Measurements of Cation-Ligand Association Constants by a Conductance Method^{1a}

by J. B. Ezell and W. R. Gilkerson^{1b}

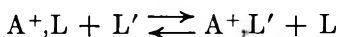
Department of Chemistry, University of South Carolina, Columbia, South Carolina 29208
(Received June 8, 1967)

The effects of several phosphine oxides on the conductances of tri-*n*-butylammonium picrate in nitrobenzene, of tri-*n*-butylmethylammonium perchlorate in *o*-dichlorobenzene, and of tri-*n*-butylmethylammonium iodide in chlorobenzene, all at 25°, have been determined. These results are used to test the validity of a titration method for determining cation-ligand association constants, to determine the effect of ligand association on cation mobility, and to investigate the effect of changing solvent on the displacement of one ligand on a cation by another.

This paper is a report of further work in our continuing investigation² of cation-ligand(solvent) association in low dielectric solvents (eq 1)



where A^+ represents the cation (quarternary or tertiary ammonium), L represents the ligand (such as amines and phosphine oxides), and A^+,L represents the cation-ligand complex. We concentrate in this paper on the following aspects of systems involving cation-ligand association: the effect of changing the solvent on the displacement of one ligand (L) in a cation complex by another (L') (eq 2), the effect of ligand association



$$K_D = K_L'/K_L = [A^+,L'][L]/[A^+,L][L'] \quad (2)$$

on ion mobility, and a detailed test of the reliability of the titration procedure (hereafter denoted method II) used in many cases³ to determine values of K_L .

Experimental Section

The salt tri-*n*-butylammonium picrate (Bu_3NHPi) was prepared and purified as before.^{2a} Tri-*n*-butylmethylammonium perchlorate was prepared and purified as before.^{2c} Methyltri-*n*-butylammonium iodide (Bu_3NMeI) was prepared by mixing equimolar quantities of tri-*n*-butylamine and methyl iodide in hexane solution, allowing the mixture to stand 12 hr at room temperature. The resulting crystals of Bu_3NMeI were filtered off and recrystallized from methanol by adding diethyl ether, mp 186–188° (lit.⁴ mp 186°). The salt was pumped down overnight *in vacuo* at 65° prior to each use. Triphenylphosphine oxide (Ph_3PO) was purified as before.^{2c} Di-*n*-butylphenylphosphine oxide was prepared and purified as before.^{2d} Tri-*n*-butylphosphine oxide (Bu_3PO) was prepared⁵ by the

addition of 1 mole of trichlorophosphine oxide to 4 moles of *n*-butyl bromide Grignard reagent in ether solution. The resulting solution was worked up in the usual manner. The solid Bu_3PO was recrystallized from hexane. The product was then twice distilled at 1 mm and dried overnight *in vacuo*, mp 67–68° (lit.⁶ mp 62–63°). The solvents *o*-dichlorobenzene (ODCB) and chlorobenzene ($PhCl$) were purified as before.^{2a} Nitrobenzene ($PhNO_2$) solvent was purified following Witschonke and Kraus,⁷ except the nitrobenzene was stored over alumina (previously fired to 1000°) after each of three distillations. The solvent was passed

(1) (a) This research was supported in part by a grant from the U. S. Army Research Office, Durham, N. C.; (b) author to whom inquiries should be addressed.

(2) (a) E. R. Ralph, III, and W. R. Gilkerson, *J. Am. Chem. Soc.*, **86**, 4783 (1964); (b) W. R. Gilkerson and E. R. Ralph, III, *ibid.*, **87**, 175 (1965); (c) W. R. Gilkerson and J. B. Ezell, *ibid.*, **87**, 3812 (1965); (d) J. B. Ezell and W. R. Gilkerson, *ibid.*, **88**, 3486 (1966); (e) W. R. Gilkerson and J. B. Ezell, *ibid.*, **89**, 808 (1967).

(3) We have used two general approaches in determining K_L . The first method (ref 2a), hereafter denoted method I, is to determine the conductances of a salt as a function of salt concentration in a series of solvent-ligand mixtures of increasing ligand concentration. Ion-pair dissociation constants for the salt in each of these solvent mixtures are then calculated using usual extrapolation techniques, and thence used to calculate ligand association constants. We believe this first method to be the most reliable. The second method is experimentally much simpler. A solution of the appropriate salt in pure solvent is titrated with increments of a solution of the ligand in the solvent, the conductance of the salt solution being determined for each increment of the ligand-solvent mixture. The conductance data are then treated to yield values of K_L . Several assumptions (ref 2d) are involved in this latter calculation. We wished to carry out a direct comparison of these two procedures for obtaining K_L .

(4) R. L. Shriner, R. C. Fuson, and D. Y. Curtin, "Systematic Identification of Organic Compounds," 4th ed, John Wiley and Sons, Inc., New York, N. Y., 1956, p 296.

(5) We wish to thank Dr. T. H. Siddall, III, of the Savannah River Laboratory, E. I. du Pont de Nemours and Co. for aid in preparation of a series of *n*-butyl-substituted phenylphosphine oxides.

(6) C. A. Blake, K. B. Brown, and C. F. Coleman, U. S. Atomic Energy Commission Report ORNL-1964, p 71, 1955.

(7) C. R. Witschonke and C. A. Kraus, *J. Am. Chem. Soc.*, **69**, 2472 (1947).

Table I: Effect of Addends on Equivalent Conductances of Ammonium Salts at 25° (*C*, moles/l.; Λ , ohm⁻¹ cm² equiv⁻¹)

10°C	A	10°C	A	10°C	A	10°C	A
Bu ₃ NHPi in PhNO ₂				Bu ₃ MeNClO ₄ in ODCB			
No Addend		0.00833 <i>M</i> in Ph ₃ PO		+0.01285 <i>M</i> Bu ₃ PO		+0.02082 <i>M</i> Bu ₃ PO	
1.584	26.40	1.621	25.46	1.343	23.45	1.379	24.22
3.325	24.62	2.813	25.03	2.656	19.06	2.603	20.21
5.829	22.78	4.091	24.62	4.120	16.41	3.739	18.00
9.550	20.78	5.374	24.26	5.548	14.73	4.821	16.51
13.430	19.27	6.571	23.94	7.129	13.41	5.807	15.46
16.910	18.19	7.888	23.61	8.512	12.53	6.656	14.73
		9.216	23.30	9.926	11.81	7.873	13.85
0.01457 <i>M</i> in Ph ₃ PO		0.02093 <i>M</i> in Ph ₃ PO		+0.03723 <i>M</i> Bu ₃ PO			
1.599	25.34	2.071	25.17	1.009	27.67		
2.793	25.02	4.277	24.72	1.994	23.75		
4.114	24.72	6.672	24.33	3.408	20.48		
5.499	24.44	8.764	24.02	4.519	18.78		
6.757	24.18	10.600	23.77	5.704	17.43		
7.945	23.96	12.820	23.46	7.056	16.23		
9.340	23.71	14.890	23.21				
0.00894 <i>M</i> Bu ₂ PhPO		0.01620 <i>M</i> Bu ₂ PhPO		No Addend		+0.00846 <i>M</i> Ph ₃ PO	
1.908	25.64	2.897	25.36	0.1670	1.624		
3.560	25.31	4.746	25.10	0.3304	1.150	1.348	0.7085
5.320	25.02	6.573	24.90	0.4769	0.9602	3.113	0.4767
7.014	24.74	8.160	24.75	0.6050	0.8544	5.244	0.3747
8.651	24.39	9.745	24.59	0.7825	0.7540	7.126	0.3266
10.147	24.29	11.360	24.44	1.994	0.4677	9.521	0.2877
11.830	24.08	12.990	24.30	4.131	0.3304	13.14	0.2512
0.02503 <i>M</i> in Bu ₂ PhPO				6.982	0.2611	16.28	0.2300
2.027	25.37			11.45	0.2123	20.98	0.2083
3.366	25.23			+0.01159 <i>M</i> Ph ₃ PO			
4.915	25.09			1.321	0.7555		
6.352	24.98			2.864	0.5251		
7.887	24.85			5.649	0.3845		
9.361	24.72			8.153	0.3266		
11.132	24.62			10.89	0.2879		
				14.24	0.2572		
				17.35	0.2373		
				21.21	0.2191		

through fired alumina^{2a} just prior to each use. The specific conductance ranged from 2 to 8×10^{-10} ohm⁻¹ cm⁻¹, 0.5% or less of the conductance of the most dilute salt solutions. Conductance measurements were carried out at 25° with cells, a bridge, and a thermostat already described.² The physical constants of the solvents at 25° are given in the order dielectric constant, density (g/cc), and viscosity (cp). PhNO₂:⁸ 34.69, 1.1977, 1.839; ODCB: 10.06,⁹ 1.3007,^{2a} 1.272;¹⁰ PhCl: 5.621,¹¹ 1.1011,^{2a} 0.752.¹²

Results

The equivalent conductances, Λ , of Bu₃NHPi at various salt concentrations in PhNO₂ with and without added Ph₃PO or Bu₂PhPO, and of Bu₃MeNClO₄ in ODCB with added Bu₃PO, and of Bu₃MeNI in PhCl with and without added Ph₃PO appear in Table I. In each case the specific conductance of the solvent has

been subtracted from that of the solution to obtain that presumed due to the salt alone. The resistances of the solutions in PhNO₂ were measured at 1, 5, and 10 kHz. Polarization was indicated by a small decrease in *R* as the oscillator frequency was increased. Resistances at infinite frequency were determined as the intercepts of plots of resistance vs. $1/\sqrt{f}$ as $1/\sqrt{f} \rightarrow 0$. These last differed from the 1 kHz values by 0.1%.

The conductance data, with the exception of those for

(8) H. Sadek and R. M. Fuoss, *J. Am. Chem. Soc.*, **76**, 5905 (1954).

(9) P. H. Flaherty and K. H. Stern, *ibid.*, **80**, 1034 (1958).

(10) F. Accascina, E. L. Swarts, P. L. Mercier, and C. A. Kraus, *Proc. Natl. Acad. Sci. U. S.*, **39**, 917 (1953).

(11) A. A. Maryott and E. A. Smith, National Bureau of Standards Circular No. 514, U. S. Government Printing Office, Washington D. C., Aug 1951.

(12) R. L. McIntosh, D. J. Mead, and R. M. Fuoss, *J. Am. Chem. Soc.*, **62**, 506 (1940).

Bu₃MeNI in PhCl, were treated by the method of Shedlovsky¹³ (eq 3), where S is the Shedlovsky function

$$1/\Delta S = 1/\Lambda^0 + \Delta S C y_{\pm}^2 / K (\Lambda^0)^2 \quad (3)$$

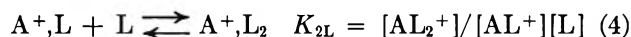
and y_{\pm}^2 is calculated from the Debye-Hückel theory. Λ_0^0 is the limiting equivalent conductance in pure solvent, while Λ_a^0 will be used to designate these values obtained in solvent-ligand mixtures. K_0 is the ion-pair dissociation constant for salt in pure solvent, while K is that in the presence of added ligand. The data were analyzed on an IBM 1620 computer; the program used was written for us by Dr. S. M. Katz. We obtain $\Lambda_0^0 = 28.62$ and $K_0 = 1.89 \times 10^{-4}$ for Bu₃NHPi in PhNO₂ at 25°. Witschonke and Kraus⁷ reported values of 28.85 and 1.90×10^{-4} , respectively, for the same system. We do not believe the 0.8% difference in the two values of Λ_0^0 to be significant. It is probably due to cell-constant error, ours or theirs. We shall be more interested in variations in Λ^0 as determined in this laboratory with a set of internally consistent conductance cells.

The ratios, $R = K/K_0$, and Λ_a^0 for Bu₃NHPi in PhNO₂ with added Ph₃PO and Bu₂PhPO appear in Figure 1, plotted vs. ligand concentration. R increases linearly with [Ph₃PO], and the slope, K_L , is listed in Table II.

Table II: Ligand Association Constants at 25°

Solvent	Cation	Ligand	K_L	K_{2L}
PhNO ₂	Bu ₃ NH ⁺	Ph ₃ PO	363	...
	Bu ₃ NH ⁺	Bu ₂ PhPO	785	13.1
ODCB	Bu ₃ MeN ⁺	Bu ₃ PO	62.5	2.6
PhCl	Bu ₃ MeN ⁺	Ph ₃ PO	70	...

R with Bu₂PhPO as ligand shows upward curvature in Figure 1, implying that more than one molecule of ligand may be binding to the cation.^{2e} If, in addition to eq 1, we add eq 4



and proceeding as in the derivation^{2a} of eq 9 of ref 2a, the conductance equation is found to be

$$1/\Delta S = (H/\Lambda_0^0 F) + (SC y_{\pm}^2 H / K_0 (\Lambda_0^0)^2 F^2) \quad (5)$$

where

$$H = 1 + K_L [L] + K_L K_{2L} [L]^2$$

and

$$F = 1 + (\Lambda_1^0 K_L [L] / \Lambda_0^0) + (\Lambda_2^0 K_L K_{2L} [L]^2 / \Lambda_0^0)$$

Λ_1^0 is the limiting equivalent conductance of the salt $AL^+ + X^-$, while Λ_2^0 is that for $AL_2^+ + X^-$.⁷ Now, $R = K/K_0 = H$ and $\Lambda_a^0 = \Lambda_0^0 F / H$. A plot of the

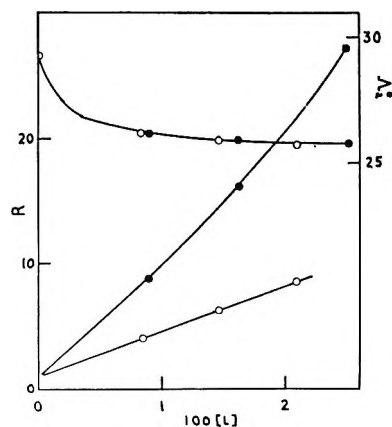


Figure 1. Bu₃NHPi in PhNO₂: O, Ph₃PO as ligand; ●, Bu₂PhPO as ligand. Lower two curves are R vs. $[L]$ plots. Upper curve is a plot of Λ_a^0 vs. $[L]$.

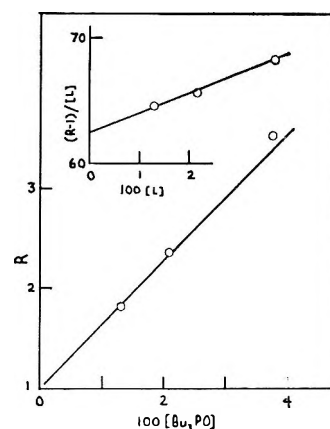


Figure 2. Bu₃MeNClO₄ in ODCB with added Bu₃PO.

quantity $(R - 1)/[L]$ vs. $[L]$ for Bu₂PhPO was made and the slope, taken to be $K_L K_{2L}$, was used to calculate the value of K_{2L} , appearing in Table II. The value of $\Lambda_1^0 = 25.5$ for Bu₃NH⁺,OPPh₃ + Pi⁻ in PhNO₂ was obtained (eq 5, with $K_{2L} = 0$) from the slope of a plot of $\Lambda_a^0 R$ vs. $[Ph_3PO]$. The values of $\Lambda_1^0 = 26.7$ and $\Lambda_2^0 = 22.6$ for Bu₂PhPO as ligand with Bu₃NHPi in PhNO₂ were obtained from the intercept and slope, respectively, of a plot of

$$(\Lambda_a^0 R - \Lambda_0^0) / [L] \text{ vs. } [L]$$

The ratios, R , for Bu₃MeNClO₄ in ODCB appear in Figure 2, plotted vs. the concentration of added Bu₃PO. Some upward curvature is evident in this graph. A plot of $(R - 1)/[L]$ vs. $[L]$ for this system is also shown in the insert in Figure 2. The intercept as $[L] \rightarrow 0$ of this latter graph is taken to be K_L . The value of K_{2L} was calculated from the slope of this graph. These association equilibrium constants appear in Table II. A value of $\Lambda_1^0 = 38.0$ for the salt Bu₃MeN⁺,OPBu₃ + ClO₄⁻ in ODCB was calculated from the slope of a plot

(13) T. Shedlovsky, *J. Franklin Inst.*, **225**, 739 (1938).

of $R(\Lambda_a^0/\Lambda_0^0)$ vs. $[\text{Bu}_3\text{PO}]$ and the prior^{2c} value of $\Lambda_0^0 = 43.87$ for the uncomplexed salt in ODCB.

The errors in the foregoing derived values of Λ_1^0 and Λ_2^0 are estimated to be no more than 2%.

The conductance of Bu_3MeNI in PhCl with and without added Ph_3PO (data of Table I) shows evidence of triple-ion formation in the 10^{-4} M range of salt concentration. These data were treated using the method of Fuoss and Kraus¹⁴ to obtain limiting values^{15,16} of $\Lambda_0^2 K$. These appear in Table III. The ratios, $R = (\Lambda_0^2 K / \Lambda_0^2 K_0)$, for these systems are plotted vs. concentration of Ph_3PO in Figure 3. The slope of this line yields a value of $K_L = 70$.

Table III: Bu_3MeNI in PhCl at 25°

$10^2[\text{Ph}_3\text{PO}]$	$10^4\Lambda_0^2 K$
0.00	4.25
0.846	6.88
1.159	7.67

Two titration experiments were performed. In one case, a 2.132×10^{-4} M solution of Bu_3MeNI in PhCl (in the conductance cell) was titrated with portions of a concentrated solution of Ph_3PO dissolved in the same salt solution. The other solution so treated was 3.561×10^{-4} M in the same salt. The ratios, $R = (g/g_0)^2$, where g_0 is the specific conductance of the solution in the absence of added ligand and g is that in the presence of added ligand, are also plotted vs. the concentration of Ph_3PO in Figure 3. The slope of the line for the highest salt concentration yields an apparent value of $K_L = 55$, while that for the lowest salt concentration yields an apparent $K_L = 56$. We have neglected possible differences in Λ_a^0 and Λ_0^0 in the foregoing treatment of the results in PhCl solvent.

Discussion

One of our objectives in this work was to test the titration method for determining values of K_L . The results in the last paragraph above show that for Bu_3MeNI with Ph_3PO in PhCl solvent, the titration results are lower than that obtained using the more reliable method I by almost 20%. There are two principal sources of error in the use of method II here: neglect of ion-atmosphere effects and neglect of effects due to triple-ion formation.¹⁷ Dilution of the salt, due to addition of ligand dissolved in pure solvent, was avoided in these experiments. Salt dilution was a factor in another set of experiments already reported.^{2d} The effect on K_L of neglect of ion-atmosphere effects can be seen most easily by considering eq 3 for small values of Λ , when it becomes eq 6

$$\Lambda_0^2 K \simeq (\Lambda^2 C) S^2 y_{\pm}^2 \quad (6)$$

The factor $S^2 y_{\pm}^2$ for the titration experiment using the

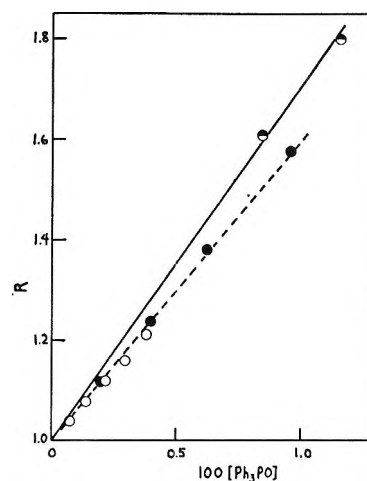


Figure 3. Bu_3MeNI in PhCl : \circ , titration of 3.561×10^{-4} M salt with Ph_3PO ; \bullet , titration of 2.132×10^{-4} M salt with Ph_3PO ; \ominus , extrapolated results, method I.

highest salt concentration is calculated to be 0.914 both at the beginning and at the end of the titration. The ratio $(g/g_0)^2$ equal to $(\Lambda^2 C)_L / (\Lambda^2 C)_{L=0}$ would then be equal to K/K_0 , if there were no triple-ion effect. Triple ions are more prevalent in iodide and bromide salt solutions than in picrate salt solutions of comparable concentrations. In the case of the most concentrated salt solution here (no ligand added), 31% of the total conductance is due to triple ions. We may estimate from data already published^{2a} that for Bu_3NHPI , a much less dissociated salt, at the same concentration in PhCl , 5–6% of the conductance is due to triple ions. In the presence of triple ions, added ligand not only must compete with solvent and anions, but also with ion pairs for the cations. Our point is that the particular salt we are using, Bu_3MeNI , exhibits as large a triple-ion effect as we are likely to encounter. We then would expect that, in most of the cases in which we shall use and have used method II, the error due to triple-ion formation will be much less than the 20% error we observe in the present case. The tertiary ammonium picrates we most often use for these measurements do not show appreciable (10%) triple-ion effects until the salt concentrations reach 10^{-3} M in PhCl solvent. A titration experiment, method II for determining values of K_L , is much easier to carry out than are the method I experiments. We conclude that as long as one is careful concerning the factors we have listed (ion-atmosphere effects, triple-ion effects, and the

(14) R. M. Fuoss and C. A. Kraus, *J. Am. Chem. Soc.*, **55**, 2387 (1933).

(15) In view of our previous experience^{2a} with iodide and bromide salts in which only one kind of triple ion was found, we tried Wooster plots,¹⁶ $\Lambda^2 C$ vs. C ; these intercepts yielded the same results as the Fuoss and Kraus treatment within 6%.

(16) C. B. Wooster, *J. Am. Chem. Soc.*, **59**, 377 (1937).

(17) The effect of triple ions is separated from ion-atmosphere effects on the same basis as the effect of ion pairing is separated from ion-atmosphere effects.

dilution effect), method II is capable of 5–10% precision in the values of K_L . This precision should be acceptable as long as one is concerned only with changes, as the ligand or cation is varied, of factors of 2 or greater in K_L .

We shall now discuss the effects of ligand association on cation mobility. The limiting equivalent conductances of the various cations have been calculated as follows: that for Bu_3NH^+ in PhNO_2 is based on the value of $\Lambda_0 = 27.9$ for Bu_4N^+ and $\lambda_0^+ = 11.17$ for Bu_4N^+ in PhNO_2 ,¹⁸ that for Bu_3MeN^+ in ODCB is based on the value of $\lambda_0^- = 23.1$ for I^- in ODCB¹⁰ and a value of $\Lambda_0 = 42.25$ for Bu_3MeNI in ODCB;^{2c} that for Bu_3MeN^+ in 1,2-dichloroethane (EC) is based on the value of $\lambda_0^- = 39.2$ for ClO_4^- in EC¹⁹ and the value $\Lambda_0 = 67.55$ for $\text{Bu}_3\text{MeNClO}_4$ in EC reported earlier.^{2c} The values so calculated appear in Table IV. We assume, with Fuoss,¹⁸ that the ionic conductances

Table IV: Cation Mobility Parameters at 25°

Cation	λ_0^+	ΔR_+ , Å
in PhNO_2		
Bu_3NH^+	11.9	
$\text{Bu}_3\text{NH}^+, \text{OPPh}_3$	8.8	1.32
$\text{Bu}_3\text{NH}^+, \text{OPBu}_2\text{Ph}$	10.0	0.71
$\text{Bu}_3\text{NH}^+, (\text{OPBu}_2\text{Ph})_2$	5.9	3.81
in ODCB		
Bu_3MeN^+	19.1	
$\text{Bu}_3\text{MeN}^+, \text{OPPh}_3$	12.3 (ClO_4^-)	1.87
$\text{Bu}_3\text{MeN}^+, \text{OPPh}_3$	12.6 (I^-)	1.74
$\text{Bu}_3\text{MeN}^+, \text{OPBu}_3$	13.2	0.52
in EC		
Bu_3MeN^+	28.4	
$\text{Bu}_3\text{MeN}^+, \text{OPPh}_3$	16.8 ^a	2.55

^a Reference 2c.

in PhNO_2 , ODCB, and EC follow Stokes' law. The Walden product then becomes $\lambda_0^+ \eta_0 = 0.8194/R_i$, where R_i is the effective hydrodynamic ion radius in angstrom units. We then calculate that $R_+ = 3.75$ Å for Bu_3NH^+ in PhNO_2 , $R_+ = 3.38$ Å for Bu_3MeN^+ in ODCB, and $R_+ = 3.70$ Å for Bu_3MeN^+ in EC. Values of ΔR_+ appearing in Table IV are increases in the effective hydrodynamic ion radii due to association with ligands, calculated in each case as the value of R_+ for the cation ligand complex minus that of the uncomplexed cation. We first note a constancy in the values of the Walden product, $\lambda_0^+ \eta_0 = 0.206$, for the symmetrical cation, Bu_4N^+ , in PhNO_2 ,¹⁸ ODCB,¹⁰ and in EC,²⁰ indicating little or no specific ion-solvent interaction and a constant value of the radius, $R_+ = 3.98$ Å. Bu_3NH^+ in PhNO_2 has an effective radius only 0.2 Å less than that of Bu_4N^+ , even though the former cation has one less bulky butyl group bonded to nitrogen.

This similarity in ion size may be due to tumbling of Bu_3NH^+ in its solvent cage, sweeping out a radius equal to that of Bu_4N^+ ; alternatively, we suggest that the equality of radii is due to a molecule of PhNO_2 solvent tightly bound to the Bu_3NH^+ by specific ion-solvent molecule interaction. The relatively small increase, $\Delta R_+ = 1.3$ Å, when Bu_3NH^+ in PhNO_2 is complexed with Ph_3PO lends support to this view. A molecule of Ph_3PO sweeps out a circle of diameter almost 7 Å, viewed perpendicularly to the P→O axis. Addition of such a bulky group should result in a greater effect than that observed if the process were a simple addition of the ligand, not involving displacement of a molecule of solvent. Adding the second molecule of Bu_2PhPO to Bu_3NH^+ in PhNO_2 results in a ΔR_+ more than five times greater than that due to the addition of the first molecule of ligand.

The values of ΔR_+ for the addition of one molecule of Ph_3PO or Bu_3PO to Bu_3MeN^+ in ODCB are not too different from those observed with Bu_3NH^+ and similar ligands in PhNO_2 solvent. Displacement of a molecule of specifically solvating ODCB from Bu_3MeN^+ appears to be occurring in these systems as well. Replacement of a hydrogen atom by a methyl group does not affect R_+ to any extent. All the cation equivalent conductances listed in Table IV are based on an arbitrary division of cation plus anion equivalent conductances,¹⁸ assuming some one salt, say tetra-*n*-butylammonium tetraphenylborate, to consist of ions of equal conductance.²¹ The consistency of the values in Table IV is indicated by the two values of λ_0^+ , 12.3 and 12.6, for $\text{Bu}_3\text{MeN}^+, \text{OPPh}_3$ obtained from values of Λ_0 of the perchlorate salt and iodide salt, respectively.

R_+ for Bu_3MeN^+ in EC solvent is 0.3 Å greater than in ODCB. ΔR_+ for $\text{Bu}_3\text{MeN}^+, \text{OPPh}_3$ is greater by 0.7 Å in EC than in ODCB. EC is more highly solvating toward cations than is ODCB, as measured^{2e} by the magnitude of the equilibrium constant, K_S , for the reaction



where S represents a specifically solvating solvent molecule. The differences between R_+ and between ΔR_+ in ODCB and EC may represent differences in the magnitude (numbers of solvating molecules) of the specific solvation, or a lability effect in which, for instance, the lifetime of a specifically solvating ODCB molecule on Bu_3MeN^+ is short, while that of an EC molecule is long compared to the time characteristic of ion mobility.

(18) R. M. Fuoss and E. Hirsch, *J. Am. Chem. Soc.*, **82**, 1013 (1960).

(19) L. F. Glyesteen and C. A. Kraus, *ibid.*, **69**, 451 (1947).

(20) D. L. Fowler and C. A. Kraus, *ibid.*, **62**, 2237 (1940).

(21) J. F. Coetzee and G. P. Cunningham, *ibid.*, **87**, 2529 (1965), report measurements that show that this particular assumption results in an error of only 2–4% in acetonitrile solvent.

We had estimated^{2d} a value of $K_L = 1600$ for Bu_3NH^+ with Ph_3PO in PhNO_2 solvent assuming that the equilibrium constant, K_D (eq 8), with py-

$$\text{Bu}_3\text{NH}^+, \text{OPPh}_3 + \text{L}' \rightleftharpoons \text{Bu}_3\text{NH}^+, \text{L}' + \text{Ph}_3\text{PO}$$

$$K_{LL'} = K_{L'}/K_L \quad (8)$$

ridine (L') does not vary from solvent to solvent. We find in the present work that K_L is 363 in PhNO_2 , almost one-fourth the previous estimate. A number of values of ligand-exchange equilibrium constants are

Table V: Effect of Solvent on Ligand Displacement

Solvent	$\text{L}' = \text{Bu}_2\text{PhPO}$	$\text{L}' = \text{Py}$	$\text{L}' = \text{MeOH}$
PhNO_2	2.16	0.017 ^c	
ODCB	1.72 ^a	0.0038 ^c	0.00023 ^b
EC	1.86 ^b		0.000014 ^c
THF	1.82 ^a		
PhCl	1.66 ^b	0.0015 ^c	

^a Reference 2d. ^b Reference 2e. ^c Reference 2a.

listed in Table V for several solvents. We see that for $\text{L}' = \text{Bu}_2\text{PhPO}$, chemically very similar to Ph_3PO , K_D is practically independent of the solvent, even though K_L for Ph_3PO varies over three orders of magnitude. The equilibrium constant for the displacement of Ph_3PO by pyridine decreases by an order of magnitude as the solvent is changed from PhNO_2 to PhCl . Methanol as a displacing ligand is ten times more effective in ODCB than in EC solvent. These latter effects, changes in K_D with changing solvent, may be due to one or more factors: changes in the interaction of the cation-ligand complex with surrounding solvent as the ligand is changed, or changes in ligand-solvent interaction as the solvent is varied. As has been remarked before,^{2d} a detailed accounting of these effects must await more information, such as determinations of the activities of the ligands in the several solvents used here. We conclude that a ligand displacement equilibrium constant, K_D (eq 2 or 8), may be assumed to be independent of solvent if the ligands involved are not too different chemically.

Differential Diffusion Coefficients of Hexamethylenetetramine

Aqueous Solutions

by L. Costantino, V. Crescenzi, and V. Vitagliano

Istituto Chimico, Università di Napoli, Naples, Italy¹

Accepted and Transmitted by The Faraday Society (June 12, 1967)

Differential diffusion coefficients of hexamethylenetetramine (HMT) aqueous solutions have been measured at two temperatures using the Gouy interferometric technique. The results can be interpreted in terms of a strong concentration-dependent hydration of the HMT molecules.

Introduction

The study of some physiochemical properties of hexamethylenetetramine (HMT) in aqueous solution has shown that the essentially nonionic tetramine is heavily solvated and that solute-solvent interactions are largely responsible for the marked deviation from ideality in these solutions.²⁻⁴

We wish to report here the results of diffusion measurements carried out on the HMT- H_2O system at two temperatures. Our diffusion coefficient data indicate that HMT behaves as a hydrated entity in water, in relation to its molal anhydrous volume. On the basis

also of the results of other measurements,^{3,4} the effect is interpreted in terms of a concentration-dependent hydration of HMT. When hydration is taken into account, a consistent, though qualitative, phenomenological relationship between diffusion coefficients and

(1) This work has been carried out with financial support of the Italian C.N.R. (Contract No. 115.1384.0.0495).

(2) G. Barone, V. Crescenzi, A. M. Liquori, and F. Quadrifoglio, *J. Phys. Chem.*, **71**, 984 (1967).

(3) V. Crescenzi, F. Quadrifoglio, and V. Vitagliano, *ibid.*, **71**, 2313 (1967).

(4) V. Crescenzi, F. Quadrifoglio, and V. Vitagliano, *Ric. Sci. Suppl.*, **37**, 529 (1967).

bulk solution viscosity results for the HMT-H₂O system as well as for a number of other systems.⁵

Experimental Section

Hexamethylenetetramine (HMT), a C. Erba (Milan, Italy) RP product, was purified by means of crystallization from ethanol. All solutions were made, by weight, using redistilled water. Diffusion experiments have been carried out by the Gouy interferometric technique, which has been widely discussed in the literature.⁶⁻⁸ The results are shown in Table I (3.66°) and Table II (24.72°). A set of density and viscosity measurements at 24.72° have also been performed to complement existing data. The experimental technique has already been described elsewhere.³ The following equations have been obtained from the experimental data by a least-square method

$$d/d_0 = 1 + 0.02943m - 0.002497m^2 + 0.0001127m^3 \pm 0.0001 \quad (m \leq 4.5) \quad (1)$$

where d/d_0 = relative density and m = molality of HMT

$$\ln \frac{\eta}{\eta_0} = \frac{0.3828c}{1 - 0.0862c}, \quad \frac{\Delta\eta}{\eta} = \pm 0.005, \quad c < 2.6 \text{ moles/l.} \quad (2)$$

where η/η_0 = relative viscosity and c = moles/l. of HMT. The density and viscosity data computed with eq 1 and 2 are perfectly consistent with other data, already reported in the literature³ for different temperatures.

Diffusion Equations. A variety of ways exist to express phenomenological diffusion equations.⁹⁻¹² Two

Table I: Diffusion Coefficients of HMT Aqueous Solutions at 3.66°

m^a	Δm^b	J_m^c	$(\Delta n/\Delta c) \times 10^2^d$	$D_0 \times 10^5^e$	$\epsilon \times 10^5^f$
0.0398	0.0796	86.66	2.40	0.3954	+0.0003
0.1213	0.0806	86.75	2.41	0.3955	-0.0002
0.2493	0.0788	82.40	2.41	0.3936	+0.0008
0.3494	0.0803	82.68	2.42	0.3950	-0.0014
0.5025	0.0761	75.81	2.42	0.3920	+0.0002
0.7487	0.0802	76.20	2.426	0.3890	+0.0010
1.0074	0.0724	65.76	2.44	0.388	-0.0003
1.4974	0.0888	73.70	2.446	0.384	-0.0003
1.9965	0.0786	60.17	2.475	0.379	0.0000
2.8921	0.0948	63.04	2.494	0.365	+0.0001
3.6874	0.0962	56.11	2.46	0.344	+0.0001

^a Average molality of each diffusion run. ^b Molality difference between the two solutions of each run. ^c Number of Gouy fringes. ^d n = refractive index, c = concentration (moles/l.), $\Delta n = J_m \lambda / a$ (a = 2.500 cm, thickness of the diffusion cell; λ = wavelength of mercury green light). ^e Differential diffusion coefficients, cm² sec⁻¹. ^f Difference between computed (eq 4, 5, 7, and 8) and experimental diffusion coefficients.

Table II: Diffusion Coefficients of HMT Aqueous Solutions at 24.72°^a

m	Δm	J_m	$(\Delta n/\Delta c) \times 10^2$	$D_0 \times 10^5$	$\epsilon \times 10^5$
0.0397	0.0793	84.59	2.34	0.7536	0.0000
0.0503	0.0804	84.73	2.31	0.7543	-0.0007
0.2513	0.0793	79.43	2.31	0.7523	+0.0003
0.2540	0.0738	77.93	2.44	0.7532	-0.0006
0.3509	0.0803	78.56	2.31	0.7516	-0.0002
0.5013	0.0802	78.48	2.38	0.7462	-0.0027
0.7505	0.0819	75.83	2.38	0.7435	0.0000
0.9927	0.0854	78.50	2.48	0.7370	+0.0004
1.0046	0.0738	65.47	2.39	0.7382	-0.0011
1.4802	0.0778	60.42	2.30	0.7270	-0.0028
2.0049	0.0795	59.26	2.43	0.7090	+0.0012
2.9083	0.0940	58.46	2.37	0.6843	+0.0013
4.0080	0.1234	67.70	2.49	0.6470	-0.0010

^a The footnotes in Table I also refer to this table.

of them, however, seem to us to be preferable for the interpretation of the phenomenological coefficients. The first, which has been recently discussed by Miller,¹³ chooses a solvent-fixed reference frame: $J_0 = 0$ (J_0 being the flow of the solvent component). The second, proposed by several authors, recently by Dunlop,¹⁴ and, in a slightly different way, by Laity,^{15,16} allows the elimination of any reference frame for describing the diffusion process.

We have treated our experimental data for the system HMT-H₂O following this second approach. The necessary thermodynamic information and the equations (3-9) which have accordingly been used for the interpretation of diffusion data for HMT in aqueous solution are reported in the Appendix. According to these data, the limiting diffusion coefficients of HMT at infinite dilution (from eq 7 and 8 of the Appendix) are: at 3.66°, $D_0 = 0.3958 \times 10^{-5}$ cm² sec⁻¹; and at 24.72°, $D_0 = 0.7535 \times 10^{-5}$ cm² sec⁻¹. These values obey the Stokes-Einstein relationship within the experimental error

(5) H. D. Ellerton, G. Reinfelds, D. E. Mulcahy, and P. J. Dunlop, *J. Phys. Chem.*, **68**, 403 (1964).

(6) C. J. Gosting, E. H. Hanson, G. Kegeles, and M. S. Morris, *Rev. Sci. Instr.*, **20**, 209 (1949).

(7) V. Vitagliano, "Introduzione Allo Studio della Diffusione," G. D'Agostino, Naples, 1959.

(8) V. Vitagliano, *Gazz. Chim. Ital.*, **90**, 876 (1960).

(9) L. Onsager, *Ann. N. Y. Acad. Sci.*, **46**, 241 (1945).

(10) S. R. De Groot, "Thermodynamics of Irreversible Processes," Interscience Publishers, Inc., New York, N. Y., 1952.

(11) S. R. De Groot and P. Mazur, "Non Equilibrium Thermodynamics," Interscience Publishers, Inc., New York, N. Y., 1962.

(12) R. P. Wendt and L. J. Gosting, *J. Phys. Chem.*, **63**, 1287 (1959).

(13) D. G. Miller, *ibid.*, **70**, 2639 (1966).

(14) P. J. Dunlop, *ibid.*, **68**, 26 (1964).

(15) R. W. Laity, *ibid.*, **63**, 80 (1959).

(16) R. W. Laity, *J. Chem. Phys.*, **30**, 682 (1959).

$$\frac{D_0\eta_0}{T} = \begin{cases} 2.275 \times 10^{-10} & \text{at } 3.66^\circ \\ 2.266 \times 10^{-10} & \text{at } 24.72^\circ \end{cases}$$

Since HMT molecules are large compared to those of the solvent, this result is not surprising. The Stokes radius of HMT, computed from the limiting diffusion coefficients, is 3.23 Å. We may correct this value using the factor proposed by Robinson and Stokes (ref 17, p 125, Figure 6.1). For a 3.23-Å radius, the correction factor would be 1.25–1.3, and in this way, we obtain for HMT a hydrodynamic volume of about 160–180 cc/mole. If the value 104 cc/mole is taken for the molar volume of HMT ($d = 1.34$ g/cc¹⁸ of solid HMT and $M = 140.19$), then an average number of three or four water molecules firmly attached per HMT molecule is obtained, in agreement with the viscosity results.³

Due cognizance being taken of the theoretical limitation underlying any correlation of diffusion and viscosity,¹³ it is nevertheless interesting to compare under this aspect the behavior of HMT with that of a number of other compounds in water. Recently Ellerton, *et al.*,⁵ have reported that the logarithm of the relative frictional coefficient (as defined in eq 9) $\ln (R_{0,1}/R_{0,1}^0)$ ($R_{0,1}$ being the frictional coefficient at infinite dilution) is a linear function of the logarithm of relative viscosity, $\ln (\eta/\eta_0)$, with a slope of about 0.8 for a variety of nonelectrolytes in water (lactamide, glycomalide, urea, α - and β -alanine, *dl*-valine) and for the system diphenyl-benzene.¹⁹

In Figure 1, a similar graph has been drawn for the relative frictional coefficients of HMT and for those of lithium ion, which is known to be strongly hydrated. It can be seen that the function

$$\ln (R_{0,1}/R_{0,1}^0) = f[\ln (\eta/\eta_0)] \quad (10)$$

is far from being a straight line in both cases, and that the frictional coefficients increase with concentration much faster than Stokes' law predicts (slope = 1).

We may try to interpret the deviation from a 0.8 slope of function (10) in terms of a more extensive hydration of HMT as compared to that of other solutes. Let \bar{h} represent the average hydration number of the HMT molecules; the true mole fraction of the solute would be

$$N_1' = \frac{m}{55.51 + m(1 - \bar{h})} \quad (11)$$

and the correct thermodynamic term would become

$$1 + \frac{d \ln f_1'}{d \ln N_1'} = \left(1 + \frac{d \ln f_1}{d \ln N_1} \right) \frac{d \ln N_1}{d \ln N_1'} \quad (12)$$

f_1' being the activity coefficient on the true mole fraction (N_1') scale. In Figure 2, eq 10 has been reported for HMT where the frictional coefficients $R_{0,1}$ have been computed through eq 6 and eq 9 assuming: (a) a constant hydration number, $\bar{h} = 3$, and (b) a variable

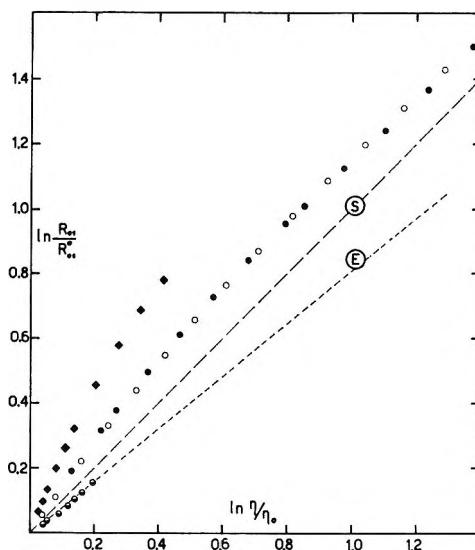


Figure 1. Logarithm of relative frictional coefficients as a function of the logarithm of relative viscosity: ●, HMT-H₂O at 3.66°; ○, HMT-H₂O at 24.72°; ◆, Li⁺ in LiCl-H₂O solutions at 25° from published diffusion data⁵ and unpublished viscosity data obtained in our laboratory for the system LiCl-H₂O; ◐, urea-H₂O;⁵ S, Stokes' rule; E, Ellerton's⁵ 0.8 slope: L. J. Gosting and D. F. Akeley, *J. Am. Chem. Soc.*, **74**, 2058 (1952); T. C. W. Mak, *J. Chem. Phys.*, **43**, 2799 (1965).

hydration number. This has been computed from the isopiestic data already reported^{3,4} according to which the following equations hold for \bar{h}

$$\bar{h} = 14.71 - 2.71m + 0.245m^2 \quad (\text{at } 3.66^\circ) \quad (13)$$

$$\bar{h} = 12.25 - 1.93m + 0.152m^2 \quad (\text{at } 24.72^\circ) \quad (14)$$

where

$$\bar{h} = \frac{55.51}{m} - \frac{a_w}{1 - a_w} \quad (15)$$

a_w being the activity of water: $\ln a_w = \varphi m/55.51$ with φ = osmotic coefficient. It can be seen (Figure 2) that a constant correction ($\bar{h} = 3$) decreases the slope of eq 10 but $\ln (R_{0,1}/R_{0,1}^0)$ does not become a linear function of $\ln (\eta/\eta_0)$. Computing the frictional coefficients with the aid of eq 11–14, a straight line is obtained for eq 10 with a slope approximately equal to 0.8, as found by Ellerton, *et al.*,⁵ for different systems. The HMT frictional coefficients behavior at both temperatures is almost the same.

We want to point out that the above-mentioned treatment is purely qualitative. No quantitative meaning may be attached to eq 13 and 14, in the sense that the hydration shell predicted by these equations for HMT must not be considered as diffusing, on the average,

(17) R. A. Robinson and R. H. Stokes, "Electrolyte Solutions," Butterworth and Co., Ltd., London, 1959.

(18) G. W. Smith, *J. Chem. Phys.*, **36**, 3081 (1962).

(19) C. L. Sandquist and P. A. Lyons, *J. Am. Chem. Soc.*, **76**, 4641 (1954).

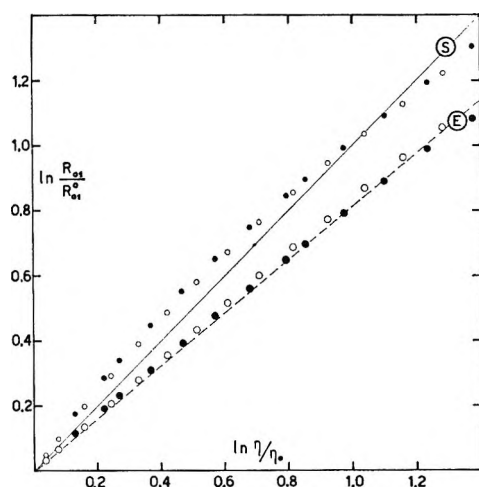


Figure 2. Logarithm of relative frictional coefficients of HMT in aqueous solution, corrected for the hydration, vs. $\ln(\eta/\eta_0)$: closed circles, 3.66°; open circles, 24.72°; small circles, $\bar{h} = 3$; large circles, \bar{h} from eq 13 and 14.

with each HMT molecule. The term \bar{h} (eq 15) furthermore is strictly connected with the "semiideal" approximate model^{3,20} as applied to HMT aqueous solutions.

At finite dilutions, our results simply suggest that a slope of eq 10 greater than 0.8 may be connected with strong concentration-dependent hydration of the solute. Sucrose and raffinose, which apparently obey the Stokes-Einstein law^{21,22} would behave in this manner because, owing to hydration, the $\ln(R_{0,1}/R_{0,1}^0)$ vs. $\ln(\eta/\eta_0)$ function has a slope higher than 0.8 (the value 1 might thus be fortuitous).

The existence of three or four water molecules strongly bound to each HMT molecule, as evaluated from our data extrapolated to infinite dilution, seems, on the other hand, a very reasonable supposition. In this connection, it is interesting to recall that in the crystalline clathrate an HMT molecule is directly connected, through hydrogen bonds, to three water molecules each of which binds other H₂O molecules in the clathrate framework.²³

Acknowledgment. The authors wish to thank Dr. Donald G. Miller for a critical reading of the manuscript.

Appendix

Equations and data which have been used in the treatment of diffusion experiments results for the HMT-H₂O system at 3.66 and 24.72° are given below.

(a) Thermodynamic terms computed from the osmotic coefficient equations reported elsewhere^{3,4} are

$$F = 1 + \frac{d \ln f_2}{d \ln N_2} = 1 + \frac{d \ln f_1}{d \ln N_1} \quad (3)$$

at 3.66°

$$F = 1 + 0.5512m + 0.01537m^2 + 0.000104m^3 \quad (4)$$

and at 24.72°

$$F = 1 + 0.4580m + 0.00806m^2 \quad (5)$$

N_1 and N_2 are the mole fractions of water and HMT, f_1 and f_2 are the corresponding activity coefficients on the mole fraction scale, and m is the molality of HMT.

(b) Thermodynamic diffusion coefficients¹⁵ are

$$D' = D_v/F \quad (6)$$

at 3.66°

$$D' \times 10^5 = 0.3958 - 0.2212c + 0.07779c^2 - 0.01793c^3 + 0.001684c^4 \pm 0.0005 \quad (7)$$

and at 24.72°

$$D' \times 10^5 = 0.7535 - 0.3423c + 0.07827c^2 - 0.008815c^3 \pm 0.0009 \quad (8)$$

where c is the HMT concentration in moles/l.

(c) Frictional coefficients according to Dunlop's treatment are

$$R_{0,1} = -\frac{RT}{D'}V_m \quad (9)$$

where V_m is the molar volume of the solution, $V_m = 1/\Sigma c_i$

(20) R. H. Stokes and R. A. Robinson, *J. Phys. Chem.*, **70**, 2126 (1966).

(21) L. J. Gosting and M. S. Morris, *J. Am. Chem. Soc.*, **71**, 1998 (1949).

(22) P. J. Dunlop, *J. Phys. Chem.*, **60**, 1464 (1956).

(23) T. C. W. Mak, *J. Chem. Phys.*, **43**, 2799 (1965).

Conformational Isomerism of 1,1'-Disubstituted Azo Compounds

by Gavriella Gabor¹ and Kedma H. Bar-Eli

Department of Chemistry, The Weizmann Institute of Science, Rehovoth, Israel (Received June 12, 1967)

The photoisomerization of 1,1'-dimethoxyazobenzene was investigated. This compound has two big substituents at the *ortho* and *ortho'* positions which might interfere with the rotation around the ring-N single bond. Photochemical steady states were obtained by irradiation at various wavelengths. The composition of these steady states and the quantum yields were calculated. The unusual results at extremely low temperatures were related to the existence of conformational isomers.

Introduction

The *cis-trans* isomerization of azobenzene by ultraviolet and visible light was extensively studied by Zimmerman² and in this laboratory.^{3,4} It was shown that the final isomeric composition depends on the temperature and the wavelength of the irradiating light,^{3,4} but is independent of initial composition of the mixture of isomers.

When bulky substituents exist in the *ortho* positions, the free rotation around the C-N single bond might be hindered,⁵ giving rise to conformational isomers. In order to prove the existence of these isomers, the photoisomerization of 1,1'-dimethoxyazobenzene was investigated.

The compositions of the photochemical steady states were independent of the compositions of the initial mixture at high temperatures. However, at liquid nitrogen temperature, 77°K, the final composition does depend on the initial composition. We relate this to hindered rotation around the C-N single bond at low temperature (77°K) and viscous medium.

Experimental Section

The hydrocarbon solvents used, methylocyclohexane, MCH, and methylocyclopentane, MCP, were purified by passage through a column of Woelm alumina. The solutions were degassed at high vacuum in the absorption cells, which were then sealed off.^{3b,4} 1,1'-Dimethoxyazobenzene was prepared as described in earlier literature.⁶

The spectrophotometric and irradiation procedures at low temperatures were described earlier.⁷ The experiments at 77°K were carried out in a copper block cooled with liquid nitrogen.

Results

The photochemistry of 1,1'-dimethoxyazobenzene is similar to that of unsubstituted azo compounds down to -120°. On irradiation, geometrical isomers are obtained. The *cis/trans* ratio at photoequilibria is

independent of the contribution of these species in the initial mixture.

The absorption spectra of the two geometrical isomers are shown in Figure 1a. The $\pi-\pi^*$ band shows a shoulder in the monosubstituted compound (around 360 m μ) which becomes a well-defined peak at 370 m μ on disubstitution (Figure 1b). The ratio between these two well-distinguished peaks at 310 and 370 m μ is a function of the temperature (Figure 2), favoring the 370-m μ peak at lower temperatures.

On photoisomerization, above -120°, well-defined isosbestic points at 415 and 440 m μ are obtained, indicating the existence of only two geometrical isomers.⁸ However, at lower temperature these isosbestic points are "smeared," and the extinction of the *cis* isomer is increased in this region. This is taken as an indication that the equilibration between the two conformational isomers of the *cis* isomer is slowed down appreciably.

Quantum yields of the photoisomerization processes were calculated as described previously.^{3b,4} The results are listed in Table I.

The decrease of ϕ_i at lower temperatures down to -150° is similar to that in unsubstituted aromatic azo compounds.^{3b} However, the equilibrium ratio *cis/trans* attained at 77°K is found to depend on the composition of the initial mixture. Starting with pure *trans*, the contribution of the *trans* at the photochemical steady state, attained by irradiation by 365-m μ monochromatic light, was 70%, while when the initial

(1) Address correspondence to this author at Tel-Aviv University, Ramat-Aviv, Tel-Aviv, Israel.

(2) G. Zimmerman, L. Chow, and U. Paik, *J. Am. Chem. Soc.*, **80**, 3528 (1958).

(3) (a) E. Fischer, *ibid.*, **82**, 3249 (1960); (b) S. Malkin and E. Fischer, *J. Phys. Chem.*, **66**, 2482 (1962).

(4) (a) G. Gabor and E. Fischer, *ibid.*, **66**, 2478 (1962); (b) G. Gabor, Y. Frei, D. Gegiou, M. Kaganowitch, and E. Fischer, *Israel J. Chem.*, **5**, 193 (1967).

(5) H. H. Jaffé and M. Orchin, *J. Chem. Soc.*, 1078 (1960).

(6) K. Brand and W. Schreiber, *Chem. Ber.*, **75B**, 156 (1942).

(7) Y. Hirshberg and E. Fischer, *Rev. Sci. Instr.*, **30**, 197 (1959).

(8) M. D. Cohen and E. Fischer, *J. Chem. Soc.*, 3044 (1962).

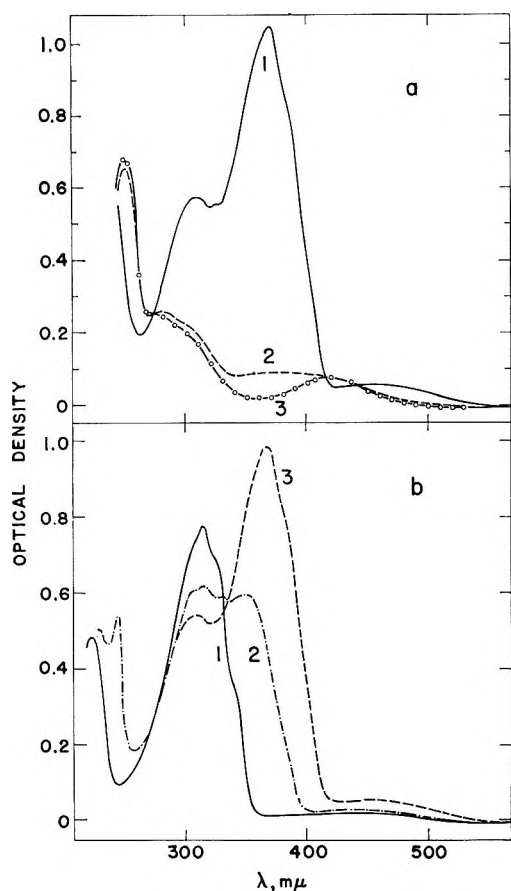


Figure 1. (a) 1,1'-Dimethoxyazobenzene $4.3 \times 10^{-5} M$ in MCH-MCP: curve 1, 100% *trans* isomer; curve 2, 95% *trans*; curve 3, 100% *cis*, calculated (E. Fischer, *J. Phys. Chem.*, in press). (b) Curve 1, *trans*-azobenzene; curve 2, *trans*-*o*-methoxyazobenzene; curve 3, *trans*-1,1'-dimethoxyazobenzene, in nonpolar solvents.

Table I: Quantum Yields in the Temperature Range -25 to -150°

Temp, $^\circ C$	ϕ_t^a		ϕ_c^b	
	λ of irradiation, μ			
	365	313	313	365
-25		0.12		0.37
-80	0.115	0.08	0.17	0.35
-110	0.086	0.047	0.28	0.27
-130	0.062	0.05	0.53	0.34
-150	0.037	0.064	0.67	0.38

^a ϕ_t is the quantum yields of the reaction *trans* \rightarrow *cis*. ^b ϕ_c is the quantum yields of the reverse reaction *cis* \rightarrow *trans*.

mixture had only 10% *trans*, the contribution of the *trans* at photoequilibrium, attained similarly, was 40%. Warming this mixture and recooling caused a slight increase of absorption in the 370-m μ range which could be further increased by irradiation at the same wavelengths.

Discussion

As the ratio of the two peaks at 310 and 370 m μ of

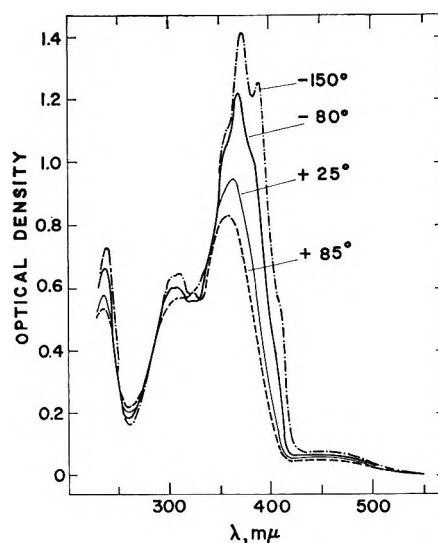


Figure 2. *trans*-1,1'-Dimethoxyazobenzene in MCH-MCP, $4.3 \times 10^{-5} M$, temperature dependence of absorption spectrum.

the *trans* isomers is a function of the temperature, we conclude that these peaks should be related to two different species, which are in thermal equilibrium with each other. We assume that these two species are the two conformational isomers having the *trans* configuration, and that the 370-m μ peak represents the more stable one, since it becomes predominant on lowering the temperature. Using van't Hoff's equation and assuming that the ratio of the extinction coefficients is temperature independent, we obtained 400 cal/mole as the enthalpy difference between the two conformational isomers A and B having the *trans* configuration.

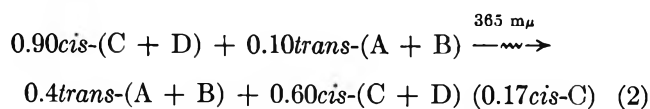
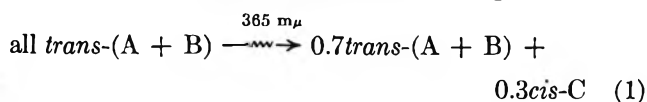
The existence of the two conformational *cis* isomers C and D is also possible. The existence of these is manifested by the "smearing" of the isosbestic points at low temperatures on photoisomerization. Similarly, substitution at the *ortho* positions in stilbene was found to interfere with the rotation around the ring-C single bond;^{5,9,10} the absorption of the π - π^* band was decreased and eventually shifted. We assume that while the absorption of C is very small at 365 m μ , the other conformational isomer D does not absorb at all at this wavelength. At high temperatures ($T > -120^\circ$) the thermal equilibrium between C and D is very fast; therefore, they take part in the photoisomerization process as one single species. However, since only species C absorbs the 365-m μ light, all *cis*-*trans* conversions are brought about *via* this species. At extremely low temperature, 77°K, the thermal equilibration becomes very slow, and since one of the conformational isomers, *i.e.*, D, does not take part in the photoisomerization by 365-m μ monochromatic light, the composition of the photochemical steady state depends on the D content of the initial mixture, as shown by

(9) R. N. Beale and E. M. F. Roe, *J. Am. Chem. Soc.*, **74**, 2304 (1952).

(10) H. Suzuki, *Bull. Chem. Soc. Japan*, **33**, 396 (1960).

the experiments carried out at 77°K. Starting with a *cis*-rich solution, only C was converted into the *trans* isomer while D remained unchanged. The C content of the solution was increased by heating to about -80°, at which the $C \rightleftharpoons D$ interconversion is very fast. After recooling the mixture to 77°K, a further quantity of C (newly obtained by thermal equilibrium at high temperatures) was converted into the *trans* isomer.

The following scheme summarizes the reactions on irradiation by 365-m μ monochromatic light at 77°K.



The last mixture contains 0.17*cis*-C assuming that at photoequilibrium the (A + B)/C ratio is the same as in reaction 1, while *cis*-D is inert to irradiation. The experiments reported here are of preliminary nature, and research is being continued on this system.

Acknowledgments. We are indebted to Dr. E. Fischer for helpful discussions, to Mr. M. Kaganowitch for synthesizing the compound, and to Mrs. N. Castell for her efficient technical assistance.

Convective Diffusion in Capillaries

by Allen R. Overman and Raymond J. Miller

Agronomy Department, University of Illinois, Urbana, Illinois 61801 (Received June 12, 1967)

A mathematical analysis and an experimental technique are developed for the study of convective diffusion in a capillary. The simplified equation relates steady-state solute concentration to measurable system parameters for a system with negligible volume change due to mixing of the species. Using the system D₂O-H₂O, with known diffusivity, the equation was tested for a low Peclet number. Experimental results support the theory. The analysis and technique presented could be employed as a means of measuring diffusion coefficients.

Convective diffusion deals with the transport of matter by the combined processes of convection and diffusion.¹ In this discussion, convection refers to laminar flow which obeys Poiseuille's law. While no exact treatment exists, because of the nature of the partial differential equation, numerous authors have presented approximate treatments appropriate to various systems.²⁻⁷ A more recent paper gives a numerical solution to the problem and discusses the range of validity of several treatments.⁸ In this paper, a simplified equation is obtained for steady state and its validity tested.

Theory

The continuity equation for convective diffusion is (cf. Taylor⁴)

$$D\left(\frac{\partial^2 C}{\partial r^2} + \frac{1}{r}\frac{\partial C}{\partial r} + \frac{\partial^2 C}{\partial x^2}\right) = \frac{\partial C}{\partial t} + V_0\left(1 - \frac{r^2}{a^2}\right)\frac{\partial C}{\partial x} \quad (1)$$

for a capillary of radius *a*, where *r*, *x*, and *t* are the radial,

longitudinal, and time variables, respectively, *C* is the solute concentration, *D* the diffusion coefficient, and *V*₀ the streaming velocity at the center of the capillary. Radial symmetry has been assumed along with independence of *D* and *V*₀ of concentration and position. Overman⁹ has proposed a simplified treatment of the system by assuming that at steady state the radial term is negligible with regard to longitudinal distribution. Flow at a point is then replaced by flow across

- (1) V. Levich, "Physicochemical Hydrodynamics," Prentice-Hall, Inc., Englewood Cliffs, N. J., 1962.
- (2) G. Hertz, *Physik. Z.*, **23**, 443 (1922).
- (3) R. Schlögl, *Z. Physik. Chem.*, **3**, 73 (1955).
- (4) G. I. Taylor, *Proc. Roy. Soc. (London)*, **A219**, 186 (1953).
- (5) R. Aris, *ibid.*, **A235**, 67 (1956).
- (6) P. G. Saffman, *J. Fluid Mech.*, **6**, 321 (1959).
- (7) W. Jost, "Diffusion of Solids, Liquids, Gases," Academic Press Inc., New York, N. Y., 1960.
- (8) V. Ananthakrishnan, W. N. Gill, and A. J. Barduhn, *A.I.Ch.E. J.*, **11**, 1063 (1965).
- (9) A. R. Overman, Ph.D. Thesis, North Carolina State University, Raleigh, N. C., 1965.

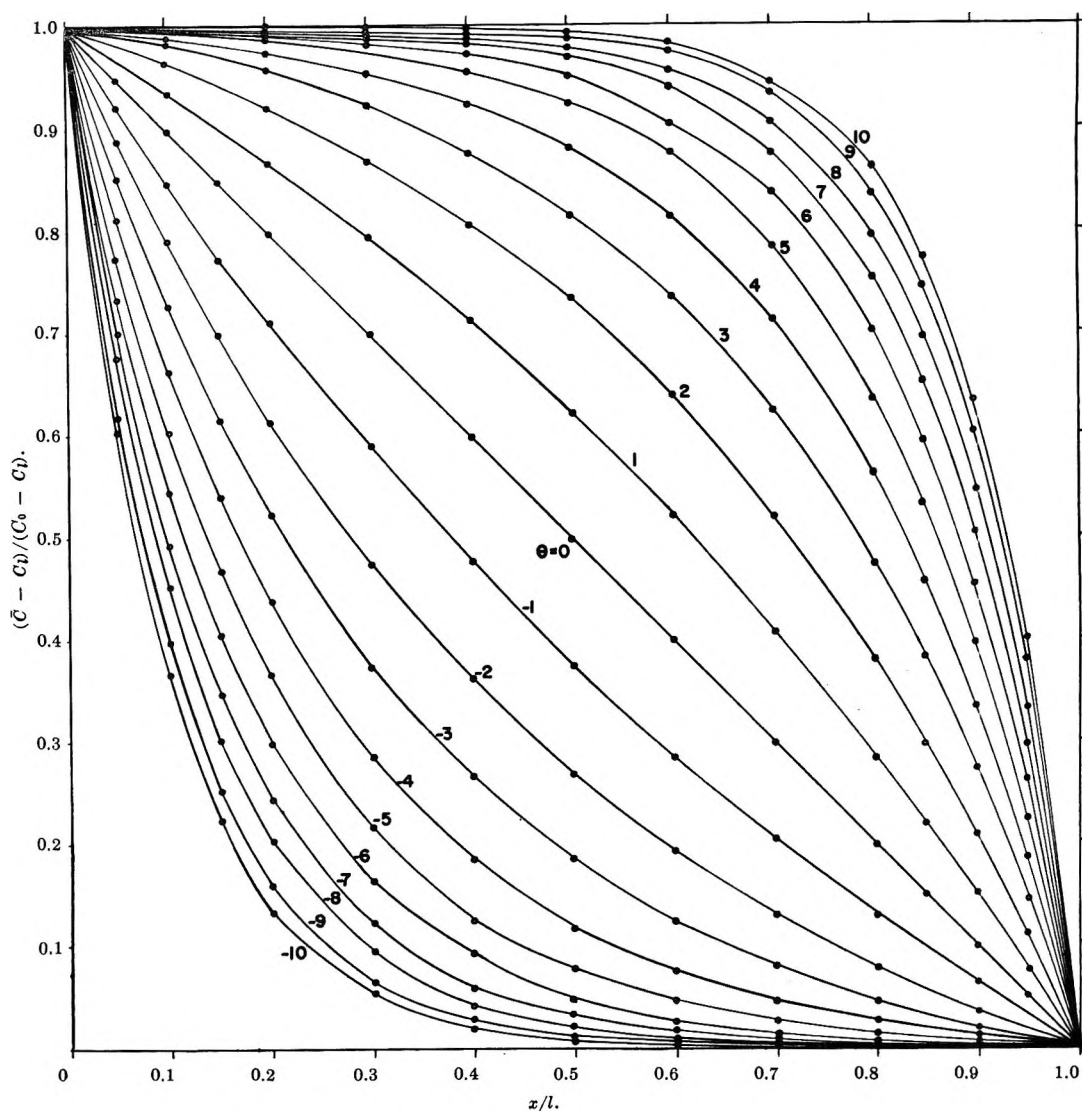


Figure 1. Distribution of a solute in a capillary due to convective diffusion. The negative numbers indicate convective flow in the opposite direction to diffusion; the positive numbers indicate that the two flows are complementary.

a plane. Utilizing linear superposition, the net-flow rate, Q_N , of solute (steady state) across a plane transverse to the longitudinal axis is

$$Q_N = CQ_L + Q_D \quad (2)$$

where Q_L and Q_D are the laminar and diffusive flow rates, respectively, taken positive with x . Using Fick's first law and the boundary conditions $C(x = 0) = C_0$ and $C(x = l) = C_l$, integration of eq 2 yields the distribution function

$$\frac{C - C_l}{C_0 - C_l} = 1 - \frac{e^{\theta x/l} - 1}{e^{\theta} - 1} \quad (3)$$

where C is the concentration at x , $\theta = lQ_L/DA = l\bar{V}_L/D$ is the Peclet number, A is the cross-sectional area of the flow capillary, l is its length, and \bar{V}_L is the average laminar velocity of the solvent. A family of curves for θ , ranging from -10 to $+10$, are shown in Figure 1. When laminar flow vanishes, the distribution

is linear as predicted by diffusion theory. With laminar flow superimposed, the distribution of solutes will depend on the direction and magnitude of that flow.

To test the validity of eq 2, the expression for average solute concentration, \bar{C}

$$\frac{\bar{C} - C_l}{C_0 - C_l} = \frac{1}{2} \left[1 + \zeta\left(\frac{\theta}{2}\right) \right] \quad (4)$$

is obtained, $\zeta(\Xi) = \coth \Xi - (1/\Xi)$ is the Langevin function. Equation 4 is shown graphically in Figure 2. For zero laminar flow, the equation reduces to the value for pure diffusion, viz., 0.5.

Experimental Section

To test the theory, a D_2O - H_2O system was utilized and the average D_2O concentration in a glass capillary was determined when concentration and pressure gradients were superimposed. The solute was D_2O , a 4% stock solution being prepared from 99.5 atom % D_2O . All-

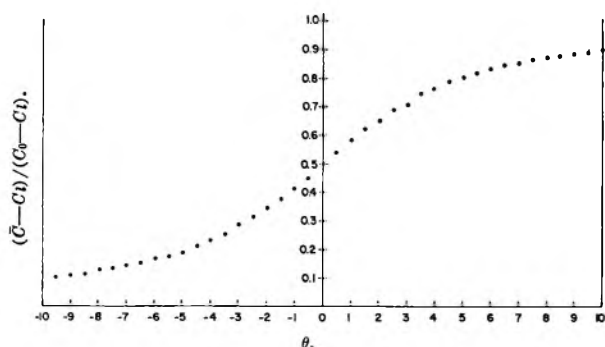


Figure 2. Plot of eq 4.

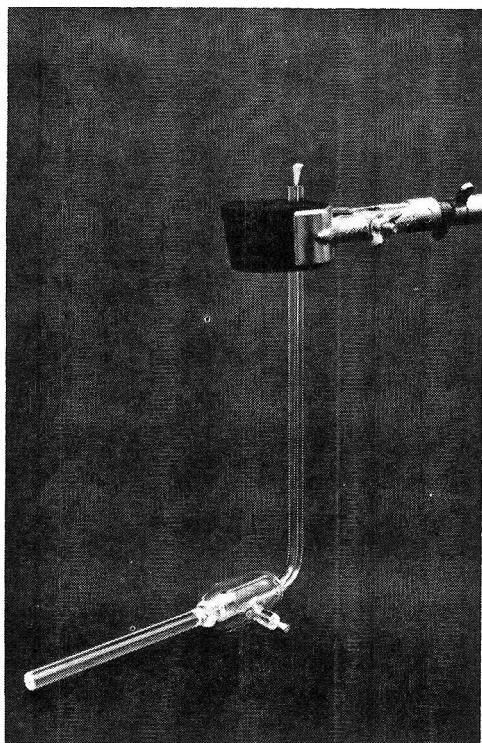
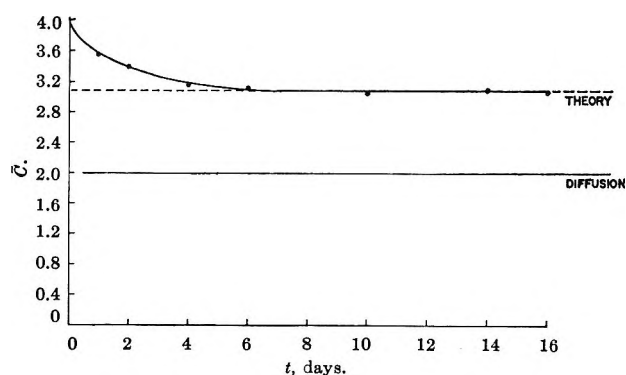


Figure 3. Glass diffusion cell.

glass cells, as shown in Figure 3 were used in the experiment. The vertical and horizontal capillaries were 1-mm precision bore, while the bulb section had a volume of about 8 cc. A capillary nipple was attached to the bulb to facilitate filling and emptying the contents. Rubber picks were used to plug the capillaries as needed.

During an experiment, the cell was submerged in a 40-l. reservoir, which in turn was mounted in a thermostat at 30.0°, with control of approximately $\pm 0.005^\circ$. The reservoir contained deionized water. Laminar flow was obtained by slowly draining the reservoir and allowing the meniscus in the vertical capillary to fall steadily. To prevent cavitation at the ends of the capillaries, the liquids were not mechanically stirred. Apparently the flow rate was adequate to provide sufficient mixing. Evaporation from the vertical capillary was minimized by gluing orifice plates to a 1-cm

Figure 4. The average concentration of D_2O in a capillary with time. Solid line is experimental; dashed line is theoretical.

section of 0.5-mm capillary and mounting these devices at the ends of the capillaries.

By using several cells, it was possible to obtain average solute concentration within the horizontal capillaries with time, thus establishing the steady state value. As samples were removed, they were placed in vials containing saturated kerosene and sealed. At the conclusion of the experiment, 10- μ l aliquots were analyzed for D_2O concentration by use of a kerosene-bromobenzene density gradient column.

That C_i is essentially constant may be established as follows. Reduction of C_i with time is by diffusion alone. Neglecting the change of solute with time in the capillary, then it may be shown that

$$\frac{C_i(t)}{C_i(0)} = e^{-DA t/lV}$$

where $C_i(t)$ and $C_i(0)$ denote C_i at time t and time zero, respectively, and V is the volume of the bulb. For this system $lV/DA = 4560$ days. For a 1% reduction in C_i , we obtain $t = 46$ days. Hence, C_i is essentially constant for the 16-day period of the experiment.

Results and Discussion

The experimental results and theoretical average concentration values are shown in Figure 4. The steady-state average concentration, \bar{C} , was 3.08%, found by averaging the last three values. The predicted \bar{C} was 3.06%, found as follows. The drainage rate was 0.920 cm/day. Using $l = 10$ cm and $D = 2.37$ cm²/day,¹⁰ $\theta = 3.88$. From Figure 2, the corresponding \bar{C} is 3.06%. The relative error was $(3.08 - 3.06)/(4.00 - 3.06) = 2\%$.

The experimental results show that the flow theory is valid and will predict the solute distribution in a system where diffusion and laminar flow are superimposed. To date, this has only been tested for a capillary, but the work is being extended to porous systems. A transient solution to the equation is also being sought.

(10) J. H. Wang, C. V. Robinson, and I. S. Edelman, *J. Am. Chem. Soc.*, **75**, 466 (1953).

Acknowledgment. Part of this work was supported by a grant from the Research Board, University of Illinois. The authors also wish to express apprecia-

tion to Professor A. H. Beavers, Agronomy Department, University of Illinois, for assistance with the density-gradient column.

Ionic Reactions of Unsaturated Compounds. I.

Polymerization of Acetylene

by Jean H. Futrell and Thomas O. Tiernan

*Aerospace Research Laboratories, Chemistry Research Laboratory,
Wright-Patterson Air Force Base, Ohio 45533 (Received June 13, 1967)*

Ion-molecule reactions of acetylene were investigated in conventional, high pressure, and tandem mass spectrometers. Evidence was obtained from ionization efficiency curves and from charge-exchange experiments for the existence of an excited molecule ion, $C_2H_2^{+*}$, with an appearance potential of about 15.9 eV, which reacts differently from the ground vibronic state ion, $C_2H_2^+$. Reactions of the individual primary ions and selected secondary, tertiary, and subsequent ions were investigated, and C_2D_2 was examined in some experiments to clarify mechanistic details and to evaluate isotope effects. A highly branched chain reaction for the ionic polymerization of acetylene is deduced from these results.

Introduction

Mass spectrometric investigations of ionic reactions in acetylene have been reported by several laboratories, using a variety of techniques¹⁻¹¹ for deducing the principal reactions involved. In two of these studies,^{7,9} a fairly complete kinetic analysis for this system over the pressure range 0.001–0.3 torr was attempted. In addition, a novel experimental approach using a 3-MeV proton beam from a Van de Graaff accelerator as an ionizing medium for source pressures to 1.3 torr was reported.¹¹ One of the striking features of these studies is the complexity of the reaction scheme of this relatively simple molecule. Moreover, it is apparent from these studies that the kinetic order, and in some cases the parent-daughter relationship, in the chain sequence of reactions is often different from that deduced from stoichiometry.

We have recently developed a high-pressure mass spectrometer system,¹² and the considerable extant body of information on ion-molecule reactions of acetylene prompted its selection as a system for evaluating the performance of the spectrometer. A tandem mass spectrometer¹³ was also used to evaluate elementary reaction steps suggested by the high-pressure results in order to define various steps in the reaction sequence. Since some of the data and deductions in

the literature are contradictory, it seems appropriate to summarize our findings as the first report of a systematic study of ion-molecule reactions of unsaturates.

Experimental Section

The apparatus and experimental procedures used in the pressure study have been described in detail else-

- (1) F. H. Field, J. L. Franklin, and F. W. Lampe, *J. Am. Chem. Soc.*, **79**, 2665 (1957).
- (2) R. Barker, W. H. Hamill, and R. R. Williams, *J. Phys. Chem.*, **63**, 825 (1959).
- (3) P. S. Rudolph and C. E. Melton, *ibid.*, **63**, 916 (1959).
- (4) R. Fuchs, *Z. Naturforsch.*, **16a**, 1026 (1961).
- (5) A. Bloch in "Advances in Mass Spectrometry II," R. M. Elliot, Ed., Pergamon Press, New York, N. Y., 1963, p 48.
- (6) E. Lindholm, I. Szabo, and P. Wilmenius, *Arkiv Fysik*, **25**, 417 (1963).
- (7) M. S. B. Munson, *J. Phys. Chem.*, **69**, 572 (1965).
- (8) J. H. Futrell and L. W. Sieck, *ibid.*, **69**, 892 (1965).
- (9) G. A. W. Derwish, A. Galli, A. Giardini-Guidoni, and G. G. Volpi, *J. Am. Chem. Soc.*, **87**, 1159 (1965).
- (10) C. E. Melton and W. H. Hamill, *J. Chem. Phys.*, **41**, 1469 (1964).
- (11) S. Wexler, A. Lifshitz, and A. Quattrochi, *Advances in Chemistry Series*, No. 58, American Chemical Society, Washington, D. C., 1966, p 200.
- (12) J. H. Futrell, T. O. Tiernan, F. P. Abramson, and C. D. Miller, unpublished data.
- (13) J. H. Futrell and C. D. Miller, *Rev. Sci. Instr.*, **37**, 1521 (1966).

where¹² and will be described only briefly. The ion source has a dual leak dual reservoir sampling system, but in the present experiments only one inlet was used. Acetylene, obtained from the Matheson Co. and purified as described previously,⁸ was introduced into the reservoir connecting to the ion source *via* a Granville-Phillips Series 213 automatic pressure controller. A static pressure tap from the ion source to an MKS Baratron Model 77H1 pressure transducer provided the reference signal to the controller, which, when energized, maintained ion-source pressure within about 1% of the selected value or ± 0.0001 torr, whichever is greater. The pressure differential from the source to pumping chamber was approximately 1000:1 and the differentially pumped analyzer pressure did not rise above 2×10^{-6} torr at 1 torr source pressure. The distance from the collimated electron beam to the source exit aperture is 0.28 cm and a field strength of 10.6 v/cm was used in these experiments.

With ionizing voltage set at 100 v and no gas in the chamber, the ionizing electron current was adjusted to approximately 5×10^{-9} amp in order to minimize space charge effects. The pressure transducer (MKS Baratron) was then zeroed on its most sensitive range. The pressure desired for a particular run was then set to four-digit precision on the pressure meter, an appropriate control range was selected, and the controller was switched on. After allowing a few minutes for source stabilization, the mass range of interest was scanned and recorded. Because of the procedure used to achieve space focus, as required for time-of-flight mass analysis, data reduction required correction for mass discrimination as described previously.¹²

Experiments with the tandem mass spectrometer followed the same format as previous studies.^{13,14} Since mass analysis of the impacting ion is an inherent characteristic of these experiments, no precautions were taken to purify gases which were used as the source of impacting ions in this instrument. Except as otherwise stated, impacting ions of kinetic energy 0–0.4 eV were used in this research. Pulse-counting techniques were used for measuring the intensities of secondary ions.

Appearance potential measurements were made on a modified Consolidated 21-103C mass spectrometer.¹⁵ Ionization efficiency curves were recorded directly by means of a Varian model F-80 X-Y recorder.

Results

Pressure Dependence of Ion Currents. The principal results of the pressure study are presented in Figures 1–3 and Tables I and II. Figure 1 illustrates the apparent chain-polymerization sequence for the major ions in the acetylene spectrum. A logarithmic pressure scale is used to emphasize both the apparently simple parent-daughter relationships and the fact that these ions constitute a gradually decreasing fraction of total

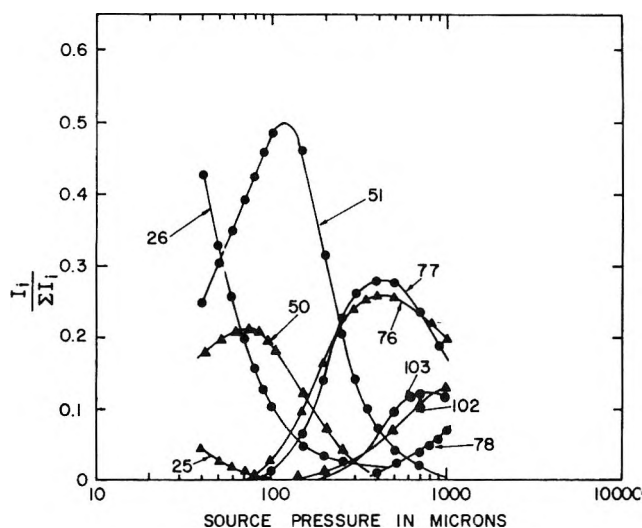


Figure 1. Mass spectrum of acetylene as a function of ion-source pressure.

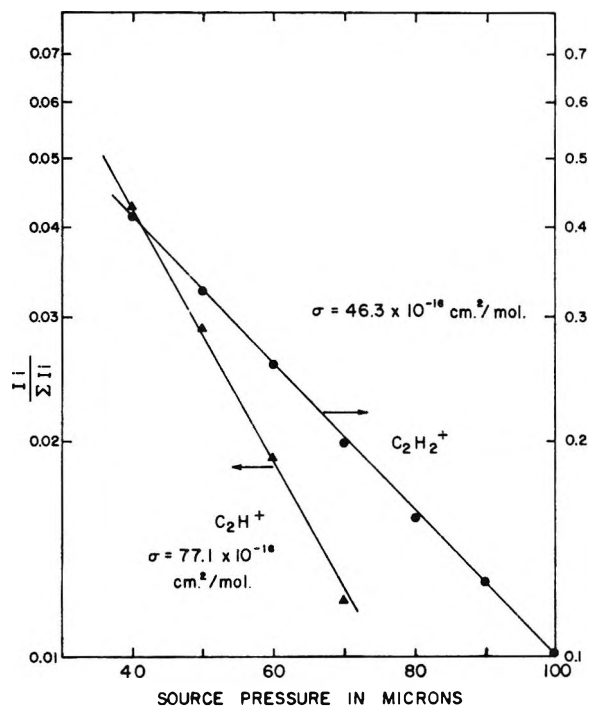


Figure 2. Semilogarithmic plots of the fractional intensities of $C_2H_2^+$ and C_2H^+ as a function of acetylene pressure.

ionization with increasing pressure. The data reproduce very well up to a pressure of about 0.4 torr all the qualitative features of the analogous Figure 3 of Derwish, *et al.*⁹ An attempt at a more quantitative comparison, using ion-path length as a scale factor was only moderately successful. However, an error in pressure measurement or ion path length of *ca.* 25%

(14) F. P. Abramson and J. H. Futrell, *J. Chem. Phys.*, **45**, 1925 (1966).

(15) K. R. Ryan, L. W. Sieck, and J. H. Futrell, *ibid.*, **41**, 111 (1964).

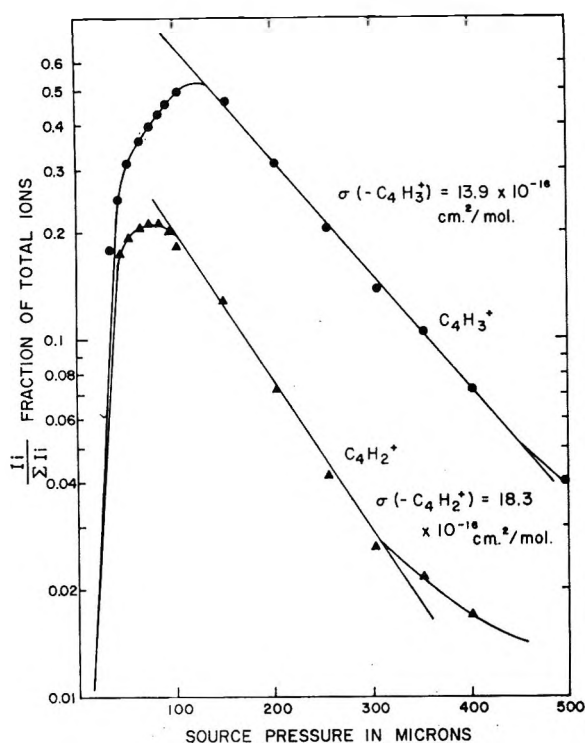


Figure 3. Semilogarithmic plots of the fractional intensities of $C_4H_2^+$ and $C_4H_3^+$ as a function of acetylene pressure.

Table I: High-Pressure Mass Spectra of Acetylene

m/e	Species	Relative intensity, %	
		70 μ	350 μ
24	C_2^+	0.3	
25	C_2H^+	1.2	
26	$C_2H_2^+$	19.9	2.0
27	$C_2H_3^+$	5.6	1.3
37	C_3H^+	0.9	
38	$C_3H_2^+$	0.9	
39	$C_3H_3^+$	1.4	2.8
50	$C_4H_2^+$	21.3	2.2
51	$C_4H_3^+$	39.8	10.6
52	$C_4H_4^+$	2.7	3.4
53	$C_4H_5^+$		5.6
61	C_5H^+	1.0	
62	$C_5H_2^+$	0.6	2.4
74	$C_6H_2^+$	1.2	
75	$C_6H_3^+$	1.0	1.2
76	$C_6H_4^+$	1.4	25.1
77	$C_6H_5^+$	0.8	26.7
86	$C_7H_2^+$		0.6
87	$C_7H_3^+$		1.6
88	$C_7H_4^+$		0.7
100	$C_8H_4^+$		1.4
101	$C_8H_5^+$		0.8
102	$C_8H_6^+$		3.9
103	$C_8H_7^+$		4.9
104	$C_8H_8^+$		1.0

in either experiment would bring the results into excellent agreement.

It is of interest to note that the ion $C_6H_6^+$ (m/e 78) appears as a relatively important ion above 0.6 torr.

Table II: Cross Sections for Reaction of Some Abundant Ions with Acetylene

Reactant ion	Cross section for 10 v/cm field strength—			
	This research ^a $\times 10^{16}$ cm ² /molecule	Lit. values $\times 10^{16}$ cm ² /molecule		
C_2^+	113	72 ^b	75 ^c	128 ^d
C_2H^+	77	70 ^b	72 ^c	153 ^d
$C_2H_2^+$	46	62 ^b	48 ^c	91 ^d
$C_4H_2^+$	18	33 ^b	46 ^d	
$C_4H_3^+$	14	18 ^b	50 ^d	

^a Distance between electron beam and ion-exit aperture, 0.28 cm. ^b Reference 9, distance between electron beam and ion-exit aperture, 0.34 cm. ^c Data from ref 7 obtained by averaging electrometer and multiplier results, which differed by a factor of 1.6. Distance between electron beam and ion-exit aperture, 0.2 cm. ^d Reference 11, distance between electron beam and ion-exit aperture, 1.0 cm.

Munson⁷ has commented on the significance of the non-observation of this ion in acetylene at elevated pressure. It is now apparent, however, that this ion does become prominent at higher pressures than those employed in the earlier work. This ion is kinetically of higher order than the other C_6 ions observed (m/e 76, 77), which are already disappearing by reaction before $C_6H_6^+$ appears.

Table I reports the mass spectrum at pressures of 0.07 and 0.35 torr. The extensive branching noted previously by Wexler, *et al.*,¹¹ is quite apparent. In addition to the even-carbon-number chains already noted there is an odd-carbon chain of much lower intensity. Another low intensity sequence is apparently initiated by the vinyl ion $C_2H_3^+$ (m/e 27), which leads to $C_4H_5^+$ (m/e 53) at 350 μ source pressure. At 1 mm, ions of m/e 140 ± 2 and 180 ± 3 of several percent relative abundance appear in addition to the ones cited in Table I as well as very low intensities of intermediate mass ions. These should probably be identified with the ions designated as $C_{11}H_{10}^+$ (m/e 142) and $C_{14}H_{14}^+$ (m/e 182) by Wexler, *et al.*,¹¹ or $C_{14}H_{12}^+$ (m/e 180) reported by Munson.⁷

In Figures 2 and 3 are presented semilogarithmic plots of the normalized intensity of the principal primary ions and first generation secondary ions, respectively. Cross sections deduced from the slopes of the straight-line portions of these curves are given in Table II, which compares our results with earlier work. Although there is considerable variation in the reported values, the results are considered to be in reasonable accord for such measurements.

Reactions of $C_2H_2^+$. That the principal primary ion in acetylene, $C_2H_2^+$, is a precursor of the principal secondary ions, $C_4H_2^+$ and $C_4H_3^+$, has been known for quite some time.^{1-5,7-11} Its possible importance as a precursor of several minor ions has been a matter of conjecture. Table III reports the results of an experi-

ment using the tandem spectrometer in which low-energy $C_2H_2^+$ ions are impacted on acetylene molecules at two different collision-chamber pressures. Although several fragments ions are observed from this interaction, the $C_4H_2^+$ and $C_4H_3^+$ ions together account for some 98% of the total products. Moreover, the results at 50 μ show clearly that the ionic polymerization of acetylene does not proceed by a simple sequence of reactions, as the $C_6H_5^+ : C_6H_4^+ : C_6H_3^+$ ratio is greatly different from the $C_4H_3^+ : C_4H_2^+ : C_4H^+$ ratio.

Table III: Reaction of $C_2H_2^+$ with C_2H_2

Product ion, <i>m/e</i>	Species	Relative intensity	
		5 μ (C_2H_2)	50 μ (C_2H_2)
27	$C^{12}C^{13}H_2^+$, $C_2H_3^+$ ^a	0.016	0.015
37	C_3H^+	0.0002	
38	$C_3H_2^+$	0.0006	0.0006
39	$C_3H_3^+$	0.0003	0.0003
49	C_4H^+	0.001	
50	$C_4H_2^+$	0.28	0.28
51	$C_4H_3^+$	0.70	0.69
74	$C_6H_2^+$		0.001
75	$C_6H_3^+$		0.005
76	$C_6H_4^+$		0.007
77	$C_6H_5^+$		0.004

^a Because secondary ions of mass 26 could not be detected in this experiment no correction of *m/e* 27 for C^{13} could be made. All other data in these tables have been corrected assuming an abundance of 1.1% C^{13} .

The ambiguity in the ion product of *m/e* 27 is easily resolved through the use of isotopically labeled reactants. Results from the reaction of $C_2H_2^+$ with C_2D_2 are given in Table IV. The ions, which would appear as *m/e* 27 for nondeuterated compounds, are now resolved into three products: $C_2D_2^+$ from simple charge exchange, C_2HD^+ from charge exchange with isotopic exchange, and the proton-transfer product, $C_2D_2H^+$. It is also noted that considerable isotopic mixing of the C_4 product ions occurs.

Lindholm and co-workers,⁶ in a study of charge exchange of a number of ions with acetylene, detected

the presence of isolated states of the acetylene molecule ion. These states also are manifested in photoionization studies,¹⁶ although they are not clearly resolved by electron impact.¹⁰ Implications of this property of acetylene have been discussed previously.⁸ In the present work, we have bombarded acetylene with ions of different recombination energies at sufficiently high pressures that secondary reactions of the ions initially produced by charge exchange may occur.¹⁷ The results of this experiment are reported in Table V. The ions Xe^+ (RE of $^2P_{1/2}$ state = 12.13 eV) and Br^+ (RE = 11.8 eV) produce $C_2H_2^+$ in the ground state, while Ar^+ (RE = 15.76 and 15.94 eV) produce $C_2H_2^+$ in an excited state. The data show that the reactions of $C_2H_2^+$ in the two states, as noted earlier by Lindholm, *et al.*,⁶ are substantially different.

Table V: Ion-Molecule Reaction Products in Acetylene Initiated by Charge Exchange

Product	Charge exchange agent		
	Ar^+	Xe^+	Br^+
$C_4H_2^+$	0.65	0.23	0.24
$C_4H_3^+$	0.35	0.77	0.76

Table VI: Reaction of C_2H^+ with C_2H_2

Product ion, <i>m/e</i>	Species	Relative intensity	
		5 μ (C_2H_2)	50 μ (C_2H_2)
26	$C_2H_2^+$	0.08	
27	$C_2H_3^+$	0.005	
37	C_3H^+	0.0005	
38	$C_3H_2^+$	0.0006	
39	$C_3H_3^+$	0.0013	
49	C_4H^+	0.013	
50	$C_4H_2^+$	0.90	0.92
51	$C_4H_3^+$	0.002	0.016
74	$C_6H_2^+$		0.007
75	$C_6H_3^+$		0.03
76	$C_6H_4^+$		0.02

Table VII: Isotopic Distribution of C_4 Ions from $C_4H_2D_2^+$ Complex

Species	Calcd distribution			Obsd
	$-X_2$	$-X$		
$C_4H_2^+$	0.02		0.02	0.02
C_4HD^+	0.14		0.14	0.14
$C_4D_2^+$, $C_4H_2D^+$	0.04	0.29	0.33	0.31
$C_4D_2H^+$		0.42	0.42	0.42

(16) R. Botter, V. H. Dibeler, J. A. Walker, and H. M. Rosenstock, *J. Chem. Phys.*, **44**, 1271 (1966).

(17) This technique was introduced explicitly in Lindholm, *Advances in Chemistry Series*, No. 58, American Chemical Society, Washington, D. C., 1966, p 14.

Table IV: Products from the Reaction of $C_2H_2^+$ with C_2D_2

Product ion, <i>m/e</i>	Species	Relative intensity
27	C_2HD^+	0.036
28	$C_2D_2^+$	0.076
29	$C_2D_2H^+$	0.014
50	$C_4H_2^+$	0.02
51	C_4HD^+	0.14
52	$C_4D_2^+$, $C_4H_2D^+$	0.31
53	$C_4D_2H^+$	0.42

Table VIII: Reaction of C_2H^+ with C_2D_2

Product ion, m/e	Species	Relative intensity
27	C_2HD^+	0.005
28	$C_2D_2^+$	0.08
29	$C_2D_2H^+$	0.007
50	C_4D^+	0.006
51	C_4HD^+	0.60
52	$C_4D_2^+$	0.31

Reactions of C_2H^+ . Experiments using mass- and energy-resolved beams of C_2H^+ analogous to those described for $C_2H_2^+$ were carried out. The results are summarized in Tables VI–VIII. The pattern is quite similar to that from $C_2H_2^+$ impact, except that essentially only $C_4H_2^+$ is formed as an ion–molecule reaction product. Somewhat surprisingly, charge transfer is about as important a reaction mode for C_2H^+ as for $C_2H_2^+$.

The complexity of the seemingly simple ionic polymerization chain for acetylene is clearly demonstrated by the higher-pressure experiment. The $C_4H_2^+$ ions do not produce $C_6H_4^+$ in an elementary reaction, as hydrogen elimination apparently occurs as the usual reaction mode. It is also noteworthy that, at the higher pressure, some $C_4H_3^+$ is also observed as a product, suggesting that stabilization of the ion–molecule complex is possible.

Reaction of Other Ions. The minor ions C_2^+ and CH^+ were also reacted with acetylene in a tandem experiment. For C_2^+ , small amounts of charge exchange (ca. 14%) and the formation of C_4H^+ (m/e 49) constitute the reaction products. For m/e 13 (ca. 60% CH^+ and 40% $C_2H_2^{2+}$, according to Munson⁷), the principal reactions are the formation of $C_3H_2^+$ and C_3H^+ plus significant amounts of charge transfer and proton transfer. With increasing pressure the $C_3H_2^+$ product is favored.

The observation of $C_6H_6^+$ as a product ion at high pressure and nonobservation as a product at the intermediate pressures where other C_6 ions predominate suggested that the reactions of $C_4H_4^+$ ions with acetylene should be studied. Table IX presents the results of bombarding acetylene with $C_4H_4^+$ ions derived from benzene. It is of interest to note that even at a pressure too low for collisional stabilization, $C_6H_6^+$ is observed as a product and the relative intensity of $C_6H_6^+$ increases with pressure. In addition, the distribution of ions bears little resemblance to that noted in the pressure experiments.

Ionization Efficiency Curves for $C_4H_2^+$ and $C_4H_3^+$. The peculiar shape of the $C_4H_2^+$ ionization efficiency curve compared with “normal” shapes for other acetylene primary and secondary ions was noted by Derwish, Galli, Giardini-Guidoni, and Volpi.⁹ These

Table IX: Products from the Reaction of $C_4H_4^+$ with $C_2H_2^a$

Product ion	Relative intensity	
	5 μ	25 μ
$C_6H_4^+$	0.096	0.125
$C_6H_5^+$	0.819	0.737
$C_6H_6^+$	0.085	0.138

^a The $C_4H_4^+$ ions were derived from electron-impact ionization of benzene. Product ions corrected for ^{13}C -isotope contribution assuming 1.1% ^{13}C in reactant molecule.

workers suggested that the structure in the curve might well be related to reaction of excited acetylene ions $C_2H_2^{+*}$ and to the parallel production of $C_4H_2^+$ from C_2H^+ primary ions. Since the branching ratios for producing $C_4H_2^+$ and $C_4H_3^+$ do appear quite different for $C_2H_2^+$ and $C_2H_2^{+*}$, it seemed worthwhile to attempt to resolve the structure of the $C_4H_2^+$ ionization efficiency curve.

A possible rationalization of the experimental curves is given in Figure 4. Solid curve A is a tracing of the experimental X–Y recorder plot of the ionization efficiency curve for $C_4H_2^+$. The ratio of $C_4H_2^+ : C_4H_3^+$ was determined in this research to be 0.45 ± 0.01 below 15-ev electron energy, in good agreement with Munson's value of 0.44 ± 0.04 .⁷ Hence the branching ratio is constant below this energy. Solid curve B is an experimental ionization efficiency curve for $C_4H_3^+$, normalized instrumentally, to the intensity of the previously traced $C_4H_2^+$ ion at 15 ev. It is noted that curves A and B superpose quite accurately, as anticipated, from threshold to 15 ev. The ionization potential for $C_2H_2^+$ is indicated on the figure to match the vanishing point for both secondary ions; i.e., there is no evidence for chemi-ionization by electron impact analogous to the photochemically produced chemi-ionizing states at 10.4 ev, reported by Koyano, Tanaka, and Omura.¹⁸

Curve C is a calculated ionization efficiency curve for estimating the intensity of $C_4H_2^+$ to be attributed to C_2H^+ . The relative intensities of the primary ions $C_2H^+ : C_2H_2^+$ was determined to be 0.196 for 25-ev electron impact. From the total reaction cross sections of Table IV and the partial cross sections for $C_4H_2^+$ production of Tables II and V, the relative contribution to the total $C_4H_2^+$ curve at 25 ev derived from C_2H^+ was deduced. This value was then used in conjunction with the concurrently measured ionization efficiency curve of C_2H^+ to construct curve C of Figure 4.

Curve D is obtained by a point-by-point subtraction of curve C from curve A. It therefore represents a “corrected” ionization-efficiency curve, which is assumed to include $C_4H_2^+$ ions, produced from $C_2H_2^+$

(18) I. Koyano, I. Tanaka, and I. Omura, *J. Chem. Phys.*, **40**, 2734 (1964).

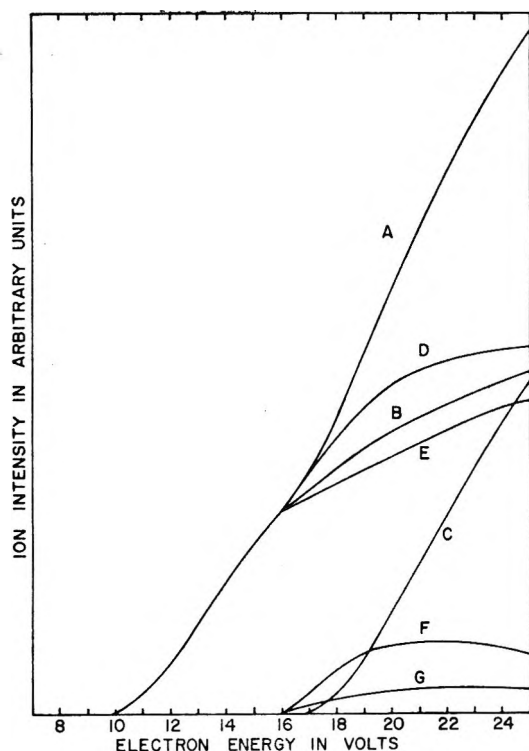


Figure 4. Ionization efficiency curves for $C_4H_2^+$ and $C_4H_3^+$ product ions in acetylene.

and $C_2H_2^{+*}$. It may be compared now with curve B, which represents $C_4H_3^+$ ions formed from the same precursor ions. The point where they diverge at ca. 16.3 eV is the point where the branching ratio changes; *i.e.*, the appearance potential of $C_2H_2^{+*}$. The value deduced, 16.3 eV, is in reasonable agreement with literature values: (possibly autoionization level) 15.5 eV,¹⁶ 14.8 eV,¹⁶ 16.27 eV,¹⁷ and 16.5 eV¹⁸ obtained from charge exchange, photoionization, photoelectron spectroscopy, and Penning ionization studies, respectively. Since ionization of acetylene is observed in these experiments using Ar^+ ions retarded to less than 0.3 eV, there must be at least a small probability of ionization down to about 15.94 eV ($^2P_{1/2} Ar^+$).

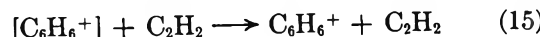
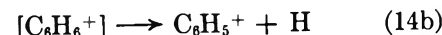
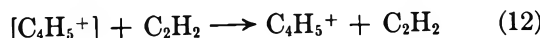
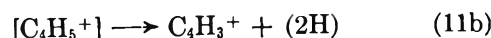
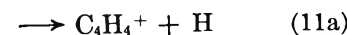
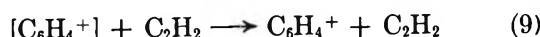
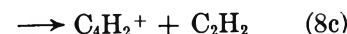
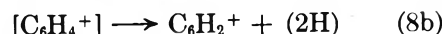
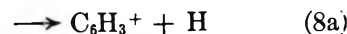
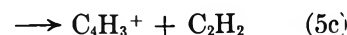
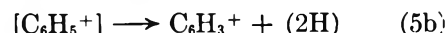
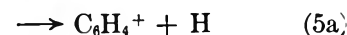
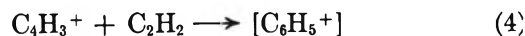
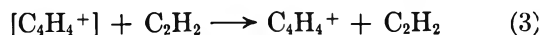
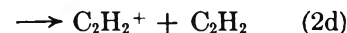
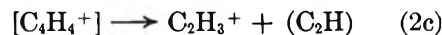
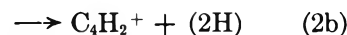
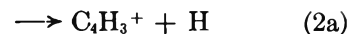
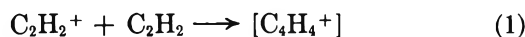
If we now assume that the branching ratio for the Ar^+ charge-exchange initiated reaction of Table V is typical of $C_2H_2^{+*}$, we may construct curve E using this ratio and a point-by-point subtraction of curve B from curve D. The resulting curve E now represents $C_4H_3^+$ and/or $C_4H_2^+$ derived from the ground-state acetylene ion $C_2H_2^+$; except for the branching ratio normalization factor, these curves should be identical. Curve F is then obtained by subtracting curve E from curve D. It represents the ionization efficiency curve for $C_4H_2^+$ derived from $C_2H_2^{+*}$. Similarly, curve G is obtained by subtracting curve E from curve B and represents the ionization efficiency curve for $C_4H_3^+$ ions produced from $C_2H_2^{+*}$. Except for a normalization factor, curves F and G should both be a measure of the ionization efficiency curve of $C_2H_2^{+*}$. The slight difference in their shapes may be the result of an ac-

cumulation of error, or it may indicate that the assumption of a constant branching ratio above 15 eV is in error.

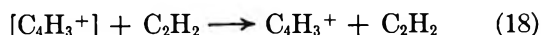
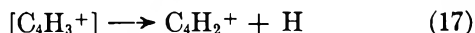
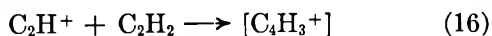
Although the circuitous procedure used here precludes a high level of confidence in the detailed resolution of these curves, it does provide a plausible deconvolution of the observed structure. Moreover, the appearance potential of $C_2H_2^{+*}$ deduced here is a rather more reliable result than the actual ionization efficiency curve, and the general features of the treatment would seem to be correct.

Discussion

The fairly complex reaction sequence required to rationalize the ionic polymerization of acetylene has been discussed in some detail by Munson,⁷ by Derwish, *et al.*,⁹ and by Wexler, *et al.*¹¹ Neglecting minor products the chain initiated by the most abundant primary ion is, through C_6 products



The second most abundant primary ion in acetylene is C_2H^+ , which initiates an analogous chain



The brackets denote a collision complex which will dissociate unless stabilized by collision.

Each step of the proposed reaction sequence has been demonstrated or can be inferred from the data presented here. In addition, other products from ion-molecule interaction of all primary ions have been reported, and a plausible reaction sequence for the odd-carbon chain and for other minor products could be written using the above scheme as a guide.

We have included in our mechanism reactions (5c and 8c), since Derwish, *et al.*,⁹ observed metastable ions corresponding to these dissociations. These workers searched for and failed to observe any metastables corresponding to $C_4H_4^+$ dissociation, and the question arises whether dissociation of this ion is so rapid that the concept of a $C_4H_4^+$ complex has any validity for this system. We believe that it does, for

the following reasons. One argument is that $C_4H_4^+$ is observed as a product ion at moderate pressures. In addition, the increasing importance of $C_6H_6^+$ at 1 torr pressure requires an abundant $C_4H_4^+$ precursor, which is difficult to account for on the basis of back reactions such as 11a.

Additional evidence for $C_4H_4^+$ is obtained in the isotopic experiment of Table IV. Both the existence of an isotopically mixed product from the back reaction and the isotopic mixing of the C_4 product ions suggest an intermediate of finite lifetime. Since both m/e 51 and m/e 53 peaks are unambiguously identified, they may be used as base points for calculating the distribution of isotopically labeled products. The results of such a calculation are summarized in Table VII. We have applied here the infinite-temperature isotope effect factors of $\sqrt{2}:1$, as discussed previously, in connection with an analogous calculation.¹⁴ The agreement is quite satisfactory, and we conclude that the concept of a stabilizable complex $C_4H_4^+$ is probably correct. The mechanism deduced seems adequate to describe the experimental results and, with minor changes, can probably be generalized to other reactive systems.

Studies of Free-Radical Species from the Reactions of Titanium(III) Ions with Hydrogen Peroxide

by Koichi Takakura and Bengt Rånby

Department of Polymer Technology, The Royal Institute of Technology, Stockholm, Sweden

Accepted and Transmitted by The Faraday Society (June 14, 1967)

Electron spin resonance studies of reaction products from titanium(III) ions with hydrogen peroxide in aqueous solutions using a flow system have shown spectra with two well-resolved peaks which are interpreted as due to $HO\cdot$ and $HO_2\cdot$ radicals, respectively. Both radicals are coordinated with $Ti(IV)$ ions and, possibly, also with other molecular species.

Since Dixon and Norman¹ observed the esr signal ascribed to hydroxyl radicals during the reaction of H_2O_2 and $TiCl_3$ in aqueous solution using a flow system, several detailed studies have been made of this reaction.

Piette, *et al.*,² have shown that the intensity ratio of the two esr signals obtained was rather sensitive to the experimental conditions for the reaction. They attributed the principal low-field peak (g value, 2.0132) to $HO_2\cdot$ radicals, and the minor high-field peak (g value,

2.0119) to $HO\cdot$ radicals. As reported earlier,³ we have also obtained the two esr signals and varied their in-

(1) W. T. Dixon and R. O. C. Norman, *Nature*, **196**, 891 (1962); *J. Chem. Soc.*, 3119 (1963).

(2) L. H. Piette, G. Bulow, and K. Loeffler, Preprint, Division of Petroleum Chemistry, American Chemical Society, Washington, D. C., April 1964.

(3) H. Yoshida and B. Rånby, paper presented at the IUPAC Symposium on Macromolecular Chemistry, Prague, 1965; *J. Polymer Sci.*, **C16**, 1333 (1967).

tensity ratios by changing the ratio of H_2O_2 to TiCl_3 . However, the assignment of the two signals has not been established so far, and conflicting proposals have been presented.

Sicilio, *et al.*,⁴ have recently confirmed the existence of two esr signals from this reaction system. On the basis of extensive kinetic evidence, they attributed the principal peak ($g = 2.0128$) observed at low field to $\text{HO}\cdot$ radicals, and the minor peak ($g = 2.0114$) to $\text{HO}\cdot$ radicals associated with Ti(IV) ions, respectively. Chiang, *et al.*,⁵ have also made a detailed esr study of the radical species formed in this system. They interpreted the signal as due to species arising from the reaction between $\text{HO}\cdot$ radicals and $\text{Ti(IV)}\text{-H}_2\text{O}_2$ complexes of different compositions. According to very recent work by Fischer,⁶ the two peaks are interpreted as due to $\text{HO}\cdot$ radicals coordinated with $\text{Ti(IV)}\text{-H}_2\text{O}_2$ complexes of different compositions. This assignment was based on the marked intensity enhancement of the two peaks on addition of the colored $\text{Ti(IV)}\text{-H}_2\text{O}_2$ complex and the observed Ti hyperfine structure.

In a series of esr investigations using a flow technique,^{3,7} we have studied the same problem in detail. In this paper, further evidence is presented that the two esr peaks are indeed due to complexes of radicals with Ti(IV) ions, which can be identified and assigned.

Experimental Section

The esr measurements were carried out as previously described^{3,7} using an X-band spectrometer (Japan Electron Optics Laboratory Co., Ltd., Model JES-3B) at room temperature ($22 \pm 2^\circ$) by applying the flow method. High-frequency field modulation (100 kc) was used with the modulation width of 0.2 gauss. The magnetic field was calibrated with pmr signals. The g values were measured with reference to the spectrum of 1,1-diphenyl-2-picrylhydrazyl in methanol solution as a standard. The flow rate of the mixed solutions was about 4 ml/sec, giving a time lag from mixing to measurement of about 0.02 sec.

The following reagents, all of analytical grade, were used: 15% titanous chloride in aqueous solution (iron free); 30% hydrogen peroxide in water, and concentrated sulfuric acid; disodium salt of ethylenediaminetetraacetic acid (EDTA), and ferrous chloride ($\text{FeCl}_2 \cdot 4\text{H}_2\text{O}$) were obtained from E. Merck AG, Darmstadt, Germany; 60% titanous tetrachloride in aqueous solution from Hopkin & Williams Ltd., England.

Results and Discussion

Under usual experimental conditions ($[\text{H}_2\text{O}_2] = 1.5 \times 10^{-1}$ mole/l.; $[\text{TiCl}_3] = 1.0 \times 10^{-2}$ mole/l.; $[\text{H}_2\text{SO}_4] = 2.0 \times 10^{-2} \sim 1.0 \times 10^{-1}$ mole/l.), we obtained two peaks in the esr spectra, a principal peak (designated as peak 1) at $g = 2.0140$ (low field) and a minor peak (peak 2) at $g = 2.0125$ (*i.e.*, at a field 2.4 gauss higher). In the absence of H_2SO_4 , two well-

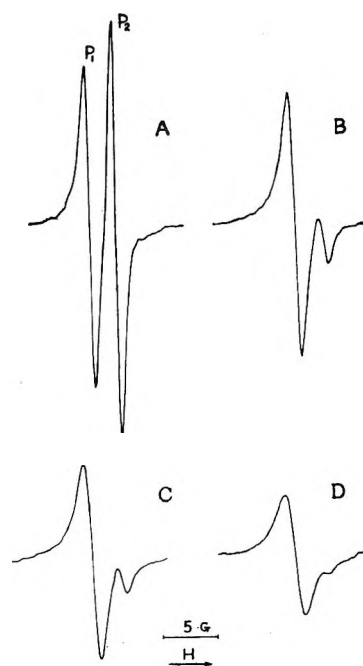


Figure 1. Effect of H_2SO_4 concentration on esr spectra obtained from reaction between H_2O_2 and TiCl_3 in aqueous solution; $[\text{H}_2\text{O}_2] = 1.5 \times 10^{-1} M$, $[\text{TiCl}_3] = 7 \times 10^{-3} M$: (A) without H_2SO_4 , pH 1.6; (B) $[\text{H}_2\text{SO}_4] = 1.1 \times 10^{-2} M$, pH 1.4; (C) $[\text{H}_2\text{SO}_4] = 4.4 \times 10^{-2} M$, pH 1.1; and (D) $[\text{H}_2\text{SO}_4] = 2.64 \times 10^{-1} M$, pH 0.5. P_1 and P_2 refer to peak 1 and peak 2, respectively.

solved intense peaks were observed with peak 2 being enhanced to greater extent than peak 1.

The addition of H_2SO_4 to the reacting solutions has a very pronounced effect on the signal intensity. Some of the results are shown in Figure 1, where the four spectra were recorded with identical esr spectrometer settings. With increasing H_2SO_4 concentration in the reaction system, the peak intensities were considerably decreased especially for peak 2, and the line width of both peaks became somewhat broader.

The ratio of $\text{H}_2\text{O}_2\text{:Ti(III)}$ also affects the signal intensity of the two peaks, as briefly described earlier.³ This is shown by experiments (Figure 2), in which the H_2O_2 and H_2SO_4 concentrations were kept constant. At the highest molar ratio of $\text{H}_2\text{O}_2\text{:Ti(III)}$ used, *i.e.*, 40, only one intense signal (peak 1) was observed (Figure 2A). With decreasing concentration ratio of $\text{H}_2\text{O}_2\text{:Ti(III)}$, however, the relative intensity of peak 1 decreased and the intensity of peak 2 increased. Finally, at the ratio of one, peak 2 became predominant with only traces of peak 1 (Figure 2D). The observed

(4) F. Sicilio, R. E. Florin, and L. A. Wall, *J. Phys. Chem.*, **70**, 47 (1966).

(5) Y. S. Chiang, J. Craddock, D. M. Mickewich, and J. Turkevich, *ibid.*, **70**, 3509 (1966).

(6) H. Fischer, personal communication; *Ber. Bunsenges. Physik. Chem.*, in press.

(7) K. Takakura and B. Rånby, *J. Polymer Sci.*, **B5**, 83 (1967); complete paper presented at the IUPAC Symposium on Macromolecular Chemistry, Brussels-Louvain, Belgium, 1967.

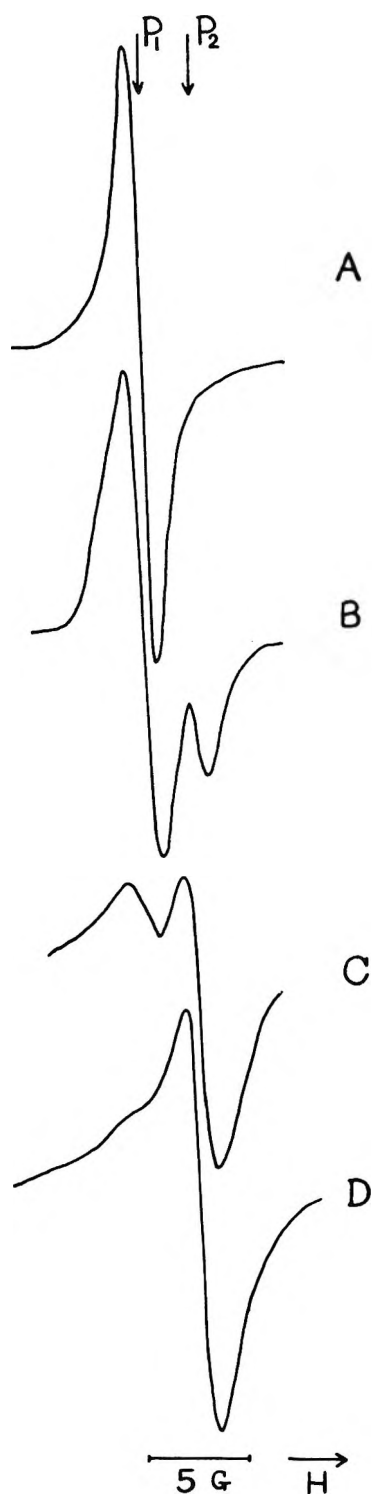


Figure 2. Effect of H_2O_2 :Ti(III) ratios on intensity of esr spectra obtained for reaction between H_2O_2 and TiCl_3 in the presence of H_2SO_4 in aqueous solution; $[\text{H}_2\text{O}_2] = 1.5 \times 10^{-1} M$, $[\text{H}_2\text{SO}_4] = 1.3 \times 10^{-1} M$ (both constant): (A) $(\text{TiCl}_3) = 3.7 \times 10^{-3} M$, (H_2O_2) : $[\text{Ti(III)}] = 40$, pH 0.80; (B) $(\text{TiCl}_3) = 1.5 \times 10^{-2} M$, (H_2O_2) : $[\text{Ti(III)}] = 10$, pH 0.68; (C) $(\text{TiCl}_3) = 7.5 \times 10^{-2} M$, (H_2O_2) : $[\text{Ti(III)}] = 2$, pH 0.50; and (D) $(\text{TiCl}_3) = 1.5 \times 10^{-1} M$, (H_2O_2) : $[\text{Ti(III)}] = 1$, pH 0.13. The spectra were recorded with identical spectrometer settings; P_1 and P_2 refer to peak 1 and peak 2, respectively.

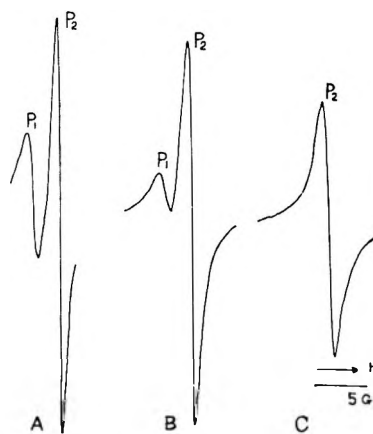
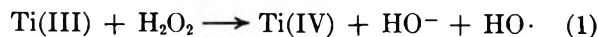


Figure 3. Effect of H_2O_2 :Ti(III) ratios on intensity of esr spectra obtained in aqueous solution for the reaction between H_2O_2 and TiCl_3 without addition of H_2SO_4 ; $[\text{H}_2\text{O}_2] = 1.4 \times 10^{-1} M$, (constant): (A) $[\text{H}_2\text{O}_2]$: $[\text{Ti(III)}] = 2$; (B) (H_2O_2) : $[\text{Ti(III)}] = 1$; and (C) $[\text{H}_2\text{O}_2]$: $[\text{Ti(III)}] = 0.5$, pH ~ 0.66 for A-C. These spectra were recorded with identical spectrometer settings.

broadening of the line width by the addition of a large amount of Ti(III) seems partly to arise from the lowering of the pH value (*cf.*, data in Figure 1).

The effects on the two peaks of variations in the H_2O_2 :Ti(III) ratio in the absence of H_2SO_4 showed similar trends. Typical spectra obtained with close to an equimolar ratio of H_2O_2 :Ti(III) are shown in Figure 3 where the concentration of H_2O_2 was kept constant at 1.4×10^{-1} mole/l. With decreasing molar ratio of H_2O_2 :Ti(III), the intensity of the two peaks tended to decrease. Peak 1, in particular, became very weak, and it disappeared completely at an H_2O_2 :Ti(III) ratio of 0.5, while peak 2 remained. It is interesting to note that in almost all cases studied (with excess of H_2O_2), the mixed solutions developed an intense yellow color. At the H_2O_2 :Ti(III) ratio of 0.5 or lower, the reacting streams became colorless. This indicates that one molecule of peroxide oxidizes two Ti(III) ions. Only peak 2 could be observed when the concentration of Ti(III) was twice the concentration of H_2O_2 or higher, *i.e.*, at H_2O_2 :Ti(III) ≤ 0.5 .

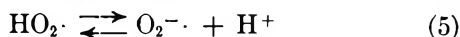
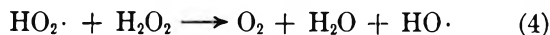
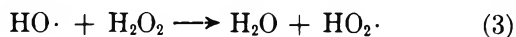
The redox reaction between Ti(III) ions and H_2O_2 is known to occur very rapidly. The one-electron reduction of H_2O_2 was found to proceed more readily by Ti(III) than that by Fe(II).⁸ These redox reactions can be formulated analogously with the well-known Fenton reagent reactions.⁹



At higher H_2O_2 :Ti(III) ratios, however, the following reactions may occur to an appreciable extent.³⁻⁵

(8) A. E. Cahill and H. Taube, *J. Am. Chem. Soc.*, **74**, 2312 (1952).

(9) C. Walling, "Free Radicals in Solution," John Wiley and Sons, Inc., New York, N. Y., 1957, p 564.



For reaction 5, $\text{HO}_2\cdot$ and $\text{O}_2^{\cdot-}$ are in equilibrium, and in strongly acidic solution the species $\text{HO}_2\cdot$ should predominate.¹⁰⁻¹²

On the basis of the reaction scheme in eq 1-5, it is suggested that the principal peak, 1, predominant at high H_2O_2 :Ti(III) ratios, is related to $\text{HO}_2\cdot$ radicals as understood from reaction 3, while peak 2, which predominates at a molar ratio of one or lower, may be related to $\text{HO}\cdot$ radicals. The formation of the species $\text{O}_2^{\cdot-}$ in measurable quantities seems to be less likely because of the strong acidity of the reaction system.

There is good evidence that $\text{HO}\cdot$ radicals are highly reactive and usually too short-lived to reach steady-state concentrations large enough for observation of their esr spectra. Livingston and Zeldes¹³ have obtained a singlet (g value of 2.015) for an aqueous H_2O_2 solution during ultraviolet irradiation in a flow system. They attributed this signal to $\text{HO}_2\cdot$ or $\text{O}_2^{\cdot-}$ species, depending upon the acidity of the system. We have observed that the radical species related to both peak 1 and peak 2 decay less rapidly than the resulting secondary radicals when organic substrates are present in this system. This indicates that the radicals from H_2O_2 are more or less stabilized. The reaction mixture of titanium salts and H_2O_2 usually develops an intense yellow to orange-red color due to formation of a stable peroxo complex between the resulting Ti(IV) ions and the excess of H_2O_2 remaining in the system. This complex is considered to be a peroxidized titanyl ion $[\text{TiO}_2 \cdot x\text{H}_2\text{O}]^{2+}$ in acid solution.¹⁴ As first proposed by Sicilio, *et al.*,⁴ it seems likely that the Ti(IV) ions are involved in complexes with $\text{HO}\cdot$ and $\text{HO}_2\cdot$ radicals resulting from the reaction of Ti(III) and H_2O_2 . In this way, these radicals could be sufficiently stabilized to be detected with the esr method. These assumptions are further supported by the following experiments.

An esr scanning of reaction mixtures containing Fe(II) and H_2O_2 showed no signal even though the $\text{HO}\cdot$ and $\text{HO}_2\cdot$ radicals are known to be formed in the reaction system. Addition of small amounts of TiCl_4 to the Fe(II)- H_2O_2 system gave, however, two intense signals which correspond exactly to peak 1 and peak 2, as previously obtained. Furthermore, the intensity of the signals increased with increasing Ti(IV) concentration. In Figure 4, a spectrum of peak 1 and peak 2 is shown. It is obtained by a rapid mixing of an FeCl_2 solution (acidified with H_2SO_4) with an H_2O_2 solution containing TiCl_4 . All these results can be interpreted to mean that $\text{HO}\cdot$ and $\text{HO}_2\cdot$ radicals generated from the reaction of Fe(II) with H_2O_2 are associated with Ti(IV) ions. The resulting free radical-Ti(IV) complexes are indicated as peak 2 and peak 1, respectively.

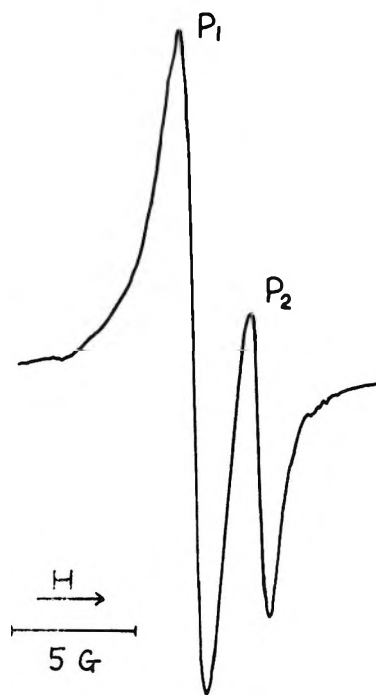


Figure 4. ESR spectrum of free radicals obtained from reaction between FeCl_2 and H_2O_2 in the presence of TiCl_4 : $[\text{H}_2\text{O}_2] = 1.5 \times 10^{-1} M$; $[\text{TiCl}_4] = 7 \times 10^{-3} M$; $[\text{FeCl}_2] = 7 \times 10^{-3} M$; and $[\text{H}_2\text{SO}_4] = 2.2 \times 10^{-2} M$.

The interpretation given here is also supported by experiments with EDTA as chelating agent, which easily forms complexes with various metal ions including titanium.^{15,16} When a 0.014 M TiCl_3 solution, containing a nearly equimolar concentration of EDTA, was mixed with a 0.26 M H_2O_2 solution in a flow system, the esr signals due to the two peaks disappeared, and the reaction mixture was almost decolorized. No radicals due to EDTA itself could be detected. This suggests that the titanium chelate with EDTA, in which EDTA is tightly bound to the Ti coordination sphere, could no longer coordinate with the resulting $\text{HO}\cdot$ and $\text{HO}_2\cdot$ radicals. It should be noted, however, that when a substrate such as vinyl acetate was added to this system containing EDTA, vinyl acetate monomer radicals appeared as in the absence of EDTA. Therefore, we may conclude that the initiating radicals that actually react with the substrate are not the species giving peak 1 and peak 2 but free $\text{HO}\cdot$ radicals which are not possible to detect in the esr spectra under these

(10) N. Uri, *Chem. Rev.*, **50**, 375 (1952).

(11) G. Czapski and B. H. Bielski, *J. Phys. Chem.*, **67**, 2180 (1963).

(12) G. Czapski and L. M. Dorfman, *ibid.*, **68**, 1169 (1964).

(13) R. Livingston and H. Zeldes, *J. Chem. Phys.*, **44**, 1245 (1966).

(14) W. C. Schumb, C. N. Satterfield, and R. L. Wentworth, "Hydrogen Peroxide," American Chemical Society Monograph No. 128, Reinhold Publishing Corp., New York, N. Y., 1955, p 656.

(15) R. Feld and P. L. Cowe, "The Organic Chemistry of Titanium," Butterworth and Co. Ltd., London, 1965, p 58.

(16) S. Fujiwara, K. Nagashima, and M. Codell, *Bull. Chem. Soc., Japan*, **37**, 773 (1964); **37**, 49 (1964).

conditions. Generally, on adding substrate to this system, the two peaks are replaced with those of the resulting substrate radicals, suggesting that the $\text{HO}\cdot$ radicals attack substrate molecules more rapidly than they form complexes with Ti(IV) .

As reported by Fischer,⁶ we also observed that addition of the colored $\text{Ti(IV)}\text{--H}_2\text{O}_2$ complex to the $\text{Ti(III)}\text{--H}_2\text{O}_2$ system enhanced the esr peaks considerably. Therefore, it cannot be ruled out in the discussion that the $\text{Ti(IV)}\text{--H}_2\text{O}_2$ complex, as such, in some cases is involved in the formation of the species giving peak 1 and peak 2. With excess of Ti(III) ions, however, peak 2 of low intensity was obtained in the absence of the colored $\text{Ti(IV)}\text{--H}_2\text{O}_2$ complex (*cf.* Figure 3C, with a $\text{H}_2\text{O}_2\text{:Ti(III)}$ ratio of 0.5).

There is additional evidence for the interpretation of peak 1 as due to $\text{HO}_2\cdot$ radicals. Saito and Bielski¹⁷ previously worked with ceric sulfate (acidified with H_2SO_4) and H_2O_2 solutions. They obtained a singlet of a line width of 27 gauss at $g = 2.016$, and attributed it to $\text{HO}_2\cdot$ radicals, presumably complexed with cerium ions according to the reaction $\text{Ce(IV)} + \text{H}_2\text{O}_2 \rightarrow \text{Ce(III)} + \text{HO}_2\cdot + \text{H}^+$. In comparison with our result for the $\text{Ti(III)}\text{--H}_2\text{O}_2$ system, the g values are nearly the same, but the line width of 27 gauss reported by Saito and Bielski is much broader. However, this difference may be ascribed to the different nature of the two metal ions as components in complexes with the $\text{HO}_2\cdot$ radicals, as suggested by Piette, *et al.*,² for the cerium- H_2O_2 sys-

tem. To test this assumption, Ti(IV) ions were added to the $\text{Ce(IV)}\text{--H}_2\text{O}_2$ system and esr measurements were carried out.

A 0.002 M ceric sulfate solution was mixed with a 0.26 M H_2O_2 solution containing 0.0140 M TiCl_4 , both acidified with 0.5 M H_2SO_4 . In this case, we obtained a narrow singlet which is identical with peak 1, instead of the reported broad singlet. This suggests that the $\text{HO}_2\cdot$ radicals formed in the reaction of Ce(IV) with H_2O_2 are coordinated faster and more strongly with Ti(IV) ions than with cerium ions. No signal corresponding to peak 2 could be observed in this case. We think, therefore, that this result is strong evidence for the identification and assignment of peak 1 to $\text{HO}_2\cdot$ radicals.

From the results obtained so far, we find evidence to conclude that peak 1 and 2 in the esr spectra observed for the $\text{Ti(III)}\text{--H}_2\text{O}_2$ system are assigned to $\text{HO}_2\cdot$ and $\text{HO}\cdot$ radicals, respectively. Both radicals are coordinated with Ti(IV) ions or $\text{Ti(IV)}\text{--H}_2\text{O}_2$ complexes.

Acknowledgments. The authors wish to thank Priv.-Dozent Dr. H. Fischer of the Deutsches Kunststoff-Institut, Darmstadt, Germany, for making his unpublished results available to us. This research was supported by MALMFONDEN—Swedish Foundation for Scientific and Industrial Development.

(17) E. Saito and B. H. J. Bielski, *J. Am. Chem. Soc.*, **83**, 4467 (1961)

Metal-Ammonia Solutions. II. Internal Reflection

Spectroscopy of Alkali Metal-Ammonia Solutions¹

by D. F. Burow and J. J. Lagowski

Department of Chemistry, The University of Texas, Austin, Texas 78712 (Received June 19, 1967)

The internal reflection spectra of alkali metal solutions in ammonia and in deuterioammonia as well as of the pure solvents were determined using silicon optics in the range 1.3–7.0 μ . The band attributed to the "solvated electron" ($\sim 1.5 \mu$) is observed at all concentrations in the blue phase but disappears for the bronze solutions. The vibrational spectrum of the solvent is observed for all solutions and does not appear to be appreciably changed from that of the pure solvent.

Introduction

The optical properties of dilute (blue) and concentrated (bronze) metal-liquid ammonia solutions have been a subject of interest for several years.² For the most part, these investigations have attempted to characterize the solute species giving rise to the band at about 1.5 μ in dilute solutions using conventional transmission techniques. The high molar absorptivity at the band maximum ($\approx 5 \times 10^4$ l. mole⁻¹ cm⁻¹)¹ has limited transmission studies to solutions less concentrated than 0.03 M.^{2b} However, the results of a front surface, specular reflection method have been reported for the blue³ and the bronze solutions.^{3,4} We present here the results of a study of metal-ammonia and metal-deuterioammonia solutions using the internal reflection technique⁵ in an attempt to understand the effect of solution of the metal on the solvent structure.

The application of conventional spectroscopic transmission methods to the study of strongly absorbing solutions requires the use of very short path-length cells and a correction for the appreciable reflection losses which occur at the solution interface. Ordinary reflection spectroscopy⁶ also suffers several disadvantages; this technique requires that the substance in question have a relatively high absorption coefficient for optimum sensitivity. The reflection spectrum cannot generally be correlated with the corresponding transmission spectrum without considerable data reduction, and in the case of liquid samples, a correction for window reflectivity must be made. The internal reflection method introduced by Fahrenfort^{5a} and developed by others^{5b-g} eliminates some of these difficulties and reduces others. In the internal reflection technique, an absorbing substance is placed in contact with an optically more dense, but still transparent, medium. Radiation is propagated through the more dense medium and is reflected at this interface; measurement of the reflectivity of this surface as a function

of frequency yields the internal reflection spectrum. A judicious choice of geometry can permit multiple reflection to occur, thereby increasing the intensity of the spectrum. The internal reflection technique has been used to advantage where conventional spectroscopic techniques cannot be readily applied.⁷ The internal reflection method still suffers the disadvantage that a direct comparison between the spectra obtained and conventional transmission spectra requires a detailed knowledge of the geometry of the interaction of the beam with the sample together with considerable numerical analysis.⁸

Experimental Section

A survey of the optical and chemical properties of substances suitable for internal reflection spectroscopy indicates that elemental silicon possesses many desirable features. Silicon has a high refractive index (*ca.* 3.5) and is transparent in the region of interest (1.3–7.0 μ). This substance can be fabricated with relative ease, and the surface will maintain an optical finish. Unlike many of the other substances that were con-

(1) Part I of this series is D. F. Burow and J. J. Lagowski, *Advances in Chemistry Series*, No. 50, American Chemical Society, Washington, D. C., 1965, p 125.

(2) (a) R. C. Douthett and J. L. Dye, *J. Am. Chem. Soc.*, **82**, 4472 (1960); (b) M. Gold and W. L. Jolly, *Inorg. Chem.*, **1**, 818 (1962); (c) W. L. Jolly and C. Hallada, *ibid.*, **2**, 1076 (1963).

(3) T. A. Beckman and K. S. Pitzer, *J. Phys. Chem.*, **65**, 1527 (1961).

(4) W. T. Cronenwett, Ph.D. Dissertation, The University of Texas, 1966.

(5) (a) J. Fahrenfort, *Spectrochim. Acta*, **17**, 698 (1961); (b) J. Fahrenfort and W. M. Visser, *ibid.*, **18**, 1103 (1962); (c) J. Fahrenfort and W. M. Visser, *ibid.*, **21**, 1433 (1965); (d) W. N. Hansen, *Anal. Chem.*, **35**, 765 (1963); (e) W. N. Hansen, *Spectrochim. Acta*, **21**, 209 (1965); (f) W. N. Hansen and J. A. Horton, *Anal. Chem.*, **36**, 783 (1964); (g) N. J. Harrick, *Ann. N. Y. Acad. Sci.*, **101**, 928 (1963).

(6) I. Simon, *J. Opt. Soc. Am.*, **41**, 3361 (1951).

(7) N. J. Harrick, *Appl. Opt.*, **5**, 1 (1966).

(8) W. N. Hansen, *Spectrochim. Acta*, **21**, 815 (1965).

sidered, silicon does not react with either anhydrous ammonia or metal-ammonia solutions.

The prism geometry was determined by the severe limitations placed on experiments involving metal-ammonia solutions and the criteria for optimum internal reflection characteristics given by Harrick.⁹ The V-shaped prism shown in Figure 1a offers a number of advantages over other designs. This type of prism can be placed directly in the beam of a commercial spectrometer without the use of auxiliary mirrors, and there is no defocusing of the beam as long as the relationship $L = nd$ is maintained; L represents the path of the beam in the prism, n is the refractive index of the prism material, and d is the distance between the entrance and exit apertures of the prism (Figure 1a). The number of reflections in a V-shaped prism is relatively large, and the number contributing to the spectrum can be modified by adjusting the height of the liquid around the prism. Rather than attempting to obtain a single, continuous V-shaped prism, two identical parallelopipeds with 30 and 150° angles were fabricated (Texas Instruments, Inc.) from transistor-grade silicon, all optical surfaces being polished flat to within 250 Å (Figure 1b). Since an adhesive inert to both ammonia and metal-ammonia solutions suitable for maintaining optical contact between the two parallelopipeds was not available, the experiments were conducted with the prisms bearing against each other. The two parallelopipeds were held together in a carriage (Figure 1c); optical contact between the prisms was undoubtedly penetrated by a thin film of the solution, but the presence of such a film could not be detected in the internal reflection spectrum. The carriage was constructed of glass using graphite prisms identical with the silicon prisms as templates. The carriage was suspended in the solution cell (Figure 2) from a glass crosspiece (Figure 1c), the exterior arms of which were ground to fit tightly within the walls of the cell. With the prisms in place, the central portion of the beam underwent 20 reflections in traversing their length.

The solution cell was permanently mounted in the sample compartment of a Perkin-Elmer Model 12B single-beam spectrometer fitted with an LiF or NaCl prism; the latter was used for measurement near 6 μ . The entire optical path from the source to the detector was sealed and purged with dry nitrogen (Figure 2). The cell, which was cooled with a Dry Ice-isopropyl alcohol slush bath, was connected to a conventional vacuum system; the temperature of the solution was measured with a calibrated thermistor probe enclosed in a glass well. The cleaning procedures, methods for preparing metal-ammonia solutions of known concentration, and the purification and handling of the alkali metals have been described previously.¹

In a typical experiment, anhydrous NH_3 or ND_3 was distilled from sodium into the cell and the volume of the liquid was determined at -70° . The cell was then

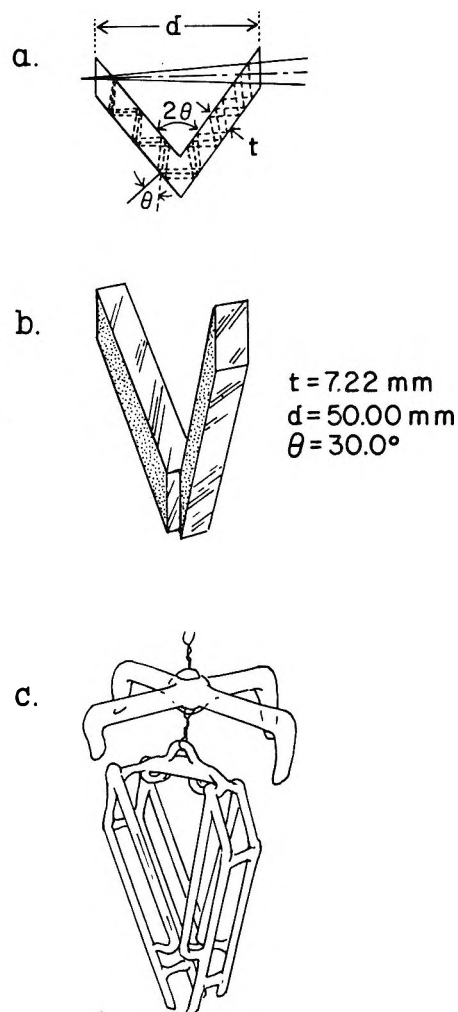


Figure 1. Internal reflection prisms: a, light path in the prism; b, geometry of the silicon prism; c, carriage for the silicon prisms.

pressurized with about 0.75 atm of dry helium to prevent condensation of ammonia onto the optical surfaces of the silicon prism which were not immersed in liquid ammonia. A carefully controlled helium pressure on the make-up side of the cell was used to raise the liquid level around the prism so that about 18 of the possible 20 reflections would be utilized when the spectrum was recorded. When a satisfactory spectrum of the solvent was obtained, the pressure on both sides of the cell was equalized, the alkali metal sample was introduced with a winch assembly,¹ and the solution was mixed by alternately pressurizing the two sides of the cell with helium. Thus, a solvent spectrum was determined immediately before the spectrum of each solution was recorded. All spectra were obtained at a constant slit width which was always in the range 0.015–0.025 cm. Because of uncontrolled bumping of the solutions at temperatures above -65° and the absorption by gaseous ammonia in the beam due to the

(9) N. J. Harrick, *Anal. Chem.*, **36**, 188 (1964).

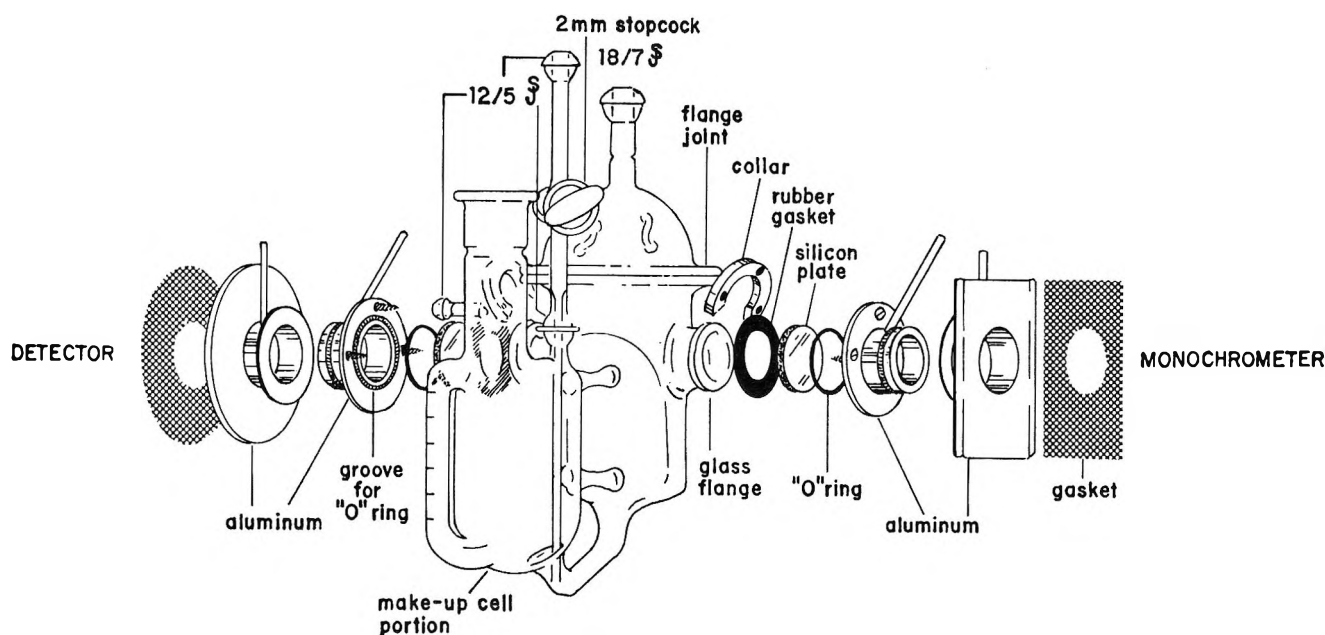


Figure 2. Internal reflection cell and cell assembly.

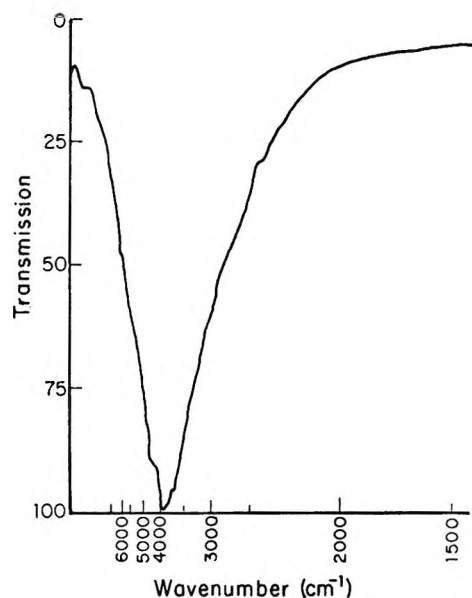


Figure 3. Internal reflection spectrum of the silicon prism.

increased vapor pressure, internal reflection spectra were not obtained at higher temperatures.

The transmission spectrum of the silicon optics in an evacuated cell is shown in Figure 3. The low signal at both high and low frequencies is due to a combination of absorption by silicon, the blackbody envelope of the infrared source, and the response of the detector. The transmission spectra of the solvents in the near-infrared region were determined in the cell previously described.¹

Results and Discussion

Internal Reflection Spectroscopy. Radiation propagated in a medium of refractive index n_1 is totally reflected from an interface with a second medium of

refractive index n_2 if the angle of incidence is greater than the critical angle, θ_c ; θ_c is given by eq 1, where $n_2 < n_1$. If the less dense medium absorbs radiation

$$\theta_c = \sin^{-1} \frac{n_2}{n_1} \quad (1)$$

from the beam at certain frequencies, total reflection is destroyed at these frequencies, reducing the beam intensity. When the radiation strikes the interface, the electromagnetic field penetrates into the less dense medium but is not propagated through it. The electric field intensity, E , beyond the interface decreases exponentially in accordance with

$$E = E_0 \exp \left\{ \frac{-\lambda x}{2\pi n_2 [\sin^2 \theta - (n_2/n_1)^2]^{1/2}} \right\} \quad (2)$$

where E_0 is the electric field strength at the interface, λ is the wavelength of the radiation *in vacuo*, θ is the angle of incidence, and x is the distance from the interface.¹⁰ The depth of penetration, $x_{1/2}$, into the less dense medium has been defined as the distance from the interface, where $E = \frac{1}{2}E_0$, and is given by

$$x_{1/2} = \frac{0.693\lambda}{2\pi n_1 [\sin^2 \theta - (n_2/n_1)^2]^{1/2}} \quad (3)$$

Under the usual conditions of obtaining internal reflection spectra, $x_{1/2} \simeq \lambda/10$, so that the electric vector associated with infrared radiation in the range of interest interacts with a layer of matter *ca.* 0.1μ thick at the interface between the two media. Thus, internal reflection techniques should prove useful in obtaining spectra of relatively concentrated metal-ammonia

(10) N. J. Harrick, *J. Opt. Soc. Am.*, **55**, 851 (1965).

Table I: The Spectra of NH₃ under Various Conditions

Assignment ^a	Gas phase, cm ⁻¹ ^b	Liquid phase, cm ⁻¹ ^c	Crystalline phase, cm ⁻¹ ^d	Adsorbed cm ⁻¹ ^e	Reflection, cm ⁻¹ ^f
ν_2	932.5 968.3	1035-1066	1060
ν_4	1626.1 1627.4	1632	1646	1635-1620	...
$2\nu_4$	3219	3220	3220
ν_1	3336.2 3337.2	3285	3223	3320-3280	3260 ^h 3280
ν_3	3443.6 3443.9	3375	3378	3410-3341	3370 ^h 3410
$\nu_1 + \nu_2$	4302 4269	4386 ^g	4360
$\nu_2 + \nu_3$	4505 4433	4470 ^g	4470
$\nu_3 + \nu_4$	5053	5000 ^g	4990
$\nu_2 + \nu_3 + \nu_4$	6016	6090 ^g	6000
$2\nu_1$	6595	6523 ^g	6400
$(2\nu_3, \nu_1 + \nu_3)$	6624				

^a Assignments of the gas phase spectra according to G. Herzberg, "Infrared and Raman Spectra of Polyatomic Molecules," D. Van Nostrand, Inc., New York, N. Y., 1945. ^b M. E. Jacox and D. E. Milligan, *Spectrochim. Acta*, **19**, 1173 (1963); G. Herzberg, ref. a. ^c Reference 11. ^d Reference 12. ^e N. W. Cant and L. H. Little, *Can. J. Chem.*, **42**, 802 (1964); V. N. Abramov, A. V. Kiselev, and V. I. Lygen, *Zh. Fiz. Khim.*, **38**, 1867 (1964); A. V. Kiselev, V. I. Lygen, and T. I. Titova, *ibid.*, **38**, 2730 (1964); M. R. Basila and T. R. Kantner, *J. Phys. Chem.*, **71**, 467 (1967). ^f Data from this investigation. ^g These bands were not within the spectral range of the equipment. ^h Assigned to adsorbed molecules.

solutions because of the very short effective pathlengths which can be attained; however, care must be exercised to distinguish between surface and bulk phenomena in interpreting the results. According to the criteria discussed by Hansen,⁸ the absorption index (*i.e.*, the imaginary portion of the complex refractive index) of metal-ammonia solutions at high concentrations is probably sufficiently large to produce a considerable distortion of the bands using the fixed angle silicon prism described here. However, qualitative observations should yield information of the nature of metal-ammonia solutions.

The Internal Reflection Spectrum of Liquid Ammonia. Examples of the internal reflection spectra of anhydrous liquid ammonia and of deuterioammonia are shown in Figure 4; the band positions and their assignments are tabulated in Tables I and II. The assignments for the isotopically different liquids have been made primarily on the basis of assignments for the gas-phase spectra and correlate well with the reported spectra and assignments for NH₃ and ND₃ in the liquid and solid states. Two bands occur in the internal reflection spectrum of ammonia in the regions associated with both ν_1 and ν_3 ; however, in each of these regions one of the bands remains after the liquid ammonia is removed from the cell and disappears when the cell is evacuated with the roughing pump at room temperature. The bands at 3260 and 3370 cm⁻¹ are assigned to the ν_1 and ν_3 modes, respectively, of ammonia molecules adsorbed on the prism surface. The assignments are within the range of frequencies observed for adsorbed ammonia molecules

Table II: The Spectra of ND₃ under Various Conditions

Assignment ^a	Gas phase, cm ⁻¹ ^b	Liquid phase, cm ⁻¹	Crystalline phase, cm ⁻¹ ^c	Reflection, cm ⁻¹ ^d
ν_2	748	...	815	...
ν_4	1191	...	1196	...
$2\nu_4$	2380	2370
ν_1	2419	2405 ^e	2318	2435 ^f
ν_3	2555	2510 ^e	2500	2490 ^f 2455
$\nu_1 + \nu_2$	3167	3175
$\nu_2 + \nu_3$	3300	3360
$\nu_3 + \nu^b$	3745	3740
$\nu_2 + \nu_3 + \nu^b$	4495	4264 ^d
$2\nu_1$	4838	4587 ^d
$2\nu_1$	4974	4822 ^d	...	4820
$(2\nu_3, \nu_1 + \nu_3)$				
$2\nu_3$	5110	5110 ^d	...	5470

^a Assignments of the gas phase spectrum according to G. Herzberg, "Infrared and Raman Spectra of Polyatomic Molecules," D. Van Nostrand, Inc., New York, N. Y., 1945. ^b M. E. Jacox and D. E. Milligan, *Spectrochim. Acta*, **19**, 1173 (1963); G. Herzberg, ref. a. ^c Reference 12. ^d Data from this investigation. ^e N. W. Cant and L. H. Little, *Can. J. Chem.*, **42**, 802 (1964). ^f Assigned to adsorbed molecules.

on various substrates (Tables I and II). The fact that these bands disappear under relatively mild conditions, *i.e.*, rough evacuation at room temperature, suggests that the adsorption energy is low compared to that in other systems (see ref. b, Table I). The internal reflection spectrum also shows a larger relative intensity for

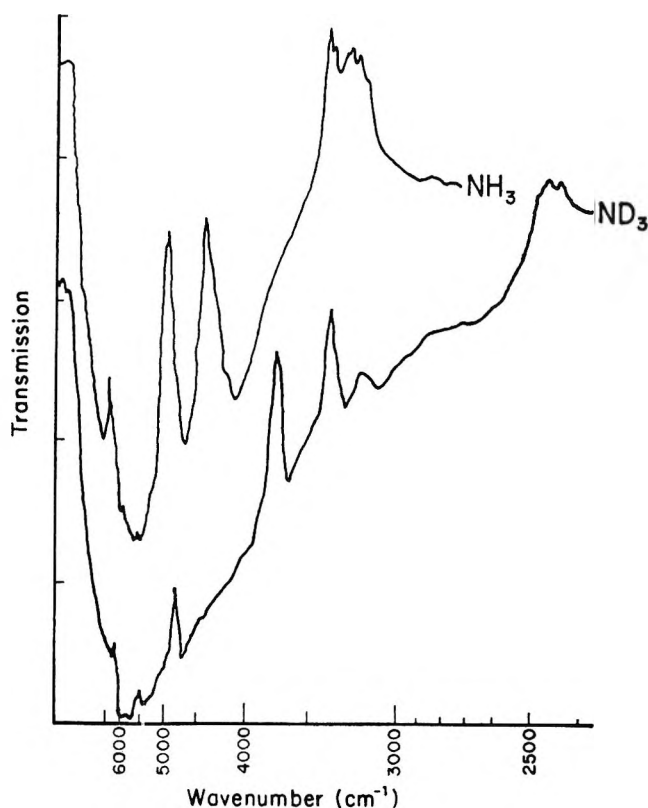


Figure 4. Internal reflection spectrum of liquid NH_3 and of liquid ND_3 .

the ν_3 vibrational mode than is observed in the gaseous spectrum, in agreement with the observations on the transmission spectrum of the liquid¹¹ and crystalline phases.¹² Failure to observe the ν_4 mode can probably be attributed to its low intensity in the liquid phase and the low transmission of silicon in this region. The larger deviation of the internal reflection bands assigned to the combination modes from the corresponding transmission bands arises from absorption effects associated with the silicon and the dispersion of the optical elements in the system.

Internal Reflection Spectra of Metal-Ammonia Solutions. The spectra of sodium solutions in anhydrous deuterioammonia (Table III) and of lithium, sodium and potassium in ammonia (Table IV) were obtained at several concentrations. The vibrational spectrum of the solvent appears to be unaffected by the presence of alkali metal sufficient to yield the blue phase. The internal reflection bands assigned to ν_1 (3280 cm^{-1}) and ν_3 (3410 cm^{-1}) occur at different positions than those observed in a specular reflectance study $\nu_1 = (3190\text{ cm}^{-1})$ and $\nu_3 = (3370\text{ cm}^{-1})$;³ however, this apparent discrepancy can probably be accounted for on the basis of a difference in the geometry of interaction of the beam with the sample in the two types of experiment. Although spectra obtained by the internal reflection method are expected to be more comparable to transmission spectra than those obtained by front sur-

Table III: Internal Reflection Spectra of Na-ND_3 Solutions at Various Concentrations

Assignment ^a	Solvent spectrum ^b	Concn, <i>m</i>		
		1.4×10^{-2}	1.4×10^{-1}	1.3
$2\nu_4$	2370
ν_1	2460 (0.81)	2430	2430	2430
ν_3	2455 (0.72)	2470	2455	2455
$\nu_1 + \nu_2$	3175 (0.15)	...	3715	3175
$\nu_2 + \nu_3$	3360 (0.81)	3385	3385	3385
$\nu_3 + \nu_4$	3740 (1.00)	3740	3760	3760
$2\nu_1$	4820 (0.56)	4820
$2\nu_3$	5470 (0.15)

^a See Table II. ^b Relative intensities indicated. The bands assigned to adsorbed molecules (2435 and 2490 cm^{-1}) are omitted; in most instances, these bands were observed in the spectrum of Na-ND_3 solutions.

face techniques, direct quantitative comparison with transmission spectra should be made with caution.⁶ The internal reflection technique permits enhancement of the weaker bands, but quantitative transformation of these data into equivalent transmission spectrum would require more sophisticated measurements so that the arguments presented here on metal-ammonia solutions are made only on the basis of the relative positions of the bands observed with a single spectroscopic technique.

A portion of the absorption band giving rise to the intense blue color characteristic of metal-ammonia solutions ($\sim 1.5\text{ }\mu$) appears as a shoulder on the high energy cutoff of the silicon prism for the most dilute solutions studied. As the concentration increases, the $1.5\text{-}\mu$ band progressively obscures the vibrational bands of the solvent without apparent major changes in the frequencies or the general shapes of these bands. The relative intensities of the set of solvent bands in a given spectrum were the same for all the spectra, although apparent changes in intensities occurred from one concentration to the next which could be attributed to an uncertainty in the immersion level of the prisms. A small portion of the sodium-ammonia solution which was prepared to be $1.4\text{ }m$ separated as the bronze phase; however, it formed a very thin film which floated on the surface of the blue solution and did not appear to contribute significantly to the spectrum. The spectra of two different concentrations of lithium and potassium in liquid ammonia are similar to those of the corresponding sodium solutions. Thus, it is evident that alkali metal-ammonia solutions do not exhibit absorption bands between 1.3 and $7.0\text{ }\mu$ other than those attributed to either the solvent or the "solvated electron."

Investigation of solutions in the concentration range

(11) I. V. Demedenkova and L. D. Shcherba, *Izv. Akad. Nauk SSSR, Ser. Fiz.*, **22**, 1122 (1959).

(12) (a) F. P. Reding and D. F. Hornig, *J. Chem. Phys.*, **19**, 594 (1951); (b) *ibid.*, **22**, 1926 (1954).

Table IV: Internal Reflection Spectra of Alkali Metal-Ammonia Solutions at Various Concentrations (*m*)

Assignment ^a	Solvent spectrum ^b	Concn, <i>m</i>								
		Na, 2 × 10 ⁻³	Li, 1.0 × 10 ⁻²	Na, 1.7 × 10 ⁻²	K, 1.0 × 10 ⁻²	Li, 1.0 × 10 ⁻¹	Na, 1.3 × 10 ⁻¹	K, 1.0 × 10 ⁻¹	Na, 1.4	Bronze, 10.3
2ν ₄	3220 (0.45)	3220	3170	3220	3230	3220	3230	3240	3240	3220
ν ₁	3280 (0.50)	3280	3280	3280	3280	3280	3230	3280	...	3300
ν ₃	3410 (0.62)	3410	3380	3410	3420	3410	3410	3400	3410	3410
ν ₁ + ν ₂	4360 (sh) (0.58)	4335	4420	4330	4320	...	(4320)	4395
ν ₂ + ν ₃	4470 (0.83)	4460	4470	4470	4470	4470	4470	4480	...	4470
ν ₃ + ν ₄	4990 (1.00)	4990	4980	4980	4990	4980	...	4980	...	4990
ν ₂ + ν ₃ + ν ₄	6000 (0.08)	...	6000	...	6000	5775
2ν ₁	6400 (0.43)	6400	6400	...	6400	6400

^a See Table I. ^b Relative intensity indicated. The bands assigned to adsorbed molecules (3260 and 3370 cm⁻¹) are omitted; in most instances these bands were observed in the spectra of metal-ammonia solutions.

encompassing the blue-bronze transition was not possible with this prism design because of the ambiguity concerning the phase in contact with the prism. Accordingly, the spectrum of an ammonia solution prepared to be 10.3 *m* in sodium was determined; with this ratio of solute to solvent the entire solution was bronze. In this solution the band attributed to the "solvated electron" is no longer discernable, in agreement with specular reflectance studies;³ however, the vibrational spectrum of liquid ammonia is observed without apparent distortion (Table IV). The significance of the broadening and shift of the relatively weak band which originally appeared in pure liquid ammonia at 6000 cm⁻¹ is not apparent, especially since the other combination bands that involve the ν₃ and ν₄ vibrations (*e.g.*, at 4470 and 4990 cm⁻¹) have not been altered. The shoulder which appears at about 4360 cm⁻¹ (ν₁ + ν₂) in pure liquid ammonia is more distinct and hence more easily defined in the bronze phase.

A notable feature of the spectrum of the bronze solution is that the intensity of the radiation transmitted by the prism in contact with the bronze solution is an order of magnitude less than that transmitted by the blue solutions. The reflectivity of the bronze sodium-ammonia solutions exceeds that of liquid mercury at the frequencies reported in this investigation.³ If reflection at the interface between the prism and the bronze solution were essentially metallic, a significant loss of energy would be apparent after 18 reflections. For example, if the reflectivity of the metal solution were 0.90, a beam of initial intensity *I*₀ would possess an intensity of 0.135-*I*₀ after 18 reflections, a decrease which is of the correct order of magnitude to account for the results obtained.

Because of the nature of the method, the vibrational modes of the molecules near the surface predominate over those of the molecules in the bulk of the sample in an internal reflection spectrum. In the case of the bronze solutions, a simple calculation illustrates that the reflected radiation penetrates to a lesser depth than occurs with weakly absorbing materials (eq 3). If metallic reflection occurs as suggested, the depth of

penetration, *x*_{1/2}, which is consistent with that calculated from eq 3, can be calculated from eq 4. The

$$I/I_0 = E^2/E_0^2 = \frac{(1/2E_0)^2}{E_0^2} = \exp(-\alpha x_{1/2}) \quad (4)$$

$$\alpha = \frac{4\pi n_2 k_2}{\lambda} \quad (5)$$

absorption coefficient, α, is given by eq 5,¹³ where *n*₂ and *k*₂ are the refractive index and the absorption index, respectively, of the sample and λ is the wavelength (measured in a vacuum) of the reflected radiation. Assuming that the optical constants of the bronze solution are similar to those of mercury,¹⁴ the depth of penetration would be an order of magnitude smaller than those expected for weakly absorbing substances calculated from eq 3. Using values for the density of ammonia and bronze sodium-ammonia solutions¹⁵ as a basis for calculation, the electromagnetic field would interact with approximately five or six molecular layers in the bronze solution compared with nearly 75 for pure ammonia. Even though the bands in the spectrum of the bronze solutions are due to molecules very near the surface, it is unlikely that ammonia molecules other than those adsorbed on the prism are in an environment drastically different from ammonia molecules in the bulk solution.

Other than the facts that the band attributed to the solvated electron is absent from the bronze solutions and the relative intensities of the bands in the spectra of the bronze solutions are less than those of the blue solutions, the internal reflection spectra of all solutions show one common characteristic; that is, the vibrational spectrum of the solvent appears to be essentially

(13) M. Born and E. Wolf, "Principles of Optics," 2nd ed, Pergamon Press, New York, N. Y., 1959.

(14) D. E. Gray, Ed., "American Institute of Physics Handbook," 2nd ed, McGraw-Hill Book Co. Inc., New York, N. Y., 1963.

(15) C. A. Kraus, E. S. Carney, and W. C. Johnson, *J. Am. Chem. Soc.*, **49**, 2206 (1927).

unchanged from that of pure ammonia. These results suggest that either the solvent structure is basically unperturbed by the dissolution of alkali metals, or that, if it is perturbed, the vibrational modes are relatively insensitive to the presence of charged species. Experi-

ments designed to investigate the validity of the latter suggestion are in progress.

Acknowledgment. We wish to thank the Robert A. Welch Foundation and the National Science Foundation for supporting this investigation.

The Proton Magnetic Resonance Spectra of Diethyl Vinylphosphonate and Substituted Vinylphosphonates

by M. P. Williamson, S. Castellano, and C. E. Griffin

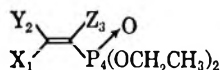
Department of Chemistry, University of Pittsburgh and Mellon Institute, Pittsburgh, Pennsylvania 15213
(Received June 20, 1967)

The proton magnetic resonance spectrum of diethyl vinylphosphonate is reported. This spectrum is of particular interest since it is an example of an ABCX type whose analysis is made possible only by virtue of the coupling of the protons to the heteronucleus. The spectra of all three isomeric diethyl chlorovinylphosphonates are also reported.

Although the nmr spectra of vinyl compounds have been of interest for a number of years,¹⁻⁴ it is only recently that the spectra of compounds containing a vinyl group attached directly to phosphorus have been examined. When this work was initiated, the only such reported analysis was that of trivinylphosphine.⁵ More recently, Maddox⁶ has examined the spectra of a number of vinylphosphines, vinylphosphine oxides, and vinylphosphine sulfides. It has been suggested that the stereochemistry of α - and β -substituted vinylphosphonic acids⁷ and esters^{8,9} can be established on the basis of the geometric dependencies of the ^1H - ^1H and ^1H - ^{31}P coupling constants. In view of the increasing interest in the effects of stereochemistry on nmr parameters in organophosphorus compounds,^{7,9,10} we wish to report here the nmr spectrum of diethyl vinylphosphonate (1). Analysis of the spectrum of 1 should yield *cis*-, *trans*-,

Experimental Section

The preparation of the samples used in this work has been described elsewhere;^{9,11} all samples were shown to be pure by glpc. After being degassed on a vacuum line, 2% tetramethylsilane (TMS) was added and the 5-mm sample tubes were sealed. The spectra were recorded on a Varian Associates A-60 spectrometer; 50-Hz sweep-width spectra were used for each region. Two spectra were recorded for each sweep direction of the magnetic field. The spectra were calibrated using



- 1, X = Y = Z = H
- 2, X = Y = H, Z = Cl
- 3, Y = Z = H, X = Cl
- 4, X = Z = H, Y = Cl

and *gem*- J_{PH} values and provide confirmation of the assignments of stereochemistry in substituted vinylphosphonates.⁷⁻⁹

- (1) C. N. Banwell and N. Sheppard, *Mol. Phys.*, **3**, 351 (1960).
- (2) W. Brügel, T. Ankel, and F. Krückeberg, *Z. Elektrochem.*, **64**, 1121 (1960).
- (3) T. Schaefer, *Can. J. Chem.*, **40**, 1 (1962).
- (4) A. A. Bothner-By in "Advances in Magnetic Resonance," Vol. I, J. S. Waugh, Ed., Academic Press, Inc., New York, N. Y., 1965, pp 195-316.
- (5) W. A. Anderson, R. Freeman, and C. A. Reilly, *J. Chem. Phys.*, **39**, 1518 (1963).
- (6) M. L. Maddox, Ph.D., Thesis, University of California, Los Angeles, Calif., 1965.
- (7) G. L. Kenyon and F. H. Westheimer, *J. Am. Chem. Soc.*, **88**, 3557 (1966).
- (8) D. C. Wysocki, Ph.D. Thesis, University of Pittsburgh, Pittsburgh, Pa., 1967.
- (9) W. M. Daniewski, M. Gordon, and C. E. Griffin, *J. Org. Chem.*, **31**, 2083 (1966).
- (10) D. J. Martin, M. Gordon, and C. E. Griffin, *Tetrahedron*, **23**, 1831 (1967).
- (11) W. M. Daniewski and C. E. Griffin, *J. Org. Chem.*, **31**, 3236 (1966).

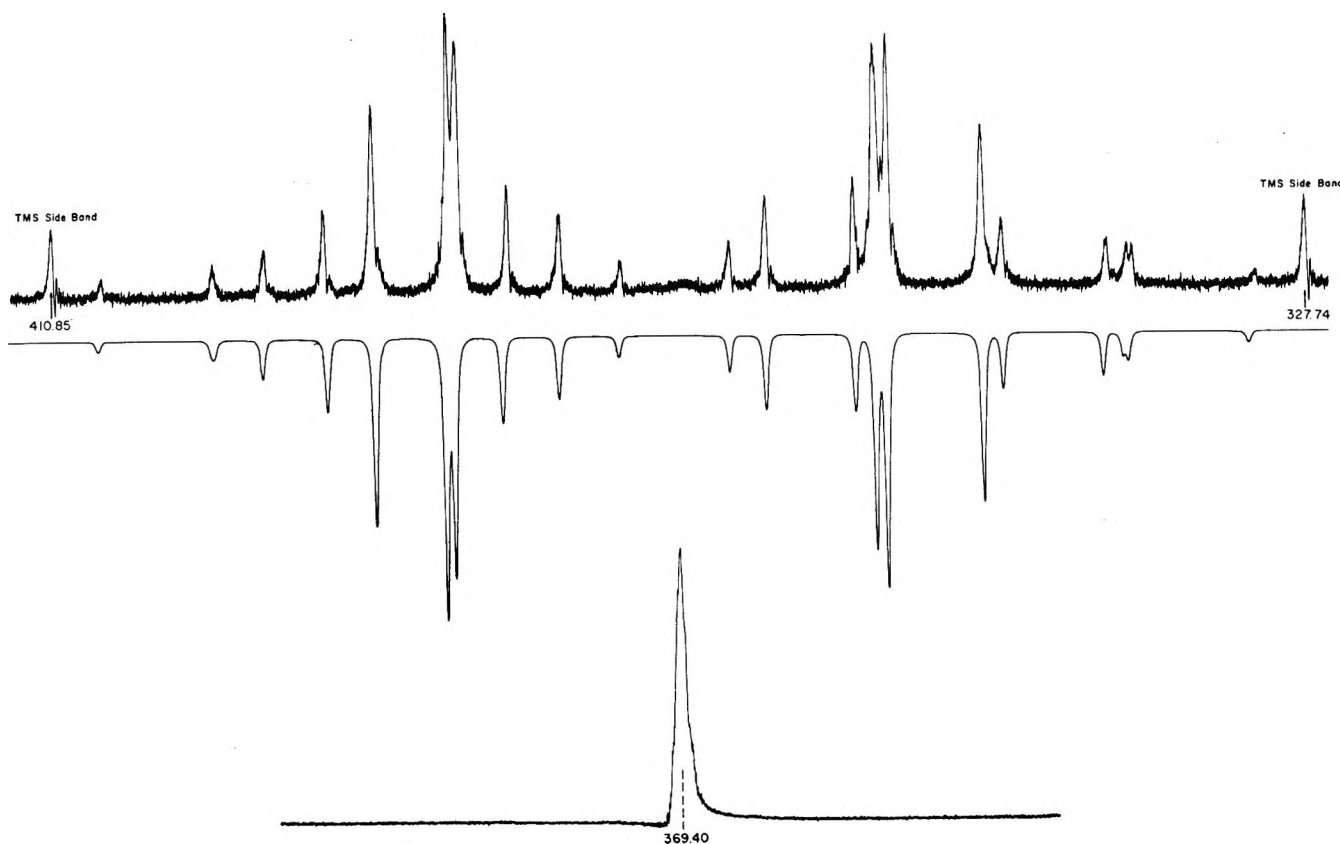


Figure 1. Upper: observed and calculated 60-MHz ^1H spectrum of diethyl vinylphosphonate (as a neat liquid); and lower: ^{31}P decoupled ^1H spectrum of diethyl vinylphosphonate. Frequencies are given in Hz from internal TMS.

the side-band technique with the aid of either a General Radio Type 1161-A frequency synthesizer or a Hewlett-Packard Model 241-A pushbutton oscillator monitored by an Anadex Model CF-200R counter-timer. Experimental line frequencies used in the analysis of the spectra were the averages of four measurements. The double-resonance experiment was performed with an nmr Specialities SD-60B Heteronuclear spin decoupler with an irradiation frequency of 24.3 MHz. Computations were performed on the IBM 7040 computer of the Carnegie Institute of Technology, Pittsburgh, Pa.

Results and Discussion

The nmr spectra of vinylphosphorus compounds are of the type ABCX,¹² provided that any long-range coupling between the vinyl group and other protons, *e.g.* ester protons in **1**, in the molecule is small. This was the case with trivinylphosphine⁶ and there is no evidence for any such coupling in **1**.

The proton spectrum of **1** is formed by the superposition of two ABC spectra, corresponding to the two spin orientations (α and β) of the ^{31}P nucleus in the magnetic field. Complete analysis of both subspectra gives all the parameters of interest. The proton-phosphorus coupling constants, because of the X approximation, enter the Hamiltonian only through the

diagonal terms giving rise to the *effective* proton chemical shifts

$$\omega_{\text{eff}}(i) = \omega(i) \pm \frac{1}{2}J(\text{ip}) \dots (i)$$

for each of the two subspectra. Because of i , the two subspectra will form a symmetrical pattern in the limit in which all the proton chemical shifts $\omega(i)$ become equal. As can be seen from the upper part of Figure 1, this is very nearly the case for the 60-MHz spectrum of **1** as a neat liquid.

The assignment of the lines of the two subspectra was carried out by a procedure previously reported¹³ and the final fit was then made on an IBM 7040 computer, which used the iterative program LAOCN3.¹⁴

It is interesting that without the coupling to the phosphorus atom, it would not be possible to carry out the spectral analysis of **1**. The near identity of the chemical shifts of the three vinyl protons of **1** was demonstrated by ^{31}P decoupling, which causes collapse of the spectrum to a broadened singlet (Figure 1).

Our analysis shows that the signs of all the coupling constants in **1** are the same. Anderson, Freeman, and

(12) C. N. Banwell and N. Sheppard, *Proc. Roy. Soc., (London)*, **A263**, 136 (1961).

(13) S. Castellano and J. S. Waugh, *J. Chem. Phys.*, **34**, 295 (1961).

(14) A. A. Bothner-By and S. Castellano, LAOCN3, Mellon Institute, Pittsburgh, Pa., 1966.

Table I: Nmr Spectral Parameters of Vinylphosphonates^a

Compound	Concn., ^b %	$\omega(1)$	$\omega(2)$	$\omega(3)$	$J(1,2)$	$J(1,3)$	$J(1,4)$	$J(2,3)$	$J(2,4)$	$J(3,4)$
$\begin{array}{c} \text{H} & \text{H} \\ & \backslash / \\ & \text{C} \\ & / \backslash \\ \text{H} & \text{P}(\text{O})(\text{OC}_2\text{H}_5)_2 \end{array}$ 1	Neat	370.519	368.615	369.050	2.341	18.734	24.945	12.688	50.363	21.950
	liquid	± 0.023	± 0.015	± 0.030	± 0.018	± 0.067	± 0.119	± 0.058	± 0.049	± 0.159
	10	371.368	361.582	358.136	2.392	18.745	24.825	12.725	50.175	20.587
		± 0.031	± 0.022	± 0.028	± 0.025	± 0.024	± 0.057	± 0.026	± 0.047	± 0.051
$\begin{array}{c} \text{H} & \text{Cl} \\ & \backslash / \\ & \text{C} \\ & / \backslash \\ \text{H} & \text{P}(\text{O})(\text{OC}_2\text{H}_5)_2 \end{array}$ 2	10	382.358	365.482		1.119		13.361		35.563	
		± 0.006	± 0.006		± 0.008		± 0.011		± 0.011	
$\begin{array}{c} \text{H} & \text{Cl} \\ & \backslash / \\ & \text{C} \\ & / \backslash \\ \text{Cl} & \text{P}(\text{O})(\text{OC}_2\text{H}_5)_2 \end{array}$ 3	50	382.945	369.517		1.458		13.259		35.664	
		± 0.020	± 0.020		± 0.026		± 0.040		± 0.040	
$\begin{array}{c} \text{H} & \text{H} \\ & \backslash / \\ & \text{C} \\ & / \backslash \\ \text{Cl} & \text{P}(\text{O})(\text{OC}_2\text{H}_5)_2 \end{array}$ 4	10		413.999	363.028				9.138	40.094	10.217
			± 0.025	± 0.025				± 0.035	± 0.050	± 0.050
	10	424.243		362.819		14.439	13.613			11.612
		± 0.016		± 0.016		± 0.021	± 0.031			± 0.031

^a All data in Hz; $\omega_0 = 60$ MHz; chemical shifts are referred to TMS as internal standard. ^b Concentrations (*v/v*) refer to solution in CCl_4 .

Reilly⁵ have shown that all the coupling constants in trivinylphosphine are positive. If the proton-phosphorus coupling constants in **1** are taken as being positive then they fit in very well with the electronegativity correlations of Banwell, Sheppard and Turner,¹⁵ and of Schaefer;³ it is therefore assumed that all the coupling constants in **1** are positive. The figures reported here for the proton-proton coupling constants in **1** agree well with those reported for trivinylphosphine,⁵ although the phosphorus-proton coupling constants in **1** are all much larger than those in trivinylphosphine. This observation is in accord with the well-known increase in the magnitude of J_{PH} for tetravalent organophosphorus compounds relative to the trivalent analogs.^{16,17} The figures obtained for *cis*- J_{PH} and *trans*- J_{PH} here are of the same magnitude as the corresponding coupling constants obtained by Maddox,⁶ Westheimer,⁷ and Wysocki.⁸ The ratio of J_{cis} to J_{trans} is of the same order as the corresponding J_{HH} ratio in vinyl compounds. It therefore appears that the assignment of stereochemistry of substituted vinylphosphonates by nmr methods possesses no inherent ambiguities or difficulties.

The nmr spectra of diethyl α -chlorovinylphosphonate (**2**) and diethyl *cis*- (**3**) and *trans*- β -chlorovinylphosphonates (**4**) have been reported⁹ but the data given were the results of first-order interpretations. We wish to report here some much more accurate data for these compounds. (See Table I.)

The spectra of the substituted vinylphosphonates (**2-4**) were analyzed as the type ABX.¹⁸ In this case, the analysis gives two sets of parameters corresponding to whether the two AB quartets arise, as in Figure 2

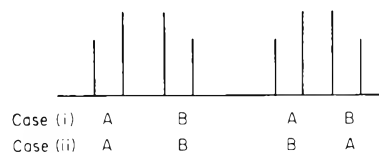


Figure 2. The AB part of the general ABX spectrum.

case i or case ii.¹⁹ One of these two sets obtained from the ABX analysis of the β -chlorovinylphosphonates (**3**, **4**) could be discarded as being implausible. However, with α -chlorovinylphosphonate (**2**) both sets were plausible and it was necessary to change the concentration in order to change the relative chemical shifts, and to carry out a second analysis.

The geminal phosphorus-proton coupling constant [$J(3,4)$] in **1** is seen to be solvent dependent, changing from 21.95 to 20.59 Hz on going from the neat liquid to a 10% (*v/v*) solution in CCl_4 . A similar medium effect has been noted for geminal ^{31}P - ^1H couplings in benzylphosphonium salts²⁰ and diethyl *cis*- β -styrylphosphonate.⁸ The geminal proton-proton coupling constant [$J(1,2)$], however, changes only slightly on making the

(15) C. N. Banwell, N. Sheppard, and J. J. Turner, *Spectrochim. Acta*, **16**, 794 (1960).

(16) C. E. Griffin, *Tetrahedron*, **20**, 2399 (1964).

(17) J. B. Hendrickson, M. L. Maddox, J. J. Sims, and H. D. Kaesz, *ibid.*, **20**, 449 (1964).

(18) J. A. Pople, W. G. Schneider, and H. J. Bernstein, "High Resolution Nuclear Magnetic Resonance," McGraw-Hill Book Co., Inc., New York, N. Y., 1959, p 132.

(19) R. J. Abraham, personal communication.

(20) M. Gordon and C. E. Griffin, *J. Chem. Phys.*, **41**, 2570 (1964).

same solvent changes. On the other hand, this same geminal coupling constant in diethyl α -chlorovinylphosphonate (**2**) is seen to change appreciably on going from 10 to 50% (*v/v*) solution in CCl_4 .

Since the completion of this work and during the preparation of this paper, the analysis of the spectrum of **1** by the use of double-quantum spectra has been reported.²¹ The results obtained by Lancaster are in substantial agreement with those reported here.

Acknowledgment. We are indebted to Dr. W. M. Daniewski for providing samples of the compounds used in this study. This work was performed using, in part, the nmr Facility for Biomedical Studies supported by a grant (FR 00292) from the National Institutes of Health.

(21) J. E. Lancaster, *Spectrochim. Acta*, **23A**, 1449 (1967).

Density and Heat of Fusion of Folded-Chain Polyethylene Crystals

by Fumiyuki Hamada, Bernhard Wunderlich,

Department of Chemistry, Rensselaer Polytechnic Institute, Troy, New York

Takuji Sumida, Seiichi Hayashi, and Akio Nakajima

Department of Polymer Chemistry, Kyoto University, Kyoto, Japan (Received June 22, 1967)

The flotation method of density determination for solution-grown crystals of polyethylene is shown to be a reliable method if sufficient care is taken in preparing the crystals for density measurement. With varying crystallization temperature and molecular weight, the measured density varied between 0.983 and 0.997 g cm^{-3} . The density is shown to vary with surface structure as well as lamellar thickness. The heat of fusion of solution-grown crystals is proportional to specific volume as long as the fold length stays constant. Different fold length crystals show different specific volume-heat of fusion relationships.

Introduction

The measurements of density and heat of fusion have been the simplest and most convenient methods for characterizing the crystallinity in melt-crystallized polymers. Folded-chain crystals grown from solution, in contrast, have proven to yield conflicting data when standard methods of density determination were used. Many different values have been reported in the literature. One group of authors¹⁻⁴ found densities in the region of 0.97 g cm^{-3} by a flotation method. These values are considerably lower than the ideal crystallographic subcell density of 1.00 g cm^{-3} and require an "amorphous content" of about 20%. On the other hand, Kawai and Keller^{5,6} obtained a value close to the ideal crystallographic density using the pycnometer method. Martin and Passaglia⁷ finally determined the density of polyethylene single crystals grown from solution, also using the pycnometer method, and obtained a density value of about 0.98 g cm^{-3} . In addition, Kawai and co-workers⁸ recently determined the density of solution-grown polyethylene single crystals, crystallized at various conditions, using the pycnom-

eter method and obtained densities between 0.99 and 1.00 g cm^{-3} , which are still higher than the values of the other authors. Table I shows a summary of measured values of density of solution-grown polyethylene single crystals. The present work was undertaken to find out more about the density of solution-grown polyethylene crystals and to reestablish density determinations as a valuable tool in structure determination. In addition, heats of fusion and melting characteristics were measured to elucidate questions of crystal perfection.

(1) B. Wunderlich and W. H. Kashdan, *J. Polymer Sci.*, **50**, 71 (1961).

(2) E. W. Fischer and G. F. Schmidt, *Angew. Chem.*, **74**, 551 (1962).

(3) E. W. Fischer and R. Lorenz, *Kolloid-Z.*, **189**, 97 (1963).

(4) J. B. Jackson, P. J. Flory, and R. Chiang, *Trans. Faraday Soc.*, **59**, 1906 (1963).

(5) T. Kawai and A. Keller, *Phil. Mag.*, **8**, 1203 (1963).

(6) T. Kawai and A. Keller, *ibid.*, **8**, 1973 (1963).

(7) G. M. Martin and E. Passaglia, *J. Res. Natl. Bur. Std.*, **70A**, 221 (1966).

(8) T. Hama, T. Goto, T. Kawai, and H. Maeda, presented at IUPAC Meeting, Tokyo, Kyoto, Japan, 1966.

Table I: Density of Polyethylene Single Crystals from Solution

Method	Author	Density
Suspension		
Centrifuge flotation	Fischer (1963)	0.96 ~ 0.97
	Flory (1963)	0.970 ~ 0.97
Flotation	Wunderlich (1961)	0.965
Dry mat		
Density gradient tube	Fischer (1963, 1966)	0.96 ~ 0.97
		0.96 ~ 0.98
Flotation	Wunderlich (1961)	0.965
Pycnometer method		
	Fischer (1963)	0.96 ~ 0.97
	Kawai, Keller (1963)	1.00
	Martin, Passaglia (1966)	0.98
	Kawai, <i>et al.</i> (1966)	0.99 ~ 1.00

Experimental Section

A. Materials. Molecular weight fractions of linear polyethylene were prepared by column fractionation⁹ (Sholex-6009, polyethylene manufactured by Japan Olefin Chem. Co., similar to Marlex-50). The viscosity average molecular weight of these fractions ranged from 8400 to 280,000. Other samples were linear polyethylene of the Marlex-50 type with an approximate viscosity average molecular weight of 60,000, polymethylene with an estimated molecular weight of 10^7 , and $n\text{-C}_{36}\text{H}_{74}$ paraffin. The paraffin was obtained from Humphrey Wilkinson Co. and was made by coupling of pure alkyl halides.

B. Crystallization. Two methods were used for the crystallization of polyethylene from solution. In one method, polyethylene was dissolved in *p*-xylene under nitrogen; the hot solution was then transferred to the crystallization vessel, which was kept at the chosen temperature and contained outgassed *p*-xylene. The final solution had a concentration of 0.1% polymer by weight. The solution was kept for 48 hr under nitrogen at the given temperature for crystallization. The resulting crystal aggregates were collected at the same temperature on a glass filter. To align the crystal lamellae as much as possible, the filtering was slowed down to take about 5 hr for 200 cm³ of suspension. The crystal mat obtained was removed from the glass filter and then dried under vacuum at 60°. The dried mat was used for density measurement in a density gradient column, for determination of heat of fusion in a scanning calorimeter, and for the determination of lamellar thickness by small angle X-ray diffraction.

The other method of crystallization was used for sample preparation for the density measurement of single crystal aggregates in suspension. The solution of polyethylene in *p*-xylene was, in this case, prepared under nitrogen, and the hot solution was then

cooled to the given crystallization temperature. After this solution was kept for 7 days at the crystallization temperature, the crystal aggregates were removed for density determination in suspension.

C. Density Measurements. Different methods were used for the density measurement of polyethylene crystals differently collected. A density gradient column was used for the density measurement of the dry mats. A modified flotation method was used for the density measurement of crystal aggregates in suspension. All measurements were carried out at 23°.

(a) Density Gradient Column Method. The liquid for the density gradient column was a mixture of monochlorobenzene and toluene. The pieces of the dry mat and a mixed liquid having a density close to that of the crystals were evacuated for 5–10 hr in a suitably shaped glass tube. The pieces of the dry mat were then immersed in the liquid mixture under vacuum. After further pumping for 3–4 hr to minimize the air bubble from the dry mat, the wet crystal mat pieces were transferred to the density gradient column. The density values obtained from any one sample showed only little variation in density (from $\pm 0.0001 \text{ g cm}^{-3}$ to $\pm 0.003 \text{ g cm}^{-3}$ for different samples).

(b) Flotation Method. A mixture of monochlorobenzene and toluene with its density close to that of the suspended crystals was prepared in a glass tube. This mixture was evacuated to eliminate all dissolved air. The polymer crystals were then transferred from the crystallization flask, which was still at the crystallization temperature. The crystals were lifted gently with the help of a wire mesh net from the crystallization flask and then immediately immersed into the liquid mixture. Thus, wet crystal aggregates were transferred to a liquid mixture for density measurement with a minimum of disturbance. The liquid mixture with the crystal aggregates was stirred carefully and again set under vacuum to eliminate air bubbles. Monochlorobenzene or toluene was added to the mixture to adjust the density to make the crystal aggregates float. This procedure was repeated for 7–30 days until the densities were matched. The density of the liquid mixture was finally determined by Mohr–Westphal balance. Any crystal aggregates which adhered to the wall of the glass tube were eliminated. When the density of the crystal aggregates and liquid mixture was nearly matched, most of the crystal aggregates floated between the top and the bottom of the liquid mixture. A few crystals, however, always rose to the top, and a few sank to the bottom. This means that the crystals have a distribution of densities and an appropriate average had to be chosen. We tried to determine the width of the distribution of the density of

(9) V. Desreux, *Rec. Trav. Chim.*, **68**, 789 (1949); P. Henry, *J. Polymer Sci.*, **36**, 3 (1959); R. Chiang, *J. Phys. Chem.*, **69**, 1645 (1965).

crystal aggregates in suspension, but failed. The estimated width of the density distribution is 0.01 to 0.02 g cm⁻³. This density distribution is somewhat dependent on the absolute value of the density of the crystal aggregates and is significantly broader than that measured in repeated determinations on the dry mat.

D. Heats of Fusion. The heats of fusion were determined with a Perkin-Elmer differential scanning calorimeter.¹⁰ Sample weights were 3–6 mg, determined to 1% accuracy on a Cahn electrobalance. The scanning rate was 5° min⁻¹. Calibration of the power input into the sample was performed by measurements of the heat of fusion of indium, anthracene, urea, and benzoic acid. The literature values of the heat of fusion of these substances are, respectively, 6.80, 38.7, 57.8, and 35.2 cal g⁻¹.^{11,12} The calibrations were repeated sufficiently often to allow an estimate of the precision. The standard deviation of a single measurement of all calibrations was $\pm 1\%$. The average value of the conversion factor of area measured to heat was 13.64 mcal cm⁻². Areas of the power-time recordings were evaluated by planimetry. The sensitivity chosen was 4X (about 4 mcal min⁻¹). The reproducibility of heats of fusion obtained was found to be better than 2%, in most cases. Difficulties in drawing the base line existed because of considerable reorganization during heating, causing a broad melting peak. These difficulties were minimized by determination of the start of melting on large amounts of substance and drawing the base line in accordance with the thus predetermined melting range. The typical melting range, as determined in this way by the first deviation from pure specific heat recording, stretched from 100 to 135°. All actual areas measured varied between 13 cm² and 23 cm². No correction^{13,14} based on the surface enthalpy of lamella of the crystals is included in the values reported.

Results

A. Paraffins. To have a check on the methods of density measurement, we determined, first, the density of single crystal aggregates of *n*-C₃₆H₇₄. The crystals were grown from methyl acetate solution at 43.3° within 2 days. The single crystals, as observed by interference microscopy, were diamond-shaped crystals with an average lateral size of 50 μ . Between 100 and 1000 layers made up the thickness of each crystal. First, the density was measured in a gradient column made of a mixture of ethyl alcohol and water. The single-crystal aggregates were transferred directly to the density gradient column using a wire-mesh net. In this way, the crystals never dried out. The obtained value of density was 0.950 g cm⁻³, a value lower than the crystallographic density. Next, the density was measured by the flotation method, as described above, starting with a mixture of ethyl alcohol and water of

density 0.950 g cm⁻³. Most of the paraffin single-crystal aggregates showed a density of 0.960 g cm⁻³, but a few aggregates showed a density of 0.965 g cm⁻³. The density 0.960 g cm⁻³ corresponds to the known crystallographic density of the orthorhombic form,¹⁵ and the density 0.965 corresponds to the crystallographic density of the monoclinic form.¹⁶ The weight of the crystals of density 0.965 g cm⁻³ was too small for X-ray diffraction analysis. Over-all the distribution of density was narrow (± 0.002 g cm⁻³) and the agreement of the calculated data from X-ray diffraction with the density measured by the flotation method was good. In contrast, the values obtained by the density gradient method were significantly less than the crystallographic density. This lower density might be due to remaining air bubbles on the surface of the single-crystal aggregates and/or to the trapped solvent between the lamellae of the crystals. Also, the density of single-crystal mats was determined by the density gradient column method. The result was 0.942 g cm⁻³, even lower than the density of the single crystals in suspension in the density gradient column. This added density defect is probably caused by the voids in single-crystal mats produced during the filtering operation.

These preliminary experiments show that the density measurement of single-crystal aggregates in suspension by the flotation method can give correct answers for small lamellar crystals, while the density gradient column seems to yield too low values.

B. Polyethylene. Table II shows the density and long period of polyethylene crystals grown from solution at various crystallization temperatures and solvents. In Figure 1, the filled circles mark the average densities of polyethylene crystal aggregates grown from *p*-xylene solution at different crystallization temperatures for a molecular weight fraction of 42,000. The open circles represent the density of dry mats of identically crystallized polyethylene measured in a density gradient column. Both sets of data show that the density increases with increasing crystallization temperature. The density values of single crystal aggregates measured in suspension are, however, significantly higher than the density values obtained from the filtered dry mats. The difference is bigger at the lower crystallization temperatures. Figure 2 shows plots of the density of polyethylene single-crystal aggregates crys-

(10) M. O'Neill, *Anal. Chem.*, **36**, 1238 (1964); E. S. Watson, M. J. O'Neill, J. Justin, and N. Brenner, *ibid.*, **36**, 1233 (1964).

(11) Landolt-Bornstein, "Zahlenwerte und Funktionen," Vol. II, 6th ed, Springer-Verlag, Berlin, 1961.

(12) For the values chosen for indium and benzoic acid see also W. Oelson, O. Oelson, and U. D. Thiel, *Z. Metallk.*, **46**, 555 (1955); G. T. Furukawa, R. E. McCoskey, and G. J. King, *J. Res. Natl. Bur. Std.*, **47**, 256 (1951).

(13) E. W. Fischer and G. Hinrichsen, *Polymer*, **7**, 195 (1966).

(14) E. W. Fischer and G. Hinrichsen, *Kolloid-Z.*, **213**, 93 (1966).

(15) V. Vand, *Acta Cryst.*, **6**, 797 (1953).

(16) H. M. M. Shearer and V. Vand, *ibid.*, **9**, 379 (1956).

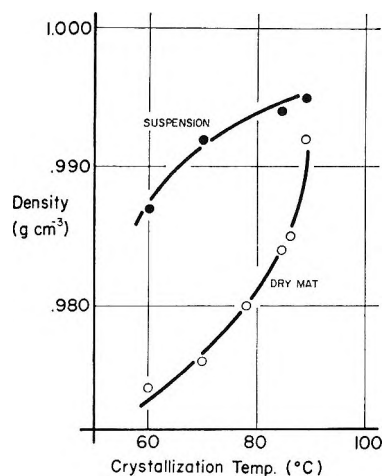


Figure 1. The effect of crystallization temperature on the density of polyethylene crystals of the same molecular weight (42,000) grown from *p*-xylene at various temperatures: filled circles represent measurements of crystal suspension by the flotation method, and open circles are the same crystals measured in the density gradient column after filtration to a dry mat.

Table II: Density of Polyethylene Crystals^a from Solution (g cm⁻³ at 23°)

Solvent used	<i>T</i> _c , °C	<i>l</i> , Å	Density gradient tube (dry mat)	Flotation method (suspension)
<i>p</i> -Xylene	89.1	151.7	0.993	0.995
	86.0	140.1	0.985	...
	84.5	...	0.984	0.994
	78.1	117.6	0.980	...
	70.0	...	0.976	0.992
	60.0	...	0.974	0.987
Decalin	83.9	121	0.981	0.997
	75.4	83.9	0.976	...
<i>n</i> -Hexadecane	106.5	181	0.990	0.992
	95.9	143	0.985	...

^a Molecular weight fraction 42,000.

tallized from *p*-xylene at 84.5° as a function of molecular weight. Filled circles again show the density of crystals in suspension and open circles show the density of dry mats. The density decreases with increasing molecular weight. Also shown in Figure 2 are a filled triangle and an open triangle which, respectively, show the density of crystal aggregates in suspension and dry mats of unfractionated Marlex 50. The filled square and the open square show the density of single-crystal aggregates in suspension and dry mats of polymethylene, respectively.

To solve the question whether high-density crystals also have a high enthalpy of fusion, the heat of fusion of solution-grown polyethylene and *n*-C₃₆H₇₄ single crystals was measured with the differential scanning

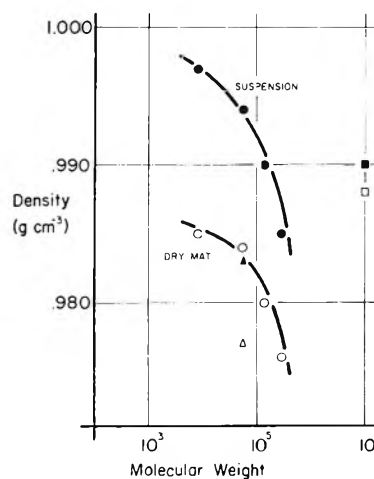


Figure 2. The effect of molecular weight on the density of polyethylene crystals grown from *p*-xylene at 84.5°; meaning of circles as in Figure 1, triangles represent unfractionated Marlex 50, and squares represent polymethylene.

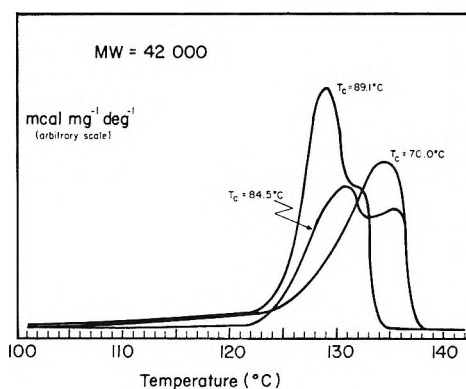


Figure 3. Melting curves for polyethylene crystals grown at 70, 84.5, and 89.1° of the same molecular weight (42,000) (heating rate, 5° min⁻¹, normalized to equal weights, not corrected for instrument lag).

calorimeter. In Figure 3 and Figure 4, some of the observed melting curves are shown. Figure 5 presents the measured heats of fusion of solution-grown polyethylene crystals, *n*-C₁₉H₄₀, *n*-C₂₅H₅₀, and *n*-C₃₆H₇₄ paraffin crystals as well as the calculated heat of fusion of *n*-C₁₀₀H₂₀₂ crystals as a function of the specific volume at 23°. Curves 1 and 2 are the results on polyethylene crystals obtained by us, curve 4 shows the heats of fusion of the paraffins, and curve 3 reproduces uncorrected data of the heat of fusion of solution grown polyethylene crystals by Fischer,^{13,14} and Hendus and Illers.¹⁷ The heats of fusion of *n*-C₁₉H₄₀ and *n*-C₂₅H₅₂ single crystals were adopted from that of the orthorhombic form reported in the literature.¹⁸⁻²⁰ The heat of

(17) H. Hendus and K. H. Illers, *Kunststoffe*, **57**, 193 (1967).

(18) A. A. Schaefer, C. J. Busso, A. E. Smith, and L. B. Skinner, *J. Am. Chem. Soc.*, **77**, 2017 (1955).

(19) F. W. Billmeyer, Jr., *J. Appl. Phys.*, **28**, 1114 (1957).

(20) M. G. Broadhurst, *J. Res. Natl. Bur. Std.*, **66A**, 241 (1963).

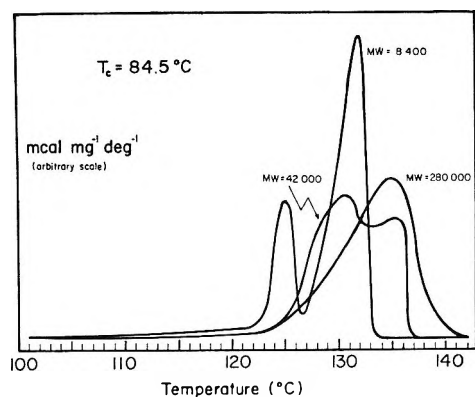


Figure 4 Melting curves for polyethylene crystals of MW 8,400, 42,000, and 280,000 crystallized at 84.5° (heating rate, 5° min⁻¹, normalized to equal weights, not corrected for instrument lag).

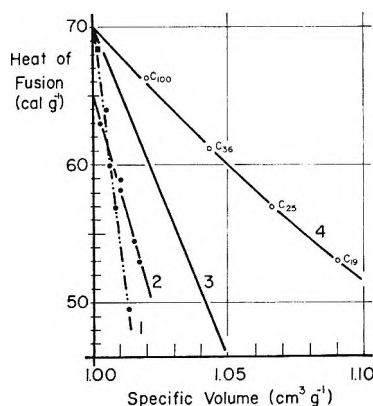


Figure 5. Plot of the measured values of the heat of fusion of polyethylene crystals grown from solution and *n*-paraffins as a function of the specific volume at 23°: curve 1, polyethylene crystals of same molecular weight (42,000) grown from *p*-xylene at various temperatures; from bottom to top: 60, 70, 84.5, and 89.1°; curve 2, polyethylene crystals of various molecular weight grown from *p*-xylene at 84.5°; from bottom to top, molecular weight: 60,000 (broad distribution), 280,000, 10⁷ polymethylene, 140,000, 42,000 and 8,400; curve 3, data on polyethylene crystal grown from solution obtained by Fischer^{13,14} and Hendus and Illers;¹⁷ curve 4, *n*-paraffin crystals of orthorhombic form.

fusion of *n*-C₁₀₀H₂₀₂ was calculated using the equation given by Flory,²¹ modified to fit the extrapolated value ($\Delta H = 980 \text{ cal mole}^{-1}$)^{13,14,17} of heat of fusion to specific volume 1.000 cm³ g⁻¹

$$\Delta H_n = 980 - \Delta C_p \Delta T - (2150/n)$$

ΔH_n is the enthalpy of fusion per CH₂ group of the paraffin of chain length *n*, ΔT is the difference between the equilibrium melting temperature of an extended chain polymer crystal of infinite molecular weight (about 142°)²² and the melting point of the *n*-paraffin homolog of chain length *n*, and ΔC_p is the difference between the heat capacity of extended chain crystals of

polyethylene²³ and the heat capacity of amorphous polyethylene.²⁴ The densities of *n*-C₁₉H₄₀, *n*-C₂₅H₅₂, and *n*-C₁₀₀H₂₀₂ were calculated from crystallographic data of the orthorhombic unit cell in the literature,²⁰ and for the density of *n*-C₃₆H₇₄, the measured density for the orthorhombic unit cell was used. The open square shows the heat of fusion of unfractionated Marlex 50 crystallized under high pressure.²⁵ The extrapolation of plot 2 to a specific volume of 1.000, which is the ideal crystallographic subcell specific volume of polyethylene, yields a heat of fusion of about 65 cal g⁻¹, while the extrapolations of curves 1, 3, and 4 to a specific volume of 1.000 cm³ g⁻¹ yield about 70 cal g⁻¹.

Discussion

A. Flotation Densities. First, we shall discuss the reliability of the flotation method as a method of density measurement of small crystal aggregates in suspension. In one set of measurements, we compared the density obtained by the flotation method directly with that obtained by the density gradient column method on the identical crystals. When the densities of the crystal aggregates and the flotation liquid were nearly matched and the aggregates floated between the top and the bottom of the liquid mixture, some of the floating crystal aggregates were carefully transferred to a density gradient column of the same liquid pair using a pipet. The density obtained in the density gradient column was often the same as in the flotation method, but occasionally somewhat lower than that obtained by the flotation method. We ascribe this inconsistency in results to the degree of care taken in transfer of the crystal. It is extremely difficult to accomplish the transfer without picking up air. In the case of dry mats, we obtained always nearly the same density by both methods. The transfer in this case is much easier because of the more compact nature of the crystals. Although the density gradient column method is subject to some error, due to the interfacial free-energy gradient present in the column,⁶ we have shown here that this error is negligible for the toluene-monochlorobenzene liquid pair. A similar conclusion was reached by Fischer for the propyl alcohol-dioxane liquid pair.^{13,14} It is noteworthy, however, that unless sufficient care is taken in preparing the sample, the density gradient method may give considerably lower density values in the case of solution-grown polyethylene crystal aggregates in suspension. In the case of poor preparation of sample for density

(21) P. J. Flory and A. Vrij, *J. Am. Chem. Soc.*, **85**, 3548 (1963).

(22) T. Arakawa, Ph.D. Thesis, Cornell University, Ithaca, N. Y., 1964.

(23) B. Wunderlich, *J. Phys. Chem.*, **69**, 2078 (1965).

(24) B. Wunderlich, *J. Chem. Phys.*, **37**, 1203 (1962).

(25) B. Wunderlich and C. M. Cormier, *J. Polymer Sci., Part A-2*, **5**, 987 (1967).

measurement, for example, by direct transfer of crystal aggregates without intermediate elimination of air by evacuation, we observed as much as 0.025 g cm^{-3} lower densities for the same materials. This lower density is probably due to air bubbles added to the surface of the single-crystal aggregates and trapped solvent between lamellae of crystals. The trapped solvent caused the density of polyethylene crystals from *p*-xylene to increase gradually, slightly with time until, after 1–2 days, a constant value was approached, while the density of polyethylene crystals from tetrachloroethylene decreased slightly, rapidly with time so that a constant value was approached after about 3 hr.

The difference between the density of crystal aggregates in suspension and that of dry mats, as shown in Figure 1 and Figure 2, is of great importance. This difference seems to be due to the voids in the dry mat. We reached this conclusion because of the following facts: (a) the density of a dry mat which was dried very well shows a slightly lower density than that dried poorly; (b) the difference between density values of crystal aggregates in suspension and as dry mats decreases with increasing crystallization temperature; (c) the collapsed crystal aggregates contain voids visible by microscopy. These voids are initially filled with solvent but cannot be refilled when the solvent was once removed by drying. The dry mats of crystals grown at higher crystallization temperature have less voids because of the more regular structure of the crystals and because of the higher temperature used for filtration. Figure 6 is an interference micrograph of a collapsed polyethylene growth spiral covered on both sides with a vacuum deposit of silver.²⁶ Several areas of irregular collapse can be seen. Similar growth spirals, observed by double beam interferometry with transmitted light, show none of these voids²⁷ since the reference beam is carried through air and thus eliminates any phase difference lack due to voids. It may be possible to improve this method by using the centrifugal force of a centrifuge instead of the weak gravitational force. This should increase the sensitivity to a change in density. Lower density values might still be obtained, however, unless similar care as described above is taken in sample preparation.⁶

Another inevitable problem in density determination of small crystals by flotation method is the selective adsorption of one of the measuring liquids. We checked, therefore, the effect of the selective adsorption on the density of crystals. The results are shown in Table III. The effect is easily measurable, but much smaller than the effect of poor sample preparation. The density is affected only in the third decimal. In the case of *n*-butyl benzoate, which has the density of 1.000 at 26°, only a single liquid was used in the flotation method. The temperature at which the crystals float between the top and the bottom of the single liquid was measured and then the density at 23° was

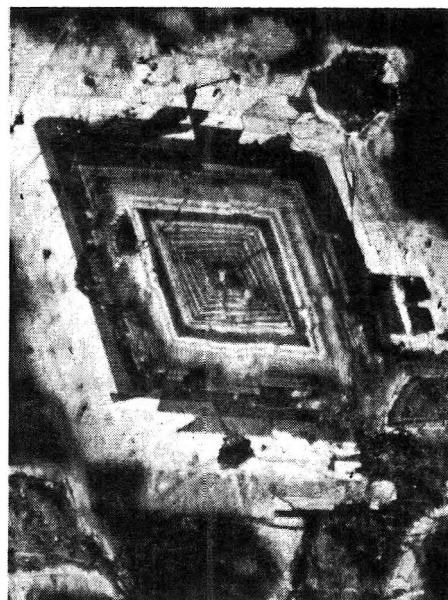


Figure 6. A top and bottom silvered polyethylene growth spiral viewed with transmitted light. The illumination is from an unfiltered mercury lamp. The long side of the photograph corresponds to 0.19 mm. The contrast is caused by interference at the top and bottom silver layer.²⁶

calculated using thermal expansion coefficients. The reproducibility of this method was not as good and the density obtained by this method may have some uncertainty.

Table III: Effects of Selective Adsorption of a Solvent in Determination of Density

Solvents used	Density measured
Carbon tetrachloride + toluene	0.998
Monochlorobenzene + toluene	0.997
Butyl benzoate	0.993
Ethyl alcohol + water	0.990

The last problem to be discussed is the increase in density caused by oxidation during the preparation of polyethylene fractions and during crystallization from solution. According to Hendus and Illers,¹⁷ a small C=O content in polyethylene may significantly affect the density and the heat of fusion of polyethylene crystals. We checked the C=O content of our crystals by determination of infrared absorption at 1720 cm^{-1} . The C=O content found was below 0.1%. The effect of C=O content in our crystals on the density and heat of fusion should therefore be small.

In summary, it has been shown that the flotation method can give reliable data if adsorbed air is elimi-

(26) P. Sullivan and B. Wunderlich, *SPE Trans.*, **4**, 315 (1964).

(27) See, for example, Figure 7 in B. Wunderlich, *J. Polymer Sci.*, **C1**, 41 (1963).

nated by careful sample preparation. Remaining systematic errors are solvent adsorption and possible oxidation. In our case (monochlorobenzene-toluene) both of these factors could give slightly higher densities. We estimate this error to be less than 0.5%.

B. Effect of Crystallization Conditions and Molecular Weight on Density. Figure 1 shows that the density of crystals of polyethylene of molecular weight 42,000 grown from *p*-xylene increases with increasing crystallization temperature. This increase in density may be caused by two effects, the decrease in the amount of (001) surface area in a crystal due to the increase of lamella thickness, and the change in the structure of the (001) surface with increasing crystallization temperature, since the subunit cell density does not vary significantly. The change of morphology of crystals grown from xylene or tetralin at various temperatures can be seen by interference microscopy²⁸ and by electron microscopy.^{4,29} At high crystallization temperature, single crystals are formed, while at low crystallization temperature, dendrites grow. In accord with this change in morphology, the melting curves as determined by the differential scanning calorimeter change, as can be seen from Figure 3. The melting curves of crystals grown from xylene solution at higher temperature show two peaks, while the melting curves of crystals from xylene grown at lower temperature show only the higher temperature peak. The interpretation can be made in conjunction with previous detailed analyses of time-dependent melting in our laboratory.^{30,31} The dendrites grown at lower temperature are less stable thermodynamically, but can recrystallize faster into crystals of larger fold length than the single crystals grown at higher temperature, which are somewhat more stable, but less mobile. The single peak at higher temperature indicates, thus, only the melting of reorganized crystals, and the double peaks show melting of crystals with less reorganization besides a portion which has reorganized more. Figure 2 shows that the density of crystals grown at 84.5° from *p*-xylene decreases with increasing molecular weight. The morphology of crystals grown from xylene also changes somewhat with increasing molecular weight.^{28,29} It is easy to form orthorhombic single crystals from polyethylene fractions of lower molecular weight, while dendrite or complicated crystals are obtained from polyethylene of high molecular weight. The fold length, however, is largely independent of molecular weight,²⁹ so that the low density in crystals of high molecular weight polyethylene must be mainly due to a change in surface structure and a possible presence of tie molecules. The effect of the molecular weight is also shown in the melting curves of polyethylene crystals grown at 84.5° from *p*-xylene in Figure 4. The melting curves of lower molecular weight crystals show two peaks, while the melting curves of crystals of polyethylene of higher molecular weight show only

one peak at the higher temperature. This indicates again that the crystals of high molecular weight of less perfect crystal structure can recrystallize faster into lamellae of larger thickness than those of low molecular weight, which have a more perfect crystal structure.

In summary, the density of crystal aggregates in suspension was found to vary between 0.983 and 0.997 g cm⁻³, according to the conditions of crystallization and the molecular weight of the sample. Most of these values are significantly higher than the values obtained by authors other than Kawai and Keller.^{5,8} Crystals grown from solution at lower temperature show low densities. Crystals of higher molecular weight and unfractionated polyethylene, grown from solution, also show lower density. This result is consistent with the data by Martin and Passaglia,⁷ but is not consistent with the result of Kawai and Keller.^{5,8} It is noteworthy that we found in all cases a few crystals having a density of nearly 1 included in the single crystal aggregates. The densities measured on the dried mats are generally lower and similar to data of Fischer.^{13,14}

C. Heats of Fusion. In Figure 5, we can see the effect of crystallization temperature and molecular weight on the heat of fusion of polyethylene. The points plotted in curve 1 show the heat of fusion of crystals of polyethylene having the same molecular weight, but different lamellar thickness because of various crystallization temperatures. The increase in heat of fusion with increasing crystallization temperature must in this case mainly be due to the decrease of the amount of lamellar (001) surface area due to the increase in fold length. The measured heat of fusion of the almost extended chain polyethylene²⁵ falls nearly on the same curve. The points plotted in curve 2 show the heats of fusion of crystals of polyethylene having various molecular weights but identical lamellar thickness because of identical crystallization temperature. The heats of fusion plotted in curve 2 increase with decreasing molecular weight. This must be due to the formation of more compact crystals with more regular surfaces with decreasing molecular weight. The difference between the extrapolated heat of fusion of curve 1 and 2 to specific volume of 1.000 cm³ g⁻¹ is about 5 cal g⁻¹. This difference is a measure of the decrease in heat of fusion on folding if the folded region of lamellae has a specific volume of 1.000 cm³ g⁻¹. Our heats of fusion agree with the heat of fusion obtained by Fischer^{13,14} and Hendus and Illers¹⁷ on similar solution-grown crystals. The discrepancy between our curves 1 and 2 and curve 3 is due to the discrepancy between

(28) B. Wunderlich, E. A. James, and T. Shu, *J. Polymer Sci.*, **A2**, 2759 (1964).

(29) V. F. Holland and P. H. Lindenmeyer, *ibid.*, **57**, 589 (1962).

(30) B. Wunderlich, P. Sullivan, T. Arakawa, A. B. DiCyan, and J. F. Flood, *ibid.*, **A1**, 3281 (1963).

(31) E. Hellmuth and B. Wunderlich, *J. Appl. Phys.*, **36**, 3039 (1965).

our density data and their density data.^{13,17} Curve 4 shows the heats of fusion of *n*-paraffins. The heat of fusion increases with increasing carbon number and approaches the value for the heat of fusion of extended chain crystals of polyethylene of high molecular weight. The difference of this curve from a similar one shown by Hendus and Illers¹⁷ is due to our use of crystallographic specific volume of paraffins.

In summary, the heat of fusion measurements support the conclusions drawn from the density measurements: Both (001) surface structure and -surface area must be considered as major factors in interpretation of crystals grown from solution. Each series of polyethylene

crystals of constant fold length has a different heat of fusion-specific-volume relation displaced from the curve for melt-crystallized polyethylene to lower heats of fusion.

Acknowledgments. The work performed at Rensselaer was supported by The National Aeronautics and Space Administration. Authors wish to express their appreciation to Mr. J. Mitchel, Jr., and Mr. C. E. Day of duPont de Nemours and Co., for giving the information about the infrared determination of carbonyl content of oxidized polyethylene. The heats of fusion were determined in cooperation with Miss C. M. Cormier and Mr. C. L. Gruner.

The Cobalt-60 γ Radiolysis of Cysteine in Deaerated Aqueous Solutions at pH Values between 5 and 6

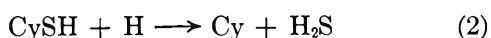
by Verna Gaye Wilkening, Manohar Lal, Meta Arends, and D. A. Armstrong

Department of Chemistry, The University of Calgary, Calgary, Alberta, Canada (Received June 23, 1967)

The major products arising from the Co⁶⁰ γ radiolysis of 10⁻² *M* cysteine (CySH) solutions at pH's in the range 5-6 are: cystine ((CyS)₂), alanine (CyH), H₂S, and hydrogen with yields of 3.4, 2.6, 2.5, and 1.1 molecules/100 ev, respectively. The reactions, which were proposed independently by El Samahy, White, and Trumbore and Armstrong and Wilkening in 1964 are consistent with the results. Nitrate ions and acetone repress the alanine and H₂S yields by identical amounts. This and other observations indicate that: (a) $G_{e_{aq}^-} = 2.5 \pm 0.2$ in 10⁻² *M* cysteine solutions; (b) reaction 4, $e_{aq}^- + \text{CySH} \rightarrow \text{Cy} + \text{SH}^-$, is the only significant reaction of e_{aq}^- with cysteine at pH 5-6; and (c) that all Cy radicals undergo reaction 5, $\text{Cy} + \text{CySH} \rightarrow \text{CyH} + \text{CyS}$. The product of the reaction between e_{aq}^- and nitrate oxidizes two cysteine molecules to cystine with the concomitant formation of nitric oxide. In the pH range employed, reaction 8, $\text{H}_2\text{O}_2 + 2\text{CySH} \rightarrow 2\text{H}_2\text{O} + (\text{CyS})_2$ is relatively slow and as a consequence there is a postirradiation oxidation of cysteine.

Introduction

The radiation chemistry of the sulfhydryl amino acid cysteine is currently a subject of considerable interest. This arises from the importance of cysteine in biological processes¹ and its extreme sensitivity to radiation damage.²⁻⁴ Recent studies⁵⁻⁷ of the γ radiolysis of aqueous solutions of cysteine have provided evidence for the reactions



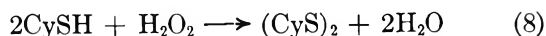
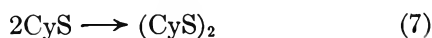
(1) J. T. Edsall and J. Wyman, "Biological Chemistry," Academic Press, Inc., New York, N. Y., 1958.

(2) S. L. Whitcher, M. Rotheram, and N. Todd, *Nucleonics*, **11**, 30 (1953).

(3) P. Markakis and A. L. Tappel, *J. Am. Chem. Soc.*, **82**, 1613 (1960).

(4) J. E. Packer, *J. Chem. Soc.*, 2320 (1963).

(5) A. El Samahy, H. L. White, and C. N. Trumbore, *J. Am. Chem. Soc.*, **86**, 3177 (1964).



In this scheme the following representations are used: Cy, the radical $\cdot\text{CH}_2\text{CH}(\text{NH}_3^+)\text{CO}_2^-$; CyH, alanine; CySH, cysteine; and $(\text{CyS})_2$, cystine. It is quite obvious that a detailed study of all product yields must be performed if the foregoing mechanism is to be substantiated. An earlier paper⁷ from this laboratory reported product yields from 1 *N* HClO₄ solutions. The objective of this investigation was to determine the yields of the major products at pH's in the range 5.0–6.0. Particular attention was given to the identification of the products arising from the reaction sequence 4 and 5. For reasons which will become apparent, the rate of the thermal reaction between 0.9×10^{-4} *M* hydrogen peroxide and 10^{-2} *M* cysteine in air-free solutions was also investigated.

Experimental Section

The thermal reaction between cysteine and hydrogen peroxide in air-free solutions was studied by the following technique. A 1.8×10^{-4} *M* neutral solution of hydrogen peroxide was prepared by the radiolysis of aerated triply distilled water. A measured aliquot of this was then placed in a 10-ml cell, which was attached by a capillary tube to a similar cell containing an equal volume of 2.0×10^{-2} *M* cysteine. The connecting tube was also attached to a standard 1-cm spectrophotometer cell. After deaeration of the two solutions by several cycles of freezing and pumping, the entire system was sealed off from the vacuum line. The two solutions were then mixed and the reaction followed spectrophotometrically for several hours by measuring the optical density due to cystine at 248 *mμ*. In a number of these experiments, the concentration of cystine at the end of the reaction was also checked with the amino acid analyzer (see below).

The details of the experimental procedures used in the radiolysis experiments have already been given.⁷ Hydrogen and hydrogen sulfide were determined by the analytical techniques already described. The yields of cystine, alanine, and residual cysteine were followed by means of a Technicon amino acid analyzer. Cystine was also determined by its absorption at 248 *mμ*. Mass spectrometric analyses of gaseous products were kindly performed for us by Dr. A. Hogg, Department of Chemistry, University of Alberta.

Results and Discussion

Products and Radical Yields. Yield-dose plots for the amino-containing products of radiolysis of 10^{-2} *M* cysteine solutions at pH 5.6 are shown in Figure 1. The concentrations of all products varied linearly with dose over the range $0\text{--}4 \times 10^{18}$ ev/ml. The *G* values, obtained from the best straight lines through

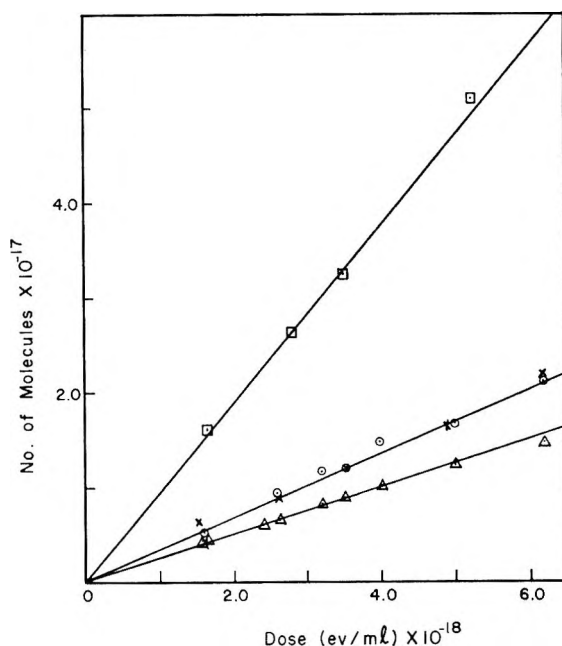


Figure 1. Yield-dose plots for the amino-containing products of radiolysis of 10^{-2} *M* cysteine solutions at pH 5.6 and at 23°: \square , cysteine consumption; \circ , cysteine by amino acid analyzer; \times , cysteine by determination of OD at 248 *mμ*; and \triangle , alanine.

the yield-dose plots, are given below with their standard deviations

$$G(\text{CyH}) = 2.6 \pm 0.2$$

$$G(\text{H}_2\text{S}) = 2.5 \pm 0.2$$

$$G(\text{H}_2) = 1.1 \pm 0.2$$

$$G((\text{CyS})_2) = 3.4 \pm 0.1$$

$$G(-\text{CySH}) = 9.3 \pm 0.2$$

The fact that the alanine and H_2S yields are equal, within experimental error, supports the view that reaction 5 is the exclusive fate of the Cy radicals formed in reactions 2 and 4. If alanine and cystine are the only major products containing the amino group, stoichiometry requires that

$$G(-\text{CySH}) = 2G((\text{CyS})_2) + G(\text{CyH}) \quad (i)$$

From the above results one obtains

$$G(-\text{CySH}) = 2(3.4) + 2.6 = 9.4$$

which demonstrates excellent material balance for the amino products when compared with the observed yield of $G(-\text{RSH}) = 9.3 \pm 0.2$. The present H_2S yield agrees well with 2.5 reported by El Samahy⁸ for $5 \times$

(6) D. A. Armstrong and V. G. Wilkening, *Can. J. Chem.*, **42**, 2631 (1964).

(7) V. G. Wilkening, M. Lal, M. Arends, and D. A. Armstrong, *ibid.*, **45**, 1209 (1967).

(8) A. El Samahy, Ph.D. Thesis, University of Delaware, Newark, Del., 1964.

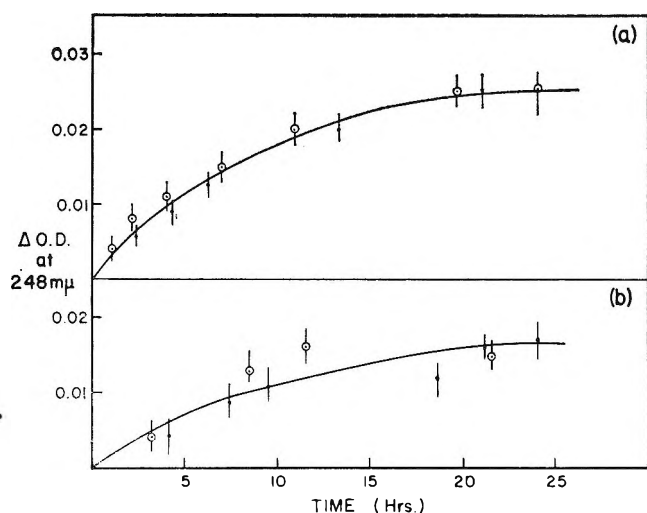


Figure 2. Reaction time curves for the H_2O_2 -cysteine reaction: (a) synthetic H_2O_2 -cysteine mixture; and (b) postirradiation reaction in an irradiated cysteine solution (see text); different size points identify separate experiments.

10^{-3} M unbuffered cysteine solutions. To the best of our knowledge, the alanine yields have not been quantitatively determined in our pH range by any other workers.

Whitcher, Rotheram, and Todd² concluded from their work that the oxidation of cysteine by H_2O_2 was negligibly slow in strongly acid solutions. This conclusion was substantiated by Packer⁴ and by our own more recent study.⁷ On the other hand, El Samahy⁸ reported that reaction 8 was very rapid in neutral solutions. The rate of this reaction was therefore determined in air-free 10^{-2} M cysteine solutions in the pH range obtaining in this study. Figure 2a shows a plot of optical density, due to the cystine absorption at 248 $\text{m}\mu$, vs. time for duplicate experiments. The initial peroxide concentration of 0.9×10^{-4} M was close to that which would have built up in the longer radiolysis experiments if no reaction with cysteine occurred. At the end of 24 hr, the reaction was 75–80% complete, and proceeding at an almost imperceptible rate. The kinetics of the reaction was not examined in very great detail, but further experiments showed that it was much slower at lower concentrations of cysteine and/or peroxide. It appears to be first order in peroxide and of fractional order in cysteine.

The reaction time curve in Figure 2a demonstrates that the oxidation of cysteine by hydrogen peroxide will be nowhere near complete under the conditions of this study, unless the irradiated samples are allowed to stand for several hours before analysis. If the solutions are analyzed immediately after a short irradiation at a very high dose rate, it should be possible to observe a postirradiation oxidation of cysteine. To confirm this, two samples of deaerated 10^{-2} M cysteine were subjected to a very high dose rate from a Philips Model MG150B/10 150-kvp constant potential X-ray machine

for a period of 10 min (the usual radiations with the 100-curie Co^{60} source lasted from 2 to 10 hr). At the end of these irradiations, the optical density had changed by 0.24 ± 0.02 unit. Further changes were then followed over a period of 24 hr. As shown in Figure 2b, the reaction time curve for the postirradiation oxidation is quite similar to that in Figure 2a. The initial peroxide concentration for the radiolysis is not very different from that obtaining in the synthesized H_2O_2 -CysSH solution.

As a standard procedure, all irradiated samples were allowed to stand for about 24 hr before analysis with the amino acid analyzer. Further changes in cystine yield beyond this time will lie within the over-all experimental error of our determinations. For practical purposes, it may therefore be assumed that 0.5 ± 0.1 (see below) molecules of cystine per 100 ev are formed in reaction 8.

The mechanism given in the Introduction requires that e_{aq}^- , H, and OH each eventually produce a thiyl radical. Consequently the total yield of cystine from reactions 7 and 8 should be given by the relationship

$$G((\text{CyS})_2) = \frac{1}{2}\{G_{\text{H}} + G_{\text{OH}} + G_{e_{\text{aq}}^-}\} + G_{\text{H}_2\text{O}_2}^{\text{M}} \quad (\text{ii})$$

Upon rearrangement one obtains

$$G_{\text{H}} + G_{\text{OH}} + G_{e_{\text{aq}}^-} = 2\{G((\text{CyS})_2) - G_{\text{H}_2\text{O}_2}^{\text{M}}\} \quad (\text{iii})$$

The experimental value of $G((\text{CyS})_2)$ is 3.4, and, allowing for the scavenging⁹ of some of the precursors of molecular peroxide in the radiation tracks, $G_{\text{H}_2\text{O}_2}^{\text{M}}$ may be taken as 0.50 in 10^{-2} M cysteine solutions. In support of this estimate, we may note that Packer⁴ obtained $G_{\text{H}_2\text{O}_2}^{\text{M}} = 0.6$ in 4.4×10^{-3} M cysteine solutions at pH 4, where reaction 8 would be much slower and $G_{\text{H}_2\text{O}_2}^{\text{M}}$ could be measured directly. Thus from expression iii, the total radical yield, $G_{e_{\text{aq}}^-} + G_{\text{H}} + G_{\text{OH}}$, is found to be 5.8.

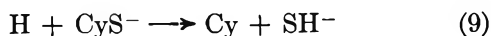
Unfortunately, the lability of the hydrogen atom on the SH group precludes isotopic labeling and the molecular hydrogen yield cannot be measured directly in cysteine solutions. Navon and Stein¹⁰ have estimated that k_1 is about $10^9 \text{ M}^{-1} \text{ sec}^{-1}$ and cysteine is also highly reactive toward e_{aq}^- .¹¹ In view of these observations, it is evident that cysteine will compete quite efficiently with radical combinations which give rise to molecular hydrogen. By analogy with nitrite⁹ and other highly reactive solutes, $G_{\text{H}_2}^{\text{M}}$ may be reduced from 0.45 to a value as low as 0.25 in 10^{-2} M cysteine solutions. Since the total hydrogen yield from these solutions is 1.1 molecules/100 ev, the yield from processes involving cysteine should be 0.65 to 0.85. This tends to be higher

(9) See Figure 5.6 of A. O. Allen, "The Radiation Chemistry of Water and Aqueous Solutions," D. Van Nostrand Co., Inc., New York, N. Y., 1961.

(10) G. Navon and G. Stein, *Israel J. Chem.*, **2**, 151 (1964).

(11) R. Braams in "Pulse Radiolysis," M. Ebert, J. P. Keene, A. J. Swallow, and J. H. Baxendale, Ed., Academic Press, London, 1965.

than the normally accepted yield of residual hydrogen atoms, $G_H = 0.60 \pm 0.05$, obtained with alcohols and formic acid as reactive solutes.¹² If one assumes $k_1/k_2 = 3.5$ as in 1 *N* acid solutions,⁷ an additional yield of ~ 0.2 hydrogen atom/100 ev must form H_2S , and the discrepancy in the apparent value of G_H would be even larger. However, in these sulfhydryl systems at pH 5–6, relatively large experimental deviations (see Figure 3) were observed in the values of $G(H_2)$ and no real significance can be attached to the above observation. Nevertheless it should be noted that Littman, Carr, and Brady¹³ found reaction 9



to be very efficient in their study of the reactions of hydrogen atoms with aqueous cysteine. This observation argues against reaction 10



being of any great importance. Since the sulfur-hydrogen bond is stronger than the sulfur-carbon bond,¹⁴ reaction 10 is also less probable than reaction 4 on thermochemical grounds. It is therefore extremely unlikely that reaction 10 could be responsible for an increase in the yield of residual hydrogen atoms in this system.

On the basis of the proposed mechanism, reactions 1, 2, 4, and 5 are the only processes leading to the formation of hydrogen, H_2S , and alanine, and it follows that

$$G(H_2) + G(H_2S) \text{ or } G(CyH) = G_H + G_e + G_{H_2}^M \quad (iv)$$

Hence, we find

$$G_H + G_e = G(H_2) + G(CyH) - G_{H_2}^M \quad (v) \\ = 3.4$$

From this and the above value of the total radical yield, G_{OH} is calculated to be 2.4, which compares favorably with values reported elsewhere.¹²

As the pH of the cysteine solutions is reduced, increasing proportions of the solvated electrons would be converted to hydrogen atoms by reaction 6. Since reaction 1 predominates over 2, it follows that this should cause the hydrogen yields to increase and those of alanine and H_2S to decrease,⁶ their values remaining identical with each other. The data presented in Figure 3 bear out these predictions. The uppermost points are values of $G_H + G_e$ calculated from expression v, using the hydrogen and alanine yields and assuming that $G_{H_2}^M$ is 0.30.¹⁵ As the pH decreases from 3.0 to 2.0 $G_H + G_e$ is seen to increase abruptly from 3.4 to 3.8. The occurrence of this increase is well established from extensive work in other systems.^{16,17} Our values of $G_H + G_e$ are larger than those observed in most other systems,^{12,16,17} the discrepancies being greatest at the higher pH's. A portion of this increase may be attributed to the high reactivity of the SH group toward

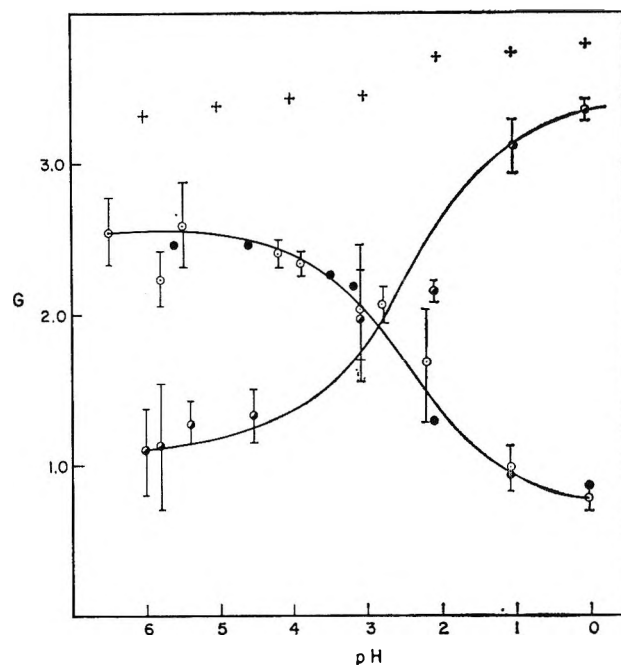
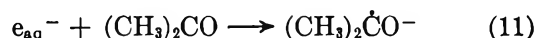


Figure 3. Effect of pH on product yields: \bigcirc , H_2S ; \bullet , alanine; and $+$, $H_2 + G_e + G_H$ (calculated from expression v, see text). The vertical lines through the H_2 and H_2S points represent the maximum deviations observed in the 3–10 replicate determinations. Standard deviations are given in the text.

all radicals and to the fact that we have employed a 10^{-2} *M* concentration, whereas radical yields have more frequently been determined at solute concentrations of 10^{-3} *M*. However, the value of $G_{e_{aq}^-}$ obtained below (2.5 ± 0.2) seems quite reasonable and the discrepancy appears to be due primarily to the high apparent value of G_H , on which we have already commented.

Competition Experiments. Trumbore and his co-workers⁶ have already shown that acetone and nitrate reduce the yield of H_2S in cysteine solutions. They attributed this to competitions between reactions 11 and 12, viz.



and reaction 4. If the proposed mechanism is correct, these scavengers should cause equivalent reductions in the alanine yields, which to the best of our knowledge

(12) See Proceedings of the Fifth Informal Conference on the Radiation Chemistry of Water, University of Notre Dame, Notre Dame, Ind., 1966, p 27 and references cited therein.

(13) F. E. Littman, E. M. Carr, and A. P. Brady, *Radiation Res.*, **7**, 107 (1957).

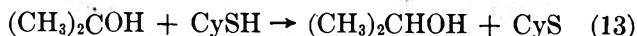
(14) H. Mackle, *Tetrahedron*, **19**, 1159 (1963).

(15) Note that the relatively small changes of ~ 0.05 molecule per 100 ev in $G_{H_2}^M$ over the pH range 0–6 [see C. H. Cheek, V. J. Linnenbom, and J. W. Swinnerton, *Radiation Res.*, **19**, 636 (1963)] has been neglected.

(16) See F. S. Dainton, *et al.*, *Trans. Faraday Soc.*, **62**, 3170 (1966), and previous related papers.

(17) E. Hayon, *Trans. Faraday Soc.*, **61**, 723 (1965).

have not been measured at pH 5.5. Also, in the case of acetone, the $(\text{CH}_3)_2\dot{\text{C}}\text{O}^-$ radical ion should be rapidly converted to the 2-hydroxyisopropyl radical, $(\text{CH}_3)_2\dot{\text{C}}\text{OH}$, which would react with the sulfhydryl group of cysteine in the same way as the Cy radical, viz.

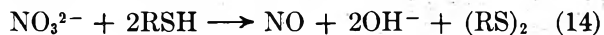


The yield of thiyl radicals and of cystine should therefore be unaffected by the presence of acetone.

Figure 4a shows the yields of cystine, H_2S , and alanine from $10^{-2} M$ cysteine solutions containing acetone at acetone:cysteine ratios in the range 0–10. As required by the mechanism, the cystine yields are independent of the amount of acetone added. In addition, the reductions in the alanine and H_2S yields are essentially equivalent. The apparent divergence at acetone:cysteine = 1 and 2 is not regarded as being significant, since there is an experimental uncertainty of ± 0.2 molecule/100 ev in both the alanine and H_2S yields.

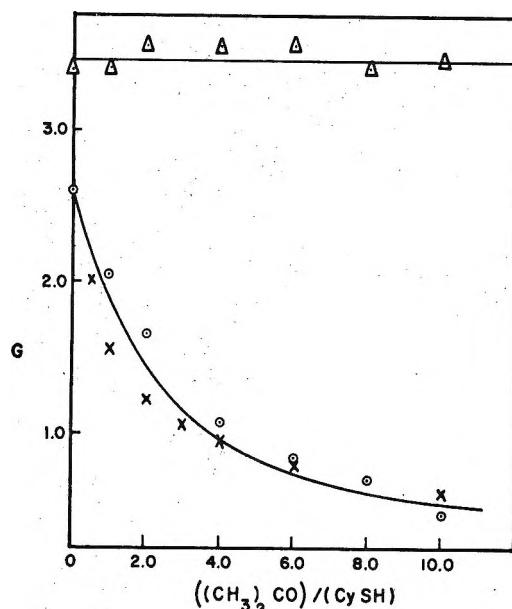
A gas-chromatographic analysis of irradiated solutions with an acetone:cysteine ratio of 5–10 showed a peak corresponding to the residual acetone and only one new peak occurring at the retention time of isopropanol. The 8-ft Poropak column was run at $\sim 66^\circ$ and the amino acids were retained. Unfortunately, the sensitivity of the flame ionization detector did not permit an accurate determination of the isopropyl alcohol yield, but $G(\text{isopropyl alcohol})$ appeared to be in the range of 2–3 as expected.

As shown in Figure 4b, the competition for e_{aq}^- between nitrate ions and cysteine also reduced the alanine and H_2S yields by equivalent amounts. However, in this case $G((\text{CyS})_2)$ increased from 3.4 toward a value of 4.7 as the nitrate concentration rose. The magnitude of this increase (≈ 1.3) is one half of the value of $G_{e_{\text{aq}}^-}$ reported in ref 18 and other recent investigations (see footnote 12). Each Cy radical formed in reaction 4 produces one CyS radical in reaction 5 and subsequently one-half of a molecule of cystine. The above increase in $G((\text{CyS})_2)$ can be explained if the product of reaction 12 gives rise to two CyS radicals or one molecule of cystine. This product is believed to be a hydrated form of NO_2^{19} or NO_3^{2-} ,²⁰ as indicated above. The observation of nitric oxide in the mass spectrum of the gaseous products from irradiated solutions containing both nitrate and cysteine provides strong support for the occurrence of

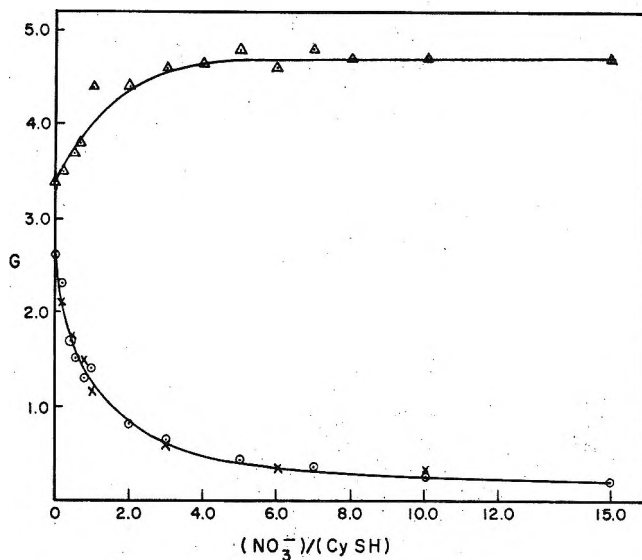


which also accounts for the formation of one molecule of cystine from each NO_3^{2-} . It should be noted that, under our conditions, nitrite ions, which are the final products of radiolysis of aqueous nitrate solutions,²⁰ do not react with cysteine at a measurable rate.

The rate constants for the reactions of hydrogen atoms with acetone and nitrate are considered to be $\sim 10^6$ and $\sim 10^7$, respectively.²¹ Since k_2 is estimated¹⁰



(a).



(b).

Figure 4. Effect of solvated electron scavengers on the product yields: (a) acetone as scavenger; and (b) NO_3^- as scavenger; (Δ , cystine, \circ , alanine, and \times H_2S).

to be about 10^8 , the scavenging of H by acetone and nitrate ions should not have been appreciable over the range of acetone and nitrate concentrations shown in Figures 4a and b. Reasonably accurate estimates of $G_{e_{\text{aq}}^-}$, k_4/k_{11} , and k_4/k_{12} may therefore be obtained from reciprocal plots of the data of these two figures, based on expression vi.

(18) C. J. Hochanadel and R. Casey, *Radiation Res.*, **25**, 198 (1965).

(19) M. Anbar in E. J. Hart, "Solvated Electron," *Advances in Chemistry Series*, No. 50, American Chemical Society, Washington, D. C., 1965.

(20) M. Daniels and E. E. Wigg, *J. Phys. Chem.*, **71**, 1024 (1967).

(21) H. A. Schwarz in "Advances in Radiation Biology," Vol. 1, L. G. Augenstein and R. Mason, Ed., Academic Press, New York, N. Y., 1964, p 17.

$$1/\Delta G(\text{H}_2\text{S}) = \{1 + k_4(\text{CySH})/k_s(\text{S})\}/G_{e_{\text{aq}}}^- \quad (\text{vi})$$

where (S) represents the scavenger concentration and k_s its rate constant for reaction with e_{aq}^- . The intercepts of the reciprocal plots gave $G_{e_{\text{aq}}}^- = 2.5$ for the acetone and 2.6 for the nitrate results. These values fall in the same range, 2.3–2.7, as most other recent determinations.^{12,18} The fact that they are equal within experimental error to $G(\text{CyH})$ and $G(\text{H}_2\text{S})$ indicates that contributions to the H_2S yields from reaction 2 cannot exceed the experimental uncertainty of 0.2 molecule/100 ev, and G_e may reasonably be set at 2.5 ± 0.2 in this system. The rate constant ratios were found to be $k_4/k_{11} = 1.95$ and $k_4/k_{12} = 1.03$. These are both twice as large as the corresponding ratios originally reported by El Samahy, White, and Trumbore.⁵ The cause of this discrepancy has not been explored, but it is to be noted that the latter workers used much lower cysteine concentrations as well as different analytical techniques. By substituting the absolute values of k_{11} ²² and k_{12} ²³ in the above ratios, k_4 is found to be $1.1 \times 10^{10} \text{ M}^{-1} \text{ sec}^{-1}$. This agrees reasonably well with $8.7 \times 10^9 \text{ M}^{-1} \text{ sec}^{-1}$ obtained by Braams¹¹ using the pulsed radiolysis technique, and there can be little doubt that reaction 4 is the predominant process by which solvated electrons react in cysteine solutions at pH 5.0–6.0.

The results reported above for 10^{-2} M cysteine solutions provide confirmation for the radiolytic mechanism based on reactions 1 to 8. Product yields from 10^{-3} M solutions are dependent on dose beyond $3 \times 10^{18} \text{ ev/ml}$. However, from the linear yield-dose plots at doses below this, $G(-\text{RSH})$, $G((\text{CyS})_2)$, and $G(\text{CyH})$ have been found to be 7.9, 2.9, and 2.2, respectively. These yields

also conform to expression i, but are significantly lower than those observed in the 10^{-2} M solutions. This is to be expected, since the competition with track reactions will not be as extensive and reaction 8 will be much slower in these more dilute cysteine solutions. $G((\text{CyS})_2)$ is in excellent agreement with that of El Samahy in $9 \times 10^{-4} \text{ M}$ solutions.⁸ The hydrogen yield from 10^{-3} M solutions rises with decreasing pH as anticipated,⁶ while the alanine yield falls. At pH 5.5 $G(\text{H}_2)$ has the same value, 1.1, in 10^{-3} M cysteine solutions as in 10^{-2} M solutions. From this one must conclude that any increase in $G_{\text{H}_2}^{\text{M}}$ resulting from the reduction in solute concentration is compensated, within experimental error, by the loss of hydrogen atoms to track reactions with radical species. As pointed out in ref 7, the H_2S yields reported by Armstrong and Wilkening⁶ are high. Further work on these is currently underway.

Acknowledgments. The authors wish to acknowledge many helpful discussions with Dr. C. N. Trumbore of the University of Delaware, Newark, Delaware. They are also indebted to the Defence Research Board of Canada for the purchase of the Technicon amino acid analyzer and for the financial support to V. G. W. and M. A. The investigation was also supported by U. S. Public Health Service Grant No. RO1-GM-14020-01MCH-B from the National Institute of General Medical Sciences, which provided the stipend for M. L.

(22) $k_{11} = 5.9 \times 10^9 \text{ M}^{-1} \text{ sec}^{-1}$; E. J. Hart, S. Gordon, and J. K. Thomas, *J. Phys. Chem.*, **68**, 1271 (1964).

(23) $k_{12} = 1.1 \times 10^{10} \text{ M}^{-1} \text{ sec}^{-1}$; J. K. Thomas, S. Gordon, and E. J. Hart, *ibid.*, **68**, 1524 (1964).

Triplet Methylene Radical Reaction with *cis*-Butene-2^{1a}

by D. F. Ring^{1b} and B. S. Rabinovitch

Department of Chemistry, University of Washington, Seattle, Washington 98105 (Received June 26, 1967)

A study of the pressure dependence of the C₆ products of the reaction between *cis*-butene-2 and triplet methylene radicals is reported. Triplet methylene was produced by collisional deactivation (in the presence of a large excess of nitrogen) of the methylene produced by the photolysis of diazomethane with 4358-A radiation at 23°, and with unfiltered light at 23 and 56°. Reaction pressures were varied from 0.3 to 3.5 atm; a constant ratio of *cis*-butene-2:diazomethane:nitrogen was maintained at 20:1:30,000. The observed pressure dependence of the product proportions indicates that alkene products arise, in part, by isomerization of the triplet dimethylcyclopropanes or diradicals, rather than exclusively by a concomitant noninterceptible formation reaction. There is a pressure dependence of the ratio of *trans*:*cis*-dimethylcyclopropane which, together with the pressure variability of products such as 3-methylbutene-1, dictates caution in the interpretation of the proportions of ³CH₂:¹CH₂ from product proportions in photolysis systems and provides an alternative interpretation of a previous finding of the authors.

Introduction

It has been reported that the ratios of products,^{2a} ¹CH₂:CH₂, and of secondary products that arise on photolysis of diazomethane and ketene in the presence of butene-2, may vary with pressure, up to several atmospheres or more.^{2b} In this connection, no information has been available on the proportions of the products that arise in pure ³CH₂-butene-2 systems at the higher pressures of interest, although Cvetanović and Duncan have reported on systematic studies at lower pressures.³ In the present investigation, diazomethane was photolyzed at 4358 Å, and with unfiltered light, in the presence of *cis*-butene-2 and excess nitrogen. The pressure of the system was systematically varied up to 3.5 atm, while constancy of composition of the reaction mixture was maintained.

Singlet methylene, which is formed upon photolysis of diazomethane, may be collisionally deactivated in the presence of excess inert gas to ground-state ³CH₂.⁴ This singlet-triplet deactivation technique can be used to produce 100% of ³CH₂ in a reaction system, provided that the system is sufficiently dilute in substrate so that the initially formed ¹CH₂ molecules undergo a sufficient number of prior collisions with the inert gas.

Experimental Section

Materials. Diazomethane (DM) was prepared by the reaction of 12 M KOH and *N*-nitrosomethylurea; it was purified by trap to trap distillation and stored in dibutyl phthalate at -196°; the samples were shielded from light at all times. Upon warming of the butyl phthalate solution, the initial-pressure fraction

was discarded in order to remove any ethane or ethylene impurities.

Phillips research grade *cis*-butene-2 (99.89%) was used without further purification; a trace of *trans*-butene-2 was the only impurity.

Airco dry nitrogen was purified by passing it through a hot copper trap, to remove oxygen, and then through two packed traps at -196°.

Apparatus and Procedure. Gas handling of the *cis*-butene-2 and nitrogen was performed on a greaseless section of the vacuum system. Diazomethane was measured out in a well-seasoned section of the vacuum system, reserved for diazomethane handling. The only reactor used was a 1000-cc Pyrex bulb, which was pumped to <10⁻⁴ mm before loading with reactants; it was well seasoned with diazomethane. The light source was a G.E. AH-6 high-pressure mercury arc lamp. Dow-Corning no. 5543 and no. 3389 filters were housed in a Pyrex water-cooled jacket; these filters and light source provided a median wavelength at 4358 Å; experiments were also performed with the unfiltered radiation of the AH-6 lamp. Reaction was carried out at 25 and 56° with mixtures of constant

(1) (a) This work was supported by the Office of Naval Research; (b) abstracted in part from the Ph.D. thesis of D. F. Ring.

(2) (a) J. W. Simons and B. S. Rabinovitch, *J. Phys. Chem.*, **68**, 1322 (1964); (b) B. S. Rabinovitch, K. W. Watkins, and D. F. Ring, *J. Am. Chem. Soc.*, **87**, 4960 (1965).

(3) F. J. Duncan and R. J. Cvetanović, *ibid.*, **84**, 3593 (1962).

(4) (a) G. Herzberg, *Proc. Roy. Soc. (London)*, **A262**, 291 (1961); *Can. J. Phys.*, **39**, 1511 (1961); (b) F. A. L. Anet, R. F. W. Bader, and A. M. Van der Auwera, *J. Am. Chem. Soc.*, **82**, 3217 (1960); (c) H. M. Frey, *ibid.*, **82**, 5947 (1960); (d) H. M. Frey, *Progr. Reaction Kinetics*, **2**, 131 (1964); (e) R. F. W. Bader and J. I. Generosa, *Can. J. Chem.*, **43**, 1631 (1965).

composition of *cis*-butene-2:DM:N₂ = 20:1:30,000. The extent of photolysis of DM was 60–95%.

Analysis. Products were separated from the nitrogen, upon completion of photolysis, by pumping the reaction mixture through packed traps at -196° . Gas chromatographic analysis was used. The analytical column was 26 ft of 15% dinonyl phthalate on 60–80 mesh Chromosorb P. Both flame and thermal detectors were used on different occasions. All products were identified with authentic samples.

Results

Nitrogen Dilution. Frey^{4d} has noted that in the identification^{4a} of the spectrum of $^3\text{CH}_2$, N₂:DM = 500:1 was employed; he proposed that about 50 collisions are required to bring $^1\text{CH}_2$ to its ground vibrational state and the remaining 400 or more collisions take $^1\text{CH}_2$ to the triplet ground state. He^{4c} has worked with dilutions of argon:*cis*-butene-2 up to 1600:1 and found that $^3\text{CH}_2$ production increased with dilution. Bell⁵ has estimated that ten times as many collisions are required to transport methylene to its ground electronic state as to deactivate vibrationally the singlet state. Bader and Generosa^{4e} have also substantiated the increase of $^3\text{CH}_2$ production with increased dilution in *cis*-butene-2:inert-gas systems in which ratios up to 950:1 were employed.

Experiments were performed here at nearly constant pressure in which the ratio of N₂:*cis*-butene-2 was varied from 500:1 to 2400:1. The relative yield of products did not appear to vary with dilution between 1200:1 and 2400:1. Thus the dilution of 1500:1, which was maintained in the present work, appears sufficient to ensure that collisional deactivation of $^1\text{CH}_2$ to $^3\text{CH}_2$ occurred.

Product Yields. The major C₅ products from the reaction of $^3\text{CH}_2$ with *cis*-butene-2 are *trans*-1,2-dimethylcyclopropane (TDMC), *cis*-1,2-dimethylcyclopropane (CDMC), 2-methylbutene-1 (2MB1), 2-methylbutene-2 (2MB2), 3-methylbutene-1 (3MB1), *trans*-pentene-2 (TP2), and *cis*-pentene-2 (CP2). In addition to these products from the photolysis reaction, the DM-*cis*-butene-2 system was found to undergo a dark reaction which produced CDMC, CP2, and 2MB2. From blank dark runs performed at several pressures, it was determined that the corrections to be applied for the dark products were virtually independent of pressure. At 23° , they amounted to 4% CDMC, 0.6% CP2, and 2% 2MB2 for the reaction with 4358-A radiation, and 4% CDMC, 1% CP2, and 2% 2MB2 with unfiltered radiation; at 56° , they were 3% CDMC, 0.8% CP2, and 2% 2MB2 with unfiltered radiation.

The experimental data are summarized in Figures 1–8. In view of the large scatter sometimes evident, subjective interpretation about trends in the data may be misleading. For this reason, we have fitted the data

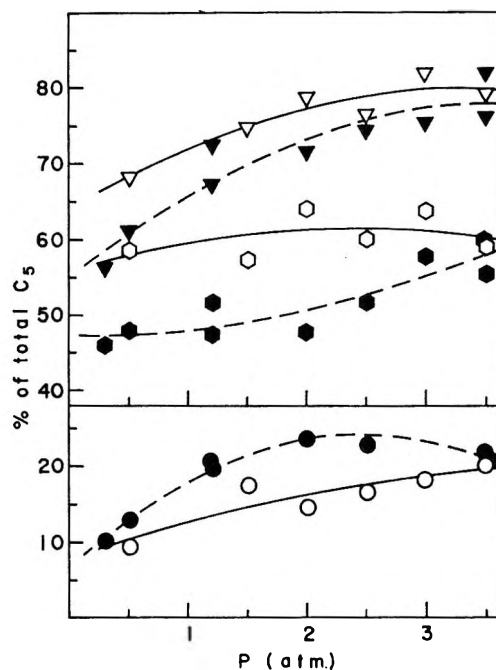


Figure 1. Variation of product composition with total pressure in the DM-*cis*-butene-2-nitrogen system at 23° for photolysis with 4358-A light (dashed line and filled points) and unfiltered AH-6 radiation (solid line and open points): total 1,2-dimethylcyclopropane, CDMC + TDMC, ∇ ; *cis*-1,2-dimethylcyclopropane, CDMC, \circ ; *trans*-1,2-dimethylcyclopropane, TDMC, \circ .

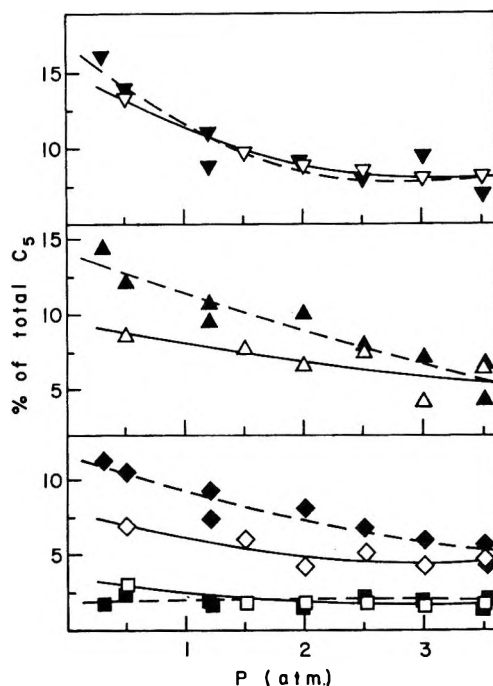


Figure 2. The change of CP2, ∇ , TP2, Δ , 3MB1, \diamond , and 2MB2, \square , with total pressure at 23° for 4358-A light (dashed line and filled points) and unfiltered AH-6 radiation (solid line and open points).

(5) J. A. Bell, *Progr. Phys. Org. Chem.*, **2**, 1 (1964).

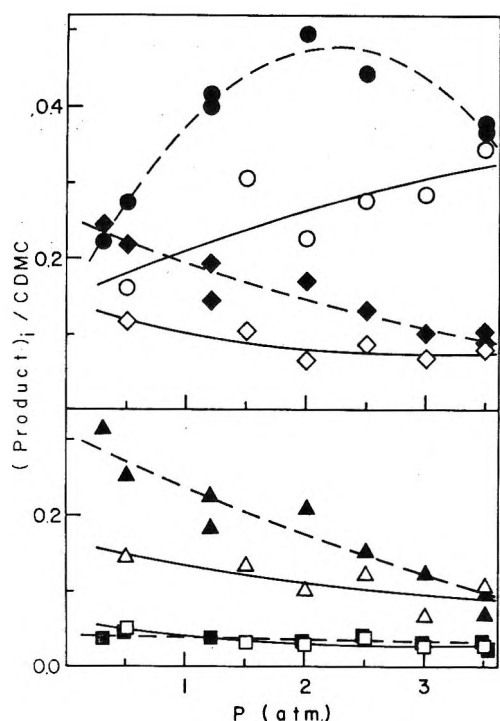


Figure 3. Variation of the ratios TDMC:CDMC, \circ , TP2:CDMC, Δ , 3MB1:CDMC, \diamond , and 2MB2:CDMC, \square , with total pressure at 23° for 4358-A light (dashed line and filled points) and unfiltered AH-6 radiation (solid line and open points).

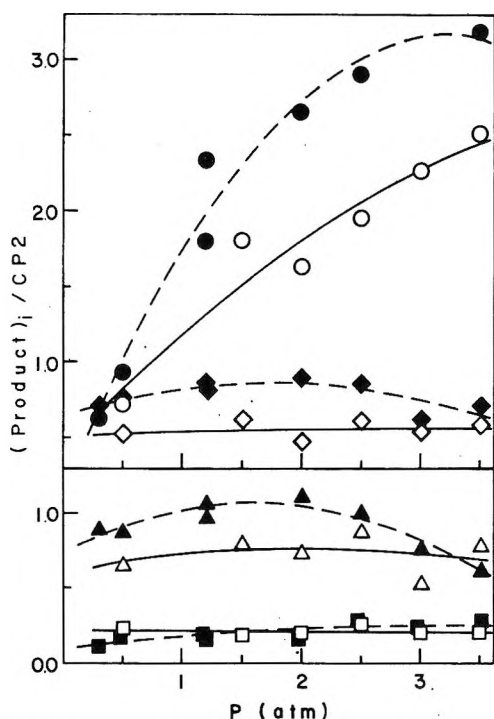


Figure 4. Variation of the ratios TDMC:CP2, \circ , TP2:CP2, Δ , 3MB1:CP2, \diamond , and 2MB1:CP2, \square , with total pressure at 23° for 4358-A light (dashed line and filled points) and unfiltered AH-6 radiation (solid line and open points).

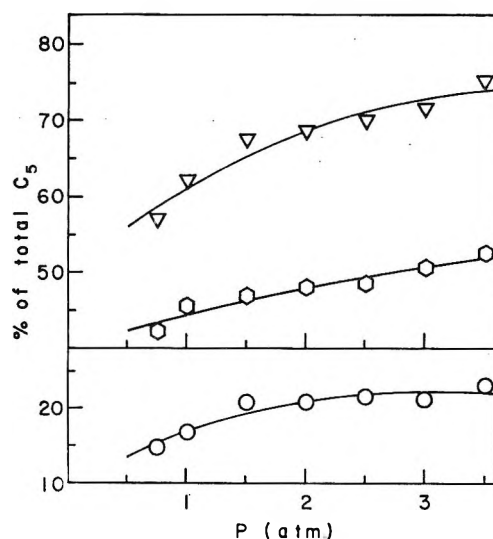


Figure 5. Change in product composition with total pressure in the DM-*cis*-butene-2-nitrogen system at 56° for photolysis with unfiltered AH-6 radiation: CDMC + TDMC, ∇ ; CDMC, \circ ; TDMC, \circ .

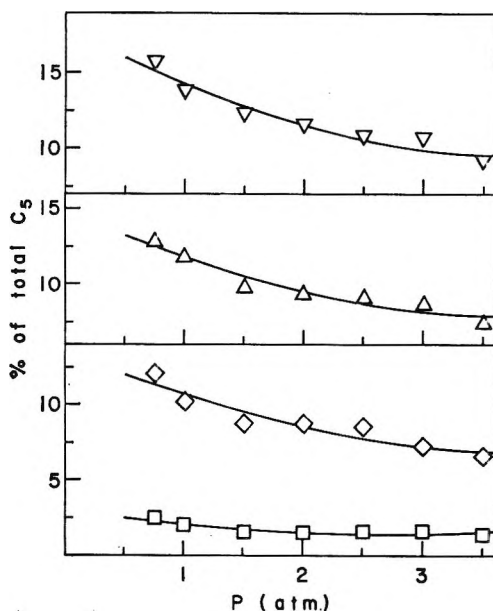


Figure 6. Variation of CP2, ∇ , TP2, Δ , 3MB1, \diamond , and 2MB1, \square , with total pressure for photolysis with unfiltered AH-6 radiation at 56°.

by least squares to a three-parameter curve, $X = a + bp + cp^2$. The curves given in the figure are these least-square fits. Solid curves associated with the open points are fits to the data from photolysis runs with unfiltered radiation; the dashed curves and filled points are for data from photolysis with 4358-A light.

The variation of the ratio (CDMC + TDMC):(total C_5) with pressure is shown in Figure 1 for the reaction at 23°; this ratio increases with pressure to a limiting value of 78% for 4358-A light and to 80% for unfiltered radiation. Figure 1 also presents the individual yields for CDMC and TDMC. Data for unfiltered and

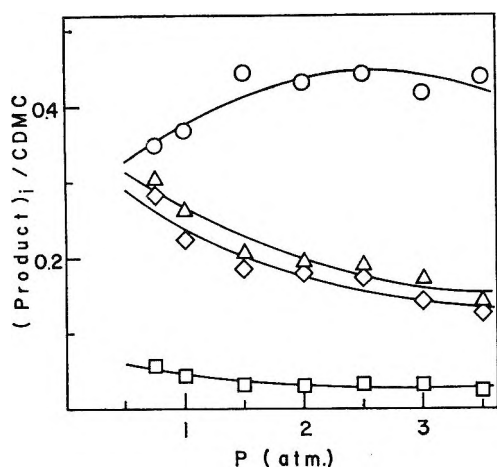


Figure 7. Pressure dependence of the ratios TDMC:CDMC, \circ , TP2:CDMC, Δ , 3MB1:CDMC, \diamond , and 2MB2:CDMC, \square , at 56° for photolysis with unfiltered AH-6 radiation.

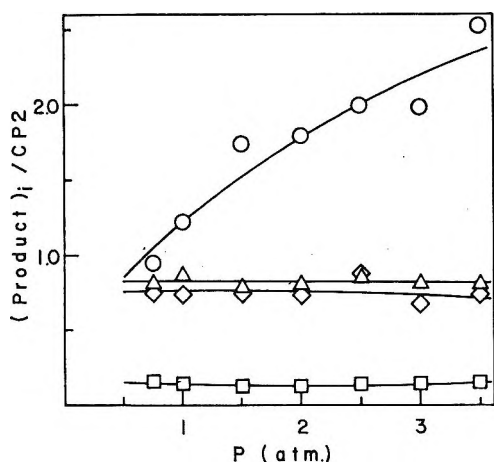


Figure 8. Variation of the ratios TDMC:CP2, \circ , TP2:CP2, Δ , 3MB1:CP2, \diamond , and 2MB2:CP2, \square , with change in pressure at 56° for photolysis with unfiltered AH-6 radiation.

filtered light show a rise to $\sim 60\%$ CDMC, while TDMC increases with pressure to 20% at 3.5 atm.

Figure 2 shows the yields of TP2, CP2, 2MB2, and 3MB1. Over the entire pressure range, 2MB2 is nearly constant at 2.0% for both 4358-A and unfiltered radiation. The compounds TP2, 3MB1, and CP2 decrease with pressure, to a plateau or minimum for the latter. The decrease of 3MB1 cannot readily be compared with the work of Bader and Generosa,^{4e} wherein they observed an increase of 3MB1 with increased pressure, but with concurrent increased inert gas and hence increased dilution; also, they worked at ratios of *cis*-butene-2:DM, which were very low (2.5:1) and which invited complicating reactions of DM. The comparison of data for the filtered and unfiltered light sources suggests some possible (but minor) real differences that may be distinguishable from experimental variability.

It is worthy of note here that there is a systematic

difference between the increase of dimethylcyclopropanes with pressure as contrasted with the decrease of alkene products; the contrast extends to both "singlet" (CDMC *vs.* CP2, 2MB2) and "triplet" (TCMC *vs.* TP2, 3MB1) products.

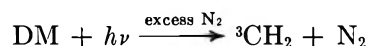
Figure 3 gives the pressure dependence of the ratio TDMC:CDMC between 0.3 and 3.5 atm. A maximum of 0.43 at 2.2 atm is noted in the 4358-A data, although the ratio with unfiltered light increases monotonically with pressure to 0.35 at 3.5 atm. These values are lower than those reported previously for the $^3\text{CH}_2$ -*cis*-butene-2 system: Frey^{4c} found TDMC:CDMC to be 0.96 at dilutions similar to those employed here; Bader and Generosa^{4e} gave a TDMC:CDMC ratio of 0.82 ; and Duncan and Cvetanovi³ reported a TDMC:CDMC value of 1.29 for mercury-photosensitized production of $^3\text{CH}_2$ from ketene; the data of Simons and Rabinovitch^{2a} tended to agree with these. This apparent discrepancy is discussed later; it led us to examine early results carefully and to repeat a number of experiments; the DM:butene ratio is lower here than that employed in other work. By contrast with the TDMC values, the ratios TP2:CDMC and 3MB1:CDMC, given in Figure 3, decrease with increasing pressure for both light sources.

Three ratios of products appear in Figure 4: TDMC:CP2, TP2:CP2, and 3MB1:CP2. The former reaches a plateau for 4358-A data and increases monotonically with pressure to nearly the same value for unfiltered light. Both TP2:CP2 and 3MB1:CP2 are approximately constant for data from both light sources, corresponding to nearly parallel pressure dependence of all alkene products.

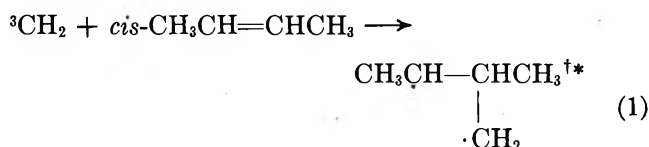
Figures 5-8 illustrate data obtained with unfiltered radiation for the DM-*cis*-butene-2 system at 56° . With little exception, the data are qualitatively similar to those in Figures 1-4.

Discussion

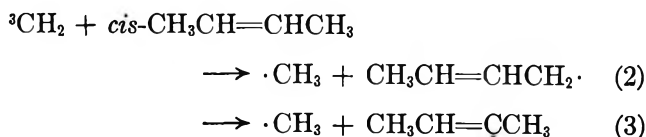
Reaction Scheme. Two initial reactions can occur after the photolysis of DM



One of these is addition to the double bond

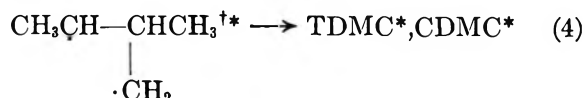


The initially formed triplet diradical^{6a} intermediate is vibrationally excited (\ast) but probably not electronically excited (\dagger), though some uncertainty exists concerning the electronic ground stage of this diradical.^{6b,c} The other reaction of $^3\text{CH}_2$ is H abstraction

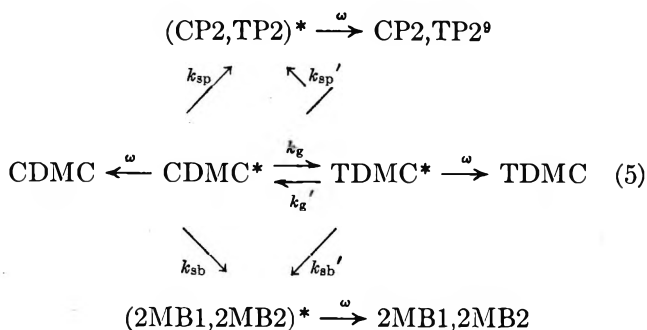


Reaction 2 should preponderate over reaction 3. A CH insertion reaction by ${}^3\text{CH}_2$ was previously reported⁷ to occur to an extent in alkane systems, but the presence of the double bond should render such reaction negligible here.

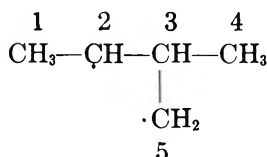
The vibrationally excited diradical formed in reaction 1 may cyclize with inversion of spin



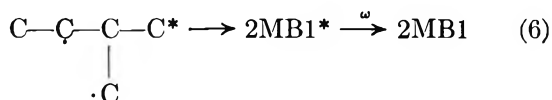
Further reactions of TDMC* and CDMC* may be summarized⁸



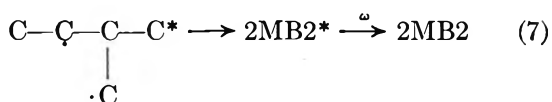
By numbering the carbon atoms



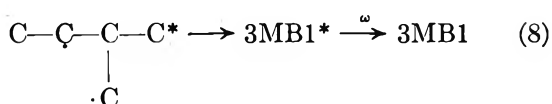
the following H- and methyl-shift reactions of the diradical species may be described:¹⁰ a 1,2-hydrogen shift from C3 to C2



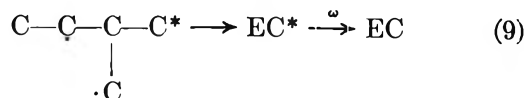
a 1,2-hydrogen shift from C3 to C5



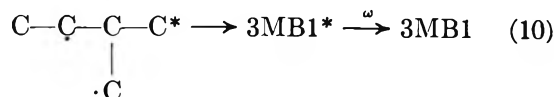
a 1,4-hydrogen shift from C1 to C5



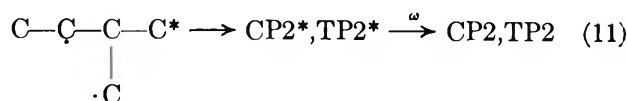
a 1,3-hydrogen shift from C4 to C2 with ring closure (ethyleyclopropane \equiv EC)



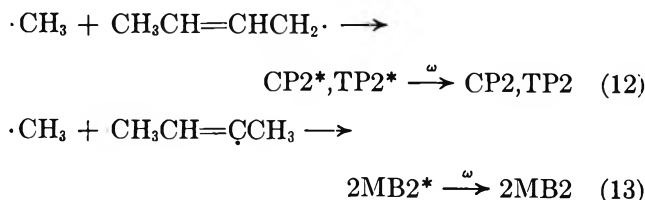
a 1,2-methyl migration by C4 to C2



and a 1,2-methyl migration by C4 to C5



Reactions 2 and 3 may lead to recombination of the initially formed radicals



Although the *cis* configuration tends to be preserved in the methallyl radical,¹¹ TP2 will also be formed by

(6) (a) The existence of a triplet diradical intermediate has been suggested by other workers: see ref 4a-c; also K. R. Kopecky, G. S. Hammond, and P. A. Leermakers, *J. Am. Chem. Soc.*, **84**, 1015 (1962); R. W. Carr and G. B. Kistiakowsky, *J. Phys. Chem.*, **70**, 118 (1966); C. McKnight and F. S. Rowland, *J. Am. Chem. Soc.*, **88**, 3179 (1966); R. J. Cvetanović, H. E. Avery, and R. S. Irwin, *J. Chem. Phys.*, **46**, 1993 (1967). (b) R. Hoffman (151st National Meeting of the American Chemical Society, Pittsburgh, Pa., March 1966, paper 109K) has reported calculations from LCAO theory, using a basis set of 2s and 2p carbon and 1s hydrogen AO's which indicate that the trimethylene diradical has a singlet ground state in which the three C's and four terminal H's are coplanar and the CCC angle is approximately 125°; the two electrons on the diradical are reported to occupy a 1,3 antibonding antisymmetric orbital; this ostensibly results in a tendency to add 1,2 to olefins and to close to cyclopropane in a conrotatory manner. The ground-state diradical has barriers to rotation of the terminal CH₂ groups, while the first excited singlet and triplet states are calculated to possess nearly free rotation for these groups. (c) H. E. Simmons, private communication to A. Mishra, *J. Am. Chem. Soc.*, **88**, 3963 (1966), carried out a Pariser-Parr-Pople calculation for trimethylene and found that the ground state is predicted to be triplet.

(7) D. F. Ring and B. S. Rabinovitch, *ibid.*, **88**, 4285 (1966).

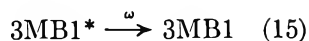
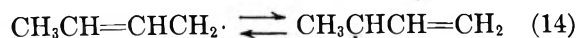
(8) H. M. Frey, *Proc. Roy. Soc. (London)*, **A251**, 575 (1959).

(9) J. A. Bell⁶ has suggested that linear pentenes may be explained if the diradical introconverts between a linear conformation (C-C-C-C) and the branched configuration formed in reaction 1, but this suggestion was questioned by G. Z. Whitten and B. S. Rabinovitch (*J. Phys. Chem.*, **69**, 4348 (1965)) on the basis of earlier results obtained by Placzek (D. W. Placzek and B. S. Rabinovitch, *Can. J. Chem.*, **43**, 820 (1965)). McKnight and Rowland^{6a} have further indicated that such a rearrangement is not a major source of pentene from dimethylcyclopropane. Very recently, Cvetanović, *et al.*,^{6a} have presented further strong evidence against the proposed introconversion.

(10) These reactions of the diradical have been suggested previously. Duncan and Cvetanović⁸ proposed the relative importance of the following reactions: 10 and 11 > 8 > 7 > 6. Reaction 9 was suggested by D. W. Setser and B. S. Rabinovitch (*Can. J. Chem.*, **40**, 1425 (1962)). Carr and Kistiakowsky^{6a} have included reaction 8 in a reaction scheme, while McKnight and Rowland^{6a} believe reactions 6, 7, 8, 10, and 11 may occur.

(11) R. F. Kubin, B. S. Rabinovitch, and R. E. Harrington, *J. Chem. Phys.*, **37**, 937 (1962).

(12). Allylic resonance can lead to 3MB1 in the following manner



In addition, other disproportionation and combination reactions of the radicals can occur to give methane, ethane, *trans*-butene-2, *cis*-butene-2, 1,2-butadiene, 3-methyl-2,5-heptadiene, 3,4-dimethyl-2,4-hexadiene, and 2,6-octadiene.

A whole host of products, many in trace or minor amounts, actually are found in this system. We have defined and limited our objective to a clarification of the major C₅ products, which conventionally have drawn the most attention and which are most closely related to the initial processes. While an exhaustive study of all of the products would assist the understanding of secondary and later radical reactions that occur, these *may* not contribute to our primary objective, and, since our interest does not extend to them *per se*, we have chosen to restrict our study to major products from C₂ through C₆.

Wavelength and Temperature Effects. The data in Figures 1-4 exhibit *possible* systematic differences for the two light sources used. Unfiltered (more energetic) radiation produced more CDMC, while enhanced relative yields of TDMC, TP2, and 3MB1 were found with 4358-Å light. The differences in product yields for the two light sources tended to lessen as the pressure was increased. It might be expected that data for both light sources would be identical, since any wavelength effect in the production of ³CH₂ should be eliminated by the subsequent collisions with the inert deactivating gas.

The observed difference, if real, could be explained if excited singlet DM[†] were capable of adding to *cis*-butene-2 in a predominantly stereospecific manner, and if the probability of this (minor) reaction were increased relative to decomposition at higher vibrational levels of DM[†]. Such reaction could, in any case, be only a minor component of the total reaction.

Comparison of the data for unfiltered radiation in Figures 1-4 with that in Figures 5-8 indicates that the yields of (CDMC + TDMC) and of CDMC are lower at 56 than at 23°, but that the yields of TDMC, CP2, TP2, and 3MB1 are higher at 56 than at 23°. These changes in yields could be rationalized by postulating that increase of temperature tends to enhance reaction of DM[†] with *cis*-butene, but that it also favors the formation of TDMC in reaction 4, if an appreciable activation energy exists for rotation about the single (C2-C3) bond in the diradical, as has been proposed.¹² Previously, Setser and Rabinovitch¹⁰ deduced that ¹CH₂ carries approximately 22-kcal excess energy from

its genesis, on the basis of $\Delta H_f^\circ(^1\text{CH}_2) = 90 \text{ kcal mole}^{-1}$. Allowance for a possible difference in heats of formation of ¹CH₂ and ³CH₂ of 5-10 kcal mole⁻¹ could reduce the exothermicity of reaction 1 to $\lesssim (110 - 29.5) \lesssim 80.5 \text{ kcal mole}^{-1}$. Depending upon the energy splitting, *x*, between singlet and triplet trimethylene, the excess internal energy of the triplet diradical might be $\lesssim (80.5 - 62 - x) = \lesssim (18.5 - x) \text{ kcal}$.

Higher temperature would also favor alkene production reactions 6-11. The above is a qualitative speculative explanation of effects whose magnitudes are not large and may even be in doubt owing to experimental scatter.

Product Trends with Pressure. The most important result of the present study concerns the consistent pressure trends of product formation found under all of the experimental conditions. The percentage of both TDMC and CDMC in the C₅ product increased with rise in pressure. By contrast, the percentage of alkenes decreased as the reaction pressure was raised; the yields of CP2, TP2, 3MB1, and 2MB2 show similar pressure dependence; the three former compounds were generated in comparable amounts, while the latter arose to a lesser extent (a few per cent) at all pressures; in addition, 2MB1 and EC were found, but only in trace amounts; each comprised less than 0.3% of the total C₅ product.

The observed pressure trends are in contrast to those observed over a similar pressure range from the ¹CH₂-*cis*-butene-2 reaction system^{4d} in which only the major product, CDMC, increased with rise of pressure while other major products, CP2 and 2MB2, remained nearly constant; TDMC, TP2, 3MB1, and 2MB2 were minor products and *decreased* with increase of pressure. The 2MB2 product is relatively the most reduced on going from a "singlet" to a "triplet" system and, of all the products, thus appears most characteristically "singlet" in nature; conventionally, CDMC and (to a lesser extent) CP2 have been thought of as characteristic "singlet" products of reaction of methylene with *cis*-butene.^{2a,4c}

The plots of ratios of the various products *vs.* CDMC indicate that TDMC:CDMC increased (to a plateau or shallow maximum) with rise of pressure, while TP2:CDMC and 3MB1:CDMC decreased and showed very similar pressure dependence (Figures 3 and 7). If the products are plotted *vs.* CP2, instead, TDMC:CP2 increases dramatically with rise in pressure while

(12) R. J. Crawford and A. Mishra (*J. Am. Chem. Soc.*, **88**, 3963 (1966)) have estimated that the linear C₅ diradical, formed upon pyrolysis of 1-pyrazolines, exhibits a bonding energy of about 8-12 kcal between the radical sites. Thus, if the diradical formed in reaction 1 is not free to rotate about the central C-C bond, the original *cis* configuration would tend to be conserved. Inasmuch as the evidence discussed in ref 9 appears to rule out a cyclized intermediate, the experimentally^{4,6} observed tendency for conservation of the original butene-2 configuration in the product cyclopropanes formed by ³CH₂ addition strongly supports the existence of a rotational barrier in the unsymmetrical diradical.

TP2:CP2 and 3MB1:CP2 are roughly constant or exhibit possible broad shallow maxima (Figures 4 and 8). Thus the pressure trends of the two sets of ratios of products, constructed relative to the two conventional "singlet" products, are dissimilar.

Interpretation of Pressure Trends. A plausible explanation of the data, which accounts for the observed trends in product yields, as well as for the contrasting trends of the two series of product ratios, is that a large fraction of products arises from isomerization reactions of the initial diradical (or triplet cyclopropane) which is formed in reaction 1 and that there is an increasing tendency for reaction 4 to be favored over reactions 6–11 as the hot diradical is collisionally deactivated.¹³ In ref 10, it is pointed out that Cvetanović, *et al.*, had proposed that the relative importance of the reactions of the diradical to produce alkenes should be 10 and 11 > 8 > 7 > 6; this proposed hierarchy is supported experimentally here. Only part of the alkene products are formed by concomitant noninterceptible initial reactions. This part includes H abstraction by ³CH₂ (reactions 2 and 3 followed by 12–15); extrapolation of the alkene proportions at highest pressures plausibly corresponds to these.

It is possible that at higher pressures the *cis* configuration in reaction 4 is favored by more rapid collisional stabilization of the initially formed diradical because of the possible existence of an appreciable activation energy for rotation around the central single bond, referred to earlier in another connection. This could help explain a leveling off or decline in the TDMC:CDMC ratio at highest pressure. At the other end, the decline of TDMC:CDMC at lower pressures prompts the following suggestion. Stereospecific CDMC formation by a reaction of DM[†] with *cis*-butene-2 may occur; a minor contribution of this kind would be more significant at lower pressures, where it provides a larger component of the total dimethylcyclopropanes because of the enhanced importance of reactions 6–11, and might account qualitatively for the observed lower pressure behavior.

Additional mention should be made of the discrepancy which exists between the low values of TDMC:CDMC found here and previous values which have appeared in the literature.^{4b,c,e} An important difference between the experimental conditions employed in this work and previous studies lies in the high ratio of *cis*-butene-2:DM used here which was 20:1 (TDMC:CDMC ~ 0.4). Other workers have used 1:10^{4b} (TDMC:CDMC ~ 6.7) through 2.5:1^{4e} (TDMC:CDMC ~ 0.8) to 4:1^{4c} (TDMC:CDMC ~ 1). In an attempt to test this possible relation between high *cis*-butene-2:DM reactant ratios and high TDMC:CDMC product ratios, experiments were performed in which the ratio of *cis*-butene-2:DM was decreased from 20:1 to 1:2; the TDMC:CDMC ratio increased to ~0.6, which is at least qualitatively con-

sistent.¹⁴ An explanation of the effect could again involve a reaction between DM[†] and *cis*-butene-2. The relative concentration of *cis*-butene-2 is decreased in going from 20:1 to 1:2 at constant pressure, and other processes of DM[†] are enhanced relative to its reaction with *cis*-butene-2. Although we are attracted to the suggested reaction between excited singlet DM[†] and *cis*-butene-2, in that such reaction helps rationalize three aspects of the data, a quantitative consistent interpretation on this basis does not seem at hand and this reaction must be considered speculative.

TDMC:CDMC as a Measure of ³CH₂ Proportion. It has been shown above that the experimental TDMC:CDMC ratio is a function of pressure even in this all-triplet system. This ratio has been employed by us^{2b} earlier as an indicator of the relative amount of ³CH₂ to ¹CH₂ reaction in ordinary ketene and DM photolysis systems. Our present results indicate that restrictions on the use of this (and similar) diagnostic

(13) Analysis was also made in this work for C₂H₄, C₂H₆, C₃H₆, C₃H₈, *n*-C₄H₁₀, and *trans*-C₄H₈-2. The data are not included here, but details may be found in ref 1b. In general, at both 23 and 56°, for both filtered and unfiltered light, the proportions of these lower products also decreased with increase of pressure. (The proportions of the total C₂-C₅ products at lowest and highest pressures were, respectively: ethylene, 43.4, 31.5%; ethane, 9.3, 4.7%; propene + propane, 5.3, 1.8%; *n*-butane, 3.4, 3.1%; and *trans*-butene-2, 6.3%, 4.1%.) This suggests that, at least in part, they too arise from decomposition reactions of excited C₅ species. All of these products (excluding *trans*-butene-2) were also found, to some extent, in blank runs that were made without substrate. Relative amounts of compounds which were formed in blank runs were: ethylene, 67.5%; ethane, 11.0%; propene, 3.4%; propane, 2.8%; cyclopropane, 1.1%; isobutane, 0.2%; *n*-butane, 0.6%; butene-1, 9.2%; 1,4-pentadiene, 1.1%; isopentane, 0.1%; neopentane, 0.1%; *n*-pentane, 0.2%; pentene-1, 1.4%; 3MB1, 0.1%; 2MB2, 1.1%; and 4-methylpentene-1, 0.1%. Excluding the ethylene product (which arises in considerable amount from the reaction of triplet methylene with DM), the C₅ products constituted approximately 56% of all C₂-C₅ products at low pressure and 80% at high pressure.

(14) A referee has suggested that the discrepancy between our data and that of others may be due, for example, to (our) analytical error. This may be so. However, we are willing to state categorically our belief that the chemistry and products of ³CH₂ systems are more complex than for ¹CH₂ systems and that high proportions of DM in triplet systems invite serious complications.

(15) NOTE ADDED IN PROOF: Experiments with *trans*-butene-2 reactant yielded: 3MB1, 4.4%; TDMC, 76.0%; TP2, 7.4%; CP2, 3.1%; CDMC, 8.2%; and 2MB2, 0.9%. These results for *cis*- and *trans*-butene-2 differ from F. S. Rowland (private communication) in regard to relative amounts of CDMC and TDMC products. Experiments on *cis*-butene-2-N₂ with an excess of added CO which removes ³CH₂ [B. A. DeGraff and B. G. Kistiakowsky, *J. Phys. Chem.*, **71**, 1553 (1967)] did not alter the proportions of CDMC and TDMC although the total C₅ yield was reduced; it seems that ¹CH₂ was not a major reaction component.

A liquid ³CH₂-*cis*-butene-2 system was produced by photolysis of DM at 23° in 200-fold excess of C₃F₈. The yields were: 3MB1, 6.1%; TDMC, 13.3%; 2MB1, 1.9%; TP2, 7.1%; CP2, 9.3%; CDMC, 60.4%; and 2MB2, 1.9%. These yields, which are characteristically "triplet," may be compared with the characteristically "singlet" products formed on photolysis of DM at 23° in neat liquid *cis*-butene-2: 3MB1, 0.2%; TDMC, 0.4%; 2MB1, 0.3%; TP2, 0.0%; CP2, 39.1%; CDMC, 47.5%; and 2MB2, 12.5%. These latter results also contrast with gas-phase results (in the absence of N₂) where some "triplet" product does arise.²

Evidently, in the presence of a liquid-phase interceptor, no inter-system crossing of excited singlet DM to a triplet surface occurs. The triplet products formed in liquid perfluoropropane can result from intersystem crossing by DM and obviously also by collisional deactivation of ¹CH₂.

ratios exist, namely, that the value of TDMC:CDMC depends on both the pressure of the system and the ratio of *cis*-butene-2:DM. This cautionary remark applies as well to much of the recent work in the literature on ordinary photolysis systems in which $^3\text{CH}_2$ has

been found. Our previous finding of an increase with pressure of the ratio TDMC:CDMC, up to a plateau or maximum, now may have an explanation other than the previously alleged variation of the $^3\text{CH}_2$: $^1\text{CH}_2$ proportion with pressure.¹⁵

Solvent-Dependent H-H Couplings in Hexachlorobicyclo[2.2.1]heptenes¹

by Stanford L. Smith and Richard H. Cox

Department of Chemistry, University of Kentucky, Lexington, Kentucky 40506 (Received June 29, 1967)

The solvent dependence of $^2J_{\text{HH}}$ and *cis* and *trans* $^3J_{\text{HH}}$ is investigated in 1,2,3,4,7,7-hexachlorobicyclo[2.2.1]heptenes substituted at the 5 position with chloro, cyano, phenyl, hydroxy, carboxyl, or acetate groups. In all six compounds, $^2J_{\text{HH}}$ decreased (in the absolute sense) in solvents of increasing dielectric constant. The magnitude of the change in $^2J_{\text{HH}}$ is similar for all compounds except the hydroxyl- and carboxyl-substituted cases where strong association effects are evident. Changes in $^3J_{\text{HH}}$ were 0.25 Hz or less in all cases. The general solvent effect (in the absence of specific association) is attributed to the solvent electric field which, in turn, is controlled by the net electric dipole of the solute molecule.

Introduction

The solvent dependence of spin-spin coupling constants in many relatively rigid molecules is now an established phenomenon whose causes and characteristics are rapidly being elucidated.^{2,3} Previous investigations have focused on geminal H-H and H-F couplings in sp^2 hybridized systems and on various single-bond couplings.^{4,5} Several examples of solvent-dependent vicinal couplings are also known, again in sp^2 hybridized systems.^{2,3,6-10} The solvent dependence of J_{gem} across C2 in 4-methyl-1,3-dioxolane² and the solvent dependence of J_{trans} in *dl*-dibromosuccinic anhydride¹¹ are the only known examples of solvent-dependent couplings in "rigid" sp^3 hybridized systems. In neither case are the results completely unambiguous. A number of investigators have noted an apparent solvent dependence of $^2J_{\text{HH}}$ in flexible systems such as 1,2-dichloro- and dibromopropanes,¹² various 1,1,2-trisubstituted ethanes,¹³ and 3,3-dimethylbutyl iodide.¹⁴ Unfortunately, it is not possible to determine whether these observed changes arise directly from some intrinsic solvent effect or indirectly from solvent-induced changes in conformer populations. In the latter event, changes in orientation of β substituents with respect to the methylene group would be expected¹⁵ to produce small changes in the geminal H-H coupling. The existence of these examples

raises potentially serious questions concerning the utilization of H-H (and H-F) couplings in the study of concentration and solvent effects on conformationally mobile systems. We therefore decided to examine the solvent dependence of $^2J_{\text{HH}}$ and *cis* and *trans* $^3J_{\text{HH}}$ in a rigid sp^3 hybridized system.

(1) A summary of this work was presented at the Southeastern Regional Meeting of the American Chemical Society, Louisville, Ky., Oct 1966.

(2) S. L. Smith and R. H. Cox, *J. Chem. Phys.*, **45**, 2848 (1966), and references therein.

(3) S. L. Smith and A. M. Ihrig, *ibid.*, **46**, 1181 (1967), and references therein.

(4) V. S. Watts and J. H. Goldstein, *J. Phys. Chem.*, **70**, 3887 (1966).

(5) H. M. Hutton, E. Bock, and T. Schaefer, *Can. J. Chem.*, **44**, 2772 (1966).

(6) R. H. Cox and S. L. Smith, *J. Mol. Spectry*, **21**, 232 (1966).

(7) S. L. Smith and A. M. Ihrig, *ibid.*, **22**, 241 (1967).

(8) H. M. Hutton and T. Schaefer, *Can. J. Chem.*, **43**, 3116 (1965).

(9) H. M. Hutton and T. Schaefer, *ibid.*, **45**, 1111 (1967).

(10) P. Laszlo and H. J. T. Bos, *Tetrahedron Letters*, 1325 (1965).

(11) L. E. Erickson, *J. Am. Chem. Soc.*, **87**, 1867 (1965).

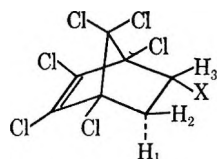
(12) H. Finegold, *J. Chem. Phys.*, **41**, 1808 (1964).

(13) E. I. Snyder, *J. Am. Chem. Soc.*, **88**, 1155 (1966).

(14) G. M. Whitesides, J. P. Sevenair, and R. W. Goetz, *ibid.*, **89**, 1135 (1967).

(15) A. A. Bothner-By in "Advances in Magnetic Resonance," Vol. 1, J. S. Waugh, Ed., Academic Press Inc., New York, N. Y., 1965, p 197.

The hexachlorobicyclo[2.2.1]heptenes, I, obtained from the Diels–Alder reaction of hexachlorocyclopentadiene with various monosubstituted olefins are ideally suited to our purpose. They have been studied previously by Williamson¹⁶ in an investigation of sub-



I, X = Cl, CN, C₆H₅, OAc, OH, CO₂H

stituent electronegativity effects on coupling constants and his results provide a check for our data. Williamson also discusses the evidence for the conformational rigidity of the bicyclo[2.2.1]heptene system.

These compounds also offer unique opportunities to clarify further the solute structural factors (other than gross hybridization) required for the solvent dependence of couplings. With rare exception¹⁷ all examples of solvent-dependent geminal H–H couplings in nondouble-bonded systems occur in molecules having a heteroatom bonded directly to the methylene group in question. Only one such case has been examined in detail.⁶ This characteristic is absent in the bicycloheptenes. Similarly, β substituents are known to affect the solvent dependence of $^2J_{HH}$ and $^3J_{HH}$ in olefins. The bicycloheptenes offer the opportunity to investigate analogous effects for sp^3 systems.

From a somewhat different viewpoint, these compounds offer some information concerning the nature of the solvent–solute interactions involved. Orientation of the solvent dipole has been shown to be a significant factor in the solvent–solute interaction(s) leading to the solvent dependence of $^2J_{HF}$. A similar dipole effect has been implicated in the solvent dependence of $^2J_{HH}$. The six chlorines located on “one side” of the hexachlorobicyclo[2.2.1]heptenes studied here provide an appreciable net dipole appropriately oriented¹⁸ to favor electron shifts away from hydrogen. If, in the absence of specific associations, the net dipole is important, then similar solvent variations should be observed for different X substituents. However, if local dipole effects are more important than the net dipole, then appreciable variations in the solvent dependence of $^2J_{HH}$ might be expected as X is changed.

The results reported below yield, at least, some information about all of these factors.

Experimental Section

The styrene, vinyl chloride, acrylonitrile, acrylic acid, and vinyl acetate Diels–Alder adducts of hexachlorocyclopentadiene were a gift from Hooker Electrochemical Co. Acid hydrolysis of the vinyl acetate adduct yielded the vinyl alcohol adduct.¹⁹ The vinyl acetate adduct was purified by vacuum distillation

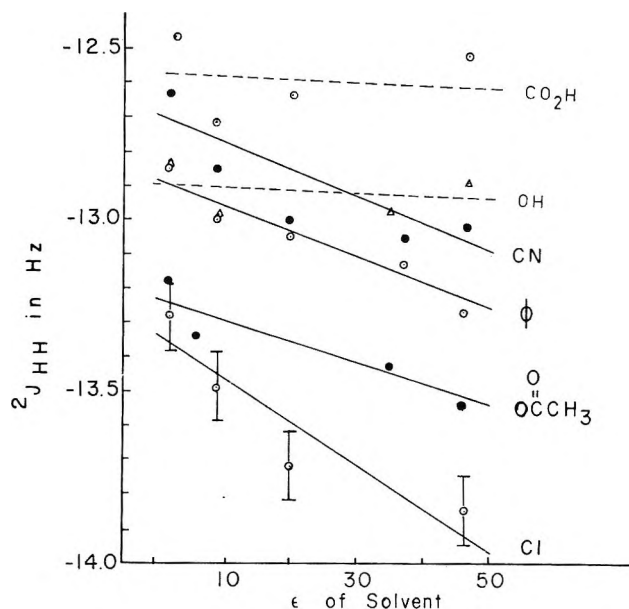


Figure 1. Plot of J_{gem} vs. solvent dielectric constant for substituted hexachlorobicyclo[2.2.1]heptenes. Vertical bars represent ± 0.1 Hz error limits.

and the remainder of the adducts were purified by vacuum sublimation. No solute impurities were observed in any of the nmr spectra. Spectro and reagent grade solvents were used without further purification. Solvent-impurity peaks were not encountered in any of the experimental spectra. Samples were prepared as 5 mole % solutions with approximately 3% tetramethylsilane (TMS) being added as internal reference and lock signal. All samples were degassed by the freeze-thaw technique and sealed under vacuum.

Spectra were obtained on a Varian HA-60-IL spectrometer operating in the frequency-sweep mode. Experimental line positions were obtained as the average of five or more independent scans and were calibrated by counting the difference in frequency of a peak from TMS with a Hewlett-Packard 521 CR frequency counter.

The proton nmr spectra of these adducts represents a slightly perturbed ABX system. Final parameters were calculated using the computer programs LAOC’N III and NMRIT. In all cases, the final parameters are good to 0.1 Hz or better (typical probable errors were 0.020–0.005 Hz).

Relative signs of the proton-coupling constants in the vinyl chloride adduct were determined using the technique of Freeman and Anderson.²⁰ Details of this decoupling work have been reported elsewhere.²¹

(16) K. L. Williamson, *J. Am. Chem. Soc.*, **85**, 516 (1963).

(17) H. M. Hutton and T. Schaefer, *Can. J. Chem.*, **41**, 684 (1963).

(18) Careful examination of Drieding models shows the dipole to lie roughly in a plane passing through the bridgehead carbons and approximately perpendicular to the plane of the bridge (C1, C7, C4).

(19) E. K. Fields, *J. Am. Chem. Soc.*, **78**, 5821 (1956).

Table I: Nmr Parameters at 60 MHz for 5-Substituted 1,2,3,4,7,7-Hexachlorobicyclo[2.2.1]heptenes in Various Solvents^a

Sub- stituent	Solvent	<i>E</i>	<i>J</i> ₁₂ (<i>gem</i>)	<i>J</i> ₁₃ (<i>trans</i>)	<i>J</i> ₂₃ (<i>cis</i>)	<i>V</i> ₁	<i>V</i> ₂	<i>V</i> ₃
Cl	C ₆ H ₁₂	1.99	-13.32	3.16	8.20	130.23	178.78	278.89
	CH ₂ Cl ₂	9.08	-13.49	3.09	8.16	137.79	186.98	287.54
	Me ₂ CO	20	-13.72	3.03	8.14	145.16	197.21	303.52
	DMSO	46	-13.85	2.97	8.19	147.46	192.33	310.55
		Max change	0.53	0.19	0.06			
CN	C ₆ H ₁₂	1.99	-12.63	4.10	9.15	137.54	168.90	216.08
	CH ₂ Cl ₂	9.08	-12.85	4.06	9.21	145.28	176.45	225.35
	Me ₂ CO	20	-13.00	4.02	9.11	160.62	186.97	252.73
	MeNO ₂	35	-13.05	3.99	9.23	154.03	184.12	238.55
	DMSO	46	-13.02	4.02	9.10	165.71	176.01	263.31
		Max change	0.42	0.11	0.12			
C ₆ H ₅	C ₆ H ₁₂	1.99	-12.85	4.27	9.16	144.20	169.04	234.34
	CH ₂ Cl ₂	9.08	-13.00	4.29	9.10	150.32	174.72	239.45
	Me ₂ CO	20	-13.05	4.19	9.12	159.31	179.13	245.54
	MeNO ₂	35	-13.13	4.37	9.12	156.32	178.37	244.50
	DMSO	46	-13.27	4.38	9.16	161.24	176.30	244.52
		Max change	0.42	0.19	0.06			
Acetate	C ₆ H ₁₂	1.99	-13.16	2.47	7.58	112.39	177.08	336.41
	C ₆ H ₅ Cl	5.6	-13.33	2.49	7.63	109.39	167.95	338.25
	C ₆ H ₅ NO ₂	32.2	-13.42	2.41	7.63	129.24	181.21	345.31
	DMSO	46	-13.54	2.48	7.68	136.90	181.91	339.77
		Max change	0.38	0.08	0.10			
CO ₂ H ^b	CCl ₄	1.99	-12.47	4.11	9.00	151.34	161.45	218.00
	CH ₂ Cl ₂	9.08	-12.71	4.12	9.07	152.76	164.72	222.49
	Me ₂ CO	20	-12.63	4.00	8.96	155.02	167.44	224.53
	DMSO	46	-12.51	3.95	8.82	148.68	162.67	220.04
		Max change	0.24	0.17	0.25			
OH ^b	C ₆ H ₁₂		-12.85	2.51	7.70	114.71	167.73	(278.5)
	CH ₂ Cl ₂	9.08	-12.98	2.48	7.72	119.39	173.59	(285.5)
	C ₆ H ₅ NO ₂	3.52	-12.96	2.36	7.58	128.77	178.67	301.45
	DMSO	46	-12.87	2.38	7.56	117.81	171.89	279.70
		Max change	0.13	0.15	0.16			

^a All values are given in hertzes from internal TMS. ^b Values for these substituents were obtained by an approximate solution; see text.

Results and Discussion

Final parameters for the nmr spectra of the adducts are given in Table I. With the exception of the vinyl alcohol and acrylic acid adducts (compounds where specific association is expected), there is a general correlation between *J*_{*gem*} and the solvent dielectric constant (Figure 1). In all cases, *J*_{*gem*} becomes more negative in solvents of increasing dielectric constant. A general correlation (with the exception of aromatic solvents) is observed between *J*_{*gem*} and the average of the chemical shifts of the two geminal protons for the styrene vinyl chloride, acrylonitrile, and vinyl acetate adducts.

The changes in the vicinal coupling constants, although quite small, are probably real. No correlation is evident between the vicinal coupling constants and any solvent parameters.

The vinyl alcohol and acrylic acid adducts present little useful information. Specific association is expected (*i.e.*, interaction of solvent with the OH in each case). In cyclohexane and methylene chloride, the X portion of the spectrum of the vinyl alcohol adduct

is broadened to such an extent that the individual lines of the quartet could not be measured accurately. Data given in Table I for the vinyl alcohol adduct in these two solvents were obtained from an ABX approximation²² using the AB portion of the spectrum. The chemical shift of the X proton in these cases is that estimated from the broad peak observed.

The minor changes observed in the vicinal couplings (if real) may be due either to general solvent effects or to very slight conformational changes in the bicyclo-[2.2.1]heptene skeleton. Thus, the generally accepted assumption that vicinal H-H couplings are not solvent dependent seems, for practical purposes, to be valid for the eclipsed conformation. There seems little reason to think the results would be significantly different for staggered conformations.

(20) R. Freeman and W. A. Anderson, *J. Chem. Phys.*, **37**, 2053 (1963).

(21) R. H. Cox and S. L. Smith, *J. Phys. Chem.*, **71**, 1809 (1967).

(22) J. W. Emsley, J. Feeney, and L. H. Sutcliffe, "High Resolution Nuclear Magnetic Resonance Spectroscopy," Pergamon Press Inc., New York, N. Y., 1965, p 357.

The measurable decrease (in the absolute sense) of J_{gem} for the chloro-, cyano-, phenyl-, and acetate-substituted compounds in solvents of increasing dielectric constant supports the previously noted correlation between the absolute sign and solvent-induced variations of geminal couplings. The magnitudes of the solvent-induced changes are about the same in these four compounds and are similar to effects observed previously. This suggests that hybridization of the carbon in the CH_2 group is not a major factor in controlling the solvent dependence of J_{gem} . It also suggests that the solvent-dependent geminal couplings observed in flexible systems arise primarily from a direct solvent effect, not from conformational changes. The smaller changes observed in the hydroxyl and carboxyl compounds undoubtedly reflect the effect of association at the β position, causing "appreciable" electronic and/or conformational changes in the molecule. Otherwise, the solvent-induced variation of J_{gem} across sp^3 hybridized carbons seems to be relatively insensitive to substituent variations of the β position.

The similarity in magnitude between the changes observed here where the CH_2 group has no heteroatom bonded to it and those changes observed in previous examples where there has been a heteroatom bonded to the CH_2 group is significant. Acidic (hydrogen-bonding) solvents are not likely to interact with an essentially aliphatic CH_2 group. Similarly, an aliphatic CH_2 group should not hydrogen bond appreciably to basic solvents. Therefore, *specific donor-acceptor interactions in the immediate vicinity of the CH_2 group are not a fundamental requirement for the existence of solvent effects on geminal coupling constants.* This is not to say that specific interactions do not cause coupling-constant variations. There is abundant evidence that they do. Rather, we wish to emphasize the existence of a general bulk solvent effect. The similarity in magnitude of the changes in J_{gem} for different β substituents implies that the net solute dipole (or at least the over-all electrical asymmetry of

the solute molecule) is more important than local dipoles or local electron distributions. This conclusion, in turn, implies that the bulk solvent effect is due to a solvent electric field whose magnitude and direction depend on the solute dipole orientation. Whether the solvent electric field arises from polarization of adjacent solvent molecules (reaction field effect), from momentary partial orientation of adjacent solvent molecules (dipole-dipole interactions, solvent Stark effects), from an unequal distribution of solvent molecules in the solvation shell, or, as seems most likely, from some combination of such phenomena cannot now be specified.

In summary, these results for the sp^3 hybridized system essentially complete a tableau as far as ϵ solute structural factors are concerned. Geminal H-H coupling constants are apparently all solvent dependent, regardless of the hybridization of the carbon involved. The only question remaining is the magnitude of the observed change which depends on the structure of the solute and on the particular solvents used.³ Vicinal H-H coupling constants may exhibit solvent dependence in a few cases. Neither the solute structural requirements nor the nature of the solvent-solute interactions necessary for solvent dependence of vicinal couplings is presently known, but the expected changes (if any) are likely to be smaller than those observed for geminal couplings. One fact, noted recently by Watts and Goldstein,⁴ is becoming increasingly apparent. Solvent-dependent coupling constants offer an extremely sensitive and unique probe for the examination of both weak solvent-solute interactions and electron redistributions within molecules in solution. Utilization of this phenomenon for such investigations should lead to significant refinement of our present theories in these areas.

Acknowledgments. The authors wish to thank the Hooker Chemical Co. for providing the compounds studied here. The financial assistance of the University of Kentucky computer is gratefully acknowledged.

Sublimation of Ammonium Perchlorate

by P. W. M. Jacobs¹ and A. Russell-Jones

Department of Chemistry, Imperial College, London, England (Received June 30, 1967)

The kinetics of the sublimation of ammonium perchlorate has been investigated over a wide range of temperatures at pressures ranging from the vapor pressure up to 1 atm. A model for the sublimation of ammonium perchlorate, which takes account both of surface diffusion and of diffusion through the gas phase, has been formulated, and a new equation describing the kinetics of sublimation has been developed. This theory is in excellent agreement with the experimental data. The evaporation coefficient, β , is strongly pressure dependent, indicating the importance of surface diffusion in the evaporation process.

I. Introduction

The first comprehensive study of the thermal decomposition of ammonium perchlorate (AP) to be published was that by Bircumshaw and Newman.^{2,3} These authors showed that at temperatures below about 300°, AP decomposes to a limited extent ($\sim 30\%$) leaving a residue which is itself AP, apparently identical chemically with the starting material but having a larger specific surface area.⁴ If the temperature is raised, sublimation of this residue occurs. Bircumshaw and Phillips⁵ made a limited study of the sublimation process and deduced from their data an activation energy for the rate of sublimation of ~ 21 kcal/mole. If the pressure of an inert gas in the reaction vessel is increased, sublimation is replaced by thermal decomposition. Galwey and Jacobs⁶ proposed that the mechanism of this thermal decomposition was dissociation of the AP into NH_3 and HClO_4 , followed by their evaporation into the gas phase, and subsequent decomposition of the perchloric acid and oxidation of ammonia in the gas phase. From their kinetic measurements,⁶ an activation energy of ~ 39 kcal/mole was deduced, but as the reaction was followed by pressure measurements, it was not clear whether the sublimation process or the gas-phase reactions were rate determining. We have therefore reinvestigated the kinetics of the sublimation and thermal decomposition of AP using the technique of weight-loss measurements. Results for the low-temperature decomposition have been described in another publication;⁷ in this paper we discuss the sublimation of the AP residue.

II. Experimental Procedure

Galwey and Jacobs⁶ had found that the rate of the thermal decomposition of AP was unaffected by the presence of molecular oxygen, and so the rate measurements at 1 atm were performed in air using a Stanton thermogravimetric balance. Measurements of weight loss under controlled atmospheres and at subatmospheric pressures were performed by measuring with a

cathetometer the change in extension of a calibrated silica spiral spring from which a compressed pellet of AP was suspended. The sensitivity of the spring was 1 mm/mg. The AP was supported on a platform suspended from the spring by a straight length of fused quartz, which passed through a short length of 3-mm capillary tubing. The side arm, through which pumping was effected, was located adjacent to the capillary and this arrangement prevented the condensation of sublimate onto the spiral. All taps and joints were greased with silicone grease. The cylindrical furnace around the reaction vessel was sited so that the AP was located in the center of the zone of constant temperature and its position was adjusted periodically during the run to maintain this position. [Pellets of 40 mg were generally used so that the change in position of the platform support during a run amounted to about 4 cm.] The low-temperature reaction was allowed to proceed to completion, first, with the system open to atmosphere to reduce sublimation to a minimum. The system was then isolated, the pressure and temperature adjusted to the required values, and the change in weight of the AP followed.

Reagent-grade AP from British Drug Houses (BDH) or Matheson Coleman and Bell (MCB) was used as received. Pellets were formed in a cylindrical stainless steel press of 3-mm bore.

III. Results

The curves for the fractional decomposition (α) of

(1) Department of Chemistry, University of Western Ontario, London, Ontario, Canada.

(2) L. L. Bircumshaw and B. H. Newman, *Proc. Roy. Soc. (London)*, **A227**, 115 (1954).

(3) L. L. Bircumshaw and B. H. Newman, *ibid.*, **A227**, 228 (1955).

(4) A. K. Galwey and P. W. M. Jacobs, *ibid.*, **A254**, 455 (1960).

(5) L. L. Bircumshaw and T. R. Phillips, *J. Chem. Soc.*, 4741 (1957).

(6) A. K. Galwey and P. W. M. Jacobs, *ibid.*, 837 (1959).

(7) J. V. Davies, P. W. M. Jacobs, and A. Russell-Jones, *Trans. Faraday Soc.*, **63**, 1737 (1967).

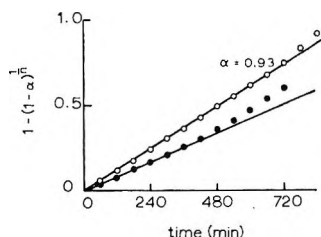


Figure 1. Test of the applicability of eq 1 and 2 to the sublimation of AP at 304°: O, eq 1; ●, eq 2.

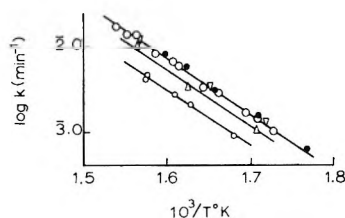


Figure 2. Arrhenius plots for the sublimation of AP, using rate constants derived from eq 2: ●, MCB AP (40-mg pellets); O, BDH AP (40-mg pellets); ▽, twice recrystallized BDH AP (40-mg pellets); Δ, BDH AP (70-mg pellets); O, BDH AP (100-mg pellets).

residue against time (t) under 1 atm of air were deceleratory in the temperature range 304–375°. If a reaction occurs on the surface at a rate proportional to the surface area and propagates inwardly at a rate $a_0 k$, where a_0 is the initial value of some characteristic size parameter (*e.g.*, the radius for a sphere of reactant), then the kinetics should conform to the contracting-volume expression

$$1 - (1 - \alpha)^{1/3} = kt \quad (1)$$

Figure 1 shows that this equation only applies over the first two-thirds of the reaction. Empirically, the exponent was altered from $1/3$ to $1/2$ when a much better representation of the data, up to $\alpha = 0.93$, was obtained. The modified equation

$$1 - (1 - \alpha)^{1/2} = kt \quad (2)$$

was therefore used to analyze the high-temperature data. Plots of $\log k$ vs. T^{-1} are shown in Figure 2. These illustrate that k is independent of the source and chemical purity of the AP, but that the rate constant decreases as the mass of the reactant is increased. The activation energy, E , is 30.6 kcal/mole. The higher value for E , found from pressure measurements, indicates that gas-phase reactions are rate determining in this temperature range and, therefore, that the rate process being followed by measurements of weight loss, is *sublimation* under 1 atm of air.

Sublimation rates under vacuo were measured, using the quartz spiral spring. The data are well fitted by eq 1 up to, at least, $\alpha = 0.90$. The applicability of this equation is illustrated in Figure 3. The activation energy is 30.0 kcal/mole. The pressure dependence of

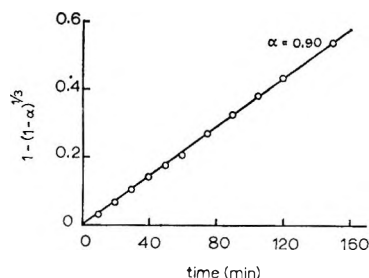


Figure 3. Test of the applicability of eq 1 to the vacuum sublimation of AP at 247.5°.

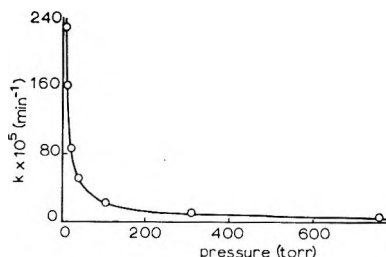


Figure 4. Variation of the sublimation rate constant k [from eq (1)] with the ambient pressure of inert gas, P .

the sublimation rate was measured at 270°. The results (Figure 4) show that there is a dramatic decrease in the rate constant [obtained from eq 1] as the pressure, P , of nitrogen is increased, but that at higher pressures the rate tends toward a constant value. The total decrease in rate as the total pressure is increased from the equilibrium pressure of AP to 1 atm is about 200-fold

IV. Theory

The sublimation of ammonium perchlorate has been found empirically to fit either of two equations, both being of the general form

$$1 - (1 - \alpha)^{1/\gamma} = kt \quad (3)$$

For vacuum sublimation, $\gamma = 3$, but as the pressure, P , of inert gas is increased, $\gamma = 2$ gives a better description of the data. We now examine the theoretical basis for these equations. The AP pellets were small cylinders, 3 mm in diameter and about 3 mm high. Since these dimensions are much smaller than those of the reaction vessel, no great error should result from approximating the shape to a sphere of radius a . Let n be the concentration (in molecules/cm³) of the subliming species at a distance r from the center of the AP, and let n_1 be the (uniform) concentration of inert gas. Sublimation of AP is dissociative but, in the steady state, the flux of ammonia through the gas phase must equal that of perchloric acid: $J_A = -D_A(\partial n_A/\partial r) = J_P = -D_P(\partial n_P/\partial r)$. It is convenient, therefore, to think of an effective mean flux, J , mean concentration gradient, $\partial n/\partial r$, and mean diffusion coefficient,

cient, D . Then because of the assumed spherical symmetry

$$\frac{\partial n}{\partial t} = -\text{div } J = \frac{D}{r^2} \frac{\partial}{\partial r} \left(r^2 \frac{\partial n}{\partial r} \right) \quad (4)$$

In the steady state, $\partial n / \partial t = 0$, so that the diffusion equation (4) has the solution

$$n = A + \frac{B}{r} \quad (5)$$

If the boundary conditions

$$\begin{aligned} n &= 0 \text{ at } r = \infty \\ n &= n_0 \text{ at } r = a \end{aligned} \quad (6)$$

are imposed, then the flux is

$$J = D n_0 / r^2 \quad (7)$$

and the rate of sublimation becomes

$$Q = -\frac{dN}{dt} = -\frac{1}{m_0} \frac{dw}{dt} = 4\pi D n_0 \quad (8)$$

where n_0 is the concentration of subliming species in the gas phase in equilibrium with the solid, N is the number of molecules of AP in the solid, m_0 is the mass of one molecule of AP, and w is the mass of the AP pellet. Equation 8 is essentially the sublimation equation of Stefan,⁸ Maxwell,⁹ and Langmuir.¹⁰

It is well known that eq 8 leads to an absurdity for spheres of very small radii; the rate of sublimation per unit area is

$$Q/4\pi a^2 = D n_0 / a \quad (9)$$

which tends to ∞ as $a \rightarrow 0$. The cause of this catastrophe is the assumption that the macroscopic diffusion equation (4) holds right up to the surface of the subliming solid [see (6)]. This difficulty was resolved by Fuchs,¹¹ who modified the Stefan-Maxwell formula (8) in the following way. If the molecules evaporating from the solid surface were unaffected by the molecules in the gas phase in any way, then the rate of sublimation, once equilibrium was attained, would be

$$Q = (4\pi a^2) \left(\frac{1}{4} \beta n_0 \bar{c} \right) \quad (10)$$

where β is the evaporation coefficient and \bar{c} is the mean velocity of the subliming molecules in the gas phase. Let the concentration in the gas phase at a distance Δ from the surface be $n^* < n_0$; the diffusion flux at $r = a + \Delta$ is then

$$J = D n^* / (a + \Delta) \quad (11)$$

and this must equal the net rate of arrival, per unit area, of subliming molecules at $r = a + \Delta$

$$\left[\frac{1}{4} a^2 \beta \bar{c} / (a + \Delta)^2 \right] (n_0 - n^*) \quad (12)$$

The Fuchs model thus considers that molecules will evaporate from the surface as though unaffected by the molecules in the gas phase, but after they travel a distance Δ , of the order of the mean free path, they start to undergo collisions and the macroscopic diffusion equation (4) applies, but with the modified boundary conditions

$$\begin{aligned} n &= 0 \text{ at } r = \infty \\ n &= n^* \text{ at } r = a + \Delta \end{aligned} \quad (6')$$

If eq 8 and 9 are solved for n^* and the result is substituted in eq 11, the rate of sublimation is given by

$$Q = 4\pi(a + \Delta)^2 J = \frac{4\pi D a n_0}{\frac{D}{a\beta\nu} + \frac{a}{a + \Delta}} \quad (13)$$

where ν has been written for $\bar{c}/4$. Note that eq 13 degenerates to eq 10, when $\Delta \gg a$, and to eq 8 when $a \gg \Delta$ and also $a \gg D/\beta\nu$. If $a \gg \Delta$, but no assumption is made as to the validity of the second inequality, $a \gg D/\beta\nu$, then eq 13 reduces to

$$Q = \frac{4\pi D a n_0}{1 + \frac{D}{a\beta\nu} \left(1 - \frac{\Delta\beta\nu}{D} \right)} \quad (14)$$

We anticipate that Δ should be of the same order as the mean free path of the subliming molecules

$$\Delta \simeq \frac{3\pi}{16} \left(\frac{D}{2\nu} \right) \quad (15)$$

The substitution (15) reduces eq 14 to

$$Q = \frac{4\pi D a n_0}{1 + \frac{D}{a\beta\nu} \left(1 - \frac{3\pi\beta}{32} \right)} \quad (16)$$

Apart from the factor $3\pi/16 \simeq 1/2$, eq 16 is the sublimation equation of Monchick and Reiss,¹² who used a nonequilibrium velocity distribution function. The experimental evidence does not permit an unequivocal decision on the correct form for Δ , although an analysis by Wright¹³ suggests that $\Delta = D/2\nu$ without the factor $3\pi/16$ is marginally the better expression for the evaporation of liquids. Therefore, for the present, we shall retain Δ as an unidentified parameter.

(8) J. Stefan, *Wien. Ber.*, **68**, 385 (1874); **83**, 545, 943 (1881); **98**, 1410 (1889).

(9) J. C. Maxwell, "Scientific Papers," Vol. 2, Cambridge University Press, London, 1890, p 638.

(10) I. Langmuir, *Phys. Rev.*, **12**, 368 (1918).

(11) N. A. Fuchs, *Physik. Z. Sowjetunion* **6**, 224 (1934); R. S. Bradley, M. G. Evans, and R. W. Whytlaw-Gray, *Proc. Roy. Soc. (London)*, **A186**, 368 (1946).

(12) L. Monchick and H. Reiss, *J. Chem. Phys.*, **22**, 831 (1954).

(13) P. G. Wright, *Discussions Faraday Soc.*, **30**, 100 (1960).

Let a_0 denote the initial radius at $t = 0$, and α the fraction sublimed at time t so that

$$1 - \alpha = a^3/a_0^3 \quad (17)$$

Substituting $(-4\pi a^2 \rho m)(da/dt)$ for Q in eq 13 gives a differential equation which is integrable by elementary methods; on using eq 17, the result is

$$\frac{\Delta}{a_0} \left\{ \frac{D}{\nu \beta \Delta} - 1 \right\} \left\{ 1 - (1 - \alpha)^{1/3} \right\} + \frac{1}{2} \left\{ 1 - (1 - \alpha)^{2/3} \right\} + \left(\frac{\Delta}{a_0} \right)^2 \ln \left\{ \frac{(1 - \alpha)^{1/3} + \frac{\Delta}{a_0}}{1 + \frac{\Delta}{a_0}} \right\} = \frac{D m n_0 t}{a_0^2 \rho} \quad (18)$$

This is an equation describing the kinetics of sublimation, which is of the form $\alpha(X_1, X_2, X_3, t) = 0$, where X_1, X_2, X_3 are the three parameters

$$\begin{aligned} X_1 &= \Delta/a_0 \\ X_2 &= (D/\nu \beta \Delta) - 1 \\ X_3 &= D m n_0 / a_0^2 \rho \end{aligned} \quad (19)$$

Equation 18 is not amenable to testing by plotting some simple function of α against t , except in certain limiting situations. Therefore a computer program was written which, using the usual least-mean-squares criterion, found the values of X_1, X_2, X_3 , giving the best fit of the equation to the experimental data.

V. Comparison with Experimental Data

That eq 18 can provide an excellent fit to the experimental data is illustrated by Figures 5 and 6. Unfortunately it is not possible, however, to determine the individual values of the three parameters with equal precision over the whole range of pressure and temperature. The third term on the left-hand side of eq 18 only contributes significantly when Δ is of the same order as a_0 . This means that, except over a narrow pressure range, only the product $X_1 X_2$ can be determined, the least-squares procedure being insensitive to the individual values of X_1 and X_2 . Furthermore, at very low pressures, $\Delta \gg a_0$, $X_1 X_2 \gg 0.5$, and eq 18 degenerates into the "contracting volume" formula, eq 1, with

$$k = \frac{X_3}{X_1 X_2} = \frac{D m n_0}{a_0 \rho \Delta \left(\frac{D}{\nu \beta \Delta} - 1 \right)} \quad (20)$$

At moderate pressures of inert gas, $P \sim 1$ atm, $\Delta \ll a_0$, and $X_1 X_2$ is of the same order as the coefficient of the second term, 0.5. Thus both terms contribute, more or less equally, explaining the fall in the value of γ when the empirical equation (3) is used to describe the kinetics of sublimation. The value $\gamma = 2$, found empirically, is clearly a compromise between the exponents of the

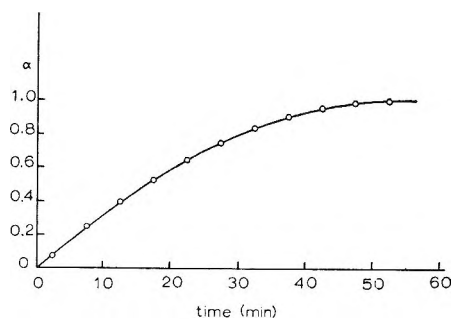


Figure 5. Test of the applicability of eq 18 to the sublimation of AP under 1 atm pressure of nitrogen at 375°: —, theory; O, experiment.

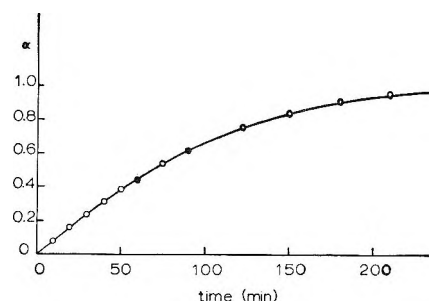


Figure 6. Test of the applicability of eq 18 to the vacuum sublimation of AP at 241°: —, theory; O, experiment.

factor $1 - \alpha$ in the first two terms in eq 18. The observed mass dependence of the sublimation rate (Figure 1) is also in accordance with eq 18, in view of the factor a_0^{-2} in the coefficient of t .

At moderate pressures, X_3 and $X_1 X_2$ can be determined separately. The only temperature-dependent factors in X_3 are n_0 and D . In the absence of detailed information about the intermolecular forces, we take the approximate expression for the coefficient of mutual diffusion

$$D = \frac{3}{8\sigma^2(n_1 + n)} \left(\frac{kT}{2\pi\mu} \right)^{1/2} \quad (21)$$

At 1 atm of pressure $n_1 \gg n$ and since $n_1 = P/kT$, $D \propto T^{3/2}$. Also $n_0 = p/kT$, where p is the partial pressure of ammonia, or perchloric acid, in equilibrium with AP, and

$$\frac{\partial \log p}{\partial T^{-1}} = - \frac{\Delta H}{2 \times 2.303R} \quad (22)$$

where ΔH is the heat of sublimation per mole of AP. The plot of $\log (X_3/T^{1/2})$ against T^{-1} should therefore be linear with the negative slope of $\Delta H/(2 \times 2.303R)$. This prediction is well fulfilled by the data, the least-squares value for $1/2\Delta H$ being 30.4 kcal/mole, which is in good agreement with the value found from an analysis of relevant thermodynamic data by Pearson¹⁴

(14) G. S. Pearson, *Advan. Inorg. Chem. Radiochem.*, **8**, 177 (1966).

(29.2 kcal/mole) and also with the value of 29 ± 1 kcal/mole, derived from direct measurements of the equilibrium dissociation pressure by Inami, Rosser, and Wise.¹⁵

The evaporation coefficient β can be calculated from X_1X_2 . From eq 19

$$X_1X_2 = \frac{\Delta}{a_0} \left(\frac{D}{\nu\beta\Delta} - 1 \right) \quad (23)$$

Since $\Delta \sim D/2\nu$, to within, at worst, a factor of 2, the term in parentheses is $(2/\beta) - 1$; anticipating that β will be $\ll 1$ when sublimation is dissociative,¹⁶ we calculate β from $D/\nu a_0 X_1X_2$ to be $\sim 5 \times 10^{-4}$. This is an average value over the temperature range 577–648°K, no temperature dependence of X_1X_2 having been detected over this range.

For the sublimation of AP under its own vapor pressure, the theory predicts [eq 20] that the plot of $\log(T^{1/2}X_3/X_1X_2)$ should be linear with slope $-1/2\Delta H/(2.303R)$. A least mean-squares analysis gives $1/2\Delta H = 29.6$ kcal/mole, in excellent agreement with the thermodynamic¹⁴ and vapor pressure¹⁵ values, and with the sublimation value found above from X_3 . If we again make the approximation of assuming $2/\beta \gg 1$, then eq 20 reduces to

$$k \simeq \frac{\nu\beta mn_0}{a_0\rho} \quad (24)$$

from which β may be calculated. The group of terms X_3/X_1X_2 may be determined with greater precision than the individual parameters, and hence there is less scatter in β , the mean value for vacuum sublimation being 0.041 ± 0.006 . The error introduced by the approximation (about 2%) is thus much less than the mean deviation and so a more accurate calculation, involving a substitution for Δ , is hardly justified.

The data for sublimation under various pressures of nitrogen at 270° were also well fitted by eq 18. Values of the evaporation coefficient determined by both of the

above methods appear in Table I. The measure of agreement is encouraging since, while neither method requires more than an order-of-magnitude knowledge of Δ (β being small enough to justify the neglect of unity in comparison with $D/\nu\beta\Delta$), X_1X_2 involves D , but not the vapor pressure, whereas the reverse is true for X_3/X_1X_2 .

Values of X_3 were also calculated at 270° from eq 19 and these are compared in Table II with the computed values obtained by fitting the experimental data to eq 18. At low pressures, $X_1X_2 \gg 0.5$ and so excellent agreement cannot be expected. Even so, this being an absolute calculation with no unknown parameters, the measure of agreement is impressive.

Table II: Values of X_3 Calculated from Eq 19 and from the Experimental Sublimation Data

P, torr	$X_3 \times 10^4, \text{ min}^{-1}$	
	Calcd	Exptl
7.75	67.6	75.1
11.0	47.8	61.1
22.0	24.1	31.4
38.0	13.9	15.5
105.0	5.05	4.97
312.0	1.70	2.07
760.0	0.69	1.16

VI. Discussion

Analysis of experimental data described in section V shows the sublimation of AP can be described very adequately in terms of Fuchs' ideas.¹¹ The new kinetic equation (18) represents the data satisfactorily and explains why the empirical laws (1) and (2) fit the experimental data in certain pressure and temperature regimes. The evaporation coefficient varies from about 4×10^{-2} for sublimation *in vacuo* to about 5×10^{-4} for sublimation under 1 atm. This can be understood in terms of the following model for the sublimation process.

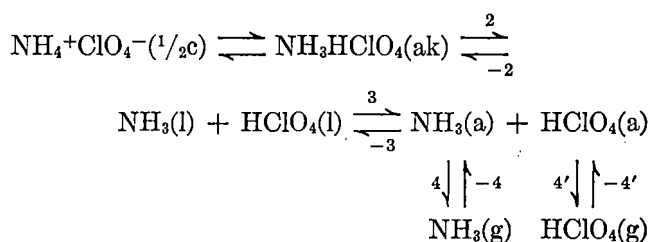
The process commences by the transfer of a proton from an NH_4^+ ion to a ClO_4^- ion at surface kink site. The NH_3 and HClO_4 molecules formed remain adsorbed at these positions for a finite time, but unless they can diffuse away to become adsorbed on separated sites away from the surface step, the proton-transfer process will reverse itself. The evaporation process is then completed by the desorption of NH_3 and HClO_4 molecules into the gas phase. This whole process may be represented by

Table I: Values of the Evaporation Coefficient, β , for (a) Vacuum Sublimation and (b) Sublimation under Various Pressures of Nitrogen at 270°

(a)		(b)		
T, °K	β	P, torr	β , from X_1X_2	β , from X_3/X_1X_2
491	0.0398	7.75	0.01007	0.00883
496	0.0417	11.0	0.00844	0.00824
502	0.0412	22.0	0.00504	0.00509
507	0.0368	38.0	0.00278	0.00274
514	0.0476	105	0.00129	0.00128
520	0.0392	312	0.00087	0.00082
528	0.0500	760	0.00020	0.00042
536	0.0414			
543	0.0294			
Mean = 0.041 ± 0.006 .				

(15) S. H. Inami, W. A. Rosser, and H. Wise, *J. Phys. Chem.*, **67**, 1077 (1963).

(16) A. P. Hardt, W. M. Foley, and R. L. Brandon, *Astronaut. Acta*, **11**, 340 (1965).



where $\frac{1}{2}\text{c}$ denotes the half-crystal site, ak the state in which the molecules are adsorbed at the kink site, l where the molecules are adsorbed at ledge sites, and a where they are adsorbed on any site on the plane surface. The importance of the ledge sites arises from the fact that it will be easier energetically for the adsorbed molecules to leave the half-crystal position by diffusing along the ledge rather than by being ejected directly onto the plane surface. The various sites involved are shown schematically in Figure 7. Clearly the reverse steps will be involved in condensation.

The importance of surface diffusion is shown by the observed pressure dependence of β . As the pressure of nitrogen is increased, nitrogen molecules will be adsorbed on the AP surface and the first sites to be affected will be just those sites (e in Figure 7) which are adjacent to kink sites. The diffusion of NH_3 and HClO_4 molecules from kink sites to ledge sites will thus be impeded. It therefore seems natural to write

$$\beta = k_1(1 - \theta) + k_2 \quad (25)$$

where k_1 relates to the diffusion to ledge sites and k_2 ($k_1 \gg k_2$) to the direct diffusion from kink sites to a sites (Figure 7). The fraction of e sites covered by adsorbed nitrogen molecules is θ . Then as $P \rightarrow 0$, $\theta \rightarrow 0$, and $\beta \rightarrow k_1 + k_2$, while as $P \rightarrow \infty$, $\theta \rightarrow 1$, and $\beta \rightarrow k_2$. The constants $k_1 + k_2$ and k_2 can therefore be found from the values of β for vacuum sublimation and for sublimation under high pressures of inert gas. The latter value is 4×10^{-4} , as found by a short extrapolation of the plot of β vs. P^{-1} to infinite pressure, and as $\beta = 0.0294$ for vacuum sublimation at 543°K , $k_1 \simeq 0.029$. Rearranging eq 25 and assuming a Langmuir adsorption isotherm for θ , P gives

$$1 - \frac{\beta - k_2}{k_1} = \theta = \frac{\chi(T)P}{1 + \chi(T)P} \quad (26)$$

where $\chi(T)$ is the product of the vibrational partition function of the adsorbed molecule $q(T)$, $\lambda_0(T)$ the absolute activity a nitrogen molecule in the gas phase at the standard pressure, and $e^{-u_0/kT}$, where u_0 is the potential energy of a nitrogen molecule adsorbed on an e site referred to that of a similar molecule at rest in the

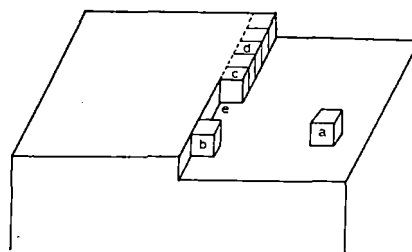


Figure 7. Schematic representation of the evaporation of AP: a, molecules adsorbed on the plane surface; b, molecules adsorbed at ledge sites; c, kink site (the half-crystal position); d, ions; e, favored sites for adsorption.

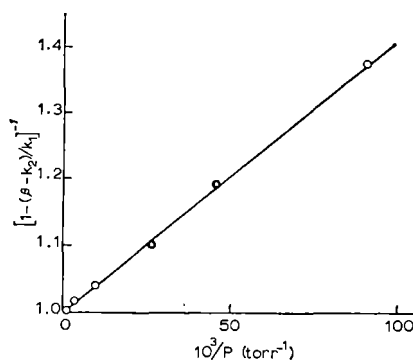


Figure 8. Test of eq 27 for the pressure dependence of β . The means by which the constants k_1 and k_2 are evaluated is explained in the text.

infinitely dilute gas as zero. Notice that θ refers to adsorption on e sites only and that u_0 (which is a negative quantity) will be several times larger in magnitude than the corresponding quantity for a sites. Equation 26 predicts that $[1 - (\beta - k_2)/k_1]^{-1}$ should be a linear function of P^{-1} , and this is confirmed by the data plotted in Figure 8.

With endothermic processes such as sublimation, one has to bear in mind the possibility of self-cooling. In connection with the thermal decomposition studies,⁶ it became necessary to correct for the weight loss due to sublimation, and so the sublimation rate under 730 torr of nitrogen was measured down to very low temperatures. These data agreed well with the extrapolation of the high-temperature data reported here and the constant activation energy for a variation in $\log k$ covering more than three decades is not to be expected if self-heating is affecting the data significantly.

Acknowledgment. We are grateful to the United Kingdom Ministry of Aviation and to the Canadian National Research Council for their support of this work.

Complexes in Calcium Phosphate Solutions¹

by A. Chughtai, R. Marshall, and G. H. Nancollas

Chemistry Department, State University of New York at Buffalo, Buffalo, New York 14214
(Received July 3, 1967)

Potentiometric measurements have been used to determine the association constants for the formation of the complexes $\text{CaH}_2\text{PO}_4^+$, CaHPO_4 , and CaPO_4^- in solutions of calcium phosphate at 25.0 and 37.0°. Approximate values of the thermodynamic functions for the association reactions are presented.

The solubilities of the various forms of calcium phosphate have been the subject of frequent study, but surprisingly little detailed work has been done in order to characterize the complex species present in solutions of this important biological mineral. A number of surface complexes, proposed from the results of solubility studies with hydroxyapatite,² have been invoked in an attempt to learn more about the growth and dissolution of bone and tooth enamel. The interpretation of such solubility data, however, is markedly dependent upon the nature and concentrations of the species present in the solutions.

Greenwald and co-workers³ were the first to recognize that the pH of solutions containing hydrogen phosphates was lowered upon the addition of calcium ions, and they calculated an association constant, $K^\circ = [\text{CaHPO}_4]/[\text{Ca}^{2+}][\text{HPO}_4^{2-}]$, of 300 l. mole⁻¹ at an ionic strength of 0.006 and at about 22°. The existence of the species CaHPO_4 was later confirmed by Gosselin and Coghlan⁴ from ion-exchange studies involving Ca^{45} . Davies and Hoyle⁵ proposed $\text{CaH}_2\text{PO}_4^+$ as the major species in calcium phosphate solutions at pH 4.54–5.17 with a thermodynamic association constant, $K^+ = [\text{CaH}_2\text{PO}_4^+]/[\text{Ca}^{2+}][\text{H}_2\text{PO}_4^-]$, lying between 11 and 12 l. mole⁻¹; their value for K° was 471–625 l. mole⁻¹ and the pH measurements were made colorimetrically. Greenwald recalculated these results⁶ and obtained $K^\circ = 230$ –982 l. mole⁻¹. The results of recent solubility studies at 37.5°, by Moreno, Gregory, and Brown⁷, of dicalcium phosphate, $\text{CaHPO}_4 \cdot 2\text{H}_2\text{O}$, in phosphoric acid solutions at pH values between 3.5 and 6.8 have been interpreted in terms of $K^\circ = 588 \pm 31$ l. mole⁻¹ at this temperature.

In view of the lack of agreement in the reported association constants, it was thought desirable to study the system by means of a precise potentiometric method over a wide range of pH. By careful control of concentrations and experimental technique, it has been possible to prepare solutions of calcium phosphate which are appreciably supersaturated and stable for at least 1 day. This has enabled potentiometric measurements to be made over a much wider range of concentration

than was previously thought possible, and, for the first time, the species CaPO_4^- has been characterized from the results of measurements at high pH.

Experimental Section

AR reagents and grade A glassware were used, and carbon dioxide was excluded from all solutions by bubbling nitrogen through the solution. Calcium chloride solutions were standardized by passing through Dowex 50-W ion-exchange resin in the hydrogen form and titrating the liberated hydrochloric acid with sodium hydroxide. Emf measurements were made at 25 ± 0.02 and $37 \pm 0.03^\circ$ with cells of the type glass electrode–solution under study–1.0 M KCl– Hg_2Cl_2 , Hg using a Beckman Research or Corning Model 12 pH meter and Beckman Type 41263 glass electrode; reproducibility was ± 0.1 mv. Each cell incorporated a pair of glass electrodes so that any irregularity in the behavior of one of them was immediately apparent. The electrode systems were standardized before and after each experiment with NBS standard buffer solutions, prepared according to Bates.⁸ 0.01 M hydrochloric acid + 0.09 M potassium chloride, pH 2.098 at 25°; 0.05 M potassium tetroxalate, pH 1.679 at 25° and 1.690 at 37°; 0.05 M potassium hydrogen phthalate, pH 4.008 at 25° and 4.028 at 37°; 0.025 M KH_2PO_4 + 0.025 M Na_2HPO_4 , pH 6.865 at 25° and 6.841 at 37°; 0.01 M sodium borate, pH 9.180 at 25° and 9.08 at 37°. Considerable care was necessary in the standardization of the electrodes for $\text{CaH}_2\text{PO}_4^+$ measurements at low pH,

(1) These studies were aided by Contract N00014-66-C0227 (NR 105-419), between the office of Naval Research, Department of the Navy, and the State University of New York at Buffalo.

(2) M. D. Francis, *Ann. N. Y. Acad. Sci.*, **131**, 694 (1965).

(3) I. Greenwald, J. Redish, and A. C. Kibrick, *J. Biol. Chem.*, **135**, 65 (1940).

(4) R. E. Gosselin and E. R. Coghlan, *Arch. Biochem. Biophys.*, **25**, 301 (1953).

(5) C. W. Davies and B. E. Hoyle, *J. Chem. Soc.*, 4134 (1953).

(6) I. Greenwald, *J. Phys. Chem.*, **67**, 2853 (1963).

(7) E. C. Moreno, T. M. Gregory, and W. E. Brown, *J. Res. Natl. Bur. Std.*, **70A**, 545 (1966).

(8) R. G. Bates, "Determination of pH," John Wiley and Sons, Inc., New York, N. Y., 1964.

particularly in the design of calomel electrode junction, owing to the increased importance of the liquid junction potential under these conditions; both potassium tetroxalate and HCl-KCl buffers were used in each experiment. In order to achieve as wide a range of concentrations as possible, six separate titration systems were studied: $\text{KH}_2\text{PO}_4 + \text{CaCl}_2$ titrated with NaH_2PO_4 ; $\text{KH}_2\text{PO}_4 + \text{Na}_2\text{HPO}_4$ with CaCl_2 ; $\text{KH}_2\text{PO}_4 + \text{CaCl}_2$ with H_3PO_4 ; Na_2HPO_4 with CaCl_2 ; Na_3PO_4 with CaCl_2 ; $\text{NaOH} + \text{H}_3\text{PO}_4$ with CaCl_2 .

Results and Discussion

The results of the potentiometric measurements over the entire ranges of concentration could be interpreted in terms of the formation of three complex species, $\text{CaH}_2\text{PO}_4^+$, CaHPO_4 , and CaPO_4^- with thermodynamic association constants K^+ , K° , and K^- , respectively. Although the existence of the ion pair NaHPO_4^- has been proposed by Smith and Alberty,⁹ Bates,¹⁰ in his extensive hydrogen electrode cell measurements with sodium phosphate buffers, could find no evidence for the presence of this species; in the present work, the interaction between Na^+ and HPO_4^{2-} ions was ignored. The concentrations of ionic species in the solutions were calculated from equations for total calcium ion concentration

$$T_M = [\text{Ca}^{2+}] + [\text{CaH}_2\text{PO}_4^+] + [\text{CaHPO}_4] + [\text{CaPO}_4^-] + [\text{CaOH}^+]$$

total phosphate concentration

$$T_P = [\text{H}_3\text{PO}_4] + [\text{H}_2\text{PO}_4^-] + [\text{HPO}_4^{2-}] + [\text{PO}_4^{3-}] + [\text{CaH}_2\text{PO}_4^+] + [\text{CaHPO}_4] + [\text{CaPO}_4^-]$$

and electroneutrality

$$2[\text{Ca}^{2+}] + [\text{H}^+] + [\text{K}^+] + [\text{Na}^+] + [\text{CaH}_2\text{PO}_4^+] + [\text{CaOH}^+] = [\text{OH}^-] + [\text{Cl}^-] + [\text{H}_2\text{PO}_4^-] + 2[\text{HPO}_4^{2-}] + 3[\text{PO}_4^{3-}] + [\text{CaPO}_4^-]$$

Values of the dissociation constants of phosphoric acid were those of Bates^{10,11} ($k_{1a} = 7.112 \times 10^{-3}$ at 25° and 6.095×10^{-3} at 37° ; $k_{2a} = 6.339 \times 10^{-8}$ at 25° and 6.562×10^{-8} at 37°), Vanderzee¹² ($k_{3a} = 4.3 \times 10^{-13}$ at 25°), and Bjerrum¹³ ($k_{3a} = 6.6 \times 10^{-13}$ at 37° ; $K(\text{CaOH}^+) = 20.0^{14}$). At low pH the concentrations $[\text{CaPO}_4^-]$, $[\text{CaHPO}_4]$, $[\text{CaOH}^+]$, $[\text{PO}_4^{3-}]$, and $[\text{OH}^-]$ are negligible and

$$[\text{H}_2\text{PO}_4^-] = \frac{T_P - 2T_M + [\text{Cl}^-] - [\text{K}^+] - [\text{Na}^+] + [\text{H}^+]}{\frac{[\text{H}^+]f_1^2}{k_{1a}} \frac{k_{2a}}{[\text{H}^+]f_2}}$$

Values of K^+ were obtained with the aid of an IBM 7044 computer by successive approximations of the ionic strength

$$I = \frac{1}{2} \left\{ [\text{H}_2\text{PO}_4^-] \left(4.0 + \frac{[\text{H}^+]f_1^2}{k_{1a}} + \frac{9.0k_{2a}}{[\text{H}^+]f_2} \right) + 3[\text{Cl}^-] - [\text{H}^+] - [\text{Na}^+] - [\text{K}^+] - T_P \right\}$$

using activity coefficients calculated from the equation $-\log f_2 = Az^2[I^{1/2}/(1 + I^{1/2})^{-0.31I}]$.¹⁵ The results of some typical experiments are given in Table I. The mean value of K^+ , $25.6 \text{ l. mole}^{-1}$ at 25° , is appreciably larger than the value of 11–12 estimated by Davies and Hoyle⁵ from colorimetric measurements.

Table I

$T_M \times 10^3$ M	$T_P \times 10^3$ M	pH	Ionic strength $\times 10^3$ M	$[\text{CaH}_2\text{PO}_4^+]$ $\times 10^4$ M	K^+ , l. mole ⁻¹
At 25°					
2.673	5.935	3.273	1.322	1.891	22.5
4.174	5.954	3.140	1.742	2.990	24.7
5.473	6.049	3.023	2.114	3.709	25.1
6.245	6.301	2.965	2.351	4.228	25.2
6.544	5.449	3.295	2.396	4.152	25.9
6.659	6.023	2.970	2.452	4.201	24.8
8.092	10.880	2.728	3.202	6.369	19.9
Mean $K^+ = 25.6 \text{ l. mole}^{-1}$; mean deviation ± 1.7 (48 determinations)					
At 37°					
2.336	5.345	3.262	1.157	2.027	31.3
3.699	5.277	3.195	1.538	2.900	30.9
4.914	5.290	3.115	1.885	3.483	29.7
5.999	6.558	2.902	2.266	4.921	31.5
6.277	5.754	3.127	2.312	4.831	31.9
6.425	5.575	2.953	2.318	4.901	34.3
Mean $K^+ = 31.9 \text{ l. mole}^{-1}$; mean deviation ± 1.6 (36 determinations)					

In the intermediate pH range, the concentrations $[\text{CaPO}_4^-]$, $[\text{PO}_4^{3-}]$, and $[\text{OH}^-]$ could be ignored, and $[\text{HPO}_4^{2-}]$ was calculated by solving the quadratic equation

$$[\text{HPO}_4^{2-}]^2 \left[\frac{K^+[\text{H}^+]f_2^2}{k_{2a}} \left(1.0 + \frac{[\text{H}^+]f_1^2f_2}{k_{1a}k_{2a}} + \frac{[\text{H}^+]f_1}{k_{2a}} \right) \right] + [\text{HPO}_4^{2-}] \left(\frac{2[\text{H}^+]f_1^2f_2}{k_{1a}k_{2a}} + \frac{[\text{H}^+]f_2}{k_{2a}} + (T_P - T_M) \frac{K^+[\text{H}^+]f_2^2}{k_{2a}} \right) + 2T_M - 2T_P - [\text{Cl}^-] + [\text{H}^+] + [\text{Na}^+] + [\text{K}^+] = 0$$

(9) R. M. Smith and R. A. Alberty, *J. Phys. Chem.*, **60**, 180 (1956).

(10) R. G. Bates and S. F. Acree, *J. Res. Natl. Bur. Std.*, **30**, 129 (1943).

(11) R. G. Bates, *ibid.*, **47**, 127 (1951).

(12) C. E. Vanderzee and A. S. Quist, *J. Phys. Chem.*, **65**, 118 (1961).

Table II: CaHPO₄ Complex Formation

$T_M \times 10^3,$ M	$T_P \times 10^3,$ M	pH	$I \times 10^3,$ M	$[CaH_2PO_4^+],$ $\times 10^4, M$	$[CaHPO_4],$ $\times 10^4, M$	$K^\circ,$ l. mole ⁻¹
25°, $K^+ = 25.6$ l. mole ⁻¹						
4.697	1.076	5.576	2.403	5.700	2.342	546
6.110	1.108	5.726	2.833	6.513	4.028	550
6.990	1.119	5.603	3.076	7.554	3.508	545
7.906	1.098	5.682	3.314	8.029	4.428	548
9.076	1.106	5.561	3.640	9.259	3.842	549
10.42	1.098	5.537	4.010	10.26	3.985	546
11.47	1.094	5.664	4.302	10.61	5.554	552
11.71	1.051	5.222	4.327	11.30	2.693	549
Mean $K^\circ = 548$ l. mole ⁻¹ ; mean deviation ± 2.8 (61 determinations)						
37°, $K^+ = 31.9$ l. mole ⁻¹						
3.407	1.107	5.566	2.062	4.857	2.178	683
4.341	1.101	5.529	2.302	6.013	2.452	681
5.978	1.092	5.475	2.732	7.872	2.798	679
7.544	1.111	5.435	3.175	9.667	3.096	679
8.937	1.103	5.404	3.552	11.00	3.253	678
10.21	1.085	5.379	3.890	12.02	3.339	678
11.85	1.102	5.473	4.361	13.20	4.582	683
12.21	1.087	5.086	4.450	14.21	2.025	689
Mean $K^\circ = 681$ l. mole ⁻¹ ; mean deviation ± 2.8 (57 determinations)						

Table III: CaPO₄⁻ Complex Formation

$T_M \times 10^4,$ M	$T_P \times 10^4,$ M	$[H^+] \times 10^{11},$ M	$[CaHPO_4],$ $\times 10^6, M$	$[CaPO_4^-],$ $\times 10^6, M$	$I \times 10^4,$ M	$[CaOH^+],$ $\times 10^6, M$	$K^- \times 10^{-6},$ l. mole ⁻¹
At 25°							
1.304	8.95	8.11	1.40	4.54	6.50	1.95	2.93
1.379	8.87	8.27	1.45	4.63	6.65	2.06	2.94
1.452	8.80	8.43	1.00	5.76	6.39	1.94	2.89
1.525	8.72	8.59	1.51	4.82	6.94	2.26	3.06
1.596	8.65	8.69	1.58	4.80	7.12	2.38	2.93
1.666	8.58	8.76	1.66	4.77	7.30	2.52	2.80
1.735	8.51	8.93	1.67	4.84	7.44	2.60	2.87
1.803	8.44	9.04	1.73	4.83	7.61	2.71	2.81
1.870	8.37	9.18	1.73	4.90	7.75	2.79	2.88
1.935	8.30	9.29	1.85	4.78	7.95	2.91	2.86
Mean $K^- = 2.9 \pm 0.1 \times 10^6$ l. mole ⁻¹							
At 37°							
1.452	8.80	3.10	2.88	3.54	6.16	6.52	3.71
1.525	8.72	3.15	3.00	3.55	6.34	6.84	3.64
1.596	8.65	3.22	3.18	3.45	6.54	7.11	3.40
1.666	8.58	3.26	3.21	3.57	6.69	7.40	3.53
1.735	8.51	3.33	3.38	3.48	6.89	7.63	3.33
1.803	8.44	3.36	3.44	3.54	7.05	7.94	3.36
1.870	8.37	3.44	3.49	3.58	7.21	8.10	3.41
1.935	8.30	3.49	3.59	3.56	7.39	8.33	3.35
Mean $K^- = 3.46 \pm 0.2 \times 10^6$ l. mole ⁻¹							

Values of K° were calculated as for K^+ using

$$I = 0.5 \left\{ [HPO_4^{2-}] \left(8.0 + \frac{2[H^+]f_1^2 f_2}{k_{1a} k_{2a}} + \frac{4[H^+]f_2}{k_{2a}} \right) + 2[Cl^-] + 2T_M - 2T_P \right\}$$

Table II summarizes the results of some typical exper-

iments at intermediate pH, and it is seen that the variation in K° over the range of accessible concentrations is very small. In experiments under supersaturated con-

(13) N. Bjerrum and A. Unmack, *Kgl. Danske Videnskab. Selskab, Mat. Fys. Medd.*, **9**, 141 (1929).
(14) C. W. Davies and B. E. Hoyle, *J. Chem. Soc.*, 233 (1951).
(15) C. W. Davies, "Ion Association," Butterworth and Co., Ltd., London, 1962.

ditions at high pH, $[\text{H}_3\text{PO}_4]$ and $[\text{CaH}_2\text{PO}_4^+]$ were negligible and $[\text{HPO}_4^{2-}]$ was calculated by successive approximations for I from the quadratic equation

$$[\text{HPO}_4^{2-}]^2 \left\{ f_2^2 K^\circ \left(1 + \frac{f_2[\text{H}^+]}{k_{2a}} + \frac{f_2 k_{3a}}{f_1 f_3 [\text{H}^+]} \right) \right\} +$$

$$[\text{HPO}_4^{2-}] \left\{ 1 + f_2^2 K^\circ (T_M - T_P) + \frac{2[\text{H}^+]}{k_{2a}} f_3 \right\} +$$

$$2T_M - 3T_P + [\text{Na}^+] +$$

$$[\text{H}^+] - [\text{Cl}^-] - [\text{OH}^-] = 0$$

The constancy of the K° values given in Table III provides supporting evidence for the presence of two complexes, CaHPO_4 and CaPO_4^- , at high pH. It was not possible to interpret the experimental data in terms of the presence of any other species such as $\text{Ca}_3(\text{PO}_4)_2$. In his calculation of K° from Bjerrum's data, Greenwald⁶ substituted values for $\log [\text{H}][\text{CaPO}_4^-]/[\text{CaHPO}_4]$ of 8.0, 8.5, and 9.0. The best consistency was obtained with the value 8.5, which can be compared with the value 8.64 of the present work. The agreement is remarkably good, in view of the differences in pH involved and of the wide range of choice of values for the dissociation of CaHPO_4 made by Greenwald. The association constant values at 25° have been used to construct the complex composition diagram given as a function of pH in Figure 1, in which the concentrations of complexes are calculated for a hypothetical system $10^{-3} M$ in both total calcium and total phosphate and at an ionic strength $0.15 M$, close to the physiological value.

The values obtained for the association constants at 25 and 37° have been used to calculate approximate thermodynamic functions for the reactions and these are given in Table IV together with estimated uncertainties.

Although direct calorimetric determination of ΔH is to be preferred to the temperature coefficient method, in these calcium phosphate systems, the range of accessible concentrations is such that the complexes, particularly CaPO_4^- at high pH, are present in too small amounts

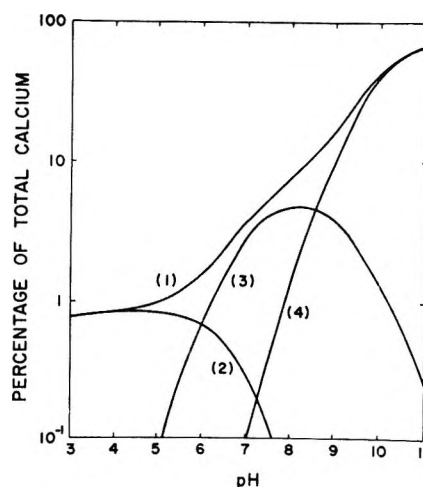


Figure 1. Concentrations of ionic species present in solutions of calcium phosphate as a function of pH for $T_M = T_P = 10^{-3} M$: (1) total complexes; (2) $[\text{CaH}_2\text{PO}_4^+]$; (3) $[\text{CaHPO}_4]$; (4) $[\text{CaPO}_4^-]$.

Table IV: Thermodynamic Functions at 25°

Reaction	$-\Delta G, \text{kcal mole}^{-1}$	$\Delta H, \text{kcal mole}^{-1}$	$\Delta S, \text{cal deg}^{-1} \text{mole}^{-1}$
$\text{Ca}^{2+} + \text{H}_2\text{PO}_4^-$	1.92 ± 0.04	3.4 ± 1.7	18 ± 6
$\text{Ca}^{2+} + \text{HPO}_4^{2-}$	3.7 ± 0.01	3.3 ± 0.6	23 ± 0.5
$\text{Ca}^{2+} + \text{PO}_4^{3-}$	8.81 ± 0.03	3.1 ± 2.0	40 ± 4

for accurate enthalpy change measurement. As is to be expected for interactions which are essentially electrostatic in nature,¹⁶ complex formation is accompanied by endothermic enthalpy changes. The complexes are stabilized through the positive entropy changes reflecting the release of solvent molecules from the cospheres of the free ions when association takes place. The ΔS values increase with increasing negative charge on the anion.

(16) G. H. Nancollas, "Interactions in Electrolyte Solutions," Elsevier Publishing Co., Amsterdam, 1966.

Osmotic Coefficients of Aqueous Solutions of Tri-*n*-alkylsulfonium Halides at 25°¹

by Siegfried Lindenbaum

Chemistry Division, Oak Ridge National Laboratory, Oak Ridge, Tennessee 37830 (Received July 3, 1967)

Osmotic coefficients measured by the gravimetric isopiestic vapor pressure equilibration method are reported for trimethyl- and tri-*n*-butylsulfonium chloride and bromide and for trimethyl-, tri-*n*-propyl-, and tri-*n*-butylsulfonium iodide. These results are compared with previously reported data on tetraalkylammonium salts. The osmotic coefficients for the sulfonium salts are in general lower than those for the corresponding ammonium salt; however, the relative order and the shape of the osmotic coefficient *vs.* concentration curves are remarkably similar. This comparison confirms the suggestion that the solution properties of these cations are largely dominated by the nature and length of the hydrocarbon substituents on the central sulfur or nitrogen atom. The suggestions previously put forward to account for the behavior of the quaternary ammonium salts, *i.e.*, water structure promotion, water structure enforced ion pairing, and micelle formation, are examined and compared in the light of the free energy behavior of the aqueous sulfonium salt solutions.

Introduction

The discovery that certain tetraalkylammonium salts crystallize from aqueous solution with large amounts of water of crystallization² and the suggestion of Frank and Wen³ that these large cations promote water structure has led to a great deal of interest and work on these solutions in recent years.⁴⁻¹⁵ Physical measurements have in general tended to support the idea that the water structure in the vicinity of these large cations is modified and promoted.¹⁶ These interpretations have been made more plausible in view of the crystal structure determinations of G. A. Jeffrey and co-workers,¹⁷⁻²⁰ who have shown that some of these compounds crystallize from aqueous solution as clathrate hydrates, in which the hydrocarbon chains of these cations are in all cases located in clathrate cages formed by an extended 4-coordinated structure of the water molecules based on pentagonal dodecahedra. Jeffrey and co-workers have reported crystal structures for clathrates formed by quaternary ammonium-, phosphonium-, and tertiary sulfonium halides. Studies of the aqueous solution chemistry of these compounds have been limited to the ammonium salts.³⁻¹⁶ The purpose of this work is to extend these studies to solutions of tertiary sulfonium halides and to determine if the thermodynamic behavior in aqueous solutions is analogous to that of the quaternary ammonium salt solutions. It was thought to be of interest to establish what generalizations, if any, can be made concerning the thermodynamic properties of aqueous solutions of compounds which form clathrate hydrates and to what extent these properties are altered by choosing a different central atom for the "onium" type cation. Studies on anion-exchange resins²¹ with tertiary sulfonium exchange sites have shown that these exchangers

have anion selectivity properties very similar to resins with quaternary ammonium exchange sites. Since in the case of the tertiary sulfonium cation only three substituents are present, it was necessary to consider the configuration of the alkyl chains. The structure of trimethylsulfonium iodide has been shown²² by

- (1) Research sponsored by the U. S. Atomic Energy Commission under contract with the Union Carbide Corp.
- (2) D. L. Fowler, W. V. Loebenstein, D. B. Pall, and C. A. Kraus, *J. Am. Chem. Soc.*, **62**, 1140 (1940).
- (3) H. S. Frank and W. Y. Wen, *Discussions Faraday Soc.*, **24**, 133 (1957).
- (4) W. Y. Wen, S. Saito, and C. Lee, *J. Phys. Chem.*, **70**, 1244 (1966).
- (5) W. Y. Wen and S. Saito, *ibid.*, **68**, 2639 (1964).
- (6) S. Lindenbaum and G. E. Boyd, *ibid.*, **68**, 911 (1964).
- (7) S. Lindenbaum, *ibid.*, **70**, 814 (1966).
- (8) D. F. Evans and R. L. Kay, *ibid.*, **70**, 366 (1966).
- (9) R. L. Kay and D. F. Evans, *ibid.*, **69**, 4216 (1965); **70**, 2325 (1966).
- (10) R. L. Kay, T. Vituccio, C. Zawoyski, and D. F. Evans, *ibid.*, **70**, 2336 (1966).
- (11) R. H. Wood, H. L. Anderson, J. D. Beck, J. R. France, W. E. deVry, and L. J. Soltzberg, *ibid.*, **71**, 2149 (1967).
- (12) H. G. Hertz and M. D. Zeidler, *Ber. Bunsenges. Physik. Chem.*, **68**, 821 (1964).
- (13) B. E. Conway and R. E. Verall, *J. Phys. Chem.*, **70**, 3952, 3961 (1966).
- (14) K. W. Bunzl, *ibid.*, **71**, 1358 (1967).
- (15) G. E. Boyd, J. W. Chase, and F. Vaslow, *ibid.*, **71**, 573 (1967); S. Lindenbaum and G. E. Boyd, *ibid.*, **71**, 581 (1967).
- (16) H. S. Frank, *Z. Physik. Chem. (Leipzig)*, **228**, 367 (1965).
- (17) D. Feil and G. A. Jeffrey, *J. Chem. Phys.*, **35**, 1863 (1961).
- (18) R. K. McMullan, M. Bonamico, and G. A. Jeffrey, *ibid.*, **39**, 3295 (1963).
- (19) G. A. Jeffrey and R. K. McMullan, *ibid.*, **37**, 2231 (1962).
- (20) P. T. Buerkens and G. A. Jeffrey, *ibid.*, **40**, 906 (1964).
- (21) S. Lindenbaum, G. E. Boyd, and G. E. Myers, *J. Phys. Chem.*, **62**, 995 (1958).
- (22) D. F. Zuccaro and J. D. McCullough, *Z. Krist.*, **112**, 401 (1959).

X-ray crystallographic methods to be pyramidal. Also, Raman spectral measurements on crystalline trimethylsulfonium chloride and bromide²³ and on aqueous solutions show that the configuration is pyramidal and not planar.

Experimental Section

Materials. Trimethylsulfonium iodide was obtained from Aldrich Chemicals; it was recrystallized from an ethanol benzene solution and analyzed gravimetrically for iodide (found, 62.13; calcd, 62.19). Trimethylsulfonium chloride and bromide were obtained by passing aqueous solutions of the iodide salt through a bed of the anion-exchange resin Dowex 1-X8 in the chloride and bromide forms, respectively. The solid chloride and bromide salts were obtained by evaporating the water at room temperature under vacuum. The white crystals obtained in each case were analyzed for chloride and bromide, respectively (chloride: found, 31.34; calcd, 31.48; bromide: found, 50.87; calcd, 50.87). Tri-*n*-butylsulfonium iodide was prepared²⁴ by treating equimolar mixtures of butyl sulfide with butyl iodide in nitromethane at 40° for 4 weeks. The nitromethane was removed under vacuum, and the remaining solid was recrystallized from ethyl acetate-ether mixtures (iodide: found, 38.39; theor, 38.42). The chloride and bromide salts were extremely hygroscopic. The aqueous solutions were therefore prepared immediately before use by ion exchange of the pure iodide. Tri-*n*-propylsulfonium iodide was prepared in the same way as the tri-*n*-butyl salt (iodide: found, 44.18; calcd, 44.03).

Isopiestic Vapor Pressure Comparisons. The isopiestic apparatus, standards, and methods used were identical with those reported earlier⁶ in a similar study on tetraalkylammonium halides. All solutions used in this study developed an odor on standing, suggesting decomposition of the sulfonium salts.²⁴ The isopiestic experiments were therefore performed as rapidly as possible. Equilibrium conditions were established by approaching equilibrium, alternately, from the high-concentration and low-concentration sides. However, fewer data were taken to establish the osmotic coefficient *vs.* concentration curve. Decomposition was more serious in dilute solutions, and erratic results were obtained in some cases below 0.5 *m*.

Thermoelectric Osmometry. Osmotic coefficients were also measured using the vapor pressure osmometer as previously described.²⁵ This method has been particularly useful for dilute solutions; however, for the sulfonium salts, erratic results were obtained on solutions less concentrated than 0.1 *m*, suggesting decomposition.

Results and Discussion

Isopiestic molalities of the sulfonium halide solutions and the solutions used as vapor pressure standards are

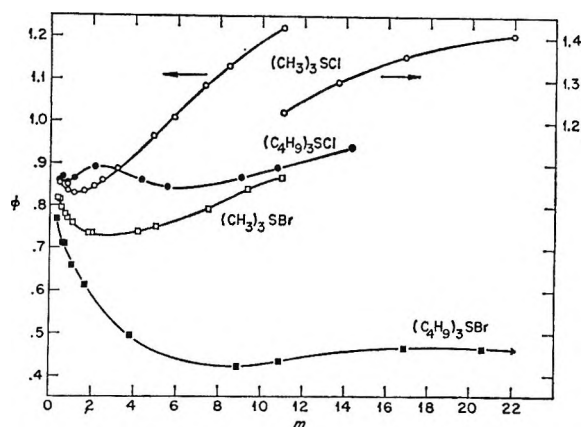


Figure 1. Osmotic coefficients of tri-*n*-alkylsulfonium chlorides and bromides.

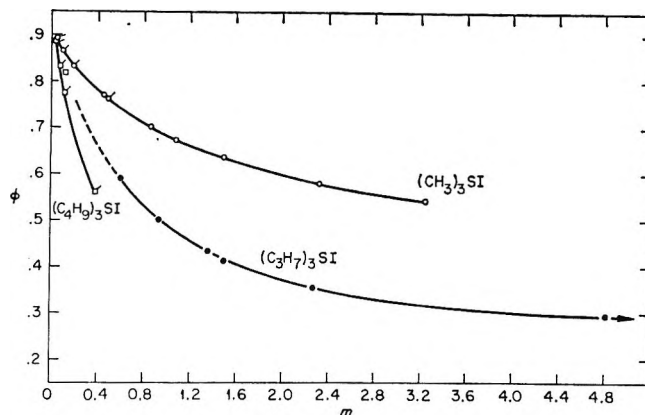


Figure 2: Osmotic coefficients of tri-*n*-alkylsulfonium iodides: \circ , \square , osmometry data; and \circ , \bullet , \square , isopiestic data.

given in Table I. Osmotic coefficients, calculated from thermoelectric osmometry data, are listed in Table II. Osmotic coefficients were calculated as before^{6,25} and are given in Figure 1 for the chloride and bromide salts and in Figure 2 for the iodide salts. Each point represents the average of two determinations. Osmotic coefficients at even values of the molality were interpolated from smooth curves drawn through the experimental data and are given in Table III. The accuracy usually attainable by the isopiestic method was not achieved in this study, especially in the dilute concentration range, owing to the problem of decomposition mentioned earlier. No attempt has been made to calculate activity coefficients, since this would require extrapolation of the data to infinite dilution and it is felt that this cannot be done in a meaningful manner with the aforementioned uncertainty in the dilute-solution region. For concentrations greater than 0.5 *m*, the values of ϕ are estimated to be accurate within ± 0.005 of the plotted points. The isopiestically

(23) K. W. Bunzl, personal communication.

(24) E. R. Kline and C. A. Kraus, *J. Am. Chem. Soc.*, **69**, 814 (1947).

(25) G. E. Boyd, A. Schwarz, and S. Lindenbaum, *J. Phys. Chem.*, **70**, 821 (1966).

Table I: Molalities of Isopiestic Solutions^a

NaCl	Me ₃ SCl	Me ₃ SI	NaCl	Bu ₃ SCl	Bu ₃ SI	Bu ₃ SBr	NaCl	Me ₃ SBr	Pr ₃ SI
0.1613	0.1613	0.1688	0.0980	...	0.1116	0.7095	0.3764	0.4244	0.5874
0.2355	0.2422	0.2590	0.1073	0.1023	0.1142	1.046	0.5066	0.5869	0.9316
0.3712	0.3994	0.4437	0.1968	0.2009		1.651	0.6305	0.7473	1.346
0.6492	0.7172	0.8553	0.2697	0.2838		3.793	0.6678	0.8008	1.498
0.7831	0.8715	1.077	0.4015	0.4295		8.875	0.8609	1.054	2.261
1.011	1.140	1.488	0.7611	0.8268		10.87	1.434	1.859	4.628
1.416	1.616	2.323				16.90	1.478	1.922	4.808
1.811	2.080	3.238	0.5466	0.5814		20.59	2.956	4.166	10.68
2.152	2.484		0.7432	0.8122		30.21	3.498	5.025	13.02
2.754	3.195		1.079	1.174			5.001	7.537	21.50
4.165	4.879		1.918	2.106			6.064	9.382	26.86
4.953	5.837		3.469	4.345			A	11.053	35.85
6.112	7.269		4.174	5.578					
B	8.417		6.108	9.087					
C	11.00		A	10.74					
D	13.63		C	14.29					
E	16.80								
F	22.01								

^a Water activities of saturated aqueous solutions used as standards: A, NaCl, $a_w = 0.7528$; B, SrCl₂, $a_w = 0.7094$; C, NH₄NO₃, $a_w = 0.6161$; D, Mg(NO₃)₂, $a_w = 0.5295$; E, K₂CO₃, $a_w = 0.4397$; and F, MgCl₂, $a_w = 0.3277$. The saturated solutions were prepared from reagent grade chemicals without further purification. The values of a_w were determined by isopiestic equilibration against solutions of H₂SO₄. The literature (R. A. Robinson and R. H. Stokes, "Electrolyte Solutions," 2nd ed, Academic Press Inc., New York, N. Y., 1959) tabulation of ϕ for H₂SO₄ and NaCl solutions was used for the calculations. Satisfactory agreement for a_w of the saturated solutions with the literature tabulation was obtained in every case except K₂CO₃.

Table II: Osmotic Coefficients from Thermoelectric Osmometry

	<i>m</i>	ϕ
Bu ₃ SCl	0.02751	0.916
	0.04736	0.911
	0.07223	0.909
	0.09759	0.908
	0.2964	0.862
	0.4781	0.855
Bu ₃ SBr	0.02999	0.948
	0.06380	0.892
	0.08219	0.876
	0.1129	0.861
	0.3442	0.769
	0.6081	0.712
Bu ₃ SI	0.03562	0.887
	0.06680	0.834
	0.1167	0.775
	0.3811	0.560
Me ₃ SCl	0.0246	0.946
	0.06835	0.906
	0.1205	0.894
	0.2145	0.872
	0.4868	0.853
Me ₃ SBr	0.0292	0.945
	0.07295	0.906
	0.1392	0.882
	0.2344	0.852
	0.5059	0.815
Me ₃ SI	0.01524	(1.015)
	0.04331	0.892
	0.08879	0.865
	0.1812	0.832
	0.4937	0.762

measured osmotic coefficients were determined by approaching equilibrium from both higher and lower water activities. The time allowed for attainment of equilibrium was between 3 and 9 days. These data all fell on the same smooth curves (Figures 1 and 2). Since each equilibration required several days, this is taken as strong evidence that the rate of decomposition in these more concentrated solutions was not sufficient to affect the results seriously. Although the data below 0.5 *m* are less accurate, they are believed to be a valid representation of the *relative* magnitudes and orders of the osmotic coefficients for the compounds compared in this study. In every case, an attempt was made to carry the measurements to the highest possible concentration. The last point on the curve for most of the compounds is therefore close to the solubility limit. Tri-*n*-butylsulfonium bromide showed no sign of crystal formation even at 30 *m*. Measurements were obtained for tri-*n*-propylsulfonium iodide beyond the range shown in Figure 2. At 21.5 *m*, $\phi = 0.277$; at 26.9 *m*, $\phi = 0.294$; and at 35.9 *m*, $\phi = 0.266$. At this concentration crystallization had not yet occurred, although it is certainly possible that this extremely viscous solution was supersaturated. Tri-*n*-butylsulfonium iodide solutions separate into two liquid phases at total concentrations higher than about 0.5 *m*. It was not determined whether the viscous phase was a supercooled liquid or a true equilibrium liquid phase at 25°.

The osmotic coefficients of Figures 1 and 2 are somewhat lower than those of the corresponding tetraalkylammonium salts.⁶ In every case, however, the relative orders and the shapes of the curves are remarkably

Table III: Osmotic Coefficients of Tri-*n*-alkylsulfonium Halides

<i>m</i>	(CH ₃) ₃ SCl	(C ₄ H ₉) ₃ SCl	(CH ₃) ₃ SBr	(C ₄ H ₉) ₃ SBr	(CH ₃) ₃ SI	(C ₄ H ₉) ₃ SI	(C ₆ H ₅) ₃ SI
0.5	0.850	0.857	0.803	0.737	0.760	(0.62) ^a	(0.51) ^a
1	0.831	0.857	0.765	0.670	0.682	0.487	
2	0.843	0.885	0.735	0.585	0.598	0.372	
3	0.875	0.888	0.726	0.526	0.550	0.325	
4	0.920	0.870	0.734	0.487		0.300	
5	0.970	0.850	0.747	0.460		0.293	
6	1.018	0.845	0.761	0.440		0.292	
7	1.070	0.850	0.780	0.429		0.291	
8	1.116	0.856	0.802	0.424		0.290	
9	1.155	0.866	0.830	0.423		0.290	
10	1.190	0.880	0.850	0.425		0.289	
11	1.225	0.895	0.865	0.434		0.288	
12	1.255	0.908		0.445		0.287	
13	1.285	0.923		0.452		0.286	
14	1.305	0.936		0.460		0.285	
15	1.325			0.463		0.285	
16	1.344			0.465		0.284	
17	1.362			0.465		0.283	
18	1.377			0.465		0.282	
19	1.391			0.465		0.281	
20	1.402			0.463		0.280	
22	1.408			0.461		0.279	
25				0.455		0.276	
30				0.447		0.272	
35						0.268	

^a Extrapolated beyond the range of the measurements.

similar. As observed previously,⁶ the osmotic coefficients of the chloride salts in dilute solution decrease with the size of the cation: (C₄H₉)₃S⁺ > (CH₃)₃S⁺. This is the order to be expected on the basis of the suggestion that these large cations promote the structuring of the solvent. The order for the bromide and iodide salts is reversed, again as previously observed for the corresponding ammonium salts. The explanation offered previously for this reversal,²⁶ that the larger anions can participate with the large cations in "water structure enforced ion pairing," is equally plausible in this case. The maximum in the curve of ϕ vs. *m* obtained for tri-*n*-butylsulfonium chloride is in almost the identical position as that observed for tetrabutylammonium chloride.⁶ The explanation offered in the latter case, and also for the low values of ϕ at high concentrations of the bromide and iodide salts, was that these large cations tend to aggregate and form micelles. Since then, the suggestion has been made^{5,16} that this lowering of the solute activity is caused by crystallite or cooperative clathrate formation. It seems likely that some form of aggregation is responsible for this lowering of the activity. The low and almost invariant values of ϕ over a large concentration range for tri-*n*-

propylsulfonium iodide (at 4.8 *m*, ϕ = 0.29, and at 36 *m*, ϕ = 0.27) also strongly suggest aggregate formation. The separation into two distinct phases noted for tri-*n*-butylsulfonium iodide may be seen as an extreme case of aggregate formation with aggregates so large that they can no longer remain dispersed in solution and, hence, coalesce to form a new phase. The exact nature of these aggregates is at present quite uncertain and is worthy of further investigation. The present work establishes that both the dilute-solution behavior and the aggregation at higher concentrations for aqueous solutions of these "onium" type salts are dominated largely by the hydrocarbon chains on the sulfur or nitrogen and to a much lesser extent on the nature and structure of the central atom of the cation.

Acknowledgments. The author acknowledges with thanks the continued interest and encouragement of Dr. G. E. Boyd. Thanks are also due to Professor R. M. Fuoss for suggesting the study of the tertiary sulfonium salts and to H. L. Holsopple for the preparation of the tri-*n*-butylsulfonium iodide.

(26) R. M. Diamond, *J. Phys. Chem.*, **67**, 2513 (1963).

Polymer Studies by Gel Permeation Chromatography. II.

The Kinetic Parameters for Styrene Polymerizations¹

by James A. May, Jr., and William B. Smith

Department of Chemistry, Texas Christian University, Fort Worth, Texas 76129 (Received July 3, 1967)

Styrene monomer was polymerized to low conversion using a range of benzoyl peroxide concentrations. The resultant polymer samples were characterized by gel permeation chromatography (gpc). Calculations made from the molecular weight distributions allowed the determination of the following kinetic parameters: chain transfer to initiator (C_I), chain transfer to monomer (C_M), and the ratio k_t/k_p^2 , where k_t and k_p are the rate constants for termination and propagation, respectively.

Introduction

The molecular weight distribution of a given polymer is well known to be a function of its mechanism of formation, and Flory² has given distribution functions which can be related to the kinetic parameters for vinyl polymerization. Until recently, it has usually been easier to determine the appropriate rate terms and to calculate molecular weight distributions rather than to suffer the difficulties and uncertainties of an experimental measurement of a weight distribution.³

The advent of gel permeation chromatography⁴ offered a rapid and potentially accurate method for ascertaining molecular weight distributions. Recently, we have demonstrated that gpc results on samples of polystyrene and polymethyl methacrylate, prepared under known kinetic conditions, were consistent with calculated distributions.⁵ These findings clearly suggest the utility of the gpc technique as a mode of studying the details of vinyl polymerization. Consequently, we have initiated a more detailed study of the styrene system with the results reported below.

Experimental Section

Styrene monomer was purified by washing three times with 10% potassium hydroxide, followed by three washes with water. After drying over calcium chloride, the styrene was carefully distilled under reduced pressure, and only the middle cut (43° (16 mm)) was retained. The benzoyl peroxide, which was used, assayed 100% by iodometric titrations in 2-propanol.

All reactions were carried out using the sealed-ampoule technique in an oil bath controlled at $60 \pm 0.1^\circ$. In every case, a known weight of benzoyl peroxide was added to a known weight of monomer, with allowance being made for the subsequent expansion of the monomer upon heating in the bath. Duplicate portions (30 ml) of the monomer-initiator mixture were placed in glass ampoules and sealed under vacuum (5×10^{-3}

mm) after a series of three freeze-thaw degassing cycles. Ampoules were withdrawn from the bath at appropriate times and plunged into an ice bath. The polystyrene was precipitated by washing the contents of the ampoules with a small amount of toluene into 3 l. of cold methanol. The polystyrene was recovered by filtration, and then it was dried to constant weight at 40° (15 mm). Evaporation of the filtrate at room temperature gave no evidence of loss of low molecular weight polymer.

Gpc Measurements. Gel permeation chromatography was carried out with the gpc Model 100 produced by Waters Associates, with the modifications that the differential refractometer ($1/64$ -in. null glass) and siphon box have been insulated and thermostated at 50°, and an automatic injection system has been added. All work was done using tetrahydrofuran as the solvent, and with the instrument operating at 50°. Solvent flow rates of ca. 0.4 ml/min were used throughout. All of the polystyrene samples chromatographed were 0.2% solutions in tetrahydrofuran, and injection times were 30 sec, *i.e.*, sample sizes of about 0.4 mg. The columns used throughout were one 4-ft section of 1×10^6 Å gel, and two 4-ft sections of 5×10^4 Å gel. Typical polystyrene samples were spread over about 30–40 ml of elution volume from the onset to completion of sample elution.

Calibration of the gpc was carried out using eleven well-characterized polystyrenes of narrow molecular

(1) Abstracted in part from a paper presented at the Fourth International Seminar on Gel Permeation Chromatography, Miami Beach, Fla., May 1967.

(2) P. J. Flory, "Principles of Polymer Chemistry," Cornell University Press, Ithaca, N. Y., 1953, pp 334–336.

(3) See, for instance, F. W. Billmeyer, *J. Polym. Sci.*, **C8**, 161 (1965).

(4) (a) J. C. Moore, *ibid.*, **A2**, 835 (1964); (b) J. C. Moore and J. G. Hendrickson, *ibid.*, **C8**, 233 (1965).

(5) Paper I: W. B. Smith, J. A. May, and C. W. Kim, *ibid.*, **A2-4**, 365 (1966).

Table I: Comparison of Gpc and Independently Determined Molecular Weights for the Standard Samples

Standard	$M_w \times 10^{-4}$	$M_w(\text{gpc}) \times 10^{-4}$	$M_n \times 10^{-4}$	$M_n(\text{gpc}) \times 10^{-4}$	M_w/M_n	M_w/M_n (gpc)
(a) PS 4190038	867	849	773	772	1.15	1.10
(b) PS 4190037	411	427	392	389	≤ 1.06	1.10
(c) PS 108	267	258	247	239	1.08	1.08
(d) PS 41984	167	165	158	160	1.06	1.03
(e) PS 103	125	124	119	116	1.05	1.07
(f) PS 41995	98.2	98.4	96.2	95.6	≤ 1.06	1.03
(g) PS 4190041	51.0	51.5	49.0	48.6	≤ 1.06	1.06
(h) PS 4190039	19.9	20.5	19.6	18.6	≤ 1.06	1.10
(i) PS 4190042	10.3	11.2	9.7	9.9	≤ 1.06	1.14
(j) Mixture of b, c, d, e, and f	214	208	159	150	1.35	1.39

weight, obtained from Waters Associates. A curve (Figure 1) was drawn through the eleven points on a plot of \log (molecular weight) at the peak *vs.* elution volume. This calibration curve was fitted by a least-squares procedure to the fifth-order polynomial $V = a + bZ + cZ^2 + dZ^3 + eZ^4 + fZ^5$, where $V = \log$ (peak molecular weight) and $Z = \text{elution volume}$. Using the analytical expression for the calibration curve, molecular weights were calculated for the standard polystyrenes. The curve was arbitrarily adjusted by minute amounts until the calculated molecular weights agreed closely with the standard values. A summary of these data is given in Table I.

All samples were run through the gpc within a period of 1 week; the calibration standards were each run three times through the gpc and interdispersed among the experimental polystyrene samples, each of which was also run three times. The calibration curve remained constant during the week, and since good results were obtained for the calculated standards, the molecular weight distributions for the experimental samples were considered to be valid. Repeated passage (five times) of the same polymer sample through the gpc for any polymer sample gave less than 5% average deviation in reproducibility of calculated molecular weights. The resolution of the columns was determined with *o*-dichlorobenzene as 1900 plates/ft or a total of 23,000 theoretical plates. The high plate counts plus the good agreement of the experimentally determined and independently determined dispersity ratio, $\bar{M}_w:\bar{M}_n$, did not indicate the need for correction due to longitudinal diffusion of the polymer samples in the gpc columns.

The gpc curves were used to calculate \bar{M}_w and \bar{M}_n , according to the method of Harmon.⁶ In order to compare the gpc curves produced by the instrument with the theoretical molecular weight distributions, the gpc data were converted to a base line linear in mer units, and the area under the curve was normalized using a procedure reported earlier.⁵ All the calculations of molecular weights and linear replot calculations

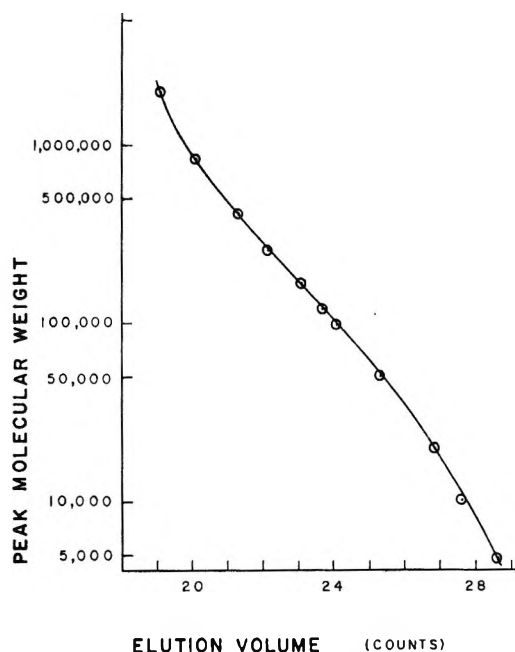


Figure 1. Calibration curve from the polystyrene standards in which the molecular weight at the peak is plotted *vs.* the elution volume. The curve is a least-squares fit of the points to a fifth-order polynomial.

were done using a computer program, which utilized as input the analytical expression for the calibration curve and readings of peak height *vs.* counts (elution volume).

Results and Discussion

Table I presents a summary of the molecular weight values given for the standard polystyrene samples and the gpc values determined for each sample based on the calibration curve derived from the whole collection. The span covered is from *ca.* 10,000 to *ca.* 900,000 in molecular weight, and the agreement with the standard was usually better than 6%, the average deviation for repeated analysis being about 5%. The fact that the ratio $\bar{M}_w:\bar{M}_n$ was consistently very close to the

(6) D. J. Harmon, *J. Polym. Sci.*, **C8**, 243 (1965).

Table II: Summary of Data

[Bz ₂ O ₂] × 10 ⁴ , M	Per cent conversion	\overline{DP}_n	P	M_w/M_n	A values		
					a	b	c
4.82	2.63 ^a	2103	0.99926	1.84	0.55	0.44	0.68
	2.63	2088	0.99922	1.82	0.40	0.37	0.62
	2.63	2032	0.99925	1.89	0.50	0.48	0.76
4.82	2.64	2342	0.99925	1.69	0.40	0.24	0.38
	2.64	2196	0.99915	1.65	0.30	0.13	0.30
	2.64	2267	0.99920	1.69	0.45	0.19	0.38
10.19	2.66	1500	0.99891	1.84	0.20	0.37	0.68
	2.66	1549	0.99884	1.71	0.25	0.20	0.42
	2.66	1665	0.99892	1.68	0.40	0.20	0.36
10.19	2.64	1521	0.99893	1.78	0.42	0.37	0.56
	2.64	1453	0.99887	1.81	0.35	0.36	0.62
	2.65	1331	0.99864	1.79	0.25	0.19	0.58
14.78	2.65	1220	0.99864	1.77	0.30	0.34	0.54
	2.65	1188	0.99867	1.87	0.30	0.42	0.74
	2.65	1274	0.99859	1.69	0.12	0.20	0.38
14.78	2.65	1207	0.99863	1.78	0.35	0.35	0.56
	2.65	1149	0.99858	1.84	0.15	0.37	0.68
	2.93	1096	0.99847	1.80	0.05	0.32	0.60
19.71	2.93	991	0.99853	1.90	0.47	0.54	0.80
	2.93	1129	0.99842	1.60	0.40	0.22	0.20
	2.90	1104	0.99840	1.69	0.07	0.23	0.38
19.71	2.90	1087	0.99835	1.67	0.15	0.21	0.34
	2.90	976	0.99841	1.86	0.20	0.45	0.72
	2.69	836	0.99823	1.87	0.20	0.52	0.74
26.14	2.69	932	0.99820	1.70	0.25	0.32	0.40
	2.69	924	0.99822	1.67	0.30	0.36	0.34
	2.69	824	0.99829	1.94	0.30	0.59	0.88
32.21	2.66	842	0.99803	1.69	0.30	0.34	0.38
	2.66	719	0.99800	1.85	0.30	0.56	0.70
	2.66	759	0.99795	1.95	0.20	0.44	0.90
43.96	2.24	649	0.99762	1.80	0.20	0.46	0.60
	2.24	720	0.99775	1.74	0.25	0.38	0.46
	2.24	681	0.99765	1.72	0.25	0.40	0.44
43.96	2.25	707	0.99767	1.70	0.20	0.35	0.40
	2.25	628	0.99759	1.78	0.20	0.49	0.56
	2.25	674	0.99768	1.73	0.35	0.44	0.46
51.99	2.30	562	0.99751	1.90	0.35	0.60	0.80
	2.30	544	0.99749	1.93	0.35	0.63	0.86
	2.26	612	0.99750	1.76	0.30	0.47	0.52
51.99	2.26	637	0.99750	1.72	0.10	0.41	0.44
	2.26	609	0.99748	1.74	0.35	0.47	0.48

^a Data having the same per cent conversion represent repetitive passes through the gpc. Data with the same initiator concentration, but different per cent conversion, represent duplicate polymerizations.

reported values over the whole range is an important indicator that good chromatographic practices were in force with zone-spreading factors reduced to a minimum. Further confirmation of the validity of the calibration is offered by the last entry in Table I for a known mixture made up from the calibration standards.

As described in the experimental section, styrene was polymerized to low conversion using various amounts of benzoyl peroxide. The reaction was conducted at 60°, a temperature at which the rate of reaction is well known.^{5,7,8} The initiator concentrations, per cent conversions, and gpc-determined values are given in Table II.

In the following discussion, the usual mechanism for

the benzoyl peroxide initiated polymerization of styrene will be assumed,^{2,8} and Flory's nomenclature will be followed. As noted previously,⁵ the instantaneous molecular weight distribution may be written as

$$W_x = Ax(1-p)^2p^{x-1} + 0.5(1-A)(x)(x-1)(1-p)^3p^{x-2}$$

where W_x is the weight fraction of polymer with x mer units, A is the fraction of material formed by chain

(7) F. R. Mayo, R. A. Gregg, and M. S. Matheson, *J. Am. Chem. Soc.*, **73**, 1691 (1951).

(8) B. Baysal and A. V. Tobolsky, *J. Polym. Sci.*, **8**, 529 (1952).

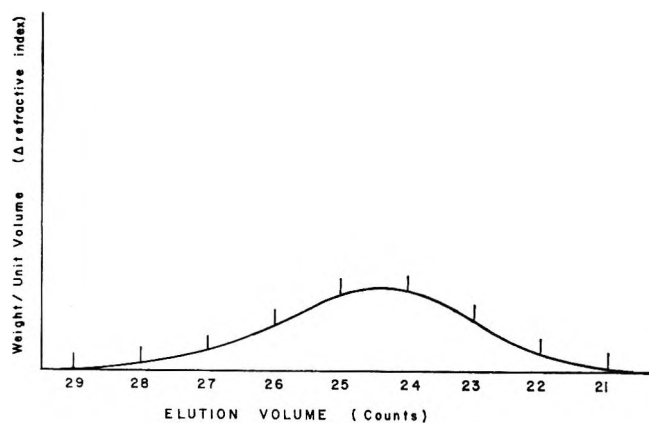


Figure 2. Experimental gel permeation chromatogram of a typical polystyrene sample. The elution volume is plotted *vs.* the weight of polymer per unit volume (arbitrary scale) on the ordinate.

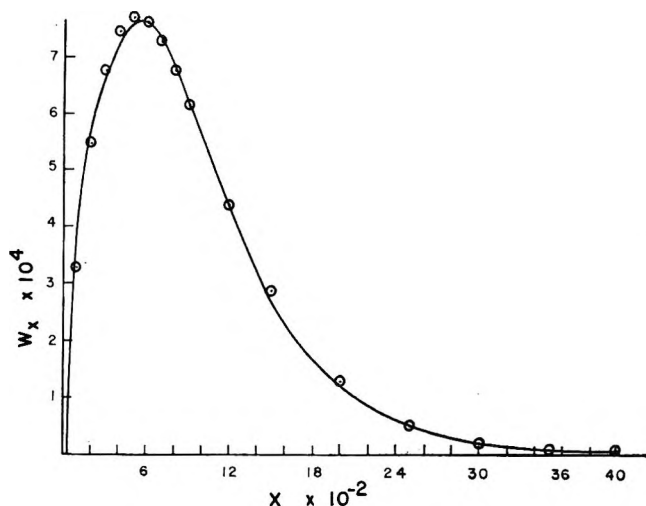


Figure 3. Normalized replot of the chromatogram shown in Figure 2 showing the weight fraction of polystyrene plotted *vs.* the number of mer units in each species. The points are calculated from the theoretical distribution given by Flory using $A = 0.65$, $p = 0.99754$.

transfer and/or disproportionation, and p is the probability that a growing chain adds one more mer unit rather than terminating. Given that termination is solely by coupling⁹ or transfer, and that transfer to polymer may be ignored at low conversions, one may write

$$1/p = 1 + (C_I[I]/[M]) + C_M + (2k_t R_p / k_p^2 [M]^2)$$

and

$$A = \frac{C_I[I] + C_M[M]}{C_I[I] + C_M[M] + (2k_t R_p / k_p^2 [M])}$$

where C_I and C_M are the chain-transfer constants to initiator and monomer, respectively, k_p and k_t are rate constants for propagation and termination, and R_p is the rate of polymerization.

The values of p and A , which characterize the molec-

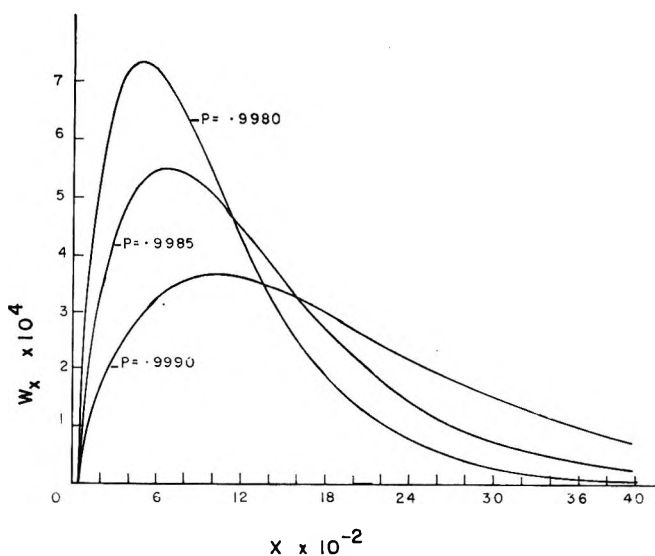


Figure 4. Theoretical molecular weight distributions, obtained by varying p values at a constant value of $A = 1.0$. The weight fraction is plotted against the number of mer units in each species.

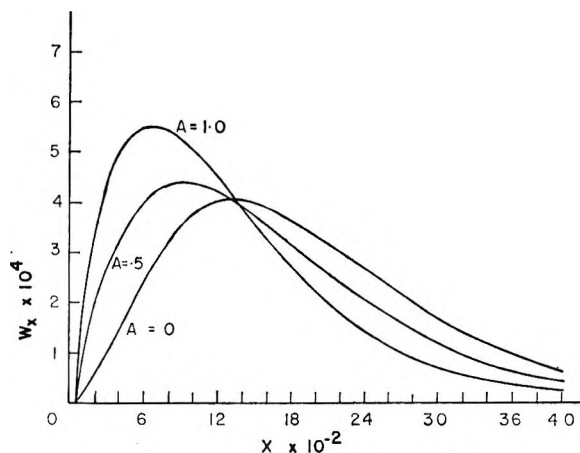


Figure 5. Theoretical molecular weight distributions, obtained by varying A values at a constant value of $p = 0.9985$. The weight fraction is plotted against the number of mer units in each species.

ular weight distribution, can be determined from the gpc data. This may be accomplished by first converting the gpc curve to a new plot linear in mer units *vs.* W_x . The replotted data were found to result in values of \bar{M}_w and \bar{M}_n which agreed within 1% of those calculated from the instrument-produced curve. A typical gpc curve and its replot are shown in Figures 2 and 3. As can be seen in Figures 4 and 5, the variation of either p or A (while the other is held constant) leads to regular variations in the distribution. Most important is the fact that the loci of the peak maxima are smooth functions (Figure 6). Comparison of the peak of a replotted gpc curve on an enlarged version of Figure 6 allowed an estimate of p and A . Sub-

(9) J. V. Bevington, H. W. Melville, and R. P. Taylor, *J. Polym. Sci.*, **14**, 463 (1954).

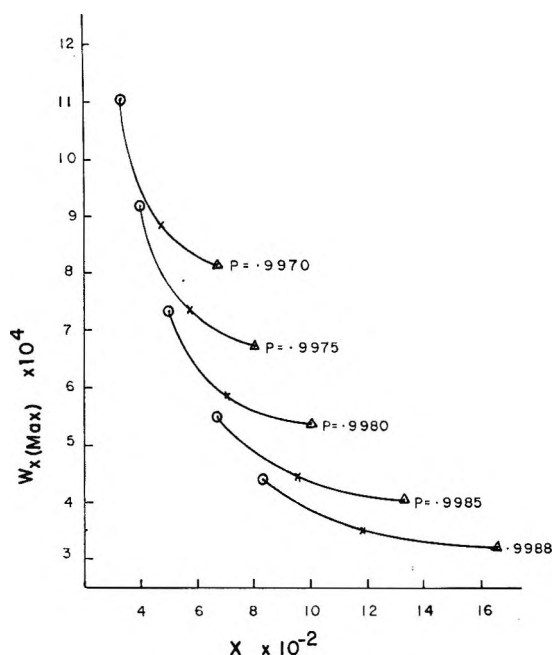


Figure 6. Loci of the maxima in the theoretical molecular weight distribution. The values of W_x and x at the maxima in the theoretical weight distributions are graphed against one another for varying values of p and A . The curves are for various values of p , whereas circles represent points where $A = 1.0$, crosses represent $A = 0.5$, and triangles represent $A = 0.0$.

sequently, the complete distribution could be calculated and compared with the experimental curve (such as shown in Figure 3). In practice, it was found that this fitting technique was quite sensitive to changes in p . However, it was estimated that values of A , so determined, were probably not accurate to better than $\pm 10\%$. The values of p and A determined for our styrene samples are reported in Table II.

In our original study,⁵ it was necessary to fit the gpc data using literature values for C_I and C_M . It was then shown that a value of k_t/k_p^2 consistent with one of several values in the literature was required. Perusal of the molecular weight distribution terms and the kinetic expression for the number-average degree of polymerization (\overline{DP}_n) suggested that data taken at several initiator concentrations would allow direct computation of these terms.

Thus

$$1/\overline{DP}_n = C_M + (C_I[I]/[M]) + (k_t R_p/k_p^2 [M]^2)$$

and subtracting this from $1/p$ one obtains

$$(1/p) - (1/\overline{DP}_n) - 1 = (k_t/k_p^2)(R_p/[M]^2) \quad (1)$$

A plot of the left side of (1) against $R_p/[M]^2$ is a straight line passing through the origin (Figure 7). A least-squares fit of the data in Table II (R_p was calculated as by Flory¹⁰) gave a value of k_t/k_p^2 of 710 ± 115 , a value in fair agreement with our previously reported value⁵ of 880 and, more importantly, in

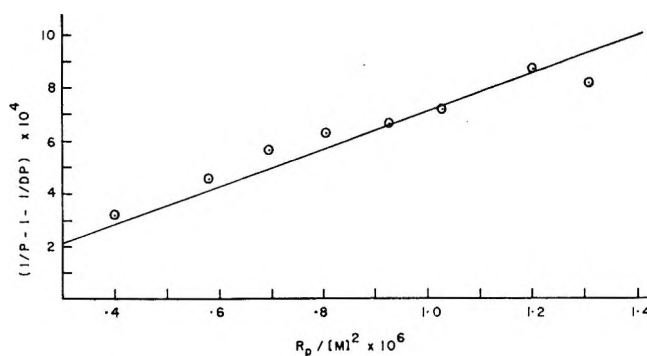


Figure 7. Graph for the determination of k_t/k_p^2 according to eq 1. The line is obtained by a least-squares fit for all the data in Table II. Each point shown on the graph represents the average of about five points.

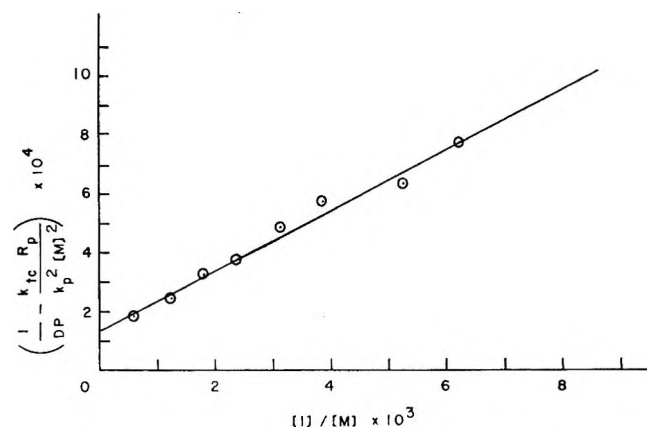


Figure 8. Graph for the determination of C_I and C_M according to eq 2. The line is obtained by a least-squares fit for all the data in Table II. Each point shown on the graph represents the average of about five points.

excellent agreement of the value of 760 recently deduced by Bevington and Sinatti¹¹ using radiochemically labeled initiator.

Utilizing the above value of k_t/k_p^2 and recasting the $1/\overline{DP}_n$ equation in the form

$$(1/\overline{DP}_n) - (k_t R_p/k_p^2 [M]^2) = (C_I[I]/[M]) + C_M \quad (2)$$

allows one to determine C_I and C_M from a plot (Figure 8) of the left-hand side of (2) against $[I]/[M]$. The results of the least-squares fit of this line are given in Table III.

By a series of substitutions it is also possible to relate C_I and C_M to A and p as

$$A(1-p)/p = (C_I[I]/[M]) + C_M \quad (3)$$

Again, a plot of the left-hand term of (3) vs. $[I]/[M]$ is linear, and a least-squares calculation gives C_I and C_M .

(10) See ref 2, p 140.

(11) J. C. Bevington and G. Sinatti, *J. Polym. Sci.*, **B4**, 7 (1966).

Table III: Values of Chain-Transfer Constants for the Benzoyl Peroxide Initiated Polymerization of Styrene at 60°

Method	C_I	$C_M \times 10^6$
Eq 2	0.101 ± 0.005	13.7 ± 1.9
Eq 3, method a	0.07 ± 0.013	24.8 ± 4.6
Eq 3, method b	0.18 ± 0.014	12.2 ± 4.7
Eq 3, method c	0.18 ± 0.025	39 ± 9
Lit. values	0.055^a	$6^{a,b}$
	0.048^b	11^c

^a Reference 7. ^b D. H. Johnson and A. V. Tobolsky, *J. Am. Chem. Soc.*, **74**, 938 (1952). ^c E. P. Bonsall, L. Valentine, and H. W. Melville, *J. Polym. Sci.*, **7**, 39 (1951).

Values of A for use in eq 3 may be determined by three methods: (a) interpolation from the molecular weight peaks and Figure 6 as described above; (b) calculation by the experimental values of \overline{DP}_n and p for a given sample and the relation $\overline{DP}_n = (2 - A)/(1 - p)$; and (c) from the value of $\overline{M}_w/\overline{M}_n$, which varies within the limits of 1.5 for all termination by coupling and 2.0 for all termination by disproportionation or chain transfer. The values of C_I and C_M from eq 3 and these various sources of A are listed in Table III.

Of the various methods for determining C_M and C_I above, the most accurate is probably the use of eq 2, which depends on the gpc-determined values of p and \overline{DP}_n , both of which can be obtained quite accurately. The use of eq 3 depends on values of A . While A is

readily determined by any of the three methods above, we found method a to be rather insensitive, and methods b and c suffer in that two gpc-determined parameters are multiplied or divided so that the errors become additive. The data in Table III indicate that the use of eq 2 results in greater precision.

As has been shown above, gel permeation chromatography allows one to determine k_t/k_p^2 , C_I , and C_M for the polymerization of styrene by means of a series of relatively simple experiments. In contrast to earlier methods, which made use of intrinsic viscosity measurements of number-average molecular weights^{7,8} and/or radioactive initiators,¹¹ this technique allows the perusal of the whole polymer sample and uses calibrations for both weight- and number-average molecular weights.

The importance of examining the whole sample has been made quite evident to us with the recent observation in these laboratories that low conversion samples of polystyrene, prepared with azobisisobutyronitrile as the initiator, possess an abnormal high molecular weight "tail" with high initiator concentrations, while benzoyl peroxide, at sufficient concentrations to give the same reaction rates, gives normal distributions. This matter is undergoing further examination at this time.

Acknowledgment. We wish to express our appreciation to the Dow Chemical Co. for support in certain aspects of this work.

Fluorine Bomb Calorimetry. XXIII. The Enthalpy of

Formation of Carbon Tetrafluoride¹

by Elliott Greenberg and Ward N. Hubbard

Chemical Engineering Division, Argonne National Laboratory, Argonne, Illinois (Received July 7, 1967)

The energy of combustion of graphite in fluorine was measured with samples of both natural and synthetic graphite. The standard enthalpy of formation, ΔH_f° , of $\text{CF}_4(\text{g})$ was calculated to be -223.04 ± 0.18 kcal mole⁻¹. Combination of this value with other thermochemical data gives -77.02 or -76.75 kcal mole⁻¹ for ΔH_f° [$\text{HF} \cdot 10\text{H}_2\text{O}(\text{l})$], depending on the auxiliary data used.

Introduction

The enthalpy of formation of CF_4 is a key thermochemical datum. CF_4 is an end product of the intensive fluorination of all organic compounds and of inorganic carbides. As such, its importance in fluorine bomb calorimetry is analogous to that of CO_2 in oxygen bomb calorimetry. The importance of $\Delta H_f^\circ(\text{CF}_4)$ led to an early direct determination (-162 kcal mole⁻¹)² and more recent indirect measurements,³⁻¹² with values ranging from -212.7 to -231 kcal mole⁻¹. The selected value of the "JANAF Tables"¹³ (-220.5) has an uncertainty of 2.5 kcal mole⁻¹ assigned to it. Domalski and Armstrong¹⁴ and the present investigators have nearly simultaneously reinvestigated the direct method of determining $\Delta H_f^\circ(\text{CF}_4)$ by burning graphite in fluorine in a high-precision calorimeter. This investigation differs from theirs in that we avoided the large contribution to the measured energy from the use of Teflon as an auxiliary combustant.

Experimental Section

Preliminary Observations and Combustion Technique. It was found that samples of graphite, exposed to fluorine at room temperature, underwent a weight increase in an ill-defined and irreproducible manner. Therefore, some means was necessary to maintain separation of the graphite from fluorine until intentional ignition was desired. It was further found that the amounts of higher fluorocarbons, C_2F_6 and C_3F_8 , formed upon combustion, decreased with increasing pressure of fluorine in the combustion chamber. At 20 atm pressure the amounts of higher fluorocarbons formed required a calorimetric correction which was only about 0.1% of the total measured heat. We, therefore, built a high-pressure two-compartment bomb,¹⁵ laboratory designation Ni-7, for this work.

Satisfactory combustions were obtained with a sample arrangement in which approximately 0.4 g of graphite flakes and several milligrams of silicon pow-

der, used as an ignitor, were contained in a nickel crucible (1.3 cm in i.d., 2 cm high, 1.5 mm in wall thickness, with a base 3.8 cm in diameter and 1 mm thick). About halfway up from the base, a ring of 1.5-mm diameter holes was drilled through the crucible wall. The height of the crucible (as well as a sintered nickel filter disk in the fluorine inlet port of the combustion compartment) was necessary to prevent scattering of the sample when fluorine was admitted to the combustion compartment. The holes in the crucible helped to improve the circulation of gases around the sample during combustion, and the relatively large base provided mechanical stability and better thermal contact with the bomb head.

(1) (a) This work was performed under the auspices of the U. S. Atomic Energy Commission. (b) For the previous paper in this series, see E. Rudzitis, H. M. Feder, and W. N. Hubbard, *Inorg. Chem.*, **6**, 1716 (1967).

(2) H. v. Wartenberg and R. Schütte, *Z. Anorg. Allgem. Chem.*, **211**, 222 (1933).

(3) H. v. Wartenberg, *ibid.*, **258**, 356 (1949).

(4) F. W. Kirkbride and F. G. Davidson, *Nature*, **174**, 79 (1954).

(5) R. S. Jessup, R. E. McCoskey, and R. A. Nelson, *J. Am. Chem. Soc.*, **77**, 244 (1955).

(6) (a) D. W. Scott, W. D. Good, and G. Waddington, *ibid.*, **77**, 245 (1955); (b) W. D. Good, D. W. Scott, and G. Waddington, *J. Phys. Chem.*, **60**, 1080 (1956).

(7) H. C. Duus, *Ind. Eng. Chem.*, **47**, 1445 (1955).

(8) C. A. Neugebauer and J. L. Margrave, *J. Phys. Chem.*, **60**, 1318 (1956).

(9) A. F. Vorob'ev and S. M. Skuratov, *Russ. J. Inorg. Chem.*, **5**, 679 (1960).

(10) (a) V. F. Baibuz, *Proc. Acad. Sci. USSR, Chem. Sect.*, **140**, 1358 (1961); (b) V. F. Baibuz and V. A. Medvedev, *Tr. Gos. Inst. Prikl. Khim.*, **49**, 84 (1962) [cf. *Chem. Abstr.*, **60**, 3555a (1964)].

(11) E. S. Domalski and G. T. Armstrong, *J. Res. Natl. Bur. Std.*, **69A**, 137 (1965).

(12) J. D. Cox, H. A. Gundry, and A. J. Head, *Trans. Faraday Soc.*, **61**, 1594 (1965).

(13) "JANAF Thermochemical Tables," The Dow Chemical Co., Midland, Mich., Sept 30, 1964.

(14) E. S. Domalski and G. T. Armstrong, *J. Res. Natl. Bur. Std.*, **71A**, 105 (1967).

(15) J. L. Settle, E. Greenberg, and W. N. Hubbard, *Rev. Sci. Instr.*, in press.

Calorimetric System. The calorimetric system consisted of the bomb, Ni-7, mentioned before, and the calorimeter, ANL-R2 (a duplicate of ANL-R1, ref 16). For the temperature measurements, we used a quartz crystal thermometer¹⁷ which has as a sensing element a quartz crystal cut in such a manner that its resonating frequency is very nearly a linear function of temperature. The resonating frequency of this thermometer is internally converted to a digitally coded temperature signal which was fed to a digital recorder (HP 562 A), together with the signal from an electronic timer (HP 5512 A), to give simultaneous print-out of time and temperature. Time was measured to 0.1 sec and temperature to 0.0001°. An auxiliary timing device initiated temperature measurements at fixed, controllable intervals. This device permitted automatic measurements on a schedule comparable to typical bomb calorimetric measurements.¹⁸ The printed data were later transferred to punched cards for computer calculation of the corrected temperature rise.

The calorimetric system was calibrated with benzoic acid (National Bureau of Standards Sample 39i) whose certified energy of combustion was 26.434 ± 0.003 abs kJoules g⁻¹ under prescribed conditions. Fifteen experiments, some preceding and some following the graphite combustions, and with temperature rises comparable to those obtained in the graphite combustions, yielded an average value for Δ (calor), the energy equivalent of the calorimetric system, of 3262.92 ± 0.46 (std dev) cal deg⁻¹.

Materials. Natural graphite, in the form of flakes, was separated from Ticonderoga graphite-bearing marble by acid leaches and flotation in methyl iodide. Graphitization and purification of these flakes was accomplished¹⁹ by heating to 3000° in nitrogen and above 2500° in chlorine. The sieved fraction between 16 and 30 mesh was retained for calorimetric combustions.

Synthetic graphite (Pyrogenics, Inc., Woodside, N. Y.) had been prepared by deposition from a carbon-bearing vapor at about 2180°, and graphitization above 3000° in an argon atmosphere. The graphite flakes were sieved, and the fraction between 16 and 30 mesh was retained for calorimetry.

The analyses of the impurities in the samples are given in Table I. Ash contents of <20 and 130 ppm, respectively, for the natural and synthetic samples, are consistent with the listed spectrochemical impurities.

X-Ray diffraction analyses of the graphite samples gave, for both samples, values of $a = 2.462$ Å and $c = 6.714$ Å ($c/a = 2.727$), indicating a hexagonal structure very close to ideal graphite ($a = 2.4612 \pm 1$ Å, $c = 6.7079 \pm 7$ Å, $c/a = 2.7255$, at 15°²⁰). The average crystallite size in the samples was estimated to be about 1000 Å. For both samples, some very faint

Table I: Impurities in the Graphite Samples^a

Impurity	Natural ^b sample, ppm	Synthetic sample, ppm
O	78	175
H	6	15
N	7	16
Cl ^c	3	...
Ca	0.5	20
Na	0.5	18
Si	10	14
Mn	N.d.	11
Fe	1	8
K	N.d.	7
Cu	0.3	7
Mg	3	5
Al	0.2	2
Ag	N.d.	1

^a Oxygen, hydrogen, and nitrogen analyses provided by Chemical Research Services, Addison, Ill.; spectrochemical analyses performed by the Union Carbide Corp., Carbon Products Division, Fostoria, Ohio. ^b Final purification of the natural graphite sample was carried out in two equal batches. Spectrochemical analyses given are the average of two similar results.

Oxygen, hydrogen, nitrogen, and chlorine analyses on the natural sample were performed after blending the two batches.

^c Determined by spark source mass spectrometry (J. A. Carter, Oak Ridge National Laboratory, Oak Ridge, Tenn.) for only the natural sample because of the use of chlorine in the purification procedure. Simultaneously obtained values for the metallic impurities do not differ significantly from those shown in the table.

lines were observed which could be attributed to the presence of a small amount (about 5%) of rhombohedral graphite. The correction²¹ to the heat of combustion for this amount would be only 0.007 kcal mole⁻¹ and is small enough to be neglected. The BET determinations of the surface area gave values of 0.1 and 0.3 m²/g, respectively, for the natural and synthetic samples.

Two samples of graphite, from completely different sources, were studied because of the importance of the enthalpy of formation of CF₄. While the natural flake graphite has a lower impurity content and might be expected to approximate more closely the ideal

(16) E. Greenberg, J. L. Settle, H. M. Feder, and W. N. Hubbard, *J. Phys. Chem.*, **65**, 1168 (1961).

(17) (a) Manufactured by the Dymec Division of Hewlett-Packard (HP), Palo Alto, Calif. (b) R. Hassun and M. C. Swiontek, *Hewlett-Packard J.*, **16**, No. 7, 1 (1965); (c) D. L. Hammond, C. A. Adams, and P. Schmidt, *Instr. Soc. Am., Trans.*, **4**, No. 4, 349 (1965).

(18) W. N. Hubbard, C. Katz, and G. Waddington, *J. Phys. Chem.*, **58**, 142 (1954).

(19) The graphitization and purification steps were carried out by the Union Carbide Corp., Carbon Products Division, Fostoria, Ohio.

(20) (a) J. B. Nelson and D. P. Riley, *Phil. Mag.*, **36**, 711 (1945); (b) J. B. Nelson and D. P. Riley, *Proc. Phys. Soc.*, **57**, 477 (1945); (c) "Structure Reports for 1947-1948," Vol. 11, A. J. C. Wilson, Gen. Ed., published for the International Union of Crystallography by A. Oosthoek, Utrecht.

(21) H. P. Boehm and R. W. Coughlin, *Carbon*, **2**, 1 (1964).

Table II: Results of Natural Graphite Combustion Experiments

Combustion no.	2	4	6	8	10	11	12	13	14
Sample introduced, g	0.39821	0.40019	0.40159	0.39782	0.40114	0.60185	0.19962	0.60018	0.20177
Unburned sample, g ^a	0.01063	0.01058	0.01407	0.01469	0.01280	0.04353	0.00654	0.02773	0.00446
1. <i>m'</i> , sample burned, g	0.38758	0.38961	0.38752	0.38313	0.38834	0.55832	0.19308	0.57245	0.19731
2. Δt_c , deg	2.21197	2.21919	2.20765	2.18371	2.20681	3.18416	1.10471	3.25546	1.12825
3. $\xi(\text{calor})(-\Delta t_c)$, cal	-7,217.48	-7,241.04	-7,203.39	-7,125.27	-7,200.64	-10,389.66	-3,604.58	-10,622.31	-3,681.39
4. $\Delta E_{\text{contents}}$, cal ^b	-12.57	-12.74	-12.55	-12.54	-12.54	-18.21	-6.31	-18.81	-6.37
5. $\Delta E_{\text{Si ignitor}}$, cal	58.65	47.19	57.71	46.41	40.71	91.46	35.96	69.75	35.82
6. $\Delta E_{\text{C-F residue}}$, cal	2.95	2.83	4.16	5.17	6.10	11.03	1.64	7.37	2.99
7. $\Delta E_{\text{C}_2\text{F}_6}$, cal	-9.05	-6.68	-5.03	-6.25	-6.53	-24.50	-1.69	-27.03	-1.69
8. $\Delta E_{\text{C}_2\text{F}_4}$, cal	-2.01	-1.21	-1.21	-1.51	-1.21	-9.48	-0.64	-12.85	-0.50
9. ΔE_{gas} , cal	-0.47	-0.45	-0.47	-0.45	-0.47	-0.62	-0.26	-0.63	-0.25
10. ΔE_{blank} , cal					-0.67				
11. $\Delta E_{\text{C}}/M(\text{sample})$ cal g ⁻¹	-18,526.88	-18,512.79	-18,480.21	-18,518.81	-18,476.72	-18,521.01	-18,523.67	-18,525.95	-18,509.25
Mean $\Delta E_{\text{C}}/M(\text{sample}) = -18,510.6 \pm 6.4$ (std dev) cal g ⁻¹									
Impurity correction = -1.6 \pm 0.2 cal g ⁻¹									
$\Delta E_{\text{C}}/M(\text{graphite}) = -18,512.2 \pm 6.4$ (std dev) cal g ⁻¹									

^a Analyzed carbon content of combustion residue. ^b The contents of the bomb included about 24.2 g of nickel.

crystal structure of graphite, the relative ease of obtaining synthetic graphite makes it more desirable as a thermochemical standard. Both samples meet the criteria recommended by Hawtin, *et al.*,²² in a critical study of the specifications for graphite to be used in the determination of its standard heat of combustion in oxygen.

Finely divided silicon powder, for use as an ignitor, was obtained from Electronic Space Products, Inc., Los Angeles, Calif. The sieved fraction finer than 400 mesh (99% pure) was used for the combustion experiments. Purified fluorine (99.94%) was prepared by distillation of fluorine in a low-temperature still.^{16,23}

Blank Experiments. The use of a two-compartment bomb requires the carrying out of blank experiments (identical with the combustion experiments except for the absence of the sample) to determine the thermal effect when fluorine is allowed to expand from the storage compartment into the combustion compartment to initiate the reaction. The thermal effect is composed of two factors—the endothermic expansion of fluorine into the evacuated combustion compartment and the exothermic reaction of fluorine with the bomb walls and/or any adsorbed moisture. The bomb was pre-conditioned by a number of typical graphite combustions and was subsequently handled in an inert-atmosphere box in order to keep the exothermic effect small and reproducible. The results of ten blank experiments, which were interspersed with the graphite combustions, gave a net endothermal effect of 0.67 ± 0.68 cal per experiment.

There was a small gain in weight of the nickel crucible (presumably due to formation of nickel fluoride) from experiment to experiment. Because the weight gain was comparable in both the blank and graphite experiments, no correction for this was made.

Experimental Procedure. The graphite sample and silicon ignitor were successively weighed into the crucible which was then taken into an inert-atmosphere box and loaded into the combustion compartment of the bomb. The sealed bomb was removed from the inert-atmosphere box, and both compartments were evacuated (usually overnight) with an oil diffusion pump. The connecting valve between the two bomb compartments was then closed, the gas storage compartment was filled with fluorine to 385 psia, and the bomb was placed in the calorimeter for the calorimetric measurements. Following the combustion experiment and recovery of the product gas for analysis, the bomb was evacuated and returned to the inert-atmosphere

(22) P. Hawtin, J. B. Lewis, N. Moul, and R. H. Phillips, *Phil. Trans. Roy. Soc. London*, A261, 67 (1966).

(23) L. Stein, E. Rudzitis, and J. L. Settle, "Purification of Fluorine by Distillation," Argonne National Laboratory, ANL-6364 (1961). (Available from Office of Technical Services, U. S. Department of Commerce, Washington 25, D. C.)

Table III: Results of Synthetic Graphite Combustion Experiments

Combustion no.	1	3	5	7	9
Sample introduced, g	0.39712	0.39909	0.39977	0.40024	0.39995
Unburned sample, g ^a	0.00458	0.00477	0.00515	0.00472	0.00622
1. m' , sample burned, g	0.39254	0.39432	0.39462	0.39552	0.39373
2. Δt_c , deg	2.24376	2.25016	2.24791	2.25668	2.25257
3. $\varepsilon(\text{calor})(-\Delta t_c)$, cal	-7,321.21	-7,342.09	-7,334.75	-7,363.37	-7,349.96
4. $\Delta E_{\text{contents}}$, cal ^b	-12.89	-12.79	-12.91	-12.83	-12.94
5. $\Delta E_{\text{Si ignitor}}$, cal	57.98	44.76	45.30	58.49	77.89
6. $\Delta E_{\text{C-F residue}}$, cal	1.65	1.07	1.57	1.87	3.03
7. $\Delta E_{\text{C}_2\text{F}_6}$, cal	-8.80	-4.59	-5.13	-5.67	-6.42
8. $\Delta E_{\text{C}_2\text{F}_8}$, cal	-2.04	-1.23	-1.07	-1.48	-1.64
9. ΔE_{gas} , cal	-0.48	-0.48	-0.47	-0.47	-0.47
10. ΔE_{blank} , cal	-0.67				
11. $\Delta E_c^\circ/M(\text{sample})$ cal g ⁻¹	-18,562.34	-18,553.51	-18,519.41	-18,517.72	-18,518.22

Mean $\Delta E_c^\circ/M(\text{sample}) = -18,534.2 \pm 9.8$ (std dev) cal g⁻¹Impurity correction = -4.5 \pm 0.6 cal g⁻¹ $\Delta E_c^\circ/M(\text{graphite}) = -18,538.7 \pm 9.8$ (std dev) cal g⁻¹^a Analyzed carbon content of combustion residue. ^b The contents of the bomb included about 24.2 g of nickel.

box for recovery of the unburned graphite residue and loading of a new sample.

Postcombustion Analyses. After each graphite combustion the bomb gases were condensed into a liquid nitrogen cooled trap. Most of the fluorine was pumped off. The gases were then transferred to a bulb containing stirred mercury for removal of the last traces of fluorine. The residual gas mixture was submitted for fluorocarbon analysis by gas chromatography (Chemical Research Services, Inc., Addison, Ill.). The total amount of higher fluorocarbons, C₂F₆ and C₃F₈, was usually of the order of 0.1 to 0.2% of the amount of CF₄. Analysis of the gases in the two compartments of the bomb, following a typical experiment, showed that the fluorocarbon products had remained in the combustion chamber, with only a trace found in the storage chamber of the bomb.

The total mass of the combustion residue was determined by the difference in the weight of the crucible before and after removal of the residue. The mass of carbon in the residue was determined by combustion to CO₂ (Clark Microanalytical Laboratory, Urbana, Ill.). The amount of fluorine in the residue was taken by difference.

Results

The results of nine combustion experiments with natural graphite and five with synthetic graphite are presented in Tables II and III, respectively. The results are expressed in terms of the defined calorie equal to 4.184 (exactly) absolute joules. The corrections to standard states were applied in the usual manner.²⁴ Most of the entries in the table are either self-explanatory or have been previously used and explained.^{24,25} The auxiliary data required for Tables II and III are given in Table IV.

Table IV: Auxiliary Data (25°)

c_p , cal deg ⁻¹ g ⁻¹		ρ , g cc ⁻¹	
C	0.1697 ^a	C	2.2667 ^d
Si	0.170 ^b	Ni	8.907 ^e
Ni	0.1061 ^c		
C_p , cal deg ⁻¹ mole ⁻¹		Atomic wt	
F ₂ (g)	5.493 ^a	C	12.01115 ^f
CF ₄ (g)	12.61 ^a		
SiF ₄ (g)	15.61 ^b		
S° , cal deg ⁻¹ mole ⁻¹		S° , cal deg ⁻¹ mole ⁻¹	
C (graphite)	1.372 ^a		
F ₂ (g)	48.44 ^a		
CF ₄ (g)	62.50 ^a		

^a National Bureau of Standards, Technical Note No. 270-1, U. S. Government Printing Office, Washington, D. C., 1965.^b National Bureau of Standards Technical Note No. 270-2, U. S. Government Printing Office, Washington, D. C., 1966.^c Supplement to R. Hultgren, R. L. Orr, and K. K. Kelley, "Selected Values of Thermodynamic Properties of Metals and Alloys," Lawrence Radiation Laboratory, University of California, Berkeley, Calif. ^d See ref 20c. ^e H. E. Swanson and E. Tatge, National Bureau of Standards Circular 539, Vol. I, U. S. Government Printing Office, Washington, D. C., 1953.^f A. E. Cameron and E. Wichers, *J. Am. Chem. Soc.*, **84**, 4175 (1962).

For calculation of item 5, the energy of combustion of pure silicon in fluorine²⁶ was taken to be 13,722 cal g⁻¹, and this value was then adjusted for impurities present in the silicon used. For calculation of item 6, the correction for the energy evolved for partial fluorine

(24) W. N. Hubbard in "Experimental Thermochemistry," Vol. II, H. A. Skinner, Ed., Interscience Publishers, London, 1962, Chapter 6.

(25) E. Greenberg, J. L. Settle, and W. N. Hubbard, *J. Phys. Chem.*, **66**, 1345 (1962).(26) S. S. Wise, J. L. Margrave, H. M. Feder, and W. N. Hubbard, *ibid.*, **67**, 815 (1963).

nation of the unburned portion of the graphite sample, the value²⁷ of -50 kcal (g-atom of fluorine) $^{-1}$ was used.

Items 7 and 8 are the respective corrections for the fact that small amounts of C_2F_6 and C_3F_8 were formed instead of CF_4 during the combustion. In each case the correction term represents the additional energy which would have been evolved if fluorination to CF_4 had occurred. For the C_2F_6 correction, the enthalpy change²⁸ for the reaction of C_2F_6 with NF_3 was combined with the enthalpy of formation²⁹ of NF_3 to obtain -125 kcal mole $^{-1}$ of C_2F_6 for the fluorination of C_2F_6 to $2CF_4$. Similarly, for the C_3F_8 correction, a value of -250 kcal mole $^{-1}$ of C_3F_8 for the fluorination of C_3F_8 to $3CF_4$ was estimated from the average bond energies in CF_4 and C_2F_6 .

For calculation of item 9, the coefficients μ and $(\partial E/\partial P)_T$ were estimated³⁰ from the intermolecular force constants for F_2 ³¹ and CF_4 .³² The coefficients as functions of composition at 25° are

$$\mu = 7.596 \times 10^{-4} (x^2 - 4.614x + 4.672) \text{ atm}^{-1} \quad (1)$$

$$(\partial E/\partial P)_T = -0.7747(x^2 - 5.574x + 6.872) \text{ cal atm}^{-1} \text{ mole}^{-1} \quad (2)$$

where x is the mole fraction of fluorine in the mixture. Because the blank correction includes the energy of expansion of fluorine from the storage chamber into the reaction chamber, the initial state of the fluorine was taken as its hypothetical condition just after expansion. For the final-state characterization, all of the fluorocarbon products and SiF_4 were considered to be in the reaction chamber of the bomb. The volumes of the storage and combustion chambers are 0.512 and 0.160 l., respectively.

Thermal corrections were made for the impurities in the samples. The correction for trace metals was made on the basis of their combustion in fluorine to their most stable fluoride. Hydrogen and an equivalent amount of oxygen were treated as moisture. Nitrogen, chlorine, and excess oxygen were treated as though uncombined. The products of combustion were considered to be HF , oxygen, nitrogen, and chlorine.

An analysis of the data (F-test) was made to see if the two series are statistically in agreement. The result of the test (4% significance level) is borderline, and it is not possible to establish with certainty whether or not there is a real difference in the results obtained for the natural and synthetic samples. In view of the barely significant result of the test and the fact that the two series overlap, we have taken the weighted mean³³ of the two series, $-18,520.4 \pm 5.4$ (std dev) cal g $^{-1}$, as the best value for the energy of combustion.

The use of widely different sample sizes in some of the combustion experiments results in considerable variation in some of the correction terms. However, these experiments are in good agreement, and we can

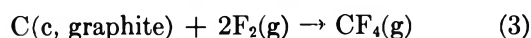
find no trend in the results with respect to mass of sample.

Derived Data. Table V presents derived standard

Table V: Derived Data for $CF_4(g)$ at 25°

Energy of formation, $\Delta E_f^\circ = \Delta E_c^\circ$	-222.45 ± 0.18 kcal mole $^{-1}$
Enthalpy of formation, ΔH_f°	-223.04 ± 0.18 kcal mole $^{-1}$
Entropy of formation, ΔS_f°	-35.75 cal deg $^{-1}$ mole $^{-1}$
Gibbs energy of formation, $\Delta G_f^\circ = \Delta H_f^\circ - T\Delta S_f^\circ$	-212.38 ± 0.18 kcal mole $^{-1}$

thermal data for the formation of carbon tetrafluoride at 25° , as shown by reaction 3.

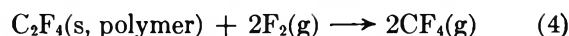


Auxiliary data required for the calculation of derived data are given in Table IV. The uncertainties given are uncertainty intervals³³ equal to twice the combined standard deviations arising from known sources.

Discussion

A comprehensive review of the literature on the enthalpy of formation of CF_4 has been presented by Domalski and Armstrong,¹⁴ and consequently will not be repeated here. The results of their experimental work ($\Delta H_f^\circ = -222.87 \pm 0.38$ kcal mole $^{-1}$) and ours are in excellent agreement despite differences in experimental technique.

Since Domalski and Armstrong's work,¹⁴ Wood, Lagow, and Margrave³⁴ determined the enthalpy of combustion of a sample of Teflon in fluorine



for which they obtained a value of -246.84 ± 0.07 kcal mole $^{-1}$. For this determination they used the same Teflon used by Good, Scott, and Waddington^{6b} in obtaining the value of -160.3 ± 0.9 kcal mole $^{-1}$ for reaction 5 by oxygen bomb calorimetry.

(27) (a) R. F. Porter and D. H. Smith, *J. Phys. Chem.*, **66**, 1562 (1962); (b) J. L. Wood, R. B. Badachhape, R. J. Lagow, and J. L. Margrave, *ibid.*, in press.

(28) G. C. Sinke, *ibid.*, **70**, 1326 (1966).

(29) (a) G. C. Sinke, *ibid.*, **71**, 359 (1967); (b) L. C. Walker, *ibid.*, **71**, 361 (1967).

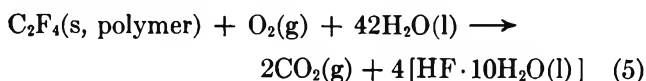
(30) J. O. Hirschfelder, C. F. Curtiss, and R. B. Bird, "Molecular Theory of Gases and Liquids," John Wiley and Sons, Inc., New York, N. Y., 1954.

(31) D. White, J. H. Hu, and H. L. Johnston, *J. Chem. Phys.*, **21**, 1149 (1953).

(32) D. R. Douslin, R. H. Harrison, R. T. Moore, and J. P. McCullough, *ibid.*, **35**, 1357 (1961).

(33) F. D. Rossini in "Experimental Thermochemistry," F. D. Rossini, Ed., Interscience Publishers, Inc., New York, N. Y., 1956, Chapter 14.

(34) J. L. Wood, R. J. Lagow, and J. L. Margrave, *J. Chem. Eng. Data*, **12**, 255 (1967).



Wood, Lagow, and Margrave combined the results of reactions 4 and 5 with Cox and Harrop's³⁵ value of $-77.367 \text{ kcal mole}^{-1}$ for $\Delta H_f^\circ_{298}[\text{HF} \cdot 10\text{H}_2\text{O}(\text{l})]$ to obtain $-223.74 \text{ kcal mole}^{-1}$ for $\Delta H_f^\circ_{298}(\text{CF}_4, \text{g})$. On the other hand, if the value of $-76.235 \text{ kcal mole}^{-1}$ ³⁶ is used for $\Delta H_f^\circ_{298}[\text{HF} \cdot 10\text{H}_2\text{O}(\text{l})]$, one obtains $-221.48 \text{ kcal mole}^{-1}$ for $\Delta H_f^\circ_{298}(\text{CF}_4, \text{g})$. Because of the uncertainty in $\Delta H_f(\text{HF}, \text{aq})$, we prefer to use our CF_4 value in the same cycle, together with values³⁶ of $\Delta H_f^\circ_{298}$ for $\text{CO}_2(\text{g})$ and $\text{H}_2\text{O}(\text{l})$, to obtain a value of $-77.02 \text{ kcal mole}^{-1}$ for $\Delta H_f^\circ_{298}[\text{HF} \cdot 10\text{H}_2\text{O}(\text{l})]$. This result is in general accord with the discussion of Domalski and Armstrong¹⁴ and the results of similar calculations of $\Delta H_f(\text{HF}, \text{aq})$ in which this laboratory's directly determined values for enthalpies of formation of binary fluorides were combined with ΔH solution values from the literature.³⁷

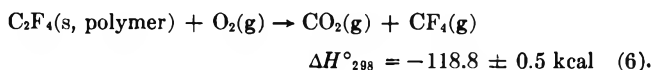
Acknowledgments. We wish to thank M. A. Kanter for supplying the Ticonderoga graphite-bearing marble and for outlining the procedure for preparation of the natural graphite sample. Thanks are also due to C. A. Natke for carrying out some preliminary experiments, H. M. Feder, R. P. Larsen, and E. Veleckis,

for helpful discussions, R. V. Schablaske, R. W. Bane, and G. W. Redding for special analyses, E. H. Van Deventer for checking the calculations, and M. Ader for editorial assistance.

(35) J. D. Cox and D. Harrop, *Trans. Faraday Soc.*, **61**, 1328 (1965).

(36) See footnote *a* of Table IV.

(37) NOTE ADDED IN PROOF. Armstrong, after reading the typescript of this paper, commented that in his paper with Domalski,¹⁴ in the paper of Wood, Lagow, and Margrave,³⁴ and in our paper, too little emphasis has been given to the fact that the enthalpy of combustion of Teflon in fluorine (reaction 4) could be combined with the enthalpy of combustion of Teflon in oxygen, when expressed as eq 6^b



to give a value for $\Delta H_f^\circ(\text{CF}_4, \text{g})$ that is independent of $\Delta H_f^\circ(\text{HF}, \text{aq})$. The result of Domalski and Armstrong for reaction 4 ($-247.92 \pm 0.07 \text{ kcal mole}^{-1}$) leads to $\Delta H_f^\circ_{298}(\text{CF}_4, \text{g}) = -223.17 \text{ kcal mole}^{-1}$; the result of Wood, Lagow, and Margrave leads to $\Delta H_f^\circ_{298}(\text{CF}_4, \text{g}) = -222.1 \text{ kcal mole}^{-1}$. Armstrong suggests the possibility that Wood, *et al.*, might have had incomplete reactions because of the low pressure of fluorine (4 atm) in their reaction vessel. This could account for a slightly less negative value for the enthalpy of combustion of Teflon and, consequently, a slightly less negative enthalpy of formation of CF_4 .

If one accepts that the result of Wood, *et al.*, is low, and uses the result of Domalski and Armstrong (even though obtained with a different sample of Teflon than that used by Good, Scott, and Waddington) to calculate $\Delta H_f^\circ_{298}[\text{HF} \cdot 10\text{H}_2\text{O}(\text{l})]$, as discussed above, the value obtained, $-76.75 \text{ kcal mole}^{-1}$, is still in general accord with the discussion.

Dose and Concentration Dependence of Hydrogen Transfer in the Radiolysis of Dilute Solutions of Cyclopropane in *n*-Hexane and Cyclohexane¹

by Stefan J. Rzad and Robert H. Schuler

Radiation Research Laboratories, Mellon Institute, Carnegie-Mellon University, Pittsburgh, Pennsylvania 15213
(Received July 10, 1967)

The radiation chemistry of ¹⁴C-cyclopropane-hexane solutions has been studied in some detail over the concentration range 10⁻⁴ to 10⁻¹ M in order to examine for possible chemical manifestation of the free-ion yield (~0.1) observed in conductivity experiments. In this system the predominant radioactive products, which appear to result from ion-molecule reactions, are propane formed by H₂ transfer (~50%) and by H transfer (~20%) and mixed nonanes (~30%). At the lower concentrations, very pronounced dose dependence of the yields are observed, which are interpreted in terms of competition of olefins formed in the radiolysis. Assuming a concentration dependence of the form $G = G_i + K\sqrt{[S]}$, a mathematical description of the dose dependence is given which allows extrapolation of the observed yields to zero dose and subsequent evaluation of the low-concentration limiting yield G_i . Similar, but less detailed, observations are also reported for cyclopropane-cyclohexane solutions, where the chemical processes seem to be considerably more complicated than for hexane solutions. The observed values of G_i for the yields of total radioactive products are ~0.05 and ~0.11, respectively, for hexane and cyclohexane. These limiting yields are of the order of magnitude of, and appear to be related to, the free-ion yields in these systems.

During recent years, measurements of electrical conductivity during the irradiation of liquid hydrocarbons²⁻⁴ have drawn attention to the yield of ions which escape geminate recombination. In the absence of an applied field, a "free-ion" yield of the order of 0.1 has been observed in a number of hydrocarbons. One of the major questions of radiation chemistry involves the chemical consequences of the reactions of ions, and, with this in mind, a number of ion-scavenging experiments have recently been carried out. Scholes and Simic,⁵ and more recently others,⁶⁻⁹ have, for example, demonstrated a yield of nitrogen from nitrous oxide-hydrocarbon solutions which appears to result from electron capture by the nitrous oxide. Presumably the positive ions formed by the radiation similarly can react with suitable ion scavengers before neutralization occurs. Williams¹⁰ has found that the irradiation of cyclohexane-ND₃ solutions gives an appreciable yield of HD and interprets this in terms of the reactions of positive hydrocarbon ions with the ND₃. Very recently Ausloos and co-workers^{11,12} have shown that the irradiation of perdeuteriocyclopropane in isopentane and other solvents results in the formation of hexadeuteriopropene, which is specifically protonated in the 1 and 3 positions. Various studies indicate that a major fraction of this propane is formed by the transfer of the H₂ to the cyclopropane in a one-step (presumably ionic)

process. With appropriately high concentrations of ion scavengers, one expects to interfere with the geminate recombination of the original ion partners, and these various studies, for the most part, have attempted to examine the nature of and the concentration dependence of this interference. At very low concentrations of ion scavengers, the free ions, which are manifest in the conductivity experiments, should contribute to and be represented by a constant limiting value of the chemical yield. Detection of these free ions by ion scavengers

(1) Supported in part by the U. S. Atomic Energy Commission; presented at the 154th National Meeting of the American Chemical Society, Chicago, Ill., Sept 10-15, 1967.

(2) A. O. Allen and A. Hummel, *Discussions Faraday Soc.*, **36**, 95 (1963); *J. Chem. Phys.*, **44**, 3426 (1966).

(3) (a) G. R. Freeman, *ibid.*, **39**, 988 (1963); (b) G. R. Freeman and J. M. Fayadh, *ibid.*, **43**, 86 (1965).

(4) W. F. Schmidt, Ph.D. Dissertation, Free University, Berlin, 1966; *Z. Naturforsch.*, in press.

(5) G. Scholes and M. Simic, *Nature*, **202**, 295 (1964).

(6) W. V. Sherman, *J. Phys. Chem.*, **70**, 667 (1966).

(7) S. Sato, R. Yugeta, K. Shinsaka, and T. Terao, *Bull. Chem. Soc. Japan*, **39**, 156 (1966).

(8) G. Meissner and A. Henglein, *Ber. Bunsenges. Physik. Chem.*, **69**, 264 (1965).

(9) K.-D. Asmus and J. M. Warman, to be published.

(10) F. Williams, *J. Am. Chem. Soc.*, **86**, 3954 (1964).

(11) A. A. Scala, S. G. Lias, and P. Ausloos, *ibid.*, **88**, 5701 (1966).

(12) P. Ausloos, A. A. Scala, and S. G. Lias, to be published.

has, however, been very elusive.¹³ The various studies carried out to date have not demonstrated a limiting yield of the order of magnitude observed in the conductivity experiments, and only in the case of the work of Williams on cyclohexane-ND₃ solutions has there been any indication at all that such a limiting yield exists.¹⁴

The present investigation represents an attempt to examine the radiation chemistry of cyclopropane in dilute hydrocarbon solutions. Attention has been focused, for the most part, on hexane where radical scavenging experiments have shown, as discussed below, that the predominant mode of transfer to cyclopropane involves H₂. Auxiliary measurements on cyclohexane, where H-atom transfer is more important and other complications seem to come into play, are also included. ¹⁴C-cyclopropane was used so that the reaction products originating from the solute could be specifically examined. Though complicated by a very pronounced dependence of yield upon dose, these experiments indicate a low-concentration limiting yield of the order of 0.05 for reaction of the cyclopropane in *n*-hexane and 0.11 in cyclohexane.

Experimental Section

Hexane and Cyclohexane. Phillips Research grade *n*-hexane and cyclohexane were passed through a column of activated silica gel and degassed on a vacuum line. These solvents were then distilled onto a fresh sodium mirror¹⁵ and, after standing, transferred on the line to a storage vessel, which to avoid any grease contamination was provided with a metal stopcock. In one case, further purification of a sample of hexane was attempted by stirring it over concentrated sulfuric acid for 72 hr. The sample was subsequently thoroughly washed with water, dried, and treated as above, and the yields of propane and nonane obtained at 10⁻⁴ *M* cyclopropane were essentially the same as obtained in the other experiments. The ultraviolet absorption spectra of the pure degassed solvents before irradiation are shown by the lower curves in Figure 1.

Because of the known¹¹ competing effects of olefins, it is important to have some indication of the possible olefinic impurity level in the starting material. The excellent transmission of the samples at 2000 Å indicates that these impurities are minimal. More quantitative estimates to the upper limits of possible olefin concentration were obtained from measurements of the extinction coefficients of typical olefins. In hexane the *cis*- and *trans*-2- and 3-hexenes have extinction coefficients of the order of 500 at 2050 Å. The maximum possible olefinic contribution to the absorbance of the purified sample is 0.02 at this wavelength. The upper limit of the concentration of these olefins in the hexane is therefore 5 × 10⁻⁵ *M*. For 1-hexene, which absorbs considerably less strongly, an estimate of <6 × 10⁻⁵ *M* is made from observations at 1900 Å, where the ex-

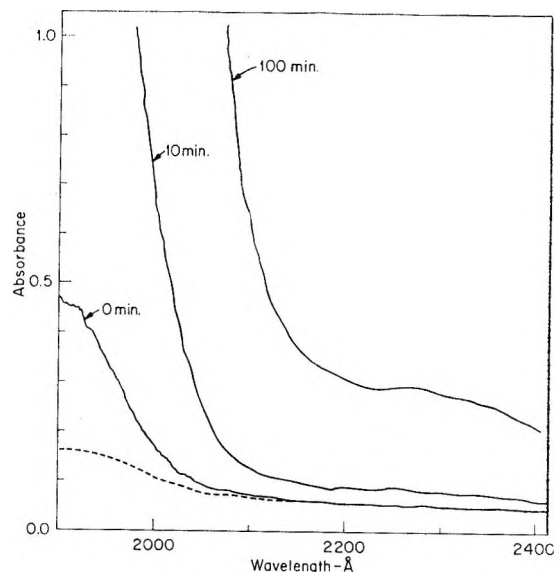


Figure 1. Absorption spectra of degassed solvents: solid curves, initial absorption of hexane and after 10 and 100 min of irradiation at 4.4×10^{17} ev(cc/min)⁻¹; dashed curve, initial absorption of cyclohexane sample.

tinction coefficient is 5000 and the possible contribution to the absorbance is 0.3. If we assume that 1-hexene is not present at a higher concentration than that of the other olefins, the absorbance at 1900 Å indicates that the olefinic impurity level in the hexane is ~10⁻⁵ *M*. The maximum possible concentration of conjugated dienes ($E = 30,000$ at 2250 Å) is 10⁻⁶ *M*. The cyclohexane sample has an even lower absorption in the region of 2000 Å and thus would appear to have an even higher purity level. From measurements on cyclohexene ($E \sim 1300$ at 2050 Å), the maximum olefin concentration is estimated to be ~10⁻⁶ *M*.

¹⁴C-Cyclopropane. ¹⁴C-Cyclopropane obtained from Nuclear Research Chemicals Inc. had a specific activity of 1.5 mcuries/mmol. It was purified gas chromatographically at room temperature using a 1250-cm column packed with 25% silicone grease on Chromosorb P. The retention times of ethylene, propylene, and cyclopropane were, respectively, 8.5, 14.5, and 21 min and afforded complete and quantitative separation of the ¹⁴C-cyclopropane. After purification and throughout the experiments, radiochromatographic analyses

(13) The initiation yield for the radiation-induced ionic polymerization of various monomers is in general stated to be in the range of 0.2 (see for example T. F. Williams, *Discussions Faraday Soc.*, **36**, 254 (1963)). We are concerned in the present study with the use of chemical scavengers in studies of the reactions of ions in saturated hydrocarbons.

(14) While Williams (see ref 10) claims that the cyclohexane-ND₃ study indicates a limiting HD yield of the order of 0.08, a more realistic extrapolation of his data would give a value of 0.02-0.03 although a further correction for the effect of olefin accumulation during irradiation would place the yield at about 0.1 again (*vide infra*).

(15) Drying of the sample is essential, since preliminary experiments in which undried material or those in which 10⁻³ mole/l. of H₂O was added, gave reaction yields only 50% of those of the dried samples.

of the ^{14}C -cyclopropane indicated no significant presence or buildup of radioactive impurities. The specific activity of the cyclopropane was determined by chromatographing a sample of measured pressure and volume under conditions identical with those used in the radiochromatographic analyses. In the experiments at $10^{-4} M$ and at low doses at $10^{-3} M$, the full specific activity was used. In the other experiments, where the sensitivity requirements were not so great, cyclopropane of a lower specific activity was prepared by dilution of the sample with inactive cyclopropane purified as described above.

Sample Preparation. Samples of approximately 10 cc of hexane or cyclohexane were distilled into cylindrical irradiation cells (10 mm i.d. \times 125 mm length) and the desired quantity of ^{14}C -cyclopropane was added. After sealing, the vapor volume was less than 1 cc. The vapor pressure of pure cyclopropane is of the order of 6 atm at room temperature so that, assuming ideal solubility, >99% of the cyclopropane should be in solution. Chromatographic analysis of the liquid phase shows that the cyclopropane is indeed in solution and that it is essentially quantitatively recovered by the syringe techniques used in handling the sample.

In certain experiments, additional liquid solutes (CCl_4 , $\text{C}_2\text{H}_5\text{I}$, 2-hexene, cyclohexene, H_2O) were added to the vacuum line by syringe injection through a silicone rubber septum. This was done to avoid exposure of the solvent to the atmosphere. Iodine was added by breaking an ampoule containing a weighed amount of the solute within the vacuum apparatus.

Sample Irradiation. The samples were irradiated at room temperature within a tubular Co^{60} source. The absorbed dose rate, determined by the Fricke dosimeter, was $4.4 \times 10^{17} \text{ ev cc}^{-1} \text{ min}^{-1}$ in *n*-hexane and $5.1 \times 10^{17} \text{ ev cc}^{-1} \text{ min}^{-1}$ in cyclohexane. Doses were in the range of 0.02–2 Mrads (10^{18} – 10^{20} ev/cc).

Radiochromatographic Analysis. After irradiation, 1 ml of the solution was taken up in a calibrated syringe and injected into a standard radiochromatographic apparatus equipped with both a thermal conductivity detector and a proportional counter.¹⁶ While cyclopropane is readily separated from propane and propylene on a silicone grease column, the latter components are not themselves resolved. Because of this, the analytical columns used consisted of a 1000-cm length packed with 25% silicone grease on a Chromosorb P followed by a 250-cm length of a "modified" silica gel. The excellent separation of the various products of interest is illustrated in the radiochromatogram shown in Figure 2. Once the cyclopropane was out of the silica gel column this column was removed and the silicone grease columns programmed up to 150° to examine the production of higher boiling radioactive products.

The amount of product generated from the ^{14}C -cyclopropane in the 1 cc of chromatographed material

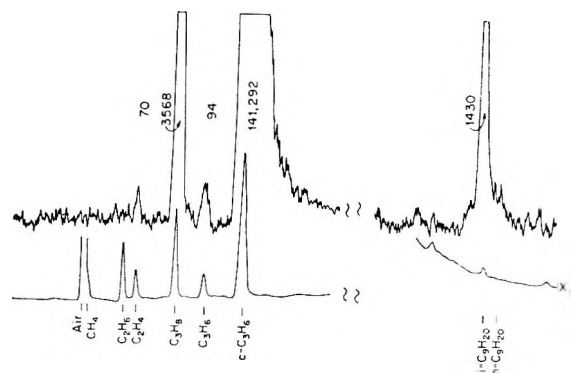


Figure 2. Radiochromatographic trace (upper curve) from $10^{-3} M$ cyclopropane in hexane after dose of $4.4 \times 10^{19} \text{ ev/cc}$. Lower trace is thermal conductivity response. Cyclopropane had a specific activity of 0.15 mcurie/mmmole (10 times diluted). Integrated count for each peak is indicated above the recorded traces.

was determined by assuming that the specific activity of the propane, propylene, and C_9 hydrocarbons was the same as that of cyclopropane. The specific activity of the ethylene produced will of course be only two-thirds that of the cyclopropane. Some C_7 hydrocarbon is produced. It seems likely that in this case only one carbon atom from the cyclopropane is incorporated and therefore that the specific activity will only be one-third that of the cyclopropane. Activities of each of the components were determined from the integrated count recorded before and after passage of a particular peak. As indicated above, comparison of the total activity with that expected from the cyclopropane initially added shows that there is little or no loss of active material in the syringe technique used for introduction of the sample into the column.

Results and Discussion

Hexane Solutions. As is seen in Figure 2, the principal radioactive product from the ^{14}C -cyclopropane-hexane solutions is propane. The particular advantage in the use of labeled cyclopropane in these experiments (in comparison with more conventional experiments) is well illustrated here by the ready observation of a number of other products which incorporate carbon from the cyclopropane. It is seen that a considerable yield of active material (of the order of 40% of that of propane) is observed in the C_9 region. Approximately 10% of this is normal nonane and most of the remaining 90% elutes with 4-methyloctane and 4-ethylheptane, which are not themselves resolved. Two very minor additional C_9 components come off just in front of these principal isomeric nonanes. Small yields of ethylene and propylene are also observed (3–4% of the propane at $10^{-3} M$). The ratio of the yield of nonanes to that of propane is essentially independent of cyclo-

(16) This apparatus is essentially that described by R. A. Holroyd and G. W. Klein, *Intern. J. Appl. Radiation Isotopes*, 13, 493 (1962).

propane concentration while those of ethylene and propylene increase somewhat at the higher concentrations (to ~ 0.15 at $10^{-1} M$). A number of other compounds are produced in small amounts (G 's of the order of 0.001 at $10^{-2} M$ cyclopropane) which are, however, observable only at higher cyclopropane concentrations and higher doses. A typical distribution found in the hexane solutions is given in Table I. Because these minor products are determined only with some difficulty, so that considerable quantitative uncertainty exists in their yields, attention has been focused in the detailed dose and concentration dependence studies, discussed below only on the propane and nonane yields.

Table I: Radioactive Products from the Radiolysis of 0.01 M ^{14}C -Cyclopropane in *n*-Hexane^a

	Total count ^b	Per cent of total activity
CH ₄	30	0.1 ^c
C ₂ H ₆	71	0.2 ^c
C ₂ H ₄	910	3.0 ^c
C ₃ H ₈	18,540	62.7 ^d
C ₃ H ₆	1,410	4.8
C ₃	100	0.3
C ₇	350	1.2 ^c
C ₉ (?)	200	0.7
<i>i</i> -C ₉ ^e	7,370	24.9
<i>n</i> -C ₉	410	1.4
C ₁₂	180	0.6

^a At a dose of 4.4×10^{19} ev/cc. ^b Integrated count from 1 cc of chromatographed sample. Initial cyclopropane activity calculated to be 1,900,000 counts. ^c In calculating the relative yields, the methane activity should be multiplied by 3 and the C₂H₆ and C₂H₄ by 1.5 to correct for the specific activity relative to the C₃ components. It is believed that the C₇ component probably contains only one carbon atom from the cyclopropane, so that a factor of 3 would apply here making the yield comparable to that of ethylene. ^d $G(\text{propane}) = 0.154$. ^e 4-Methyloctane + 4-ethylheptane.

At the lower concentrations the formation of the two principal products is not linear with dose, but decreases considerably as is illustrated in Figure 3. Upon reflection, this falloff in yield is not surprising, since at doses of the order of 10^{19} ev/cc the olefins formed by the irradiation will build up to concentrations comparable to that of the cyclopropane initially added. Since it is known from the studies of Ausloos and co-workers^{11,12} that olefins react at rates similar to that of cyclopropane, these olefins will presumably compete and decrease the yield from the cyclopropane. The importance of the olefin buildup is indicated in Figure 1 by the strongly increased absorption in the region of 2000 Å. A rough estimate of a G of 4.7 was made for the olefin yield from the linear rate of increase of absorbance of 2050 Å.¹⁷ This estimate is somewhat higher

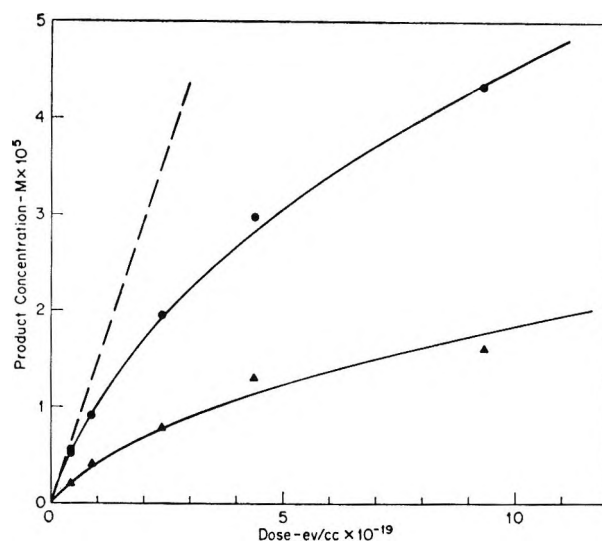


Figure 3. Dose dependence of the product propane (●) and nonane (▲) concentration from a $10^{-3} M$ solution of cyclopropane in hexane. Curves are for the integrated yields as given by the product of (V) and the total absorbed dose.

than the total unsaturation yield of the order of 3.5 reported by Hardwick¹⁸ and by Widmer and Gaumann,¹⁹ but, of course, strong contributions from diene formation would make the estimate from the ultraviolet measurements too high. The broad absorption seen in Figure 1 at wavelengths longer than 2100 Å is apparently due to the formation of a small amount of diene. From the measured extinction coefficient of 1,3-hexadiene (which has a spectrum similar to that found in the irradiated sample), its yield is estimated to be only 0.01. Taking $G = 3.5$, the olefin production rate is $2.55 \times 10^{-6} M/\text{min}$. At the highest dose, reported in Figure 3, at the end of the experiment, the olefin has built up to a concentration of the order of 5 times that of the added cyclopropane.

In order to obtain some idea of the relative reaction rates of the olefins, one experiment was carried out in which $10^{-3} M$ *trans*-hexene-2 (the predominant olefin produced from hexane) was added to a solution of $10^{-3} M$ cyclopropane in the hexane. The propane yield decreased from 0.076 to 0.039. Using the detailed equations from the concentration dependence described below, it is estimated from this observed decrease that the *trans*-hexene-2 is 2.7 times more effective than the cyclopropane. It can be seen, therefore, that at concentrations of $10^{-3} M$ and below, significant competing concentrations of olefins will be built up in even a few minutes irradiation, and that the observed yield will

(17) This estimate was made by assuming that the ratio of hexenes was as given by Hardwick¹⁸ and by Widmer and Gaumann¹⁹ and by weighting the extinction coefficients accordingly.

(18) T. J. Hardwick, *J. Phys. Chem.*, **64**, 1623 (1960).

(19) H. Widmer and T. Gaumann, *Helv. Chem. Acta*, **46**, 945, 2766 (1963).

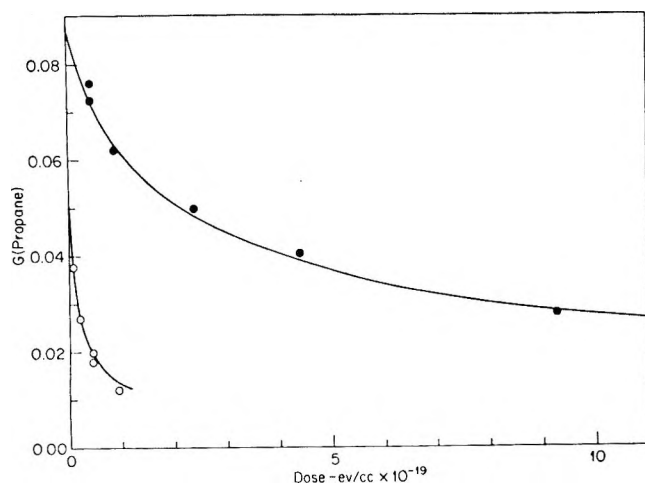


Figure 4. Yield of propane at 10^{-2} (●) and 10^{-4} (○) *M* cyclopropane in hexane as a function of dose. Curves are calculated from (V) with the parameters having the values given in the text.

as a result already be considerably lower than the initial yield.

Because of the strong dependence of yield on dose, a detailed description of the dose and concentration dependence can be arrived at only with some difficulty. The available data, however, allow one to proceed by successive approximations to obtain such a description. It is seen that the yield data given in Figure 4 for 10^{-2} and 10^{-4} *M* cyclopropane solutions can be reasonably extrapolated to zero dose to give values of approximately 0.085 and 0.050, respectively. One run at 10^{-2} *M* at a dose of 4×10^{18} ev/cc, where little dose dependence is expected, gave a propane yield of 0.20. Both the studies of Williams and of Ausloos on positive ion reactions and, more recently, work in these laboratories with electron scavengers (CH_3I and CH_3Cl)²⁰ indicate that at intermediate concentrations, where the yields are in the range of 0.1–1, the reaction yields are very nearly proportional to the square root of the solute concentrations. A plot of the above mentioned propane yields as a function of the square root of the cyclopropane concentration is linear with, however, an intercept of the order of 0.03. In the following it is assumed, therefore, that the dependence on solute concentration ($[\text{S}]$) is described by a relationship of the form^{21, 21a, 22}

$$G = G_i + K\sqrt{[\text{S}]} \quad (\text{I})$$

where G_i represents a concentration-independent yield.

The total effective solute concentration at any time during the irradiation will be given by the sum of the concentration of the cyclopropane added ($[\Delta]$) and the product of the total concentrations of olefins produced (i.e., PD , the production rate times the dose) and the effectivity of the reactions of these olefins relative to the cyclopropane, f . The total yield of ionic reactions should therefore be given by

$$G = G_i + K\sqrt{[\Delta] + f[PD]} \quad (\text{II})$$

and should be distributed between the reactants to give

$$G(\text{propane}) =$$

$$\left\{ G_i(\text{propane}) + K\sqrt{[\Delta] + f[PD]} \right\} \left\{ \frac{[\Delta]}{[\Delta] + f[PD]} \right\} \quad (\text{III})$$

The observed yield of product at any dose will be the integral of this quantity averaged over the dose

$$G_{\text{obsd}} = \frac{1}{D} \left\{ \int_0^D G_i \frac{[\Delta]}{[\Delta] + f[PD]} dD + \int_0^D K \frac{[\Delta]}{[\Delta] + f[PD]^{1/2}} dD \right\} \quad (\text{IV})$$

The integrations of eq IV are readily carried out to give

$$G_{\text{obsd}} = G_i \frac{[\Delta]}{f[PD]} \ln \left[1 + \frac{f[PD]}{[\Delta]} \right] + K[\Delta]^{1/2} \left\{ \frac{2[\Delta]}{f[PD]} \left[\left(\frac{f[PD]}{[\Delta]} + 1 \right)^{1/2} - 1 \right] \right\} \quad (\text{V})$$

Using approximate values of G_i and K (0.03 and 1.6, respectively) obtained from the preliminary plot of (I), the dose dependence was determined from (V) in terms of the remaining parameter fP . Taking the above indicated value of f (2.7) and the olefin production rate (2.55×10^{-5} *M* min⁻¹), this parameter becomes 6.9×10^{-5} *M* min⁻¹ or, in the proper units, 1.57×10^{-22} *M* (ev/cc)⁻¹. Evaluation of (V) with these parameters gives a dose dependence of the form observed and allows a more accurate extrapolation to zero dose with the extrapolated values being fairly insensitive to the choice of the parameters used in this evaluation. Using these extrapolated values in a plot of the form of (I), G_i is found to be 0.033 and K to be 1.60. The upper

(20) K.-D. Asmus, J. M. Warman, and R. H. Schuler, to be published.

(21) Equation I must be regarded as an empirical description of the dependence of yield upon solute concentration and is based on an assumed existence of a low-concentration limiting yield, G_i , and an observed dependence on $\sqrt{[\text{S}]}$, as found at solute concentrations of 10^{-4} to 10^{-2} *M*. An adequate quantitative theoretical treatment of the dependence of the yield upon solute concentration, based on a mechanistic description of the competition between the ion recombination and scavenging processes, does not at the moment exist though recent attempts in this direction (G. R. Freeman, *J. Chem. Phys.*, **43**, 93 (1965); **46**, 2822 (1967); J. W. Buchanan and F. Williams, *ibid.*, **44**, 4377 (1966)) would appear to give a dependence qualitatively in accord with the observed results.

(21a) NOTE ADDED IN PROOF. A. Hummel (private communication) has recently considered the problem of competition between ion scavenging and recombination and has shown that an equation of the form of (I) should be applicable at low scavenger concentrations.

(22) The decrease in yield with dose (or that observed upon the addition of a second solute), in itself, shows that the yield is proportional to something less than the first power of the solute concentration.

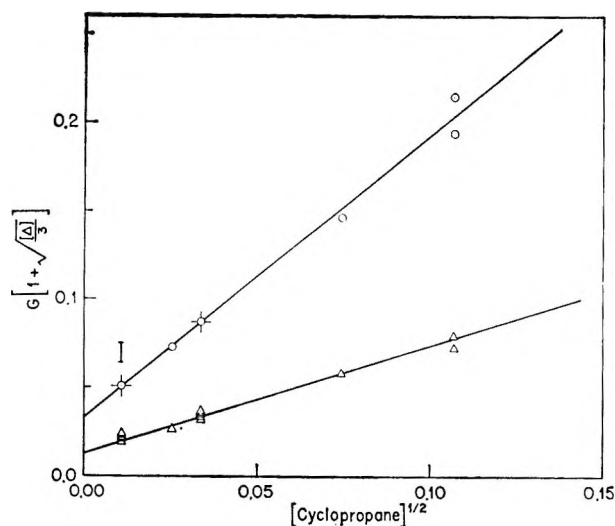


Figure 5. Dependence of the observed zero dose yields of propane (O) and nonane (Δ) upon the concentration of cyclopropane in hexane: flagged points refer to extrapolation of Figure 4; bracketed values at $\sqrt{A} = 10^{-2}$ gives estimates of the increased zero dose yields which would be observed at this concentration should the solvent initially contain between 1 and 2×10^{-6} M olefin.

solid curve in Figure 4 gives the dose dependence of the yield as calculated from (V) with these values taken for the parameters G_i and K and fP taken as 1.72×10^{-22} M (ev/cc) $^{-1}$, as determined from the best fit of the data at 10^{-3} M. Since this analysis of the data is, to a large extent, a matter of curve fitting, it is important to note that these same values of the parameters also describe the dose dependence at 10^{-4} M quite well.

The over-all concentration dependences of the propane and nonane yields are given in Figure 5, where the individual yields have been corrected to zero dose according to (V). At the higher concentrations, the yield must approach some limiting value so that a falloff from the square-root dependence is expected. In the case of a number of electron scavengers, this falloff is described quite well by a dependence of the form²⁰

$$G = G_{\infty} \left(\frac{1}{1 + \sqrt{[S]/A}} \right)$$

from which $G(1 + \sqrt{[S]/A})$ is expected to be proportional to $\sqrt{[S]}$. One experiment at 10^{-1} M gave a propane yield of 0.55, which is essentially as predicted by (I). The correction term $(1 + \sqrt{[S]/A})$ cannot, therefore, be very much larger than unity at the lower concentrations and is taken into account in Figure 5, assuming $A = 3$ (a 5% correction at 10^{-2} M).

Some Comments on the Nature of the Reaction in Hexane. In order to obtain some information on the nature of the reaction, a number of experiments with additional solutes were carried out in hexane and are reported in Table II. Perhaps one of the most im-

Table II: Reaction of Cyclopropane in the Presence of Other Solutes^a

Second solute	Solute concentration $\times 10^4$	C ₂ H ₄	C ₃ H ₆	C ₄ H ₈	C ₅
...	...	0.0029	0.076	0.0030	0.028
I ₂ ^b	0.79	0.0030	0.044	0.0023	0.024
C ₆ H ₁₂ ^c	1.15	0.0044	0.039	0.0026	0.018
C ₂ H ₅ I ^d	124	0.0008	0.0038	0.0012	0.0022
CCl ₄	104	0.0015	0.193	0.0031	0.082

^a Cyclopropane concentration, 1.15×10^{-3} M; dose, 4.4×10^{18} ev/cc. ^b $G(n\text{-propyl iodide}) = 0.020$; no observable isopropyl iodide is formed. ^c *trans*-2-hexene. ^d $G(n\text{-propyl iodide}) = 0.0021$; active pentane < 0.001 .

portant aspects to be examined is that involving possible contributions from radical reactions. Presumably, hydrogen atom (or proton transfer) could result in the formation of propyl radicals which could then form propane by hydrogen atom abstraction, nonane by combination with the hexyl radicals present, or propane and propylene by disproportionation with the other radicals formed. In the latter case, the ratio of each of the disproportionation-combination reactions with the predominant secondary hexyl radicals is estimated from the product entropies²³ to be ~ 0.15 . The low propylene yield indicates that radical disproportionation and therefore, also, combination processes are relatively unimportant and cannot be a major source of the propane and nonanes observed. Presumably, any propyl radicals formed at the low intensities employed here would, for the most part, abstract hydrogen²⁴ (though a small fraction could contribute to the nonane product). The experiment in which iodine was added demonstrates that, in fact, little of the nonane or propylene is formed *via* the production of propyl radicals. The propane yield is reduced by some 40% with the concomitant production of a somewhat lesser amount of active propyl iodide. The total propane + propyl iodide + nonane activity decreases to 85% of that observed from the iodine-free sample. The iodine interferes, therefore, to a small extent with the positive ion reactions. The propyl iodide observed comprises 31% of the total propane + propyl iodide. A contribution to the yield of propane of 0.024, or about 20% of the over-all reaction of the cyclopropane, is attributed to the intermediary production of propyl radicals. The low value of this contribution, together with the absence of isopropyl iodide, shows that any addition of hydrogen atoms, either directly to the cyclopropane or to propylene (active propylene builds up to only 10^{-6} M in this experiment) in a secondary process, cannot

(23) R. A. Holroyd and G. W. Klein, *J. Phys. Chem.*, **67**, 2273 (1963).

(24) R. H. Schuler and R. R. Kuntz, *ibid.*, **67**, 1004 (1963).

be of major significance. At these low concentrations of solutes the hydrogen atoms are, of course, expected to abstract from the solvent.

The results with *trans*-2-hexene have been commented on above. The relative effectivity of the hexene ($f' = 2.7$) was calculated from (V), taking into account an additional constant, $f'[\text{C}_6\text{H}_{12}]$, in the concentration terms to account for competition of this solute. It is also noted that the addition of the hexene does not result in an increase in the propylene, which would be protected from possible secondary reactions in this case. Presumably the propylene yield represents an initial yield.

One experiment was carried out with ethyl iodide as a second solute. The purpose of this experiment was the production *in situ* of ethyl radicals which then, it was thought, would react with any propyl radicals present to form active pentane. The iodide, however, decreased the over-all yield of active products by 90%. Pentane was not observed, but instead a small yield of active propyl iodide was found which again amounted to about one-third of the total C_3 activity. Since it is known that, at this concentration, alkyl radicals abstract iodine from alkyl iodides,²⁵ the propyl iodide presumably was formed by a process which resulted in an interchange of the identity of the radicals. The large reduction in the yield of products produced from cyclopropane shows that, like iodine, the alkyl iodides are good positive ion scavengers.

Scala, Lias, and Ausloos have found¹¹ that the addition of carbon tetrachloride in the region 0.1–1 *M* increases the yield of propane from 0.7 to 2.7 for a solution of 0.3 *M* cyclopropane in isopentane. It was argued that this increase in yield results from the trapping of electrons by the carbon tetrachloride with a resultant increase in the lifetime of the positive ions. It is conceivable, therefore, that the addition of CCl_4 to the dilute cyclopropane solutions might result in an enormous increase in yield. One experiment with 10^{-3} *M* cyclopropane and 10^{-1} *M* CCl_4 , reported in Table II, gave only a 2.5-fold increase in the propane and nonane yields. While the involvement of ionic reactions according to the above argument is indicated, it is noted that the yield in the presence of the carbon tetrachloride is still very dependent on the cyclopropane concentration and does not represent a saturation value. The lifetime of the intermediates seems to be increased, but the probability of reaction with the cyclopropane is still considerably less than unity. Interestingly, the propylene yield observed in this experiment is identical with that of the CCl_4 free sample.

In summary, the three predominant reactions of cyclopropane present in hexane seem to be transfer of an H_2 and H-atom entity to cyclopropane (of the order of 50% and 20%, respectively) and the addition of a C_3H_6 unit directly to hexane in what appears to be a nonradical process (of the order of 30%). The effect

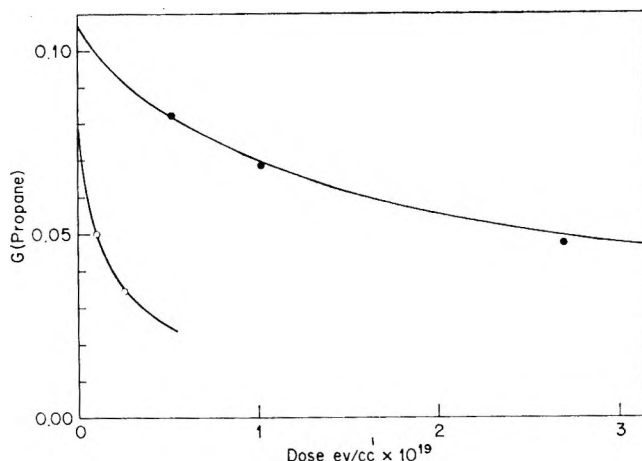


Figure 6. Dose dependence of the propane yields from cyclopropane in cyclohexane at 10^{-4} (○) and 10^{-3} (●) *M*. Curves are calculated from (V) with the parameters having the values given in the text.

of the various solutes indicates very strongly that the precursor of a predominant fraction of each of these processes is a hexane ion. It would appear, from differences in the concentration dependences, that other modes of energy transfer may well be responsible for the formation of ethylene, propylene, and other minor products.

Cyclohexane Solutions. Preliminary experiments on cyclopropane–cyclohexane solutions indicate that the contributions from intermediary production of propyl radicals (iodine scavenging experiments show that propyl radicals are precursors of 55% of the propane) and the formation of minor products are somewhat more important than in the case of hexane solutions. Propane is, however, still the principal product and accounts for ~60% of the total reaction at 10^{-4} *M*. A strong dependence in the importance of the minor products on concentration makes it appear that this case is considerably more complicated than is the case of hexane, and further more detailed investigations on the nature of the reactions are currently in progress. With the above background on the hexane solutions in mind, a number of experiments were carried out to briefly examine the dose and concentration dependence in dilute solution. Since they amplify the results from the hexane studies to a certain extent, they are reported here.

The data obtained at 10^{-3} and 10^{-4} *M* on the dose dependence of the yield of propane are presented in Figure 6. These data are seen to be very similar in form to those of Figure 4. In one experiment at 10^{-3} *M*, in which 10^{-3} *M* cyclohexene was also added, the propane yield was found to be 37% of that from the olefin-free sample. From this, $f(\text{cyclohexene})$ is ~3. Taking $G \sim 3.9$, as estimated from the rate of increase

(25) R. H. Schuler, *J. Phys. Chem.*, **61**, 1472 (1957).

of absorption at 2050 Å, a preliminary value of fP of $1.9 \times 10^{-22} \text{ M (ev/cc)}^{-1}$ was obtained. A yield of propane of 0.177 was observed at $1.09 \times 10^{-2} \text{ M}$ cyclopropane (at a dose of $5.1 \times 10^{18} \text{ ev/cc}$) which together with estimates of the zero dose limits from Figure 6 served to allow preliminary evaluation of G_i and K . Finally, from a best fit of the data, values of $fP = 1.96 \times 10^{-22} \text{ M (ev/cc)}^{-1}$, $G_i = 0.065$ and $K = 1.25$ were obtained for propane formation. The solid curves of Figure 6 were calculated from (V) using these parameters. Again, the same parameters fit the observations at the two concentrations.

Possible Significance of the Parameter G_i . Dividing the low-concentration limiting yield of propane from the hexane solutions (0.033) by the fractional contribution of this product (0.63), a total limiting yield of 0.05 is obtained. The various conductivity experiments give a room-temperature free-ion yield of 0.09–0.10.²⁻⁴ The many difficulties inherent in attempts to use ion-scavenging processes to measure free-ion yields from hydrocarbons are obvious from the contents of this paper. Quantitative chemical manifestation of the reaction of these ions will appear in only the most detailed examination of these systems. In particular, the presence of even a trace quantity of olefin would have a very pronounced effect on the extrapolation of the data of Figure 5. It is estimated that in the experiments at 10^{-4} M cyclopropane, the presence of 10^{-5} M olefin would reduce the observed zero dose yield by 25%. The limits of the heavy bracket in the figure (at $[\Delta] = 10^{-4}$) represent the zero dose yield if the observed value is corrected for reaction with an assumed background olefin concentration of 1 and $2 \times 10^{-5} \text{ M}$. It is seen that extrapolation from the values obtained at higher concentrations, where the yields will be relatively little affected by 10^{-5} M olefin, will result in an appreciable increase in G_i . A value of the total limiting yield of 0.08 is therefore reasonably in accord with an initial olefin impurity level $\sim 10^{-5} \text{ M}$. The directly observed value of 0.05 is, undoubtedly, only a lower limit to the actual value of this limiting yield.

In the case of the cyclohexane solutions, where conductivity measurements give a free ion yield in the range 0.06–0.10,^{3b,4} another difficulty occurs in that G_i for propane (0.065) seems to represent a much less well-defined fraction of the ionic reactions. Taking the 60% observed at 10^{-4} M as representative, the total limiting yield is 0.11. However because of the several large sources of error possible here, error limits of ± 0.03 should be assigned to this value. The higher limiting yield of propane observed in this case, together with the indication that the purity level seems to be better than that in the case of hexane, lends greater credence to the above argument that the G_i observed for hexane is somewhat low.

It is not completely clear whether these total low-concentration limiting yields are merely artifacts result-

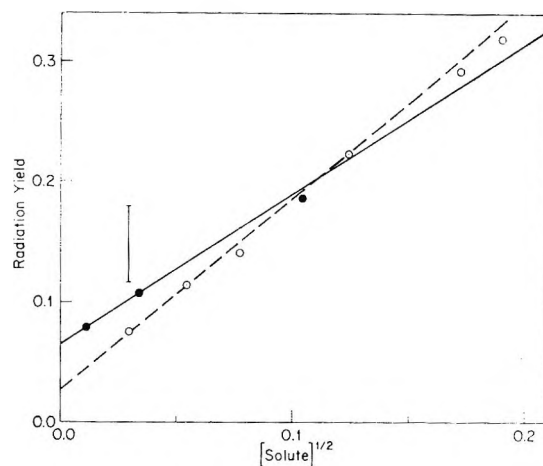


Figure 7. Concentration dependence of the yields of propane from cyclopropane-cyclohexane solutions observed at zero dose (●) and of HD from ND_3 -cyclohexane solutions observed at $3.3 \times 10^{19} \text{ ev/cc}$ (○). The latter data are taken from the work of Williams (cf. ref 10). Bracketed values give estimates of the zero dose yields at $\sqrt{[\text{ND}_3]} = 0.03$, should the applicable corrections be similar to those described here and the relative effectivity of olefin between 1 and 2 times that of ND_3 .

ing from the treatment of the data or whether they can be truly identified with the yields of ions which have not undergone geminate recombination and which are presumably responsible for the conductivity observed during irradiation. It is reasonable, however, to identify the present values of G_i with the yield of free ions. In fact, given any sort of efficiency for the reaction of ions with the solute, one expects that this reaction will compete with the homogeneous recombination of ions²⁶ and thus give a low concentration limiting yield of the magnitude observed.

As mentioned in the introduction, of the various ion-scavenging studies carried out to date, only the work of Williams on ND_3 in cyclohexane has indicated a low-concentration limiting yield. A reasonable extrapolation of the data presented by Williams (see Figure 7), gives an apparent $G_i(\text{HD})$ of 0.02–0.03. Since doses of $3.3 \times 10^{19} \text{ ev/cc}$ were used, the yields measured at the lower concentrations presumably were suppressed to a certain extent by dose effects of the form reported in the present study. The extent to which the zero dose yield might be increased is indicated by the bracketed values in the figure at $[\text{ND}_3] = 10^{-3} \text{ M}$. The limiting HD yield is certainly somewhat higher than that given by a direct extrapolation of the data in Figure 7 and may well be reasonably in accord with a value of ~ 0.1 . It is seen that at higher concentrations the yields for the ND_3 and cyclopropane reactions virtually overlap each other, indicating common precursors which react with not too different rate constants.

(26) The concentration of these ions will be $\sim 10^{-10} \text{ M}$ at the dose rates used here.

From the above it is seen that any more meaningful attempt to probe the production of free ions with ion scavengers will have to be carried out at concentrations of the order of $10^{-5} M$ and below. This, in turn, means that only very limited doses (<1000 rads) can be

used, that the solvents must be ultrapure (maximum impurity levels of the order of $10^{-7} M$), and, of course, that detection sensitivities must be extremely high. These criteria can be met in only the most rigorous of experiments.

Computed Activation Energies and Rate Constants for Forward and Reverse Transfers of Hydrogen Atoms¹

by S. W. Mayer and L. Schieler

Aerospace Corporation, El Segundo, California (Received July 14, 1967)

Activation energies were computed for 324 gas-phase hydrogen-atom transfers between atoms of atomic numbers 1 through 19 (excluding the inert gases) as well as Br and I. Eighteen exchange reactions and 153 reverse reactions were included. A modification of the Johnston-Parr method that considers the temperature region in which the activated complex can be expected to obey small-vibration theory was used to calculate rate constants and rate-equation parameters from 298 to 2500°K. Comparison of computed E_0 and k with experiment show satisfactory agreement over this temperature range, except for the $H_2 + O = H + OH$ transfer. The E_0 and k values for forward and reverse reactions agree very well with theory. Contributions of the activated-complex vibrations and tunneling are discussed briefly.

I. Introduction

In a recent investigation,² the method of Johnston and Parr³ was applied to the computation of rate constants for hydrogen-atom transfers between atoms of atomic number 1 through 11 (excluding He and Ne). The Johnston-Parr treatment was applied to the calculation of only 47 of the 66 transfers listed,² since the square of the Boltzmann average vibrational amplitude of the activated complex was larger than 2π at 1000°K for the other 19 transfers. In this work, the activation energies and rate constant parameters were computed for 324 gas-phase transfers (and are summarized in Table I). The Johnston-Parr method is an *a priori* calculation, involving no adjustable parameters. It used bond properties such as bond energy, vibrational wavenumber, and bond length. Recent supplements to the JANAF Thermochemical Tables⁴ were used as the source of the data needed in these computations, with the consequence that significant changes were made in some bond energies relative to those used previously. The new bond energies ($-\Delta H^\circ_0$ of formation from the gaseous atoms) are: BH, 78.2; BeH, 52.7; LiH, 57.5; NH, 83.2; and OH, 101.3 kcal/

mole. The present work includes the atoms of Mg, Al, Si, P, and S. Molecular parameters for the diatomic hydrides of these atoms are presented in Table II with those for NH, which has a revised vibrational wavenumber.⁴

The computer program previously employed was limited to reactions in the exothermic direction. The program was improved for the present work, and it can also be used for activation energy and rate constant calculations in the endothermic direction of transfer reactions. This improvement permits questions⁵ to be answered relative to the agreement (Table III) of computed rate constants in the forward and

(1) This research supported by the U. S. Air Force under Contract No. AF 04(695)-1001.

(2) S. W. Mayer, L. Schieler, and H. S. Johnston, *J. Chem. Phys.*, **45**, 385 (1966).

(3) H. S. Johnston and C. Parr, *J. Am. Chem. Soc.*, **85**, 2544 (1963).

(4) D. R. Stull, Ed., "JANAF Thermochemical Tables, and Supplements," Dow Chemical Co., Midland, Mich., 1966.

(5) W. E. Wilson, comment on paper by S. W. Mayer, L. Schieler, and H. S. Johnston, "Proceedings of the Eleventh International Symposium on Combustion," The Combustion Institute, Pittsburgh, Pa., 1967, p 632.

Table I: Computed E_0 , $10^{-11}A$, b , and $\log k_{1000^\circ K}$ for 324 H-Atom Transfers

	AlH	BH	BeH	HBr	CH	HCl	HF	H ₂	HI	KH	LiH	MgH	NH	NaH	OH	PH	SH	SiH
	64.3	78.2	52.7	86.6	80.0	102.2	134.8	103.3	70.4	43.2	57.5	45.8	83.2	57.3	101.3	71.8	85.9	42.9
Al	3.8 0.20 1.21 13.08	16.6 4.3 0.72 10.16	4.0 1.8 0.72 12.54	29.9 1.4 0.76 8.88	27.8 0.10 1.07 11.49	27.8 1.9 0.75 6.62	45.6 4.4 0.73 7.11	42.9 32. 0.73 5.28	14.3 0.03 1.40 10.53	7.2 0.52 0.94 11.95	7.2 0.32 1.14 11.51	3.0 2.1 0.67 12.68	21.8 3.6 0.70 8.90	47.3 1.8 0.75 12.28	45.3 1.3 0.80 3.66	8.0 14. 0.5 C	22.7 13. 0.5 C	2.2 1.5 0.67 12.70
B	2.8 2.5 0.72 12.93	5.8 18. 0.5 C	2.4 2.5 0.67 12.89	16.7 0.05 1.27 9.88	8.1 1.05 0.77 11.49	30.9 1.2 0.77 6.62	60.2 5.7 0.58 0.64	29.5 14. 0.73 7.89	7.7 0.78 0.82 11.66	2.2 3.0 0.70 13.11	7.2 0.55 0.98 12.11	0.3 11. 0.5 C	6.8 0.94 0.68 12.20	2.2 4.1 0.68 13.18	24.8 4.2 0.67 8.23	2.6 1.8 0.71 12.82	7.3 0.89 0.81 11.77	1.1 6.5 0.5 C
Be	15.4 5.1 0.72 10.49	27.5 12. 0.67 8.08	11.9 0.40 1.05 11.20	37.0 9.4 0.68 5.91	35.2 1.1 0.79 5.59	51.7 14. 0.67 3.18	84.2 32. 0.67 -4.33	51.3 92. 0.5 C	19.8 11. 0.67 9.71	4.8 65. 0.5 C	21.3 0.80 1.04 9.36	6.5 0.69 0.95 12.26	30.6 27. 0.5 C	8.8 0.53 1.12 12.15	49.0 24. 0.5 C	19.5 32. 0.5 C	33.5 30. 0.5 C	5.8 1.2 0.74 12.08
Br ⁺	7.5 0.66 0.71 11.30	8.1 0.04 1.25 11.55	3.3 1.3 0.67 12.42	0.4 8.6 0.5 C	3.25 0.02 1.22 12.23	15.9 9.9 0.5 C	48.5 21. 0.5 C	19.2 9.3 0.68 10.15	0.3 8.9 0.5 C	12.7 0.35 0.77 10.08	11.6 0.52 0.82 10.63	3.4 0.82 0.67 12.18	0.0 6.7 0.5 C	9.0 0.76 0.71 11.04	14.9 5.8 0.5 11.04	1.8 1.7 0.67 12.85	0.1 6.0 0.5 C	1.6 3.2 0.5 C
C	12.2 0.55 1.00 11.08	6.2 0.81 1.06 12.72	8.2 1.7 0.76 11.73	10.0 0.20 1.22 11.77	35.2 0.13 1.13 11.77	51.7 52. 0.5 C	84.2 24. 0.67 2.02	51.3 63. 0.68 9.23	19.8 6.8 0.69 13.11	4.8 0.85 0.94 11.11	21.3 0.63 1.04 10.08	6.5 3.8 0.68 12.97	30.6 27. 0.5 C	8.8 1.4 0.86 11.40	49.0 24. 0.5 C	19.5 32. 0.5 C	33.5 30. 0.5 C	5.8 1.2 0.68 12.36
Cl	7.8 0.79 0.70 11.28	6.9 0.72 0.74 11.58	2.4 2.0 0.67 12.79	0.4 0.10 0.5 C	0.6 3.2 0.5 C	0.6 11. 0.5 C	33.2 9.2 0.7 12.77	5.9 11. 4.7 C	0.5 11. 0.5 C	12.6 0.42 0.76 10.15	7.4 1.4 0.5 11.62	1.1 5.7 0.5 C	0.3 6.5 0.71 C	9.8 0.78 0.5 10.88	0.1 2.0 0.67 13.30	2.3 1.7 0.67 12.72	0.9 6.4 0.5 C	1.7 3.3 0.5 C
F	5.6 0.9 0.69 11.80	3.6 1.6 0.67 12.46	2.5 1.3 0.67 12.58	0.4 9.5 0.5 C	1.8 1.0 0.67 12.60	0.6 9.3 0.5 C	1.1 0.35 0.99 13.28	1.2 12. 0.67 13.52	0.4 11. 0.5 C	9.9 0.43 0.77 10.78	8.5 0.91 0.72 11.26	0.6 5.2 0.5 C	1.0 5.2 0.5 C	8.0 0.67 0.73 11.26	0.3 4.6 0.5 C	1.9 1.7 0.67 12.80	0.6 5.7 0.5 C	1.9 3.0 0.5 C
H	4.0 5.5 0.58 12.90	4.4 3.9 0.71 12.76	1.3 16. 0.5 C	2.7 8.3 0.67 13.33	2.4 2.4 0.67 12.87	4.8 2.5 0.77 12.67	34.2 11. 0.67 6.58	8.9 5.8 0.78 12.15	1.6 15. 0.67 13.68	4.6 5.6 0.70 12.82	6.1 4.1 0.5 12.43	1.8 21. 0.5 C	1.5 7.1 0.68 13.52	4.0 6.5 0.68 12.18	4.3 1.6 0.76 12.63	1.9 6.9 0.67 13.42	2.8 4.6 0.67 13.11	0.4 13. 0.5 C
I	8.2 0.02 1.34 11.53	15.3 0.62 0.82 9.92	2.3 1.8 0.67 12.76	16.6 8.9 0.5 C	13.0 0.82 0.68 10.11	32.1 11. 0.5 C	64.7 10. 0.5 C	34.2 60. 0.67 7.55	0.1 8.8 0.5 C	12.1 0.47 0.74 10.23	11.1 0.09 1.16 10.99	2.7 5.9 0.5 C	13.0 7.5 0.5 C	7.6 0.98 0.69 11.42	31.0 6.6 0.5 C	3.4 1.4 0.67 12.40	15.4 6.5 0.5 C	0.9 3.4 0.5 C
K	28.4 0.77 0.98 7.61	38.7 2.1 0.89 5.53	14.6 16. 0.5 C	56.3 0.67 0.94 1.34	48.9 0.17 0.94 2.81	71.6 0.93 0.94 -2.13	99.9 1.8 0.79 -9.90	64.7 42. 0.79 0.86	39.4 0.81 0.88 4.93	12.4 0.18 1.32 11.53	25.9 0.48 1.18 8.53	11.2 0.10 1.30 11.44	45.9 2.1 0.85 3.85	12.4 0.24 1.29 11.53	63.5 1.8 0.87 -1.97	37.0 1.2 0.84 5.49	52.9 1.3 0.83 2.00	9.4 0.05 1.28 11.49
Li	17.9 0.29 1.15 10.01	27.9 0.78 1.01 7.84	16.8 0.22 1.08 9.92	40.8 0.69 0.93 4.72	40.2 0.09 1.15 4.60	52.1 2.9 0.78 2.42	85.8 16. 0.83 -5.21	51.8 16. 0.80 3.31	24.1 0.10 1.26 8.51	11.6 0.31 1.14 11.36	20.5 0.43 1.10 9.46	11.2 0.35 1.00 11.79	38.3 0.17 1.15 5.30	10.2 0.38 1.11 7.70	48.7 3.1 0.76 11.30	25.1 0.12 1.19 8.18	36.3 1.0 0.83 5.56	16.1 0.21 0.96 9.68
Mg	21.5 9.1 0.67 9.26	32.6 43. 0.5 C	13.7 1.1 0.96 10.90	43.8 15. 0.67 4.62	37.2 4.1 0.69 5.57	57.5 46. 0.5 C	89.7 41. 0.5 C	59.0 123. 0.5 C	27.2 48. 0.5 C	8.6 0.27 1.27 12.38	19.8 1.6 1.00 9.88	3.4 0.24 0.20 13.23	39.1 15. 0.43 5.60	7.9 0.35 0.25 12.52	56.7 25. 0.5 C	29.4 5.7 0.69 7.40	43.2 7.1 0.68 4.45	8.6 0.16 1.07 11.53
N	2.9 2.4 0.69 12.79	1.7 0.99 0.91 13.34	0.5 2.1 0.5 C	2.4 9.8 0.5 C	3.0 0.11 1.04 12.49	19.3 20. 0.5 C	52.5 16. 0.5 C	21.6 30. 0.67 C	0.4 23. 0.5 C	5.9 1.2 0.76 12.04	12.7 0.26 1.00 10.65	1.7 0.91 0.67 12.95	0.1 0.1 0.91 13.66	7.6 2.1 0.75 11.70	18.3 9.7 0.5 C	6.7 1.0 0.73 11.73	1.2 12. 0.5 C	5.3 0.91 0.67 11.83
Na	22.8 2.1 0.77 8.67	33.0 1.0 0.91 6.80	14.4 0.21 1.16 10.63	48.4 1.5 0.82 3.04	43.4 0.23 0.99 3.84	64.7 1.7 0.83 -1.49	95.6 2.6 0.86 -7.10	59.9 42. 0.77 1.78	30.8 1.7 0.77 6.83	8.3 0.18 1.28 12.78	20.4 0.47 1.13 9.60	6.4 0.12 1.22 12.32	43.4 1.5 0.85 4.23	8.3 0.22 1.25 12.28	55.0 14. 0.5 C	30.7 1.6 0.77 6.80	43.7 2.4 0.73 4.04	5.7 0.17 0.99 11.93
O	8.3 1.1 0.73 11.40	1.5 4.2 0.67 13.30	0.6 9.3 0.5 C	0.3 19. 0.5 C	1.5 3.8 0.67 12.85	0.8 15. 0.5 C	33.7 6.1 0.80 13.41	6.1 22. 0.5 C	0.1 22. 0.5 C	5.3 1.2 0.73 12.11	4.8 2.4 0.71 12.46	1.3 10. 0.5 C	0.1 23. 0.5 C	1.0 0.21 0.5 C	0.1 0.49 0.97 13.56	10.2 0.97 0.71 12.94	1.9 2.3 0.67 12.94	9.6 0.62 0.68 10.75
P	0.7 21. 0.5 C	9.0 3.6 0.71 11.73	0.8 12. 0.5 C	16.7 5.4 0.67 10.08	14.6 0.34 0.85 9.89	32.3 11.0 0.67 6.98	64.5 19.0 0.5 C	33.3 55.0 0.67 7.47	2.1 3.3 0.67 13.08	8.3 1.2 0.75 11.49	10.8 0.22 1.11 11.32	3.3 1.6 0.67 12.49	18.0 1.8 0.74 9.53	6.1 1.9 0.71 12.08	39.8 1.7 0.73 4.73	0.4 0.06 1.27 13.51	15.8 3.6 0.67 10.11	1.5 6.7 0.5 C
S	1.1 20. 0.5 C	0.5 1.7 0.81 13.75	0.5 11. 0.5 C	0.9 20. 0.5 C	0.7 0.07 1.11 12.96	17.0 17. 0.5 C	49.4 18. 0.5 C	20.0 34. 0.68 10.19	0.1 21. 0.5 C	11.6 1.3 0.73 11.08	7.9 1.7 0.76 11.78	3.0 1.8 0.67 12.61	0.0 13. 0.5 C	5.0 2.6 0.68 12.36	17.4 4.4 0.67 9.86	1.7 3.4 0.67 13.18	0.9 4.1 0.67 13.42	1.5 6.5 0.5 C
Si	23.6 10. 0.67 8.84	36.4 51. 0.5 C	15.9 3.1 0.74 10.26	45.3 52. 0.5 C	41.7 3.9 0.68 4.52	60.9 53. 0.5 C	93.6 48. 0.5 C	60.3 145. 0.5 C	28.6 56. 0.5 C	9.6 0.29 1.19 11.95	30.7 1.9 0.91 7.30	11.5 0.30 1.04 11.08	45.6 9.7 0.68 4.12	10.1 1.2 0.93 11.66	68.1 6.3 0.71 -1.06	3.0 36. 0.5 C	44.5 32. 0.5 C	0.8 0.09 1.25 13.54

reverse direction with experimental equilibrium constants. The improved program also permits the computation of the characteristic temperature (Table III) for the bending vibration of the linear triatomic activated complex and the rate-equation parameters at that temperature. Computed activation energies and rate-constant data for exchange reactions (*i.e.*, trans-

fers of an H atom between two atoms of the same element) were obtained in the present work, whereas none were obtained in the preceding investigation.²

II. Results and Discussion

Table I represents an effort to condense into one page the computed activation energy and rate con-

Table II: Bond Parameters^a for Several Hydride Gases

	Bond energy, ^b kcal/mole	Bond length, Å	Vibrational wavenumber cm ⁻¹
AlH	64.34	1.648	1682.6
MgH	45.8	1.731	1496
NH	83.2	1.038	3315
PH	71.83	1.433	2380
SH	85.88	1.350	2700
SiH	42.9	1.520	2042.4

^a See ref 3. ^b $-\Delta H^\circ_0$ of formation from atoms in the gas phase.

$$k = A \times 10^{11} T^b \exp(-E_0/RT) \text{ cc/mole-sec} \quad (3)$$

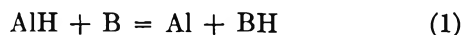
For most of the reactions of Table I, A was calculated in accordance with the Johnston-Parr method. It has been pointed out,² however, that it would be preferable to calculate A on the basis of a collision treatment for those reactions that have a computed Boltzmann average vibrational amplitude, l_ϕ , for the bending mode of the activated complex, greater than $(2\pi)^{1/2}$ at 1000°K. Such reactions are denoted in Table I by the symbol C at the bottom of the box that corresponds to the appropriate pair of reactants; A was then calculated in accordance with the collision treatment followed in the preceding investigation²

Table III: Comparison of Experimental Values with Calculated Results^a

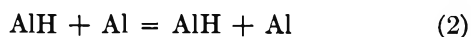
Reactants	HCl + H	HBr + H	HI + H	H ₂ + H	H ₂ + O
Computed E_0 , kcal/mole	4.8	2.7	1.6	8.9	6.1
Obsd E_0 , kcal/mole	4.5 ^b	2.9 ^b	1.3 ^c	8.7 ^d	10.2 ^e
$10^{-9} \times$ computed k , 298°K	6.3	370	4600	0.015	2.7
$10^{-9} \times$ obsd k , 298°K	29	390	8100	0.07	0.001
$10^{-12} \times$ computed k , 1000°K	4.7	22	68	1.4	7.0
$10^{-12} \times$ observed k , 1000°K	6.0	13	37	1.8	0.24
$10^{-12} \times$ computed k , 2500°K	41	92	200	42	160
$10^{-12} \times$ observed k , 2500°K	33	37	60	63	11
$10^{13} F_\phi$, ergs/radian ²	4.69	2.95	1.72	3.99	3.45
T for $l_\phi = (2\pi)^{1/2}$, °K	3400	2140	1250	2890	2490
$\theta_b = 1.44\omega_{\text{bend}}$, °K	766	501	323	995	763
ω_{sym} , cm ⁻¹	1761	2347	2233	2328	1736
A_{coll} , 10^{11} cc/mole-sec	40	45	53	38	37
$i^{-1} \omega_{\text{antisym}}$, cm ⁻¹	1012	496	305	1693	1373
Tunneling factor, 298°K	3.1	1.1	1.2	22	6
Log (k_t/k_r) , 1000°K	-0.10	3.18	6.13	0	0.20
Log K_c , JANAF, 1000°K	-0.02	3.24	6.55	0	0.06

^a k is expressed in units of cc/mole-sec. ^b R. M. Fristrom and A. A. Westenberg, "Flame Structure," McGraw-Hill Book Co., Inc., New York, N. Y., 1965, p 355. ^c J. H. Sullivan, *J. Chem. Phys.*, **30**, 1292, 1577 (1959). ^d See ref 6, p 162. ^e A. A. Westenberg and N. de Haas, *J. Chem. Phys.*, **46**, 490 (1967).

stant data for 324 reactions, which otherwise would have required about six pages of conventional tabular format. Each box of computed data corresponds to the H-atom transfer from the hydride reactant in the heading to the atom listed on the left side of the table. As an example, the box for AlH and B corresponds to the reaction



The box for BH and Al corresponds to the reverse direction of this reaction. And the box for AlH and Al represents, of course, the exchange reaction



The first entry in each box is the activation energy, E_0 , in kcal/mole, as computed by the Johnston-Parr method. The second entry in the box is the computed frequency factor, A , in units of 10^{11} cc/mole-sec for the modified Arrhenius form² of the rate-constant equation (3).

$$A_{\text{coll}} = 6.85(R_{\text{AH}} + R_{\text{BH}})^2 \left(\frac{1}{m_{\text{AH}}} + \frac{1}{m_{\text{B}}} \right)^{1/2} \times \left(\frac{g_{\text{BH}} g_{\text{A}}}{g_{\text{AH}} g_{\text{B}}} \right)^{1/2} \sigma_{\text{AH}} \quad (4)$$

where R denotes bond length in angstroms, AH and B are the reactants, m is mass in molecular weight units, g is the electronic multiplicity, and σ is the symmetry number. Equation 4 was used for all reactions for which F_ϕ , the computed force constant of the bending vibration in the activated complex, was less than 1.38×10^{-13} erg/radian². In these reactions, l_ϕ was larger than $(2\pi)^{1/2}$ at 1000°K, since

$$l_\phi = (2\pi k_0 T / F_\phi)^{1/2} \text{ radians} \quad (5)$$

where k_0 is Boltzmann's constant. For these rigid-sphere collision cases, the third item in each box was 0.5 because this entry corresponds to b , which determines the pre-exponential temperature dependence of

eq 3. For all other reactions, the third item, b , was calculated in accordance with the Johnston-Parr activated complex treatment at the bending-vibration characteristic temperature, θ_b , which equals $1.439 \omega_{\text{bend}}$ (ref 6). The last entry in the box was the logarithm of the computed rate constant at 1000°K , for those cases not treated by the collision theory. Tunneling corrections were not included in these rate constant computations.

In Table I, the bond energy (kcal/mole) for each hydride is tabulated below the formula for the hydride at the heading of each column. These data on bond energies are helpful in discerning some general characteristics of the computed results, in addition to distinguishing between the exoenergetic and endoenergetic direction of each reaction. One characteristic of the computed data is that, for exoenergetic reactions, the Johnston-Parr method is usually applicable for computing rate constants when the computed activation energy exceeds 1.1 kcal/mole. Also, the computed activation energies in the endoenergetic direction agree very well (within an average deviation of less than 0.1 kcal/mole) with the rule that E_0 in the endoenergetic direction exceeds E_0 in the exoenergetic direction by an amount equal to the absolute value of the difference in bond energies between the reactant and product hydrides. Consequently, the rate constants at 1000°K for endoenergetic reactions exhibit a very wide distribution (from 10^{-10} to 10^{13} cc/mole-sec), but those for the exoenergetic reactions fall within a narrower range (from 10^{10} to $10^{13.5}$ cc/mole-sec). The computed results do not support, however, the method suggested by Hirschfelder⁷ for estimating E_0 . For example, computed E_0 for the exoenergetic reactions of HI range from 0.1 to 7.7, whereas 5.5% of the bond energy (*i.e.*, the suggested Hirschfelder approach) equals 3.9 for each of these HI reactions.

Computed activation energies are compared with experimentally observed activation energies, in Table III, for those H transfers that have been the subject of rate investigations over a wide range of temperatures. It can be seen that, except for the $\text{O} + \text{H}_2$ transfer, the agreement between computed and experimental E_0 is remarkably good, with an average deviation of less than 0.2 kcal/mole. The deviation from the mean for the $\text{O} + \text{H}_2$ reaction, however, is 2 kcal/mole. For the reactions of H with HCl, HBr, HI, or H_2 , the computed rate constants at 298°K (Table III) without tunneling corrections were all somewhat lower than the experimental values. This is consistent with the view that tunneling can have a major effect on H-atom transfer rates at 298°K , although the effect at 1000 or 2500°K is relatively minor.³ (The tunneling correction at 298°K will be discussed later.) For the $\text{O} + \text{H}_2$ case, the computed E_0 is less than the observed E_0 and thus overrides the tunneling effect at 298°K , with the result that the computed rate con-

stant is larger than the observed rate constant. (A possible explanation of the deviation between computed and observed E_0 for the $\text{O} + \text{H}_2$ reaction is discussed in terms of increased spin repulsion near the end of this paper.) The computed and observed rate constants for these reactions at 1000°K differ from the mean by an average factor of only 1.27, which is excellent in view of the usual uncertainties in rate constant measurements at 1000°K .

Agreement between computed and experimental k 's at 2500° is good, although the experimental and theoretical rate constants are probably less reliable at such high temperatures. The temperatures at which the bending l_ϕ^2 of the activated complex theoretically begins to exceed the unreasonably² large value of 2π radians are listed in Table III. The $\text{HI} + \text{H}$ and $\text{HBr} + \text{H}$ reactions attain this temperature at 1250 and 2140°K , but the other three reactions do not reach this temperature at 2500°K . Consequently, it may be anticipated that the computed k 's at 2500°K for the $\text{HI} + \text{H}$ and $\text{HBr} + \text{H}$ reactions would not show as good agreement with observed k 's at 2500°K as do the other three reactions; this is borne out by the rate constant data in Table III. The characteristic temperature of bending θ_b is listed in Table III. Small vibration theory will usually be obeyed well by bending vibrations at this temperature θ_b , but will not be followed as well at higher temperatures. For this reason, the value of b in eq 3 was calculated at θ_b , since b is dependent on the vibrational bending wavenumber of the activated complex and is not computed correctly (unless anharmonic terms for the complex can be introduced) at vibrational amplitudes that exceed the limits of small vibration theory. The values of θ_b in Table III are all less than 1000°K , but agreement between computed and observed k at 1000°K of the first four reactions is excellent. This suggests that θ_b does not represent a practical upper temperature limit for activated complex theory, and the limit may be nearer the temperature at which $l_\phi = (2\pi)^{1/2}$. It is perhaps significant, however, that the two reactions, $\text{HBr} + \text{H}$ and $\text{HI} + \text{H}$, that exhibit the lowest values of θ_b and F_ϕ^\ddagger also show the best agreement with experiment at 298°K and the poorest agreement at 1000° and 2500°K , among the first four reactions.

It can be seen in Table I that the values of b , as computed by activated complex theory, vary from 0.67 to about 1.3. This variation is dependent on the vibrational wavenumbers of the activated complex and the reactants since the temperature dependence of the preexponential factor in eq 3, as computed by absolute rate theory, is determined by the vibrational partition

(6) H. S. Johnston, "Gas Phase Reaction Rate Theory," Ronald Press Co., New York, N. Y., 1966, p 91.

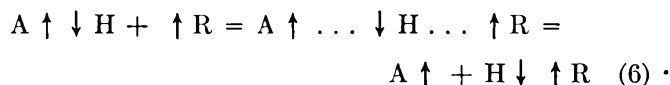
(7) J. O. Hirschfelder, *J. Chem. Phys.*, **9**, 645 (1941).

functions and a $T^{-1/2}$ factor.⁸ For the $\text{HBr} + \text{H}$ and $\text{HI} + \text{H}$ reactions, b does not exceed 0.67, since the symmetric stretching vibrational wavenumber ω_{sym} of the complex and the vibrational wavenumber of the reactant are large enough so that their partition functions have not increased significantly above unity at θ_b . For the $\text{H}_2 + \text{O}$ reaction, however, b is 0.80, inasmuch as ω_{sym} (Table III) is 1746 cm^{-1} , which is low enough so that the vibrational partition function for stretching is appreciably higher than 1.0 at θ_b . The vibrational wavenumber of the H_2 reactant is large enough (4405 cm^{-1}) so that it does not significantly affect b at θ_b for the $\text{H}_2 + \text{O}$ reaction. The value of b should not exceed 1.5 in these transfer reactions, since that is the limit attained at temperatures high enough so that all the vibrational partition functions reach their classical value.

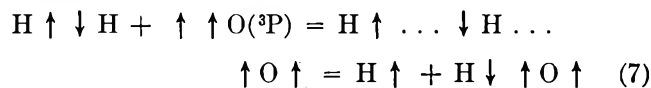
The frequency factor, A_{coll} , calculated in accordance with the collision treatment, eq 4, is listed in Table III. It is evident that the corresponding A in Table I, calculated by the Johnston-Parr activated complex method, is generally smaller than A_{coll} . The solid-angle ratio² for reaction, $l_p^2/4\pi$, and the fact that b_{coll} is 0.5 for hard spheres, contribute to making A smaller than A_{coll} . Table III lists the tunneling factors at 298°K , calculated on the basis of the Eckart barrier (ref 6, p 43 ff), and the computed wavenumbers of the antisymmetric vibration of the complex. It is apparent that the tunneling corrections usually improve the agreement between the computed and observed rate constants at 298°K . Johnston⁶ has pointed out that tunneling corrections higher than 10 should probably not be used, and that the accuracy of tunneling factor calculations has not been established. The last row of Table III lists the logarithm of the equilibrium constant at 1000°K , as obtained from data in the JANAF thermochemical tables.⁴ These values compare very well (Table III) with the logarithms of the ratio of the computed forward rate constant to the computed rate constant in the reverse direction. The average deviation from the mean between K_c and k_f/k_r at 1000°K is less than 15%, which is very high accuracy for rate data. This deviation arises from the usual neglect of anharmonicity and electronic excitation in theoretical rate constant calculations, whereas they are considered in the JANAF thermodynamic calculations.

If the following modification is made to the triplet repulsion considerations of Johnston and Parr,³ the

previously mentioned disagreement between computed and experimental E_0 for the $\text{H}_2 + \text{O}$ reaction is considerably reduced. Johnston and Parr pointed out that a repulsion potential energy contribution to E_0 for H-atom transfers can arise because the electron spin of the unpaired electron of the attacking radical R has the same direction as the spin of the bonding electron on the atom A to which the H atom is initially attached. The direction of electron spin is indicated by the arrows in this model of the reaction



The triplet repulsion between A and R in the transition state was based on that of the nonbonded H_2 ($^3\Sigma_u^+$) state. This model³ is directly applicable if the attacking radical has only one unpaired electron, as in doublet Cl, Br, I, or H. When the attacking radical is triplet $\text{O}(^3\text{P})$ it can be expected that the spin repulsion will be higher because the *two* unpaired electrons of triplet $\text{O}(^3\text{P})$ repel the nontransferred hydrogen atom



If the tentative simple assumption is made that the repulsion is doubled because of the two unpaired electrons on $\text{O}(^3\text{P})$, the computed E_0 for the $\text{O}_2 + \text{H}$ reaction becomes 11.2 kcal/mole. The computed rate constants, at 298, 1000, and 2500°K then become 4×10^5 , 3×10^{11} , and 3×10^{13} cc/mole-sec, respectively. Comparison with the corresponding data in the last column of Table III shows that this type of consideration of increased repulsion does provide considerably better agreement between observed and computed results. When experimental rate data become available for transfer reactions in which triplet or quartet ground states of C, N, P, S, or Si are the attacking atoms, it will be interesting to see whether there are indications of increased spin repulsion.

Acknowledgment. The authors are indebted to H. S. Johnston of the University of California, Berkeley, for valuable correspondence.

(8) S. Glasstone, K. J. Laidler, and H. Eyring, "Theory of Rate Processes," McGraw-Hill Book Co., Inc., New York, N. Y., 1941, p 203.

Infrared Spectra of Kaolin Mineral-Dimethyl Sulfoxide Complexes

by S. Olejnik, L. A. G. Aylmore, A. M. Posner, and J. P. Quirk

*Department of Soil Science and Plant Nutrition, University of Western Australia, Nedlands, Western Australia
(Received July 17, 1967)*

Dimethyl sulfoxide (DMSO) intercalates into the kaolin minerals and increases the basal spacing $d(001)$ from 7.14 Å to approximately 11.16 Å. The rate of intercalation has been measured and found to increase in the order: halloysite > kaolinite > dickite. An explanation of the observed intercalation rates based on the structure of the kaolin minerals and the numbers of interlayer hydrogen bonds is given. The infrared spectra of the kaolin minerals-DMSO complexes were examined. DMSO hydrogen bonds *via* its oxygen atom to the clay hydroxyl surface. The hydrogen bonding involves predominantly the 3690-cm^{-1} hydroxyls of the clay and results in the appearance of sharp peaks at approximately 3658, 3535, and 3499 cm^{-1} . Deuteration of the complex confirms that these peaks are due to perturbed hydroxyls. A model consistent with the infrared and X-ray data is suggested to account for the bonding of the DMSO to the internal surfaces of the clay.

Introduction

Intercalation of potassium acetate and certain other compounds into kaolinite has been examined by a number of workers,¹⁻⁴ using measurements of the change in basal spacing. Infrared techniques were also used by Ledoux and White^{3,4} to determine the nature of the bonding of these molecules to kaolinite.

The compounds examined by Ledoux and White,^{3,4} potassium acetate, hydrazine, formamide and urea, can be classed as protic type compounds; that is, they can either accept or donate protons with suitable molecules to form hydrogen bonds. They can therefore hydrogen bond to both the hydroxyl and oxygen surfaces of kaolinite.

Dimethyl sulfoxide (DMSO) is classed as a dipolar aprotic solvent. It has a large dipole moment (4.3 D.)⁵ and is a proton acceptor, not having any labile hydrogens that it can donate; hence it can only hydrogen bond with suitable donors.

Preliminary X-ray studies indicated that DMSO intercalates into kaolinite with an increase of the basal spacing $d(001)$ to 11.16 Å. The infrared spectrum of intercalated DMSO was deemed of interest: first, because of the unusual properties of DMSO, and secondly, because of the possibility of its hydrogen bonding to the hydroxyl surfaces of kaolinite.

Experimental Section

Kaolinite and dickite were obtained from Ward's Natural Science Establishment Inc. and are the standard clay minerals No. 9 and 15 of API Project No. 49, respectively. X-Ray diffraction showed the kaolinite to be well crystallized with no oxide impurities and a $d(001)$ of 7.14 Å. The dickite contains a small amount of unidentified impurity, and its $d(001)$ spacing is 7.15

Å. A sample of hydrated halloysite was kindly supplied by the Government Chemical Laboratories and originated from near Boorabbin, Western Australia. Electron microscopy revealed it to have the characteristic tubular morphology of halloysites and its $d(001)$ spacing is 10.01 Å.

Other kaolinites used originated from Clackline and Rocky Gully, Western Australia. The Rocky Gully kaolinite, which is a *b*-axis disordered form, contains some iron oxides and gibbsite as impurity⁶ and was used in the K^+ saturated form. A dickite from Pottsville, Pa., was also examined. The Pottsville dickite is a coarse crystalline material and some of it was used as received. A sample was gently ground before use, but even so its particle size was considerably greater than $2\text{ }\mu$. The specific surface areas of the clay minerals were determined by application of the BET method to low-temperature nitrogen sorption isotherms and are given in Table I.

Homoionic samples of the clays (Na^+ saturated form) were prepared by the method of Posner and Quirk,⁷ and the $<2\text{ }\mu$ esd fraction was obtained by sedimentation in distilled water at pH 8.6. Meta-halloysite was prepared by freeze-drying a portion of the

(1) K. Wada, *Am. Mineralogist*, **46**, 78 (1961).

(2) A. Weiss, W. Thielepape, G. Goring, W. Ritter, and H. Schafer *Intern. Clay Conf.*, **1**, 287 (1963).

(3) R. L. Ledoux and J. L. White, *J. Colloid Interface Sci.*, **21**, 127 (1966).

(4) R. L. Ledoux and J. L. White, *Proc. Intern. Clay Conf.*, **1**, 361 (1966).

(5) A. J. Parker, *Quart. Rev. (London)*, **16**, 163 (1962).

(6) D. Muljadi, Ph.D. Thesis, University of Adelaide, 1964.

(7) A. M. Posner and J. P. Quirk, *Proc. Roy. Soc. (London)*, **A278**, 35 (1964).

hydrated halloysite paste and then heating at 140° for 13 hr. It gave a $d(001)$ spacing of 7.34 Å.

Table I: Specific Surface Areas of Kaolin Minerals

	Specific surface area, m ² /g
API No. 9 kaolinite (Na ⁺)	17.7
Clackline kaolinite (Na ⁺)	27.04
Rocky Gully kaolinite (K ⁺)	40.0
Boorabbin halloysite (Na ⁺)	76.27
API No. 15 dickite (Na ⁺)	8.23
Pottsville dickite (natural)	1.01
Pottsville dickite (ground)	13.39

BDH laboratory reagent grade DMSO was dried over molecular sieve Type 5A with intermittent shaking for several days, then distilled through a short fractionating column at reduced pressure. The first few milliliters of distillate was discarded. No water was present in the DMSO as shown by the infrared spectrum of a thin liquid film between AgCl plates forming the cell. Heavy water, of high isotopic purity 99.75% by weight of D₂O, was supplied by the Australian Institute of Nuclear Science and Engineering.

DMSO (2 ml) was added to 20 mg of kaolinite (pre-dried over P₂O₅) and the suspension shaken in an end-over-end shaker at 20 ± 2° for various lengths of time. To obtain uniform oriented clay films for the infrared studies, a portion of the suspension was evaporated onto AgCl disks in a vacuum desiccator at approximately 0.05 mm pressure till all the liquid disappeared. Continuous evacuation, up to 15 hr at 0.005 mm, did not remove intercalated DMSO and had negligible effect on the infrared spectra.

Infrared spectra were recorded with a Perkin-Elmer Model 337 double-beam infrared spectrometer. For the orientation studies, a mask was placed around the disk to eliminate nonuniformity of the clay film near the disk edges. The orientation spectra were all recorded for the same clay film and so are comparable. The clay films on the AgCl disks were unprotected from atmospheric moisture, since the spectra obtained were unaffected by standing in air for a considerable length of time.

X-Ray measurements were obtained using a Philips PW-1010 X-ray generator and Model PW-1050 diffractometer, using iron filtered Co K α radiation at 40 kv and 15 ma and a scanning rate of 0.5° 2 θ /min.

For the kinetic studies, a sample of the clay suspension in DMSO was spread on an unglazed porcelain tile to form a uniform thin layer, covered with thin polythene film to prevent drying and moisture adsorption, and X-rayed. Integrated peak intensities were obtained by the method of Norrish and Taylor⁸

for minimizing background errors, after correcting the recorder peak heights to the same scale factor of the recorder, and assuming the peak half-width does not change significantly with peak height for different scale factors of the diffractometer. X-Ray spacings were also determined on the specimens used for the infrared measurements.

Results

I. Kaolinite A. Rate of Intercalation. Intercalation of DMSO into kaolinite results in a considerable portion of the clay expanding from a basal spacing $d(001)$ of 7.14–11.16 Å. The $d(001)$ value obtained, 11.16 Å, is close to the reported value of 11.18 Å.⁹ The proportion expanded increases with the time of contact with DMSO, suggesting that the rate of intercalation is governed by time-dependent factors. However, even after several months, there is still some clay with a $d(001)$ of 7.14 Å left.

Figure 1 shows a plot of the ratio $I_{(001)\text{complex}} / (I_{(001)\text{complex}} + I_{(001)\text{kaolinite}})$ vs. time for DMSO and several water–DMSO mixtures. The use of this relationship assumes approximately the same degree of particle orientation for both the expanded and unexpanded forms and for different specimens. The figure shows an initial rapid expansion of portion of the kaolinite to $d(001)$ of 11.16 Å, followed by a slower rate of expansion of the remainder. The process is obviously enhanced by the presence of water, which must act as a catalyst in promoting the expansion since its spectrum is never observed together with that of the intercalated DMSO. There appears to be an optimum water content favorable to expansion of approximately 9% (v/v), beyond which the presence of water decreases the rate of expansion of kaolinite.

B. Infrared Spectra. The infrared spectrum of the API-9 kaolinite–DMSO complex, after 38 days shaking, is shown in Figure 2 together with the spectra of kaolinite and liquid DMSO. Hydroxyl stretching bands at 3690, 3664, 3646, and 3617 cm⁻¹ are observed for the kaolinite and correspond to those at 3695, 3670, 3650, and 3620 cm⁻¹, reported previously.^{3,10,11} Vibrational assignments of kaolinite in the low-frequency region are based on those of Farmer and Russell,¹² viz., 1117, 1035, and 1016 cm⁻¹ to in-plane SiO vibrations; 941 and 917 cm⁻¹ to AlOH vibration; 797, 789, 751, and 693 cm⁻¹ to vibrations of the gibbsite-like layers of kaolinite; and 542, 476, 434, and 421 cm⁻¹ to SiOAl skeletal vibrations.

(8) K. Norrish and R. M. Taylor, *Clay Minerals Bull.*, **5**, 98 (1962).

(9) S. Gonzalez Garcia and M. Sanchez Camazano, *Anales Edafol. Agronol.* (Madrid), **24**, 495 (1965).

(10) R. L. Ledoux and J. L. White, "Proceedings of the 13th National Conference on Clays and Clay Minerals," Pergamon Press, London, 1966, p 289.

(11) J. M. Serratosa, A. Hidalgo, and J. M. Vinas, *Intern. Clay Conf.*, **1**, 17 (1963).

(12) V. C. Farmer and J. D. Russell, *Spectrochim. Acta*, **20**, 1149 (1964).

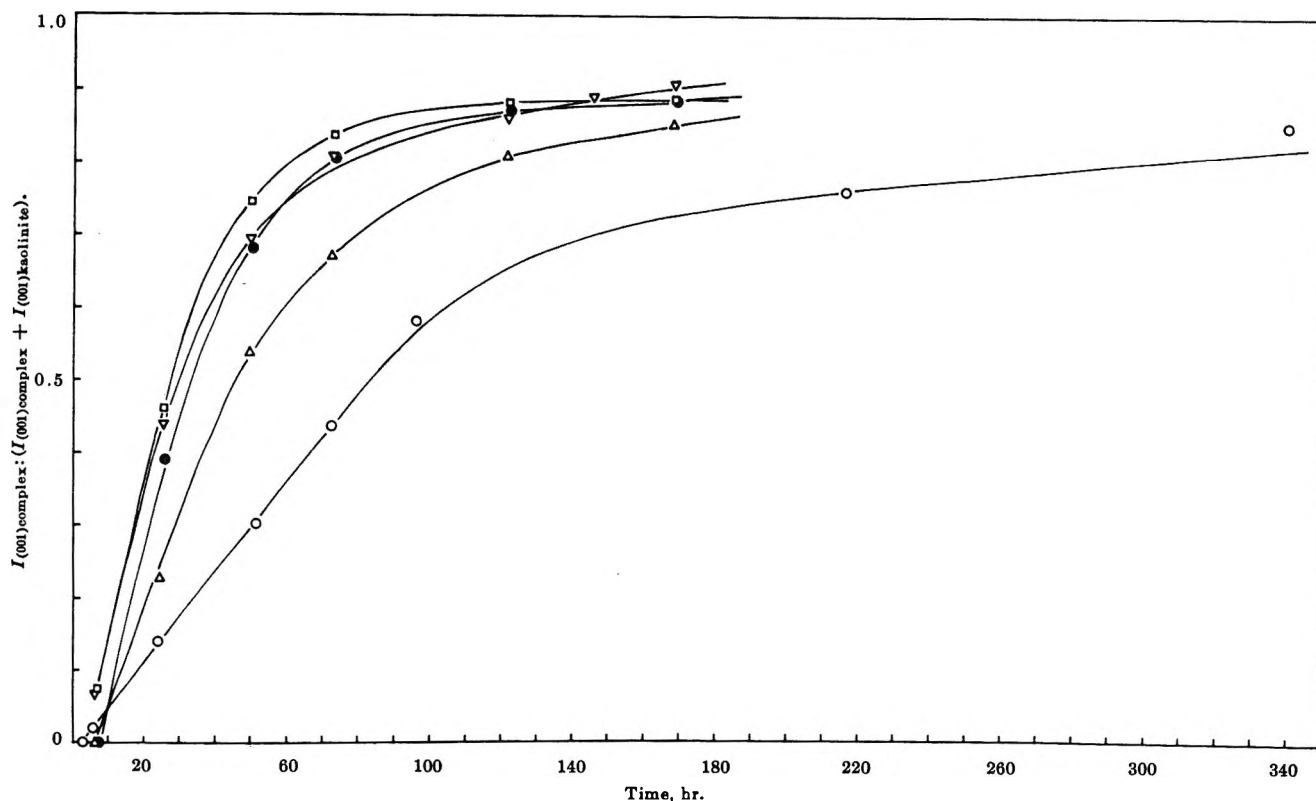


Figure 1. Rate of intercalation of DMSO into API-9 kaolinite in DMSO and water-DMSO solutions: Δ , 0.99% H_2O ; ∇ , 4.77% H_2O ; \square , 9.09% H_2O ; \bullet , 20% H_2O ; and \circ , pure DMSO.

Table II: Vibrational Frequency Assignments of DMSO, Cm^{-1}

Liquid		Solution ^c	Vapor ^d	Assignment
a	b			
2994	2965	3000	2973	Asym CH stretching
2913	2880	2918	2908	Sym CH stretching
1445	1412-1436	1436	1440	Asym CH_3 deformation
1414		1416	1419	
1320		1404	1405	
1303	1312	1325	1319	Sym CH_3 deformation
1288	1007-1075	1306	1304	
1057		1291	1287	SO stretching
		1055	1102	
		1012	1016	
			1006	CH_3 rocking
953	950	946	929	
929	930	921	915	
896	897	887	898	Asym CS stretching
699	696	690	689	
669	665	661	672	Sym CS stretching

^a This work. ^b Salonen.¹³ ^c In chloroform and carbon disulfide solvents. ^d F. A. Cotton and W. D. Horrocks.¹⁵

The infrared spectrum of the liquid DMSO used here is similar to that published by Salonen,¹³ with the exception that he obtained broad bands at approximately 3430 and 1650 cm^{-1} due to incomplete removal of water from his sample. Vibrational assignments have been made for the liquid,¹³ in dilute solution in chloroform and carbon disulfide,¹⁴ and in the vapor phase.¹⁵ Although the vibration frequencies differ slightly, the

assignments are similar and are given in Table II, together with the present results.

Sharp absorption bands appear at 3658, 3535, and

(13) A. K. Salonen, *Ann. Acad. Sci. Fennicae*, **67A**, 5 (1961).

(14) F. A. Cotton, R. Francis, and W. D. Horrocks, *J. Phys. Chem.*, **64**, 1534 (1960).

(15) F. A. Cotton and W. D. Horrocks, *Spectrochim. Acta*, **17**, 134 (1961).

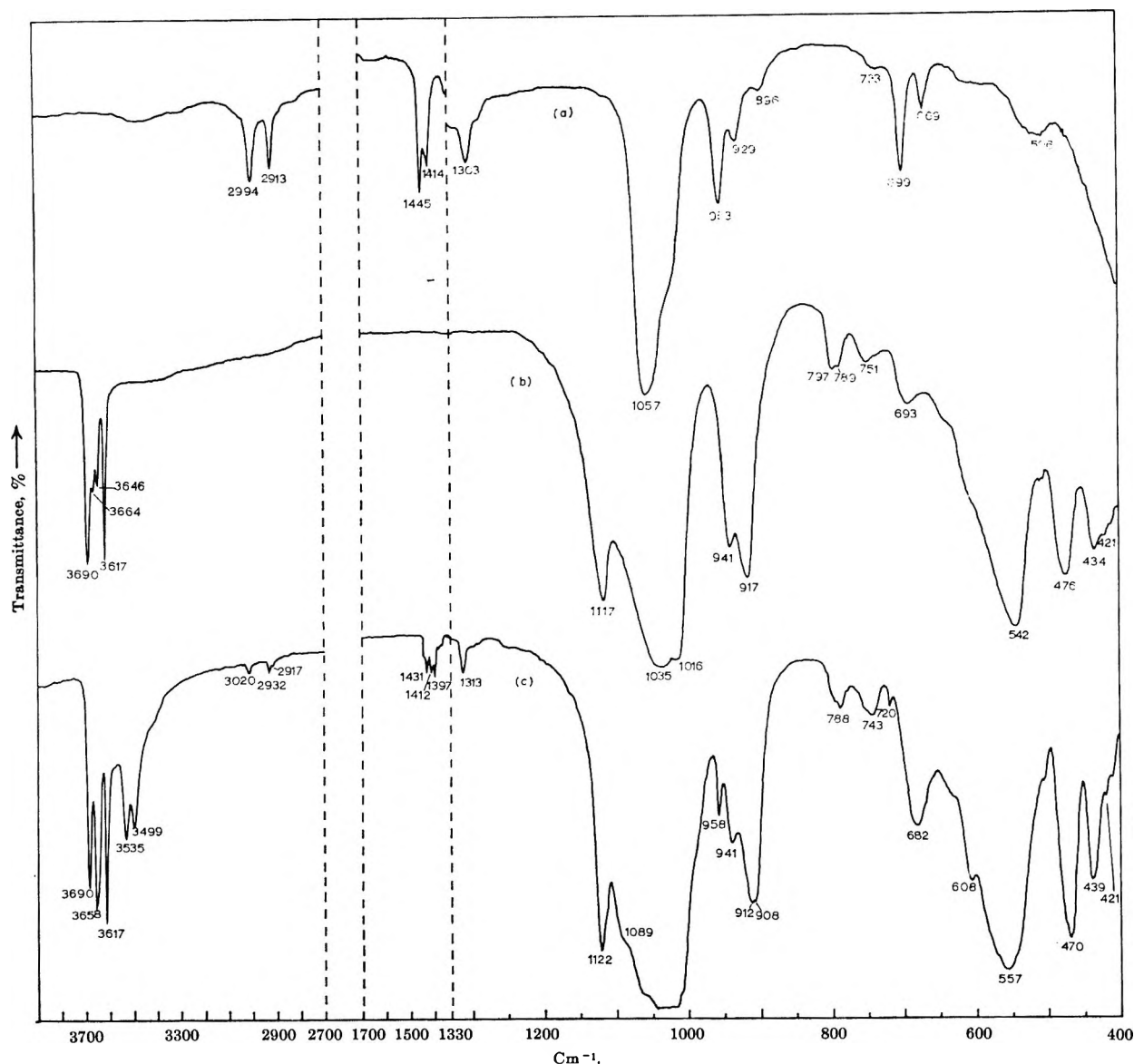


Figure 2. Infrared spectra of (a) liquid DMSO, (b) API-9 kaolinite, and (c) API-9 kaolinite-DMSO complex.

3499 cm^{-1} in the infrared spectrum of the complex. These peaks increase in intensity with time as the 3690-cm^{-1} peak intensity decreases. An increasing sharpness and delineation of the shoulder at approximately 1089 cm^{-1} and the peak at 608 cm^{-1} , and also a marked intensity decrease of the AIOH vibration of 941 and 917 cm^{-1} occur with the amount of DMSO intercalated, the 941-cm^{-1} peak decreasing more than the 917-cm^{-1} peak. These results indicate that bonding of DMSO is to the hydroxyl surface of the kaolinite sheets. Intercalation of DMSO shifts the perpendicular modes of kaolinite at 751 and 693 to 743 and 682 cm^{-1} , respectively, with an intensity increase. The other kaolinites showed similar behavior to the API-9 kaolinite in the appearance of sharp peaks at around 3655 , 3530 , and 3497 cm^{-1} .

C. Effect of Heating and Evacuation on the Complex. Continuous evacuation of the API-9 complex on a AgCl

disk for 2 hr over silica gel slowly removes the DMSO, increasing slightly the 3690-cm^{-1} peak intensity while decreasing the 3658 -, 3535 -, and 3499-cm^{-1} peak intensities. Longer evacuation, up to 15 hr, restores the original hydroxyl peaks of kaolinite, except for an additional small peak at 3540 cm^{-1} (Figure 3). Although the X-ray patterns show that evacuation over silica gel for several hours collapses most of the kaolinite to a $d(001)$ of 7.14 \AA , the infrared spectra still show the presence of some DMSO on the kaolinite. Peaks in other regions of the infrared associated with the complex gradually disappear on evacuation. Removal of DMSO from the complex apparently causes some irreversible changes in the kaolinite structure, as the infrared spectrum after evacuation is not the same as for the original kaolinite (compare Figures 2b and 3). Heating the DMSO complex has the same effects as evacuation over silica gel, the rate of removal of the

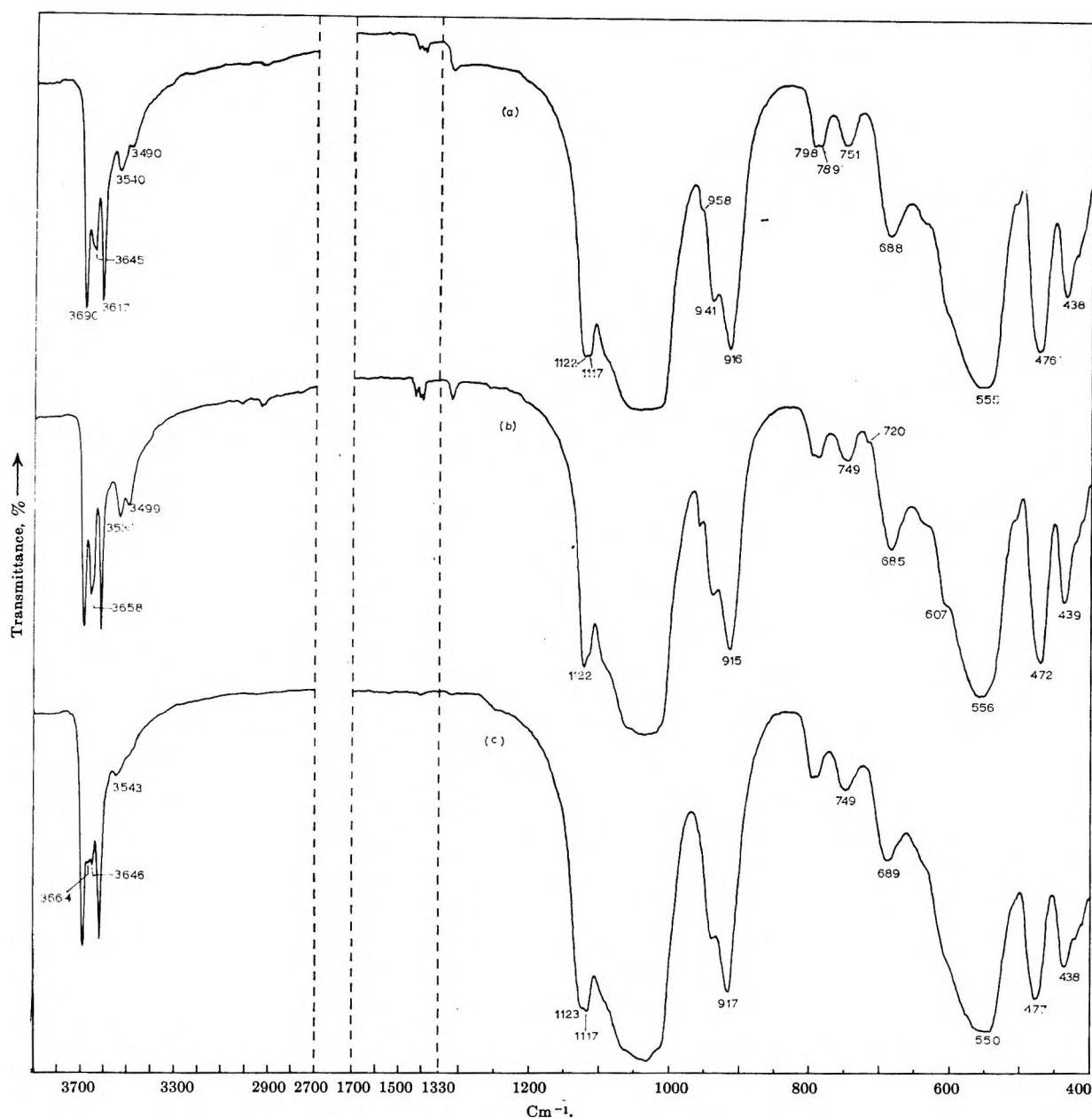


Figure 3. Infrared spectra of kaolinite-DMSO complex (a) evacuated over silica gel approx 5 hr, (b) heated 65° for 30 min, and (c) heated 100° for 15 min.

DMSO depending on the temperature of heating. A slight peak appears at 3543 cm^{-1} and remains even after heating for 9 hr at 105°.

D. Deuteration of the Kaolinite-DMSO Complex. Only a small amount of OH-OD exchange occurred after 7 days when the clay was expanded by DMSO containing 10% D_2O . However, considerably more exchange took place after 2 months (Figure 4d). If the clay-DMSO complex is washed with pure D_2O for 3 1-hr periods, partial deuteration of the kaolinite takes place and effects complete removal of intercalated DMSO with a collapse of $d(001)$ to 7.14 Å. Figure 4a, b, c shows the successive stages in this deuteration. The X-ray patterns demonstrate that complete removal of DMSO and collapse of the $d(001)$ spacing occurs only

during the third wash. Apart from a shift of some peak positions due to deuteration, washing with D_2O or H_2O appears to restore the kaolinite to its original form, unlike evacuation or heating.

Peaks at 2623 and 2597 cm^{-1} appear in the deuterated DMSO complex. The isotopic ratio of frequencies $\nu\text{OH}:\nu\text{OD}$ to the 3535- and 3499- cm^{-1} peaks is 1.3477 and 1.3473, respectively. Hence, the 3535- and 3499- cm^{-1} peaks are due to perturbed hydroxyls on the kaolinite surface hydrogen bonded to DMSO. It appears that only the 3690- cm^{-1} hydroxyls of kaolinite are largely involved in hydrogen bonding. A peak at 2672 cm^{-1} is attributed to deuteration of the inner hydroxyls, Figure 4d.¹⁰

E. Pleochroism of the Kaolinite-DMSO Complex.

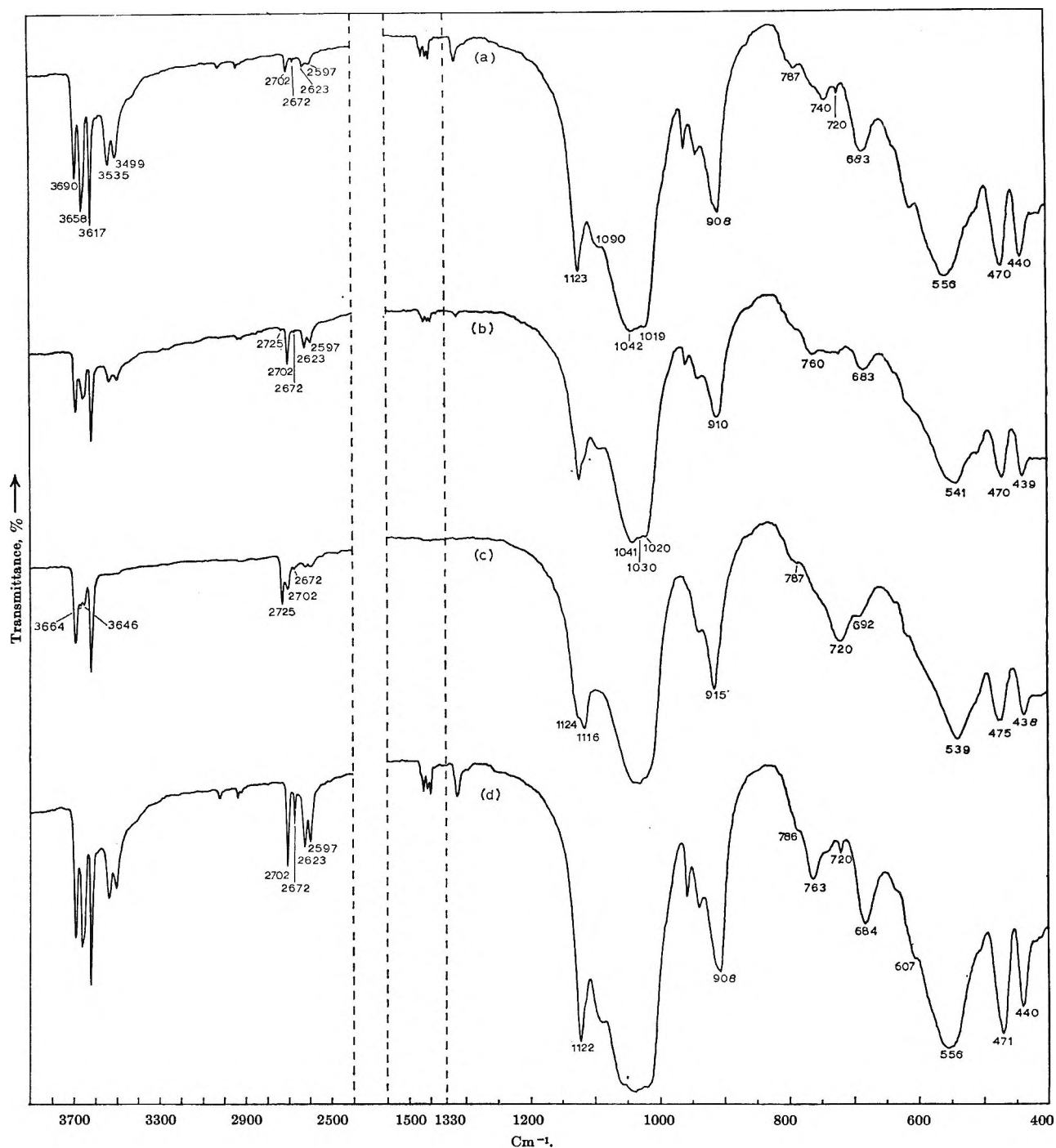


Figure 4. Infrared spectra of deuterated kaolinite-DMSO complex: (a) kaolinite-DMSO complex washed with D_2O for 1.25 hr; (b) D_2O in (a) replaced by fresh D_2O and washed for a further hour; (c) as (b) and washed for another hour; and (d) kaolinite treated for 2 months with DMSO containing 10% D_2O .

The pleochroism of an oriented film of the kaolinite-DMSO complex on an AgCl disk was examined at several angles of incidence. The pleochroism of the peaks is essentially the same in the hydroxyl region of the complex as in pure kaolinite, indicating that the dipole moment change of the perturbed hydroxyls, which are hydrogen bonded, is much the same as in the original unexpanded kaolinite. A shoulder at approximately 3646 cm^{-1} appears to be slightly more pleochroic than the 3658-cm^{-1} peak.

II. Halloysite. A. Infrared Spectra. Intercalation of DMSO into hydrated halloysite displaces the interlamellar water and expands halloysite to $d(001)$ of 11.13 Å , as in kaolinite. Metahalloysite similarly expands to 11.16 Å , though more slowly than hydrated halloysite. The infrared spectra of the halloysite-DMSO complex and hydrated halloysite are shown in Figure 5. The interlayer water of the hydrated halloysite is shown by the bands at approximately 3440 and at 1630 cm^{-1} . The infrared spectrum of fully

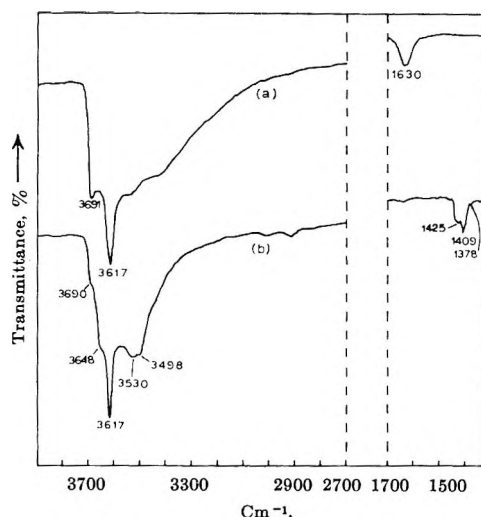


Figure 5. Infrared spectra of (a) hydrated halloysite, and (b) hydrated halloysite-DMSO complex.

hydrated halloysite was difficult to obtain by the method used.

Two hydroxyl bands were observed in halloysite at 3691 and 3618 cm^{-1} ; they correspond to bands at 3695 and 3620 cm^{-1} , respectively, previously reported^{10,11} for halloysite. A broad band from approximately 3498 to 3530 cm^{-1} and two shoulders at 3690 and 3648 cm^{-1} are seen in the infrared spectrum of the halloysite-DMSO complex. The broad-band contour suggests that it consists of two slightly broadened overlapping peaks, just unresolved by the instrument and thereby appearing as one (compared with Figure 2c for the kaolinite-DMSO complex). Intercalation of DMSO into the kaolin clays therefore involves hydrogen bonding between the 3690- cm^{-1} hydroxyls and DMSO, as shown by the similar infrared spectra and reduction of the 3690- cm^{-1} peaks in the kaolinite-DMSO and halloysite-DMSO complexes.

B. Deuteration and Heating of the Halloysite-DMSO Complex. Analogous behavior to the kaolinite-DMSO complex is observed for the halloysite-DMSO complex on D_2O washing for hourly periods or heating. Heating collapses the halloysite to $d(001)$ of 7.34 Å. A weak band at approximately 3665 and a shoulder at 3641 cm^{-1} appear in the heated sample. These bands could be the halloysite analogs of the kaolinite peaks at 3664 and 3646 cm^{-1} , respectively. Washing the meta-halloysite-DMSO complex with water rehydrates the halloysite and the $d(001)$ spacing collapses from 11.16 to 9.97 Å; Wada¹ similarly rehydrated meta-halloysite using potassium acetate.

III. Dickite. The unground Pottsville dickite gave no intercalation of DMSO even after 3 months. Intercalation of DMSO took place with the ground Pottsville and API-15 dickites with the $d(001)$ spacing increasing to 11.14 Å. However, the intercalation rate is much slower than with kaolinite. Virtually no expansion occurs after 8 days and even after 40 days the ratio

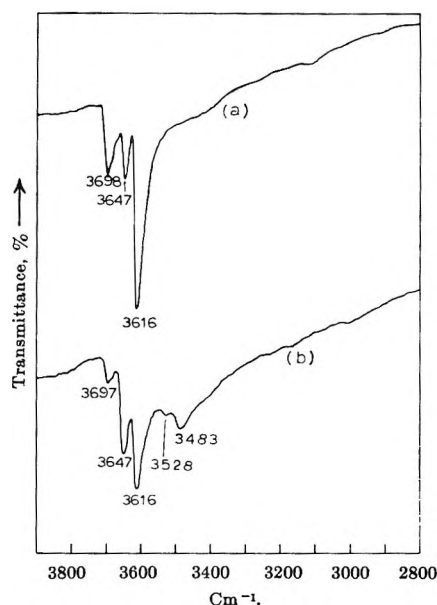


Figure 6. Infrared spectra of (a) Pottsville dickite, and (b) Pottsville dickite-DMSO complex.

$I_{(001)\text{complex}} : (I_{(001)\text{complex}} + I_{(001)\text{dickite}})$ is only 0.339 (compare with 0.72 for kaolinite after 7 days, Figure 1).

The infrared spectrum of the dickite-DMSO complex is essentially similar to the kaolinite-DMSO complex spectra (Figure 6) with a few slight differences. The two new peaks at 3528 and 3483 cm^{-1} appear broader and more intense for the same amount of expansion, compared to their kaolinite counterparts, and the 3483 cm^{-1} peak is the stronger. There is also an intensity increase of the peak at 3647 cm^{-1} and a decrease in the 3698- cm^{-1} peak intensity. The infrared spectrum of the API-15 dickite-DMSO complex is less distinct but essentially similar to the others.

No evidence could be obtained of any intercalation of DMSO into gibbsite or goethite, presumably because of the stronger interlayer hydrogen bonding in gibbsite.

Discussion

A. Nature of the Hydroxyl Interactions. The interesting feature of the infrared spectrum of intercalated DMSO is the appearance of sharp peaks in the regions of 3658, 3535, and 3499 cm^{-1} and decreased intensity of the peak at about 3690 cm^{-1} . In contrast, the intercalation of potassium acetate, hydrazine, formamide, and urea markedly decreases the 3695-, 3670-, and 3650- cm^{-1} peak intensities^{3,4,10} and new broader bands at lower frequencies are seen instead. To explain these observations, Ledoux and White^{3,4,10} propose hydrogen bonding between these hydroxyls and the intercalated molecules.

The intensity increase of the 3658-, 3535-, and 3499- cm^{-1} peaks occurs simultaneously with an intensity decrease of the 3690- cm^{-1} peak as more DMSO is intercalated. Removal of DMSO and collapse to

$d(001)$ of 7.14 Å, by heating, restores the original hydroxyl peaks of kaolinite. Hence, bonding of DMSO to kaolinite involves only the 3690-cm^{-1} hydroxyls and is responsible for the appearance of peaks at 3658, 3535, and 3499-cm^{-1} .

It is suggested that intercalation of DMSO results from the DMSO breaking the interlayer hydrogen bonds and reforming them with itself. In addition, new hydrogen bonds are formed. The sharpness of the new peaks at 3535 and 3499-cm^{-1} and marked increase in intensity at 3658-cm^{-1} is uncommon for hydrogen bonding. The DMSO hydrogen bonds to some of the 3690-cm^{-1} hydroxyls *via* its oxygen atom (see below) and gives rise to the hydroxyl peaks at 3535 and 3499-cm^{-1} . Crystal-field effects, caused perhaps by distortion in the kaolinite lattice, symmetry factors, or degeneracy of the vibrations, cause two relatively sharp peaks instead of one broad band to be observed. The geometry of the system may also permit different arrangements of the DMSO oxygens with respect to the hydroxyl layer leading to a splitting of the bands.

Dimethyl sulfoxide hydrogen bonds *via* its oxygen atom and so may be relatively mobile between the layers compared to substances such as formamide that bond to both the hydroxyl and oxygen surfaces of kaolinite and are restricted in their mobility. The DMSO will arrange itself to give the least expansion consistent with minimum interaction between adjacent molecules. This may lead to some of the oxygen atoms of DMSO being positioned in a similar situation with respect to the hydroxyl layer as the oxygen atoms of the adjacent tetrahedral layer in unexpanded kaolinite. The increase in number of such weak hydrogen bonds would result in the increased intensity of the 3658-cm^{-1} band. Its broadened band width compared to the 3690-cm^{-1} peak is consistent with a slight shift to lower frequencies of the 3690-cm^{-1} peak.

The reduced crystallinity and randomness in structure of halloysite probably does not allow such marked splitting to occur, resulting in two closely overlapping bands at 3530 and 3498-cm^{-1} and a shoulder at approximately 3648-cm^{-1} , instead of the sharper peaks observed for the kaolinite-DMSO complex. Two bands at 3528 and 3483-cm^{-1} , corresponding to those obtained for the kaolinite couple at 3535 and 3499-cm^{-1} , respectively, are also observed for the ground Pottsville dickite complex. Their large intensity and overlap may be related to the frequency shift resulting from an increase in bond strength, once entry of DMSO has been gained. The appearance of the 2725-cm^{-1} peak and simultaneous disappearance of the 2623- and 2597-cm^{-1} peaks upon deuteration, when all the DMSO has been washed out, (Figure 4c) is further evidence that bonding of DMSO to kaolinite predominantly involves the 3690-cm^{-1} hydroxyls of kaolinite.

B. Bonding Interactions of DMSO. Bonding of DMSO can occur either through the sulfur or oxygen

atoms.¹⁶ Bonding *via* the oxygen may involve the resonance form $\text{R}_2\text{S}^+-\text{O}^-$, which lowers the S-O vibration frequency and is the most likely.¹⁴ An examination of the broad band at approximately 1030-cm^{-1} in a thin sample of the kaolinite complex shows that it may be composed of three overlapping peaks at 1042, 1030, and 1019-cm^{-1} , with the 1042-cm^{-1} peak the strongest. If two of these are the in-plane SiO vibrations corresponding to the 1035 and 1016-cm^{-1} vibrations of kaolinite, the other could be the SO stretching vibration of DMSO. From a comparison of relative intensities and assuming a slight upward frequency shift of the SiO vibration, the SO stretch in the complex is assigned to the 1030-cm^{-1} peak. The results for dickite in this region support the above assignment of peaks. A peak at 720-cm^{-1} in the kaolinite-DMSO complex is assigned to the asymmetric CS stretching occurring at 699-cm^{-1} (Table II) in liquid DMSO. The downward frequency shift of the SO stretching vibration and the absence of the symmetric CS vibration¹² shows that hydrogen bonding of DMSO to the hydroxyl surfaces of the clay takes place *via* the oxygen atom, rather than the sulfur atom.

A shoulder at 2917-cm^{-1} appears on the symmetric CH stretching vibration of 2932-cm^{-1} , and the asymmetric CH bending mode is split into three components of approximately equal intensity in the kaolinite complex (Figure 2c). The halloysite complex is similar except for the asymmetric bending vibration peak intensities, which are in the reverse order to that in liquid DMSO (compare Figures 2a and 5b). Clearly the CH bonds of DMSO in the complexes are perturbed by the clay lamellae in different ways, depending upon the clay. The upward frequency shift of the CH stretching vibration in all the complexes is difficult to reconcile with the possibility of $\text{CH}\cdots\text{O}$ hydrogen bonding to the tetrahedral oxygen layer.

The interlayer space of 3.96 Å (11.16–7.2 Å) (MacEwan's "Δ value")¹⁷ is less than the dimensions of the DMSO molecule, since the diameter of the methyl group alone is 4.0 Å.¹⁸ Some "keying" of the DMSO molecules into the kaolinite surface must therefore occur, especially when the DMSO molecular structure is considered to consist of a trigonal pyramid with sulfur at the apex.¹⁹ An orientation consistent with the X-ray and infrared data is one where the sulfur atom points toward the tetrahedral oxygen layer and the pyramid base is nearly parallel to the hydroxyl surface. Hence, weak $\text{C-H}\cdots\text{O}$ hydrogen bonds may exist, but these are masked and cannot be seen. Vig-

(16) M. J. Bennett, F. A. Cotton, and D. L. Weaver, *Nature*, **212**, 286 (1966).

(17) D. M. C. MacEwan, *Trans. Faraday Soc.*, **44**, 349 (1948).

(18) L. Pauling, "Nature of the Chemical Bond," Cornell University Press, Ithaca, N. Y., 1960, p 260.

(19) R. Thomas, C. B. Shoemaker, and K. Eriks, *Acta Cryst.*, **21**, 12 (1966).

orous removal of DMSO, as by heating, may cause permanent distortions in the tetrahedral oxygen layer, hence the broadened appearance of some SiO vibrations, compared to the original kaolinite.

C. Intercalation Rates and Interlayer Bonding. Intercalation rates of DMSO into the kaolin minerals may reflect variations in the strength of interlayer bonding related to the degree of order in the structures. Intercalation is slowest with dickite, the most crystalline kaolin polymorph with probably the strongest interlayer hydrogen bonding, intermediate with kaolinite, and fastest with halloysite, the least crystalline polymorph with very weak hydrogen bonding (if any) between the lamellae. The infrared spectra of the uncomplexed kaolin minerals in the hydroxyl stretching region indicate that the strength and number of interlayer hydrogen bonds increases from halloysite through kaolinite to dickite. For example, the peak in the region of 3650 cm^{-1} increases markedly in this order. This is in the same order as the rates of intercalation.

Some variation in the intercalation rate is also observed between the kaolinites themselves. Intercalation in Clackline kaolinite appears to be faster than in API-9 kaolinite, whereas that in Rocky Gully kaolinite is somewhat slower, in spite of its significantly higher surface area. Removing the iron oxides from the Rocky Gully kaolinite by treatment with dithionite²⁰ does not increase the intercalation rate. Grinding of the Pottsville dickite increases the rate of intercalation more than would be expected from the decrease in particle size. Also the finer API-15 dickite intercalates at much the same rate as the ground Pottsville dickite, despite the larger specific surface area of the latter. In general, it would appear that factors other than particle size have a significant effect on the intercalation rate of DMSO into the kaolin minerals. From the above, it appears that grinding produces other changes in particle morphology which allow a faster penetration of the DMSO.

The presence of water also affects the intercalation rates into kaolinite. The rate increases up to a certain water content and then falls. Apparently, water may break up the cyclic hydrogen bonded structure of liquid DMSO⁵ allowing the individual molecules, with perhaps some attached water molecules, to act in opening up the lamellae. Without water, the rate appears to be governed by the availability of single DMSO molecules and hence intercalation is slower. With more than the optimum amount of water present, the DMSO molecules may again be further intermolecularly bonded with the water molecules and the intercalation rate decreases.

A tentative explanation of the reason for the hydration of halloysite and not kaolinite may be attempted. The crystalline lattice distortions of the lamellae in halloysite may result in conditions favorable to the weak bonding of water to the interlamellar surfaces. Once water is removed and interlayer bonds formed, halloysite behaves similarly to kaolinite with regard to intercalation of DMSO. If, however, water can reenter the interlamellar spaces with the help of an external agent, *e.g.*, DMSO, the water-surface bonds are reformed and halloysite hydrates. The lesser degree of lamellae distortion and absence of water in the infrared spectra of kaolinite complexes, confirmed by the D₂O washings, favor the explanation given. Further evidence comes from the work of Wada,²¹ who found that kaolinite forms a partial water complex and dickite none at all.

Acknowledgment. The authors wish to express their thanks to Dr. L. H. Little of the Chemistry Department, University of Western Australia, for helpful discussions.

(20) T. L. Deshpande, Ph.D. Thesis, University of Adelaide, 1964.

(21) K. Wada, *Am. Mineralogist*, **50**, 924 (1965).

Infrared Spectra of the Beryllium Halides

by Alan Snelson

IIT Research Institute, Chicago, Illinois 60616 (Received July 18, 1967)

The infrared spectra of BeCl_2 , BeBr_2 , and BeI_2 have been observed in the spectral range 4000–200 cm^{-1} using the matrix isolation technique. Two frequencies were recorded for the chloride and bromide and one for the iodide. Assuming a linear geometry for these molecules, the frequencies were assigned as follows: BeCl_2 , $\nu_3 = 1135$ and $\nu_2 = 250 \text{ cm}^{-1}$; BeBr_2 , $\nu_3 = 1010$ and $\nu_2 = 220 \text{ cm}^{-1}$, and BeI_2 , $\nu_3 = 873$. The unobserved and infrared inactive frequencies have been estimated for all the beryllium halides.

Introduction

In a recent investigation¹ using the matrix isolation technique, the infrared spectra of beryllium fluoride and beryllium chloride were reported. Two frequencies were observed for the former in the spectral region 4000–200 cm^{-1} and were assigned to ν_3 and ν_2 . For the latter, only one frequency ν_3 was observed. The entropy of BeF_2 calculated using this frequency assignment agreed well with that obtained experimentally from thermodynamic data. A similar entropy calculation for BeCl_2 in which the bending frequency ($\nu_2 = 240 \text{ cm}^{-1}$) was estimated by assuming the ratios of the stretching to bending force constants to be the same in both BeF_2 and BeCl_2 was not satisfactory. Using the thermodynamic data for BeCl_2 , ν_2 may be calculated at 150 cm^{-1} , suggesting that the technique of transferring force constants ratios in similar molecules may be unsatisfactory for BeCl_2 . Subsequent studies in this laboratory, however, have shown that the single-beam spectrometer (Perkin-Elmer 12B) used in the beryllium chloride investigation had rather poor resolution in the spectral region 250–200 cm^{-1} , and that absorption bands in this region could have been missed. If this were the case for BeCl_2 , then the thermodynamically derived entropy would be in error. To resolve these difficulties, a reexamination of the beryllium chloride spectrum was undertaken, using a Perkin-Elmer 621 spectrophotometer. In addition, the spectra of beryllium bromide and iodide were also investigated.

Experimental Section

The matrix-isolation cryostat, molecular-beam furnace, and experimental procedures used in this investigation were essentially the same as that described by the author in a previous paper,¹ and only those details peculiar to the present experiments are given. Beryllium chloride was supplied by A. D. Mackay and was purified prior to use by sublimation in a stream of hydrogen chloride. Beryllium bromide and iodide were prepared by passing analytical reagent grade bromine and iodine vapor, respectively, over heated beryllium

metal powder. The latter was supplied by K and K Laboratories with an indicated purity of 99%. The halides were sublimed once prior to use.

Graphite effusion tubes were used to contain the halides, and in all cases the unsaturated vapor was super-heated at about 700° to decrease the concentration of polymeric species being trapped in the matrix. Research grade neon and argon, supplied by Matheson Co., were used to form the matrices. Deposition rates of halide and matrix were of the same order as in previous experiments. The spectra were recorded on a Perkin-Elmer 621 infrared spectrophotometer. The reported frequencies are believed accurate to $\pm 1 \text{ cm}^{-1}$.

Results

Beryllium Chloride (Figure 1A). Under the best conditions of isolation, $M/H \approx 6000$ for a neon matrix, two strong absorption bands occurred at a and d, together with two very weak features at b and c. The latter were comparable in intensity to the bands at a and d under poor conditions of isolation ($M/H \approx 500$). In addition, other features also appeared. The bands at b and c are assigned to polymeric material. This may have been present in the beryllium chloride vapor; the degree of superheating used in the experiment being insufficient to dissociate the polymeric material completely. Alternatively, polymeric material may have been formed due to incomplete isolation of the monomer during the trapping process in the matrix. The ratios of the intensities of the bands at a and d under various conditions of isolation remained constant to within $\pm 5\%$ and these two features are assigned to monomeric beryllium chloride.

Beryllium Bromide (Figure 1B). The spectrum of beryllium bromide in a neon matrix is analogous to that of beryllium chloride. Two strong and two weak absorption bands at a, d and b, c, respectively, appeared under the best isolation conditions. The latter increased markedly in intensity under poor conditions of isolation. The features at b and c are assigned to poly-

(1) A. Snelson, *J. Phys. Chem.*, **70**, 3208 (1966).

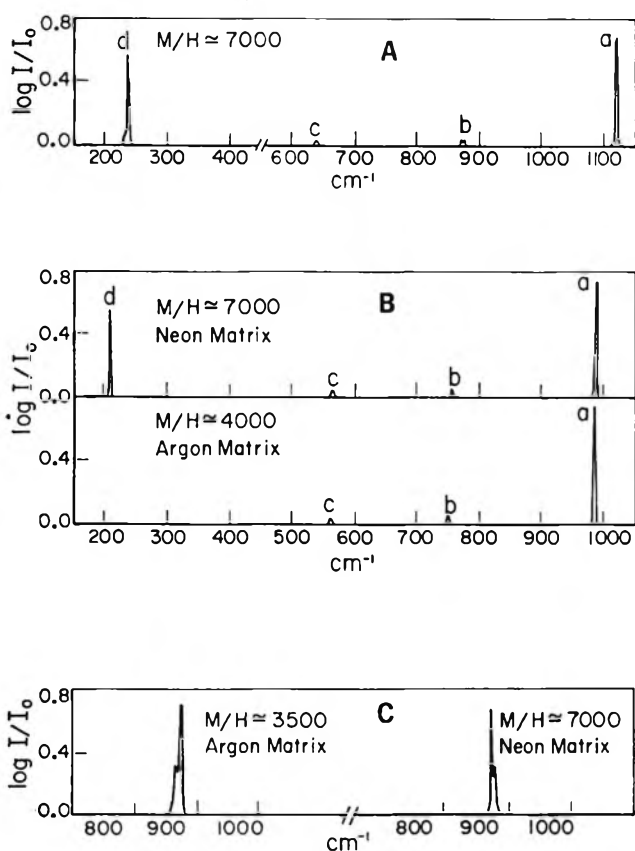


Figure 1. Infrared spectra of beryllium halides: A, beryllium chloride in a neon matrix; B, beryllium bromide in neon and argon matrices; C, beryllium iodide in neon and argon matrices.

meric material, and those at a and d to monomeric beryllium bromide. The spectrum of beryllium bromide vapors in an argon matrix is similar to that in neon except that the absorption band at d in the latter matrix does not appear. This is presumably due to a larger frequency shift in the argon matrix resulting in this band lying below 200 cm^{-1} .

Beryllium Iodide (Figure 1C). The spectrum of beryllium iodide was recorded only under conditions of good isolation. In both the neon and argon matrices, an absorption feature with several maxima occurred at about 870 cm^{-1} . These maxima are believed to be due to matrix effects, and the band is assigned to monomeric beryllium iodide.

Discussion

Recent studies by Klemperer, *et al.*,²⁻⁴ using the electric quadrupole deflection of molecular beams to detect dipole moments, indicate that all the beryllium halides are linear symmetric triatomic molecules. This type of molecule has two infrared-active vibrations, assigned to ν_3 , the asymmetric stretching mode, and ν_2 , the bending mode. Of the four absorption bands attributed to monomeric beryllium chloride and bromide from the experimental data, the two higher frequencies are assigned to ν_3 , and the two lower fre-

quencies to ν_2 . The one frequency observed for beryllium iodide is assigned to ν_3 . In Table I, the observed matrix frequencies are listed, together with estimated gas-phase values obtained using the simple procedure indicated previously.¹ In the beryllium iodide spectrum, the main maximum of the absorption band in the argon matrix lies at a higher frequency than the comparable maximum in the neon matrix. This contrasts

Table I: Frequencies of BeCl_2 , BeBr_2 , and BeI_2

	BeCl_2		BeBr_2		BeI_2
	ν_2	ν_3	ν_2	ν_3	ν_3
Neon	238	1122	207	993	878, 872
Argon		1108 ^a		985	877, 867
Estimated gas phase frequencies	250	1135	220	1010	873

^a See ref 1.

with the behavior of the other alkaline earth halides for which matrix spectra are available, the frequencies shifting further to the red in the order neon < argon < krypton. Beryllium iodide appears to be undergoing a blue shift, and the estimated "gas-phase frequency" in Table I is simply taken as the average of the four matrix frequencies.

In Table II, the vibrational frequencies and force constants of all the beryllium halides are listed. In

Table II: Valence Force Constants of the Beryllium Halides

	cm^{-1}			10^4 dynes/cm		
	ν_1	ν_2	ν_3	k	k/l^2	$k_1/(k/l^2)$
BeF_2	(680) ^b	345	1555	5.15	0.12	43
BeCl_2	(390)	250	1135	3.28	0.07	47
BeBr_2	(230)	220	1010	2.53	0.06	42
BeI_2	(160)	(175)	873	1.96	0.04 ^a	44 ^a

^a The values were estimated. ^b Calculated values.

the last column, the ratios of the stretching to bending force constant for the fluoride, chloride, and bromide are seen to be of similar magnitude. This gives some confidence to the estimated value of the bending force constant calculated for beryllium iodide using the mean of the observed values for the other halides, $k_1/(k/l^2) = 44$.

The values of ν_1 were calculated using the simple valence force field approximation; however, a better estimate of these frequencies might be obtained if the

(2) L. Wharton, R. A. Berg, and W. Klemperer, *J. Chem. Phys.*, **39**, 2023 (1963).

(3) A. Buchler, J. L. Stauffer, W. Klemperer, and L. Wharton, *ibid.*, **39**, 2299 (1963).

(4) A. Buchler, J. L. Stauffer, and W. Klemperer, *ibid.*, **40**, 3471 (1964).

interaction constants k_{12} were known. Linnet and Hoare⁵ have shown that the expression

$$k_{12} = 3k_1 \frac{(r_{A-B}^t - r_{A-B}^d)}{r_{A-B}^t}$$

is obeyed fairly well for triatomic molecules, r_{A-B}^t and r_{A-B}^d being the bond lengths between the atoms A and B in the triatomic and diatomic species, respectively. The bond lengths in all the beryllium dihalides were determined by Akishin, *et al.*,⁶ but for the monohalides only the value for BeF has been observed experimentally.⁷ It is thus necessary to estimate bond lengths for the remaining diatomic beryllium halides. For BeCl, the relationship given by Herschbach and Laurie,⁸ relating the internuclear distance, r , to the vibrational force constant, k , may be used. From spectroscopic data⁹ on BeCl, $k = 3.01 \times 10^5$ dynes cm^{-1} . Substituting into the expression $r = 2.02 - 0.53 \log k$, a value of $r = 1.77$ Å is obtained. A similar calculation for BeF with $k = 5.75 \times 10^5$ dynes cm^{-1} and $r = 1.73 - 0.47 \log k$, gives $r = 1.37$ Å, in good agreement with the experimental value of 1.361 Å, and suggests that the value of r calculated for BeCl is probably good to about $\pm 1\%$. Estimation of the bond lengths for BeBr and BeI cannot be made using the same approach since no spectroscopic data are available for these species. Instead, use is made of a relationship which appears to hold for some gaseous diatomic halides. The ratios of the bond distances MF/MCl, MF/MBr, and MF/MI in certain groups of halides are quite constant. For M = Na, K, Rb, and Cs, the above ratios fall in the range 0.811 ± 0.006 , 0.767 ± 0.004 , and 0.711 ± 0.004 , respectively. The same ratios for M = Li and Al are 0.774 ± 0.001 , 0.721 ± 0.001 , and 0.654 ± 0.001 . Unfortunately, the only other diatomic halides for which accurate bond distances are available are those of hydrogen. The ratios are, 0.719, 0.649, and 0.572, which do not fall into either of the other two groups. The ratios for the alkali metals, Na, K, Rb, and Cs are constant to approximately $\pm 1\%$, while those for Li and Al are good to about 0.5%. The ratio of the bond lengths of BeF/BeCl is 0.769 which, within the accuracy of the estimated bond length for BeCl, suggests that the diatomic beryllium halides are similar to the lithium and aluminum species and enables the bond lengths of BeBr and BeI to be calculated at 1.89 and 2.08 Å, respectively, with an estimated error of $\pm 3\%$.

In Table III, the above data on the beryllium halides are summarized. The frequencies of the diatomic

Table III: Molecular Constants of the Beryllium Halides

Bond	r , Å, diatomic	r , Å, triatomic	$(\delta^{\text{tri}} - \delta^{\text{di}})$, Å	ν_1 , diatomic
BeF	1.361	1.43	0.07	1247
BeCl	1.77	1.77	0.00	835
BeBr	1.89	1.92	0.03	(750)
BeI	2.12	2.08	-0.04	(680)

species in parentheses were calculated using the estimated bond lengths and the formulas of Herschbach. They are believed to be accurate to ± 50 cm^{-1} . The difference in bond lengths $r^{\text{tri}} - r^{\text{di}}$ is significant for the BeF bonds, but the values of 0.00, 0.03, and -0.04 Å for BeCl, BeBr, and BeI can probably best be taken to indicate that within the estimated error of the bond lengths, the differences are close to zero and do not justify making a calculation of k_{12} . The value of k_{12} calculated for BeF₂ is 0.76×10^6 dynes cm^{-1} resulting in $\nu_1 = 770$ cm^{-1} . Using this frequency assignment, the calculated entropy of BeF₂ is 68.1 eu at 880°K, agreeing with the observed value of 69.0 ± 2.0 eu¹⁰ at the same temperature. A similar calculation for the entropy of BeCl₂ gives 66.6 eu at 500° compared to observed values of 69.2 ± 2.0 or 68.2 ± 2 eu.¹⁰ It is clear that the spectroscopic data favor the lower value, and that the agreement between the calculated and observed values, though not as good as with BeF₂, is satisfactory. Finally, it must be stressed that in view of the uncertainties in the methods of estimating bond lengths and frequencies for the beryllium halides, the values of the infrared inactive symmetrical stretching frequencies ν_2 , reported here for the triatomic species must be regarded as somewhat speculative until more accurate data are available.

Acknowledgment. The author gratefully acknowledges the support of the Air Force Office of Scientific Research in funding this study.

(5) J. W. Linnet and M. F. Hoare, *Trans. Faraday Soc.*, **45**, 844 (1949).

(6) P. A. Akishin, V. P. Spiridonov, and G. A. Sobolev, *Dokl. Akad. Nauk SSSR*, **118**, 1134 (1958).

(7) G. Herzberg, "Molecular Spectra and Molecular Structure. I. Spectra of Diatomic Molecules," D. Van Nostrand Co., Inc., New York, N. Y., 1950.

(8) D. R. Herschbach and V. M. Laurie, *J. Chem. Phys.*, **35**, 458 (1961).

(9) M. M. Novikov and L. N. Tunitskii, *Opt. Spectry.*, **8**, 396 (1960).

(10) D. L. Hildenbrand, L. P. Theard, E. Murad, and F. Ju, *Aeronutronic Final Report No. U-3068*, 1965.

Energy Transfer in Radiolysis of Rare Gas-C₂F₆ Liquid Mixtures

by Alicja Sokolowska and Larry Kevan

Department of Chemistry, University of Kansas, Lawrence, Kansas 66044 (Received July 18, 1967)

The liquid-phase γ radiolysis of C₂F₆ with Xe, Kr, and Ar has been investigated as a function of the fraction of energy deposition in the rare gas in the presence and absence of O₂ as a radical scavenger. All energy-transfer efficiencies are smaller by a factor of 2-3 than those found previously in the gas phase. The energy-transfer efficiencies in the absence of O₂ are similar for Xe and Ar, and twice as great for Kr. It is suggested that this reflects the correspondence between ionic states of Kr₂⁺ and C₂F₆⁺, and that charge transfer contributes to the energy-transfer process. In the presence of O₂, no energy-transfer contribution to nonscavengeable products is observed; this implies that excitation transfer processes are inefficient or are quenched by O₂.

Introduction

Energy transfer in radiolysis of rare gas-C₂F₆ mixtures has been previously studied in the gas phase.¹ It was shown that the over-all energy-transfer efficiency depended on the difference between the recombination energies of C₂F₆ and a given rare gas, and it was suggested that charge-transfer processes would show such behavior. C₂F₆ is suitable for such studies since its recombination energy (14-16 ev) lies within the range of recombination energies (12-24 ev) spanned by the rare gases. Recent mass spectrometric studies on charge-transfer cross sections of rare gas ions with C₂F₆ confirm that the cross sections are largest when the recombination energy difference is small.² In this paper, we extend the macroscopic radiolysis approach for studying energy transfer to the liquid phase. The liquid phase radiolysis of C₂F₆ has been previously studied³ to provide a suitable background. C₂F₆ radiolysis in liquid Xe, Kr, and Ar is reported here. The effect of phase on total energy-transfer efficiency and evidence for the role of charge transfer in the liquid phase are discussed.

Experimental Section

C₂F₆ (Air Products Inc.) quoted as 99.9% pure contained <0.02 mole% CF₃Cl as impurity; it was rigorously degassed before using. O₂ (Air Products Inc., extra dry grade) and Xe, Kr, and Ar (Air Products Inc., research grade) were used as received.

Samples were prepared by condensing C₂F₆ + R (rare gas) or C₂F₆ + R + O₂ into 8-cm Pyrex capillary ampoules of 2-mm i.d. and 7-mm o.d. with liquid nitrogen. Samples with C₂F₆ + Xe and C₂F₆ + Kr were kept for 12 hr, and samples with C₂F₆ + Ar were kept for 2 hr at -80° for mixing before irradiation.

Irradiations were performed with Co⁶⁰ γ rays at -80° with a Dry Ice-acetone bath and at -130° with precooled N₂ gas. The dose rate was 0.6 Mrad/hr

to H₂O (35°); monthly corrections for decay were made. Nominal irradiation doses were about 3 Mrads. The dose to a ferrous sulfate dosimetry solution was corrected by the total mass energy absorption coefficient of the sample mixture to give the total dose absorbed by the sample. In the xenon mixtures, an 11% correction for the photoelectric effect was included. Yields are reported as *G* values, the number of product molecules per 100 ev absorbed by the entire mixture. The fraction of radiation energy absorbed by the rare gas (*F*) was calculated according to eq 1

$$F_r = D_m(f_r n_r S_r) / (f_r n_r S_r + f_c n_c S_c) \quad (1)$$

where *D_m* is the total radiation dose absorbed by the mixture, *f* is weight fraction, *n* is electrons per gram, *S* is stopping power per electron, subscript *r* refers to rare gas, and subscript *c* refers to C₂F₆.

Product analysis was done by gas chromatography with thermal conductivity detection on a 2 m, 0.25 in. silica gel column at 35 and 80° and on a 4 m, 0.25 in. silica gel column at 35, 90, and 120°. Standard samples were used for calibration.

Results

The radiolysis products of liquid C₂F₆ at low doses (less than 10 Mrads) are CF₄, C₂F₈, and C₄F₁₀.³ The yields are linear with dose to greater than 10 Mrads. Figures 1-3 show these product yields as a function of the fraction of radiation energy (*F*) absorbed in the rare gas for Xe, Kr, and Ar, respectively. Table I shows directly measured mole fractions, *X*, and the corresponding calculated *F* parameter. The xenon and krypton mixtures were irradiated at -80° and the argon mixtures at -130°. Some krypton mixtures were

(1) L. Kevan, *J. Chem. Phys.*, **44**, 683 (1966).

(2) D. Smith and L. Kevan, to be published.

(3) A. Sokolowska and L. Kevan, *J. Phys. Chem.*, **71**, 2220 (1967).

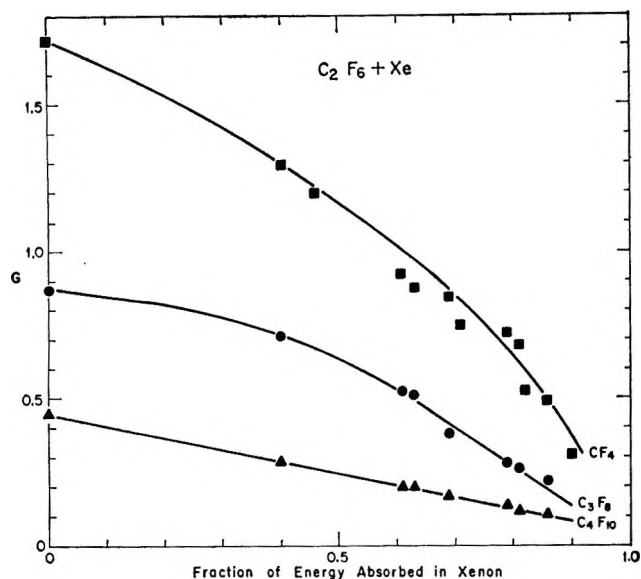


Figure 1. Radiolysis product yields (G) in C_2F_6 -Xe liquid mixtures at -80° vs. F , the fraction of energy absorbed by Xe.

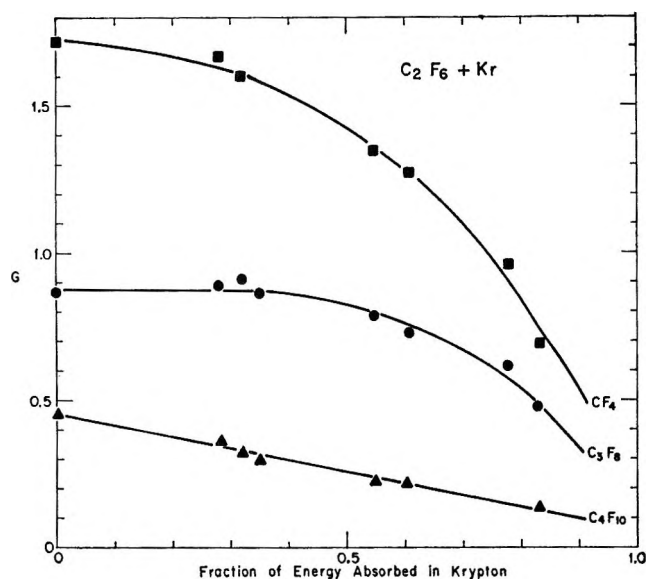


Figure 2. Radiolysis product yields (G) in C_2F_6 -Kr liquid mixtures at -80° vs. F , the fraction of energy absorbed by Kr.

also irradiated at -130° and gave similar results to the runs at -80° . All data points represent averaged values of 2-4 runs with deviations of $\pm 12\%$ or less. All of the product yields decrease as F increases, but the relative product ratios are not greatly changed. For 100% energy transfer from the rare gas to C_2F_6 , and for an invariant product distribution, the product G values should be constant. For 0% energy transfer, the G values should decrease linearly to 0.0 at $F = 1.0$. An intermediate behavior is observed which indicates partial energy transfer.

In the presence of O_2 as a free radical scavenger, about 60% of CF_4 , 100% of C_3F_8 (except in Ar mixtures), and 100% of C_4F_{10} are scavenged. Figures 4-6 show CF_4

Table I: Correspondence between Mole Fraction (X) and Fraction of Energy Absorbed (F) for Rare Gases in Rare Gas- C_2F_6 Mixtures

Xenon		Krypton		Argon	
X	F	X	F	X	F
0.53	0.40	0.48	0.28	0.50	0.20
0.59	0.46	0.53	0.32	0.70	0.36
0.73	0.61	0.56	0.35	0.77	0.44
0.79	0.69	0.74	0.55	0.82	0.52
0.87	0.79	0.78	0.61	0.87	0.62
0.89	0.82	0.89	0.78	0.89	0.67
0.91	0.86	0.92	0.83	0.92	0.73

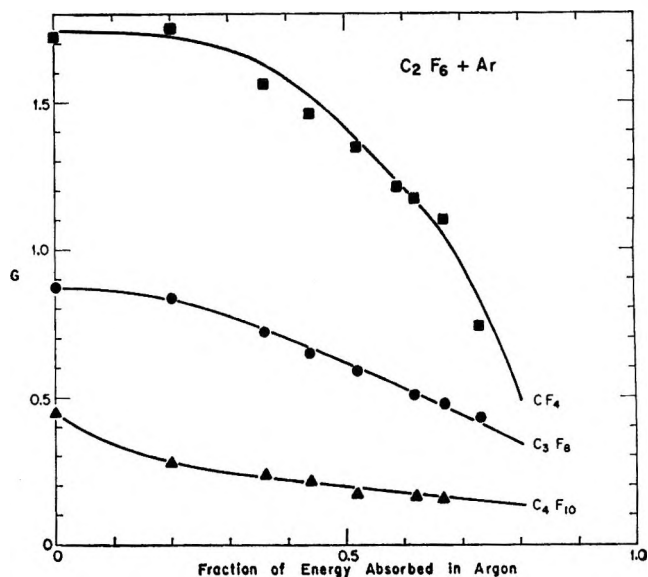


Figure 3. Radiolysis product yields (G) in C_2F_6 -Ar liquid mixtures at -130° vs. F , the fraction of energy absorbed by Ar.

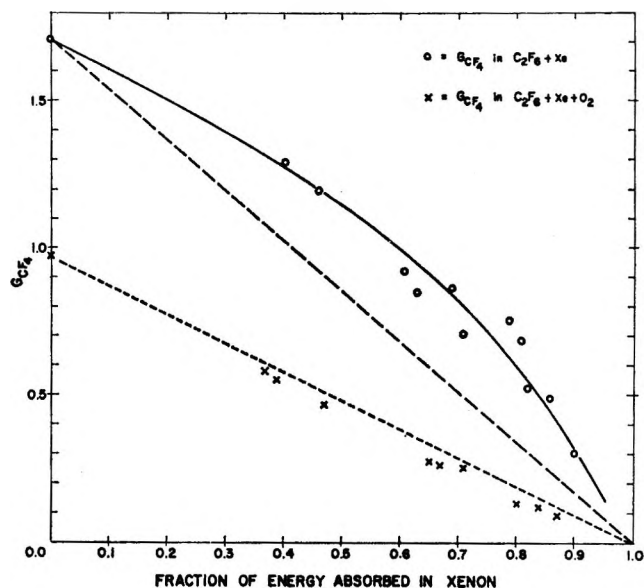


Figure 4. CF_4 radiolysis yields (G) in C_2F_6 -Xe liquid mixtures with (\times) and without (O) O_2 scavenger vs. F , the fraction of energy absorbed by Xe.

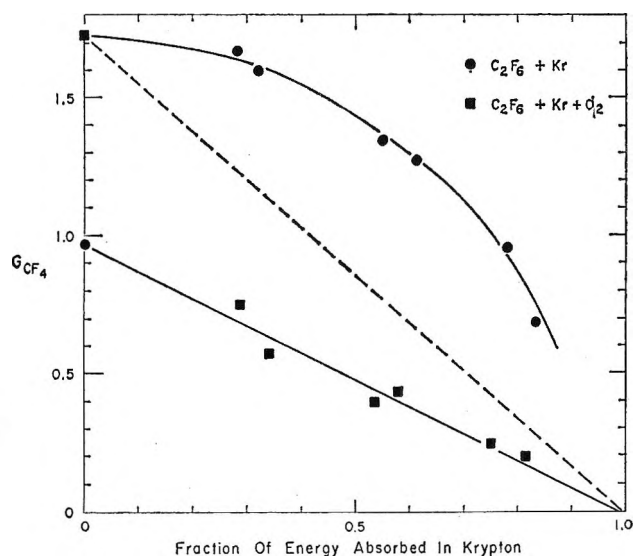


Figure 5. CF₄ radiolysis yields (G) in C₂F₆-Kr liquid mixtures with (■) and without (●) O₂ scavenger vs. F , the fraction of energy absorbed by Kr.

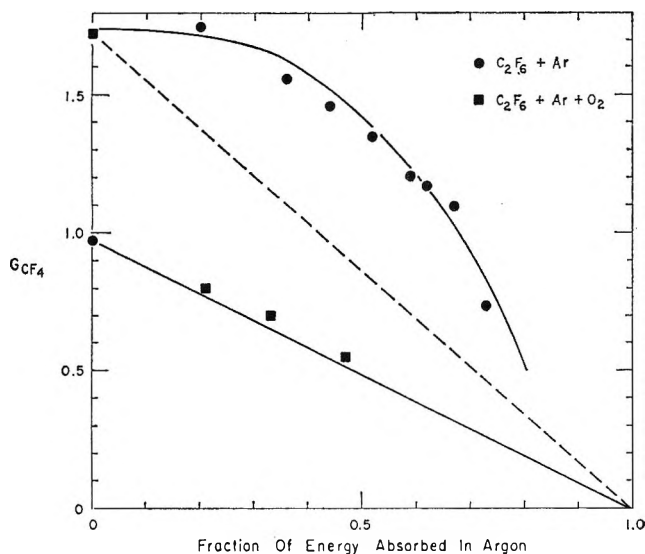


Figure 6. CF₄ radiolysis yields (G) in C₂F₆-Ar liquid mixtures with (■) and without (●) O₂ scavenger vs. F , the fraction of energy absorbed by Ar.

yields in the absence and presence of O₂ vs. F in Xe, Kr, and Ar mixtures, respectively. The dotted line represents the 0% energy-transfer line for unscavenged CF₄. Note that the nonscavengeable CF₄ yields in all cases decrease linearly to 0.0 at $F = 1.0$. Thus, although the total CF₄ yield indicates occurrence of energy transfer, nonscavengeable CF₄ is not produced by the energy-transfer process.

In C₂F₆ + Ar + O₂ mixtures, a large gas chromatographic peak ($G \sim 3$) appeared at the C₃F₈ retention time. Mass spectrometric analysis showed that the peak was largely, if not entirely, C₃F₈. This behavior was not observed in Xe or Kr mixtures.

The variation of the total carbon yield in the products is shown in Figure 7. The dashed horizontal and di-

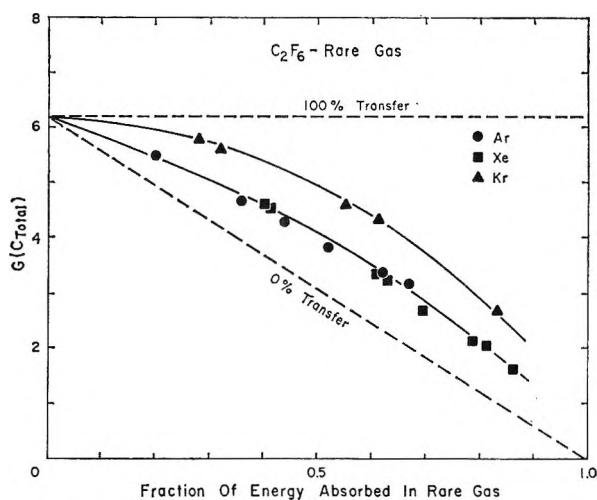


Figure 7. Total radiolysis yield in C₂F₆-rare gas liquid mixtures vs. F , the fraction of energy absorbed by the rare gas.

agonal lines represent 100% and 0% energy transfer. To determine energy-transfer efficiency in quantitative terms, the total carbon yield in products is used as an indicator of the extent of energy transfer. This method is independent of variation in product distribution. Transfer efficiency is then defined by eq 2

$$\% \text{ transfer efficiency} = [G_m - G_c(1 - F)]100/G_0 \quad (2)$$

where subscripts m and c refer to mixture and C₂F₆, respectively. Transfer efficiencies at different F values are given in Table II.

Table II: Energy-Transfer Efficiencies in Radiolysis of Liquid Rare Gas-C₂F₆ Mixtures^a

F	Xe-C ₂ F ₆ , ^b %	Kr-C ₂ F ₆ , ^b %	Ar-C ₂ F ₆ , ^c %
0.3	38	76	38
0.5	33	61	33
0.7	23	43	23
0.8	18	34	18

^a Nominal dose 3 Mrads. ^b At -80°. ^c At -130°.

Discussion

Figure 7 shows that significant energy transfer is observed in liquid C₂F₆-rare gas mixtures. At large values of F , where most of the radiation energy is absorbed by the rare gas (R), one must consider what rare gas species are formed from which energy may be transferred. This has been discussed for liquid rare gases;⁴ it was concluded that all R* states above the appearance potential of R₂⁺ react to yield R₂⁺, that the majority of R⁺ reacts to yield R₂⁺ in liquid mixtures in

(4) R. Koob and L. Kevan, "The Chemistry of Ionization and Excitation," G. R. A. Johnson and G. Scholes, Ed., Taylor and Francis, Ltd., London, 1967, pp 141-150.

which the rare gas is in excess, and that low-lying R^* states mostly react to yield excimers, R_2^* . Thus, it may be initially postulated that energy transfer in liquid rare gas mixtures occurs mostly from R_2^+ and to a lesser extent from R_2^* .

The observed transfer efficiency is maximum for Kr and 50% less for both Xe and Ar. In contrast to this, the energy available for transfer from R_2^+ and R_2^* increases monotonically from Xe to Ar. A similar maximum transfer efficiency was observed in the gas phase¹ for Kr and Ar compared to Xe, Ne, and He when energy transfer from all the rare gases was examined. The gas-phase maximum transfer efficiency was interpreted as an indication of the importance of charge transfer, since the recombination energies of Kr^+ (14.0, 14.7 eV) and Ar^+ (15.7, 15.9 eV) are near the expected ionization potential of C_2F_6 . (Although the C_2F_6 parent ion is not observed in the mass spectrum, CF_3^+ has the lowest appearance potential at 14.0–14.7 eV.^{2,5}) A similar interpretation seems to be applicable in the liquid phase, except that the energy-transfer maximum appears at Kr instead of Ar.

Although dimeric rare gas ions have appearance potentials about 1 eV lower than monoatomic ions, the diatomic ion bond strength is about 1 eV. In a liquid-phase encounter of R_2^+ and C_2F_6 , the total energy of R_2^+ is available for excitation of C_2F_6 . For Kr, this is 14.0 eV, and for Ar, it is 15.7 eV. The shift in the transfer maximum from Ar in the gas to Kr in the liquid probably reflects a lowered ionization potential by 1–2 eV in the liquid. An important conclusion is that energy-transfer probability from a given rare gas is closely correlated with the lowest ionic states of C_2F_6 and is observed in both liquid and gaseous phases.

In the liquid phase, the energy-transfer efficiencies are high, but not as high as those observed in the gas phase. To compare, at $F = 0.5$, the transfer efficiencies for Xe, Kr, and Ar are 55, 94, and 98% in the gas¹ vs. 33, 61, and 33% in the liquid. The ionic mobilities are about 1000-fold less in the liquid compared to the gas^{6,7} so it is not surprising that the transfer efficiencies are less in the liquid.

The oxygen-scavenged systems (Figures 4–6) illustrate that only radical precursors to the products are produced by the energy-transfer process. Products without thermal free radical precursors (nonscavengable products) are measured in the presence of oxygen; these show no enhancement by energy transfer. In liquid C_2F_6 radiolysis, CF_4 is produced by a radical process (40%) and a nonradical process (60%). Part of the nonradical process is thought to be molecular elimination of CF_4 from excited C_2F_6 . The noninvolvement of nonradical processes in C_2F_6 decomposition resulting from energy transfer can be interpreted in at least two ways. One, energy transfer from excited rare gas states to C_2F_6 is inefficient and little excited C_2F_6 is formed by the energy-transfer process. Two, oxygen quenches the excited rare-gas states and prevents energy transfer from them. These interpretations cannot be distinguished at present; in fact, both are supported by other experimental data. Preliminary experiments⁸ on gas-phase Kr-sensitized photolysis of C_2F_6 have not shown molecular CF_4 to be formed; this implies that energy transfer from R^* and R_2^* to C_2F_6 is highly inefficient. On the other hand, excimer emission from R_2^* in liquid rare gases is strongly quenched by oxygen.⁹ At any rate, energy transfer from rare gases in R - C_2F_6 liquid radiolysis gives quite a different energy distribution deposited in C_2F_6 than does direct radiolysis.

Acknowledgment. We wish to thank the U. S. Atomic Energy Commission and the Petroleum Research Fund of the American Chemical Society for financial support of this research. This is AEC Document No. C00-1528-16.

(5) D. Smith and L. Kevan, *J. Chem. Phys.*, **46**, 1586 (1967).

(6) H. T. Davis, S. A. Rice, and L. Meyer, *ibid.*, **37**, 947 (1962).

(7) F. E. Niles and W. W. Robertson, *ibid.*, **43**, 1076 (1965).

(8) L. Kevan, K. Norland, and N. S. Viswanathan, unpublished results.

(9) J. Jortner, L. Meyer, S. A. Rice, and E. G. Wilson, *J. Chem. Phys.*, **42**, 4250 (1965).

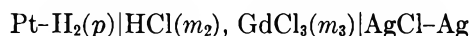
Electromotive Force Studies in Aqueous Solutions at Elevated Temperatures. IX. The Thermodynamic Properties of Hydrochloric Acid-Gadolinium Chloride Mixtures¹

by M. H. Lietzke and R. W. Stoughton

Oak Ridge National Laboratory, Oak Ridge, Tennessee (Received July 19, 1967)

The activity coefficient of HCl in HCl-GdCl₃ mixtures has been studied to 150°. At constant temperature and ionic strength, the logarithm of the activity coefficient of HCl in the mixtures varies linearly with the ionic strength fraction of GdCl₃ in conformity with Harned's rule. The activity coefficient of GdCl₃ in the mixtures was calculated by using the parameters describing the variation of the logarithm of the activity coefficient of HCl in the mixtures and those for the variation of the activity coefficient of GdCl₃ with ionic strength in pure GdCl₃ solutions at 25°. In contrast to the activity coefficient of LaCl₃ which showed a decrease with ionic strength fraction of HCl, that of GdCl₃ showed an increase at total ionic strengths of 0.5 and 1.0.

This investigation into the thermodynamic properties of HCl-GdCl₃ mixtures was undertaken in order that a comparison might be made between the properties of a mixture of HCl and a higher rare earth chloride and those of HCl-LaCl₃ mixtures which had been studied previously.² In the present study, emf measurements of the cell



have been combined with values of the activity coefficient of GdCl₃³ to compute the thermodynamic properties of both HCl and GdCl₃ in HCl-GdCl₃ mixtures.

Experimental Section

The high-temperature, high-pressure experimental apparatus and the preparation of electrodes and solutions were the same as described previously.^{4,5} Since this apparatus was built for moderate accuracy over a wide temperature range rather than for maximum accuracy at low temperatures, the accuracy in the latter range is not as great as that claimed by other investigators.⁶ The emf measurements were carried out in the temperature range 25–150° in solutions of total ionic strengths 0.5 and 1.0 in which the ratio of HCl to GdCl₃ was varied. The emf values taken at the same temperature were reproducible to *ca.* ±0.5 mv. No drift of emf with time was observed.

Results and Discussion

Each emf value was corrected to 1.00 atm of hydrogen pressure as described previously.² Then the corrected emf values, *E*, at each ionic strength were plotted as a function of temperature and the values corrected to the

round values of the temperature, 25, 60, 90, 125, and 150°. The temperature of measurement was never more than 1° from the corresponding round temperature. These corrected values are given in Table I.

The activity coefficients, γ_{\pm} , of HCl at each temperature and set of concentrations in the mixtures were evaluated by using the Nernst equation and previous values⁷ of the standard potential, *E*°, of the Ag, AgCl electrode, except that 0.2223 v was used instead of 0.2220 v at 25°. In eq 1, *m*₂ and *m*₃ are the molalities

$$E = E^\circ - \frac{RT}{\mathcal{F}} \ln [m_2(m_2 + 3m_3)] - \frac{RT}{\mathcal{F}} \ln \gamma_{\pm} \quad (1)$$

of HCl and LaCl₃, respectively, while *T* is the absolute temperature, *R* is the gas constant, and \mathcal{F} is the Faraday.

A plot of $\ln \gamma_{\pm}$ vs. ionic strength fraction of GdCl₃ was made at each temperature and at the total ionic strengths 0.5 and 1.0. Also included in these plots were the values for pure HCl⁷ at all temperatures. In all cases the plots were linear within experimental error in conformity with Harned's rule.

(1) Research sponsored by the U. S. Atomic Energy Commission under contract with the Union Carbide Corp.

(2) M. H. Lietzke and R. W. Stoughton, *J. Phys. Chem.*, **71**, 662 (1967).

(3) F. H. Spedding and I. S. Yaffe, *J. Am. Chem. Soc.*, **74**, 4751 (1952).

(4) R. S. Greeley, W. T. Smith, Jr., R. W. Stoughton, and M. H. Lietzke, *J. Phys. Chem.*, **64**, 652 (1960).

(5) M. B. Towns, R. S. Greeley, and M. H. Lietzke, *ibid.*, **64**, 1861 (1960).

(6) H. S. Harned and B. B. Owen, *ibid.*, **64**, 456 (1960).

(7) M. H. Lietzke and R. W. Stoughton, *ibid.*, **68**, 3043 (1964).

Table I: Values of the Emf in Volts for the Cell, Pt-H₂(p)|HCl(*m*₂), GdCl₃(*m*₃)|AgCl-Ag, and Deviations^a of the Emf Values Calculated from Smoothed Activity Coefficients

<i>m</i> ₂	<i>m</i> ₃	Temp, °C				
		25	60	90	125	150
0.3551	0.0280	0.2840	0.2672	0.2484	0.2238	0.2037
		+11	+1	-6	+9	+24
0.2224	0.0515	0.2992	0.2834	0.2657	0.2422	0.2215
		+13	+3	-2	+13	+12
0.1230	0.0619	0.3180	0.3030	0.2870	0.2650	0.2465
		+2	-17	-21	-8	+1
0.7407	0.0448	0.2460	0.2264	0.2055	0.1775	0.1547
		+8	+8	+7	+13	+14
0.5497	0.0942	0.2555	0.2360	0.2160	0.1900	0.1670
		+12	+7	+8	-22	+10
0.1897	0.1473	0.2871	0.2730	0.2551	0.2320	0.2100
		-17	0	-8	-1	-30

^a The deviations are given below each emf as observed emf values less the values calculated from smoothed activity coefficients. Thus, a positive deviation indicates that the emf reported here is algebraically larger.

Expressions for γ_{\pm} of HCl and GdCl₃ in the Mixtures. The smoothing of the activity coefficients of HCl and the calculation of the activity coefficients of the GdCl₃ in the mixtures were carried out in the same way as in the HCl-LaCl₃ study.² The excess free energy of the solution G^e , i.e., excess over the molality and Debye-Hückel terms, was expressed as

$$\frac{G^e}{RT} = 2n_2 \ln \gamma_2^e + 4n_3 \ln \gamma_3^e = 2 \sum_{ij} B_{ij} \frac{n_i n_j}{w} + 2 \sum_{ijk} C_{ijk} \frac{n_i n_j n_k}{w^2} \quad (2)$$

where n represents the number of moles of each solute, w is the number of kilograms of water, and the sums are taken over each solute $i, j, k = 2$ (for HCl) to 3 (for GdCl₃). B_{ij} and C_{ijk} are interaction coefficients to be determined from the data.

Then for the HCl

$$2 \ln \gamma_2^e = \frac{\bar{G}_2^e}{RT} = \frac{\partial}{\partial n_2} \left(\frac{G^e}{RT} \right) = 4 \sum_i B_{2i} m_i + 6 \sum_{ij} C_{2ij} m_i m_j \quad (3)$$

while for the LaCl₃

$$4 \ln \gamma_3^e = \frac{\bar{G}_3^e}{RT} = 4 \sum_i B_{3i} m_i + 6 \sum_{ij} C_{ij3} m_i m_j \quad (4)$$

On expanding the sums on the right-hand sides of eq 3 and 4 and dividing both sides by 2.30259 eq 5 and 6 are obtained.

$$\log \gamma_2^e = 2I \left[B_{22} + \left(\frac{B_{23}}{6} - B_{22} \right) X_3 \right] + 3I^2 \left[C_{222} + \left(\frac{C_{223}}{3} - 2C_{222} \right) X_3 + \left(C_{222} + \frac{C_{233}}{36} - \frac{C_{223}}{3} \right) X_3^2 \right] \quad (5)$$

and

$$\log \gamma_3^e = I \left[\frac{B_{33}}{6} + \left(B_{23} - \frac{B_{33}}{6} \right) X_2 \right] + \frac{I^2}{2} \left[\frac{C_{333}}{12} + \left(C_{233} - \frac{C_{333}}{6} \right) X_2 + \left(\frac{C_{333}}{12} + 3C_{223} - C_{233} \right) X_2^2 \right] \quad (6)$$

In eq 5 and 6, X represents the ionic strength fraction of the designated component in the mixture and I represents the ionic strength of the solution given by $I = m_2 + 6m_3$. Since, as mentioned above, Harned's rule appears to hold for the HCl in the mixtures, the coefficient in parentheses of the X_3^2 term in eq 5 is zero.

The total $\ln \gamma_e$ is obtained by adding the Debye-Hückel term to eq 5 and 6. This term was assumed to be $s\rho^{1/2}\sqrt{I}/(1 + 1.5\sqrt{I})$ for the HCl and $3s\rho^{1/2}\sqrt{I}/(1 + 1.5\sqrt{I})$ for the GaCl₃ where s is the limiting slope for a univalent ion and ρ is the density of water which corrects the ionic strength to a volume basis as required by the Debye-Hückel theory.

The activity coefficients of HCl in the HCl-GdCl₃ mixtures were fitted by the method of least squares using eq 5 with the coefficient of the X_3^2 term set to zero. As in the case of the HCl-LaCl₃ mixture,² it was found possible to express the B coefficients with equations of the type

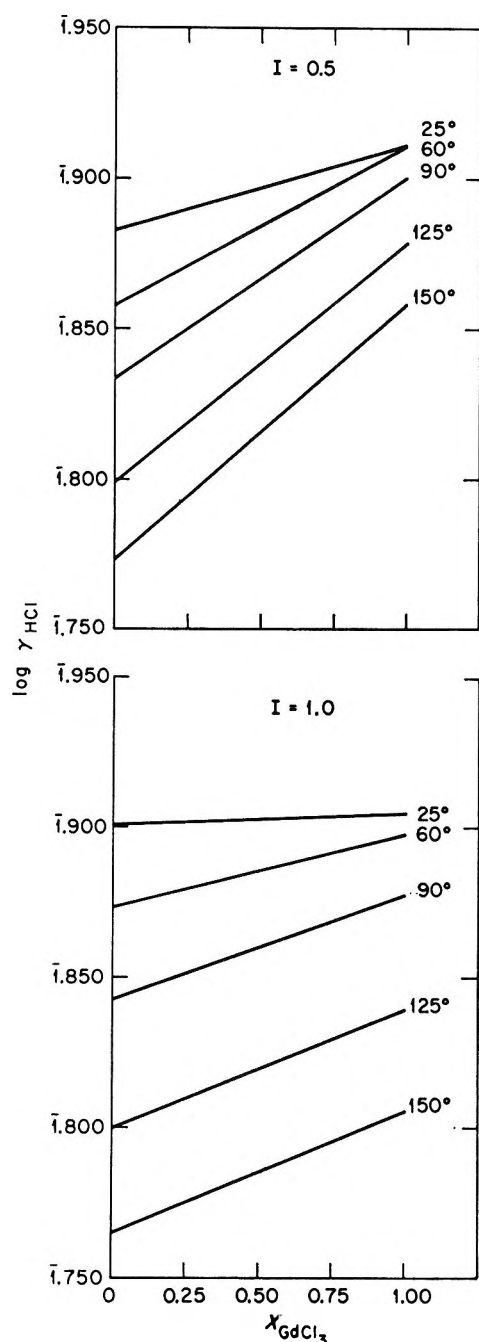
$$B_{iq} = B'_{iq} + (B''_{iq}/T) + B'''_{iq} \ln T \quad (7)$$

and the C coefficients with equations of the type

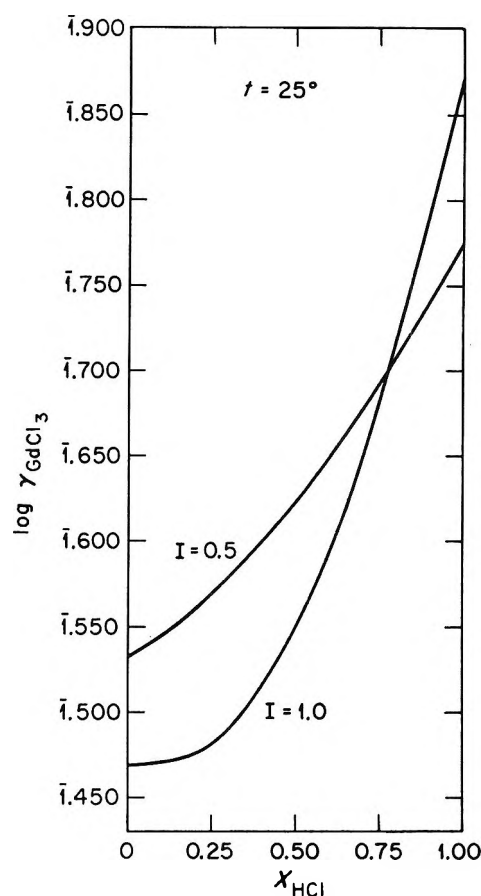
$$C_{ijk} = C'_{ijk} + (C''_{ijk}/T) \quad (8)$$

Thus, in this system also, the contribution of the B terms is much more important than the C terms (at least in the ionic strength range studied) and hence the difficulty in determining as many parameters in the C coefficients.

The values of B'_{22} , B''_{22} , B'''_{22} , B'_{23} , B''_{23} , B'''_{23} , C'_{222} , C''_{222} , C'_{223} , and C''_{223} were obtained directly by the least-squares fit, while the values of C'_{233} and C''_{233} were obtained by application of Harned's rule: $C_{222} + (C_{233}/36) - (C_{223}/3) = 0$. The additional parameters needed for calculating $\ln \gamma_3^e$ by eq 6, namely, the coefficients B_{33} and C_{333} , were evaluated by the method of least squares using activity coefficient data on pure GdCl₃ solutions.³ Unfortunately, the activity coefficient of GdCl₃ has been measured only in solutions more

Figure 1. $\log \gamma_{\text{HCl}}$ vs. X_{GdCl_3} in HCl-GdCl₃ mixtures.

dilute than those being investigated in the present study. However, since Gd and Eu are adjacent members of the rare earth series, the activity coefficients of the chlorides are probably very little different in 0.1 and 0.2 *m* solution. (In fact, the activity coefficients of LaCl₃ and EuCl₃ differ by only 1% at 0.1 *m* and by 2.5% at 0.2 *m*.) Hence, in lieu of any values for GdCl₃ solutions at 0.1 and 0.2 *m*, activity coefficient values for EuCl₃⁸ at 0.1 and 0.2 *m* were used along with those of GdCl₃ at lower concentrations in the least-squares estimation of B_{33} and C_{333} . Since the activity coefficient of GdCl₃ has been measured at 25° only, it was possible to compute the activity coefficient of GdCl₃

Figure 2. $\log \gamma_{\text{GdCl}_3}$ vs. X_{HCl} in HCl-GdCl₃ mixtures.

in the HCl-GdCl₃ mixtures at this temperature only.

The parameters for calculating the various B and C coefficients of eq 5 and 6 (so as to give the common logarithm of the activity coefficients) are shown in Table II. Activity coefficients of HCl and GdCl₃ in the mixtures at $I = 0.5$ and 1.0 , calculated using these parameters, are shown in Figures 1 and 2. Since the experimental solutions used were not at exactly $I = 0.5$ and 1.0 , the activity coefficient values calculated from the observed emf values are not shown in the figure. However, values of the emf E were calculated using the previously determined E° values and the B and C values for the smoothed activity coefficients (Table II) for each experimental point. The algebraic difference between the observed E values and those calculated are given below the observed E values in Table I.

The relationship between the B and C coefficients as defined by eq 7 and 8 and the α coefficient of Harned's rule is given by eq 9. In this equation, α_{23} is the co-

$$\alpha_{23} = 2\left(B_{22} - \frac{B_{23}}{6}\right) + 3I\left(2C_{222} - \frac{C_{223}}{3}\right) \quad (9)$$

(8) R. A. Robinson and R. H. Stokes, "Electrolyte Solutions," Academic Press Inc., New York, N. Y., 1955, p 487.

efficient designated by Harned as α_{12} . When eq 9 is solved at 25° using the parameters given in Table II, then the values of α_{23} shown in Table III are obtained. The values of α_{23} for HCl in HCl-LaCl₃ and HCl-CeCl₃⁹ mixtures are also shown for comparison. Qualitatively, the values of α_{23} appear to decrease in going from LaCl₃ to GdCl₃.

Table II: Parameters of B and C Coefficients (Eq 7 and 8) for the HCl-GdCl₃ System over the Range 25–150°

$B'_{22} = 2.41185$	$B''_{22} = -67.2133$	$B'''_{22} = -0.372759$
$B'_{23} = 28.8136$	$B''_{23} = -1598.56$	$B'''_{23} = -3.99226$
$C'_{222} = 0.0663522$	$C''_{222} = -21.9425$	
$C'_{223} = -0.225857$	$C''_{223} = 22.6755$	
$C'_{233} = -5.09896$	$C''_{233} = 1062.04$	
$B_{33} = 0.863658$		$C_{333} = -1.56670$

Table III: Values of α_{23} for HCl

	$I = 0.5$	$I = 1.0$
HCl-LaCl ₃	0.1061	0.0991
HCl-CeCl ₃	...	0.0870
HCl-GdCl ₃	-0.0569	-0.00372

It is interesting to compare the activity coefficient behavior observed in the HCl-GdCl₃ system with that obtained in the previous HCl mixtures studied.^{2,10,11} In the case of the HCl-GdCl₃ mixtures, at all temperatures and ionic strengths investigated the plots of $\log \gamma_{\text{HCl}}$ vs. X_{GdCl_3} have a positive slope; *i.e.*, the values of α_{23} are all negative. In contrast, the corresponding

plots for the HCl-BaCl₂ and the HCl-LaCl₃ mixtures all show negative slopes. The activity coefficient behavior of the HCl in the HCl-GdCl₃ system more nearly resembles the behavior in the HCl-NaCl system at $I = 0.4$ at temperatures above 25°, where again the slopes are all positive. Except for the difference in sign of the α_{23} values, both the HCl-LaCl₃ and the HCl-GdCl₃ systems are similar in that the greatest change in activity coefficient behavior of the HCl occurs between 25 and 60°. As far as the activity coefficient behavior of the salt in the mixtures is concerned, the plots of $\log \gamma_{\text{GdCl}_3}$ vs. X_{HCl} most nearly resemble those of $\log \gamma_{\text{NaCl}}$ vs. X_{HCl} in that in both systems the activity coefficient of the salt increases more rapidly in the mixtures at higher total ionic strength. In fact the activity coefficient of the salt at infinite dilution in the acid is higher in each case in the mixture of higher ionic strength (*i.e.*, the same "cross-over" behavior shown in Figure 2 at 25° is shown by NaCl in the HCl-NaCl mixtures). The opposite behavior is observed in the mixtures containing higher fractions of salt (at the same ionic strengths).

The excess partial and total partial thermodynamic quantities for both the HCl and GdCl₃ in the HCl-GdCl₃ mixtures may be readily evaluated using the expressions previously reported.²

Acknowledgment. The authors wish to express their sincere appreciation to John T. Turk and to J. D. Porterfield for performing the experimental emf measurements.

(9) C. M. Mason and D. B. Kellam, *J. Phys. Chem.*, **38**, 689 (1934)

(10) M. H. Lietzke, H. B. Hupf, and R. W. Stoughton, *ibid.*, **69**, 2395 (1965).

(11) M. H. Lietzke and R. W. Stoughton, *ibid.*, **70**, 756 (1966).

Sound Velocities, Adiabatic Compressibilities, and Free Volumes in Aniline Solutions

by D. D. Deshpande and L. G. Bhatgadde

Department of Chemistry, Indian Institute of Technology, Powai, Bombay, India (Received July 20, 1967)

The adiabatic compressibilities of aniline in benzene, toluene, carbon tetrachloride, chlorobenzene, dioxane, and acetone have been determined at 25, 35, and 45° from the measurements of densities and velocities of sound in these solutions. Eyring's model has been extended to the case of solutions to calculate the free volumes in solutions using the relationship $V_f = V(C_g/C_L)^3$. The excess compressibilities of all of the systems except aniline-dioxane have the same sign as that of excess volume, while the sign of excess free volume and excess volume is the same for all of the six systems studied. The magnitude of excess free volume is much smaller than excess volume. When the free volume is expressed as $V_f = 4/3\pi N(V_a/Y)^3$, where V_a is the available volume, it is found that even the excess available volume differs widely from excess volume. It is shown that only in special cases, depending on the size and collision factors of unlike molecules, can the excess volume and the excess available volume be identical.

There are a number of papers on the measurements of ultrasonic velocities in and adiabatic compressibilities of binary liquid-liquid mixtures.¹⁻¹² The deviations from a rectilinear dependence of velocities and compressibilities on the mole fractions are explained as due to difference in size of the molecules and the strength of interactions between them. Many authors¹⁰⁻¹² compare the excess adiabatic compressibilities with the differences in the boiling points of solutes and solvents—taken as a rough measure of interaction between the two species. Some investigators^{7,10} compare the sign of excess compressibility with that of excess volume or excess entropy. Using Jacobson's approach, some authors^{5,7,12} have calculated the excess free lengths. No one has, however, given any consideration to the calculation of free volumes in mixtures and the calculation of excess free volumes therefrom.

In the present study, we have obtained ultrasonic velocities, densities, adiabatic compressibilities, and free volumes for six liquid-liquid systems representing different types and degrees of interactions. Aniline has been chosen as a solute, since recently we have measured the excess thermodynamic properties of aniline solutions in several solvents.¹³⁻¹⁵

Experimental Section

The liquids used were obtained from E. Merck and were further purified by standard methods described by Weissberger.¹⁶ Densities and refractive indices of pure liquids agreed closely with the literature values.^{16,17} Synthetic mixtures were prepared by mixing the weighed amounts of triple distilled liquids in stop-

pered flasks. Densities were measured in the temperature range of 22 to 45°, using a Lipkin's double stem pycnometer with a volume of 18 ml, as described previously.¹⁴ Ultrasonic velocities were measured by observing Hiedemann's secondary interference pattern in a microscope.¹⁸ The liquid was contained in an optical glass cell and was excited by an X-cut quartz

- (1) P. Tuomikoski and V. Nurmi, *Comment. Phys. Math. Helsingf.*, **10**, 11 (1940).
- (2) I. Gabriel and G. Poianni, *Ricerca Sci.*, **24**, 1039 (1954).
- (3) I. G. Mikhailov, *Dokl. Akad. Nauk SSSR.*, **81**, 779 (1951).
- (4) R. Parshad, *Indian J. Phys.*, **16**, 1, 307 (1942).
- (5) M. V. Kaulgud, *Acustica.*, **10**, 316 (1960).
- (6) H. Sackmann and A. Bockzek, *Z. Physik Chem. (Frankfurt)*, **29**, 329 (1961).
- (7) M. V. Kaulgud, *ibid.*, **36**, 365 (1963).
- (8) E. A. Moelwyn-Hughes and D. I. R. Low, *Proc. Roy. Soc. (London)*, **A267**, 384 (1962).
- (9) E. A. Moelwyn-Hughes and P. L. Thorpe, *ibid.*, **268**, 574 (1964).
- (10) R. J. Fort and W. R. Moore, *Trans. Faraday Soc.*, **61**, 2102 (1965).
- (11) K. C. Reddy, S. V. Subrahmanyam and J. Bhimasenachar, *ibid.*, **58**, 2352 (1962).
- (12) K. C. Reddy, S. V. Subrahmanyam, and J. Bhimasenachar, *J. Phys. Soc. Japan*, **19**, 559 (1964).
- (13) D. D. Deshpande and M. V. Pandya, *Trans. Faraday Soc.*, **61**, 1858 (1965).
- (14) D. D. Deshpande and M. V. Pandya, *ibid.*, in press.
- (15) D. D. Deshpande and M. V. Pandya, unpublished data.
- (16) A. Weissberger, "Techniques of Organic Chemistry," Vol. 7, Interscience Publishers, Inc., New York, N. Y., 1959.
- (17) J. Timmermans, "Physico-Chemical Constants of Pure Organic Compounds," Vol. 1, Elsevier Publishing Co., Amsterdam, The Netherlands, 1950; Vol. 2, 1965.
- (18) E. Hiedemann and Ch. Bachem, *Z. Physik.*, **91**, 418 (1934); **94**, 68 (1935).

crystal of 1-Mc frequency, driven by a Hartley oscillator at its third harmonic. For the sake of thermostating, the cell was placed in a double walled metal jacket with glass windows. The temperature was controlled to $\pm 0.01^\circ$ in the range of 20 to 50° . A parallel beam of monochromatic light was passed through the cell in a direction at right angles to the propagation of sound waves. The distance between consecutive fringes corresponds to half-wavelength, and this is evaluated by observing 50–100 fringes in a traveling microscope (Soviet NZA-2), reading to 0.001 mm and provided with a calibrated glass scale. This method of measurement is rapid and compares in accuracy with that of an interferometer.^{10,19} The frequency was determined by a signal corps BC221 frequency meter. The maximum uncertainty in our velocity measurements is 0.20%. The ultrasonic velocities in pure liquids compare well with the literature values. The densities are accurate to 1 part in 10^4 . The maximum error in the adiabatic compressibility values is $\pm 0.4\%$. The error in mole fraction is not more than 0.05%.

Results

The results on ultrasonic velocities, C_L , densities, d , adiabatic compressibilities, β_s , and free volumes, V_f , as obtained from eq 2 for pure liquids and mixtures at 25, 35, and 45° are given in Tables I–VI. In these tables, the first column gives x_1 , the mole fraction of aniline.

The velocity data have been fitted to eq 1

Table II: System Aniline + Toluene

x_1	t , °C	C_L , m/sec	d , g/ml	$\beta_s \times 10^6$, atm ⁻¹	V_f , ml/mole
0.00	25	1303	0.8623	68.4	0.258
	35	1265	0.8529	73.3	0.294
	45	1229	0.8435	78.5	0.336
0.0889	25	1334	0.8746	64.2	0.237
	35	1289	0.8651	69.6	0.275
	45	1243	0.8556	75.7	0.322
0.3139	25	1397	0.9075	56.5	0.200
	35	1352	0.8980	60.9	0.230
	45	1307	0.8885	65.9	0.267
0.3999	25	1425	0.9204	53.5	0.184
	35	1380	0.9108	57.7	0.213
	45	1335	0.9016	62.2	0.242
0.4928	25	1451	0.9345	50.9	0.174
	35	1408	0.9251	54.5	0.199
	45	1366	0.9157	58.6	0.231
0.5953	25	1484	0.9500	47.8	0.164
	35	1443	0.9407	51.1	0.190
	45	1403	0.9322	54.5	0.208
0.7282	25	1516	0.9716	44.8	0.147
	35	1474	0.9624	47.8	0.167
	45	1432	0.9533	51.2	0.191
0.8086	25	1547	0.9848	42.4	0.137
	35	1505	0.9758	45.3	0.155
	45	1462	0.9668	48.4	0.177
1.00	25	1634	1.0174	37.3	0.113
	35	1594	1.0088	39.5	0.127
	45	1554	1.0002	41.9	0.143

Table I: System Aniline + Benzene

x_1	t , °C	C_L , m/sec	d , g/ml	$\beta_s \times 10^6$, atm ⁻¹	V_f , ml/mole
0.00	25	1295	0.8737	69.1	0.285
	35	1248	0.8631	75.4	0.334
	45	1200	0.8525	82.5	0.393
0.1951	25	1357	0.9033	60.9	0.237
	35	1313	0.8930	65.8	0.274
	45	1269	0.8827	71.2	0.319
0.4050	25	1422	0.9350	53.6	0.196
	35	1381	0.9248	57.4	0.224
	45	1340	0.9146	61.7	0.257
0.5068	25	1455	0.9500	50.4	0.179
	35	1417	0.9400	53.7	0.203
	45	1378	0.9300	57.3	0.230
0.6037	25	1491	0.9648	47.2	0.163
	35	1447	0.9556	50.6	0.185
	45	1404	0.9464	54.4	0.212
0.8015	25	1565	0.9912	41.7	0.134
	35	1525	0.9822	44.4	0.152
	45	1485	0.9732	47.2	0.172
1.00	25	1634	1.0174	37.3	0.113
	35	1594	1.0088	39.5	0.127
	45	1554	1.0002	41.9	0.143

$$C_L = a_0 + a_1x_1 + a_2x_1^2 + a_3x_1^3 \quad (1)$$

where a_0 , a_1 , a_2 , and a_3 are constants whose values are evaluated by the least-square method. The values of these constants are given in Table VII.

Discussion

According to Eyring and co-workers,²⁰ the free volume in liquids can be calculated from the velocity of sound in liquids, C_L , and that in the vapor, C_g , by the relation

$$V_f = V(C_g/C_L)^3 \quad (2)$$

The same equation may be used to calculate the free volume in liquid mixtures provided C_g for the vapor mixtures is known. Even for the calculation of free volume in pure liquids, one should not depend on the experimental value of C_g , as the thermal relaxation in the vapors causes the velocity dispersion. One has to

(19) F. T. Gucker, C. L. Chernick, and P. R. Chowdhury, *Proc. Natl. Acad. Sci. U. S.*, **55**, 12 (1966).

(20) H. Eyring and J. O. Hirschfelder, *J. Phys. Chem.*, **41**, 249 (1937); J. O. Hirschfelder, D. P. Stevenson, and H. Eyring, *J. Chem. Phys.*, **5**, 896 (1937); J. C. Kincaid and H. Eyring, *ibid.*, **5**, 587 (1937); **6**, 620 (1938).

Table III: System Aniline + Carbon Tetrachloride

z_1	t , °C	C_L , m/sec	d , g/ml	$\beta_s \times 10^6$, atm ⁻¹	V_f , ml/mole
0.00	25	919	1.5842	75.8	0.313
	35	888	1.5650	82.0	0.365
	45	858	1.5458	89.1	0.423
0.2037	25	1012	1.4775	67.0	0.275
	35	983	1.4619	71.7	0.314
	45	954	1.4463	77.0	0.359
0.3941	25	1116	1.3730	59.3	0.236
	35	1086	1.3591	63.2	0.268
	45	1057	1.3452	67.4	0.305
0.5244	25	1202	1.2995	53.9	0.205
	35	1172	1.2868	57.3	0.234
	45	1141	1.2741	61.1	0.265
0.6000	25	1253	1.2545	51.4	0.192
	35	1225	1.2425	54.4	0.216
	45	1196	1.2305	57.5	0.243
0.8043	25	1437	1.1327	43.3	0.147
	35	1399	1.1222	46.1	0.167
	45	1360	1.1117	49.3	0.189
1.00	25	1634	1.0174	37.3	0.113
	35	1594	1.0088	39.5	0.127
	45	1554	1.0002	41.9	0.143

Table IV: System Aniline + Chlorobenzene

z_1	t , °C	C_L , m/sec	d , g/ml	$\beta_s \times 10^6$, atm ⁻¹	V_f , ml/mole
0.00	25	1264	1.1009	57.6	0.200
	35	1226	1.0900	61.8	0.228
	45	1189	1.0791	66.4	0.260
0.1991	25	1320	1.0848	53.6	0.182
	35	1284	1.0745	57.2	0.208
	45	1247	1.0642	61.2	0.238
0.4005	25	1381	1.0684	49.7	0.165
	35	1346	1.0585	52.9	0.188
	45	1311	1.0486	56.3	0.213
0.5038	25	1412	1.0599	48.0	0.158
	35	1379	1.0496	50.8	0.178
	45	1346	1.0393	53.8	0.200
0.6070	25	1453	1.0512	45.6	0.148
	35	1419	1.0416	48.3	0.167
	45	1384	1.0320	52.4	0.188
0.8045	25	1542	1.0345	41.2	0.129
	35	1501	1.0254	43.9	0.146
	45	1460	1.0163	46.8	0.165
1.00	25	1634	1.0174	37.3	0.113
	35	1594	1.0088	39.5	0.127
	45	1554	1.0002	41.9	0.143

use, therefore, the static value of the velocity of sound C_g obtained from the equation

$$C_g = \left\{ \frac{C_p}{C_v} \frac{RT}{M} \left[1 + \frac{9}{128} \frac{PT_c}{P_c T} \left(1 - 6 \frac{T_c^2}{T^2} \right) \right] \right\}^{1/2} \quad (3)$$

Table V: System Aniline + Dioxane

z_1	t , °C	C_L , m/sec	d , g/ml	$\beta_s \times 10^6$, atm ⁻¹	V_f , ml/mole
0.00	25	1344	1.0269	54.6	0.194
	35	1299	1.0156	59.1	0.226
	45	1254	1.0043	64.1	0.263
0.1061	25	1379	1.0279	51.2	0.181
	35	1338	1.0171	54.9	0.207
	45	1297	1.0063	59.1	0.238
0.1980	25	1412	1.0285	48.8	0.168
	35	1368	1.0181	52.5	0.194
	45	1324	1.0077	56.6	0.224
0.3924	25	1474	1.0284	44.8	0.149
	35	1434	1.0187	47.8	0.170
	45	1394	1.0090	51.0	0.194
0.4466	25	1492	1.0276	43.7	0.144
	35	1451	1.0179	46.7	0.164
	45	1410	1.0082	50.0	0.187
0.4929	25	1507	1.0271	42.9	0.140
	35	1465	1.0173	45.9	0.160
	45	1423	1.0075	49.1	0.183
0.5982	25	1536	1.0259	41.3	0.133
	35	1495	1.0165	44.0	0.152
	45	1454	1.0071	47.0	0.172
0.6982	25	1563	1.0243	40.0	0.127
	35	1522	1.0148	42.6	0.144
	45	1480	1.0054	45.4	0.163
0.7965	25	1590	1.0215	38.7	0.121
	35	1547	1.0127	41.3	0.135
	45	1503	1.0039	44.1	0.157
1.00	25	1634	1.0174	37.3	0.113
	35	1594	1.0088	39.5	0.127
	45	1554	1.0002	41.9	0.143

in which we have included the correction for the non-ideality of vapors using Berthelot's equation. Using Dobratz's²¹ method, we have calculated C_p and C_v of the vapors at 25, 35, and 45° and have used them in eq 3 to obtain C_g . As an approximation, C_g for the mixture of vapors has been assumed to be additive. If V is the experimental molar volume of the liquid mixture, and C_L is the experimental velocity in the mixture, eq 2 can be used to calculate the molar free volume in the mixture. The excess molar free volume can be calculated as

$$V_f^E = V_f - x_1 V_{f_1} - x_2 V_{f_2} \quad (4)$$

Table VIII gives the free volumes in liquids at 25°; the free volumes in mixtures are included in Tables I-VI. Table IX gives the excess properties of nearly equimolar mixtures at 25°.

It is interesting to compare the excess free volumes with the excess volumes for these systems. According

(21) C. J. Dobratz, *Ind. Eng. Chem.*, **33**, 759 (1941).

Table VI: System Aniline + Acetone

z_1	t , °C	C_L , m/sec	d , g/ml	$\beta_s \times 10^6$, atm ⁻¹	V_f , ml/mole
0.00	25	1168	0.7851	93.3	0.465
	35	1123	0.7736	102.5	0.553
	45	1078	0.7621	112.8	0.658
0.2012	25	1292	0.8504	70.4	0.319
	35	1252	0.8399	76.0	0.367
	45	1212	0.8294	82.1	0.425
0.3038	25	1349	0.8792	62.5	0.268
	35	1308	0.8689	67.3	0.309
	45	1266	0.8586	72.6	0.358
0.4042	25	1399	0.9046	56.5	0.231
	35	1361	0.8947	60.4	0.263
	45	1323	0.8848	64.6	0.301
0.5040	25	1452	0.9274	52.4	0.198
	35	1409	0.9179	54.9	0.228
	45	1367	0.9084	58.9	0.262
0.5958	25	1487	0.9461	47.8	0.178
	35	1447	0.9369	51.0	0.203
	45	1407	0.9277	54.5	0.231
0.7012	25	1529	0.9673	44.3	0.157
	35	1493	0.9579	46.9	0.177
	45	1457	0.9485	49.7	0.200
0.8502	25	1586	0.9924	40.0	0.132
	35	1543	0.9833	42.7	0.150
	45	1500	0.9742	45.6	0.171
1.00	25	1634	1.0174	37.3	0.113
	35	1594	1.0088	39.5	0.127
	45	1554	1.0002	41.9	0.143

Table VII: Constants of the Eq 1

Solvent	t , °C	a_0	a_1	a_2	a_3
Benzene	25	1295.9	283.7	80.5	-25.8
	35	1248.0	314.6	34.7	-3.1
	45	1200.6	345.4	-11.0	19.7
Toluene	25	1302.1	378.0	-271.4	223.7
	35	1262.6	336.5	-179.3	171.7
	45	1223.8	289.8	-77.5	114.3
Carbon tetra- chloride	25	918.5	292.0	759.5	-343.4
	35	888.6	413.8	182.8	109.0
	45	857.7	435.3	135.5	125.0
Chlorobenzene	25	1264.4	249.6	77.8	42.8
	35	1226.3	274.2	32.5	60.8
	45	1188.9	262.6	120.2	-37.8
Dioxane	25	1343.1	347.6	-17.2	-39.8
	35	1298.7	370.6	-66.3	-9.7
	45	1254.3	393.6	-115.4	20.4
Acetone	25	1167.8	665.1	-238.0	38.6
	35	1123.0	690.1	-275.6	55.4
	45	1078.3	715.7	-313.1	72.1

Table VIII: Comparison of Free Volumes of Pure Liquids at 25°

Liquid	C_g , m/sec	B , ml/mole	S	V_f	
				From eq 2, ml/mole	From eq 5, ml/mole
Benzene	190.5	26.2	2.77	0.285	0.267
Toluene	174.7	32.0	2.72	0.258	0.276
Carbon tetra- chloride	135.6	30.7	2.52	0.313	0.308
Chlorobenzene	157.8	32.4	2.67	0.200	0.147
Dioxane	176.3	21.7	3.32	0.194	0.206
Acetone	215.5	20.3	2.67	0.465	0.737
Aniline	177.2	34.0	2.21	0.133	0.141

to the physical concept of free space in liquids, the excess volume of a nonideal mixture is attributed to the increase or decrease of free space in liquids on mixing. However, one should not immediately jump to the conclusion that the excess free volume will be identical with the excess volume. Table IX clearly shows that they are different, although the sign is always the same. The precise difference between the excess free volume and excess volume can be explained from the definition of free volume. Following Bondi²²

$$V_f = \frac{4}{3}\pi N(V_a/Y)^3 \quad (5)$$

where Y is the surface area per mole of molecules and V_a is the molar available volume. That the excess available volume can in some cases, but not always, be identical with excess volume, is shown later.

If B is the geometrical volume of molecules, the surface area will be $(36\pi NB^2)^{1/3}$. B can be evaluated from molecular radius as $\frac{4}{3}\pi Nr^3$ or can be reasonably equated with the molar refraction. We have used the latter method and have evaluated B using atomic contributions, following Schaaffs.²³

The available volume, V_a , can be expressed in various ways. Following Bondi,²² $V_a = V - V_w$, V_w being the van der Waals volume to be obtained from kinetic collision cross sections or from X-ray diffraction measurements. Following Jacobson,²⁴ $V_a = V - V_0$, V_0 being the volume at absolute zero to be obtained from the relation $V_0 = V(1 - T/T_c)^{0.3}$. Bondi's method gives free volumes much higher than that given by eq 2, while that of Jacobson gives a much lower value. In order to obtain comparable results on free volumes by eq 2 and eq 5, we prefer to calculate the available volume as

$$V_a = V - SB \quad (6)$$

(22) A. Bondi, *J. Phys. Chem.*, **58**, 929 (1954); **68**, 441 (1964).

(23) W. Schaaffs, *Z. Physik*, **114**, 110 (1939); **115**, 69 (1940); *Z. Physik. Chem.*, **194**, 39, 66 (1944); *Ergebn. exakt. Naturw.*, **25**, 109 (1951); "Molekular Akustik," Springer-Verlag, Berlin, Germany, 1963.

(24) B. Jacobson, *Acta Chem. Scand.*, **6**, 1485 (1952).

Table IX: Excess Properties of Mixtures at 25°

Solvent	z_1	C_L^E , m/sec	$\beta_s^E \times 10^4$, atm ⁻¹	V^E , ml/mole	$V_f^E,^a$ ml/mole	$V_a^E,^b$ ml/mole
Benzene	0.5068	-12	-2.7	-0.240	-0.020	-8.54
Toluene	0.4928	-15	-2.2	-0.188	-0.013	-8.81
Carbon tetra- chloride	0.5244	-91	-1.7	-0.314	-0.005	+5.38
Chlorobenzene	0.5038	-38	+0.6	+0.139	+0.003	-4.85
Dioxane	0.4929	+20	+3.2	-0.438	-0.013	-9.89
Acetone	0.5040	+49	-12.7	-1.157	-0.089	-10.61

^a From eq 4. ^b From eq 8.

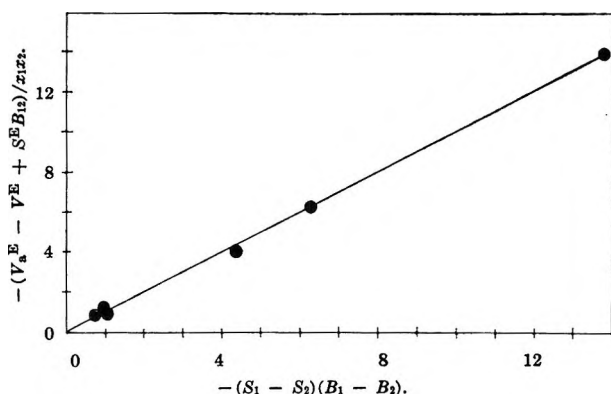


Figure 1. Test of eq 11.

where S is the collision factor, so that SB corresponds to the excluded volume. If the molecules are regarded as hard spheres, S will be simply 4. But since in reality the molecules cannot be regarded as hard spheres, due to forces prevailing between them, S will deviate from the value of 4. The value of S can be obtained by two methods. (i) The van der Waals constant, b , as used in Berthelot's equation is related to the critical volume by $b = V_c/4$. Since $b = SB$, it follows that $S = V_c/4B$. (ii) Starting from van der Waals' equation, Schaaffs²³ expresses velocity of sound in liquid as where

$$C_L = C_\infty SB/V \quad (7)$$

$C_\infty = 1600$ m/sec. This relationship is very useful to evaluate S for pure liquids, and we have used it for mixtures also. Both of the above methods give almost identical results for S for all liquids other than aniline. In the case of aniline, $S = 2.74$, as obtained from eq 7. This leads to negative available volume for aniline. This deviation must be due to the associated nature of liquid aniline. We have, therefore, preferred the calculation of S in the case of aniline from critical volume, and this gives $S = 2.21$. The free volumes of pure liquids calculated from eq 2 and 5 are given in Table VIII and show a reasonable agreement. For acetone, the free volume given by eq 5 is much higher than that given by eq 2. Because of only approximate agreement of

magnitudes of free volumes for pure liquids, there is no point in the calculation of free volumes of mixtures by using eq 5 for the sake of comparison.

As pointed out earlier, from the concept of available volume, we can explain the difference between the excess volume and the excess available volume. Expressing the excess available volume V_a^E as

$$\begin{aligned} V_a^E &= (V_{a12})_{\text{exptl}} - (V_{a12})_{\text{ideal}} \\ &= (V_{a12})_{\text{exptl}} - x_1 V_{a1} - x_2 V_{a2} \end{aligned} \quad (8)$$

where x_1 and x_2 are mole fractions. For evaluation of $(V_{a12})_{\text{exptl}}$, it is necessary to know S_{12} and B_{12} . B_{12} can be obtained from the values of pure components as $B_{12} = x_1 B_1 + x_2 B_2$. In case of S_{12} , $(S_{12})_{\text{ideal}} = x_1 S_1 + x_2 S_2$, and $(S_{12})_{\text{exptl}}$ can be evaluated from eq 7 using experimental sound velocity in the mixture, experimental molar volume of mixture V_{12} , and B_{12} . This leads to the definition of excess value of the collision factor S^E for the mixture

$$(S_{12})_{\text{exptl}} = x_1 S_1 + x_2 S_2 + S^E \quad (9)$$

Eq 8 can be expanded as

$$\begin{aligned} V_a^E &= (V_{12} - S_{12} B_{12})_{\text{exptl}} - \\ &\quad x_1 (V_1 - S_1 B_1) - x_2 (V_2 - S_2 B_2) \end{aligned}$$

After rearranging and knowing that $V_{12} - x_1 V_1 - x_2 V_2 = V^E$, this gives

$$V_a^E = V^E - S_{12} B_{12} + x_1 S_1 B_1 + x_2 S_2 B_2 \quad (10)$$

If

$$S_{12} B_{12} = (x_1 S_1 + x_1 S_2 + S^E)(x_1 B_1 + x_2 B_2)$$

is substituted in eq 10, after rearrangement we get

$$V_a^E = V^E + x_1 x_2 (S_1 - S_2)(B_1 - B_2) - S^E B_{12}$$

or

$$V_a^E - V^E + S^E B_{12} = x_1 x_2 (S_1 - S_2)(B_1 - B_2) \quad (11)$$

Since $(S_1 - S_2)(B_1 - B_2)$ is a constant for the given system, the quantities on the left-hand side of eq 11 would symmetrically vary with composition. Equation 11 shows that V_a^E and V^E will be identical only if

$S^E = 0$ and either $S_1 = S_2$ or $B_1 = B_2$. As a test of eq 11, the plot of $(V_a^E - V^E + S^E B_{12})/x_1 x_2$ vs. $(S_1 - S_2)(B_1 - B_2)$ gives a straight line for these six systems, as shown in Figure 1.

Fort and Moore¹⁰ have reported that the excess compressibility becomes increasingly negative as the strength of interaction between unlike molecules increases. The difference in the boiling points of the two components is a rough measure of the strength of interaction. With the exception of aniline-dioxane, the excess compressibilities of these systems vary according to the boiling points of solvents. The excess compressibility for aniline-acetone mixtures is highly negative, thus suggesting a strong interaction leading to a complex formation through a N-H...O bond. Though similar complex formation is possible between aniline

and dioxane, from the positive excess compressibility observed, one may apparently conclude that the interaction between aniline and dioxane is very weak. We have observed, however, that the heat of mixing of the aniline-dioxane system is highly negative (exothermic) and a complex formation is possible.¹⁵ Instead of excess compressibilities, therefore, the excess free volumes should be compared with the strength of interaction. Our results show that the sign of excess free volume for these six systems is identical with that of excess volume and also with that of excess entropy.^{14,15}

Acknowledgment. Our thanks are due to the Council of Scientific and Industrial Research for financial support to this work and for the award of a research scholarship to L. G. B.

The Crystal Structure of Dipotassium Tetranitroethide

by Maurice Dyke and Ronald L. Sass

Department of Chemistry, William Marsh Rice University, Houston, Texas (Received July 20, 1967)

The structure of dipotassium tetranitroethide, $K(NO_2)_2CC(NO_2)_2K$, has been determined by single crystal X-ray diffraction techniques. The compound crystallizes in the centrosymmetric space group C2/c with cell constants of $a = 13.03$ Å, $b = 7.56$ Å, $c = 13.55$ Å, and $\beta = 140.87^\circ$. Each unit cell contains four molecules, with the anions centered on twofold rotation axes. Atomic and thermal vibration parameters were refined by the isotropic least-squares method to give a final structure with an R value of 12.3%. The configuration of each carbon atom and its three substituents is planar within experimental error. There is a twisting of the nitrogen atoms about the C-C molecular axis to produce an angle of 63.1° between the N-C-N planes in the tetranitroethide anion. The C-C bond distance is 1.43 Å.

Introduction

In previous investigations, the crystal structures of the stable carbanion salts ammonium tricyanomethide,¹ pyridinium dicyanomethylide,² and potassium *p*-nitrophenyldicyanomethide³ were determined. It was thought that the structure determination of dipotassium tetranitroethide, $K(NO_2)_2CC(NO_2)_2K$, would be an interesting extension of the previous work because this salt contains a polynitro-substituted dicarbanion.

Experimental Section

Dipotassium tetranitroethide was prepared from the reaction of tribromonitromethane with an anhydrous ethanol solution of potassium iodide by the method of Hunter.⁴ Well formed rhombohedral single

crystals of dipotassium tetranitroethide were obtained by leaving loosely covered beakers of a saturated solution, prepared from the purified salt and water, at room temperature in a refrigerator until the crystals formed.

Crystals with a diameter of about 0.2 mm were selected as specimens for X-ray diffraction analysis and mounted on glass fibers. Weissenberg and rotational photographs showed the dipotassium tetranitroethide unit cell to be monoclinic with cell constants of $a = 13.03 \pm 0.02$ Å, $b = 7.56 \pm 0.02$ Å, $c = 13.55 \pm 0.02$ Å, and $\beta = 140.87 \pm 0.50^\circ$. The c axis was found to be

- (1) R. Desiderato and R. Sass, *Acta Cryst.*, **18**, 1 (1965).
- (2) C. Bugg and R. Sass, *ibid.*, **18**, 591 (1965).
- (3) C. Bugg and R. Sass, in press.
- (4) C. Hunter, *J. Chem. Soc.*, 543 (1923).

coincident with the needle axis of the crystal, while the b axis was perpendicular to the needle axis and coincident with the shorter edge diagonal of the needle.

All reflections with $h + k = 2n + 1$ were absent, indicating a C-centered unit cell. Systematic absences were also observed for $h0l$ reflections with $l = 2n + 1$, which showed the presence of a c glide plane perpendicular to the b axis.

The centrosymmetric space group $C2/c-C_{2h}^6$ and the noncentrosymmetric space group $Cc-C_s^4$ are the only monoclinic space groups containing symmetry elements consistent with the above absences. These space groups cannot be distinguished from each other on the basis of systematic absences. However, refinement of a trial structure derived from the assumption of a centrosymmetric structure indicates that $C2/c$ is the correct space group for dipotassium tetranitroethide.

An experimental density determination by the flotation method using a mixture of CH_2Br_2 and CCl_4 gave a value of 2.24 g/cc. Comparison of this value with the theoretical density of 0.58 g/cc for each molecule in the unit cell showed the multiplicity to be four.

Integrated intensities for 530 independent reflections were recorded on multiple films using a Nonius integrating Weissenberg camera and nickel-filtered Cu $K\alpha$ radiation. Weissenberg data were obtained around the b axis for $k = 0$ through 4, and around the c axis for $l = 0$ through 6. The integrated intensity values were measured with a Welch Densichron densitometer. Corrections were applied for the Lorentz, polarization, and Tunnell effects. No corrections were made for absorption and extinction.

Our initial assumption of $C2/c$ cell symmetry with eightfold general positions and the observed multiplicity of four implied that the center of each tetranitroethide anion was on a twofold axis or a center of symmetry in a unit cell containing one potassium ion at each of eight general positions. Synthesis of the $[010]$ Patterson projections yielded a heavy peak at $\mu = 0.75$ and $w = 0.60$, from which the x and z trial parameters of the potassium ion were obtained. The $[010]$ superposition projection was calculated *via* the α_{gen} synthesis,⁵ using these trial parameters and the relative intensities of the observed $h0l$ reflections. An image of a tetranitroethide anion centered on a twofold axis was located in the superposition projection. The positions of the peaks in this image were used to calculate the x and z anion parameters for a two-dimensional trial structure. A least-squares refinement of these parameters reduced R from an initial value of 39% to a final value of 16%.

Heavy-atom peaks in the three-dimensional Patterson synthesis showed the y parameter of the potassium ion to be ± 0.092 or ± 0.408 , with the choice of sign serving to determine the direction of the positive b axis in the coordinate system. The Patterson function's

inherent twofold ambiguity in the numerical value of the heavy-atom y parameter was resolved by testing the related trial structures for agreement with the experimental data. The anion y parameters for the three-dimensional trial structure were obtained from packing considerations and the knowledge that the anion must possess a twofold rotation axis.

Results

A three-dimensional isotropic least-squares refinement was used to reduce the R of the trial structure from 43 to 12.3%. The calculation was done with an IBM 7094 computer, using the least-squares analysis program ORFLS written by Busing, Martin, and Levy.⁶ Unobserved reflections were omitted from the refinement. During the latter stages of the refinement, the original unit weighting scheme was abandoned in favor of a modified Hughes weighting scheme. With this scheme, w was set equal to $1/F^2$ for all F 's larger than $4F_{min}$. For all other F 's, a w of $16F_{min}^2/F^4$ was used.⁷ Table I gives the final atomic parameters obtained by the refinement and their estimated standard deviations.

Table I: Final Atomic Parameters for $K_2C_2N_4O_8$

Atom	x	y	z	B
C2	0.5621 (14)	0.5459 (16)	0.3335 (13)	0.45 (19)
O1	0.4144 (13)	0.7313 (14)	0.3173 (12)	1.62 (19)
O2	0.6274 (14)	0.6177 (18)	0.5431 (14)	2.67 (24)
O3	0.7322 (11)	0.4054 (15)	0.3553 (11)	1.33 (17)
O4	0.8270 (12)	0.4750 (15)	0.5701 (12)	1.49 (18)
N1	0.5371 (13)	0.6359 (15)	0.4042 (13)	0.82 (19)
N2	0.7098 (13)	0.4692 (15)	0.4216 (12)	0.51 (17)
K	0.3725 (3)	0.0999 (5)	0.3012 (4)	0.96 (7)

Discussion

Figure 1 shows the $[010]$ projection of the crystal structure of dipotassium tetranitroethide. The interatomic distances and angles in the tetranitroethide di-

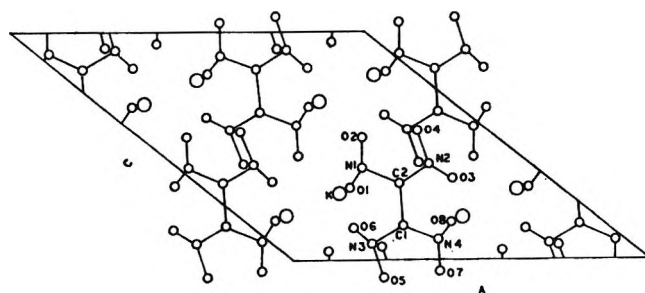


Figure 1. Projection $[010]$ of dipotassium tetranitroethide.

(5) G. N. Ramachandran and S. Roman, *Acta Cryst.*, **12**, 957 (1959).

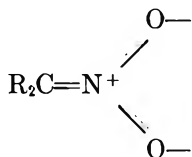
(6) W. R. Busing, K. O. Martin, and H. A. Levy, "ORFLS, a FORTRAN Crystallographic Least-Squares Program," ORNL-TM-305, Oak Ridge National Laboratory, Oak Ridge, Tenn, 1962.

(7) A table of observed and calculated structure factors can be obtained by writing to the authors.

Table II: Interatomic Dimensions in $K_2C_2N_4O_8$

Distance	Å	Angle	Deg
C1-C2	1.43 (2)	O1-N1-O2	121 (2)
C2-N1	1.40 (2)		
C2-N2	1.38 (2)	O3-N2-O4	119 (2)
N1-O1	1.24 (2)		
N1-O2	1.23 (2)	O1-N1-C2	116 (2)
N2-O3	1.24 (2)		
N2-O4	1.27 (2)	O3-N2-C2	119 (2)
N1-N2	2.43 (2)		
N2-N4	3.06 (2)	O2-N1-C2	122 (2)
N1-N3	3.06 (2)		
O1-O2	2.15 (2)	O4-N2-C2	120 (2)
O3-O4	2.17 (2)		
O1-O6	2.87 (2)	N1-C2-N2	121 (2)
O3-O8	2.87 (2)		
O1-O3	4.49 (2)	N1-C2-C1	120 (2)
O1-O4	3.98 (2)		
O2-O3	4.04 (2)	N2-C2-C1	118 (2)
O2-O4	2.57 (2)		

anion are shown in Table II. In nitromethane, the C-N and N-O bond lengths are 1.46 and 1.21 Å, respectively.⁸ Thus, there is a lengthening of the N-O bond and a shortening of the C-N bond in the tetranitroethide ion. These changes may be attributed to resonance interactions of the type



Perhaps the most striking feature of the tetranitroethide anion's structure is the twist of the nitrogen

atoms about the C1-C2 molecular axis to produce an angle of 63.1° between the N1-C2-N2 and N3-C1-N4 planes. The O1-N1-O2 and O3-N2-O4 planes make angles of 13.0 and 6.3° with the N1-C2-N2 plane, respectively.

Atom N1 is 0.017 Å above the O1-C2-O2 plane, while N2 is 0.035 Å below the O3-C2-O4 plane. The carbon atom C2 is 0.040 Å below the plane of its substituents N1, N2, and C1, indicating a planar carbanion configuration within the limits of the experimental error.

The variations in the configurations of the two nitro groups may be due to forces in the crystal lattice, since each of the nitro-group oxygens is in a different chemical environment in the lattice. Each oxygen atom has two potassium ions as its nearest intermolecular atomic neighbors with corresponding O-K distances of 2.81 and 2.87 Å for O1, 2.79 and 3.00 Å for O2, 2.68 and 2.85 Å for O3, and 2.76 and 2.84 Å for O4. The shortest O-O intermolecular distance is 3.09 Å across a center of symmetry. The shortest K-C approach is 4.00 Å. The minimum O-K distance of 2.68 Å is consistent with the values of 2.73 Å in potassium *p*-nitrophenyldicyanomethide,³ 2.70 Å in dipotassium nitroacetate,⁹ and 2.68 Å in potassium bicarbonate.¹⁰

Acknowledgments. This work was supported by grants from the National Aeronautics and Space Administration and the Robert A. Welch Foundation of Houston, Texas. The 7094 computer calculations were done at the Common Research Computer Facility located in the Texas Medical Center and supported by USPH Grant FR-00254.

(8) L. O. Brockway, J. Y. Beach, and L. Pauling, *J. Am. Chem. Soc.*, **57**, 2693 (1935).

(9) D. Sutor, F. J. Lelewellyn, and H. S. Moslen, *Acta Cryst.*, **7**, 145 (1954).

(10) I. Nitta, Y. Tomiie, and C. H. Koo, *ibid.*, **5**, 292 (1952).

Estimation of the Isomerization Rate of Nitrous Acid¹

by I. C. Hisatsune

Department of Chemistry, Whitmore Laboratory, The Pennsylvania State University,
University Park, Pennsylvania 16802 (Received July 24, 1967)

The rate constant for the unimolecular isomerization of *cis*-nitrous acid to the *trans* acid has been calculated by using the transition-state model. The one-dimensional potential-energy function for the barrier to internal rotation of the HO group and the necessary force constants and structural parameters of the transition complex were obtained from an earlier infrared study of isotopic nitrous acids. Quantum correction arising from the penetration of the potential barrier does not appear to be important. Over the temperature range from 0 to 50°, the calculated rate constants fit the Arrhenius form $1.33 \times 10^{13} \exp(-10.9 \text{ kcal}/RT) \text{ sec}^{-1}$ and $1.21 \times 10^{13} \exp(-11.0 \text{ kcal}/RT) \text{ sec}^{-1}$ for HNO_2 and DNO_2 , respectively. The isomerization half-life is about three orders of magnitude shorter than that of the formation of the acids from NO , NO_2 , and H_2O .

Introduction

A quantitative kinetic study of the rapid gas-phase equilibrium, $\text{NO} + \text{NO}_2 + \text{H}_2\text{O} = 2\text{HNO}_2$, has not been reported, but Wayne and Yost² have found that the forward reaction at about 24° has a half-life as short as 14 msec. Since the infrared spectra of all species in this equilibrium, including those of the *cis*- and *trans*-nitrous acids as well as of other oxides like N_2O_3 , N_2O_4 , and HNO_3 , which may be present in the equilibrium system, are well known, this reaction may be suitable for study by the technique of rapid-scan infrared spectroscopy reported recently by Jensen and Pimentel.³ However, during the temperature dependence study of the infrared bands of isomeric nitrous acids,⁴ it was noted that the isomerization of the acid also appears to be very rapid. If this isomerization rate is indeed rapid and comparable to the rate of formation of the acid, then the interpretation of the kinetic data for the equilibrium may not be possible at the present time, since one can conceive of three possible competing equilibria in addition to those involving N_2O_3 , N_2O_4 , and HNO_3 . (Equilibria for the latter three oxides can be minimized by using higher temperatures and lower partial pressures of the reactants.) Thus, an *a priori* estimation of the isomerization rate of nitrous acid will be helpful before one undertakes the experimental study of the formation equilibrium.

In the present paper, the unimolecular rate constant for the isomerization of *cis*-nitrous acid to the *trans* molecule has been calculated. A transition state model⁵ was employed from which the rate constant is given by

$$k = \Gamma^*(kT/h)(F^\ddagger/F) \exp(-\Delta E_0/RT) \quad (1)$$

where the various symbols have the usual meanings. Structural parameters, vibrational frequencies, and

the potential-energy function separating the two isomers were taken or estimated from our earlier work on nitrous acid.⁴ The transmission correction, Γ^* , was calculated by fitting an unsymmetrical Eckart potential-energy function⁶ to the rotational barrier. Johnston and Heicklen⁷ have transformed the Eckart potential into a convenient form to calculate tunneling corrections, and their results were used here.

Results

The fundamental vibrational frequencies of the isotopic *cis*-nitrous acids observed in our earlier study⁴ are listed in Table I. The structure of the *cis* isomer is not known, but the structure of the *trans* acid from microwave spectroscopy⁸ is reported to be planar with $r(\text{HO}) = 0.954 \text{ \AA}$, $r(\text{N}-\text{O}) = 1.433 \text{ \AA}$, $r(\text{N}=\text{O}) = 1.177 \text{ \AA}$, $\angle \text{HON} = 102^\circ 3'$, and $\angle \text{ONO} = 110^\circ 39'$. The principal moments of inertia given in the table for our molecules were derived by assuming the same *cis* structure as was used before: namely, $r(\text{HO}) = 0.96 \text{ \AA}$, $r(\text{N}-\text{O}) = 1.46 \text{ \AA}$, $r(\text{N}=\text{O}) = 1.20 \text{ \AA}$, $\angle \text{HON} = 104^\circ$, and $\angle \text{ONO} = 114^\circ$.

The rotational barrier potential function between

(1) Work supported by Grant AP-18 from the National Center for Air Pollution Control, U. S. Public Health Service.

(2) L. G. Wayne and D. M. Yost, *J. Chem. Phys.*, **19**, 41 (1951).

(3) R. J. Jensen and G. C. Pimentel, *J. Phys. Chem.*, **71**, 1803 (1967).

(4) G. E. McGraw, D. L. Bernitt, and I. C. Hisatsune, *J. Chem. Phys.*, **45**, 1392 (1966).

(5) S. Glasstone, K. J. Laidler, and H. Eyring, "The Theory of Rate Processes," McGraw-Hill Book Co., Inc., New York, N. Y., 1941.

(6) C. Eckart, *Phys. Rev.*, **35**, 1303 (1930).

(7) H. S. Johnston and J. Heicklen, *J. Phys. Chem.*, **66**, 532 (1962); in the reference, the term in brackets in eq 15 should be $[\alpha_1(\xi - 1) + \alpha_2]^{1/2}$.

(8) A. P. Cox and R. L. Kuczkowski, *J. Am. Chem. Soc.*, **88**, 5071 (1966).

Table I: Vibrational Frequencies (cm^{-1}) and Principal Moments of Inertia (amu \AA^2)

	<i>cis</i> - HNO ₂	<i>cis</i> - DNO ₂	HNO ₂ ±	DNO ₂ ±
ν_1 (OH)	3424	2525	3544	2581
ν_2 (N=O)	1640	1625	1628	1628
ν_3 (H-O-N)	1261	1008	1263	1001
ν_4 (N-O)	853	814	849	797
ν_5 (O-N-O)	608	601	634	626
ν_6 (torsion)	638	504	(611i) ^a (705i) ^b	(466i) ^a (538i) ^b
I_1	6.158	7.244	6.134	6.952
I_2	41.15	42.08	41.57	43.96
I_3	47.31	49.33	46.10	48.00

^a Torsion force constant = -0.1604 mdyne $\text{\AA}/\text{radian}^2$; see text. ^b Torsion force constant = -0.2134 mdyne $\text{\AA}/\text{radian}^2$; see text.

the *trans* and the *cis* isomers was deduced previously from the infrared spectra⁴ to be

$$2V(\text{kcal/mole}) = 1.17(1 - \cos \theta) + 11.27(1 - \cos 2\theta) - 0.78(1 - \cos 3\theta) \quad (2)$$

where $\theta = 0^\circ$ corresponds to the *trans* isomer minimum potential energy, which is 0.389 kcal/mole below the *cis* minimum. Since the barrier maximum was at $\theta = 86^\circ$ from the *cis* minimum, this angle was taken for the nonplanarity of the transition complex, i.e., the angle between the planes defined by ONO and HON in the complex. The remaining structural parameters of the complex were taken to be essentially intermediate between those of the *cis* and *trans* acids: $r(\text{HO}) = 0.96$ \AA , $r(\text{N-O}) = 1.45$ \AA , $r(\text{N=O}) = 1.20$ \AA , $\angle \text{HON} = 103^\circ$, and $\angle \text{ONO} = 112^\circ$. The principal moments of inertia of the complex, listed in Table I, were calculated with these parameters.

Once the structure of the transition complex is fixed, its vibrational frequencies can be calculated from estimated force constants. In the present case, the *cis* "overlay" force constants, derived earlier from least-squares fitting of both the *cis* and *trans* acid fundamental frequencies, were used (See Table III of ref 4). The calculated frequencies for the normal and the heavy-acid transition complex are given in Table I. Two sets of imaginary torsional frequencies are also listed here, and these were calculated from two different negative torsional force constants whose origin is described below.

The cosine rotational barrier given by eq 2 is illustrated in Figure 1 by the solid curve. Here, the potential energy is in units of $V^* = 11.15$ kcal/mole and the torsional angle $x = \theta$ is in radians. These notations, as well as the subsequent ones in this section, are the same as those used by Johnston and Heicklen.⁷ In order to estimate the tunneling corrections for this

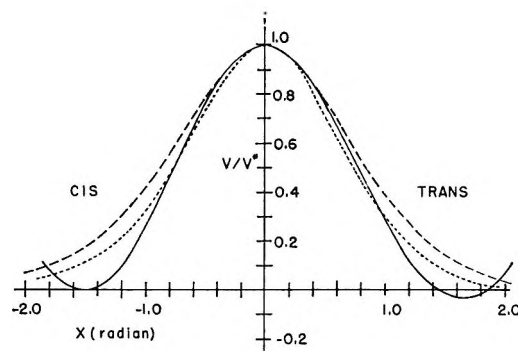


Figure 1. Rotational potential-energy barrier in nitrous acid: the solid curve is the cosine barrier, and the dashed and dotted curves are Eckart potential functions with force constants of -0.1604 and -0.2134 mdyne $\text{\AA}/\text{radian}^2$, respectively.

rotational barrier, an unsymmetrical Eckart potential function

$$V = -Ay(1 - y)^{-1} - By(1 - y)^{-2} \quad (3)$$

for which the transmission coefficient, κ , is given by a closed form was fitted to the cosine barrier. Here, A and B are functions of barrier heights from the *cis* and *trans* minima, respectively, and y is an exponential function of x , the barrier height, and the force constant at the barrier maximum. The second derivative at the maximum of the cosine barrier gives a value of -0.1604 mdyne $\text{\AA}/\text{radian}^2$ for the latter force constant. The resulting Eckart function is shown in Figure 1 by the dashed curve. Since this function is broader than the cosine barrier, a second Eckart potential function was derived by fitting the barrier maximum, the inflection point on the *cis* side of the cosine barrier, and the two barrier minima. For this function, which is illustrated by the dotted curve in Figure 1, the force constant at the barrier maximum was -0.2134 mdyne $\text{\AA}/\text{radian}^2$.

The quantum-mechanical transmission coefficient, derived from the two force constants described above, is shown as a function of scaled initial energies in Figure 2. The classical transmission coefficient would be a step-function at $E/V^* = 1.0$. It is apparent that

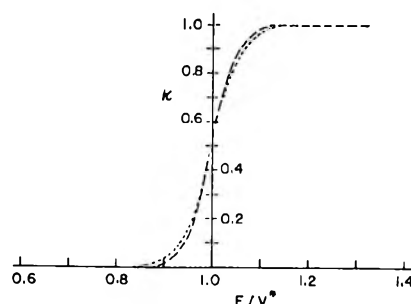


Figure 2. Transmission coefficient for Eckart potential functions; the dashed and dotted curves are for force constants of -0.1604 and -0.2134 mdyne $\text{\AA}/\text{radian}^2$, respectively.

Table II: Calculated Rate Constants

T, °K	$k \times 10^{-4}, \text{sec}^{-1}$		k_b/k_d
	HNO ₂	DNO ₂	
273	2.46	2.00	1.23
283	4.99	4.09	1.22
293	9.67	7.94	1.22
298	13.2	10.9	1.21
303	17.9	14.8	1.21
313	32.1	26.5	1.21
323	55.2	45.7	1.21

* tunneling is significant only when the energy of the reactant molecule is within about 10% of the barrier maximum.

Johnston and Heicklen⁷ have also tabulated quantum correction factors Γ^* , obtained by integrating the transmission coefficients over a Boltzmann distribution of incident molecules. These correction factors are expressed in terms of α 's and u^* , which are proportional, respectively, to the ratio of barrier height to the imaginary frequency and to the ratio of the imaginary frequency to the absolute temperature. Examination of the tabulated results indicates that for a given set of α 's, the correction factor increases as u^* becomes larger, i.e., larger imaginary frequencies and lower temperatures. In our case, the largest imaginary frequency given in Table I corresponds to $u^* = 3.4$ at 25°. For this value of u^* , the published table extends only to $\alpha = 20$, while our α 's are near 35 and 41 for the two Eckart potential functions. However, the numerical trend in the table suggests that the quantum correction factor in the present case must be at most about two and more probably less. Since the variation, at a given temperature, of experimental rate constants for complex reactions is of this order, eq 1 can be used without the Γ^* to get a reasonable estimate of the isomerization rate constants. Results calculated on this basis are presented in Table II.

Over the temperature range from 0 to 50°, which appears to be a convenient range to study experimentally the nitrous acid formation and isomerization reactions, the calculated isomerization rate constants listed in Table II for HNO₂ and DNO₂ fit well the Arrhenius

form of $1.33 \times 10^{13} \exp(-10.9 \text{ kcal}/RT) \text{ sec}^{-1}$ and $1.21 \times 10^{13} \exp(-11.0 \text{ kcal}/RT) \text{ sec}^{-1}$, respectively.

The only experimental result with which our calculated rate constants can be compared appears to be that from a study of the decomposition of chloroformic acid by Jensen and Pimentel.³ These authors found this reaction to be first order and interpreted their results on the basis of a rate-determining step involving the isomerization of the *cis*-chloroformic acid to the *trans* acid. The rate constant they obtained over the temperature range from 15 to 70° was $5 \times 10^{13} \exp(-14 \text{ kcal}/RT) \text{ sec}^{-1}$. Since the rotational barrier in *cis*-chloroformic acid is probably very similar to that in *cis*-formic acid, which in turn has a barrier⁹ 2.2 kcal/mole greater than that in *cis*-nitrous acid, the result obtained by Jensen and Pimentel suggests that our calculated rate constants are reasonable.

As was stated in the Introduction, there has been no quantitative kinetic study of the formation of nitrous acid from NO, NO₂, and H₂O. However, Wayne and Yost² have reported that the formation half-life at about 24° can be as short as 14 msec, and that the reaction rate at the same temperature is approximately 10^{-2} atm/sec when the partial pressures of the reactants are all about 10^{-2} atm. The calculated isomerization half-life of *cis*-nitrous acid, on the other hand, is about 5 μsec at 25°, and if the partial pressure of the *cis* acid is about 10^{-2} atm, then the isomerization rate will be about 10^3 atm/sec. Thus, even though the results of Wayne and Yost may be opened to question because their experimental points show considerable scatter, it appears, at the present time, that the isomerization reaction of nitrous acid is faster by about five orders of magnitude than the rate of formation of the acid from NO, NO₂, and H₂O.

Acknowledgments. I am grateful to Dr. D. L. Bernitt of our Computation Center for calculating the vibrational frequencies of the transition complex, and to Professor Julian Heicklen for helpful discussions. It is a pleasure to acknowledge the continued financial support of our studies by the National Center for Air Pollution Control.

(9) D. L. Bernitt, K. O. Hartman, and I. C. Hisatsune, *J. Chem. Phys.*, **42**, 3553 (1965).

Diffusion Potential Decay Accompanying Transient-State

Diffusion of Electrolytes in Ideal Solutions¹

by Gary E. Spalding

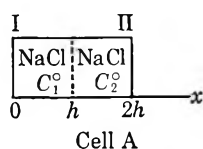
UT-AEC Agricultural Research Laboratory, Oak Ridge, Tennessee² 37830 (Received July 26, 1967)

A new relationship describing single electrolyte diffusion in closed ideal systems has been derived. This relationship, which applies at the boundaries of a closed system, is $\partial\psi/\partial t = \alpha(\partial^2\psi/\partial x^2)$ where ψ is the electric potential and α is a rate constant. The equation was tested by using a potentiometric technique and by obtaining a measure of electrolyte flux. Agreement between theory and experiment was excellent.

This work was prompted by a need for a treatment of diffusion in complex systems which is at once general, readily applicable, and of predictive value. Before considering complex systems directly, it seemed reasonable to inquire whether there exist relationships for ideal systems which have not been recognized; if one were found then perhaps it would also hold for nonideal systems. This is a report on what is thought to be a previously unrecognized relationship describing diffusion in ideal electrolyte solutions.

Theory

Let us, for clarity, consider a particular example—the diffusion of NaCl at an initial concentration, C_1^0 , into NaCl at a lower initial concentration, C_2^0 . Cell



A illustrates the initial and boundary conditions of a diffusion cell. The system is closed, with walls I and II at $x = 0$ and $x = 2h$; $x = h$ is the plane of contact between half-cells and the x direction is that in which diffusion occurs.

If one considers the driving force for diffusion of a species (be it charged or uncharged) to be the electrochemical potential gradient of that species, one can readily show, as did Karreman and Eisenman³ that

$$J_i = -D_i C_i \left(\frac{d \ln a_i}{dx} + \frac{z_i F}{RT} \frac{d\psi}{dx} \right) \quad (1)$$

where J_i is the flux, D_i the diffusion coefficient, C_i the concentration, z_i the valence, and a_i the activity of species i . R is the gas constant, T the absolute temperature, F the Faraday, and ψ the electric potential. For an ideal system, $a_i = C_i$ and eq 1 becomes

$$J_i = -D_i \left(\frac{dC_i}{dx} + \frac{z_i F C_i}{RT} \frac{d\psi}{dx} \right) \quad (2)$$

which is the Nernst-Planck equation.⁴

Considering the solutions in Cell A to be ideal, one can write a Nernst-Planck equation for each of the diffusible species.

$$J_{Na} = -D_{Na} \left(\frac{dC_{Na}}{dx} + \frac{FC_{Na}}{RT} \frac{d\psi}{dx} \right) \quad (3)$$

$$J_{Cl} = -D_{Cl} \left(\frac{dC_{Cl}}{dx} - \frac{FC_{Cl}}{RT} \frac{d\psi}{dx} \right)$$

Combining electroneutrality conditions

$$J_{Na} = J_{Cl} \quad (4)$$

$$C_{Na} = C_{Cl} = C_{NaCl} = C$$

with eq 3, and writing the result in differential form, one can find that

$$d\psi = k d \ln C \quad (5)$$

where

$$k = -\frac{RT}{F} \frac{D_{Na} - D_{Cl}}{D_{Na} + D_{Cl}} = \text{constant} \quad (6)$$

Differentiating eq 5 partially with respect to time yields

(1) This paper is published with the permission of the Director of the University of Tennessee Agriculture Experiment Station, Knoxville, Tenn.

(2) Operated by the Tennessee Agricultural Experiment Station for the U. S. Atomic Energy Commission under Contract No. AT-40-1-GEN-242.

(3) G. Karreman and G. Eisenman, *Bull. Math. Biophys.*, **24**, 413 (1962).

(4) F. Helfferich, "Ion Exchange," McGraw-Hill Book Co., Inc., New York, N. Y., 1962.

$$\frac{\partial \psi}{\partial t} = \frac{k}{C} \frac{\partial C}{\partial t} \quad (7)$$

Differentiating eq 5 twice with respect to x and multiplying by the diffusion coefficient of NaCl, α ,⁵ gives

$$\alpha \frac{\partial^2 \psi}{\partial x^2} = \frac{k\alpha}{C} \frac{\partial^2 C}{\partial x^2} - \frac{k\alpha}{C^2} \left(\frac{\partial C}{\partial x} \right)^2 \quad (8)$$

If we specify that eq 8 is to be applied only at the cell boundaries I and II, where $\partial C / \partial x = 0$, it simplifies to

$$\alpha \frac{\partial^2 \psi}{\partial x^2} = \frac{k}{C} \alpha \frac{\partial^2 C}{\partial x^2} \quad (9)$$

Equations 7 and 9 may now be combined with Fick's second law

$$\frac{\partial C}{\partial t} = \alpha \frac{\partial^2 C}{\partial x^2} \quad (10)$$

yielding

$$\frac{\partial \psi}{\partial t} = \alpha \frac{\partial^2 \psi}{\partial x^2} \quad (11)$$

Equation 11 is integrable and is subject to experimental test. Although the derivation places eq 11 on as firm a foundation, in ideal systems, as are Fick's law and the Nernst-Planck equations, it must be remembered that it is applicable only in closed-system diffusion where there is no flux across the boundaries. The above derivation is readily extended, under the assumption of ideality, to all electrolyte solutions containing a single electrolyte.

Basis of Experimental Tests of Eq 11

Sodium chloride solution in the concentration range 0.2–0.7 M is sufficiently ideal to be an excellent test system. In this range, its diffusion coefficient is very constant, $\alpha = 1.476 \pm 0.002 \times 10^{-5}$ cm²/sec.⁶ From molal activity-coefficient data at six points over the range of 0.2–0.7 m ,⁶ molar concentrations and activities were calculated, and a linear least-squares regression of activity on concentration was computed. The regression equation was

$$a_{\text{NaCl}} = 0.6494C_{\text{NaCl}} + 0.0186 \quad (12)$$

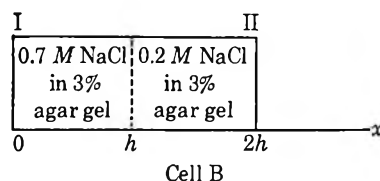
The average deviation of a_{NaCl} (regression) from a_{NaCl} was found to be 0.0005 and the maximum deviation 0.0010. Thus, to a close approximation, one may consider a_{NaCl} to be a linear function of concentration, and eq 10 can be written

$$\frac{\partial a_{\text{NaCl}}}{\partial t} = \alpha \frac{\partial^2 a_{\text{NaCl}}}{\partial x^2} \quad (13)$$

Using the Guggenheim assumption that Cl activity equals the mean activity of NaCl, eq 13 can be written

$$\frac{\partial a_{\text{Cl}}}{\partial t} = \alpha \frac{\partial^2 a_{\text{Cl}}}{\partial x^2} \quad (14)$$

Cell B was used in our experiments to test the validity of eq 11. Ag–AgCl electrodes were placed at planes I



and II, and the cell potential, E , was measured continuously with time as diffusion occurred.

Equations 11 and 14 will now be used to predict the time variation of E accompanying diffusion. The difference between the electric potentials at I and II is the diffusion potential, E_d

$$E_d = \psi_{\text{II}} - \psi_{\text{I}} \quad (15)$$

Solving eq 11 under the constraints of Cell B,⁷ applying the solution at I and II, and combining with eq 15 leads one to

$$E_d = \frac{4E_d^0}{\pi} S \quad (16)$$

where $E_d^0 = (\psi_{\text{II}}^0 - \psi_{\text{I}}^0)$ is the diffusion potential at the time the half-cells are brought together ($t = 0$), and

$$S = \sum_{n=0}^{\infty} \frac{(-1)^n}{2n+1} \exp[-(2n+1)^2(\pi/2h)^2\alpha t] \quad (17)$$

In addition to the diffusion potential, there exists a Nernst potential

$$E_N = \frac{RT}{F} \ln \frac{a_{\text{Cl,I}}}{a_{\text{Cl,II}}} \quad (18)$$

Integrating eq 14, applying the result at I and II, and combining with eq 18 yields

$$E_N = \frac{RT}{F} \ln \frac{\frac{1}{2}(a_{\text{Cl,I}}^0 + a_{\text{Cl,II}}^0) + \frac{2}{\pi}(a_{\text{Cl,I}}^0 - a_{\text{Cl,II}}^0)S}{\frac{1}{2}(a_{\text{Cl,I}}^0 + a_{\text{Cl,II}}^0) - \frac{2}{\pi}(a_{\text{Cl,I}}^0 - a_{\text{Cl,II}}^0)S} \quad (19)$$

From eq 12 and the Guggenheim assumption, $a_{\text{Cl,I}}^0$ and $a_{\text{Cl,II}}^0$ are found to be 0.4731 and 0.1484 M , respectively. Substituting these values in eq 19 and rearranging gives

(5) The symbol α has been used in place of the usual D because, in extending this treatment to complex systems, α is not always associated with a particular D . We shall not treat such extension here, as the experimental basis for it is not complete and is as yet inconclusive.

(6) R. A. Robinson and R. H. Stokes, "Electrolyte Solutions," Academic Press, Inc., New York, N. Y., 1955.

(7) Methods of solving such equations are given in many text and reference books including: H. S. Carslaw and J. C. Jaeger, "Conduction of Heat in Solids," Oxford University Press, London, 1959.

$$E_N = \frac{RT}{F} \ln \frac{1 + 0.6652S}{1 - 0.6652S} \quad (20)$$

The initial diffusion potential, E_d^0 , is (under the assumption made on Cl activity) experimentally obtainable from the initial cell potential, E^0 , and the initial Nernst potential, $E_N^0 = 29.79$ mv

$$E_d^0 = E^0 - 29.79 \quad (21)$$

At this point, it is convenient to anticipate the results and report that E^0 for our experimentally determined potentiometric decay curves was 22.96 mv leading to a calculated E_d^0 of -6.83 mv. Substituting this value into eq 16, and adding eq 16 and 20 one obtains, for the time dependence of E

$$E = -8.696S + \frac{RT}{F} \ln \frac{1 + 0.6652S}{1 - 0.6652S} \quad (22)$$

Figure 1 shows the theoretical decay curve of E , and those of E_d and E_N . The time axis is not labeled because its scale will depend upon the constant, $(\pi/2h)^2\alpha$, in eq 17. The figure serves to emphasize that E_d and E_N cannot be measured independently; only E can be measured.

Since E_d cannot be measured independently of E_N , testing eq 22 must be considered an indirect test of eq 11. It is felt, however, that such a test is valid since the assumptions leading to the Nernst potential decay, eq 20, are straightforward and are not expected to be significantly violated. Inasmuch as the correctness with which E is partitioned into E_N and E_d can be questioned, it was deemed advisable to supplement potentiometric decay curves with an independent measure of α .

A measure of NaCl flux in Cell B can be obtained by separating the half-cells after diffusion has occurred for a given time and determining the fraction of total NaCl which is in the right-hand half-cell, F . This value can be compared with the value⁸ of F predicted by the potentiometric decay curves and eq 10

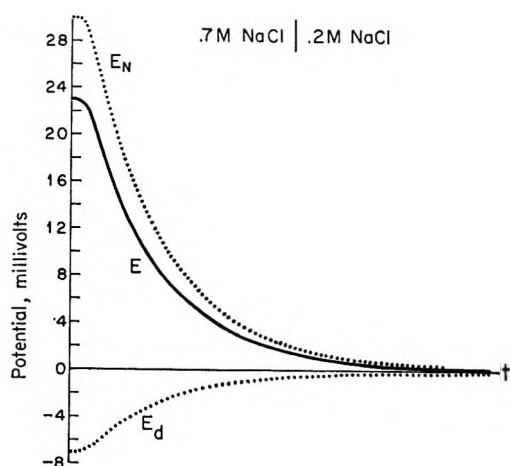


Figure 1. E , E_N , and E_d theoretical decay curves.

$$F = \frac{1}{2} \left(1 - \frac{8}{\pi^2} \frac{C_1^0 - C_2^0}{C_1^0 + C_2^0} S' \right) = \frac{1}{2} (1 - 0.4503S') \quad (23)$$

where

$$S' = \sum_{n=0}^{\infty} \frac{1}{(2n+1)^2} \exp[-(2n+1)^2(\pi/2h)^2\alpha t] \quad (24)$$

and $(\pi/2h)^2\alpha$ is the value obtained by fitting eq 22 to the observed decay curves.

Testing eq 23 may be considered an independent test of eq 20, and eq 20 and 22 lead to an independent test of eq 16, hence of eq 11.

Experimental Section

A diffusion cell was fabricated from Plexiglas and cylindrical silver rod as shown in Figure 2. The silver rod was potted into the Plexiglas with ferule cement, and then the silver-cement-Plexiglas surface was machined to a flat clean plane. This was followed by polishing the surface with fine emery powder and removing the powder by repeatedly washing with distilled water and polishing with absorbent tissue.

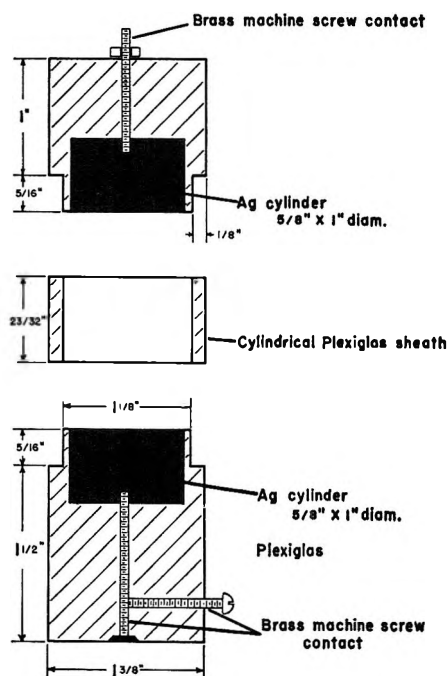


Figure 2. Cross-sectional view of diffusion cell.

A Plexiglas sheath was fitted over the electrode and filled with 0.1 M HCl. The electrode was plated for 3 min at 5 ma/cm² against a Pt electrode dipped into the HCl. The electrode was washed with distilled water and then dried and lightly polished with absorbent tissue. The drying was not found to be detrimental to electrode performance and was necessary in order to use

(8) A derivation of (23) for the case where $C_2^0 = 0$ is given by A. Klute and J. Letey, *Soil Sci. Soc. Amer. Proc.*, **22**, 213 (1958).

the electrode without disturbing the composition of half-cells. The asymmetry potential between two electrodes prepared in this manner was immediately 0.08 mv and very stable. Following each use, the electrodes were rinsed thoroughly with distilled water, and then dried and polished with absorbent tissue.

The half-cells were 3% agar gels of 0.2000 and 0.7000 *M* NaCl. To prepare gels, 50.00 ml of NaCl solution was added to 1.500 g of dry agar⁹ in a 125-ml conical flask, and the flask was loosely stoppered and held in boiling water for 4 min to melt the agar. The agar was stored in tightly stoppered 4-ml vials.

Half-cells were molded in a 1.125-in. i.d. \times 0.2822 cm thick Plexiglas ring held between two glass slides. The ring was placed on a glass slide and a vial of melted agar (1.5 min in boiling water) was poured into it. A second slide was placed on the ring causing excess agar to overflow. The reproducibility of molding half-cells was found, by weighing, to always be within $\pm 1\%$ and usually within $\pm 0.3\%$.

Ten minutes after pouring, the agar half-cell was transferred directly from the mold to the electrode surface of the diffusion cell. The transfer was easily made without introducing air pockets and with apparently complete wetting of the electrode surface. A Plexiglas sheath was placed over the electrode and agar and was stoppered. The half-cells were allowed to remain at least 1 hr in a constant temperature box at $25 \pm 0.1^\circ$ before a diffusion run was started.

The diffusion run was started by bringing the half-cells together with 0.7 *M* NaCl agar on the bottom and 0.2 *M* NaCl agar on top. The sheath of the top half-cell was removed and the half-cell inserted into the sheath of the bottom, that sheath becoming common to both. The bottom sheath had a 0.0825-in. hole in the wall at the plane where the half-cells met; the hole was ordinarily closed with tape, but was opened in order to allow air to escape so the half-cells could easily be brought into contact.

At the moment half-cells were brought together, a Beckman 10-in. potentiometric recorder was started and the cell potential was recorded continuously with time. A Leeds and Northrup Model K-2 potentiometer, equipped with a large stable storage battery, was used to buck out a precisely known portion of the cell potential so that the remainder could be read by the recorder at a full scale sensitivity of 10 mv, allowing one to estimate the potential to 0.01 mv. When the recorder pen approached going off-scale, the bucking voltage was changed by 10 mv to return it to full scale.

Besides obtaining complete potentiometric decay curves, some of the diffusion runs were interrupted after given times, the half-cells split apart, and NaCl was determined in each half-cell using a Na²² tracer. To ensure identical specific radioactivity in the 0.2 and 0.7 *M* NaCl half-cells, 0.2 *M* NaCl was prepared by dilution of labeled 0.7 *M* NaCl. Half-cells were counted in flat-

bottom tubes in a NaI scintillation crystal having a 1.375-in. well diameter. Extensive preliminary data showed that NaCl could always be determined within $\pm 1\%$ using this method; determinations were usually good to within $\pm 0.5\%$.

Results and Discussion

Seven complete potentiometric decay curves were obtained for the interdiffusion of 0.7 and 0.2 *M* NaCl in 3% agar gels. At infinite time (6 hr could be considered infinite in these experiments) an asymmetry potential was always observed between the Ag-AgCl electrodes. Six of the runs showed 0.07 ± 0.03 mv and the other 0.18 mv asymmetry potential at infinite time. It was assumed that the electrode asymmetry potential was constant throughout each run and the recorder trace was corrected for its value at infinite time. Using this correction, the average E^0 for the seven decay curves was 22.96 mv; this value was previously used in arriving at eq 22.

In order to compare the observations with the curve predicted by eq 22, it was necessary to analyze the curves to determine the value of $(\pi/2h)^2\alpha$ which produces the best fit between eq 22 and the observations. While α in 0.2–0.7 *M* NaCl is known to be 1.476×10^{-5} cm²/sec,⁶ and h was fixed at 0.2822 cm, these values are not applicable to our diffusion cell because of the presence of agar. Agar makes the diffusion path tortuous, and hence makes h appear larger than it was measured to be. The method used to analyze the decay curves is outlined in the Appendix. The result of that analysis showed $(\pi/2h)^2\alpha$ to be 0.02588 ± 0.00016 min⁻¹ (or 4.313×10^{-4} sec⁻¹), hence (using $\alpha = 1.476 \times 10^{-5}$ cm²/sec) the effective half-cell length, h , was 0.2906 cm, which is 3.0% greater than the measured value. The data analysis also indicated that a zero time correction of 0.03 min should be added to all observed times to correct for a small amount of mixing which takes place as the half-cells are brought into contact. Thus the particular solution for S , which is substituted into eq 22, is

$$S = \sum_{n=0}^{\infty} \frac{(-1)^n}{2n+1} \exp[-(2n+1)^2 \times (0.02588)(t+0.03)] \quad (25)$$

where t is in minutes.

Table I presents the results of seven experimental runs compared with results predicted by eq 22 and 25. The average of the seven observations is obviously in excellent agreement with predicted values, the largest deviation being 0.03 mv. Reproducibility of decay curves is evident from the average deviations of experimental from theoretical values, usually 0.04 mv or less.

(9) Difco Certified Agar, Control 493973.

Table I: Theoretical and Observed Decay of E (mv at 25°)^a

t , min	E , theoretical	E , obsd
0.00	22.96	22.96 ± 0.03
6.92	22.43	22.43 ± 0.03
9.24	21.58	21.56 ± 0.04
11.56	20.49	20.47 ± 0.03
13.88	19.30	19.30 ± 0.04
16.20	18.11	18.11 ± 0.04
18.52	16.96	16.96 ± 0.04
20.84	15.87	15.87 ± 0.04
23.16	14.85	14.86 ± 0.04
25.47	13.90	13.91 ± 0.04
27.79	13.01	13.03 ± 0.04
30.11	12.19	12.19 ± 0.04
32.43	11.42	11.43 ± 0.05
34.75	10.71	10.71 ± 0.04
40.54	9.14	9.15 ± 0.05
46.34	7.82	7.84 ± 0.05
52.14	6.70	6.70 ± 0.04
57.94	5.74	5.74 ± 0.05
69.53	4.24	4.22 ± 0.04
81.12	3.13	3.11 ± 0.03
92.71	2.32	2.29 ± 0.04
104.31	1.71	1.69 ± 0.02
115.90	1.27	1.25 ± 0.02

^a The observed value is the average of seven runs. The error indicated is the average deviation of observed from theoretical values.

The results of the F value (F is the fraction of NaCl in the initially more dilute half-cell) determinations are given in Table II and compared with the values predicted by (23) and (24), where $(\pi/2h)^2\alpha$ is 0.02588 min⁻¹ and 0.03 min was added to observed times. Deviations between observed and predicted F values are well within the experimental error in determining NaCl.

The close agreement between theoretical decay curves and F values and the corresponding observations is considered to be ample evidence that E was correctly partitioned by our treatment, and constitutes an experimental verification of eq 11.

Table II: Predicted and Observed Values of F at Different Times

t , min	F , predicted	F , obsd
5.72	0.299	0.302
9.71	0.322	0.321
14.50	0.345	0.347
18.77	0.361	0.359
24.67	0.381	0.382
31.55	0.401	0.403
40.44	0.421	0.422
51.55	0.441	0.442
66.31	0.460	0.461
93.64	0.480	0.481

Preliminary potentiometric data have been obtained which indicate that eq 11 may have wide validity. Systems examined include: (a) interdiffusion of two differing electrolytes, and (b) interdiffusion of differing cations in ion-exchange resin membranes, coupled with significant transient fluxes of free electrolyte. In these cases, the interpretation of α is not as straightforward as in ideal systems containing but one electrolyte; α cannot be identified with a particular diffusion coefficient. Work is continuing along this line.

Acknowledgment. I wish to express appreciation to Mrs. Viola Gibbons for technical assistance and to Mr. Don White for fabricating the diffusion cell.

Appendix

Analysis of Potentiometric Decay Curves. Since agar was used in diffusion half-cells, it was not possible to use the known diffusion coefficient of NaCl and measured length of a half-cell to calculate the correct value of $(\pi/2h)^2\alpha$ to use in eq 22. The presence of agar creates a tortuous diffusion path and makes the half-cell length appear longer than its measured length. Thus, it was necessary to find $(\pi/2h)^2\alpha$ by fitting the experimental decay curves to a hypothetical solution of eq 22.

Equation 22 was first evaluated at twenty-two different times using a hypothetical value, $(\pi/2h)^2\alpha = 0.03 \text{ min}^{-1}$. Table III is a representation of the data and calculations used; E is the cell potential calculated at different hypothetical times, t_β . Real times, t , corresponding to the hypothetically calculated E values were read from recorder traces and averaged for seven experimental runs.

Table III: Representation of Calculations and Data Used to Find $(\pi/2h)^2\alpha$

E	t_β	t	t_e	w	t_R
E_1	$t_{\beta 1}$	t_1	$t_{e 1}$	w_1	$t_{R 1}$
E_2	$t_{\beta 2}$	t_2	$t_{e 2}$	w_2	$t_{R 2}$
E_3	$t_{\beta 3}$	t_3	$t_{e 3}$	w_3	$t_{R 3}$
...
...
...

If eq 22 is correct, then it is evident that

$$0.03t_\beta = (\pi/2h)^2\alpha t \tag{1A}$$

In order to allow for the possibility that mixing takes place as the half-cells are brought together, a time increment, Δt , must be added to observed times,¹⁰ hence

$$0.03t_\beta = (\pi/2h)^2\alpha(t + \Delta t) \tag{2A}$$

(10) L. G. Longworth, *J. Am. Chem. Soc.*, **69**, 2510 (1947).

or

$$t = \frac{0.03}{(\pi/2h)^2\alpha} t_\beta - \Delta t \quad (3A)$$

Since t is a linear function of t_β , $(\pi/2h)^2\alpha$ and Δt can be evaluated from a linear regression analysis of t on t_β . Since the slope of decay curves varies greatly, the precision with which t is known also varies. Hence, it is necessary to weight t values in such a manner as to obtain a constant variance before computing a linear regression. This was done by assuming a constant variance of E values and determining the amount of uncertainty in t , t_e , corresponding to a given uncertainty in E . A weighted linear least-squares regression of t on t_β was then computed according to Steele and Torrie,¹¹ using weighting factors, $w = (1/t_e)^2$. The regression equation obtained was

$$t = 1.159t_\beta - 0.03 \quad (4A)$$

Comparing eq 4A and 3A it is seen that $(\pi/2h)^2\alpha = 0.02588 \text{ min}^{-1}$ and $\Delta t = 0.03 \text{ min}$.

Equation 4A was used to calculate the regression estimates of real time, t_R , which should be identical with t if eq 22 is correct and there were no experimental error. The times reported in Table I are the regression values. To obtain Table I E values, the recorder traces were read at each time listed and were averaged for the seven experimental runs. The deviation of each E value from the theoretical value was calculated and the average deviation for each point is listed in Table I. Based on the average deviation observed, the estimated error in the regression slope was found, using a graphical method, to be ± 0.007 . The corresponding error in $(\pi/2h)^2\alpha$ is ± 0.00016 , so that $(\pi/2h)^2\alpha = 0.02588 \pm 0.00016 \text{ min}^{-1}$.

(11) R. G. D. Steele and J. H. Torrie, "Principles and Procedures of Statistics," McGraw-Hill Book Co., Inc., New York, N. Y., 1960.

Light Scattering and Refractometry of a Monodisperse

Polymer in Binary Mixed Solvents

by K. Okita, A. Teramoto, K. Kawahara, and H. Fujita

Department of Polymer Science, Osaka University, Toyonaka, Japan (Received July 27, 1967)

Equilibrium properties of a polymer in mixed solvents are affected by the preferential adsorption of a particular solvent component on the polymer molecule. In this study, using monodisperse poly- α -methylstyrene as a polymer sample, the parameter characterizing this effect was evaluated in two mixed solvent systems, toluene-1-butanol and benzene-cyclohexane, from light-scattering and refractive index measurements. As required by the thermodynamic theory on multicomponent systems, the values obtained from these two independent measurements agreed well with one another, irrespective of the molecular weight of the polymer sample and the wavelength of light used. The tendency that the good solvent component (toluene and benzene in the present case) is preferentially adsorbed on the polymer was much stronger in the toluene-1-butanol system than in the benzene-cyclohexane one. Apparent second virial coefficients derived from the light-scattering data, using the familiar Zimm plot, were corrected for the effect of the preferential adsorption of solvent by use of the method indicated in the current theory of scattered light photometry. It was found that the corrected values stood in good agreement with the second virial coefficients derived from osmotic pressure measurements over a range of composition of the mixed solvent in which both light-scattering and osmotic pressure data were taken. Finally, for the highest molecular weight sample ($\bar{M}_w \div 1.4 \times 10^6$), the mean-square radii of gyration of the polymer molecule at various compositions of the two mixed solvent systems were calculated from data for the angular dependence of scattered light by making use of a very recent theory due to Yamakawa, and a correlation of the resulting values with the corresponding light-scattering second virial coefficients was discussed.

Introduction

Since the pioneering work of Ewart, *et al.*,¹ many authors have concerned themselves with the theoretical²⁻⁵ and experimental⁶⁻¹⁰ aspects of light-scattering behavior of polymer molecules dissolved in mixed solvents. The emphasis of these studies was generally put on the consideration of the preferential adsorption of solvent molecules on the polymer solute. However, there still remain many problems which have to be elucidated for a more complete understanding of light-scattering phenomena in multicomponent systems. For example, thermodynamic theory on such systems⁵ tells that refractometry should yield the same information for the preferential adsorption of solvent as does the light-scattering experiment, but no experimental check on this point appears to have been reported by previous authors. A rigorous thermodynamic relation exists which enables one to evaluate the correct second virial coefficient of a ternary solution from an "apparent" second virial coefficient, which would be obtained if the given light-scattering data were analyzed in terms of the method known to be valid for binary solutions.⁵ Theory also indicates

that the correct second virial coefficient so obtained should agree with the osmotic second virial coefficient derived from osmotic pressure data by the usual method, *i.e.*, the one which is almost universally employed for binary systems.⁵ None of the previous publications, however, has dealt with an experimental demonstration of this theoretical prediction. Finally, mention may be made of the fact that, very recently, an explicit expression for the angular dependence of light scattered from a ternary solution has first become available

- (1) R. H. Ewart, C. P. Roe, P. Debye, and J. R. McCartney, *J. Chem. Phys.*, **14**, 687 (1946).
- (2) W. H. Stockmayer, *ibid.*, **18**, 58 (1950).
- (3) J. G. Kirkwood and R. J. Goldberg, *ibid.*, **18**, 54 (1950).
- (4) H. Eisenberg, *ibid.*, **36**, 1837 (1962).
- (5) E. F. Casassa and H. Eisenberg, *Advan. Protein Chem.*, **19**, 287 (1964).
- (6) B. E. Read, *Trans. Faraday Soc.*, **59**, 382 (1960).
- (7) H. Lange, *Makromol. Chem.*, **63**, 209 (1963); *Kolloid-Z.*, **199**, 128 (1964); **201**, 123 (1965).
- (8) C. Strazielle and H. Benoit, *J. Chim. Phys.*, **58**, 678 (1961).
- (9) H.-G. Elias and O. Etter, *Makromol. Chem.*, **58**, 56 (1963).
- (10) J. M. G. Cowie and S. Bywater, *J. Macromol. Chem.*, **1**, 581 (1966).

through a theoretical study of Yamakawa.¹¹ The availability of this expression now enables one to determine the statistical radii of polymer molecules in mixed solvents.

The study reported in this paper was initiated in order to examine three topics suggested from the above discussion on ternary systems. They are (1) to check the thermodynamic equivalence of scattered light photometry and refractometry with reference to the preferential adsorption of solvent, (2) to evaluate the second virial coefficient of a ternary system both from scattered light photometry and osmometry, and (3) to determine the statistical radius of a polymer in mixed solvents by the use of Yamakawa's theory for the angular dependence of scattered light. To this end, we have chosen "monodisperse" poly- α -methylstyrene as a polymer solute and two pairs of good and poor solvents as mixed solvents. The use of a very narrow distribution polymer such as this is essential for the purposes of the present study, since otherwise the final conclusions to be derived will be obscured by polydispersity effects, the extent of which may not be readily estimated in many cases.

Theoretical Section

First, we shall summarize necessary thermodynamic equations for the analysis of a ternary system, confining ourselves to the case in which a monodisperse polymer (component 2) is dissolved in a mixed solvent composed of a good solvent (component 1) and a poor solvent (component 3). It is assumed that no volume change occurs on mixing of these three components. This is equivalent to treating the partial specific volume of each component to be independent of the composition of the system. The subsequent treatment mainly follows the recent formulation of Casassa and Eisenberg⁵ on the thermodynamics of multicomponent systems.

The osmotic pressure, π , which is set up between a ternary solution and its mixed solvent when they are separated by a membrane permeable only to the solvent components is expanded in power of c_2 to give

$$\pi/RTc_2 = 1/M_2 + A_2^{(C)}c_2 + \text{higher terms in } c_2 \quad (1)$$

Here R is the gas constant, T is the absolute temperature of the system, c_2 is the equilibrium concentration of polymer in grams per ml of solution, M_2 is the molecular weight of the polymer component, and $A_2^{(C)}$ is the osmotic second virial coefficient of the solution.

The molal refractive index increment of the ternary solution considered, at given temperature T and pressure P , depends on whether the addition of the polymer component 2 is carried out at a fixed chemical potential of component 3 or at a fixed composition of the same component. The two kinds of refractive index increment are related with one another by the equation

$$(\partial n/\partial m_2)_{T,P,\mu_3} = (\partial n/\partial m_2)_{T,P,m_3} + \Gamma(\partial n/\partial m_3)_{T,P,m_2} \quad (2)$$

where m_i ($i = 2, 3$) is the molality of component i , μ_i is the molar chemical potential of component i , and Γ is the molal "adsorption" parameter defined by

$$\Gamma = (\partial m_3/\partial m_2)_{T,P,\mu_3} \quad (3)$$

For experimental work with polymer solutes it is convenient to use the gram per ml concentration (*i.e.*, the c -scale concentration) instead of the molality concentration. Furthermore, our primary interest may be confined to the value of Γ at the limit of zero concentration of polymer. In terms of the c -scale concentration, eq 2 gives at infinite dilution of polymer

$$(\partial n/\partial c_2)^0_{T,P,\mu_3} = (\partial n/\partial c_2)^0_{T,P,c_3} + \Gamma_o^0 \phi_1^0 (\partial n/\partial c_3)^0_{T,P} \quad (4)$$

where Γ_o^0 is related to Γ^0 by

$$\Gamma_o^0 = (M_3/M_2)\Gamma^0 \quad (5)$$

and ϕ_1^0 is the volume fraction of component 1 in the solution at infinite dilution of polymer. The superscript 0 in these expressions indicates the value to be taken at this limiting state. The parameter Γ_o^0 may be interpreted as representing the number of grams of component 3 preferentially adsorbed on one gram of polymer component 2 at the limit of zero concentration of the latter component.

We define the excess scattering R as the reduced intensity of light scattered from a solution minus that from its solvent which is at the same temperature, pressure, and solvent composition as in the solution, and denote its value in the direction of the incident beam of light by R_0 . Then, if we apply the fluctuation theory of light scattering on multicomponent systems due mainly to Stockmayer² and Kirkwood, *et al.*,³ to the particular ternary system considered, the following equation is derived for R_0

$$\frac{K[(\partial n/\partial c_2)^0_{T,P,c_3}]^2 c_2}{R_0} = \frac{1}{M_{2,app}} + 2A_{app}^{(C,R)}c_2 + \text{higher terms in } c_2 \quad (6)$$

where K stands for $2\pi^2 n^2/N_A \lambda_0^4$, with n being the refractive index of the solution; N_A , the Avogadro number; and λ_0 the wavelength of the incident light under vacuum. The quantities $M_{2,app}$ and $A_{app}^{(C,R)}$ are the apparent molecular weight and apparent second virial coefficient, respectively, and are related to M_2 and the light-scattering second virial coefficient of the solution $A_2^{(C,R)}$ by the following equations

$$M_{2,app} = \Omega^2 M_2 \quad (7)$$

$$A_{app}^{(C,R)} = \Omega^{-2} A_2^{(C,R)} \quad (8)$$

(11) H. Yamakawa, *J. Chem. Phys.*, **46**, 973 (1967).

where

$$\Omega = 1 + \phi_1^0 \Gamma_\theta^0 \frac{(\partial n / \partial c_3)^0_{T,P}}{(\partial n / \partial c_2)^0_{T,P,c_3}} \quad (9)$$

The light-scattering second virial coefficient $A_2^{(C,R)}$ is identical with the osmotic second virial coefficient $A_2^{(C)}$ for a monodisperse polymer in a single solvent, but both are different, in the case of ternary solutions, by an additional term which is generally negligible except in the circumstances where $A_2^{(C)}$ is very close to zero. It was one of the purposes of the present study to check this theoretically predicted closeness of $A_2^{(C)}$ and $A_2^{(C,R)}$ with experiments using nearly monodisperse samples of polymer.

Equation 4 provides a basis for determining the parameter Γ_θ^0 from measurements of refractive index increments, while combination of eq 7 and 9 enables one to calculate this parameter from light-scattering measurements, provided that M_2 is known in advance. One of the motivations to the present study was to evaluate Γ_θ^0 from these two independent experiments and compare the resulting values.

Finally, we present Yamakawa's expression¹¹ for the angular dependence of the intensity of light scattered from a ternary solution of the kind considered here. Writing the excess scattering at the angle of observation θ as R_θ , it reads

$$\lim_{c_2 \rightarrow 0} (K_2 c_2 / R_\theta)^{1/2} = (1/M_{2,app})^{1/2} [1 + (8\pi^2/3\lambda_0^2) \times \langle S^2(c_3) \rangle \sin^2(\theta/2) + \text{higher terms in } (1/\lambda_0^2) \langle S^2(c_3) \rangle \sin^2(\theta/2)] \quad (10)$$

subject to the restricting condition that

$$0.8 < M_{2,app}/M_2 < 1.2 \quad (11)$$

In eq 10, $K_2 = K[(\partial n / \partial c_2)^0_{T,P,c_3}]^2$, and $\langle S^2(c_3) \rangle$ denotes the mean-square radius of gyration of a polymer molecule in a mixed solvent in which component 3 is at the c -scale concentration c_3 ; all other symbols have the same meaning as in the preceding lines. Equation 10 has the same form as the corresponding equation for a polymer in a single solvent, except for the true molecular weight of polymer being replaced here by the apparent molecular weight, $M_{2,app}$. Thus we find that the desired value of $\langle S^2(c_3) \rangle$ may be determined by treating light-scattering data in terms of the usual Zimm plot,¹² provided that the value of $M_{2,app}$, estimated from the ordinate intercept of the plot, is found to obey condition 11. The M_2 value necessary for this judgment may be determined directly from the light-scattering measurement with a suitably chosen single solvent.

Experimental Section

Polymer Sample and Solvent. Four samples of poly- α -methylstyrene prepared by the anionic polymerization technique were kindly put at our disposal

Table I: Characterization Data for Poly- α -methylstyrene Samples Used^a

Sample code	$\bar{M}_w \times 10^{-4}$ (at 436 m μ)	$\bar{M}_n \times 10^{-4}$	$[\eta]$, dl/g
I	13.9	12.8	0.497
II	19.9	19.0	0.658
III	48.6	44.4	1.175
IV	141	...	2.660

^a Determined in benzene at 25°, excepting \bar{M}_w for sample I, which was obtained in cyclohexane at 39°.

Table II: Characterization Data for Solvents Used

Solvent	Bp, °C	n_{25}^{25}	$\partial n / \partial c$, ml/g ^a
Benzene	80.1	1.5196	0.1238 \pm 0.0008
Cyclohexane	80.7	1.4262 (39°)	0.1967 \pm 0.0048 (39°)
Toluene	110.6	1.5153	0.1307 \pm 0.0007
1-Butanol	117.7	1.4069	...
Ethylene dichloride	83.4	1.4528	0.1764 \pm 0.0009

^a Specific refractive index increment for poly- α -methylstyrene at 25° and for wavelength 436 m μ .

by the courtesy of Mr. T. Fujimoto of the Department of Synthetic Chemistry, Nagoya University, who stated that they may be regarded as essentially monodisperse with respect to molecular weight.¹³ Each sample was purified by repeated precipitation, freeze-dried from a benzene solution, and further dried for 2 days in a vacuum oven at 90° immediately before use. The weight-average and number-average molecular weights of these samples, determined in appropriate single solvents, are given in Table I. Unfortunately, sample III is not homogeneous enough with respect to molecular weight. In fact, ultracentrifugal patterns of this sample in cyclohexane exhibited a small shoulder on the centripetal side of the maximum refractive index gradient. However, this sample was used without effecting further fractionation.

Cyclohexane, benzene, and toluene were refluxed over sodium metal for several hours and then fractionally distilled. 1-Butanol was distilled after refluxing over barium oxide. Relevant characterization data of these organic liquids are compiled in Table II.

The following two pairs of good and poor solvents (or nonsolvents) for poly- α -methylstyrene were chosen as the mixed solvent systems to be studied: toluene (bp 110.6°)–1-butanol (bp 117.7°) and benzene (bp 80.1°)–cyclohexane (bp 80.7°). The choice of a pair of solvents which have nearly the same boiling points is important for minimizing the variation of compo-

(12) B. H. Zimm, *J. Chem. Phys.*, **16**, 1093 (1948).

(13) T. Fujimoto, N. Ozaki, and M. Nagasawa, *J. Polymer Sci., Part A-2*, **3**, 2259 (1965).

sition due to the evaporation of solvents. Each mixture was prepared gravimetrically, and the c -scale concentration of each component was calculated using the density of the mixture. The c -scale concentration of the polymer in a mixed solvent was calculated also using the density of the solvent, not of the solution. This procedure may be justified, as far as we are concerned only with very dilute solutions of the polymer component.

Osmotic Pressure. A Mechrolab 502 high-speed membrane osmometer was used for samples in single solvents, and several glass osmometers of the Zimm-Myerson type were used for the studies with mixed solvents. Adequately conditioned gel cellophane membranes were used in either osmometer. All measurements were made at 25°. The osmotic equilibrium was generally attained after about 4 days, except in experiments with mixed solvents containing a relatively large portion of cyclohexane, where it took about 10 days for the equilibrium to be reached. When checked refractometrically, no detectable change occurred in the composition of the mixed solvent placed outside the osmometer during the entire interval of an osmotic experiment. The leakage of the polymer from the osmometer cell was not observable, either. Therefore, the polymer concentration in each solution before being subjected to the osmotic experiment was used in analyzing the data obtained.

Refractive Index and Refractive Index Increment. Refractive-index measurements were made with the aid of a Bausch and Lomb precision sugar refractometer. Refractive indices at 25° for wavelengths 436 and 546 m μ were determined over the complete range of composition of mixed solvent. The values for each component solvent are given in Table II.

A differential refractometer was constructed, for the purpose of the present study, following the design which had been reported by Schulz, *et al.*¹⁴ The modification from the original design was that the sector angle of the solution compartment in the cell was changed from 60 to 30° and that the lens immediately before the photomultiplier was omitted. The necessary volume of liquid for each measurement was about 2 ml either for solution or solvent. The advantage over the differential refractometer of the Debye type¹⁵ and that of the Brice type¹⁶ is in that the cell portion can be thermostated easily and an exact reproducible positioning of the cell is readily achieved without sacrifice of the sensitivity. The apparatus was calibrated with aqueous solutions of sucrose (at 546 m μ)¹⁷ and of potassium chloride (at 436 and 546 m μ).¹⁸ The calibration constants so determined for light of wavelength 546 m μ agreed with one another to within $\pm 0.3\%$.

The necessary data for the calculation of Γ_θ^0 in terms of eq 4 are the values of $(\partial n/\partial c_3)_{T,P}^0$, $(\partial n/\partial c_2)_{T,P,c_3}^0$, and $(\partial n/\partial c_2)_{T,P,\mu_3}^0$. The first derivative may be deter-

mined by measuring, at given temperature and pressure, the refractive index increment between two mixed solvents having slightly different compositions. For the second derivative, one must prepare a polymer solution in which component 3 has the same c -scale concentration as in the given mixed solvent. In practice, this cannot be done exactly. Hence, in this work, we used polymer solutions in which component 3 had the same molality as in the given mixed solvents. The error introduced by this substitution into the measurement of the second derivative becomes smaller as the polymer concentration is lowered. The conditions required for the determination of the third derivative are even more difficult to obtain experimentally. Therefore, we were content with adopting the following approximation. Namely, we dialyzed a given solution against its mixed solvent using the cell of an osmometer, transferred the equilibrated solution into the cell of the differential refractometer together with the dialyzate, and then measured the refractive index increment of one over the other at given temperature and pressure. It can be shown that the derivative so determined differs from that to be obtained at fixed T , P , and μ_3 by a factor which may be safely ignored if the molecular weight of the dissolved polymer is sufficiently high.

These measurements were all performed at 25° and under atmosphere pressure, using light of wavelengths 436 and 546 m μ .

Density. Densities of solvent mixtures, needed for the calculation of the c -scale concentrations of solvent and polymer components, were measured at 25° and at a number of compositions covering the necessary range by making use of a bicapillary pycnometer which had a capacity of about 24 ml.

Light Scattering. A Shimadzu light-scattering photometer equipped with a temperature-regulating water jacket was used. Measurements were made at 25° for samples II, III, and IV, using unpolarized light of wavelengths 436 and 546 m μ . Data were taken at angles of observation θ ranging from 35 to 135°, and treated in terms of the Zimm plot.¹² For sample IV, the measurements were made only at 436 m μ and the analysis of data was made by plotting values for $(K_2c_2/R_\theta)^{1/2}$ against either c_2 at fixed θ or $\sin^2(\theta/2)$ at fixed c_2 .

Results and Discussion

A. Adsorption Parameter. As explained in the Theoretical section, the parameter Γ_θ^0 characterizing the preferential adsorption of a particular solvent on the polymer molecule at infinite dilution may be evaluated

(14) G. V. Schulz, O. Bodmann, and H.-J. Cantow, *J. Polymer Sci.*, **10**, 73 (1953).

(15) P. P. Debye, *J. Appl. Phys.*, **17**, 392 (1946).

(16) B. A. Brice and M. Halwer, *J. Opt. Soc. Am.*, **41**, 1033 (1951).

(17) L. J. Gosting and M. Morris, *J. Am. Chem. Soc.*, **71**, 1988 (1949).

(18) A. Kruis, *Z. Physik. Chem.*, **34B**, 13 (1936).

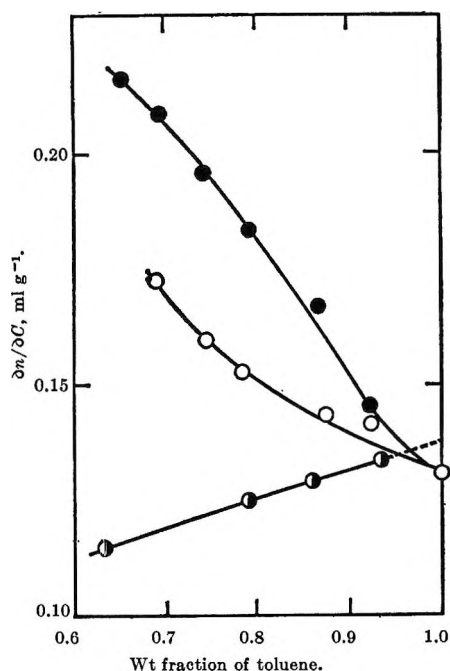


Figure 1. Specific refractive index increments for sample I in the mixture of toluene and 1-butanol at 25° as a function of the weight fraction of toluene: ●, $(\partial n/\partial c_2)^0_{T,P,\mu_4}$; ○, $(\partial n/\partial c_2)^0_{T,P,\lambda}$; ●, $-(\partial n/\partial c_3)^0_{T,P}$.

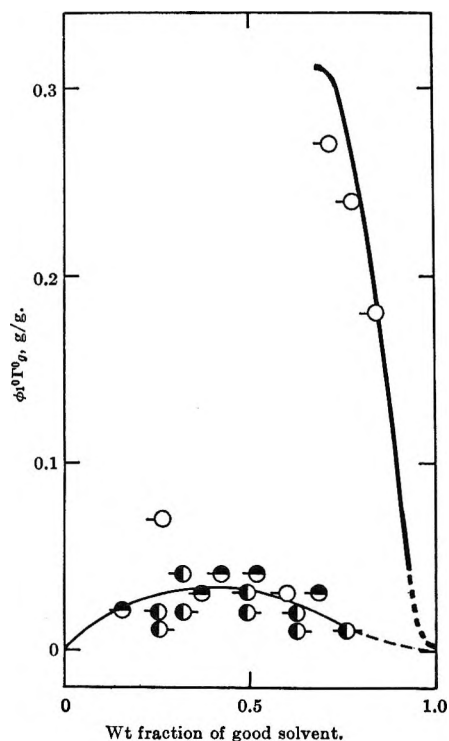


Figure 2. Composition dependence of $\Gamma_e^0\phi_1^0$. The solid lines show the results from the measurements of refractive index increments: thick line, toluene-1-butanol system; thin line, benzene-cyclohexane system. The points indicate values derived from light-scattering measurements: ●, with sample II; ●, with sample III; ○, with sample IV. Left pips indicate the values at wavelength 436 mμ and right pips the ones at wavelength 546 mμ.

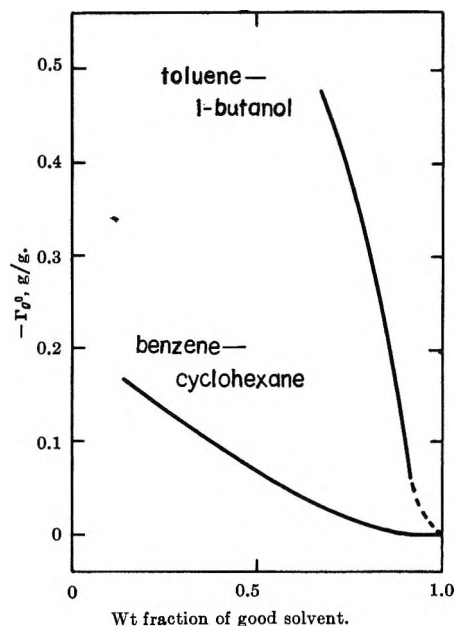


Figure 3. Composition dependence of the preferential absorption coefficient Γ_e^0 , calculated from the solid lines in Figure 2.

either from data for refractive index increments (eq 4) or from light-scattering data (eq 7 and 9).

The measurements of the refractive index increment with the toluene-1-butanol mixture were made only for one polymer sample (I) at weight fractions of 1-butanol less than about 0.3; the addition of the nonsolvent component beyond this limit caused phase separation of the solution and thus did not permit us to perform the measurement. By way of example, the data obtained for wavelength 436 mμ are plotted as a function of the weight fraction of the good solvent component (toluene) in Figure 1. Similar data were obtained from the measurements on the same system with light of wavelength 546 mμ. The calculation of $\phi_1^0\Gamma_e^0$ from these data with eq 4 was made after they had been smoothed as shown by the solid curves in Figure 1, and it was found that the calculated values for wavelengths 436 and 546 mμ gave virtually coincident curves when plotted against the weight fraction of toluene. The average of them is depicted as a thick line in Figure 2. For the benzene-cyclohexane system, the measurements were made with this and other samples, and the calculation of $\phi_1^0\Gamma_e^0$ was also effected after the experimental data had been smoothed suitably. The results as a function of the weight fraction of benzene were nearly independent not only of the wavelength of light, but also of the molecular weight of the polymer sample. The thin solid curve in Figure 2 shows their average. Figure 3 indicates Γ_e^0 as a function of the weight fraction of either toluene or benzene derived from the solid curves depicted in Figure 2. The values of ϕ_1^0 needed in this calculation were computed assuming that no volume change occurs on mixing of the component liquids in either of the two systems studied.

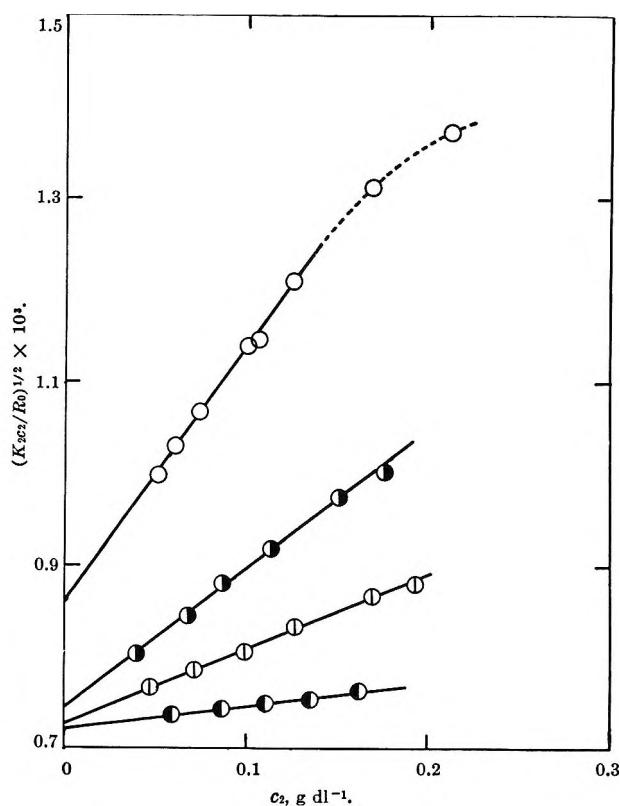


Figure 4. Concentration dependence of the excess scattering at zero angle of observation for sample IV in the mixture of toluene and 1-butanol at 25°: O, 1.0; O, 0.838; ◐, 0.777; ●, 0.718. These figures denote the weight fractions of toluene in the mixture.

Values of $(K_2c_2/R_0)^{1/2}$ for sample IV in the toluene-1-butanol mixture at 25° are plotted against the polymer concentration c_2 in Figure 4, wherein each line corresponds to different solvent composition. It is seen that the ordinate intercept of the indicated line, which equals the reciprocal square root of the apparent molecular weight, $M_{2,app}$, lowers as the amount of the poor solvent component in the mixed solvent increases. Taking the apparent molecular weight for the system containing toluene only as the true molecular weight, M_2 , of the dissolved polymer and using the smoothed refractometric data shown in Figure 1, one can calculate $\phi_1^0\Gamma_\phi^0$ from these light-scattering data by means of eq 7 and 9. The resulting values are plotted in Figure 2 for comparison with the refractometric measurements. This figure also indicates the values for $\phi_1^0\Gamma_\phi^0$ derived from light-scattering data on the same, as well as lower, molecular-weight samples in the benzene-cyclohexane system at 25°. It is seen that for a given mixed solvent both refractometry and scattered-light photometry yield essentially identical values for the adsorption parameter, irrespective of the molecular weight of polymer and the wavelength of light used for the experiments. Although the definitive conclusion must be reserved in view of the considerable scatter of the data points from light-scattering measurements, this result may be taken as a substantial support to the

theoretically predicted equivalence of refractometry and scattered light photometry with respect to the absorption coefficient.

In either mixed solvent studied here, the parameter Γ_ϕ^0 is negative, and its absolute magnitude for the

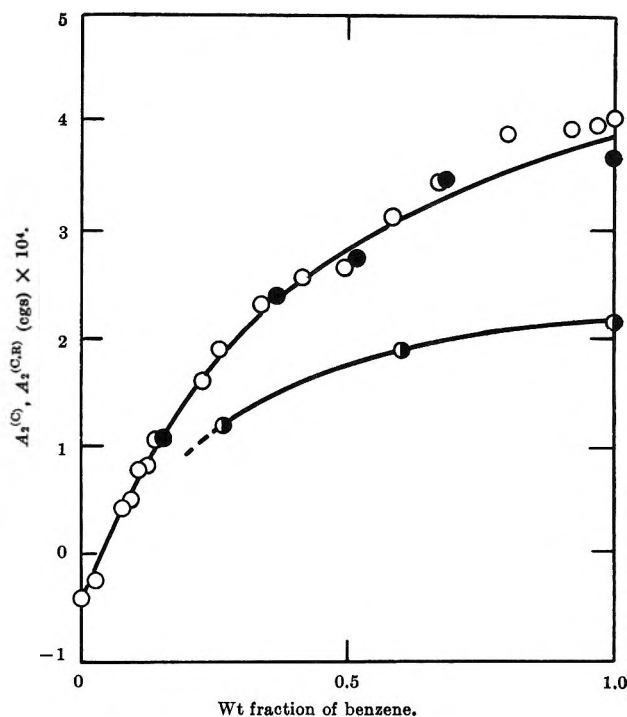


Figure 5. Osmotic second virial coefficient (O) and light-scattering second virial coefficient (●) for sample II in the mixture of benzene and cyclohexane at 25°. The half-filled points show the light-scattering second virial coefficients for sample IV in the same mixed solvent.

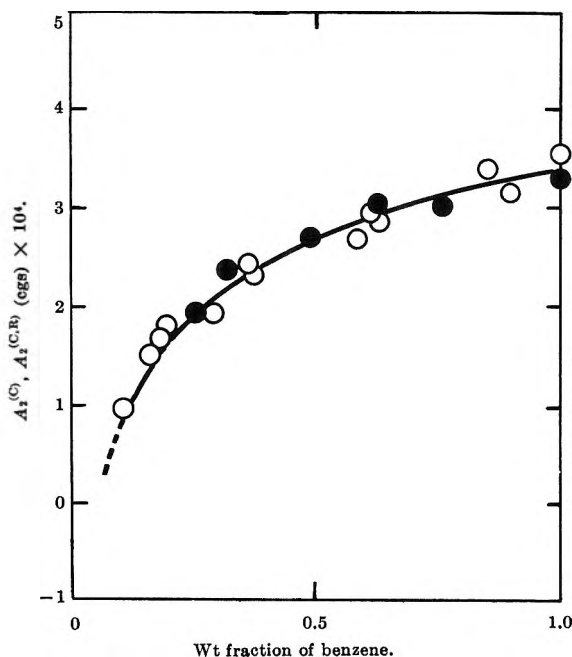


Figure 6. Comparison of the osmotic and light-scattering second virial coefficients for sample III in the mixture of benzene and cyclohexane at 25°.

benzene-cyclohexane system is much smaller than that for the toluene-1-butanol system, when compared at the same weight fraction of the good solvent component: benzene in the former system and toluene in the latter one. A negative Γ_p^0 implies, in the present case, that the molecules of component 3, *i.e.*, the poor-solvent component, are expelled from the domain surrounding the polymer molecule, or, conversely, the good-solvent component is preferentially adsorbed on the polymer component. A marked difference in the absolute value of Γ_p^0 between the two mixed solvent systems may be accounted for by the fact that 1-butanol is a nonsolvent and cyclohexane is simply a poor solvent for poly- α -methylstyrene, while both toluene and benzene may have similar solvent powers for this polymer species.

B. Second Virial Coefficient. Figures 5 and 6 show comparisons of $A_2^{(C)}$ and $A_2^{(C,R)}$ for samples II and III in the mixture of benzene and cyclohexane at 25°. Here $A_2^{(C)}$ is the osmotic second virial coefficient defined in eq 2, and $A_2^{(C,R)}$ is the light-scattering second virial coefficient obtained by correcting the experimentally determined $A_{app}^{(C,R)}$ for the effect of preferential adsorption. The agreement indicated in these graphs may be taken to substantiate the theoretical prediction that the correction of $A_{app}^{(C,R)}$ for the preferential adsorption by eq 8 should yield a second virial coefficient which agrees with the osmotic second virial coefficient, provided the polymer is "monodisperse." However, we wish to reserve the definite argument, because, as demonstrated above, the values of Γ_p^0 for the benzene-cyclohexane system are not large enough for a critical test of this theoretical prediction to be made and, moreover, sample III is not homogeneous enough with respect to molecular weight. Figure 5 includes $A_2^{(C,R)}$ values for sample IV in this mixed solvent. The corresponding $A_2^{(C)}$ could not be determined with precision, since the molecular weight of the sample was too high to make an accurate osmotic pressure measurement

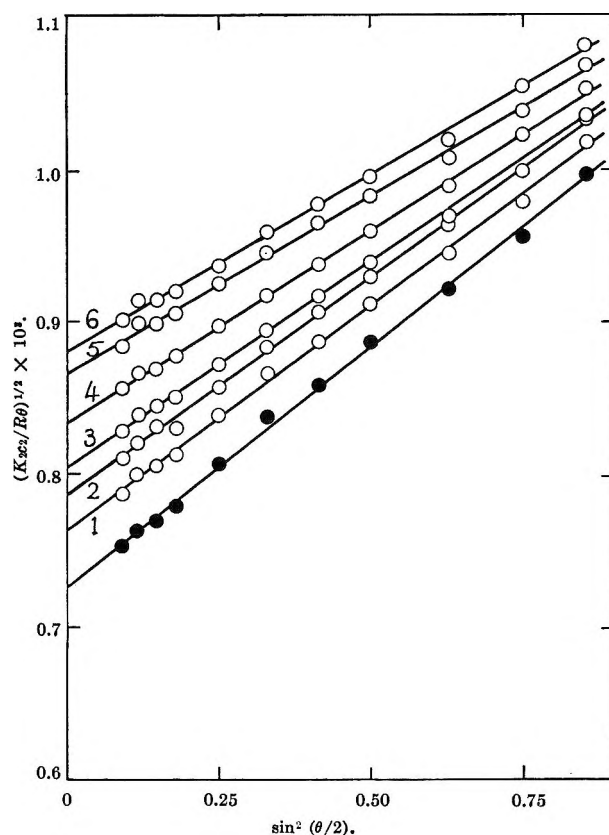


Figure 7. Angular dependence of the excess scattering for sample IV in the mixture of toluene and 1-butanol at 25° and for light of wavelength 436 mμ; weight fraction of toluene is 0.777: O, at nonzero concentrations of polymer (g dl⁻¹); (1) $c_2 = 0.04637$; (2) $c_2 = 0.07109$; (3) $c_2 = 0.09864$; (4) $c_2 = 0.1263$; (5) $c_2 = 0.1695$; (6) $c_2 = 0.1932$; ●, at zero concentration of polymer (extrapolated).

possible. Table III summarizes results from light-scattering measurements on sample IV in the two mixed solvents studied and in one pure solvent, ethylene dichloride. The values for $M_{2,app}$, given in the second column, are ones which have been used to calculate Γ_p^0 by means of eq 7.

C. Mean-Square Radius of Gyration. The presentation of data for the angular dependence of scattered light is confined here to sample IV, because the other samples were too low in molecular weight for their mean-square radii of gyration to be determined with confidence from the experimental results obtained. Figure 7 shows some of the angular dependence data for sample IV in the form of $(Kc_2/R\theta)^{1/2}_{c_2=0}$ plotted against $\sin^2(\theta/2)$. The values for the mean-square radius of gyration $\langle S^2 \rangle$ calculated from the slopes of the indicated lines using eq 10 are listed on the last column of Table III. The data in the other solvent systems were treated in the same way, and the results are also listed in Table III.

It is to be noted in this table that the restricting condition 11 is satisfied with the data obtained in the benzene-cyclohexane system, whereas it is not so even in the relatively narrow range of composition of the

Table III: Light Scattering Data for Sample IV

w_1^a	$M_{2,app} \times 10^{-6}$	$A_2^{(C,R)} \times 10^4$ cgs	$\langle S^2 \rangle^{1/2}$, Å
Toluene-1-Butanol			
1.00	1.33	2.33	470
0.8380	1.80	1.49	419
0.7773	1.90	0.817	375
0.7188	1.92	0.25	319
Benzene-Cyclohexane			
1.00	1.41	2.15	477
0.6011	1.50	1.87	455
0.2662	1.52	1.19	410
0	1.36 ^b	0.0 ^b	313 ^b
Ethylene Dichloride			
	1.34	1.53	450

^a Weight fraction of good solvent. ^b Measured at 39°.

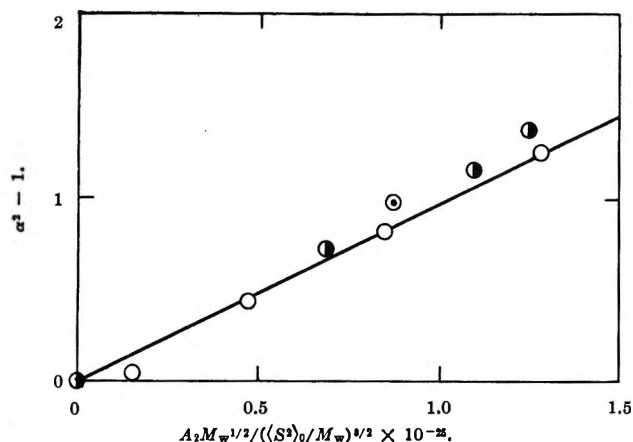


Figure 8. Application of Berry's plot to the present data taken with sample IV in two mixed solvents and in one pure solvent: ●, in benzene-cyclohexane; O, in toluene-1-butanol; ○, in ethylene dichloride. See the text for the notations on the ordinate and abscissa axes. The solid line drawn has a slope of 0.95.

toluene-1-butanol system, where $M_{2,app}$ exceeded $1.2 M_2$ even at the lowest of the poor solvent contents treated. At present, in these circumstances, we cannot argue anything about the correctness of $\langle S^2 \rangle$ deduced by the use of Yamakawa's theory. In fact, we have no positive reason to discard the data obtained, since condition 14, imposed by Yamakawa, is not necessarily founded on the decidedly acceptable ground.

Berry¹⁹ has demonstrated for monodisperse polysty-

rene in single pure solvents that the second virial coefficient, A_2 , and the mean-square radius of gyration, $\langle S^2 \rangle$, were empirically correlated by the relation

$$A_2 M^{1/2} = \frac{4N_A \pi^{1/2} (\langle S^2 \rangle_0 / M)^{1/2}}{(134/105)} (\alpha^2 - 1) \quad (12)$$

where M is the molecular weight of the solute polymer, and the expansion factor α is defined by $\alpha^2 = \langle S^2 \rangle / \langle S^2 \rangle_0$, with $\langle S^2 \rangle_0$ being the value of $\langle S^2 \rangle$ under θ conditions.

We were interested in whether the present data for $\langle S^2 \rangle$ and A_2 summarized in Table III follow this empirical relation. To examine this problem, we calculate the necessary values of α with a value of $9.8 \times 10^{-12} \text{ cm}^2$ being taken as $\langle S^2 \rangle_0$ for sample IV. This value of $\langle S^2 \rangle_0$ is the average of measurements in cyclohexane at 39° , which is equal or quite close to the reported θ temperatures for poly- α -methylstyrene in this solvent.²⁰ The results of calculation are plotted in Figure 8, and it can be seen that our data on ternary solutions also follow a linear relation as predicted by eq 12. In fact, the straight line in the figure represents eq 12 and has a slope of 0.951; the empirical value obtained for this slope by Berry¹⁹ was 0.97. At present, we are not yet in a position to be able to discuss the significance of this agreement.

(19) G. C. Berry, *J. Chem. Phys.*, **44**, 4550 (1967).

(20) J. M. G. Cowie, S. Bywater, and D. J. Worsfold, *Polymer* (London), **8**, 105 (1967).

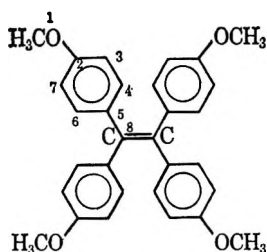
Electron Spin Resonance Spectrum of Tetrakis(*p*-methoxyphenyl)ethylene Cation Radical

by Jorge A. Valenzuela and Allen J. Bard¹

Department of Chemistry, The University of Texas, Austin, Texas 78712 (Received August 2, 1967)

The electron spin resonance (esr) spectrum of the tetrakis(*p*-methoxyphenyl)ethylene (TAE) cation radical, prepared by treatment with methanesulfonic acid with methylene chloride as a solvent, is given. The experimental coupling constants were found to be in good agreement with those calculated using molecular orbital theory, assuming non-planarity of the molecule, with the methoxyphenyl groups rotated out of the plane of the ethylenic bond by about 32°. A semiempirical approach proposed by Adrian to calculate the theoretical twist angle yielded a value of 34°.

Several years ago, Buck, *et al.*,² observed that tetrakis(*p*-methoxyphenyl)ethylene (tetra-*p*-anisylethylene or TAE) reacted with bromine to form a blue solution which exhibited an undescribed esr signal. At the



same time, Buckles and Womer³ studied, spectrophotometrically, the interaction of bromine with TAE in ethylene chloride, and the blue solution obtained was attributed to the formation of donor-acceptor complexes, where TAE was the electron donor. Later, Buckles, *et al.*,⁴ described in detail the interaction of TAE with several electron acceptors, observing the characteristic blue solution. Buck, *et al.*,⁵ in a study of the system Lewis acid (aluminum chloride)-nitro compound (nitromethane) as a strong electron acceptor, reported that the reaction of TAE with this system produced a divalent positive ion yielding an identical ultraviolet absorption spectrum to that of the perchlorate salt in nitromethane.

The rather easy formation of this diamagnetic dipositive ion with a number of oxidants leads to difficulty in preparing the cation radical of TAE in the absence of appreciable amounts of either parent or dication. The result is that most esr spectra arising from the oxidation of TAE are characterized by a broad unresolved singlet, probably arising from rapid electron exchange between the radical and dipositive cation. Similar effects have been noted in esr studies of hydrocarbon cation radicals.⁶

This study was undertaken to investigate what conditions would lead to a well-resolved spectrum of TAE radical cation, and as a part of a study of the effects of configuration on esr spectra.⁷ No previous interpretation of the esr spectrum of TAE cation radical has been reported.⁸

Results and Discussion

Preparation of TAE Cation Radical. A systematic investigation of a number of reported techniques for oxidation of aromatic hydrocarbons was undertaken in an attempt to find conditions for optimum resolution in the esr spectrum of TAE. When the antimony pentachloride in methylene chloride solution oxidation method⁹ was employed, only a single broad line with no trace of resolved hyperfine structure was observed. Oxidation with concentrated sulfuric acid⁹ produced a spectrum with a small amount of resolution, but it was still not sufficient for a satisfactory analysis. Malachuk, Marcoux, and Adams¹⁰ recently demonstrated

(1) To whom all correspondence and requests for reprints should be directed.

(2) H. M. Buck, J. H. Lupinski, and L. I. Oosterhoff, *Mol. Phys.*, **1**, 196 (1958).

(3) R. E. Buckles and W. D. Womer, *J. Am. Chem. Soc.*, **80**, 5055 (1958).

(4) R. E. Buckles, R. E. Erickson, J. D. Snyder, and W. B. Person, *J. Am. Chem. Soc.*, **82**, 2444 (1960).

(5) H. M. Buck, W. Bloemhoff, and L. J. Oosterhoff, *Tetrahedron Letters*, **9**, 5 (1960).

(6) I. C. Lewis and L. S. Singer, *J. Chem. Phys.*, **43**, 2712 (1965).

(7) (a) L. O. Wheeler, K. S. V. Santhanam, and A. J. Bard, *J. Phys. Chem.*, **70**, 404 (1966); (b) *ibid.*, **71**, 2223 (1967).

(8) Professor Robert E. Buckles, University of Iowa, Iowa City, Iowa, reported in a private communication, 1966, the observation of a 59-line spectrum during the oxidation of TAE.

(9) (a) S. I. Weissman, E. De Boer, and J. J. Conradi, *J. Chem. Phys.*, **26**, 963 (1957); (b) G. J. Hoijtink and W. P. Weijland, *Rec. Trav. Chim.*, **76**, 836 (1957).

(10) P. A. Malachuk, L. S. Marcoux, and R. N. Adams, *J. Phys. Chem.*, **70**, 2064 (1966).

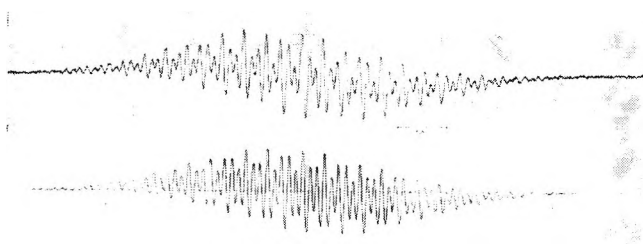


Figure 1. (a) Top: esr spectrum of TAE cation radical produced by methanesulfonic acid oxidation in methylene chloride. The sweeping field is increasing from the left to the right. (b) Bottom: calculated spectrum using constants given in the last row of Table I with a line width of 0.084 gauss.

that 1 *M* methanesulfonic acid in nitrobenzene solution was a useful solvent for oxidations of aromatic hydrocarbons. The use of methanesulfonic acid as an oxidant employing methylene chloride as a solvent, because of higher solubility of TAE in it, produced a well-resolved spectrum of approximately 67 lines (Figure 1). Electrochemical oxidation of 10^{-4} *M* solutions of TAE in vacuum-degassed methylene chloride–0.2 *M* tetra-*n*-butylammonium perchlorate solutions at a platinum electrode showed esr spectra with some hyperfine structure, which were the same as poorly resolved spectra obtained from the methanesulfonic acid oxidation.

Assignment of Spectrum. The following assignment of coupling constants (in gauss) has been made: $a_{\text{H}}(1) = 0.43 \pm 0.02$ (12 hydrogens), $a_{\text{H}}(3,7) = 0.28 \pm 0.02$ (8 hydrogens), and $a_{\text{H}}(4,6) = 1.16 \pm 0.02$ (8 hydrogens).¹¹ All anisyl groups are assumed equivalent in the molecule. A computer-simulated spectrum using these coupling constants and assuming a line width of 84 mgauss and 100% Lorentzian line shape is also shown in Figure 1.

Molecular Orbital Calculations. In order to correlate the experimental splitting assignments with a theoretical molecular model, calculations of π -e spin density were performed using simple Hückel LCAO–MO^{12,13} and McLachlan MO–SCF¹⁴ procedures. The McLachlan method is an approximate self-consistent configuration-interaction modification of the Hückel LCAO–MO method.

Two problems arise in carrying out these calculations. The first involves assignment of the coulomb integral (α_0) and the resonance integral (β_{CO}) associated with the oxygen atoms. The second involves accounting for the steric interactions between the *o*-hydrogens on the anisyl groups, which force the molecule out of a planar configuration.

Coulomb and Resonance Integrals. The values of α_0 and β_{CO} are generally given by equations of the following type¹³

$$\alpha_{\text{CO}} = \alpha_{\text{C}} + \delta_{\text{O}}\beta_{\text{CC}}$$

$$\beta_{\text{CO}} = \gamma_{\text{CO}}\beta_{\text{CC}}$$

where α_{C} and β_{CC} are the coulomb and resonance integrals, respectively, for benzene, and δ_{O} and γ_{CO} are the coulomb and resonance integral parameters (sometimes denoted h_{O} and k_{CO}).¹³ We have employed the values $\delta_{\text{O}} = 2.0$ and $\gamma_{\text{CO}} = 0.8$, suggested by Streitwieser¹³ and used by Zweig, Hodgson, and Jura,¹⁵ in correlating esr and polarographic data of methoxybenzenes. Pullman¹⁶ has suggested similar parameters ($\delta_{\text{O}} = 2.0$, $\gamma_{\text{CO}} = 0.9$). Walter¹⁷ has recently proposed quite different values of these parameters, based on optimization of parameters for fitting esr coupling constants in 1-picryl-2,2-bis(*p*-methoxyphenyl)hydrazyl and related compounds. Because of the number of adjustable parameters which had to be employed in this optimization, we feel Walter's values are less applicable to the present work.

The oxygen also modifies the coulomb integral on carbon 2 (α_2) by an inductive or direct effect, which is sometimes taken into account by equations such as

$$\alpha_2 = \alpha_{\text{C}} + \delta_{\text{C}}'\beta_{\text{CC}}$$

with $\delta_{\text{C}}' = \delta\delta_{\text{O}}$, where δ , the auxiliary inductive parameter, is given values in the order of 0.1. In this study, δ_{C}' was taken as zero. The $-\text{OCH}_3$ group is regarded as $-\ddot{\text{O}}$, contributing two electrons to the π system.¹⁸

The resonance integral parameter for the ethylenic double bond, $\gamma_{\text{C}=\text{C}}$, was assigned a value of 1.1. This parameter was calculated from the relation between the bond order and the bond length of a bond by the equation

$$r_{ij} = a - bp_{ij}$$

where r_{ij} is the bond length between atom *i* and *j*, p_{ij} is the corresponding bond order, and *a* and *b* are adjustable parameters.¹⁹ The parameters suggested by Coulson and Golembiewski,²⁰ $a = 1.517$ and $b = 0.180$, were employed. From the bond length, we estimated $\gamma_{\text{C}=\text{C}}$ using the relation of Mulliken.^{13,21} We repeated this procedure until a self-consistent bond

(11) The assignment of this spectrum is not unique, and other combinations of proton coupling constants for 8,8,12 or even 4,4,6 could probably fit the spectrum as well. The proposed assignment is mainly based on molecular-orbital calculations.

(12) E. Hückel, *Z. Physik*, **70**, 204 (1931).

(13) A. Streitwieser, Jr., "Molecular Orbital Theory for Organic Chemists," John Wiley and Sons, Inc., New York, N. Y., 1961.

(14) A. D. McLachlan, *Mol. Phys.*, **3**, 233 (1960).

(15) A. Zweig, W. G. Hodgson, and W. H. Jura, *J. Am. Chem. Soc.*, **86**, 4124 (1964).

(16) B. Pullman and A. Pullman, "Quantum Biochemistry," Interscience Publishers Inc., New York, N. Y., 1963.

(17) R. I. Walter, *J. Am. Chem. Soc.*, **88**, 1930 (1966).

(18) G. W. Wheland, *ibid.*, **64**, 900 (1942).

(19) L. Salem, "The Molecular Orbital Theory of Conjugated Systems," W. A. Benjamin, Inc., New York, N. Y., 1966, pp 137, 138.

(20) C. A. Coulson and A. Golembiewski, *Proc. Phys. Soc.*, **78**, 131 (1961).

(21) R. S. Mulliken, *J. Chim. Phys.*, **46**, 375 (1949); R. S. Mulliken, C. A. Rieke, D. Orloff, and H. Orloff, *J. Chem. Phys.*, **17**, 1248 (1949); R. S. Mulliken, *J. Phys. Chem.*, **56**, 295 (1952).

length was obtained, and found a bond order of 0.8519 and a bond length of 1.364 Å. We should point out that the choice of relation between the resonance integral and the bond length does not significantly affect the results, and the differences in the value of $\gamma_{C=C}$ obtained with different procedures are below the limits of accuracy of our calculations. These calculations were done assuming planar configuration. The small changes in the C=C bond length when the molecule is considered nonplanar are too small to affect the value of the resonance integral significantly.

Steric Effects. Steric strain caused by repulsion of the orthohydrogens (*i.e.*, 4,6), especially between the anisyl groups located on the different ethylene carbons, can be alleviated by stretching or bending of the anisylethylene carbon (C₅-C₈) bonds, by rotation about the C₅-C₈ bonds, and by rotation about the ethylenic bond. The calculation performed here assumes all of the steric strain is relieved by rotation about the C₅-C₈ bonds. A similar assumption has been used in calculations involving phenyl-substituted anthracenes⁷ and is somewhat justified by the calculations of Favini and Simonetta.²² Even admitting only rotation about the C₅-C₈ bonds, the strain can be eased by a small rotation of all of the anisyl groups out of the plane of the ethylene bond or by a larger displacement of the two *trans*-related anisyl groups leaving the two remaining *trans*-anisyl groups in the plane of the ethylene bond. Jones²³ favored the second possibility in a study which compared the ultraviolet absorption spectrum of tetraphenylethylene with that of *trans*-stilbene. However, in a more detailed analysis of the spectra by the molecular orbital method, Suzuki²⁴ found that the configuration in which all groups are rotated out the plane of the ethylenic bond was a more reasonable one. Favini and Simonetta²² employed a similar model with good success. Therefore, a model in which all anisyl groups are equivalent was adopted here. The resonance integral for the C₅-C₈ bond (β_θ) was evaluated from the equation $\beta_\theta = \beta_{\theta=0} \cos \theta$,^{7,25,26} where $\beta_{\theta=0}$ is the value of the resonance integral in the planar configuration at the same internuclear distance. The bond order and bond length for the C₅-C₈ bond was calculated in the same manner as that of the C=C bond. From these values, 0.2775 and 1.464 Å, a value of $\beta_{\theta=0} = 0.9 \beta_{CC}$ was obtained. The McLachlan¹⁴ calculations were carried out following the Hückel MO calculations, employing a λ value of 1.10.

Results. Values of the spin densities (ρ) were calculated for various θ values; typical results based on a Hückel MO calculations are shown in Figure 2. The calculated ρ values were compared with those derived from the experimental coupling constants (a_H) using: McConnell's relation,²⁷ $a_H = Q\rho$, with $Q = 35.7$, calculated by Lewis and Singer⁶ using a least-squares fitting procedure for about 12 cation radicals; Colpa-Bolton's relation,^{28,29} $a_H = -(Q\rho \pm K\rho^2)$, where $Q =$

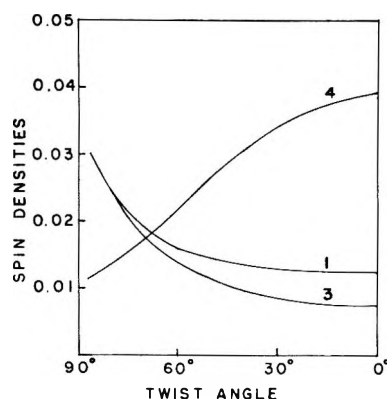


Figure 2. Plot of the Hückel spin densities as a function of the twist angle (θ) for TAE. The numbers correspond to the positions of atoms in the TAE molecule.

Table I

	Position		
	1	3	4
Hückel spin density ^a	0.0128	0.0085	0.0337
McLachlan spin density ^b	0.0088	-0.0075	0.0416
a_H , gauss ^c	0.46	0.30	1.20
a_H , gauss ^d	0.31	0.27	1.49
a_H , gauss ^e	0.35	0.23	0.92
a_H , gauss ^f	0.24	0.20	1.14
a_H , gauss ^g	0.58	0.29	1.16
Experimental a_H , gauss	0.43 ± 0.02^h	0.28 ± 0.02^h	1.16 ± 0.02

^a Calculated using $\theta = 32^\circ$. ^b Calculated using $\theta = 32^\circ$ and $\lambda = 1.1$. ^c Calculated using the McConnell equation, where $Q = 35.7$, and Hückel spin densities. ^d Calculated using the McConnell equation, where $Q = 35.7$, and McLachlan spin densities. ^e Calculated using the Colpa-Bolton equation, where $Q = 27$ and $K = 12$, and Hückel spin densities. ^f Calculated using the Colpa-Bolton equation, where $Q = 27$ and $K = 12$, and McLachlan spin densities. ^g Calculated using the Giacometti, *et al.*, equation, where $Q_1 = 31.5$ and $Q_2 = 7$, and Hückel spin densities. ^h Assigned to this position on the basis of analogy with Hückel molecular-orbital theory.

27 and $K = 12$; and Giacometti, Nordio, and Pavan's relation,³⁰ $a_H = Q_1\rho \pm Q_2 \left| \sum_j c_i c_j \right|$, where $Q_1 = 31.5$ and $Q_2 = 7$.

The calculated values are shown in Table I. It was

- (22) G. Favini and M. Simonetta, *Theoret. Chim. Acta*, **1**, 294 (1963).
- (23) R. N. Jones, *J. Am. Chem. Soc.*, **65**, 1818 (1943).
- (24) H. Suzuki, *Bull. Chem. Soc. Japan*, **33**, 389 (1960).
- (25) H. Preuss, *Z. Naturforsch.*, **12a**, 603 (1957).
- (26) M. J. S. Dewar, *J. Am. Chem. Soc.*, **74**, 3345 (1952).
- (27) H. M. McConnell, *J. Chem. Phys.*, **24**, 632, 764 (1956); H. M. McConnell and H. H. Dearman, *ibid.*, **28**, 51 (1958); H. M. McConnell and D. B. Chesnut, *ibid.*, **28**, 107 (1958).
- (28) J. P. Colpa and J. R. Bolton, *Mol. Phys.*, **6**, 273 (1963).
- (29) J. R. Bolton, *J. Chem. Phys.*, **43**, 309 (1965).
- (30) G. Giacometti, P. L. Nordio, and M. V. Pavan, *Theoret. Chim. Acta*, **1**, 404 (1963).

found that the best fit between experimental and theoretical coupling constants is obtained when the methoxyphenyl groups are rotated out of the plane of the ethylenic bond by about 32° . The technique of comparing the ratio of the experimental coupling constants with the ratio of the corresponding spin densities at different values of the angle θ' also yields an angle of about 32° .

Molecular Geometry of TAE

We have already pointed out that TAE cannot have a planar structure because of steric hindrance. This steric effect in overcrowded molecules has been studied extensively^{22,31-35} and many theoretical procedures have been proposed to calculate their structures. Most of these procedures consider that this steric strain can be released by a twisting around a C-C bond. We have similarly assumed, in the case of TAE, that this steric strain can be released by rotation of the anisyl groups out of the plane of the ethylenic bond.

To calculate the steric interaction energy in TAE, we have used a method proposed by Eyring^{36,37} based on the valence bond approximation of perfect pairing. According to this procedure, the steric interaction for two hydrogen atoms is given by the equation

$$E_s = {}^1/4 {}^1\Sigma + {}^3/4 {}^3\Sigma$$

where E_s is the steric interaction energy, and ${}^1\Sigma$ and ${}^3\Sigma$ are the energies of the lowest single and triplet states of the hydrogen molecule.³³ These energies are known as a function of the internuclear separation.³⁸

Adrian³¹ calculated the geometrical configuration of triphenylmethyl, biphenyl, stilbene, and azobenzene using the Eyring method to get the steric interaction energy and the valence bond method to obtain the resonance energy. He plotted the steric and resonance energies as functions of the twist angle and added them together; the minimum of this resulting energy yielded the effective resonance energy at the equilibrium angle. In general, we followed the same procedure here, but calculating the resonance energies using the Hückel molecular orbital method. To calculate the resonance energies we use the equation

$$E_r'(\text{twist angle}) = E_r(\text{twist angle}) - E_r(90^\circ)$$

where we actually obtain the difference in resonance energy between a partially and completely twisted molecule.³¹ The effective resonance energy E_t will be the addition of E_s and E_r' at the different θ . These energies are given in Figure 3. This treatment, therefore, predicts the anisyl groups in TAE are rotated out of the plane by an angle of about 34° , and the effective resonance energy is about -7 kcal/mole.³⁹ A similar treatment has been used for phenyl-substituted anthracenes, with a discussion of the limitation of the approach.⁴⁰

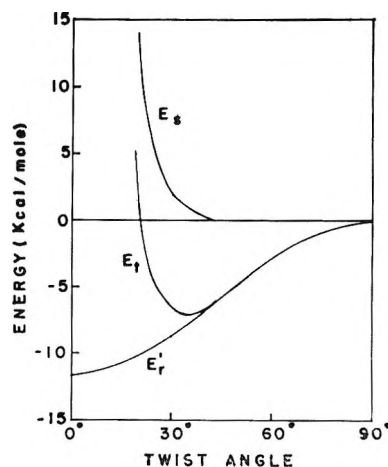


Figure 3. The steric energy (E_s), the resonance energy (E_r), and the effective resonance energy (E_t) for the TAE as functions of the twist angle.

Conclusions

The angle obtained by the theoretical approach and by esr agree very well within the limits of accuracy of these calculations. Considering all the approximations performed both in the theoretical approach and in the Hückel molecular orbital method to correlate the esr coupling constants, we conclude that, at first approximation, the most stable configuration for TAE involves the anisyl groups rotated out of the plane of the ethylenic bond by about 32° . A very recent publication by Baenziger, Buckles, and Simpson⁴¹ on the crystal structure of the dichloriodate (I) salt of the tetra-*p*-anisyl-ethylene dication showed that the anisyl groups are rotated 28.2° out of the plane of the ethylenic bond in the crystal structure.

Experimental Section

TAE was provided by Dr. E. A. Chandross (Bell Laboratories) and was used as received; its purity was established by carbon-hydrogen analysis, visible and ultraviolet spectroscopy, and melting point determination. Methanesulfonic acid and methylene chloride

(31) F. J. Adrian, *J. Chem. Phys.*, **28**, 608 (1958).

(32) C. A. Coulson and M. A. Ali, *J. Chem. Soc.*, 1558 (1959).

(33) C. A. Coulson and C. W. Haigh, *Tetrahedron*, **19**, 527 (1963).

(34) A. Golebiewski and A. Parczewski, *Theoret. Chim. Acta*, **7**, 171 (1967).

(35) T. H. Goodwin and D. A. Morton-Blake, *ibid.*, **1**, 458 (1963).

(36) H. Eyring, *J. Am. Chem. Soc.*, **54**, 3191 (1932).

(37) C. A. Coulson, "Valence," 2nd ed, Oxford University Press, London, 1961, p 174.

(38) J. O. Hirschfelder and J. W. Linnett, *J. Chem. Phys.*, **18**, 130 (1950).

(39) The β used in this work was that also used by Adrian (see ref 31), -17 kcal/mole. See G. W. Wheland, "Resonance in Organic Chemistry," John Wiley and Sons, Inc., New York, N. Y., 1955, p 132.

(40) L. O. Wheeler, Ph.D. Dissertation, The University of Texas, 1967.

(41) N. C. Baenziger, R. E. Buckles, and T. D. Simpson, *J. Am. Chem. Soc.*, **89**, 3405 (1967).

were obtained from Aldrich Chemical Co. and were used without further purification.

The cation radical was prepared by dissolving about 10–15 mg of TAE in 1–2 ml of methylene chloride and treating this solution with 2–3 ml of methanesulfonic acid. A red solution is produced. The solution was stirred for at least 10 min and nitrogen was bubbled through it. The solution was then transferred to a flat Varian aqueous sample cell. This red solution obtained was very stable, lasting at least 1 week. The reaction of TAE with sulfuric acid, on the other hand, leads very quickly to a blue color.

A Varian Associates V-4502 spectrometer employing 100-kc field modulation and a Varian V-153C Klystron (output, 300 mW) were used. The field sweep was calibrated by using Fremy's salt in one side of a V-4532 dual sample cavity. The high and the low field coupling constants for the Fremy's salt were taken as

13.160 ± 0.008 and 13.101 ± 0.004 , based on measurements obtained in this laboratory by Mr. T. V. Atkinson.

The Hückel and McLachlan molecular orbital calculations were done on a Control Data Corp. 6600 computer. The theoretical simulated spectrum was calculated on the CDC computer and plotted on the CDC 160 plotter.

Acknowledgment. The support of this research by the Robert A. Welch Foundation and the National Science Foundation (GP-6688X) is gratefully acknowledged. The esr instrument was purchased with funds provided by the National Science Foundation (GP-2090). We extend these acknowledgments to Mr. T. V. Atkinson and Dr. L. O. Wheeler for helpful discussions, to Dr. E. A. Chandross for the sample of TAE, and to Professor R. E. Buckles for communicating his work on TAE in advance of publication.

Carbon-13 Nuclear Magnetic Resonance Studies of 3-Substituted Pyridines

by H. L. Retcofsky and R. A. Friedel

*Pittsburgh Coal Research Center, U. S. Department of the Interior, Bureau of Mines,
Pittsburgh, Pennsylvania 15213 (Received August 4, 1967)*

Carbon-13 magnetic shieldings for eight 3-substituted pyridines are reported and compared with those of the corresponding monosubstituted benzenes. Thirty of the forty carbon shieldings measured in the spectra of the pyridines yield substituent effects that are within ± 1.3 ppm of those found for the benzenes. Shieldings of the carbons in the 6 position in the pyridines are shown to reflect electron release or withdrawal by substituent groups.

Introduction

Carbon-13 magnetic shieldings in substituted benzenes have recently received considerable attention.¹ The effects of substituents on ring carbon shieldings are nearly additive, except in cases where steric interactions are pronounced, and often reflect specific electronic properties of the substituents. No corresponding studies of six-membered aromatic ring heterocyclic molecules have been reported, although data for azines and selected methylazines² and protonated diazines³ have appeared. A C¹³ nmr study of monosubstituted pyridines was undertaken in this laboratory to determine whether or not these compounds could be treated analogously to the benzenes. We wish here to report carbon shieldings for eight 3-substituted pyridines which constitute the second phase of this investiga-

tion. Substituents studied included weak electron-releasing groups and moderate to strong electron-attracting groups. Pyridines bearing strong electron-releasing groups in the 3-position were not studied since these were either not available or not sufficiently soluble in suitable solvents for C¹³ nmr studies. A similar study of 4-substituted pyridines has recently been reported.⁴

(1) Numerous papers reporting carbon shieldings in substituted benzenes have appeared. Typical examples are: (a) H. Spiess and W. G. Schneider, *J. Chem. Phys.*, **35**, 731 (1961); (b) P. C. Lauterbur, *J. Am. Chem. Soc.*, **83**, 1838 (1961); (c) K. S. Dhami and J. B. Stothers, *Can. J. Chem.*, **43**, 479 (1965); (d) G. B. Savitsky, *J. Phys. Chem.*, **67**, 2723 (1963); (e) G. E. Maciel and J. J. Natterstad, *J. Chem. Phys.*, **42**, 2427 (1965).

(2) P. C. Lauterbur, *ibid.*, **43**, 360 (1965).

(3) A. Mathias and V. M. S. Gil, *Tetrahedron Letters*, 3163 (1965).

(4) H. L. Retcofsky and R. A. Friedel, *J. Phys. Chem.*, **71**, 3592 (1967).

Experimental Section

The nmr spectra were obtained at a spectrometer frequency of 15.085 MHz and were of the rapid passage dispersion mode variety. Details of the experimental procedure have been reported previously.⁴ The compounds studied were all obtained commercially and contained only naturally occurring carbon-13. 3-Iodopyridine and 3-cyanopyridine were examined as saturated solutions in carbon tetrachloride; all other measurements were made on neat liquids.

Results and Spectral Assignments

Magnetic shieldings of all carbon atoms in the compounds investigated are given in Table I. Spectral assignments are unambiguous only for C-3 carbons since these resonances appear as single lines under the experimental conditions employed. All other aromatic

Table I: Carbon-13 Magnetic Shieldings in 3-Substituted Pyridines (ppm from CS₂)

Substituent	Aromatic carbons					Others
	CH-2	C-3	CH-4	CH-5	CH-6	
H ^a	43.1	69.2	57.3	69.2	43.1	
CH ₃ ^a	43.2	59.9	56.4	69.6	45.9	174.8 (CH ₃)
CH ₂ CH ₃	43.4	54.3	58.8	69.6	45.7	166.9 (CH ₂) 178.3 (CH ₃)
COCH ₃	43.6	61.2	58.2	69.4	39.8	-3.8 (C=O) 166.9 (CH ₃)
CHO	41.5	61.4	57.3	68.7	38.5	1.5 (C=O)
Cl	44.8	61.0	56.1	68.3	44.8	
Br	42.3	72.1	54.5	68.2	45.0	
I	37.2	95.8	48.9	67.5	44.6	
CN	40.0	82.5	53.2	69.0	40.0	76.2 (CN)

^a Data from ref 2.

carbon resonances appear as doublets due to large one-bond C¹³-H spin-spin couplings. Assignments of the doublets to specific carbon atoms are based upon the known assignments in pyridine² and the substituent effects established for monosubstituted benzenes^{1a,c} and 4-substituted pyridines.⁴ In addition, use was made of the fact that C¹³-H spin coupling constants for carbons adjacent to the heterocyclic atom in pyridine² and pyrrole^{5,6} are considerably larger than those of the other ring carbons. Assignments for the carbons in the 4 and 5 positions are fairly certain since these give rise to resonances that lie in distinct regions of the spectrum. For the most part, substituent effects on shieldings are expected to be smaller than the chemical shift differences among the various ring carbon atoms.

Discussion

Ring Carbon Shieldings. Since substituents in 3-substituted pyridines are located *meta* to the nitrogen atom, little if any resonance interaction between the two occurs, and the substituent effects may be expected to

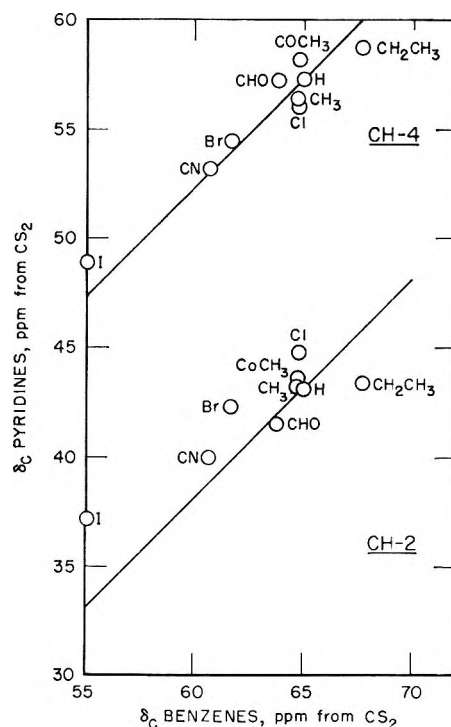


Figure 1. Magnetic shieldings of the carbon atoms *ortho* to substituents in 3-substituted pyridines and monosubstituted benzenes.

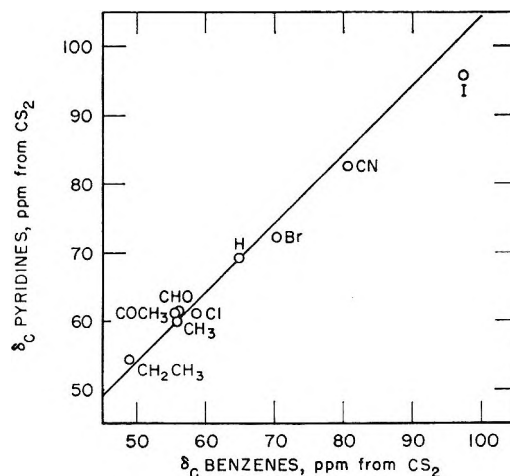


Figure 2. Magnetic shieldings of the substituted carbon atoms in 3-substituted pyridines and monosubstituted benzenes.

follow trends already established for monosubstituted benzenes. Figures 1 and 2, in which representative pyridine shieldings are plotted as a function of the corresponding benzene shieldings, clearly show that this is true at least to a first approximation. The solid lines in the figures represent pyridine shieldings calculated by algebraically adding the pertinent substituent effect for the monosubstituted benzene to the known shieldings in pyridine. It may be concluded that the

(5) T. F. Page, T. Alger, and D. M. Grant, *J. Am. Chem. Soc.*, **87**, 5333 (1965).

(6) K. Tori and T. Nakagawa, *J. Phys. Chem.*, **68**, 3163 (1964).

the most interesting ones are those of CH-6, which may be considered as being *para* to the substituent. These carbons are sufficiently far removed from the substituent to be relatively free from its inductive and magnetic anisotropy effects. Unlike the *para* carbons in monosubstituted benzenes, the CH-6 carbons in pyridines are adjacent to a more highly electronegative atom. This is known to reduce the electron density at this position in the parent compound. Nevertheless, the shieldings of these carbons are very nearly linearly related to Hammett's chemical reactivity parameters σ_p (Figure 3) as was also found for the *para* carbons in monosubstituted benzenes.^{1a} No substituent effect at the CH-6 position in the pyridines differed by more than experimental uncertainty from the corresponding effect in the benzene derivative. It must be noted, of course, that the present study was limited to fewer substituents

than were included in the benzene investigation and that no strong electron-releasing groups were included.

Other Carbon Shieldings. Magnetic shieldings of carbon atoms within the substituents for the cyano, acetyl, and formyl compounds (Table 1) are identical within experimental error with those found for the corresponding 4-substituted pyridines. For the alkyl substituents, the α -carbon atoms are more highly shielded than those in either the 4-substituted pyridines or the monosubstituted benzenes.

Acknowledgments. The authors wish to thank F. R. MacDonald (Laramie Petroleum Research Center, Bureau of Mines) for supplying many of the samples, G. P. Thompson (Pittsburgh Coal Research Center, Bureau of Mines) for valuable technical assistance, and C. E. Griffin (University of Pittsburgh) for helpful discussions.

The Ultraviolet Spectrum of the Nitrate Ion in Molten Mixtures of Alkali Metal Nitrates^{1a}

by Charles R. Boston, David W. James,^{1b} and G. Pedro Smith

*Metals and Ceramics Division, Oak Ridge National Laboratory, Oak Ridge, Tennessee 37830
(Received August 7, 1967)*

The effects of composition and temperature on the first ultraviolet band of the nitrate ion in molten mixtures of alkali metal nitrates are described. The energy of the band maximum E_{\max} is a linear function of mole fraction for NaNO_3 - RbNO_3 and KNO_3 - RbNO_3 mixtures and shows small positive deviations from linearity for LiNO_3 - NaNO_3 , LiNO_3 - KNO_3 , and LiNO_3 - CsNO_3 . The f number shows moderate negative deviations from linearity for all mixtures. With increasing temperatures E_{\max} decreases and f increases.

Introduction

The energy and intensity of the first ultraviolet band of the nitrate ion are strongly influenced by surrounding cations in molten salt media. The present paper fills in an important gap in our information about this behavior.

Smith and Boston² showed that for melts of the pure alkali metal nitrates the energy of the band maximum is approximately a linear function of the reciprocal of the cationic radius. They rationalized this behavior in terms of a Coulomb interaction between the nearest-neighbor cations and the charge cloud on the nitrate ion. Extension of this study to multicharged cations with rare-gas electronic configurations presented difficulties

because nitrate melts containing large fractions of such cations are not chemically stable. Therefore, Smith and Boston³ studied nitrate mixtures in which the multicharged cations were substantially diluted with alkali metal cations.

These authors³ assumed that the band energy for a mixture could be linearly interpolated from the band energies of the pure components by using a particular concentration scale. However, it was clear from their

(1) (a) Research sponsored by the U. S. Atomic Energy Commission under contract with the Union Carbide Corporation. (b) Department of Chemistry, University of Queensland, Brisbane, Australia.

(2) G. P. Smith and C. R. Boston, *J. Chem. Phys.*, **34**, 1396 (1961).

(3) G. P. Smith and C. R. Boston, *Discussions Faraday Soc.*, **32**, 14 (1961).

data that this interpolation is only approximate, but it was not clear just how large an error was involved. In the present paper, the validity of this postulate is quantitatively tested for binary mixtures of alkali metal nitrates, most of which can be studied over the entire composition range.

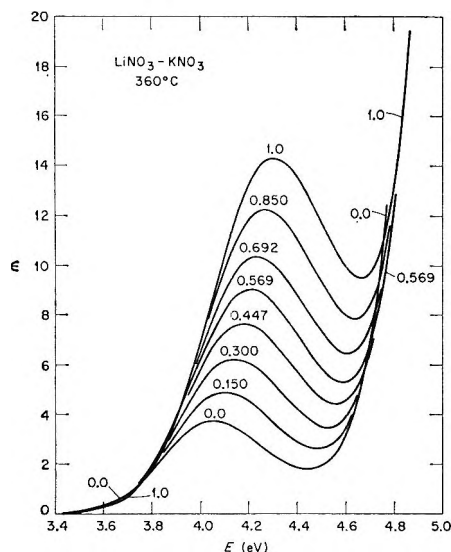


Figure 1. Spectra of LiNO_3 - KNO_3 mixtures at 360°C . Numbers on each spectrum give the mole fraction of LiNO_3 .

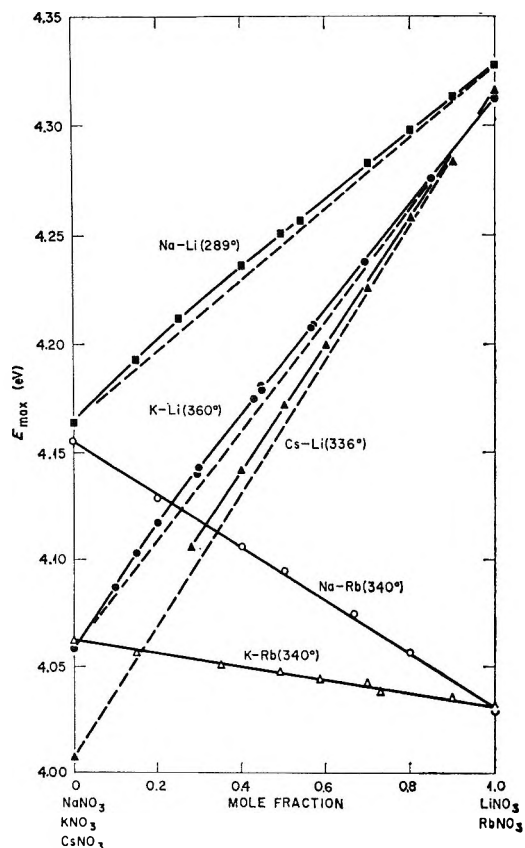


Figure 2. Effect of composition on the energy of the band maximum. Each curve is labeled with the constituent cations and the temperature.

Results and Discussion

Experimental and computational procedures were like those already published.² Estimation of f numbers was based on the Lowry-Hudson band shape model.

The systems studied were LiNO_3 - NaNO_3 , LiNO_3 - KNO_3 , LiNO_3 - CsNO_3 , NaNO_3 - RbNO_3 , and KNO_3 - RbNO_3 . Lithium nitrate-rich mixtures of LiNO_3 and CsNO_3 tend to decompose at temperatures above the melting point of CsNO_3 . Therefore, measurements on these mixtures were restricted to low temperatures and did not extend above 75 mole % CsNO_3 . For purposes

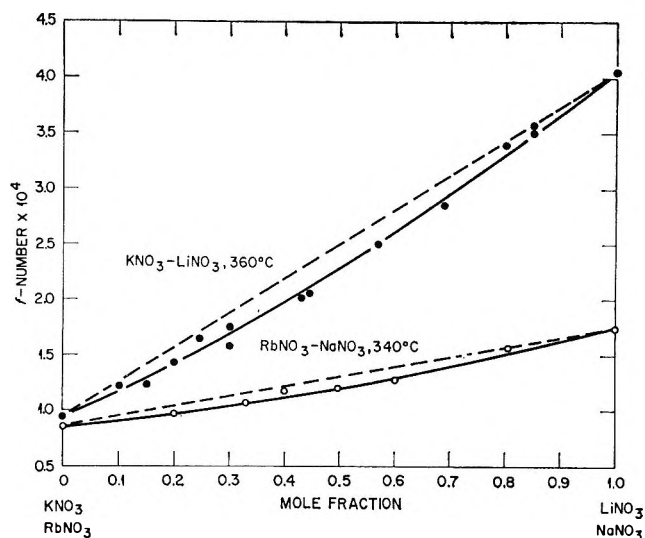


Figure 3. Effect of composition on the f number for typical systems.

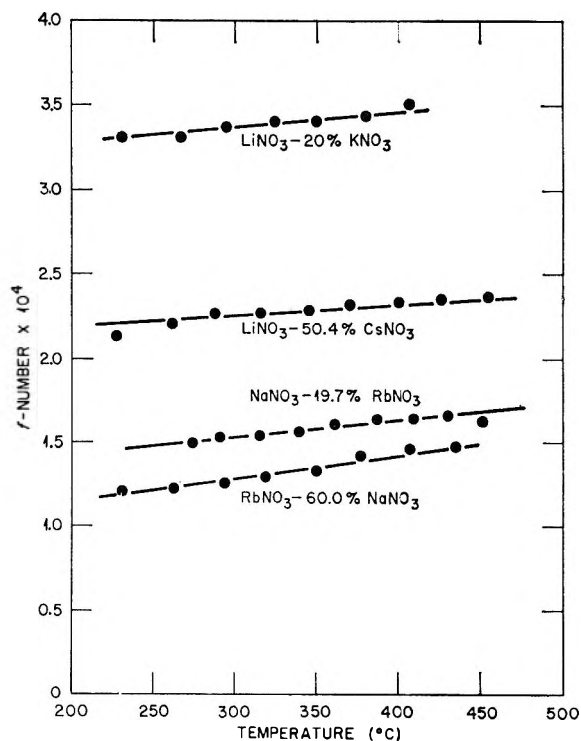


Figure 4. Effect of temperature on the f number for typical compositions.

of comparison, the spectrum of CsNO_3 was extrapolated below the melting point.

Figure 1 shows a typical set of spectra, that for LiNO_3 - KNO_3 mixtures at 360° . With increasing LiNO_3 content, the band maximum shifts toward higher energies and the intensity increases substantially.

Figure 2 shows the shift in the energy of the band maximum E_{max} as a function of composition for all systems studied. Solid lines follow the course of the data while dashed lines connect the points for the pure materials. For KNO_3 - RbNO_3 and NaNO_3 - RbNO_3 the two systems that do not contain LiNO_3 , E_{max} is a linear function of mole fraction over the entire composition range. For the three mixtures that contain LiNO_3 , E_{max} shows small positive deviations from linearity.

The effect of temperature on E_{max} is small and of the same magnitude for mixtures as for pure nitrates (-10^{-4} ev/deg). For example, E_{max} for the LiNO_3 - KNO_3 eutectic (43 mole % LiNO_3) was measured at eight temperatures from 138 to 400° . To within experimental error it was a linear function of temperature with a slope of -1.7×10^{-4} ev/deg.

Typical examples of the effect of composition on the f number are given in Figure 3. There are small to moderate negative deviations from linearity in all cases. In general, the f number increases with increasing temperature, but the magnitude of the effect varies with system composition. Typical examples are given in Figure 4.

These data fit quite well with the pattern of systematic effects that Smith and Boston^{2,3} have reported previously. They showed that E_{max} for the pure alkali metal nitrates and binary mixtures of these nitrates with up to 25-60 mole % of $\text{Ba}(\text{NO}_3)_2$, $\text{Sr}(\text{NO}_3)_2$, $\text{Ca}(\text{NO}_3)_2$, and $\text{La}(\text{NO}_3)_3$ was approximately represented by the relation

$$E_{\text{max}} = A \sum_i \frac{z_i}{r_i} \bar{N}_i + B$$

where A and B are empirical constants that are the same for all systems and depend only on temperature; z_i , r_i , and \bar{N}_i are the formal charge, crystal radius, and electrical equivalent fraction, respectively, of the i th species of cation.

The data presented here show that the above relation also holds approximately for binary mixtures of alkali metal nitrates. The small curvature in the E_{max} vs. composition relations for mixtures containing LiNO_3 is of similar magnitude to the corresponding curvature in this relation for mixtures containing multicharged cations.

We conclude that the effect of composition on E_{max} is approximately an additive function of cationic composition for the mixtures of alkali metal nitrates.

The lowest energy electronic band of NO_3^- is very weak. If it is a singlet-singlet transition as we suppose, the high symmetry of NO_3^- (D_{3h}) must play an important role in fixing the selection rule. For example, the more plausible assignments are $n \rightarrow \pi^*$ ($A_1' \rightarrow A_1''$ and $A_1' \rightarrow E''$), $n \rightarrow \sigma^*$ ($A_1' \rightarrow A_2'$), and $\pi \rightarrow \sigma^*$ ($A_1' \rightarrow E''$). All of these transitions are forbidden as electric dipole processes and can be observed only when the nitrate ion is suitably perturbed by vibrations or an asymmetric environment. Such vibrational perturbations undoubtedly account for the observed increase in f with temperature. However, mixed nitrates provide more opportunities for asymmetric arrangements of cations about NO_3^- than pure nitrates. For that reason, it is surprising that f shows only moderate deviations from a linear composition dependence and that these deviations are negative.

Isosbestic Points and Internally Linear Spectra

Generated by Changes in Solvent Composition or Temperature^{1a}

by Jorulf Brynstad and G. Pedro Smith^{1b}

Metals and Ceramics Division, Oak Ridge National Laboratory, Oak Ridge, Tennessee 37830
(Received August 7, 1967)

We show that isosbestic points generated by changes in temperature or solvent composition may be formed under a wider variety of conditions than previously recognized, so that the rules previously proposed for interpreting these points in terms of the number of absorbing species or the number of independent reaction parameters are unreliable. Examples of experimental cases in which these rules break down are cited. We also point out that in most applications it is more useful to show that spectra are linearly related than to show that they have isosbestic points.

Introduction

The presence or absence of isosbestic points in a set of spectra generated by changing the composition or temperature of a liquid system is often used as evidence regarding the number of absorbing species or the number of independent reaction parameters. The most complete isosbestic point theories are those by Cohen and Fischer,² and Morrey.³ We shall show these theories to be incomplete and partly wrong, and shall cite experimental results that illustrate some of the deficiencies. In so doing, we do not single out these authors for special criticism. On the contrary, we cite them because their treatments are the most complete thus far.

Cohen and Fischer² showed that isosbestic points may occur in a system containing several absorbing species when the variation in concentration of all these species is linearly related by a single reaction parameter. They then generalized on this result and concluded that the existence or absence of isosbestic points provides a basis for distinguishing between systems in which the absorbing species are interrelated by a single reaction parameter and those requiring more than one such parameter. They also considered the effect which changes in temperature or solvent composition have on the spectra of such systems. They pointed out that these changes will, in general, not only shift the chemical equilibrium but also alter the shapes of the absorption bands, so that one would expect to find isosbestic points only for limited ranges of variations in temperature or solvent composition.

Recently, Angell and Gruen^{4,5} applied the Cohen-Fischer type of model to large temperature variations under the assumption that the effects of temperature on band shapes could be ignored. They proposed that the presence of temperature-generated isosbestic points implies the presence of two absorbing species in equilibrium,

while their absence implies the presence of a single such species which is continuously distorted by changing temperature.

The Cohen-Fischer and Angell-Gruen treatments overlooked the possibility that the effect of temperature (or solvent composition) on the spectra of species that are not in chemical equilibrium might be of a unique type that generates isosbestic points. Morrey³ experimentally demonstrated that just this behavior sometimes occurs in the case of temperature variations. He measured the effect of temperature on the spectra of several systems that plausibly contained a single absorbing species and showed, first, that isosbestic points are formed on *both* the absorbance and absorptivity scales over wide temperature ranges, and, second, that the absorbance and absorptivity at any wavelength are linear functions of temperature. He proposed a phenomenological theory of this behavior and concluded, among other things, that only one species contributes to the absorbance at a given temperature-generated isosbestic point, and that any equilibrium involving this species is not appreciably affected by temperature changes.

In all of these theories it is taken for granted that isosbestic points occur only if the spectra are linearly interrelated. That this is not a generally valid assumption is illustrated by the measurements of Angell and Gruen,⁴ who published several sets of spectra that have well-defined isosbestic points but that are not

(1) (a) Research sponsored by the U. S. Atomic Energy Commission under contract with the Union Carbide Corp. (b) Oak Ridge National Laboratory and Department of Chemistry, University of Tennessee, Knoxville, Tenn.

(2) D. M. Cohen and E. Fischer, *J. Chem. Soc.*, 3044 (1962).

(3) J. R. Morrey, *J. Phys. Chem.*, **66**, 2169 (1962); **67**, 1569 (1963).

(4) C. A. Angell and D. M. Gruen, *ibid.*, **70**, 1601 (1966).

(5) C. A. Angell and D. M. Gruen, *J. Am. Chem. Soc.*, **88**, 5192 (1966).

even approximately linearly interrelated. We shall treat this problem, but we shall also show that even when the spectra are known to be linearly interrelated, still the Cohen-Fischer and Morrey theories are inadequate and misleading. Furthermore, we shall contend, in opposition to Angell and Gruen, that the absence of isosbestic points provides no evidence one way or the other concerning the number of species.

Definitions

The absorbance, $A = \log(I_0/I)$, of a liquid system is a function of the wavelength λ , the path length, and a set of N macroscopic parameters that uniquely fix the state of the system (temperature, pressure, external fields, composition, etc.). We denote these N parameters $\{X_k\}_N$.

It is convenient to factor A as follows

$$A = A(\lambda, \{X_k\}_N) = E(\lambda, \{X_k\}_N)/V(\{X_k\}_N) \quad (1)$$

where V is the volume of the system. The quantity E is related to the formal absorptivity ϵ_f via the expression $\epsilon_f = E/M$, where M is the mass parameter for a component that gives rise to the absorbing entities under consideration. We designate the external parameters in a reference state as $\{X_k^0\}_N$ and the spectrum of the reference state as

$$\begin{aligned} A^0 &= A^0(\lambda, \{X_k^0\}_N) \\ E^0 &= E^0(\lambda, \{X_k^0\}_N) \end{aligned}$$

When one of the external parameters, say X_j , is changed so that $X_j = X_j^0 + \Delta X_j$, the resultant change in the absorbance can be written

$$A(\lambda, X_j) = A^0 + \Delta A(\lambda, \Delta X_j)$$

with similar expressions for E and V , namely

$$\begin{aligned} E(\lambda, X_j) &= E^0 + \Delta E(\lambda, \Delta X_j) \\ V(X_j) &= V^0 + \Delta V(\Delta X_j) \end{aligned}$$

We say that a set of spectra has an X_j -generated isosbestic point on the E (or A) scale at a wavelength λ_i if ΔE (or ΔA) is zero at λ_i for all values of ΔX_j over a specified range.

There are a number of well established cases⁶⁻¹⁰ in which a set of spectra may be described by the relation

$$E = E^0[1 + h(\lambda)g(\Delta X_j)] \quad (2)$$

where g is a monotonous function of ΔX_j . We refer to such sets as internally linear because any spectrum that conforms to eq 2 can be expressed as a linear combination of any two other members of the set. That is

$$\begin{aligned} E_i(\lambda) &= (1 - \beta_i)E_1(\lambda) + \beta_i E_2(\lambda) \\ &= E^0\{1 + h(\lambda)[(1 - \beta_i)g(\Delta X_j^{(1)}) + \beta_i g(\Delta X_j^{(2)})]\} \end{aligned} \quad (3)$$

where β_i is a number, and $\Delta X_j^{(1)}$ and $\Delta X_j^{(2)}$ are the values of X_j at which $E_1(\lambda)$ and $E_2(\lambda)$, respectively, were measured.

Role of Internal Linearity in Isosbestic Point Theories

In the Cohen-Fischer² and Morrey³ theories, and in all previous theories as well, isosbestic points appear as a mathematical consequence of internal linearity, so that these theories are, in fact, theories of internal linearity. According to the Cohen-Fischer model, isosbestic points occur only if the spectra are of the type specified by eq 2. Morrey³ concluded that temperature-generated isosbestic points occur only if a special form of eq 2 is obeyed (his eq 11). The possibility that isosbestic points can be caused by functional forms other than those in accord with eq 2 has been overlooked or else ignored as physically improbable. As a result, the observation of isosbestic points is commonly considered a sufficient proof that the system behaves in accordance with some theory of internal linearity.

The fallacy in such an approach is easily recognized by realizing that although internal linearity is a sufficient condition for isosbestic points, it is by no means a necessary condition. For example, if E (or A) is any monotonous function of X_j at all wavelengths, isosbestic points will occur at wavelengths where $\partial E/\partial X_j = 0$. (Equation 2 is a particularly simple class of functions monotonous in X_j .) There may also be cases where isosbestic points occur "accidentally" without underlying monotony at all wavelengths. Not only are there no *a priori* physical reasons for excluding these possibilities, but in the recent literature there are a number of examples in which isosbestic points are observed without internal linearity. Angell and Gruen⁴ present several such sets. The danger in this situation is illustrated by the fact that these authors proceed to use these isosbestic points as evidence for a Cohen-Fischer² type of situation, *i.e.*, as if the spectra were internally linear.

Since isosbestic points are not reliable indicators of internal linearity, other methods must be employed to test for this property. Several methods are possible and two have been published^{7,9} that can be used whether isosbestic points are present or not.

We conclude that isosbestic points are not sound evidence for anything, although they may serve as eye-catching indicators of *possible* internal linearity. The question of whether or not internal linearity is reliable evidence of something will be treated in the remainder of this paper.

Existence Conditions for Internally Linear Sets of Spectra

We consider first systems which obey the relation of additive absorbances, that is

(6) Examples are given in ref 3 and 7-10.

(7) J. Brynestad, C. R. Boston, and G. P. Smith, *J. Chem. Phys.*, **47**, 3179 (1967).

(8) J. Brynestad and G. P. Smith, *ibid.*, **47**, 3190 (1967).

(9) C. R. Boston and G. P. Smith, *J. Phys. Chem.*, **66**, 1178 (1962).

(10) G. P. Smith, C. R. Boston, and J. Brynestad, *J. Chem. Phys.*, **45**, 829 (1966).

$$E = \sum_{i=1}^C \epsilon_i(\lambda, \{X_k\}_N) n_i(\{X_k\}_N) = \sum_{i=1}^C \epsilon_i n_i \quad (4)$$

where ϵ_i and n_i are the absorptivity and number of moles, respectively, of the i th species in the system. Both ϵ_i and n_i are, in the general case, functions of the external parameters $\{X_k\}_N$. Equation 4 can be expected to hold for dilute solutions or absorbing species that do not interact. This equation can be recast in terms of a reference state designated by E^0 , ϵ_i^0 , and n_i^0 as

$$\begin{aligned} E^0 &= \sum_{i=1}^C \epsilon_i^0 n_i^0 \\ E &= \sum_{i=1}^C (\epsilon_i^0 + \Delta\epsilon_i)(n_i^0 + \Delta n_i) \\ &= E^0 + \sum_{i=1}^C (n_i^0 \Delta\epsilon_i + \epsilon_i^0 \Delta n_i) + \sum_{i=1}^C \Delta\epsilon_i \Delta n_i \quad (5) \end{aligned}$$

In the following, we discuss the more important conditions under which systems that obey eq 4 will give rise to internal linearity.

A. Case I: All $\Delta\epsilon_i = 0$, All $\Delta n_i \neq 0$. In this model case, the absorptivities of the individual species are invariant with respect to the external parameter in question, X_j . Equation 5 reduces to

$$E = E^0 + \sum_{i=1}^C \epsilon_i^0 \Delta n_i \quad (6)$$

Suppose that in a specific instance all the Δn_i are linearly related, *i.e.*

$$\Delta n_i = k_i \Delta\xi = k_i g(\Delta X_j) \quad (7)$$

where the k_i are constants (stoichiometric coefficients), finite or zero. Then eq 6 gives

$$E = E^0 + \left(\sum_{i=1}^C \epsilon_i^0 k_i \right) g(\Delta X_j) = E^0 [1 + h(\lambda) g(\Delta X_j)] \quad (8)$$

where $h(\lambda) = (1/E^0) \sum (i) \epsilon_i^0 k_i$. Hence, we obtain an equation of the same type as eq 2, the internal linearity relation. Isosbestic points occur when $\sum (i) \epsilon_i^0 k_i = 0$.

This case is the same as that discussed by Cohen and Fischer.² It applies when there is only one chemical equilibrium in the system, in which case the n_i are linearly interrelated. It automatically includes the situation in which there is an arbitrary number of species that do not take part in the equilibrium. For these species, $\Delta n_i = 0$ and their spectra are included in E^0 .

A basic requirement for this model to be applicable is that the absorptivities ϵ_i be invariant with respect to the variable parameter, X_j . If X_j is a composition parameter, the species must obey the Bouguer-Beer law to within experimental tolerance. If X_j is the temperature (or pressure), the ϵ_i must be insensitive to changes in temperature (or pressure) to within experi-

mental tolerance. If there are no good reasons for believing that these conditions are fulfilled, it is not valid to assume that observed internal linearity proves that a Cohen-Fischer type of mechanism is operative.

There are many valid examples of internal linearity of the Case I type generated by composition changes, and these are discussed by Cohen and Fischer.² Also, an example of the Case I type generated by temperature changes is presented by Angell and Gruen.⁵ These authors report a set of spectra with one temperature-generated isosbestic point for nickel complexes in concentrated aqueous solutions of magnesium chloride (their Figure 3a), and they use the isosbestic point as evidence of a temperature dependent two-species equilibrium. Their spectra also appear to be internally linear, in accordance with the requirements of the Cohen-Fischer model. Note, however, that in Morrey's³ theory, the same experimental behavior is used as evidence that only one absorbing nonreacting species is present. We look more closely at this discrepancy in the section that follows.

B. Case II: All $\Delta n_i = 0$, All $\Delta\epsilon_i \neq 0$. In this case the absorptivities ϵ_i are not invariant with respect to X_j , whereas the amounts of the absorbing species are constant, *i.e.*, these species do not participate in chemical equilibria. Equation 5 reduces to

$$E = E^0 + \sum_{i=1}^C n_i^0 \Delta\epsilon_i \quad (9)$$

Obviously, if the spectrum of a single species behaves according to eq 2, then the absorptivity must be of the same functional type, *i.e.*

$$\epsilon_i = \epsilon_i^0 [1 + h(\lambda) g(\Delta X_j)] \quad (10)$$

Now there is no known physical reason to expect that the spectrum of a pure species should in general have this particularly simple form with separable λ and X_j dependence. Therefore, one might expect internal linearity of the Case II type to be rather rare except, possibly, for special types of optical transitions. Furthermore, if there are several species, the only way of converting eq 9 into a relation with internal linearity (eq 2) is for the ϵ_i of all of the species to have the form of eq 10 and also the same X_j dependence, that is

$$\epsilon_i = \epsilon_i^0 [1 + h_i(\lambda) g(X_j)] \quad (11)$$

This would lead to

$$\begin{aligned} E &= E^0 + g(\Delta X_j) \left(\sum_{i=1}^C h_i(\lambda) n_i^0 \right) \\ &= E^0 [1 + h(\lambda) g(\Delta X_j)] \quad (12) \end{aligned}$$

where $h(\lambda) = 1/E^0 [\sum (i) h_i(\lambda) n_i^0]$. We do not expect eq 12 to be fulfilled very often except in cases where all of the absorbing species are "similar."

There are a substantial number of examples of internal linearity generated by changes in temperatures that cannot be rationalized in a satisfactory way as in

terms of Case I, so that one is forced to conclude that Case II applies. In the known instances where a Case II situation is suspected, the spectra are internally linear, or almost so, on both the A and E scales over most of the wavelength range and A and E at a fixed wavelength are linear functions of temperature. This behavior was first pointed out by Morrey.³ He presumed that this behavior would hold at all wavelengths, but we have recently found that in λ regions where the relative change $\Delta E/E^0$ (or $\Delta A/A^0$) is not small compared to unity, linearity tends to break down. An empirical explanation for this behavior is as follows. A condition for observing temperature-generated isosbestic points on the A scale is that E must have the same temperature dependence as the volume V at given wavelengths, i.e., $\Delta E/E^0 = \Delta V/V^0$, and in order to have isosbestic points on the E scale, ΔE must be zero at given wavelengths. This can be accounted for by assuming that in these cases E has the same, or almost the same, type of temperature dependence as V at all wavelengths. Since it is commonly true that the volume expansion coefficient $\alpha = 1/V(\partial V/\partial T)_p$ is approximately constant for liquids over substantial temperature ranges, and hence

$$V \approx V_0 \exp(\alpha \Delta T)$$

this would require that

$$E \approx E_0 \exp[h(\lambda) \Delta T] \quad (13)$$

with isosbestic points on the E scale wherever $h(\lambda) = 0$, and on the A scale wherever $h(\lambda) = \alpha$. Moreover, if $\alpha \Delta T$ and $h(\lambda) \Delta T \ll 1$ at all wavelengths, eq 13 will be experimentally indistinguishable from

$$E \approx E^0 [1 + h(\lambda) \Delta T] \quad (14a)$$

and

$$A \approx A^0 \{1 + [h(\lambda) - \alpha] \Delta T\} \quad (14b)$$

Spectra obeying eq 14 are not only internally linear, but they are also linear functions of temperature at any fixed wavelength. It is important to note that temperature-generated internal linearity for species in chemical equilibrium (Case I situation) will not, in general, have these characteristics because concentration changes caused by a shift in a chemical equilibrium are usually not linear with respect to the temperature. Thus, in the previously mentioned example of a two-species equilibrium reported by Angell and Gruen⁵ (their Figure 3a), the spectra are apparently internally linear but they are obviously not linear with respect to temperature.

A typical example of internal linearity with respect to temperature when there is no chemical equilibrium (Case II situation) is given by the spectra of molten CsCl , 20 mole % NiCl_2 , which have been measured from 5000 to 27,000 cm^{-1} over a 300° range.¹⁰ To within experimental uncertainty, this set of spectra is in-

ternally linear on both the A and E scales with a linear temperature dependence between 5000 and about 19,000 cm^{-1} . Four isosbestic points occur in this range, and $\Delta A/A^0$ and $\Delta E/E^0$ are everywhere fairly small. Above 19,000 cm^{-1} , $\Delta E/E^0$ and $\Delta A/A^0$ are not small for a 300° change in temperature, and both the linearity and the internal linearity break down. Several other examples of this kind of temperature dependence are known.

Although eq 13 leads to eq 14 if $h(\lambda) \Delta T$ is small, it should not be assumed that an experimental verification of eq 14 proves that E has the functional form of eq 13. There are numerous other functional forms that would give the linear temperature dependence specified by eq 14 to within a good approximation, and we do not single out eq 13 as more probable than other functions. On the contrary, an examination of the spectra available to us indicates that deviations from eq 14 are not in accord with eq 13. We conclude, therefore, that linear temperature dependence of the absorptivity in given wavelength ranges is only approximate, and that, when it occurs, the physical reasons for this simple behavior are as yet unknown.

There are insufficient data to decide whether or not linear temperature dependence of absorptivities is a common phenomenon. If it turns out to be a common phenomenon, then the observation of linear temperature dependence cannot be used as evidence regarding the number of species, because a sum of absorptivities that are all linear with respect to the temperature will also be linear. This is contrary to Morrey's³ conclusion that isosbestic points caused by linear temperature dependence are evidence for only one absorbing species. The flaw in his argument was the assumption that if several species are present, the spectrum of each, individually, must have isosbestic points at the same wavelengths as the composite spectrum.

As yet, all cases of temperature-generated internal linearity that have been interpreted as being due to a Case II type of mechanism have also shown a linear dependence on temperature. However, one cannot exclude the possibility, contrary to Morrey's³ conclusions, that temperature-generated internal linearity of the Case II type may occur without a linear temperature dependence. One would, of course, expect to find such internal linearity on the E scale, but not on the A scale.

Both Cohen and Fischer² and Morrey³ overlooked the possibility that changes in the spectra caused by changes in solvent composition may cause internal linearity of the Case II type. However, recent studies of nickel ions in molten chlorides^{7,8} provide examples of composition-generated internal linearity that cannot be explained satisfactorily in terms of a chemical equilibrium (Case I situation), so that one is led to conclude that it is caused by Case II type behavior. An example is provided by nickel centers in molten LiCl-KCl mixtures at high temperatures.⁷ The spec-

tra form internally linear sets when the solvent composition is isothermally varied over modest ranges. This fact taken by itself might indicate a Case I type of situation in which the absorbing species have composition invariant spectra. However, when the temperature of such mixtures is varied at constant composition, temperature linearity in accordance with eq 14 is observed. This indicates either a Case II type of situation in which the spectra of the species present are temperature dependent, or else a Case I type of chemical equilibrium between species which have temperature-invariant spectra. Thus, if a Case I type of situation were present, the spectra of the individual absorbing species would have to be invariant with respect to both composition and temperature changes and if this were so, the temperature-generated and composition-generated spectra would have to have the same internally linear forms with temperature-generated and composition-generated isosbestic points at the same wavelengths. This unique behavior, however, is not observed so that these spectra cannot signify a Case I type of situation. We are left to conclude that a Case II type of situation is present with composition-generated internal linearity that obeys eq 2 and temperature-generated linearity that obeys eq 14. Furthermore, in the present example, there is additional experimental evidence which indicates that only one kind of nickel center is present in the system. The same type of behavior has been observed for nickel centers in KCl-MgCl_2 mixtures at high temperatures.⁸

C. Other Types of Internal Linearity. In the preceding discussion, only situations for which the law of additive absorbances, eq 4, is valid were considered. There are a number of situations, however, for which eq 4 is not applicable, and other situations in which it is impossible to decide whether eq 4 is valid or not. A condition for the validity of eq 4 is that no absorbing species influence the spectrum of any other species. This requirement is necessary because interaction effects among species cannot be ascribed unambiguously to individual species. Therefore, eq 4 can be strictly valid only for solutions sufficiently dilute in the absorbing species so that any one of these species does not influence the solvent environment of any other.

It would be inappropriate to assume that internal linearity will occur only in situations for which the law of additive absorbances (eq 4) is valid. Therefore, the verification of internal linearity cannot be used as evidence of the fulfillment of the law of additive absorbances. Internal linearity in situations for which

the law of additive absorbances is not valid cannot be properly discussed or evaluated in terms of simple models so that it is impossible to anticipate the numerous conditions under which they might occur.

Absence of Isosbestic Points

Cohen and Fischer² concluded that the existence or absence of isosbestic points provides a basis for distinguishing between systems whose compositions are defined by a single reaction parameter and those requiring more than one such parameter. In other words, they inferred that the absence of isosbestic points could be used as evidence for two or more simultaneous chemical equilibria. Angell and Gruen^{4,6} used the presence of isosbestic points as evidence of two species in chemical equilibrium, in accordance with the Cohen-Fischer model, whereas they used the absence of isosbestic points as evidence for only one species, in opposition to the Cohen-Fischer model. In view of these statements, it seems necessary to point out that the absence of isosbestic points cannot be used as evidence for anything, unless one can be sure that each species in the system behaves as required by the model employed.

A condition for the validity of Cohen and Fischer's statement is that the absorptivity of each species present be invariant with respect to the external parameter in question, but there should be numerous systems in which this ideal behavior does not hold. In such instances, internal linearity and isosbestic points will not be observed irrespective of the number of reaction parameters or nonreacting species, so that *the absence of isosbestic points has no practical value whatsoever.*

Concluding Remarks

We have shown that in terms of available theoretical models that it is more useful to test sets of spectra for internal linearity than for isosbestic points, although even internal linearity is, by itself, insufficient evidence to verify theoretical models so that additional information is always necessary in order to arrive at safe conclusions.

Even though our analysis includes all the situations we know to be important, it does not include all of the possible ways that internal linearity might arise. Furthermore, neither we nor anyone else has considered the numerous possibilities for forming isosbestic points when the spectra are not internally linear, although experimental examples of this behavior are known.

Kinetics of Aluminum Ion Hydrolysis in Dilute Solutions¹

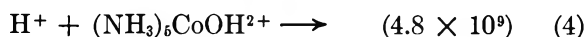
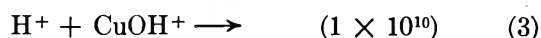
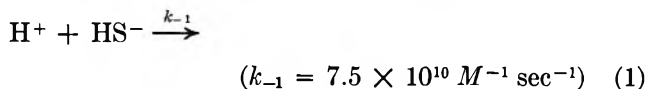
by Lloyd P. Holmes, David L. Cole, and Edward M. Eyring²

Department of Chemistry, University of Utah, Salt Lake City, Utah 84112 (Received August 7, 1967)

Dissociation field effect relaxation times in dilute aqueous aluminum chloride have been measured and attributed to the perturbation of the hydrolysis equilibrium $\text{Al}^{3+} + \text{H}_2\text{O} \xrightleftharpoons[k_{-1}]{k_1} \text{AlOH}^{2+} + \text{H}^+$ rather than complexing or dimerization equilibria. At 25° the specific rate $k_{-1} = (4.4 \pm 0.5) \times 10^9 \text{ M}^{-1} \text{ sec}^{-1}$ at an ionic strength $\mu \cong 1 \times 10^{-3} \text{ M}$. This result is consistent with measured rate constants for other essentially diffusion-controlled protolytic reactions $\text{H}^+ + \text{M}^{(n+)-1} \rightarrow$ for which n varies from 0 to 3.

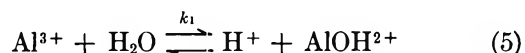
Introduction

Several years ago, DeMaeyer and Kustin³ generalized on the basis of the then available kinetic data that the rate constant for the essentially diffusion-controlled reaction between a proton and a species $\text{M}^{(n+)-1}$ in water would decrease by a factor of 0.3 to 0.5 for each positive charge added to the reaction partner $\text{M}^{(n+)-1}$. As evidence, they cited the following kinetic results⁴⁻⁶



Using the dissociation field effect relaxation method, we recently determined⁷ the rate constant of the reaction $\text{H}^+ + \text{UO}_2\text{OH}^+ \xrightarrow{k_{-1}}$ to be $k_{-1} = (1.65 \pm 0.33) \times 10^{10} \text{ M}^{-1} \text{ sec}^{-1}$ at 25°, in satisfactory agreement with the above results. An overwhelming body⁸ of evidence supports the validity of the Smoluchowsky-Debye-Eigen equation⁸ for the limiting value of a diffusion-controlled reaction which is, in fact, the theoretical basis for the DeMaeyer-Kustin generalization. Had a significant discrepancy with theory occurred in the case of uranyl hydrolysis, it would have been logical to seek an explanation in steric peculiarities of the UO_2OH^+ ion rather than to dispute the generalization.

With the above considerations as background, we recently undertook a dissociation field effect (dfe) relaxation method⁹ kinetic study of the aluminum hydrolysis



in dilute aqueous aluminum chloride solutions. In addition to revealing whether unusual steric factors limit the rate of the reverse reaction, we anticipate that the rate constants k_1 and k_{-1} reported below

will aid in unraveling the kinetics of complexing reactions of aluminum ion¹⁰ that are to some extent obscured by aluminum ion hydrolysis and polymerization.

In an equilibrium study involving pH and conductance measurements, Frink and Peech¹¹ found that the monomeric hydrolysis mechanism of eq 5 adequately described the chemistry of dilute aqueous aluminum chloride. In the total concentration range $C_0 = 10^{-5}$ to 10^{-2} M there was no evidence of dimer, $\text{Al}_2(\text{OH})_2^{4+}$, or higher polymers being present. They also were able to rule out the presence of aluminum chloride complexes. At 25° they found the thermodynamic hydrolysis constant to be

$$K_1 = \frac{10^{-\text{pH}} a_{\text{AlOH}^{2+}}}{a_{\text{Al}^{3+}}} = 10^{-5.02} \text{ M} \quad (6)$$

In this expression $a_{\text{Al}^{3+}} = \gamma_{\text{Al}^{3+}}[\text{Al}^{3+}]$ is the activity of aluminum ion. They calculated the activity coefficients $\gamma_{\text{Al}^{3+}}$, $\gamma_{\text{AlOH}^{2+}}$, and $\gamma_{\text{H}^+} = 10^{-\text{pH}}/[\text{H}^+]$ from the extended Debye-Hückel equation for water at 25°

$$-\log \gamma_i = \frac{0.509 z_i^2 \sqrt{\mu}}{1 + (0.33 \times 10^8 \sigma_i \sqrt{\mu})} \quad (7)$$

(1) This research was supported in part by NIH Grant No. AM-06231 and by NIH Grant No. 1805FRO7092-01.

(2) To whom communications should be addressed.

(3) L. DeMaeyer and K. Kustin, *Ann. Rev. Phys. Chem.*, **14**, 5 (1963).

(4) M. Eigen and K. Kustin, *J. Am. Chem. Soc.*, **82**, 5952 (1960).

(5) E. Grunwald, P. J. Karabatsos, R. A. Kromhout, and E. L. Purlee, *J. Chem. Phys.*, **33**, 556 (1960).

(6) M. Eigen and W. Kruse, *Z. Naturforsch.*, **18b**, 18 (1963).

(7) D. L. Cole, E. M. Eyring, D. T. Rampton, A. Silzars, and R. P. Jensen, *J. Phys. Chem.*, **71**, 2771 (1967).

(8) M. Eigen and L. DeMaeyer, "Technique of Organic Chemistry," Vol. VIII, Part II, S. L. Friess, E. S. Lewis, and A. Weissberger, Ed., Interscience Publishers, Inc., New York, N. Y., 1963, pp 1031-1050.

(9) See ref 8, pp 988-1001.

(10) K. Kustin, E. R. Ehrenfeld, and E. M. Reinheimer, Abstracts, 144th National Meeting of the American Chemical Society, Los Angeles, Calif., April 1963, p 18k.

(11) C. R. Frink and M. Peech, *Inorg. Chem.*, **2**, 473 (1963).

where z_i is the ionic charge, μ is the ionic strength, and the value of the parameter σ_i is 9×10^{-8} cm for Al^{3+} , AlOH^{2+} , and H^+ following Kielland.¹² To a very good first approximation, the ionic strength in these solutions is given by¹¹

$$\mu = 6C_0 \quad (8)$$

Experimental Section

J. T. Baker reagent grade $\text{AlCl}_3 \cdot 6\text{H}_2\text{O}$ was weighed and dissolved in distilled, Deeminized, boiled water to make a 10^{-2} M stock solution. The exact concentration of aluminum(III) was determined to be $(1.0011 \pm 0.0018) \times 10^{-2}$ M using a gravimetric technique involving precipitation with 8-quinolinol. This result was further verified by atomic absorption analysis (Perkin-Elmer Model 303). Aliquots of this stock solution were then added to water having a specific conductance of 1.4×10^{-7} ohm $^{-1}$ cm $^{-1}$ prepared by an electrophoretic ion exclusion technique.¹³ This and all subsequent operations were carried out under an atmosphere of Linde high purity dry nitrogen. The pH of sample solutions was determined with a Beckman 1019 Research pH Meter using a Beckman 41263 glass electrode and a 39071 calomel electrode.

We have described the construction and operation of our dfe apparatus elsewhere in considerable detail.^{7,14} In essence, a square 30-kv pulse of 7–12 μsec duration developed with a coaxial line is applied to a specially constructed Wheatstone bridge, one arm of which consists of a platinum in glass cell containing the aqueous aluminum chloride sample solution. The interelectrode distance is 0.3 cm. The sudden jump of the electric field intensity from 0 to approximately 10^5 v/cm perturbs the weak electrolyte equilibrium, eq 5, giving rise to an exponential decay in ionic conductance to that characteristic of the high electric field condition. This relaxation time τ is recorded on a Tektronix 535A oscilloscope as a voltage vs. time curve using Tektronix P6015 high voltage probes and a Tektronix Type W differential-input preamplifier.

To check the performance of our dfe apparatus, we ran frequent blanks as well as a 3×10^{-2} M aqueous veronal solution for which our average measured relaxation time of 1.85 μsec was in excellent agreement with the value of 1.9 μsec reported by Eigen, *et al.*¹⁵

Results and Discussion

In Table I we have assembled molarities of H^+ and AlOH^{2+} calculated from the known total concentration C_0 , the experimental pH, eq 6–8, and the additional condition

$$C_0 \cong [\text{Al}^{3+}] + [\text{AlOH}^{2+}] \quad (9)$$

Also shown in Table I are our experimental dfe relaxation times τ . For an equilibrium such as that of eq 5, the appropriate expression for the relaxation time is¹⁶

$$\tau^{-1} = k_1 + k_{-1}([\text{H}^+] + [\text{AlOH}^{2+}]) \quad (10)$$

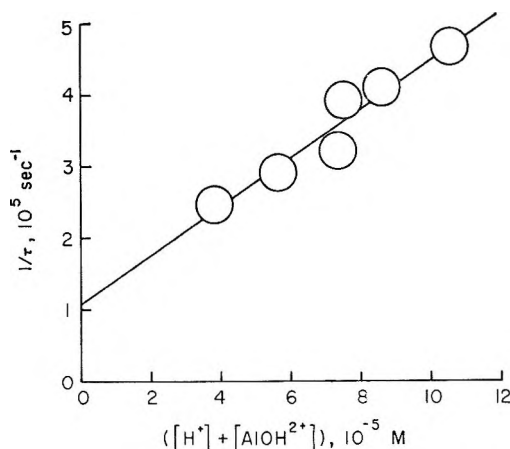


Figure 1. Plot of the reciprocal of the experimental dissociation field effect relaxation time τ vs. the sum of the hydrogen ion and AlOH^{2+} ion concentration at 25° . The points are experimental data, and the straight line is a least-squares fit of the data.

In Figure 1 we have plotted τ^{-1} vs. $[\text{H}^+] + [\text{AlOH}^{2+}]$. The slope of the least-squares straight line drawn through the data points is $k_{-1} = 3.37 \times 10^9 \text{ M}^{-1} \text{ sec}^{-1}$ and the intercept is $k_1 = 1.09 \times 10^5 \text{ sec}^{-1}$. The quotient $k_1/k_{-1} = 3.23 \times 10^{-5} \text{ M}$ is in fair agreement with eq 6. In principle, with values of τ for a more extended range of C_0 we would expect even better agreement between k_1/k_{-1} and K_1 . There are, however, compelling experimental reasons for limiting the range of C_0 . At values of C_0 appreciably higher than $4 \times 10^{-4} \text{ M}$, heating of the highly conducting sample solution by repeated high voltage pulses causes the bridge balance to drift markedly with consequent decreased reliability of the τ 's. At values of C_0 much below $5 \times 10^{-5} \text{ M}$, the maximum pulse duration of 12 μsec obtainable with all the coaxial cable available to us is not long enough to establish unequivocally the base line of the exponential conductance decay curves. Actually, the aluminum chloride solution is supersaturated with $\text{Al}(\text{OH})_3$ at dilutions greater than $C_0 = 10^{-5} \text{ M}$ according to Frink and Peech;¹¹ this in itself would preclude any significant extension of our τ^{-1} vs. concentration plot in the direction of higher dilutions even if more coaxial cable were available.

As is evident from the standard deviations of the τ 's shown in Table I, there is no reasonable basis for assuming that $k_1/k_{-1} = [\text{H}^+][\text{AlOH}^{2+}]/[\text{Al}^{3+}] = 3.23 \times 10^{-5} \text{ M}$ is more accurate than $K_1 = 10^{-5.02}$ of Frink and Peech.¹¹ Thus there is no justification for an iterative redetermination of $[\text{AlOH}^{2+}]$, k_{-1} , and so

(12) J. Kielland, *J. Am. Chem. Soc.*, **59**, 1675 (1937).

(13) W. Haller and H. C. Duecker, *J. Res. Natl. Bur. Std.*, **64A**, 527 (1960).

(14) D. T. Rampton, L. P. Holmes, D. L. Cole, R. P. Jensen, and E. M. Eyring, *Rev. Sci. Instr.*, **38**, 1637 (1967).

(15) M. Eigen, G. Ilgenfritz, and W. Kruse, *Chem. Ber.*, **98**, 1623 (1965).

(16) See ref 8, pp 901–905.

Table I: Calculated Molar Concentrations and Experimental Dissociation Field Effect Relaxation Times in Dilute Aqueous Aluminum Chloride at 25°

C_0^a $10^{-4} M$	pH ^b	$\sqrt{\mu}^c$ $10^{-2} M^{1/2}$	$\gamma_{Al^{3+}}^d$	$[H^+]^e$ $10^{-5} M$	$[AlOH^{2+}]^f$ $10^{-5} M$	τ_i^g μsec	n^h	k_{-1}^i $10^9 M^{-1} \text{sec}^{-1}$
4.004	4.256	4.90	0.636	5.83	4.73	2.16 ± 0.17	6	4.08
2.503	4.296	3.88	0.694	5.28	3.35	2.44 ± 0.44	6	4.34
2.002	4.379	3.47	0.718	4.34	3.19	2.55 ± 0.07	3	4.69
1.502	4.292	3.00	0.766	5.27	2.10	3.12 ± 0.34	4	3.89
1.001	4.432	2.45	0.786	3.81	1.84	3.45 ± 0.26	3	4.45
0.501	4.598	1.73	0.840	2.57	1.27	4.06 ± 0.13	4	5.21
								4.44 ± 0.53^j

^a Total molar concentration of aluminum chloride. ^b Glass electrode pH of the sample solution. ^c Square root of the same solution ionic strength $\mu \cong 6C_0$. ^d Activity coefficient of aluminum ion calculated from the extended Debye-Hückel relation, $-\log \gamma_i = [(0.509z_i^2\sqrt{\mu})/(1 + 0.33 \times 9\sqrt{\mu})]$. ^e Concentration of hydrogen ion $[H^+] = 10^{-\text{pH}}/\gamma_{H^+}$ where γ_{H^+} is calculated from the same Debye-Hückel form. ^f Concentration of $AlOH^{2+}$ calculated from eq 3 and 4 of the text. ^g Average experimental dissociation field effect relaxation time with standard deviation calculated from the range. ^h Number of independent determinations of the relaxation time. ⁱ Rate constant in water at 25° for the reaction $H^+ + AlOH^{2+} \rightarrow Al^{3+} + H_2O$. ^j Average rate constant with standard deviation calculated from the range.

on. A calculation of k_{-1} from each data point using the relation

$$k_{-1} = \tau^{-1} \left([H^+] + [AlOH^{2+}] + \frac{10^{-5.02}\gamma_{Al^{3+}}}{\gamma_{H^+}\gamma_{AlOH^{2+}}} \right)^{-1} \quad (11)$$

is instead preferable. The resulting values of k_{-1} are given in the last column of Table I. The average is $k_{-1} = (4.4 \pm 0.5) \times 10^9 M^{-1} \text{sec}^{-1}$. Although there is a systematic trend in $\sqrt{\mu}$, there is not a corresponding continuous trend to lower values of k_{-1} with decreasing $\sqrt{\mu}$. We would anticipate this latter trend from the fact that $z_{AZB} = +2$ in the Brønsted-La Mer relation¹⁷

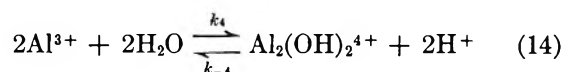
$$\log k = \log k_0 + 1.02z_{AZB}\sqrt{\mu} \quad (12)$$

If the true value of k_{-1} at $\sqrt{\mu} = 3 \times 10^{-2} M^{1/2}$ were $4.4 \times 10^9 M^{-1}$, the expected values of k_{-1} at the two limits of our experimental range would be $4.8 \times 10^9 M^{-1} \text{sec}^{-1}$ at $C_0 = 4 \times 10^{-4} M$ and $4.1 \times 10^9 M^{-1} \text{sec}^{-1}$ at $C_0 = 5 \times 10^{-5} M$. Both of these values lie within the limits of our experimental error and further emphasize the approximate nature of individual values of k_{-1} in Table I.

Before weighing the significance of the average value of k_{-1} , we must convincingly lay to rest the possibility that any other equilibrium in the system is responsible for the observed τ 's. The equilibrium $H^+ + OH^- \xrightleftharpoons{k_2} H_2O$ is clearly excluded since even the lowest¹⁸ of the reported values of k_2 , $7.2 \times 10^{10} M^{-1} \text{sec}^{-1}$, would give rise to τ 's nearly an order of magnitude shorter than those we have measured. Complexing of aluminum ion by chloride ion



and dimerization of aluminum ion



also suggest themselves as explanations for our measured relaxation times.

Kraus and co-workers^{19,20} found that at 25° even in 12 M HCl there is no evidence of complexing of Al(III) by chloride ion. As we noted earlier, the pH measurements of Frink and Peech confirm this conclusion.¹¹ If, however, we ignore the equilibrium evidence and plot our kinetic data in terms of the equation

$$\tau^{-1} = k_{-3} + k_3([Al^{3+}] + [Cl^-]) \quad (15)$$

we obtain a roughly linear plot with positive slope $k_3 \approx 2 \times 10^8 M^{-1} \text{sec}^{-1}$ and intercept $k_{-3} \approx 2 \times 10^5 \text{sec}^{-1}$. The quotient $k_{-3}/k_3 \approx 10^{-3} M^{-1}$ erroneously predicts detectable concentrations of $AlCl^{2+}$. However, the most persuasive argument against the importance of the complexing equilibrium, eq 13, is the improbability of so large a value of k_3 , as we show below.

Eigen^{21,22} briefly espoused the notion that ions showing strong hydrolysis such as Fe^{3+} , Be^{2+} , and Al^{3+} do not belong to the broad class for which the rate constant for replacement of a water molecule by a ligand L depends primarily on the rate of water exchange rather than the nature of L. The irregularities of Fe^{3+}

(17) C. W. Davies, *Progr. Reaction Kinetics*, **1**, 161 (1961).

(18) G. C. Barker and D. C. Sammon, *Nature*, **213**, 65 (1967).

(19) G. E. Moore and K. A. Kraus, *J. Am. Chem. Soc.*, **72**, 5792 (1950).

(20) K. A. Kraus, F. Nelson, and G. W. Smith, *J. Phys. Chem.*, **58**, 11 (1954).

(21) M. Eigen, "Advances in the Chemistry of the Coordination Compounds," S. Kirschner, Ed., The Macmillan Co., New York, N. Y., 1961.

(22) M. Eigen, *Pure Appl. Chem.*, **6**, 97 (1963).

substitution that misled Eigen have since been attributed to concurrent reaction pathways involving Fe^{3+} and the more rapidly substituted FeOH^{2+} rather than apparent ligand specificity.²³ Thus for ligands such as Cl^- , Br^- , SCN^- , SO_4^{2-} , and HN_3 , all the rate constants for the $\text{Fe}^{3+} + \text{L} \rightarrow$ reaction lie in the range 4.0 to $6.37 \times 10^3 \text{ M}^{-1} \text{ sec}^{-1}$ and for the $\text{FeOH}^{2+} + \text{L} \rightarrow$ reaction in the range 3×10^3 to $3 \times 10^5 \text{ M}^{-1} \text{ sec}^{-1}$ at 25° .^{23,24} The only analogous data²⁵ for Al^{3+} indicate a rate constant of at most $10^2 \text{ M}^{-1} \text{ sec}^{-1}$ for the complexing reaction $\text{Al}^{3+} + \text{SO}_4^{2-} \rightarrow \text{AlSO}_4^+$. Thus a rate constant as large as $2 \times 10^8 \text{ M}^{-1} \text{ sec}^{-1}$ for the reaction $\text{Al}^{3+} + \text{Cl}^- \rightarrow \text{AlCl}^{2+}$ or even $\text{AlOH}^{2+} + \text{Cl}^- \rightarrow \text{AlOHCl}^+$ is completely implausible.

To test the possibility that the dimerization equilibrium, eq 14, is responsible for the measured τ 's, we used the following equilibrium constant²⁶

$$10^{-6.27} = \frac{[\text{Al}_2(\text{OH})_2^{4+}][\text{H}^+]^2}{[\text{Al}^{3+}]^2} \quad (16)$$

valid at 25° and $\mu \approx 0$. This relation we combined with eq 6, 7, and 8, the measured pH, and the condition

$$C_0 = [\text{Al}^{3+}] + [\text{AlOH}^{2+}] + 2[\text{Al}_2(\text{OH})_2^{4+}] \quad (17)$$

to calculate concentrations of Al^{3+} , AlOH^{2+} , $\text{Al}_2(\text{OH})_2^{4+}$ and H^+ . The expression for the relaxation time of the dimerization equilibrium, eq 14, is

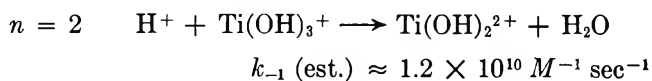
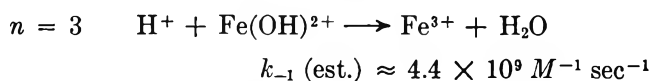
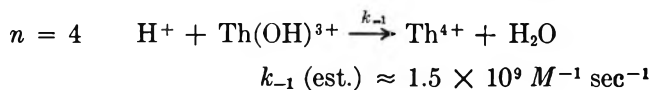
$$\frac{1}{4[\text{Al}^{3+}]\tau} = k_4 + k_{-4} \left(\frac{[\text{H}^+]^2 + 4[\text{H}^+][\text{Al}_2(\text{OH})_2^{4+}]}{4[\text{Al}^{3+}]} \right) \quad (18)$$

A plot of our experimental data in terms of eq 18 yields a shotgun pattern the linear least-squares fit of which has a negative slope $k_{-4} = -2.24 \times 10^4 \text{ M}^{-2} \text{ sec}^{-1}$ and an intercept $k_4 = 2.12 \times 10^9 \text{ M}^{-1} \text{ sec}^{-1}$. The scatter of the data and the negative rate constant provide adequate grounds for rejecting the dimerization equilibrium, eq 14, as the origin of our experimental relaxation times.

Drawing an analogy to the aqueous uranyl nitrate system for which the equilibrium constants²⁷ for mono-

meric hydrolysis, $K_1 = 2 \times 10^{-6}$, and dimerization, $K_2 = 1.2 \times 10^{-6}$, at 25° are quite similar to $\text{Al}(\text{III})$ and for which the dimerization rate constant²⁸ $k_4 \cong 116 \text{ M}^{-1} \text{ sec}^{-1}$ at 25° and $\mu = 0.1 \text{ M}$, we would predict an aluminum ion dimerization rate constant $k_4 \approx 10^2 \text{ M}^{-1} \text{ sec}^{-1}$ in water at 25° .

Having assured ourselves that the experimental relaxation times of Table I relate to the monomeric hydrolysis equilibrium, eq 5, we should note that a rate constant $k_{-1} = 4.4 \times 10^9 \text{ M}^{-1} \text{ sec}^{-1}$ is quite consistent with the rate constants cited by DeMaeyer and Kustin.³ In fact, the generalization that $k_{-1}(n+1)/k_{-1}(n) \approx 0.4$ for reactions of the type $\text{H}^+ + \text{M}^{(n+)-1} \xrightarrow{k_{-1}}$ appears to work so well that we can, for instance, predict with considerable confidence that at 25° in water



Available equilibrium data^{29,30} on aqueous thorium(IV) indicate that we could use the dfe relaxation technique to verify this predicted k_{-1} . On the other hand, the technically more interesting titanium equilibrium is unsuited for such an experiment since $\text{Ti}(\text{OH})_3^+$ is not observed³¹ at $\text{pH} > 0.3$.

(23) D. Seewald and N. Sutin, *Inorg. Chem.*, **2**, 643 (1963).

(24) M. Eigen and R. G. Wilkins, "Mechanisms of Inorganic Reactions," *Advances in Chemistry Series*, No. 49, R. F. Gould, Ed., American Chemical Society, Washington, D. C., 1965, pp 55-67.

(25) B. Behr and H. Wendt, *Z. Elektrochem.*, **66**, 223 (1962).

(26) H. Kubota, *Dissertation Abstr.*, **16**, 864 (1956).

(27) C. F. Baes, Jr., and N. J. Meyer, *Inorg. Chem.*, **1**, 780 (1960).

(28) M. P. Whittaker, E. M. Eyring, and E. Dibble, *J. Phys. Chem.*, **69**, 2319 (1965).

(29) S. Heitanen and L. G. Sillen, *Acta Chem. Scand.*, **13**, 533 (1959).

(30) E. Matijevic, M. B. Abramson, K. F. Schulz, and M. Kerker, *J. Phys. Chem.*, **64**, 1157 (1960).

(31) J. Beukenkamp and K. D. Herrington, *J. Am. Chem. Soc.*, **82**, 3025 (1960).

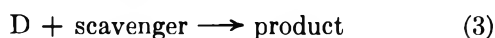
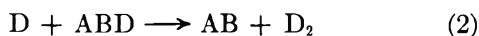
The Photochemistry of NCS^- in Solution

by M. Luria and A. Treinin

Department of Physical Chemistry, The Hebrew University, Jerusalem, Israel (Received August 7, 1967)

The photochemistry of NCS^- was investigated at wavelengths within its charge-transfer-to-solvent (CTTS) absorption band. Only a small yield of solvated electrons was detected; most of the excited ions dissociate to give CN^- (or HCN) + S pairs, which undergo efficient cage recombination. The increase of the quantum yield with NCS^- concentration is ascribed to self-scavenging: NCS^- scavenges the sulfur atom from the cage. This mechanism is verified by the use of allyl alcohol as a foreign scavenger for S atoms. The photolysis is strongly affected by varying the acidity around pH 7.5. This is attributed to acid-base equilibrium involving the excited ion.

The photochemistry of several molecules with 16 valence electrons appears to proceed by the following mechanism (in several cases concurrently with other mechanisms)



where AB is a stable molecule with 10 valence electrons (*e.g.*, N_2 , CO) and D is a six-electron intermediate (*e.g.*, NH, S, O), which may be either in its singlet or triplet state. D_2 is either stable or reacts



This scheme is applicable to the following molecules in the gas phase: carbon oxysulfide,¹ ketene,² nitrous oxide,³ diazomethane and diazirine,⁴ and probably HN_3 .⁵ In the case of N_3^- in solution, the solvent participates, probably by protonating the excited ion.⁶

The ion NCS^- is isoelectronic with OCS. However, the spectra of these molecules are rather dissimilar: the main absorptions of OCS and NCS^- above 200 m μ are due to $\pi \rightarrow \pi$ and charge-transfer-to-solvent (CTTS) transitions, respectively.^{1,7} In all the cases reported so far, the CTTS state yields solvated electrons; this determines the photochemistry of the halide ions⁸ and of polyatomic anions which are stable to bond rupture.⁹ However, for ions such as NCS^- and N_3^- , the excitation energy may be efficiently utilized to break the weak bonds. This has recently been verified in the case of N_3^- .¹⁰ Here we present the results for the photolysis of NCS^- . Previous work on this subject¹¹ is rather obsolete and seemed to require revision, employing new scavenger techniques.

Experimental Section

Light Sources. For 2537 Å, the low-pressure mercury arc lamp was used. The 1849-Å line was filtered out by

a 1-cm layer of 1 M KCl solution contained in a silica cell. Change of light intensity in the range $2\text{--}4 \times 10^{-5}$ einstein $\text{l}^{-1} \text{min}^{-1}$ was achieved by varying the position of the lamp with respect to the reaction vessel. Uranyl oxalate was employed for actinometry. For 2288 Å, a Cd/1 Osram lamp was used and differential actinometry with uranyl oxalate was carried out.¹²

Solutions and Procedure. Potassium thiocyanate of Analar grade was used without further purification, since recrystallization had no effect on our results. Moreover, at variance with previous work,¹¹ the same results were obtained with sodium and ammonium thiocyanates. Allyl alcohol was distilled under vacuum in an all-glass still. Some oxidation product, formed by ordinary distillation, was found to interfere. It could be identified by its absorption peaking at about 320 m μ . Water was redistilled from alkaline permanganate and then from dilute phosphoric acid. All other materials used were of Analar grade. Acetate, phosphate, and borate buffers, at about 10^{-2} M, were used to keep the pH constant within ± 0.05 unit. All experiments were carried out at 23°, and, unless otherwise stated, the solutions were not evacuated.

(1) H. E. Gunning and O. P. Strausz, "Advances in Photochemistry," Vol. 4, Interscience Publishers, Inc., 1966, p 143.

(2) G. B. Kistiakowsky and N. W. Rosenberg, *J. Amer. Chem. Soc.*, **72**, 321 (1950).

(3) J. P. Doering and B. H. Mahan, *J. Chem. Phys.*, **36**, 1682 (1962).

(4) H. M. Frey, *Advan. Photochem.*, **4**, 225 (1966).

(5) A. O. Beckman and R. G. Dickinson, *J. Amer. Chem. Soc.*, **50**, 1870 (1928); **52**, 124 (1930).

(6) I. Burak and A. Treinin, *ibid.*, **87**, 4031 (1965).

(7) E. Gusarsky and A. Treinin, *J. Phys. Chem.*, **69**, 3176 (1965).

(8) J. Jortner, M. Ottolenghi, and G. Stein, *ibid.*, **68**, 247 (1964).

(9) J. Barrett, M. F. Fox, and A. L. Mansell, *ibid.*, **69**, 2996 (1965);

M. Halmann and I. Platzner, *ibid.*, **70**, 2281 (1966); E. Hayon and J. J. McGarvey, *ibid.*, **71**, 1472 (1967).

(10) I. Burak, M. Mautner, D. Shapira, and A. Treinin, to be published.

(11) K. Jablczynski and H. Jablczynska, *Roczniki Chem.*, **10**, 579 (1930); *Bull. Soc. Chim.*, **49**, 877 (1931).

(12) M. Ottolenghi, *J. Amer. Chem. Soc.*, **85**, 3557 (1963).

An alcohol-phosphate mixture ($8 \times 10^{-2} M$ KH_2PO_4 , $10^{-2} M$ Na_2HPO_4 , and $1 M$ methanol) was used to scavenge electrons;¹³ in these experiments, the solutions were thoroughly evacuated and the amount of H_2 determined as described elsewhere.⁶

Analytical Methods. The photolysis was usually followed by determining the amount of CN^- produced. The alkali picrate method,¹⁴ properly standardized, was used for this purpose. NCS^- (up to $8 M$) and allyl alcohol (up to $4 M$) interfere little with this method (within $\pm 5\%$). The analysis was carried out as follows: 10 ml of 1% picric acid and 1 ml of 5% Na_2CO_3 were added to 10 ml of the irradiated solution, and the mixture heated in boiling water for 10 min. Then it was diluted to 100 ml and the absorbance measured at $540 m\mu$ (ϵ 2100 $M^{-1} \text{cm}^{-1}$). Sulfur was determined by extracting with chloroform and measuring the absorbance of the extract at $265 m\mu$ (ϵ 825 $M^{-1} \text{cm}^{-1}$). Sulfate was determined as BaSO_4 after leaving the solution for 24 hr until all the sulfur had back reacted with CN^- .

Results

The photolysis yields CN^- , sulfur, and little sulfate. (The latter is not produced in air-free solutions). The quantum yield of CN^- , φ_{CN^-} , decreases with irradiation time. This is due to: (a) inner filter effect of sulfur, especially at relatively low NCS^- concentration; (b) a fast back reaction (there is also a slow back reaction which is responsible for the gradual disappearance of the products after irradiation). The photolysis could be entirely suppressed by addition of CN^- . Still, at short irradiation times (up to 10 min) the yields were nearly linear with time, and so the initial quantum yields φ_i could be readily determined. The initial quantum yield, φ_i , increases with NCS^- concentration up to some limiting value ϕ_s , as shown in Figure 1 for two pH values. It appears that the pH has a pronounced effect on the photolysis, the yield increases with decrease of pH in a way that resembles

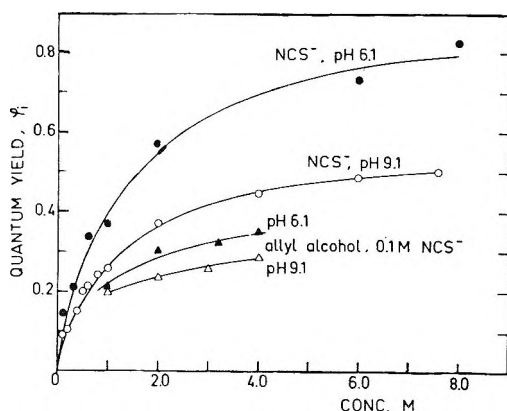


Figure 1. The effect of NCS^- and allyl alcohol concentrations on the quantum yield at pH 6.1 and 9.1.

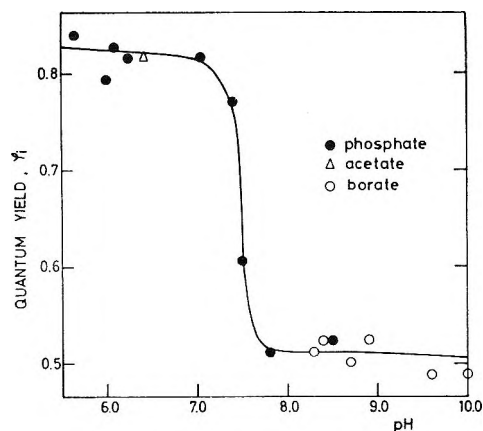


Figure 2. The effect of pH on the photolysis of $8 M$ NCS^- solutions.

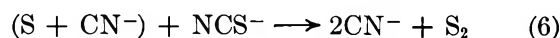
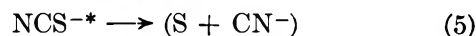
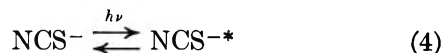
a neutralization curve. This is shown in Figure 2, where the results for $8 M$ NCS^- are recorded.

The photolysis of NCS^- in pure ethanol was studied and found to closely resemble that of basic aqueous solutions ($\text{pH} > 8$). However, allyl alcohol exerts a pronounced effect even at relatively small concentrations. It suppresses the formation of sulfur and its effect on φ_i (at $0.1 M$ NCS^-) is shown in Figure 1: φ_i increases with the allyl alcohol concentration and approaches a limiting value $\phi_a \sim \phi_s/2$.

Irradiation at $229 m\mu$ gives rise to higher yields, but no new features are revealed. At this wavelength, air-free solutions were also investigated. The evacuation had little effect on the quantum yields. In presence of the alcohol-phosphate mixture, some H_2 was produced, but φ_{H_2} was only 6% of φ_{CN^-} and it hardly changed when (NCS^-) was raised from 10^{-3} to $10^{-2} M$. The latter result is consistent with previous reports that NCS^- is a rather poor electron scavenger.¹⁵ Light intensity has no effect on φ_i .

Discussion

The results are consistent with the following mechanism



where parenthesis represents the solvent cage. Here we ignore acid-base equilibria and assume that all species involved are in their basic form. This problem will be discussed later.

The above mechanism resembles that proposed for

(13) J. Jortner, M. Ottolenghi, J. Rabani, and G. Stein, *J. Chem. Phys.*, **37**, 2488 (1962).

(14) F. B. Fisher and J. S. Brown, *Anal. Chem.*, **24**, 1440 (1952).

(15) E. J. Hart, S. Gordon, and J. K. Thomas, *J. Phys. Chem.*, **68**, 1524 (1964).

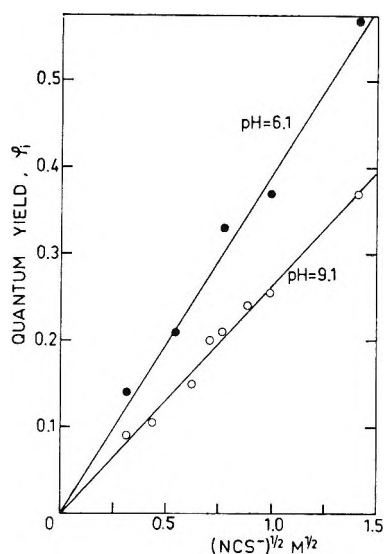


Figure 3. Noyes' relation for diffusion controlled scavenging.

the photolysis of OCS ,¹ but now it involves efficient cage recombination. It is a fine example of self-scavenging, where NCS^- itself scavenges the sulfur atom from the cage. For this reason, φ_i decreases with decrease of NCS^- concentration, approaching zero at $(\text{NCS}^-) = 0$ (Figure 1). On raising the concentration, a limiting yield is approached $\varphi_s = 2\phi_p$, where ϕ_p is the primary dissociation yield (the factor 2 accounts for the production of 2 molecules of CN^- by the scavenging reaction (6)). Noyes' equation for diffusion-controlled scavenging¹⁶

$$\varphi_i = \varphi_r + A(\text{NCS}^-)^{1/2}$$

is obeyed over a considerable range of concentrations (Figure 3). By a suitable choice of ϕ_p for each pH value, the data could be fitted to the general equation proposed by Jortner, Ottolenghi, and Stein¹⁷

$$\log(1 - \varphi_i/\phi_s) = B + C(\text{NCS}^-)^{1/2}$$

over the whole range of concentrations (Figure 4). The intercept ($B = 0$) and slope of the line appear to be independent of the pH, and from their values we obtain $\varphi_r = 0$ and $a(\pi k_6)^{1/2} = 0.20 \text{ M}^{-1/2}$, where φ_r

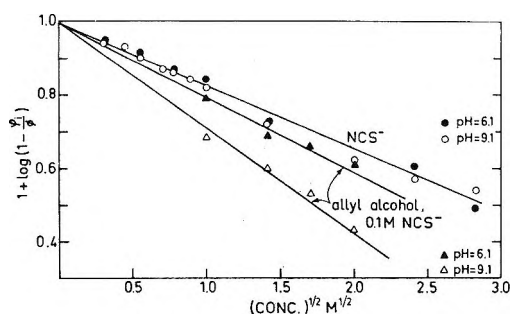
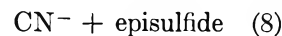
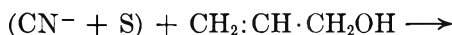


Figure 4. The J-O-S¹⁷ relation for diffusion-controlled scavenging. (ϕ is the limiting yield. For NCS^- alone $\phi = \phi_s$ was taken to be 1.2 and 0.77 at pH 6.1 and 9.1, respectively. For the allyl alcohol plots, $\phi = \phi_s/2$).

is the residual yield, k_6 is the rate constant of reaction 6, and a is a parameter characteristic of the cage (it specifies the recombination probability of the dissociation pairs). Thus, the scavenging reaction (6) and the cage parameters are pH independent. On the other hand, the primary dissociation yield, ϕ_p (so determined as to give the best agreement with the J. O. S. equation), does depend on the pH: $\phi_p(\text{pH } 6.1)/\phi_p(\text{pH } 9.1) \sim 1.5$. This is also evident from the plots of Noyes' equation (Figure 3): the ratio of the slopes of the lines ($A = 2\phi_p a(\pi k_6)^{1/2}$) for these pH values is close to 1.5. At $8 \text{ M } \text{NCS}^-$, the value of φ_i is about 70% of ϕ_s , and so Figure 2 may be used to show the dependence of ϕ_p on pH.

Reaction 6 is energetically plausible. The heats of formation of S and S_2 , as recently determined,¹ are 66 and 30.5 kcal, respectively, and so the scavenging of $\text{S}(^3\text{P})$ by NCS^- is exothermic to the extent of ~ 16 kcal (with $\text{S}(^1\text{D})$, the reaction is more exothermic, by 26.4 kcal).

Olefins are known to scavenge sulfur atoms to form episulfides and mercaptans.¹ This explains the effect of allyl alcohol on the photolysis

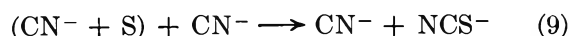


With increase of allyl alcohol concentration, a limiting yield ϕ_a is approached, which should equal ϕ_p , since only one molecule of CN^- is produced by reaction 8. And indeed our results indicate that $\phi_a \sim \phi_s/2$ (Figure 1), and this strongly supports the proposed mechanism. Moreover, with the values of ϕ_p derived as previously discussed, the data for the allyl alcohol experiments could be fitted to the equation

$$\log(1 - \varphi_i/\phi_p) = C(\text{allyl alcohol})^{1/2}$$

for allyl alcohol concentration higher than 1 M . At lower concentrations, there is competition between NCS^- and the alcohol, since they differ only little in their rates of scavenging. ($0.1 \text{ M } \text{NCS}^-$ solutions were used because at lower concentrations there is no total light absorption at $254 \text{ m}\mu$.) The Jortner¹⁷ plots for allyl alcohol also give $\varphi_r = 0$ (which is reasonable), but it appears that the alcohol scavenges sulfur a little better than NCS^- , and that the rate constant k_8 of reaction 8 is somewhat pH dependent. Thus the values of k_8/k_6 are 2.7 and 1.3 at pH 9.1 and 6.1, respectively. The reason for this variation with pH is still not clear.

The product CN^- also acts as a scavenger for the sulfur atom. The fast back reaction is probably

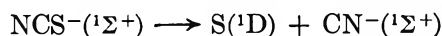


(16) R. M. Noyes, *J. Amer. Chem. Soc.*, **77**, 2042 (1955).

(17) J. Jortner, M. Ottolenghi, and G. Stein, *J. Phys. Chem.*, **66**, 2029 (1962).

Reactions between CN^- and the sulfur polymers also take place¹⁸ but they are relatively slow. They are responsible for the postradiation effects.

The zero value of φ_r at 254 $m\mu$ means that in absence of scavenger, the reunion of the dissociation products is very efficient. This indicates that they are separated with little excess of energy. The energy of the dissociation

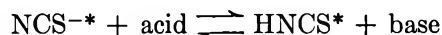


is *ca.* 106 kcal, *i.e.*, only 6.5 kcal less than the energy provided by 254 $m\mu$ photons. (But if intersystem crossing leads to the formation of $\text{S}(^3\text{P})$, the excess of energy may be 33 kcal.) With 229- $m\mu$ photons, the energy imparted is larger by 12.5 kcal, and indeed both φ_r and ϕ_p appear to be larger at this wavelength. However, the actinometry is not very reliable at 229 $m\mu$ and so quantitative conclusions cannot yet be obtained.

Both wavelengths investigated are within the CTTS band of NCS^- . Nevertheless, only a small yield of solvated electrons could be detected. Internal conversion or intersystem crossing appear to efficiently compete with the dissociation of the CTTS state to NCS^- radicals and solvated electrons. It was found that ^1D sulfur atoms react with paraffins by insertion.¹ The absence of any distinct effect of ethanol on the photolysis of NCS^- suggests that the sulfur atoms are formed in their triplet state. Still, they may be formed in their ^1D state and undergo fast deactivation by collisions. Moreover, there is no evidence for the reaction of $\text{S}(^1\text{D})$ with alcohols. Theoretically, CTTS transitions may readily lead to triplets, since in the

CTTS state the electron is detached from the radical and so spin reversal may be efficient.

Finally, the effect of pH on the photolysis should be considered. In the pH region studied, practically all the thiocyanate is present as NCS^- , and indeed no change of optical absorption could be detected in this region. On the other hand, the pH dependence of the photolysis suggests that some acid-base equilibrium does play a prominent role in the mechanism. That equilibrium is attained is proved by the observation that the nature of the buffer has no effect. We believe that the excited ion is involved in the following equilibrium



and that the primary dissociation yield ϕ_p of HNCS^* is higher than that of NCS^* . HNCS^* appears to be a weak acid with $\text{p}K \sim 7.5$ (Figure 2). According to the foregoing discussion, the excited states involved in this equilibrium may be triplets.

The sulfate formed in aerated solutions is probably due to oxidation of atomic sulfur; *i.e.*, O_2 competes with other scavengers present on the sulfur atoms. This view is supported by the observation that the yield of SO_4^{2-} decreases with the thiocyanate concentration and at 8 *M* NCS^- no SO_4^{2-} could be detected.

Acknowledgments. We are indebted to Dr. M. Ottolenghi for some valuable discussions and gratefully acknowledge the support of this research by the U. S. Army (Contract No. DAJA37-67-C-01767).

(18) P. D. Bartlett and R. E. Davis, *J. Amer. Chem. Soc.*, **80**, 2513 (1958).

The Enthalpy of Fusion of Linear Polyethylene¹

by L. Mandelkern, A. L. Allou, Jr., and M. Gopalan

Department of Chemistry and Institute of Molecular Biophysics, Florida State University, Tallahassee, Florida
(Received August 10, 1967)

The enthalpy of fusion of molecular weight fractions of linear polyethylene, crystallized under a variety of controlled conditions, has been measured. For samples crystallized in the bulk, the enthalpy of fusion is very dependent on the molecular weight. For a given crystallization procedure, there is a monotonic decrease in this quantity with increasing molecular weight, so that a wide range of values are observed. A comparison of the degree of crystallinity calculated from enthalpy of fusion and density measurements indicates a very good agreement for samples which are never cooled below the initial crystallization temperature. However, for samples which are subsequently cooled to room temperature, the enthalpy measurements give lower values for the degree of crystallinity than does the density. This result is attributed to the small-size crystallites which form on cooling and the associated contribution from the interfacial enthalpy. In contrast to the above results, the enthalpy of fusion of crystals formed from dilute solution is independent of molecular weight and depends only on the crystallite size. The interfacial enthalpy and entropy of such crystals, calculated from the experimental data, are discussed in terms of different morphological models that have been proposed.

Introduction

The melting of a collection of crystalline long-chain molecules has been demonstrated to be a first-order phase transition.² However, for a variety of morphological reasons, broad fusion curves and depressed melting temperatures are characteristically observed.^{2,3} In addition, there is usually a significant lowering in the values of the pertinent thermodynamic quantities, such as the density³ and enthalpy of fusion.^{4,5} The more detailed reasons for these deviations from idealized behavior can be attributed to the finite size of the crystals in the chain direction,⁶ the molecular nature of the interfacial region,⁶ and the conformational differences and associated thermodynamic properties of the chain units in the interzonal regions which connect crystallites.^{6,7} Thus it has been shown that thermodynamic,^{3,5} mechanical,⁶ and spectral properties⁸ are very sensitive to morphological detail, so that a large range in properties can be observed, depending on the details of the crystallization process. Controlled changes in the crystallite size and interfacial region can be achieved by utilizing molecular weight fractions and varying the crystallization conditions, particularly the crystallization temperature.

A detailed study of thermodynamic properties should enable the development of a better understanding and insight into the molecular nature of the interfacial and interzonal regions and how they depend on the mode of crystallization. Modern developments in instrumentation have allowed enthalpies of fusion to be measured utilizing very small amounts of material.^{4,9,10} Thus

the properties of molecular weight fractions of high polymers, where the supply of the sample is invariably limited, can be studied. In the present paper, we report the results and analysis of enthalpy of fusion measurement on fractions of linear polyethylene encompassing a very wide molecular weight range. The crystallizations were conducted under a variety of controlled conditions from both the melt of the pure polymer and also from very dilute solutions. By these methods, it was possible to obtain samples which possessed a range in crystallite sizes and a diversity of interfacial structures and properties. A preliminary report of the results for bulk samples, crystallized at a high temperature and subsequently cooled to room temperature, has been previously given.⁴

Experimental Section

With one exception, molecular weight fractions of linear polyethylene were used in this study. The frac-

(1) This work was supported in part by the Army Research Office (Durham) and the Division of Biology and Medicine, Atomic Energy Commission.

(2) L. Mandelkern, "Crystallization of Polymers," McGraw-Hill Book Co., Inc., New York, N. Y., 1964.

(3) J. G. Fatou and L. Mandelkern, *J. Phys. Chem.*, **69**, 417 (1965).

(4) L. Mandelkern, J. G. Fatou, R. Denison, and J. Justin, *J. Polymer Sci.*, **B3**, 803 (1965).

(5) L. Mandelkern, *ibid.*, **C15**, 129 (1966).

(6) L. Mandelkern, J. M. Price, M. Gopalan, and J. G. Fatou, *ibid.*, **A2-4**, 385 (1966).

(7) R. Chiang and P. J. Flory, *J. Am. Chem. Soc.*, **83**, 2857 (1961).

(8) T. Okada and L. Mandelkern, *J. Polymer Sci.*, **A2-5**, 239 (1967).

(9) E. S. Watson, M. J. O'Neill, J. Justin, and N. Brenner, *Anal. Chem.*, **36**, 1233 (1964).

(10) A. P. Gray and K. Casey, *J. Polymer Sci.*, **B2**, 381 (1964).

tionation procedure and characterization of the fractions have been previously described in detail.³ The viscosity average molecular weights ranged from 1.20×10^4 to 1.47×10^6 . To investigate, the influence of very high molecular weight on the properties of an unfractionated sample of $M_\eta = 7 \times 10^6$ was also studied.

The specimens for study were crystallized either from the pure melt or from very dilute solutions. Two distinctly different kinds of procedures were utilized for the bulk crystallization. In all cases, however, the samples were first melted at 155–160° for 20 min and then the crystallization procedure initiated. In one kind of experiment, the samples were crystallized at a predetermined temperature for a given period of time and then cooled to room temperature. In the other category, the samples were crystallized in the calorimeter and, simultaneously, in a dilatometer at a given temperature for a predetermined time and never cooled below the crystallization temperature. The time for the crystallization was set so that the accelerated portion of the transformation was completed and the protracted crystallization was taking place.² The resulting data, discussed below, indicate that a definite distinction must be made between these crystallization procedures.

In one set of experiments, involving bulk crystallization, the specimens were wrapped in aluminum foil and immediately transferred from the high-temperature thermostat to water at 23°. For the crystallization at elevated temperature, which involved long times, the samples were crystallized isothermally in sealed evacuated tubes. One series was maintained at 130° for 30–40 days and cooled to room temperature over a 24-hr period. Other specimens were crystallized at 120° for 5–7 days and then cooled to room temperature. The crystallization at intermediate temperatures was carried out the same way. The times of crystallization were adjusted based on crystallization kinetic studies,^{2,11} so that no additional significant crystallization was expected at the crystallization temperatures.

The samples, thus prepared, particularly those crystallized at 130° for long times, were monitored for possible oxidation by the examination of the infrared absorption spectra in the region 1709–1729 cm^{-1} . Except in a few instances, where the specimens were discarded, the samples displayed no evidence of oxidation. Samples which were oxidized, either inadvertently or deliberately, are characterized by abnormally high densities and low enthalpies of fusion and thus become easily recognizable.

Crystals were also prepared from dilute (0.05–0.1%) solutions of *p*-xylene. The crystallization was carried out, isothermally, in the temperature range 60–90° for periods of time varying from 3 days to 3 weeks, depending on the crystallization kinetics. The precipitate was separated from the supernatant either by cooling to room temperature and then filtering, or by filtering

at the crystallization temperature and then cooling. The same results were obtained by either procedure. The samples were dried *in vacuo* at 45°.

For all the samples cooled to room temperature, the densities were determined at 25° in a toluene–dioxane gradient column, which was calibrated with glass floats. The densities could be measured to $\pm 0.0005 \text{ g/cc}$. As has been previously reported,³ the densities of samples thus determined agree to better than 3 parts per 1000 with corresponding samples in a dilatometer which had undergone similar crystallization procedures. The densities of the samples, which were never cooled below the crystallization temperature, were determined from the dilatometer readings.

The crystallite thickness, at room temperature, of the dilute-solution prepared specimens was determined from low-angle X-ray diffraction measurements using a Rigaku-Kenki camera. The well-defined maxima were converted to linear dimensions by means of Bragg's law. The experimental uncertainty is estimated to be $\pm 4^\circ \text{\AA}$.

The heats of fusion were measured with a Perkin-Elmer DSC-1 or DSC-1B differential scanning calorimeter.⁹ Typical examples of the calorimeter's performance and the resulting data, for both bulk and solution crystallized samples, have already been given in detail.^{4,12} The operation of the instrument was adjusted so that the area under the fusion curve was always in the range of 10 in.² To properly delineate the area to be measured, cognizance must be taken of the onset of fusion at a temperature below which the major portion of the melting occurs.¹² At a heating rate of 5°/min, the measured enthalpy of fusion per gram was independent of the mass used in the range 3–17 mg. The uncertainty of the results under these conditions, for repetitive experiments utilizing the same sample, was well within the range of $\pm 1 \text{ cal/g}$. An uncertainty in the base-line delineation exists when smaller size samples are used. Under these latter conditions, there is a larger experimental error. Sample sizes in the range of 3 mg were used in this work but in selected controlled experiments increasing sample weights were also studied. Within the range cited, identical values for the enthalpies of fusion were obtained with heating rates of either 5 or 10°/min. The value of the heat of fusion of the polymer sample was determined by comparing the area under its fusion curve with that obtained with a known weight of indium heated under the same conditions.

The dilatometric procedures employed here have already been described in detail.^{3,13,14} The density and

(11) J. G. Fatou and L. Mandelkern, unpublished results.

(12) L. Mandelkern and A. L. Allou, Jr., *J. Polymer Sci.*, **B-4**, 447 (1966).

(13) P. J. Flory, L. Mandelkern, and H. K. Hall, *J. Am. Chem. Soc.*, **73**, 2532 (1951).

(14) L. Mandelkern and P. J. Flory, *ibid.*, **73**, 3206 (1951).

specific volume measurements were converted to a degree of crystallinity by means of the relation and constants given by Chiang and Flory.⁷

Results and Discussion

Bulk Crystallized Samples. The enthalpies of fusion and densities that were obtained for the samples crystallized isothermally from the pure melt for extended time periods and then cooled to room temperature are summarized in Figures 1 and 2, respectively. The quantities of interest are plotted against the logarithm of x , the number of CH_2 units per chain, for the different crystallization temperatures. The more extensive data that are given here for samples crystallized at 130° are very similar to the preliminary results previously reported⁴ and the trends discerned earlier are further substantiated. At this latter crystallization temperature, for x equal to or less than approximately 3×10^3 , the plotted densities and enthalpies of fusion are comparable to the values expected for a large macroscopic crystal. From the dimensions of the unit cell,¹⁵ the density should be 1.00 at room temperature. An enthalpy of fusion 69 ± 1 cal/g is also expected from independent analyses and experiment.^{16,17} Densities as high as 0.99 and enthalpies of fusion of 66 cal/g are directly observed in this molecular weight range. As the molecular weight is in-

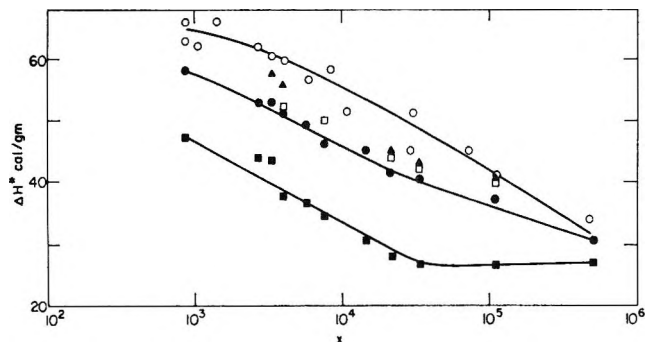


Figure 1. Plot of enthalpy of fusion, ΔH^* as a function of chain length x for samples initially crystallized at indicated temperatures and cooled to room temperature; crystallization temperatures: \circ , 130° ; \blacktriangle , 126° ; \square , 124° ; \bullet , 120° ; and \blacksquare , 23° .

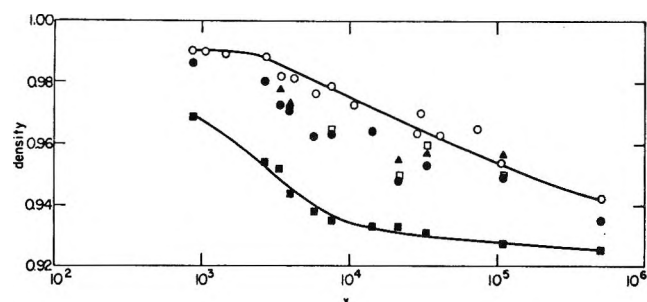


Figure 2. Plot of density as a function of chain length x for samples initially crystallized at indicated temperatures and cooled to room temperature; crystallization temperatures: \circ , 130° ; \blacktriangle , 126° ; \square , 124° ; \bullet , 120° ; and \blacksquare , 23° .

creased, however, these quantities decrease monotonically. For the highest molecular weight sample studied here, the density has been reduced to 0.94 and the enthalpy of fusion to 34 cal/g. Thus, despite the very stringent conditions of high temperature and long crystallization times, a wide range in values, which depend on molecular weight, is observed for these thermodynamic quantities.

At the lower temperatures of crystallization, which are characterized by more rapid rates of crystallization, there is also a systematic change in the density and enthalpy of fusion with molecular weight. For $x \leq 10^5$, these quantities decrease with the lowering of the crystallization temperature at a given molecular weight. There is, therefore, a corresponding decrease with increasing chain length, at a fixed crystallization temperature. However, when x exceeds 2×10^4 , the change with molecular weight becomes very small so that the curve representing the data intersects and joins the one delineating the results for crystallization at 130° . For the samples which were quickly transferred from the melt to room temperature, this intersection has not as yet occurred over the molecular weight range presently available for study. The trends in the data indicate that this intersection will occur for a molecular weight of the order of 10^7 . The density and enthalpy of fusion expected at this point are 0.925 g/cc and 25 cal/g, respectively. These latter values are actually observed for quenched specimens of the highest molecular weight sample and represent the lowest values that have been reported for linear polyethylene. These low values are obtained from a crystallization procedure wherein the samples spend a minimal time at the elevated temperature. These results must, therefore, be a consequence of the crystallization process and the morphology that results and cannot be attributed to any oxidation during crystallization.

Hendus and Illers¹⁸ have recently reported enthalpy of fusion measurements for molecular weight fractions which were slowly cooled from the melt to room temperature. Although this is a relatively undefined crystallization procedure, the slow cooling process does insure that some crystallization occurs at elevated temperatures. Their results are qualitatively similar to those reported here. For $M_w \leq 4 \times 10^4$, the enthalpies of fusion are slightly greater than 60 cal/g, but not as high as those in Figure 1 for the 130° crystallization. As the molecular weight increases beyond this value, the enthalpy of fusion monotonically decreases. For $M = 1 \times 10^6$, the enthalpy of fusion has decreased to 35 cal/g. For the lower molecular weights, the enthalpy of fusion results correspond to those obtained

(15) C. W. Bunn, *Trans. Faraday Soc.*, **35**, 482 (1939).

(16) F. A. Quinn, Jr., and L. Mandelkern, *J. Am. Chem. Soc.*, **80**, 3178 (1958); **81**, 6533 (1958).

(17) M. G. Broadhurst, *J. Res. Natl. Bur. Std.*, **66A**, 241 (1963).

(18) H. Hendus and K. H. Illers, *Kunststoffe*, **57**, 193 (1967).

Table I: Thermodynamic Parameters for Samples Crystallized in Calorimeter

Mol wt	T_c , °C	t , min	Crystallized in calorimeter				Cooled to room temperature			
			ΔH^* , cal/g	$(1 - \lambda)\Delta H$	$(1 - \lambda)d^a$	Ratio	ΔH^*	$(1 - \lambda)\Delta H$	$(1 - \lambda)d$	Ratio
7×10^6	125	140	18.8	0.27	0.28	0.96				
		317	20.7	0.29	0.29	1.0				
		1087	21.5	0.30	0.30	1.0				
	123	20	15.6	0.22	0.22	1.0				
		100	17.1	0.24	0.26	0.92				
	120	22	25.0	0.35	0.34	1.0	30.5	0.43	0.60	0.72
4.7×10^5	125	1065	35.7	0.50	0.53	0.94				
	123	720	38.0	0.54	0.53	1.0	41.5	0.59	0.71 ^b	0.83
3.7×10^5	128	1140	37.4	0.52	0.53	0.98				
	127	960	37.6	0.53	0.55	0.96	44.0	0.62	0.74	0.84
2×10^5	128	900	46.04	0.65	0.67	0.97				
	128	2467	49.1	0.69	0.70	0.99	54.3	0.77	0.81	0.95
5.6×10^4	128	975	52.6	0.74	0.76	0.97	56.6	0.81	0.83	0.98

^a Determined from dilatometer measurements under the same conditions of crystallization temperature and time. ^b Crystallized initially at 120°.

by isothermal crystallization at 126° and subsequent cooling to room temperature. For the higher molecular weights, the results are similar to those obtained after crystallization at 130°. Of major interest is the confirmation of the influence of molecular weight on the enthalpy of fusion and the further demonstration of the relatively low values obtained for the highest molecular weights studied.

The data for the samples crystallized in the calorimeter and never cooled to room temperature are summarized in Table I. Also given in the table are the values obtained after cooling to room temperature over a 24-hr period. Because of the unduly long times that are involved, the crystallization in the calorimeter could not be conducted at 130°. The densities are reported in terms of the degree of crystallinity, calculated according to the relation⁷

$$(1 - \lambda)_d = \frac{\bar{V}_A - \bar{V}}{\bar{V}_A - \bar{V}_c} \quad (1)$$

Here \bar{V}_A is the specific volume of the completely amorphous polymer, \bar{V}_c the corresponding quantity for the crystalline polymer, and \bar{V} is the specific volume of the actual system. The values of ΔH^* and the density are, as expected, much lower than those obtained under similar initial crystallization conditions with subsequent cooling to room temperature.^{3,4} The increases that occur in these quantities upon cooling, which is a consequence of further crystallization, become more pronounced as the molecular weight is increased. This is in accord with a previous report of the densities obtained after isothermal crystallization at 130°.³ In these latter experiments, for example, when $M = 1.5 \times 10^6$, the degree of crystallinity increases from 0.37 to 0.70 upon cooling. On the other hand, for $M = 2 \times 10^4$, the relatively small change of from only 0.82 to 0.96 is observed. An examination of the data,

prior to the cooling of the samples, indicates that the thermodynamic quantities depend on molecular weight in a manner qualitatively similar to that which has been cited above. The measured enthalpy of fusion decreases from 52.6 to 20 cal/g, under comparable crystallization conditions, as the molecular weight is increased. Similar changes are observed in the density.

It is of interest to examine the enthalpy of fusion data in terms of the molecular nature of the crystalline state that is actually formed. A formal and general expression can be developed which describes the enthalpy difference between the crystalline polymer and the pure melt for various morphologies that can evolve. We consider a system of n crystallites, which are uniform in size and which contain ρ crystalline sequences each of length ζ . The degree of crystallinity $1 - \lambda$ is defined as

$$1 - \lambda = \frac{n\zeta\rho}{N_0} \quad (2)$$

where N_0 is the total number of units in the system.

If H is defined as the enthalpy per unit, prior to complete fusion, then

$$N_0H = (N_0 - n\zeta\rho)H_a + n\zeta\rho(1 - \alpha)H_c + \alpha n\zeta\rho H_d + 2n\rho\Delta H_e \quad (3)$$

Here H_a is the enthalpy per unit of the noncrystalline units, which are identified with the enthalpy of a unit in the pure melt; H_c is the corresponding enthalpy per unit in the completely crystalline state; α is the fraction of units per sequence, within the interior of the crystal which is defected, each such unit contributing an excess enthalpy H_d ; and ΔH_e is the enthalpy deficiency per sequence at the terminus of each crystalline sequence. It is equivalent to the enthalpic contribution to the interfacial free energy and as such contains

the contribution of the chain units which comprise the interfacial region. Equation 3 can be rewritten as

$$\Delta H^* = (1 - \lambda) \left(\Delta H_u - \frac{2\Delta H_e}{\zeta} + \alpha \Delta H_d \right) \quad (4)$$

Here ΔH^* is the measured enthalpy of fusion per repeating unit, ΔH_u is the corresponding quantity for fusion of a completely crystalline polymer, and ΔH_d is defined as $H_e - H_d$. Equation 4 contains contributions from a variety of sources and indicates many reasons why the observed enthalpy of fusion can be less than the value expected for a large completely crystalline nondefected substance.

In the absence of internally defected structures, eq 4 reduces to

$$\Delta H_u - \frac{\Delta H^*}{1 - \lambda} = \frac{2\Delta H_e}{\zeta} \equiv B \quad (5)$$

If the degree of crystallinity calculated from enthalpy measurements is defined in a manner analogous to that of eq 1, namely that

$$(1 - \lambda)_{\Delta H} = \frac{\Delta H^*}{\Delta H_u} \quad (6)$$

then eq 5 becomes

$$1 - \frac{(1 - \lambda)_{\Delta H}}{(1 - \lambda)_d} = \frac{2\Delta H_e}{\zeta \Delta H_u} \quad (7)$$

Inherent in the definitions of $(1 - \lambda)_d$ and $(1 - \lambda)_{\Delta H}$ that have been given above are the assumption that the contributions of the ordered and nonordered regions are additive. In addition, any possible contribution from the interfacial region to the quantity in question is tacitly neglected. A similarly defined degree of crystallinity can be obtained from infrared absorption^{8,19} and from wide-angle X-ray diffraction.^{19,20} It has recently been shown that for linear polyethylene samples which encompass a very wide range in density, there is very good accord between the values of the degree of crystallinity calculated from the density, wide-angle X-ray,^{19,20} and infrared absorption^{8,19} data. For these cases, therefore, there is either no significant contribution from the interfacial regions or these contributions are self-compensating. The latter circumstance would be a highly unlikely coincidence.

The data reported here for the density and enthalpy of fusion under a variety of crystallization conditions can also be used as a basis of comparison between $1 - \lambda$, as defined by eq 1 and 6. We consider first the data, summarized in Table I, for the samples never cooled below the crystallization temperature. Under these circumstances, as can be seen from columns 5 and 6 in the table, there is excellent accord between the two quantities over a range of $1 - \lambda$ from about 0.75 to 0.20. In this and subsequent calculations, ΔH_u has been taken to be 70 cal/g. Consequently, it must be

concluded that the term $(2\Delta H_e)/(\zeta \Delta H_u)$ must be negligibly small in these cases. This conclusion implies the existence of either a large value of ζ or a characteristically small value of the ratio $\Delta H_e/\Delta H_u$.

In order to pursue the matter in more detail, these latter quantities must be independently determined. All the required information is not available at present. There are, however, some data with respect to the molecular weight dependence of crystallite sizes, as determined from electron microscope studies of replicas of fracture surfaces.⁶ These results are limited, however, for samples crystallized at 130° for long time periods and then cooled to room temperature. Characteristic lamella-like crystallites are observed over the complete molecular weight range and the sizes in the chain direction were found to be dependent on chain length. The size analysis that was made⁶ was restricted to the thickest or largest size grouping of lamella present. It was observed, however, that for $M > 5.6 \times 10^4$, thinner lamella were also present, their profusion increasing with molecular weight. For molecular weights corresponding to $x \leq 1-2 \times 10^3$, the average size ζ corresponds very closely to the chain length x . Such crystallites have been termed extended chain crystals. As x increases to 4×10^3 , the crystallite thickness increases from about 600 to 900 units, so that the ratio of crystallite size to chain length decreases to about 0.2. With a further increase in molecular weight to 5.7×10^5 (the upper molecular weight limit of the electron microscope measurements), the crystallite thickness reaches an upper limit of about 1000-1200 CH₂ units. The ratio of the crystallite size to extended chain length thus becomes very small. The above represents the only available experimental data concerned with crystallite sizes that are pertinent to the problem at hand.

A reasonable assumption can be made that the larger sizes that were observed are representative of the crystallites formed at the elevated temperature of crystallization.^{2,21} Hence, for the higher molecular weights, since ζ is of the order of 10^3 , rather large values of the ratio $\Delta H_e/\Delta H_u$ can be tolerated and still allow for concordance in the degree of crystallinity calculations. For example, if $\Delta H_e/\Delta H_u = 10$, $(1 - \lambda)_{\Delta H}/(1 - \lambda)_d = 0.98$, which is consistent with the experimental observation. Thus, even a value as high as 10,000 cal/mole of sequences for ΔH_e would not reflect itself in a disparity in the degree of crystallinity calculations. For the lower molecular weights, when ζ becomes comparable to x , there must be a change in interfacial structure consistent with the extended chain crystals that are formed. A reduction in ΔH_e , accompanying the lowered crystallite size, would allow for the observed experimental agreement between the

(19) H. Hendus and G. Schnell, *Kunststoffe*, **51**, 69 (1960).

(20) M. Gopalan and L. Mandelkern, *J. Polymer Sci.*, **5B**, 925 (1967).

(21) M. R. Gopalan and L. Mandelkern, *J. Phys. Chem.*, in press.

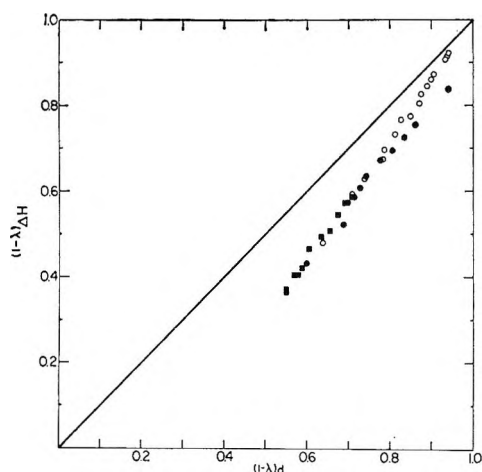


Figure 3. Plot of degree of crystallinity calculated from enthalpy measurements as a function of same quantity calculated from density for samples initially crystallized at indicated temperature and cooled to room temperature; crystallization temperatures: O, 130°; ●, 120°; and □, 23°.

calculated degrees of crystallinity in this molecular-weight range. Since the exact crystallite sizes or size distributions under these conditions of crystallization are not known, a more detailed analysis cannot be given at present. However, the magnitude involved and the change suggested in ΔH_e with molecular weight is consistent with the values for the interfacial free energy.^{6,22} Two independent studies^{6,22} of the dependence of the melting temperature on crystallite size and molecular weight have yielded concordant results for the interfacial free energies to be assigned the mature crystallites. For molecular weights greater than 5×10^4 , an asymptotic value of between 8000 and 9000 cal/mole of crystalline sequences was obtained for the interfacial free energy of the crystallites formed. As the molecular weight decreased, with the concomitant increase in the ratio ζ/x , the interfacial free energy decreases and reaches a value slightly less than 5000 cal/mole for the lowest molecular weight of interest in the present work.

A comparison of the degrees of crystallinity for the samples crystallized at the elevated temperatures and then cooled to room temperature are summarized in Figure 3. It is clear from the figure that these results are quite different from those just discussed for specimens never cooled below the crystallization temperature. Except at the very high levels of crystallinity, which are obtained with the lowest molecular weights studied, there is a significant disparity between the two different methods of calculation the degree of crystallinity. The calculations based on the enthalpy of fusion measurements consistently yield lower values than those obtained from the density measurements utilizing the Chiang-Flory⁷ specific volume of 1.17 cm³/g for the completely amorphous polymer at 25°. Utilizing the slightly lower value 1.16 cm³/g that has been suggested^{18,19} for this specific volume reduces this dif-

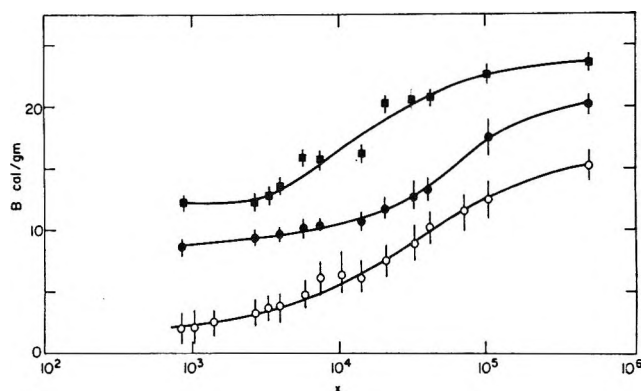


Figure 4. Plot of quantity B as function of chain length x for samples initially crystallized to elevated temperature and then cooled to room temperature; crystallization temperatures: O, 130°; ●, 120°; and ■, 23°.

ference slightly. The divergence between the two sets of values becomes larger as the level of crystallinity becomes smaller. The concordance previously noted between the degrees of crystallinity obtained from density, infrared absorption, and wide-angle X-ray diffraction is for samples cooled to room temperature. The enthalpy of fusion measurements are thus unique at present in yielding lower values for the degree of crystallinity for this particular mode of crystallization.

The differences between the two basically different kinds of crystallization procedures, as manifested by a comparison of the data in Table I and Figure 3, cannot be attributed either to the samples or the technique of measurements, since they are identical in both cases. Neither can the range in the level of crystallinity be involved, since there is a significant overlapping in these values. The difference must therefore reside in the crystallization procedure with a major contribution thus expected to come from the properties of the crystallites formed on cooling. For example, for the samples initially crystallized at 130°, a much higher proportion of the crystallinity eventually developed is found in the higher molecular weight samples as compared to the lower ones. Concomitantly, the disparity in the calculations is greater for the higher molecular weight fractions. On cooling, much smaller size crystallites are expected, since the sizes are primarily controlled by nucleation processes^{2,21} and thus on the crystallization temperature. Since extended chain crystals will now not be formed, except in the extreme of very low molecular weight, a compensation or lowering of the value of ΔH_e would not be anticipated. Consequently, there could be a major contribution to the measured enthalpy of fusion from the term $(2\Delta H_e)/\zeta \equiv B$. In this event, the simple additivity law, as embodied in eq 6, would not be valid to calculate the degree of crystallinity. Values of the quantity B , calculated according to eq 5, are plotted in Figure 4 as a function

(22) J. M. Schultz, W. H. Robinson, and G. M. Pound, *J. Polymer Sci.*, **A2-5**, 511 (1967).

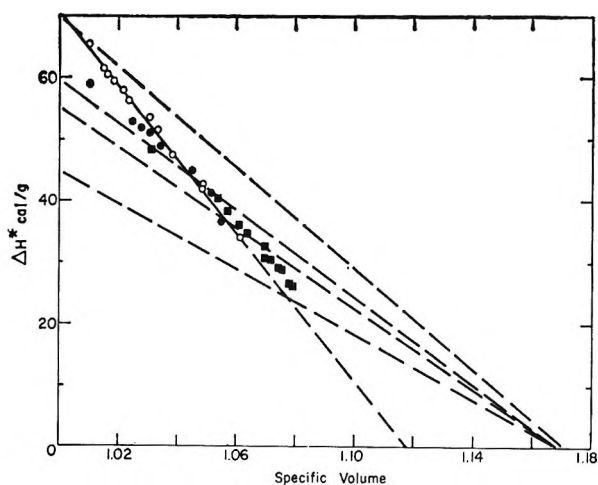


Figure 5. Plot of enthalpy of fusion as function of specific volume; dashed straight lines (curves 1-4 from top to bottom, respectively) calculated according to eq 8 for $B = 0$, curve 1; $B = 10$, curve 2; $B = 15$, curve 3; and $B = 25$, curve 4. Crystallization conditions are the same as in preceding figures.

of molecular weight for each of the crystallization temperatures. Although the values of B are definitely dependent on the crystallization temperature, the qualitative dependence on molecular weight is the same in all cases. Relatively constant values are calculated for the lower molecular weights, but a rapid increase occurs when x exceeds 3×10^4 . For $x > 10^5$, an asymptotic value of B , which is characteristic of each crystallization temperature, appears to be reached. For a given molecular weight, the value of B decreases with an increase in the initial crystallization temperature. The quenched samples have the largest values of B consistent with the low crystallization temperature and the accompanying small crystallite sizes. For example, a value of B of 10 cal/g corresponds to a ratio of 0.86 for the calculated degrees of crystallinity. As this ratio becomes smaller, the greater the molecular weight and the lower the crystallization temperature become. A consistent interpretation of the data can then be found in the contribution of the interfacial enthalpy of the crystallites formed on cooling to the measured enthalpy of fusion. A more quantitative analysis requires more detailed information with respect to the crystallite sizes initially formed as well as those formed on cooling, since the melting of all the crystallites in the system at room temperature contribute to the enthalpy of fusion.

Although the degree of crystallinity data just described is unique in not being in agreement, it should be realized that the disparity is a consequence of a particular crystallization procedure which introduces small crystallites into the system. Processes, such as annealing or much slower cooling, which minimize the latter effect, should lead to more concordant results. It is clear, however, from a variety of methods, that relatively low levels of crystallinity are achieved at room

temperature for the higher molecular weights. This conclusion makes mandatory the presence of chain units in random conformation which connect crystallites.^{5,7,8}

From the above discussion, it follows that a plot of ΔH^* against the specific volume does not necessarily have to be linear as has been supposed.^{18,23} Neither would it be expected to be represented by a unique function which encompasses all the data. This is seen analytically by combining eq 1 and 5 to give

$$\Delta H^* = \frac{\bar{V}_A - \bar{V}}{\bar{V}_A - \bar{V}_\infty} (\Delta H_u - B) \quad (8)$$

A linear relation between ΔH^* and \bar{V} is only to be expected when B is a constant. Since the quantity $2\Delta H_u/\zeta$ depends on the crystallite morphology and size, the latter condition will not in general be fulfilled. The data in Figure 4 indicate that there will be a wide variation in B , depending on the crystallization conditions. In Figure 5, plots of ΔH^* as a function of \bar{V} are given for the hypothetical situation of B being a constant. Curve 1 is for the case of $B = 0$ and the straight line drawn has the property that for the completely crystalline polymer $\bar{V} = 1.00$, $\Delta H^* = 70$ cal/g, while for the completely amorphous polymer at room temperature $\Delta H^* = 0$, $\bar{V} = 1.17$. This straight line corresponds to the case where the calculated degrees of crystallinity are in agreement. The data for the samples never cooled below the crystallization temperature lie on this straight line. The other straight lines in the figure represent increasingly higher values of B . Although all the curves originate from the point $\Delta H^* = 0$, $\bar{V} = 1.17$, the expected values of ΔH^* corresponding to $\bar{V} = 1.00$ decreases as B increases. The experimental results for the samples cooled to room temperature are also plotted in the figure. As can be anticipated from the data in Figure 4, there is no simple pattern to the plots. Each point in the plot occupies a position corresponding to the appropriate value of B . The data for samples crystallized at 120° or quenched to room temperature cannot be represented linearly. In this grouping, based on the data at the lower specific volumes, an exceptionally low value for ΔH^* , corresponding to the pure crystal, is extrapolated. With increasing specific volume, the points correspond to increasing values of B . An extrapolation to $\Delta H^* = 0$, $\bar{V}_A = 1.17$ is suggested along the lines of B approximately equal to 20-25. On the other hand, the data for samples initially crystallized at 130° can be empirically represented by a straight line, which originates at $\Delta H^* = 70$ cal/g, $\bar{V} = 1.00$, and yields an extrapolated value of $\bar{V} = 1.12$ corresponding to $\Delta H^* = 0$. This specific volume is much less than the value of 1.17 that is expected for the completely amorphous polymer. This empirical linear relation is a result of the low, but not negligible, values of B that are char-

acteristic of the lower specific volumes and the fact that the asymptotic value of B has not been reached for a sufficient number of samples to indicate the change in slope and the approach to the ultimate value of $\Delta H^* = 0$, $\bar{V} = 1.17$. The expectation that there is not a common linear relation is thus confirmed by the experimental data. The results just cited are another manifestation of the effect of small-size crystals on yielding differing values of the degree of crystallinity calculated from density and enthalpy measurements.

Crystals Formed from Dilute Solution. When crystallized from dilute solution, polymers display the characteristic platelet or lamella habit. The lamella are usually about 100 Å thick and the width, or lateral dimension, is of the order of about a micron.²⁴ It has been well established that the chain axes are preferentially oriented normal to the wide faces of the lamella.²⁴ Hence, a given molecule must traverse a crystallite many times. Based primarily on the visual observation of the electron micrographs, it has been presumed that this interface is comprised of regularly folded chains,²⁴ with a minimum number of units consistent with the potentials hindering bond rotation participating in the folded structure. For linear polyethylene, this involves five bonds in *gauche* orientation.²⁵ On the other hand, a wide variety of physical measurements indicates that about 15–20% of the chain units must be in nonordered conformations.^{26–32} The presence of such a large number of noncrystalline chain units leads to the conclusion that a disordered amorphous overlayer is present.^{26,27} This latter conclusion is also consistent with the electron micrographs that have been presented. It, therefore, becomes a matter of interest to see if enthalpy of fusion measurements of crystals formed from dilute solution can help elucidate this problem.

A detailed report of the course of fusion of such crystals has already been given.¹² The fusion process is relatively broad¹² and characterized by partial melting and recrystallization before final melting occurs.^{12,27} The onset of melting is detected at relatively low temperatures, ranging from 100 to 110°, depending on the molecular weight and the crystallization temperature.¹² Extreme care must, therefore, be exercised in evaluating the enthalpy of fusion from the experimental data to properly account for the contribution to the fusion of this low-temperature region. It is also important that a distinction be made between isothermally crystallized samples which have never been heated above the crystallization temperature, after separation from the mother liquor, and those which have been heated or annealed at an elevated temperature. In the latter case, partial melting and recrystallization is known to occur.^{12,27} The necessity for making this distinction has not always been recognized in interpreting experimental data.^{18,23,33} If this is not made, different crystallite morphologies with different interfacial

Table II: Properties of Crystals Formed from Dilute Xylene Solutions

$M\eta$	T_c , °C	d , Å	ΔH^* , cal/g	Density, g/cc
19,000	60	99	48.3	0.968
	70	104	47.6	0.975
	85	130	53.3	0.983
	90	148	53.7	0.985
45,000	60	101	47.2	0.967
	70	106	49.2	0.975
	85	129	52.2	0.9801
	90	149	54.9	0.9837
300,000	70	112	51.1	0.9698
	70	112	52.2	0.9728
	85	129	53.0	0.9730
	90	146	54.5	0.9774
1,200,000	90	148	54.6	0.9792
	70	112	51.8	0.973
	90	148	54.7	0.9775

structures are being analyzed simultaneously. We limit ourselves here to a discussion of the properties of crystals which have not been annealed.

The enthalpy of fusion data and other related properties for the molecular weight fractions crystallized isothermally from dilute xylene solutions are summarized in Table II.

There are certain salient features in the data listed in Table II. In striking contrast to samples crystallized from the melt, ΔH^* is now essentially independent of molecular weight over the range of 1.9×10^6 – 1.2×10^8 that has been studied here. The values of ΔH^* given in the table are about 10% lower than the differential thermal analysis measurements reported by Fischer and Hinrichsen²³ for unfractionated polyethylene and two measurements involving fractions. This discrepancy may be due to the different experimental methods used or the inclusion of an additive constant to each measurement in the latter work. The validity of these enthalpy measurements is discussed below. The enthalpy of fusion is primarily dependent on the crystallization temperature and increases as this temperature increases. Concomitant with an increased crystallization temperature, there is also a significant increase in the crystallite thickness which is also

(24) A. Keller, *Phil. Mag.*, **2**, 1171 (1957); A. Keller, *Makromol. Chem.*, **34**, 1 (1959).

(25) J. D. Hoffman, *Soc. Plastic Eng.*, **4**, 315 (1964).

(26) P. J. Flory, *J. Am. Chem. Soc.*, **84**, 2857 (1962).

(27) E. W. Fischer and G. Schmidt, *Angew. Chem.*, **74**, 551 (1962).

(28) J. B. Jackson, P. J. Flory, and R. Chiang, *Trans. Faraday Soc.*, **59**, 1906 (1963).

(29) W. O. Statton and P. H. Geil, *J. Appl. Polymer Sci.*, **3**, 357 (1960).

(30) W. P. Slichter, *J. Appl. Phys.*, **32**, 2339 (1961).

(31) A. Peterlin, G. Meinel, and H. G. Olf, *J. Polymer Sci.*, **B-4**, 399 (1966).

(32) T. Okada and L. Mandelkern, *ibid.*, **B-4**, 1043 (1966).

(33) V. F. Holland, *J. Appl. Phys.*, **35**, 59 (1964).

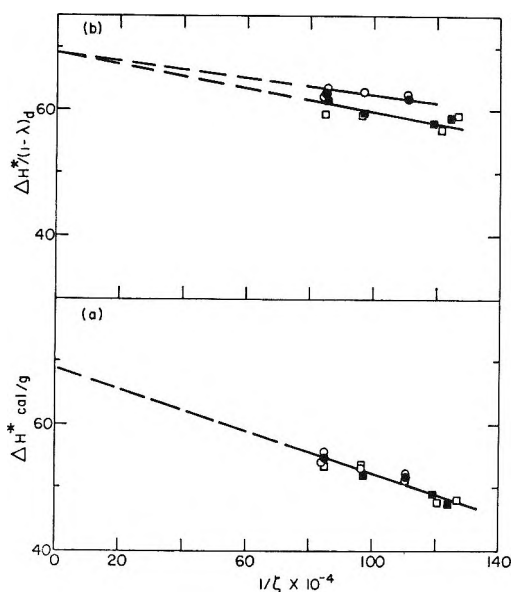


Figure 6. (a) Plot of enthalpy of fusion, ΔH^* , as a function of $1/\zeta$ for molecular weight fractions crystallized from dilute xylene solutions: $M = 1.2 \times 10^6$, \bullet ; $M = 3 \times 10^5$, \circ ; $M = 4.5 \times 10^4$, \blacksquare ; and $M = 1.9 \times 10^4$, \square ; and (b) plot of quantity $\Delta H^*/(1-\lambda)_d$ as a function of $1/\zeta$ for molecular weight fractions crystallized from dilute xylene solutions: $M = 1.2 \times 10^6$, \bullet ; $M = 3 \times 10^5$, \circ ; $M = 4.5 \times 10^4$, \blacksquare ; and $M = 1.9 \times 10^4$, \square .

molecular weight independent in the range studied. This increase in crystallite thickness is well known, and the size-temperature relation reported here agrees very well with those given by others.^{2,34-36} It should be noted that the crystallite sizes are all in the range of about 100 Å.

The density of the samples agrees very well with the range reported by the vast majority of other investigators.^{23,27,28,37,38} An increase in the density is observed with increasing crystallization temperature. There appears to be a small but detectable decrease in density for the two highest molecular weight fractions when compared with the lower molecular weights for the same crystallization temperatures. Despite the disparity in the enthalpy measurements, the density-crystallite size-molecular weight relations agree very well with those given by Fischer and Hinrichsen.²³

For a regularly structured interface, exemplified by regularly folded chains, $1 - \lambda$ is by necessity unity. Equation 5 can, therefore, be rewritten as

$$\Delta H^* = \Delta H_u - \frac{2\Delta H_e}{\zeta} \quad (9)$$

Hence a plot of ΔH^* against $1/\zeta$ should be linear, giving an intercept equal to ΔH_u and slope equal to $2\Delta H_e$. In making this analysis, it must be realized that only a limited range of values for ζ is experimentally available. This limitation will obviously hamper any thermodynamic analysis wherein the crystallite size assumes a dominant role. The appropriate plot, ac-

cording to eq 9, is given in Figure 6a. Within the restricted values of $(1/\zeta)$ that are available, the data are well represented by a straight line. The intercept corresponding to $1/\zeta = 0$ is 69 ± 1 cal/g,³⁹ which is in good accord with the expected value for ΔH_u . From the slope of the straight line ΔH_e is found to be $10,500 \pm 1500$ cal/mole of sequence. In a purely formal manner, the enthalpy of fusion data are thus consistent with a regularly folded interface in that eq 9 is obeyed.

However, the value deduced for the interfacial enthalpy must also be consistent with the model. For an interface comprised of regularly folded chains, ΔH_e has been estimated to be 1500 cal/mole.²⁵ Hence the experimental values are much larger than the theoretical value required to justify a surface of regularly folded chains. Although an admittedly very long extrapolation is involved, the intercept is so close to the theoretically expected value so as to rule out any major contribution from size independent internal defects.

The data of Fischer and Hinrichsen,²³ previously referred to, have a very similar functional form when plotted in this manner. The straight line representing their data parallels the one in Figure 6a, but is displaced upward. The intercept, corresponding to $1/\zeta = 0$, is equal to 77 cal/g. This is an abnormally high value for ΔH_u which evades any theoretical explanation at present. It is a consequence of the higher experimental values reported for ΔH^* and must raise some concern in regard to these values.

From solubility studies of mature crystallites formed in dilute solution, the interfacial free energy has been found to be 1900 cal/mole²⁸ of crystalline sequence. This result is independent of any model assumed for the crystallite morphology. From the experimental interfacial enthalpy deduced above for the regularly folded model, the corresponding interfacial entropy is 22 eu/mole of sequence. For a fold consisting of five CH_2 units, more than 4 eu would have to be assigned to each chain unit in the interface. This appears to be an unduly high value since the entropy of fusion per CH_2 unit is only 2.3 eu.^{2,16}

The enthalpy of fusion data can also be analyzed according to the model of a finite-size crystal with an amorphous or noncrystalline overlayer.^{26,27} In this case, the chain does not necessarily return to the crystal with the sequences juxtaposed. The loops are of variable length, and the chain units are in nonordered conformation. For this model, eq 5 is valid and the ap-

(34) V. F. Holland and P. Lindenmeyer, *J. Polymer Sci.*, **57**, 589 (1962).

(35) F. P. Price, *J. Chem. Phys.*, **35**, 1884 (1961).

(36) A. Keller and A. O'Connor, *Polymer*, **1**, 163 (1960).

(37) E. W. Fischer and R. Lorenz, *Kolloid-Z.*, **189**, 97 (1963).

(38) G. M. Martin and E. Passaglia, *J. Res. Natl. Bur. Std.*, **70A**, 221 (1966).

(39) The significance of this intercept is only valid for the highest molecular weights. For the lower molecular weight fractions, there would have to be a discontinuity for this model when ζ becomes comparable with the extended chain length.

propriate plots are given accordingly in Figure 6b.⁴⁰ Here the degree of crystallinity is again calculated from the measured density. The data can again be represented by straight lines which extrapolate to 69 ± 1 cal/g. The data for the two lowest molecular-weight fractions are displaced slightly below those for the higher molecular weight. Although this slight divergence could be real, it might also very well be a reflection of the extreme sensitivity of the plotted data to the calculated degree of crystallinity. An interfacial enthalpy of 4500 ± 1000 cal/mole is deduced from the plot in Figure 6b. It is significantly less than the corresponding value for the regular chain model. The interfacial entropy is now found to be about 6 eu per crystalline sequence. If the interface is comprised of about 10–20 units per sequence, then the interfacial entropy per unit is very small and consistent with a disordered interfacial structure.

The enthalpy of fusion data, for crystals formed from dilute solution, are formally or algebraically consistent with either of the two major crystallite morphologies

considered. The choice from solely the point of view of the enthalpy measurements depends on the value of ΔH_u and ΔS_u appropriate to the particular molecular structure. The interfacial enthalpy and entropy that are deduced appear to be much too high to be reconcilable with a regular folded-chain structure. The parameters for an irregular structured interface are, however, acceptable ones. The data and this latter conclusion are thus compatible and consistent with the diversity of other physical measurements previously cited for similar constituted crystalline systems.^{26,32}

The degrees of crystallinity calculated from the density data are always higher than the corresponding value obtained from the enthalpy of fusion data with neglect of the interfacial contribution. This is expected, from the discussion in the previous section, because of the small crystal sizes and the value of the interfacial enthalpy that has been deduced.

(40) There is a question as to the crystallite thickness to use here with respect to the low angle maxima. However, a reduction of the spacings by 5–10 Å does not sensibly alter the analysis.

The Radius of the Draining Film beneath a Drop

Approaching a Plane Interface

by S. Hartland

Chemical Engineering Department, The University of Nottingham, Nottingham, England
Accepted and Transmitted by The Faraday Society (May 8, 1967)

The radius of the draining film beneath a drop approaching a plane interface through an immiscible fluid may be obtained from the Bashforth and Adams tables¹ in terms of the size of the drop and its physical properties relative to the surrounding fluid. Derjaguin and Kussakov² have obtained an expression relating these quantities when the drop size is very small. This agrees with the lower limit of the Bashforth and Adams relationship, but should not be used outside the region for which it was experimentally verified.

When a drop of heavy fluid approaches a plane interface through an immiscible light fluid, the drop deforms as shown in Figure 1 so that a film of light fluid is trapped between the drop and the plane. (With a gas bubble in a liquid, Figure 1 would be inverted.) The rate of approach of the drop to the plane is controlled by the rate of drainage of the liquid in this film. When the film becomes sufficiently thin at some point, it ruptures and the drop wets the plane. The final static-equilibrium position is then obtained, and this depends on the angle of contact between the fluids and

the plane. The shape of such a static drop has been tabulated by Bashforth and Adams¹ in terms of the physical properties and the radius of curvature at the top of the drop. Only the period before rupture is considered here, and equilibrium refers to the conditions when the overall dimensions of the draining film become substantially constant. This dynamic-equilib-

(1) F. Bashforth and J. C. Adams, "An Attempt to Test the Theories of Capillary Action," Cambridge University Press, London, England, 1883.

(2) Derjaguin and Kussakov, *Acta Physicochim. URSS*, **10**, 25 (1939).

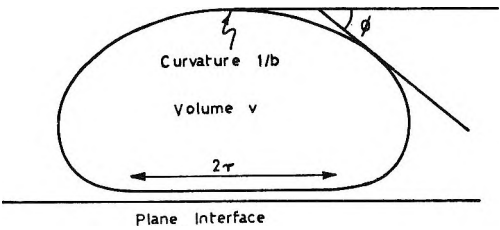


Figure 1. Dimensions of a drop approaching a plane interface through an immiscible fluid.

rium position is equivalent to a static-equilibrium position, in which the angle of contact is 180° measured through the heavy fluid.

The radius of contact, r , between the drop and the draining film is a function of the drop volume, v , the acceleration due to gravity, g , the density difference between the two phases, $\Delta\rho$, and their interfacial tension, σ . Applying the usual methods of dimensional analysis yields

$$r/v^{1/3} = f(cv^{2/3}) \tag{1}$$

Table I^a

B	$cv^{2/3}$	$r/v^{1/3}$	$0.313\sqrt{cv^{2/3}}$
0.125000	0.301048	0.166661	0.172404*
0.250000	0.564301	0.222571	0.236039*
0.500000	1.013051	0.287626	0.316260
0.750000	1.390273	0.328240	0.370492
1.000000	1.717773	0.357482	0.411824
1.500000	2.270092	0.398520	0.473424
2.000000	2.728432	0.427099	0.519021
2.500000	3.122133	0.448770	0.555206
3.000000	3.468276	0.466101	0.585175
4.000000	4.058136	0.492663	0.632983
5.000000	4.551311	0.512558	0.670343
6.000000	4.976373	0.528323	0.700947
7.000000	5.350668	0.541331	0.726830
8.000000	5.685527	0.552344	0.749228
10.000000	6.266299	0.570213	0.786564
12.000000	6.759543	0.584347	0.816935
14.000000	7.189149	0.595970	0.842495
16.000000	7.569927	0.605812	0.864519
20.000000	8.223761	0.621765	0.901081
24.000000	8.773353	0.634390	0.930704
28.000000	9.248103	0.644779	0.955553
32.000000	9.666497	0.663565	0.976929
40.000000	10.379672	0.667840	1.012326
48.000000	10.974839	0.679158	1.040945
56.000000	11.486291	0.688484	1.064924
64.000000	11.935088	0.696369	1.085529
72.000000	12.335301	0.703216	1.103579
80.000000	12.696457	0.709249	1.119618
88.000000	13.026023	0.714617	1.134056
96.000000	13.328725	0.719458	1.147157
100.000000	13.471468	0.721702	1.153284

^a Values of $cv^{2/3}$ and $r/v^{1/3}$ calculated from Bashforth and Adam's tables. Only the values of $0.313\sqrt{cv^{2/3}}$ marked with an asterisk are within the experimental range of Derjaguin and Kussakov.

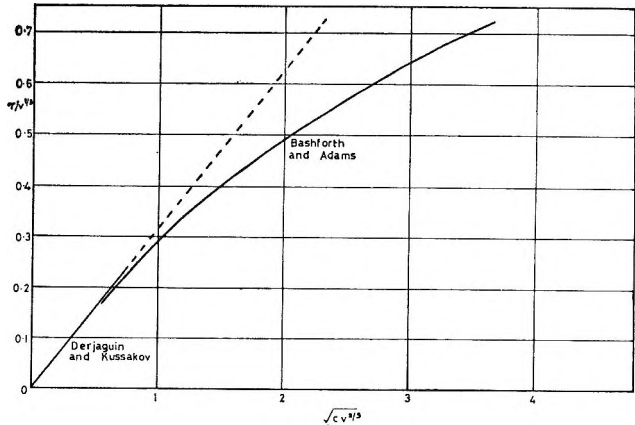


Figure 2. The relationship between the radius of the draining film and the physical properties and size of a drop approaching a plane interface. (Equation 4 is represented by a broken line outside the range for which it was experimentally verified.)

where $c = \Delta\rho g/\sigma$. Introducing the radius of curvature, b , at the top of the drop, this may be written

$$\frac{r}{b} / \left(\frac{v}{b^3}\right)^{1/3} = f \left\{ B \left(\frac{v}{b^3}\right)^{2/3} \right\} \tag{2}$$

where $B = cb^2$.

Bashforth and Adams tabulated r/b and v/b^3 as functions of ϕ for different values of B (here r and v are, respectively, the radius at, and the volume up to, the angle ϕ). When $\phi = 180^\circ$, it is thus possible to obtain corresponding values of $r/v^{1/3}$ and $cv^{2/3}$ as shown in Table I. These are plotted in Figure 2. Knowing the drop volume and physical properties enables the radius of contact to be obtained from this graph. The lowest point on the curve corresponds to a value of $cv^{2/3}$ of 0.30, and the highest point to a value of 13.5.

Because of the radial pressure gradient in the draining film, and because the liquid–fluid interface must deform if there is a pressure difference across it, a variation in film thickness with position is to be expected. Using an interference technique, Derjaguin and Kussakov² have observed a “dimple” in the base of air bubbles approaching a glass plate through water. The draining film is thinnest at the edge of the film where there is a barrier ring, the radius of which does not change with time. A similar effect has been observed by others.^{3–6} The presence of a dimple will increase the apparent volume of the drop and so experimentally determined values of r may differ slightly from those deduced from the Bashforth and Adams tables.

Assuming the bubble to remain substantially spherical, Derjaguin and Kussakov balance the force due to

(3) D. Platikanov, *J. Phys. Chem.*, **68**, 3619 (1964).
(4) P. S. Prokhorov, *Discussions Faraday Soc.*, **18**, 41 (1954).
(5) R. S. Allan, G. E. Charles, and S. G. Mason, *J. Colloid Sci.*, **16**, 150 (1961).
(6) G. D. M. MacKay and S. G. Mason, *Can. J. Chem. Eng.*, **41**, 203 (1963).

the average excess pressure in the draining film against the net buoyancy force acting on the bubble and hence obtain

$$r = \left(\frac{3v}{4\pi}\right)^{2/3} \left(\frac{2}{3} \frac{\Delta\rho g}{\sigma}\right)^{1/2} \quad (3)$$

This may be rewritten

$$r/v^{1/3} = 0.313(cv^{2/3})^{1/2} \quad (4)$$

which is also plotted in Figure 2 and values of $0.313 (cv^{2/3})^{1/2}$ are given in Table I.

It can be seen that eq 4 is the limiting case of the Bashforth and Adams relationship when r approaches zero, which is to be expected as the experiments of Derjaguin and Kussakov covered a range of values of $cv^{2/3}$ up to about 0.6. When $cv^{2/3}$ is greater than this amount (that is for practically the whole range of the Bashforth and Adams tables), the value of r is less than that predicted by eq 4. This equation has been used by many authors⁷⁻⁹ to obtain an estimate of the radius of the film beneath drops and bubbles approaching flat plates and liquid-liquid interfaces. The above discus-

sion emphasizes that it should not be used outside the range of values of $cv^{2/3}$ for which it was experimentally verified.

Nomenclature

b	Radius of curvature at top of drop
$c = \Delta\rho g/\sigma$	Group characterizing physical properties of drop relative to surrounding fluid
g	Acceleration due to gravity
r	Radius of draining film beneath drop
v	Volume of drop
$B = cb^2$	Dimensionless number
$\Delta\rho$	Difference in density between drop and surrounding fluid
σ	Interfacial tension between drop and surrounding fluid
ϕ	Angle of drop surface with horizontal (measured from top of drop)

(7) G. E. Charles and S. G. Mason, *J. Colloid Sci.*, **15**, 236 (1960).

(8) T. Gillespie and E. K. Rideal, *Trans. Faraday Soc.*, **52**, 173 (1956).

(9) S. P. Frankel and K. J. Mysels, *J. Phys. Chem.*, **66**, 190 (1962).

The Gaseous Photolysis of the Methylene cycloalkanes

by R. K. Brinton

Department of Chemistry, University of California, Davis, California (Received March 1, 1967)

The direct and $\text{Hg}(6^3\text{P}_1)$ photolyses of methylenecyclopropane result in the production of ethylene and acetylene in about equal quantities. The reactions proceed cleanly with essentially no polymer formation, but small amounts of allene and hydrogen are also formed in addition to the main products. Behavior of the reactants in the presence of added oxygen indicates that the mechanism is intramolecular rather than the result of radical processes. The quantum yields of decomposition of the $\text{Hg}(6^3\text{P}_1)$ reaction decrease as the pressure of the methylenecyclopropane is increased, and the quantum-yield data are consistent with a deactivation-decomposition mechanism involving two excited states being deactivated by the methylenecyclopropane molecule. Methylenecyclobutane decomposes by the direct photolytic process, in a similar fashion, to produce ethylene and allene in equivalent quantities. The effect of added oxygen also suggests an intramolecular mechanism, but no quantitative quantum-yield data were obtained. Photolysis of the methylenecyclopentane, on the other hand, did not produce detectable decomposition products. Speculation concerning the details of ring scission and rearrangement for the two smaller homologs is made and possible explanations are given for the lack of reactivity of methylenecyclopentane.

A detailed study of the direct photolysis of the methylenecycloalkanes has not been made, although certain experimental evidence relevant to the problem has been obtained in connection with other studies.¹

Loeffler, Eberlin, and Pickett, in the course of their examination of the ultraviolet absorption spectra of small ring hydrocarbons, observed that methylenecyclobutane decomposed rather readily under irradiation and they were able to identify ethylene as one of the decomposition products.

DeMaré, Strausz, and Gunning in a detailed study of the $\text{Hg}(6^3\text{P}_1)$ -sensitized decomposition of methylenecyclobutane vapor determined ethylene and allene to be formed in equal quantities along with smaller amounts of hydrogen, methylcyclobutane, isoprene, and 1,4-pentadiene. They discussed the mechanism in terms of a vibrationally excited triplet state subject to a stepwise deactivation or decomposition *via* two or more reaction modes.

The decomposition of an activated methylenecyclopropane molecule formed by the addition of methylene to allene has been investigated in detail by Frey.² The main products of this decomposition were ethylene and acetylene ($\approx 60\%$), butadiene-1,3 ($\approx 20\%$), dimethylacetylene ($\approx 10\%$), and ethylacetylene ($\approx 10\%$), although the relative amounts of these products were dependent on pressure and to a lesser extent on the mode of formation of the methylene group added to the allene molecule.

Two investigations carried out independently by Chesick³ and Brandaur, Short, and Kellner⁴ were con-

cerned with the pyrolysis of methylenecyclobutane. Both studies indicated that the pyrolytic products were cleanly ethylene and allene and the activation energy of the first-order decomposition reaction was 63.3 and 61.5 kcal mole⁻¹, respectively.

Recently a study made in this laboratory⁵ on the photolysis of the aliphatic allenimines indicated that the decomposition was, for the main part, intramolecular processes from one or more excited species. The present study was initiated to determine if the methylenecycloalkanes, with structures quite similar to the allenimines, would follow a similar type mechanism on direct photolysis. Evidence from Frey's investigation² of the activated methylenecyclopropane molecule in which several paths are followed and the product distribution is somewhat variable would seem to show that the mechanism is quite complex. On the other hand, the $\text{Hg}(6^3\text{P}_1)$ -sensitized^{1b} decomposition and the pyrolysis^{3,4} of methylenecyclobutane follow a much simpler intramolecular mechanism to a large degree.

Experimental Section

Direct photolyses in this investigation were carried out with a fused-silica cylindrical cell, 31 mm in diam-

(1) (a) B. B. Loeffler, E. E. Eberlin, and L. W. Pickett, *J. Chem. Phys.*, **28**, 345 (1958); and (b) G. R. DeMaré, O. P. Strausz, and H. E. Gunning, *Can. J. Chem.*, **44**, 953 (1966).

(2) H. M. Frey, *Trans. Faraday Soc.*, **57**, 951 (1961).

(3) J. P. Chesick, *J. Phys. Chem.*, **65**, 2170 (1961).

(4) R. L. Brandaur, B. Short, and S. M. E. Kellner, *J. Am. Chem. Soc.*, **84**, 3411 (1962).

(5) R. K. Brinton, *J. Phys. Chem.*, **68**, 2652 (1964).

eter by 249 mm (189 cm²). These irradiations were made with an end-on 1000-w water-cooled Hanovia ac hydrogen arc. No optical system or filter was used, but the design of the lamp produced a beam collimated, at least to a limited degree. The absorption characteristics of methylenecyclopropane, given below, and the short-wavelength cutoff of fused silica limit the absorption to the region 1750–2450 Å.

	Wavelength, Å				
	2400	2350	2300	2250	2200
Absorption	12	59	237	840	1135

Methylenecyclobutane and methylenecyclopentane absorb in a similar fashion.

Mercury (6³P₁) sensitized photolyses were carried out by use of a low-pressure mercury arc of 30 cm in length, operated at a constant current of 100 ma ac. Light was taken from an end-on window, filtered through a 2-mm Vycor plate, and roughly collimated by use of a fused-silica lens and restrictive apertures. Light intensities were determined by using *n*-butane as an actinometer. Actinometer determinations were made after two or three methylenecyclopropane photolyses, and only small differences could be detected in the lamp intensity. The quantum yield of hydrogen from *n*-butane at room temperature (25°) and a pressure of 200 mm was taken as $\Phi_{H_2} = 0.50$, from the data of Bywater and Steacie.⁶ Complete quenching was assumed for both the *n*-butane and methylenecyclopropane at all pressures. A few mercury-sensitized experiments were carried out with a helical Vycor tubing low-pressure mercury arc of about 1 m in length, whose axis was placed parallel to the cell axis. Use of this intense source allowed rather high percentage decompositions in relatively short periods. The lamp was operated at 100 ma ac, and variation in the absorbed intensity was obtained by altering the distance between the lamp and the cell. In all sensitized experiments, a pool of mercury lay along the bottom of the absorption cell.

Products from both the direct and sensitized experiments were separated by temperature fractionation using Ward stills and a gas-buret collector in a greaseless vacuum system. The noncondensable gases were collected from a trap at −210° and the C₂H₂–C₂H₄–C₃H₄ fraction at −155°. In general, the noncondensable fraction was very small (0.1–0.2 μ mole) and was contaminated by small amounts of residual gases, mainly N₂, from the system. Because of the small sample size, analysis was not made except for the few irradiations carried to substantial per cent decomposition. The size of this noncondensable fraction, however, fixes an upper limit for H₂ production in the various photolyses. It was noted, in general, that its size was fairly constant and thus experiments with larger C₂H₂–C₂H₄–C₃H₄ yields indicated smaller upper limits for H₂ yield. The fraction separated at −155°, containing mainly C₂H₂

and C₂H₄, always had small amounts of methylenecyclopropane, CO₂ (not completely degassed from the starting material), and C₃H₄. The small amount of C₃H₄ (allene) was difficultly volatilized at −155° and thus a possibility existed for traces to remain behind in the residue. Thus, the yield of C₃H₄ determined by analysis is of lower reproducibility than those of C₂H₂ and C₂H₄.

Analysis of the light-gas fractions was made by a Consolidated 21-103 or 21-104 mass spectrometer. The residue containing the unreacted cycloalkane was analyzed by gas chromatography (2 m \times 4 mm in diameter column of adiponitrile on firebrick, temperature, 0°–ambient). Residue samples from photolyses of methylenecyclopentane were also chromatographed through a 500-ft, 0.03-in. i.d. stainless steel capillary column, coated with General Electric 96 (50) silicone fluid.

Methylenecyclopropane was prepared by the method described by Anderson,⁷ from a commercial sample of chloroisobutene. Final purification was made by a successive fractionation on three different preparative gas chromatographic columns. Elimination of some of the C₄H₈ isomers (especially bicyclobutane) was difficult. The final product contained less than a detectable 0.03% impurity.

Methylenecyclopentane was obtained from the API; gas chromatograms made on several columns and under varying conditions did not reveal anything except trace impurities.

Methylenecyclobutane was purified from commercially available samples (60–80% purity). By use of successive fractionation on different gas chromatographic columns, a product of purity greater than 99.95% was obtained.

Results

Products produced in the methylenecycloalkane photolyses are summarized in Tables I and II. In the case of methylenecyclopropane irradiated with the hydrogen arc, ethylene and acetylene are produced in closely comparable amounts; C₂H₂:C₂H₄ = 0.97 \pm 0.015 for MCP-1, 4, 5, 6, a ratio differing from unity by no more than the experimental error of the determination, although the slightly lesser yield of C₂H₂ may well be real and significant. For the series of mercury-sensitized experiments at varying pressure, MCP-7, 8, 9, 10, 11, 12, 13, C₂H₂:C₂H₄ = 0.941 \pm 0.017, clearly demonstrating that the yield of C₂H₄ is greater than C₂H₂ under all of the pressure conditions tested. In addition, no systematic change in ratio seems to accompany the pressure variation. Oxygen added to the system in the direct photolysis (MCP-3) produced an appreciable yield of CO₂, CO₂:C₂H₄ = 1.38, but the C₂H₂:C₂H₄ ratio was

(6) (a) S. Bywater and E. W. R. Steacie, *J. Chem. Phys.*, **19**, 172 (1951); and (b) S. Bywater and E. W. R. Steacie, *ibid.*, **19**, 319 (1951).

(7) B. C. Anderson, *J. Org. Chem.*, **27**, 2720 (1962).

Table I: Methylene cyclopropane Photolysis Products

	Temp, °C	P, mm	Arc	Decomp, %	Rate, ^a C ₂ H ₄	Relative yields (C ₂ H ₄) = 1.00		
						C ₂ H ₂	C ₃ H ₄ ^c	H ₂
MCP-1	25	131	H ₂ helical	0.10	8.4	0.98	0.024	<0.14
MCP-2	25	137	2537	0.50	160	0.92	0.122	<0.09
MCP-3 ^b	25	130	H ₂	0.05	4.5	0.90 ^b	0.029 ^b	...
MCP-4	25	136	H ₂	0.59	22.4	1.01	0.028	<0.09
MCP-5	150	132	H ₂	0.71	23.9	0.97	0.020	<0.04
MCP-6	25	29.5	H ₂	0.34	0.54	0.97	0.023	<0.18
MCP-7	25	508	2537	0.01	1.07	0.95	0.096	<0.16
MCP-8	25	302	2537	0.03	1.80	0.89	0.085	<0.10
MCP-9	25	250	2537	0.05	2.12	0.95	0.147	<0.09
MCP-10	25	164	2537	0.04	3.23	0.96	0.098	<0.06
MCP-11	25	100	2537	0.19	3.92	0.96	0.124	<0.07
MCP-12	25	30.4	2537	1.10	6.50	0.95	0.100	<0.03
MCP-13	25	10.2	2537	0.16	7.52	0.94	0.139	<0.07

^a Mole cm⁻³ sec⁻¹ × 10¹³. ^b 5.4 mm of O₂ added. ^c C₃H₄ = allene.

Table II: Methylene cyclobutane Photolysis Products

	Temp, °C	Arc	P, mm	Decomp, %	Rate, ^a C ₂ H ₄	Relative yields		
						C ₂ H ₄	C ₃ H ₄ ^b	H ₂
MCB-2	25	2537 helical	153	12.5	525.0	1.00	0.36	0.029
MCB-3	25	H ₂	145	0.11	1.95	1.00	0.97	<0.024
MCB-4	25	H ₂	106	0.15	0.65	1.00	0.97	<0.051
MCB-5 ^c	25 ^c	H ₂	52	0.58	...	1.00 ^c	0.99 ^c	...
MCB-6	25	H ₂	132	...	1.91	1.00	1.01	...
MCB-7	150	H ₂	126	0.47	1.81	1.00	0.93	<0.038

^a Mole cm⁻³ sec⁻¹ × 10¹². ^b C₃H₄ = allene. ^c 4.8 mm of O₂ added.

not significantly affected. Under the conditions of irradiation, oxygen absorbs to some extent, and the CO₂ yield must be the result of excited oxygen molecule and/or oxygen atom interaction with the substrate.

Allene, C₃H₄, was present in the products of both the direct and mercury-sensitized experiments, but to a much lesser extent for the direct trials. The relative yields, C₃H₄:C₂H₄, are 0.025 ± 0.0015 and 0.111 ± 0.015, respectively, and in both cases there does not appear to be any systematic change with experimental conditions. Reasons for the rather large statistical experimental errors have been discussed in the Experimental Section.

The yield of hydrogen in the various photolyses was not, in general, directly analyzed because of the very small size of the noncondensable gas fraction as mentioned earlier. The values appearing in Table I represent upper limits. It is certain, from the data, that a maximum limit is less than 10% of the C₂H₄ yield, and it is probable that 3% is a more realistic value for both the direct and mercury-sensitized decompositions. Such a relatively small yield is surprising in view of the very energetic light absorbed in the direct photolysis and the common occurrence of hydrogen in the mercury-photosensitized decomposition of hydrocarbons. Com-

parison of MCP-4 (25°) and MCP-5 (150°) shows little difference in the products, except for the somewhat smaller hydrogen yield at the higher temperature. Careful examination of the residues from the photolysis by gas chromatography on several different columns indicated only two small peaks not present in the starting material. These products (unidentified) were approximately 2.3 and 0.48% as abundant as the ethylene produced in the corresponding more volatile fraction.

No measure of the quantum efficiency of the direct photolysis was made because of the wide spectrum of absorbed radiation from the hydrogen arc and the difficulty of quantitative measurement of absorbed intensities at these short wavelengths. Table III lists the quantum yields of C₂H₄, C₂H₂, and C₃H₄ for the series of mercury (6³P₁)-sensitized photolyses MCP-7, 8, 9, 10, 11, 12, 13, in which the methylenecyclopropane was varied from 508 to 10.2 mm. The quantum yields of all three products increase in a regular fashion as the pressure is lowered.

The direct photolyses of methylenecyclobutane at 25° with the hydrogen arc, MCB-3, 4, 6, produced C₂H₄ and C₃H₄ (allene) in equal amounts to within the experimental accuracy of the product analyses. The ef-

Table III: Methylenecyclopropane Photolysis Products

	Quantum yields			
	C ₂ H ₄	C ₂ H ₂	C ₃ H ₄	C ₂ H ₄ + ½C ₃ H ₄
MCP-7	0.0112	0.0106	0.0011	0.0112
MCP-8	0.0188	0.0166	0.0016	0.0174
MCP-9	0.0220	0.0210	0.0032	0.0226
MCP-10	0.0325	0.0312	0.0032	0.0328
MCP-11	0.0408	0.0393	0.0051	0.0419
MCP-12	0.0679	0.0641	0.0068	0.0675
MCP-13	0.0758	0.0711	0.0105	0.0763

fect of oxygen addition in MCP-5 was similar to its action on methylenecyclopropane; CO₂ was formed to an appreciable extent (CO₂:C₂H₄ = 0.29), but the ratio C₃H₄:C₂H₄ was unaffected. Comparison of MCP-6 (25°) and MCP-7 (150°), photolyses, conducted under identical conditions except for temperature, indicates that the relative yield of C₃H₄ is somewhat lower (*ca.* 7%) at the higher temperature. Examination of the residue of MCP-6 by gas chromatography did not reveal any peaks not present in the starting material. The residue of the high-temperature photolysis (MCP-7) indicated two products, 9.1 and 3.6% as large as the C₂H₄ produced in that experiment.

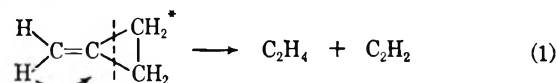
The yield of H₂ was, if anything, lower for methylenecyclobutane than for methylenecyclopropane. The rather large nonvolatile fraction of MCP-2 (mercury sensitized) indicated H₂:C₂H₄ = 0.029. The upper limit of H₂ yields in the direct photolyses are of this same magnitude.

Methylenecyclopentane did not photolyze to any extent, even on prolonged exposure to radiation from the hydrogen arc. Exposure times sufficient to produce 5–10% decomposition on the other two methylenecycloalkanes produced negligible amounts of volatile gases, H₂ and C₂H₄. Gas chromatography of the remainder of the photolyzed material, both in the adiponitrile column and in the very efficient 500-ft capillary column, did not reveal any new peaks in this residue greater than about 0.1% of the substrate. Further, the mass spectra of the reaction material before and after irradiation were identical to within the limits of experimental reproducibility of such spectra. Although the absence of a rearranged isomer of methylenecyclopentane in the residue fraction is not definitely proven, it seems unlikely that any appreciable amount of such a substance would have escaped detection by the methods used.

Irradiation of the methylenecyclopentane by the intense helical low-pressure arc with mercury vapor present produced a very small yield of hydrogen but no ethylene was detected. Small peaks were present in the gas chromatogram of the residual fraction made on the adiponitrile column, but certainly the decomposition yield of methylenecyclopentane was several orders of magnitude less than the corresponding decompositions of methylenecyclopropane or -cyclobutane.

Discussion

Methylenecyclopropane. It is of interest to compare the behavior of the excited methylenecyclopropane molecule observed in the present study to that reported by Frey.² In his experiments, the excited molecule was formed by addition of methylene to allene. Methylene was formed by photolysis of ketene at 3130 Å as well as diazomethane at 3660 and 4358 Å, and the results were qualitatively similar regardless of the mode of methylene formation. The methylenecyclopropane molecule formed in this manner is presumably in a highly excited vibrational state and decomposes by a number of different paths wherein acetylene and ethylene, butadiene-1,3, methylallene, dimethylacetylene, and ethylacetylene are the decomposition products. In the present study, the excited methylenecyclopropane formed with approximately 125–160 kcal mole⁻¹ of energy by absorption of ultraviolet radiation is initially in an excited singlet state. Although the process for the decomposition of the excited singlet has not been demonstrated in these experiments, a possible mechanism involves internal conversion and/or collisional deactivation to the first excited singlet state and a concerted intramolecular rearrangement to acetylene and ethylene. This entails a hydrogen shift and the breaking of two bonds.



An alternate mechanism is the formation of a biradical intermediate, suggested by Nangia and Benson⁸ as a common precursor to thermal and photochemical decompositions and rearrangements of small ring hydrocarbons. In the case of the direct photolysis, the lack of evidence as to the energies of available excited states, probabilities of intersystem crossover, and the effect of pressure on the decomposition makes further speculation as to the details of the mechanism pointless. However, the independence of the ratio of C₂H₂:C₂H₄ from oxygen gas added to the system argues strongly for an intramolecular mechanism to the exclusion of a free radical path for the formation of these products. Whether such an oxygen effect also forbids a triplet excited state as the precursor to these products is not at all certain.⁹

The extensive quantitative yield data for the mercury-sensitized decomposition of methylenecyclopropane allow a more detailed consideration of the excited state for this process and the subsequent mechanisms leading to deactivation and/or product formation. Quantum yields of C₂H₄, C₂H₂, and C₃H₄ for MCP-7, 8, 9, 10, 11, 12, 13 are listed in Table III. Several conclusions seem justified from these data.

(a) The decrease in quantum yield of all products with pressure increase of methylenecyclopropane is

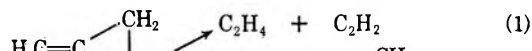
(8) P. Nangia and S. W. Benson, *J. Am. Chem. Soc.*, **84**, 3411 (1962).

(9) D. W. Setser, D. W. Placzek, R. J. Cvetanović, and B. S. Rabinovitch, *Can. J. Chem.*, **40**, 279 (1962).

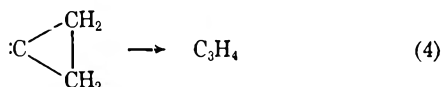
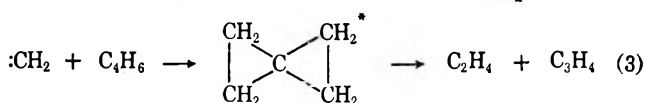
strong evidence for the existence of an excited molecule with appreciable lifetime. The substrate acts as a third body deactivator in competition with a first-order decomposition process.

(b) The small, but definite excess of C_2H_4 over C_2H_2 formed in the products indicates that the process is more complex than the simple intramolecular split shown in 1.

(c) The rather constant values of $C_2H_2:C_2H_4 = 0.941 \pm 0.017$ and $C_3H_4:C_2H_4 = 0.111 \pm 0.015$ without any trend with change in substrate pressure suggest that a single excited state has two possible decomposition paths, one leading to C_2H_4 plus C_2H_2 , reaction 1, and a second step producing C_3H_4 and additional C_2H_4 . A reasonable type of decomposition mechanism is

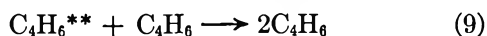
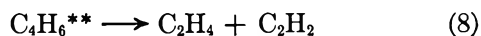
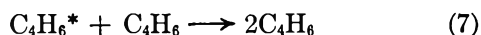


(2)



Such a process would require: (i) that, as indicated above, the relative yields of C_2H_4 , C_2H_2 , and C_3H_4 be constant regardless of substrate pressure, and (ii) the stoichiometry $C_2H_4 = C_2H_2 + \frac{1}{2}C_3H_4$. Table III indicates that probably, within the experimental error, such a stoichiometry is at least consistent with the data. Insertion of the methylene group into a C-H bond is of course an alternate to reaction 3. Although the insertion process should be minor as compared to 3, such a reaction would perhaps upset the proposed stoichiometry.

Figure 1 shows the variation of $1/\Phi_{C_2H_2}^{1/2}$ as a function of methylenecyclopropane pressure. This form of data display was chosen to test out the following excited-state deactivation-decomposition mechanism, similar to the treatment used by Callear and Cvetanović¹⁰ for the Hg (6^3P_1)-sensitized decomposition of C_2H_4 .



It is seen that the fit of the data to a straight line is reasonable considering the accuracy of the analyses. It should be pointed out that a *single* excited-state deactivation-decomposition mechanism, which requires a linear relationship between $1/\Phi_{C_2H_2}$ and the pressure of the substrate, does not give nearly as good a fit to the

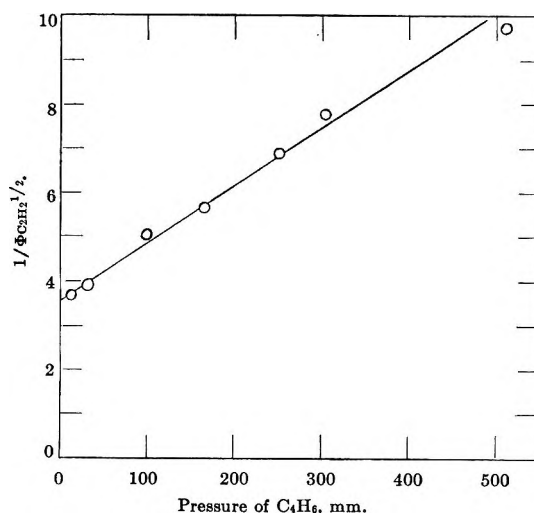


Figure 1. Methylenecyclopropane photolysis, the variation in the quantum yield of acetylene with pressure.

derived data as does the double excited-state mechanism given above. Although kinetic data of this type do not really furnish sufficient proof of such a complex mechanism, it is interesting to note that this reaction scheme is consistent with what is known concerning Hg(6^3P_1)-sensitized mechanisms for olefinic compounds in general, *i.e.*, that the initial excited state is not the one leading to intramolecular decomposition.¹¹ Following the method of Callear and Cvetanović,¹⁰ wherein the assumption is made that $k_6/k_7 = k_8/k_9$, and using a value for $k_7 = k_9 = 6 \times 10^{14} \text{ cm}^3 \text{ mole}^{-1} \text{ sec}^{-1}$ (the approximate collisional frequency), one obtains a lifetime of about 10^{-10} sec for the excited states, $C_4H_6^*$ and $C_4H_6^{**}$, from the slope and intercept of Figure 1.

The direct photolysis of butadiene-1,3, as well as its mercury-sensitized decomposition, have been investigated in detail.¹² This compound, an isomer of methylenecyclopropane, follows an extremely complex decomposition mechanism with several primary steps, multiple products, and considerable polymerization. In contrast to this behavior, methylenecyclopropane decomposes by a rather simple mechanism into C_2H_4 and C_2H_2 for over 90% of the total reaction, and small amounts of C_3H_4 , H_2 , and unidentified substances make up the remainder of the products. It should be pointed out that methylenecyclopropane does not have valence tautomeric forms similar to butadiene-1,3, and, for this reason, rearrangement products must involve hydrogen atom transfer to give products such as those observed by Frey.² The excited state responsible for this type of reaction both for methylenecyclopropane² and buta-

(10) A. B. Callear and R. J. Cvetanović, *J. Chem. Phys.*, **24**, 873 (1956).

(11) R. J. Cvetanović, *Progr. Reaction Kinetics*, **2**, 85 (1964).

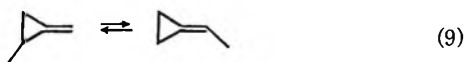
(12) (a) J. Collin and F. P. Lossing, *Can. J. Chem.*, **35**, 778 (1957); (b) R. Srinivasan, *J. Am. Chem. Soc.*, **82**, 5063 (1960); (c) I. Haller and R. Srinivasan, *J. Chem. Phys.*, **40**, 1992 (1964); (d) R. Srinivasan, *Advan. Photochem.*, **4**, 113 (1966); (e) I. Haller and R. Srinivasan, *J. Am. Chem. Soc.*, **88**, 3695 (1966).

diene-1,3^{12c} has been assumed to be a vibrationally activated ground state. The absence of rearrangement products in the direct photolysis would indicate that a highly excited ground state is unimportant to the photolytic process of methylenecyclopropane.

One of the striking features of the methylenecyclopropane photolysis is the virtual absence of polymer as a product. As many as ten photolytic experiments could be conducted without visible coating on the cell windows. On the other hand, polymer is one of the major products of butadiene-1,3 photolysis and its formation has been attributed^{12d} to secondary absorption by primary products of the butadiene, mainly allene-type compounds. Experiments conducted in the present study were limited to quite low per cent conversions (<0.6%). It is probable that higher conversions would have led to polymerization through absorption by acetylene.

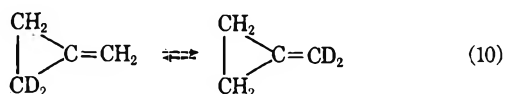
The similarity of decomposition behavior of methylenecyclopropane in direct and mercury-sensitized irradiation, on first consideration, seems contrary to the generalizations made by Placzek and Rabinovitch¹³ concerning the differences to be expected in decomposition mechanisms for excited singlet and triplet states. However, the excited singlets considered by these authors were the result of methylene being added to double bonds. This process, in all probability, leads to a highly vibrationally excited ground singlet state as already indicated in Frey's² treatment of the methylenecyclopropane excited state. It is quite clear that the direct photolysis of methylenecyclopropane does not produce an excited ground singlet. The similarity of the direct photolytic products to those of the sensitized process suggest that the final excited state, which undergoes a split into C₂H₄ and C₂H₂, may be the same for both processes.

Valence tautomerism in the methylenecyclopropane system was demonstrated by Chesick¹⁴ in an investigation of the pyrolysis of 2-methylmethylenecyclopropane.



This reaction was shown to be an equilibrium between two first-order reactions of about equal activation energies, approximately 40 kcal mole⁻¹. Further evidence as to the nature of this type of interconversion has been furnished by the work of Bell,¹⁵ who studied the pyrolysis of methylenecyclopropane-d₂ at about 200°.

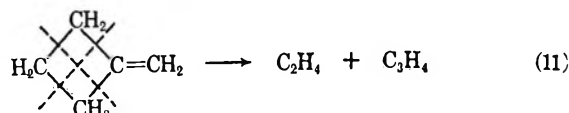
Under these conditions the isomerization



proceeds with an activation energy of 40–45 kcal mole⁻¹.

It is evident from the above investigations that the methylene groups in the activated state are quite labile. These activation energies are appreciably below the 47–57 kcal mole⁻¹ calculated¹⁴ for the unassisted opening of the strained cyclopropane ring and argue strongly against a biradical form in the activated complex. In addition, the lack of decomposition products in either of these two studies indicates that another activated complex of higher energy is required to allow formation of products such as acetylene and ethylene. This may well be the biradical form as suggested by Nangia and Benson.⁸ Whether the isomerization equilibrium can also exist in the photoexcited state can only be determined by experiments with labeled methylenecyclopropane. A similar type of process was used to explain the aliphatic allenimine photolysis.⁵

Methylenecyclobutane. The photodecomposition of methylenecyclobutane proceeds in a manner analogous to that of methylenecyclopropane with a simple formation of ethylene and allene accounting for more than 95% of the process. Decomposition may occur directly in two equivalent ways by the breaking of a pair of carbon-carbon bonds in the ring



without a requirement of hydrogen atom transfer. The uncomplicated nature of the products, just as in the case of the pyrolysis,^{3,4} may indicate that the photoexcited state is similar to the thermally activated state, but such an argument is not compelling. An excited state of much greater energy could decompose in a similar fashion. The valence tautomer, spirobicyclopentane, could not be detected in the products. This is not surprising on the basis of the work of Flowers and Frey,¹⁶ showing it to be at least thermally unstable with respect to methylenecyclobutane.

The ratio of C₃H₄:C₂H₄ is taken to be 1.0, within experimental error, just as in the case of C₂H₂:C₂H₄ for the direct methylenecyclopropane photolysis. The low value of the ratio for MCB-2 in which the mercury-sensitized reaction was carried to 12.5% decomposition may possibly be explained by photopolymerization reactions of allene in the system. Effects produced by adding oxygen and raising the temperature to 150° are about the same as in the methylenecyclopropane case and can be interpreted in a similar fashion.

The Hg(6³P₁)-sensitized photolysis of methylenecyclobutane studied in detail by DeMaré, *et al.*,^{1b} produced products similar to those of the direct photolysis studied herein. These workers also followed the

(13) D. W. Placzek and B. S. Rabinovitch, *Can. J. Chem.*, **43**, 820 (1965).

(14) J. P. Chesick, *J. Am. Chem. Soc.*, **85**, 2720 (1963).

(15) J. A. Bell, personal communication.

(16) M. C. Flowers and H. M. Frey, *J. Chem. Soc.*, 5550 (1961).

production of hydrogen quantitatively, as well as the other minor products mentioned earlier. The excited states leading to decomposition were assumed to be triplet biradicals, although other types of excited states were not ruled out by the experimental evidence. The quantum yields for the $\text{Hg}(6^3\text{P}_1)$ decomposition of methylenecyclobutane were approximately a factor of tenfold greater than the $\text{Hg}(6^3\text{P}_1)$ decomposition of methylenecyclopropane determined in the present study. This would infer that the excited methylenecyclopropane molecule has a lifetime considerably greater than the corresponding excited methylenecyclobutane, since one would not expect the methylenecyclopropane molecule to be a more efficient deactivator than methylenecyclobutane.

Methylenecyclopentane. Lack of detectable photolytic products, except for very small amounts of hydrogen and some unidentified residue products, on irradiation of methylenecyclopentane is surprising in view of the ready decomposition of the smaller homologs. This behavior indicates that the photoexcited state must be extremely stable to decomposition processes and is deactivated with high probability to the ground state.

The valence tautomer, spirobicyclohexane, would be predicted, on basis of ring strain considerations, to be much more unstable than the substrate and, therefore, an unlikely product. Other isomerization reactions all involve hydrogen atom shifts. Necessity for hydrogen transfer in the isomerization reactions of all three of the methylenecycloalkanes investigated could offer an explanation for the absence of products resulting from such reactions in the photolysis products. In the case of methylenecyclopentane, a split into two smaller decomposition products requires somewhat less likely reactions than for the two other cycloalkanes studied. Double-ring scission reactions can be formulated forming C_2H_2 , C_2H_4 , and C_3H_4 as possible fragments. Accompanying these products, however, must be strained ring compounds or ones requiring hydrogen transfer reactions.

Acknowledgment. This investigation was supported by a grant-in-aid from the National Science Foundation. Appreciation is also expressed to this same agency for funds furnished for the purchase of the mass spectrometer used in some of the analytical procedures.

Infrared Absorption at $21\ \mu$ of Carbon Monoxide Adsorbed on Silica-Supported Platinum

by J. K. A. Clarke, G. M. Farren, and H. E. Rubalcava¹

*Department of Chemistry, University College, Dublin, Ireland
Accepted and Transmitted by The Faraday Society (June 12, 1967)*

An absorption band of carbon monoxide adsorbed on silica-supported platinum has been observed at $476\ \text{cm}^{-1}$. This band is assigned to the carbon-platinum stretching vibration of the adsorbed species. The results are reported of a force-constant calculation for a potential-energy function, which includes interaction between the C-O stretch and the C-Pt stretch. The interaction constant is unusually large. The stretching force constants for the C-O band and the C-Pt are, respectively, larger and smaller than those previously obtained for related systems by calculations neglecting bond-bond interaction. Details of the technique for improving the transmission of silica-supported metal disks beyond $8\ \mu$ are discussed.

Introduction

In spectroscopic studies of carbon monoxide adsorbed on metals, the region beyond $15\ \mu$ is of special interest, for it is in this region that absorption may arise due to excitations of vibrational modes which strongly involve the carbon-metal bonds. Such in-

vestigations should therefore be particularly valuable in yielding information about these bonds and about the adsorption process itself. We report here our observation of absorption at $21\ \mu$ due to carbon monoxide

(1) To whom correspondence regarding this paper should be addressed.

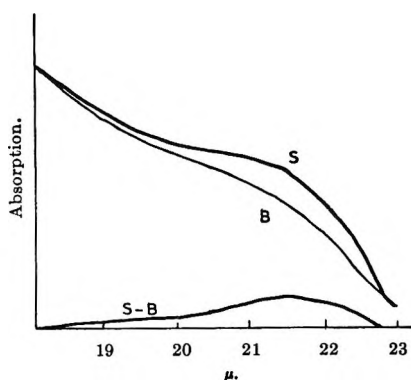


Figure 1. Absorption due to the carbon-platinum stretching vibration of carbon monoxide adsorbed on silica-supported platinum. The curves show the averaged results of nine separate runs, as described in the text: S is the spectrum, B is the background, and S - B is the graphical difference.

adsorbed on silica-supported platinum; we assign this band to the carbon-platinum stretching vibration. Figure 1 is a smoothed plot of the nine separate spectra which were obtained as discussed below. This information and that obtained from the 5- μ spectra of $C^{12}O^{16}$ and $C^{13}O^{16}$ adsorbed on silica-supported platinum²⁻⁴ yield values of the stretching and of the stretch-stretch interaction force constants for the adsorbed species. Previous investigators⁵ of related systems did not include a stretch-stretch interaction force constant in the functions used to describe the potential energy of the adsorbed species. In fact, this constant is not negligible, hence earlier conclusions regarding the bonding in the adsorbed species must be reconsidered in view of the present results.

Experimental Section

The adsorbent used was in the form of a compressed disk, containing 10 mg/cm² of silica with 10%, by weight, platinum dispersed in ten impregnations according to the methods described earlier.⁶ Ammonium chloroplatinate, prepared from spectrographically standardized metal as supplied by Johnson, Matthey, and Co., Ltd., was used as the source of metal; the silica was Cabosil (300-350 m²/g), and the carbon monoxide, supplied by the British Oxygen Co., was 99.95% pure.

Since the 21- μ band was very weak, it was recorded using a high scale expansion, and the resulting signal-to-noise ratio was poor. The results reported here are based on three separate experimental sequences. Each involved reducing the adsorbent, recording three background spectra, adsorbing the carbon monoxide at 1 torr, and recording three spectra with the adsorbed species present. The disk was thoroughly cleaned between sequences. At room temperature, the clean disks transmitted about 5% of the incident 21- μ radiation, but in the presence of carbon monoxide, or of other gases, at pressures greater than 0.01 torr, they became virtually opaque. We have discovered that the transmission of these disks increases with temperature:

at 250°, they transmit about 40% of the incident 21- μ radiation. When the carbon monoxide was admitted into the cell, the disk was cooled and its transmittance decreased, but when the temperature was restored to 250°, the transmission was sufficient to obtain spectra. Concurrent examination of the 5- μ region showed a normal high-coverage (about 90%) absorption due to the adsorbed carbon monoxide.

The *in situ* cell is, essentially, of a conventional design,⁴ and the methods for cleaning the adsorbent are also conventional.⁴ The spectra were obtained with a Grubb-Parsons Spectromaster using the slit program Program 10. An evacuated cell was used in the reference beam to compensate for absorption by atmospheric water, and the monochromator compartment was purged with dry air.

Discussion

We assume that the structure of the adsorbed species is that of a linear XYZ molecule with the carbon atom bonded to the metal. Contributions to the potential energy by displacements parallel to the CO axis are given, neglecting anharmonicity, by eq 1.

$$2V = F_{CO}S_{CO}^2 + F_{CM}S_{CM}^2 + 2fS_{CO}S_{CM} \quad (1)$$

S_{CO} and S_{CM} are the CO and the C-Pt stretching displacements, F_{CO} and F_{CM} , and f are the corresponding stretching and stretch-stretch interaction force constants. This system has two axial normal modes of vibration: the high frequency mode, ν_3 , is largely a C-O stretching deformation, but it contains a small out-of-phase contribution from the C-M stretching and absorbs near 5 μ ;²⁻³ the low frequency mode, ν_1 , is mostly a C-Pt stretching vibration with an in-phase contribution from the CO stretch. Given values of ν_3 for $C^{12}O$ and for $C^{13}O$, and of ν_1 for $C^{12}O$, the three force constants can be calculated by standard methods.⁷ Unfortunately, the value of ν_1 to be used is not immediately obvious. To eliminate the effects of intermolecular interactions between adsorbed molecules, it is best to use the frequencies for the zero-coverage limit; these are known for ν_3 , but the corresponding value for ν_1 is not known because of the experimental limitations already described. Unpublished work in this laboratory³ suggests that the surface-coverage dependence of the frequency of ν_3 is due to coupling between the adsorbed molecules by interactions which depend on the

(2) R. P. Eischens, S. A. Francis, and W. A. Pliskin, *J. Phys. Chem.*, **60**, 194 (1956).

(3) J. K. A. Clarke, G. M. Farren, and H. E. Rubalcava, unpublished data.

(4) L. H. Little, "Infrared Spectra of Adsorbed Species," Academic Press, New York, N. Y., 1966.

(5) C. W. Garland, R. C. Lord, and P. F. Troiano, *J. Phys. Chem.*, **69**, 1188 (1965).

(6) J. K. A. Clarke, G. M. Farren, and H. E. Rubalcava, *J. Phys. Chem.*, **71**, 2376 (1967).

(7) E. B. Wilson, J. C. Decius, and P. C. Cross, "Molecular Vibrations," McGraw-Hill Book Co., Inc., New York, N. Y., 1955.

transition moments associated with ν_3 . If the same is true for ν_1 , then the required frequency at the zero-coverage limit will be only slightly less than the observed value of 476 cm^{-1} . A small difference is reasonable in view of the fact that such shifts decrease with a decrease in transition moments, and these vary as the square root of the integrated intensity.⁷ Since ν_1 is much weaker than ν_3 , for which the zero-coverage frequency lies 35 cm^{-1} below the high-coverage limit,^{2,3} 10 cm^{-1} is used as a conservative estimate of the amount by which the frequency of ν_1 decreases as the surface coverage changes from high to low. Accordingly, we have used the observed values of 2038 and 1991 cm^{-1} for $\nu_3(\text{C}^{12}\text{O})$ and $\nu_3(\text{C}^{13}\text{O})$ and an estimated value of 466 cm^{-1} for $\nu_1(\text{C}^{12}\text{O})$ in the calculation of the force constants. These are given in Table I. However, the conclusions discussed below are not critically dependent on small changes in the frequencies used in the calculations; the force constants were evaluated, using both high and low coverage values of ν_3 as a function of ν_1 at 10 cm^{-1} in-

energy difference between the asymmetric and the symmetric vibrational levels. An increase in f shifts ν_1 upward and ν_3 downward. Thus, if F_{CO} and F_{CM} are evaluated under the assumption that f is zero, the resulting values for these two stretching force constants will be, respectively, smaller and larger than the values which result when f takes its best value, *i.e.*, when f is positive. Ideally, our three force constants should be compared with a similar set for molecular platinum carbonyls of known structure, but we have found no published investigations which give such information. The force constant calculations of Jones⁹ for $\text{Mo}(\text{CO})_6$ and for $\text{Ni}(\text{CO})_4$ appear to be the best available for the present purpose; the relevant constants from his calculations are also given in Table I. The value obtained here for F_{CO} is approximately equal to those obtained by Jones, indicating greater similarity between the C-O bond of the adsorbed species and that of molecular metal carbonyls than had been suggested by earlier results.^{1,5} The values of F_{CM} and f are substantially higher for the adsorbed carbonyls than for the molecular carbonyls. This larger value of F_{CM} implies, insofar as force constants are measures of bond energies, that the C-Pt bond of these chemisorbed species is stronger than those of the molecular metal carbonyls discussed by Jones. Similarly, the stretch-stretch interaction is considerably larger in the adsorbed species.

These differences may well be due to the fact that on metal crystals the bonding electrons may, in effect, come from a large number of metal atoms, whereas in the case of the molecular metal carbonyls considered the bonding involves one metal atom.

In considering the validity of the foregoing analysis, at least two questions arise. The first is whether the assignment of the $21\text{-}\mu$ band is correct. If ν_1 absorbs at a much lower frequency, *i.e.*, beyond the region where measurements were possible, then the resulting values of F_{CM} and of f would be similar to those discussed by Jones. We are inclined to reject this possibility for the following reasons. The spectrum reported by Garland, *et al.*,⁵ shows a relatively sharp absorption at 477 cm^{-1} , and a broader weaker band at 570 cm^{-1} which they assigned to the Pt-C-O bending modes. This assignment is in agreement with recent spectroscopic studies of molecular metal carbonyls.¹⁰ We saw no absorption near 570 cm^{-1} , although a very weak broad band could have easily been lost due to the poor signal-to-noise level which prevailed.

The second question concerns a more fundamental matter: our treatment, and those of Eischens, *et al.*,² and of Garland, *et al.*,⁵ neglect interactions between

Table I: Force Constants^a of Carbon Monoxide Adsorbed on Platinum and of Related Metal Carbonyls

System	F_{CO}	F_{CM}	f	Ref
CO-Pt(SiO ₂)	17.16	3.51	1.34	This study
CO-Pt(SiO ₂)	16	4.5	...	2
CO-Pt	15.6	4.1	...	5
Mo(CO) ₆	17.0	1.82	0.63	9
Ni(CO) ₄	17.55	2.09	0.33	9

^a Units are mdynes/Å.

tervals from 426 to 496 cm^{-1} without substantial change. The effective mass of atom Z was also varied to correspond to one, two, or four platinum atoms, with a resulting variation in the force constants small enough to neglect. The results given are those for the case of four platinum atoms.

Table I includes results from two earlier studies of related systems. Eischens, *et al.*,² examined the $5\text{-}\mu$ spectrum of a mixture of C^{12}O and C^{13}O adsorbed on silica-supported platinum, and from the results predicted that ν_1 should occur near $20\text{ }\mu$. Subsequently, Eischens and Pliskin⁸ reported absorption at $21\text{ }\mu$ by carbon monoxide adsorbed on platinum dispersed on potassium bromide. Garland, *et al.*,⁵ observed absorption at $21\text{ }\mu$ by carbon monoxide adsorbed on platinum films formed by evaporating the metal in the presence of the gas. Both groups assigned the $21\text{-}\mu$ absorption to the carbon-platinum stretching vibration. The difference between our set of force constants and those obtained by the previous workers, even though there is little difference in the frequencies used, is due to the manner in which the interaction constant f affects the

(8) R. P. Eischens and W. P. Pliskin, "Advances in Catalysis," Vol. X, Academic Press, New York, N. Y., 1958.

(9) L. H. Jones, *J. Chem. Phys.*, **36**, 2375 (1962).

(10) R. W. Cattrell and R. J. H. Clark, *J. Organometal. Chem.*, **6**, 167 (1966), and references cited therein.

lattice modes of the platinum and molecular modes of the adsorbed carbon monoxide. Grimley¹¹ has treated the general problem of the vibrations of adsorbed molecules by a method which includes the interactions between lattice modes and molecular modes. In applying his treatment to the data obtained by Eischens' group^{2,8} he estimated, also neglecting intramolecular interactions, that ν_1 was shifted about 30 cm⁻¹ upward by platinum lattice modes at 156 cm⁻¹, *i.e.*, Grimley's

calculation suggests that the unperturbed value of ν_1 lies at about 446 cm⁻¹. When our value of ν_1 is corrected by the same amount, the values 17.01, 3.01, and 1.09 mdynes/Å are obtained for F_{CO} , F_{CM} , and f , respectively. These values tend toward those obtained by Jones,⁹ but they still suggest a strong interaction between the platinum crystallites and the adsorbed carbon monoxide.

(11) T. B. Grimley, *Proc. Phys. Soc. (London)*, **79**, 1203 (1962).

Solubility of Water in Compressed Nitrogen, Argon, and Methane

by M. Rigby and J. M. Prausnitz

Department of Chemical Engineering, University of California, Berkeley, California 94720
(Received August 8, 1967)

The vapor-phase solubility of water was measured in compressed nitrogen, argon, and methane at 25, 50, 75, and 100° and at various pressures between 20 and 100 atm. The volumetric properties of the vapor mixtures were described by the virial equation of state, and second virial cross coefficients were obtained from the solubility data.

The solubility of a liquid in a gas at low pressures may be calculated from the vapor pressure of the liquid. Raoult's law yields an expression for the mole fraction, y_1 , of the liquid component in the gaseous phase

$$y_1 = \frac{(1 - x_2)P^s}{P} \quad (1)$$

where x_2 is the mole fraction of the gaseous component dissolved in the liquid, P^s is the vapor pressure of the (pure) liquid, and P is the total pressure.

At low pressures, x_2 is negligibly small and the solubility is given directly by the ratio of the vapor pressure of the liquid to the total pressure. At high pressures, approaching the critical pressure of the mixture, the nonideality of the liquid phase becomes important in determining the vapor-phase solubility. However, in the intermediate pressure range with which this work is concerned, the critical factor determining the solubility is the nonideality of the vapor phase.

The equilibrium of a binary system consisting of a heavy (liquid) component 1 and a light (gaseous) component 2 is governed by the equation

$$f_i^L = f_i^V \quad (2)$$

where $i = 1, 2$, f_i is the fugacity of component i , and the superscripts L and V refer, respectively, to the liquid and vapor phases. The fugacities may be related to

the experimental quantities pressure, P , temperature, T , and the liquid and vapor compositions x and y to give

$$y_i \phi_i P = \gamma_i^{(P^r)} x_i f_i^{0(P^r)} \exp \int_{P^r}^P \frac{\bar{v}_i^L dP}{RT} \quad (3)$$

where ϕ_i is the vapor-phase fugacity coefficient, $\gamma_i^{(P^r)}$ is the liquid-phase activity coefficient, $f_i^{0(P^r)}$ is the reference fugacity of component i at T and at the reference pressure P^r , and \bar{v}_i^L is the liquid partial molar volume.

In the temperature range 25–100°, the solubility in water of argon, nitrogen, and methane is very small, and to a good approximation we may take $\gamma_1^{(P^r)} = 1$ and $\bar{v}_1^L = v_1^L$ (pure). In the pressure range under consideration here, liquid water is essentially incompressible. The mole fraction of water in the gas may therefore be written

$$y_1 = \frac{(1 - x_2)f_1^{0(P^r)}}{\phi_1 P} \exp \left(\frac{v_1^L(P - P^r)}{RT} \right) \quad (4)$$

Since x_2 is very small compared to unity, the vapor-phase solubility is determined primarily by the fugacity coefficient ϕ_1 . This may be calculated from the virial equation of state.

$$\ln \phi_1 = \frac{2}{v}(y_2 B_{12} + y_1 B_{11}) + \dots - \ln \left(\frac{Pv}{RT} \right) \quad (5)$$

where v is the vapor molar volume, B_{11} is the second virial coefficient of water, and B_{12} is the second virial cross coefficient. Under the conditions used in this study, $y_1 \ll y_2$, and, as a result, ϕ_1 is strongly dependent on B_{12} . Measurements of y_1 yield values of ϕ_1 through eq 4, and it is, therefore, possible to derive values of B_{12} from these data. Since $x_2 \ll 1$, sufficiently accurate values of $(1 - x_2)$ may be estimated from solubility data in the literature.

In general, a measurement of y_1 accurate to 1% gives rise to an uncertainty in B_{12} of around ± 6 ml/mole at 20 atm and ± 3 ml/mole at 40 atm. However, in view of the omission of higher terms in eq 5, the total uncertainties may be slightly larger. In particular, contributions from the third virial coefficients complicate the calculations at higher pressures. It is, in principle, possible, from very accurate measurements over a wide pressure range, to derive values of the third virial cross coefficients C_{112} and C_{122} . However, the uncertainties in third virial coefficients for the pure components and the limited accuracy of the present measurements have not permitted the derivation of these quantities, although corrections (using estimated values of the coefficients) have been applied in deriving values of B_{12} .

Neglecting terms of C_{112} and C_{122} leads to an apparent B_{12} which changes with pressure at constant temperature. This change, almost entirely from contributions due to C_{122} , is around 5 ml/mole in the pressure range studied at 25° and about 2 ml/mole at 100°. The effect of omitting the term in C_{112} is essentially negligible under the conditions used here.

Experimental Section

The solubility of water in compressed gases was measured using a flow system very similar to that of Benson,¹ shown schematically in Figure 1.

A steady supply of high-pressure gas was obtained from two cylinders connected by a manifold. The gas passed through a regulator, R, designed for controlled pressures up to 1500 psia. Two equilibrium cells, C, connected in series were used to ensure saturation of the gas. The cells were constructed of 2.5-in. stainless-steel pipe capped at each end and sealed with O rings. A detail drawing of an equilibrium cell is given in Figure 2. The water was contained within the cells in Pyrex liners, and the gas was dispersed from a sintered glass bubbler at the bottom of the cell. To prevent entrainment of the liquid from the equilibrium cell, several layers of glass beads were placed on a Teflon support at the top of the water in each cell. These caused the finely dispersed gas to form large bubbles before breaking the surface. In addition, a Teflon plate was placed $\frac{1}{4}$ in. below the outlet tube of the cell to

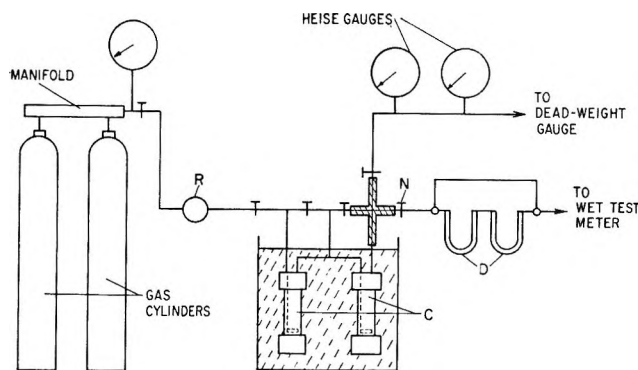


Figure 1. Schematic diagram of the apparatus.

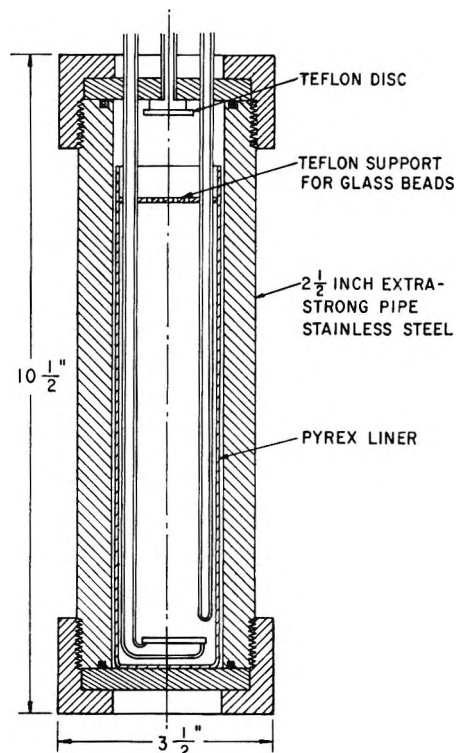


Figure 2. Equilibrium cell.

prevent spray from escaping. The cells were immersed in a constant-temperature bath, controlled to $\pm 0.01^\circ$. Temperature measurement was by calibrated mercury thermometers in thermowells in the equilibrium cells with an estimated accuracy of $\pm 0.02^\circ$.

On leaving the second cell, the vapor was led to a needle expansion valve, N, at which the pressure was reduced to approximately 1 atm. The section of tubing between the cell and the expansion valve was maintained at a temperature 10–20° above the bath temperature to prevent condensation. The pressure in the second equilibrium cell was measured using an Aminco dead-weight gauge. In experiments with nitrogen and argon, an oil separator was used, and a bellows separa-

(1) J. M. Prausnitz and P. R. Benson, *A.I.Ch.E. J.*, **5**, 161 (1959).

tor was employed for methane. The uncertainty in pressure measurement was not more than 0.3% at the lowest pressures (around 20 atm) and was smaller at the higher pressures.

After expansion, the vapor mixture was passed through two drying tubes, D, containing anhydrous magnesium perchlorate. This material has been shown² to be one of the most effective chemical desiccants, leaving a residual water concentration of less than 2 $\mu\text{g/l}$. The gas was then saturated with water and passed through a calibrated wet test meter, after which it was vented to the atmosphere.

Before making a measurement, gas was allowed to flow through the system for several hours in order to reach a steady state. The drying tubes were weighed with a total uncertainty of approximately 0.4 mg and the gas was then passed for a suitable period. The flow was then diverted around the drying tubes, which were weighed. Most experiments were planned to deposit at least 200 mg of water, yielding an uncertainty in the measurement of around 0.5%. It was generally observed that the first drying tube removed about 98% of the total water in the gas, indicating that the gas leaving the second tube was dry within the limits of the desiccant. In cases where the water concentration was very small, a correction (never exceeding 0.2%) was made to the weight of water deposited in order to take account of the equilibrium concentration of water in contact with magnesium perchlorate. The maker's calibration of the wet test meter was checked and agreement within 0.5% was found. Gas-flow rates used were normally in the range 20–40 l. of expanded gas per hour. No systematic variation of the analyses with flow rate was observed, indicating that the gas leaving the second equilibrium cell was completely saturated and that entrainment was not occurring.

The measurements of water concentration were generally reproducible within $\pm 0.5\%$ and are probably accurate within 1%, except at the lowest concentrations where the uncertainty may be slightly larger. With data of this accuracy, it was possible to derive second virial cross coefficients with an uncertainty of about ± 5 ml/mole.

Materials

Airco dry nitrogen containing less than 0.2% impurity was used. The argon was Matheson prepurified grade containing less than 0.002% of impurity. Gold Label Matheson methane, for which the manufacturer's analysis indicated an impurity of at most 100 ppm, was used. Degassed distilled water was used in all measurements.

Results

The measured mole fractions of water in compressed nitrogen, argon, and methane are given in Table I. The mole fractions listed are mean values of two or

Table I: Solubility of Water in Compressed Gases

T , °C	Pressure, atm	y_1 , exptl	y_1 , calcd	B_{12} , ml/mole
Nitrogen				
25.0	22.20	0.001529	0.001531	-40 ± 6
	30.50	0.001149	0.001149	
	38.19	0.000941	0.000943	
50.0	20.81	0.00626	0.00621	-28 ± 5
	36.93	0.00368	0.00365	
	59.04	0.00242	0.00242	
	75.99	0.001956	0.001957	
75.0	41.66	0.01009	0.01006	-20 ± 4
	60.35	0.00721	0.00723	
	88.55	0.00523	0.00522	
100.0	56.42	0.01994	0.01995	-15.5 ± 3
	78.44	0.01503	0.01491	
	100.19	0.01218	0.01219	
Argon				
25.0	20.10	0.001660	0.001657	-37 ± 6
	32.44	0.001067	0.001065	
	45.45	0.000784	0.000790	
50.0	20.21	0.00631	0.00631	-25 ± 5
	40.00	0.003328	0.003324	
	60.86	0.002275	0.002278	
75.0	31.57	0.01292	0.01284	-20 ± 4
	45.97	0.00908	0.00905	
	61.44	0.00694	0.00695	
100.0	55.50	0.01971	0.01971	-14 ± 3
	69.40	0.01606	0.01607	
	91.50	0.01258	0.01255	
Methane				
25.0	23.23	0.001483	0.001481	-63 ± 6
	30.11	0.001175	0.001174	
	40.02	0.000915	0.000919	
50.0	29.75	0.004474	0.004465	-46 ± 5
	47.75	0.002921	0.002923	
	67.28	0.002185	0.002185	
75.0	30.80	0.01335	0.01335	-37 ± 4
	54.01	0.00803	0.00803	
	66.39	0.00671	0.00672	
100.0	56.66	0.01992	0.01991	-30 ± 3
	70.95	0.01643	0.01633	
	92.25	0.01309	0.01306	

more determinations. Also given in Table I are the mole fractions calculated with eq 5, together with the values of B_{12} selected to give the closest agreement with the experimental data. Solubility data for the gases in water used in the calculations were taken from the literature.^{3–5} Table II contains the pure-component second virial coefficients and the values of the vapor pressure of water used. Although the values of B_{22} do not appear explicitly in eq 5, they are required in the calculation of the vapor molar volume. The uncer-

(2) F. Trusel and H. Diehl, *Anal. Chem.*, **35**, 674 (1963).

(3) H. A. Pray, C. E. Schweichert, and B. H. Minnich, *Ind. Eng. Chem.*, **44**, 1146 (1952).

(4) T. J. Morrison and N. B. Johnstone, *J. Chem. Soc.*, 3441 (1954).

(5) O. L. Culbertson and J. J. McKetta, *J. Petrol. Technol.*, **3**, 223 (1951).

Table II: Pure-Component Properties

T , °C	B , ml/mole				P^s_{water} , atm
	Nitrogen ^a	Argon ^a	Methane ^a	Water ^b	
25	-4.8	-15.6	-43.4	-1165	0.03126
50	-0.3	-11.1	-34.7	-803	0.1217
75	+3.4	-7.2	-27.9	-590	0.3804
100	+6.3	-3.9	-21.7	-454	1.000

^a J. H. Dymond, "Compilation of Second and Third Virial Coefficients," Physical Chemistry Laboratory, Oxford University, 1964. ^b J. P. O'Connell, Dissertation, University of California, Berkeley, Calif., 1967.

tainties in the values of B_{11} are of the order ± 30 ml/mole, but the consequent uncertainties in B_{12} are much smaller because of the low mole fraction of water vapor.

The selected values of the virial cross coefficients lead to calculated values of y_1 , which are in excellent agreement with the experimental results. The uncertainties in B_{12} decrease with increasing temperature, since the increased water vapor pressure permitted the use of higher total pressures.

In making comparison with the results of other workers, a convenient graphical representation is obtained by plotting $y_1 P / P^s$ vs. P . Under the conditions used here, this function is linear within the experimental uncertainty and has a positive slope which decreases with increasing temperature. This behavior corresponds to the normal trend to more ideal behavior at higher temperatures.

Bartlett⁶ has studied the nitrogen-water system at 50° and Saddington and Krase⁷ have made measurements in the temperature range 50–230°. These results have been discussed by Webster.⁸ In Figure 3, the data of this work and points at 50° and 51 atm by the above workers are compared. The solid lines are calculated values. There is a 6% difference between Bartlett and Saddington and Krase at 51 atm, and the disagreement is more pronounced at higher pressures.

The results of this work are in good agreement with Bartlett's data. The data of Saddington and Krase do not give constant values of B_{12} at a given temperature and different pressures; also, the fugacity coefficients ϕ_1 derived from their data do not vary smoothly with temperature and pressure. No previous work appears to have been reported for the argon-water system.

Figure 4 shows the data for the methane-water system. Also indicated are the data of Olds, Sage, and Lacey⁹ at 71.1 and 104.4°. Their values at 104.4° are in good agreement with our results, although the value at 26.37 atm lies about 1% above our line. It seems probable that the low-temperature and low-pressure data of these workers are less reliable than their results at higher temperatures and pressures. Their two data at 37.8° around 80 atm show considerable irregularity and have been omitted from their

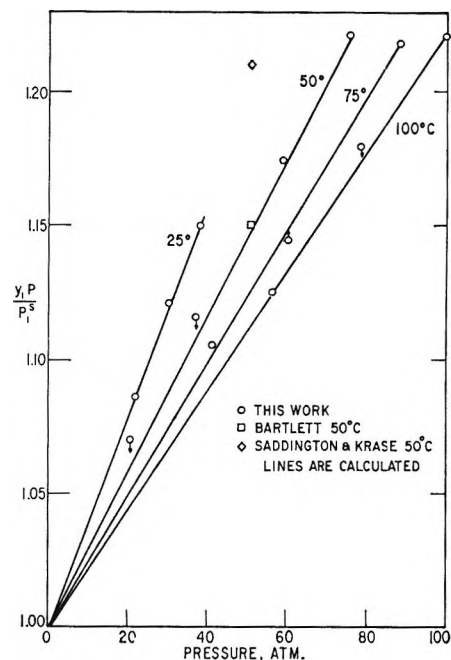


Figure 3. Solubility of water in nitrogen.

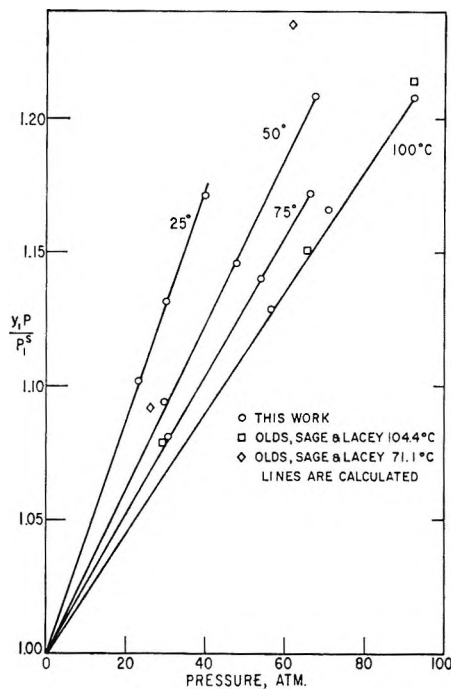


Figure 4. Solubility of water in methane.

Figure 3. However, the smoothed data of these workers at 37.8 and 71.1°, obtained by interpolation from values at higher pressures, show considerable

(6) E. P. Bartlett, *J. Am. Chem. Soc.*, **49**, 65 (1927).

(7) A. W. Saddington and N. W. Krase, *ibid.*, **56**, 353 (1934).

(8) T. J. Webster, *Discussions Faraday Soc.*, **15**, 243 (1953).

(9) R. H. Olds, B. H. Sage, and W. N. Lacey, *Ind. Eng. Chem.*, **34**, 1223 (1942).

disagreement with our results. The low-pressure data at 71.1° are shown in Figure 4, and suggest a slope intermediate between our results at 25 and 50°. At 50 atm, their data are about 4% higher than those derived from our values, and the discrepancy at 37.8° is larger. In view of the smoothness of our data, and the irregularities previously noted in those of Olds,

Sage, and Lacey, the new results are probably more reliable.

Acknowledgment. The authors are grateful to the Office of Saline Water, U. S. Department of the Interior, for financial support and to the Computer Center, University of California, Berkeley, for the use of its facilities.

Sorption of Vapors by Sepiolite

by A. J. Dandy

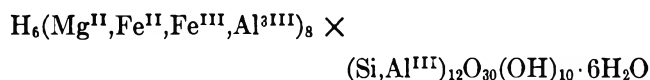
Makerere University College, University of East Africa, Kampala, Uganda, East Africa

Accepted and Transmitted by The Faraday Society (March 30, 1967)

The sorption by outgassed sepiolite of nitrogen at -197 and -184° , of oxygen at -184° , and of ammonia, methylamine, and ethylamine at 0 , 25 , and 41° has been studied. Uptakes of nitrogen and oxygen were measured volumetrically; uptakes of the other three vapors were measured by means of a silica helix. The BET surface area of sepiolite is increased by outgassing at 70 instead of at 25° . The areas calculated from isotherms for N_2 at -197 and -184° , for O_2 at -184° , and for CH_3NH_2 and $C_2H_5NH_2$ at 0° all lie in the range 354 – 383 m^2/g , but that calculated from NH_3 sorption data at 0° is 747 m^2/g . Prior heating of sepiolite in air or *in vacuo* at 300° considerably reduces the area available to nitrogen. The isosteric heat of N_2 sorption is 2.2 kcal/mole at "monolayer" coverage; values for the polar vapors increase in the order of increasing basic strength of sorbate. Differential entropies of sorption have been calculated. There are sudden changes in these functions at corresponding coverages. The results are interpreted in terms of adsorption on the external surface of sepiolite and partial penetration of the lattice "channels" of sepiolite.

Introduction

Sepiolite possesses properties which make it important as a molecular sieve and as a sorbent of gases and vapors.¹ It is a magnesium trisilicate of ideal formula $H_4Mg_9Si_{12}O_{30}(OH)_{10} \cdot 6H_2O$ and has structural similarities to attapulgite (palygorskite), which is also an important industrial sorbent. The main deposits of sepiolite are at Eski shehir (Turkey), Amboseli (Tanzania), and Vallecas (Spain). Nagy and Bradley² have proposed a structure for sepiolite. An important feature of this structure is the existence of "channels" which traverse the crystals. These channels are thought to be wider in sepiolite than in attapulgite, the dimensions being about 5.6×11.0 Å. Sepiolite samples used in the present work were obtained from Amboseli and have a chemical constitution very similar to that of Vallecas sepiolite, of approximate formula



Barrer and Mackenzie³ found that large amounts of nitrogen, *n*-pentane, and isopentane were rapidly sorbed by sepiolite at temperatures near their respective boiling points, but that neopentane was sorbed to a lesser extent. They concluded that lattice penetration by these molecules was not important or was very limited. Müller and Koltermann⁴ investigated the flow of various gases through a column of sepiolite at 20° and atmospheric pressure. While CO_2 , SO_2 , *n*- C_4H_{10} , CCl_3 -

- (1) R. H. S. Robertson, *Chem. Ind.* (London), 1492 (1957).
- (2) B. Nagy and W. F. Bradley, *Am. Mineralogist*, **40**, 855 (1955).
- (3) R. M. Barrer and N. Mackenzie, *J. Phys. Chem.*, **58**, 560 (1954).
- (4) K. P. Müller and M. Koltermann, *Z. Anorg. Allgem. Chem.*, **36**, 341 (1965).

NO_2 , and $n\text{-C}_4\text{H}_9\text{OH}$ were strongly sorbed, no sorption of CO and N_2 could be observed. They state that N_2 and CO can pass freely through the channels of the sepiolite structure and conclude that the latter have a diameter of 6–8 Å.

It was of interest to extend these investigations by studying the sorption of molecules of differing sizes and polarities by sepiolite at various temperatures. The results yield information concerning the nature and availability of the surface.

Experimental Section

* Sepiolite was obtained from Amboseli, Tanzania, and was identified by X-ray and chemical analysis. In all cases, the analyses show the mineral to be a very pure sepiolite. The DTA curves were similar to those found for Vallecas sepiolite, although a sharp peak at 850° was not observed. Samples were ground to between 30 and 40 BS mesh.

Cylinder nitrogen and oxygen were purified and dried. Ammonia, methylamine, and ethylamine were prepared by heating NH_4Cl , $\text{CH}_3\text{NH}_2 \cdot \text{HCl}$, and $\text{C}_2\text{H}_5\text{NH}_2 \cdot \text{HCl}$, respectively, with soda lime. All solids were previously degassed *in vacuo*. The vapors were purified by passage over CaO , soda lime, and NaOH , and by repeated fractionation; they were stored over fresh CaO . Vapor pressure measurements showed that the temperatures of liquid N_2 and liquid O_2 were -197 and -184° , respectively, at the prevailing atmospheric pressure (ca. 66 cm).

The sorption isotherms of N_2 at -197 and at -184° , and of O_2 at -184° were determined in a standard volumetric apparatus. Pressures were measured by means of a mercury manometer connected to the sorption vessel *via* a solid CO_2 -acetone cold trap. A silica helix was used to measure gravimetrically the sorption of NH_3 , CH_3NH_2 , and $\text{C}_2\text{H}_5\text{NH}_2$ on sepiolite. It had an extension of 63.7 cm when fully loaded at 2.5 g. The sensitivity over the measured range was about 17.95 cm/g and was checked between runs. The extensions were independent of temperature in the range 0 – 70° , and buoyancy corrections were negligible, except at pressures higher than 30 cm, when they were very small. A cathetometer, reading to 0.001 cm, was used to measure the extension of the helix and the mercury manometer levels. The balance case was kept at a constant temperature by immersion in a thermostated water bath (constant to $\pm 0.1^\circ$) or in ice. An oil diffusion pump backed by a Speedivac rotary oil pump was used to evacuate the apparatus to about 5×10^{-6} mm, as measured by a McLeod gauge (bulb capacity, 310 ml; capillary, 1 mm) and a Speedivac Pirani gauge.

Results and Discussion

Surface Area and Water Removal. Figure 1 illustrates typical N_2 and O_2 isotherms on outgassed sepiolite samples. Variation of the outgassing periods from 1

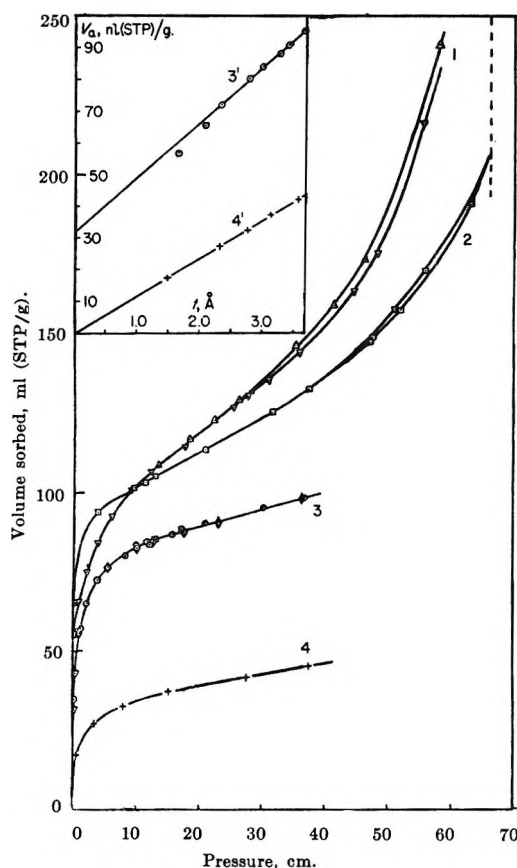


Figure 1. 1, Sorption of O_2 on sepiolite at -184° : ∇ , sorption; Δ , desorption; outgassed 1 hr at 96° ; 2, sorption of N_2 on sepiolite at -197° : outgassed 24 hr at 70° ; 3, sorption of N_2 on sepiolite at -184° : \odot , outgassed 1 hr at 96° ; \diamond , outgassed 24 hr at 70° ; 4, sorption of N_2 on sepiolite at -184° : outgassed 1 hr at 300° , dotted line represents P_0 for curves 1 and 2; inset, V_a [ml(STP)/g] vs. t plots for curves 3 and 4.

to 24 hr had negligible effect on the reproducibility of isotherms. The outgassing procedure was standardized to 24 hr at 70° for the majority of the later experiments. The isotherms were type II in the Brunauer classification and yielded good straight lines up to $P/P_0 = 0.2$, when plotted according to the BET equation. BET surface areas were calculated from N_2 isotherms at -197 and -184° , and from O_2 isotherms at -184° , on sepiolite samples subjected to various outgassing procedures. The results are presented in Table I. The cross-sectional area of a N_2 molecule was taken as 16.2 \AA^2 at -197° and as 16.9 \AA^2 at -184° , and that of O_2 was taken as 14.1 \AA^2 at -184° .

Caution is required in interpreting these results, particularly as micropore filling may be occurring in the initial stages of the isotherms; this will be discussed later. However, they are expressed as BET surface areas for convenience, and some general conclusions can be drawn from a comparison of the values. The areas calculated for samples outgassed at 70 and 96° were reproducible, and those derived from N_2 isotherms are in good agreement with each other; it is not possible to make a true comparison of these with the result

Table I: BET Surface Areas of Sepiolite Samples

Preheating in air	Outgassing procedure	BET area, m ² /g	Isotherm
...	48 hr at 25°	354	N ₂ at -184°
...	24 hr at 70°	380	N ₂ at -184°
...	24 hr at 70°	375	N ₂ at -197°
...	1 hr at 96°	375	N ₂ at -184°
...	3 hr at 96°	378	N ₂ at -184°
...	48 hr at 25°	310	O ₂ at -184°
...	1 hr at 96°	352	O ₂ at -184°
...	1 hr at 300°	195	N ₂ at -184°
...	1 hr at 400°	196	N ₂ at -184°
1 hr at 100°	5 min at 25°	330	N ₂ at -184°
1 hr at 200°	5 min at 25°	328	N ₂ at -184°
1 hr at 300°	5 min at 25°	158	N ₂ at -184°
1 hr at 500°	5 min at 25°	158	N ₂ at -184°
1 hr at 700°	5 min at 25°	157	N ₂ at -184°

calculated from the oxygen isotherm, owing to the uncertainty in the values of N₂ and O₂ molecular cross-sectional areas. The highest surface areas reported here are higher than those previously reported for sepiolite obtained from other sources.^{1,3,4} Nevertheless, the relationship between surface area and heat pretreatment (water loss) is similar to that found by Barrer and Mackenzie,³ who heated sepiolite samples *in vacuo*; the surface area is increased by outgassing at 70° rather than at 25° and is markedly decreased by heating in air or *in vacuo* above 200°. (The low area obtained for samples preheated in air at 300°, compared with that for sepiolite heated at 300° *in vacuo*, may be partly due to sorption of atmospheric moisture during transfer to the sorption apparatus in the former case.) The density of sepiolite samples as received was 2.086 g/ml. This rose to about 2.7 g/ml on outgassing at 70°, and was accompanied by a loss in weight of about 19% (based on the outgassed weight). Heating in air at 100° caused a loss in weight of about 14.5%. It has been reported⁵ that six molecules of adsorbed water and one molecule of coordinated water per half-cell are lost easily on heating. Between 250 and 350°, a further two half-molecules of coordinated water are lost, and a structure transformation takes place at about 350°.

Outgassing or heating sepiolite at temperatures up to 200° thus removes water and makes more surface available for the adsorption of nitrogen. This may be interpreted in terms of at least partial penetration of the lattice channels by N₂. The O₂ molecules appear to penetrate these channels to about the same extent. The decrease in the BET surface area of sepiolite, which occurs when samples are heated above 200°, may be due to sealing of the channel entrances, though Barrer³ has tentatively suggested that the cause may be the smoothing of surface corrugations. Müller⁴ has shown that sorption data for the large molecules *n*-C₄H₁₀ (estimated

cross-sectional area 37.6 Å²) yield a low value for the surface area of sepiolite (163 m²/g, compared with a value of 331 m²/g derived from the uptakes of CO₂ (16.9 Å²) and SO₂ (24.4 Å²). This low value may represent the "external" surface, excluding the surface in the channels. It compares with the value of 196 m²/g for sepiolite heated *in vacuo* at 300 or 400° (Table I). At such temperatures, therefore, the microporous structure may partially collapse, leaving only the external surface accessible to nitrogen. This view is supported by a comparison of the N₂ isotherms at -184° for sepiolite outgassed at 96° and sepiolite preheated at 300° (curves 3 and 4 in Figure 1). The former curve exhibits a much steeper slope in the initial stages than does curve 4; it has been suggested⁶ that a steep slope in this initial region indicates micropore filling by the adsorbate on microporous solids. The application of the BET equation may then evaluate external surface plus micropore volume, though the application of the BET equation itself in these circumstances is of uncertain validity.

de Boer, *et al.*,⁷ have suggested that plots of V_a (volume sorbed, ml (STP)/g) *vs.* the thickness of the adsorbed layer, t , may yield information concerning the pores of sorbents. The thickness of the sorbed layer, t , may be put equal to $16.43 V_a/A$ for N₂ at -184°, assuming a liquid density of 0.76 g/ml. The inset in Figure 1 is t plots based on the ideal shape for N₂ sorption at -184° on sepiolite outgassed at 300° (plot 4'); the assumption is made that for this sample the BET surface area, A , of 195 m²/g represents the external surface. Plot 3' for N₂ sorption on sepiolite outgassed at 70 or 96° is linear after an initial steep rise; the linear section cuts the ordinate at $V_a = 32$ ml. No physical significance can be given to the t plot values in this case, but the shape of plot 3' suggests that micropores are being filled in the initial section.^{8,9} de Boer relates the slopes of t plots to the external surface areas of sorbents. The slope of the linear portion of 3' is greater than that of 4'; hence large pores or surface corrugations, in addition to micropores, may be destroyed by heating sepiolite samples at 300°.

Dubinin has modified the Polanyi potential theory¹⁰ for microporous solids, and has derived¹¹ the isotherm equation

(5) J. L. Martin-Vivaldi and J. Cano-Ruiz, National Academy of Science of Spain, National Research Council Publication No. 456, 1956, p 177.

(6) S. J. Gregg and K. S. W. Sing, "Adsorption, Surface Area, and Porosity," Academic Press, London, 1967, p 208.

(7) B. C. Lippens, B. G. Linsen, and J. H. de Boer, *J. Catalysis*, **3**, 32 (1964); B. C. Lippens and J. H. de Boer, *ibid.*, **4**, 319 (1965); J. H. de Boer, B. G. Linsen, and Th. J. Osinga, *ibid.*, **4**, 643 (1965); J. H. de Boer, *et al.*, *J. Colloid Interface Sci.*, **21**, 405 (1966).

(8) R. E. Day and G. D. Parfitt, *Trans. Faraday Soc.*, **63**, 708 (1967).

(9) R. F. Horlock and P. J. Anderson, *ibid.*, **63**, 717 (1967).

(10) M. Polanyi, *ibid.*, **28**, 316 (1932).

(11) M. M. Dubinin, *Chem. Rev.*, **60**, 235 (1960).

$$\log V_a = \log (V_0) - D(\log P_0/P)^2 \quad (1)$$

where V_a = volume uptake of adsorbate, V_0 = total volume of micropores, and D is a constant. Figure 2 illustrates Dubinin plots for N_2 sorption at -184 and -197° on sepiolite samples outgassed at 70 or 96° . The results satisfy the Dubinin equation in the initial stages of N_2 uptake.

Extrapolation of the lines gives intercepts which correspond to uptake volumes approximately the same as the volumes at BET monolayer coverage, found by applying the BET equation. However, the interpretation of V_0 remains uncertain. The fact that the Dubinin equation is obeyed suggests that N_2 does have partial access to micropores with overlapping force fields for sepiolite samples outgassed at 96° .

The isosteric heat of adsorption of N_2 on sepiolite was calculated from the adsorption isotherms at -197 and -184° , using the Clausius-Clapeyron equation. The value was 2.2 kcal/mole in the region of BET monolayer coverage.

Sorption of Polar Vapors. The sorption of NH_3 , CH_3NH_2 , and $C_2H_5NH_2$ by sepiolite at 0 , 25 , and 41° was studied. Fresh samples of sepiolite were outgassed at 70° for at least 24 hr before each run. Typical results are shown in Figures 3, 4, and 5. Points on any isotherm were reproducible after raising and lowering the temperature through the range 0 – 41° . With the exception of $C_2H_5NH_2$ at 0° at high relative pressures, the isotherms were all reversible, although long periods of evacuation at 70° were necessary to completely remove any of these vapors from sepiolite samples.

The $C_2H_5NH_2$ isotherm at 0° shows definite hysteresis effects. Experimental points were determined after many days to allow the system to reach equilibrium.

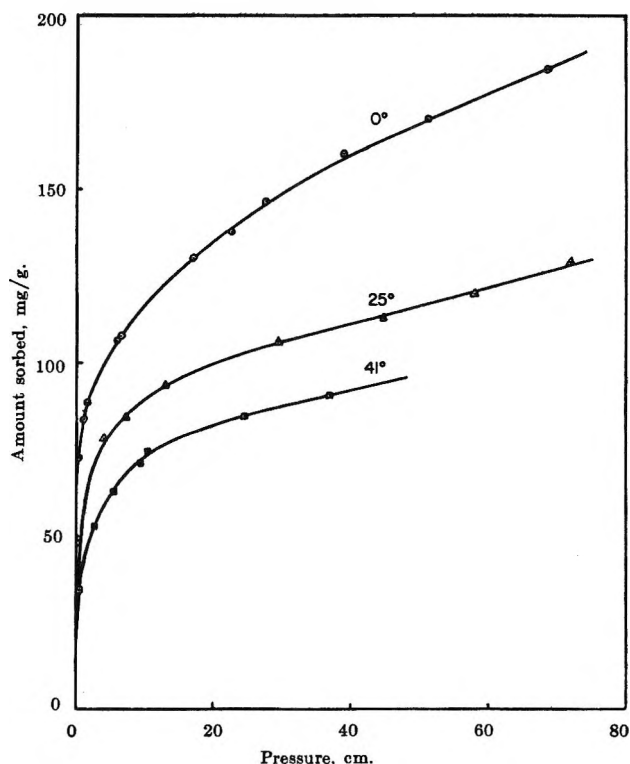


Figure 3. Sorption of NH_3 on sepiolite outgassed at 70° .

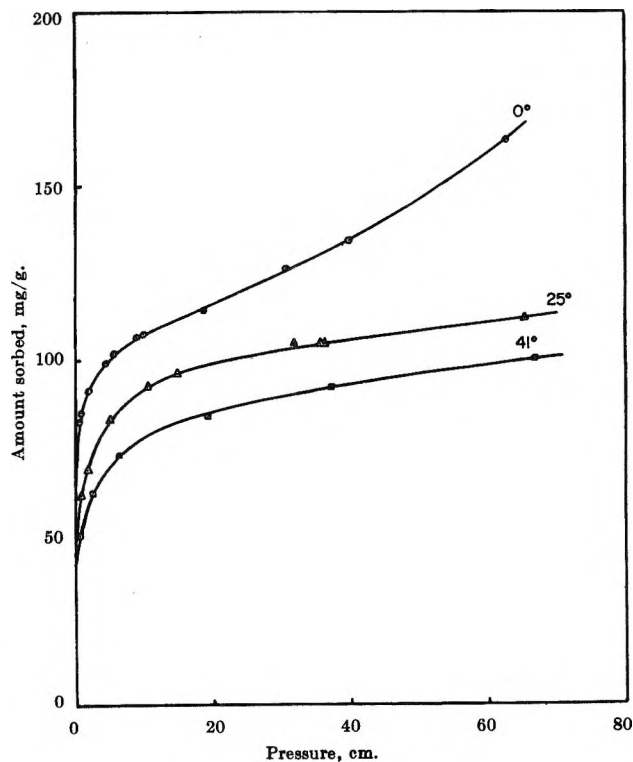


Figure 4. Sorption of CH_3NH_2 on sepiolite outgassed at 70° .

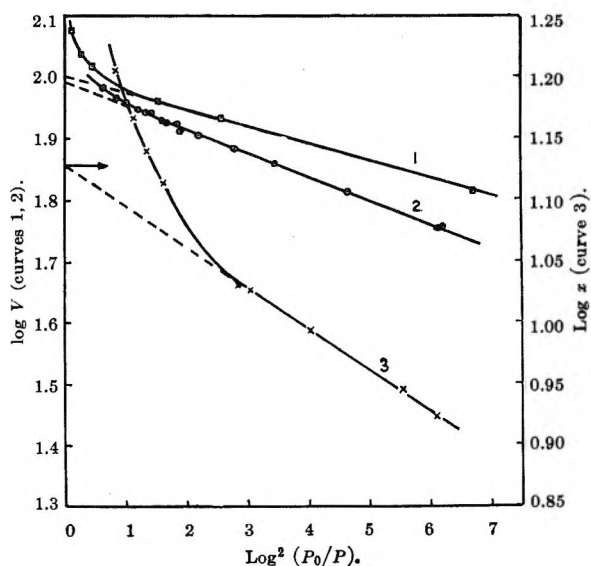


Figure 2. Dubinin plots of vapor sorption on sepiolite: 1, N_2 at -197° ; 2, N_2 at -184° (sepiolite outgassed at 70 or 96°); 3, NH_3 at 0° (sepiolite outgassed at 70°).

In general, equilibria were achieved only after several hours. This effect indicates lattice penetration by sorbate molecules. The relative pressures achieved with NH_3 and CH_3NH_2 at the temperatures studied

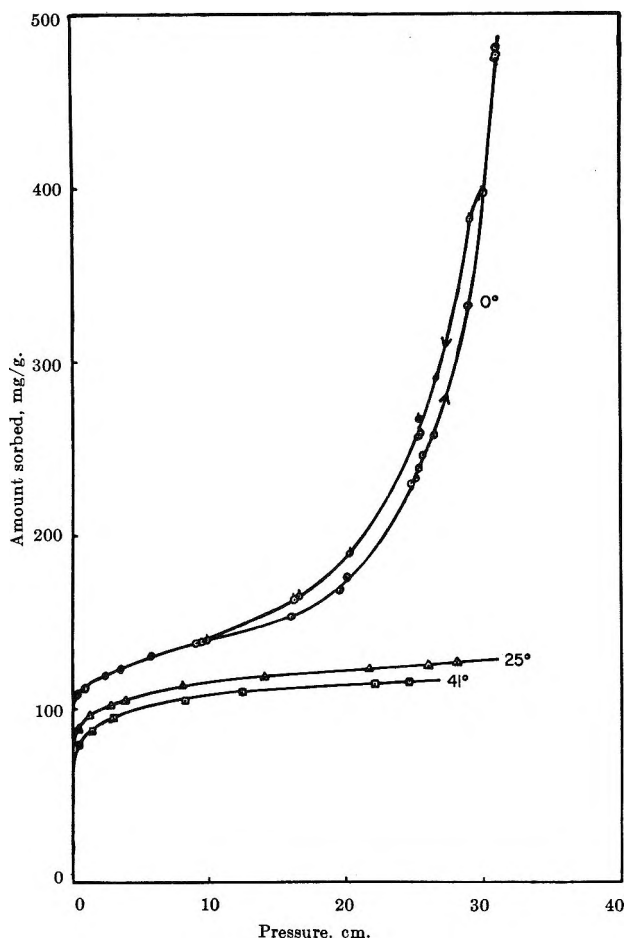


Figure 5. Sorption of $\text{C}_2\text{H}_5\text{NH}_2$ on sepiolite outgassed at 70° .

were not high enough for hysteresis effects to be detected.

The data obtained at 0° were plotted according to the BET equation and yielded good straight lines up to $P/P_0 = 0.2$. Surface areas of sepiolite were calculated from these plots, using the equation¹²

$$\sigma = 1.091(M/Nd)^{2/3} \quad (2)$$

(M = molecular weight and d = density of liquid sorbate) to calculate σ , the cross-sectional areas of sorbate molecules. The results are presented in Table II, which also includes relevant data for the three vapors taken from the literature.

BET surface areas of sepiolite calculated from CH_3NH_2 and $\text{C}_2\text{H}_5\text{NH}_2$ isotherms are in general agreement with the values calculated from N_2 and O_2 isotherms (see Table I). However, the ammonia isotherm yields the very high value of $747 \text{ m}^2/\text{g}$. This may represent the failure of the BET equation to give meaningful surface areas in this case; alternatively, the channels in the sepiolite structure may be penetrated to a much greater extent by NH_3 than by the other vapors because of greater accessibility due to small molecular size and relatively strong interaction with the surface. Estimates of the dimensions of the channel openings

Table II: Constants for NH_3 , CH_3NH_2 , and $\text{C}_2\text{H}_5\text{NH}_2$, and BET Surface Areas for Sepiolite Calculated from Vapor Sorption Isotherms at 0°

	NH_3	CH_3NH_2	$\text{C}_2\text{H}_5\text{NH}_2$
Critical temperature	130°	160°	183°
Boiling point	-33°	-7°	$+15^\circ$
$\text{p}K_b$	4.75	3.37	3.27
ΔH of evaporation, kcal/mole	-5.5	-6.4	-6.6
P_0 at 0° , cm	323.6	100.4	37.2
Molecular cross-sectional area, \AA^2	13.7	19.4	24.4
BET surface area of sepiolite, m^2/g	747	383	370

have been given as $6\text{--}8 \text{ \AA}$ in diameter⁴ and as $5.6 \times 11.0 \text{ \AA}^2$. The NH_3 molecule has an estimated diameter of about 4 \AA at 0° . The Dubinin plot for NH_3 uptake at 0° (Figure 2) yielded an intercept corresponding to $x_0 = V_0/d = 136 \text{ mg/g}$, compared to the BET monolayer uptake of 154 mg/g . Such intercepts have been interpreted as representing the micropore volume filled by capillary condensation at low relative pressures as a result of the overlap of strong force fields in the micropores of the adsorbent.^{11,13}

Barrer and Mackenzie³ measured a large uptake of NH_3 on the mineral attapulgite, which has a structure similar to sepiolite. They interpreted this result as due to lattice penetration by NH_3 , but stated that N_2 did not enter the lattice of that mineral at all. The difference in the surface areas of attapulgite calculated from N_2 and isooctane-molecule isotherms was ascribed

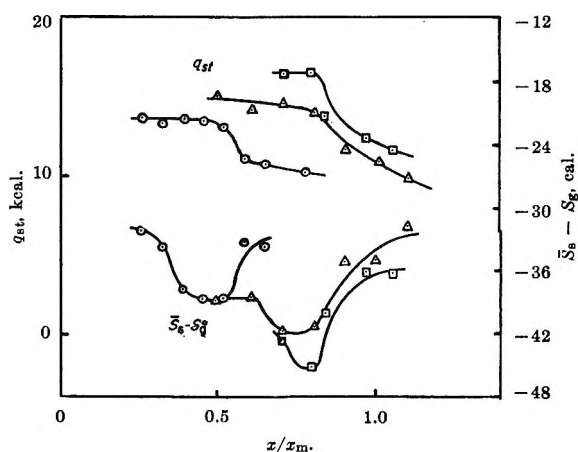


Figure 6. Molar isosteric heats and differential entropies of sorption on sepiolite: \circ , NH_3 ; Δ , CH_3NH_2 ; \square , $\text{C}_2\text{H}_5\text{NH}_2$. x_m is BET monolayer uptake.

(12) P. H. Emmett and S. Brunauer, *J. Am. Chem. Soc.*, **59**, 1553 (1937).

(13) T. G. Lamond and H. Marsh, *Carbon*, **1**, 281 (1964).

to imperfect packing of the large isooctane molecules on corrugations of the surface of attapulgite. Such corrugations may also exist on the sepiolite surface. However, it is clear that the uptake of N_2 increases with progressive water removal, presumably from the lattice channels. N_2 , CH_3NH_2 , and $C_2H_5NH_2$ all appear to have access to approximately the same amount of surface. These results may therefore indicate that the channels are at least partially accessible to molecules of cross-sectional areas less than approximately 25 \AA^2 .

Thermodynamic Functions. Isosteric heats of adsorption, q_{st} , were calculated by applying the Clausius-Clapeyron equation to the isotherms at 0, 25, and 41° . Differential entropies of adsorption, \bar{S}_s , relative to the molar entropy of gaseous adsorbate at one atmosphere pressure, S_G° , were calculated from the equation

$$\bar{S}_s - S_G^\circ = -q_{st}/T - R \ln P \quad (3)$$

Values of the isosteric heats and differential entropies of sorption are presented in Figure 6. The error in q_{st} values is estimated to be $\pm 0.7 \text{ kcal/mole}$, which imposes an error of about $\pm 2.5 \text{ cal}$ in the values of \bar{S}_s . In addition, the uncertainties inherent in the BET method introduce errors in calculations of surface coverage for different vapors.

All the values of q_{st} are high relative to the latent heats of liquefaction, which are all about 6 kcal/mole , and they increase in the order of increasing basic strength of the sorbate. Interaction of sorbate with the sepiolite surface is facilitated by increasing basic strength of sorbate; this interaction may thus take place at specific acidic sites on the surface.

Acknowledgments. The author is indebted to the British Ceramic Research Association and the Geological Survey Unit, Dodoma, Tanzania, for X-ray analysis of sepiolite samples.

A Light-Scattering Study of the Effect of Temperature on the Micellar Size and Shape of a Nonionic Detergent in Aqueous Solution

by D. Attwood

Department of Pharmacy, University of Strathclyde, Glasgow, Scotland, United Kingdom

Accepted and Transmitted by The Faraday Society (April 6, 1967)

Light scattering and viscosity methods have been used to determine changes in size and shape of the micelles in aqueous solutions of heptaoxyethylene glycol monohexadecyl ether at temperatures above the threshold temperature. The concentration dependence of turbidity in dilute solutions is more pronounced than reported previously and is not due to contributions to the nonideality of the solutions arising from the presence of maxima or minima in the consolute boundaries. The micelle molecular weight increases exponentially with temperature, and the angular dependence of scattered light indicates a rod-like model at all temperatures. The systems are shown to be non-Newtonian at high temperatures, and viscosity results obtained using a Couette viscometer show anomalous concentration dependence, indicative of micellar growth at low concentrations. An empirical interpretation of the viscosity data yields asymmetry values in agreement with those from light scattering. Micellar hydration is calculated from a combination of the viscosity and light-scattering data, and the structure of the micelles is discussed.

Introduction

Previous measurements of the temperature-dependent changes in the micelle molecular weight (mmw) in aqueous solutions of heptaoxyethylene glycol monohexadecyl ether (abbreviated to Hn_7) have indicated a threshold temperature above which a rapid increase in

the mmw occurs and pronounced micellar asymmetry develops.¹

In the present investigation, a more detailed study has been made of the changes in micellar size and shape

(1) P. H. Elworthy and C. McDonald, *Kolloid-Z.*, **195**, 16 (1964).

in aqueous solution using light-scattering and viscosity techniques, and a model has been suggested for the micelles at elevated temperatures.

In common with other nonionic surfactants,²⁻⁹ solutions of Hn₇ exhibit an initial rapid increase in turbidity as the concentration is increased above the critical micelle concentration (cmc), and this increase has been explained in terms of micellar growth by the association of small micellar units, using the mass action theory.⁸ Extrapolation of the light-scattering data to determine the mmw of the small micellar unit is, however, difficult because of the magnitude of the upward curvature of the light-scattering plots. A light-scattering photometer has been constructed enabling precise measurements to be made at lower concentrations than was previously possible, in an attempt to determine the extrapolated mmw with greater certainty.

It has recently been suggested¹⁰ that the temperature and concentration dependent changes in turbidity for this and other nonionic surfactants are explicable in terms of the solution nonideality associated with the presence of consolute boundaries in these systems. The temperature range over which the Hn₇-water system exists as one isotropic solution is limited by two consolute boundaries: an upper cloud point and a lower Krafft point. This paper reports on the concentration dependence of the two boundaries and relates the light-scattering results to this in the light of these suggestions.

Experimental Section

Materials. 3,6,9,12,15,18,21 - Heptaoxaheptatriacontan-1-ol (heptaoxyethylene glycol monohexadecyl ether, Hn₇) was synthesised and purified as described previously.⁸ The ethylene oxide content was determined using the method of Siggia, *et al.*,¹¹ and a value of 55.6% obtained in agreement with the theoretical value (55.9%).

Light Scattering. A light-scattering photometer was constructed, similar in design to the Sofica instrument, but fitted with an automatic scanning device and recording system. The cylindrical light-scattering cell (Brice Phoenix catalog No. C-101) was immersed in a bath of liquid paraffin, the refractive index of which was adjusted to that of the glass of the cell ($n = 1.475$) to minimize parasitic reflections at the cell walls. The optical systems were telecentric¹² and designed so that the photomultiplier did not "see" past the edges of the incident beam. The photomultiplier tube (E.M.I. 6097B) was driven in a 110° arc about the center of the cell at the rate of 30°/min, and the output was fed into a Honeywell Brown 0-5 mv strip-chart recording potentiometer. An extremely stable response was obtained, the variation in the scale reading being less than 0.5% at the highest sensitivity used. Microswitches accurately positioned around the base of the instrument were activated by the rotation of the photomultiplier tube and operated an auxiliary pen on the recorder,

placing angle marks at 10° intervals. An automatically operated camera shutter in the path of the incident beam enabled the dark current of the photomultiplier tube to be recorded in between the measurements of scattered intensity. Measurement of the angular dependence of the fluorescence of an aqueous solution of Rhodamine 6G (B.D.H.) was used to check the positioning of the microswitches. The absence of stray light over the angular range 40°-140° was verified by the measurement of the light scattering from clarified benzene. The temperature of the cell assembly was controlled to within $\pm 0.1^\circ$.

The instrument was calibrated at wavelengths of 4358 and 5461 Å, using Ludox colloidal silica according to the method suggested by Maron and Lou.¹³ The usual precautions were taken to avoid errors in the measurements of the turbidity of the Ludox suspensions due to the scattering of light by the Ludox particles.¹⁴ In particular, it was found necessary to considerably reduce the acceptance angle of the spectrophotometer (Unicam S.P. 600) to prevent measurement of the light scattered in the forward direction.¹⁵ A weight-average molecular weight of 3.1×10^5 was obtained for a polystyrene fraction supplied by the National Chemical Laboratory in agreement with a quoted value of 3.0×10^5 .

The surfactant solutions were clarified by ultrafiltration through 0.22-μ Millipore filters, and light-scattering measurements were made at 4358 Å. Concentrations were determined interferometrically after filtration using a Hilger-Rayleigh interference refractometer.

Viscosity. Measurements at 35° using capillary viscometers (Cannon-Fenske No. 50 and 100 and a suspended level viscometer) indicated non-Newtonian behavior. Viscosity determinations at all temperatures were therefore carried out using a Couette viscometer,¹⁶ thermostated to within $\pm 0.05^\circ$ and with a variable shear rate between 0 and 40 sec⁻¹.

(2) L. M. Kushner and W. D. Hubbard, *J. Phys. Chem.*, **58**, 1163 (1954).

(3) L. M. Kushner, W. D. Hubbard, and A. S. Doan, *ibid.*, **61**, 371 (1957).

(4) J. M. Corkill, J. F. Goodman, and R. H. Ottewill, *Trans. Faraday Soc.*, **57**, 1627 (1961).

(5) R. R. Balmbra, J. S. Clunie, J. M. Corkill, and J. F. Goodman, *ibid.*, **58**, 1661 (1962).

(6) R. R. Balmbra, J. S. Clunie, J. M. Corkill, and J. F. Goodman, *ibid.*, **60**, 979 (1964).

(7) K. Kuriyama, *Kolloid-Z.*, **180**, 55 (1962).

(8) P. H. Elworthy and C. B. Macfarlane, *J. Chem. Soc.*, 907 (1963).

(9) J. M. Corkill, J. F. Goodman, and T. Walker, *Trans. Faraday Soc.*, **63**, 759 (1967).

(10) K. W. Herrmann, J. G. Brushmiller, and W. L. Courchene, *J. Phys. Chem.*, **70**, 2909 (1966).

(11) S. Siggia, A. C. Starke, J. J. Garis, and C. R. Stahl, *Anal. Chem.*, **30**, 115 (1958).

(12) L. Kushner, *J. Opt. Soc. Am.*, **44**, 155 (1954).

(13) S. H. Maron and R. L. H. Lou, *J. Polymer Sci.*, **14**, 29 (1954).

(14) W. Heller and R. M. Tabibian, *J. Colloid Sci.*, **12**, 25 (1957).

(15) G. F. Lothian and F. P. Chappel, *J. Appl. Chem.*, **1**, 475 (1951).

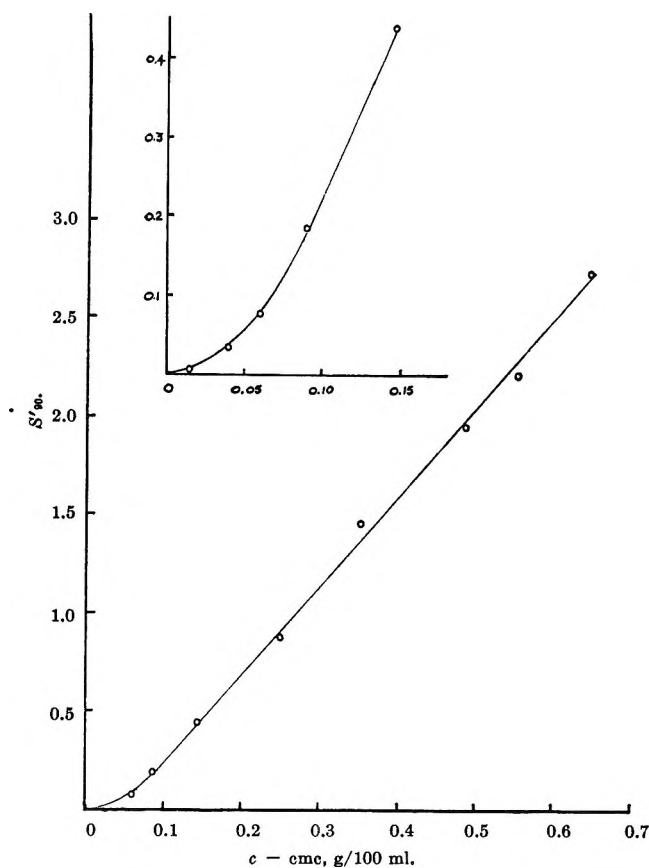


Figure 1. Excess scattering intensity at $\theta = 90^\circ$ as a function of the concentration of micelles for Hn_7 at 25° .

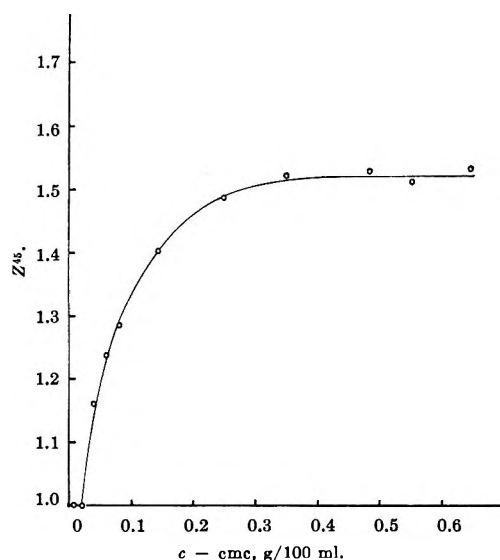


Figure 2. The dissymmetry of the scattering envelope of solutions of Hn_7 at 25° as a function of the concentration of micelles.

Phase Studies. The phase behavior of the Hn_7 -water system was examined over the concentration range $6 \times 10^{-4} \text{ g ml}^{-1}$ – $6 \times 10^{-3} \text{ g ml}^{-1}$. The cloud points of a series of solutions of known concentration were determined by sealing the solutions in small glass tubes fitted with a thermometer and gently heating

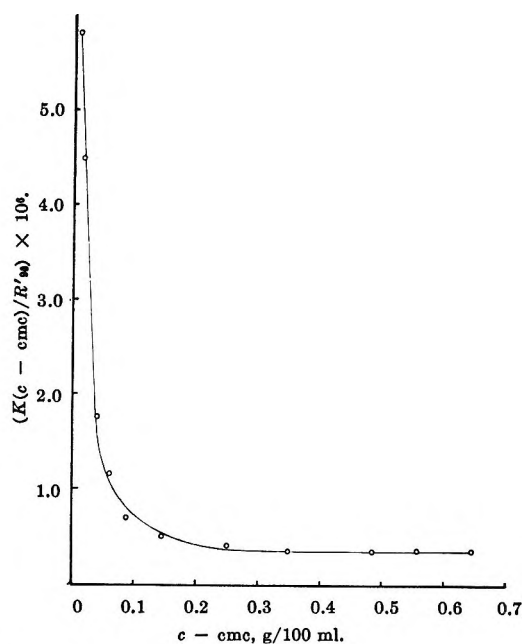


Figure 3. Debye plot for Hn_7 at 25° .

them in a temperature-controlled water bath. The concentration dependence of the Krafft point was investigated by a similar method, using a refrigerated thermostat bath to cool the solutions. Phase separation in both cases was marked by the first appearance of turbidity in the solutions.

Results and Discussion

Concentration Dependence of Micelle Molecular Weight.

Figure 1 shows the variation of S'_{90} with the micellar concentration at a temperature of 25° , where S'_{90} is the intensity of the light scattered by aqueous Hn_7 solutions at an angle of 90° , in excess of that from solutions at the cmc ($9.4 \times 10^{-7} \text{ g ml}^{-1}$ as determined by surface tension measurements¹⁷). Similar plots were obtained at other temperatures up to 35° and all show a positive curvature at low concentrations (less than $1 \times 10^{-3} \text{ g ml}^{-1}$). The dissymmetry, Z^{45} , of the scattering envelope, expressed as the ratio of the excess scattering intensity at an angle of 45° to that at 135° , also shows a concentration dependence (Figure 2) for concentrations less than $3 \times 10^{-3} \text{ g ml}^{-1}$. The S'_{90} values plotted in Figure 1 have been corrected for the effect of this dissymmetry. As a consequence of the curvature in the S'_{90} vs. $(c - \text{cmc})$ graphs, the Debye plots show a very pronounced upward curvature at concentrations below approximately $2 \times 10^{-3} \text{ g ml}^{-1}$ (Figure 3). For systems such as the Hn_7 - H_2O systems which show consolute boundaries, concentration-dependent changes in $K(c - \text{cmc})/R'_{90}$ may be due not only to changes in mmw, but also to extreme nonideality if measurements

(16) A. G. Ogston and J. E. Stanier, *Biochem. J.*, **53**, 4 (1953).

(17) P. H. Elworthy and C. B. Macfarlane, *J. Pharm. Pharmacol.*, **14**, 100T (1962).

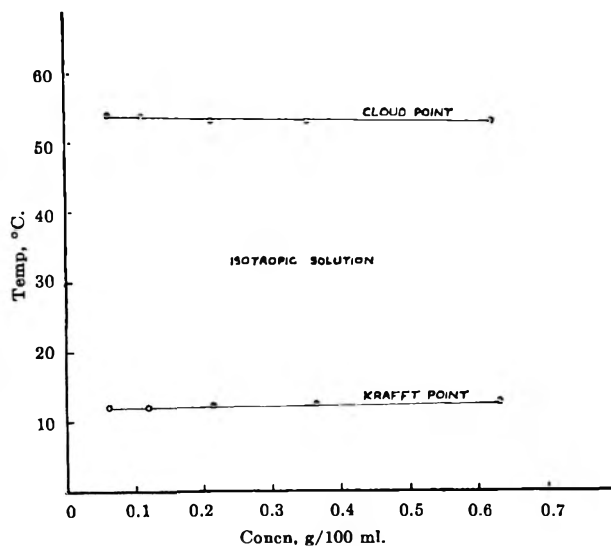


Figure 4. Concentration dependence of the consolute boundaries for the $\text{Hn}_7\text{-H}_2\text{O}$ system.

are made in the vicinity of maxima or minima in the consolute boundaries.¹⁰ Figure 4 shows the absence of a critical concentration in either of the phase boundaries for concentrations as low as $0.6 \times 10^{-3} \text{ g ml}^{-1}$, and it is concluded that the light-scattering behavior is indicative of an increase in micellar size and asymmetry with concentration, until a constant mean size and shape is attained.

Many workers^{2,3,5,6,8,9} have suggested that increase in size occurs by the association of small micelles formed at the cmc, and for several surfactants the size of the aggregating units has been determined by extrapolation of curved light-scattering plots to the cmc.^{8,9} A mmw of 3.27×10^5 has been obtained in this way for the Hn_7 system.⁸ The experimentally obtained curvature at low concentrations shown in Figure 3 is, however, more pronounced than the extrapolated curvature from which this mmw value was derived. Consequently, a much lower mmw is indicated (less than 80,000), although it is not possible to assign an accurate value because of the uncertainty of extrapolation of the available data. Errors arising from the presence of any dust in the solutions become appreciable as the solution scatter approaches that of the solvent and, consequently, the lower concentration range at which precise measurements can be made is limited.

The mmw's of the large micellar species in aqueous solutions of nonionic detergents have been determined by two methods. Linear Debye plots have been obtained using the light-scattering cmc (determined by linear extrapolation of the S'_{90} vs. c graphs) rather than the surface tension cmc, and extrapolated to give the mmw in the usual way.^{1,5,10,18} Alternatively, the mmw has been calculated from the horizontal portion of the light-scattering graphs, plotted as in Figure 1 using the surface tension cmc.^{4,6} There is little significant differ-

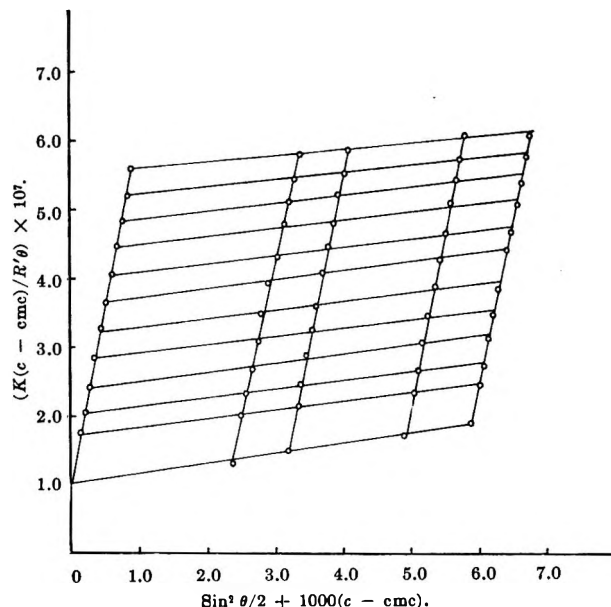


Figure 5. Zimm plot for Hn_7 at 35° .

ence in the mmw values obtained using either of these methods for the Hn_7 system. In the present investigation, the size and shape of the large micelles were determined using the Zimm method. The concentration range was restricted to between $4 \times 10^{-3} \text{ g ml}^{-1}$ and $6 \times 10^{-3} \text{ g ml}^{-1}$, which corresponds to the linear portion of the Debye plots. Graphs of $K(c - \text{cmc})/R'_\theta$ vs. $\sin^2(\theta/2) + 1000(c - \text{cmc})$, where c = surfactant concentration in g ml^{-1} ; R'_θ = reduced intensity at an angle θ , in excess of that scattered by solution at the cmc; K = optical constant; and cmc = critical micelle concentration as determined by surface tension measurements, were extrapolated linearly to $c = \text{cmc}$ and $\theta = 0^\circ$ to obtain the weight-average mmw (see Figure 5).

Temperature Dependence of Micellar Size and Shape. The light-scattering data obtained for the large micellar species at a series of temperatures above the threshold temperature (22°) are summarized in Table I. An exponential increase in mmw with increasing temperature is observed (see Figure 6) which is similar to that reported for other polyoxyethylene nonionic detergents above their threshold temperatures.^{1,5,6,18} The mmw of 1.4×10^6 determined at 25° is in agreement with the

Table I: Light-Scattering Data for Hn_7

Temp, $^\circ\text{C}$	$d\eta/dc$, ml/g	mmw $\times 10^{-5}$	Radius of gyration, A	Length, A	Axial ratio (anhydrous rod)
22	0.135	1.00	412	1370	34
25	0.135	1.43	512	1690	38
30	0.135	3.04	775	2580	51
35	0.135	4.86	987	3230	60

(18) P. H. Elworthy and A. T. Florence, *Kolloid-Z.*, **204**, 105 (1965).

value obtained in a previous investigation⁸ in which the large micelles were shown to be composed of 3.6 small micellar units of mmw 3.3×10^5 (thus having a mmw of 1.2×10^6).

The experimental values of $P^{-1}(\theta)$ (the reciprocal particle-scattering factor) were plotted as a function of $\sin^2(\theta/2)$ and compared with similar plots for particles of known shape, calculated using theoretical equations for spheres, rods, and mono- and polydisperse coils. At all temperatures, graphs of this type show that the micellar shape is best represented by a rod, but the experimental curves in all cases lie below the theoretical curves calculated for this shape (see Figure 7) indicating

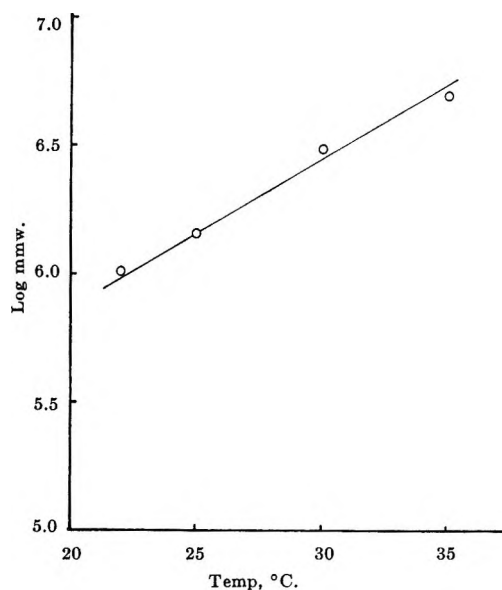


Figure 6. Temperature dependence of the micelle molecular weight of Hn_7 .

polydispersity of micellar size.¹⁹ Values for the lengths of the rods were assigned on the basis of the best fit of the experimental data at low scattering angles with that calculated for rods of definite length. A linear increase in the rod length with increasing temperature is observed (see Figure 8).

Viscosity Results. Measurements made using a suspended level viscometer indicated an increase in viscosity with temperature, similar to that previously reported¹ for temperatures less than 30°. Further temperature increase resulted in an apparent fall in the limiting viscosity number, although the solutions appeared visibly to become more viscous. Measurements at 35° using Cannon-Fenske viscometers of varying capillary diameter indicated a dependence of viscosity on the rate of shear. Consequently, viscosity measurements at all temperatures were made using a Couette viscometer and extrapolated to zero shear rate. Viscosity-concentration graphs showing an abrupt change of slope at a concentration of approximately 2×10^{-3} g ml⁻¹ were obtained at each temperature (Figure 9). The steeply

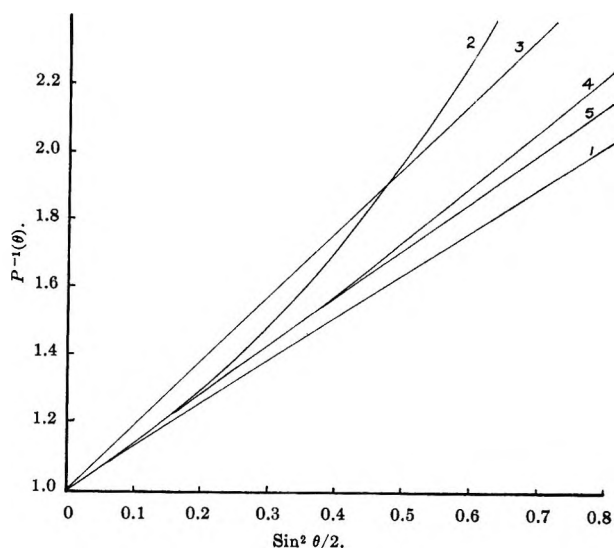


Figure 7. The reciprocal particle scattering factor $P^{-1}(\theta)$ as a function of angle θ for (1) Hn_7 and for (2) sphere, (3) polydisperse coil, (4) monodisperse coil, and (5) rod of the same radius of gyration.

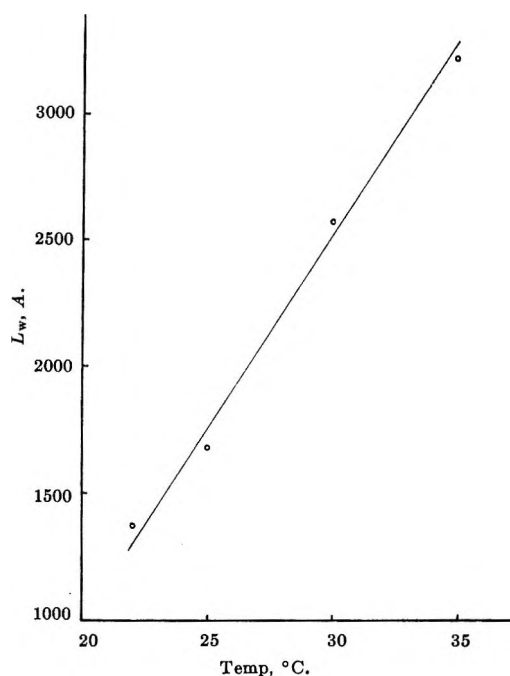


Figure 8. Variation of the length of the micelles of Hn_7 with temperature.

rising portion of the curve can be described by a polynomial expansion in $(c - c')$ of the type

$$\eta(\text{rel}) = 1 + A(c - c') + B(c - c')^2$$

where c' is the concentration obtained by extrapolation of this portion of the graph. If it is assumed that c' represents the concentration at which large micelles are first observed, and this seems reasonable from the light-scattering results, then the above equation rep-

(19) M. Goldstein, *J. Chem. Phys.*, **21**, 1255 (1953).

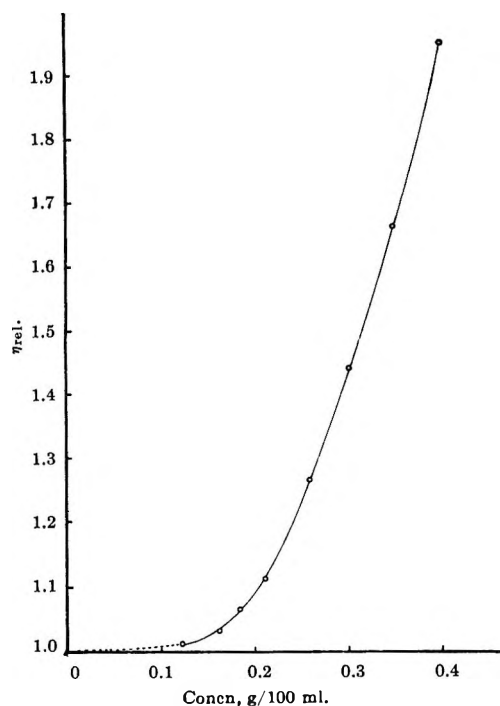


Figure 9. Concentration dependence of relative viscosity of H_{n7} solutions at 35°.

resents the concentration dependence of the viscosity of the large micellar species. On this basis, the constants A and B were tentatively equated with $[\eta]$, the limiting viscosity number of the large micelles, and $k'[\eta]^2$ (where k' is the Huggins constant), respectively. Values of A and B were evaluated by least-squares methods and are given in Table II. Axial ratios calculated from the limiting viscosity numbers, using an anhydrous rod as a micellar model, were of the same order as the values obtained from light scattering. A temperature-independent value of approximately 1.0 was obtained for the Huggins constant, which is not an unreasonable value for a rod of this asymmetry.²⁰ Measurements at very low concentrations were insufficiently precise to enable the viscosity-concentration graphs to be extrapolated to the cmc, and hence estimation of the asymmetry of the small micellar units was not possible. It is interesting to note that the type of graph shown in Figure 9 is not obtained when capillary viscometers are used, and this is possibly due to disturbance of the aggregation process under high shear rates.

Table II: Viscosity Data for H_{n7}

Temp, °C	Apparent limiting viscosity number $[\eta]$	Huggins constant, k'	Axial ratio (anhydrous rod)
25	107	1.5	44
30	176	0.9	61
35	260	1.0	74

Micellar Model. The micellar hydration (W , grams of H_2O per gram of H_{n7}) was calculated from a combination of the light-scattering and viscosity data using an equation proposed by Oncley.²¹

$$|\eta| = \nu(\bar{v} + WV_1^0)$$

A value for the density of H_{n7} at each temperature was calculated from the molar volumes of heptaoxyethylene glycol and hexadecane, a procedure which for other members of the hexadecyl series has yielded good agreement with experimentally determined values.¹ The partial molal volumes in the micellar state of nonionic detergents of similar chain length to H_{n7} have been shown to approximate closely to their molal volumes in the pure liquid state²² and there is, therefore, little error introduced in equating the partial specific volume, \bar{v} , of H_{n7} with its reciprocal density as calculated above. Values of the viscosity increment, ν , were calculated from the light-scattering data. The micellar dimensions, determined by light scattering assuming an anhydrous rod model, were converted to the corresponding values for an anhydrous prolate ellipsoid of equivalent volume, thereby enabling values of ν to be obtained from the Mehl, Oncley, and Simha²³ tables in the usual way. The values obtained for hydration in this way are necessarily speculative because of the assumptions made in the treatment of the viscosity data. However, they are similar to those obtained previously using vapor-pressure methods²⁴ and show the same tendency to increase with increasing temperature (see Table III). The H_{n7} micelles are composed of a hydrocarbon core with the polyoxyethylene chains projecting into the aqueous phase. For an idealized model, in which the hydrocarbon chains are radially oriented with their centers along the long axis of the rod, the radius of the hydrocarbon core, r_b , can be approximately equated with the length of the hexadecane chains. A value of

Table III: Dimensions of H_{n7} Micelles Assuming a Hydrated Rod Model

Temp, °C	Hydration (g of H_2O /g of H_{n7})	Hydrated micellar volume, $A^3 \times 10^{-6}$	Micellar radius, A	r_e , A^a
25	0.3	3.2	25	11
30	0.4	6.8	29	15
35	0.5	12.4	35	21

^a r_e = radial length of micelle occupied by the polyoxyethylene chain. Values for the micellar length are given in Table I.

(20) F. Eirich and J. Riseman, *J. Polymer Sci.*, **4**, 417 (1949).

(21) J. L. Oncley, *Ann. N. Y. Acad. Sci.*, **41**, 121 (1940).

(22) A. T. Florence, *J. Pharm. Pharmacol.*, **18**, 384 (1966).

(23) J. W. Mehl, J. L. Oncley, and R. Simha, *Science*, **92**, 132 (1940).

(24) P. H. Elworthy and C. B. Macfarlane, *J. Chem. Soc.*, 311 (1964).

13.8 Å has been calculated¹ for the latter using a formula proposed by Taylor,²⁵ which takes into account the restricted rotation about the C-C bonds of the hydrocarbon chain. The radial lengths of the polyoxyethylene regions, r_e , calculated by subtraction of r_h from the total radius of the hydrated micelles, are given in Table III. The gradual increase in r_e with increasing temperature continues the trend observed with the micelles below the threshold temperature,¹ and indicates a

gradual extension of the polyoxyethylene chain toward its fully extended length (26 Å).

Acknowledgments. The author is indebted to Professor P. H. Elworthy for his advice and encouragement, and wishes to thank Mr. G. Cochrane for constructing the light-scattering apparatus and Dr. J. E. Mathews for advice during its development.

(25) W. Taylor, *J. Chem Phys.*, **16**, 257 (1948).

Volume Dependence of the Equation of State for Rubber Elasticity: Poly(dimethyl siloxane)

by A. V. Tobolsky and L. H. Sperling

Department of Chemistry, Princeton University, Princeton, New Jersey (Received May 22, 1967)

The exact equation of state for rubber elasticity has been the subject of much recent work, both theoretical and experimental. In order to evaluate the volume dependence suggested in recent equations,^{1,5} a swelling technique has been employed. In this manner the value of the volume dependence parameter γ has been estimated to be +0.33 for poly(dimethyl siloxane) swollen with silicone oil. The significance of previous thermoelastic work on this polymer is discussed in the light of the present result.

Introduction

It has recently been suggested that the equation of state for rubber elasticity should be somewhat modified as¹

$$f = C \left(\frac{V_0}{V} \right)^\gamma \left[\frac{L}{L_0} - \frac{V}{V_0} \left(\frac{L_0}{L} \right)^2 \right] \quad (1)$$

Equation 1 is such that it should also be applicable to stretched swollen rubbers. In this case, the symbols of eq 1 are defined as follows: f equals force, L_0 equals original unstretched unswollen length at 1 atm, V_0 equals original unstretched unswollen volume at 1 atm, and L and V refer to the final length and volume of the stretched swollen sample at 1 atm. The quantity γ is a new empirical parameter suggested in ref 1; if this is zero, eq 1 is the same as prior equations.²⁻⁵ The quantity C is a function of temperature but not of volume. Its molecular interpretation in terms of network parameters is well known, especially if γ is zero. (See Appendix I.) Independent of detailed molecular interpretation of C , γ can be regarded as a parameter which permits a volume-dependent front factor in eq

1; it was introduced on an empirical basis to be evaluated by experiment.

In the experiments to be discussed below, it will be assumed that the unstretched swollen volume V' is very nearly the same as V , the stretched swollen volume, at least when compared to the difference between V_0 and V .

(In deriving eq 1 it is assumed that dilational or hydrostatic pressure is applied as necessary at all times during the stretching process, so that the stretching always occurs at volume V . The original swelling may be regarded as similar to dilational pressure.)

In eq 1, the measurable quantities are f , L_0 , L , V_0 , and T . As stated above, V' is assumed essentially equal to V for numerical purposes, and V' is readily mea-

(1) A. V. Tobolsky and M. C. Shen, *J. Appl. Phys.*, **37**, 1952 (1966).

(2) P. J. Flory, *Trans. Faraday Soc.*, **57**, 829 (1961).

(3) A. V. Tobolsky, D. W. Carlson, and N. Indictor, *J. Polymer Sci.*, **54**, 175 (1961).

(4) (a) W. R. Krigbaum and R. J. Roe, *Rubber Chem. Technol.*, **38**, 1039 (1965); (b) G. Gee, *Polymer*, **1**, 373 (1966).

(5) L. H. Sperling and A. V. Tobolsky, *J. Macromol. Chem.*, **1**, 799 (1966).

sured. It will be shown below that the quantity C is easily eliminated in the evaluation of γ . (Note small corrections discussed in Appendix I.)

The system poly(dimethyl siloxane)–silicone oil was chosen for the first examination because: (1) we have previously studied the thermoelastic properties of this elastomer;⁵ and (2) silicone oil is an athermal,⁶ relatively nonvolatile swelling agent for silicone rubber.

Experimental Details, Results, and Discussion

Silicone oils of two differing viscosities (50 and 2 cSt) were used to make samples with V/V_0 ranging from 1.4 to 4.6 for the swollen polymer. The samples were swollen to equilibrium for the first observations. Subsequently, the samples were partly deswollen and the measurements were repeated. The observations were made in air, with a small amount of silicone oil placed in a standard relaxation box⁷ to retard sample evaporation. A highly swollen polymer in equilibrium with solvent will absorb more solvent when stretched,⁸ but over-all weight gains were not observed in these experiments. The unswollen polymer was also studied. All of the polymers were cut in the form of narrow rectangular strips.

Stress–time curves at constant length were determined near room temperature, approximately 22°. Extensions of $L/L_0 \cong 1.1$ were employed. In all cases a value of equilibrium stress was obtained with the method of Chasset and Thirion.^{9,10} By use of this method, unswollen samples were observed for several days until the equilibrium stress was nearly attained; swelling much reduced the time needed for a reasonable approach to equilibrium.

In each case, dimensions of the samples were measured and the samples were weighed before and after relaxation. This latter procedure was a precaution against slight evaporation. While weight losses were usually small, after very long times the stress of swollen samples appeared to increase slightly; this was attributed to sample shrinkage and was a limitation to the technique employed.

The calculation of γ was carried out in the following manner. We consider samples having the same value of V_0 and L_0 , though swollen to different extents. Starting with eq 1, it is convenient to introduce a new parameter

$$A = \frac{f}{C \left[\frac{L}{L_0} - \frac{V}{V_0} \left(\frac{L_0}{L} \right)^2 \right]} \quad (2)$$

where the quantity A_0 may be employed to represent the value of A for the unswollen polymer. Division of A by A_0 yields the ratio

$$\frac{A_0}{A} = \left(\frac{V}{V_0} \right)^\gamma \quad (3)$$

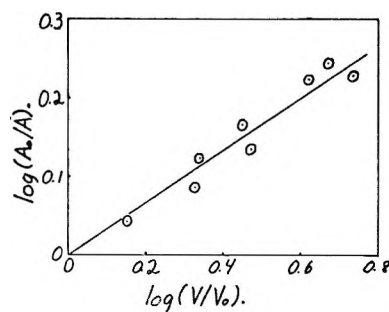


Figure 1. Plot of $\log(A_0/A)$ vs. $\log(V/V_0)$ for poly(dimethyl siloxane) rubber swollen by silicone oil.

after noting that $(V_0/V_0)^\gamma = 1$. Equation 3 suggests that a plot of $\log(A_0/A)$ vs. $\log(V/V_0)$ would yield γ directly as the slope of the expected straight line.

Figure 1 shows a plot of $\log(A_0/A)$ vs. $\log(V/V_0)$ for poly(dimethyl siloxane) elastomer swollen with silicone oil. The slope yields $\gamma = 0.33 \pm 0.04$. These determinations were made at $L/L_0 = 1.1$ and should be extended to other values of L/L_0 .

A nonzero value of γ affects the interpretation of thermoelastic data^{1,5} (stress–temperature measurements at constant length). This type of measurement can be related to the variation of the mean-square end-to-end distance of the equivalent free chain at volume V_0 , $\overline{r_f^2}_{V_0}$, with temperature provided γ is known. For poly(dimethyl siloxane), $\epsilon' = R d \ln \overline{r_f^2}_{V_0} / d(1/T)$ can now be computed. Using data in the literature,⁵ $\epsilon' = -28$ cal/mole. This indicates a very small energy difference between rotational isomers in the poly(dimethyl siloxane) chain, if interdependence of bond rotational states is (cautiously) neglected.^{11,12}

The value of the present experiment lies in the relative ease of evaluating γ from eq 1. The change of volume with elongation or with pressure is very small,^{13,14} but with swelling the volume can be altered at will over a considerable range.

There have been numerous studies on the elastic properties of swollen polymers.^{15–18} However, it

(6) J. E. Mark and P. J. Flory, *J. Am. Chem. Soc.*, **86**, 138 (1964).

(7) A. V. Tobolsky, "Properties and Structure of Polymers," John Wiley and Sons, Inc., New York, N. Y., 1960, p 143.

(8) T. L. Hill, "An Introduction to Statistical Thermodynamics," Addison-Wesley Publishing Co., Inc., Reading, Mass., 1960, p 414.

(9) R. Chasset and P. Thirion, "Physics of Non-Crystalline Solids," North-Holland Publishing Co., Delft, 1964, p 345.

(10) L. H. Sperling and A. V. Tobolsky, to be published.

(11) A. Ciferri, *Trans. Faraday Soc.*, **57**, 846, 853 (1961).

(12) U. Bianchi, E. Patrone, and M. Galpiaz, *Makromol. Chem.*, **84**, 230 (1965).

(13) G. Gee, J. Stern, and L. R. G. Treloar, *Trans. Faraday Soc.*, **46**, 1101 (1950).

(14) F. G. Hewitt and R. L. Anthony, *J. Appl. Phys.*, **29**, 1411 (1958).

(15) G. Gee, *Trans. Faraday Soc.*, **42**, 584 (1946).

(16) M. C. Shen and A. V. Tobolsky, *J. Polymer Sci.*, **A2**, 2513 (1964).

appears to be difficult to make a quantitative analysis of γ from this literature.

The volume dependence of the front factor in eq 1 has been introduced in the form $(V_0/V)^\gamma$. This particular form makes calculation of many of the thermoelastic properties relatively simple. Although γ has been found to be a constant for poly(dimethyl siloxane) elastomer, there is no guarantee that the volume dependence of the front factor will be equally simple for other polymers.

An elegant extension of the volume dependent front factor was given by Ciferri, Smith, and Bashaw,¹⁹ who pointed out that γ can be expressed in a more general manner. They wrote the equation of state in the form

$$f = B \left[\frac{L}{L_0} - \frac{V}{V_0} \frac{L_0^2}{L^2} \right] \quad (4)$$

where all terms except B have the same meaning as in eq 1. The quantity B was assumed to depend upon both V and L . Applying the well-known thermoelastic relation, it was shown that

$$\frac{f_e}{f} = -T \left[\frac{\partial \ln (f/T)}{\partial T} \right]_{P,L} + \frac{VT}{f} \left(\frac{\partial f}{\partial V} \right)_{L,T} \beta \quad (5)$$

where f_e is the energetic component of the stress and $\beta = (\partial V / \partial T)_{P,V} / V$. Combining eq 4 and 5 yields

$$\frac{f_e}{f} = -T \left[\frac{\partial \ln (f/T)}{\partial T} \right]_{P,L} - \frac{\beta T}{\left[\frac{L^3}{L_0^3} \frac{V_0}{V} - 1 \right]} + \left(\frac{\partial \ln B}{\partial \ln V} \right)_{L,T} \beta T \quad (6)$$

Comparison with ref 1 shows

$$\gamma = - \left(\frac{\partial \ln B}{\partial \ln V} \right)_{L,T} \quad (7)$$

where γ need no longer be constant.

If the Mooney equation is applicable, Ciferri, Smith, and Bashaw have also derived a relation among γ and the Mooney constants C_1 and C_2 .

A Molecular Interpretation of γ . We present here an interpretation of γ which emphasizes polymer-solvent interactions during swelling. Equation 1 may be written in a more detailed molecular form, applicable to networks under pressure (plus or minus), or to swollen networks.^{1,5}

$$f = \frac{N_0 k T}{L_0} \left(\frac{\bar{r}_{i^2 v_0}}{\bar{r}_{f^2 v_0}} \right) \left(\frac{\bar{r}_{f^2 v_0}}{\bar{r}_{f^2 v}} \right) \left[\frac{L}{L_0} - \frac{L_0^2}{L^2} \frac{V}{V_0} \right] \quad (8)$$

The quantity $\bar{r}_{f^2 v_0} / \bar{r}_{f^2 v}$ which appears in eq 8 is the only term that relates to γ . It is interesting to consider that this quantity may be a function of volume because of the varying solvent-polymer interactions at different degrees of swell. It has been suggested that a

network chain in the unswollen polymer may be considered as having Θ solvent unperturbed dimensions, whereas a network chain in the polymer highly swollen by oligomer may be considered to be in a nearly athermal solvent.^{20,21}

In solution, the mean-square end-to-end distance of polymer chains compared to the unperturbed distance (in a Θ solvent) is given by²⁰

$$r^2 / r_0^2 = \alpha^2 \quad (9)$$

where α is the swelling or expansion factor.

If the solvent is a low molecular weight species of the polymer, the following equation has been suggested²¹ for dilute solutions

$$\alpha^5 - \alpha^3 = K Z^{1/2} / X_s \quad (10)$$

where $K \cong 1$, Z is the degree of polymerization of the linear polymer, and X_s is that of the solvent.

It would be very interesting if an equation for α could be developed for concentrated solutions and swollen networks. Such a relation could then be applied to eq 8.²²

Acknowledgments. We wish to acknowledge the support of the Office of Naval Research. We also wish to thank Dr. A. C. Martellock of the General Electric Company, Waterford, N. Y., for the preparation of the poly(dimethyl siloxane) elastomer.⁵

Appendix I

Further treatment of the parameter C is desirable here from a theoretical point of view, and also to show how to handle the data if V_0 and L_0 are not exactly the same in all samples. A particular molecular interpretation of the parameter C gives the following^{1,5}

$$C = \frac{N_0 k T}{L_0} \frac{\bar{r}_{i^2 v_0}}{\bar{r}_{f^2 v_0}} \quad (A1)$$

where N_0 equals the number of network chains in the sample, kT equals Boltzmann's constant times temperature, and $\bar{r}_{i^2 v_0}$ equals the mean-square end-to-end distance of the actual network chains at volume V_0 . L_0 and $\bar{r}_{f^2 v_0}$ were defined in the text.

Slight variations in L_0 and V_0 occurred. Noting that V_0 is proportional to N_0

$$C = \frac{\text{constant} \times V_0 k T}{L_0} \frac{\bar{r}_{i^2 v_0}}{\bar{r}_{f^2 v_0}} \quad (A2)$$

(17) A. Oplatka and A. Katchalsky, *Makromol. Chem.*, **92**, 251 (1966).

(18) P. J. Flory, *Chem. Rev.*, **35**, 51 (1944).

(19) A. Ciferri, K. J. Smith, Jr., and R. N. Bashaw, private communication.

(20) P. J. Flory, "Principles of Polymer Chemistry," Cornell University Press, Ithaca, N. Y., 1953.

(21) P. J. Flory, *J. Chem. Phys.*, **17**, 303 (1949).

(22) NOTE ADDED IN PROOF. Utilizing eq 26' of ref 21, we have derived a value of $\gamma = 0.40$ for a special case.

If L_0 and V_0 are constant, the value of C appearing in eq 2 and 3 is a constant. Slight variations in L_0 and V_0

affect C as shown in eq A2. This variation of C can be accounted for in eq 2 and 3.

On the Kinetics and Mechanism of the Thermal Decomposition of Methane in a Flow System¹

by H. B. Palmer, J. Lahaye, and K. C. Hou

Department of Fuel Science, The Pennsylvania State University, University Park, Pennsylvania 16802
(Received July 31, 1967)

The rate of thermal decomposition of methane has been studied in a flow system at temperatures from 1323 to 1523°K. The experimental data are generally in close agreement with a recent, similar study by Eisenberg and Bliss. However, a different interpretation is given to the results. In particular, it is concluded that nucleation of carbon in the gas phase causes the decomposition to accelerate because of heterogeneous decomposition of methane on the nuclei. The conclusion is supported experimentally. A qualitative model of the pyrolysis process is presented and discussed.

Introduction

The kinetics and mechanism of the homogeneous thermal decomposition of methane should be completely understood by now, but they are not. Decomposition in more or less conventional static and flow systems has been studied for many years. Kramer and Happel² have reviewed a number of those studies. Results of three of them are included in Figure 1, an Arrhenius plot of some reported first-order rate constants. The line through the results from flow and static systems is expressed by

$$\log k(\text{sec}^{-1}) = 13.0 - 18.6 \times 10^3/T \quad (1)$$

corresponding to an activation energy of 85 kcal.

Shock tube data,^{3,4} when combined with the results of measurements of the rate of carbon film formation from pyrolyzing methane,⁵ yield a quite different result

$$\log k(\text{sec}^{-1}) = 14.6 - 22.5 \times 10^3/T \quad (2)$$

corresponding to an activation energy of 103 kcal. This line is also shown in Figure 1, as is the result from rapid compression experiments reported recently by Kondratiev,⁶ which agrees well with eq 2.

In the hope of understanding the discrepancy between these expressions, we have carried out some new measurements of the thermal decomposition rate using a conventional flow system. Since doing so, we have become aware of a recent and detailed study of Eisen-

berg and Bliss⁷ (hereafter referred to as (EB)) in which a similar flow reactor was used. We shall refer to their work throughout this paper.

Experimental Section

The experimental system has been described elsewhere.⁸⁻¹⁰ It is basically a hot porcelain tube of 5-mm i.d., having a long plateau in its temperature profile. Methane at concentrations in the neighborhood of 10% by volume is carried into the reactor in a stream of helium at a total pressure of about 740 torr. Products are analyzed by gas chromatography using a 5-ft silica gel column at 50°.

(1) Work supported in part by a grant from the J. M. Huber Corp.

(2) L. Kramer and J. Happel, "The Chemistry of Petroleum Hydrocarbons," Vol. II, B. T. Brooks, S. S. Kurtz, C. E. Boord, and L. Schmerling, Ed., Reinhold Publishing Corp., New York, N. Y., 1955, Chapter 25, p 71.

(3) (a) G. B. Skinner and R. A. Ruehrwein, *J. Phys. Chem.*, **63**, 1736 (1959); (b) H. S. Glick, "Seventh Symposium (International) on Combustion," Butterworth and Co. Ltd., London, 1959, p 98.

(4) V. Kevorkian, C. E. Heath, and M. Boudart, *J. Phys. Chem.*, **64**, 964 (1960).

(5) H. B. Palmer and T. J. Hirt, *ibid.*, **67**, 709 (1963).

(6) V. N. Kondratiev, "Tenth Symposium (International) on Combustion," The Combustion Institute, Pittsburgh, Pa., 1965, p 319.

(7) B. Eisenberg and H. Bliss, *Chem. Eng. Progr., Symp. Ser.*, **63**, No. 72, 3 (1967).

(8) H. B. Palmer and F. L. Dormish, *J. Phys. Chem.*, **68**, 1553 (1964).

(9) K. C. Hou and H. B. Palmer, *ibid.*, **69**, 858 (1965).

(10) K. C. Hou and H. B. Palmer, *ibid.*, **69**, 863 (1965).

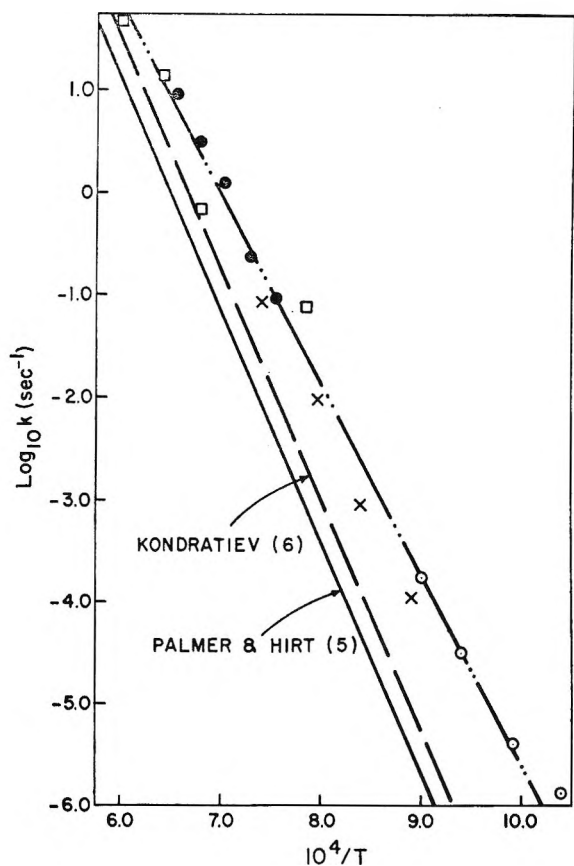


Figure 1. Arrhenius plot of first-order rate constants for the decomposition of methane: squares, from the work of D. Rudder and H. Biederman, *Bull. Soc. Chim. France*, **47**, 710 (1930); crosses, P. S. Shantarovich and B. V. Pavlov, *Zh. Fiz. Khim.*, **30**, 811 (1956); open circles, L. S. Kassel, *J. Am. Chem. Soc.*, **54**, 3949 (1932); solid circles, apparent rate constants derived from the present study (see Discussion). Solid line is eq 2.

In the present study, methane has been introduced into the tube at concentrations between 1 and 20% by volume in the helium. Residence times ranging from 0.1 to 0.9 sec have been employed over the temperature range 1323–1523°K. The available wall surface area of the reactor has been varied twofold by shifting from the single cylindrical tube to a porcelain tube containing four holes of smaller diameter.

In the latter stages of the work, the effect of added naphthalene has been studied. Naphthalene of high purity is introduced into the helium stream at a volume fraction of approximately 0.01 by bubbling the carrier gas through molten $C_{10}H_8$ at 80°.

The purity of the helium is above 99.995%, but nevertheless it is passed through hot copper wool to ensure the complete absence of oxygen. The methane is CP grade (Matheson), purity 99% minimum. According to a mass spectrometric analysis, the principal impurity is argon. A small amount of ethane is present. Its upper limit is estimated from the analysis to be 0.3%.

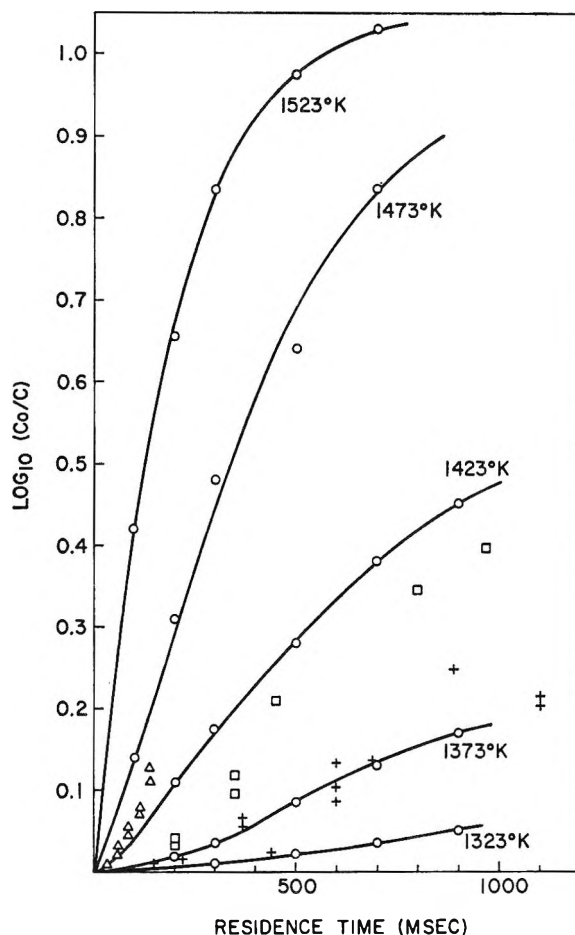


Figure 2. Kinetic results at five temperatures, at input concentrations close to 10 mole %. The results of Eisenberg and Bliss⁷ are shown for comparison, as follows: crosses, 1371°K, 15–25 mole %; squares, 1409°K, 15 mole %; triangles, 1458°K, 15 mole %.

Results and Discussion

The basic data on the fraction of CH_4 decomposed as a function of time agree remarkably well with the results of EB.⁷ Figure 2 shows our results at five temperatures and the results at the three temperatures employed by EB. The two studies taken together establish the general character of the rate behavior for methane decomposing in a flow system: the reaction accelerates and then decelerates. A steady rate appears only momentarily, as an inflection. At low temperatures, one sees only the acceleration. At high temperatures, the induction period is short and is difficult to observe, though it undoubtedly is present.

Our observations on the effect of CH_4 concentration on the rate are typified by Figure 3, which shows a slightly increasing extent of decomposition as the input concentration rises, except at the longer times, where there seems to be no effect. However, even at the shorter times the apparent effect is very slight and may be specious. The concentration effect reported by EB was considerably larger, but it seems to be subject to

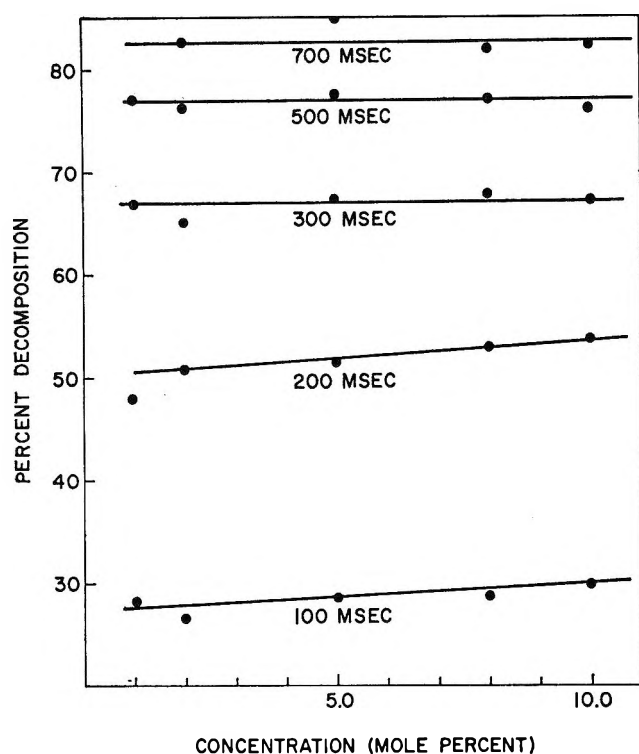


Figure 3. The effect of input concentration at 1473°K, showing the extent of decomposition as a function of the input concentration, at five fixed residence times.

some question, as it relies heavily upon one experimental point (see Figure 5 of their paper).

We do not insist that the reaction is simple first order, kinetically. On the contrary, it clearly is complex, exhibiting as it does an induction period and then a deceleration that develops strongly as decomposition proceeds. Nevertheless, the over-all kinetic order of the decomposition, throughout its course, is very close to unity.

On the effect of surface-to-volume ratio of the reactor, the present study provides confirmation of EB's tentative conclusion that there is essentially no effect. In Figure 4 are shown the results at two temperatures at which pairs of runs have been made using two reactors: reactor A, a single porcelain cylinder of 5-mm inner diameter, and reactor B, a porcelain rod having four 2.4-mm holes instead of the single large one. The alteration of S/V by about a factor of 2 is not as large a change as one might like, but the data are in such good agreement that the conclusion is clear.

EB determined the time-dependent behavior of the three principal gaseous hydrocarbon products, C_2H_6 , C_2H_4 , and C_2H_2 . We have carried out similar determinations and agree with EB that ethane production is always small, and that it goes through a maximum at relatively short contact times. The maximum seems to match up fairly well with the end of the acceleration in the reaction. For C_2H_4 and C_2H_2 , we obtain the same general shape of the time dependences as EB.

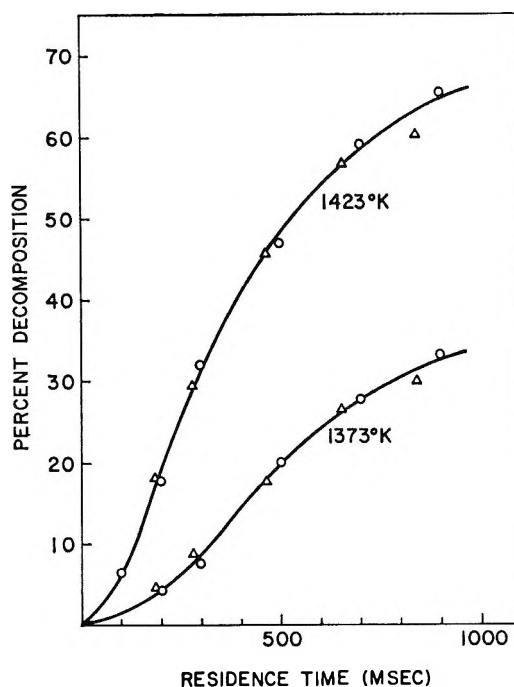


Figure 4. Effect of surface-to-volume ratio: circles, reactor A; triangles, reactor B. $(S/V)_B = 2 \times (S/V)_A$. Input concentration for 1423°K runs was 10%; for 1373°K runs, 16%.

Our yields of acetylene agree quite well with theirs, but yields of ethylene do not. EB find acetylene rising to considerably larger concentrations than ethylene at all three of their temperatures (1371, 1409, and 1458°K) and find the relative magnitudes of the two to be essentially independent of the input concentration. However, we find that ethylene tends to exceed acetylene when the temperature is below about 1420°K and the input concentration is less than about 10% CH_4 . Increasing the input concentration enhances the C_2H_2 yield relative to C_2H_4 , but at 1373°K the yield of C_2H_2 is still well below that of C_2H_4 when the input is 13% CH_4 .

In Figure 5 are shown the yields of C_2 hydrocarbon products obtained by us at 1373°K and $[CH_4]_0 = 13.1\%$, and those obtained by EB at 1371°K. In view of the agreement on the extent of decomposition (Figure 2) as a function of time, we believe the difference in products is largely a reflection of the difference in cooling rates at the end of the hot zone. EB used a nitrogen-quench method that provided cooling rates several times greater than ours. In both studies the cooling rates were sufficient to freeze reaction steps of high activation energy quite promptly. However, in our reactor, processes of low activation energy, such as perhaps various hydrogenation processes, may continue and affect the product distribution markedly, shifting it toward a distribution characteristic of a lower temperature and perhaps enhancing the yield of hydrocarbons, as opposed to carbon and hydrogen. One

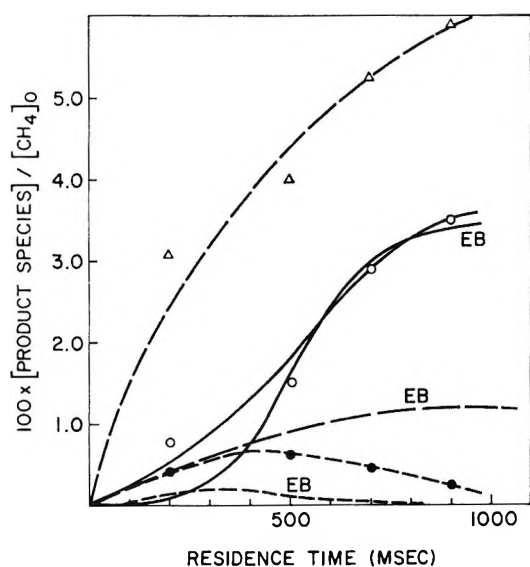


Figure 5. Conversion of original methane to C_2 hydrocarbons at $1373^\circ K$: initial concentration, 13 mole %; short dashes, ethane; long dashes, ethylene; solid lines, acetylene. Curves labeled EB are constructed by averaging the results from ref 7 at $1371^\circ K$ and initial concentrations of 15 and 25 mole %.

notes that among the C_2 hydrocarbons, C_2H_4 tends to be favored over C_2H_2 at temperatures below about $1150^\circ K$, and C_2H_6 becomes the more prominent the lower the temperature. This seems to be broadly consistent with the rationalization suggested. Neither EB nor we have determined the carbon formation. Vitreous carbon deposits on the reactor wall, and a small amount of soot escapes from the reactor. Quantitative determination would be extremely inaccurate.

Effects of the additives, H_2 and C_2H_6 , have not been studied by us (note, however, that our CH_4 may have contained as much as 0.3% C_2H_6). EB found inhibition by H_2 and acceleration by C_2H_6 . Their study of H_2 was systematic and is supported by other, earlier work.¹¹ The observation on C_2H_6 addition consisted of one experiment. Nevertheless, qualitatively, the effect appears unquestionably real. It is supported also by earlier work in flow reactors^{12,13} but not by shock tube studies.^{3a} The previously discussed agreement of our basic rate data with EB leads us to conclude that we may have overestimated the possible C_2H_6 content of our CP grade methane.

Later, an explanation is proposed for the difference between the data from shock tubes and from flow reactors. First, let us reconsider the sources of the rate constant expressions given in the Introduction. Equation 1 is found by fitting data from flow systems and from static systems. In view of the acceleration-deceleration behavior exemplified by the data in Figure 2, how can a first-order rate constant be obtained? The answer is clear: one can draw reasonably good straight lines through the several collections of points, ignoring the decelerations. From the slopes, one ob-

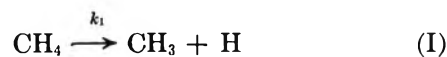
tains the rate constants shown on the Arrhenius plot in Figure 1. They agree very well with eq 1, but not, of course, with eq 2.

However, these are not fundamental rate constants for a homogeneous reaction. At best, they represent some combination of rate constants. The shock tube data, which do not show an acceleration,^{3a} yield fundamental rate constants. These should be compared with flow system data at very short times, before the reaction has accelerated appreciably. Unfortunately, we cannot obtain these from a system of the present type. All that can be said is that the behavior is fully compatible with a rate that commences at the value given by eq 2 and then accelerates.

In their study of methane decomposition, Palmer and Hirt^{5,14} used a flow reactor, but instead of measuring concentrations in the exiting gas stream, they followed the rate at which carbon deposited on the wall. It is their rate constants that, in combination with shock tube data, specify eq 2. Their residence times were comparable to those in the present study. One must ask why they did not observe an acceleration and why their rate constants appear to be of the order of those that might apply at the commencement of reaction in the present system.

Before presenting a hypothesis, let us summarize the pertinent points above the decomposition. (a) It begins relatively slowly, accelerates, then decelerates. (b) The rate is approximately first order despite its complex behavior. (c) Vitreous carbon deposits on the wall; small amounts of soot and tars collect at the exit. (d) The main gaseous products are C_2H_2 and C_2H_4 , with lesser quantities of C_2H_6 . (e) H_2 inhibits the decomposition; ethane accelerates it. (f) The rate is not appreciably affected by the S/V ratio.

EB do not agree with point b. They believe the decomposition to be of order distinctly greater than unity and to be homogeneous. Accordingly, they construct a mechanistic model that involves a nonsteady-state chain. By suitably choosing rate constants, they are able to fit their observations at one temperature. Their success in doing this is interesting, but we consider some features of their mechanism to be questionable; for example, although the mechanism creates hydrogen atoms, no subsequent reactions of H atoms are included. Perhaps the most obvious difficulty with their treatment is that fitting their results requires that the rate constant for the initial reaction



be approximately 0.1 times the value given by eq 2.

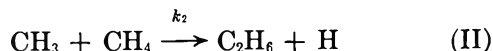
(11) J. E. Germain and C. Vaniscotte, *Bull. Soc. Chim. France*, 319 (1958).

(12) J. E. Germain and C. Vaniscotte, *ibid.*, 964 (1958).

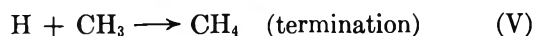
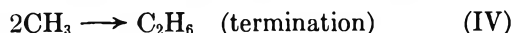
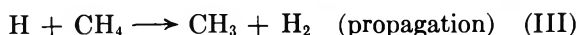
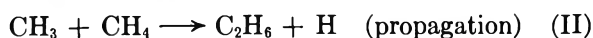
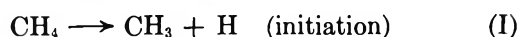
(13) I. A. Schneider, *Z. Physik. Chem.*, **223**, 234 (1963).

(14) T. J. Hirt and H. B. Palmer, *Carbon*, **1**, 65 (1963).

The only ways to reconcile this with shock tube data are to suggest either that the activation energy for reaction I is much larger than 103 kcal or that there was a chain length of about 10 under the shock tube reaction conditions. The chain length argument is the only one that seems conceivable, but it would require that the reaction



be very fast. Skinner has considered this possibility (the rate has not been measured) and has rejected it by estimating the probable value of the rate constant. It can also be ruled out on another basis. If reaction II is important, a chain results. If it is not in a steady state, then an acceleration of the rate should have been observed in the shock tube experiments, but it was not. If there is a steady-state chain, it is very probably represented by



Whether one chooses (IV) or (V) as the ending reaction (IV is more probable), the reaction order will be close to or equal to 1.5, but in the shock tube experiments it was found to be accurately equal to unity.

Thus, it seems necessary to look for an explanation of the acceleration of the rate in a flow system that is based upon a process other than a homogeneous chain reaction. The obvious possibility that comes to mind is acceleration by a heterogeneous process, namely nucleation of soot. Soots are known to contain a large concentration of spin centers and should present active surfaces for heterogeneous decomposition of CH_4 in contrast to the vitreous carbon on the wall. Tesner¹⁵ has in fact studied the heterogeneous decomposition of methane on carbon black, using an electron microscopic technique.

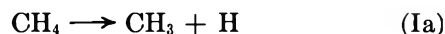
Acceleration by added C_2H_6 might then simply be a consequence of its more rapid decomposition, with accompanying formation of soot. The inhibition by added H_2 is also qualitatively understood on this basis.

If nuclei are significant, then one should be able to accelerate the reaction very strongly by adding a hydrocarbon that nucleates with great rapidity. Accordingly, we added naphthalene in one experiment. The reaction temperature was not known accurately, but it was steady. At a concentration of 10% CH_4 and a residence time of about 0.8 sec, the extent of decomposition without added naphthalene was 1.2%. Addition of 1% naphthalene (by running the helium through a vaporizer) increased the decomposition to 37.2%. Sooting

was heavy. When the naphthalene addition was discontinued, the decomposition reverted to 3.8%. The inability to return completely to the original low figure was probably due to the large amount of carbon black that clung to the reactor wall.

Thus addition of a small quantity of an active soot-former increased the rate by roughly a factor of 30. This very striking effect convinces us that nucleation in the gas phase is indeed responsible for the acceleration of the reaction as observed in flow systems.

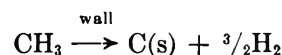
Since the kinetics of nucleation in sooting systems are not understood, we cannot propose a detailed mechanism that includes it. A general model can be suggested, however. It includes: (a) homogeneous decomposition



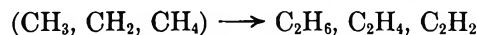
and/or



((Ia) seems the more probable); (b) deposition of carbon on the wall



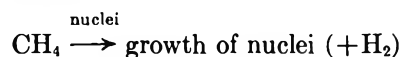
(c) formation of light hydrocarbons



(d) nucleation



(e) and heterogeneous decomposition



According to this model, shock tube measurements yield the rate of the homogeneous first step because nuclei do not form in time to influence the rate appreciably. Carbon deposition measurements also yield this rate because the principal fate of CH_3 is to disappear at the wall, when the system is of small diameter. This process is not perfectly efficient, however, and some CH_3 survives to form light hydrocarbons and, eventually, soot nuclei. The reaction then accelerates. The rate of wall deposition is not appreciably affected by the nucleation because the total surface area presented by the nuclei is very small relative to the wall area, and most of the CH_3 continues to deposit carbon on the wall. However, CH_4 is much more stable than CH_3 ; it does not decompose efficiently on the vitreous carbon deposit on the wall, but does decompose well on the active surfaces presented by the nuclei. Deceleration occurs as hydrogen accumulates and as the nuclei age and become less active. A decrease in activity of

(15) P. A. Tesner, "Seventh Symposium (International) on Combustion," Butterworth and Co. Ltd., London, 1959, p 546.

this type has been observed in the flame studies of Bonne, *et al.*¹⁶

Conclusions

Studies of hydrocarbon pyrolysis in flow systems have much technological utility, but they will yield fundamental information on homogeneous reaction rates only with great difficulty. Other types of reactions, including reactions involving hydrocarbons, can be effectively studied in flow systems if the enormous complication presented by sooting phenomena can be avoided.

The present study of methane pyrolysis shows it to be an example of a system that is very sensitive to the

effect of nucleation. The accumulation of evidence from this and other studies, particularly the valuable contribution of Eisenberg and Bliss, had led us to the conclusion that the controversy over the rate constant for the first-order homogeneous decomposition of methane is a consequence of the kinetic complications in flow- and static-system studies. On this basis, we believe that eq 2 must be chosen as the best available representation of the rate constant for the homogeneous first step in the decomposition mechanism.

(16) U. Bonne, K. H. Homann, and H. Gg. Wagner, "Tenth Symposium (International) on Combustion," The Combustion Institute, Pittsburgh, Pa., 1965, p 503.

Surface Tension of Liquid Cadmium Chloride-Alkali Chloride Systems

by G. Bertozzi¹ and G. Soldani¹

Materials Department, Electrochemistry Group, Euratom CCR, Petten, Holland

Accepted and Transmitted by The Faraday Society (March 13, 1967)

Surface tension measurements have been carried out on four cadmium-alkali metal chloride systems, from the melting point up to 650°, and the results are given in the form of linear equations for each mixture. All the surface tension isotherms are S shaped. The behavior of the systems is discussed in terms of associated entities in pure CdCl₂ and complex anions in the mixtures. The effect of temperature is also taken into account.

Introduction

The study of molten cadmium halide-alkali halide liquid mixtures is not only interesting because of the association phenomena which occur in them, but also because it could provide indications on the structure of pure liquid CdCl₂.

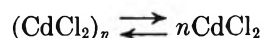
The structure of pure liquid cadmium chloride is not yet well understood and is still open to discussion. In Bues' opinion,² the Raman spectrum of liquid CdCl₂ maintains the peak of the solid polymer up to 100° above the melting point, thus indicating the presence in the liquid of an appreciable degree of polymerization.

However, its low viscosity and high vapor pressure do not agree with this point of view; they seem rather to suggest a molecular structure similar to that of the mercuric halides, but with a much higher degree of ionization. In fact, the electrical conductivity of molten CdCl₂ is similar to that of the alkaline earth halides, while that of HgCl₂ is 10⁴ times lower.

The dominant ionic species present must be the monatomic ions, since the frequencies corresponding to

the two possible complex ions (CdCl)⁺ and (CdCl₃)⁻ do not appear in the vibrational spectrum of molten CdCl₂.³

The principal equilibria which follow could be



the associated entities (CdCl₂)_n being so small and their concentration so low that no effect on the viscosity results. A structure of this type was proposed by Bockris and Angell.⁴

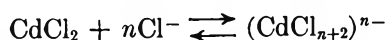
On addition of Cl⁻ ions, a different ionization process takes place

(1) Address correspondence to the authors at Euratom CCR, Ispra, Italy.

(2) W. Bues, *Z. Anorg. Allgem. Chem.*, **279**, 104 (1955).

(3) D. W. James in "Molten Salt Chemistry," M. Blander, Ed., 1964, p 515.

(4) J. O. M. Bockris and C. A. Angell, *Electrochim. Acta*, **1**, 308 (1959).

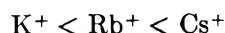


which results in the formation of complex anions.

Many authors have studied the mixtures of CdCl_2 with the alkali metal chlorides using various techniques.⁵⁻⁹ The results have confirmed the presence of the complex ions $(\text{CdCl}_{n+2})^{n-}$, where n is 1, 2, or 4, following the composition.

Unfortunately, however, only the systems with potassium and sodium salts have been extensively investigated, and the effect of a gradual change in the alkali metal size has not been emphasized.

As a rule, we observe that the stability of a complex, $\text{C}_x(\text{BA})_y$ (where C is an alkali or alkaline earth metal ion, B is a metal of the Ib or IIb group, and A is a simple anion) increases with increasing the size and decreasing the charge of the cation C; *i.e.*, the covalent character of the B-A interaction increases when the polarizing power of the cation C decreases. This trend already has been pointed out by Thurmond,¹⁰ in connection with $(\text{Ag-Li})\text{Br}$ and $(\text{Ag-Rb})\text{Br}$ mixtures, and so, it should be possible to predict *a priori* that the stability of cadmium complexes will be low with lithium and sodium salts, and will increase in the order



Since complex ions or other molecular species are likely to be surface active, the surface properties should be suitable for investigating their presence in melts.

In the present work, the results of measurements on the surface tension of cadmium chloride-alkali chloride systems are discussed, and the effect of changing the alkali metal radius is outlined.

Experimental Section

The surface tension measurements were performed by the Wilhelmy slide method, previously tested by us in a wide series of research on surface properties of ionic melts.¹¹⁻¹⁴

Analytical grade salts were dried by heating in air up to 400° for about 4 hr. The mixtures were prepared by weighing the predetermined quantities of the components in a platinum crucible, which was then placed in the furnace inside a small cylindrical cell of alumina. The lid of the cell had a small bore through which the suspension wire passed, so the liquid-vapor equilibrium was easily retained and the CdCl_2 losses were negligible. However, the high vapor pressure of CdCl_2 forced us to limit the working temperature at about 650°, so that the measurements were not carried out in a wide temperature range; this fact also hindered the study of mixtures in the range 80-100 mole % of alkali chloride.

The surface tension isotherms of these systems do not have a simple shape. Several experimental points were, therefore, necessary in order to draw the curves correctly; all the compositions 10, 20, 30, ... 80

mole % were investigated. Results were reproducible within 1%.

Results

The surface tension of pure CdCl_2 is a linear function of the temperature in the range from the melting point up to 650°; the corresponding equation is

$$\gamma = 99.1 - 0.023t$$

This result agrees within 1% with the data of Ellis, *et al.*¹⁵ We emphasize the fact that the temperature coefficient is particularly low in comparison with the values of 0.06-0.08 dyne/(cm deg), which it has normally for molten salts.

The results of the surface tension measurements are given in Table I in the form of constants for linear equations of the type $\gamma = A - Bt$.

We notice that small amounts of alkali chloride are sufficient to raise the temperature coefficient, which

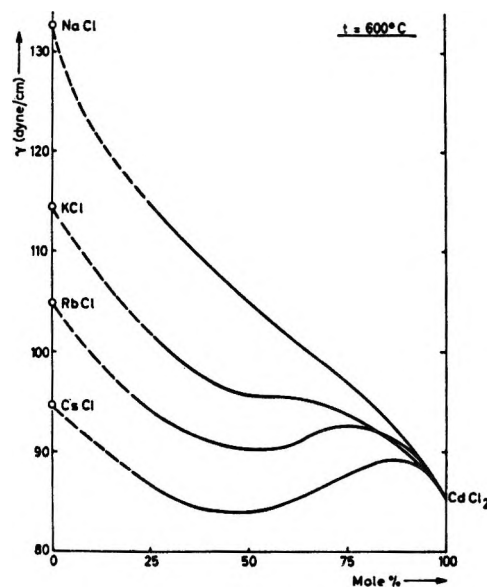


Figure 1. Surface tension isotherms at 600° for cadmium chloride-alkali chloride systems.

(5) (a) M. F. Lantratov and A. F. Alabyshev, *J. Appl. Chem. USSR*, **26**, 321 (1953); (b) H. Bloom and E. Heymann, *Proc. Roy. Soc. (London)*, **A188**, 392 (1947).

(6) N. K. Boardman, A. R. Palmer, and E. Heymann, *Trans. Faraday Soc.*, **51**, 277 (1955).

(7) M. Tanaka and K. Balasubramanyam and J. O. M. Bockris, *Electrochim. Acta*, **8**, 621 (1963).

(8) R. B. Ellis and A. C. Freeman, *J. Phys. Chem.*, **69**, 1443 (1965).

(9) H. Bloom and S. B. Tricklebank, *Australian J. Chem.*, **19**, 187 (1966).

(10) C. D. Thurmond, *J. Am. Chem. Soc.*, **75**, 3928 (1953).

(11) G. Bertozzi and G. Sternheim, *J. Phys. Chem.*, **68**, 2908 (1964).

(12) G. Bertozzi, *ibid.*, **69**, 2606 (1965).

(13) G. Bertozzi and G. Soldani, *ibid.*, **70**, 1838 (1966).

(14) G. Bertozzi and G. Soldani, *ibid.*, **71**, 1536 (1967).

(15) R. B. Ellis, J. E. Smith, W. S. Wilcox, and E. H. Crook, *ibid.*, **65**, 1186 (1961).

Table I

Alkali chloride, mole %	(Cd-Na)Cl		(Cd-K)Cl		(Cd-Rb)Cl		(Cd-Cs)Cl	
	A	B	A	B	A	B	A	B
10	113.9	0.038	114.0	0.040	120.5	0.050	122.1	0.055
20	124.0	0.048	125.2	0.054	128.2	0.060	125.9	0.062
30	128.5	0.050	131.8	0.062	132.1	0.066	127.0	0.067
40	137.4	0.060	134.5	0.065	131.4	0.068	128.3	0.072
50	142.8	0.063	137.7	0.070	131.1	0.068	126.1	0.070
60	144.0	0.059	135.5	0.064	130.8	0.066	126.5	0.070
70	144.8	0.054	137.8	0.063	128.8	0.060	124.7	0.066
80	***	***	***	***	***	***	125.5	0.062

reaches a maximum at an approximately equimolar composition, then decreases again.

Surface tension isotherms at 600° are shown in Figure 1. The dotted parts of the curves correspond to the region in which the melting point of the mixture is higher than the working temperature; likewise, the surface tensions of pure alkali chlorides at 600° have been calculated by linear extrapolation below the melting points. Although destitute of any real significance, these values enable us to draw the isotherms in the whole range of compositions.

All of the four isotherms are S shaped, with a positive deviation from linearity in the CdCl_2 -rich region and a negative deviation in the remaining region.

The extent of the deviations increases with the size of the alkali metal ion. The isotherm for the (Cd-Na)Cl system deviates only slightly from linearity, and the inflexion is not very marked. The other three curves exhibit large deviations from linearity. In all of them, a minimum and a maximum are present. The larger the radius of the alkaline ion, the more the maximum is shifted toward high CdCl_2 concentrations.

Discussion

1. *Effect of Alkali Chloride Additions.* Let us take into account, for comparison, the lead chloride-alkali chloride systems. They are known to contain the pyramidal PbCl_3^- ions, similar to the CdCl_3^- , as it has been recently shown by Raman spectra investigations.^{7,16}

The surface tensions of the lead chloride-alkali chloride systems were investigated by Dahl and Duke;¹⁷ the isotherms exhibit a minimum, whose deepness increases when the size of the alkali metal ion increases (Figure 2).

We want to emphasize that no positive deviations appear; these exist only in the cadmium halide systems, and are a peculiar feature of them.

Positive deviations of the activity of CdCl_2 at low alkali chloride concentrations ($x = 0.1$) were found by Lantratov and Alabyshev by emf investigations.⁵

It is quite generally accepted that small additions of alkali chloride to liquid CdCl_2 result in the breakdown

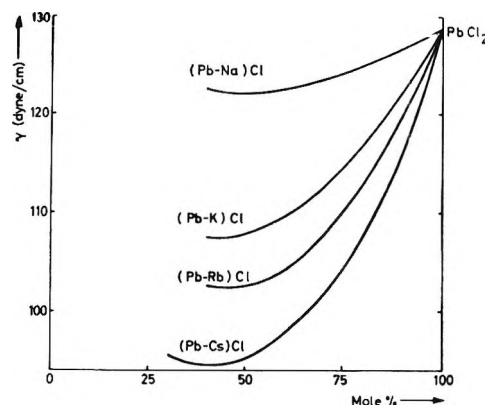


Figure 2. Surface tension isotherms for lead chloride-alkali chloride systems (from data of ref 17).

of the associated $(\text{CdCl}_2)_n$. These entities in pure CdCl_2 are likely to be surface active because of their large size and covalent character. They may be responsible for the low surface tension and its temperature coefficient; thus, their dissociation may account for the rapid increase of the surface tension upon dilution with alkali chlorides, so leading to positive deviations from linearity.

No similar associated entities exist in liquid lead chloride, which has a much more ionic character; no further dissociation can result in it when alkali chlorides are added. An excess of Cl^- will remove the Pb^{2+} ions by fixing them in the complex PbCl_3^- ; this latter, being surface active, will decrease the surface tension.

Let us consider the isotherm of the (Cd-Cs)Cl system (Figure 1). The surface tension of CdCl_2 is increased by small additions of CsCl following the mechanism we have illustrated, until a maximum is reached at 12 mole % of CsCl. Then, the complex ions CdCl_3^- , which gradually form at the expense of Cd^{2+} and Cl^- , make the surface tension decrease. After reaching a minimum at an equimolar composition, the surface tension increases again, up to pure CsCl.

(16) K. Balambrahmanyam and L. Nanis, *J. Chem. Phys.*, **40**, 2657 (1964).

(17) J. L. Dahl and F. R. Duke, USAEC Report ISC-923, 1958.

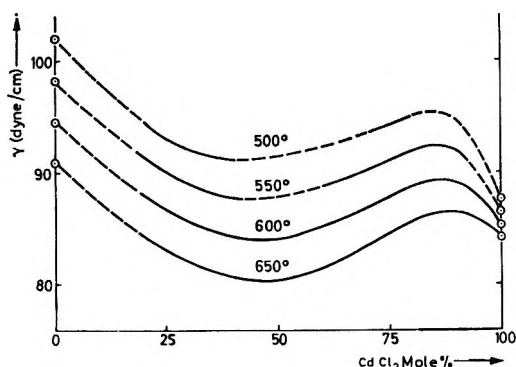


Figure 3. Surface tension isotherms for the (Cd-Cs)Cl system at various temperatures.

When the size of the alkali metal ion is varied by replacing cesium with rubidium, the shape of the isotherm changes slightly; the minimum becomes less deep, and the maximum is shifted toward higher alkali chloride concentrations. This means that—the alkali chloride concentration being equal—the CdCl_3^- concentration is lower with Rb^+ than with Cs^+ ; in other words, replacing cesium with rubidium causes the complex anion to become less stable.

On going from rubidium to potassium, the isotherm changes further in the same way; the maximum and minimum are no longer distinct, but overlap in a horizontal inflexion at the composition of an approximately equimolar mixtures.

At least, in the (Cd-Na)Cl system, maximum and

minimum have disappeared, and a slight inflexion only is present.

We may therefore point out that really the stability of the complex anions decreases gradually from cesium to sodium, in agreement with the considerations outlined in the Introduction.

By observing the phase diagrams of these systems,¹⁸ we may notice that the larger the alkali metal is, the higher and sharper the peak of the congruent MeCdCl_3 compound. If this may be regarded as a rough indication of the stability of the complex, we clearly find a parallelism between this trend and our previous conclusions.

2. *Effect of Temperature.* In Figure 3, the surface tension isotherms of the (Cd-Cs)Cl system at various temperatures are shown. It appears that with increasing temperature the maximum flattens.

We may understand this behavior by making the assumption that pure cadmium chloride contains some associated entities, which are likely to be thermally dissociated, so that their concentration diminishes by increasing temperature. Thus, the dissociating effect of the alkali chloride will be less and less remarkable as the associated entities disappear upon heating.

Probably, if it were possible to work at higher temperatures, pure CdCl_2 would no longer contain any associated group, and no positive deviation would appear in the surface tension isotherms; these would have the same shape as those of the PbCl_2 systems.

(18) E. Degurnov, *Dokl. Akad. Nauk SSSR*, **64**, 517 (1949).

NOTES

Desorption of Cumene from Silica-Alumina Catalysts

by Yutaka Kubokawa and Hisashi Miyata

Department of Applied Chemistry, University of Osaka Prefecture, Sakai, Osaka, Japan (Received March 23, 1967)

The kinetics of cumene cracking on silica-alumina catalysts have been investigated by many workers. As for the chemisorption of cumene on silica-alumina, there seem to have been no studies made of the heat of adsorption. Only the heat values on catalytically active sites have been estimated approximately from the kinetics of the reaction.¹ In a previous work,² it

has been shown that desorption rate measurements can give unambiguous information on the heat of adsorption over a wide range for a given chemisorption system. In the present work similar measurements have been carried out for cumene adsorbed on silica-alumina.

Experimental Section

Materials. A silica-alumina catalyst containing 13% alumina was obtained from the Shokubaikasei Co. It has a BET surface area of 448 m²/g. Cumene

(1) C. D. Prater and R. M. Lago, *Advan. Catalysis*, **8**, 298 (1956); W. B. Horton and R. W. Maatman, *J. Catalysis*, **3**, 113 (1964).

(2) Y. Kubokawa, *Bull. Chem. Soc. Japan*, **33**, 546, 550, 555, 739, 747, 936 (1960); *J. Phys. Chem.*, **67**, 769 (1963); **69**, 2676 (1965); Y. Kubokawa and O. Toyama, *Bull. Chem. Soc. Japan*, **64**, 1407 (1962); Y. Kubokawa, S. Takashima, and O. Toyama, *J. Phys. Chem.*, **68**, 1244 (1964).

was purified by passing it through silica gel heated to 100°. Ammonia was obtained from the thermal decomposition of ammonium chloride and purified by fractional distillation.

Apparatus and Procedure. A conventional constant volume apparatus was used. In order to measure the rate of desorption, two traps were attached to the reaction vessel. After the adsorption of cumene at room temperature, the desorption experiment was started by immersing the trap in liquid nitrogen. By using the two traps alternately, the desorption could be continued without interruption. The amounts of cumene collected in the trap were determined by gas chromatography. From the amounts desorbed in a definite time the rates of desorption were determined. During the rate measurements the temperature of the catalyst was lowered abruptly and the rates before the temperature drop were extrapolated to those for the small amount adsorbed after the temperature drop. Thus, the rates at the two temperatures corresponding to the same amount adsorbed and the activation energy of desorption could be obtained. Afterward, the temperature of the catalyst was raised in stages, and similar measurements were carried out at each stage.

Results and Discussion

The activation energies of desorption of cumene from a silica-alumina catalyst are shown in Figure 1. It is seen that in the temperature range 20–60° the activation energy of desorption E_d ranges from 12 to 18 kcal/mole, while above 60° it increases markedly with increasing desorption temperature up to 40 kcal/mole. It was found that above 60° the desorption products contained benzene, suggesting that the decomposition of cumene had occurred. According to the work of Horton and Maatman,¹ who investigated the kinetics of cumene cracking on silica-alumina, the heat of adsorption of cumene on active sites is only 9.5 kcal/mole, much less than the E_d values shown in Figure 1.³

After various amounts of ammonia were adsorbed on silica-alumina, similar additional experiments were carried out, the results of which are again shown in Figure 1. It is seen that the plots of E_d against the amount of cumene adsorbed for the catalysts before and after the ammonia adsorption nearly coincide, although no decomposition of cumene took place after the ammonia adsorption of 4.08 cc/g. This suggests that cumene adsorption on silica-alumina is unaffected by the ammonia adsorption; *i.e.*, most of the cumene adsorption is not associated with the acidity of silica-alumina. With regard to the cumene adsorption on the active sites for the decomposition, it should be noted that the sites with a high heat of adsorption such as 40 kcal/mole still remain active after the ammonia adsorption. It can be concluded that the sites on which a strong adsorption of cumene occurs are not the same as the

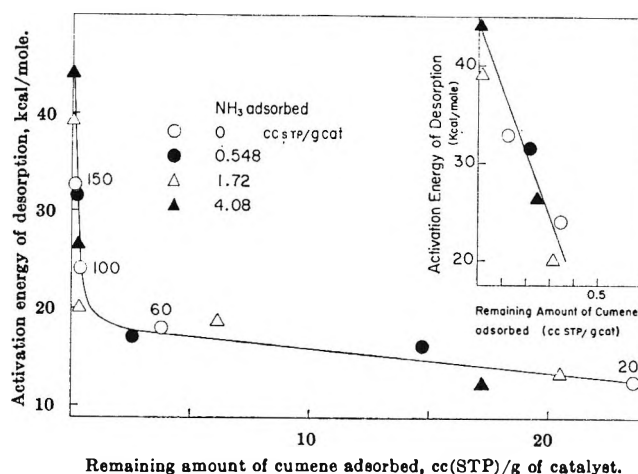


Figure 1. Activation energy of desorption of cumene. Figures indicate the temperature of desorption.

strongly acidic sites, *i.e.*, the most active sites for the reaction.

In the temperature range where the decomposition of cumene occurs, the activation energy of decomposition was determined by measuring the benzene content in the decomposition products in a similar manner to the measurements for the activation energy of desorption. The results are shown in Table I. As an ex-

Table I: Activation Energy of Cumene Decomposition

Temp. °C	Activation energy, kcal/mole		Remaining amount of cumene adsorbed, cc(STP)/ g of catalyst
	Desorption	Decomposition	
60	16.7	20.5	4.71
100	24.1	32.2	0.312
150	32.9	41.9	0.033

ample, the rate data used to calculate the activation energy of decomposition are given in Figure 2. The rate shown in this figure was found to be in fair agreement with that expected from the data of cumene cracking at high temperatures given by Pansing and Malloy.⁴ It is seen that the activation energy of decomposition is increased with increasing temperature, *i.e.*, with increasing E_d values. With regard to the nature of such an increase in the activation energy of decomposition, further studies are now in progress. At present it seems very difficult to predict whether a similar increase in the activation energy will occur in the

(3) In view of a rapid establishment of the adsorption equilibrium, it may be certain that cumene adsorption on silica-alumina is a nonactivated type.

(4) W. F. Pansing and J. B. Malloy, *Ind. Eng. Chem., Proc. Design Develop.*, **4**, 181 (1965).

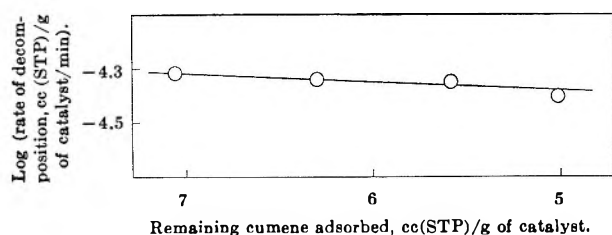


Figure 2. The rates of decomposition of cumene at 60°. The rate of decomposition at 40° for the cumene adsorbed of 4.17 cc was found to be 5.64×10^{-8} cc (STP)/g of catalyst, min. Comparison of the rates at both temperatures corresponding to the same amount adsorbed (4.17 cc) leads to an activation energy of 20.5 kcal/mole.

usual flow method, owing to a marked difference in the experimental conditions, *e.g.*, the reaction temperature or the coverage of cumene during the reaction.

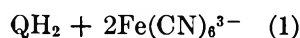
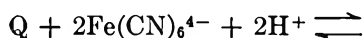
Kinetics of Ferrocyanide Reduction of Quinones

by S. A. Levison^{1a} and R. A. Marcus^{1b}

Department of Chemistry, Polytechnic Institute of Brooklyn, Brooklyn, New York (Received July 10, 1967)

We describe here the kinetics of ferrocyanide reduction of 2,5-dichloro-, benzo-, and 2,5-dimethylquinones (denoted below by I, II, III) in 1 *M* KCl. Reagent materials were used where available and the hydroquinones of I and III were synthesized by SnCl₂ reduction and recrystallization. Slightly alcoholic solutions of quinones^{2,3} in 1 *M* KCl were deoxygenated, placed in blackened vessels at 27°, and then in a 10-cm path Beckman cell. Buffered 1 *M* KCl ferrocyanide at 27° was added and the rate was measured from ferrocyanide disappearance at 420 mμ or disappearance of I at 275 mμ, using a Beckman.⁴

The acid dissociation constants of H₂Fe(CN)₆²⁻ and HFe(CN)₆³⁻ in 1 *M* KCl were measured with a Beckman (260–280 mμ) at concentrations of $0.4\text{--}4.5 \times 10^{-5}$ *M* and found to be 0.32 ± 0.02 and $(4.7 \pm 0.2) \times 10^{-3}$ *M*, respectively^{1a}. The equilibrium constant, *K*, of



was measured from the formal potentials *E*₀' of the two half-cells using a Leeds and Northrup potentiometer. The *E*₀' (relative to sce) of the ferrocyanide system in 1 *M* KCl was 0.22 V, and those for I, II, and III in 1 *M* KCl were 0.47, 0.44, and 0.34 V yielding *K*'s of $(2.8 \pm 0.5) \times 10^8$, $(3.1 \pm 0.5) \times 10^7$, and $(1.1 \pm 0.2) \times 10^4$ *M*⁻², respectively. (The anions in (1) are largely paired with *K*⁺; concentrations throughout this paper

include all species, paired or unpaired.) *E*₀' for ferroferri was constant from pH 3.7 to 6.7 and *E*₀' for Q–QH₂ was constant from pH 2 to 6.7. (These *E*₀'s were defined by *E* = *E*₀' and *E* = *E*₀' + 2.3(*RT*/*F*)pH, respectively, for the systems in the cited pH ranges, for equal concentration of oxidized and reduced forms.)

The stoichiometric equation (1) was confirmed spectrophotometrically by determining the amount of Fe(CN)₆³⁻ formed in excess quinone and then in excess Fe(CN)₆⁴⁻.^{1a} The reaction order was investigated by (1) pseudo-first-order plots with ferrocyanide in large excess, and (2) when no reagent was in large excess, by determining best tangents to amount reacted *vs.* time plots. The slopes and known concentrations yielded apparent second-order *k*'s [= rate/(ferro)_s(Q)_s, where *s* denotes stoichiometric].

All *k*'s were constant at fixed (ferri)_s/(ferro)_s at pH 2.74 to 4.74. Typical data for I and II are plotted in Figures 1 and 2.⁵ The *k*'s for III were constant in this range of ratios. The (ferro)_s was varied from 0.3 to 4, 0.2 to 2, and 1 to 10 ($\times 10^{-4}$ *M*), respectively, and the (Q)'s from 0.1 to 1, 1 to 5, and 1 to 10 ($\times 10^{-5}$ *M*). All data obeyed

$$\frac{1}{k} = \frac{1}{k_1'} + \frac{C(\text{ferri})_s}{(\text{ferro})_s} \quad (2)$$

and are summarized in Table I: *k*₁' is fairly insensitive to pH in the range (2.74 to 3.74) where it was measured.⁶ *C* ∝ (*H*⁺)⁻¹ for I, and *C* ∝ (*H*⁺)^{-1.4} for II.

Table I: Summary of Kinetic Data^a

pH	I (2,5-Dichloroquinone)		II (Benzoquinone)		III (2,5-Dimethylquinone)	
	<i>k</i> ₁ ' × 10 ⁻⁴	<i>C</i> × 10 ³	<i>k</i> ₁ ' × 10 ⁻⁴	<i>C</i> × 10 ³	<i>k</i> ₁ '	<i>C</i>
2.74	3.6	0.036	3.7	0.014	36	<i>b</i>
3.74	3.6	0.39	3.7	0.54	26	<i>b</i>
4.74	...	2.7	...	20.	...	5
5.74			...	390.		

^a Units for *k*₁' and *C*⁻¹ are (*M* min)⁻¹. ^b Not measured.⁶

(1) (a) S. A. Levison, Ph.D. Thesis, Polytechnic Institute of Brooklyn, June 1962. (b) Address correspondence to this author at Noyes Chemical Laboratory, University of Illinois, Urbana, Ill.

(2) I and III were dissolved in ethanol because of slow dissolution in water and were diluted to 1.0 to 0.01% alcoholic content, a variation without effect on potentials or reaction rates.

(3) Versene, 10⁻⁶ *M*, added to the ferrocyanide solution to remove a slight turbidity, perhaps due to Pb₂Fe(CN)₆, did not affect rates.

(4) In the kinetically important time of 10 min, a Δ*T* (0.7°) was estimated to cause a minor increase of 7% in rate.

(5) When (ferri)_s/(ferro)_s changed during reaction in pseudo-first-order data, a mean was used. In ref 1a, *C* and *E* in Table 32 should be interchanged.

(6) A flow system would permit determination of *k*₁' at pH 4.74 and 5.74 by permitting measurements at very low conversions and hence at very low mean (ferri)_s/(ferro)_s ratios. For compound III at pH 2.74 and 3.74, only initial rates were measured and no effort was made to determine *C*. Those initial rates were unchanged when (ferro)_s was increased from 1 to 10 × 10⁻⁴ *M*.

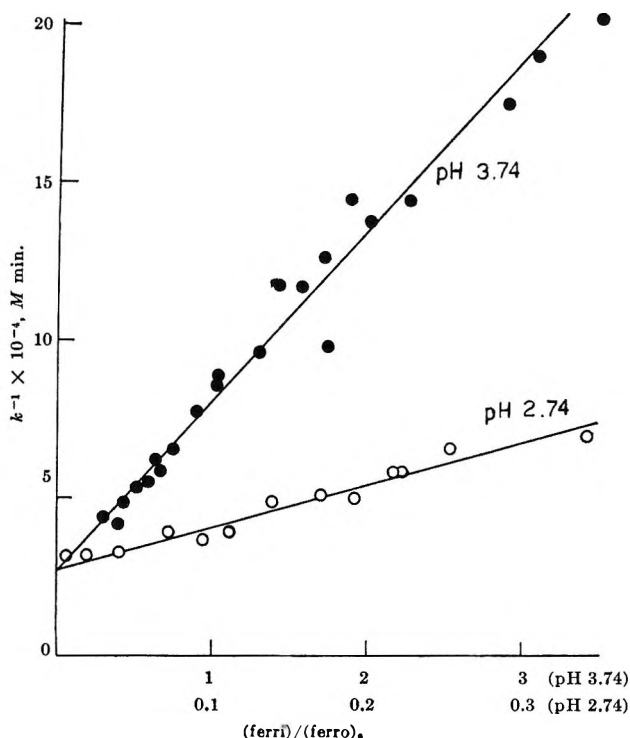


Figure 1. Depression of rate constants by ferricyanide at pH 2.74 and 3.74 (benzoquinone). At pH 2.74, (ferro) = 20 μ M and (Q) = 50 μ M. At pH 3.74, (ferro) = 20 and 10 μ M and (Q) = 10 μ M.

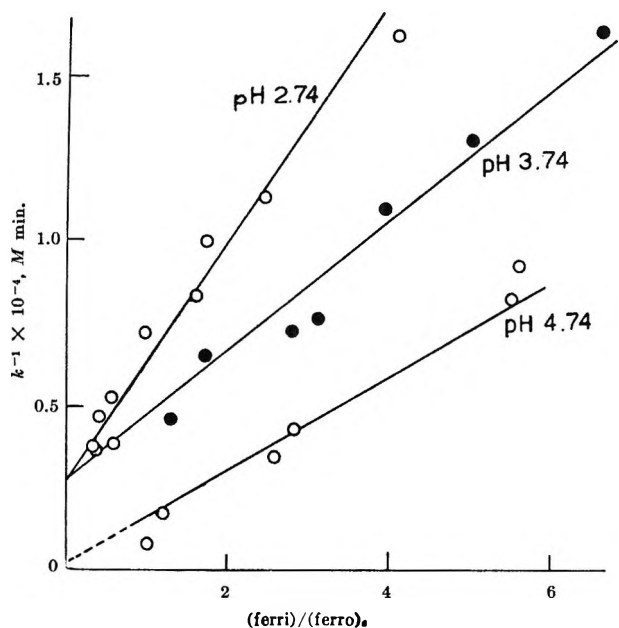
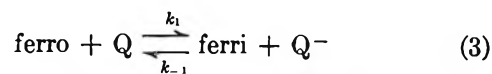


Figure 2. Depression of rate constants by ferricyanide at pH 2.74, 3.74, and 4.74 (2,5-dichloroquinone). For pH 4.74, the ordinate numerals should be multiplied by 5. For pH 3.74 and 4.74, the abscissa numerals should be multiplied by $1/20$ and by $1/40$, respectively. Various values of (Q) and (ferro) were used.

With a pK of 2.3, the unprotonated form of ferro predominates ($\geq 70\%$) in pH 2.74 to 3.74 and, since k_1' was pH independent in this range, the principal elementary step involves unprotonated ferro and quinone.

Thus, it cannot involve H-atom transfer. Using a steady-state treatment for



and $\text{Q}^- + \text{H}^+ \rightleftharpoons \text{QH}'$, $\text{Ferro} + \text{QH}' \xrightleftharpoons[k_2]{k_1'} \text{QH}^- + \text{ferri}$, one obtains (2) with $k_1' = 2k_1$, and $C = k_{-1}K_{\text{QH}}/2k_1k_2(\text{H}^+)$, where K_{QH} is the acid dissociation constant for QH' . [(ferro)_s = (ferro) in this range.] The mechanism agrees with $C \propto (\text{H}^+)^{-1}$ for I. To explain $C \propto (\text{H}^+)^{-1.4}$ for II, one can add reactions such as $\text{QH}' + \text{HFe}(\text{CN})_6^{3-}$ or $\text{Q}^- + \text{H}_2\text{Fe}(\text{CN})_6^{2-}$.

The $\Delta F^{\circ'}$ values in Table II were computed from

$$\Delta F^{\circ'} = -RT \ln (KK_{\text{QH}_2}K_{\text{QH}} - K_{\text{S}})^{1/2} \quad (4)$$

where K_{QH_2} and K_{QH} are acid dissociation constants of the hydroquinone and of its anion, and K_{S} refers to $\text{Q} + \text{Q}^{2-} \rightleftharpoons 2\text{Q}^-$. K was given earlier and the other constants in (4) are known.⁸ The $\Delta F^{\circ'}$ in Table II were calculated from $k_1' = 10^{11} \exp(-\Delta F^*/RT) \text{ M}^{-1} \text{ sec}^{-1}$. For comparison with other data, we extrapolate these $\Delta F^{\circ'}$ to $\Delta F^{\circ'} = 0$ using⁹

$$\Delta F^* = \Delta F_0^*(1 + \Delta F^{\circ'}/4\Delta F_0^*)^2 \quad (5)$$

The $\Delta F^*_{\text{calcd}}$ in Table II were obtained using $\Delta F_0^* = 8.4 \text{ kcal mole}^{-1}$.

Table II: Kinetic and Thermodynamic Data for $\text{Q} + \text{Fe}(\text{CN})_6^{4-}$ Reaction 3

Quinone	k_1' , (M min) ⁻¹	$\Delta F^{\circ'}$, kcal mole ⁻¹	$\Delta F^{\circ'}$ expt., kcal mole ⁻¹	$\Delta F^*_{\text{calcd}}$, kcal mole ⁻¹
2,5-Dichloro	1.9×10^4	5.7	11.7	11.5
Benzo	1.9×10^3	9.1	13.1	13.6
2,5-Dimethyl	1.3×10^1	12.5	16.1	15.8

We may compare this ΔF_0^* with that which we estimate from one-electron oxidation of the anion (IH_2^-) of 2,6-dichlorophenol indophenol by ferricyanide and one-electron reduction of a cation (IH_2^+) of leuco 2,3-dichlorophenol indophenol by ferrocyanide.¹⁰ The

(7) $\Delta F^{\circ'}$ is the " $\Delta F^{\circ'}$ " of (3) for the given T and medium.

(8) C. A. Bishop and L. K. S. Tong, *J. Am. Chem. Soc.*, **87**, 501 (1965).

(9) This relation is motivated by the electron transfer theory in *J. Chem. Phys.*, **43**, 679 (1965), *J. Phys. Chem.*, **67**, 853 (1963), etc. As noted there, the theory does not exclude ion-paired systems. ΔF_0^* (i.e., ΔF^* extrapolated to zero $\Delta F^{\circ'}$) depends on intrinsic reorganization terms, $1/\lambda$, on work terms, and now on ion-pair constants. This ΔF_0^* , according to theory, equals $1/2[\Delta F^*(\text{ferro-ferri exchange}) + \Delta F^*(\text{Q-Q}^- \text{ exchange})]$ when the work terms are small. (Compare eq A42, Appendix VIII, of the 1965 article. Our extrapolation based on (5) permitted the fulfillment of the linear $\Delta F^{\circ'}$ condition in that Appendix.) When the work terms are not small, this ΔF_0^* is still a useful property for characterizing intrinsic reactivities of different series of substrates towards a given reagent in a given medium.

(10) H. Diebler, *Z. Elektrochem.*, **67**, 396 (1963). (11° and $\mu = 0.1 \text{ M}$).

corresponding ΔF^*_{expt} are 4.6 and 2.8 kcal mole⁻¹ and, we estimate,¹¹ the corresponding $\Delta F^0'$ are -1.8 and -3.2 kcal mole⁻¹. Thereby, the ΔF^0_* is *ca.* 5 kcal mole⁻¹. That is, the indophenols are intrinsically more reactive than the quinones. Several explanations could be offered, based on differences in molecular sizes and on a milder rearrangement of bond lengths for the larger conjugated system. However, comparisons with ΔF^0_* 's of related systems would be useful first.

(11) The $\Delta F^0'$'s for the IH_2^- and IH_2^+ reactions are $-RT \ln (K_a/K_a^2K)^{1/2}$ and $-RT \ln (K_aKK_a')^{1/2}$, where K , K_a , K_a' and K_a'' refer to $\text{IH} + 2\text{Fe}(\text{CN})_6^{4-} + 2\text{H}^+ \rightleftharpoons \text{IH}_3 + 2\text{Fe}(\text{CN})_6^{3-}$, $\text{IH}_3 \rightleftharpoons \text{IH}_2^- + \text{H}^+$, $\text{IH}_3 + \text{IH} \rightleftharpoons 2\text{IH}_2^+$ and $\text{IH}_2^+ \rightleftharpoons \text{IH} + \text{H}^+$, respectively. In ref 10, $K_a = 1 \times 10^{-7} M$ and $K_a' = 0.3 M$. In O. Tomicek, "Chemical Indicators," Butterworth and Co. Ltd., London, 1951, p 156, $K = 3.6 \times 10^8 M^{-2}$. K_a for phenol blue, an analog of the dichloro compound, is *ca.* 2×10^{-3} , using data in G. Schwarzenbach and L. Michaelis, *J. Am. Chem. Soc.*, **60**, 1667 (1938).

Osmotic Coefficients of Tungstosilicic Acid¹

by J. S. Johnson, Jr., and R. M. Rush

Chemistry Division, Oak Ridge National Laboratory,
Oak Ridge, Tennessee (Received July 21, 1967)

The heteropolyacid $\text{H}_4\text{SiW}_{12}\text{O}_{40}$ has attracted considerable interest as one of the few known examples of a strong 1:4 electrolyte and as a well-characterized monodisperse solute of molecular weight between those of simple electrolytes and such large species as proteins. Some years back we measured the activity coefficients of tungstosilicic acid in dilute aqueous solution (0.004–0.04 *M*) by equilibrium ultracentrifugation and found that turbidities calculated from these activity coefficients agreed with our light scattering measurements.² These turbidities were substantially lower than some earlier measurements in the literature.³ Since then, there have been reports of several other studies in related areas, and the controversy has, if anything, widened.

A group (KKOM)⁴ associated with Kerker remeasured turbidities and included higher concentrations than our measurements. Their values fell between ours and those of Kronman and Timasheff.³ They calculated water activities from turbidities, and claimed agreement with some preliminary values obtained isopiesticly by Tyree and co-workers at the University of North Carolina (UNC). The turbidities they calculated from the isopiestic measurements were 6–10% lower than their measured values. However, differences between turbidities measured in the various laboratories are considerably greater.

Scatchard and Yoest at the Massachusetts Institute of Technology (MIT) also carried out some isopiestic measurements, and in collaboration with the UNC group, published⁵ an analysis of both sets (MIT–UNC).

They concluded that some early low concentration UNC points, which appeared to extrapolate to lower activity coefficient values than we obtained by ultracentrifugation, were in error, that the ultracentrifugation and isopiestic methods were in reasonably good agreement, and that their values were substantially different from KKOM over the entire concentration range.

Shortly before their paper appeared, a second Kerker group (KOK) published another study⁶ of water activities of tungstosilicic acid solutions, this time measured with a vapor-phase osmometer. This set of values fell between KKOM and MIT–UNC. Pelzer and Schönert⁷ have recently published osmotic coefficients of aqueous $\text{HCl-H}_4\text{SiW}_{12}\text{O}_{40}$ solutions. Although no two-component tungstosilicic acid solutions were included in their study, they concluded that their data indicated closer agreement at low concentrations with the preliminary UNC osmotic coefficients than with our ultracentrifugation values.

From this summary, it is apparent that there is no general agreement concerning the free energies of tungstosilicic acid–water solutions. Although equilibrium ultracentrifugation and the MIT–UNC study are consistent, the scatter of the data makes further study desirable, and the rejection of low-concentration points from the preliminary UNC study should be confirmed. Resolution of these conflicts with other laboratories is desirable, not only because of the widespread interest in this system, but also because a suggestion we made,² that $\text{H}_4\text{SiW}_{12}\text{O}_{40}$ solutions might be useful in calibration of light scattering photometers for measurements of aqueous solutions, depends on knowledge of the non-ideality of the system. We have therefore carried out isopiestic measurements extending both higher and lower in concentration (from 0.02 to 1.3 *m*) than previously made by this technique.

Experimental Section

The isopiestic equipment and the techniques of measurement have been described previously.⁸ Sodium chloride solutions were used as standards, and two cups were used for each solution and standard; the concentration of solutions in each of the duplicates for each

(1) Research sponsored by the U. S. Atomic Energy Commission under contract with Union Carbide Corporation.

(2) J. S. Johnson, K. A. Kraus, and G. Scatchard, *J. Phys. Chem.*, **64**, 1967 (1960).

(3) M. J. Kronman and S. N. Timasheff, *ibid.*, **63**, 629 (1959).

(4) M. Kerker, J. P. Kratochvil, R. H. Ottewill, and E. Matijevic, *ibid.*, **67**, 1097 (1963).

(5) S. Y. Tyree, Jr., R. L. Angstadt, F. C. Hentz, Jr., R. L. Yoest, and G. Scatchard, *ibid.*, **70**, 3917 (1966).

(6) J. P. Kratochvil, L. E. Oppenheimer, and M. Kerker, *ibid.*, **70**, 2834 (1966).

(7) H. Pelzer and H. Schönert, *Ber. Bunsenges. Physik. Chem.*, **70**, 897 (1966).

(8) R. M. Rush and J. S. Johnson, *J. Chem. Eng. Data*, **11**, 590 (1966).

point was initially set to be different by appropriate addition of water. At equilibrium, molalities (m) in the duplicates agreed within 0.12% for all but two pairs (deviations <0.4%), except at the lowest concentration, where agreement was within 0.6% for four solutions and 2% for the other two. Averages for the two cups are reported. Equilibration times ranged from 3 days for the high concentrations to 3 weeks at the low concentration end.

Since some of the discrepancies in earlier results may arise from differences in the starting material, we have used $\text{H}_4\text{SiW}_{12}\text{O}_{40}$ from two sources. One (BA) is the reagent grade material of Baker and Adamson, the supplier of most of the solute used in our ultracentrifugation and light scattering work.² The other was prepared at the University of North Carolina⁹ by the procedure they used to make the material for their study, and for some of the KKOM work. These samples were used as received (BA-O and UNC-O); after recrystallization from water (the middle crop of crystals), followed by drying over desiccant (BA-RD and UNC-RD); and after recrystallization, the stock solution being made from damp, undried crystals (BA-R). Solutions made from the dried materials (BA-RD and UNC-RD) and the UNC-O (which had also been dried during preparation⁵) over a period of time deposited a light sediment, not enough to affect the composition appreciably; no such precipitation was noted with BA-O or BA-R.

Three analyses were carried out on stock solutions prepared from these materials or on a weight dilution. Two analyses were made by evaporation of duplicate samples to dryness, ignition at 800°, and weighing as $\text{SiO}_2 \cdot 12\text{WO}_3$; the third was by density measurement of a dilute solution, and from density, calculation of its composition.² The widest variation of the three analyses for a sample was equivalent to about $\pm 0.2\%$ in water content of this sample's concentrated stock, which contained about 27% water (*ca.* 0.95 m).

Results and Discussion

The molalities of the solutions at solvent activity equilibrium are given in Table I. From these values,

Table I: Isopiestic Molalities

NaCl	Tungstosilicic acid				
	BA-O	BA-R	BA-RD	UNC-O	UNC-RD
5.6260	1.2938	1.2873	1.2961	1.2780	1.2700
2.5972	0.7496	0.7475	0.7508	0.7424	0.7392
1.3404	0.4614	0.4604	0.4618	0.4579	0.4564
0.8374	0.3192	0.3188	0.3196	0.3174	0.3165
0.55294	0.2258	0.2254	0.2260	0.2247	0.2242
0.43316	0.1826	0.1824	0.1830	0.1823	0.1818
0.41432	0.1753	0.1751	0.1754	0.1745	0.1742
0.19096	0.08742	0.08734	0.08751	0.08730	0.08716
0.08580	0.04079	0.04081	0.04084	0.04064	0.04068
0.04161	0.02022	0.02008	0.01992	0.01977	0.01982

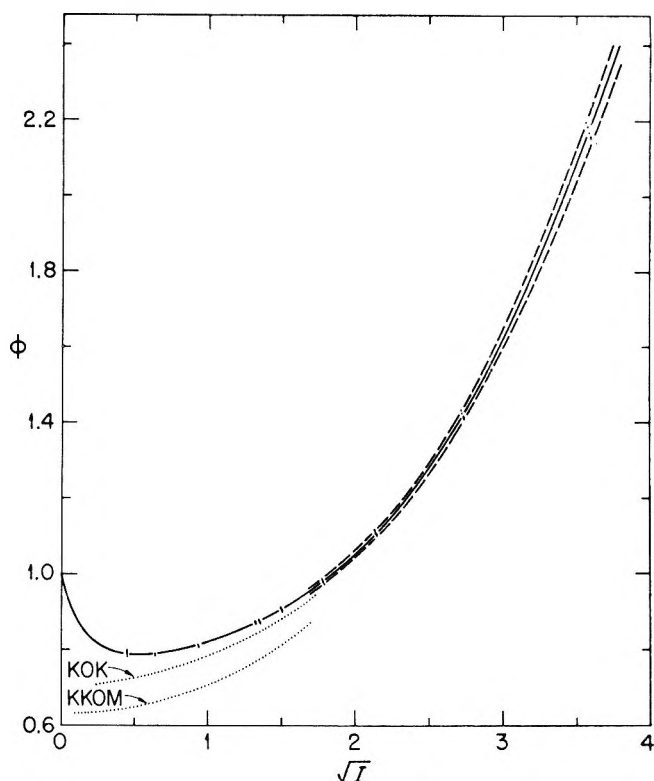


Figure 1. Osmotic coefficients of tungstosilicic acid. Solid line calculated from best least-squares fit to data. Dashed lines represent the maximum probable uncertainty in the tungstosilicic acid analysis.

osmotic coefficients ϕ_{TSA} of tungstosilicic acid were computed with the equation

$$\phi_{\text{TSA}} = \frac{2m_{\text{NaCl}}\phi_{\text{NaCl}}}{5m_{\text{TSA}}} \quad (1)$$

the osmotic coefficient of the standard being taken from the equation previously reported (ref 8, eq 3). Values of ϕ_{TSA} are given in Figure 1, along with the curve computed from the following equation obtained by a least-squares fit of all our data

$$\phi_{\text{TSA}} = \phi^{\text{DH}} + 0.0254I + 0.00799I^2 - 0.000165I^3 \quad (2)$$

$$\phi^{\text{DH}} = 1 - \frac{(4)(1.17082)}{a^3I} \times$$

$$\left[1 + aI^{1/2} - \frac{1}{1 + aI^{1/2}} - 2 \ln(1 + aI^{1/2}) \right] \quad (3)$$

where $I = 10m_{\text{TSA}}$, the distance of closest approach parameter a was found to be 2.499 by the least-squares fit, and the standard deviation $\sigma = 0.012$ in ϕ_{TSA} . On each side of the computed curve, dashed curves indicate the effect on ϕ_{TSA} of the maximum probable uncertainty

(9) We thank F. C. Hentz, Jr., for supplying us with samples of tungstosilicic acid.

in concentration, taken to be the widest scatter for a single sample (see Experimental Section).

The tungstosilicic acid molalities in isopiestic equilibrium appear to be consistently lower (ϕ_{TSA} higher) for the UNC samples than for the BA, and the individual values fall in the order UNC-RD, UNC-O, BA-R, BA-O, BA-RD except for the two most dilute concentrations. In view of the uncertainty of the analyses, however, we doubt the significance of these differences in ϕ between samples.

Since Figure 1 of ref 5 summarizes earlier isopiestic data, we have not reproduced these here; the curve computed from eq 2, however, agrees with the curve adopted by MIT-UNC as most representative of all their results (their eq 1b) within 0.01 in ϕ_{TSA} over their experimental concentration range. Our converged least-squares value of $a = 2.499$ is the same as 2.5 adopted from the ultracentrifugation data.² Since at the upper concentration limit of the centrifugation study, the power series terms of eq 2 contribute about 0.02 to $\ln \gamma_{\pm}/d \ln m_{\text{TSA}}$ (Figure 1, ref 2 or Figure 2, ref 5), the difference in a is not as small as comparison of these numbers implies, but the agreement is nevertheless gratifying.

In Figure 1, we compare the values of KOK⁶ calculated from their equation for water activity (since they gave no experimental points and do not specify the lower concentration limit of their study, we do not know the extent of the gap between $\phi = 1$ at $m = 0$ and their lowest experimental concentration). We also present values obtained from an equation obtained from the KKOM results.⁵ Ours disagree with those of KOK, and even more with those of KKOM. It is perhaps worth mentioning that there is a substantial difference between the values of KOK and KKOM, contrary to the authors' implication⁶ that the two sets of values agree well except at the low concentration end. Apparently, the differences were overlooked because the water activity graphs by which they visualized their results are less sensitive to deviations than osmotic coefficients.

In summary, we see no reason to modify in any substantial way our conclusions concerning the free energies of water-tungstosilicic acid solutions. With respect to their use as light scattering standards, we feel that activity coefficients are adequately known for this purpose. However, the agreement between osmotic coefficients obtained with various samples here, both those from which precipitation took place and those which were apparently stable, suggests that there may be further problems with decomposition which might affect turbidities more seriously than water activities.

Acknowledgments. We thank Professor George Scatchard for helpful discussions and Neva Harrison for technical assistance.

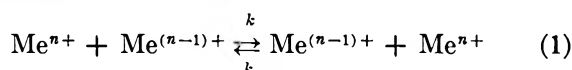
Electronic Conduction in Aqueous Solution

by Harald Dahms

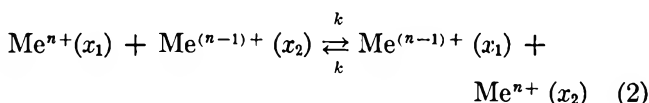
IBM Watson Research Center, Yorktown Heights, New York 10598
(Received July 31, 1967)

Diffusion, migration, and convection of ions are the three well-known mechanisms of charge transport in aqueous solution. However, electron-transfer processes can contribute to charge transfer if the solution contains an oxidation-reduction system. The possibility of charge transport by electron transfer appears to have been mentioned only by Levich,¹ who considered briefly the case of an electric field gradient. Here, the electronic conductivity due to concentration gradients, as well as electric field gradients, will be discussed for two types of oxidation-reduction systems.

The electron-transfer reaction



can be written for our purposes in the form

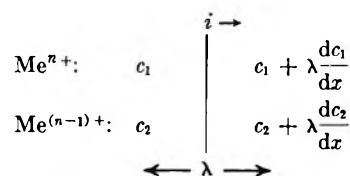


where x_1, x_2 is the position of the ion in solution in reference to the direction of current conduction. This reaction will contribute to current conduction if $x_1 \neq x_2$ and if there is an electrochemical potential gradient in the x direction. The quantity $x_2 - x_1 = \lambda$ is the average distance of electron transfer in the x direction.

Electronic Conduction Due to Concentration Gradients

Let the concentration gradient of Me^{n+} be dc_1/dx and that of $\text{Me}^{(n-1)+}$ be dc_2/dx , where c_1 and c_2 are given in moles/cm³. In two adjoining segments of the solution, the average concentrations are then as shown in Scheme I.

Scheme I



The flux of electrons/cm² across the boundary in the forward direction is

$$i_t = Fk\lambda c_1 \left(c_2 + \lambda \frac{dc_2}{dx} \right) \quad (3)$$

where i_t is the current density (left to right) in amp

(1) V. G. Levich in *Advan. Electrochem. Electrochem. Eng.*, **4**, 314 (1966).

cm^{-2} , F is Faraday's constant in coulombs equiv $^{-1}$, k is the rate constant of electron exchange in $\text{cm}^3 \text{sec}^{-1} \text{mole}^{-1}$ (eq 1), λ is the effective electron-transfer distance in the x direction in cm, c_1 is the concentration of Me^{n+} , and c_2 is the concentration of $\text{Me}^{(n-1)+}$, both in moles cm^{-3} .

The electron flow in the opposite direction is

$$i_b = Fk\lambda c_2 \left(c_1 + \lambda \frac{dc_1}{dx} \right) \quad (4)$$

where i_b is the current density (right to left) in amp cm^{-2} ; k , F , c_1 , c_2 , and λ are as given above.

The net flow of current is

$$i_e = i_t - i_b = Fk\lambda^2 \left(c_1 \frac{dc_2}{dx} - c_2 \frac{dc_1}{dx} \right) \quad (5)$$

The direction of current flow depends, of course, on the direction (*i.e.*, the sign) of the concentration gradients.

Under common experimental conditions, the two concentration gradients are very often approximately equal and opposite in sign since the flow of matter to and from the electrode has to be identical

$$\frac{dc_2}{dx} = -\frac{dc_1}{dx} = \frac{dc}{dx} \quad (6)$$

In this case, the current flow is

$$i_e = Fk\lambda^2 \frac{dc}{dx} (c_1 + c_2) \quad (7)$$

Let us now consider the magnitude of electronic conduction in comparison to conduction due to ionic diffusion. Since concentration gradients are present, there will be charge transfer by ionic diffusion according to

$$i = F \left(-D_1 \frac{dc_1}{dx} + D_2 \frac{dc_2}{dx} \right) \quad (8)$$

where D_1 and D_2 are the diffusion coefficients in $\text{cm}^2 \text{sec}^{-1}$. If the two concentration gradients are equal and opposite in sign (eq 6), and $D = D_1 = D_2$, eq 8 reduces to

$$i = 2FD \frac{dc}{dx} \quad (9)$$

The ratio of currents carried by electron transfer and ionic diffusion is

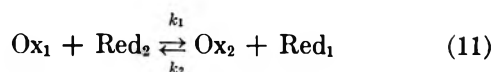
$$\frac{i_e}{i_i} = \frac{k\lambda^2(c_1 + c_2)}{2D} \quad (10)$$

where i_e is the electron conduction according to eq 7 and i_i is the ionic conduction according to eq 9.

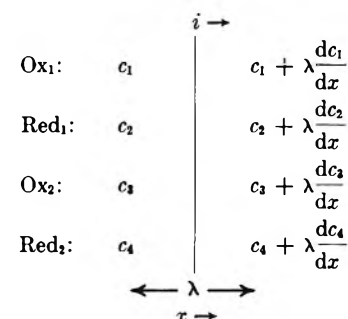
We can estimate the contribution of electronic conduction by inserting literature data into eq 10. For the electron exchange $\text{Fe}(o\text{-phen})_3^{3+} + e = \text{Fe}(o\text{-phen})_3^{2+}$, $k \sim 10^8 \text{ cm}^3 \text{mole}^{-1} \text{sec}^{-1}$,² the range of elec-

tron transfer is estimated from molecular dimensions $\lambda = 5 \times 10^{-8} \text{ cm}$, $D = 5 \times 10^{-6} \text{ cm}^2 \text{sec}^{-1}$,³ and concentrations of $10^{-4} \text{ mole cm}^{-3}$ are assumed. For these data: $i_e = 5 \times 10^{-6} i_i$. Hence, the contribution of electronic conduction is small.

Rate constants of electron transfer for reactions $\text{Ox} + e = \text{Red}$ (eq 1) have only been measured up to values of $10^8 \text{ cm}^3 \text{mole}^{-1} \text{sec}^{-1}$.⁴ However, some electron-transfer reactions of the type $\text{Red}_1 + \text{Ox}_2 = \text{Red}_2 + \text{Ox}_1$ are considerably faster. Several workers⁵⁻⁷ have reported second-order rate constants higher than $10^{12} \text{ cm}^3 \text{sec}^{-1} \text{mole}^{-1}$. The fact that these rate constants are higher is in accordance with the Marcus theory.⁸ We will, therefore, now consider electronic conduction in solutions containing a system of the type (see Scheme II)



Scheme II



Referring to Scheme 2, the forward current is given by

$$i_t = F\lambda \left[k_1 c_1 \left(c_4 + \lambda \frac{dc_4}{dx} \right) + k_2 c_3 \left(c_2 + \lambda \frac{dc_2}{dx} \right) \right] \quad (12)$$

and the current in the opposite direction is given by

$$i_b = F\lambda \left[k_1 c_4 \left(c_1 + \lambda \frac{dc_1}{dx} \right) + k_2 c_2 \left(c_3 + \lambda \frac{dc_3}{dx} \right) \right] \quad (13)$$

The net current is, then

$$i_e = i_t - i_b = F\lambda^2 \left(k_1 c_1 \frac{dc_4}{dx} + k_2 c_3 \frac{dc_2}{dx} - k_1 c_4 \frac{dc_1}{dx} - k_2 c_2 \frac{dc_3}{dx} \right) \quad (14)$$

Again, if (see comment to eq 6)

- (2) E. Eichler and A. C. Wahl, *J. Am. Chem. Soc.*, **80**, 4145 (1958).
- (3) I. M. Kolthoff and J. J. Lingane in "Polarography," Interscience, Publishers, Inc., New York, N. Y., 1952.
- (4) H. Strehlow, *Ann. Rev. Phys. Chem.*, **16**, 167 (1965).
- (5) J. Halpern, R. J. Legard, and R. Lumry, *J. Am. Chem. Soc.*, **85**, 680 (1963).
- (6) R. Campion, N. Purdie, and N. Sutin, *ibid.*, **85**, 3528 (1963).
- (7) P. Hurwitz and K. Kustin, *Inorg. Chem.*, **3**, 823 (1964).
- (8) R. A. Marcus, *Ann. Rev. Phys. Chem.*, **15**, 155 (1964).

$$\frac{dc_2}{dx} = -\frac{dc_1}{dx}; \quad \frac{dc_4}{dx} = -\frac{dc_3}{dx} \quad (15)$$

then eq 14 reduces to

$$i_e = F\lambda^2 \left((k_3c_3 + k_1c_4) \frac{dc_2}{dx} + (k_1c_1 + k_2c_2) \frac{dc_4}{dx} \right) \quad (16)$$

Let us compare the ionic and the electronic currents. The ionic diffusion current is

$$i_i = 2FD \left(\frac{dc_2}{dx} + \frac{dc_4}{dx} \right) \quad (17)$$

assuming that all diffusion coefficients are equal and also taking eq 15 into account. In order to evaluate the possible contribution of electronic current, we insert the following data into eq 16 and 17: $k_1 = 10^{12} \text{ cm}^3 \text{ sec}^{-1} \text{ mole}^{-1}$, $k_2 = 4 \times 10^{12} \text{ cm}^3 \text{ sec}^{-1} \text{ mole}^{-1}$ as experimentally observed for the system tris(4,7-dimethyl-1-10-phenanthroline)iron(II) and hexachloroiridate(IV).⁵ From molecular dimensions, we estimate $\lambda = 10^{-7} \text{ cm}$; the concentrations we assume as $c_2 = c_4 = 10^{-4} \text{ mole cm}^{-3}$, $c_1 = 10^{-5} \text{ mole cm}^{-3}$, $c_3 = 2.5 \times 10^{-6} \text{ mole cm}^{-3}$; $dc_2/dx = 10^{-2} \text{ mole cm}^{-4}$, $dc_4/dx = 10^{-2} \text{ mole cm}^{-4}$; $D = 10^{-5} \text{ cm}^2 \text{ sec}^{-1}$. With these values we obtain

$$i_e = 0.13i_i$$

It should be noted that there is an upper limit for the contribution of the electronic current to the total current. This upper limit is due to the fact that the electron-transfer rate constants k_1 and k_2 will approach diffusion control.⁹ In fact, the rate constant values given in the latter example are less than one order of magnitude below the diffusion limit.

Electronic Conductivity Due to Electric Field Gradient

Referring again to Schemes I and II, we will consider the case that all concentration gradients are zero. An electric field gradient V (v cm^{-1}) is now applied with current flowing in the forward direction

$$i_f = F\lambda k c_1 c_2 \exp\left(+\frac{\alpha F V \lambda}{RT}\right) \quad (18)$$

and in the reverse direction

$$i_b = F\lambda k c_1 c_2 \exp\left(-\frac{\alpha F V \lambda}{RT}\right) \quad (19)$$

where α is the free energy fraction between initial and activated state, R is the gas constant, T is absolute temperature, and all other quantities are as defined previously.

Taking into account that $2\alpha \sim 1$ and developing the exponential term into a series, we obtain for the net current

$$i_e = i_f - i_b = F^2 \lambda^2 k c_1 c_2 \frac{V}{RT} \quad (20)$$

Equation 20 can be compared with the one derived

by Levich.¹ Except for obvious errors (k is used in the same equation to represent both Boltzmann's constant and the rate constant, Avogadro's number is missing), the two equations are essentially identical except that Levich's equation contains the average distance of electron transfer while the equation derived here is expressed in terms of the component in the x direction of the transfer.

For the faster system represented by Scheme II, the electronic current is

$$i_e = \frac{F^2 \lambda^2 V}{RT} (k_1 c_1 c_4 + k_2 c_2 c_3) \quad (21)$$

The corresponding ionic currents are given by

$$i_i = V \Sigma \Lambda_i c_i n_i \quad (22)$$

where Λ is the equivalent conductance in $\text{ohm}^{-1} \text{ cm}^2 \text{ equiv}^{-1}$, c is the concentration in moles cm^{-3} , and n is the valency of ion, so that the ratio of electronic over ionic current is for a simple redox system (Scheme I)

$$\frac{i_e}{i_i} = \frac{F^2 \lambda^2 k c_1 c_2}{RT \Sigma \Lambda_i c_i n_i} \quad (23)$$

and for the faster redox system (Scheme II)

$$\frac{i_e}{i_i} = \frac{F^2 \lambda^2 (k_1 c_1 c_4 + k_2 c_2 c_3)}{RT \Sigma \Lambda_i c_i n_i} \quad (24)$$

We will now evaluate the order of magnitude of the electronic current with respect to the ionic current. Using the same data as above and assuming an equivalent conductance $\Lambda = 50 \text{ cm}^2 \text{ ohm}^{-1} \text{ equiv}^{-1}$,¹⁰ we obtain $i_e = 7 \times 10^{-3} i_i$.

Only aqueous solutions have been considered here since electron-exchange reactions have been mostly studied in this medium. It is, however, obvious that these considerations apply to other solvents. Although difficulties in studying electronic conduction will arise from the fact that it constitutes only part of the total conduction, these studies are of interest since rate constants as well as ranges of electron transfer enter into the equations discussed above.

(9) P. Debye, *Trans. Electrochem. Soc.*, **82**, 265 (1942).

(10) R. A. Robinson and R. H. Stokes in "Electrolyte Solutions," Butterworth and Co. Ltd., London, 1959.

Solute-Solvent Interactions: Ethyl Acetate in Water

by J. H. Stern and A. Hermann

Department of Chemistry, California State College,
Long Beach, California 90804 (Received August 1, 1967)

Recently, some studies have been made to examine possible correlations of the change in heat capacity

($\Delta C_{p,2}^{\circ}(g)$), resulting from the solution of various gases in water, with structural changes in the surrounding medium.¹

Frank and Evans² proposed that the solution of gases which are nonpolar or contain large nonpolar groups, in water, favors those iceberg forms of water which most easily can accommodate the solutes. An increase in temperature of the solution thus requires additional energy in order to melt the solute-induced iceberg forms of the water, and, thus, large positive values of $\Delta C_{p,2}^{\circ}(g)$ should be observed.

In this note, $\Delta C_{p,2}^{\circ}(g)$ for the solution of gaseous ethyl acetate (EtOAc(g)) in water is reported, based on calorimetric enthalpies of solution of EtOAc(l) between 15 and 50° combined with its values of $C_{p,2}^{\circ}(l)$ and $C_{p,2}^{\circ}(g)$.

Experimental Section

Calorimeter and Measurements. The calorimeter,³ materials, and experimental procedure⁴ have been described previously. All runs were carried out within $\pm 0.20^{\circ}$ of the reported temperatures.

Results and Discussion

The means of the observed enthalpies of solution of liquid ethyl acetate in water, ΔH_2° obsd, with their standard deviations, σ , are recorded in Table I. No variation in enthalpies over the reported final molality range, m_f , was observed within the limits of the over-all estimated uncertainty. The value at 298° has been reported previously.⁴ The calculated enthalpies, ΔH_2° -(calcd), are from eq 1, with values of the constants determined by the least-squares method, using weighting factors equal to $1/\sigma^2$

$$\Delta H_2^{\circ} = -126.23 + 0.7581T - 0.001148T^2 \quad (1)$$

The estimated uncertainty of enthalpies calculated from eq 1 is ± 0.1 kcal/mole.

Table I: Enthalpies of Solution of Ethyl Acetate(l) in Water

Runs	$m_f \times 10^3$	$T, ^{\circ}\text{K}$	$-\Delta H_2^{\circ}$ obsd, kcal/mole	$-\Delta H_2^{\circ}$ -(calcd), kcal/mole
3	5-10	288	3.22 ± 0.03	3.12
23 (4)	2-10	298	2.23 ± 0.01	2.17
9	6-10	313	1.52 ± 0.02	1.41
6	8-12	323	1.08 ± 0.02	1.13

The $\Delta C_{p,2}^{\circ}$ in cal/deg mole for the above solution process is obtained directly from the temperature derivative of eq 1

$$\Delta C_{p,2}^{\circ}(l) = C_{p,2}^{\circ} - C_{p,2}^{\circ}(l) = 758.1 - 2.296T \quad (2)$$

where $C_{p,2}^{\circ}$ and $C_{p,2}^{\circ}(l)$ are the heat capacities of EtOAc(aq) and EtOAc(l), respectively. The latter

quantity⁵ combined with $\Delta C_{p,2}^{\circ}(l)$ at 25° yields a calculated value for $C_{p,2}^{\circ}$ of 116 cal/deg mole. This together with the calculated $C_{p,2}^{\circ}(g)$ ⁶ gives the calculated change in heat capacity $\Delta C_{p,2}^{\circ}(g)$, 92 ± 5 cal/deg mole, upon solution of EtOAc(g) in water. The large positive value of $\Delta C_{p,2}^{\circ}(g)$ supports the dynamic solution model for nonpolar gases discussed earlier.

Group additivity methods have been very successful in the prediction of thermodynamic properties of gaseous organic compounds.⁶ It would be of interest to obtain similar additive group contributions to $C_{p,2}^{\circ}$ since these in turn could be used to estimate heat capacities of other aqueous nonelectrolytes. Meaningful values of group contributions could be calculated if sufficient and accurate supporting data were available. It appears that there are no $C_{p,2}^{\circ}$ data for compounds containing methyl, ethyl, and carboxyl groups, and that there is a general lack of data for organic solutes in water.

Lower order approximation methods of bond and atomic property additivity⁶ have also been useful in the gaseous state. Analysis of $C_{p,2}^{\circ}$ values for methane and ethane^{1b,6} shows that these two approaches fail for even these two simple hydrocarbon solutes. Further studies with a variety of aqueous nonelectrolytes have been initiated.

Acknowledgment. The authors wish to thank Dr. L. Brooks and K. Baier for assistance with the least-squares calculation, and Dr. R. H. Wood for fruitful discussion. The financial assistance of the National Science Foundation is gratefully acknowledged.

(1) (a) H. S. Frank and W. Wen, *Discussions Faraday Soc.*, **24**, 133 (1957); (b) L. A. D'Orazio and R. H. Wood, *J. Phys. Chem.*, **67**, 1435 (1963).

(2) H. S. Frank and M. W. Evans, *J. Chem. Phys.*, **13**, 507 (1945).

(3) J. H. Stern and C. W. Anderson, *J. Phys. Chem.*, **68**, 2528 (1964).

(4) J. H. Stern and A. Hermann, *ibid.*, **71**, 306 (1967).

(5) Landolt-Bornstein, "Zahlenwerte und Funktionen," "Kalorische Zustandsgrößen," Part 4, Springer-Verlag, Berlin, Germany, 1961, p 526.

(6) S. W. Benson and J. H. Buss, *J. Chem. Phys.*, **29**, 546 (1958).

Properties of Organic-Water Mixtures. VIII.

Dielectric Constants of N,N-Dialkylamides

Containing Water¹

by C. F. Coleman

Chemical Technology Division, Oak Ridge National Laboratory, Oak Ridge, Tennessee (Received August 4, 1967)

Dielectric constants of a series of amides at varying water contents were measured to test correlation with

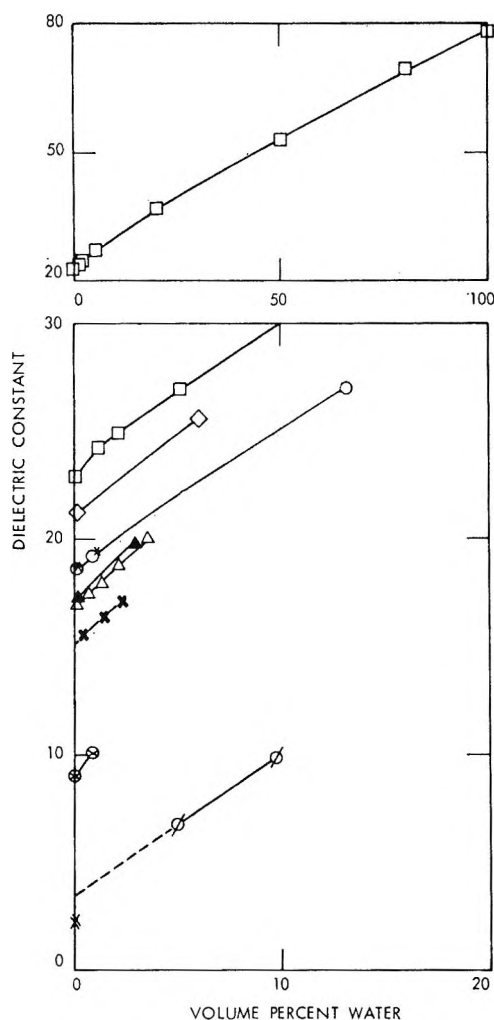


Figure 1. Dielectric constants of N,N-dialkylamide-water mixtures; \square , dipropylacetamide; \diamond , dipropylpropionamide; \circ , dibutylacetamide; $*$, dibutylacetamide saturated with NaCl; \otimes 50.3 vol. % dibutylacetamide-49.7 vol. % diethylbenzene; \blacktriangle , diisobutylpropionamide; \triangle , dibutylpropionamide; \times , diethyldecanamide; ϕ , tetraethylphthalamide; \times , diethylbenzene.

the previously reported activity coefficients (γ_{\pm}^*) of sodium and potassium chlorides in these same amides.² Of these amides, dipropylacetamide is miscible in all proportions with water at 25°, and its dielectric constant was measured over the entire range. The plot against volume per cent water (Figure 1) is smooth and nearly linear. The curves for the other amides (up to saturation except for tetraethylphthalamide) parallel the dipropylacetamide curve. Dilution of dibutylacetamide by 50% with diethylbenzene decreased the dielectric constant by about 50%. The dielectric constant found for diethylbenzene (2.35) is close to the literature value for benzene (2.27).³

If the amido groups provide the main contribution to the inductive capacity in the absence of water, and if the volume occupied per amido group is about the same in each compound, the dielectric constants extrapolated to zero water content should be proportional to the

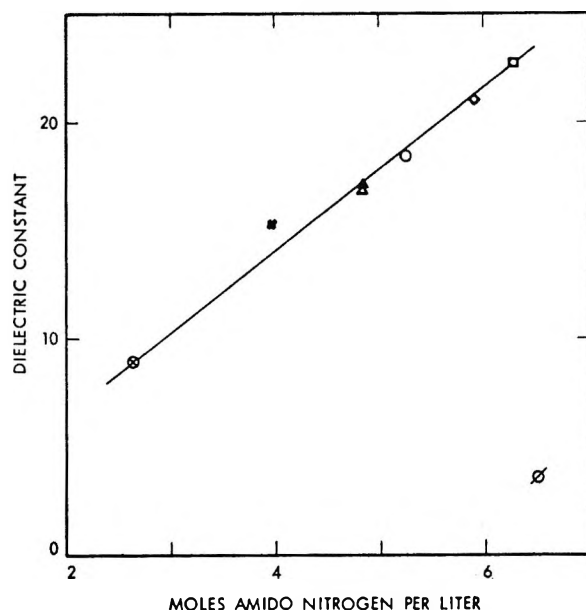


Figure 2. Dielectric constants at zero water content vs. molarity of amido nitrogen; symbols as defined in Figure 1.

moles of amido nitrogen per liter. Figure 2 shows that this is approximately true for the monoamides, including the dibutylacetamide diluted with hydrocarbon. The much lower value for tetraethylphthalamide probably reflects internal cancellation of the dipoles of the two amido groups.

Lanier⁴ reported a theoretically based correlation of salt activity coefficients γ_{\pm}^* with dielectric constants that approaches linearity and shows different slopes in mixtures of different organic compounds with water, where γ_{\pm}^* is the value of γ_{\pm}^* extrapolated to infinite dilution of the salt at each composition of the organic-aqueous mixture.

In the measurement of activity coefficients² in the amides examined here, the water-amide ratio as well as the salt concentration was different in each test, precluding direct extrapolation of γ_{\pm}^* to infinite dilution of the salt. Instead, values of γ_{\pm}^* were estimated by calculating the ratio $\gamma_{\pm}^*/\gamma_{\pm}$ from the Debye-Hückel equation

$$-\log \gamma_{\pm} = Az_{+}z_{-}\sqrt{I}/(1 + aB\sqrt{I})$$

A and B were adjusted for the dielectric constant of each mixture, and a was taken arbitrarily as 2.5×10^{-8} . The resulting curves for sodium chloride (Figure 3) lie

(1) Research sponsored by the Office of Saline Water, U. S. Department of the Interior, under Union Carbide Corporation's contract with the U. S. Atomic Energy Commission. Preceding paper in series: A. E. Marcinkowsky, H. O. Phillips, and K. A. Kraus, "VII. Self-Diffusion Coefficients of Na^+ in Ethylene Glycol-water and Glycerine-Water Mixtures," *J. Phys. Chem.*, in press.

(2) C. F. Coleman, *J. Phys. Chem.*, **69**, 1377 (1965).

(3) A. A. Maryott and E. R. Smith, National Bureau of Standards Circular 514, U. S. Government Printing Office, Washington, D. C., 1951.

(4) R. D. Lanier, *J. Phys. Chem.*, **69**, 2697 (1965).

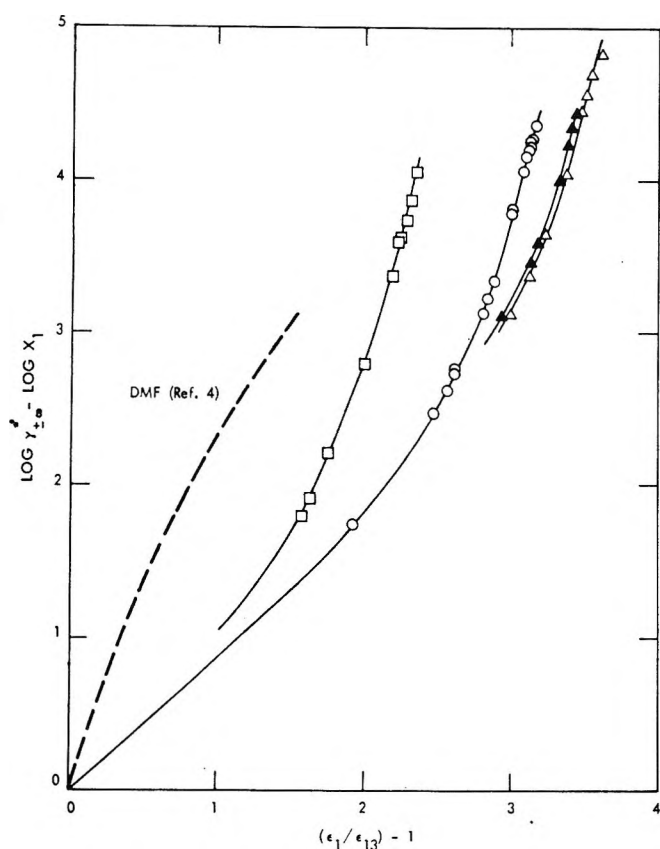


Figure 3. Correlation of NaCl activity coefficients with dielectric constants of amides containing water; symbols as defined in Figure 1; X_1 = mole fraction of water; ϵ_1 and ϵ_{13} = respective dielectric constant of water and of aqueous-organic mixture; DMF, dimethylformamide; the function $(\epsilon_1/\epsilon_{13}) - 1$ is identical with the function $(1 - \rho)/\rho$, $\rho = \epsilon_{13}/\epsilon_1$ used in ref 4.

in the same general direction as does Lanier's curve for sodium chloride in dimethylformamide (DMF, included in Figure 3), but they are concave upward, instead of downward as were most of Lanier's curves. The curvatures are compatible with smooth extension to the point (0,0) for pure water, which is the limiting member of each series. The results for potassium chloride are similar.

Experimental Section

The amides were described previously.² Capacitances were measured with the equipment (except the cell) described by McDowell and Allen,⁵ a General Radio Type 716-CS1 bridge plus Type 722-NQ precision capacitor, permitting direct reading of up to 2300 μf . All measurements were made at 1 Mc/sec. The cell, following a design used by Fuoss,⁶ was made of stainless steel and Teflon, plus a thin glass disk to provide a wettable surface under the Teflon. It was calibrated with 1,2-dichloroethane, ϵ 10.36 at 25° (ref 3), and gave satisfactory measurements on known compounds (see Table I). The cyclohexane (spectral grade) was dried in a molecular sieve column; the dichloroethane and acetonitrile were dried with calcium

Table I

Compound	Dielectric constant at 25°	
	Measd (10 ⁶ cps)	Lit. ⁴ (static)
Cyclohexane	2.02	2.015
Methanol	32.66	32.63
Nitrobenzene	34.8	34.82
Acetonitrile	35.9	36.0
Water	78.5	78.54

sulfate and then distilled, the methanol was rectified in a 4-ft Podbielniak column, and the nitrobenzene was fractionally crystallized.

Acknowledgment. It is a pleasure to thank J. P. Eubanks for extensive technical assistance.

- (5) W. J. McDowell and K. A. Allen, *J. Phys. Chem.*, **63**, 747 (1959).
 (6) J. E. Lind, Jr., and R. M. Fuoss, *ibid.*, **65**, 999 (1961).

Experimental Determination of the Electronic Absorption Spectrum Ascribable to the O_2^- Ion Adsorbed on Porous Glass

by Hiroshi Tsubomura, Naoto Yamamoto, Hiroyasu Sato, Kunio Yoshinaga, Hideyuki Ishida, and Kiyoshi Sugishima

Department of Chemistry, Faculty of Engineering Science, Osaka University, Toyonaka, Osaka, Japan
 (Received August 3, 1967)

A tube of porous glass¹ 3–4 cm long and with an outer diameter of 11 mm was placed in a vacuum line. N,N,N',N'-tetramethyl-*p*-phenylenediamine (TMPD) was adsorbed onto it, and the absorption spectrum of the glass was measured with light incident across the tube. The absorption spectrum obtained was essentially that of the TMPD molecule itself. The sample was then irradiated with a high-pressure mercury lamp. The absorption spectrum arising from the irradiation is shown in Figure 1. In the visible region, it has three characteristic bands readily identified with those of TMPD^+ and another band with a maximum at 4200 Å (hereafter called the Y band). The intensity of the Y band produced under various conditions is proportional to the intensity of the TMPD^+ band. The specimen also gives an esr pattern shown in Figure 2 (curve a), which is regarded to be the sum of the symmetric esr

(1) Made and kindly donated by Central Research Laboratories, Mitsubishi Electric Corp., Amagasaki, Japan. It is prepared by treating alkali borosilicate glass with strong acid, and said to have pores with fairly uniform diameter, 30–100 Å. The surface area is measured to be about 271 m²/g. The glass is slightly opaque.

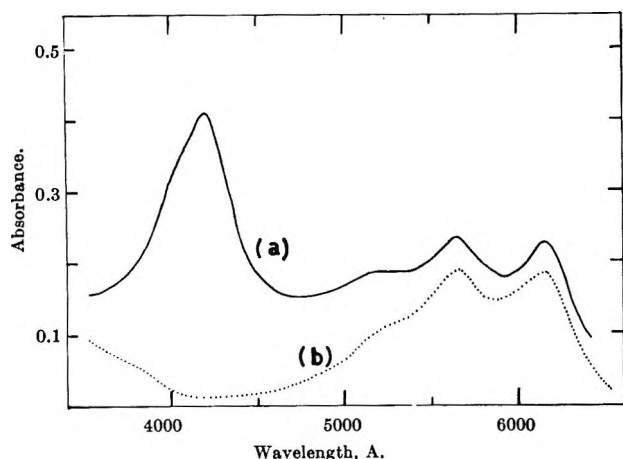


Figure 1. Curve 1: the electronic absorption spectrum of TMPD adsorbed on porous glass and irradiated by ultraviolet light. Curve b: that of TMPD^+ (Br^-) in an ethanol solution.

spectrum centered at $g = 2.003$ for TMPD^+ and another spectrum with considerably large anisotropic g factors (curve b). The latter seems to be in accordance with the spectrum assigned to the O_2^- ion formed on the surface of zinc oxide.^{2,3}

It has been confirmed that the irradiation of porous glass itself causes neither a special electronic spectrum nor an esr spectrum.

The intensity of the Y band depends much on the treatment of the porous glass before adsorption. The results in Figure 1 are for the glass activated at about 500° for several hours under vacuum. With higher temperature and longer time of activation, the intensity of the band decreases. By a similar experiment using the glass treated with hydrogen gas at 500° , both the TMPD^+ band and the Y band appear only faintly. To the contrary, the introduction of pure, dry oxygen (10 mm pressure) into the vacuum line for about 1 min increases to a large extent the intensities of both absorption bands produced by irradiation.⁴

In the case where an aromatic hydrocarbon (A) as well as TMPD is adsorbed on the porous glass, there is a marked effect on the intensity of the photochemically formed Y band. For the case of anthracene, terphenyl, or naphthalene used as (A), the Y band disappears and, instead, the spectrum corresponding to the A^- anion appears. For the case of fluorene, both the Y band and the band of fluorene $^-$ appear. For the case of diphenyl, no spectrum of diphenyl $^-$ appears but the Y band does appear. These results are in good accord with the sequence of the electron affinities of the aromatic hydrocarbons. The species related to the Y band, therefore, may be roughly regarded to have an electron affinity nearly the same as that of fluorene.

Similar photoionization experiments using N,N-dimethyl-*p*-phenylenediamine instead of TMPD resulted in the appearance of the Y band as well as those for the phenylenediamine cation.

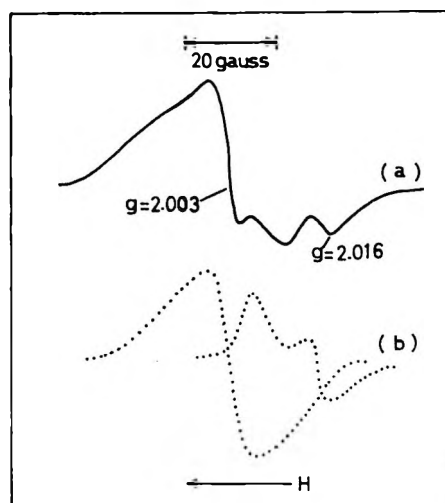


Figure 2. Curve a: the esr spectrum of irradiated TMPD adsorbed on porous glass. Curve b: the spectrum is tentatively divided into two components in such a way that their sum agrees with curve a.

All the above results seem to suggest fairly strongly that the carrier for the Y band is O_2^- .

The photoionization of TMPD in low temperature matrices has been extensively studied.^{5,6} It is concluded that photoionization under near-ultraviolet light is caused by a two-step mechanism *via* the lowest triplet state. For the present case, therefore, it is reasonable to suppose that electrons are ejected from TMPD by a two-step excitation. Our present results suggest that the electrons thus ejected return quickly to TMPD^+ unless an acceptor, O_2 or an aromatic, traps it.

Thompson and Kleinberg⁷ reported many years ago that alkali superoxides formed in liquid ammonia showed a band at about 3800 Å, which they assigned to O_2^- . We prepared potassium superoxide and measured the absorption spectrum of its solution in liquid ammonia. No absorption peak has been found, but an absorption arising monotonically to 3000 Å has been obtained.

(2) For example, R. J. Kokes, *Proc. 3rd Intern. Congr. Catalysis, Amsterdam, 1964*, 1, 484 (1965); J. H. Lunsford and J. P. Jayne, *J. Chem. Phys.*, **44**, 1487 (1966).

(3) According to McLachlan, *et al.*, the O_2^- ion in an aqueous solution shows an ultraviolet absorption spectrum at about the same region of wavelength as the Y band, but its esr spectrum is quite different from that obtained in the present paper: A. D. McLachlan, M. C. R. Symons, and M. G. Townsend, *J. Chem. Soc.*, 952 (1959).

(4) Under humid conditions, TMPD^+ is instantaneously formed by the introduction of oxygen. Under strictly dry conditions, no TMPD^+ is formed with the introduction of oxygen until the specimen is irradiated.

(5) N. Yamamoto, Y. Nakato, and H. Tsubomura, *Bull. Chem. Soc. Japan*, **40**, 451 (1967), and papers cited therein.

(6) K. D. Cadogan and A. C. Albrecht, *J. Chem. Phys.*, **43**, 2550 (1965); G. E. Johnson, W. M. McClain, and A. C. Albrecht, *ibid.*, **43**, 2911 (1965); W. M. McClain and A. C. Albrecht, *ibid.*, **43**, 465 (1965).

(7) J. K. Thompson and J. Kleinberg, *J. Am. Chem. Soc.*, **73**, 1243 (1951). We are indebted to Professor Kleinberg for detailed information on his work published a long time ago.

Rolfe, *et al.*,⁸ recently reported a broad absorption spectrum at 2500 Å, together with a fluorescence spectrum which they assign to O_2^- in the crystal of alkali halides fused in an oxygen atmosphere. Also, Czapski and Dorfman⁹ assigned the absorption band at about 2400 Å obtained by the pulse radiolysis of the H_2O-O_2 system to O_2^- . These two results seem to offer reliable data for the spectrum of the O_2^- ion. Our spectrum, though at a different wavelength, may also be valid, because the position of the spectrum may be susceptible to the environment. Another alternative is that our Y band might be the first band of O_2^- , which is much weaker than the second band, which may be the spectra found by the above authors. (In our experiment, no absorption band below 3500 Å can be measured.)

(8) J. Rolfe, F. R. Lipsett, and W. J. King, *Phys. Rev.*, **123**, 447 (1961).

(9) G. Czapski and L. M. Dorfman, *J. Phys. Chem.*, **68**, 1169 (1964).

Interpretation of Infrared Spectra of Chemisorbed Hydrogen and Deuterium

by W. Hayden Smith, H. C. Eckstrom, and F. B⁻r

Department of Chemistry, University of Kentucky,
Lexington, Kentucky (Received August 29, 1967)

Results obtained by one of these writers (F. B.) for D_2 on rhodium and previously published but uninterpreted data for H_2 on rhodium¹ may be correlated using a recently proposed group theoretical method² and the observed isotopic shift to verify the origin of the bands.

As noted by Pickering and Eckstrom,¹ numerous absorptions are observed in the Rh- H_2 system in the presence of a few torr of gas. Upon evacuation of the system only the absorptions listed in Table I persist. These may be considered as due to chemisorbed hydrogen and deuterium in a tightly held form. A decrease in reflectivity in presence of the gas phase partially remains upon evacuation as further evidence of chemisorbed hydrogen (or deuterium).

Several investigators³⁻⁵ have studied the chemisorption of hydrogen on atomically clean single crystal substrates. In all cases, the evidence has indicated an atomic rather than a molecular mode of absorption for hydrogen on these substrates. The infrared results of Becker and Gobeli⁴ for atomic hydrogen chemisorbed on single crystal silicon surfaces would indicate that infrared absorption arising from an Rh-H stretch should be expected in the 2000-2200- cm^{-1} region for the Rh- H_2 system. In the case of D_2 , the isotope effect should lower the Rh-D stretches to a frequency of approximately $\nu(Rh-H)/\sqrt{2}$. The observation of a group

Table I: Absorptions for H_2 and D_2 on Rhodium (after Evacuation)

H_2^a	D_2
4372	...
3384	
3200	
3154	
2995	
2930	...
2879	
2766	
2734	
2711	
2193	1584
2187	1564
2163	1556
2131	1538
2118	1533
2114	1528
2058	1518
	1506
	1447
	1409

^a See ref 1.

of bands for the Rh- H_2 system at 2114-2193 cm^{-1} , and a displaced group at 1506-1584 cm^{-1} for the Rh- D_2 system provides a convincing assignment of these bands as due to chemisorbed hydrogen. The observation of a number of bands in each region is ascribed to the polycrystalline nature of the Rh mirrors used in these experiments. Such mirrors exhibit a random crystallographic orientation and relatively different adsorption sites on each type of face exposed.

The Σ_g^+ vibrational motions of gas phase $D_{\infty h}$ molecules can create no varying dipole at low pressures and hence are infrared inactive. In the case of the evacuated rhodium-hydrogen system,¹ an absorption is found at 4372 cm^{-1} . This band lies near the Σ_g^+ stretching motion of gas phase hydrogen at 4160 cm^{-1} . Because these bands are at the limits of observability,¹ intensity considerations make the observation of overtones unlikely, unless they are in position to allow Fermi resonance or some other intensity enhancement to occur. For this reason, we do not assign 4372 cm^{-1} as a possible overtone of the 2100- cm^{-1} bands.

Before proposing an assignment of the 4372- cm^{-1} band, we first must discuss the symmetry properties of H_2 chemisorbed upon a crystalline substrate, and show that the molecular stretching mode is thereby formally

(1) H. L. Pickering and H. C. Eckstrom, *J. Phys. Chem.*, **63**, 512 (1959).

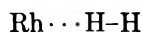
(2) W. H. Smith and H. C. Eckstrom, *J. Chem. Phys.*, **46**, 3657 (1967).

(3) J. A. Becker, *Solid State Phys.*, **7**, 379 (1958).

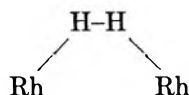
(4) G. E. Becker and G. W. Gobeli, *J. Chem. Phys.*, **38**, 2942 (1963).

(5) P. J. Estrup and J. Anderson, *ibid.*, **45**, 2254 (1966).

allowed in the infrared spectrum. It is clear that the mode of adsorption should be a linear one



in order that a nearly gas phase hydrogen stretching frequency will persist. A bridged mode of adsorption like



would clearly allow more H-H, Rh-H vibrational coupling interactions than a linear mode of adsorption with the consequence of lowering the frequency of the H-H stretch. As an example, consider hydrogen chemisorbed in a linear fashion upon a rhodium (110) crystallographic face. Using the group theoretical procedures,² the following correlation mapping (Table II) is derived for the vibrational motions, assuming a gas phase $\text{Rh} \cdots \text{H}-\text{H}$ molecule, and yields an infrared active A' species for the molecular stretching mode of H_2 at the adsorption site. A similar result holds for other infrared crystallographic faces; *i.e.*, the mode becomes active.

Table II: Hydrogen Chemisorbed Linearly upon a Rhodium (110) Crystallographic Face^a

	Correlation mapping		
	Molecular group $C_{\infty v}$	Site group C_s	Factor group $C_s(\text{plml})$
ν_1, ν_3, z	Σ^+	A'	A'
ν_2, R_x, R_y, X, Y	Π	A', A''	A', A''

^a All species infrared and Raman active. R_x species non-existent for linear absorption.

The experimental conditions precluded a determination of true line widths. This was due to the low resolution necessitated by the reduced transmission resulting from the large number of reflections needed to observe these extremely weak adsorptions. Nevertheless, the single line at 4372 cm^{-1} indicates either that the H-H stretching frequency is not strongly dependent upon the crystallographic orientation of the adsorbing surface or that linear adsorption is only occurring on certain crystallographic faces which do not differ too greatly in the density of atoms exposed. The latter choice is preferable since the observations, to be discussed below, lead to the conclusion that at least two modes of adsorption occur under these experimental conditions. It has been demonstrated that a given crystallographic surface will adsorb molecules in different structures depending upon the extant experimental conditions.⁶ When the conditions change, the structures are found to

be reversibly interchangeable. Further, a linear mode of adsorption upon crystal faces with a very different atom density or arrangement would be expected to exhibit large frequency shifts due to the change in intermolecular interactions. The possibility that such shifts are all less than the resolution limit of 40 cm^{-1} certainly cannot be ruled out at this point. Nevertheless, we conclude that the 4372-cm^{-1} band is due to hydrogen, molecularly chemisorbed in a linear fashion on the rhodium film upon certain undetermined, but similar crystallographic faces.

It is significant that we are here proposing a molecular adsorption mode for H_2 , whereas the previously mentioned investigations³⁻⁵ detected only an atomic mode of adsorption. This will lead us to an alternate, and preferable, explanation for the bands found in the 2000 cm^{-1} region in the present experiments.

A review of the experimental conditions³⁻⁵ reveals that these studies on single crystal substrates were carried out in ultrahigh vacua on atomically clean surfaces. The infrared studies being discussed here did not meet these stringent conditions, being conducted at pressures of $\sim 10^{-6}$ torr. It is well known that at such pressures an almost immediate oxygen coverage is formed from the residual gas. This would have been sufficient to remove and/or cover the sites where hydrogen might be dissociated. We are left with the observed result that only molecular hydrogen may be adsorbed in such cases.

This conclusion implies strongly that the 2000-cm^{-1} bands are only accidentally coincident with the Si-H stretch observed by Becker⁴ since dissociation of hydrogen is now precluded under the experimental conditions of Bär and Eckstrom and Pickering and Eckstrom.⁷

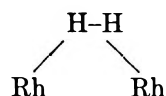
Again referring to a correlation mapping (Table III)

Table III: Bridged Hydrogen on a (110) Rhodium Crystallographic Face^a

	Correlation mapping		
	Molecular group C_{2v}	Site group C_2	Factor group $C_{2v}(\text{pgg})$
z	A_1	A	A_1, A_2
R_x	A_2	A	A_1, A_2
X, R_y	B_1	B	B_1, B_2
Y, R_x	B_2	B	B_1, B_2

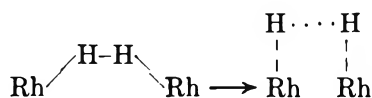
^a All modes are infrared and Raman active, except A_2 which is Raman active only.

for a rhodium (110) surface with hydrogen chemisorbed in a bridged mode



we find that both the Rh-H, and H-H stretches are shown to be infrared active species. The general result again is that whatever geometry is assumed, the non-degenerate stretching modes are infrared active, and consist of a single line per type of adsorbing face, unless split by the correlation field.² The infrared spectra listed in Table I contain a number of lines in the 3000-cm⁻¹ region which have not been assigned. A possible assignment presents itself if these bands are considered to be the perturbed H-H stretches associated with a

Rh $\begin{array}{c} \diagup \text{H-H} \diagdown \\ \text{Rh} \end{array}$ Rh bridged structure. The 2000-cm⁻¹ bands have essentially the same interpretation given at first, that of being Rh-H stretches, but now, due to the bridged structure are capable of vibrational coupling with the higher frequency H-H motions of the same symmetry species. The corresponding motions of the metal-hydrogen bond in these two extremes may be considered analogous ones in which the H-H interaction of neighboring protons on the surface is changed from a molecular bond to an atom-atom interaction term.



Again, since the metal-H frequency is so similar in both cases, it is clear that special sites must be responsible for dissociation, which then diffuse mobile hydrogen atoms onto the observed sites. In the case of the atomic mode of adsorption, the H \cdots H motions will be included among the lattice modes predicted in the correlation mappings, Tables II and III, and should be observable optically.

In the 3000- and 2000-cm⁻¹ regions the large number of bands observed can be attributed to multiple crystallographic sites available on the polycrystalline films, each exhibiting as would be expected a different perturbation of the fundamentals discussed above.

The discussion herein applies a group theoretical model to the discussion of spectra for H₂ and D₂ on polycrystalline rhodium substrates, and predicts the existence of certain fundamentals lying outside the region available to the investigators. A theoretical discussion of experimental problems in these regions has been given to indicate how these data may be obtained.⁶

Acknowledgment. This work was supported in part by U. S. Atomic Energy Commission Contract No. AT-(40-1)-2948.

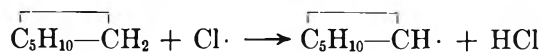
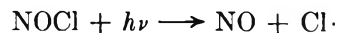
Quantum Yield of Photonitrosation of Cyclohexane under a Flash Lamp

by Kuya Fukuzawa and Hajime Miyama

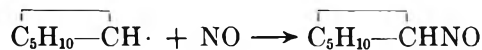
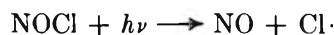
Basic Research Laboratories, Toyo Rayon Co., Ltd.,
Kamakura, Japan (Received August 22, 1967)

Baumgartner, *et al.*,¹ reported the quantum yield of photonitrosation of cyclohexane as 1.48, while Shimokawa, *et al.*,² reported a rather contradictory value of 0.7 for the same reaction.

To explain these data the former believes that the reaction proceeds *via* the following chain mechanism



The latter, however, assumes the scheme



Thus the quantum yield must necessarily be smaller than or at best equal to unity.

There seems to be no compromise between these two observations and further investigations still to be awaited. We therefore performed this photoreaction under an intense flash lamp. Our conclusion is that the quantum yield is about 0.65 ± 0.20 even under intense light.

Experimental Section

The reaction vessel used in this work was of a triply walled, coaxial type with a flash lamp mounted at the center. The inner chamber was filled with a filter solution, and the outer chamber with a solution of cyclohexane. A photomultiplier was attached to the outer surface to serve as a monitor. The flash light was separated into peak wavelengths of 3600, 4100, and 5050 Å by means of water solutions of cupric and cobaltous sulfate, cupric nitrate, and cupric and calcium chloride, respectively.

A 0.006 *M* solution of potassium ferrioxalate³ was filled in the reaction chamber to measure the absolute number of incident light quanta at 3600 Å, which together with the monitoring photomultiplier enabled us

(1) P. Baumgartner, A. Deschamps, and C. Roux-Guerraz, *Compt. Rend.*, **259**, 4021 (1964).

(2) Y. Shimokawa, *et al.*, *Kogyo Kagaku Zasshi*, **68**, 937 (1965).

(3) C. A. Parker, *Proc. Roy. Soc. (London)*, **A220**, 104 (1953).

(6) H. C. Eckstrom and W. H. Smith, *J. Opt. Soc. Am.*, **57**, 1132 (1967).

to determine the number of light quanta at the longer wavelengths.

Nitrosyl chloride was bubbled into a cyclohexane solution saturated with gaseous hydrochloric acid. The concentration of nitrosyl chloride was *ca.* 1%. In order to determine the extent of the photoreaction, resulting oxime hydrochloride was treated with chlorine to give chloronitrosocyclohexane, the absorption of which was measured at 6500 Å. The experimental error involved in the whole procedure was estimated to be within $\pm 30\%$.

Results summarized in Table I show that the quantum yield as measured at the three wavelengths was

Table I

Wave-length, Å	Oxime produced, M	Light quanta absorbed, M	Quantum yield
3600	0.83×10^{-4}	1.22×10^{-4}	0.68
3600	0.76×10^{-4}	1.22×10^{-4}	0.62
4100	1.39×10^{-4}	2.02×10^{-4}	0.69
4100	1.18×10^{-4}	2.00×10^{-4}	0.59
5050	0.86×10^{-4}	1.36×10^{-4}	0.63
5050	0.87×10^{-4}	1.30×10^{-4}	0.67

invariable within experimental error. The fact that the values obtained are less than unity does not necessarily exclude the chain mechanism. Our observation, however, seems to support Shimokawa's mechanism.

The Treatment of End Effects in a Markov Chain Model of the Configurational Properties of Long-Chain Molecules

by S. G. Whittington and P. J. Williams

Unilever Research Laboratory, The Frythe, Welwyn, Hertshire, England (Received August 30, 1967)

The majority of treatments of the configurational properties of long-chain molecules have begun with the assumption that the properties of the molecule are sufficiently well represented by the properties of a self-avoiding random walk on a regular lattice. The mathematical difficulties introduced by the self-avoiding condition can be avoided by approximating the self-avoiding walk by a first-order homogeneous Markov chain. In Mazur's treatment,¹ the self-avoiding condition is introduced by including an absorbing state in the Markov chain and by averaging only over the transient states of the chain. The approach can be adapted to include end effects and then proves to be a reasonably

accurate way of estimating the number of relatively short self-avoiding walks.

The relative positions of the monomer units in the molecule are represented by the successive states of a Markov chain. The Markov chain contains an absorbing state, and transitions into this state correspond to configurations of infinite energy (normally where two monomer units occupy the same lattice point). Suppose that the states of the Markov chain are labeled $(1, 2, \dots, m)$ where 1 and m are the absorbing and initial state, respectively. Let $p_{ij}^{(n)}$ be the n -step transition probability from state i to state j and let $p_{ij}^{(1)}$ be written p_{ij} . The $(m \times m)$ transition probability matrix $\mathbf{P} = (p_{ij})$ may be partitioned as

$$\mathbf{P} = \begin{pmatrix} 1 & \mathbf{0} \\ \mathbf{R} & \mathbf{Q} \end{pmatrix} \quad (1)$$

where \mathbf{Q} is the transition probability matrix between all nonabsorbing states, \mathbf{R} is the column vector of transition probabilities into the absorbing state, and $\mathbf{0}$ is a zero-row vector. A particular configuration of the molecule will then be represented by a realization of the Markov chain, *i.e.*, by a vector of the form $(m, i_1, i_2, \dots, i_n)$. If, at the r th step the absorbing state is reached, the corresponding vector is $(m, i_1, i_2, \dots, i_{r-1}, 1, 1, \dots, 1)$.

Suppose that the coordination number of the lattice is c and that walks with adjacent steps in opposite directions are forbidden; then the number of otherwise unrestricted walks is

$$c(c-1)^{n-1} \simeq (c-1)^n \quad (2)$$

The probability (p^*) that a walk, starting in state m will not have reached the absorbing state 1 in n steps is

$$p^* = 1 - p_{m1}^{(n)} \quad (3)$$

so that the number of walks, $f(n)$, not reaching the absorbing state is given by

$$f(n) = p^*(c-1)^n \quad (4)$$

To the level of approximation of this treatment, this is the number of self-avoiding walks.

$p_{m1}^{(n)}$ can readily be expressed² in terms of the eigenvalues and eigenvectors of \mathbf{P} , leading to the expression

$$p_{m1}^{(n)} = \sum_{j=1}^m \frac{\lambda_j^n \alpha_{mj} \beta_{j1}}{\mathbf{y}_j \cdot \mathbf{x}_j} \quad (5)$$

where λ_j is the j th eigenvalue of \mathbf{P} and \mathbf{x}_j and \mathbf{y}_j are the corresponding right and left eigenvectors. α_{mj} is the m th element of \mathbf{x}_j and β_{j1} is the first element of \mathbf{y}_j .

If the eigenvalues are numbered in decreasing order

(1) J. Mazur, *J. Chem. Phys.*, **41**, 2556 (1964).

(2) L. Takacs, "Stochastic Processes," Methuen and Co. Ltd., London, 1962, p 9.

of magnitude, then making use of the special form of \mathbf{P} , the expression reduces to

$$p_{m_1} = 1 + \frac{\lambda_2^n \alpha_{m_1}(\mathbf{s} \cdot \mathbf{R})}{(\lambda_2 - 1)(\mathbf{s} \cdot \mathbf{r})} + 0(\lambda_3^n) \quad (6)$$

where \mathbf{s} and \mathbf{r} are the left and right eigenvectors of \mathbf{Q} corresponding to the eigenvalue λ_2 . Provided that the terms $0(\lambda_3^n)$ can be neglected, the expression for $f(n)$ becomes

$$f(n) = \frac{\lambda_2^n \alpha_{m_1}(\mathbf{s} \cdot \mathbf{R})(c - 1)^n}{(1 - \lambda_2)(\mathbf{s} \cdot \mathbf{r})} \quad (7)$$

An approximate transition probability matrix was set up for the two-dimensional hexagonal lattice, using a state-labeling scheme similar to that adopted by Mazur.¹ The value of λ_2 was calculated to be 0.96, which compares quite well with the value of 0.93 obtained by lengthy Monte Carlo calculations.³ Values of $f(n)$, for $n \sim 10$, agreed to within 10% with exact enumeration results.

(3) F. T. Wall, L. A. Hiller, and W. F. Atchison, *J. Chem. Phys.*, **23**, 913 (1955).

Quantum Theoretical Treatment of Equilibrium Chemical Rate Processes

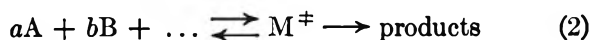
by Shang Jeong Yao¹ and Bruno J. Zwolinski

Thermodynamics Research Center, Department of Chemistry, Texas A&M University, College Station, Texas 77843
(Received September 7, 1967)

The equilibrium chemical rate processes, as treated by Eyring's statistical thermodynamic formalism, is reexamined. The usual expression for the velocity is

$$\begin{aligned} \left[\begin{array}{c} \text{forward} \\ \text{reaction} \\ \text{velocity} \end{array} \right] &= \left[\begin{array}{c} \text{probability} \\ \text{factor for} \\ \text{reaction} \end{array} \right] \times \\ v &= \kappa \times \\ \left[\begin{array}{c} \text{frequency of} \\ \text{approach to} \\ \text{the barrier} \end{array} \right] &\times \left[\begin{array}{c} \text{equilibrium} \\ \text{concentration of} \\ \text{activated complexes} \\ \text{crossing to the right} \\ \text{of the barrier} \end{array} \right] \quad (1) \\ \bar{\nu} &\times C_M^\ddagger \end{aligned}$$

For the reaction-activated complex equilibrium system, the usual assumption is made



Thus, with the standard definition of ordinary equilibrium constant K and a specific rate constant \bar{k} , the velocity expression is given by

$$v = \kappa \bar{\nu} C_M^\ddagger = \kappa \bar{\nu} K C_A^a C_B^b \dots = \bar{k} C_A^a C_B^b \dots \quad (3)$$

where the rate constant, \bar{k} , is defined as

$$\bar{k} = \kappa \bar{\nu} K = \kappa \bar{\nu} (Q_{\ddagger}^{\circ \ddagger} / K^\ddagger) \quad (4)$$

In line with Eyring's convention and molecular thermodynamic formalism, the term $(Q_{\ddagger}^{\circ \ddagger} / K^\ddagger)$ is defined for an activated complex as

$$\begin{aligned} K &= \frac{C_M^\ddagger}{C_A^a C_B^b \dots} = \\ (Q_{\ddagger}^{\circ \ddagger}) &\frac{Q_{\ddagger}^{\circ \ddagger} \frac{3N-1}{2}}{(Q_A^{\circ})^a (Q_B^{\circ})^b \dots} \exp[-\epsilon_0/kT] = Q_{\ddagger}^{\circ \ddagger} / K^\ddagger \quad (5) \end{aligned}$$

The partition function for the activated complex will always differ in form from that for a stable molecule in at least one vibrational degree of freedom, $Q_{\ddagger}^{\circ \ddagger}$, namely, the one along the reaction coordinate or channel. Now this special or unusual degree of freedom is considered as a harmonic vibration with an **imaginary frequency**, $\nu^\ddagger = (1/2\pi)(f^\ddagger/\mu^\ddagger)^{1/2} = i\nu$, where ν is a real frequency and is associated with a positive force constant f . The $f^\ddagger = (\partial^2 U / \partial q^2)_0 < 0$ is the unusual force constant of the imaginary mode oscillating in an inverted parabolic potential

$$U = \frac{1}{2!} \left(\frac{\partial^2 U}{\partial q^2} \right)_0 q^2 = \frac{1}{2} f^\ddagger q^2 = -\frac{1}{2} f q^2 \quad (6)$$

and μ^\ddagger is the reduced mass of the imaginary oscillator. The special partition function per degree of freedom, $Q_{\ddagger}^{\circ \ddagger}$, is evaluated as follows.

For a bound system associated with negative total energy, both of its potential and kinetic energies must be negative (see Figure 1). The Hamiltonian for a harmonic oscillator associated with an inverted parabolic potential can be written as

$$H^\ddagger = -\frac{p^2}{2\mu^\ddagger} + \frac{1}{2} f^\ddagger q^2 = -\frac{p^2}{2\mu^\ddagger} - \frac{1}{2} f q^2 \quad (7)$$

or

$$\begin{aligned} -H^\ddagger = H &= \frac{p^2}{2\mu^\ddagger} + \frac{1}{2} f q^2 = \\ &\frac{p^2}{2\mu^\ddagger} + \frac{1}{2} \mu^\ddagger (2\pi\nu)^2 q^2 \quad (8) \end{aligned}$$

where

$$\nu = \frac{1}{2\pi} (f/\mu^\ddagger)^{1/2} \quad (9)$$

The right-hand side of eq 8 is essentially the Hamiltonian, H , of an ordinary harmonic oscillator.

The eigenvalues of H are well known; *i.e.*

$$E_n = (n + 1/2)h\nu \quad (10)$$

(1) Robert A. Welch Foundation Postdoctoral Fellow.

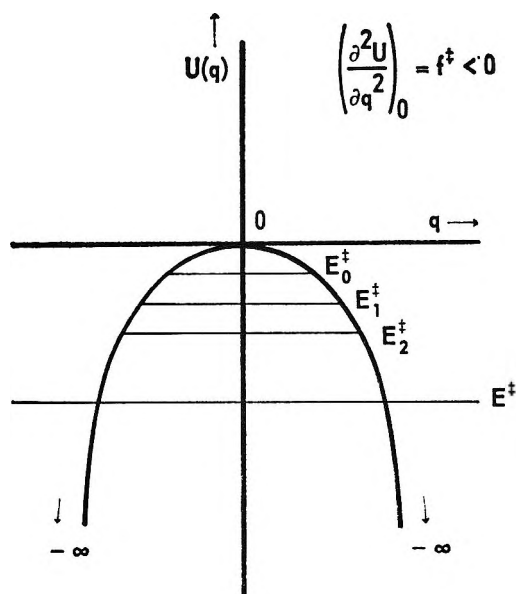


Figure 1. A sketch for an inverted parabolic potential

$$U = \frac{1}{2!} \left(\frac{\partial^2 U}{\partial q^2} \right)_0 q^2 = \frac{1}{2} f^{\ddagger} q^2 = -\frac{1}{2} f q^2$$

Therefore, the eigenvalues of the defined Hamiltonian H^{\ddagger} are in our particular case

$$E_n^{\ddagger} = -(n + \frac{1}{2})h\nu \quad (11)$$

The details of this solution are given in the Appendix.

It is obvious that for negative energy levels, the Boltzmann distribution of particles can be written straightforwardly as

$$\frac{N_i}{N_j} = \exp \left[\frac{1}{kT} (E_i - E_j) \right] \quad (12)$$

Consequently, the partition function for the negative energy levels can be written as

$$Q_s^{\circ \ddagger} = \sum_{n=0}^{\infty} e^{+E_n^{\ddagger}/kT} = \sum_{n=0}^{\infty} e^{-(n+1/2)h\nu/kT} = \frac{e^{-1/2 h\nu/kT}}{1 - e^{-h\nu/kT}} \quad (13)$$

The rate constant is then determined to have the general form

$$\tilde{k} = \kappa \bar{\nu} Q_s^{\circ \ddagger} K^{\ddagger} = \kappa \bar{\nu} \left[\frac{e^{-1/2 h\nu/kT}}{1 - e^{-h\nu/kT}} \right] K^{\ddagger} \quad (14)$$

From this general expression, the high-temperature rate constant is obtained as

$$\tilde{k}_{H.T.} = \kappa \frac{\bar{\nu}}{\nu} \left(\frac{kT}{h} \right) K^{\ddagger} \quad (15)$$

for $h\nu_j \geq kT \gg h\nu$ where $j = 1, 2, \dots, 3N - 7$ for non-linear molecules.

The harmonic frequency, $\nu = (1/2\pi)\sqrt{f/\mu^{\ddagger}}$, provides us knowledge of the magnitude of $(\partial^2 U/\partial q^2)_0$ of the

parabolic potential near its minimum which is the same as the absolute magnitude of the $(\partial^2 U/\partial q^2)_0 = f^{\ddagger}$ of the inverted parabolic potential near its maximum. From this knowledge, the curvature of the potential barrier can be estimated.

If the frequency of passage across the barrier ($\bar{\nu}$) which characterizes decomposition is equal to the absolute magnitude of the frequency of the imaginary mode, i.e., $|i\nu| = \nu$, then

$$\tilde{k}_{H.T.} = \kappa \left(\frac{kT}{h} \right) K^{\ddagger} \quad (16)$$

which reduces to the same form obtained originally by Eyring² in 1935 as well as obtained *via* the application of Marcellin's rate formula.³

After completion of this note, Dr. Richard J. Eden of Cambridge University was kind enough to inform us that he heard Professor R. Peierls refer to the same negative energy solution for an imaginary harmonic oscillator in a lecture in England some time ago.

Appendix

The negative energy can be obtained from a tentatively called energy reversal solution of the Schroedinger equation. The Schroedinger equation in its coordinate-time representation has the form

$$i\hbar \frac{\partial \Psi(\vec{r}, t)}{\partial t} = -\frac{\hbar^2}{2\mu} \nabla^2 \Psi(\vec{r}, t) + U\Psi(\vec{r}, t) = E\Psi(\vec{r}, t) \quad (a)$$

In case the potential U is real, the complex conjugate and the energy reversed expression for the Schroedinger equation is of the form

$$\left[i\hbar \frac{\partial \Psi(\vec{r}, t)}{\partial t} \right]^* = [-E\Psi(\vec{r}, t)]^* = -\left[-\frac{\hbar^2}{2\mu} \nabla^2 \Psi(\vec{r}, t) + U\Psi(\vec{r}, t) \right]^* \quad (b)$$

which has the invariant form

$$i\hbar \frac{\partial \Psi'(\vec{r}, t)}{\partial t} = E\Psi'(\vec{r}, t) \quad (c)$$

where

$$\Psi'(\vec{r}, t) = [\varphi(\vec{r})e^{-i(-E)t/\hbar}]^* = \varphi^*(\vec{r})e^{-iEt/\hbar} \quad (d)$$

The harmonic oscillation in an inverted parabolic potential can then be interpreted as an ordinary harmonic oscillation associated with a negative energy. This special harmonic oscillation is physically realizable since it satisfies the Schroedinger equation.

(2) S. Glasstone, K. J. Laidler, and H. Eyring, "Theory of Rate Processes," McGraw-Hill Book Co., Inc., New York, N. Y., 1940.

(3) M. R. Marcellin, Thesis, University of Paris, 1914, Gauthiers-Villars, Paris (1914); *Ann. Phys.*, **3**, 158 (1915).

COMMUNICATIONS TO THE EDITOR

Comment on "Fast Reactions of Polar Molecules in Processes with No Activation Energy"

Sir: In a recent paper, Walton¹ has calculated the rates of several radical recombinations and ion-molecule reactions using a modified absolute rate theory formulation. He proposes a transition-state model in which the reacting species are confined to a square potential well. The energy of the system within this well is quantized and given by $E_n = n^2 h^2 / 8m^* R^2$, where m^* is the reduced mass. The corresponding expression in the well-known Gorin² model is the centrifugal potential or kinetic energy of rotation $E_J = J(J+1)h^2 / 8\pi^2 m^* R^2$, where J is the angular momentum quantum number. Reasonably enough, Walton proceeds to maximize the total energy of the system, which is the sum of the quantized energy E_n and the attractive potential, and finds in the case of radical recombinations

$$E_c = n^3 h^3 / 2^{7/2} 3^{1/2} (m^*)^{3/2} \lambda^{1/2}$$

where λ is the coefficient of R^{-6} in the long-range attractive potential. Next, using this value of E_c , Walton evaluates the partition function

$$f_n = \int_{n=0}^{\infty} g_n e^{-E_c(n)/kT} dn$$

and proceeds in the usual way³ to derive the expression for the rate constant, which differs from the Gorin result by a factor of π^2 .³

It is the evaluation of the partition function, f_n , to which our comments are directed. Although Walton does not in any way discuss the degeneracy factor g_n , his results imply that the value $g_n = 2n$ has been used.

In our view, the problem as discussed by Walton involves a model in which a pair of particles undergoing reaction are treated as a single particle of mass equal to the reduced mass of the pair, in a square well potential along the line joining the two centers. A problem of this type may be easily reduced to a solution of the Schroedinger equation with the radial part only. In fact, the use of the energy expression $E_n = (n^2 h^2) / (8m^* R^2)$ is rather suggestive of such an approach. It is well known from quantum mechanics⁴ that such a problem may be visualized as a one-dimensional motion bounded on one side, for which it can be shown that the eigenvalues are nondegenerate. Hence it appears to us that the use of $2n$ as a degeneracy factor in the calculation of the partition function requires some further justification. It appears as well, from standard expressions⁵ for particles in a spherical cavity, that the

above equation for energy results in a case where $l = 0$, for which the degeneracy is unity. If higher values of l are used, then the expression for the energy E_n would be different and the results would differ from those obtained by Walton.

In the following communication,⁶ Walton further elaborates on his activated complex model from which we find the following.

(a) With $g_n = 1$ the evaluation of the integral for the partition function, f_a , for a single particle (radical), A, leads to

$$f_a = 2^{7/2} 3^{-1/2} \Gamma(1/3) \lambda^{1/3} M_a^{1/2} (kT)^{1/3} / h$$

which differs from Walton's result. Furthermore, the total partition function for two particles, A and B, should be the product of the individual partition functions, f_a and f_b . The latter does not appear to be the case in Walton's expression for f_{total} .

(b) It is also pointed out⁶ that we may consider the radicals in the transition state as a single entity confined to a square potential well which exists when both species are present and it is shown that analogous expressions to those discussed in (a) result.

(1) J. C. Walton, *J. Phys. Chem.*, **71**, 2763 (1967).

(2) E. Gorin, *Acta Physicochim. U.R.S.S.*, **6**, 691 (1938).

(3) S. Glasstone, K. J. Laidler, and H. Eyring, "The Theory of Rate Processes," McGraw-Hill Book Co., Inc., New York, N. Y., 1941, p 260.

(4) L. D. Landau and E. M. Lifshitz, "Quantum Mechanics," Addison-Wesley Publishing Co., Inc., Reading, Mass., 1958, p 109.

(5) W. Kauzmann, "Quantum Chemistry," Academic Press Inc., New York, N. Y., 1957, p 187.

(6) J. C. Walton, *J. Phys. Chem.*, **72**, 375 (1968).

DEPARTMENT OF CHEMISTRY
THE UNIVERSITY OF CALGARY
CALGARY, ALBERTA, CANADA

E. TSCHUIKOW-ROUX
R. PAUL

RECEIVED SEPTEMBER 7, 1967

Reply to Comment on "Fast Reactions of Polar Molecules in Processes with No Activation Energy," by E. Tschuikow-Roux and R. Paul

Sir: The path of a radical combination reaction proceeds from two separate species $A\cdot$ and $B\cdot$, via the transition state, to the single product molecule AB. The high rate constant and absence of activation energy of these combinations suggests that in the transition

state the species are well separated, and that the transition state resembles the separate radicals more than the final product.

In the transition state model I proposed,¹ the species $A\cdot$ and $B\cdot$ are confined, as a single entity, in the square potential well. Consider first the artificial situation of radical $A\cdot$ alone in the well, where it undergoes a one-dimensional motion bounded on one side.² The quantized energy of the system is $En = n^2h^2/8M_aR^2$, where M_a is the mass of radical $A\cdot$. The maximum total energy of the system is given by

$$E_c = n^3h^3/2^{7/2}3^{1/2}M_a^{1/2}\lambda^{1/2}$$

and the partition function f_a is found from

$$f_a = \sum_{n=0}^{\infty} g_n e^{-E_c(n)/kT} dn$$

As Tschuikow-Roux and Paul point out,² the degeneracy factor, g_n , is unity and the evaluated partition function is

$$f_a = 2^{1/2}\Gamma(1/3)\lambda^{1/6}M_a^{1/2}(kT)^{1/3}/h$$

Now on adding radical $B\cdot$ to the potential well, a second partition function f_b is obtained.

$$f_b = 2\Gamma^{2/3}(1/3)\lambda^{1/3}M_b^{1/2}(kT)^{1/3}/h$$

The total partition function f_{total} becomes

$$f_{\text{total}} = 2^{10/3}\Gamma(2/3)\lambda^{1/3}(M_aM_b)^{1/2}(kT)^{2/3}/h^2$$

When the radicals are considered as a single entity confined in the well, which exists only when both species are present, use of the degeneracy factor $g_n = 1$ leads to the analogous expression for the partition function

$$f_{\text{partial}} = 2^{4/3}\Gamma(1/3)\lambda^{1/3}(M^*)^{1/2}(kT)^{1/3}/h$$

but two degrees of freedom must be allowed to the transition state in the critical coordinate, which is motion in the potential well. The total partition function f_{total} is therefore

$$f_{\text{total}} = 2^{10/3}\Gamma(2/3)\lambda^{1/3}M^*(kT)^{2/3}/h^2$$

as given in ref 1.

If two degrees of freedom are not allowed to the transition state, its condition corresponds to a single product molecule AB in the potential well, which is contrary to the initial assumption for radical combinations and not appropriate for this situation. Two radicals together, as a single entity, are required to produce the transition state, but the initial premise of a "loose" transition state is fulfilled by allowing them to move independently within the transition state potential well.

The use of a degeneracy factor of unity, when applied

as above, does lead to the expression for the rate constant originally given¹ and similar in form to the rate expression derived by Gorin.³

CHEMISTRY DEPARTMENT
UNIVERSITY OF DUNDEE
DUNDEE, SCOTLAND

J. C. WALTON

RECEIVED SEPTEMBER 27, 1967

A Low-Temperature, High-Pressure Hydrate of *n*-Tetrabutylammonium Halides¹

Sir: In the course of an investigation of the electrical conductivity of aqueous solutions of tetraalkylammonium halides under high hydrostatic pressure and in the temperature range 0–20°, we found that as the pressure was increased the resistance of an 0.10 *M* solution of *n*-tetrabutylammonium bromide abruptly increased by several orders of magnitude. The sample was depressurized, removed from the apparatus, and visual inspection revealed an ice-like solid, which subsequently melted. The temperature of the sample at the time of solidification was several degrees in excess of the expected freezing point. The results of further preliminary tests are summarized in Table I. As the pressure is increased, the pressure at which the resistance suddenly rises is listed as the solidification pressure, while, as the pressure is decreased, the pressure at which the resistance abruptly drops is listed as the melting pressure. The inequality of the two pressures may be a reflection of adiabatic compression and expansion thermal effects and/or the slowness of the phase transitions inasmuch as these qualitative measurements were hurriedly made. Similar results were observed in the chloride salt, while the iodide is insufficiently soluble to make an 0.10 *M* solution.

Table I: Melting and Freezing Pressures for $(n\text{-C}_4\text{H}_9)_4\text{N}^+\text{Br}^-$

Temp, °C	Solidification pressure, kg/cm ²	Melting pressure, kg/cm ²
8	No solidification	Up to 4470
6	3300	2700
4	2000	1300
2	2000	1300

The solid is presumably some kind of hydrate. The fact that a solution so dilute solidifies would indicate that the salt is hydrated with a large number of water molecules. Fowler, Loebenstein, Pall, and Kraus²

(1) J. C. Walton, *J. Phys. Chem.*, **71**, 2763 (1967).

(2) E. Tschuikow-Roux and R. Paul, *ibid.*, **72**, 375 (1968).

(3) E. Gorin, *Acta Physicochim. URSS*, **6**, 691 (1938).

(1) This work was supported by the Office of Naval Research.

(2) D. L. Fowler, W. V. Loebenstein, D. B. Pall, and C. A. Kraus, *J. Am. Chem. Soc.*, **62**, 1140 (1940).

prepared the hydrates $(n\text{-C}_4\text{H}_9)_4\text{NOH}\cdot 31\text{H}_2\text{O}$ and $(n\text{-C}_4\text{H}_9)_4\text{NF}\cdot 18\text{H}_2\text{O}$ and they note that "no salts of ions other than tetra-*n*-butylammonium and tetraisoamylammonium have been found that form high hydrates." Wen and Saito³ also found that the concentration dependence of the partial molal volume of $(n\text{-C}_4\text{H}_9)_4\text{NBr}$ exhibited peculiar behavior. Similarly, we found that the tetramethyl-, -ethyl-, and -propyl bromides, chlorides, and iodides did not exhibit freezing under pressure. The solubility of some of the iodides, however, does decrease at high pressure, as evidenced by a slower increase in resistance and the precipitation of white crystals, but this slow precipitation of a fine powder contrasts so sharply with the near-instantaneous solidification throughout the $(n\text{-C}_4\text{H}_9)_4\text{NBr}$ solution into a semiclear mass, that it seems unlikely that the latter phenomenon is also the result of a pressure-induced decrease in solubility rather than hydrate formation. The crystal structure of the higher hydrates of *n*-tetrabutylammonium salts is believed to be a polyhedral clathrate-type cage.^{4,5}

The apparent stabilization of the present hydrate substance by pressure is quite extraordinary for usually the application of pressure destroys the coulombic hydration atmosphere of normal ions.^{6,7} The implication of the present finding is that, unlike the Frank-Wen cluster-like *total* coulombic hydration atmosphere of "normal" ions,⁸ the *hydrophobic hydration atmosphere* of the $(n\text{-C}_4\text{H}_9)_4\text{N}^+$ ion is more dense than the liquid water at some great distance from the ion. That is to say, the present results constitute further evidence that the local water structure near hydrophobic ions, molecules, or segments of molecules is fundamentally different from the local water structure near "normal" ions and charge sites.

(3) W. Y. Wen and S. Saito, *J. Phys. Chem.*, **68**, 2639 (1964).

(4) R. K. McMullan and G. A. Jeffrey, *J. Chem. Phys.*, **31**, 1231 (1959); **42**, 2725 (1965).

(5) R. K. McMullan, M. Bonamico, and G. A. Jeffrey, *ibid.*, **39**, 3295 (1963).

(6) R. A. Horne, *Nature*, **200**, 418 (1963).

(7) R. A. Horne, *Adv. High Pressure Res.*, in press.

(8) R. A. Horne and J. D. Birkett, *Electrochim. Acta*, **12**, 1153 (1967).

ARTHUR D. LITTLE, INC.
CAMBRIDGE, MASSACHUSETTS 02140

R. A. HORNE
R. P. YOUNG

RECEIVED AUGUST 7, 1967

On the Mechanism of Preannihilative

Electrochemiluminescence

Sir: In the following communication,¹ Chandross and Visco have proposed that thermodynamic arguments make the hypothesis of direct electrogeneration of

triplets dubious. We have suggested this process as a possible source of some emission under some circumstances.² Although we are aware of no definite evidence of such heterogeneous generation of excited states, we do not feel that it can be ruled out purely on the basis of their arguments.

The failure¹ of Chandross and Visco to observe emission from rubrene in benzonitrile until both the stable cation and anion were generated is in conflict with the results of Chang, Lytle, Roe, and Hercules,³ who found emission while oxidizing the rubrene anion in *the same solvent* at potentials as far negative as -0.2 V vs. sce. This is more than 1 V short of the R^+-R half-wave potential and cannot possibly be accounted for by Nernstian generation of R^+ followed by an ion-annihilation process.⁴

The assignment of cation decomposition products as being responsible for preannihilative emission¹ is untenable with regard to the cited works,^{2,5} since the investigations were made with sequences of potentials such that cations were not produced in the test solution until after the preannihilative emission was measured.⁶

As to whether our assignment of the phenanthrene phosphorescence emission is "questionable," Weller and Zachariasse⁷ have found such emission for chrysene under not dissimilar conditions and also note that, in the presence of paramagnetic species such as ion radicals, the radiative lifetimes of triplet states may be decreased many orders of magnitude.⁷

The main item in the paper,¹ "the thermodynamic arguments which make the hypothesis of direct electrogeneration of triplet dubious," is also worthy of comment. The thermodynamics described are a simple extension of the considerations made by Weller⁸ and others.⁹ However, the relative rates of emission and electrode reaction are unknown. It is evident that, because of the paramagnetic environment, the rate of emission has become quite rapid.⁷ Because the competing rate of triplet electron transfer at an electrode has not been experimentally measured, nothing can be said with certainty about the possibility of triplet quenching *via* heterogeneous electron transfer.

(1) E. A. Chandross and R. E. Visco, *J. Phys. Chem.*, **72**, 378 (1968).

(2) D. L. Maricle and A. H. Maurer, *J. Am. Chem. Soc.*, **89**, 188 (1967).

(3) J. Chang, F. E. Lytle, D. K. Roe, and D. M. Hercules, Symposium on Electrochemical Processes and the Energy States of Electrons, Schloss Elmau, April 23-29, 1967. CITCE Abstracts, p 71.

(4) D. K. Roe, private communication.

(5) A. Zweig, D. L. Maricle, J. S. Brinen, and A. H. Maurer, *ibid.*, **89**, 473 (1967).

(6) D. L. Maricle, A. Zweig, A. Maurer, and J. Brinen, CITCE Symposium 1967, Elman, Germany; *Electrochem. Acta*, in press.

(7) A. Weller and K. Zachariasse, *J. Chem. Phys.*, **46**, 4984 (1967).

(8) H. Leonhardt and A. Weller, *Ber. Bunsenges. Physik. Chem.*, **67**, 791 (1963).

(9) J. Feitelson and N. Shaklay, *J. Phys. Chem.*, **71**, 2582 (1967).

Finally, the comment¹ on the triplet quenching of 1,3,5-hexatriene neglected the fact that we had noted similar reservations about active olefins used as quenchers.⁵ We also noted⁵ that 1,3,5-hexatriene failed to quench 1,3,4,7-tetraphenylisobenzofuran preannihilative fluorescence emission.^{5,10} The ion radicals of the latter should be as reactive toward the triene as the phenanthrene anion radical. This is, therefore, still uncontested evidence for triplet quenching in the phenanthrene system and lack of triplet quenching in the isobenzofuran system.

(10) A. Zweig, A. K. Hoffmann, D. L. Maricle, and A. H. Maurer, *Chem. Comm.*, 106 (1967).

CENTRAL RESEARCH DIVISION
AMERICAN CYANAMID COMPANY
STAMFORD, CONNECTICUT 06904

ARNOLD ZWEIG
DONALD L. MARICLE

RECEIVED AUGUST 21, 1967

On Preannihilation Electrochemiluminescence and the Heterogeneous Electrochemical Formation of Excited States

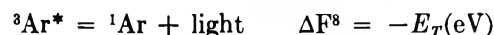
Sir: There have been two recent communications discussing the mechanism of preannihilation electrochemiluminescence (ECL). The first paper,¹ which described a study of rubrene in dimethylformamide (DMF), suggested that a portion of the observed fluorescent emission "may be due to direct generation of the triplet in a heterogeneous electron-transfer step," *via* electron transfer directly to or from the appropriate radical ion of the hydrocarbon, followed by triplet-triplet annihilation (TTA). The second paper² reported observation of luminescence assigned to phenanthrene phosphorescence upon electrooxidation of the phenanthrene radical anion in DMF solution and implied that the same generation of triplets occurred. We shall discuss some of our experimental results as well as some simple thermodynamic arguments which make the hypothesis of direct electrogeneration of triplets dubious.

We consider first the case of rubrene in DMF.³ Our studies in this solvent,⁴ although not as extensive as those of the above authors,¹ indicated that the preannihilation light is about 1% of that generated upon cation-anion annihilation.⁵ We were concerned about these results because we had previously⁵ studied 9,10-diphenylanthracene and 9,10-dimethylanthracene in acetonitrile, where the respective cations and anions are stable, and had failed to observe any preannihilation ECL. We have now studied rubrene extensively at Pt electrodes in benzonitrile.⁶ This system has the advantage over DMF that both the rubrene cation and anion are very stable, as determined by chrono-

potentiometry and cyclic voltammetry. In marked contrast to results in DMF, there was *no* luminescence in benzonitrile until both cations and anions were generated. We see no reason why the heterogeneous generation of triplets should be so solvent dependent. In DMF we have detected solvent decomposition products formed by reaction with radical cations, even though the potential never reached the normal oxidative decomposition of the solvent. Thus, results obtained in DMF for oxidations which occur much above the *see* potential are to be viewed with caution.

We have no disagreement with the postulation of fluorescence arising from homogeneous TTA. We have no comment on the assignment of the broad emission from phenanthrene as its phosphorescence, although we note that Ar^- and Ar^+ are likely to be efficient diffusion-controlled quenchers of $^3\text{Ar}^*$. However, we feel that the observations of Zweig, *et al.*,² cannot be explained on the basis of direct formation of $^3\text{Ar}^*$ at metal electrodes *via* reduction of Ar^+ or oxidation of Ar^- . Marcus⁷ suggested recently that, on theoretical grounds, the electrochemical formation of excited states at metal electrodes is unlikely.

We shall show with thermodynamic arguments that, at electrode potentials sufficient to form $^3\text{Ar}^*$ from Ar^+ or Ar^- , $^3\text{Ar}^*$ would necessarily be quenched *via* electron exchange with the electrode. Consider the following



We may now calculate couples for $^3\text{Ar}^*$



Values for representative hydrocarbons are given in Table I.

Standard potentials for couples involving $^3\text{Ar}^*$ define potential ranges over which $^3\text{Ar}^*$ would be electroactive. Since E_T is always positive, ${}^3\epsilon_{\text{ox}}$ is always less positive than ${}^1\epsilon_{\text{ox}}$ while ${}^3\epsilon_{\text{red}}$ is more positive than ${}^1\epsilon_{\text{red}}$. At potentials above ${}^3\epsilon_{\text{ox}}$, $^3\text{Ar}^*$ would be oxidized

(1) D. L. Maricle and A. H. Maurer, *J. Am. Chem. Soc.*, **89**, 188 (1967).

(2) A. Zweig, D. L. Maricle, J. S. Brinen, and A. H. Maurer, *ibid.*, **89**, 473 (1967).

(3) D. M. Hercules, R. C. Lansbury, and D. K. Roe, *ibid.*, **88**, 4578 (1966).

(4) R. E. Visco, E. A. Chandross, and J. W. Longworth, unpublished results.

(5) R. E. Visco and E. A. Chandross, *J. Am. Chem. Soc.*, **86**, 5350 (1964); E. A. Chandross, J. W. Longworth, and R. E. Visco, *ibid.*, **87**, 3259 (1965).

(6) R. E. Visco, E. A. Chandross, and R. Sonner, to be published.

(7) R. A. Marcus, *J. Chem. Phys.*, **43**, 2654 (1965).

Table I^a

	Naphthalene	Anthracene	Phenanthracene	Rubrene
E_S^b ($^1\text{Ar}^*$)	3.8	3.2	3.5	2.3
E_T ($^3\text{Ar}^*$)	+2.6	+1.8	+2.7	+1.2 ^c
$^1\epsilon_{\text{red}}^d$	-2.6	-2.0	-2.5	-1.4
$^1\epsilon_{\text{ox}}^e$	+1.5	+1.1	+1.5	+1.0 ^f
$^3\epsilon_{\text{ox}}$	-1.1	-0.7	-1.2	-0.2
$^3\epsilon_{\text{red}}$	0.0	-0.2	+0.2	-0.2

^a E_T is the energy difference between $^3\text{Ar}^*$ and ^1Ar and is positive. $\Delta F = nF\epsilon$, but we discuss only cases where $n = 1$ and ϵ (V) is equal directly to $-\Delta F$ (eV). The entropy term due to degeneracy of the triplet is small and is neglected. ^b E_S (eV) is the energy of the 0-0 fluorescence band. The rubrene value is estimated from the absorption spectrum. ^c Estimated, based on 10,250 cm^{-1} (1.27 eV) found for tetracene by S. P. McGlynn, M. R. Padhye, and M. Kasha, *J. Chem. Phys.*, **23**, 593 (1955). ^d Except for rubrene,^{1,6} G. J. Hoijtink, *Rec. Trav. Chim.*, **74**, 1525 (1955). ^e Except for rubrene,^{1,6} E. S. Pysh and N. C. Yang, *J. Am. Chem. Soc.*, **85**, 2124 (1963).

to Ar^+ . However, at potentials below $^1\epsilon_{\text{ox}}$, Ar^+ will be reduced to ^1Ar . Thus, in the range between $^3\epsilon_{\text{ox}}$ and $^1\epsilon_{\text{ox}}$, $^3\text{Ar}^*$ will be quenched by the electrode *via* electron transfer reactions. A parallel argument for the conversion of $^3\text{Ar}^*$ to ^1Ar *via* Ar^- demonstrates that the triplet will be quenched at electrode potentials between $^3\epsilon_{\text{red}}$ and $^1\epsilon_{\text{red}}$.

For the hydrocarbons cited in the table, it is obvious that $^3\epsilon_{\text{ox}}$ is generally lower than $^3\epsilon_{\text{red}}$. Therefore, $^3\text{Ar}^*$ at the electrode must be quenched over the potential range from $^1\epsilon_{\text{ox}}$ to $^1\epsilon_{\text{red}}$. This is a general conclusion for hydrocarbons smaller than tetracene, because the separation between $^1\epsilon_{\text{ox}}$ and $^1\epsilon_{\text{red}}$ is usually a few tenths of a volt greater than E_S , while $E_T > 1/2 E_S$. If $E_T < 1/2 E_S$, $^3\epsilon_{\text{ox}}$ will not lie below $^3\epsilon_{\text{red}}$ and $^3\text{Ar}^*$ would be stable over some narrow potential range. Then, however, TTA to give $^1\text{Ar}^*$ would be impossible.

These arguments also lead to the conclusion that the recently discussed⁸ heterogeneous generation of $^1\text{Ar}^*$ is impossible. Further, it will not be possible to determine oxidation and/or reduction potentials for externally generated excited states.

The only assumption involved in this argument is that the standard rate constants for electrochemical reactions involving $^3\text{Ar}^*$ are comparable to those for the similar reactions of ^1Ar . These rates would then be sufficiently fast that a nonequilibrium, steady-state concentration of $^3\text{Ar}^*$ could not be maintained. The standard rate constants for charge transfer to or from aromatic hydrocarbons are among the largest electrochemical rate constants known.^{9,10}

Preannihilation ECL of rubrene in DMF, starting from either Ar^+ or Ar^- , was observed¹ beyond certain critical potentials and continued up to the potentials for the usual ECL. This is inconsistent with the thermodynamic arguments presented here. Even if triplets could be formed at Pt electrodes over some

narrow range, the intensity of the preannihilation light arising from TTA should decrease with increasing electrode polarization. The phenanthrene case² is similar. Triplet phenanthrene could not be formed under the conditions cited² and, if Ar^- or solvent decomposition had not occurred, *the only electrochemical process possible is oxidation of Ar^-* . The luminescence might be phenanthrene phosphorescence, but an explanation other than the electrooxidation of Ar^- to $^3\text{Ar}^*$ is required. The necessity of invoking other reactions makes the spectrum assignment questionable.

The arguments presented² involving homogeneous quenchers are inconclusive. It is necessary to have a triplet quencher which is not only electroinactive, as hexatriene is, but is also inert to the foreign radicals which we feel are responsible for the homogeneous luminescent reaction. 1,3,5-Hexatriene does not meet this requirement because of its high reactivity.

In summary, we have demonstrated that $^3\text{Ar}^*$ cannot be formed by electron transfer at metal electrodes and that other explanations are required for preannihilation ECL. We believe that decomposition products are responsible in some way for the unusual observations in DMF, results which we have not found when the system is stable.

In response to the rebuttal to be published with this paper, we urge the reader to examine the pertinent references. We reiterate that the single kinetic assumption involved in the thermodynamic arguments is a reasonable one and, further, that after consideration of what is known about the electrochemistry of aromatic hydrocarbons, there is no reason to suppose that charge transfer between a triplet and an electrode should be anything but fast. Thus, any preannihilation luminescence observed must be a consequence of reactions involving impurities or decomposition products, rather than heterogeneous generation of excited states.

(8) A. Zweig, A. K. Hoffmann, D. L. Maricle, and A. H. Maurer, *Chem. Comm.*, 106 (1967).

(9) M. E. Peover and B. S. White, *J. Electroanal. Chem.*, **13**, 93 (1967).

(10) P. Malachuk, T. Miller, T. Layhoff, and R. Adams, *Proceedings of the Symposium on Exchange Reactions at Brookhaven National Laboratory*, Upton, N. Y., 1965, p 157. See also P. Malachuk, Ph.D. Thesis, University of Kansas, 1966.

BELL TELEPHONE LABORATORIES
MURRAY HILL, NEW JERSEY 07971

EDWIN A. CHANDROSS
ROBERT E. VISCO

RECEIVED AUGUST 29, 1967

Comments on the Paper "Solubilization of a Water-Insoluble Dye as a Method for Determining Micellar Molecular Weights" by Hans Schott

Sir: Schott¹ concluded from some measurements of the solubility of an organic dye in aqueous solutions of a

nonionic surfactant that the limit of solubilization was one dye molecule per surfactant micelle. He recently suggested² that if this limit were general, it could serve as the basis of a new method of determining micellar molecular weights. One would merely have to saturate an aqueous surfactant solution with a "water-insoluble" dye, filter to remove unsolubilized dye, and measure the absorbancy. Combining this information with the molar extinction coefficient of the dye and the critical micelle concentration of the surfactant, one could then calculate the ratio of the moles of aggregated surfactant (total moles of surfactant minus that present at the critical micelle concentration) to moles of solubilized dye. This ratio would represent the average number of surfactant molecules (ions) per micelle, *i.e.*, the aggregation number. Since the calculation would not be charge dependent, the method would have a decided advantage over techniques such as light scattering and ultracentrifugation where this is not the case.

Although Schott's dye solubilization procedure gave aggregation numbers for two nonionic detergents which agreed well with values provided by light scattering, it yielded an aggregation number for sodium decylsulfonate some seven times larger than that rendered by light scattering.³ The light-scattering value is undoubtedly low, since no correction for micellar charge was made. However, it is extremely unlikely that a charge correction could reduce the disagreement significantly.

Schott² stated that a possible source of error in the dye solubilization procedure is the assumption that the solubilization ratio, *i.e.*, the number of micelles per solubilized dye molecule at saturation, is unity. He subsequently dismissed this possibility, at least in the case of sodium decylsulfonate, by pointing out that a solubilization ratio smaller than unity would increase the discrepancy between the dye solubilization and light-scattering aggregation numbers and by remarking that "solubilization ratios greater than one are extremely unlikely for highly purified detergents."

It is my view that the assumption of unit solubilization ratio is the weak point in the dye-solubilization procedure for calculating aggregation numbers. A unit solubilization ratio may be a good approximation for the nonionic detergents used by Schott, but it cannot be valid generally. Kinetic considerations force one to conclude that the micelle is a dynamic entity whose size fluctuates about some equilibrium value. The ability of a surfactant monomer unit to enter into or leave the micelle structure must also be possessed by a dye molecule. The probability that a dye molecule will escape from the micelle in which it is solubilized in a specified time interval is not zero. The lower the barrier to escape, the shorter is the average time of residency of a dye molecule in a micelle, the greater is the fraction of "empty" micelles in solution, and the higher is the solubilization ratio. If the escape barrier is very high and there is room in each micelle

for only one dye molecule, the solubilization ratio will be only slightly greater than unity. If the barrier is low, the solubilization ratio will be appreciably greater than unity. Presumably, the latter situation pertains in the sodium decylsulfonate solutions which Schott examined.

Conditions are conceivable for which the solubilization ratio would be less than unity, *i.e.*, for which there would be on the average more than one solubilized dye molecule per micelle. Whereas a spherical micelle might not be able to accommodate more than a single dye molecule, a rod-like micelle would not be so restricted.

Schott² found aggregation numbers of 128, 124, 131, and 101 by his dye-solubilization procedure for micelles of sodium lauryl sulfate in 0, 0.03, 0.10, and 0.40 *m* sodium chloride, respectively. The first three values are somewhat larger than those obtained at corresponding sodium chloride concentrations by other investigators.⁴ The last value, however, is appreciably lower than all published aggregations for the surfactant in 0.40 *m* sodium chloride. The drop in aggregation number when the sodium chloride concentration is increased to 0.40 *m* is contrary to the usual observation⁴⁻⁷ that the addition of simple salts to solutions containing ionic surfactants is accompanied by an increase in the aggregation number. I suggest that Schott's experiments with sodium lauryl sulfate are best explained by solubilization ratios greater than unity in the dilute sodium chloride solutions and a ratio less than unity in the 0.40 *m* sodium chloride solution. In other words, the ratio has some dependence on the supporting electrolyte concentration.

(1) H. Schott, *J. Phys. Chem.*, **68**, 3612 (1964).

(2) H. Schott, *ibid.*, **70**, 2966 (1966).

(3) H. V. Tartar and A. L. M. Lelong, *ibid.*, **59**, 1185 (1955).

(4) See Figure 8 in E. W. Anacker, R. M. Rush, and J. S. Johnson, *ibid.*, **68**, 81 (1964).

(5) K. Granath, *Acta Chem. Scand.*, **4**, 103 (1950).

(6) J. N. Phillips and K. J. Mysels, *J. Phys. Chem.*, **59**, 325 (1955).

(7) W. Prins and J. J. Hermans, *Koninkl. Ned. Akad. Wetenschap. Proc.*, **B59**, 298 (1956).

DEPARTMENT OF CHEMISTRY
MONTANA STATE UNIVERSITY
BOZEMAN, MONTANA 59715

E. W. ANACKER

RECEIVED SEPTEMBER 5, 1967

Reply to Comments on the Paper "Solubilization of a Water-Insoluble Dye as a Method for Determining Micellar Molecular Weights," and Remarks on Molecular Weight Determination of Charged Micelles by Light Scattering

Sir: The solubilization limit of one molecule of Orange OT per micelle was found for the nonionic detergents

1-dodecanol-28 ethylene oxide units, $C_{12}(EO)_{28}$,¹ $C_{12}(EO)_{16}$,² and $NPh(EO)_{30}$,³ where NPh is branched nonylphenol. This was shown by the agreement of the micellar molecular weights (mmw) determined by dye solubilization, calculated on the assumption of unit solubilization ratio, with the mmw determined by light scattering or ultracentrifugation. Micelles of $C_{18}(EO)_{18}$ were found to contain three dye molecules at saturation, since the mmw determined by light scattering was 2.99 times greater than the mmw calculated from dye solubilization on the assumption of unit solubilization ratio. This is due to the larger hydrocarbon core of micelles of the latter detergent (calculated radius, 24 Å) as compared to radii between 15 and 18 Å calculated for the hydrocarbon cores of micelles of the three previous detergents.

Disagreement between mmw determinations by dye solubilization and by light scattering is found for charged micelles of anionic² and cationic³ detergents in water and at low concentrations of supporting electrolyte. Dye solubilization measurements indicate that the mmw values of sodium decanesulfonate ($SDSO_3$), sodium dodecyl sulfate (SDS),² dodecyl trimethyl ammonium bromide (DTAB), and cetyl pyridinium chloride (CPyC)³ are essentially constant and independent of the concentration of added electrolyte, up to the point where the micelles show appreciable polydispersity according to equilibrium ultracentrifugation.⁴ At that point, there is a slight decrease in mmw, probably indicating a rearrangement of the micelles.

Light-scattering measurements, on the other hand, indicate an apparent increase in mmw with increasing electrolyte concentration until this concentration becomes high enough to suppress or swamp the effective charge of the micelles. At that point, further increase in electrolyte concentration produces no further increase in mmw (see references listed in ref 4). The dye-solubilization mmw of SDS and DTAB at electrolyte concentrations low enough to leave the micelles predominantly monodisperse^{2,3} are in good agreement with the light-scattering mmw determined in swamping electrolyte.⁴

To account for the discrepancy in mmw of ionic detergents at less than swamping electrolyte concentrations, Anacker suggests that the solubilization ratio depends on the concentration of added electrolyte. This seems unlikely in view of the following. The dye has negligible solubility in water and in solutions of $NaCl$ and Na_2SO_4 (less than 2×10^{-9} mole/l.), probably because the hydroxyl is internally hydrogen bonded to the azo group, but is moderately soluble in solvents of low or medium polarity. Therefore, the solubilized dye molecules are probably located in the hydrocarbon core of the micelles, out of contact with the aqueous phase.

An alternative explanation for the discrepancy is given by Hutchinson's treatment of light scattering.⁵ Hutch-

inson concludes that (a) light-scattering measurements of charged micelles in solutions containing little or no supporting electrolyte give information on the charge rather than on the size of the micelles; (b) the correct mmw is obtained by light scattering only in the presence of swamping electrolyte, where the situation is essentially nonionic; and (c) the mmw is unchanged by the addition of electrolyte. This points to the need for much more extensive corrections in interpreting light scattering by multicomponent systems involving charged particles than are presently made, a viewpoint which has received considerable support recently.⁶⁻⁹

The concept of a small, constant, and integral number of solubilized molecules per micelle at saturation, independent of the concentration of detergent and of added electrolytes, was established by G. Spencer Hartley thirty years ago.¹⁰ For Orange OT, we found this number to be unity for all detergents mentioned here, except for $C_{18}(EO)_{18}$ and CPyC, where it is 3. This concept can readily be reconciled with Anacker's kinetic considerations if one considers that the solubilized dye molecules act as nuclei for micelle formation. When a micelle containing a dye molecule dissociates, most likely a few detergent molecules remain attached to this dye molecule. This aggregate then acts as the nucleus around which another micelle forms.

The reason why light-scattering determinations of the mmw of charged micelles at less than swamping concentrations of supporting electrolyte are low is probably connected with the downward curvature occurring in the light-scattering plots of polymeric polyelectrolytes at low concentrations. Plots of the kind shown in Figure 1, where H is an optical constant, τ the turbidity, and c the polymer concentration, have been reported for a variety of polyelectrolytes such as sodium polymethacrylate,¹¹ bovine serum albumin,¹² phosphotungstic,¹³ and silicotungstic acids.^{9,13,14} Going from swamping concentration of added salt to 0.1 M and to water results in progressively steeper decreases in Hc/τ with decreasing polyelectrolyte concentration,

- (1) H. Schott, *J. Phys. Chem.*, **68**, 3612 (1964).
- (2) H. Schott, *ibid.*, **70**, 2966 (1966).
- (3) H. Schott, *ibid.*, **71**, 3611 (1967).
- (4) E. W. Anacker, R. M. Rush, and J. S. Johnson, *ibid.*, **68**, 81 (1964).
- (5) E. Hutchinson, *J. Colloid Sci.*, **9**, 191 (1954).
- (6) A. Vrij and J. Th. G. Overbeek, *ibid.*, **17**, 570 (1962).
- (7) R. K. Bullough, *Proc. Roy. Soc. (London)*, **A275**, 271 (1963).
- (8) E. F. Casassa and H. Eisenberg, *Advan. Protein Chem.*, **19**, 287 (1964).
- (9) J. P. Kratochvil, L. E. Oppenheimer, and M. Kerker, *J. Phys. Chem.*, **70**, 2834 (1966).
- (10) G. S. Hartley, *J. Chem. Soc.*, 1968 (1938).
- (11) A. Oth and P. Doty, *J. Phys. Chem.*, **56**, 43 (1952).
- (12) P. Doty and R. F. Steiner, *J. Chem. Phys.*, **20**, 85 (1952).
- (13) M. Kerker, J. P. Kratochvil, R. H. Ottewill, and E. Matijevic, *J. Phys. Chem.*, **67**, 1097 (1963).
- (14) M. J. Kronman and S. N. Timasheff, *ibid.*, **63**, 629 (1959).

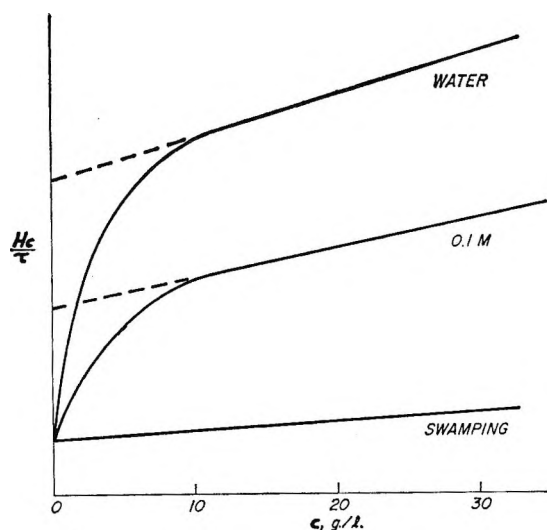


Figure 1. Light-scattering plot for polyelectrolytes.

owing to strong repulsive forces between the polyions.¹⁴ Only the curve in swamping concentration of added salt is linear over the whole range of polyelectrolyte concentration. Extrapolating the linear portions of the plots in water to zero concentration results in intercepts with the ordinate which are from 3 to 6 times greater than the actual intercepts. Therefore, molecular weights calculated from the extrapolated intercepts would be from three to six times too small.

For light-scattering plots of detergents, one uses the concentration of micelles, *i.e.*, the over-all detergent concentration minus the critical micelle concentration (cmc). Since turbidity is proportional to the square of the mass of the scattering particle, the light-scattering contribution of micelles will be far greater than that of monomers, dimers, trimers, and other submicellar ag-

gregates of detergent molecules. However, such small aggregates may be able to exert repulsive forces far greater in proportion to the repulsive forces exerted by micelles than their contribution to turbidity is in proportion to the turbidity caused by micelles, owing to binding of counterions in the latter.^{15,16} Thus, the downturn in the Hc/τ vs. c curve for detergents in water with decreasing detergent concentration would not be expected to occur at a very low concentration of micelles, *i.e.*, just above the cmc, but at a still lower over-all detergent concentration, where there is a very low concentration of submicellar aggregates as well. This latter concentration can only be reached below the cmc, *i.e.*, after disappearance of the micelles. This hypothesis explains (a) why Hc/τ vs. c plots for ionic association colloids in water do not show the downturn at low concentration of micelles which is observed for low concentrations of nonassociated polyelectrolytes, and (b) why the light-scattering mmw of ionic micelles determined in water is from two to seven times smaller than the correct mmw, found by dye solubilization in water and at low electrolyte concentrations, and by light scattering in swamping electrolyte.

Since swamping electrolyte concentrations are of the order of 0.1–0.3 M ,⁹ and the cmc values of the common ionic detergents in water are about ten times smaller, the concentration of nonmicellar detergent is far too small to swamp the effective charge of the micelles.

(15) A. P. Brady and D. J. Salley, *J. Am. Chem. Soc.*, **70**, 914 (1948).

(16) K. J. Mysels and C. I. Dulin, *J. Colloid Sci.*, **10**, 461 (1955).

U. S. FOREST PRODUCTS LABORATORY
MADISON, WISCONSIN 53705

HANS SCHOTT

RECEIVED OCTOBER 30, 1967